frontiers | Research Topics

Coastal environmental and ecological data analysis

Edited by
Meilin Wu, Yu-Pin Lin, Biraja Kumar Sahu and
Ana Carolina Ruiz-Fernández

Published in
Frontiers in Marine Science

FRONTIERS EBOOK COPYRIGHT STATEMENT

The copyright in the text of individual articles in this ebook is the property of their respective authors or their respective institutions or funders. The copyright in graphics and images within each article may be subject to copyright of other parties. In both cases this is subject to a license granted to Frontiers.

The compilation of articles constituting this ebook is the property of Frontiers.

Each article within this ebook, and the ebook itself, are published under the most recent version of the Creative Commons CC-BY licence. The version current at the date of publication of this ebook is CC-BY 4.0. If the CC-BY licence is updated, the licence granted by Frontiers is automatically updated to the new version.

When exercising any right under the CC-BY licence, Frontiers must be attributed as the original publisher of the article or ebook, as applicable.

Authors have the responsibility of ensuring that any graphics or other materials which are the property of others may be included in the CC-BY licence, but this should be checked before relying on the CC-BY licence to reproduce those materials. Any copyright notices relating to those materials must be complied with.

Copyright and source acknowledgement notices may not be removed and must be displayed in any copy, derivative work or partial copy which includes the elements in question.

All copyright, and all rights therein, are protected by national and international copyright laws. The above represents a summary only. For further information please read Frontiers' Conditions for Website Use and Copyright Statement, and the applicable CC-BY licence.

ISSN 1664-8714
ISBN 978-2-83251-576-1
DOI 10.3389/978-2-83251-576-1

About Frontiers

Frontiers is more than just an open access publisher of scholarly articles: it is a pioneering approach to the world of academia, radically improving the way scholarly research is managed. The grand vision of Frontiers is a world where all people have an equal opportunity to seek, share and generate knowledge. Frontiers provides immediate and permanent online open access to all its publications, but this alone is not enough to realize our grand goals.

Frontiers journal series

The Frontiers journal series is a multi-tier and interdisciplinary set of open-access, online journals, promising a paradigm shift from the current review, selection and dissemination processes in academic publishing. All Frontiers journals are driven by researchers for researchers; therefore, they constitute a service to the scholarly community. At the same time, the *Frontiers journal series* operates on a revolutionary invention, the tiered publishing system, initially addressing specific communities of scholars, and gradually climbing up to broader public understanding, thus serving the interests of the lay society, too.

Dedication to quality

Each Frontiers article is a landmark of the highest quality, thanks to genuinely collaborative interactions between authors and review editors, who include some of the world's best academicians. Research must be certified by peers before entering a stream of knowledge that may eventually reach the public - and shape society; therefore, Frontiers only applies the most rigorous and unbiased reviews. Frontiers revolutionizes research publishing by freely delivering the most outstanding research, evaluated with no bias from both the academic and social point of view. By applying the most advanced information technologies, Frontiers is catapulting scholarly publishing into a new generation.

What are Frontiers Research Topics?

Frontiers Research Topics are very popular trademarks of the *Frontiers journals series*: they are collections of at least ten articles, all centered on a particular subject. With their unique mix of varied contributions from Original Research to Review Articles, Frontiers Research Topics unify the most influential researchers, the latest key findings and historical advances in a hot research area.

Find out more on how to host your own Frontiers Research Topic or contribute to one as an author by contacting the Frontiers editorial office: frontiersin.org/about/contact

Coastal environmental and ecological data analysis

Topic editors

Meilin Wu — South China Sea Institute of Oceanology, Chinese Academy of Sciences (CAS), China

Yu-Pin Lin — National Taiwan University, Taiwan

Biraja Kumar Sahu — National Institute of Oceanography, Council of Scientific and Industrial Research (CSIR), India

Ana Carolina Ruiz-Fernández — National Autonomous University of Mexico, Mexico

Citation

Wu, M., Lin, Y.-P., Sahu, B. K., Ruiz-Fernández, A. C., eds. (2023). *Coastal environmental and ecological data analysis*. Lausanne: Frontiers Media SA.

doi: 10.3389/978-2-83251-576-1

Table of contents

06 Editorial: Coastal environmental and ecological data analysis
Meilin Wu, Yu-Pin Lin, Ana Carolina Ruiz-Fernández and Biraja Kumar Sahu

10 Evaluation of Site Suitability for Artificial Reefs Deployment in Southeast Coast of India Using Geographical Information System as a Management Tool
Dilip Kumar Jha, Vikas Pandey, J. Santhanakumar, P. Sathish Kumar, S. Venkatnarayanan, J. Prince Prakash Jebakumar, G. Dharani and R. Vijaya

18 Seasonal Variation of Food Web Structure and Stability of a Typical Artificial Reef Ecosystem in Bohai Sea, China
Shengpeng Li, Ruyue Wang, Yueming Jiang, Yanyu Li, Lin Zhu and Jianfeng Feng

27 Switch of Bacteria Community Under Oxygen Depletion in Sediment of Bohai Sea
Xiaoxiao Guo, Guisheng Song, Yanying Li, Liang Zhao and Jing Wang

40 Distribution, Diversity, and Abundance of Nitrite Oxidizing Bacteria in the Subterranean Estuary of the Daya Bay
Wei Sun, Lijing Jiao, Jiapeng Wu, Mingken Wei and Yiguo Hong

53 Phytoplankton Species Diversity Patterns and Associated Driving Factors in China's Jiulong River Estuary: Roles That Nutrients and Nutrient Ratios Play
Feiyang Ge, Zhiyuan Ma, Bin Chen, Yu Wang, Xiaoqian Lu, Shenqun An, Dian Zhang, Wanting Zhang, Weiwei Yu, Wenxuan Han, Xingguang Yu, Zhenghua Liu and Fangfang Kuang

70 Discrepant Effects of Oceanic Advection in the Evolution of SST Anomalies in the South China Sea During El Niño of Different Intensities
Fuan Xiao, Dongxiao Wang, Qiaoyan Wu, Wei Song, Lili Zeng, Qiang Xie and Yan Wang

85 Differences of Macroalgal Consumption by Eight Herbivorous Coral Reef Fishes From the Xisha Islands, China
Peng Wu, Teng Wang, Yong Liu, Chunhou Li, Yayuan Xiao, Shannan Xu, Tingting Han, Lin Lin and Qiumei Quan

99 Comparative Study of Nitrogen Cycling Between a Bay With Riverine Input and a Bay Without Riverine Input, Inferred From Stable Isotopes
Chunqing Chen, Qibin Lao, Youli Shen, Guangzhe Jin, Fajin Chen, Qizhong Su, Xuetie Lei, Xin Zhou, Xuan Lu, Qingmei Zhu and Guoqiang Liu

116 Community Structure of Benthic Macrofauna and the Ecological Quality of Mangrove Wetlands in Hainan, China
Ping Li, Jingli Liu, Jiankun Bai, Yifan Tong, Yuchen Meng, Xiaoping Diao, Ke Pan, Xiaoshan Zhu and Guanghui Lin

125 Variations and Environmental Controls of Primary Productivity in the Amundsen Sea
Jianlong Feng, Delei Li, Jing Zhang and Liang Zhao

140 Plankton Metabolism in Coastal Waters of the Guangdong-Hong Kong-Macao Greater Bay: Regional Variance and Driving Factors
Liangkui Zhang, Gang Li, Chenhui Xiang, Yadong Huang, Xiaoming Fu, Chuanyang Zheng, Zheng Wang, Zhiyuan Ouyang and Xingyu Song

154 Impact of Environmental Regulation on Coastal Marine Pollution—A Case of Coastal Prefecture-Level Cities in China
Jintao Ma, Qiuguang Hu and Xinyi Wei

167 Conditions of Mainland China's Island Ecosystems and Associated Influencing Factors: Integrated Assessment of 42 Typical Island Ecosystems
Zhiyuan Ma, Weiwei Yu, Wanting Zhang, Feiyang Ge, Bin Chen, Wenjia Hu, Dian Zhang, Jianji Liao, Hao Huang, Yuanmin Sun and Haiping Huang

179 Ecological Distribution and Diversity of Key Functional Genes for Denitrification in Surface Sediments of the Northern South China Sea: Implications for Potential N_2O Emissions
Hua Xiang, Yiguo Hong, Jiapeng Wu and Aimin Long

191 Contaminant Characteristics and Influencing Factors of Heavy Metals in Seawater and Sediments in a Typical Mariculture Bay in South China
Qibin Lao, Shangjun Cai, Peng Huang, Fajin Chen, Qizhong Su, Xuetie Lei, Xin Zhou, Chunqing Chen, Qingmei Zhu, Xuan Lu and Guoqiang Liu

205 Organic Enrichment Induces Shifts in the Trophic Position of Infauna in a Subtropical Benthic Food Web, Hong Kong
Wenzhe Xu, Paul K. S. Shin and Jun Sun

214 Impacts of Human Activities and Environmental Changes on Spatial-Seasonal Variations of Metals in Surface Sediments of Zhanjiang Bay, China
Fengxia Zhou, Mengqi Xiong, Shuangling Wang, Sheng Tian, Guangzhe Jin, Fajin Chen, Chunqing Chen, Xuan Lu, Qingmei Zhu and Yafei Meng

230 Application of Microalgae Assemblages' Parameters for Ecological Monitoring in Mangrove Forest
Aniefiok Ini Inyang, You-Shao Wang and Hao Cheng

245 Linkages Between Optical and Molecular Signatures of Dissolved Organic Matter Along the Yangtze River Estuary-to-East China Sea Continuum
Xingnian Sun, Penghui Li, Yuping Zhou, Chen He, Fang Cao, Yuntao Wang, Quan Shi and Ding He

257 Distribution, Sources, and Biogeochemistry of Carbon Pools (DIC, DOC, and POC) in the Mangrove-Fringed Zhangjiang Estuary, China
Ran Yan, Jianxiang Feng, Yuming Wang, Linxi Fu, Xiangxin Luo, Lixia Niu and Qingshu Yang

269 Investigation of Coastal Water Characteristics Along the Southeast Coast of India: A Multivariate Approach
Dilip Kumar Jha, Vikas Pandey, Chandrasekaran Muthukumar, Ponnusamy Sathish Kumar, Srinivas Venkatnarayanan, Jebarathnam Prince Prakash Jebakumar and Gopal Dharani

275 Effects of decabromodiphenyl ether (BDE-209) on a mangrove plant, *Kandelia obovata* and the uptake, translocation and accumulation of BDE-209
Ying Wang, Yi-Tong Du and Nora Fung-Yee Tam

284 Sources of nitrate in a heavily nitrogen pollution bay in Beibu Gulf, as identified using stable isotopes
Shangjun Cai, Qibin Lao, Guangzhe Jin, Chunqing Chen, Xin Zhou, Qingmei Zhu and Xuan Lu

299 Characteristics of Dissolved Organic Matter in a Semi-closed Bay in Summer: Insights from Stable Isotope and Optical Analyses
Yafeng Zhong, Gang Pan, Hui Zhao and Chao Wang

310 Incorporating coastal blue carbon into subnational greenhouse gas inventories
Peng Zhao, Song Ge, Dinghua He, Cairong Zhong, Boyan Wang, Xiaokang Wang, Fengxia Wang and Shuhji Kao

320 Effect of cyclonic storm *Vardah* on the community structure and ecosystem functioning of macrobenthic fauna in the intertidal region of South Andaman Islands
Nosad Sahu, Raj Kiran Lakra and Ganesh Thiruchitrambalam

329 Biological–physical oceanographic coupling influencing particulate organic matter in the South Yellow Sea
Congcong Guo, Shu Yang, Weidong Zhai, Yao Niu and Chunli Liu

353 Seasonal variations in biochemical and stable isotope compositions of particulate organic matter in two contrasting temperate coastal lagoons of Korea
Dong-Young Lee, Jung Hyun Kwak, Tae Hee Park, Hee Yoon Kang, Dongyoung Kim, Sungmin Hwang and Hyun Je Park

368 Coastal environmental and atmospheric data reduction in the Southern North Sea supporting ecological impact studies
Lőrinc Mészáros, Frank van der Meulen, Geurt Jongbloed and Ghada El Serafy

frontiers | Frontiers in Marine Science

TYPE Editorial
PUBLISHED 20 January 2023
DOI 10.3389/fmars.2022.1126086

Check for updates

OPEN ACCESS

EDITED AND REVIEWED BY
Hans Uwe Dahms,
Kaohsiung Medical University, Taiwan

*CORRESPONDENCE
Meilin Wu
mlwu@scsio.ac.cn

SPECIALTY SECTION
This article was submitted to Marine Pollution, a section of the journal Frontiers in Marine Science

RECEIVED 17 December 2022
ACCEPTED 30 December 2022
PUBLISHED 20 January 2023

CITATION
Wu M, Lin Y-P, Ruiz-Fernández AC and Sahu BK (2023) Editorial: Coastal environmental and ecological data analysis. *Front. Mar. Sci.* 9:1126086. doi: 10.3389/fmars.2022.1126086

COPYRIGHT
© 2023 Wu, Lin, Ruiz-Fernández and Sahu. This is an open-access article distributed under the terms of the Creative Commons Attribution License (CC BY). The use, distribution or reproduction in other forums is permitted, provided the original author(s) and the copyright owner(s) are credited and that the original publication in this journal is cited, in accordance with accepted academic practice. No use, distribution or reproduction is permitted which does not comply with these terms.

Editorial: Coastal environmental and ecological data analysis

Meilin Wu[1,2,3]*, Yu-Pin Lin[4], Ana Carolina Ruiz-Fernández[5] and Biraja Kumar Sahu[6]

[1]State Key Laboratory of Tropical Oceanography, South China Sea Institute of Oceanology, Chinese Academy of Sciences, Guangzhou, China, [2]Southern Marine Science and Engineering Guangdong Laboratory (Guangzhou), Guangzhou, China, [3]Innovation Academy of South China Sea Ecology and Environmental Engineering, Chinese Academy of Sciences, Guangzhou, China, [4]Department of Bioenvironmental Systems Engineering, National Taiwan University, Taipei, Taiwan, [5]Instituto de Ciencias del Mar y Limnología, Unidad Académica Mazatlán, Universidad Nacional Autónoma de México, Mazatlán, Mexico, [6]Integrated Oceanography Division, National Institute of Oceanography, Goa, India

KEYWORDS

coastal environment, coastal water quality, temporal and spatial variation, long-term ecology, anthropogenic effects

Editorial on the Research Topic
Coastal environmental and ecological data analysis

The coastal seas are one of the most important areas of the ocean and land. Approximately 3 billion people – about half of the world's population – live within 60 km of the coastline. At the same time, a total of 14 of the world's 17 largest cities are located along coasts (Brown and Hausner, 2017). Pervasive environmental pollution and occurrence of natural disasters in the coastal waters result in serious environmental and ecological problems. Eutrophication, hypoxia, and other adverse effects caused by anthropogenic activities are recognized as growing problems in many estuaries and coastal areas around the world. Hence, implementing regular monitoring programs is paramount to help understand the spatial and temporal variations of coastal water quality, with the purpose to prevent and mitigate marine pollution.

Long-term ecological monitoring networks have been established in coastal areas to evaluate eutrophication and other environmental problems like harmful algal blooms (HABs), heavy metal pollution and their biomagnifications, etc, and this measurement of hydro-chemical variables and biological indicators in the coastal environment will aid better understanding of aquatic environment. These monitoring programs produce huge datasets, and it becomes really difficult to extract latent meaningful information from these datasets. To extract the latent meaningful information, chemometrics, multivariate statistical analysis and different biotic indices for biodiversity data are used. It may include factor analysis, cluster analysis, discriminant analysis, self-organizing maps, artificial neural network, canonical correspondence analysis, redundancy analysis and many biotic indices (Wu and Wang, 2007; Wu et al., 2009a; Wu et al., 2009b; Wu et al., 2010; Dong et al., 2010a; Dong et al., 2010b; Wu et al., 2011; Wu et al., 2012a; Wu et al., 2012b; Wu et al., 2012c; Ling et al., 2014; Wu et al., 2015a; Wu et al., 2015b; Wu et al., 2016; Wu et al., 2020). These methods identify the spatial and temporal variation of water quality in coastal waters and help to elucidate the processes involved in it. The multivariate statistical analysis identifies different

patterns in the datasets and provides meaningful underlying information which would be rather difficult just seeing the raw data or using traditional statistics techniques.

The aim of this Research Topic is to explore the recently used or newly developed methodologies involving chemometrics, multivariate analysis or biotic indices, with an emphasis on Land-Ocean Interactions in the Coastal Zone, to solve the environmental and ecological problems.

Multivariate statistical analysis

The multiple ecosystemic services of the coastal zone are at risk owing to the development of human activities and the occurrence of natural extreme events. Firstly, coastal environment and ecosystems receive the excessive fluxes of waste water discharges and residues that promote eutrophication, ocean acidification, hypoxia, HABs, heavy metal pollution and their biomagnifications, etc. Secondly, the occurrence of extreme events such as storms and typhoon in the coastal zones is increasing. Thirdly, relevant coastal carbon sinks, such as to mangrove, seagrass and coral reefs are under stronge pressure due to global change. These changes also support the need to measure hydro-chemical variables and biological indicators. Analysis of variance (ANOVA-one way) showed significant ($p < 0.05$) spatial variation for depth, slope, seawater current, salinity, chlorophyll-a, benthic density, and diversity of coral reef in the southeast coast of India. The geographical information system (GIS) based model output showed space allocation for artificial reef deployment; that will help to conserve the fish stock and support the fishermen in the coastal regions (Jha et al.). Statistical analysis including principal component analysis, combined with the subterranean estuary dynamic variation, indicated that dissolved organic carbon (DOC), salinity, and ammonium concentrations along the sediment depths was related with the vertical community distribution of the Nitrospira species in Daya Bay, South China Sea (Sun et al.). Jiulong River estuary of Chian was subdivided into three subregions, including the upper (Area I), middle (Area II), and lower reaches (Area III) of the estuary. The diversity patterns of phytoplankton were shown to vary at different scales, in different seasons and in different indices in Jiulong River estuary. It is noteworthy that the significant roles that nutrients and nutrient ratios played in shaping phytoplankton diversity patterns and the nutrient balance were characterized by excess nitrogen (N) and silicon (Si) and limited phosphorus (P), which could potentially cause diatom blooms (Ge et al.). Based on canonical correspondence analysis, it was deduced that the variations of the community structure and potential functions of microbes in expanding marine hypoxic area in Bohai Sea could be influenced by depth, $NO2–$ concentration and DO availability (Guo et al.). Non-metric multidimensional scaling and an analysis of similarities revealed significant seasonal and spatial differences among macroinvertebrate assemblages in Hainan, China (Li et al.). Multivariate analysis revealed that the dynamics of phytoplankton alpha-diversity and algal pollution indices was influenced by environmental conditions (e.g., nutrients) particularly by trophic states changes (Inyang et al.). Cluster analysis revealed that composition of the macroalgae consumed by eight fish species from Xisha Islands,China, was always grouped together (Wu et al.). The Amundsen Sea was divided into nine bioregions by cluster analysis in the Antarctic (Feng et al.). A self-organizing map analysis using the environmental data revealed that the spatiotemporal variations in salinity and nutrient concentrations differed significantly between the two lagoon systems in two contrasting temperate coastal lagoons of Korea. Canonical correlation analysis highlighted that the POM properties differed according to physicochemical factors in two contrasting temperate coastal lagoons of Korea (Lee et al.). Multivariate tool indicated that except near-shore sites, there is a good seawater quality at Thanjavur in the southeast coast of India (Jha et al.). Temporal changes in faunal assemblages were evidenced through multivariate technique in the intertidal region of South Andaman Islands (Sahu et al.)

Data mining and ecosystem modelling

Studies using big data methods are alsoi included in this special issue. Loop analysis revealed that the heaviest feedback loops are the interactions among benthos, zooplankton, and phytoplankton; and the predator-prey negative interaction strength between zooplankton and phytoplankton dominated the stability of an artificial reef, whether in summer or autumn in the Bohai Sea (Li et al.). The maximum gross primary producti-on and community respiration occurred in the estuarine plume of the Guangdong-Hong Kong-Macao Greater Bay Areain summer, while in winter the more active metabolisms of plankton community occurred in the Daya Bay by principal component analysis (Zhang et al.). Wth a model on the basis of the nonlinear impact of environmental regulation on coastal marine environmental pollution, the level of environmental regulation and the degree of coastal marine pollution in 46 coastal prefecture-level cities in China from 2004 to 2016 was identified in the coastal prefecture-level cities ofChina (Ma et al.). In subtropical waters of Hong Kong, it was found that some omnivorous infauna shifted from a mainly carnivorous diet at the unpolluted site to a largely herbivorous diet at the organically polluted site by standard deviation of nearest neighbour distance (Xu et al.). The first (second) warming peak is warmer than the second (first) one for super (other) El Niño composite in the South China Sea (Xiao et al.). Chen et al. used mixing model and concluded that atmospheric deposition contributes to the nitrate pool in water and that the impact of atmospheric deposition on the whole Beibu Gulf is relatively consistent.

The ecological distribution profiles of the nirS, nosZ I, and nosZ II gene communities varied with water depth, and denitrification genes in shallow-sea and deep-sea sediments differed in their sensitivity to environmental factors in the South China Sea (Xiang et al.). The estimates of the resuspended fraction of the proportion of resuspended particles in total suspended matter showed a substantial uncertainty of 50% in summer, likely owing to the potential errors of model parameter estimation and the influence of other unexplored biophysical processes such as biological degradation, upwelling, and monsoons, combined a simplified ecosystem model and vertical mixing model (Guo et al.). Island ecosystem conditions were influenced by both natural and anthropogenic factors as well as area size, population, and gross domestic product (GDP) in the 42 typical, representative islands

within China's coastal regions (Ma et al.). The data reduction potentials and explanatory value of these methods are showcased and important atmospheric variables affecting the chlorophyll-a concentration are identified in the Dutch Wadden Sea (Mészáros et al.).

Seasonal variations in the concentration of heavy metals were found in both seawater and sediment from Qinzhou Bay, as a result of seasonal hydrological change, biological activity, and human influence (Lao et al.). The combined assessment results of enrichment factor, contaminated factor and the percentages of acid soluble fraction indicated that surface sediments of Zhanjiang Bay were generally contaminated by Cd and Zn,and that their concentrations may pose medium to high risk to the environment (Zhou et al.). CO_2 emission from mangrove deforestation and N_2O emission from shrimp aquaculture in coastal aeras may offset the efforts of coastal wetlands conservation and restoration in the Hainan province of China (Zhao et al.). Mangrove plants could take up and accumulate PBDEs; and although BDE-209 is less toxic than other congeners, it is more difficult to be removed by mangrove systems (Wang et al.). Biogeochemical processes have little impact on nitrate dual isotopes under heavy nitrogen pollution, and isotopes are an ideal proxy for tracing nitrogen sources in Beibu Gulf, China (Cai et al.). There were many sources of organic matter in the bay, including inputs of soil, algae, and sewage. Influenced by freshwater input, dissolved organic matter decreased from the upper to the outer zone in Zhanjiang Bay (Zhong et al.). The combination of the untargeted FT-ICR MS approach and optical techniques could be valuable for studying the DOM sources and transformation in large river estuarine systems along the Yangtze River Estuary-to-East China Sea Continuum (Sun et al.). The source of the particulate organic carbon is overwhelmingly the mariculture, averagely accounting for 42.7% in the flood season and 52.6% in the dry season, mainly in the form of microalgae in Zhangjiang Estuary (Yan et al.).

Contribution and perspectives

In this special issue, we introduce the Research Topic "*Coastal Environmental and Ecological Data Analysis*" to analyze the structure and functioning of diverse coastal ecosystems around global, adressing topics related with water quality, mangrove, coral reef and CO_2 emissions. Experimental data for mining is important in the law and theory of the science. Outputs of these big database can improve the knowledge of us. In the 29 papers, the special issue provides a better understanding of the data monitoring, data analysis, and data integration. Thus, the knowledge of this special issue is by no means a closed chapter. In particular, we hope for significant insights from the novel big data, which can provide a high level of scientific, administrative and financial integration of coastal environmental and ecological sciences.

Author contributions

All authors listed have made a substantial, direct and intellectual contribution to the work, and approved it for publication.

Acknowledgments

We thank all the reviewers and scientists who contributed to this Research Topic.

Conflict of interest

The authors declare that the research was conducted in the absence of any commercial or financial relationships that could be construed as a potential conflict of interest.

Publisher's note

All claims expressed in this article are solely those of the authors and do not necessarily represent those of their affiliated organizations, or those of the publisher, the editors and the reviewers. Any product that may be evaluated in this article, or claim that may be made by its manufacturer, is not guaranteed or endorsed by the publisher.

References

Brown, G., and Hausner, V. H. (2017). An empirical analysis of cultural ecosystem values in coastal landscapes. *Ocean. Coast. Manage.* 142, 49–60. doi: 10.1016/j.ocecoaman.2017.03.019

Dong, J. D., Zhang, Y. Y., Wang, Y. S., Wu, M. L., Zhang, S., and Cai, C. H. (2010a). Chemometry use in the evaluation of the sanya bay water quality. *Braz. J. Oceanogr.* 58 (4), 339–352. doi: 10.1590/S1679-87592010000400008

Dong, J. D., Zhang, Y. Y., Zhang, S., Wang, Y. S., Yang, Z. H., and Wu, M. L. (2010b). Identification of temporal and spatial variations of water quality in sanya bay, China by three-way principal component analysis. *Environ. Earth Sci.* 60 (8), 1673–1682. doi: 10.1007/s12665-009-0301-4

Ling, J., Wu, M. L., Chen, Y. F., Zhang, Y. Y., and Dong, J. D. (2014). Identification of spatial and temporal patterns of coastal waters in sanya bay, south China Sea by chemometrics. *J. Environ. Inf.* 23 (1), 37–43. doi: 10.3808/jei.201400255

Wu, Z. Z., Che, Z. W., Wang, Y. S., Dong, J. D., and Wu, M. L. (2015b). Identification of surface water quality along the coast of sanya, south China Sea. *PloS One* 10 (4), e0123515. doi: 10.1371/journal.pone.0123515

Wu, M. L., Ling, J., Long, L. J., Zhang, S., Zhang, Y. Y., Wang, Y. S., et al. (2012b). Influence of human activity and monsoon dynamics on spatial and temporal hydrochemistry in tropical coastal waters (Sanya bay, south China Sea). *Chem. Ecol.* 28 (4), 375–390. doi: 10.1080/02757540.2011.650167

Wu, M. L., and Wang, Y. S. (2007). Using chemometrics to evaluate anthropogenic effects in daya bay, China. *Estuar. Coast. Shelf. Sci.* 72 (4), 732–742. doi: 10.1016/j.ecss.2006.11.032

Wu, M. L., Wang, Y. T., Cheng, H., Sun, F. L., Fei, J., Sun, C. C., et al. (2020). Phytoplankton community, structure and succession delineated by partial least square regression in daya bay, south China Sea. *Ecotoxicology* 29 (6), 751–761. doi: 10.1007/s10646-020-02188-2

Wu, M. L., Wang, Y. S., and Gu, J. D. (2015a). Assessment for water quality by artificial neural network in daya bay, south China Sea. *Ecotoxicology* 24 (7-8), 1632–1642. doi: 10.1007/s10646-015-1453-5

Wu, M. L., Wang, Y. S., Sun, C. C., Sun, F. L., Cheng, H., Wang, Y. T., et al. (2012a). Monsoon-driven dynamics of water quality by multivariate statistical methods in daya bay, south China Sea. *Oceanolog. Hydrobiolog. Stud.* 41 (4), 66–76. doi: 10.2478/s13545-012-0040-0

Wu, M. L., Wang, Y. S., Sun, C. C., Wang, H. L., Dong, J. D., and Han, S. H. (2009a). Identification of anthropogenic effects and seasonality on water quality in daya bay, south China Sea. *J. Environ. Manage.* 90 (10), 3082–3090. doi: 10.1016/j.jenvman.2009.04.017

Wu, M. L., Wang, Y. S., Sun, C. C., Wang, H. L., Dong, J. D., Yin, J. P., et al. (2010). Identification of coastal water quality by statistical analysis methods in daya bay, south China Sea. *Mar. Pollut. Bull.* 60 (6), 852–860. doi: 10.1016/j.marpolbul.2010.01.007

Wu, M. L., Wang, Y. S., Sun, C. C., Wang, H. L., Lou, Z. P., and Dong, J. D. (2009b). Using chemometrics to identify water quality in daya bay, China. *Oceanologia* 51 (2), 217–232. doi: 10.5697/oc.51-2.217

Wu, M.-L., Wang, Y.-S., Wang, Y.-T., Sun, F.-L., Sun, C.-C., Cheng, H., et al. (2016). Seasonal and spatial variations of water quality and trophic status in daya bay, south China Sea. *Mar. Pollut. Bull.* 112 (1-2), 341–348. doi: 10.1016/j.marpolbul.2016.07.042

Wu, M. L., Zhang, Y. Y., Dong, J. D., Cai, C. H., Wang, Y. S., Long, L. J., et al. (2012c). Monsoon-driven dynamics of environmental factors and phytoplankton in tropical sanya bay, south China sea. *Oceanolog. Hydrobiolog. Stud.* 41 (1), 57–66. doi: 10.2478/s13545-012-0007-1

Wu, M. L., Zhang, Y. Y., Dong, J. D., Wang, Y. S., and Cai, C. H. (2011). Identification of coastal water quality by self-organizing map in sanya bay, south China Sea. *Aquat. Ecosyst. Health Manage.* 14 (3), 291–297. doi: 10.1080/14634988.2011.604273

frontiers in Marine Science

ORIGINAL RESEARCH
published: 25 January 2022
doi: 10.3389/fmars.2021.817975

Evaluation of Site Suitability for Artificial Reefs Deployment in Southeast Coast of India Using Geographical Information System as a Management Tool

Dilip Kumar Jha[1], Vikas Pandey[1], J. Santhanakumar[1], P. Sathish Kumar[1], S. Venkatnarayanan[1], J. Prince Prakash Jebakumar[2], G. Dharani[1] and R. Vijaya[2]*

[1] Ocean Science and Technology for Islands, National Institute of Ocean Technology, Ministry of Earth Sciences, Government of India, Chennai, India, [2] Coastal and Environmental Engineering, National Institute of Ocean Technology, Ministry of Earth Sciences, Government of India, Chennai, India

OPEN ACCESS

Edited by:
Meilin Wu,
South China Sea Institute of Oceanology, Chinese Academy of Sciences (CAS), China

Reviewed by:
Satheeswaran Thangaraj,
Incheon National University, South Korea
Ganesh T,
Pondicherry University, India
Prashanthi Devi Marimuthu,
Bharathidasan University, India

***Correspondence:**
Dilip Kumar Jha
dilipjhaniot@gmail.com

Specialty section:
This article was submitted to Marine Pollution, a section of the journal Frontiers in Marine Science

Received: 18 November 2021
Accepted: 15 December 2021
Published: 25 January 2022

Citation:
Jha DK, Pandey V, Santhanakumar J, Sathish Kumar P, Venkatnarayanan S, Jebakumar JPP, Dharani G and Vijaya R (2022) Evaluation of Site Suitability for Artificial Reefs Deployment in Southeast Coast of India Using Geographical Information System as a Management Tool. Front. Mar. Sci. 8:817975. doi: 10.3389/fmars.2021.817975

A planned artificial reef (AR) deployment program as part of a fisheries enhancement might be a useful tool for managers to supplement traditional ways to utilize available space and augment local productivity. Several AR deployment initiatives have been carried out globally, but they are rarely subjected to a rigorous site selection process. We created a site selection procedure in this study that includes systematic stages including exclusion mapping, underwater visual transect, benthic composition, seawater quality, and comparative visual mapping. This research focused on restoring the fishing grounds for artisanal fishermen by deploying AR along the southeast coast of India. The results of each stage in the procedure enabled us to choose suitable locations at a target depth with low wave action, no slope, and a good substrate capable of supporting an AR. Analysis of variance (ANOVA-one way) showed significant ($p < 0.05$) spatial variation for depth, slope, seawater current, salinity, chlorophyll-a, benthic density, and diversity. The geographical information system (GIS) based model output showed space allocation for AR deployment. The GIS methodology for site selection was developed to be easily adaptable to the demands of diverse artificial reef programs. The integrated strategy has proven to be a successful regulatory intervention for AR deployment practices in order to facilitate coastal restoration and management.

Keywords: artificial reef, fishery, coastal, GIS, Tamil Nadu

INTRODUCTION

The artificial reef (AR) is a submerged structure deliberately placed on the seabed to mimic the functions of a natural reef, such as protecting, regenerating, concentrating, and enhancing marine organism stock, and serves as a part of the natural ecosystem (FAO, 2015). The earliest recorded AR was from the 1830s, when logs from huts were used off the coast of South Carolina, United States, to improve fishing (Weisburd, 1986). The first scientifically planned reefs were deployed in 1974

off the Adriatic coast of central Italy (Fabi and Fiorentini, 1994). However, in the Indian scenario, AR was first reported on the Coromandel Coast (Hornell, 1924), whereas the first AR construction was carried out off Puthiyathura village in 1953, and further organized efforts to deploy ARs were initiated from 1980 onward (Sreekanth et al., 2019).

Despite widespread usage of AR as a mitigating tool for restoring fisheries, they are rarely subjected to a thorough site selection protocol before deployment. Though there are site selection guidelines, they primarily focus on physical factors (shipping channels, fishing, or substrate) and methods for obtaining permits (Figley, 2005). The majority of scientific effort is focused on studying AR after deployment to obtain time-series data of community dynamics (Reed et al., 2006; Thanner et al., 2006). Although these findings are important for evaluating the effectiveness of AR, they typically do not provide the required information to develop a standard protocol for reef placement, management, and mitigation plans. Poor site selection is one of the most common causes of failure of AR deployment programs (Tseng et al., 2001; Kennish et al., 2002).

Exclusion mapping (Kaiser, 2006) is one of the most commonly utilized methods for selecting suitable locations and screening out unsuitable ones. However, it does not provide the physical and biological data needed to comprehend the ecology of a prospective AR site. Seawater currents, waves, substrate stability, seawater quality, and existing benthic fauna are key factors in site selection (Spieler et al., 2001; Duzbasilar et al., 2006; Mousavi et al., 2015). It is well known that exclusion mapping may account for the majority of these features, nevertheless very few studies have been carried out (Barber et al., 2009) that combine them with physical and biological field data to determine site suitability. Site selection is a complex process in which the role of geographical information systems (GIS) is well established (Moeinaddini et al., 2010; Mousavi et al., 2015; Jha et al., 2017).

Coral reefs on the southeast coast of India (Tamil Nadu) are located in Palk Bay (PB) and in the Gulf of Mannar (GoM) (Muley et al., 2000), which accounts for 94.3 sq km in which reef flat and reef vegetation comprise 64.9 and 13.7 sq km, respectively (Department of Ocean Development and Space Application Centre, 1997). It is reported that the GoM and PB harbor about 117 species belonging to 40 genera of coral and support the fisheries production in the region (Raghuraman et al., 2013). However, in recent times, there has been a decline in traditional fishing due to which artisanal fishermen are facing severe problems such as lower catch (Vijayanand et al., 2007). In addition, factors such as trawling (James, 1994) and damage to benthic habitats (Murugan and Durgekar, 2008) have also exacerbated the decline in annual total fish catch along the southeast coast of India (Tamil Nadu). Considering the above facts, the present research focussed on systematic site selection protocols for fishery restoration and conserving the ecosystem in the southeast coast of India (Tamil Nadu). Hence, an integrated site selection method was established before the deployment to ensure long-term success of AR in supporting the local fishery. The objectives of the present study are to (1) use exclusion mapping as the first stage for selecting target locations for AR deployment; (2) develop a comprehensive record of physical and biological parameters for each location based on quantitative *in situ* data; and (3) *in situ* and satellite data comparison for selected parameters for the site suitability to develop a simple site selection protocol that could easily be adapted in other coastal environments.

MATERIALS AND METHODS

Study Area Description

Tamil Nadu has a coastline of 1,076 km and stretches along the Bay of Bengal, the Indian Ocean, and the Arabian Sea. It constitutes about 15% of the total coastal length of India, covering PB and the GoM, which is one of the major coral-rich areas located along the southeast coast of India. Five coastal districts, namely, Thanjavur (THA), Pudukottai (PUD), Ramanathapuram (RAM), Thoothukudi (THO), and Tirunelveli (TIR), were studied for the site suitability of AR deployment (**Figure 1A**).

Exclusion Mapping

The site selection is an important step towards the AR deployment process and the restoration of fisheries in the selected coastal regions. In this study, systematic approaches were used for AR site selection: (1) Exclusion mapping (bathymetry, wave, cost-effective distances, and discharge points), (2) quantitative transect survey, and 3) constructing a GIS model (Barber et al., 2009). Sites that were too shallow or deep ($<$5.0 m or $>$15.1 m), had strong waves ($>$1.5 m), beyond the cost-effective distance (12 km), and within 1 km of the discharge point (i.e., shore) were eliminated from further consideration (**Table 1**).

The data for bathymetry was sourced from the General Bathymetric Chart of the Ocean (GEBCO) portal (spatial resolution of 30 Arc seconds). The average significant wave height (SWH) (spatial resolution of 0.25 degree) data was collected from the Indian National Centre for Ocean Information Services (INCOIS) over 1 year period. The depth and wave data were interpolated using the inverse distance weighted (IDW) method (Chang, 2006). We also generated buffer layers for the cost-effective distance (12 km) to incorporate that layer into the exclusion mapping model. To analyze such sites, a buffer layer of discharge locations (1 km) was also built. However, the buffer layer was not represented in the exclusion model. The criteria and sub-criteria for deploying AR are given in **Table 2**.

Quantitative Transect Survey

After completing the initial site selection process using exclusion mapping (first step), the GIS model output was validated by conducting field sampling in suitable locations from January 2020 to April 2020. During the field survey, the bathymetry data of the suitable locations were measured by a multi-beam sonar system using a fishing trawler at 42 locations. Depth was corrected for tidal elevations and values were expressed with reference to chart datum (FAO, 2015). The seawater current was measured by deploying a current meter (RCM9) by following the protocols of FAO (2015). The slope was calculated based on the difference between the depths of measured points and the distance between

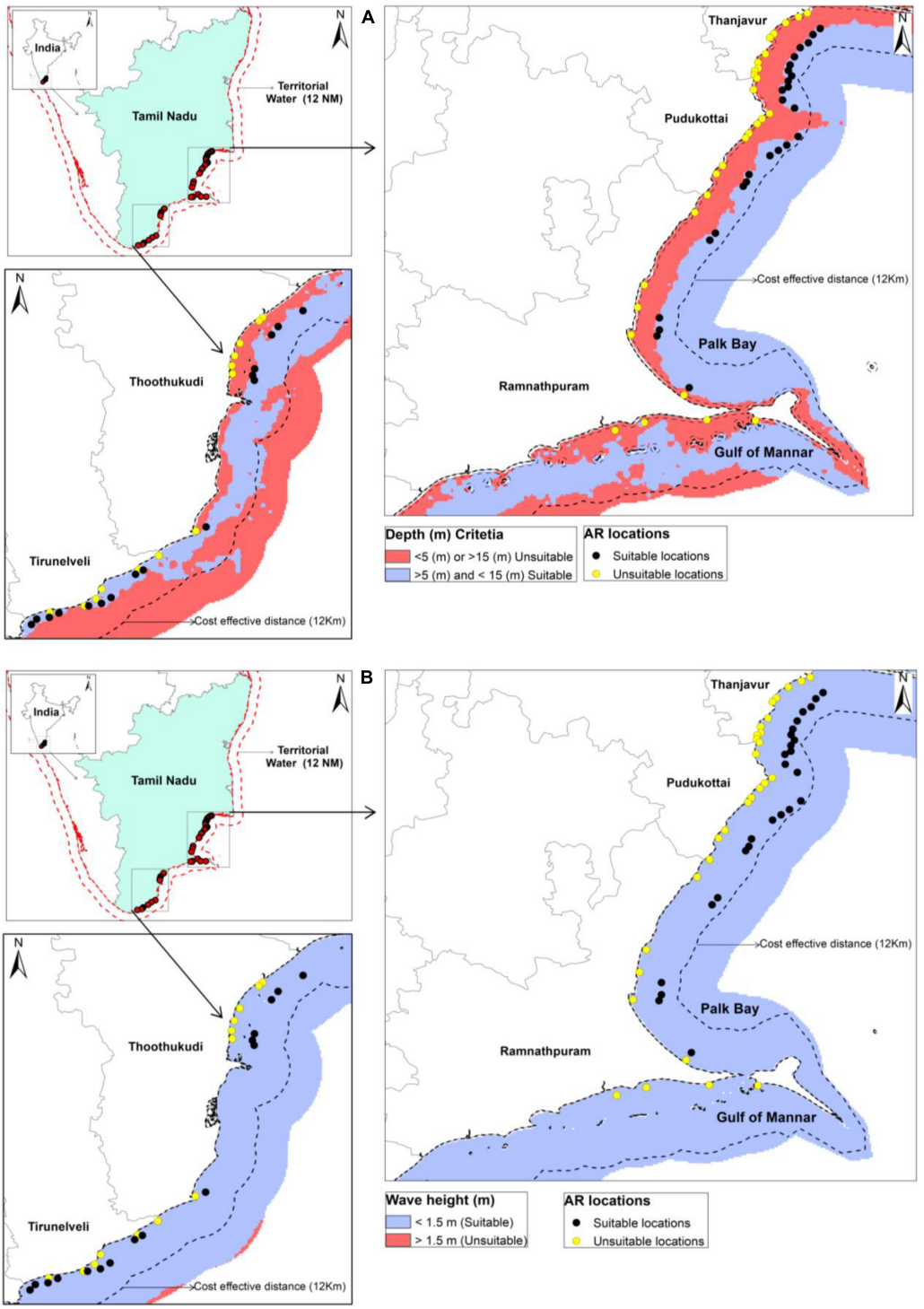

FIGURE 1 | Exclusion mapping model for AR deployment along the Tamil Nadu coast. Data layer indicates unsuitable (red) and suitable (blue) for **(A)** bathymetry and **(B)** wave height produced through the GIS reclassification tool.

those points. After initial exclusion, slope angles below 5° were considered for the AR deployment (Barber et al., 2009).

To determine the composition of the substrate at each site, underwater surveys using self-contained underwater breathing apparatus (SCUBA) were conducted along three 25-m transects at each site. The parallel transects were carried out at the 25 m × 25 m footprint for AR deployment. Each diver collected data on one side of the transect until the entire transect had

been sampled (Barber et al., 2009). The viability of each site was discussed, and barren areas without seagrass or coral reef beds were selected for AR deployment among the sensitive ecosystem.

Sediment texture was determined in the field laboratory using the wet sieving and pipette method, and grain size fractions were obtained by dry sieving through a stack of 8 sieves ranging from 2 to 0.063 mm mesh sizes (Holme and McIntyre, 1984). To identify benthic fauna, sediment samples were collected using a Van-Veen grab having a surface area of 0.16 m^2, and each sample was identified up to the lowest possible taxonomic level using standard taxonomic literature, and their density was expressed as ind/m^2.

Geographical Information System Model

Considering the diversity of the data and the variety of scales on which all criteria can be measured, the values contained in the different thematic layers were transformed into comparable classes by following the reclassification tool of GIS (Malczewski, 2006). This data layer was used to identify suitable sites for the AR deployment. Out of 84 tentative locations, 42 locations that fell within these criteria were delineated as "suitable" locations and were further investigated. The average sea surface temperature (SST), sea surface salinity (SSS), total suspended matter (TSM), and chlorophyll-a (chl-a), data were collected (spatial resolution of 0.25 degree) from the INCOIS. In addition to that, the above parameters were also collected during the quantitative survey (*in-situ*) from the surface using a GOFLO sampler by a boat sampling. The sampling positions were geo-coded by using a hand-held GPS (Garmin eTrex Vista; ± 5 m). The SST and SSS were measured onboard by calibrated multi-parameter water quality instruments (Hanna HI9829). The TSS was determined by filtering 1 L of seawater through pre-dried and pre-weighed (0.45 μm Millipore GF/C) filter paper and washed with Milli-Q water to remove salt content (APHA [American Public Health Association], 2005). The chl-*a* was analyzed by a spectrophotometric method (Parsons et al., 1992). The TSS and chl-a samples were analyzed in the field laboratory and data were recorded after the analysis was completed. The samples were analyzed in triplicates, and quality control procedures were followed by careful standardization and blank measurements. One-way ANOVA was employed to test the spatial variations (station-wise) of physicochemical parameters. A geo-database of the above parameters was developed and imported to Arc GIS software (ver. 9.3.1). The parameters were interpolated using the IDW method (Chang, 2006). In this study, uniform class ranges and color codes were adopted for the maps generated through interpolation.

TABLE 1 | Reclassification values for bathymetry, wave height, cost-effective distance, and discharge points data used in the exclusion mapping model (adapted and modified from Barber et al., 2009).

Original value	Reclassified value	Reasoning for reclassification
Bathymetry		
5.0–15.0 m	Suitable	Ideal larval settlement and safe SCUBA diving depth
0.0–4.9 m >15.1 m	Unsuitable	Navigational concerns, wave action, and too deep for many larvae, and SCUBA
Wave		
<1.5 m	Suitable	Ideal wave action for fish and larval settlement
>1.5 m	Unsuitable	Affect the larval settlement and fish activity
Cost-effective distance		
<12 KM	Suitable	Safe for traditional or artisanal fishermen
>12 KM	Unsuitable	Unsafe for traditional fishermen
Discharge points		
>1 km	Suitable	Provide good water quality for the ecosystem
<1 km	Unsuitable	Not conducive for ecosystem rebuilding

TABLE 2 | Description of criteria and sub-criteria for artificial reef deployment (adapted and modified from Barber et al., 2009; Kapetsky et al., 2013; Mousavi et al., 2015; Jha et al., 2017).

Criteria	Sub criteria	Recommended limit
Exclusion mapping	Bathymetry	>5 m and <15 m
	SWH	<1.5 m
	Cost effective distance	<12 km
	Distance from sewage points	>1 km
Quantitative transect survey	Bottom slope	<5°
	Seawater current	10–75 cm/s
	Bottom type	Hard or solid bottom
	Benthos	Density and diversity
Constructing GIS model	Water temperature	26–32°C
	Salinity	29–35 PSU
	Suspended solids	<50 mg/L
	Chlorophyll-a	<5 mg/m^3

RESULTS AND DISCUSSION

Eighty-four locations were considered for the exclusion modeling for the AR deployment; only 42 sites met the site selection criteria. These locations were within a 12 km radius of cost-effective distance and in the 5–15 m water depth range, conforming to accessibility criteria (**Table 1**). Similar results were also reported in which potential sites were within 11 km radius of the nearest shore, and in the 6–15 m mean water depth range at Massachusetts Bay (Barber et al., 2009). In the present study, none of the sites were located in the shipping route marked on navigational charts. A raster classification categorized depth layers into two classes (<5 m and >15 m = unsuitable, and >5 m and <15 m = suitable). Based on the threshold value of depth, the unsuitable and suitable areas have been represented in red and blue, respectively (**Figure 1A**). The cost-effective distance is very useful since the ARs give an excellent chance for impoverished artisanal fishermen who can't afford a net can easily use a hook and line, to earn their livelihood by venturing to the AR areas for fishing (Kasim Mohamad et al., 2015). While, the optimal depth range helps in larval settlement on the AR structure (Duzbasilar et al., 2006). The spatial variation of depth was significant ($p < 0.05$, $F = 59.755$) in the present study. A buffer layer of 12 km was used for showing the accessible sites as per the cost-effective distance criteria, whereas a 12NM buffer was used for clipping the inaccessible territorial waters for artisanal and traditional

fishermen. Further, wave height is another important technical criteria for AR deployment, because frequent high waves in the region will hamper ecosystem restoration (James and Slaski, 2006). Few areas in the offshore environment in Thoothukudi and Tirunelveli had wave heights of more than 1.5 m, as seen in **Figure 1B**, and those areas were eliminated from further investigation. The GIS model supported exclusion mapping and allowed us to eliminate 50% of prospective locations for the AR deployment.

The physical (slope, seawater current, and bottom type) and biological factors (benthos) played a vital role in the site selection process. In the present study, after initial screening through exclusion mapping, slope angles below 5° were considered suitable for the AR deployment. Similar results were reported in which slope angles below 5° were considered for the AR deployment at Massachusetts Bay (Barber et al., 2009). Similarly, optimum seawater current also plays a vital role in delivering nutrients and larvae to the newly deployed AR, as well as

TABLE 3 | Details of the Artificial Reefs deployed locations along the Tamil Nadu coast.

Latitude	Longitude	Name of the villages	Depth (m)	Slope angle (degree)	Seawater current (cm/s)	Bottom type	Benthic Taxa (nos.)	Benthos density (ind/m^2)
10.2518	79.3708	Keelathottam	5.77	0.03	12	Coarse sand	24	2,808
10.2495	79.3567	Kollukadu	5.00	0.01	14	Medium sand	23	2,340
10.2387	79.3535	Chinnamanai	5.01	0.03	20	Coarse sand	18	1,989
10.2026	79.3421	Sethubhavachathiram	5.00	0.22	15	Coarse sand	24	2,769
10.1873	79.3203	Karankuda	5.27	0.14	14	Coarse sand	28	2,457
10.1546	79.3027	Adaikathevan	5.49	0.07	11	Coarse sand	22	2,145
10.1444	79.2992	Manthiripattinam	5.83	0.10	14	Coarse sand	22	2,847
10.1339	79.3000	Somanathanpattinam	5.44	0.13	11	Medium sand	21	3,588
10.1169	79.3073	Vallavanpattinam	5.66	0.01	22	Coarse sand	26	2,145
10.1052	79.3056	Sembiyanmahadevipattinam	5.80	0.05	20	Coarse sand	19	2,574
10.0971	79.3053	Kattumavadi	5.65	0.09	12	Coarse sand	18	1,989
10.0715	79.3057	Krishnajipattinam	6.00	0.03	27	Medium sand	15	1,911
10.0586	79.3207	Kodiyakarai	6.00	0.11	27	Fine sand	15	2,145
9.9780	79.3443	Ponnagaram	5.50	0.07	28	Medium sand	18	2,964
9.9562	79.3148	Ammapattnam	6.13	0.03	18	Coarse sand	28	1,585
9.9432	79.2935	Pudukudi	5.71	0.05	20	Coarse sand	28	2,379
9.9302	79.2715	Kottaipattinam	5.88	0.03	21	Coarse sand	29	1,819
9.8826	79.2174	R. Pudupattinam	6.02	0.05	22	Coarse sand	26	1,507
9.8635	79.2103	Arasanagaripattinam	6.00	0.02	20	Coarse sand	31	1,936
9.8529	79.2022	Enathi	5.81	0.02	24	Medium sand	30	1,989
9.7342	79.1290	Pasipattinam	5.25	0.07	26	Coarse sand	34	1,936
9.7258	79.1170	Dhamodharapattinam	5.25	0.24	29	Coarse sand	36	1,936
9.5196	78.9830	Thiruppalaikudi	5.25	0.01	21	Coarse sand	38	1,351
9.4886	78.9826	Devipattinam	5.50	0.09	24	Medium sand	32	1,741
9.4735	78.9765	Mudiveranpatti	5.50	0.06	20	Coarse sand	31	1,390
9.3404	79.0573	Alaikathavalasai	6.50	0.06	18	Medium sand	45	1,897
9.0287	78.3670	Indiranagar	6.50	0.07	20	Fine sand	45	1,209
8.9788	78.2812	S.M Valasi	5.00	0.02	20	Coarse sand	43	1,429
8.9685	78.2701	Keelamundal	7.30	0.17	18	Medium sand	41	1,585
8.8366	78.2415	Vembar	5.60	0.06	20	Coarse sand	32	1,326
8.8278	78.2324	Keelavaipar	5.70	0.03	19	Very coarse sand	34	1,429
8.8136	78.2374	Sippikulam	6.20	0.05	15	Medium sand	16	1,663
8.3928	78.0950	Tharuvaikulam	8.90	0.03	34	Coarse sand	25	1,404
8.2700	77.9129	Vellaipatti	8.60	0.11	18	Very coarse sand	21	1,950
8.2580	77.8904	Siluvaipatti	7.20	0.22	47	Coarse sand	26	1,741
8.1792	77.7894	Kulasekarapattinam	5.50	0.17	24	Very fine sand	16	1,819
8.1563	77.7527	Kuduthalai	11.50	0.24	29	Very coarse silt	16	1,131
8.1360	77.6412	Uvari	12.00	0.07	26	Medium sand	19	1,209
8.1135	77.5977	Thoomaiyarpuram	9.50	0.29	16	Coarse sand	26	1,450
8.1754	77.7965	Idinthakarai	12.00	0.21	30	Fine sand	16	3,666
8.1387	77.6469	Perumanal	14.50	0.17	20	Coarse sand	21	1,560
8.1215	77.5975	Kootapulli	14.00	0.07	15	Medium sand	30	1,638

maintaining a well-oxygenated environment (Duzbasilar et al., 2006). The suggested seawater current ranges from 10 to 75 cm/s (Mousavi et al., 2015). However, in the present study, it ranged from 11 to 47 cm/s and its spatial variation was significant ($p < 0.05$, $F = 3.317$).

Hard-bottom habitat is critical to several life stages of commercially important species like lobster, crabs, marine finfish, and other species of invertebrates (Wahle and Steneck, 1992; Tupper and Boutilier, 1995; Packer et al., 1999). The bottom type in selected locations was categorized as: (1) very coarse sand, (2) coarse sand, (3) medium sand, (4) fine sand, (5) very fine sand, and (6) very coarse silt, which can support the deployment of AR. Apart from the good bottom substrate, the natural larval supply such as benthic fauna promotes the rebuilding of the newly deployed AR ecosystem (Pratt, 1994). We observed a total of 81 taxa of benthic fauna represented by a wide range of taxonomic groups namely Polychaeta, Amphipoda, Isopoda, Cumacea, Ostracoda, Nematoda, Bivalvia, Gastropoda, Echinoidea, Nemertea, and Cephalochordata (Pandey et al., 2022). The substratum heterogeneity and habitat complexity lead to higher diversity and abundance of the benthic community, which in turn supports the ecosystem formation around the ARs (Pandey et al., 2018; Pandey and Ganesh, 2019). The taxa and density of benthos varied from 15 to 45 and 1,131–3,666 ind/m^2, respectively. The spatial variation of taxa ($p < 0.05$, $F = 12.923$) and density ($p < 0.05$, $F = 6.083$) was significant. The details of the selected site with its location, depth, slope angle, seawater current, bottom type, benthic taxa, and density are given in **Table 3**.

Comparative Water Quality Model

The IDW spatial interpolation technique was used to generate spatial maps (**Figures 2A–H**) for recommended environmental variables (TSS, SST, SSS, and Chl-a). The range of *in-situ* TSS concentration was 14–40 mg/L (**Figure 2A**), whereas (**Figure 2B**) satellite-derived data ranged from 2.72 to 61.69 mg/L. Similarly, SST (26.61–29.99°C) (**Figure 2C**), SSS (28.38–34.38 PSU) (**Figure 2E**), and chl-a (0.03–0.49 mg/m^3) (**Figure 2G**) showed variation in the present study. However, the spatial variation was significant for SSS ($p < 0.05$, $F = 8.001$) and chl-a ($p < 0.05$, $F = 4.558$). Satellite derived data for SST, SSS, and chl-a, varied from 26.35 to 29.09°C (**Figure 2D**), 31.87–34.72 PSU (**Figure 2F**), and 0.24–2.07 mg/m^3 (**Figure 2H**), respectively. The average value calculated for satellite data indicates that higher concentrations were noticed in the nearshore regions, whereas it was well within the site selection criteria at the selected locations in the offshore waters. The higher TSS could be attributed to the freshwater input from many perennial rivers (i.e., Krishna, Godavari, and Mahanadi) and several seasonal rivers (i.e., Palar, Vellar, and Coleroon) in the nearshore region (Shanthi et al., 2013). A range of values are represented by color codes for mapping the area that visualizes the concentration of specific parameters and shows the comparison. Visual interpretation is an easy method to depict and explain the dispersion pattern of environmental parameters (Lillesand and Kiefer, 1979) in a broader perspective, like AR deployment. This type of comparative study will help to select the suitable parameters that are available through satellite datasets for the better coverage

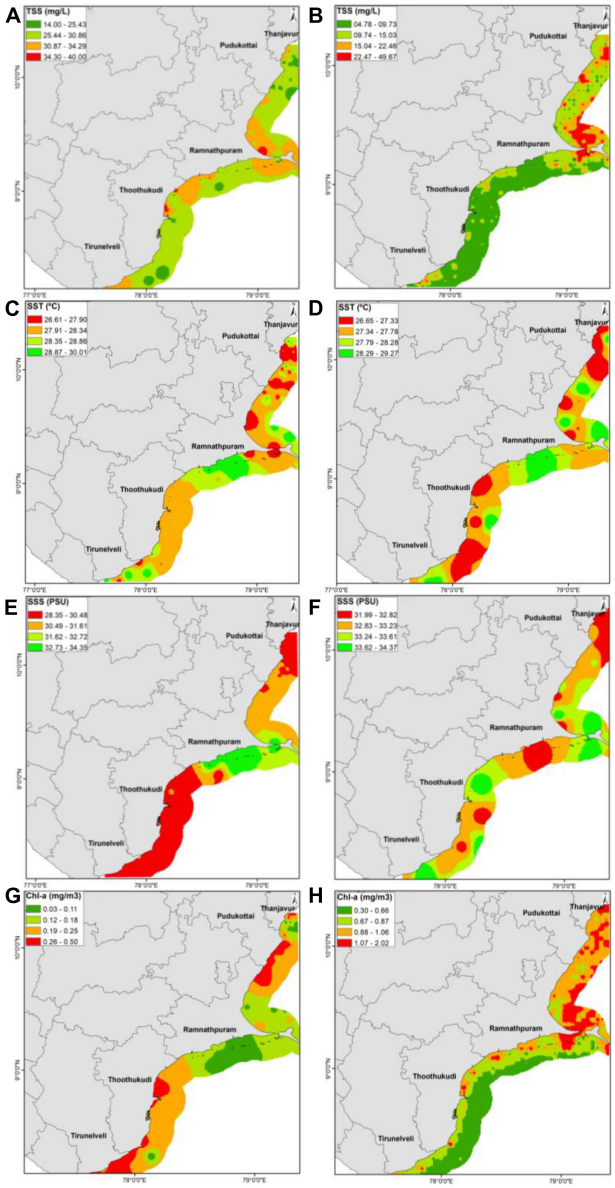

FIGURE 2 | (A–H) *In-situ* **(A,C,E,G)** and satellite **(B,D,F,H)** data comparison along the Tamil Nadu coast.

and management of a long coastline. *In-situ* and satellite data validation is well reported for selected physicochemical parameters, e.g., chlorophyll-a, in southeast coast of India and it revealed good correlation coefficient ($r^2 = 0.89$) (Selvavinayagam et al., 2003). Though the present study was limited to site suitability for AR deployment, earlier reports on the post-deployment study indicated a higher aggregation of juvenile fishes at the AR site along the Tamil Nadu coast.[1]

A systematically planned site selection approach contributes to the development of an ecosystem around the AR, which in

[1]https://www.newindianexpress.com/cities/chennai/2020/nov/13/artificial-reefs-deployed-in-record-time along chennai-coast-come-to-life-2223346.html

turn promotes sustainable rural technology highly suitable for the livelihood enhancement of artisanal and traditional coastal fishermen (Kasim Mohamad et al., 2015). It is claimed that biomass output in the ARs regions ranges between 2.5 and 5 tons per year, with biodiversity products/ecosystem services valued at USD 190,000 per year (Kasim Mohamad et al., 2015). Increase productivity by reducing fishermen's reliance on natural coral reefs; it also promotes a healthy ornamental fish population, ecotourism, and natural resource conservation. Thorough monitoring of environmental factors is critical for the deployment of ARs in suitable sites. Yet, there is little data on the pre-deployment of ARs in India and globally. The current study will provide a good understanding of physical factors such as seawater quality, and benthic diversity at the pre-deployment stage of ARs in fisheries depleted coastal regions for promoting conservation and improving livelihoods through ecosystem services by enhancing 20% catch adjacent to ARs compared to sites away from the ARs in the Indian (Philipose, 1996) and global scenarios (Fabi and Fiorentini, 1994). The integrated approach will also aid in the development of a management strategy for site appropriateness prior to the deployment of ARs, resulting in improved outcomes and benefits to coastal society.

CONCLUSION

An integrated approach (exclusion mapping and quantitative transect survey) in combination with GIS proved to be a simple and systematic method to support AR site selection and deployment in the coastal environment. The deployment of ARs in the tropical coastal environment is critical for restoring the fisheries activities in depleted coastal areas. Finding a suitable site for AR deployment is an important step in the whole process. The study developed distinctive exclusion maps which supported screening out the non-potential sites for AR deployment. Results revealed that out of 84 tentative sites, only 50% met the site selection criteria. Considering the recent depletion in fish catch, especially for artisanal fishermen, a comprehensive plan needs to be evolved to initiate a systematic site selection approach before AR deployment. This will help to conserve the fish stock and support the fishermen in the coastal regions. Although Tamil Nadu was selected as the study area, the systematic site selection approach developed would be useful to other maritime nations, especially in the tropical regions.

DATA AVAILABILITY STATEMENT

The original contributions presented in the study are included in the article/supplementary material, further inquiries can be directed to the corresponding author/s.

AUTHOR CONTRIBUTIONS

DJ: conceptualization, sampling design, and data validation, GIS modeling, and writing – original draft. VP: sample collection, laboratory analysis, and data processing. JS: SCUBA diving and underwater data collection. PS and SV: field investigation and analysis. JJ: co-ordination of study and reviewing the data. GD: reviewing the manuscript, suggestion, and project management. RV: reviewing the manuscript, guidance, and project management. All authors contributed to the article and approved the submitted version.

ACKNOWLEDGMENTS

We are grateful to the Ministry of Earth Sciences, Government of India, for providing support to carry out the present study. We are thankful to G. A. Ramadass, Director, NIOT, Chennai, for his constant encouragement, support, and guidance. We show our gratitude to M. V. Ramana Murthy, Scientist-G, for their guidance and support for this study. We thank the Rural Development and Panchayat Raj Department, Government of Tamil Nadu, and Department of Fisheries and Fishermen Welfare, Government of Tamil Nadu for their kind support during the study. We are thankful to T. Srinivasa Kumar, Director, INCOIS, E. Pattabhi Rama Rao, Head, Data Modelling Group, INCOIS, and R. Venkat Shesu, Scientist-D, INCOIS for sharing data. We are also thankful to our colleagues S. Ragumaran, G. Nanadhagopal, and B. Ranjan Babu for their kind support during the fieldwork. Further, we extend our gratitude to the scientific and supporting staff of MBT, NIOT, Chennai, India, for their kind support during this study.

REFERENCES

APHA [American Public Health Association] (2005). *Standard Methods for the Examination of Water and Wastewater*, 21th Edn. Washington, D.C: American Works Association and Water Environmental Federation.

Barber, J. S., Chosid, D. M., Glenn, R. P., and Whitmore, K. A. (2009). A systematic model for artificial reef site selection. *New Zeal. J. Mar. Freshw. Res.* 43, 283–297. doi: 10.1080/00288330909510001

Chang, K. T. (2006). *Introduction To Geographic Information Systems*, 3rd Edn. New Delhi: Tata McGraw Hill, 325–327.

Department of Ocean Development and Space Application Centre (1997). *Coral Reef Maps Of India*. Ahmedabad: Department of Ocean Development and Space Application Centre.

Duzbasilar, F. O., Lok, A., Ulas, A., and Metin, C. (2006). Recent developments on artificial reef applications in Turkey: hydraulic experiments. *Bull. Mar. Sci.* 78, 195–202.

Fabi, G., and Fiorentini, L. (1994). Comparison of an artificial reef and a control site in the Adriatic Sea. *Bull. Mar. Sci.* 55, 538–558.

FAO (2015). *Practical Guidelines For The Use Of Artificial Reefs In The Mediterranean And The Black Sea: Studies and Reviews No.96.ISSN 1020-9549*. Rome: FAO.

Figley, B. (2005). *Artificial Reef Management Plan For New Jersey*. Trenton, NJ: New Jersey Department of Environmental Protection, Division of Fish and Wildlife, 130.

Holme, N. A., and McIntyre, A. D. (1984). *Methods For The Study Of Marine Benthos*. Oxford: Blackwell Scientific Publication, 334.

Hornell, J. (1924). The fishing methods of the Madras Presidency. *Madras Fish. Bull.* 18, 60–66.

James, M. A., and Slaski, R. (2006). *Appraisal of the Opportunity For Offshore Aquaculture In UK waters. Report of Project FC0934 Commissioned by Defra and Sea fish from FRM Ltd., 119 pp*. Available online at:

www.seafish.org/media/Publications/Offshore_Aquaculture_Compiled_Final_Report.pdf (accessed December 10, 2012).

James, P. S. B. R. (1994). "Endangered, vulnerable and rare marine fish and animals: threatened fish of India," in *Threatened Fish Of India*, eds P. V. Dehadrai, P. Das, and S. R. Varma (Allahabad: NATCON), .271–295.

Jha, D. K., Rajaprabhu, G., Kirubagaran, R., Sendhil Kumar, R., Dharani, G., Das, A. K., et al. (2017). Estimation of potential zones for offshore mariculture in the Indian Sea using geographical information system as a management tool. *J. Coast. Conserv.* 21, 893–902. doi: 10.1007/s11852-017-0556-y

Kaiser, M. J. (2006). The louisiana artificial reef program. *Mar. Policy* 30, 605–623. doi: 10.1016/j.marpol.2005.04.005

Kapetsky, J. M., Aguilar-Manjarrez, J., and Jenness, J. (2013). *A Global Assessment Of The Potential For Offshore Mariculture Development From A Spatial Perspective.* FAO Fisheries and Aquaculture Technical Paper No. 549. Rome: FAO, 181.

Kasim Mohamad, H., Syda Rao, G., Rajagopalan, M., Vivekanandan, E., Mohanraj, G., Kandasami, D., et al. (2015). *Ecosystem Services By Artificial Reef Structures In The Marine Environment Along The Tamil Nadu Coast*. Available online at: https://www.researchgate.net/publication/281117456 (accessed June 9, 2021).

Kennish, R., Wilson, K. D. P., Lo, J., Clarke, S. C., and Laister, S. (2002). Selecting sites for large-scale deployment of artificial reefs in Hong Kong: constraint mapping and prioritization techniques. *ICES J. Mar. Sci.* 59, S164–S170. doi: 10.1006/jmsc.2002.1209

Lillesand, T. M., and Kiefer, R. W. (1979). *Remote Sensing And Image Interpretation*. New York, NY: Wiley.

Malczewski, J. (2006). GIS-based multicriteria decision analysis: a survey of the literature. *Int. J. Geogr. Inf. Sci.* 20, 703–726. doi: 10.1080/13658810600661508

Moeinaddini, M., Khorasani, N., Danehkar, A., Darvishsefat, A. A., and Zienalyan, M. (2010). Siting MSW landfill using weighted linear combination and analytical hierarchy process (AHP) methodology in GIS environment (case study: Karaj). *Waste Manag.* 30, 912–920. doi: 10.1016/j.wasman.2010.01.015

Mousavi, S. H., Danehkar, A., Reza Shokri, M., Poorbagher, H., and Azhdari, D. (2015). Site selection for artificial reefs using a new combine multi-criteria decision-making (MCDM) tools for coral reefs in the Kish Island – Persian Gulf. *Ocean Coast. Manag.* 111, 92–102. doi: 10.1016/j.ocecoaman.2015.03.004

Muley, E. V., Subramanian, B. R., Venkataraman, K., and Wafar, M. (2000). "Status of coral reefs of India," in *Proceedings of the 9th International Coral Reef Symposium* Bali, 360.

Murugan, A., and Durgekar, R. (2008). *Beyond the Tsunami: Status of Fisheries in Tamil Nadu, India: A Snapshot of Present and Long-term Trends*. Bangalore: UNDP/UNTRS, 75.

Packer, D. B., Cargnelli, L. M., Griesbach, S. J., and Shumway, S. E. (1999). *Sea scallop, Placopecten magellanicus, Life history, and Habitat characteristics.* Essential Fish Habitat Source Document, NOAA Technical Memorandum NMFS-NE-134. Washington, DC: NOAA, 30.

Pandey, V., and Ganesh, T. (2019). Spatial and temporal variability in the vertical distribution of gastropods on the rocky shores along the east coast of South Andaman Island, India. *Mar. Biodivers.* 49, 633–645. doi: 10.1007/s12526-017-0838-5

Pandey, V., Ganesh, T., and Satyam, K. (2018). Habitat heterogeneity determines the structural properties of intertidal gastropod assemblages in a pristine tropical Island ecosystem. *Indian J. Geo Mar. Sci.* 47, 846–853.

Pandey, V., Jha, D. K., Sathish Kumar, P., Santhanakumar, J., Venkatnaraynan, S., Prince Prakash Jebakumar, J., et al. (2022). Effect of multiple stressors on the functional traits of sub-tidal macrobenthic fauna: a case study of the southeast coast of India. *Mar. Pollut. Bull.* doi: 10.1016/j.marpolbul.2022.113355

Parsons, T. R., Maita, Y., and Lalli, C. M. (1992). *A Manual of Chemical and Biological Methods for Sea Water Analysis*. Oxford, NY: Pergamon Press.

Philipose, K. K. (1996). Artificial reefs habitat enhancement and increasing fisheries potential. *CMFRI Bull.* 48, 4–7.

Pratt, J. R. (1994). Artificial habitats and ecosystem restoration: managing for the future. *Bull. Mar. Sci.* 55, 268–275.

Raghuraman, R., Raghunathan, C., and Venkataraman, K. (2013). "Present status of coral reefs in india," in *Ecology and Conservation of Tropical Marine Faunal Communities*, eds K. Venkataraman, C. Sivaperuman, and C. Raghunathan (Berlin: Springer). doi: 10.1007/978-3-642-38200-0_23

Reed, D. C., Schroeter, S. C., Huang, D., Andersen, T. W., and Ambrose, R. F. (2006). Quantitative assessment of different artificial reef designs in mitigating losses to kelp forest fishes. *Bull. Mar. Sci.* 78, 133–150.

Selvavinayagam, K., Surendran, A., and Ramachandran, S. (2003). Quantitative study on chlorophyll using IRS-P4 OCM data of Tuticorin coastal waters. *J. Indian Soc. Rem. Sens* 31, 227–235. doi: 10.1007/BF03030829

Shanthi, R., Poornima, D., Raja, S., Vijayabaskara Sethubathi, G., Thangaradjou, T., Balasubramanian, T., et al. (2013). Validation of OCM-2 sensor performance in retrieving chlorophyll and TSM along the southwest Bay of Bengal coast. *J. Earth Syst. Sci.* 122, 479–489. doi: 10.1007/s12040-013-0286-y

Spieler, R. E., Gilliam, D. S., and Sherman, R. L. (2001). Artificial substrate and coral reef restoration: what do we need to know what we need. *Bull. Mar. Sci.* 69, 1013–1030.

Sreekanth, G. B., Lekshmi, N. M., and Singh, N. P. (2019). Can artificial reefs enhance the inshore fishery resources along indian coast? A critical review. *Proc. Natl. Acad. Sci. India Sect. B Biol. Sci.* 89, 13–25. doi: 10.1007/s40011-017-0861-0

Thanner, S. E., Mclnosh, T. L., and Blair, S. M. (2006). Development of benthic and fish assemblages on artificial reef materials compared to adjacent natural reef assemblages in Miami-Dade County, Florida. *Bull. Mar. Sci.* 78, 57–70.

Tseng, C., Chen, S., Huang, C., and Liu, C. (2001). GIS-assisted site selection for artificial reefs. *Fish. Sci.* 67, 1015–1022. doi: 10.1046/j.1444-2906.2001.00356.x

Tupper, M., and Boutilier, R. G. (1995). Effects of habitat on settlement, growth, and post-settlement survival of Atlantic cod (*Gadus morhua*). *Can. J. Fish. Aquat. Sci.* 52, 1834–1841. doi: 10.1139/f95-176

Vijayanand, P., Murugan, A., Saravanakkumar, K., Ajmalkhan, S., and Rajagopal, S. (2007). Assessment of lobster resources along Kanyakumari (Southeast coast of India). *J. Fish. Aquat. Sci.* 2, 387–394. doi: 10.3923/jfas.2007.387.394

Wahle, R. A., and Steneck, R. S. (1992). Habitat restriction in early benthic life: experiments on habitat selection and in situ predation with the American lobster. *J. Exp. Mar. Biol. Ecol.* 157, 91–114. doi: 10.1016/0022-0981(92)90077-N

Weisburd, S. (1986). Artificial reefs. *Sci. News* 130, 59–61. doi: 10.2307/3971028

Conflict of Interest: The authors declare that the research was conducted in the absence of any commercial or financial relationships that could be construed as a potential conflict of interest.

Publisher's Note: All claims expressed in this article are solely those of the authors and do not necessarily represent those of their affiliated organizations, or those of the publisher, the editors and the reviewers. Any product that may be evaluated in this article, or claim that may be made by its manufacturer, is not guaranteed or endorsed by the publisher.

Copyright © 2022 Jha, Pandey, Santhanakumar, Sathish Kumar, Venkatnarayanan, Jebakumar, Dharani and Vijaya. This is an open-access article distributed under the terms of the Creative Commons Attribution License (CC BY). The use, distribution or reproduction in other forums is permitted, provided the original author(s) and the copyright owner(s) are credited and that the original publication in this journal is cited, in accordance with accepted academic practice. No use, distribution or reproduction is permitted which does not comply with these terms.

frontiers in Marine Science

BRIEF RESEARCH REPORT
published: 02 February 2022
doi: 10.3389/fmars.2022.830324

Seasonal Variation of Food Web Structure and Stability of a Typical Artificial Reef Ecosystem in Bohai Sea, China

*Shengpeng Li[1], Ruyue Wang[2], Yueming Jiang[2], Yanyu Li[2], Lin Zhu[2] and Jianfeng Feng[2]**

[1] School of General Education, Tianjin Foreign Studies University, Tianjin, China, [2] College of Environmental Science and Engineering, Nankai University, Tianjin, China

The last 30 years have witnessed the degradation and loss of function in the ecosystem of the Bohai Sea, China. Great efforts, such as artificial reefs, have been used to restore the ecosystem of the Bohai Sea in recent years. In this study, we examined the seasonal variation of food webs in artificial reefs of Juehua Island by the Ecopath model. Results showed that the number of species, range of trophic level, energy cycle proportion, energy complexity, nutrition transfer efficiency, and ecosystem maturity have increased from summer to autumn. However, the food web stability of artificial reefs has no obvious change from summer to autumn. Loop analysis revealed that the heaviest feedback loops are the interactions among benthos, zooplankton, and phytoplankton, and the predator-prey negative interaction strength between zooplankton and phytoplankton dominated the stability of the artificial reef, whether in summer or autumn. This study suggests that stability is a more robust indicator for ecosystem assessment and could provide useful information in future restoration plans of the marine ecosystem.

Keywords: Bohai Sea, Ecopath, feedback loop, food web, stability

OPEN ACCESS

Edited by:
Meilin Wu,
South China Sea Institute of Oceanology, Chinese Academy of Sciences (CAS), China

Reviewed by:
Wenzhe Xu,
Tianjin University of Science and Technology, China
Hongxia Ming,
National Marine Environmental Monitoring Center, China

****Correspondence:***
Jianfeng Feng
fengjf@nankai.edu.cn

Specialty section:
This article was submitted to Marine Pollution, a section of the journal Frontiers in Marine Science

Received: *07 December 2021*
Accepted: *11 January 2022*
Published: *02 February 2022*

Citation:
Li S, Wang R, Jiang Y, Li Y, Zhu L and Feng J (2022) Seasonal Variation of Food Web Structure and Stability of a Typical Artificial Reef Ecosystem in Bohai Sea, China. Front. Mar. Sci. 9:830324. doi: 10.3389/fmars.2022.830324

INTRODUCTION

The Bohai Sea ecosystem is an important nursery and feeding ground for coastal species and now is under tremendous pressure due to economic and social development. Studies have shown that over the past decades the Bohai Sea ecosystem has rapidly degraded and lost its function to a great extent due to overfishing and eutrophication. In recent years, great efforts (e.g., artificial reef) have been used in slowing down, halting, and finally reversing the environmental deterioration of the Bohai Sea. Thus, understanding the change of structure and stability of the ecosystem under restoration projects is critical for future restoration plans.

Natural communities of species embody complex interrelationships between the structure of the interspecific interaction network, the dynamics of the populations of species, and the stability of the system as a whole. It is particularly important to study the food web embedded in each interaction network because trophic interactions are the main channels of energy flow in all ecosystems (Curtin and Prellezo, 2010). However, it is a challenge to quantify the ecosystem properties, especially for the coastal ecosystem with multiple stressors. The Ecopath with Ecosim (EwE) modeling approach[1]

[1]http://www.ecopath.org

is a suitable tool to assess the food web characteristics and is being widely used for the analysis of exploited aquatic ecosystems. For example, based on the EwE modeling, a total of 23 functional groups were modeled based on a year-round trawl survey of the Bohai Sea conducted in 2016 (Rahman et al., 2019). An overview of the trophic structure and flow of the Bohai Sea ecosystem was also illustrated by 13 functional groups using the data collected from April 1982 to May 1983 (Tong et al., 2000). To quantify the historical ecosystem changes in the Bohai Sea, the Ecopath models were developed in three periods (1982–1983, 1992–1993, and 1998–1999). The trends in the structure, maturity, and keystone species of the Bohai Sea ecosystem from 1982 to 1999 were assessed, and planning management measures were proposed (Zheng and You, 2014). A comparative study was carried out on the changes in the food web structure of 17 functional groups between 1982 and 1992 (Zhang and Lin, 2009). Studies also showed that the decadal decline in the mean trophic level of the biomass in the Bohai Sea is more apparent than the decline of the mean trophic level of the catch extracted from that sea (Liang and Pauly, 2020). A recent study investigated the steady-state trophic models in different seasons of a newly created artificial coastal oyster reef within the Luanhe River estuary in the Bohai Sea, which could help fisheries managers to understand whether the ecosystem function of artificial oyster reef habitat is consistent throughout the seasons and to assess the reasonability of the current fishing production policy which varies with seasons (Min and Xin, 2021). Although the structures of the ecosystem are often assessed, the stability is seldom considered, especially for the real ecosystem.

Due to particular features (e.g., isolation and ocean currents) of land and sea in the island, the island ecosystem is more sensitive and vulnerable, prone to degrade for disturbance, and difficult to recover (Leclerc et al., 2020). Therefore, taking Juehua Island as an example, we examined the seasonal variation of food web structure and stability. The Juehua Island in this case is different from other study areas in previous studies, in that artificial reefs are thrown into the seawater for recovery ecosystem (de Vries et al., 2013). Since stability is very important to ecosystem function, current manifestations of anthropological stresses on ecosystems have heightened the need to understand and predict the stability of ecosystems (MacArthur, 1955; Paine, 1966). Considering the previous scenarios of ecological changes, we aimed to present the seasonal ecological changes in Juahua Island in summer and autumn of 2019 using the Ecopath mass-balance model (Christensen et al., 2005) and estimate their stability by Jacobian community matrix (May, 1972; Stone and Lewi, 2001; Tang et al., 2014; Jacquet et al., 2016). We also investigated the most dangerous omnivorous loop and the decisive factor of food web stability (Neutel et al., 2002, 2007; Mitchell and Neutel, 2012; Neutel and Thorne, 2015, 2016).

MATERIALS AND METHODS

Study Area

Located in Liaodong Bay in the north Bohai Sea, the Juehua Island (40.5°N, 120.8°E) is a typical nearshore island ecosystem (**Figure 1**), with its seacoast encircled by reef and its shallow water of 10- to 15-m depth and a feature of the mixed semidiurnal tide with a mean tidal range of about 2.06 m. The artificial reefs were deposited in 2018.

Sampling and Analysis

Phytoplankton, zooplankton, benthos, and nekton in monitoring stations were sampled and tested according to "Specifications for Oceanographic Survey—Part 6: Marine Biological Survey" (GB12763.6-2007). Zooplankton was collected with NORPAC plankton net (mesh 300 μm) by horizontal towing method at 1.5-m depth, and phytoplankton samples were collected with Kitahara plankton net (mesh 80 μm) using exactly the same method as zooplankton sampling. The net was towed from south to north at a 2-knot boat speed in 5 min. Samples were preserved in 250-cc plastic bottles and fixated with 1% Lugol's solution. Chlorophyll *a* concentration was measured in 1 L sampled seawater and collected by the filtration of the seawater. Marine sediments were extracted by a bottom grab sampler with 0.05 m^2. The preserved sediment sample was washed through the sieves of 63- and 500-μm mesh opening to remove sand and clay from the sample. Then, the floatation technique in silica colloidal (LudoxTM) with 1.15 of specific gravity was used to extract meiobenthos from fine particles in the residue on a 63-μm mesh sieve. The extracted meiobenthos was washed with filtered freshwater through a 63-μm mesh sieve. The residue on a 63-μm mesh sieve was moved into a mixture of 10% glycerin and 90% ethanol solution in a plastic bottle. Nektons were collected by 8-m trawls at a stable boat speed in 30–60 min.

Species identification of phytoplankton, zooplankton, and meiobenthos was performed with an optical microscope, and Chlorophyll *a* was determined by spectrophotometry. Phytoplankton biomass was transformed on the basis of Chlorophyll *a* concentration, and zooplankton biomass is calculated as follows:

$$P_z = \frac{m_z}{V} \times L, \tag{1}$$

where P_z is biomass on the unit area (mg/m^2), m_z is the wet weight of zooplankton, V is filtered water amount (m^3), and L is the length of rope.

Benthos biomass is computed as follows:

$$P_d = \frac{m_d}{S} \tag{2}$$

where P_d is benthos biomass on the unit area (mg/m^2), m_d is the wet weight of benthos, and S is the opening area of the bottom grab sampler (m^2).

Nekton biomass is estimated by stock density method with the following formula:

$$P_n = \frac{c}{q \times \alpha} \tag{3}$$

where P_n is nekton biomass on the unit area (kg/km^2), c represents trawl yields per hour (kg/h), α is sweep area per hour (km^2/h) that equals the product of expanded width of net mouth (km) and trawl speed (km/h), and q is capture efficiency whose

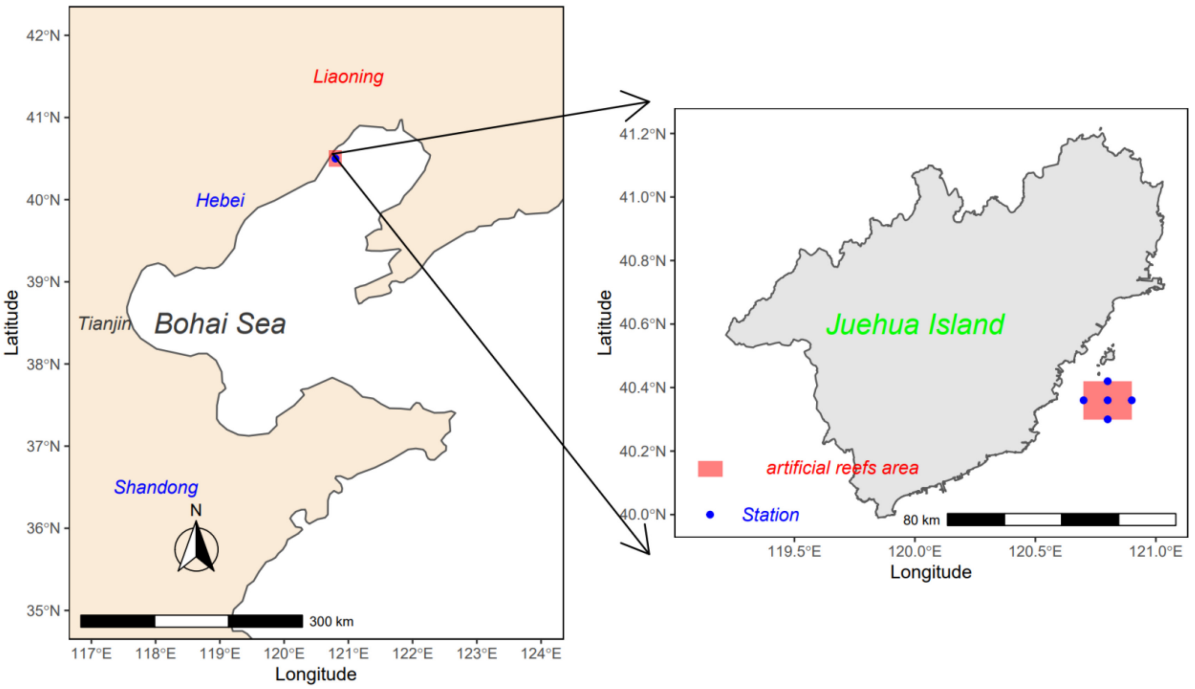

FIGURE 1 | Monitoring stations in the artificial reef ecosystem near Juehua Island in the Bohai Sea.

default value is 0.5. All biomass is unified at the wet weight ($t \cdot km^{-2}$).

Model Analysis

Based on survey datum of Juehua Island in summer and autumn of 2019, food web models were established to analyze the structure and functional variation of community matrices by EwE. The food web stability of artificial reefs was evaluated by the Ecosim models driven by Ecopath, and consequently, the effect of ecological restoration can be assessed.

Functional Groups

In total, 12 functional groups and 16 functional groups in summer and autumn, respectively (**Table 1**), were identified according to division rules that are essentially the same to ensure the comparability of the two seasons. *Charybdis japonica* is further classified into juvenile and adult groups in autumn for more precise diet proportion since it plays an important role in the autumn survey and has a different diet during growth.

Model Parameters

For the Ecopath model of Juehua Island, the input data include biomass (B), production/biomass ratio (P/B), consumption/biomass ratio (Q/B), ecotrophic efficiency (EE), diet composition, and fishery landings. B is estimated based on the marine survey. P/B and Q/B ratios are primarily referenced to the values of nearby Ecopath parameters seawater. Most EE values are estimated by the model. Diet composition is initially assigned according to *Fishbase* and stomach content analysis.

TABLE 1 | Functional groups of Juehua Island ecosystem in summer and autumn of 2019.

No.	Summer	Autumn
1	*Cynoglossus joyneri*	*Cynoglossus joyneri*
2	*Setipinna taty*	*Setipinna taty*
3	Gobiidae	Gobiidae
4	Engraulidae	*Platycephalus indicus*
5	*Charybdis japonica*	*Paralichthys olivaceus*
6	Other crabs	*Larimichthys polyactis*
7	Shrimps	*Engraulidae*
8	Cephalopod	*Charybdis japonica* (juvenile)
9	Other benthos	*Charybdis japonica* (adult)
10	Zooplankton	Other benthos
11	Phytoplankton	Shrimps
12	Detritus	Cephalopod
13		Other benthos
14		Zooplankton
15		Phytoplankton
16		Detritus

The landing data are collected primarily from peer-reviewed publications, stock assessments, and government reports.

Model Calibration

There is an energy balance equation between input and output in the Ecopath model that adheres to ecological and thermodynamics law. EE and Q/B ratio are tested for a valid range which requires $0 < EE \leq 1$ and $0.1 < P/Q < 0.3$. If EE is greater than 1, the corresponding functional group has undergone overhunting and overfishing. P/Q lie in 0.1 and 0.3 as the

consumption of most organisms is generally believed to be 10–30% of its production. For functional groups without balance energy, P/B, Q/B ratios, and diet matrix are adjusted until all EEs reach a reasonable level to ensure energy flow balance.

Pedigree coefficient (P) is defined to indicate the uncertainty of input parameters and model quality in Ecopath. The coefficient P is defined as follows:

$$P = \sum_{i=1}^{n} \frac{I_{ij}}{NLG}, \tag{4}$$

where I_{ij} is the pedigree coefficient of functional group i and input parameter j that may be B, P/B ratio, Q/B ratio, and diet matrix (DC_{ij}). While statistics in Morissette et al. (2006) showed that all pedigree coefficients of 150 Ecopaths from all over the world are between 0.16 and 0.68, the pedigree coefficients are 0.38 and 0.44, which testify the credibility and reliability of o ur model.

Food Web Traits and Stability Metrics

Food Web Traits

The Ecopath model can calculate multiple indicators for the evaluation of ecosystem functioning that include intrinsic structure and external pressure. We chose four complexity metrics (i.e., richness, connectance, omnivory index, and interaction strength), two energy recycling metrics (i.e., Finn's cycling index and Finn's mean path length), three maturity metrics (i.e., total net primary production, the ratios of total primary production (TPP) with total respiration, and ascendency), and two fishery metrics (i.e., fishery efficiency and mean trophic level of catches). Food web structure is depicted by complexity, energy recycling, and maturity metrics, and fishery metrics represent environmental pressure. All data are transferred by a natural logarithm to satisfy the normal distribution hypothesis.

Stability Metrics

This study focuses on two widely discussed categories of stability metrics: local stability and non-local stability. The former indicates the stability of the ecosystem near the equilibrium point. It is quantified by $\mathrm{Re}(\lambda_{max})$ that is the real part of the maximum eigenvalue of community matrix C, with a smaller value suggesting higher local stability. Lotka–Volterra interaction coefficient (α_{ij}), representing the effect of predator j on the *per capita* growth rate of prey i, is estimated as follows:

$$\alpha_{ij} = -\frac{\left(Q/B\right)_j \cdot DC_{ij}}{B_i}, \tag{5}$$

α_{ji}, representing the effect of prey i on the *per-capita* growth rate of predator j, is estimated as follows:

$$\alpha_{ji} = -e_{ji} \cdot \alpha_{ij}, \tag{6}$$

where,

$$e_{ji} = \frac{(P/B)_j}{\left(Q/B\right)_j} \tag{7}$$

is the predator conversion efficiency.

Since we focused only on interspecific interactions, diagonal elements α_{ii} are set to zero. Community matrix C is obtained through multiplying interaction matrix $A = [\alpha_{ij}]$ by corresponding biomass and

$$C = \begin{pmatrix} 0 & \frac{DC_{ij} \cdot (P/B)_j \cdot B_j}{B_i} \\ -\left(Q/B\right)_j \cdot DC_{ij} & 0 \end{pmatrix}. \tag{8}$$

The non-local stability reflects the overall characteristics of the ecosystem responding to relatively large perturbations. To simulate external disturbance, we increased fishing effort by 50% in Ecosim, which is observed as a moderate impact of fishing (Marco and Wolff, 2002; Adam et al., 2015). The disturbance remains constant during the first 10 years, then decreases to the baseline, and continues for the next 70 years (Marcelo et al., 1997). The three aspects of non-local stability are measured based on the ratio of simulated biomass to initial values (Pérez-España and Arreguın-Sánchez, 1999). Resistance reflects the ability of an ecosystem to maintain its original state in the context of disturbances. It is calculated as the reciprocal of the magnitude of biomass change (the difference between the maximum and minimum biomass values during the simulation). Resilience is defined as the speed at which species return to initial values after perturbations (Pimm and Lawton, 1978), and the resilience of an ecosystem depends on the least resilient species (Blanche et al., 2015). It is computed as the inverse tangent of the ratio of the magnitude of biomass change to recovery time (the time required to recover to original biomass values) (Pérez-España and Arreguın-Sánchez, 1999). Variability is the variance of biomass during simulation, which is quantified as the coefficient of variation of population biomass (the SD of population biomass divided by the mean value).

RESULTS AND DISCUSSION

Food Web Traits

Functional groups increase from 11 to 15, corresponding to summer and autumn in 2019, and species with a high trophic level, such as *platycephalus*, *Paralichthys olivaceus*, and less yellow croakers, are found in autumn but not in summer (**Table 2**). As is suggested in most marine surveys, the species in summer are believed to be more plentiful than in autumn, since migratory fish schools enter the Bohai area for food in spring and leave in autumn. However, our research tells a different story: the species in autumn are more diversified than in summer. One possible reason for our paradoxical results is that marine living are attracted to the artificial reef that provides more suitable habitats and thus biodiversity in the artificial reef is enhanced. The other contributing factor may be the fishing moratorium in summer that leads to the recovery of fish richness and fish resources. The omnivory index and the connectance index are almost the same in summer and autumn, whereas a minimal decrease in food web connectance could be observed from summer to autumn in 2019.

The recycling metrics Finn cycling index (FCI) and Finn mean path length (FML) have increased by 112.97 and 16.36%

TABLE 2 | Food web trait metrics of artificial reef of Juehua Island in summer and autumn of 2019.

Classification	Metrics	Summer	Autumn
Complexity	Number of groups(NLG)	11	15
	Connectance (CI)	0.46	0.40
	Omnivory index (SOI)	0.23	0.21
	Interaction strength (ISI)	0.58	7.37
Recycling	Finn cycling index (FCI) (%)	10.33	22.00
	Finn mean path length (FML)	2.68	3.12
Maturity	Total primary production/total respiration (TPP/TR)	1.76	1.07
	Total primary production/total biomass (TPP/TB)	63.66	45.71
	Ascendency (A/C) (%)	32.21	34.44
Fishery	Total catches (TC) (t/km^2)	0.84	0.85
	Mean trophic level of the catch (MTLc)	2.87	2.90
	Gross efficiency (GE)	0.00	0.00

TABLE 3 | Food web stability of artificial reef of Juehua Island in summer and autumn of 2019.

Category	Stability metrics	Summer	Autumn
Local Stability	Re(λ_{max})	0.15	0.16
Non-local stability	Resistance	1.54	1.57
	Resilience	0.90	0.59
	Variability	0.01	0.05

from summer to autumn, respectively, which indicates obvious promotion of matter recycling proportion, organic matter flow, and cycling diversity in autumn compared with that of summer. A longer cycle period and a slower cycle are manifested in autumn. Maturity metrics TPP/TR (the best indicator for food web maturity) and TPP/TB show a decrease from summer to autumn. Results showed that the artificial reef near Juehua Island has good maturity with TPP/TR of 1.76 and 1.07 in summer and autumn, respectively, and maturity in autumn is higher than that in summer.

Food Web Structure

The food web of artificial reef of Juehua Island mainly consists of graze and detritus food chain. During summer, twelve functional groups of artificial reef occupy three trophic levels (assessed by EwE) with a range of 1.00–3.63 where *Cynoglossus joyneri* has the highest trophic (**Figure 2A**). In contrast, in autumn, 16 groups are divided into four levels with a range of 1.00–4.20 where *P. olivaceus* is at the top of the food chain (**Figure 2B**). The bottom of food webs from summer to autumn remains the same: detritus, phytoplankton, zooplankton, and other benthos.

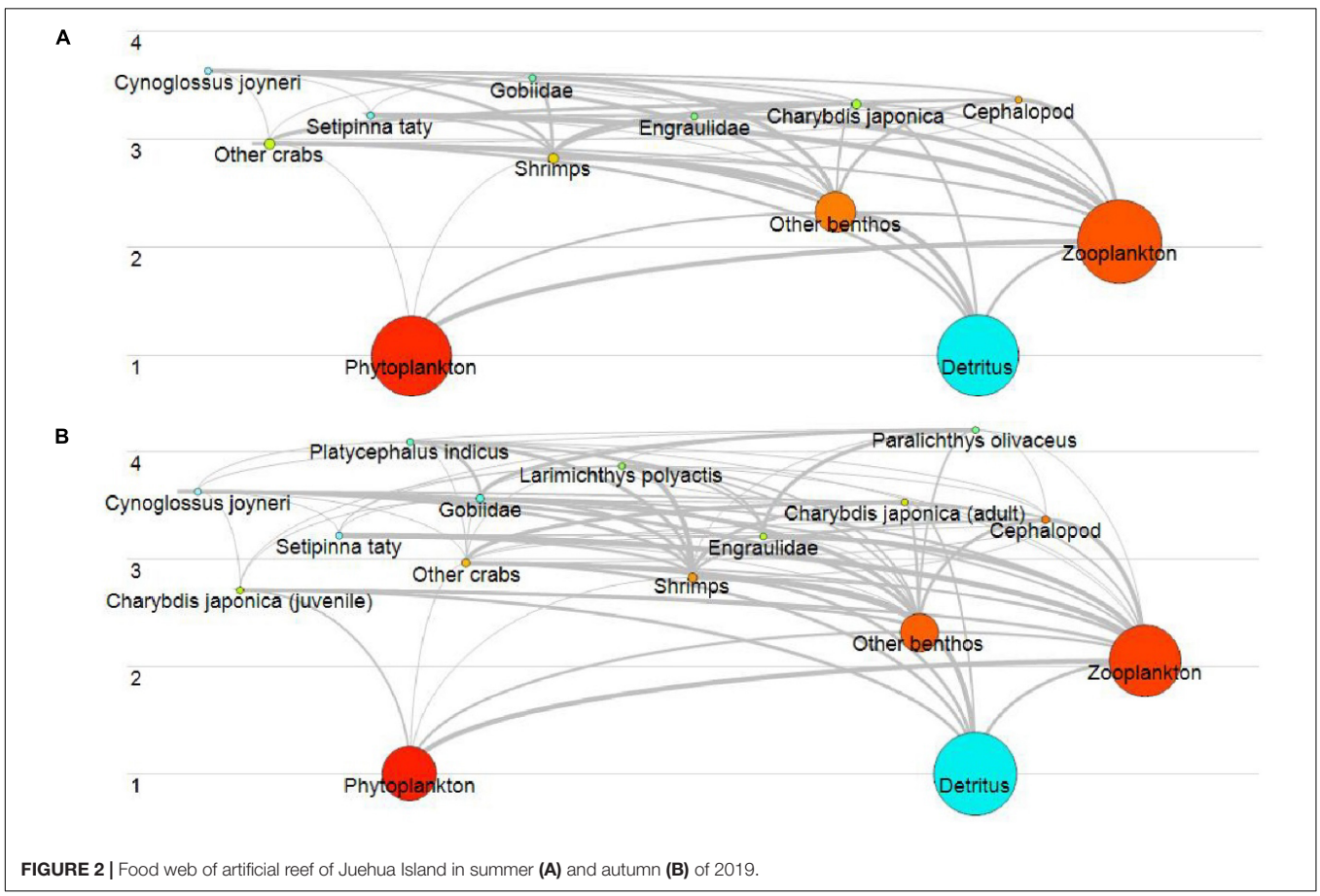

FIGURE 2 | Food web of artificial reef of Juehua Island in summer **(A)** and autumn **(B)** of 2019.

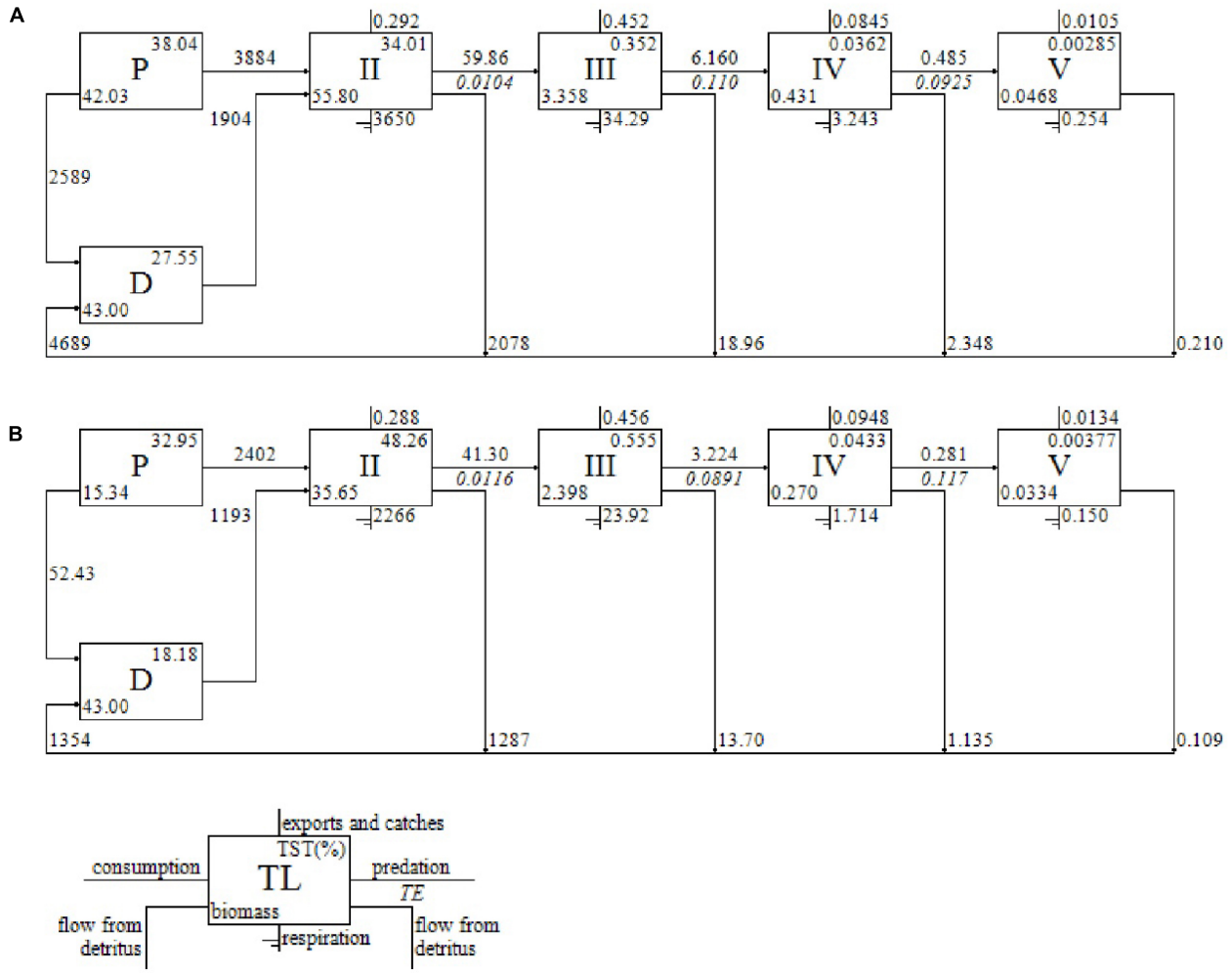

FIGURE 3 | Energy flows of the artificial reef food web in summer **(A)** and autumn **(B)** of 2019.

Food Web Stability

The food web stability, local and non-local, decreases mildly from summer to autumn since Re(λ_{max}), resilience, and variability in autumn are higher than in summer, whereas resistance got worse at the same time (**Table 3**). The result did not support the assumption that artificial reefs can improve food web stability in Juehua Island. This occurs because the restoring time is too short to let the fish community arrive at equilibrium. As artificial reefs planning started in September, 2018 and the release launch took place in January, 2019, the time from reefs launching to this marine survey is less than 1 year. In most cases, it takes 4–5 years for the fish community to reach its steady-state after artificial reefs are thrown into the ocean bottom since reefs would generate some disturbance on fishes and invertebrate communities nearby. To precisely evaluate the recovering effect and stability promotion of the sea area near Juehua Island after the launch of artificial reefs, a tracking survey must be conducted along the long-term scale until a stable point of the community is reached.

Food Web Function

The energy flow proportions of phytoplankton to the total energy in the summer and autumn of 2019 are greater than that of detritus (**Figure 3**), which indicates that the food web of reefs in Juehua Island is dominated by the graze food chain. Trophic levels I and II take 65.59 and 34.01% of the total energy in summer and take 51.41 and 48.26% in autumn, respectively, which shows that the energy flows in Juehua Island give priority to lower trophic species, and the energy flows between level III and above are poorer for the absence of high-trophic marine living, although the use of detritus and primary production in the ecosystem is improving from summer to autumn.

Energy flow efficiencies were approximate and improved a bit from summer to autumn (**Table 4**), whereas they are less than Lindeman's efficiency of 10%. The efficiencies from trophic level II to level III in summer and autumn are both around 1%, which manifests that low efficiency from trophic level II to level III is the main cause of the inefficiency of the total food web. The low resource of trophic level III cannot consume

TABLE 4 | Energy flow efficiencies of the artificial reef food web in summer and autumn of 2019.

Trophic level	Summer	Autumn
II	1.04%	1.16%
III	11.04%	8.91%
IV	9.25%	11.65%
V	4.45%	8.04%
Total	4.74%	4.93%

explosive growth biomass of level II since there is a great rise in plankton, benthos near reefs, and filter feeder adhering to fish reefs as a result of expanding habitat space and enough bait of artificial reefs. There is a transferring bottleneck from trophic level II to level III for its low efficiency. New species in autumn, such as *platycephalus* and *P. olivaceus* with trophic level IV that feeds on *C. joyneri*, *Setipinna taty*, goby, and anchovy, speed up the consumption of living in trophic level III, but the flow efficiency from level III to level IV declined from summer to autumn. This may be caused by the catch reduction of trophic level III biomass. Energy flow efficiency from level IV to level V has a slight increase due to additional fishery of high trophic species. In brief, the lack of high trophic species brings about the low energy flow efficiency in Juehua Island although the efficiency goes up slightly from summer to autumn. To get the normal efficiency of energy flows in Juehua Island, the resource of high trophic species must be enhanced for a long time.

Food Web Loop Analysis

Loop weights of the community matrix are almost symmetric at zero for a given length, and their absolute values decrease with length increasing (**Figures 4C,D**), which means that long loops relatively contain many weak links. The three-species omnivory feedback loop has a maximum weight that is close to four in summer (**Figure 4C**) and exceeds four in autumn (**Figure 4D**). The maximum weight loops that are considered as the most dangerous ones for food web stability are both other benthos, zooplankton, and phytoplankton in summer and autumn in Juehua Island of 2019 (**Figures 4A,B**), which confirms the conclusion that lower trophic level is dominant in the food web of Juehua Island. The largest interaction strength −81.2 is from zooplankton to phytoplankton, whereas the mean interaction

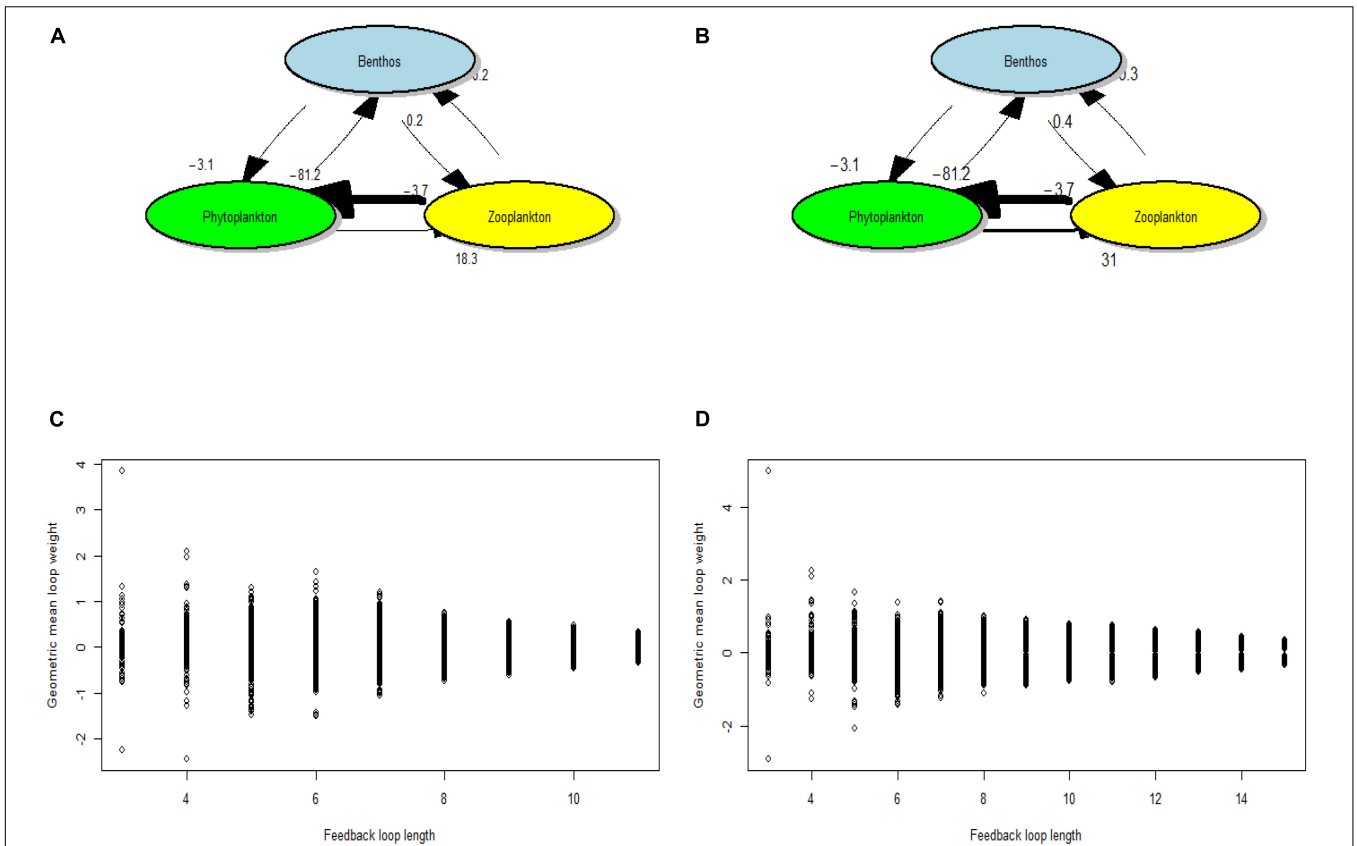

FIGURE 4 | The mean loop weights that are defined as the geometric mean of the values of the interaction strengths in the loop and their maximum of different lengths in the summer and autumn in Juehua Island of 2019. The maxima both occur at the smallest omnivory feedback loop (length three). **(A)** Benthos, zooplankton, and phytoplankton have maximum loop weight among all loops in the summer of 2019 in Juehua Island since the interaction strength from zooplankton to phytoplankton is –81.2 that far outweigh the other interaction strengths. **(B)** The maximum weight loop in autumn is the same as the one in summer. **(C)** All loop weights of different lengths in summer. **(D)** All loop weights of different lengths in autumn.

strength is 3.6 in summer and autumn. To improve food web stability in Juehua Island, one effective method is to reduce the predator-prey negative interaction strength between zooplankton and phytoplankton by promoting zooplankton biomass.

CONCLUSION

Artificial reefs are often used to restore the degraded marine ecosystem. This study analyzed the seasonal variations, structure, stability, and function of a typical artificial reef food web. We found that the structure (species number, trophic level, and interaction), function (energy cycle proportion, energy complexity, and energy transfer efficiency), and maturity of the food web increased from summer to autumn. However, no significant change for food web stability was found between the two seasons, which is possibly due to the relatively slow process for stability restoration. Furthermore, the feedback loop analysis revealed that interaction strengths in the omnivorous feedback loop (benthos, zooplankton, and phytoplankton) are the maximum loop, which suggests that the predator-prey negative interaction strength between zooplankton and phytoplankton dominates the stability of the artificial reef, whether in summer or autumn. This study also suggests that stability is a more robust indicator for ecosystem assessment and could provide useful information in future restoration plan of the marine ecosystem.

DATA AVAILABILITY STATEMENT

The original contributions presented in the study are included in the article/supplementary material, further inquiries can be directed to the corresponding author.

AUTHOR CONTRIBUTIONS

SL, RW, and YJ: formal analysis. SL: investigation. LZ and JF: resources. JF: supervision. All authors have read and agreed to the published version of the manuscript.

FUNDING

This study was supported by the National Key R&D Program of China (2018YFC1406403).

REFERENCES

Adam, G., Lavery, P. S., and Lonzano-Montes, H. (2015). Trophic implications and faunal resilience following one-off and successive disturbances to an *Amphibolis griffithii* seagrass system. *Mar. Pollut. Bull.* 94, 131–143. doi: 10.1016/j.marpolbul.2015.03.001

Blanche, S. B., Baird, D., Asmus, H., Asmus, R., Bacher, C., Pacella, S. R., et al. (2015). Trophic networks: how do theories link ecosystem structure and functioning to stability properties? A review. *Ecol. Ind.* 52, 458–471. doi: 10.1016/j.ecolind.2014.12.017

Christensen, V., Walters, C., and Pauly, D. (2005). "Ecopath with ecosim: a User's guide," in *Fisheries Centre, University of British Columbia, Vancouver, Canada and ICLARM*, Penang, 01.

Curtin, R., and Prellezo, R. (2010). Understanding marine ecosystem based management: a literature review. *Marine Policy* 09, 821–830. doi: 10.1016/j.marpol.2010.01.003

de Vries, F. T., Thébault, E., Liiri, M., Birkhofer, K., Tsiafouli, M., Bjørnlund, L., et al. (2013). Soil food web properties explain ecosystem services across European land use systems. *Proc. Natl. Acad. Sci. U.S.A.* 110, 14296–14301. doi: 10.1073/pnas.1305198110

Jacquet, C., Moritz, C., Morissette, L., Legagneux, P., Massol, F., Archambault, P., et al. (2016). No complexity-stability relationship in empirical ecosystems. *Nat. Commun.* 71:12573. doi: 10.1038/ncomms12573

Leclerc, C., Courchamp, F., and Bellard, C. (2020). Future climate change vulnerability of endemic island mammals. *Nat. Commun.* 11:4943. doi: 10.1038/s41467-020-18740-x

Liang, C., and Pauly, D. (2020). Masking and unmasking fishing down effects: the Bohai Sea (China) as a case study. *Ocean Coast. Manag.* 184:105033.

MacArthur, R. (1955). Fluctuations of animal populations and a measure of community stability. *Ecology* 07, 533–536. doi: 10.2307/1929601

Marcelo, V., Mackinson, S., Sloman, K., and Pauly, D. (1997). The stability of trophic mass-balance models of marine ecosystems: a comparative analysis. *Ecol. Model.* 100, 125–134. doi: 10.1016/s0304-3800(97)00150-6

Marco, O., and Wolff, M. (2002). Dynamical simulation of mass-balance trophic models for benthic communities of north-central Chile: assessment of resilience time under alternative management scenarios. *Ecol. Model.* 148, 277–291. doi: 10.1016/s0304-3800(01)00454-9

May, R. (1972). Will a large complex system be stable. *Nature* 09, 413–414. doi: 10.1038/238413a0

Min, X., and Xin, Y. (2021). Seasonal analysis of artificial oyster reef ecosystems: implications for sustainable fisheries managemen. *Aquacul. Int.* 29, 167–192. doi: 10.1007/s10499-020-00617-x

Mitchell, E., and Neutel, A.-M. (2012). Feedback spectra of soil food webs across a complexity gradient, and the importance of three-species loops to stability. *Theor. Ecol.* 05, 153–159. doi: 10.1007/s12080-011-0143-z

Morissette, L., Hammill, M. O., and Savenkoff, C. (2006). The trophic role of marine mammals in the northern gulf of st. lawrence. *Mar. Mamm. Sci.* 22, 74–103. doi: 10.1111/j.1748-7692.2006.00007.x

Neutel, A.-M., Heesterbeek, J. A., and De Ruiter, P. C. (2002). Stability in real food webs: weak links in long loops. *Science* 296, 1120–1123. doi: 10.1126/science.1068326

Neutel, A.-M., Heesterbeek, J. A., van de Koppel, J., Hoenderboom, G., Vos, A., Kaldeway, C., et al. (2007). Reconciling complexity with stability in naturally assembling food webs. *Nature* 11, 599–602. doi: 10.1038/nature06154

Neutel, A.-M., and Thorne, M. (2015). Linking saturation, stability and sustainability in food webs with observed equilibrium structure. *Theor. Ecol.* 9, 73–81.

Neutel, A.-M., and Thorne, M. A. (2016). Beyond connectedness: why pairwise metrics cannot capture community stability. *Ecol. Evol.* 6, 7199–7206. doi: 10.1002/ece3.2461

Paine, R. (1966). Food web complexity and species diversity. *Am. Nat.* 01, 65–75. doi: 10.1086/282400

Pérez-España, H., and Arreguın-Sánchez, F. (1999). Complexity related to behavior of stability in modeled coastal zone ecosystems. *Aquat. Ecosyst. Health Manag.* 2, 129–135. doi: 10.1111/jeb.13524

Pimm, J. H., and Lawton, S. L. (1978). On feeding on more than one trophic level. *Nature* 275, 542–544.

Rahman, M. F., Qun, L., Xiujuan, S., Chen, Y., Ding, X., and Liu, Q. (2019). Temporal changes of structure and functioning of the bohai sea ecosystem: insights from ecopath models. *Thalassas* 10, 625–641.

Stone, I. D., and Lewi, R. (2001). Complexity can enhance stability in competitive systems. *Ecol. Lett.* 6, 397–400.

Tang, S., Pawar, S., and Allesina, S. (2014). Correlation between interaction strengths drives stability in large ecological networks. *Ecol. Lett.* 17, 1094–1100. doi: 10.1111/ele.12312

Tong, L., Tang, Q., and Pauly, D. (2000). A preliminary approach on mass-balance ecopath model of the Bohai Sea. *Chin. J. Appl. Ecol.* 07, 435–440.

Zhang, Q., and Lin, X. S. (2009). Comparative study on the changes of the Bohai Sea ecosystem structure based on Ecopath model between ten years. *Acta Ecol. Sin.* 07, 3613–3620.

Zheng, T., and You, X. (2014). On structure and maturity changes of the Bohai Sea ecosystem during the 1980s–1990s. *Aquat. Ecosyst. Health. Manag.* 17, 186–195.

Conflict of Interest: The authors declare that the research was conducted in the absence of any commercial or financial relationships that could be construed as a potential conflict of interest.

Publisher's Note: All claims expressed in this article are solely those of the authors and do not necessarily represent those of their affiliated organizations, or those of the publisher, the editors and the reviewers. Any product that may be evaluated in this article, or claim that may be made by its manufacturer, is not guaranteed or endorsed by the publisher.

Copyright © 2022 Li, Wang, Jiang, Li, Zhu and Feng. This is an open-access article distributed under the terms of the Creative Commons Attribution License (CC BY). The use, distribution or reproduction in other forums is permitted, provided the original author(s) and the copyright owner(s) are credited and that the original publication in this journal is cited, in accordance with accepted academic practice. No use, distribution or reproduction is permitted which does not comply with these terms.

frontiers in Marine Science

ORIGINAL RESEARCH
published: 10 February 2022
doi: 10.3389/fmars.2022.833513

Switch of Bacteria Community Under Oxygen Depletion in Sediment of Bohai Sea

*Xiaoxiao Guo[1], Guisheng Song[2], Yanying Li[1], Liang Zhao[3] and Jing Wang[1]**

[1] Tianjin Key Laboratory of Animal and Plant Resistance, Tianjin Key Laboratory of Conservation and Utilization of Animal Diversity, Tianjin Normal University, Tianjin, China, [2] School of Marine Science and Technology, Tianjin University, Tianjin, China, [3] College of Marine and Environmental Sciences, Tianjin University of Science and Technology, Tianjin, China

Regular oxygen depletion is occurring every summer in the depression area of the Bohai Sea. The community structure and potential functions of microbes in expanding marine hypoxic area are of great importance due to their roles in biogeochemical cycling. In this study, the diversity and distribution of bacteria based on 16S rRNA gene in sediment along an inshore-offshore transect across the oxygen-depletion area in the Bohai Sea was investigated in June, July and August of 2018 by employing high-throughput sequencing. Results revealed that the bacteria community was dominated by Proteobacteria (42.67%), Actinobacteria (14.13%), Chloroflexi (13.02%), Acidobacteria (8.01%), and Bacteroidetes (6.30%). During oxygen depletion, the bacteria community from inshore site A3 subjected to dramatic variation from June to August, but the composition tended to be stable in sites from the depression area along the transect. Distinct switch of bacteria from aerobic to anaerobic group was observed when the DO concentration <4.2 mg/L, typically represented by dominance of *Anaerolineaceae* in August sample. Further, KEGG prediction by PICRUSt confirmed the variations by showing significant difference in functional pathways, especially the nitrogen metabolisms, before and after DO depletion ($p < 0.05$). These variations could be influenced by depth, NO_2^- concentration and DO availability based on RDA analysis. The details in diversity and composition of bacteria under continually observation provide insights into both instant and long-term response of bacteria community to oxygen depletion, and the distinct functional switch under this process expands our knowledge on the metabolic character of bacteria in worldwide hypoxia areas.

Keywords: Bohai Sea, sediment, oxygen depletion, 16S rRNA, community switch, function prediction

OPEN ACCESS

Edited by:
Meilin Wu,
South China Sea Institute of Oceanology, Chinese Academy of Sciences (CAS), China

Reviewed by:
Hualong Wang,
Ocean University of China, China
Lei Yan,
Heilongjiang Bayi Agricultural University, China

****Correspondence:***
Jing Wang
jwang_hku@163.com

Specialty section:
This article was submitted to Marine Pollution, a section of the journal Frontiers in Marine Science

Received: *11 December 2021*
Accepted: *06 January 2022*
Published: *10 February 2022*

Citation:
Guo X, Song G, Li Y, Zhao L and Wang J (2022) Switch of Bacteria Community Under Oxygen Depletion in Sediment of Bohai Sea. Front. Mar. Sci. 9:833513. doi: 10.3389/fmars.2022.833513

INTRODUCTION

As a vital part of marine ecosystem, sediments are impacted by geological, hydrodynamical, physicochemical and biological processes (Köster and Meyer-Reil, 2001) and acting as both source and sink of adsorbed nutrients (Zhou et al., 2017), heavy metals (Dou et al., 2013), and persistent hydrophobic organics (Lofrano et al., 2017). The microbes that living in the sediments are responsible for various biogeochemical transformations and organic matter decomposition by means of uptake and release of chemicals (Petro et al., 2017). Due to excessive anthropogenic

nitrogen inputs resulted from application of synthetic nitrogenous fertilizers and industry activity, nitrogen pollution in coastal ecosystem has led to deleterious ecological changes (Canfield et al., 2010; Cui et al., 2013). The negative effects including eutrophication and harmful algal blooms (Anderson et al., 2002; Bricker et al., 2008), expanding hypoxia and anoxic zones (Diaz and Rosenberg, 2008; Paulmier and Ruiz-Pino, 2009; Breitburg et al., 2018) are increasing in high frequency. Additionally, as a key environmental factor, dissolved oxygen (DO) affects biochemical processes of marine organisms and also acts as one of the vital drivers in the global carbon and nitrogen cycling (Voss et al., 2013; Mahaffey et al., 2020). Bacteria is an important contributor to the net loss of fixed nitrogen in oxygen minimum zones (OMZ) of oceans (Lam et al., 2009; Ward et al., 2009; Stramma et al., 2020). At the same time, some autotrophic denitrifying bacteria and anaerobic ammonium oxidizing (anammox) bacteria are also involved in the fixation of carbon dioxide (CO_2) by activating electron acceptors: the former fixes CO_2 while reducing sulfur, forming compounds with nitrate; the latter fixes CO_2 while oxidizing ammonium plus nitrite to dinitrogen, both of which are under anaerobic environment (Koeve and Kähler, 2010).

Certain bacterial community are sensitive enough to be an indicator when inferring bacteria changes under hypoxic environment (Wright et al., 2012), such as Proteobacteria, Bacteroidetes, Actinobacteria, and Planctomycetes. Some members belonging to the suboxic-related phyla can use electron acceptors as an alternative to oxygen, by which mechanisms driving changes in the bacterial community to response oxygen depletion or totally lack of dissolved oxygen. Therefore, the community composition of bacteria and unique biogeochemical cycling processes in hypoxic area have been extensively studied in recent years (Beman and Carolan, 2013; Li et al., 2014; Fuchsman et al., 2019; Sen et al., 2021). Certain bacteria have been reported to be adapted for low-oxygen environments, such as SAR11 bacteria, NC10 bacteria and Protochlorococcus (Füssel et al., 2012; Padilla et al., 2016), which are related to ocean hypoxia and nitrogen loss and generally distributed in the core hypoxic area with high abundance (Thiele et al., 2019) or intensive activity (Tsementzi et al., 2016). In addition, some investigations have determined the metabolic basis for SAR11 and confirmed their role as a model to study the carbon and nitrogen cycles in the OMZs (Tsementzi et al., 2016; Bertagnolli and Stewart, 2018; Ruiz-Perez et al., 2021). However, direct clues on the effects of oxygen depletion on bacterial diversity and metabolism are still limited. Therefore, to explore the response mechanism of the functional bacterial groups in hypoxia environment is of great importance.

It is a common method to achieve information about bacteria diversity and abundance by profiling the 16S-rRNA gene. Moreover, examining the functions of bacterial communities is critical for estimating and understanding of how bacterial communities respond to the changes of ecosystem (Ward et al., 2017; Escales et al., 2019). Recent investigations on functional potential prediction of bacteria by employing PICRUSt2 in different environments, including soils (Toole et al., 2021), seawater (Xue et al., 2021), marine sediment (Su et al., 2018) are in help to decipher the detailed function variations successfully. In addition, benefiting from the function prediction of bacteria from the 16S rRNA gene sequences solely, diverse unknown microbes could be identified phylogenetically (Tsaban et al., 2021). With the unique contribution of each clade to Kyoto Encyclopedia of Genes and Genomes (KEGG) pathways are developed, PICRUSt2 prediction is increasingly applied in microbial ecology studies.

Bohai Sea, with an area of 77,000 km^2 and the average water depth of 18 m, is semi-enclosed and located in northern China. It is characterized by a long water exchange half-life as much as 17–21 months (Hao et al., 2002; Luo et al., 2021). Due to the long-term impact of industry and agriculture, heavy metal pollution and excessive inorganic nitrogen has been accumulated in the Bohai Sea (Duan and Li, 2017; Mu et al., 2017), which led to severe eutrophication and the formation of oxygen-deficient zone in the central Bohai Sea (Zhao et al., 2017). Microbes are suffering from severe ecological pollution but also argued to be key for remediation since the denitrification bacteria could remove excessive nitrogen from marine environment. Based on current study on microbial composition, Proteobacteria and Bacteroidetes are widely distributed in Bohai Sea sediments (Wang et al., 2013, 2014; Li et al., 2017), with temperature and DO are the key impacting factors. Moreover, other environmental vital drivers such as salinity (Lv et al., 2016) and pH (Zhang et al., 2017) have been proved to determine bacterial communities also. However, to the best of our knowledge, the detailed information on bacteria diversity in the coastal Bohai Sea sediments remain limited, and none of the above studies put emphasize on the variation of bacterial communities under hypoxia in sediment of Bohai Sea.

In this study, the diversity and distribution of bacteria along one transect covering inshore and oxygen-depleted offshore area of Bohai Sea were investigated from June to August, 2018. By employing 16S rRNA gene high-throughput sequencing, in combination with metagenomic analysis, bacteria diversity, distribution, phylogeny and functions during oxygen depletion was evaluated and predicted. Furthermore, key environmental factors driving the bacterial communities were discussed. All of which provide insights into the relationship between oxygen depletion and relating microbial functions.

MATERIALS AND METHODS

Sample Collection

Samples were collected in four cruises carried out in June, July, early and late August of 2018, respectively, in the Bohai Sea along one inshore-offshore transect (A3–A7:39.38°–39.69°N, 119.63° –120.55°E) (**Figure 1**), details of sampling site and date were listed in **Supplementary Table 1**. The sediment samples were collected in stainless steel 0.1 m^2 GyO'Hara box corer, and the top 1–2 cm surface sediment were gently scraped off before subsampling were made after homogenization. All the samples were stored in sterilized 60 ml centrifuge tubes and frozen in liquid nitrogen immediately. It is worth to note that samples were attached to dry ice during transportation and then stored at –80°C until DNA extraction.

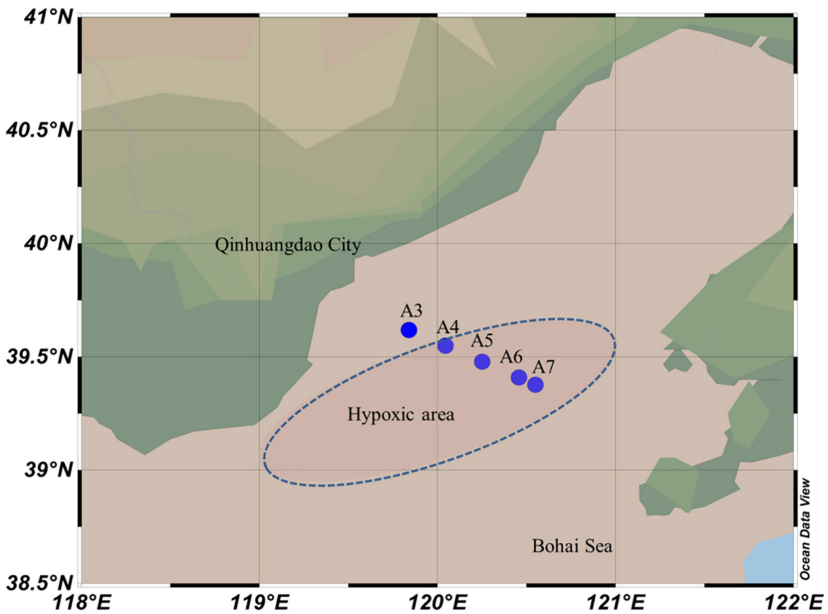

FIGURE 1 | Map showing the sampling sites in Bohai Sea along inshore—offshore transect. The blue dash line oval showing the reported hypoxic area.

Physic-Chemical Parameters

At each site, the salinity, dissolved oxygen (DO), pH, and temperature of seawater was recorded *in situ* by employing the SeaBird model SBE9 conductivity-temperature-depth (CTD) recorder (Sea-Bird Electronics). The pore water from sediment cores were obtained by centrifuging at 6,000 r/min and poisoned by $HgCl_2$ before analysis. Concentration of ammonium, nitrite and nitrate were determined by using a AA3 nutrient Auto Analyzer.

DNA Extraction and High-Throughput Sequencing

The DNA extraction and PCR amplification were following the published procedures (Wang et al., 2019) with replacement of primer sets targeting the V3, V4 region of 16S rRNA gene. Phylogenetically diagnostic sequences were amplified using the universal primers 338F (5′-ACTCCTACGGGAGGCAGCA-3′) and 806R (5′-GGACTACHVGGGTWTCTAAT-3′) (Dai et al., 2016). High-throughput sequencing was performed using Illumina MiSeq system (Illumina MiSeq, United States).

Statistical Analysis

The OTUs (operational taxonomic units) were defined by 97% identity for taxonomy assignment using Uclust method (Edgar, 2010). Rarefaction analysis was performed for all the OTUs using Mothur (version v.1.30) and R with the aim to ensure the amount of the sequences was as reasonable as possible (**Supplementary Figure 1**). Mothur software was then used to evaluate the species richness and alpha diversity index of the samples (Shannon, Simpson, ACE and Chao 1). Beta diversity at phylum level was calculated between the five sites and four sampling time using non-metric multidimensional scaling analysis (NMDS) based on binary-jaccard distance using the R (3.6.3). Phylogenetic analysis of the representative sequences from dominant OTU (top 18 OTUs of 16S rRNA gene) was conducted with the software of MEGA7.0. Neighbor-joining tree of the representative OTUs and the reference sequences from NCBI GenBank was established with 1,000 replicates of bootstrap value. Bacterial community dynamics at generic level with eight environmental variables (Temperature, salinity, pH, DO, NO_3^-, NO_2^-, NH_4^+) were analyzed using canonical correspondence analysis (CANOCO v.5.02) and mapped with R language vegan package. Significance test was conducted using one-way ANOVA by employing SPSS 17.0.

Functional Prediction of Bacteria by PICRUSt

Functional potential of microbial communities in sediment samples were predicted using PICRUSt (phylogenetic investigation of communities by reconstruction of unobserved states) (Langille et al., 2013). PICRUSt is a bioinformatics tool that predicts the functional composition of a metagenome using 16S rRNA gene sequences and a reference genome database. Sequences used for PICRUSt prediction were clustered into OTUs (97% similarity) against the Greengenes 13.5 database using QIIME2 software (version 2.9.1). Then the rarefied OTU table was used for normalization of 16S rRNA gene copy numbers. The normalized OTU table and the KEGG database were compared to obtain different function files for each sample. Finally, PICRUSt was used to obtain information at three pathway levels. The KEGG orthology (KO) genes that involved in nitrogen transformation in the KEGG database were compared with the PICRUSt function prediction results, and the

KO related to nitrogen metabolism with the gene copy numbers in the respective sample was selected for analysis.

Nucleotide Sequences Accession Numbers

The annotated nucleotide sequences of 16S rRNA gene were deposited to NCBI under accession numbers SRR17253936-SRR17253955.

RESULTS

Biogeochemical Characteristics of Bohai Sea

In total, 20 sediment samples were collected from 5 sites and 3 months along inshore-offshore transect covering oxygen depletion area (**Supplementary Table 1**). The hydrological parameters (except depth and NO_3^-) showed significant variation before and after DO depletion ($p < 0.05$, **Supplementary Table 1**), but no significance was observed among sites within each sampling time. As shown in **Supplementary Figure 2**, both DO and salinity decreased in August, especially in the reported oxygen depletion area (sites A4–A7 in this study). At the same time, concentration of NO_2^- and NH_4^+ were also accumulated in August. The variation of NO_3^- concentrations was not significant in sediment across sampling time, and the highest value occurred in August A5 site, which was also core of the oxygen-depletion zone.

Community Composition of Bacteria During Oxygen Depletion

By applying high-throughput sequencing targeting V3, V4 region of bacterial 16S rRNA gene, 1,198,861 reads and 77,560 clean reads were achieved from 20 samples. Based on 97% similarity, 8,032 OTUs were identified by reference from NCBI. A rarefaction curve was plotted with 34,070 sequences for each sample (**Supplementary Figure 1**). The community composition revealed by 16S rRNA gene at phylum level and genus level was shown in **Figure 2**. In general, Proteobacteria dominated by 42.67% among all the detected communities, followed by Actinobacteria (14.13%), Chloroflexi (13.02%), Acidobacteria (8.01%), Bacteroidetes (6.30%), and Gemmatimonadetes (2.95%). Phylum of Proteobacteria was mainly composed of classes Gammaproteobacteria, Deltaproteobacteria, and Alphaproteobacteria, among which, Gammaproteobacteria obviously was the most dominant class (19.12%). The relative proportion of every phylum within each sample was changing between sampling sites and time. Proteobacteria was most abundant in A3826 (56.75%), but overall, they tend to distribute in offshore sites (**Figure 2B**). From A3 to A5, Chloroflexi was less than Actinobacteria in June and July, but greater than Actinobacteria when time turned to August. But this variation was observed in the offshore samples A6 and A7. With their location in the reported core hypoxia area, the relative abundance of these phylum kept constant along the four sampling times. Phylum Firmicutes was only abundant in A3 and A4 sites before the oxygen began to deplete. For the dominant phylum, strong variation was observed in inshore sites, and their relative composition tend to be stable in the offshore and core hypoxia sites.

Switch of bacteria was observed after oxygen depletion. Members of class Acidimicrobiia under phylum Actinobacteria were dominant in June and July, genus *Woeseia* (9.61%) of Proteobacteria was dominant and evenly distributed at all sites across all sampling time, and their dominance was replaced by the anaerobic bacteria *Anaerolineaceae* that belonging to Chloroflexi by 12.5% in August (**Figure 2A**). In addition, specific genera including *Amphiplicatus*, *Ellin6067*, *Dokdonella*, *Defluviimonas* from Proteobacteria, *OLB12,* and *Rikenella* from Bacteroidetes, *Lactobacillus* from Firmicutes and *Mucispirillum* from Deferribacteres, most of which were aero-tolerant or anaerobic bacteria, were also detected as a result of oxygen depletion with first occurrence in August samples.

The spatial distribution of bacteria was evaluated by non-metric multidimensional scaling (NMDS) analysis based on the binary-jaccard method (**Figure 3**). Samples from the same sites were clustered together, while samples from different sampling time were separately distributed. Among which, samples from A6 and A7 overlapped with each other, which suggested the high similarity of community composition of bacteria in A6 and A7.

Spatiotemporal Variations of Alpha Diversity

ACE and Chao 1 indices showed that the greatest diversity of 16S rRNA gene was observed at the offshore site A6 in June and July, while the lowest value occurred at the nearest inshore site A3 in Late-August. The diversity indices decreased slightly in the reported core oxygen depletion sites when oxygen began depleted, but decreased sharply in site A3, which subjected to low DO only in this study. The indices of Shannon and Simpson showed consistent trend with ACE and Chao1. Spatially, the diversity of the 16S rRNA gene was higher at offshore sites than the inshore; temporally, higher diversity was appeared in June, and decreased in August. As shown in **Table 1**, the differences observed was not significant between sites or sampling times ($p > 0.05$).

Functional Prediction of Bacteria by PICRUSt

Community prediction using PICRUSt was performed to determine the function of the observed bacteria. Based on the KEGG database, 6 categories of biological metabolic pathways were obtained, including metabolism, genetic information processing, environmental information processing, cellular processes, human diseases and organismal systems. Metabolism, genetic information processing and environmental information processing appeared to be the primary components, accounting for 51.88, 20.22, and 11.12% of all components, respectively. An analysis on the secondary functional levels of predicted genes identified 39 sub-functions, with relative abundance greater than 1% are shown in **Figure 4A**. A large proportion of the microbial functions were found in carbohydrate metabolism (9.76%),

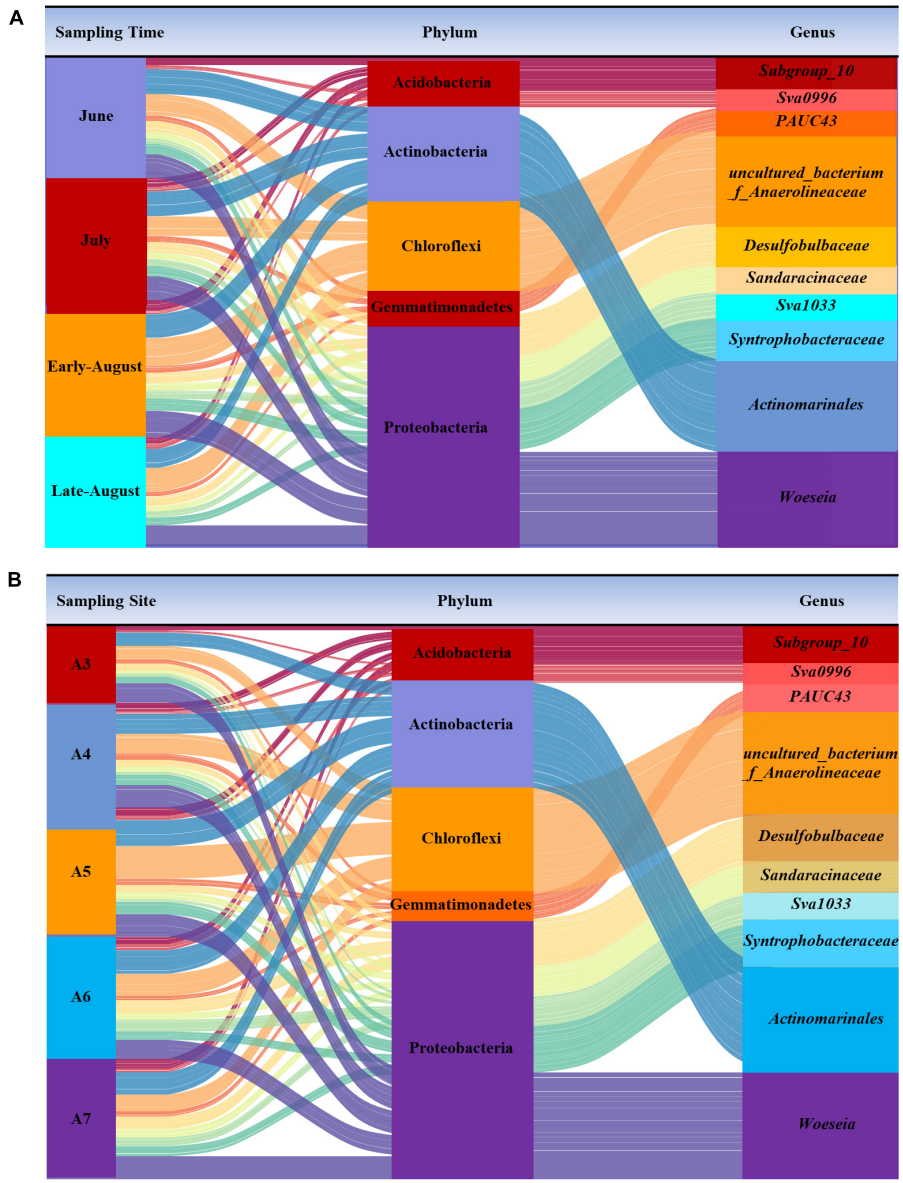

FIGURE 2 | The community composition of dominant bacteria at phylum and genus level from each sampling time **(A)** and site **(B)**.

amino acid metabolism (9.63%), membrane transport (9.40%), energy metabolism (9.11%), replication and repair (8.78%), translation (6.09%), metabolism of cofactors and vitamins (5.37%), and nucleotide metabolism (4.23%). The results showed that the relative abundance of bacteria in the carbohydrate metabolism and membrane transport was higher in the nearshore station (DO sufficient area). The abundance of bacteria in relatively offshore sites (DO depletion area) was high in other functional pathways that account for a relatively large proportion.

To gain more insight into nitrogen metabolism, the functional genes that involved in nitrogen metabolism were analyzed further and 31 KOs relating to nitrogen metabolism with the corresponding gene copy numbers in the sample were selected (**Figure 4B**). Results showed that a majority of the genes were significantly differentiated among the sites ($p < 0.05$) (**Supplementary Table 2**). KO predictions K00366 (*nirA*), K00367 (*narB*), and K02575 (*narK*), which were associated with denitrification pathway, were highly abundant in oxygen-depleted sites for each month. Surprisingly, other denitrification related genes were abundant in nearshore sites, including K00371 (*narH*), K00370 (*narG*), K00374 (*narI*), K00363 (*nirD*), K00362 (*nirB*), where the content of DO was not depleted, but the dominance was weak. Additionally, during the transition period between non-hypoxia and hypoxia (sample from July), the expression of functional genes related to denitrification decreased significantly in sites A3 and

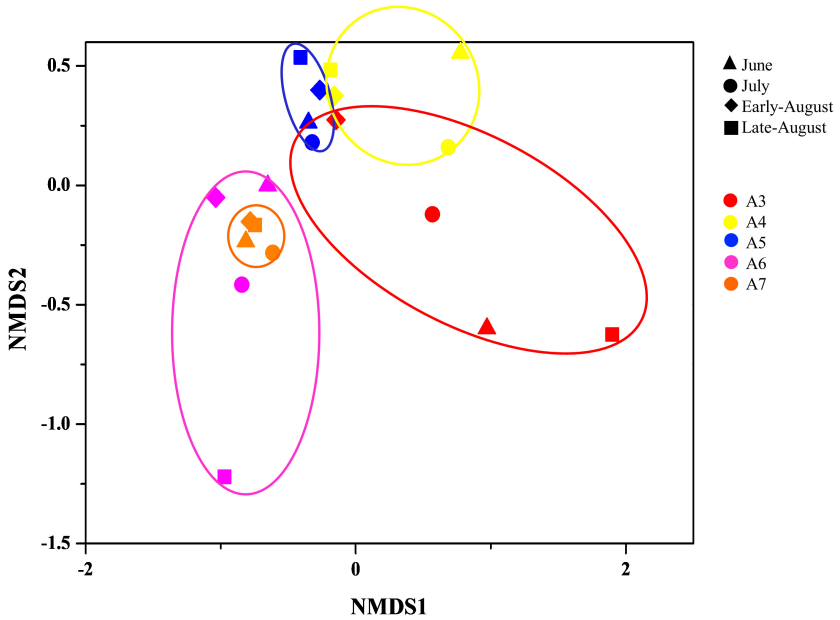

FIGURE 3 | Non-metric multidimensional scaling (NMDS) plot depicting phylum-level bacteria composition of each sample from different sampling time and site. (Axis define 2D space that allows the best spatial representation of sample distance, based on binary-jaccard distance with stress = 0.154. The points in different color represent sampling sites, different symbol represent sampling time, and the distance between points represents the degree of difference).

A4 ($p < 0.05$) (**Supplementary Table 2**), which were only slightly recovered in August. The KOs responsible for nitrogen fixation were found to be abundant in offshore sites and August samples (DO-depleted areas) for the following genes: K01915 (*glnA*), K04751 (*glnB*), and K04752 (*glnK*), while differences in expression of functional genes were not significant in these samples.

TABLE 1 | Alpha diversity index of 16S rRNA.

Sample ID	Shannon	Simpson	ACE	Chao1
A3611	0.98	7.46	554.39	557.22
A4611	0.99	7.67	554.12	574.50
A5611	0.98	7.14	590.18	599.21
A6611	0.98	7.17	584.99	612.79
A7611	0.99	7.30	591.21	602.00
A3719	0.99	7.70	553.64	563.46
A4719	0.99	7.82	564.73	572.25
A5719	0.98	7.21	585.98	601.12
A6719	0.98	7.15	604.10	606.90
A7719	0.99	7.37	586.25	586.00
A3808	0.98	7.29	586.75	589.68
A4808	0.98	7.32	565.93	584.00
A5808	0.98	7.15	563.31	590.50
A6808	0.98	6.95	570.63	593.00
A7808	0.99	7.30	575.53	587.52
A3826	0.97	6.34	448.81	468.00
A4826	0.98	7.42	576.34	597.75
A5826	0.97	6.98	581.70	603.12
A6826	0.98	7.25	553.67	584.89
A7826	0.99	7.32	559.15	555.89
	p	*p*	*p*	*p*
Sampling Time	0.10	0.09	0.16	0.28
Site	0.11	0.07	0.46	0.42

Environmental Drivers on Community Compositions of Bacteria

RDA (redundancy analysis) was performed to find out the relationship between the environmental parameters and bacterial structure (**Figure 5**). Identified phylum along with 8 environmental variables (Depth, Temperature, salinity, pH, NO_3^-, NO_2^-, NH_4^+, DO) were analyzed using CANOCO. The length of an environmental parameter arrow in the sorting diagram indicated the strength of the relationship of that variable with community composition. For the first two RDA dimensions, 53.57 and 72.50% of the environmental variables were explained for the total variance, and the results showing that depth ($p < 0.01$), DO and NO_2^- ($p < 0.05$) were the key impact factors shaping the community composition encoded by 16S rRNA gene. NO_2^- and temperature were positively correlated with the samples in site A7, indicating the microbial communities from this site were significantly influenced by these two parameters. Depth and NO_3^- were positively correlated with samples from A5 and A6, and DO mainly influenced samples from A3 and A4. Further, a triplot revealed that Chloroflexi, Acidobacteria were positively correlated with NO_3^- and depth. The most abundant phylum, Proteobacteria was highly influenced by NO_2^- and temperature. In general, the concentration of nitrogen was key to the bacterial communities in the studied area.

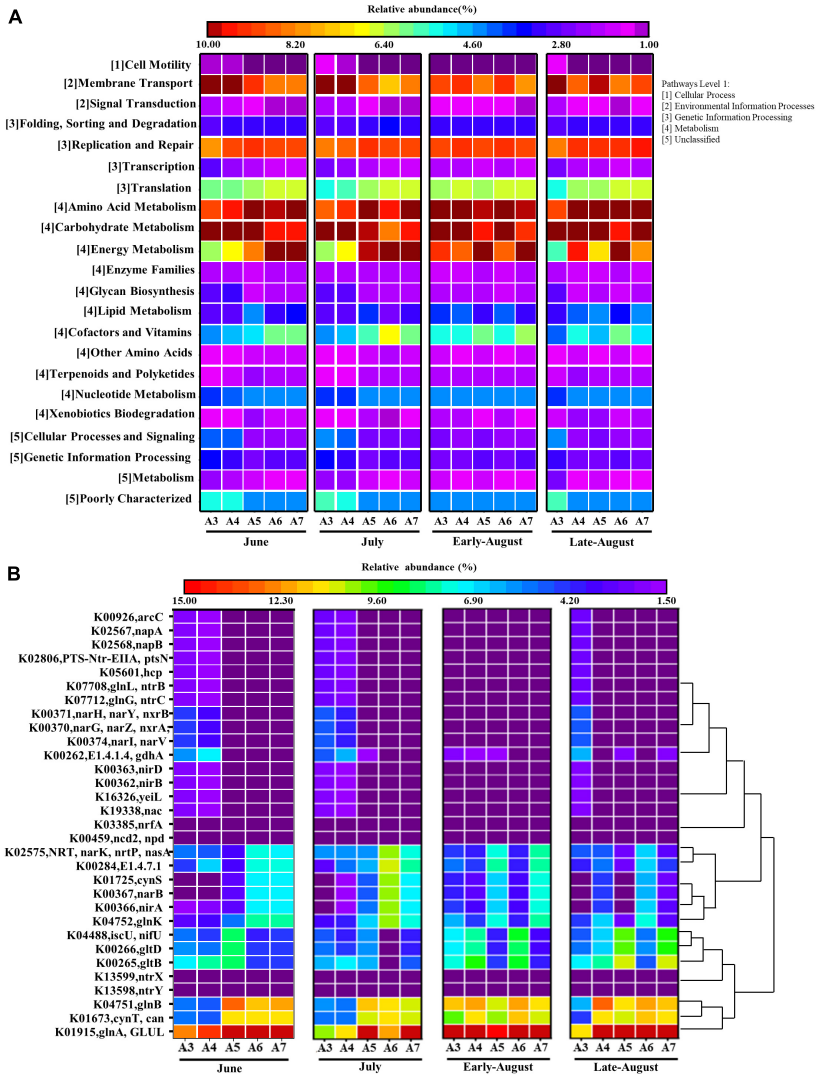

FIGURE 4 | Heatmap profiles showing the functional categories (KEGG level 2) of bacteria communities predicted by PICRUSt analysis **(A)** and nitrogen metabolism-related KO based on predicted gene copy **(B)** in each sampling time and site. (Rows represent the 22 KEGG orthology (KO) functions, columns represent the twenty samples, and the color intensity in the heatmap represents the relative abundance (%) of the functional genes. Pathways are displayed on the *y* axis, the number (1–5) in front of pathway names correspond to the number (1–5) of Pathways Level 1 shown on the right).

These results suggested that the distribution of bacteria was affected by multiple environmental factors rather than a single parameter.

DISCUSSION

Switch of Bacteria Community in Response to Oxygen Depletion

The ocean OMZs were found extending globally, typical OMZ had been reported from the Indian Ocean (Arabian Sea, the Bay of Bengal), the Pacific Ocean and the Atlantic (Namibian upwelling) (Stramma et al., 2008; Wright et al., 2012; Schmidtko et al., 2017). Under the increasing pressure of anthropogenic activity and climate change, oxygen depletion zone began to occur in central Bohai Sea (Zhai et al., 2012, 2020; Wei et al., 2019), with a regular occurrence every August ranging from 1.07 to 3.60 mg/L (bottom layer water) in the past 10 years. In our monthly investigation from June to August covering marginal and central Bohai Sea in 2018, although the disturbance by typhoon Yagi (landed on August 11 and continued until August 16, 2018) braked the layers and vertical mixing increased the DO content of the reported oxygen-depleted area, the gradually depletion of DO was also observed from July to August, and the lowest value was 4.2 mg/L in the reported hypoxic sites.

With key roles in metabolism played by marine microbes, dissolved oxygen had been confirmed to be an important

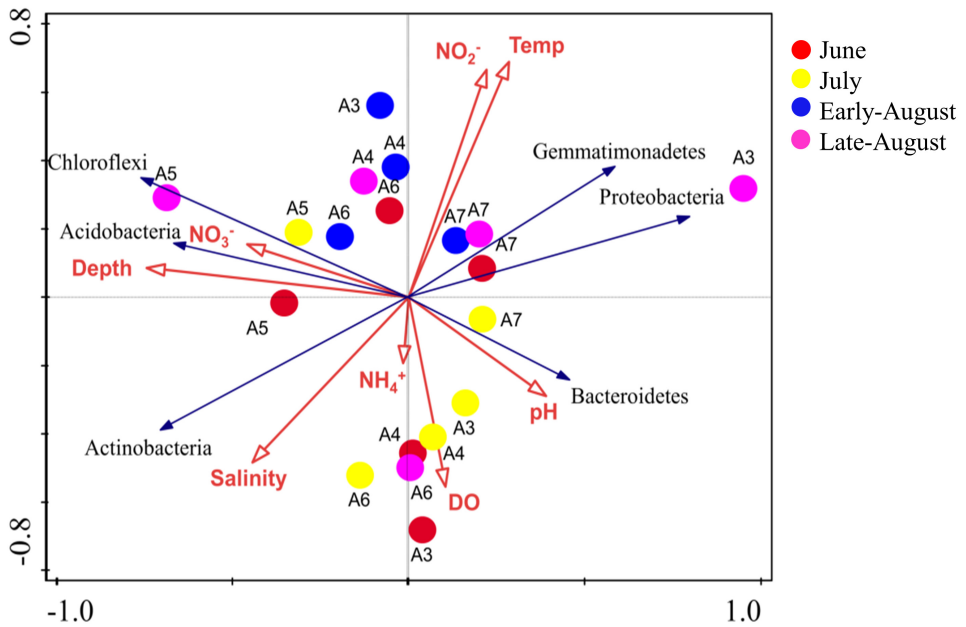

FIGURE 5 | Redundancy analysis (RDA) shows the relationship between environmental variables and the bacteria communities.

impacting factor and further influence the microbial biogeochemical cycling in marine sediment (Durbin and Teske, 2012; Spietz et al., 2015; Lipsewers et al., 2017). The instant variations of bacteria composition in Bohai Sea sediment during the depletion of oxygen were revealed by our monthly investigations. Distinct switch of dominant groups, such as the continuous change of dominant groups from Acidimicrobiia in June, *Woeseiaceae* in July and Anaerolineae in August (**Figure 2A**), revealed the specific response of bacteria to oxygen depletion. Anaerolineae could thrive in anaerobic, organic carbon-enriched environments, and in turn, eutrophic and anoxic conditions in the marine sediment favored the proliferation of this group of bacteria (Moncada et al., 2019). Anaerolineae had been reported in the middle and deeper layers of the hypoxic coral reef sand (Red Sea), further indicating their preference to the oxygen depletion environment (Schöttner et al., 2011; Andreote et al., 2012), which was also in accordance with our study by showing dominance only in oxygen-depleted August samples. Switch of bacteria under depletion of oxygen was also reflected by the occurrence of the anaerobic species, including *Rikenella* (Abe et al., 2012), *Lactobacillus* (Marcial-Coba et al., 2018), and *Mucispirillum* (Herp et al., 2019). Although they were rare species, their instant response to oxygen depletion in our study were evidences for their potential ecological role in Bohai Sea. Furthermore, switch of bacteria also included some strictly aerobic species, such as *Amphiplicatus*, which was also a thermophilic bacterium (Zhen-Li et al., 2014). It could be suspected that the high temperature rather than DO facilitated their occurrence in August in inshore sites. Additionally, combined with the results from functional prediction, genes involved in denitrification were abundant in DO sufficient sites. *Ellin6067* had been reported as a group of significant ammonia oxidizing bacteria (Podlesnaya et al., 2020) and could be inhibited by activity when DO content was low (Huang et al., 2018). The only occurrence of both *Amphiplicatus* and *Ellin6067* in August in our study indicated that oxygen might not be a limiting factor but could be an indicator for their distribution in marine environment. Moreover, the distribution and diversity of bacteria was also influenced as a function of sediment annum or impacted by seasonality (Laverock et al., 2014; Ebah et al., 2016; Huang et al., 2018). Although in general the abundance and diversity of bacteria in June and July were higher than in August, the difference was not significant ($p > 0.05$), possibly because the short interval for our sampling time limited the transport and sedimentation of sediment since it was an inter-annual or seasonal event.

Diversity and Distribution of Bacteria in Bohai Sea Sediment

Bacteria in marine sediments had been widely studied, Proteobacteria, Actinobacteria, Chloroflexi, Acidobacteria and Bacteroidetes were revealed to be the main component in marine environment (Kerfahi et al., 2014; Walsh et al., 2016; Hoshino et al., 2020; Wang et al., 2020; Peng et al., 2021). But generally, and also obviously, the dominant groups varied due to the influence of geographical locations and environmental factors (Antunes et al., 2020). Compared to changes in relative abundance on a sampling time scale, Proteobacteria, Actinobacteria and Chloroflexi were evenly distributed among the studied sites, however, Acidobacteria and Bacteroidetes varied along the transect (**Figure 2B**). Acidobacteria, that were dominated in nearshore sites (A3 and A4), had been revealed to be involved in nitrate reduction process (Kielak et al., 2016).

This may also be the reason for the high abundance of genes that mediate the denitrification process in nearshore sites (**Figure 4B**). Bacteroidetes had been reported to be preponderant in nutrient-rich waters (Gomes et al., 2019), which also in support of our results that the abundance of Bacteroidetes was higher in the nutrient-rich sites regardless of the sampling time. Most of the sequences assigned to phylum Actinobacteria belonged to class Acidimicrobiia, and two most representative OTUs were classified as uncultured Actinobacterium (previously classified as OM1 clade), an eosinophilic family (Goodfellow et al., 2012; Chen et al., 2016). This group of bacteria was usually abundant in high salinity and pH sediments, and related to the capability of metabolizing hydrocarbon compounds (Queiroz et al., 2020). Their great abundance in the studied sites might contribute to the degradation of severe oil pollution in the coast of Bohai Sea (Liu et al., 2016; Yu et al., 2018). *Woeseia*, which belonging to Proteobacteria and most abundant in the inshore sediments of the Bohai Sea, had the capability for both aerobic and anaerobic growth (Du et al., 2016). For oxygen-independent respiration, *Woeseia* may take part in a truncated denitrification pathway which including periplasmic dissimilatory nitrite and the membrane-bound nitric oxide reductase by employing NirS and NorB gene, respectively (Mußmann et al., 2017). This ubiquitous and abundant group might substantially contribute to nitrous oxide emissions from coastal sediments due to its truncated denitrification which revealed by our nitrogen gene function prediction results that the inshore sediments had more functional genes which playing role in denitrification. In addition, it proved that the role of coastal sediments in nitrogen loss made more contribution than assumed, and may account for a large part of the global oceanic powerful emission of greenhouse gas nitrous oxide.

Aiming to figure out the origin or the phylogenetic distance of bacteria in Bohai Sea sediment, with special focus on the oxygen depletion sites, the phylogenetic analysis was further performed with dominant sequences (top 18 OTUs) and the reference sequences from GenBank by constructing Neighbor-joining tree. Results revealed that bacteria from Bohai Sea oxygen depletion

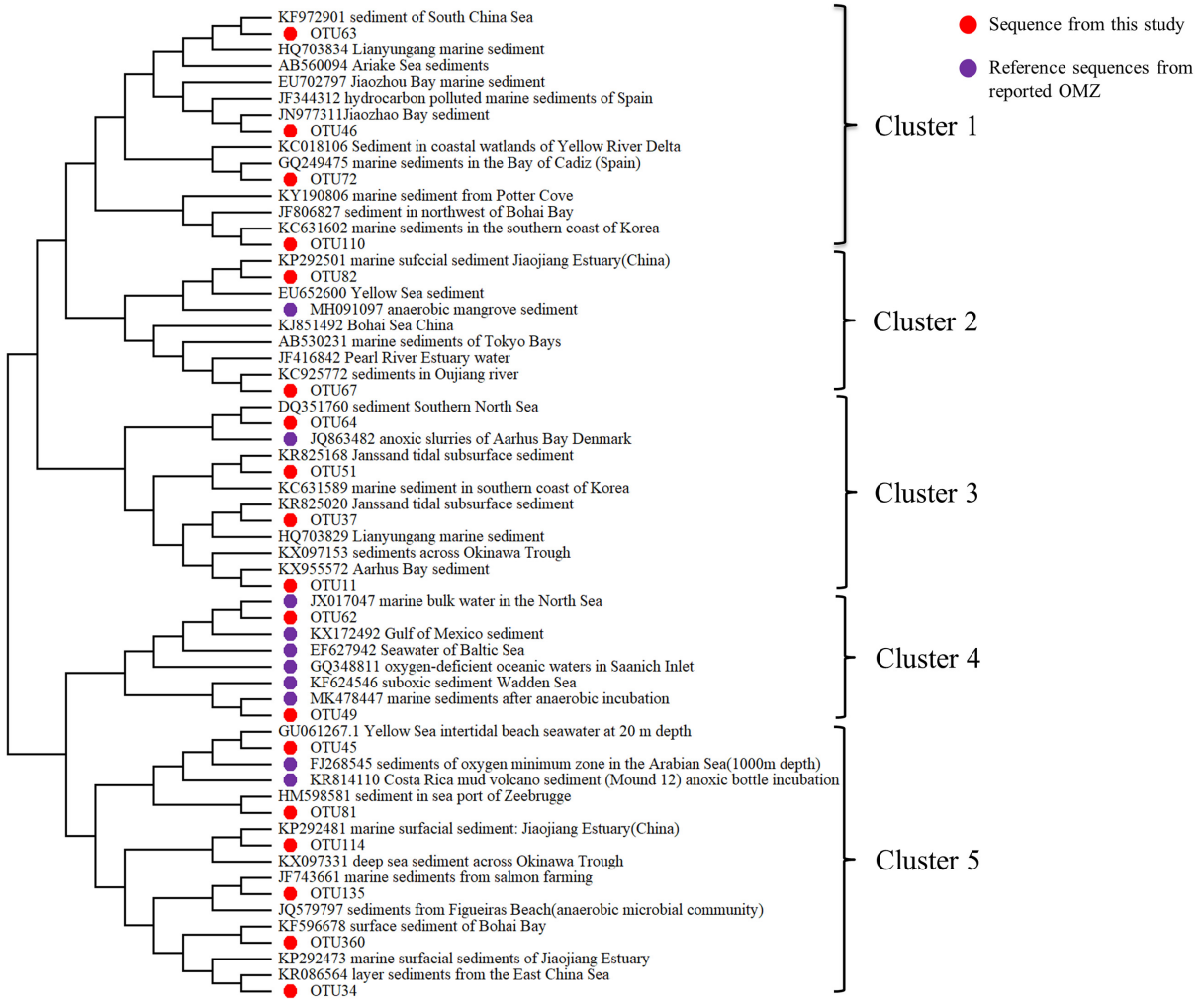

FIGURE 6 | Neighbor-joining phylogenetic tree of the dominant OTUs (Top 18) in the sediment samples of Bohai Sea (Bootstrap values were 1,000 replicates).

sites had a diverse phylogenetic relationship with bacteria in typical OMZs, such as the Yangtze River estuary, the Gulf of Mexico, the Arabian Sea, the west coast of the Indian Ocean, the North Indian Ocean, and the Bay of Bengal (**Figure 6**). Moreover, novel hypoxic-adapted species in the sediments of Bohai Sea were also predicted, such as OTU64, OTU82, which were grouped with reported OMZ species but formed a unique clade in the phylogenetic tree. Anaerolineae and SAR11, represented by OTU45, OTU62, respectively, clustered together with most of the sequences from OMZs. As mentioned above, Anaerolineae was strictly anaerobic, which was a typical and specific bacterium in the Bohai Sea oxygen depletion area. While for SAR11 members, which were group of aerobic Alphaproteobacteria, had the ability to assimilate nitrogen-rich organic compounds by allocating surrounding resources when experiences nitrogen stress (Smith et al., 2013). Therefore, this group of bacteria could function as a specific object for research on nitrogen cycle in hypoxic zone. Moreover, due to the close geographic distance, a high degree of kinship of Bohai Sea sediment with the sediment sequences in Jiaozhou Bay, the Yellow Sea and the South China Sea were revealed from the phylogenetic tree.

Environmental Factors Shaping the Community Composition

As early as decades ago, a number of studies supported the view that different depth would be associated with changes in sediment bacterial community composition (Urakawa et al., 2000; Haglund et al., 2003). At present, Huang et al. (2018) mentioned that nitrification bacteria were highly abundant in shallow sediments, which may explain our result that high abundant functional gene related to nitrification were observed in offshore sites where sampling depth was shallower. Additionally, NO_2^- played a key role in shaping bacterial community. As an important substrate in the nitrogen cycle, nitrite participates in the nxr-mediated NO_2^- to NO_3^- nitrification process and denitrification pathway mediated by nir which reducing NO_2^- to NO (Zumft, 1997). Nitrite contents and sampling depth may make influence on nitrogen transforming bacteria, especially the nitrifier and denitrifier communities. Furthermore, a recent study found that the nitrogen transforming microbial communities in the hypoxia area and non-hypoxic area of the Yangtze River Estuary are different (Wu et al., 2019), which was highly consistent with our study, that denitrifiers prefer non-hypoxia area and genes involved in nitrification dominant in oxygen depletion area. Dissolved oxygen content substantially influenced bacterial structure and potential function with the discovery and expansion of the global ocean hypoxic zone.

CONCLUSION

During the occurrence of oxygen depletion from June to August, distinct community switch of bacteria was observed in the sediment of Bohai Sea. Members of class Acidimicrobiia and genus *Woeseia* affiliating with Gammaproteobacteria dominated before oxygen depletion, while Anaerolineae affiliating with Chloroflexi was absolutely dominant in August when DO $<$ 4.2 mg/L. Occurrence of anaerobic rare species after oxygen depletion indicated their potential roles in Bohai Sea sediment. Spatially, Proteobacteria distributed evenly from inshore to offshore regardless of sampling time, however, relative abundance of Actinobacteria and Bacteroidetes varied among inshore sites but tended to be stable in offshore sites. Firmicutes was only abundant in nearshore and oxygen sufficient samples. KEGG pathways prediction by bacterial community showed significant variation before and after DO depletion ($p < 0.05$). the Predicted functional genes involved in nitrogen metabolism revealed abundant denitrification pathways in both oxygen rich (inshore) and depleted samples (offshore), while nitrogen fixation pathway was only abundant in oxygen-depleted sites. Local environmental factors including depth, NO_2^- together with DO play important roles in shaping bacterial community ($p < 0.05$). Variations in diversity and distribution of bacteria communities over oxygen depletion in the sediment of Bohai Sea provided detailed insights into bacterial response to world expending OMZs.

DATA AVAILABILITY STATEMENT

The datasets presented in this study can be found in online repositories. The names of the repository/repositories and accession number(s) can be found below: https://www.ncbi.nlm.nih.gov/sra/PRJNA789710, SRR17253936-SRR17253955.

AUTHOR CONTRIBUTIONS

JW: conceptualization. XG: experimental operation. XG and YL: writing—original draft preparation. JW and GS: writing—review, editing, and funding acquisition. GS and LZ: field sampling. All authors read and approved the final manuscript.

FUNDING

This study was supported by the Natural Science Foundation of Tianjin City (5KK19004), the National Natural Science Foundation of China (52070143, 42076033, and 41506182), and the Doctoral Foundation of Tianjin Normal University (043135202-XB1714).

ACKNOWLEDGMENTS

We thank the crews for their help and cooperation during the cruises.

SUPPLEMENTARY MATERIAL

The Supplementary Material for this article can be found online at: https://www.frontiersin.org/articles/10.3389/fmars.2022.833513/full#supplementary-material

REFERENCES

Abe, K., Ueki, A., Ohtaki, Y., Kaku, N., Watanabe, K., and Ueki, K. (2012). *Anaerocella delicata* gen. nov., sp. nov., a strictly anaerobic bacterium in the phylum Bacteroidetes isolated from a methanogenic reactor of cattle farms. *J. Gen. Appl. Microbiol.* 58, 405–412. doi: 10.2323/jgam.58.405

Anderson, D. M., Glibert, P. M., and Burkholder, J. M. (2002). Harmful algal blooms and eutrophication: nutrient sources, composition, and consequences. *Estuaries* 25, 704–726. doi: 10.1007/BF02804901

Andreote, F. D., Jiménez, D. J., Chaves, D., Dias, A. C. F., Luvizotto, D. M., Dini-Andreote, F., et al. (2012). The microbiome of Brazilian mangrove sediments as revealed by metagenomics. *PLoS One* 7:e38600. doi: 10.1371/journal.pone.0038600

Antunes, J. T., Sousa, A. G., Azevedo, J., Rego, A., Leão, P. N., and Vasconcelos, V. (2020). Distinct temporal succession of bacterial communities in early marine biofilms in a portuguese atlantic port. *Front. Microbiol.* 11:1938. doi: 10.3389/fmicb.2020.01938

Beman, J. M., and Carolan, M. T. (2013). Deoxygenation alters bacterial diversity and community composition in the ocean's largest oxygen minimum zone. *Nat. Commun.* 4:2705. doi: 10.1038/ncomms3705

Bertagnolli, A. D., and Stewart, F. J. (2018). Microbial niches in marine oxygen minimum zones. *Nat. Rev. Microbiol.* 16, 723–729. doi: 10.1038/s41579-018-0087-z

Breitburg, D., Levin, L. A., Oschlies, A., Grégoire, M., Chavez, F. P., Conley, D. J., et al. (2018). Declining oxygen in the global ocean and coastal waters. *Science* 359:6371. doi: 10.1126/science.aam7240

Bricker, S. B., Longstaff, B., Dennison, W., Jones, A., Boicourt, K., Wicks, C., et al. (2008). Effects of nutrient enrichment in the nation's estuaries: a decade of change. *Harmful Algae* 8, 21–32. doi: 10.1016/j.hal.2008.08.028

Canfield, D. E., Glazer, A. N., and Falkowski, P. G. (2010). The evolution and future of Earth's nitrogen cycle. *Science* 330, 192–196. doi: 10.1126/science.1186120

Chen, P., Zhang, L., Guo, X., Dai, X., Liu, L., Xi, L., et al. (2016). Diversity, biogeography, and biodegradation potential of actinobacteria in the deep-sea sediments along the southwest Indian ridge. *Front. Microbiol.* 7:1340. doi: 10.3389/fmicb.2016.01340

Cui, S., Shi, Y., Groffman, P. M., Schlesinger, W. H., and Zhu, Y. G. (2013). Centennial-scale analysis of the creation and fate of reactive nitrogen in China (1910–2010). *Proc. Natl. Acad. Sci. U S A.* 110, 2052–2057. doi: 10.1073/pnas.1221638110

Dai, T., Zhang, Y., Tang, Y., Bai, Y., Tao, Y., Huang, B., et al. (2016). Identifying the key taxonomic categories that characterize microbial community diversity using full-scale classification: a case study of microbial communities in the sediments of Hangzhou Bay. *FEMS Microbiol. Ecol.* 92:fiw150. doi: 10.1093/femsec/fiw150

Diaz, R. J., and Rosenberg, R. (2008). Spreading dead zones and consequences for marine ecosystems. *Science* 321, 926–929. doi: 10.1126/science.1156401

Dou, Y., Li, J., Zhao, J., Hu, B., and Yang, S. (2013). Distribution, enrichment and source of heavy metals in surface sediments of the eastern Beibu Bay, South China Sea. *Mar. Pollut. Bull.* 67, 137–145. doi: 10.1016/j.marpolbul.2012.11.022

Du, Z. J., Wang, Z. J., Zhao, J. X., and Chen, G. J. (2016). *Woeseia oceani* gen. nov., sp. nov., a chemoheterotrophic member of the order Chromatiales, and proposal of *Woeseiaceae fam*. nov. *Int. J. Syst. Evol. Microbiol.* 66, 107–112. doi: 10.1099/ijsem.0.000683

Duan, X., and Li, Y. (2017). Distributions and sources of heavy metals in sediments of the Bohai Sea, China: a review. *Environ. Sci. Pollut. Res.* 24, 24753–24764. doi: 10.1007/s11356-017-0330-6

Durbin, A. M., and Teske, A. (2012). Archaea in organic-lean and organic-rich marine subsurface sediments: an environmental gradient reflected in distinct phylogenetic lineages. *Front. Microbiol.* 3:168. doi: 10.3389/fmicb.2012.00168

Ebah, E., Tersagh, I., and Okpokwasili, G. C. (2016). Studies on seasonal variation and effect of heavy metal pollution on microbial load of marine sediment. *Am. J. Mar. Sci.* 4, 4–10.

Edgar, R. C. (2010). Search and clustering orders of magnitude faster than BLAST. *Bioinformatics* 26, 2460–2461. doi: 10.1093/bioinformatics/btq461

Escales, A., Hale, L., Voordeckers, J., Yang, Y. F., Firestone, M., Alvarez-Cohen, L., et al. (2019). Microbial functional diversity: from concepts to applications. *Ecol. Evol.* 9, 12000–12016. doi: 10.1002/ece3.5670

Fuchsman, C. A., Palevsky, H. I., Widner, B., Duffy, M., Carlson, M. C., Neibauer, J. A., et al. (2019). Cyanobacteria and cyanophage contributions to carbon and nitrogen cycling in an oligotrophic oxygen-deficient zone. *ISME J.* 13, 2714–2726. doi: 10.1038/s41396-019-0452-6

Füssel, J., Lam, P., Lavik, G., Jensen, M. M., Holtappels, M., Günter, M., et al. (2012). Nitrite oxidation in the Namibian oxygen minimum zone. *ISME J.* 6, 1200–1209. doi: 10.1038/ismej.2011.178

Gomes, J., Khandeparker, R., Meena, R. M., and Ramaiah, N. (2019). Bacterial community composition markedly altered by coastal hypoxia. *Indian J. Microbiol.* 59, 200–208. doi: 10.1007/s12088-019-00790-5

Goodfellow, M., Kämpfer, P., Busse, H. J., Trujillo, M. E., Suzuki, K. I., Ludwig, W., et al. (2012). *Bergey's Manual® of Systematic Bacteriology: Volume Five the Actinobacteria, Part A*. New York, NY: Springer. doi: 10.1007/978-0-387-68233-4

Haglund, A. L., Lantz, P., Törnblom, E., and Tranvik, L. (2003). Depth distribution of active bacteria and bacterial activity in lake sediment. *FEMS Microbiol. Ecol.* 46, 31–38. doi: 10.1016/S0168-6496(03)00190-9

Hao, W., Tian, T., and Feng, Z. (2002). Numerical study on the water exchange of the Bohai Sea: simulation of the half-life time by dispersion model. *J. Ocean Univ. China* 32, 519–525.

Herp, S., Brugiroux, S., Garzetti, D., Ring, D., Jochum, L. M., Beutler, M., et al. (2019). Mucispirillum schaedleri antagonizes *salmonella* virulence to protect mice against colitis. *Cell Host Microbe* 25, 681–694. doi: 10.1016/j.chom.2019.03.004

Hoshino, T., Doi, H., Uramoto, G. I., Wörmer, L., Adhikari, R. R., Xiao, N., et al. (2020). Global diversity of microbial communities in marine sediment. *Proc. Natl. Acad. Sci. U S A.* 117, 27587–27597. doi: 10.1073/pnas.1919139117

Huang, S., Chen, C., and Jaffé, P. R. (2018). Seasonal distribution of nitrifiers and denitrifiers in urban river sediments affected by agricultural activities. *Sci. Total Environ.* 642, 1282–1291. doi: 10.1016/j.scitotenv.2018.06.116

Kerfahi, D., Hall-Spencer, J. M., Tripathi, B. M., Milazzo, M., Lee, J., and Adams, J. M. (2014). Shallow water marine sediment bacterial community shifts along a natural CO2 gradient in the Mediterranean Sea off Vulcano. Italy. *Microb. Ecol.* 67, 819–828. doi: 10.1007/s00248-014-0368-7

Kielak, A. M., Barreto, C. C., Kowalchuk, G. A., van Veen, J. A., and Kuramae, E. E. (2016). The ecology of Acidobacteria: moving beyond genes and genomes. *Front. Microbiol.* 7:744. doi: 10.3389/fmicb.2016.00744

Koeve, W., and Kähler, P. (2010). Heterotrophic denitrification vs. autotrophic anammox–quantifying collateral effects on the oceanic carbon cycle. *Biogeosciences* 7, 2327–2337. doi: 10.5194/bg-7-2327-2010

Köster, M., and Meyer-Reil, L. A. (2001). Characterization of carbon and microbial biomass pools in shallow water coastal sediments of the southern Baltic Sea (Nordrügensche Bodden). *Mar. Ecol. Prog. Ser.* 214, 25–41. doi: 10.3354/meps214025

Lam, P., Lavik, G., Jensen, M. M., van de Vossenberg, J., Schmid, M., Woebken, D., et al. (2009). Revising the nitrogen cycle in the Peruvian oxygen minimum zone. *Proc. Natl. Acad. Sci. U S A.* 106, 4752–4757. doi: 10.1073/pnas.0812444106

Langille, M. G. I., Zaneveld, J., Caporaso, J. G., Knights, D., Reyes, J. A., et al. (2013). Predictive functional profiling of microbial communities using 16S rRNA marker gene sequences. *Nat. Biotechnol.* 31, 814–821. doi: 10.1038/nbt.2676

Laverock, B., Tait, K., Gilbert, J. A., Osborn, A. M., and Widdicombe, S. (2014). Impacts of bioturbation on temporal variation in bacterial and archaeal nitrogen-cycling gene abundance in coastal sediments. *Environ. Microbiol. Rep.* 6, 113–121. doi: 10.1111/1758-2229.12115

Li, J., Li, N., Li, F., Zou, T., Yu, S., Wang, Y., et al. (2014). Spatial diversity of bacterioplankton communities in surface water of northern South China Sea. *PLoS One* 9:e113014. doi: 10.1371/journal.pone.0113014

Li, Y., Wu, C., Zhou, M., Wang, E. T., Zhang, Z., Liu, W., et al. (2017). Diversity of cultivable protease-producing bacteria in Laizhou bay sediments, Bohai Sea, China. *Front. Microbiol.* 8:405. doi: 10.3389/fmicb.2017.00405

Lipsewers, Y. A., Vasquez-Cardenas, D., Seitaj, D., Schauer, R., Hidalgo-Martinez, S., Sinninghe Damsté, J. S., et al. (2017). Impact of seasonal hypoxia on activity and community structure of chemolithoautotrophic bacteria in a coastal sediment. *Appl. Environ. Microbiol.* 83:e03517-16. doi: 10.1128/AEM.03517-16

Liu, X., Guo, M., Wang, Y., Yu, X., Guo, J., Tang, C., et al. (2016). Assessing pollution-related effects of oil spills from ships in the Chinese Bohai Sea. *Mar. Pollut. Bull.* 110, 194–202. doi: 10.1016/j.marpolbul.2016.06.062

Lofrano, G., Libralato, G., Minetto, D., De Gisi, S., Todaro, F., Conte, B., et al. (2017). In situ remediation of contaminated marinesediment: an overview. *Environ. Sci. Pollut. Res.* 24, 5189–5206. doi: 10.1007/s11356-016-8281-x

Luo, C., Lin, L., Shi, J., Liu, Z., Cai, Z., Guo, X., et al. (2021). Seasonal variations in the water residence time in the Bohai Sea using 3D hydrodynamic model study and the adjoint method. *Ocean Dyn.* 71, 157–173. doi: 10.1007/s10236-020-01438-5

Lv, X., Ma, B., Yu, J., Chang, S. X., Xu, J., Li, Y., et al. (2016). Bacterial community structure and function shift along a successional series of tidal flats in the Yellow River Delta. *Sci. Rep.* 6:36550. doi: 10.1038/srep36550

Mahaffey, C., Palmer, M., Greenwood, N., and Sharples, J. (2020). Impacts of climate change on dissolved oxygen concentration relevant to the coastal and marine environment around the UK. *MCCIP Sci. Rev.* 2002, 31–53.

Marcial-Coba, M. S., Cieplak, T., Cahú, T. B., Blennow, A., Knøchel, S., and Nielsen, D. S. (2018). Viability of microencapsulated Akkermansia muciniphila and Lactobacillus plantarum during freeze-drying, storage and in vitro simulated upper gastrointestinal tract passage. *Food Funct.* 9, 5868–5879. doi: 10.1039/C8FO01331D

Moncada, C., Hassenrück, C., Gärdes, A., and Conaco, C. (2019). Microbial community composition of sediments influenced by intensive mariculture activity. *FEMS Microbiol. Ecol.* 95:fiz006. doi: 10.1093/femsec/fiz006

Mu, D., Yuan, D., Feng, H., Xing, F., Teo, F. Y., and Li, S. (2017). Nutrient fluxes across sediment-water interface in Bohai Bay Coastal Zone. China. *Mar. Pollut. Bull.* 114, 705–714. doi: 10.1016/j.marpolbul.2016.10.056

Mußmann, M., Pjevac, P., Krüger, K., and Dyksma, S. (2017). Genomic repertoire of the Woeseiaceae/JTB255, cosmopolitan and abundant core members of microbial communities in marine sediments. *ISME J.* 11, 1276–1281. doi: 10.1038/ismej.2016.185

Padilla, C. C., Bristow, L. A., Sarode, N., Garcia-Robledo, E., Ramírez, E. G., Benson, C. R., et al. (2016). NC10 bacteria in marine oxygen minimum zones. *ISME J.* 10, 2067–2071. doi: 10.1038/ismej.2015.262

Paulmier, A., and Ruiz-Pino, D. (2009). Oxygen minimum zones (OMZs) in the modern ocean. *Prog. Oceanogr.* 80, 113–128. doi: 10.1016/j.pocean.2008.08.001

Peng, X., Su, H., Cai, R., and Han, Y. (2021). Wide-bound salt tolerance of the inocula from marine sediment and their specific microbial community. *Environ. Res.* 197:111119. doi: 10.1016/j.envres.2021.111119

Petro, C., Starnawski, P., Schramm, A., and Kjeldsen, K. U. (2017). Microbial community assembly in marine sediments. *Aquat. Microb. Ecol.* 79, 177–195. doi: 10.3354/ame01826

Podlesnaya, G. V., Krasnopeev, A. Y., Potapov, S. A., Tikhonova, I. V., Shtykova, Y. R., Suslova, M. Y., et al. (2020). Diversity of nitrifying bacteria in microbial communities from water and epilithic biofilms of the Lake Baikal littoral zone. *Limnol. Freshw. Biol.* 3, 1008–1010. doi: 10.31951/2658-3518-2020-A-4-1008

Queiroz, L. L., Bendia, A. G., Duarte, R. T. D., das Graças, D. A., da Silva, A. L. D. C., Nakayama, C. R., et al. (2020). Bacterial diversity in deep-sea sediments under influence of asphalt seep at the São Paulo Plateau. *Antonie Van Leeuwenhoek* 113, 707–717. doi: 10.1007/s10482-020-01384-8

Ruiz-Perez, C. A., Bertagnolli, A. D., Tsementzi, D., Woyke, T., Stewart, F. J., and Konstantinidis, K. T. (2021). Description of Candidatus Mesopelagibacter carboxydoxydans and Candidatus Anoxipelagibacter denitrificans: Nitrate-reducing SAR11 genera that dominate mesopelagic and anoxic marine zones. *Syst. Appl. Microbiol.* 44:126185. doi: 10.1016/j.syapm.2021.126185

Schmidtko, S., Stramma, L., and Visbeck, M. (2017). Decline in global oceanic oxygen content during the past five decades. *Nature* 542, 335–339. doi: 10.1038/nature21399

Schöttner, S., Pfitzner, B., Grünke, S., Rasheed, M., Wild, C., and Ramette, A. (2011). Drivers of bacterial diversity dynamics in permeable carbonate and silicate coral reef sands from the Red Sea. *Environ. Microbiol.* 13, 1815–1826. doi: 10.1111/j.1462-2920.2011.02494.x

Sen, K., Bai, M., Sen, B., and Wang, G. (2021). Disentangling the structure and function of mycoplankton communities in the context of marine environmental heterogeneity. *Sci. Total Environ.* 766:142635. doi: 10.1016/j.scitotenv.2020.142635

Smith, D. P., Thrash, J. C., Nicora, C. D., Lipton, M. S., Burnum-Johnson, K. E., Carini, P., et al. (2013). Proteomic and transcriptomic analyses of "Candidatus Pelagibacter ubique" describe the first PII-independent response to nitrogen limitation in a free-living Alphaproteobacterium. *mBio* 4:e00133-12. doi: 10.1128/mBio.00133-12

Spietz, R. L., Williams, C. M., Rocap, G., and Horner-Devine, M. C. (2015). A dissolved oxygen threshold for shifts in bacterial community structure in a seasonally hypoxic estuary. *PLoS One* 10:e0135731. doi: 10.1371/journal.pone.0135731

Stramma, L., Johnson, G. C., Sprintall, J., and Mohrholz, V. (2008). Expanding oxygen-minimum zones in the tropical oceans. *Science* 320, 655–658. doi: 10.1126/science.1153847

Stramma, L., Schmidtko, S., Bograd, S. J., Ono, T., Ross, T., Sasano, D., et al. (2020). Trends and decadal oscillations of oxygen and nutrients at 50 to 300 m depth in the equatorial and North Pacific. *Biogeosciences* 17, 813–831. doi: 10.5194/bg-17-813-2020

Su, Z., Dai, T., Tang, Y., Tao, Y., Huang, B., Mu, Q., et al. (2018). Sediment bacterial community structures and their predicted functions implied the impacts from natural processes and anthropogenic activities in coastal area. *Mar. Pollut. Bull.* 131, 481–495. doi: 10.1016/j.marpolbul.2018.04.052

Thiele, S., Basse, A., Becker, J. W., Lipski, A., Iversen, M. H., and Mollenhauer, G. (2019). Microbial communities in the nepheloid layers and hypoxic zones of the Canary current upwelling system. *MicrobiologyOpen* 8:e00705. doi: 10.1002/mbo3.705

Toole, D. R., Zhao, J., Martens-Habbena, W., and Strauss, S. L. (2021). Bacterial functional prediction tools detect but underestimate metabolic diversity compared to shotgun metagenomics in southwest Florida soils. *Appl. Soil Ecol.* 168:104129. doi: 10.1016/j.apsoil.2021.104129

Tsaban, T., Stupp, D., Sherill-Rofe, D., Bloch, I., Sharon, E., Schueler-Furman, O., et al. (2021). CladeOScope: functional interactions through the prism of clade-wise co-evolution. *NAR Genom Bioinform.* 3:lqab024. doi: 10.1093/nargab/lqab024

Tsementzi, D., Wu, J., Deutsch, S., Nath, S., Rodriguez-R, L. M., Burns, A. S., et al. (2016). SAR11 bacteria linked to ocean anoxia and nitrogen loss. *Nature* 536, 179–183. doi: 10.1038/nature19068

Urakawa, H., Yoshida, T., Nishimura, M., and Ohwada, K. (2000). Characterization of depth-related population variation in microbial communities of a coastal marine sediment using 16S rDNA-based approaches and quinone profiling. *Environ. Microbiol.* 2, 542–554. doi: 10.1046/j.1462-2920.2000.00137.x

Voss, M., Bange, H. W., Dippner, J. W., Middelburg, J. J., Montoya, J. P., and Ward, B. (2013). The marine nitrogen cycle: recent discoveries, uncertainties and the potential relevance of climate change. *Philos. T. R. Soc. B.* 368:20130121. doi: 10.1098/rstb.2013.0121

Walsh, E. A., Kirkpatrick, J. B., Rutherford, S. D., Smith, D. C., Sogin, M., and D'Hondt, S. (2016). Bacterial diversity and community composition from seasurface to subseafloor. *ISME J.* 10, 979–989. doi: 10.1038/ismej.2015.175

Wang, J., Kan, J., Qian, G., Chen, J., Xia, Z., Zhang, X., et al. (2019). Denitrification and anammox: understanding nitrogen loss from Yangtze Estuary to the east China sea (ECS). *Environ. Pollut.* 252, 1659–1670. doi: 10.1016/j.envpol.2019.06.025

Wang, L., Liu, L., Zheng, B., Zhu, Y., and Wang, X. (2013). Analysis of the bacterial community in the two typical intertidal sediments of Bohai Bay, China by pyrosequencing. *Mar. Pollut. Bull.* 72, 181–187. doi: 10.1016/j.marpolbul.2013.04.005

Wang, L., Zheng, B., Nan, B., and Hu, P. (2014). Diversity of bacterial community and detection of nirS-and nirK-encoding denitrifying bacteria in sandy intertidal sediments along Laizhou Bay of Bohai Sea. China. *Mar. Pollut. Bull.* 88, 215–223. doi: 10.1016/j.marpolbul.2014.09.002

Wang, M., Noor, S., Huan, R., Liu, C., Li, J., Shi, Q., et al. (2020). Comparison of the diversity of cultured and total bacterial communities in marine sediment using culture-dependent and sequencing methods. *Peer J.* 8:e10060. doi: 10.7717/peerj.10060

Ward, B. B., Devol, A. H., Rich, J. J., Chang, B. X., Bulow, S. E., Naik, H., et al. (2009). Denitrification as the dominant nitrogen loss process in the Arabian Sea. *Nature* 461, 78–81. doi: 10.1038/nature08276

Ward, C. S., Yung, C. M., Davis, K. M., Blinebry, S. K., Williams, T. C., Johnson, Z. I., et al. (2017). Annual community patterns are driven by seasonal switching between closely related marine bacteria. *ISME J.* 11, 1412–1422. doi: 10.1038/ismej.2017.4

Wei, Q., Wang, B., Yao, Q., Xue, L., Sun, J., Xin, M., et al. (2019). Spatiotemporal variations in the summer hypoxia in the Bohai Sea (China) and controlling mechanisms. *Mar. Pollut. Bull.* 138, 125–134. doi: 10.1016/j.marpolbul.2018.11.041

Wright, J. J., Konwar, K. M., and Hallam, S. J. (2012). Microbial ecology of expanding oxygen minimum zones. *Nat. Rev. Microbiol.* 10, 381–394. doi: 10.1038/nrmicro2778

Wu, D. M., Dai, Q. P., Liu, X. Z., Fan, Y. P., and Wang, J. X. (2019). Comparison of bacterial community structure and potential functions in hypoxic and non-hypoxic zones of the Changjiang Estuary. *PLoS One* 14:e0217431. doi: 10.1371/journal.pone.0217431

Xue, J., Shi, K., Chen, C., Bai, Y., Cui, Q., Li, N., et al. (2021). Evaluation of response of dynamics change in bioaugmentation process in diesel-polluted seawater via high-throughput sequencing: degradation characteristic, community structure, functional genes. *J. Hazard. Mater.* 403:123569. doi: 10.1016/j.jhazmat.2020.123569

Yu, F., Xue, S., Zhao, Y., and Chen, G. (2018). Risk assessment of oil spills in the Chinese Bohai Sea for prevention and readiness. *Mar. Pollut. Bull.* 135, 915–922. doi: 10.1016/j.marpolbul.2018.07.029

Zhai, W. D., Zheng, L. W., Li, C. L., Xiong, T. Q., and Wang, S. Y. (2020). *Changing Nutrients, Dissolved Oxygen and Carbonate System in the Bohai and Yellow Seas, China*. Singapore: Springer. doi: 10.1007/978-981-15-4886-4_8

Zhai, W., Zhao, H., Zheng, N., and Xu, Y. (2012). Coastal acidification in summer bottom oxygen-depleted waters in northwestern-northern Bohai Sea from June to August in 2011. *Chin. Sci. Bull.* 57, 1062–1068. doi: 10.1007/s11434-011-4949-2

Zhang, H., Zheng, S., Ding, J., Wang, O., and Liu, F. (2017). Spatial variation in bacterial community in natural wetland-river-sea ecosystems. *J. Basic Microbiol.* 57, 536–546. doi: 10.1002/jobm.201700041

Zhao, H. D., Kao, S. J., Zhai, W. D., Zang, K. P., Zheng, N., Xu, X. M., et al. (2017). Effects of stratification, organic matter remineralization and bathymetry on summertime oxygen distribution in the Bohai Sea. China. *Cont. Shelf Res.* 134, 15–25. doi: 10.1016/j.csr.2016.12.004

Zhen-Li, Z., Xin-Qi, Z., Nan, W., Wen-Wu, Z., Xu-Fen, Z., Yi, C., et al. (2014). *Amphiplicatus metriothermophilus* gen. nov., sp. nov., a thermotolerant alphaproteobacterium isolated from a hot spring. *Int. J. Syst. Evol. Microbiol.* 64, 2805–2811. doi: 10.1099/ijs.0.062471-0

Zhou, F., Gao, X., Zhang, Y., Yuan, H., Song, J., Liu, K., et al. (2017). Potential mobility of inorganic nutrients and its controls at the sediment-water interface in the main path of Kuroshio Current off eastern Taiwan. *Mar. Pollut. Bull.* 119, 270–276. doi: 10.1016/j.marpolbul.2017.04.002

Zumft, W. G. (1997). Cell biology and molecular basis of denitrification. *Microbiol. Mol. Biol. Rev.* 61, 533–616. doi: 10.1128/mmbr.61.4.533-616.1997

Conflict of Interest: The authors declare that the research was conducted in the absence of any commercial or financial relationships that could be construed as a potential conflict of interest.

Publisher's Note: All claims expressed in this article are solely those of the authors and do not necessarily represent those of their affiliated organizations, or those of the publisher, the editors and the reviewers. Any product that may be evaluated in this article, or claim that may be made by its manufacturer, is not guaranteed or endorsed by the publisher.

Copyright © 2022 Guo, Song, Li, Zhao and Wang. This is an open-access article distributed under the terms of the Creative Commons Attribution License (CC BY). The use, distribution or reproduction in other forums is permitted, provided the original author(s) and the copyright owner(s) are credited and that the original publication in this journal is cited, in accordance with accepted academic practice. No use, distribution or reproduction is permitted which does not comply with these terms.

frontiers in Marine Science

ORIGINAL RESEARCH
published: 17 February 2022
doi: 10.3389/fmars.2022.822939

Distribution, Diversity, and Abundance of Nitrite Oxidizing Bacteria in the Subterranean Estuary of the Daya Bay

*Wei Sun[1,2], Lijing Jiao[2], Jiapeng Wu[2], Mingken Wei[1] and Yiguo Hong[2]**

[1] College of Biological and Food Engineering, Guangdong University of Petrochemical Technology, Maoming, China, [2] Key Laboratory for Water Quality and Conservation of the Pearl River Delta, Ministry of Education, Institute of Environmental Research at Greater Bay Area, Guangzhou University, Guangzhou, China

OPEN ACCESS

Edited by:
Meilin Wu,
South China Sea Institute of Oceanology, Chinese Academy of Sciences (CAS), China

Reviewed by:
Hui Wang,
Shantou University, China
Yuchun Yang,
Sun Yat-sen University, China
Yonggang Yang,
Guangdong Institute of Microbiology, Guangdong Academy of Science, China
Jing Wang,
Tianjin Normal University, China

***Correspondence:**
Yiguo Hong
yghong@gzhu.edu.cn

Specialty section:
This article was submitted to Marine Pollution, a section of the journal Frontiers in Marine Science

Received: *26 November 2021*
Accepted: *18 January 2022*
Published: *17 February 2022*

Citation:
Sun W, Jiao L, Wu J, Wei M and Hong Y (2022) Distribution, Diversity, and Abundance of Nitrite Oxidizing Bacteria in the Subterranean Estuary of the Daya Bay. Front. Mar. Sci. 9:822939. doi: 10.3389/fmars.2022.822939

The oxidation of nitrite to nitrate as the second step of nitrification is vital for the global nitrogen cycle, and the genus *Nitrospira* is the most widespread nitrite-oxidizing bacteria (NOB) in diverse natural ecosystems. However, our understanding of *Nitrospira* distribution and their response to dynamic environmental parameters is still limited in the subterranean estuary (STE), a special environment of the mixed zone between land and sea. In this study, *Nitrospira* communities were collected within 5–10 cm depth intervals of sediments with the physiochemical gradients along the transections of the Daya Bay (DYB) from the landward member to the seaward member. The abundance, community structure of *Nitrospira,* and their potentially influencing environmental factors were investigated using Q-PCR, the high throughput sequencing targeting *Nitrospira nxr*B gene, and biostatistics analyses. The abundance of *Nitrospira* showed uniform distribution along the transections, but significantly decreasing variations were observed from the surface (<20 cm) to the bottom (>20 cm) of sediments. The community diversity and structure of *Nitrospira* also displayed a remarkable vertical distribution in the DYB (STE), although no significant differences were observed along the transections of STE. *Nitrospira marina* (*N. marina*) predominated in the sediments, *Candidatus Nitrospira bockiana* (*Ca. N. bockiana*), and *Candidatus Nitrospira defluvii* (*Ca. N. defluvii*) were the main *Nitrospira* species, and *Candidatus Nitrospira lenta* (*Ca*. *N. lenta*) and *Nitrospira japonica* (*N. japonica*) also existed with relatively low abundance in the DYB (STE). These findings revealed that *Nitrospira* species (*Ca. N. defluvii*, *Ca*. *N. lenta*, and *N. japonica*) derived from activated sludge was also widespread in natural habitats and deduced that the STE may be affected by the pollution derived from terrigenous human activities. The statistical analysis combined with the STE dynamic variation indicated that dissolved organic carbon (DOC), salinity, and ammonium along the sediment depths attributed to the vertical community distribution of the *Nitrospira* species. In summary, the vertical distribution of *Nitrospira* and their response to the dynamic physicochemical parameters imply their important role in the nitrite oxidation of the STE and provide insights into the niche differentiation and diversely physiologic metabolism of NOB.

Keywords: nitrite oxidization, *Nitrospira*, diversity, subterranean estuary, Daya Bay

INTRODUCTION

The subterranean estuary (STE), an unconfined aquifer mixed with land fresh water and seawater, is the transition zone between land underground runoff and the ocean in the surface estuary (Moore, 1999). Due to the influence of tides, waves, and other geochemical factors, the STE forms a dynamic redox state, which leads to the occurrence of complex biogeochemical reactions and makes the STE become a very active and strong area of biogeochemical reactions (Santos et al., 2009). The inorganic nitrogen in the STE comes from both the input of freshwater groundwater and the mineralization products of organic matter input through seawater circulation (Santos et al., 2009). Therefore, the STE is a key "Filter" of nitrogen compounds derived from terrestrial and marine ecosystems. In recent years, some studies have confirmed that groundwater discharge, especially the submarine groundwater discharge (SGD) of the STE, contributed a large part of the nutrients (especially the nitrogen budget) input to coastal water and has an important impact on the coastal ecosystem (Moore, 1996; Hwang et al., 2005; Lee and Kim, 2007; Smith and Swarzenski, 2012; Sáenz et al., 2012).

A large amount of nitrogen transformation occurred in the STE based on the analysis of geochemical processes in multiple sites (Santos et al., 2009). Nitrification is a process in which microorganisms oxidize ammonia to nitrite and further oxidize nitrite to nitrate. It is an important part of the global nitrogen cycle and plays an important role in maintaining the operation of natural ecosystems (Zehr and Kudela, 2011; Kuypers et al., 2018). Nitrification is generally considered to be catalyzed by two kinds of functional microorganisms: ammonia-oxidizing microorganisms (AOM) and nitrite-oxidizing bacteria (NOB). Compared with the research on AOM, little cognition about NOB has seriously restricted our understanding of the nitrification process and related functional groups.

Nitrite oxidizing bacteria includes seven effectively recognized genera (Daims et al., 2016). Among these NOB genera, *Nitrospira* belongs to phylum *Nitrospirae* (Ehrich et al., 1995), which forms an independent branch in phylogenetic analysis, and is considered to be the most diverse and ubiquitous in natural and engineered ecosystems (Fujitani et al., 2013; Park et al., 2017), such as soils, marine sponge, geothermal spring, acid mine drainage, estuary, and subtropical forest (Bartosch et al., 2002; Off et al., 2010; Lebedeva et al., 2011; Ramanathan et al., 2017; Hou et al., 2018; Han et al., 2020). In addition, *Nitrospira* may be involved in soil nitrification more actively than *Nitrobacter* by DNA-stable isotope probing (SIP) investigation (Xia et al., 2011). These results suggest *Nitrospira* plays a predominant role in the nitrite oxidation process and ecological balance in natural ecosystems (Han et al., 2021). However, the community structure and diversity distribution characteristics of *Nitrospira* are still limited in the STE.

A series of primers targeting the 16S rRNA gene was used to analyze *Nitrospira* in the environments, but the genetic diversity of *Nitrospira* makes most primers unable to amplify all subgroups or may amplify non-specific sequences (Pester et al., 2014). Functional genes *nxr*A, *nxr*B, and *nxr*C of NOB, respectively, encode the expression of subunits α, β, and γ of nitrite oxidoreductase (NXB). The multicopies of the *nxr*B gene in *Nitrospira* may benefit the synthesis of NXB and the transmission of the electronic respiratory chain and accelerate the metabolism and consumption of nitrite in the environments (Hong et al., 2020). In addition, when the nitrite increased in the environment after the starvation treatment, the *nxr*B expression of *Candidatus Nitrospira defluvii* (*Ca. N. defluvii*) increased significantly, while the 16S rRNA expression did not change significantly (Lücker et al., 2010). This result further indicates that the functional gene *nxr*B is more suitable than 16S rRNA for the biological analysis of *Nitrospira*.

In this study, sediment samples were collected from the DYB (STE) and the community characteristics of *Nitrospira* were investigated using the *nxr*B gene of *Nitrospira* by high throughput sequencing. Q-PCR assays were employed to analyze the abundance of *Nitrospira.* The potential key environmental factors influencing the *Nitrospira* distribution and abundance in the STE sediments were identified by multivariate statistical and correlation analyses. The understanding of the community structure and characteristics of *Nitrospira* in the special habitat of the STE will expand the current cognition of the NOB distribution characteristics.

MATERIALS AND METHODS

Sample Collection

The STE mentioned in this study belongs to the shallow type. Sedimentary columns were obtained from the STE in Renshan District, DYB (E 114.80° and N 22.82°) in September 2016. The DYB is a semi open bay in the north of the South China Sea, and its northeast Bay is also a small semi open bay with a maximum width of 2 km (Jiao et al., 2018). The intertidal zone selected in this study is located in the lower reaches of farmland and the population accumulation area of Renshan. Due to the confluence of two small seasonal rivers near the DYB, the overlying water of the intertidal zone is actually saltwater with a mix of terrestrial fresh water and seawater.

After obtaining the sediment column by vibracoring technique, the sediment columns were pushed out, placed on the plastic paper, and marked, respectively, as D1, D2, D3, and D4 from the landward member to the seaward member. The sediments in the sampling profile were heterogeneous. Some areas were mainly sand and gravel, while some areas were mainly silt. Therefore, the depths of different sediment columns were limited by the sediment characters in some areas under the same conditions. The depths of four sedimentary columns D1–D4 were 110, 90, 90, and 80 cm, respectively. The surface and the bottom sediments were, respectively, defined as depth $<$20 cm and $>$20 cm. The sampling location and sampling map are shown in **Figure 1** as our previous report (Jiao et al., 2018). The name of the sample was marked by the sediment column and depth, as shown in **Figure 1**. For core D1, every 5 cm sediment section from 5 to 90 cm was mixed as one sample named from D1_5 to D1_90, while every 10 cm sediment section from 90 to 110 cm was named D1_100 and sample D1_110, respectively. For

core D2, core D3, and core D4, every 10 cm sediment section was mixed as one sample with the same naming policy. The above sediment column of 5 or 10 cm length was taken as a sample, collected, and sealed in a plastic bag, stored in a refrigerator at −20°C, and transported to the laboratory. After the samples were transported to the laboratory, they were separated into two parts for use. One part of the samples were centrifuged to obtain pore water, which was used to determine the physical and chemical parameters of sediments. The other samples were stored at −80°C for DNA extraction and molecular biological analysis.

Determination of Environmental Parameters

Oxidation reduction potential (ORP) of sediment samples was measured by SG2 pH meter (SevenGo^{TM}, Mettler Toledo, Switzerland). The nitrogen nutrients were measured after the samples were transported back to the laboratory. The concentrations of NO_3^-, NO_2^-, and NH_4^+ were determined by the continuous and rapid determination method with small systems established by our laboratory (Wu et al., 2016; Guan et al., 2017).

DNA Extraction

About 0.3 g (wet weight) sediment from each sample was used for DNA extraction using the PowerSoil DNA Isolation Kit (MO BIO Laboratories, Inc., Switzerland). The total genomic DNA extracted was dissolved in 50 μl nuclease-free water, and the concentration and quality of DNA were determined by Nanodrop^{TM} Lite spectrophotometer (Thermo Scientific, Wilmington, ME, United States), and then stored in a refrigerator at −20°C for further study.

Quantitative PCR

The quantitative PCR (Q-PCR) for functional gene *nxr*B of *Nitrospira* was carried out by Roche LightCycler 480 Real-Time PCR using SYBR Green as a fluorescence dye (Promega, Switzerland) with primer set Nxr f27 (5′-GAGGAGCGGCATCCGAAGT-3′), Nxr r617 (5′-GGCABCGRTTCTGGTCG-3′) as optimized in the previous study, which has proven showing good coverage of *Nitrospira* in environmental samples (Hong et al., 2020). The correlation coefficient R^2 of the Q-PCR standard curve was in the range of 0.989–0.995, and the amplification efficiency was 94.9–101%.

PCR Amplification and High Throughput Sequencing

Functional gene *nxr*B of *Nitrospira* was amplified using primers Nxr f27/Nxr r617 which can effectively explore the diversity of *Nitrospira* (Hong et al., 2020). Barcode and adaptor sequences were designed and ligated to the 5′-end of the sequencing forward primers for distinguishing samples in the pyrosequencing runs. The PCR reaction mixtures contained the following components: 12.5 μl GoTaq Green Master Mix (Promega, United States), 0.5 μl primers, 1 μl DNA, and 10.5 μl H_2O. The PCR protocol was as follows: initial denaturation at 95°C for 2 min, 32 cycles at 95°C for 45 s, 62°C for 45 s, 72°C for 45 s, and a final extension at 72°C for 5 min. The PCR mixture products were purified using the Agarose Gel DNA Extraction Kit (TaKaRa MiniBEST) and were then prepared for the Illumina MiSeq sequencing.

The quality of purified PCR products was controlled by a 2200 tape station system (Agilent Technologies, Santa Clara, CA, United States). The sequencing process was performed by the Ion Torrent PGM sequencer (life technologies, Grand Island, NY, United States) and the sample library with a barcode on 316 chips. The sequences were assigned to different samples according to barcodes after a series of high-quality controls.

Processing and Analysis of High Throughput Sequencing Data

Nitrospira functional gene *nxr*B sequences were analyzed by standard operating procedures using Mothur (V.1.35.1)[1] (Schloss et al., 2009). In short, the effective original data can be obtained by de-barcoding, de-noising, and pruning the sample sequences. At first, the sequences less than 380 bp in length can be removed, the quality of the sequence was controlled by utilizing the command of the screen.seqs and unique.seqs, and the search and removal of chimera were conducted by the command combinations of pre.cluster, chimera.uchime, and remove.seqs. The effective sequences were compared with the reference database established before, and the final sequences obtained from preprocessing were divided into different operational taxonomic units (OTUs) by the cut-off value of 91% similarity established before (Hong et al., 2020). After removing the rare OTU (sequence number <0.1 ‰ total sequence number), the Shannon–Wiener curve and α diversity-related parameters, such as Chao1 index, Shannon index, and Simpson index, can be generated from the files generated by Mothur. The Shannon index curve was drawn by OriginPro 2017 to verify the sampling depth.

Phylogenetic Analysis

Operational taxonomic units with representative sequences of more than 0.1% of total sequences were defined as the dominant OTUs. The dominant OTUs and seed database were integrated into a FASTA file and imported into MEGA7. The sequences were aligned by running ClustalW. The phylogenetic analysis of the sequences was carried out by using the neighbor-joining method and the phylogenetic tree was constructed. The bootstrap test was set to repeat 1,000 times, and the bootstrap value was not less than 50%. Then, phylogenetic analysis of the representative sequences from dominant OTUs was customized by Evolview (He et al., 2016). Combining the abundance distribution of OTU in each sample with the clustering results, the heat map was drawn to identify similarities and differences in species distribution among samples by the software GraphPad Prism 7.

Biostatistical Analysis

The physical and geochemical parameters of each sample and the clustering and abundance distribution information of dominant OTUs in each sample were integrated into two sheets of the same excel file and imported into Canoco

[1]https://mothur.org/wiki/MiSeq_SOP

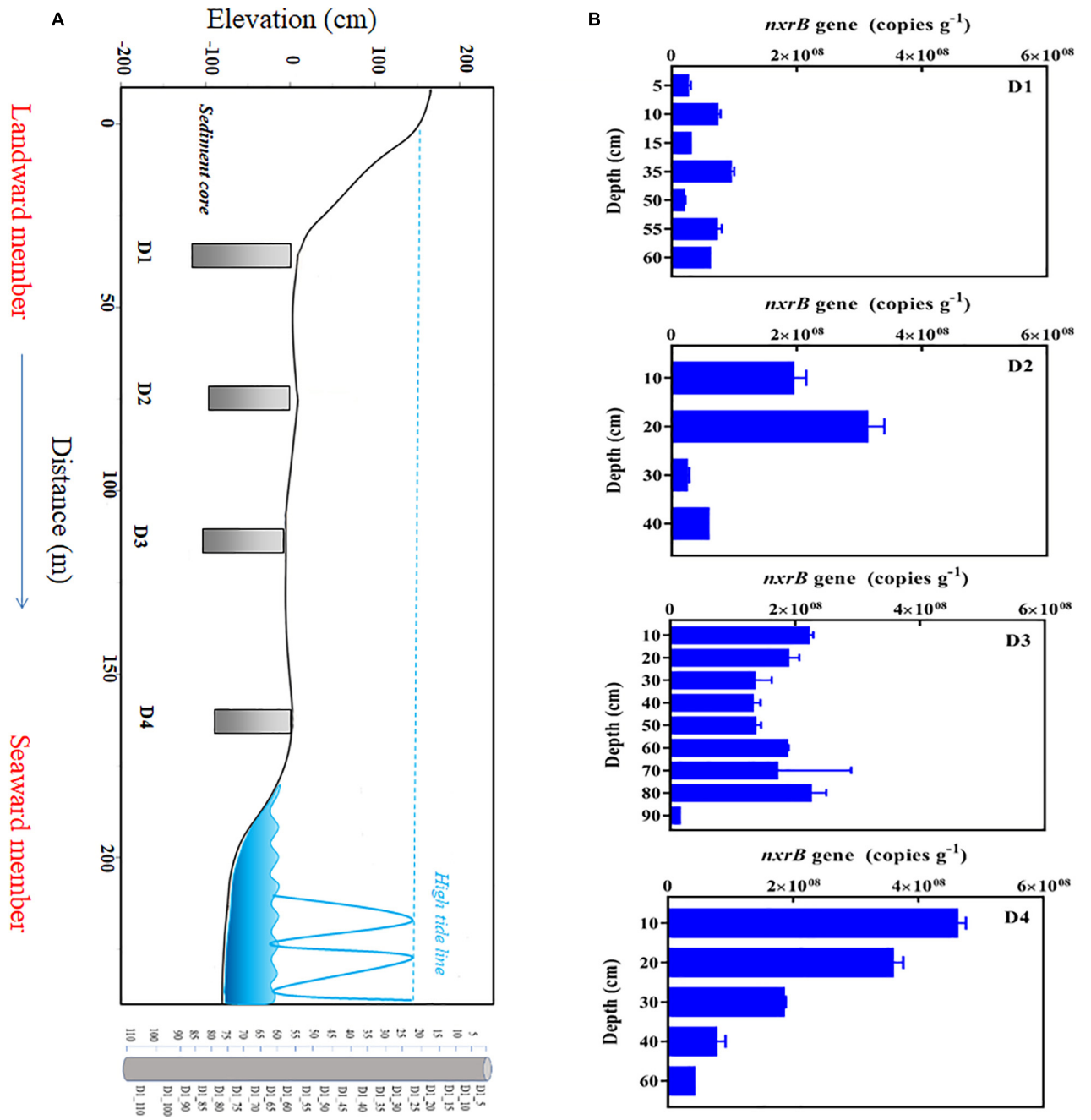

FIGURE 1 | Sampling sites **(A)** and *nxrB* gene abundance of *Nitrospira* the DYB (STE) **(B)**. D1, D2, D3, and D4 (from landward member to seaward member) stands for sediment cores with a depth of 110, 90, 90, and 80 cm, respectively. As shown in core D1, eveiy 5 cm sediment section was mixed as one sample named from D1_5 to D1_90, while eveiy 10 cm sediment section from 90 to 110 cm respectively named D1_100 and sample D1_110. For core D2, Core D3 and core D4, eveiy 10 cm sediment section was mixed as one sample with the same naming policy.

(version: 5.0). Principal component analysis (PCA) was used to analyze the distribution characteristics of the *Nitrospira* community structure. Redundancy analysis (RDA) was used to analyze the main physical and geochemical parameters affecting the distribution of the *Nitrospira* community structure. Pearson correlation analysis was used to analyze statistically significant correlations between the abundance distribution of dominant OTUs, the abundance of *nxr*B gene, and physical and geochemical parameters by R language. The differentiation of the *Nitrospira* abundance and the diversities between the surface and the bottom sediments was tested by the one-way ANOVA using SPSS (version 22.0). A two-tailed *t*-test was used to detect the significant effects of environmental parameters on the diversity, abundance, and distribution of *Nitrospira* in different samples

with *P*-values of 0.05 or 0.01 by using SPSS (version 22.0). The differences among community structures of the *nxr*B gene were tested by multiresponse permutation procedure (MRPP; Zimmerman et al., 1985) analysis using Vegan in R package with permutation 999.

Nucleotide Sequence Accession Numbers

The accession number CAR005397 of sequences generated in this study has been reported to GSA DATA ADMIN.

RESULTS

Physical and Geochemical Environmental Parameters of the Study Profile

The physical and geochemical parameters of pore water in the sedimentary column were shown in **Supplementary Table 1** as our previous report (Jiao et al., 2018). The salinity of the pore water in this study profile ranged from 19 to 30 psu. The salinity of bottom sediments was higher than that of upper sediments, and that of landward member (D1) was higher than that of seaward member (D4). The ORP presented an increasing trend along with the depth and ranged between −385 mv and −76 mv. The concentrations of NO_3^- varied from 0.00 to 44.07 μmol L^{-1}, and the average concentration of the study profile was 4.90 μmol L^{-1}. The concentrations of NO_2^- varied from 0.13 to 27.29 μmol L^{-1}, and the average concentration of the study profile was 2.60 μmol L^{-1}. The nitrogen concentrations were high (i.e., NO_3^- concentration 44.07 μmol L^{-1} and NO_2^- – concentration 27.29 μmol L^{-1}) in the surface sediment (0–10 cm) of D3_10, which may be due to the sampling randomness. In the whole study profile, the NH_4^+ concentrations varied from 0.78 to 19.18 μmol L^{-1} with an average concentration of 5.15 μmol L^{-1}.

Abundance Distribution of *Nitrospira nxr*B Gene in the Daya Bay Subterranean Estuary

The abundance distributions of the *Nitrospira nxr*B gene in the DYB (STE) are shown in **Figure 1**. Overall, the abundances of the *nxr*B gene in the sediments of the DYB (STE) ranged from 1.47×10^7 to 4.61×10^8 copies g^{-1}. Among the four sediment columns, the abundance of *nxr*B gene in sediment column D1 was relatively low compared with the other sediment columns and ranged from 1.90×10^7 copies g^{-1} to 9.36×10^7 copies g^{-1} along the sediment depths. The *nxr*B gene cope number in sediment column D2 ranged from 2.57×10^7 copies g^{-1} to 3.14×10^8 copies g^{-1}, and showed a reducing trend from the surface to bottom sediments. The abundance of the *nxr*B gene in sediment column D3 was relatively high and fluctuated in the range of 10^8 orders of magnitude except for the lowest abundance at 80–90 cm profile. The abundance of the *nxr*B gene fluctuated from 4.61×10^8 copies g^{-1} in the surface layer (D4_10) to 4.07×10^7 copies g^{-1} in the deep layer (D4_60) in sediment column D4 and showed the decreasing trend with depth. There was insignificant variation ($F = 2.88$, $P > 0.05$) in the abundance variation of the *nxr*B gene among the four sediment columns, which indicated that *Nitrospira* bacteria were uniformly distributed in the DYB (STE) from the landward member to the seaward member. However, the *nxr*B gene abundance varied significantly along the sediment depth in the DYB (STE) ($F = 5.96$, $P < 0.05$) with higher abundance in the surface sediments than the bottom sediments.

Diversity and Richness Analysis of *Nitrospira* in DYB (Subterranean Estuary) Based on High-Throughput Sequencing of *nxr*B Gene

Every sediment sample screened 2,500 sequences with a total of 25 sediment samples for diversity analysis. Some samples with too few sequences (sequence number <1000) were removed to avoid affecting the subsequent diversity analysis. A total of 68,594 high-quality sequences were obtained through the pretreatment of the Mothur platform. The sequences with similarities greater than 91% were classified as the same OTU (Hong et al., 2020) and 689 OTUs were obtained by cluster analysis. After removing the rare OTU (sequence number <6), *Nitrospria* in the sediment samples of the DYB (STE) could be divided into 62 OTUs according to the *nxr*B gene, accounting for 98.82% of the total sequence number. The top 20 OTUs in sediments of the DYB (STE) (the sequence number of OTUs more than 0.1%) were defined as the dominant OTUs, which accounted for 97.63% of the total sequence number. The calculation results of sample richness and diversity index (**Supplementary Table 2**) showed that the coverage of *Nitrospira* in all samples was higher than 99.55%, which reflected the reliability of diversity index results. Moreover, the Shannon curve tended to be flat with the increase of sequencing depth as shown in **Supplementary Figure 1**, which indicated that the amount of sequencing data in the sediments of the DYB (STE) was large enough to reflect the vast majority of microbial information in the samples and can be used for the subsequent diversity and community structure analysis of *Nitrospira*.

The OTU number of *Nitrospira* ranged from 16 to 40 among the sediment samples. Although the OTU number did not show significant variations from the landward member to the seaward member ($F = 1.95$, $P = 0.16$), it generally decreased from the surface to the bottom sediments ($F = 5.49$, $P < 0.05$) with the exception of sediment column D1_5 with the lowest value 16. The highest OTU number was detected in sediment column D2_10. In general, the Shannon index also decreased from the surface to the bottom sediment ($F = 15.18$, $P < 0.05$) except for sediment column D1_5 with the lowest Shannon index of 1.08. The higher Shannon indexes were, respectively, observed in sediment columns D3 (D3_10) and D4 (D4_10) with values of 2.08 and 2.02. The Chao1 and Simpson indexes showed a similar changing variation as the OTU number and Shannon index among samples from the surface to the bottom sediment ($F = 5.49$, $P < 0.05$; $F = 8.01$, $P < 0.05$). Overall, the *Nitrospira* diversities of the surface sediments were generally higher than those of the bottom sediments in the DYB (STE).

Phylogenetic and Community Distribution Analysis of *Nitrospira* in DYB (Subterranean Estuary)

The representative sequences of dominant OTUs and reference sequences were extracted and the phylogenetic tree was constructed, as shown in **Figure 2**. The obtained *nxr*B genes of *Nitrospira* shared 83.58 to 94.17% identity with each other and 84.92 to 95.84% similarity with the sequences matched with the known *Nitrospira* genus in the Genbank. All retrieved sequences could be divided into seven branches that could be affiliated to the known genus *Nitrospira*. OTU04 was affiliated to *Nitrospira marina* (*N. marina*), with 95.84% similarity. OTU01, OTU02, and OTU12 also showed a close relationship with *N. marina* with up 90.42% similarity. OTU06 was closely related

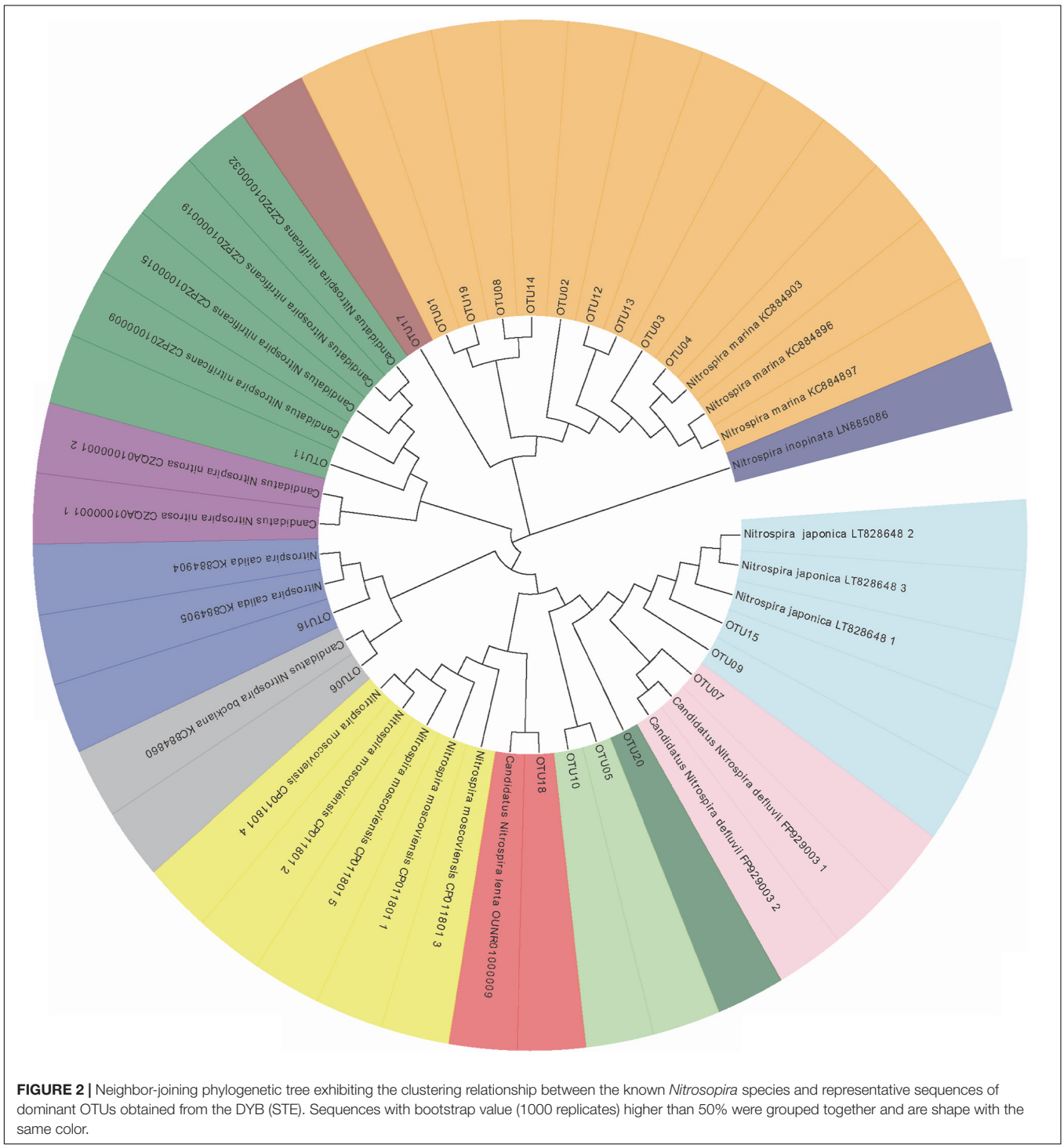

FIGURE 2 | Neighbor-joining phylogenetic tree exhibiting the clustering relationship between the known *Nitrosopira* species and representative sequences of dominant OTUs obtained from the DYB (STE). Sequences with bootstrap value (1000 replicates) higher than 50% were grouped together and are shape with the same color.

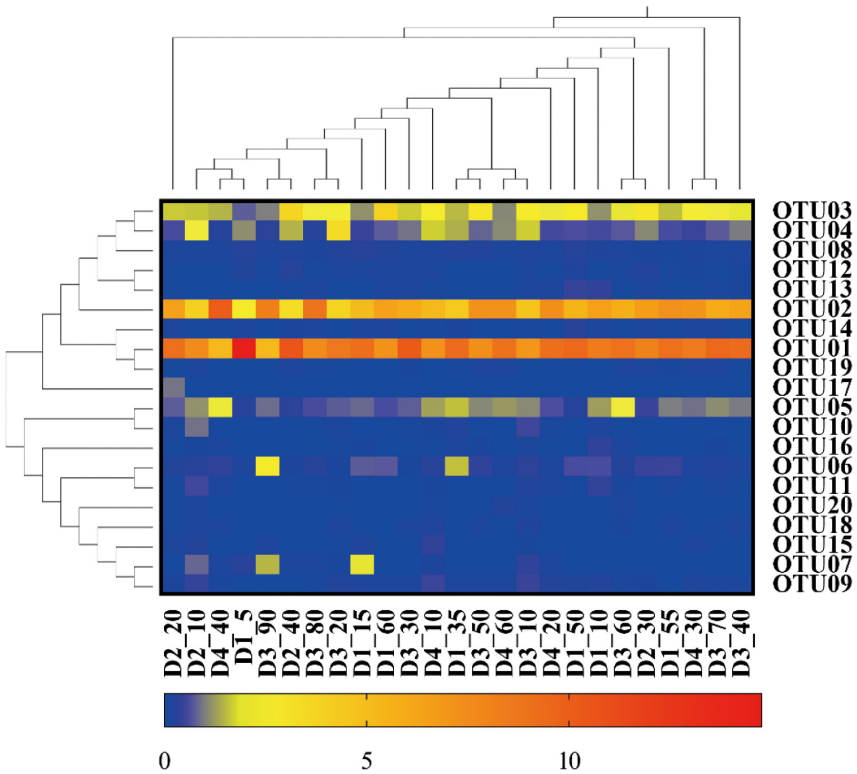

FIGURE 3 | Heat map of *Nitrospira* in sediment of the DYB (STE). DI, D2, D3, and D4 stands for sediment cores with a depth of 110, 90, 90, and 80 cm, respectively. As shown in core DI, every 5 cm sediment section was mixed as one sample named from D15 to DI_90, while sample DI_100 and sample DI_110 represent sediment sections from 90 to 100 cm and from 100 to 110 cm, respectively. For core D2, Core D3 and core D4, every 10 cm sediment section was mixed as one sample with the same naming policy. The 20 dominant OTUs in sediments of the DYB (STE) (OTUs of sequence number >0.1%) were clustered, which accounted for 97.63% of the total sequence number.

to *Candidatus Nitrospira bockiana* (*Ca. N. bockiana*). OTU07 was affiliated with *Candidatus Nitrospira defluvii* (*Ca. N. defluvii*) with 93.33% similarity. OTU11 was clustered with *Candidatus Nitrospira nitrifcans* (*Ca. N. nitrifcans*) with 89.38% similarity. OTU9 and OTU15 were closely related to *Nitrospira japonica* (*N. japonica*) with 90.83 and 94.38% similarity, respectively. OTU16 was affiliated with *Nitrospira calida* (*N. calida*) with 91.25% similarity. OTU18 was closely affiliated to *Candidatus Nitrospira lenta* (*Ca. N. lenta*) *with* 90.00% similarity. The remaining OTUs (OTU03, 05, 08, 10, 13, 14, 17, 19, and 20) shared low similarity and did not group closely with the known *Nitrospira* genus, whereas they still clustered distinctly with *Nitrospira*. A heat map based on the abundance distribution and clustering results of dominant OTUs (**Figure 3**) showed that OTU01, OTU02, OTU03, OTU04, OTU05, and OTU08 were widespread in all samples, while OTU06 and OTU07 mainly existed in the bottom and surface sediments, respectively, which suggested that the *Nitrospira* community should be distinct along the sediment depth.

The overall community composition and relative abundance of *Nitrospira* species based on phylogenetic clustering analysis were exhibited in **Supplementary Figure 2**. Among the seven known classified *Nitrospira* genus, *N. marina, Ca. N. bockiana and Ca. N. defluvii* were the main *Nitrospira* species, with the relative abundance proportion 78.41, 2.21, and 1.06%, respectively. *N. marina is* commonly distributed and predominated in all sediment samples. Although the distribution of *Ca. N. bockiana* was also ubiquitous in all sediment samples, its heterogeneous distribution among the surface and bottom sediments was exhibited with relatively high abundance in the bottom sediments of D1_35, D1_60, D2_30, D3_90, and D4_40. However, *Ca. N. defluvii* did not ubiquitously distribute in all samples and exhibited the opposite changing trend compared with *Ca. N. bockiana*. The relative abundance of *Ca. N. defluvii* was higher in the surface sediments of D1_15, D2_10, D3_10, and D4_10 with the exception of D3_90, and *Ca. N. defluvii* was not detected in nine samples from the bottom sediments. Furthermore, a significant difference ($P < 0.05$, **Supplementary Table 3**) was discovered in the community composition of *Nitrospira* between the surface sediments and bottom sediments, although no significant difference (D1/D2, D1/D3, D1/D4, D2/D3, D2/D4, D3/D4, all of $P > 0.05$) existed in the community composition of *Nitrospira* from the landward member D1 to the seaward member D4.

The difference of community structure among samples was performed by PCA as shown in **Figure 4**. The contribution rates of the first and second components in PCA were 31.92 and 19.72%, respectively. The surface sediment columns of D1,

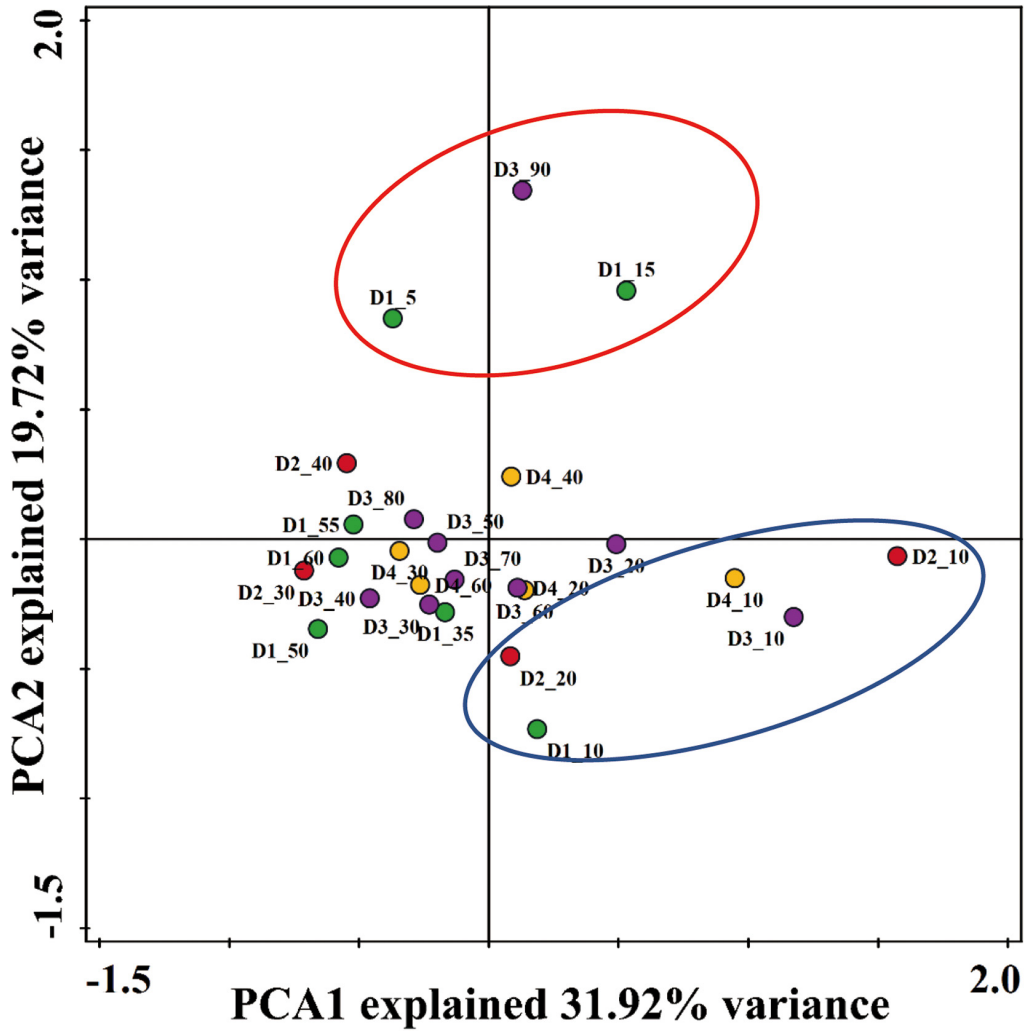

FIGURE 4 | Principal component analysis (PCA) of *Nitrospira* nxrB gene sequences retrieved from sediments of the DYB (STE). Horizontal and vertical axes represent the first two dimensions, axis 1 and axis 2, respectively.

D2, D3, and D4 (D1_10, D2_10, D2_20, D3_10, and D4_10) except D1_5 and D1_15 were gathered together, while most of the bottom sedimentary samples except D3_90 were grouped together. The analysis of MRPP indicated that the *Nitrospira* community structure from the DYB (STE) was not significantly different on the total level (all, $P > 0.05$, **Supplementary Table 3**), whereas there was a significant inconsistent community structure of *Nitrospira* between the surface and the bottom sediments (Surface/Bottom, $P = 0.044$).

Relationship Between Environmental Factors and *Nitrospira* Community Structure in the DYB (Subterranean Estuary)

The correlation between the community structure of *Nitrospira* based on main OTUs and environmental factors was analyzed by RDA, which showed that the analysis model was invalid based on the Monte Carlo test ($F = 1.2$, $p > 0.05$). That is to say, the environmental factors determined in this study could not adequately explain the composition of *Nitrospira* community structure in the sediments of Daya Bay (STE), and other environmental factors which were not determined might affect the distributions of *Nitrospira* community structure. The correlations between environmental factors and diversity indexes of Daya Bay STE were plotted and shown in **Figure 5**. Shannon index was positively correlated with nitrite ($r = 0.41$, $p < 0.05$). The number of OTU was negatively correlated with salinity ($r = -0.57$, $p < 0.01$), and significantly decreased with depth ($r = -0.40$, $p < 0.05$). The abundance of *nxr*B gene was positively correlated with nitrate ($r = 0.407$, $p < 0.05$) and significantly negatively correlated with ammonium ($r = -0.42$, $p < 0.05$) and salinity ($r = -0.48$, $p < 0.05$), but did not significantly correlate with nitrite.

The correlations between environmental factors and dominant OTUs were calculated by the Pearson correlation

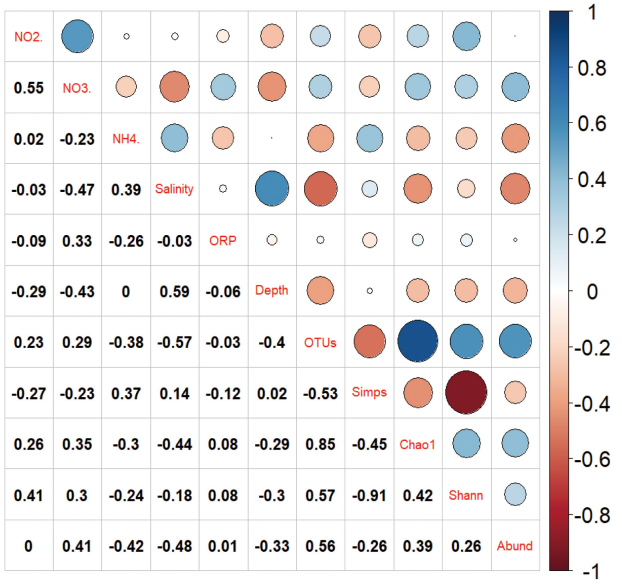

FIGURE 5 | Pearson correlation analysis of environmental parameters and diversity. Chao1 stands for Chao1 estimator, Shann stands for Shannon index, Simps stands for Simpson index, N02 stands for nitrite, N03 stands for nitrate and NH4 represents ammonia, OTUs represents the number of OTU and Abund stands for the abundance of *nxrB* gene. Blue and red denote positive and negative correlations, respectively. The *r*-values of pearson correlation analysis were shown in the grid.

analysis. The data with statistically significant correlation was shown in **Supplementary Table 4** in the **Supplementary Information**. OTU02, OTU08, and OTU14 were positively correlated with depth, ammonium, and salinity, respectively, while OTU04 was negatively correlated with depth. OTU06 was positively correlated with salinity and increased with depth. OTU09 was positively correlated with nitrate and nitrite and decreased with depth. OTU18 was positively correlated with nitrite concentration.

DISCUSSION

Distributions of *Nitrospira* Community Structure in the DYB (Subterranean Estuary)

There are at least six lineages of *Nitrospira* according to the phylogenetic analysis of 16S rRNA gene sequences (Daims and Wagner, 2018). *N.* marina belonging to the so-called *Nitrospira* lineage IV (Daims et al., 2001) has been detected previously in saltwater aquaria (Hovanec et al., 1998), marine biofilters (Tal et al., 2003), and marine recirculation aquaculture system (Foesel et al., 2008). In addition, *N. marina* was also the major group in the sediments of Nanliu (NL) River Estuary (Zhao et al., 2021) and in the water column of the Pearl River in winter (Hong et al., 2021). *N. marina* was predominant and ubiquitous in the DYB (STE), which predicted the potentially important role of *N. marina* in nitrite oxidation during nitrification in the STE. The genome and proteome of the first marine *Nitrospira* isolate indicate that *N.* marina is highly metabolically versatile, which might enable it to adapt to life in the oxic marine environments and even survive under conditions unfavorable for aerobic nitrite oxidation with fluctuating levels of electron acceptors and donors (Bayer et al., 2021).

Candidatus Nitrospira bockiana and *N. calida* belonging to the *Nitrospira* lineages V and VI, respectively, are considered to be strict chemolithoautotrophic species and organotrophic growth of these two species is not observed (Lebedeva et al., 2008, 2011). Their relatively low abundances in the DYB (STE) may infer that rich organic matter exists in the land–sea interface, which might adversely affect the development and growth of these two species. *Ca. N. defluvii* belonging to *Nitrospira lineages* I was most important for sewage treatment (Lücker et al., 2010) and was also found in the downstream river of wastewater discharge area (Cébron and Garnier, 2005). *Ca. N. defluvii* was first detected in the waters of PRE which likely resulted from land source pollution (Hong et al., 2021). *Ca. N. lenta* and *N. japonica* belonged to *Nitrospira lineages* II mainly inhabited in activated sludge from wastewater treatment plants (Ushiki et al., 2013; Boris et al., 2015), while *Ca. N. lenta* also dominated in the waters of PRE (Hong et al., 2021). *Ca. N. defluvii, Ca. N. lenta,* and *N. japonica* were all present with relatively low abundance in Daya Bay (STE). These findings revealed that members of *Nitrospira* lineage I was also widespread in natural habitats, and confirmed the versatile distribution of representatives of *Nitrospira* lineage II (Boris et al., 2015). On the other hand, it can be deduced that STE may be affected by the pollution derived from terrigenous human activities. The discharge of domestic wastewater from the population and the agricultural gathering area may lead to organic pollution in the STE. The emergence of anammox *Ca. Kuenenia* in this study profile (Jiao et al., 2018) also proved this view.

The discovery of comammox (with the capability for the complete oxidation of ammonia to nitrate in a single organism) has fundamentally overthrown the conventional understanding of the nitrification process with two-step (Daims et al., 2015). All comammox *Nitrospira* found in natural ecosystems was so far identified in representatives of *Nitrospira* lineage II (Zhao et al., 2021). However, comammox *Nitrospira* generally dominates the ammonia oxidation in acidic soils (Hu et al., 2021), and appears to be absent in marine systems (Daims et al., 2015; Bayer et al., 2021). The general existence of comammox *Nitrospira* in a wide range of coastal wetlands and Chongming eastern intertidal sediments indicates the potential role of comammox *Nitrospira* in the estuarine coastal system (Sun et al., 2020, 2021). OTU11 affiliated to *Ca. N. nitrifcans* belonged to comammox with a low proportion in the DYB (STE). This may be due to the amplification limit of primers, and *amo*A gene of comammox might broaden our cognition of comammox in the STE. Groundwater flow and chemical transport in STE are potentially important implications for chemical fluxes from aquifers to coastal waters (Robinson et al., 2007). How different types of nitrifiers respond to the dynamic changes may provide new insights into the ecological niche specificity of nitrifying microorganisms in STE. Therefore,

the detection of comammox *Nitrospira* in Daya Bay (STE) deserves further study.

Environmental Factors Affecting the Abundance and Distribution of *Nitrospira* in Subterranean Estuary

A distinctly vertical pattern of *Nitrospira* distribution was revealed considering the surface to the bottom zones of the STE sediments. The abundance of the *nxr*B gene was maintained in the range of 10^7–10^8 copies g^{-1} in the DYB (STE) sediments, which was 1–2 orders of magnitude lower than that of NOB in surface sediments (0–5 cm) in the Nanliu River estuary (10^8–10^{10}) (Zhao et al., 2021). Moreover, apparent depth-related differentiation of abundance was detected in the DYB (STE), which resembles previous studies with the lowest microbial abundance in the anaerobic zone (depth of 80–100 cm) in sediments of STE located at Gloucester Point (GP-STE), the beach of Virginia, United States (Hong et al., 2019). In addition, the *Nitrospira* diversity indexes (Shannon, Chao1, and Simpson) were all obviously higher on the surface than the bottom sediments. Although the predominant of *N.* marina may lead to the little differentiation in *Nitrospira* community among the sediments from the landward member to the seaward member of the STE, the distribution of *Ca. N. defluvii* and *Ca. N. bockiana* showed the opposite changing trend along with depths. Moreover, the overall community structure exhibited significant differences along the sediment depths based on MRPP and PCA analysis. The vertical distribution of bacteria at GP-STE suggested the predictable changes in permeable STE sediment from surface to bottom layers (Hong et al., 2019). Therefore, the vertical distribution of *Nitrospira* seems to be shaped with the gradient variation of physiochemical parameters along with the sediments' depths, such as salinity, organic matter, and nitrogen species.

Salinity is one of the most important factors which impacts the community composition and distribution of nitrifying microorganisms in ecosystems (Zhao et al., 2021). The lower diversity of *Nitrospira* is exhibited in bottom sediments with relatively high salinity at the DYB (STE). A less diverse microbiology community appeared to be associated with salinity in most cases (Hong et al., 2019). *N. marina* affiliated to lineage IV has widely adapted to variable salinity (Zhao et al., 2021), which may make it widely present in salinity ecosystems, including deep sea, estuary area, and saline soils (Pester et al., 2014; Hong et al., 2021; Li et al., 2021; Zhao et al., 2021). *Ca. N. bockiana* affiliated with LineageVmight also adapt to salinity, due to its positive relationship with salinity in DYB (STE) (**Supplementary Table 3**). Lineage II (*N. japonica* and *Ca. N. lenta*) were also the main groups with the adaption of variable salinity, while Lineage I (*Ca. N. defluvii*) appeared to be less adaptable salt than Lineage II and IV (Zhao et al., 2021). This may be also one of the reasons for the higher abundance of *Ca. N. defluvii* in the surface sediments of the STE with relatively low salinity. However, salinity could interact with the other environmental parameters. Salinity showed positive relationships with the contents of ammonium in this study (**Figure 5**). Salinity could control ammonium concentrations by influencing its absorption onto sediment and then play an important role in shaping the community distribution of nitrifying microorganisms (Li et al., 2015). In addition, different cations are also affected by salinity, which deserves attention (Zhao et al., 2021). *Nitrospira* community variation in agriculture soils was found to be significantly affected by potassium levels (Luo et al., 2020).

The study profile of the DYB (STE) was the typical submarine groundwater discharge (SGD) area. SGD is an important component of the global water balance and the rates of SGD play important role in biogeochemical cycling with coastal ecosystems (Smith et al., 2008; Anderson and Emanuel, 2010). Even though up to 96% of total SGD is marine water recirculating through the nearshore by the processes of wave setup and tidal oscillations (Anderson and Emanuel, 2010), fresh SGD is an important pathway of nutrients as a result of biogeochemical additions across the mixing zone of STE (Santos et al., 2009). About 25% of dissolved organic carbon (DOC) and 50% of total nitrogen (TN) inputs were transported by this pathway, and the remainder was associated with a one-dimensional vertical seawater recirculation along a seepage face (Santos et al., 2009). Considering that the sampling sites were located downstream of the population and agricultural accumulation areas, the abundant DOC and nitrogen species in the STE originated from fresh SGD transportation may be important factors affecting the growth, abundance, and distribution of *Nitrospira*. Han et al. (2018) found that manure could increase the activity and abundance of *Nitrospira* in the red soil by providing organic matter. *N. marina* benefit from additions of undefined organic carbon substrates, has adaptations to resist oxidative, osmotic, and is thus chemoorganotroph but not an obligate chemolithoautotroph (Bayer et al., 2021). In addition, the predominance of *N.* marina might be a general characteristic of ammonium-limited systems (Foesel et al., 2008). Ammonium concentration was relatively low throughout the transect in the DYB (STE), which may be due to the metabolization of ammonium along the flow path in the intertidal subsurface with permeability and long residue time (Jiao et al., 2018). The abundance of the *nxr*B gene and distribution of OTU02 were both significantly correlated with ammonium in the DYB (STE). Ammonium was also reported to be the most important factor influencing *Nitrospira* distribution in the water column of the PRE (Hong et al., 2021). Therefore, DOC and ammonium concentrations regulated by the dynamics of the STE may be the main factors driving the community composition and distribution of *Nitrospira* in the DYB (STE).

The pH, which was not determined in this study, may also be a factor affecting the growth of *Nitrospira* and was a potential factor affecting the distribution of *Nitrospira* in the DYB (STE). Low soil pH could accelerate the ionization of ammonium ions, which will affect the ammonia oxidation activity by reducing the available substrate for ammonia oxidizing microorganisms (Han et al., 2018). Due to the spatial dependence of ammonia oxidation and nitrite oxidation, low pH may affect soil NOB activity (Han et al., 2018). In addition, dissolved oxygen (DO) also plays important role in the niche differentiation of functional

microorganisms (Hong et al., 2019). DO was responsible for the *Nitrospira* distribution in the PRE estuary (Hong et al., 2021). *Ca. N. defluvii* may be inhibited by the elevated DO, which is likely related to the evolutionary history, evolved from anaerobic ancestors (Lücker et al., 2010; Hong et al., 2021). Due to the permeability of the STE sediments (Santos et al., 2009), the gradient DO along the sediment depth may affect the *Nitrospira* distribution in the DYB (STE).

Although *Nitrospira* based on functional gene level could represent the diversity and community distribution of NOB in natural habitats, it is necessary to measure the rate of nitrite oxidation *in situ* and measure the flux during the nitrite oxidation process. On this basis, the contribution of *Nitrospira* to the process of nitrite oxidation and the internal relationship between *Nitrospira* and nitrite oxidation could be explored. At present, there are some controversies about the determination methods of nitrite oxidation rate (Daims et al., 2001) and the determination of nitrite oxidation rate needs to be further optimized in the future.

CONCLUSION

In this study, the abundance, diversity, and community structure of *Nitrospira* along sediment depths at the DYB (STE) were detected by using high-throughput sequencing of the *Nitrospira nxr*B gene. From the surface to the bottom sediments, the abundance and diversity of *Nitrospira* showed a vertical decreasing trend. Although the *Nitrospira* community showed little differentiation from landward member to seaward member of the DYB (STE), a prominent spatial shift in composition was detected between the surface and bottom sediments. Seven known *Nitrospira* species were detected in the DYB (STE), but *N. marina* were predominant, and *Ca. N. bockiana* and *Ca. N. defluvii* were the main groups. Such observation not only reflected the wide distribution of various *Nitrospira* species along the depths but might also be associated with the physiologies of *Nitrospira* with the adaption and response to the dynamic environmental parameters in the STE. Salinity, DOC, and ammonium were predicted to be the important factors affecting the *Nitrospira* distribution combined with statistical analysis and dynamic characteristics of SGD transportation in STE. These findings may broaden our new insights into the niche differentiation of *Nitrospira* under the dynamic and complex changes and provide a guide for future studies on the functional activity and ecological status of *Nitrospira* in STE environments.

DATA AVAILABILITY STATEMENT

The datasets presented in this study can be found in online repositories. The names of the repository/repositories and accession number(s) can be found below: National Genomics Data Center (NGDC), part of the China National Center for Bioinformation (CNCB) [accession: CRA005397].

AUTHOR CONTRIBUTIONS

YH was responsible for the conceptualization. LJ was responsible for the experimental operation. WS and LJ prepared and wrote the original draft. YH, WS, and MW wrote, reviewed, and edited the manuscript. JW and LJ are responsible for field sampling. YH and WS funded the acquisition. All authors read and approved the final manuscript.

FUNDING

This work was funded by the National Natural Science Foundation of China (Nos. 42006137 and 31870100), Basic and Applied Basic Research Foundation of Guangdong Province (Nos. 2019B1515120066 and 2020A1515110597), Guangdong Key Area R&D Program (2018B020205002), Scientific Research Fund of talent introduction of Guangdong University of Petrochemical Technology (2019rc108), and Demonstration of harmless treatment of shrimp tail water in high-place pond [Letter of Agricultural Bureau in Maoming, Guangdong (2019) NO. 440].

ACKNOWLEDGMENTS

The authors would like to thank the reviewers for their valued criticism and suggestions.

SUPPLEMENTARY MATERIAL

The Supplementary Material for this article can be found online at: https://www.frontiersin.org/articles/10.3389/fmars.2022.822939/full#supplementary-material

REFERENCES

Anderson, W. P., and Emanuel, R. E. (2010). Effect of interannual climate oscillations on rates of submarine groundwater discharge. *Water Resour. Res.* 46:W05503. doi: 10.1029/2009WR008212

Bartosch, S., Hartwig, C., Spieck, E., and Bock, E. (2002). Immunological detection of Nitrospira-like bacteria in various soils. *Microb. Ecol.* 43, 26–33. doi: 10.2307/4287571

Bayer, B., Saito, M. A., Mcilvin, M. R., Luecker, S., and Santoro, A. E. (2021). Metabolic versatility of the nitrite-oxidizing bacterium *Nitrospira marina* and its proteomic response to oxygen-limited conditions. *ISME J.* 15, 1025–1039. doi: 10.1038/s41396-020-00828-3

Boris, N., Sandra, O., Holger, D., and Eva, S. (2015). Improved isolation strategies allowed the phenotypic differentiation of two *Nitrospira* strains from widespread phylogenetic lineages. *FEMS Microbiol. Ecol.* 91, 1–11. doi: 10.1093/femsec/fiu031

Cébron, A., and Garnier, J. (2005). *Nitrobacter* and *Nitrospira* genera as representatives of nitrite-oxidizing bacteria: detection, quantification and growth along the lower seine river (France). *Water Res.* 39, 4979–4992. doi: 10.1016/j.watres.2005.10.006

Daims, H., and Wagner, M. (2018). Nitrospira. *Trends Microbiol.* 26, 462–463.

Daims, H., Lebedeva, E. V., Pjevac, P., Han, P., Herbold, C., Albertsen, M., et al. (2015). Complete nitrification by *Nitrospira* bacteria. *Nature* 528, 504–509. doi: 10.1038/nature16461

Daims, H., Lücker, S., and Wagner, M. (2016). A new perspective on microbes formerly known as nitrite-oxidizing bacteria. *Trends Microbiol.* 24, 699–712. doi: 10.1016/j.tim.2016.05.004

Daims, H., Nielsen, J. L., Nielsen, P. H., Schleifer, K. H., and Wagner, M. (2001). In situ characterization of Nitrospira-like nitrite oxidizing bacteria active in wastewater treatment plants. *Appl. Environ. Microbiol.* 67, 5273–5284. doi: 10.1128/AEM.67.11.5273-5284.2001

Ehrich, S., Behrens, D., Lebedeva, E., Ludwig, W., and Bock, E. (1995). A new obligately chemolithoautotrophic, nitrite-oxidizing bacterium, *Nitrospira moscoviensis sp*. nov. and its phylogenetic relationship. *Arch. Microbiol.* 164, 16–23. doi: 10.1007/BF02568729

Foesel, B. U., Gieseke, A., Schwermer, C., Stief, P., Koch, L., Cytryn, E., et al. (2008). *Nitrosomonas* Nm143-like ammonia oxidizers and *Nitrospira marina*-like nitrite oxidizers dominate the nitrifier community in a marine aquaculture biofilm. *FEMS Microbiol. Ecol.* 63, 192–204. doi: 10.1111/j.1574-6941.2007.00418.x

Fujitani, H., Aoi, Y., and Tsuneda, S. (2013). Selective enrichment of two different types of *Nitrospira*-like nitrite-oxidizing bacteria from a wastewater treatment plant. *Microbes. Environ.* 28, 236–243. doi: 10.1264/jsme2.ME12209

Guan, F. J., Hong, Y. G., Wu, J. P., Wang, Y., Bin, L. Y., Tang, B., et al. (2017). A fast sodium hypobromite oxidation method for the sequential determination of ammonia nitrogen in small volume. *Ecol. Sci.* 36, 42–48.

Han, S. H., Zeng, L. Y., Luo, X. S., Xiong, X., Wen, S. H., Wang, B. R., et al. (2018). Shifts in Nitrobacter- and Nitrospira-like nitrite-oxidizing bacterial communities under long-term fertilization practice. *Soil Biol. Biochem.* 124, 118–125. doi: 10.1016/j.soilbio.2018.05.033

Han, S., Huang, Q., and Chen, W. (2021). Partitioning nitrospira community structure and co-occurrence patterns in a long-term inorganic and organic fertilization soil. *J. Soil Sediment* 21, 1–10. doi: 10.1007/s11368-020-02813-x

Han, S., Tan, S., Wang, A. C., Chen, W. L., and Huang, Q. Y. (2020). Deciphering belowground nitrifier assemblages with elevational soil sampling in a subtropical forest ecosystem (Mount Lu. China). *FEMS Microbiol. Ecol.* 96, 1–11. doi: 10.1093/femsec/fiz197

He, Z., Zhang, H., Gao, S., Lercher, M. J., Chen, W. H., and Hu, S. (2016). Evolview v2: an online visualization and management tool for customized and annotated phylogenetic trees. *Nucleic Acids Res.* 44, W236–W241. doi: 10.1093/nar/gkw370

Hong, Y. G., Jiao, L. J., and Wu, J. P. (2020). New primers, taxonomic database and cut-off value for processing nxrB gene high-throughput sequencing data by MOTHUR. *J. Microbiol. Meth.* 173:105939. doi: 10.1016/j.mimet.2020.105939

Hong, Y. G., Wu, J. P., Jiao, L. J., Hu, Y. H., Ye, F., Wang, Y., et al. (2021). Shifts in the abundance and community composition of particle-associated and free-living *Nitrospira* across physicochemical gradients in the Pearl River Estuary. *Estuar. Coast* 44, 1931–1945. doi: 10.1007/s12237-021-00909-2

Hong, Y. G., Wu, J. P., Wilson, S., and Song, B. (2019). Vertical stratification of sediment microbial communities along geochemical gradients of a subterranean estuary located at the gloucester beach of virginia, united states. *Front. Microbiol.* 9:3343. doi: 10.3389/fmicb.2018.03343

Hou, L., Xie, X., Wan, X., Kao, S. J., Jiao, N., and Zhang, Y. (2018). Niche differentiation of ammonia and nitrite oxidizers along a salinity gradient from the Pearl River estuary to the South China Sea. *Biogeosci. Discuss.* 15, 5169–5187. doi: 10.5194/bg-2018-189

Hovanec, T. A., Taylor, L. T., Blakis, A., and DeLong, E. F. (1998). *Nitrospira* like bacteria associated with nitrite oxidation in freshwater aquaria. *Appl. Environ. Microbiol.* 64, 258–264. doi: 10.1002/abio.370180412

Hu, J. H., Zhao, Y. X., Yao, X. W., Wang, J. P., Zheng, P., Xi, C. W., et al. (2021). Dominance of comammox nitrospira in soil nitrification - sciencedirect. *Sci. Total Environ.* 780:146558. doi: 10.1016/j.scitotenv.2021.146558

Hwang, D. W., Kim, G., Lee, Y. W., and Yang, H. S. (2005). Estimating submarine inputs of groundwater and nutrients to a coastal bay using radium isotopes. *Mar. Chem.* 96, 61–71. doi: 10.1016/j.marchem.2004.11.002

Jiao, L. J., Wu, J. P., He, X., Wen, X. M., Li, Y. B., and Hong, Y. G. (2018). Significant microbial nitrogen loss from denitrification and anammox in the land-sea interface of low permeable sediments. *Int. Biodeter. Biodegr.* 135, 80–89. doi: 10.1016/j.ibiod.2018.10.002

Kuypers, M., Marchant, H. K., and Kartal, B. (2018). The microbial nitrogen-cycling network. *Nat. Rev. Microbiol.* 16, 263–276. doi: 10.1038/nrmicro.2018.9

Lebedeva, E. V., Alawi, M., Maixner, F., Jozsa, P. G., Daims, H., and Spieck, E. (2008). Physiological and phylogenetic characterization of a novel lithoautotrophic nitrite-oxidizing bacterium, '*Candidatus Nitrospira Bockiana*'. *Int. J. Syst. Evol. Micr.* 58, 242–250. doi: 10.1099/ijs.0.65379-0

Lebedeva, E. V., Off, S., Zumbrägel, S., Kruse, M., Shagzhina, A., and Lücker, S. (2011). Isolation and characterization of a moderately thermophilic nitrite oxidizing bacterium from a geothermal spring. *FEMS Microbiol. Ecol.* 75, 195–204. doi: 10.1111/j.1574-6941.2010.01006.x

Lee, Y. W., and Kim, G. (2007). Linking groundwater-borne nutrients and dinoflagellate red-tide outbreaks in the southern sea of Korea using a Ra tracer. *Estuar. Coast. Shelf S.* 71, 309–317. doi: 10.1016/j.ecss.2006.08.004

Li, J., Nedwell, D. B., Beddow, J., Dumbrell, A. J., Mckew, B. A., Thorpe, E. L., et al. (2015). *Amo*A gene abundances and nitrification potential rates suggest that benthic ammonia-oxidizing bacteria and not archaea dominate N cycling in the Colne Estuary, United Kingdom. *Appl. Environ. Microbiol.* 81, 159–165. doi: 10.1128/AEM.02654-14

Li, X., Wan, W., Zheng, L., Wang, A., Luo, X., Huang, Q., et al. (2021). Community assembly mechanisms and co-occurrence patterns of nitrite-oxidizing bacteria communities in saline soils. *Sci. Total Environ.* 772:145472. doi: 10.1016/j.scitotenv.2021.145472

Lücker, S., Wagner, M., Maixner, F., Pelletier, E., Koch, H., Vacherie, B., et al. (2010). A *Nitrospira* metagenome illuminates the physiology and evolution of globally important nitrite-oxidizing bacteria. *Proc Natl. Acad. Sci. U.S.A.* 107, 13479–13484. doi: 10.1073/pnas.1003860107

Luo, X., Wang, A., Hou, C., Han, S., Huang, Q., and Chen, W. (2020). The limited effects of carbonaceous material amendments on nitrite-oxidizing bacteria in an Alfisol. *Sci. Total Environ.* 734:139398. doi: 10.1016/j.scitotenv.2020.139398

Moore, W. S. (1996). Large groundwater inputs to coastal waters revealed by 226Ra enrichments. *Nature* 380, 612–614. doi: 10.1038/380612a0

Moore, W. S. (1999). The subterranean estuary: a reaction zone of ground water and sea water. *Mar. Chem.* 65, 111–125. doi: 10.1016/S0304-4203(99)00014-6

Off, S., Alawi, M., and Spieck, E. (2010). Enrichment and physiological characterization of a novel Nitrospira-like bacterium obtained from a marine sponge. *Appl. Environ. Microbiol.* 76, 4640–4646. doi: 10.1128/aem.00320-10

Park, M. R., Park, H., and Chandran, K. (2017). Molecular and kinetic characterization of planktonic *Nitrospira* spp. selectively enriched from activated sludge. *Environ. Sci. Technol.* 51, 2720–2728. doi: 10.1021/acs.est.6b05184

Pester, M., Maixner, F., Berry, D., Rattei, T., Koch, H., Lücker, S., et al. (2014). NxrB encoding the beta subunit of nitrite oxidoreductase as functional and phylogenetic marker for nitrite-oxidizing *Nitrospira*. *Environ. Microbiol.* 16, 3055–3071. doi: 10.1111/1462-2920.12300

Ramanathan, B., Boddicker, A. M., Roane, T. M., and Mosier, A. C. (2017). Nitrifier gene abundance and diversity in sediments impacted by acid mine drainage. *Front. Microbiol.* 8:2136. doi: 10.3389/fmicb.2017.02136

Robinson, C., Li, L., and Barry, A. D. (2007). Effect of tidal forcing on a subterranean estuary. *Ade. Water Resour.* 30, 851–865. doi: 10.1016/j.advwatres.2006.07.006

Sáenz, J. P., Hopmans, E. C., Dan, R., Henderson, P. B., Charette, M. A., Schouten, S., et al. (2012). Distribution of anaerobic ammonia-oxidizing bacteria in a subterranean estuary. *Mar. Chem.* 13, 7–13. doi: 10.1016/j.marchem.2012.04.004

Santos, I. R., Burnett, W. C., Dittmar, T., Suryaputra, I., and Chanton, J. (2009). Tidal pumping drives nutrient and dissolved organic matter dynamics in a gulf of mexico subterranean estuary. *Geochim. Cosmochim. AC.* 73, 1325–1339. doi: 10.1016/j.gca.2008.11.029

Schloss, P. D., Westcott, S. L., Ryabin, T., Hall, J. R., Hartmann, M., Hollister, E. B., et al. (2009). Introducing mothur: open-source, platform-independent, community-supported software for describing and comparing microbial communities. *Appl. Environ. Microb.* 75, 7537–7541. doi: 10.1128/AEM.01541-09

Smith, C. G., and Swarzenski, P. W. (2012). An investigation of submarine groundwater-borne nutrient fluxes to the west florida shelf and recurrent harmful algal blooms. *Limnol. Oceanogr.* 57, 471–485. doi: 10.4319/lo.2012.57.3.0896

Smith, C. G., Cable, J. E., and Martin, J. B. (2008). Episodic high intensity mixing events in a subterranean estuary: effects of tropical cyclones. *Limnol. Oceanogr.* 53, 666–674. doi: 10.2307/40006450

Sun, D., Liu, M., Hou, L., Zhao, M., Tang, X., Zhao, Q., et al. (2021). Community structure and abundance of comammox nitrospira in chongming eastern intertidal sediments. *J. Soil Sediment* 21, 3213–3224. doi: 10.1007/s11368-021-02940-z

Sun, D., Tang, X., Zhao, M., Zhang, Z., Hou, L., Liu, M., et al. (2020). Distribution and diversity of comammox *Nitrospira* in coastal wetlands of China. *Front. Microbiol.* 11:589268. doi: 10.3389/fmicb.2020.589268

Tal, Y., Watts, J. E. M., Schreier, S. B., Sowers, K. R., and Schreier, H. J. (2003). Characterization of the microbial community and nitrogen transformation processes associated with moving bed bioreactors in a closed recirculated mariculture system. *Aquaculture* 215, 187–202. doi: 10.1016/S0044-8486(02)00372-1

Ushiki, N., Fujitani, H., Aoi, Y., and Tsuneda, S. (2013). Isolation of nitrospira belonging to sublineage ii from a wastewater treatment plant. *Microbes. Environ.* 28, 346–353. doi: 10.1264/jsme2.me13042

Wu, J. P., Hong, Y. G., Guan, F., Wang, Y., Tan, Y., Yue, W., et al. (2016). A rapid and high-throughput microplate spectrophotometric method for field measurement of nitrate in seawater and freshwater. *Sci. Rep.* 6:20165. doi: 10.1038/srep20165

Xia, W., Zhang, C., Zeng, X., Feng, Y., Weng, J., Lin, X., et al. (2011). Autotrophic growth of nitrifying community in an agricultural soil. *ISME J.* 5, 1226–1236. doi: 10.1038/ismej.2011.5

Zehr, J. P., and Kudela, R. M. (2011). Nitrogen cycle of the open ocean: from genes to ecosystems. *Annu. Rev. Mar. Sci.* 3, 197–225. doi: 10.1146/annurev-marine-120709-142819

Zhao, M. Y., Tang, X. F., Sun, D. Y., Hou, L. J., Liu, M., Zhao, Q., et al. (2021). Salinity gradients shape the nitrifier community composition in Nanliu River estuary sediments and the ecophysiology of comammox Nitrospira inopinata. *Sci. Total Environ.* 795:148768. doi: 10.1016/j.scitotenv.2021.148768

Zimmerman, G. M., Goetz, H., and Mielke, P. W. (1985). Use of an improved statistical method for group comparisons to study effects of prairie fire. *Ecology* 66, 601–611. doi: 10.2307/1940409

Conflict of Interest: The authors declare that the research was conducted in the absence of any commercial or financial relationships that could be construed as a potential conflict of interest.

Publisher's Note: All claims expressed in this article are solely those of the authors and do not necessarily represent those of their affiliated organizations, or those of the publisher, the editors and the reviewers. Any product that may be evaluated in this article, or claim that may be made by its manufacturer, is not guaranteed or endorsed by the publisher.

Copyright © 2022 Sun, Jiao, Wu, Wei and Hong. This is an open-access article distributed under the terms of the Creative Commons Attribution License (CC BY). The use, distribution or reproduction in other forums is permitted, provided the original author(s) and the copyright owner(s) are credited and that the original publication in this journal is cited, in accordance with accepted academic practice. No use, distribution or reproduction is permitted which does not comply with these terms.

frontiers in Marine Science

ORIGINAL RESEARCH
published: 08 March 2022
doi: 10.3389/fmars.2022.829285

Phytoplankton Species Diversity Patterns and Associated Driving Factors in China's Jiulong River Estuary: Roles That Nutrients and Nutrient Ratios Play

Feiyang Ge[1,2], Zhiyuan Ma[2,3], Bin Chen[2,3], Yu Wang[2], Xiaoqian Lu[1], Shenqun An[1], Dian Zhang[2], Wanting Zhang[2], Weiwei Yu[2,3], Wenxuan Han[1]*, Xingguang Yu[2], Zhenghua Liu[2] and Fangfang Kuang[2]*

[1] Beijing Key Laboratory of Biodiversity and Organic Farming, China Agricultural University, Beijing, China, [2] Third Institute of Oceanography, Ministry of Natural Resources, Xiamen, China, [3] Key Laboratory of Marine Ecological Conservation and Restoration, Ministry of Natural Resources, Xiamen, China

OPEN ACCESS

Edited by:
Meilin Wu,
South China Sea Institute of Oceanology (CAS), China

Reviewed by:
Mi Sun Yun,
Tianjin University of Science & Technology, China
Jianfeng Feng,
Nankai University, China

***Correspondence:**
Weiwei Yu
yuweiwei@tio.org.cn
Wenxuan Han
hanwenxuan@cau.edu.cn

Specialty section:
This article was submitted to Marine Pollution, a section of the journal Frontiers in Marine Science

Received: 05 December 2021
Accepted: 02 February 2022
Published: 08 March 2022

Citation:
Ge F, Ma Z, Chen B, Wang Y, Lu X, An S, Zhang D, Zhang W, Yu W, Han W, Yu X, Liu Z and Kuang F (2022) Phytoplankton Species Diversity Patterns and Associated Driving Factors in China's Jiulong River Estuary: Roles That Nutrients and Nutrient Ratios Play. Front. Mar. Sci. 9:829285. doi: 10.3389/fmars.2022.829285

Understanding diversity patterns and associated driving factors are the critical topics in macroecology and conservation biology. Phytoplankton are highly susceptible to environmental changes in estuaries, particularly eutrophication. This study examined phytoplankton alpha and beta diversity using investigation data in May (springtime), August (summer) and November (autumn) 2009 in China's Jiulong River estuary, where it was easily polluted because of considerable discharge from a highly dense human population and low self-purification capacity with its limited river basin area, potentially resulting in eutrophication and then influencing phytoplankton diversity. Potential influencing factors were also explored, including dissolved oxygen, salinity, nutrients, nutrient ratios, geographic and hydrologic distance, and so on. The results indicated that Shannon's index (*H'*) and Pielou's index (*J*) decreased from the estuary's upper to middle and then increased from middle to lower reaches, Simpson's (*D*) observed the opposite trend and species number (*S*) gradually increased from the estuary's upper to lower reaches. For beta diversity, all the indices showed a gradual decrease trend from the estuary's upper to lower reaches, where also, turnover dominated beta diversity for all seasons. It is noteworthy that the significant roles that nutrients and nutrient ratios played in shaping phytoplankton diversity patterns and the nutrient balance were characterized by excess nitrogen (N) and silicon (Si) and limited phosphorus (P), which could potentially cause diatom blooms. Findings also showed that decreasing Si concentrations can help to reduce overall pollution levels as well as the restoration of the estuary's ecosystem better than just reducing N alone. Accordingly, this study advocates for the protection of the entire estuary system with particular emphasis on its upper reaches. Moreover, greater attention should also be paid to impacts associated with N input and nutrient ratio trade-offs to the prospective watershed management of this estuary. This study

provides a practical approach to explore estuarine diversity in a comprehensive way, which can inform effective biodiversity conservation and also be applied to other marine ecosystems to better guide sustainable management and conservation practices.

Keywords: phytoplankton, diversity pattern, nutrient ratio, nutrient, driving factors

INTRODUCTION

Reducing biodiversity loss has become a global issue on both land and sea (Blowes et al., 2019; Pinsky et al., 2019; Cooper et al., 2020; Trisos et al., 2020). The Earth is presently experiencing an extinction crisis that is largely the result of anthropogenic exploitation, which has caused widespread changes in the global distribution of organisms (Chapin et al., 2000), where roughly one million species are threatened with extinction (Balvanera, 2019). The biodiversity of ocean systems is higher than terrestrial systems, while the rate of loss in marine biodiversity occurs much quicker compared to terrestrial biodiversity caused by climate change and anthropogenic impacts (Blowes et al., 2019; Pinsky et al., 2019; Cooper et al., 2020; Trisos et al., 2020). Furthermore, a decline in marine biodiversity has caused to reduction or loss of some ocean or coastal ecosystem services and functions (Blowes et al., 2019; Pinsky et al., 2019; Cooper et al., 2020; Paul et al., 2020; Trisos et al., 2020).

Estuaries act as transitional zones between brackish and freshwater, where intense material exchanges take place among terrestrial, riverine, and marine ecosystems, subsequently playing a critical role in biogeochemical cycling (Srichandan et al., 2019). High diversity and productivity are critical characteristic of estuarine systems (Dursun and Tas, 2019), which comprise of various ecosystem services and a high natural capital value (Costanza et al., 1997). However, estuaries are susceptible to a variety of natural and anthropogenic disturbances (Gillanders et al., 2011; Atwood et al., 2012; Bucci et al., 2012; O'Brien et al., 2016). It has been estimated that greater than 60% of the world's population and two-thirds of mid- to large-sized cities are distributed within and around estuarine and coastal areas (Ma and Mao, 2014; O'Brien et al., 2016). Over the past half century, intensive anthropogenic disturbances have dramatically increased nutrient inputs into estuaries from inland sources, causing widespread eutrophication (Nixon, 1995; NRC (National Research Council), 2000; Rabalais, 2002; Ho et al., 2019) that ultimately results in the degradation of habitats and a decrease in biodiversity (NRC (National Research Council), 2000; Bricker et al., 2008; Zhao et al., 2010; Clark et al., 2015). Accordingly, nutrient pollution in estuaries and associated effects have garnered increasing attention throughout the world (Liu and Shen, 2001; Li et al., 2014; Paerl et al., 2014; Wallace et al., 2014; Fennel and Testa, 2018; Barletta et al., 2019; Wurtsbaugh et al., 2019).

Being both the most important primary producer and the fundamental component of the food web, phytoplankton are an essential constituent of marine ecosystems (Dursun and Tas, 2019). However, phytoplankton is susceptible to nutrient concentrations (Redfield, 1934; Paerl et al., 2007), whose biomass and patterns will be dramatically altered in the presence of such nutrients. To some extent, the composition, structure, function, and spatiotemporal distribution of phytoplankton indicate the environmental quality status and the biological integrity of aquatic ecosystems (Ekwu and Sikoki, 2006). In macroecology and conservation biology, it is critical to understand phytoplankton spatial diversity patterns (Collen et al., 2013). In doing so, previous studies primarily focused on alpha and gamma diversity (Muylaert et al., 2009; Rochelle-Newall et al., 2011; Guo et al., 2014; Bharathi and Sarma, 2019; Dursun and Tas, 2019), while little attention has been paid to beta diversity. Although both alpha and gamma diversity are indicative of species richness, their spatial scales dramatically differ, where the former refers to in-site diversity (i.e., local species pools) and the latter refers to overall diversity (i.e., regional species pools). Notably differing from alpha and gamma diversity, beta diversity refers to between-site diversity across different habitats, ecosystems, or regions (Whittaker, 1960), which reflect community construction processes as well as biodiversity formation and maintenance (Condit et al., 2002; Kraft et al., 2011; Legendre and De Cáceres, 2013; Li et al., 2016). Given the considerable habitat gradients of estuarine systems (e.g., that associated with salinity levels), beta diversity (used in conjunction with alpha and gamma diversity) and associative patterns provide much more informative results. This approach is key to understanding estuarine response to anthropogenic activities.

Numerous studies have documented many factors that contribute to phytoplankton diversity, which mostly include alpha diversity, such as salinity (Elliot and Whitfield, 2011; Mousing et al., 2016; Bode et al., 2017; Stefanidou et al., 2020), nutrients (Bode et al., 2017), organic matter variables (Bode et al., 2017), hydromorphology (Elliot and Whitfield, 2011), sunlight (Wang et al., 2020), and spatial structure (Moresco et al., 2017; Yang et al., 2017). However, there is only limited information on potential factors that influence beta diversity patterns (Mousing et al., 2016; Moresco et al., 2017; Yang et al., 2017; Stefanidou et al., 2020; Wang et al., 2020), and even less on the different factors between alpha and beta diversity. It is important to note that the significant role that nutrients concentrations play in phytoplankton diversity is widely recognized among researchers (Huppert et al., 2002, 2005; Ji et al., 2016). Additionally, although nutrient ratios have attracted considerable attention from the scientific community, the role they play in natural ecosystems is not well understood (Redfield, 1934; Falkowski and Davis, 2004; Koeve and Kähler, 2010; Mills and Arrigo, 2010; Weber and Deutsch, 2010; Peñuelas et al., 2013). This is because relevant studies have mostly conducted controlled experiments (Chislock et al., 2014; Xu et al., 2014; Thrane et al., 2016; Jacquemin et al., 2018; Schulhof et al., 2019; Bach et al., 2020; Zhou et al., 2021).

The Jiulong River estuary is one of China's most important estuarine systems. It is characterized by an extremely dense human population (13.39 million) that subsists within a limited river basin area (1.47×10^4 km^2) (Fujian Provincial Bureau of Statistics, 2020), which roughly corresponds to approximately 41% of the areas of the Hudson River basin, Canada, under a population density equivalent to New York City, United States. A highly dense human population in conjunction with highly intensive anthropogenic activities pose great pressure on the Jiulong River estuary, where annual dissolved inorganic nitrogen (DIN) flux is 8.278×10^4 t·yr^{-1}, soluble reactive phosphorus (SRP) flux is 0.195×10^4 t·yr^{-1}, and dissolved silica (DSi) flux is 17.831×10^4 t·yr^{-1} (Wu et al., 2017), which may shape and influence phytoplankton diversity patterns, given that phytoplankton are the most sensitive aquatic community to nutrient pollution. This study used the Jiulong River estuary as the study area to (i) examine spatial patterns of phytoplankton species diversity along estuary to offshore gradients, using both alpha and beta diversity; to (ii) explore potential factors that shape diversity patterns, particularly within an environmental context, and to test whether differences exist between alpha and beta diversity; and to (iii) evaluate the relative roles that nutrient concentrations and nutrient ratios play in shaping diversity patterns.

MATERIALS AND METHODS

Study Area

The Jiulong River estuary is situated along China's southeastern coast at the southern point of the East China Sea. This estuary originates from Longyan and Zhangzhou cities, with a total length of 1,923 km and a basin area of 1.47×10^4 km^2 (**Figure 1**; Huang, 2008). Nutrient and pollutant runoff flows into the estuary through three tributaries, namely, the Beixi River, the Xixi River, and the Nanxi River, which together strongly impact the Jiulong River estuary. The estuary is comprised of several ecosystems, such as mangrove, salt marsh, tidal flats, and brackish water, which provide important spawning ground habitats for many marine organisms. In 1988, the Jiulong River Estuary Provincial Mangrove Reserve (with a total area of 420.2 ha) was established to protect its mangrove ecosystem, wetland waterfowl community, and endangered wildlife. The Jiulong River estuary is an also important habitat for the Indo-Pacific humpback dolphin (*Sousa chinensis*), which the IUCN Red List of Threatened Species has classified as "Vulnerable." The estuary also acts as a migratory "stopover" for thousands of migratory waterfowls in the East Asian–Australasian Flyway.

Methodological Approach

The study approach is provided in **Figure 2**. First, species diversity indices were selected and calculated, including alpha and beta diversity. Then, a quantile-quantile test (i.e., Q–Q test) was used to verify data normality of alpha diversity, while Ordinary Kriging was used to map distribution. At the same time, the study area was divided into different subregions based on salinity clustering and geographical characteristics, and beta diversity distribution was mapped for pairwise site and subregion comparisons. Finally, Pearson's r was applied to calculate the relationship between environmental variables and diversity indices, after which optimal equations were obtained by means of stepwise regression, which was used to identify critical environmental factors that contribute to spatial patterns in phytoplankton diversity.

Data Sources

The phytoplankton and environmental data used in this study were obtained from Yu et al. (2012). These data were collected at 21 locations along the estuary during three field campaigns, namely, in May (springtime), August (summer), and November (autumn) 2009 (**Figure 1**). All samples were obtained during low tide. Niskin bottles (5 L) was used to collect water samples, where two water depths were conducted, i.e., surface samples at a water depth below 5 m and bottom samples at a water depth above 5 m. Three duplicate samples were also collected from each location.

Phytoplankton organisms contained in the samples were then transferred to glass sampler bottles and fixed in a 2% glutaraldehyde solution. Referring to traditional phytoplankton identification systems (Jin and Chen, 1960; Hu et al., 1980; Tomas, 1997), species identification and phytoplankton enumeration were conducted using an epifluorescence microscope. The original phytoplankton species data supporting Yu et al. (2012) were provided in the **Supplementary Table 2**.

The environmental data of 15 variables were extracted from the Figures of Yu et al. (2012), including pH, dissolved oxygen (DO), chemical oxygen demand (COD), temperature (T), salinity (Sal), water depth (WD), Total nitrogen (TN), DIN (i.e., the sum total of ammonium, nitrate, and nitrite), silicate (SiO_4^--Si), nitrate (NO_3^--N), nitrite (NO_2^--N), ammonium (NH_4^+-N), total phosphorus (TP), dissolved inorganic phosphorus (DIP), suspended particulate matter (SPM). A multi-parameter probe (YSI 6600 V2) was used to measure pH and DO. A conductivity-temperature-depth (CTD) system was used to measure T, Sal, and WD. Samples used for nutrient concentration measurements were kept in 2 L plastic bottles at −4 °C and measured within a 12 h period at a laboratory. TN, DIN, SiO_4^--Si, NO_3^--N, NO_2^--N, NH_4^+-N, TP, DIP, SPM, and COD were measured following the National Standard of the Oceanographic Survey of China (GB/T 12763.4-2007). Other environmental variables were also calculated based on the above procedure, including the dissolved inorganic nitrogen (DIC) to phosphorus (P) ratio (N/P), the TN to TP ratio (TN/TP), the silicon (Si) to P ratio (Si/P), and the Si to DIN ratio (Si/N).

Hydrologic data used to calculate the hydrologic distance was extracted from Jing et al. (2011), including hydrologic direction and velocity.

Statistical Analysis

The phytoplankton diversity indices selected for this study cover both alpha and beta diversity. For alpha diversity, four typical and widely used indices were selected, including the Shannon index ($H^{'}$), Simpson's index (D), Pielou's evenness index (J), and the Species number (S) index. For beta diversity, this study used the

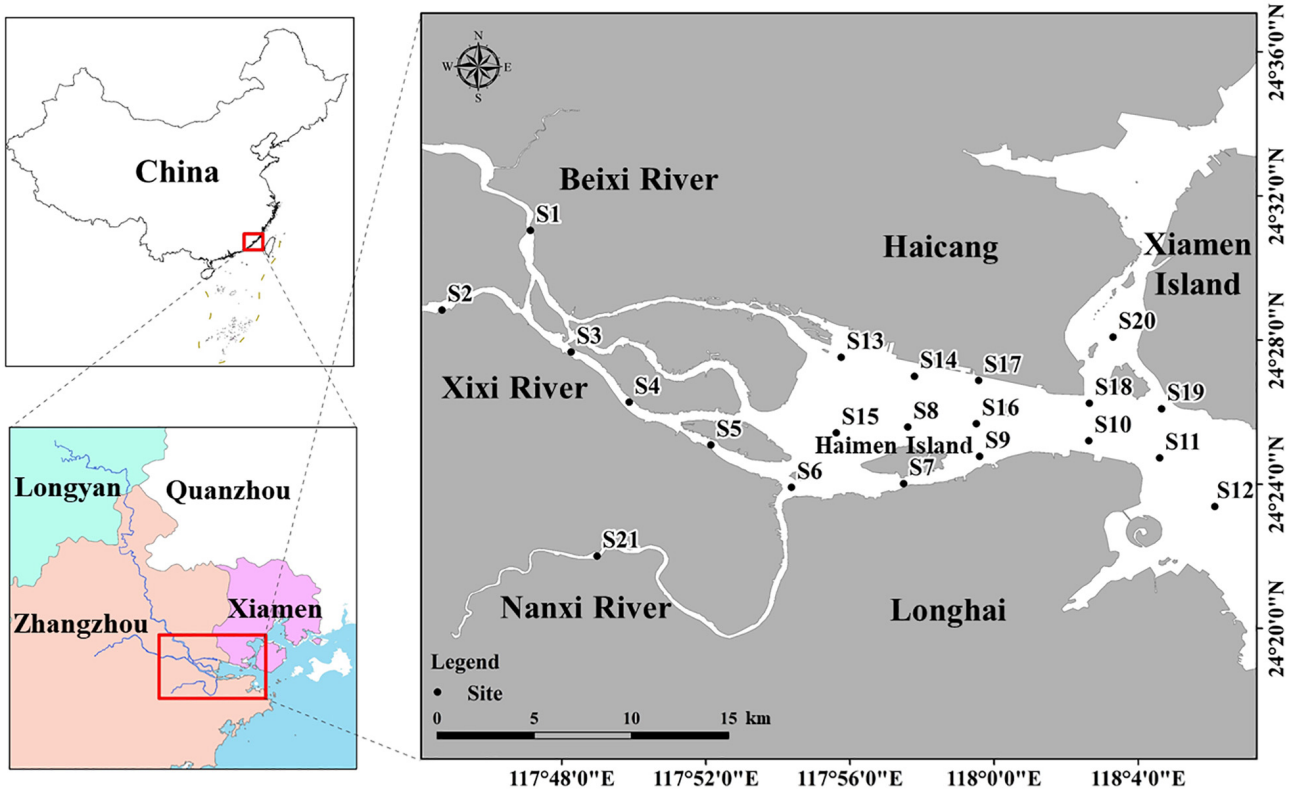

FIGURE 1 | Study area and sampling sites of Jiulong River estuary.

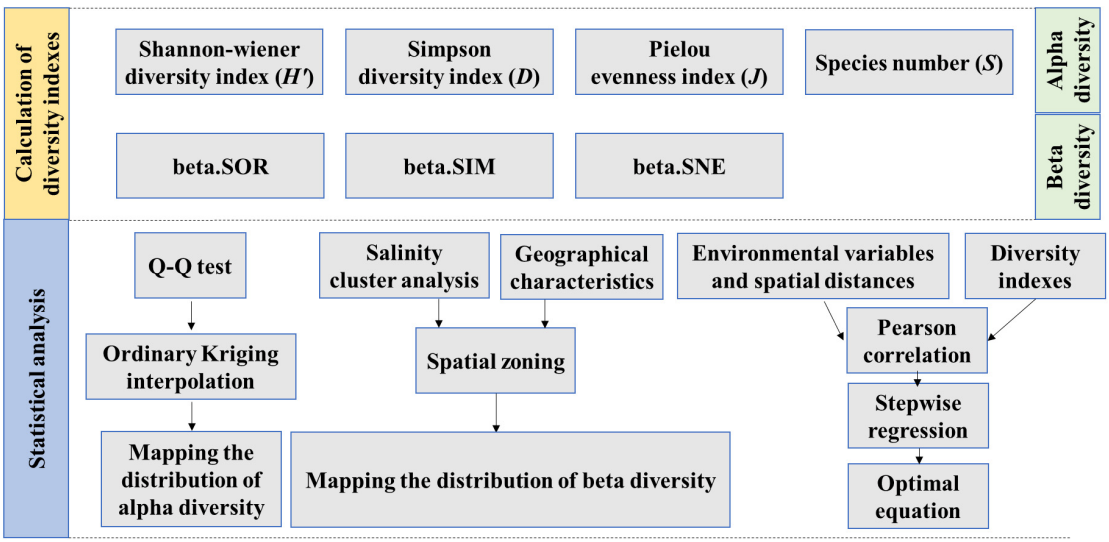

FIGURE 2 | Methodology flowchart.

BAS approach (Baselga, 2010, 2012) to calculate and decompose beta diversity, where the Sørensen pairwise dissimilarity index (*beta.SOR*) was first calculated and then decomposed to a turnover value (*beta.SIM*) and a nestedness value (*beta.SNE*). **Supplementary Table 1** provides the diversity index equations, which were conducted in the packages "vegan" and "beta.part" of R 4.0.2 (Baselga and Orme, 2012).

Spatial subdivision was conducted to further quantify the diversity distribution. The salinity clustering results showed that five distinctive groups were found according to their geographic

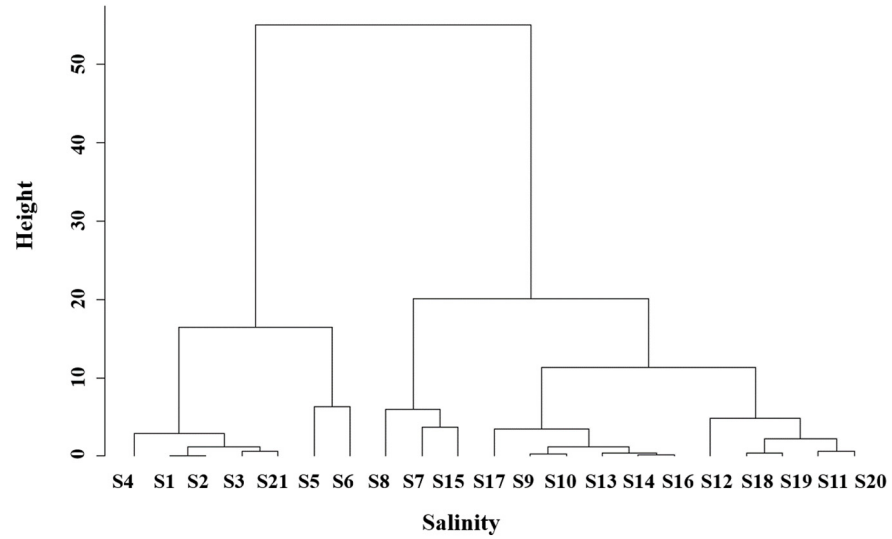

FIGURE 3 | The hclust (Average Linkage Clustering) of the sites according to the salinity.

location, i.e., tributary (S1–S4, S21), river mouth (S5, S6), southern part of middle estuary (S7, S8, S15), northern and eastern part of middle estuary (S9, S10, S13, S14, S16, S17) and outer estuary (S11, S12, S18–S20) (**Figure 3**). Based on salinity clustering groups, combined with the consideration of sampling sites number balance, the study area was subdivided into three subregions, including the upper (Area I), middle (Area II), and lower reaches (Area III) of the estuary (**Figure 4**).

Results from the Q–Q test indicated that alpha diversity data followed normal distribution (see **Supplementary Figure 1**), suggesting that Ordinary Kriging was applicable in mapping the distribution of alpha and gamma diversity, where a linear function was selected as the semi-variant model used in Ordinary Kriging, given that the linear function was optimal for accuracy of cross-validation evaluation. A pairwise site comparison of beta diversity was mapped using a connective line, and averages were used to represent the beta diversity of each subregion. The "ggplot2" package in R 4.0.2 was used to conduct the Q–Q test. ArcGIS 10.7 was used to conduct Ordinary Kriging and biodiversity mapping.

Pearson's *r* was used to quantify relationships between environmental and geographic parameters and diversity indices, which was conducted to identify the driving factors of phytoplankton diversity patterns in the Jiulong River estuary. In total, 63 datasets obtained from three field campaigns were used to analyze correlations between environmental variables and alpha diversity. In total, 210 datasets, covering data from three field campaigns that were mixed among any two sites, were used to analyze correlations between beta diversity and environmental and geographic variables, where differences in environmental variables among pairwise site comparisons were used, while geographic distance and hydrologic distance were used to represent geographic variables, which were, respectively, obtained using the point distance tool of proximity analysis and SDM toolbox incorporating the north and east components of mean flow velocity at 6 h during low tide (because of a regular semidiurnal tide in Jiulong River estuary, Liu, 2012) as the cost resistance surface in ArcGIS 10.7. Additionally, based on Pearson's *r* results, stepwise regression was conducted to obtain optimal equations between variables and diversity indices after data was normalized. This was done to enhance comparisons at the same scale. Forest plots were used to visualize the coefficient strength of key variables in the optimized equation. Pearson's *r*, normalization, stepwise regression, and forest plots were conducted in packages "corrplot," "clusterSim," "car," "grid," "magrittr," "checkmate," and "forestplot" in R 4.0.2, respectively.

RESULTS

Spatial Patterns of Phytoplankton Alpha Diversity

Supplementary Table 3 and **Figure 5** provide the overall spatial variation of phytoplankton alpha diversity indices across three seasons. Shannon index (*H'*) values ranged from 2.23 to 3.51 (2.90 average), where the highest value was measured at S11 (i.e., at the lower reaches of the estuary) and the lowest value was measured at S8 (i.e., at the middle reaches of the estuary). Simpson's index (*D*) values ranged from 0.15 to 0.71 (0.28 average), where the highest value was measured at S1 (i.e., at the upper reaches of the Beixi River estuary) and the lowest value was measured at S3 (i.e., at the upper reaches of the Xixi River estuary). Pielou's evenness (*J*) values ranged from 0.55 to 0.84 (0.67 average), where the highest value was measured at S3 (i.e., at the upper reaches of the Xixi River estuary) and the lowest value was measured at S20 (i.e., the lower reaches of the estuary). Species number (*S*) values ranged from 27 to 59 (45 average), where the highest value was measured at S19 (i.e., the lower reaches of the estuary) and the lowest value was measured at S4 (i.e., the upper reaches of the estuary).

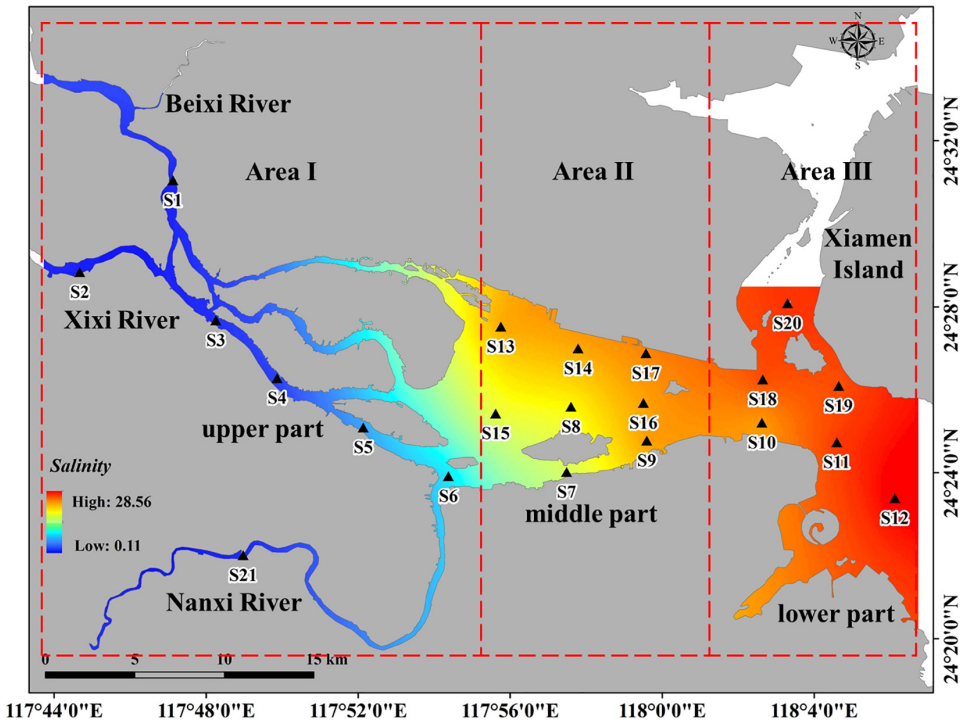

FIGURE 4 | The sub-regions of study area.

Results generally showed a wide range of values in all alpha diversity indices, indicating significant spatial variation among the different sites. A similar gradient was observed in *H'* and *J* values, which gradually decreased from upper to middle and then increased from the middle to lower reaches of the estuary (**Supplementary Table 3** and **Figures 5A,B**). *D* gradually decreased from the upper to lower reaches of the estuary (**Supplementary Table 2** and **Figure 5C**). Conversely, *S* gradually increased from the upper to lower reaches of the estuary (**Supplementary Table 3** and **Figure 5D**). Among the different subregions, the highest *H'* and *S* values were observed in Area III, the highest *J* value was observed in Area I, and the highest *D* was observed in Area II.

Season variations of spatial patterns were observed (**Supplementary Table 3**). The highest *H'* value was found in autumn (3.43 average), followed by spring (2.79 average) and summer (2.46 average), where spatial patterns varied greatly across different seasons, i.e., *H'* value in spring decreased from upper to lower reaches of estuary, while the opposite trend was found in autumn. The highest *J* value was found in autumn (0.75 average), followed by spring (0.70 average) and summer (0.56 average), where their spatial patterns were similar with *H'*. The highest *D* value was found in summer (0.42 average), followed by spring (0.24 average) and autumn (0.19 average), where their spatial patterns were nearly opposite to *H'* and *J*. The *S* values in autumn (24 average) and summer (23 average) were higher than that in spring (16 average), with an increasing spatial trend from upper to lower reaches of estuary for all three seasons.

Spatial Patterns of Phytoplankton Beta Diversity

Pairwise beta diversity site comparisons are shown in **Figure 6**. The *beta.SOR* values ranged from 0.27 to 0.81 (0.4 average), and this large range indicated significant variation between the different sites. A gradual decreasing trend was observed from the upper to lower reaches of the estuary. The highest *beta.SOR* value was observed between S3 (the Xixi River) and S21 (the Nanxi River) at the upper reaches of the estuary, characterized by a low hydrologic exchange between these two different tributaries. On the other hand, the lowest *beta.SOR* value was observed between S10 and S20 at the lower reaches of the estuary, characterized by a small geographic distance and a high hydrologic exchange.

Supplementary Table 3 show the beta diversity of each subregion and associated components. *beta.SOR* values ranged from 0.34 to 0.51 (0.4 average); *beta.SIM* values ranged from 0.31 to 0.43 (0.35 average); *beta.SNE* values ranged from 0.03 to 0.07 (0.05 average). *beta.SOR*, *beta.SIM*, and *beta.SNE* values exhibited the same distribution pattern, namely, a deceasing trend from the upper to lower reaches of the estuary, where the highest value was measured at Area I and the lowest value was measured at Area III. Furthermore, *beta.SIM* dominated *beta.SNE* regardless of the area (i.e., the upper, middle, or lower reaches of the estuary), indicating that species turnover was dominant.

The seasonal similarities and differences of beta diversity patterns were provided in the **Supplementary Table 3**. The same pattern was observed for *beta.SOR* and *beta.SIM*, where temporally, their values in summer and spring were slightly

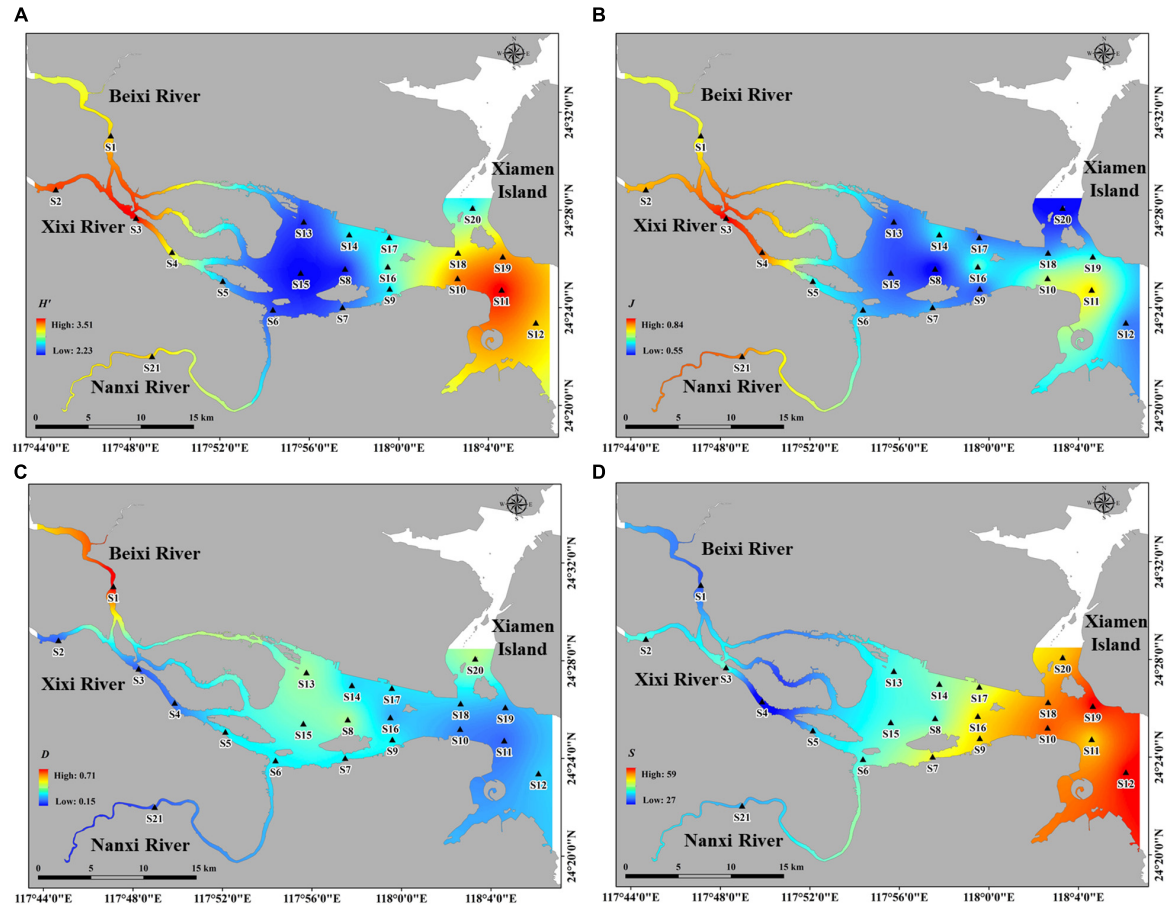

FIGURE 5 | The spatial distribution patterns of alpha diversity and species number. **(A)** Shannon-wiener diversity index. **(B)** Pielou evenness index. **(C)** Simpson diversity index. **(D)** Species number. The darker color indicates the higher diversity.

higher than that in autumn, and spatially, the highest value was found at Area I and the lowest value was found at Area III, indicating a deceasing trend from the upper to lower reaches of the estuary for all three seasons. Fluctuations in *beta.SNE* values differed from the other two indices, it showed inconsistent spatial trends across different seasons, where the highest value was found in Area III in spring, while Area II observed the highest value in summer and autumn. It was noted that *beta.SIM* value was greatly higher than *beta.SNE* across all subregions and seasons, indicating that species turnover was dominant.

Relationships Between Phytoplankton Biodiversity and Environmental and Spatial Variables

Pearson's r values between phytoplankton alpha diversity and environmental variables are shown in **Figure 7A**. Results showed that H' significantly and negatively correlated to T ($r = -0.45$; $p < 0.01$) and NO_2^--N ($r = -0.46$; $p < 0.01$). J significantly and negatively correlated to T ($r = -0.31$, $p < 0.01$), Sal ($r = -0.28$; $p < 0.01$), NO_2^--N ($r = -0.46$; $p < 0.01$), and positively correlated to NO_3^--N ($r = 0.32$; $p < 0.01$), and DIN ($r = 0.26$; $p < 0.01$). D positively correlated to T ($r = 0.32$; $p < 0.01$). Compared to the other alpha diversity indices, S was affected by more environmental variables, where the top six environmental variables that showed a high correlation were Sal ($r = 0.61$; $p < 0.01$), WD ($r = 0.59$; $p < 0.01$), and pH ($r = 0.36$; $p < 0.01$) and those showing a negative correlation were COD ($r = -0.45$; $p < 0.01$), NO_3^--N ($r = -0.44$; $p < 0.01$), and DIN ($r = -0.4$; $p < 0.01$).

The development of optimal regression equations between phytoplankton alpha diversity indices and environmental variables indicated that alpha diversity was influenced by interactions among several environmental factors, and their parameters and coefficients are shown in **Supplementary Figure 2**. The equation for H' parameterized with T and NO_2^--N (adjusted $R^2 = 0.27$; $p < 0.001$; Akaike information criterion [AIC] = −19); J parameterized with Sal and NO_2^--N (adjusted $R^2 = 0.41$; $p < 0.001$; AIC = −31); D parameterized with T (adjusted $R^2 = 0.09$; $p < 0.001$; AIC = −6). By contrast, more parameters were included in the S equation, which parameterized with WD, Sal, NO_3^--N, and TN:TP (adjusted $R^2 = 0.58$; $p < 0.001$; AIC = −48), among which salinity, nutrients (NO_3^--N) and nutrients ratio (TN:TP) were the

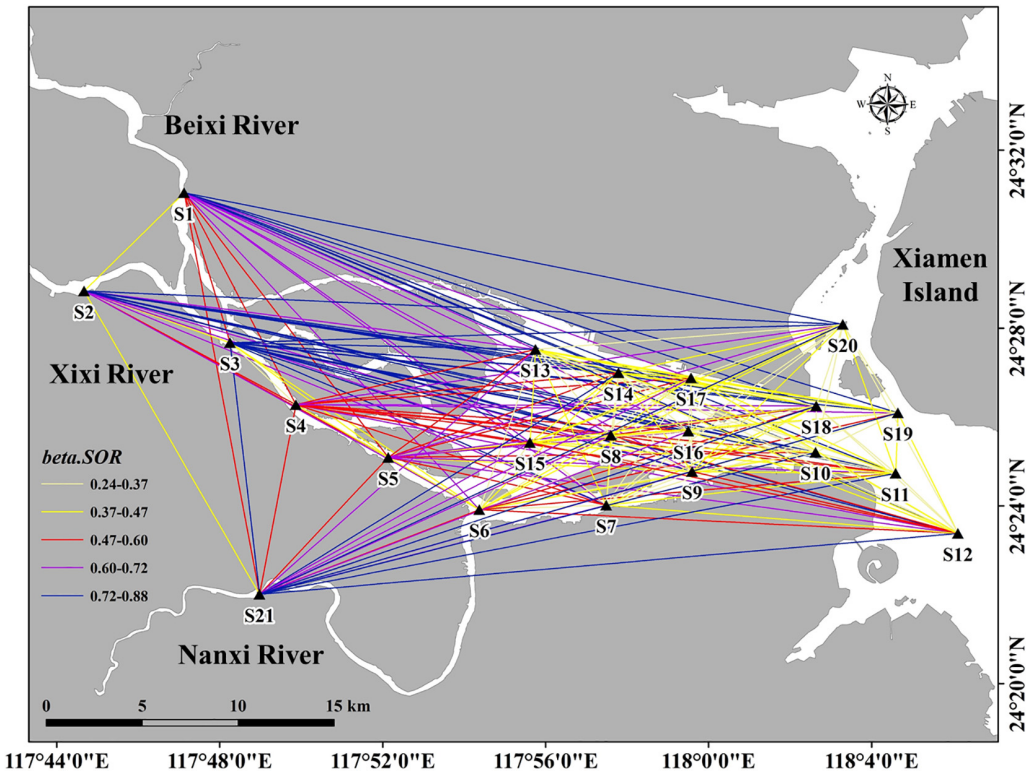

FIGURE 6 | The spatial distribution of pairwise-site beta diversity (*beta.SOR*).

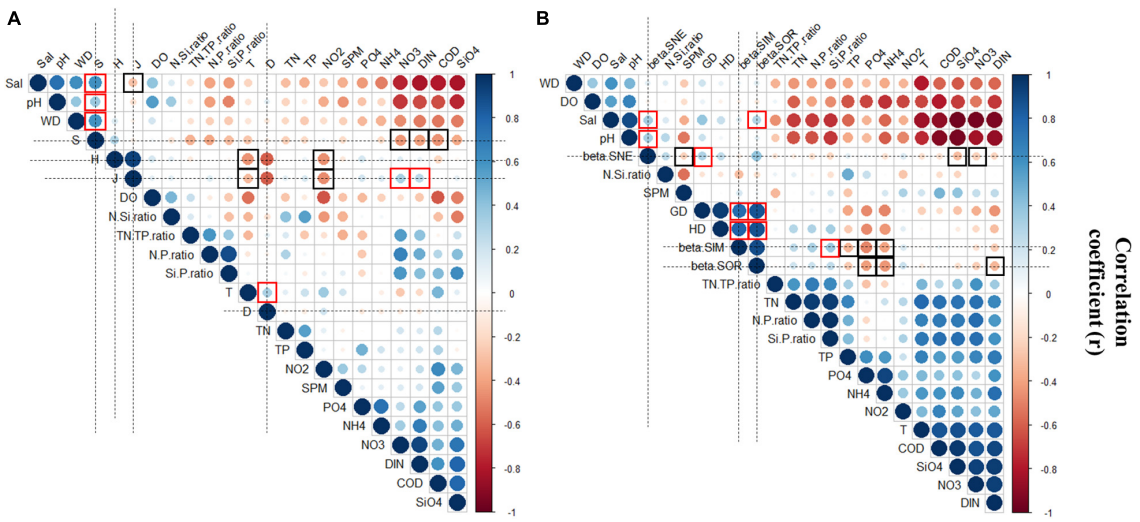

FIGURE 7 | The Pearson's correlation coefficient matrix between diversity and environmental variables and spatial distances. **(A)** The Pearson's correlation coefficient matrix between alpha diversity and environmental variables. **(B)** The Pearson's correlation coefficient matrix between beta diversity and environmental variables and spatial distances. Red represented negative correlations, and blue represented positive correlations. The size of circle indicated the strength of correlation.

most influential environmental variables, yielding high absolute coefficient values. In general, results indicated that *H'*, *D*, and *J* were strongly affected by temperature, salinity, and nutrients, while *S* was mainly affected by salinity, nutrients and nutrient ratios, including NO_3^--N and TN:TP. Low and negative AIC values in all equations indicated the goodness-of-fit of the equations shown above.

Pearson's *r* between phytoplankton beta diversity and environmental variables are shown in **Figure 7B**. Results showed that much more environmental variables significantly influenced

beta.SIM, the top four that showed high correlations were PO_4^{-}-P ($R^2 = -0.48$; $p < 0.01$), NH_4^{+}-N ($R^2 = -0.39$; $p < 0.01$), Si:P ($R^2 = 0.37$; $p < 0.01$) and TP ($R^2 = -0.34$; $p < 0.01$). The correlation strength of the top five (i.e., between *beta.SNE* and environmental variables) was as follows: Sal ($R^2 = 0.34$; $p < 0.01$), pH ($R^2 = 0.32$; $p < 0.01$), SiO_4^{-}-Si ($R^2 = -0.30$; $p < 0.01$), NO_3^{-}-N ($R^2 = -0.23$; $p < 0.01$), and SPM ($R^2 = -0.22$; $p < 0.01$). Analogously, *beta.SOR* correlated to NH_4^{+}-N ($R^2 = -0.44$; $p < 0.01$), PO_4^{-}-P ($R^2 = -0.42$; $p < 0.01$), Sal ($R^2 = 0.28$; $p < 0.01$) and DIN ($R^2 = -0.33$; $p < 0.01$). Additionally, all beta diversity indices significantly and positively correlated to geographic distance (*beta.SOR*, $R^2 = 0.85$, $p < 0.01$; *beta.SIM*, $R^2 = 0.76$, $p < 0.01$; *beta.SNE*, $R^2 = 0.31$, $p < 0.01$), and hydrologic distance (*beta.SOR*, $R^2 = 0.86$, $p < 0.01$; *beta.SIM*, $R^2 = 0.81$, $p < 0.01$; *beta.SNE*, $R^2 = 0.24$, $p < 0.01$).

The optimal regression equations between phytoplankton beta diversity indices and environmental and spatial variables were subsequently developed, and their parameters and coefficients are shown in **Supplementary Figure 3**. The equation for *beta.SIM* parameterized to the nutrients (PO_4^{-}-P, TP, DIN), nutrients ratio (Si:P) and spatial variables (GD, HD) (adjusted $R^2 = 0.78$; $p < 0.001$; AIC = −313), where the nutrients ratio (Si:P) was the crucial parameter with a higher absolute coefficient value. *beta.SNE* parameterized to nutrients (SiO_4^{-}-Si), nutrients ratio (Si:P and N:Si), others (Sal, COD, SPM), and spatial variables (HD) (adjusted $R^2 = 0.51$; $p < 0.001$; AIC = −143), among which nutrients (SiO_4^{-}-Si) was the most influential environmental variables with the highest absolute coefficient value. *beta.SOR* parameterized to nutrients (NO_3^{-}-N, NH_4^{+}-N, TN, and DIN), and spatial variables (GD, HD) (adjusted $R^2 = 0.83$; $p < 0.001$; AIC = −366), among which nutrients (NO_3^{-}-N, NH_4^{+}-N, TN, and DIN) were the most influential environmental variables with high absolute coefficient values. Low and negative AIC values for all equations indicated the goodness-of-fit of the equations shown above.

DISCUSSION

Diversity Patterns Incorporating Alpha and Beta Diversity

Phytoplankton species diversity in the Jiulong River estuary was calculated at two different scales, namely, alpha and beta diversity, where alpha diversity reflects with-in site diversity and beta diversity reflects between-site diversity between sites or subregions. Different diversity scales represent fundamental aspects of biological communities (Socolar et al., 2016), and this is due to the different constructs and mathematical expressions among the various indices.

For overall alpha diversity across three seasons, *H'* and *J* values decreased from the upper to middle and then increased from middle to lower reaches of the Jiulong River estuary. *D* exhibited the opposite trend, and *S* gradually increased from the upper to lower reaches of the Jiulong River estuary Alpha diversity patterns were observed to be complex, and this was due to their multiple indices, which differ in their theoretical foundation and interpretation (Morris et al., 2014). Moreover, *H'* was equally sensitive to rare and abundant species; *J* emphasized evenness; *D* was sensitive in the presence of abundant species; *S* was sensitive to rare species (Shannon, 1948; Simpson, 1949; Pielou, 1969; Peet, 1974; Magurran, 1988; Krebs, 1998; Morris et al., 2014). Observed patterns in the different diversity indices indicated that species abundance was relatively evenly distributed in the upper reaches of the estuary, a greater number of abundant species was observed in the tributary estuary, while a greater number of rare species was observed in the lower reaches of the estuary.

For overall beta diversity across three seasons, *beta.SOR*, *beta.SIM*, and *beta.SNE* values exhibited a general gradient, gradually decreasing along with an increase in salinity gradients from the upper to the lower reaches of the estuary. This trend also reflects the strength of environmental gradients under the hypothesis that diversity is greater in heterogeneous environments. In other words, the standard deviation of most environmental variables in the upper reaches of the estuary was higher than corresponding values in the middle or lower reaches, including T, DO, SPM and all nutrients and nutrient ratios except for NO_2^{-}-N (**Supplementary Table 4**). Analogously, beta diversity patterns of the three subregions showed that their variations gradually decreased from the upper reaches (Area I) to the middle reaches (Area II) to the lower reaches (Area III) of the estuary (*beta.SOR*: $\Delta_{I-II} = 0.146$, $\Delta_{I-II} = 0.024$; *beta.SIM*: $\Delta_{I-II} = 0.114$, $\Delta_{I-II} = 0.014$; *beta.SNE*: $\Delta_{I-II} = 0.032$, $\Delta_{I-II} = 0.01$). Results indicated that phytoplankton communities in the hyposaline upper reaches of the estuary were the most diverse and heterogeneous in species composition, while hypersaline communities were the least diverse and most homogeneous. Besides, there was not seasonal difference in spatial pattern of *beta.SOR* and *beta.SIM*, which was consistent with the decreasing gradient aforementioned from the upper to the lower reaches of the estuary. Slight seasonal variation was found for *beta.SNE*, but *beta.SNE* value was largely lower than *beta.SIM* (see **Supplementary Table 3**).

Beta diversity decomposition can help clarify processes associated with phytoplankton community construction, which typically decompose into species replacement (or turnover) and richness differences or nestedness (i.e., species gain or loss) (Harrison et al., 1992; Williams, 1996). The relative importance of these two components may help us better understand the underlying mechanisms that shape and maintain community diversity distribution patterns (Baselga, 2010; Podani and Schmera, 2011; Fu et al., 2019). In this study, beta diversity patterns in the Jiulong River estuary were mostly dominated by turnover (spring: 90%, summer: 90%, autumn: 88%), which appears to be a common phenomenon across a wide range of taxa in estuary or marine ecosystems, such as macrobenthos (Alsaffar et al., 2017), aquatic plant communities (Bertuzzi et al., 2018), and marine fish (Liggins et al., 2015).

When alpha and beta diversity was combined, although species richness increased along with gradients (i.e., from the upper to lower reaches of the estuary), phytoplankton composition became more homogeneous as environmental differences decreased (see **Supplementary Table 4**). With-in and between-site variation are both important to comprehensively

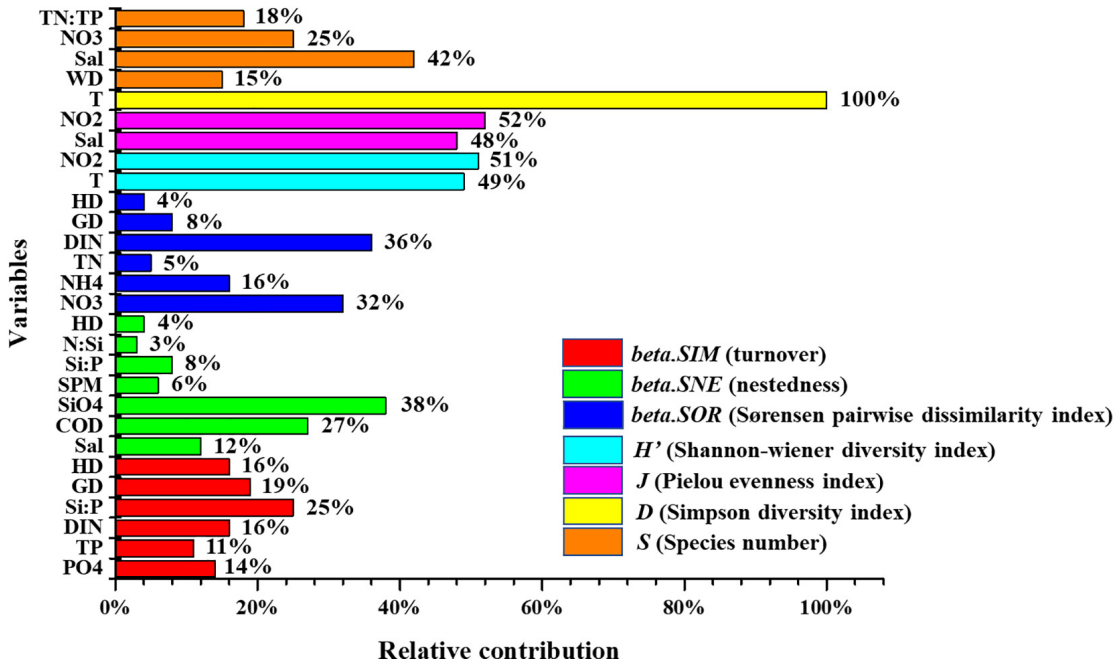

FIGURE 8 | Relative contribution of environmental variables and spatial distances to phytoplankton diversity of the overall.

explore biodiversity patterns. Since the different scales and the different levels of biodiversity make it relatively complex, a single index cannot reasonably be used to explore diversity patterns. Although a variety of diversity indices have been developed to express various aspects of biodiversity, there is no consensus on which diversity index is best (Socolar et al., 2016). Different indices will yield different diversity patterns, showing different aspects of the same natural phenomenon. In Jiulong River estuary, our study indicated that the species richness of phytoplankton was relatively higher in the lower estuary, while phytoplankton was more diverse and heterogeneous in species composition in the upper estuary, informing flexible conservation strategies in line with different objectives. Thus, it is better to explore diversity patterns hierarchically, incorporating both alpha and beta diversity with various other indices.

Key Factors That Shape Phytoplankton Diversity Patterns

Pearson's *r* and stepwise regression results indicated that a few variables correlated to diversity patterns. To more comprehensively identify key factors, this study quantified relative contributions by calculating the absolute coefficient percentage value to all statistically significant variables ($p < 0.001$) obtained from the optimal regression equations (see **Supplementary Figure 2** and **Figure 3**). Results showed that environmental variables, including T, NO_2^--N, Sal, N:P, and Si:P, were the key determinants that shaped alpha diversity patterns in the Jiulong River estuary (see **Supplementary Figure 2**). Differences were observed among the different indices, namely, NO_2^--N and T in *H'* contributed 51 and 49%, NO_2^--N and Sal in *J* contributed 52 and 48%, respectively, while a greater number of environmental determinants in *S* were observed, including Sal (42%), NO_3^--N (25%), TN:TP (18%), and WD (15%) (**Figure 8**).

For *beta.SOR*, *beta.SIM*, and *beta.SNE*, environmental and spatial factors drove beta diversity, where the total contributions of environmental variables were 88, 65, and 96% and that of spatial variables were 12, 35, and 4%, respectively (**Figure 8**). Key environmental determinants of *beta.SOR* included DIN (36%), TN (5%), NO_3^--N (32%), and NH_4^+-N (16%), followed by spatial variables (12%, GD: 8%; HD: 4%). Environmental variables contributed of *beta.SIM* the highest were Si:P (25%), DIN (16%), PO_4^--P (14%), and TP (11%), followed by spatial variables (35%, HD:16%, GD: 19%). Compared to the low spatial variables contribution (4%, HD) of *beta.SNE,* environmental variables played a significant role, namely, SiO_4^--Si (38%), COD (27%), Sal (12%), Si:P (8%), SPM (6%), and N:Si (3%). Although phytoplankton beta diversity was shaped by the limited contribution of spatial variables in the Jiulong River estuary, which could admittedly be due to the relatively small spatial scale of our study, a significant correlation was observed between beta diversity and spatial distance (**Figures 8**, **9**), which is in agreement with findings from previous studies across various taxa in estuary ecosystems (Josefson and Göke, 2013; Josefson, 2016).

Combined with the key factors that influenced alpha and beta diversity, our study found that environmental factors significantly influenced alpha and beta diversity. Moreover, beta diversity was also influenced by spatial distances. Although many studies have shown a strong relationship between spatial distance and beta diversity respective to different taxa in estuarine systems, such as phytoplankton (Josefson and Göke, 2013), benthic invertebrates (Josefson and Göke, 2013), and bivalve mollusks

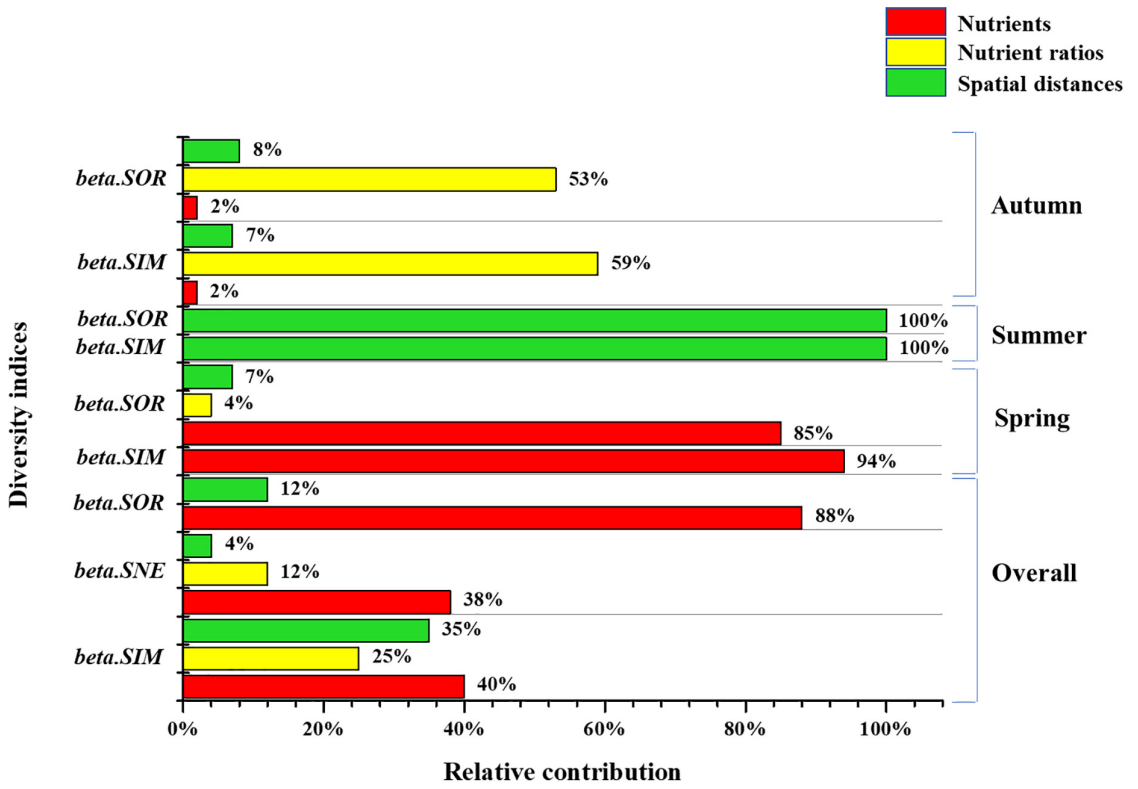

FIGURE 9 | Relative contributions of nutrients, nutrient ratios and spatial distances in beta diversity.

(Chust et al., 2013), most of these studies focused on passive dispersal or less mobile species, and the relationship between distance and highly mobile species in estuarine systems is not yet clear. In our study, compared with environmental variables, spatial distance (geographic and hydrologic distance) showed a lower contribution, for example, only about 12% contribution of spatial distances to the beta.SOR (**Figure 9**), which might be mainly because of the limited spatial scale in Jiulong River estuary. Thus, it was worthy to examine the contribution of spatial distance to phytoplankton beta diversity in a larger scale in further studies.

Roles of Nutrients and Nutrient Ratios in Shaping Phytoplankton Diversity Patterns

Our study found high correlations between phytoplankton diversity indices and environmental variables of nutrients and nutrient ratios in the Jiulong River estuary, indicating that nutrients and nutrient ratios contributed significantly to phytoplankton biodiversity patterns, which is in agreement with findings from previous studies conducted in similar estuarine environments (Schoor et al., 2008; Li et al., 2010; Huang et al., 2013; Chu et al., 2014; Zhang et al., 2015; Anselme et al., 2018). The relative contribution was quantified by calculating the percentage of the absolute coefficient value of all relevant variables that yielded a statistically significant value ($p < 0.001$) from optimal regression equations (see **Figures 9**, **10**). Results showed that nutrients contributed 25, 52, 51, 40, 38, and 88% to *S*, *J*, *H'*, *beta.SIM*, *beta.SNE*, and *beta.SOR*, respectively, while nutrients ratio contributed 17, 12, and 25% to *S*, *beta.SNE*, and *beta.SIM*, respectively (**Figures 9**, **10**). In general, nutrients and nutrient ratios contributed significantly to beta diversity and overwhelmingly to alpha diversity, where nutrient ratios influenced *S*, *beta.SIM* and *beta.SNE* and nutrients significantly influenced *beta.SOR*.

The results indicated that key variables with greatest contribution to beta diversity varied among different seasons, i.e., nutrients in spring, spatial distances in summer and nutrient ratios in autumn, respectively (see **Supplementary Table 4**). The seasonal difference above might due to the variation of specific variable, such greatest variation of nutrients (TN and TP) found in spring, nutrient ratios (N:P and Si:P) in autumn; by contract, the variation was slight for environmental variables in summer, so spatial distance played a more important role in shaping communities differences between sites (**Figure 9**).

Previous studies conducted on nutrient ratios primarily focused on N:P and Si:P (Schoor et al., 2008; Li et al., 2010; Huang et al., 2013; Chu et al., 2014; Zhang et al., 2015), while relatively few focused on Si:N (Li et al., 2010; Chu et al., 2014). Justić et al. (1995) proposed that P limitation could potentially occur under conditions where Si:P > 22 and N:P > 22, N limitation could potentially occur under conditions where N:P < 10 and N:Si < 1,

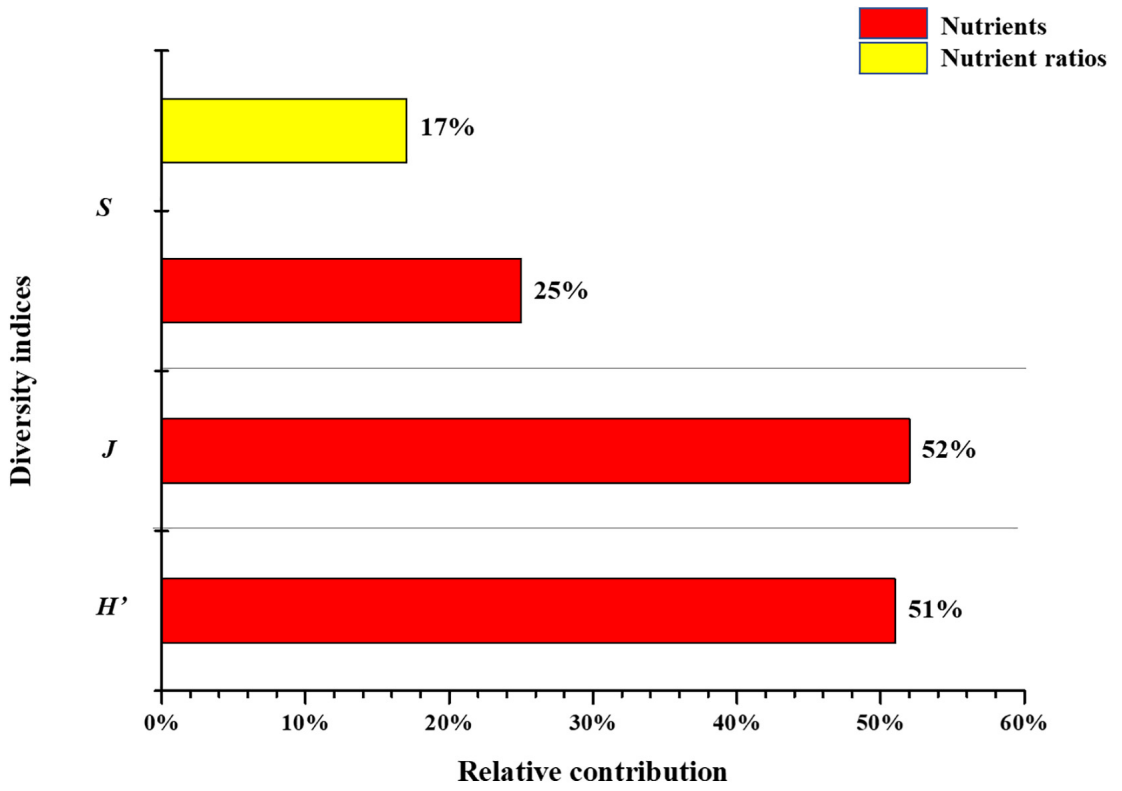

FIGURE 10 | Relative contributions of nutrients and nutrient ratios in alpha diversity.

and Si limitation could potentially occur under conditions where Si:P < 10 and N:Si > 1. In our study, P limitation could potentially occur under conditions of high Si:P and N:P in the Jiulong River estuary, where the former ranged from 19 to 933 (118 average) and the latter ranged from 16 to 322 (51 average) (**Figure 11**). Additionally, the fact that both N:P and Si:P exceeded a value of 10 at all sampling sites (**Figure 11**), the probability of Si and N limitation was low. Our study found that P was a potential limiting factor in the Jiulong River estuary, while the estuary was clearly N-enriched, Si-enriched, and P-limited.

The same nutrient ratio phenomenon was observed in the Yangtze River and Pearl River estuaries, being the two largest and most densely populated and economically developed estuaries in China, where Si:P and N:P values exceeded the recommended threshold (22) (Yin et al., 2001; Li et al., 2010), indicating that similar to the Jiulong River estuary, they were also N-enriched, Si-enriched, and P-limited. However, compared to these two large estuaries, Si:P, N:P, and N:Si values in the Jiulong River estuary were all lower (**Figure 12**), indicating that the nutrient condition of the Jiulong River estuary was more balanced than these estuaries, even with respect to the general condition along the Chinese coast (**Figure 12**).

Given that different phytoplankton species differ in their nutrient demands, nutrient concentrations and nutrient ratios may affect phytoplankton diversity (Redfield, 1934; Paerl and Justić, 2013). Additionally, N and P are essential nutrients for all phytoplankton species (Paerl and Justić, 2013), while Si is mostly specific to diatoms (Officer and Ryther, 1980). Taking this into account, we inferred that N played a more important role in phytoplankton diversity patterns than P and Si in the Jiulong River estuary. This is because of a nutrient concentration imbalance in different elements characterized by enriched N, limited P, and specifically Si. We also found that diatoms became more prevalent in the Jiulong River estuary as Si concentrations increased, where diatoms accounted for large proportion of species composition of the phytoplankton community (i.e., 90% in summer and 87% in autumn). Therefore, nutrient concentrations and nutrient ratios may influence phytoplankton diversity patterns. Accordingly, more attention should be paid to trade-offs among nutrient elements instead of just solely focusing on specific nutrient concentrations.

Recommended Jiulong River Estuary Ecosystem Management Practices

Increasingly, beta diversity has been used to guide biodiversity conservation, such as the design of protected areas, the identification of priority areas, and the establishment of ecological corridors (Cody, 1986; Thomas, 1990; Harrison et al., 1992; Pimm and Gittleman, 1992; Nekola and White, 1999; Myers et al., 2000; Wu et al., 2010; Fattorini, 2011). The two beta diversity components reflect two different

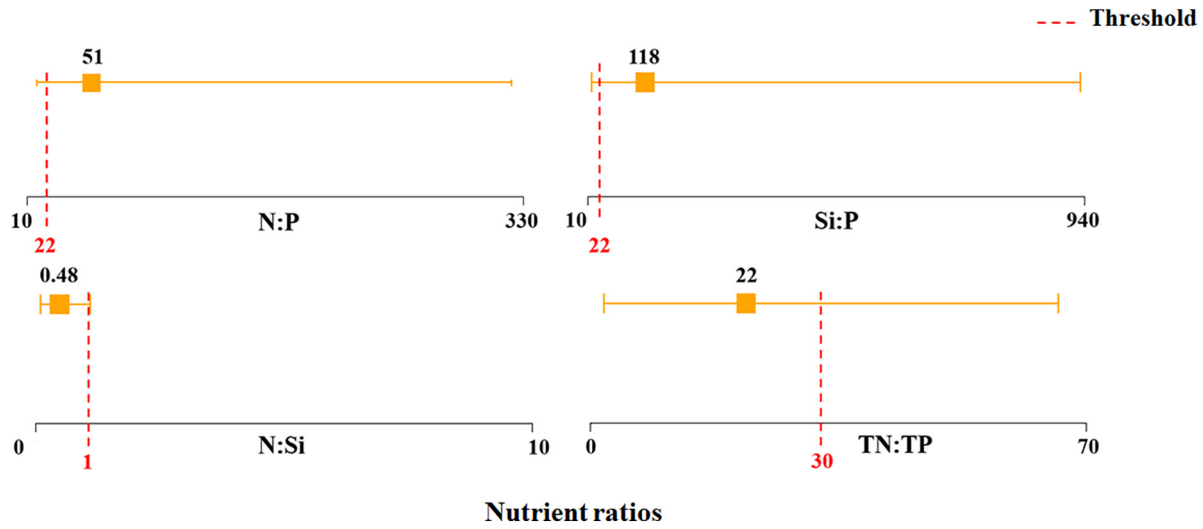

FIGURE 11 | The range and average of nutrient ratios. Yellow line represented the range values of nutrient ratio in Jiulong River Estuary, and yellow square represented their average. Red dashed line represented the threshold of nutrient ratios to inform potential P, N, and Si limitation (Justić et al., 1995).

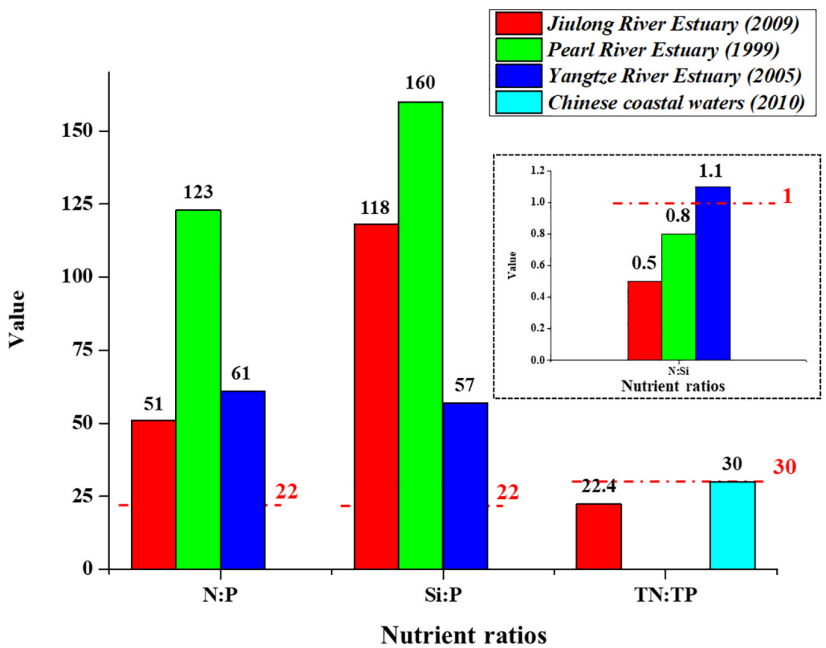

FIGURE 12 | The average of nutrient ratios in Yangtze River Estuary (Li et al., 2010), Pearl River Estuary (Yin et al., 2001), Jiulong River Estuary and Chinese coastal waters (Wang et al., 2021). Red dashed line represented the threshold of nutrient ratio to inform potential P, N, and Si limitation (Justić et al., 1995).

or even opposite processes in community construction (Gaston and Blackburn, 2000; Baselga, 2012); thus, beta diversity decomposition should be incorporated into biodiversity conservation rather than accounting for beta diversity alone (Angeler, 2013). Baselga (2010) suggested that when turnover dominates, the entire area should be protected, while when nestedness dominates, only sites or areas with the highest species richness should be protected to conserve the entire area. On this account, the entire Jiulong River estuary should be protected due to its dominant turnover pattern (accounting for 85%). Additionally, when using alpha and beta diversity, more attention should be paid to conserving diverse species composition of phytoplankton in the upper reaches, and protecting its species abundance in the lower reaches.

This study showed that the Jiulong River estuary is N-enriched, Si-enriched, and P-limited, where an excess in N and Si may lead to eutrophication and impact phytoplankton

diversity. Compared to the Yangtze River and Pearl River estuaries, the nutrient status in the Jiulong River estuary was more balanced. Phytoplankton take up extraneous nutrients at a fixed ratio (Redfield ratio: C:N:P = 106:16:1; Redfield, 1934) to meet their own growth and survival requirements, and diatoms specifically require Si in addition to C, N, and P, absorbing Si and N on a 1:1 M basis (Officer and Ryther, 1980). Although there is a strong consensus that N is the primary cause of eutrophication in aquatic marine ecosystems (Paerl, 2009; Cosme et al., 2015), the relatively high Si (compared to N) in the Jiulong River estuary poses a potential algal bloom threat. With an increase in Si concentrations in the Jiulong River estuary, the composition of phytoplankton species richness gradually led to the dominance of diatoms. For example, diatoms accounted for roughly 90% of phytoplankton species richness in our study, which may impact phytoplankton diversity. Therefore, instead of solely focusing on reducing N pollution, it is recommended to also reduce Si concentrations during ecosystem restoration initiatives. This will help restructure the phytoplankton community and prevent algal blooms (via diatoms).

CONCLUSION

Phytoplankton is one of the most susceptible aquatic organisms to environmental change in estuaries, especially regarding eutrophication. In this study, phytoplankton diversity patterns and their potential factors (particularly nutrient concentrations and nutrient ratios) were examined, using both alpha and beta diversity in the Jiulong River estuary, China. Our study indicated that diversity patterns were shown to vary at different scales, in different seasons and in different indices in Jiulong River estuary, where the phytoplankton species richness was higher in autumn and in the lower estuary, while phytoplankton was more diverse and heterogeneous in its composition in the upper estuary, highlighting that it is better to explore diversity patterns hierarchically to inform an effective conservation strategy. Environmental factors had a significant influence on both alpha and beta phytoplankton diversity in Jiulong River estuary, particularly nutrient concentrations and nutrient ratios, characterized by an excess in N and Si but limited P. Our findings provide an important information to enhance biodiversity conservation in Jiulong River estuary in a comprehensive way, and also offer a practical approach and analytically based information to protect estuarine or even other marine ecosystem diversity, which can be applied to other estuaries to better guide sustainable management and conservation practices.

DATA AVAILABILITY STATEMENT

The raw data supporting the conclusions of this article will be made available by the authors, without undue reservation.

AUTHOR CONTRIBUTIONS

FG: perform the research. FG, WY, and WH: methodology, data wrangling, and project administration. FG, YW, XL, SA, DZ, WZ, and FK: data analyze. XY, ZM, and ZL: resources and data collection. WY, WH, ZM, and BC: supervision. BC, XY, and WY: funding acquisition. All authors contributed to the conceptualization, writing, review, and editing of the manuscript, and read and agreed to the published version of the manuscript.

FUNDING

This article was funded by the National Key research and Development Program of China (2017YFA0604902), the National Natural Science Foundation of China (42076163 and 42176171), and Marine Public Welfare Project of China (200805064).

SUPPLEMENTARY MATERIAL

The Supplementary Material for this article can be found online at: https://www.frontiersin.org/articles/10.3389/fmars.2022.829285/full#supplementary-material

REFERENCES

Alsaffar, Z., Cúrdia, J., Borja, A., Irigoien, X., and Carvalho, S. (2017). Consistent variability in beta-diversity patterns contrasts with changes in alpha-diversity along an onshore to offshore environmental gradient: the case of red sea soft-bottom macrobenthos. *Mar. Biodiv.* 49, 247–262. doi: 10.1007/s12526-017-0791-3

Angeler, D. G. (2013). Revealing a conservation challenge through partitioned long-term beta diversity: increasing turnover and decreasing nestedness of boreal lake metacommunities. *Divers. Distrib.* 19, 772–781. doi: 10.1111/ddi.12029

Anselme, C. M., Gisele, F. Y. G., Jules, R. N. N., Manfred, D. B., Fils, M. O., and Raphaël, O. (2018). Assessment of water quality in the lower nyong estuary (cameroon, atlantic coast) from environmental variables and phytoplankton communities composition. *Afr. J. Environ. Sci. Technol.* 12, 198–208. doi: 10.5897/ajest2017.2454

Atwood, T. B., Wiegner, T. N., and MacKenzie, R. A. (2012). Effects of hydrological forcing on the structure of a tropical estuarine food web. *Oikos* 121, 277–289. doi: 10.1111/j.1600-0706.2011.19132.x

Bach, L. T., Paul, A., Boxhammer, T., von der Esch, E., Graco, M., Schulz, K., et al. (2020). Factors controlling plankton community production, export flux, and particulate matter stoichiometry in the coastal upwelling system off Peru. *Biogeosciences* 17, 4831–4852. doi: 10.5194/bg-17-4831-2020

Balvanera, P. (2019). Societal burdens of nature loss. *Science* 366, 184–185. doi: 10.1126/science.aaz1433

Barletta, M., Lima, A. R. A., and Costa, M. F. (2019). Distribution, sources and consequences of nutrients, persistent organic pollutants, metals and microplastics in south American estuaries. *Sci. Total Environ.* 651, 1199–1218. doi: 10.1016/j.scitotenv.2018.09.276

Baselga, A. (2010). Partitioning the turnover and nestedness components of beta diversity. *Glob. Ecol. Biogeogr.* 19, 134–143. doi: 10.1111/j.1466-8238.2009.00490.x

Baselga, A. (2012). The relationship between species replacement, dissimilarity derived from nestedness, and nestedness. *Glob. Ecol. Biogeogr.* 21, 1223–1232. doi: 10.1111/j.1466-8238.2011.00756.x

Baselga, A., and Orme, C. D. L. (2012). betapart: an R package for the study of beta diversity. *Methods Ecol. Evol.* 3, 808–812. doi: 10.1111/j.2041-210x.2012.00224.x

Bertuzzi, T., Pires, M. M., and Maltchik, L. (2018). Drivers of the beta diversity of aquatic plant communities along a latitudinal gradient in southern Brazilian coastal ponds. *J. Veg. Sci.* 30, 281–290. doi: 10.1111/jvs.12711

Bharathi, M. D., and Sarma, V. S. (2019). Impact of monsoon-induced discharge on phytoplankton community structure in the tropical Indian estuaries. *Reg. Stud. Mar. Sci.* 31:100795. doi: 10.1016/j.rsma.2019.100795

Blowes, S. A., Supp, S. R., Antão, L. H., Bates, A., Bruelheide, H., Chase, J. M., et al. (2019). The geography of biodiversity change in marine and terrestrial assemblages. *Science* 366, 339–345. doi: 10.1126/science.aaw1620

Bode, A., Varela, M., Prego, R., Rozada, F., and Santos, M. D. (2017). The relative effects of upwelling and river flow on the phytoplankton diversity patterns in the ria of a coruña (NW Spain). *Mar. Biol.* 164:93. doi: 10.1007/s00227-017-3126-9

Bricker, S. B., Longstaff, B., Dennison, W., Jones, A., Boicourt, K., Wicks, C., et al. (2008). Effects of nutrient enrichment in the nation's estuaries: a decade of change. *Harmful Algae.* 8, 21–32. doi: 10.1016/j.hal.2008.08.028

Bucci, A. F., Ciotti, ÁM., Pollery, R. C. G., de Carvalho, R., de Albuquerque, H. C., and Simões, L. T. S. (2012). Temporal variability of chlorophyll-a in the São vicente estuary. *Braz. J. Oceanogr.* 60, 485–499. doi: 10.1590/s1679-87592012000400007

Chapin, F. S. III, Zavaleta, E. S., Eviner, V. T., Naylor, R. L., Vitousek, P. M., Reynolds, H. L., et al. (2000). Consequence of changing biodiversity. *Nature* 405, 232–242. doi: 10.1038/35012241

Chislock, M. F., Sharp, K. L., and Wilson, A. E. (2014). Cylindrospermopsis raciborskii dominates under very low and high nitrogen-to-phosphorus ratios. *Water Res.* 49, 207–214. doi: 10.1016/j.watres.2013.11.022

Chu, T. V., Torréton, J. P., Mari, X., Nguyen, H. M. T., Pham, K. T., Pham, T. T., et al. (2014). Nutrient ratios and the complex structure of phytoplankton communities in a highly turbid estuary of Southeast Asia. *Environ. Monit. Assess.* 186, 8555–8572. doi: 10.1007/s10661-014-4024-y

Chust, G., Albaina, A., Aranburu, A., Borja, Á, Diekmann, O. E., Estonba, A., et al. (2013). Connectivity, neutral theories and the assessment of species vulnerability to global change in temperate estuaries. *Estuar. Coast. Shelf Sci.* 131, 52–63. doi: 10.1016/j.ecss.2013.08.005

Clark, G. F., Kelaher, B. P., Dafforn, K. A., Coleman, M. A., Knott, N. A., Marzinelli, E. M., et al. (2015). What does impacted look like? High diversity and abundance of epibiota in modified estuaries. *Environ. Pollut.* 196, 12–20. doi: 10.1016/j.envpol.2014.09.017

Cody, M. L. (1986). "Diversity, rarity, and conservation in mediterranean-climate regions," in *Conservation Biology: The Science of Scarcity and Diversity*, ed. M. E. Soulé (Sunderland, MA: Sinauer Associates), 122–152. doi: 10.1016/j.scitotenv.2016.09.097

Collen, B., Whitton, F., Dyer, E. E., Baillie, J. E. M., Cumberlidge, N., Darwall, W. R. T., et al. (2013). Global patterns of freshwater species diversity, threat and endemism. *Glob. Ecol. Biogeogr.* 23, 40–51. doi: 10.1111/geb.12096

Condit, R., Pitman, N., Leigh, E. G. Jr., Chave, J., Terborgh, J., Foster, R. B., et al. (2002). Beta-diversity in tropical forest trees. *Science* 295, 666–669. doi: 10.1126/science.1066854

Cooper, G. S., Willcock, S., and Dearing, J. A. (2020). Regime shifts occur disproportionately faster in larger ecosystems. *Nat. Commun.* 11:15029. doi: 10.1038/s41467-020-15029-x

Cosme, N., Koski, M., and Hauschild, M. Z. (2015). Exposure factors for marine eutrophication impacts assessment based on a mechanistic biological model. *Ecol. Modell.* 317, 50–63. doi: 10.1016/j.ecolmodel.2015.09.005

Costanza, R., d' Arge, R., de Groot, R., Farber, S., Grasso, M., Hannon, B., et al. (1997). The value of the world's ecosystem services and natural capital. *Nature* 387, 253–260. doi: 10.1038/387253a0

Dursun, F., and Tas, S. (2019). Variations in abundance and diversity of phytoplankton in the surface waters of the golden horn estuary (sea of marmara). *J. Mar. Biol. Assoc. U.K.* 99, 279–290. doi: 10.1017/s0025315418000073

Ekwu, A. O., and Sikoki, F. D. (2006). Phytoplankton diversity in the cross river estuary of nigeria. *J. Appl. Sci. Environ. Mgt. March.* 10, 89–95. doi: 10.4314/jasem.v10i1.17296

Elliot, M., and Whitfield, A. K. (2011). Challenging paradigms in estuarine ecology and management. *Estuar. Coast. Shelf Sci.* 94, 306–314. doi: 10.1016/j.ecss.2011.06.016

Falkowski, P. G., and Davis, C. S. (2004). Natural proportions. *Nature* 431:131. doi: 10.1038/431131a

Fattorini, S. (2011). Insect rarity, extinction and conservation in urban rome (italy): a 120-year-long study of tenebrionid beetles. *Insect. Conserv. Divers.* 4, 307–315. doi: 10.1111/j.1752-4598.2010.00129.x

Fennel, K., and Testa, J. M. (2018). Biogeochemical controls on coastal hypoxia. *Annu. Rev. Mar. Sci.* 11, 4.1–4.26. doi: 10.1146/annurev-marine-010318-095138

Fu, H., Yuan, G., Jeppesen, E., Ge, D., Li, W., Zou, D., et al. (2019). Local and regional drivers of turnover and nestedness components of species and functional beta diversity in lake macrophyte communities in China. *Sci. Total Environ.* 687, 206–217. doi: 10.1016/j.scitotenv.2019.06.092

Fujian Provincial Bureau of Statistics (2020). *The Statistical Bulletin of National Economic and Social Development of Fujian Province*. Fuzhou: Fujian Daily News. 2019.

Gaston, K. J., and Blackburn, T. M. (2000). *Pattern and Process in Macroecology*. Oxford: Blackwell Science.

Gillanders, B. M., Elsdon, T. S., Halliday, I. A., Jenkins, G. P., Robins, J. B., and Valesini, F. J. (2011). Potential effects of climate change on *Australian estuaries* and fish utilising estuaries: a review. *Mar. Freshw. Res.* 62:1115. doi: 10.1071/mf11047

Guo, P., Shen, H., and Wang, J. (2014). Species diversity, community structure and distribution of phytoplankton in the changjiang estuary during dry and flood periods. *J. Mar. Biol. Assoc. U.K.* 94, 459–472. doi: 10.1017/s0025315413001641

Harrison, S., Ross, S. J., and Lawton, J. H. (1992). Beta diversity on geographic gradients in britain. *J. Anim. Ecol.* 61, 151–158. doi: 10.2307/5518

Ho, J. C., Michalak, A. M., and Pahlevan, N. (2019). Widespread global increase in intense lake phytoplankton blooms since the 1980s. *Nature* 574, 667–670. doi: 10.1038/s41586-019-1648-7

Hu, H., Li, Y., Wei, Y., Zhu, H., Chen, J., and Shi, Z. (1980). *Algae in Fresh Waters of China*. Shanghai: Shanghai Science and Technology Press.

Huang, W., Zhu, X., Chen, Q., He, Q., Liao, Y., Du, P., et al. (2013). Seasonal variability of phytoplankton community structure in relation to different nitrogen-phosphorus ratios in the southern coastal waters of zhejiang, China. *J. Ocean Univ. China* 12, 577–588. doi: 10.1007/s11802-013-2192-y

Huang, X. (2008). Hydrological characteristics of jiulong river basin. *Hydraul. Sci. Technol.* 1, 16–20.

Huppert, A., Blasius, B., and Stone, L. (2002). A model of phytoplankton blooms. *Am. Nat.* 159, 156–171. doi: 10.1086/324789

Huppert, A., Blasius, B., Olinky, R., and Stone, L. (2005). A model for seasonal phytoplankton blooms. *J. Theor. Biol.* 236, 276–290. doi: 10.1016/j.jtbi.2005.03.012

Jacquemin, C., Bertrand, C., Oursel, B., Thorel, M., Franquet, E., and Cavalli, L. (2018). Growth rate of alpine phytoplankton assemblages from contrasting watersheds and N-deposition regimes exposed to nitrogen and phosphorus enrichments. *Freshw. Biol.* 63, 1326–1339. doi: 10.1111/fwb.13160

Ji, X., Yuan, S., and Zhu, H. (2016). Analysis of a stochastic model for algal bloom with nutrient recycling. *Int. J. Biomath.* 9:1650083. doi: 10.1142/s1793524516500832

Jin, D., and Chen, Z. (1960). *Benthtic Diatoms in China Sea*. Beijing: Ocean Press.

Jing, C., Zhu, X., Bao, X., and Song, D. (2011). Three dimensional tidal current numerical simulation based on FVCOM in and around Xiamen bay. *J. Oceanogr. Taiwan Strait.* 30, 103–113. doi: 10.3969/J.ISSN.1000-8160.2011.01.016

Josefson, A. B. (2016). Species sorting of benthic invertebrates in a salinity gradient – importance of dispersal limitation. *PLoS One* 11:e0168908. doi: 10.1371/journal.pone.0168908

Josefson, A. B., and Göke, C. (2013). Disentangling the effects of dispersal and salinity on beta diversity in estuarine benthic invertebrate assemblages. *J. Biogeogr.* 40, 1000–1009. doi: 10.1111/jbi.12047

Justić, D., Rabalais, N. N., Turner, R. E., and Dortch, Q. (1995). Changes in nutrient structure of river-dominated coastal waters: stoichiometric nutrient balance

and its consequences. *Estuar. Coast. Shelf Sci.* 40, 339–356. doi: 10.1016/s0272-7714(05)80014-9

Koeve, W., and Kähler, P. (2010). Balancing ocean nitrogen. *Nat. Geosci.* 3, 383–384. doi: 10.1038/ngeo884

Kraft, N. J. B., Comita, L. S., Chase, J. M., Sanders, N. J., Swenson, N. G., Crist, T. O., et al. (2011). Disentangling the drivers of β-diversity along latitudinal and elevational gradients. *Science* 333, 1755–1758. doi: 10.1126/science.1208584

Krebs, C. J. (1998). *Ecological Methodology*. Menlo Park, CA: Benjamin/Cummings.

Legendre, P., and De Cáceres, M. (2013). Beta diversity as the variance of community data: dissimilarity coefficients and partitioning. *Ecol. Lett.* 16, 951–963. doi: 10.1111/ele.12141

Li, H., Tang, H., Shi, X., Zhang, C., and Wang, X. (2014). Increased nutrient loads from the changjiang (yangtze) river have led to increased harmful algal blooms. *Harmful Algae.* 39, 92–101. doi: 10.1016/j.hal.2014.07.002

Li, X., Liu, Y., Liu, Y., Xu, Y., Yang, Y., and Shen, Z. (2016). Impacts of geographical distances and environmental differences on the beta diversity of plant communities in the dry-hot valley of the yuanjiang river. *Biodiv. Sci.* 24, 399–406. doi: 10.17520/biods.2015245

Li, Y., Li, D., Tang, J., Wang, Y., Liu, Z., and He, S. (2010). Long-term changes in the changjiang estuary plankton community related to anthropogenic eutrophication. *Aquat. Ecosyst. Health. Manag.* 13, 66–72. doi: 10.1080/14634980903579942

Liggins, L., Booth, D. J., Figueira, W. F., Treml, E. A., Tonk, L., Ridgway, T., et al. (2015). Latitude-wide genetic patterns reveal historical effects and contrasting patterns of turnover and nestedness at the range peripheries of a tropical marine fish. *Ecography* 38, 1212–1224. doi: 10.1111/ecog.01398

Liu, X., and Shen, H. (2001). Estimation of dissolved inorganic nutrients fluxes from the changjiang river into estuary. *Sci. China Ser. B.* 44, 135–141. doi: 10.1007/bf02884819

Liu, Z. (2012). *Sediment Characteristics, Transport Patterns and Their Environmental Response in the Xiamen Sea*. Available online at: https://kns.cnki.net/KCMS/detail/detail.aspx?dbname=CMFD2012&filename=1012376101.nh (accessed May 23).

Ma, T., and Mao, L. (2014). Adaptation strategies for climate change in foreign estuarine cities and implications for China. *World Environ.* 2, 60–63.

Magurran, A. E. (1988). *Ecological Diversity and Its Measurement*. Bangor: University College of North Wales.

Mills, M. M., and Arrigo, K. R. (2010). Magnitude of oceanic nitrogen fixation influenced by the nutrient uptake ratio of phytoplankton. *Nat. Geosci.* 3, 412–416. doi: 10.1038/ngeo856

Moresco, G. A., Bortolini, J. C., Dias, J. D., Pineda, A., Jati, S., and Rodrigues, L. C. (2017). Drivers of phytoplankton richness and diversity components in *Neotropical floodplain* lakes, from small to large spatial scales. *Hydrobiologia*. 799, 203–215. doi: 10.1007/s10750-017-3214-3

Morris, E. K., Caruso, T., Buscot, F., Fischer, M., Hancock, C., Maier, T. S., et al. (2014). Choosing and using diversity indices: insights for ecological applications from the german biodiversity exploratories. *Ecol. Evol.* 4, 3514–3524. doi: 10.1002/ece3.1155

Mousing, E. A., Richardson, K., Bendtsen, J., Cetiniæ, I., and Perry, M. J. (2016). Evidence of small-scale spatial structuring of phytoplankton alpha- and beta-diversity in the open ocean. *J. Ecol.* 104, 1682–1695. doi: 10.1111/1365-2745.12634

Muylaert, K., Sabbe, K., and Vyverman, W. (2009). Changes in phytoplankton diversity and community composition along the salinity gradient of the Schelde estuary (belgium/the netherlands). *Estuar. Coast. Shelf Sci.* 82, 335–340. doi: 10.1016/j.ecss.2009.01.024

Myers, N., Mittermeier, R. A., Mittermeier, C. G., da Fonseca, G. A. B., and Kent, J. (2000). Biodiversity hotspots for conservation priorities. *Nature* 403, 853–858. doi: 10.1038/35002501

Nekola, J. C., and White, P. S. (1999). The distance decay of similarity in biogeography and ecology. *J. Biogeogr.* 26, 867–878. doi: 10.1046/j.1365-2699.1999.00305.x

Nixon, S. W. (1995). Coastal marine eutrophication: a definition, social causes, and future concerns. *Ophelia*. 41, 199–219. doi: 10.1080/00785236.1995.10422044

NRC (National Research Council) (2000). *Clean Coastal Waters: Understanding and Reducing The Effects of Nutrient Pollution*. Washington, DC: National Academies Press.

O'Brien, A., Townsend, K., Hale, R., Sharley, D., and Pettigrove, V. (2016). How is ecosystem health defined and measured? A critical review of freshwater and estuarine studies. *Ecol. Indic.* 69, 722–729. doi: 10.1016/j.ecolind.2016.05.004

Officer, C., and Ryther, J. (1980). The possible importance of silicon in marine eutrophication. *Mar. Ecol. Prog. Ser.* 3, 83–91. doi: 10.3354/meps003083

Paerl, H. W. (2009). Controlling eutrophication along the freshwater–marine continuum: dual nutrient (n and p) reductions are essential. *Estuar. Coast.* 32, 593–601. doi: 10.1007/s12237-009-9158-8

Paerl, H. W., and Justić, D. (2013). *Estuarine ecology*. Hoboken, NJ: Wiley-Blackwell.

Paerl, H. W., Hall, N. S., Peierls, B. L., and Rossignol, K. L. (2014). Evolving paradigms and challenges in estuarine and coastal eutrophication dynamics in a culturally and climatically stressed world. *Estuar. Coast.* 37, 243–258. doi: 10.1007/s12237-014-9773-x

Paerl, H. W., Valdes-Weaver, L. M., Joyner, A. R., and Winkelmann, V. (2007). Phytoplankton indicators of ecological change in the eutrophying pamlico soundsystem, north carolina. *Ecol. Appl.* 17, S88–S101. doi: 10.1890/05-0840.1

Paul, C., Hanley, N., Meyer, S. T., Fürst, C., Weisser, W. W., and Knoke, T. (2020). On the functional relationship between biodiversity and economic value. *Sci. Adv.* 6:eaax7712. doi: 10.1126/sciadv.aax7712

Peet, R. K. (1974). The measurement of species diversity. *Annu. Rev. Ecol. Syst.* 5, 285–307. doi: 10.2307/2096890

Peñuelas, J., Poulter, B., Sardans, J., Ciais, P., van der Velde, M., Bopp, L., et al. (2013). Human-induced nitrogen–phosphorus imbalances alter natural and managed ecosystems across the globe. *Nat. Commun.* 4:2934. doi: 10.1038/ncomms3934

Pielou, E. C. (1969). *An Introduction to Mathematical Ecology*. New York: Wieley-Interscience.

Pimm, S. L., and Gittleman, J. L. (1992). Biological diversity: where is it? *Science* 255:940. doi: 10.1126/science.1546290

Pinsky, M. L., Eikeset, A. M., McCauley, D. J., Payne, J. L., and Sunday, J. M. (2019). Greater vulnerability to warming of marine versus terrestrial ectotherms. *Nature* 569, 108–111. doi: 10.1038/s41586-019-1132-4

Podani, J., and Schmera, D. (2011). A new conceptual and methodological framework for exploring and explaining pattern in presence-absence data. *Oikos* 120, 1625–1638. doi: 10.1111/j.1600-0706.2011.19451.x

Rabalais, N. N. (2002). Nitrogen in aquatic ecosystems. *Ambio*. 31, 102–112.

Redfield, A. C. (1934). *On The Proportions of Organic Derivations in Sea Water and Their Relation To The Composition of Plankton*. Liverpool: University Press of Liverpool.

Rochelle-Newall, E. J., Chu, V. T., Pringault, O., Amouroux, D., Arfi, R., Bettarel, Y., et al. (2011). Phytoplankton distribution and productivity in a highly turbid, tropical coastal system (bach dang estuary, vietnam). *Mar. Pollut. Bull.* 62, 2317–2329. doi: 10.1016/j.marpolbul.2011.08.044

Schoor, A., Selig, U., Geiß-Brunschweiger, U., Schaible, R., Schumann, R., Schubert, B., et al. (2008). Phytoplankton diversity and photosynthetic acclimation along a longitudinal transect through a shallow estuary in summer. *Mar. Ecol. Prog. Ser.* 364, 31–46. doi: 10.3354/meps07452

Schulhof, M. A., Shurin, J. B., Declerck, S. A. J., and Van de Waal, D. B. (2019). Phytoplankton growth and stoichiometric responses to warming, nutrient addition and grazing depend on lake productivity and cell size. *Glob. Chang Biol.* 25, 2751–2762. doi: 10.1111/gcb.14660

Shannon, C. (1948). A mathematical theory communication. *Bell Syst. Tech. J.* 27, 379–423.

Simpson, E. H. (1949). Measurement of diversity. *Nature* 163:688.

Socolar, J. B., Gilroy, J. J., Kunin, W. E., and Edwards, D. P. (2016). Sparse data necessitate explicit treatment of beta-diversity: a reply to bush. *Trends Ecol. Evol.* 31, 338–339. doi: 10.1016/j.tree.2016.02.019

Srichandan, S., Baliarsingh, S. K., Prakash, S., Lotliker, A. A., Parida, C., and Sahu, K. C. (2019). Seasonal dynamics of phytoplankton in response to environmental variables in contrasting coastal ecosystems. *Environ. Sci. Pollut. Res.* 26, 12025–12041. doi: 10.1007/s11356-019-04569-5

Stefanidou, N., Katsiapi, M., Tsianis, D., Demertzioglou, M., Michaloudi, E., and Moustaka-Gouni, M. (2020). Patterns in alpha and beta phytoplankton diversity along a conductivity gradient in coastal mediterranean lagoons. *Diversity* 12:38. doi: 10.3390/d12010038

Thomas, C. D. (1990). Fewer species. *Nature* 347:237. doi: 10.1038/347237a0

Thrane, J. E., Hessen, D. O., and Andersen, T. (2016). The impact of irradiance on optimal and cellular nitrogen to phosphorus ratios in phytoplankton. *Ecol. Lett.* 19, 880–888. doi: 10.1111/ele.12623

Tomas, C. R. (1997). *Identifying Marine Phytoplankton*. New York: Academic Press.

Trisos, C. H., Merow, C., and Pigot, A. L. (2020). The projected timing of abrupt ecological disruption from climate change. *Nature* 580, 1–6. doi: 10.1038/s41586-020-2189-9

Wallace, R. B., Baumann, H., Grear, J. S., Aller, R. C., and Gobler, C. J. (2014). Coastal ocean acidification: the other eutrophication problem. *Estuar. Coast. Shelf Sci.* 148, 1–13. doi: 10.1016/j.ecss.2014.05.027

Wang, H., Zhao, D., Chen, L., Giesy, J. P., Zhang, W., Yuan, C., et al. (2020). Light, but not nutrients, drives seasonal congruence of taxonomic and functional diversity of phytoplankton in a eutrophic highland lake in China. *Front. Plant Sci.* 11:179. doi: 10.3389/fpls.2020.00179

Wang, J., Bouwman, A. F., Liu, X., Beusen, A. H. W., Van Dingenen, R., Dentener, F., et al. (2021). Harmful algal blooms in chinese coastal waters will persist due to perturbed nutrient ratios. *Environ. Sci. Technol. Lett.* 8, 276–284. doi: 10.1021/acs.estlett.1c00012

Weber, T. S., and Deutsch, C. (2010). Ocean nutrient ratios governed by plankton biogeography. *Nature* 467, 550–554. doi: 10.1038/nature09403

Whittaker, R. H. (1960). Vegetation of the siskiyou mountains. *Oregon California. Ecol. Monogr.* 30, 279–338. doi: 10.2307/1948435

Williams, P. H. (1996). Mapping variations in the strength and breadth of biogeographic transition zones using species turnover. *Proc. R. Soc. Lond. B.* 263, 579–588. doi: 10.2307/50680

Wu, F., Yang, X., and Yang, J. (2010). Additive diversity partitioning as a guide to regional montane reserve design in Asia: an example from yunnan province, China. *Divers. Distrib.* 16, 1022–1033. doi: 10.1111/j.1472-4642.2010.00710.x

Wu, G., Cao, W., Huang, Z., Kao, C. M., Chang, C., Chiang, P., et al. (2017). Decadal changes in nutrient fluxes and environmental effects in the jiulong river estuary. *Mar. Pollut. Bull.* 124, 871–877. doi: 10.1016/j.marpolbul.2017.01.071

Wurtsbaugh, W. A., Paerl, H. W., and Dodds, W. K. (2019). Nutrients, eutrophication and harmful algal blooms along the freshwater to marine continuum. *WIREs. Water* 6:e1373. doi: 10.1002/wat2.1373

Xu, H., Paerl, H. W., Qin, B., Zhu, G., Hall, N. S., and Wu, Y. (2014). Determining critical nutrient thresholds needed to control harmful cyanobacterial blooms in eutrophic lake taihu, China. *Environ. Sci. Technol.* 49, 1051–1059. doi: 10.1021/es503744q

Yang, Y., Hu, R., Lin, Q., Hou, J., Liu, Y., Han, B., et al. (2017). Spatial structure and β-diversity of phytoplankton in tibetan plateau lakes: nestedness or replacement? *Hydrobiologia*. 808, 301–314. doi: 10.1007/s10750-017-3433-7

Yin, K., Qian, P., Wu, M. C. S., Chen, J. C., Huang, L., Song, X., et al. (2001). Shift from P to N limitation of phytoplankton growth across the pearl river estuarine plume during summer. *Mar. Ecol. Prog. Ser.* 221, 17–28. doi: 10.3354/meps221017

Yu, X., Liu, Z., Ma, Z., and Chen, B. (2012). *Jiulong Jianghekou Shengtai Huanjing Zhuangkuang Yu Shengtai Xitong Guanli*. Beijing: Ocean Press.

Zhang, W., Sun, J., Nie, H., Jiang, G., and Tao, J. (2015). Seasonal and spatial variations of nutrient and the response of phytoplankton in PRE and adjacent sea areas. *Acta Ecol. Sinica.* 35, 169–179. doi: 10.5846/stxb201308262158

Zhao, D., Zhang, F., Wang, H., Liu, F., and Suo, A. (2010). Driving forces and management strategies for estuaries in northern China. *Front. Earth Sci.* 4:51–58. doi: 10.1007/s11707-010-0004-x

Zhou, Y., Yang, X., Wang, Y., Li, F., Wang, J., and Tan, L. (2021). Exogenous nutrient inputs restructure phytoplankton community and ecological stoichiometry of eastern Indian Ocean. *Ecol. Indic.* 127:107801. doi: 10.1016/j.ecolind.2021.107801

Conflict of Interest: The authors declare that the research was conducted in the absence of any commercial or financial relationships that could be construed as a potential conflict of interest.

Publisher's Note: All claims expressed in this article are solely those of the authors and do not necessarily represent those of their affiliated organizations, or those of the publisher, the editors and the reviewers. Any product that may be evaluated in this article, or claim that may be made by its manufacturer, is not guaranteed or endorsed by the publisher.

Copyright © 2022 Ge, Ma, Chen, Wang, Lu, An, Zhang, Zhang, Yu, Han, Yu, Liu and Kuang. This is an open-access article distributed under the terms of the Creative Commons Attribution License (CC BY). The use, distribution or reproduction in other forums is permitted, provided the original author(s) and the copyright owner(s) are credited and that the original publication in this journal is cited, in accordance with accepted academic practice. No use, distribution or reproduction is permitted which does not comply with these terms.

frontiers in Marine Science

ORIGINAL RESEARCH
published: 23 March 2022
doi: 10.3389/fmars.2022.871458

Discrepant Effects of Oceanic Advection in the Evolution of SST Anomalies in the South China Sea During El Niño of Different Intensities

Fuan Xiao[1,2,3], Dongxiao Wang[3,4], Qiaoyan Wu[2], Wei Song[5], Lili Zeng[6], Qiang Xie[5] and Yan Wang[7]*

[1] School of Geography and Remote Sensing, Guangzhou University, Guangzhou, China, [2] State Key Laboratory of Satellite Ocean Environment Dynamics, Second Institute of Oceanography, Ministry of Natural Resources (MNR), Hangzhou, China, [3] Southern Marine Science and Engineering Guangdong Laboratory (Zhuhai), Zhuhai, China, [4] School of Marine Sciences, Sun Yat-Sen University, Zhuhai, China, [5] Institute of Deep-Sea Science and Engineering, Chinese Academy of Sciences, Sanya, China, [6] State Key Laboratory of Tropical Oceanography, South China Sea Institute of Oceanology, Chinese Academy of Sciences, Guangzhou, China, [7] Department of Ocean Science, The Hong Kong University of Science and Technology, Hong Kong, Hong Kong SAR, China

OPEN ACCESS

Edited by:
Meilin Wu,
Chinese Academy of Sciences, China

Reviewed by:
Xuhua Cheng,
Hohai University, China
Xiao-Hua Zhu,
Ministry of Natural Resources, China

***Correspondence:**
Dongxiao Wang
dxwang@mail.sysu.edu.cn

Specialty section:
This article was submitted to Marine Pollution, a section of the journal Frontiers in Marine Science

Received: 08 February 2022
Accepted: 02 March 2022
Published: 23 March 2022

Citation:
Xiao F, Wang D, Wu Q, Song W, Zeng L, Xie Q and Wang Y (2022) Discrepant Effects of Oceanic Advection in the Evolution of SST Anomalies in the South China Sea During El Niño of Different Intensities. Front. Mar. Sci. 9:871458. doi: 10.3389/fmars.2022.871458

Observed different evolutions of SST anomalies in the South China Sea (SCS) between super and other El Niño events are revealed. The results suggest that the first (second) warming peak is warmer than the second (first) one for super (other) El Niño composite. Mixed layer heat budget analysis indicates that during the first warming period, the vertical advection induced by the anomalous anticyclone in the SCS (SCSAC) warms the SST in the central SCS through the basin-scale downwelling motion for super El Niño composite. In contrast, the positive shortwave radiation anomalies from atmosphere into ocean associated with the reduced total cloud cover contribute the most warming SST for other El Niño composite. During the cooling period, the horizontal linear cold advection associated with a large west-east SST gradient anomaly and climatological western boundary currents plays the most important role in rapid cooling SST for super El Niño composite. However, the nonlinear warm advection associated with the northward current anomalies and anomalous SST gradient in the western SCS maintains the SCS SST for other El Niño composite. During the second warming period, the net surface heat flux anomalies act as a damping process, while the warming process could be attributed to the vertical warm advection. Specially, the SCSAC weakens but the anomalous easterly winds strengthen to suppress the upwelling off the coast of southeast Vietnam for other El Niño composite. The anomalous ocean circulations and associated advections are related to the development of SCSAC, which could be largely attributed to the SST anomalies in the Indian Ocean. In contrast with previous studies, our results highlight the role of ocean dynamics in the evolution of SCS SST anomalies during El Niño of different intensities.

Keywords: South China Sea, sea surface temperature, El Niño intensity, ocean advection, anomalous anticyclone over the SCS, air–sea interaction, Indian Ocean

1 INTRODUCTION

The South China Sea (SCS), which is located between the western Pacific Ocean and the Indian Ocean, is the largest marginal sea in the northwest Pacific. Abundant water exchange and complex atmospheric processes make the SCS susceptible to the Pacific and Indian Oceans but quite different from them (Liu et al., 2004; Chiang et al., 2018). Observational analyses have shown that the sea surface temperature in the SCS (SCS SST) exhibit abundance of multiple timescales from seasonal to decadal variabilities, which are largely modulated by the East Asian monsoon, El Niño–Southern Oscillation (ENSO), Interdecadal Pacific Oscillation, and global warming (Shen and Lau, 1995; Tomita and Yasunari, 1996; Ose et al., 1997; Chu et al., 1999; Klein et al., 1999; Qu, 2001; Chen et al., 2003; Wang et al., 2006a; Yu and Qu, 2013; Wu et al., 2014; Cheng et al., 2016; Cheng et al., 2017; Cheng et al., 2019; Xiao et al., 2020a; Liang et al., 2021). Among them, the impact of ENSO on the SCS SST on the interannual timescale has been widely studied.

There are two main processes for ENSO to affect the SCS SST. One is called the "atmospheric bridge": the Walker circulation is weakened with the development of El Niño to modulate the SCS SST through surface heat flux (Trenberth et al., 1998; Klein et al., 1999; Wang et al., 2000; Alexander et al., 2002). Zhang et al. (1996) proposed that an anomalous anticyclone over the western North Pacific (WNPAC) could be a critical linkage between East Asian climate and El Niño. Wang et al. (2000) indicated that the formation of the WNPAC during the late fall of the El Niño developing phase and the local atmosphere–ocean interaction (wind–evaporation–SST feedback) could support the WNPAC to persistent. Xie et al. (2009) proposed another maintenance mechanism of the WNPAC *via* the Indian Ocean capacitor effect, namely the tropical Indian Ocean warming following the El Niño event could force a warm equatorial Kelvin wave to the east to maintain the WNPAC. These theories could explain the continuous warming SST in the SCS during El Niño decaying phase. Another process is called "oceanic channel". The only deep channel that connects the SCS and the Pacific is the Luzon Strait (Qu et al., 2004; Tian et al., 2006). The SCS SST anomalies could be modulated by the ENSO-induced ocean dynamical processes through the Luzon Strait (Qu et al., 2004; Wang et al., 2006b). For example, Wang et al. (2002) found that the extreme warm event in 1997/1998 was triggered mainly by the warm advection caused by the southerly wind anomalies, but the weakened throughflow from the Luzon Strait maintained the warming SST. Xiao et al. (2018) reported two subsurface extreme warming events, which were related to the warm water advected from the Kuroshio current.

According to the above theories, some features and mechanisms of the SCS SST associated with the El Niño were proposed. Wang et al. (2006a) pointed out that following an El Niño event the evolution of the SCS SST shows a double-peak feature. The net heat flux anomalies contribute to the first warming peak, while geostrophic heat advection is the major factor in producing the second warming peak. Chen et al. (2007) demonstrated that the rapid warming of the SCS during fall of a strong El Niño was mainly attributed to the increased solar heating in October and decreased latent heat flux in November–December, respectively, which are both induced by the evolution of the WNPAC. The influence of the different types of El Niño on SCS SST has also been studied (Liu et al., 2014; Tan et al., 2016; Liang et al., 2021). For instance, the SCS may warm throughout the basin during the eastern Pacific El Niño, while during the central Pacific El Niño the SCS warming only occurs to the west of 115°E. Tan et al. (2016) investigated the influences of three types of El Niño on the SCS during developing autumn. They pointed that the positive latent heat flux (positive anomalous *Qnet* and its components indicate that the ocean gains heat from the atmosphere to warm the SST, and vice versa) contributed to the warm SCS SST anomalies for canonical El Niño and El Niño Modoki I, whereas the cold SST anomalies are found for El Niño Modoki II induced by negative latent heat flux.

As summarized above, previous studies mainly focused on the impact of the El Niño and its diversity on the SCS SST. Yet little is known about the impacts of El Niño of different intensities on the SCS SST. The purpose of this study is to investigate different evolutions of SCS SST anomalies between super and other El Niño events and the corresponding physical mechanisms. In addition, different from previous studies, this study focuses on the role of ocean advection in the evolution of SCS SST in response to the El Niño with different intensities.

The remainder of this paper is organized as follows. The data and methodology are set out in *Section Data and Methods*. In *Section Results*, we show the spatiotemporal difference of SCS SST in response to El Niño with different intensities, a detailed mixed layer heat budget analysis, and the large scale forcing from the Indian Ocean. Finally, a discussion and the main conclusions are given in *Section Conclusions and Discussion*.

2 DATA AND METHODS

2.1 Data

In this study, observed monthly SST data are collected from the National Oceanic and Atmospheric Administration (NOAA) daily optimum interpolation SST datasets version 2 (OISSTv2, Reynolds et al., 2007). To detect the possible associated mechanisms for controlling the SST variation, the subsurface ocean temperature and three-dimensional currents from Simple Ocean Data Assimilation (SODA version 3.4.2) reanalysis data are used (Carton et al., 2018). The quality of SST in SODA3.4.2 has been validated against observations in OISSTv2 from previous studies (Xiao et al., 2020b; Xiao et al., 2020c). Atmospheric variables are obtained from the European Centre for Medium-Range Weather Forecasts Reanalysis Interim (ERA-Interim, Dee et al., 2011), namely, the longwave radiation, shortwave radiation, latent heat flux, sensible heat flux, total cloud cover, and horizontal wind fields. We choose ERA-Interim because the ocean model used to produce SODA was forced by ERA-Interim. All datasets covered the period of 1982–2018 and all anomalous values are calculated based on the climatological data for the period of 1982–2018. Linear trends for all variables have been moved before analyses.

According to monthly Niño3.4 index (area-averaged SST anomalies over 5°S–5°N, 120°–170°W) from 1982 to 2018, three strongest El Niño events with the Niño 3.4 index exceeding 2.5°C (referred to super El Niño events: 1982/83, 1997/98, 2015/16) and the remaining eight events (referred to other El Niño events 1986/87, 1987/88, 1991/92, 1994/95, 2002/03, 2006/07, 2009/10, 2014/15) are chosen for analysis.

2.2 Mixed Layer Heat Budget

In this study, mixed layer heat budget analysis is a very important method to examine the atmospheric heat flux and oceanic advection controlling changes in SST quantitatively. Following Li et al. (2002), the mixed layer temperature tendency equation is written as:

$$\underbrace{\frac{\partial T_m^{'}}{\partial t}}_{SST\ \ tendency} = -(\underbrace{V^{'}\cdot\nabla\bar{T}_m + \bar{V}\cdot\nabla T_m^{'}}_{horizontal\ \ linear\ \ adv}) - \underbrace{(V^{'}\cdot\nabla T_m^{'})}_{horizontal\ \ nonlinear\ \ adv} - \underbrace{(W\cdot\nabla T_m)^{'}}_{vertical\ \ adv} + \underbrace{\left(\frac{Q_{net}}{\rho C_p H}\right)^{'}}_{heat\ \ flux} + \underbrace{\underset{\sim}{R}}_{residual} \quad (1)$$

where T_m is the mixed layer averaged temperature, which is a good proxy for SST in the mixed layer heat budget analysis; V and W are the horizontal and vertical current velocities averaged in the mixed layer, respectively; ρ is the reference density for seawater (1,027 kg m^{-3}); C_p is the specific heat capacity of seawater (4,007 J $°C^{-1}$ kg^{-1}); H denotes the mixed layer depth, which is defined here as the depth at which the temperature is 0.5°C lower than the SST (Monterey and Levitus, 1997); and R represents the residual term from unaccounted effects like diffusion, turbulent mixing, and errors in other terms. The overbar and prime denote the climatological mean and the deviation from the mean, respectively.

The Q_{net} is the net surface heat flux at the sea surface:

$$Q_{net} = SWR + LWR + LHF + SHF \quad (2)$$

Where LWR is the net surface longwave radiation flux, LHF is the latent heat flux, SHF is the sensible heat flux, and SWR is the difference between the net surface shortwave radiation flux and unabsorbed shortwave radiation penetrating through the mixed layer base. Following Halliwell (2004), SWR is calculated as follows:

$$SWR = SWR_{surf} - SWR_{pen} = SWR_{surf} - SWR_{surf}\times\left(Re^{-\frac{H}{\beta_1}} + (1-R)e^{-\frac{H}{\beta_2}}\right) \quad (3)$$

Where R is red light fraction, β_1 and β_2 are the penetration depth scales of red and blue light, respectively. In this study, coefficients R, β_1, and β_2 are chosen to be 0.58, 0.35, and 23, respectively, according to the water transparency properties in the SCS (Seow and Tozuka, 2019).

3 RESULTS

3.1 Spatiotemporal Difference of SCS SST in Response to ENSOs

The 2-year evolutions of the monthly SST anomalies in the main part of SCS (10°–20°N, 109°–118°E) from developing to decaying phases of three super El Niño events are shown in **Figure 1A**. The results indicate that the SCS experienced continuous abnormal warming since developing summer to autumn. In contrast, the SCS SST anomalies reveal great differences among eight other El Niño events (**Figure 1B**). Each impact of El Niño on the SCS is expected to be unique.

In order to elucidate the temporal variations of SCS SST anomalies during El Niño events clearly, we averaged the SCS SST anomalies for three super El Niño events and eight other El Niño events, respectively (**Figures 2A, B**). We use years 0 and +1 to represent El Niño developing and decaying years, respectively. A prominent feature of the SCS SST anomalies is a double peak following super El Niño events, which is consistent with Wang et al. (2006a). The first and second peaks occur in January and August during subsequent year of the El Niño with the average SST anomalies of 0.99°C and 0.58°C in the boreal winter [D(0)JF(+1)] and summer [JJA(+1)], respectively (**Figure 2C**). From the standard deviation of the winter SST anomalies for these super El Niño events, the first peak has a larger standard deviation, indicating that each impact of super El Niño on the SCS also has its uniqueness (**Figures 2A, C**). For example, we discussed that the early and extreme SCS SST anomalies in boreal autumn 2015 were different from the other two super El Niño events, which were modulated by the Indian Ocean (Xiao et al., 2020b). For eight other El Niño events, the SCS SST anomalies also display a double peak, but the amplitudes are much weaker than those for super El Niño events (**Figure 2B**). The first and second peaks occur in March and August during subsequent year of the El Niño with the average SST anomalies of 0.14°C and 0.33°C in the boreal winter [D(0)JF(+1)] and summer [JJA(+1)], respectively (**Figure 2D**). Compared with the difference between **Figures 2A, B**, a continuous warming from Aug(0) to Jan(+1) (+0.94°C in 6 months) and a rapid cooling Feb (+1) to Apr(+1) (−0.83°C in 3 months) make the first peak warmer than the second one for super El Niño events. In contrast, a very slowly warming from Sep(0) to Mar(+1) (+0.36°C in 7 months) and a continuous warming from Apr(+1) to Aug(+1) (+0.47°C in 5 months) make the second peak warmer than the first one for other El Niño events.

The spatial distributions of the SCS SST and 975hPa wind anomalies for super and other El Niño events are shown in **Figure 3**. The anomalous anticyclone in the SCS (SCSAC) establishes in SON(0) and maintains until MAM(+1) for super El Niño events. A basin-scale warming occurs throughout the super El Niño life cycle. As mentioned above, the first peak in D(0)JF(+1) is much warmer than the second peak in JJA(+1) (**Figures 3B, D**). The maximum warming centers of the first and

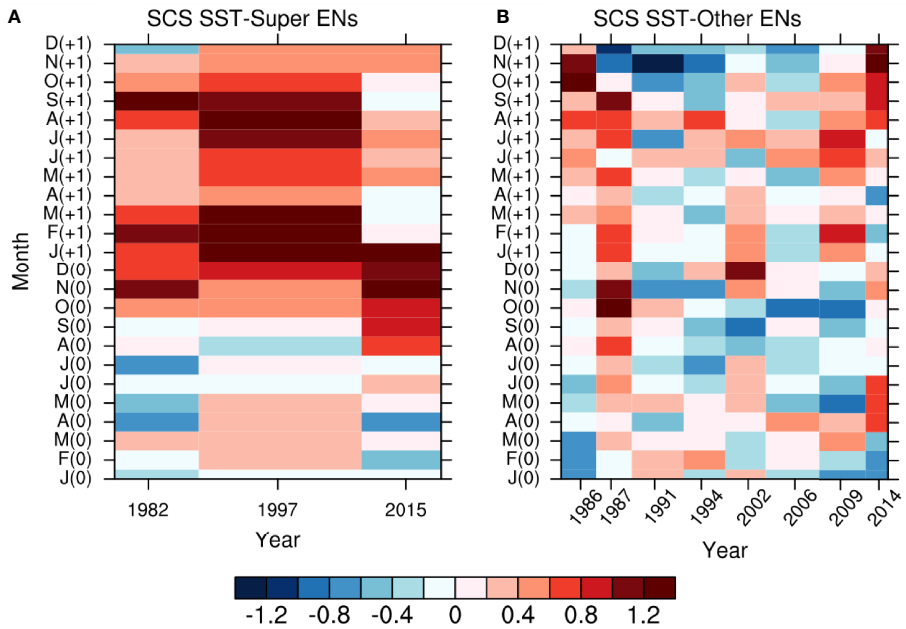

FIGURE 1 | **(A)** Time series of the SST anomaly over the SCS (10–20°N, 109–118°E) during three super El Niño events (Unit: °C). **(B)** Same as in **(A)** but for eight other El Niño events. "(0) and (1)" indicate the developing year and the decaying year for El Niño.

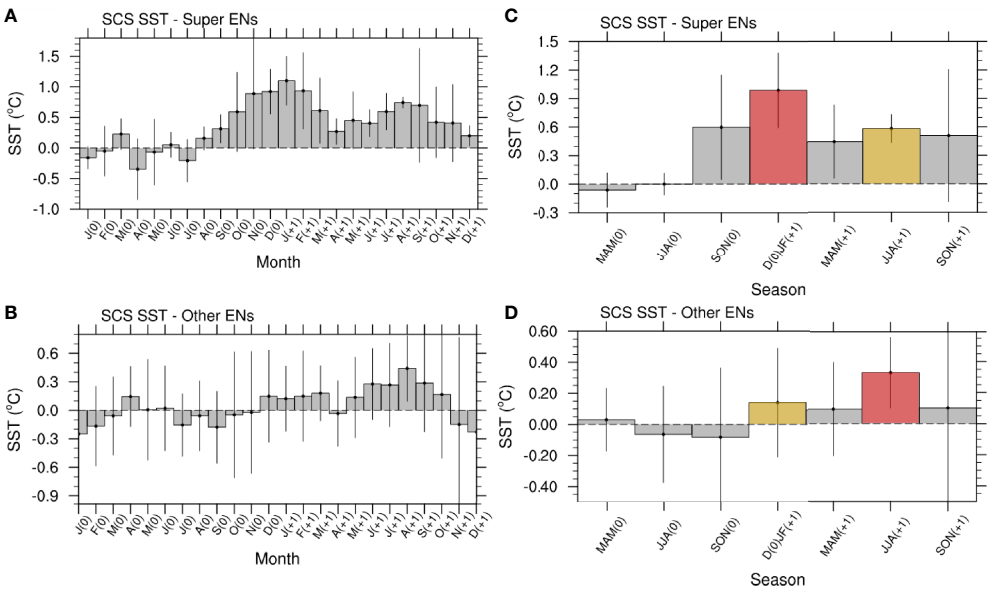

FIGURE 2 | **(A)**. Gray bars indicate two-year SST anomaly evolutions averaged over the SCS (10–20°N, 109–118°E) for super El Niño composite and the error bars indicate ±1 standard deviations of every month. **(B)** Same as in **(A)** but for the other El Niño composite. **(C, D)** Same as in **(A, B)** but for the seasonal mean. The red shading and yellow shading in **(C, D)** indicate the warming peaks, and the red one is the warmest.

second peaks are located in the western and eastern SCS, respectively. For other El Niño events, the SCSAC establishes in D(0)JF(+1), about one season later than that for super El Niño events (**Figure 3F**). It appears that the warming center occurs in the southern SCS during first peak and develops to be a basin-scale warming pattern during second peak (**Figures 3F, H**). We can conclude that the first (second) peak was 0.41°C (0.19°C) warmer than the second (first) one for super (other) El Niño

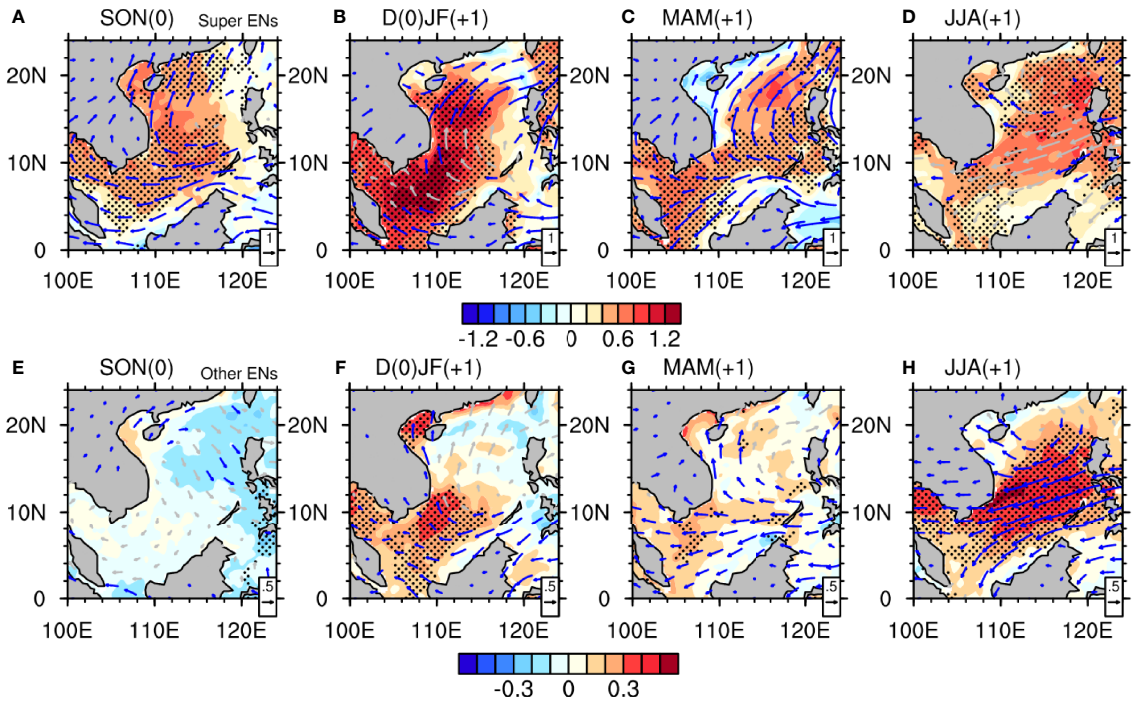

FIGURE 3 | Composited SST anomalies (shading; unit: °C) and 975-hPa wind anomalies (vector; unit: m/s) during **(A)** SON(0), **(B)** D(0)JF(+1), **(C)** MAM(+1), and **(D)** JJA(+1) for super El Niño events. **(E–H)** Same as in **(A–D)** but for other El Niño events composite. The black dots and blue vectors indicate the composite exceeding the 90% significance level based on Student's *t*-test.

events, indicating that the impact of non-super El Niño events on the SCS mainly occurs in decaying summer of El Niño events (**Figures 2C, D**).

3.2 Mixed Layer Heat Budget Analysis

To assess the local atmospheric and oceanic processes that contribute to the SCS SST anomalies during super and other El Niño years, the mixed layer heat budget is carried out based on Equations (1)–(3). For super El Niño composite, the cumulative SST tendencies are similar to the SST anomalies (**Figures 2A**, **4A**). The three-dimensional oceanic advection and *Qnet* are positive contributions to warm the SCS SST until Dec(0), the contribution of oceanic warm advection is larger than the surface heat flux during the continuous warming period. Then oceanic advection serves to rapidly reduce in the SCS SST from Jan(+1) to Mar(+1) and turns to warm the SCS SST after Apr(+1) again. That the SST starts to cool down after second warming peak could be attributed to the negative *Qnet* anomalies. However, the positive *Qnet* seems to make the same contribution to SCS SST warming as the three-dimensional warm oceanic advection until Mar(+1) for other El Niño composite. The *Qnet* anomalies turn to be negative from Aug(+1) and contribute to the SCS SST cooling, although the advection still maintains a positive contribution. Compared with super El Niño events, the residual term in the mixed layer heat budget for other El Niño events is larger (**Figures 4A, B**). As mentioned above, we can divide the development of the SCS SST anomalies during super El Niño events into three stages. Period 1 is the rapid warming stage in OND(0), short for P1. Period 2 is the sharp cooling stage in JFM(+1), short for P2. Period 3 is the second warming stage in JJA(+1), short for P3.

The components of *Qnet* and three-dimensional oceanic advection are discussed in detail. For P1, it is found that the LHF, SHF, and LWR anomalies act as thermodynamic damping terms in the *Qnet*. The positive SWR anomalies are responsible for the positive *Qnet* (**Figure 5A**). These results are inconsistent with Wang et al. (2006a); Liu et al. (2014) and Tan et al. (2016). They concluded that the LHF related to the wind speed was the most important contributor to *Qnet* averaged on the SCS basin-scale. In fact, their results also demonstrate that the LHF or *Qnet* only played an important role in the northern SCS, the importance of ocean circulation was reduced because their results were based on whole SCS (see **Figure 5** of Liu et al., 2014 and **Figure 8** of Tan et al., 2016). Therefore, the spatial distributions of *Qnet*, SWR, and LHF are shown in **Figure 6**. The positive *Qnet* anomalies occur in the northern SCS, weak positive and even negative *Qnet* anomalies occur over south of 16°N (**Figure 6A**). Interestingly, the SWR and LHF anomalies show opposite patterns in **Figures 6B, C**. The positive *Qnet* anomalies in the northern SCS are attributed to the positive LHF anomalies associated with reduced wind speed (**Figure 7C**). It is because the climatological wind during OND in the SCS is northeasterly, the anomalous southwesterly wind in the northern SCS related to the SCSAC could weaken the climatological northeasterly wind. Thus, the weakened surface

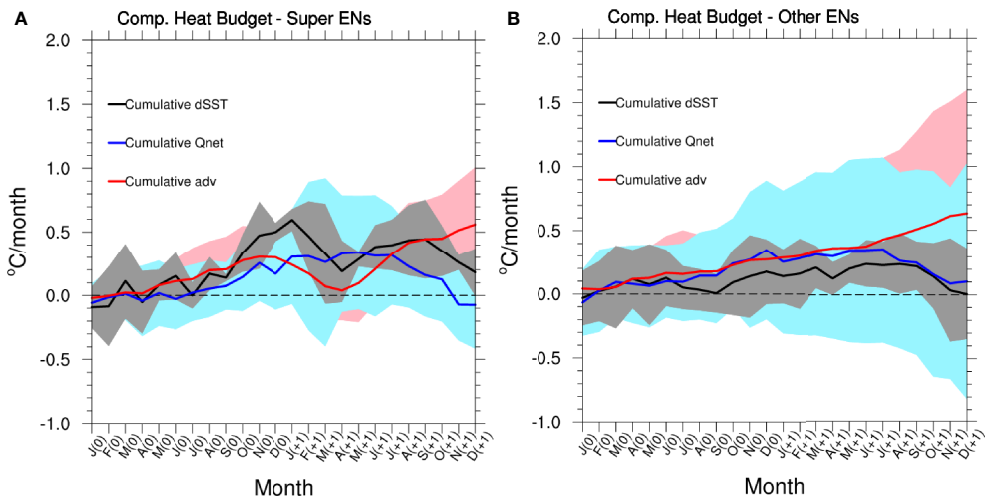

FIGURE 4 | **(A)** Mixed layer heat budget results averaged over the SCS for super El Niño composite. The black line is the cumulative mixed layer temperature tendency (dSST), and the blue and red lines indicate the cumulative net surface heat flux (Qnet) and three-dimensional advections (adv), respectively. Shading indicates ±1 standard deviations of every month. **(B)** Same as in **(A)** but for other El Niño composite.

wind speed reduces heat loss from the ocean to warm the SCS (**Figures 3A–C**). The positive SWR and negative LHF anomalies offset each other, which contributes to the weak positive or even negative *Qnet* anomalies over south of 16°N. It is seen that the positive SWR anomalies are also related to the SCSAC. The SCSAC-induced descending motion could suppress convective activity and significantly reduce the total cloud cover, leading to increased solar heating (**Figure 7A**). For other El Niño events, it is found that the LHF anomalies are positive instead of exerting the damping effect for super El Niño composite (**Figure 5B**). The positive *Qnet* anomalies occur over the whole SCS but concentrate over the eastern part (**Figure 6D**). The positive SWR anomalies associated with reduced total cloud cover play a dominant role in positive *Qnet* (**Figures 6E**, **7B**). The LHF anomalies are weaker than that for super El Niño composite because the wind speed anomalies relative to climatology are insignificant (**Figures 6F**, **7D**).

As a result, the thermodynamic process (*Qnet*) could only account for most rapid warming in the northern and eastern SCS for super El Niño composite. What causes the warming in the central-western SCS? To answer this question, the dynamic processes of the oceanic advection term are analyzed. **Figure 5C** displays that the vertical advection plays a positive role in warming the SST for super El Niño composite, while the horizontal linear advection plays a damping role. We further decompose the horizontal linear advection into horizontal advection of mean temperature by anomalous currents (MTAC) and horizontal advection of anomalous temperature by mean currents (ATMC). Although the horizontal advection of MTAC shows a warming effect, the horizontal advection of ATMC causes a stronger cooling in the western SCS (**Figure 8A**). Therefore, the net effect of ATMC and MTAC is that the linear horizontal advection plays a damping role during the first warming period (**Figure 5C**). The climatological wind stresses in the SCS are northeasterly and the wind stress curl in the central SCS is positive induced by the cyclonic circulation (**Figure 9A**). For super El Niño composite, it is clear that the significant SCSAC-induced negative wind stress curl occur in the central SCS (**Figure 9B**). The Sverdrup relation was used to connect the ocean circulation and wind stress curl in the SCS (Sverdrup, 1947; Liu et al., 2001; Xiao et al., 2018; Xiao et al., 2019). According to the Sverdrup theory, the anomalous Sverdrup transport is forced mainly by the negative wind stress curl anomalies and is balanced by weakened western boundary current transports, which forms an anomalous anticyclonic circulation in the SCS. The anomalous wind stress curl induced-anomalous anticyclone leads to basin-scale downwelling motion to make the SST warming in the central SCS, and this is why the vertical advection is the main contributor for warming the SCS SST. For other El Niño composite, the vertical advection is also important than the horizontal advection for warming the SST, but weaker than the contribution of *Qnet* (**Figure 5D**). The mechanism of the vertical advection is similar to that for super El Niño events, but the wind stress and its curl anomalies are weaker due to late establishment of SCSAC (**Figures 3A, B**, **9C**).

For P2, rapid cooling process occurs for super El Niño composite rather than other El Niños. This is mainly due to the difference in oceanic advection, the contribution of *Qnet* anomalies is very weak and can be ignored (**Figure 4**). Thus, only the role of oceanic advection will be discussed during P2. The decomposed advection terms show that the both the decreased horizontal linear and nonlinear advections cool the SST for super El Niño composite, especially the linear term (**Figure 5C**). Further decomposition indicates that the horizontal advection of ATMC is the major factor (**Figure 8A**). Then, the detailed analyses of the horizontal advection are clearly demonstrated by the distribution of the SST and mixed-layer averaged currents (**Figures 10A–C**). The SST anomalies and mean mixed layer

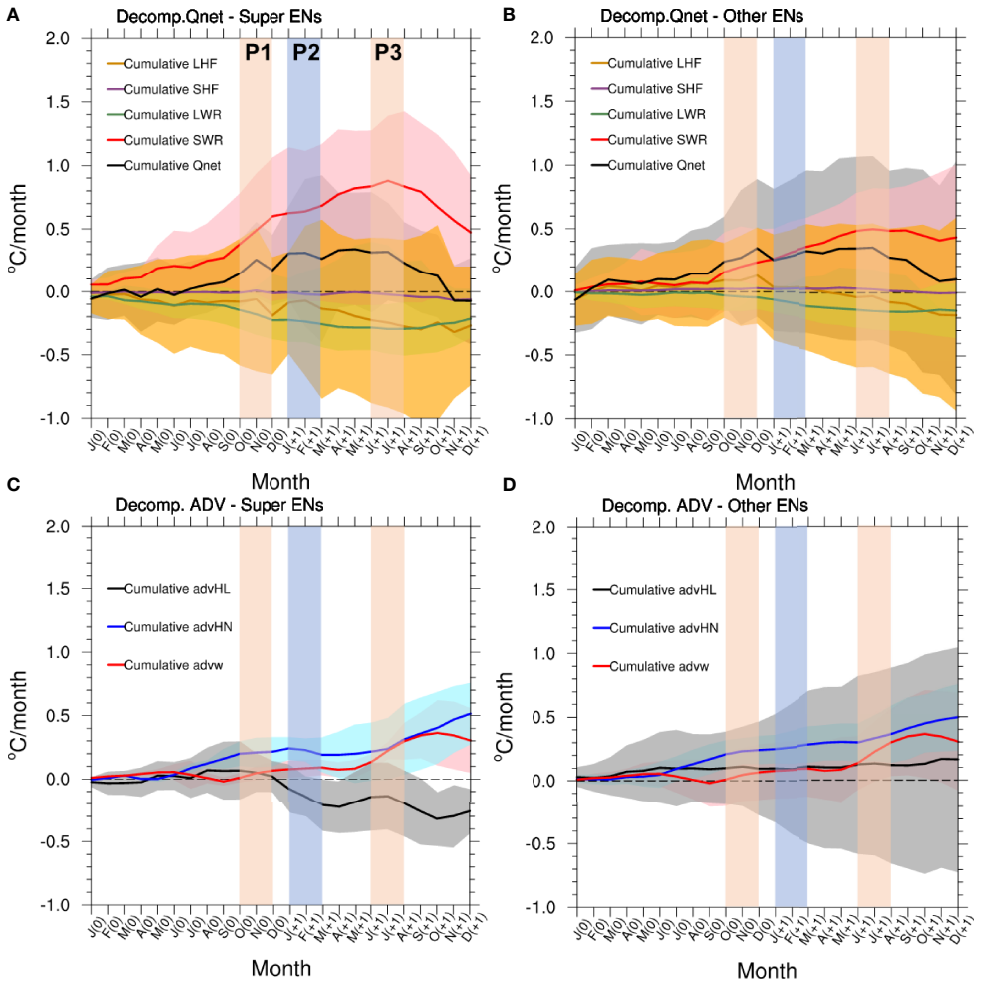

FIGURE 5 | **(A)** The orange, purple, green, red, and black lines indicate the cumulative latent heat flux (LHF), sensible heat flux (SHF), longwave radiation flux (LWR), shortwave radiation flux (SWR), and net surface heat flux (Qnet) for super El Niño composite, respectively. **(B)** Same as in **(A)** but for other El Niño composite. **(C)** The black, blue, and red lines indicate the cumulative linear horizontal advection (advHL), nonlinear horizontal advection (advHN), and vertical advection (advw) for super El Niño composite, respectively. **(D)** Same as in **(C)** but for other El Niño composite. Shading indicates ±1 standard deviations of every month.

averaged currents over JFM(+1) for super El Niño composite are shown in **Figure 10A**. Due to accelerated warming in previous months, the spatial distribution of the SST anomalies show a west-east gradient with the maximum warming SST concentrated in the western SCS. Then, the strong climatological western boundary currents drive more cool water from the northeastern and southeastern SCS to the central-western regions (**Figure 10A**). The mean SST and mixed layer averaged currents anomalies over JFM(+1) are shown in **Figure 10C**. The anomalous currents in the central SCS flow mainly along the isotherm, indicating that there is no thermal exchange between cold and warm water. However, there are anomalous southeasterly currents in the western part of the Luzon Strait bringing the cold water to the eastern SCS. Therefore, the horizontal linear advection of the MTAC remains as a negative contribution. Lastly, the SST anomalies and mixed layer averaged currents anomalies over JFM(+1) are shown in **Figure 10E**, indicating the horizontal nonlinear advection. As mentioned above, it is obviously seen that the anomalous southwesterly currents drive anomalous cold water from eastern SCS to the central part. Consistent with the decomposition of mixed layer heat budget analysis, the horizontal advection of ATMC is the largest contributor due to the strongly intensified ocean currents and large influence range. For other El Niño composite, the reduced SST only occurs in Apr (+1) which means the SST anomalies have been maintained during P2 (**Figure 2B**). As in previous analyses, only the role of oceanic advection is discussed. Further decomposition results demonstrate that the major contributor to maintaining the SST anomalies was the horizontal nonlinear advection, while the horizontal linear and vertical advections had little impact (**Figure 5B**). As the two components of the horizontal advection, the negative ATMC and positive MTAC offset each other during P2 (**Figure 8B**). Different configurations of SST and currents are shown in the right panels of **Figure 10**. The

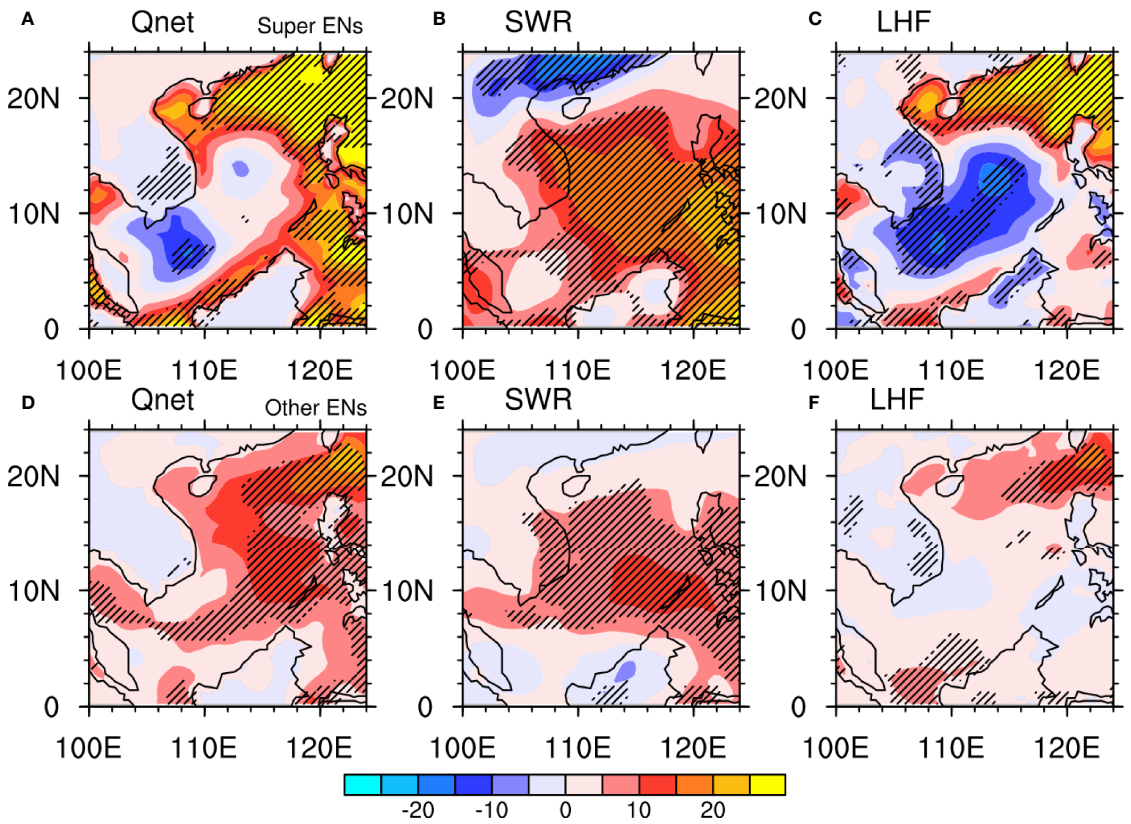

FIGURE 6 | **(A)** The *Qnet* anomalies, **(B)** SWR, and **(C)** LHF anomalies averaged over OND(0) for super El Niño composite (Unit: W/m^2). **(D–F)** Same as in **(A–C)** but for other El Niño composite. The composite results exceeding the 90% confidence level are hatched based on Student's *t*-test.

climatological western boundary currents drive a cold advection to cool the SST in the central and western SCS, which is similar to that of super El Niños, but the cold advection is weaker due to a weak west-east gradient in the northern-central SCS with the maximum warming SST concentrated in the southern SCS (**Figure 10D**). The mean SST and mixed layer averaged currents anomalies over JFM(+1) in **Figure 10D** display some obviously contrasts between **Figure 10C**. The anomalous currents in the western SCS flow across the isotherm, indicating that the warm advection drive warm water from the western SCS to the north, although the SST gradient in the western SCS is not as large as that in the eastern part (**Figure 10D**). Thus, the two components of linear advection counteract each other in the western SCS like those analyzed before. Lastly, both the northward currents anomalies and maximum SST gradient are located in the western SCS, resulting in warm advection effect to make the SCS SST unreduced during P2. Based on the above analyses, the rapid cooling in JFM(+1) for super El Niños could be attributed to the continuous warming-induced large SST gradient during the first warming peak.

For P3, the mechanisms for SST warming for super and other El Niños are very similar. The *Qnet* anomalies act as a damping role to cool the SST, so the second warming period in other El Niños could be attributed to the oceanic warm advection (**Figure 4**). Further decomposition results show that the vertical warm advection controls most of the total advection (**Figures 5C, D**). This process is very easy to understand: the SCSAC weakened but the anomalous easterly winds strengthened to reduce the upwelling over the SCS, especially off the coast of southeast Vietnam (**Figures 3D, H**, Xie et al., 2003). It is clear that the maximum warming center is located in the same region of easterly winds for other El Niños. The second warming rate for super El Niños is smaller than that of other El Niños because the horizontal advection of ATMC offsets the warming partially (**Figure 8A**).

3.3 Large-Scale Forcing From the Indian Ocean

Based on above analyses, it is understood that the thermodynamic and dynamic processes related to the SST warming and cooling are directly associated with SCSAC. Previous studies have demonstrated that the life cycle of the SCSAC is tightly tied to the phase of El Niño. On average, the SCSAC forms during El Niño developing fall and establishes during winter, maintains during the subsequent spring and summer, then decays (Wang et al., 2000; Wang and Zhang, 2002;

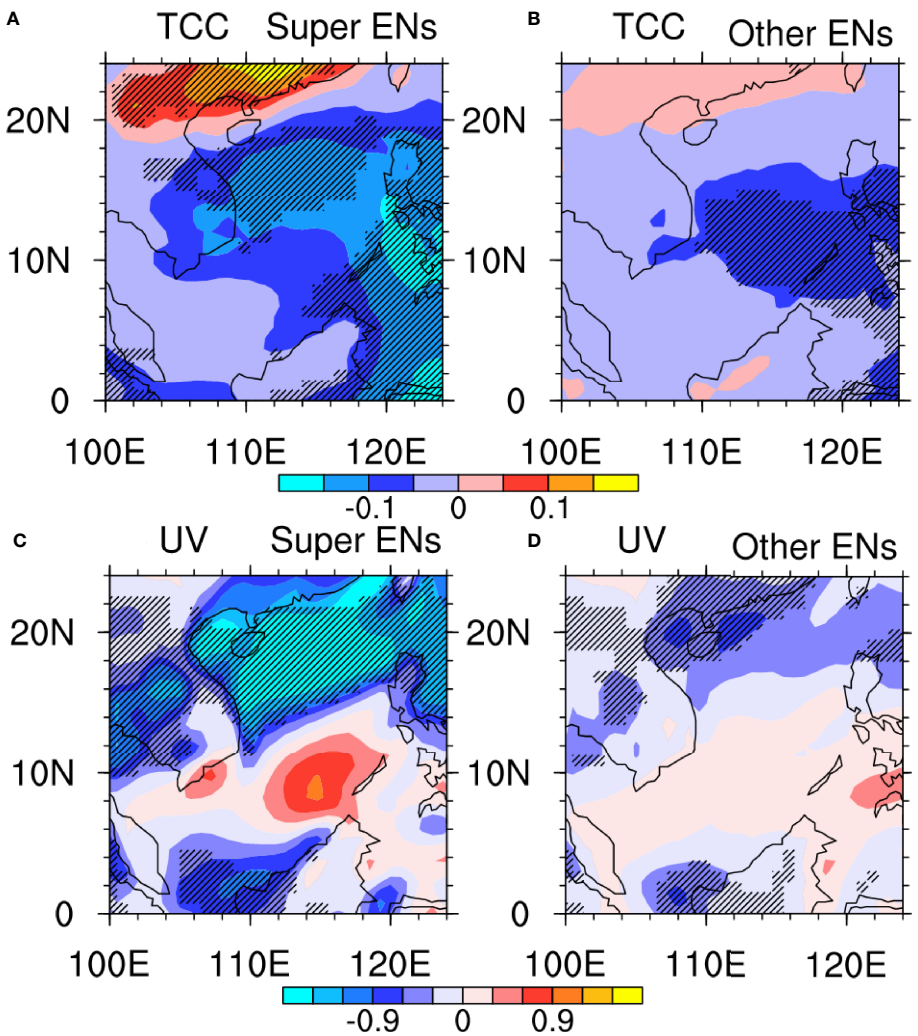

FIGURE 7 | **(A)** The total cloud cover (TCC) anomalies averaged over OND(0) for super El Niño composite. **(B)** Same as in **(A)** but for other El Niño composite. **(C)** The wind speed anomalies averaged over OND(0) for super El Niño composite (Unit: m/s). **(D)** Same as in **(C)** but for other El Niño composite. The composite results exceeding the 90% confidence level are hatched based on Student's *t*-test.

Wang et al., 2003; Kim and An, 2019). It is shown that the warming SST anomalies in the central-eastern Pacific (CEP) reach maximum in OND(0) and gradually retreat eastward in following seasons for super El Niño events (**Figures 11A–D**). While the warming SST anomalies in the CEP also reach maximum in OND(0) but gradually retreat westward in following seasons for other El Niños (**Figures 11E–H**). It has been widely accepted that the establishment of SCSAC in OND (0) for super El Niño events could be largely attributed to the cold SST anomalies in the WNP associated with El Niño, especially in the Maritime Continent region, by a Rossby wave-like response (**Figure 11A**, Matsuno, 1966; Gill, 1980; Watanabe and Jin, 2002; Xiao et al., 2020b). In contrast, a weak SCSAC starts to establish in OND(0) for other El Niños. Relative vorticity is used to quantify the intensity of SCSAC. The evolution of the relative vorticity anomalies display that the rapid establishment of SCSAC in Oct(0) for super El Niños (**Figure 12A**). In JFM(+1), the SCSAC moves eastward, along with eastward withdrawal of the cyclonic anomalies extending from the CEP, indicating the formation of WNPAC for super El Niños (**Figure 11B**). This WNPAC could be maintained until AMJ(+1), then rapid weakens in JAS(+1) (**Figures 11C, D**, and **12A**). In contrast, the SCSAC fully establishes in JFM(+1) for other El Niños, the relative vorticity over the SCS also reaches its minimum in Mar(+1) in **Figure 12A**. Then the continuous easterly wind anomalies extend from the central Pacific to the entire Indian Ocean for other El Niños, as opposed to a strong WNPAC for super El Niños (**Figure 11F**), and decay in JAS(+1). Xie et al. (2009) proposed one maintenance mechanism of the WNPAC *via* the Indian Ocean capacitor effect, namely the tropical Indian Ocean warming following the El Niño event could force a warm equatorial Kelvin wave to the east to

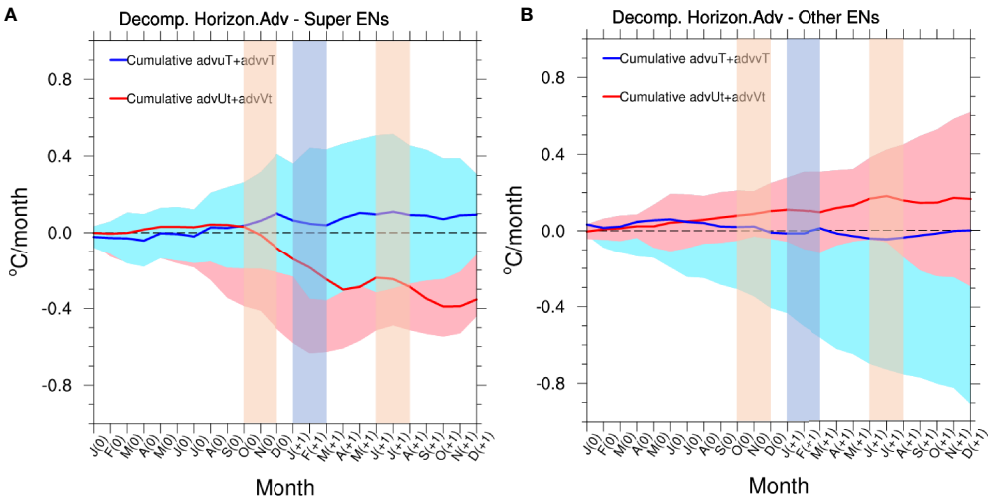

FIGURE 8 | **(A)** The blue and red lines indicate the cumulative horizontal advection of mean temperature by anomalous currents (advuT + advvT) and horizontal advection of anomalous temperature by mean currents (advUt + advVt) for super El Niño composite, respectively. **(B)** Same as in **(A)** but for other El Niño composite. Shading indicates ±1 standard deviations of every month.

maintain the WNPAC. In this study, the Indian Ocean also plays an important role in the discrepant evolutions of SST anomalies in the SCS between super and other El Niño events. The significantly Indian Ocean warming basin mode (IOBM) occurs from OND(0) to AMJ(+1) for super El Niño composite, IOBM could strengthen the SCSAC through the warm equatorial Kelvin wave, indicating its important role in establishment and maintenance of WNPAC (**Figures 11A–C**). The IOBM index (area-averaged SST anomalies over 20°S–20°N, 40°–100°E) in **Figure 12B** also shows a continuous warming until Apr(+1), which is consistent with the intensity of SCSAC (correlation coefficient is −0.84) for super El Niños, then the IOBM and SCSAC decay in JAS(+1). In contrast, the IOBM occurs from AMJ(+1) to JAS(+1) for other El Niño composite, and is later and weaker than that of super El Niños (**Figures 11E–H**). It is noteworthy that the IOBM reaches its peak in JAS(+1), indicating that the Indian Ocean is warmer than during super El Niños. The warm Indian Ocean enhances the SST gradient between the WNP and Indian Ocean to contribute the second warming stage though easterly wind anomalies in the SCS (**Figures 11H**, **12B**).

4 CONCLUSIONS AND DISCUSSION

Previous studies mainly focused on the impact of the El Niño and its diversity on the SCS SST. In this study, observed different evolutions of SCS SST anomalies between super and other El Niño events were revealed by the composite analyses. The SCS SST anomalies have two warming peaks in the El Niño mature winter and decaying summer. The SCS starts to warm in Aug(0) and lasts more than one year for super El Niño composite. However, for other El Niño composite, the SCS warms later in Dec(0) and the warming intensity is weaker. Another prominent feature is that the first (second) warming peak warmer than the second (first) one for super (other) El Niños, indicating that the different impacts of El Niño with different intensities on the SCS SST. Then, according to the SCS SST variation, three different warming and cooling stages are compared by carrying out the mixed layer heat budget analysis.

During the first warming period, the positive LHF anomalies induced by reduction of wind speed could only account for the rapid warming in the northern SCS. The reduced total cloud cover-induced positive SWR anomalies and enhanced wind speed-induced negative LHF anomalies offset each other in the central SCS. Further analysis displays that the established SCSAC-induced vertical advection warms the SST in the central SCS through the basin-scale downwelling motion for super El Niños. In contrast, the positive SWR anomalies associated with the reduced total cloud cover contribute the most warming SST for other El Niños, and the vertical warm advection is less important.

During the cooling period, the oceanic advections are more important than the *Qnet* term. The horizontal linear advection of ATMC plays the most important role in rapid cooling SST for super El Niño composite. The SST anomalies show a west-east gradient with the maximum warming SST concentrated in the western SCS due to accelerated warming in previous months. The western boundary currents drive more cold water from the northeastern and southeastern SCS to the central-western regions to cool the SCS. In contrast, the cold advection of ATMC is weak due to small west-east SST gradient and offset by the warm advection of MTAC for other El Niño composite. Both the northward currents anomalies and maximum SST gradient are located in the western SCS, resulting in warm advection effect to make the SCS SST not reduce during this stage.

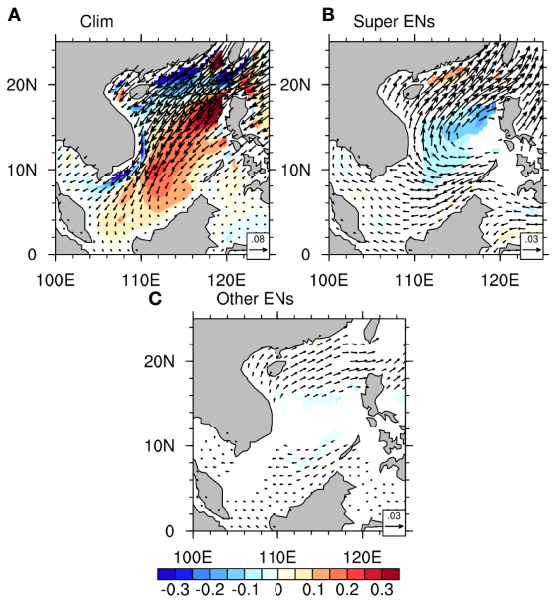

FIGURE 9 | **(A)** Climatological wind stress (vectors, unit: N/m^2) and wind stress curl (shading, unit: $\times 10^{-6}$ N/m^3) over OND(0). **(B)** Same as in **(A)** but for the wind stress and wind stress curl anomalies for super El Niño composite. **(C)** Same as in **(B)** but for other El Niño composite. Shaded areas and vectors in **(B, C)** are only shown for the results exceeding the 90% confidence level based on Student's *t*-test.

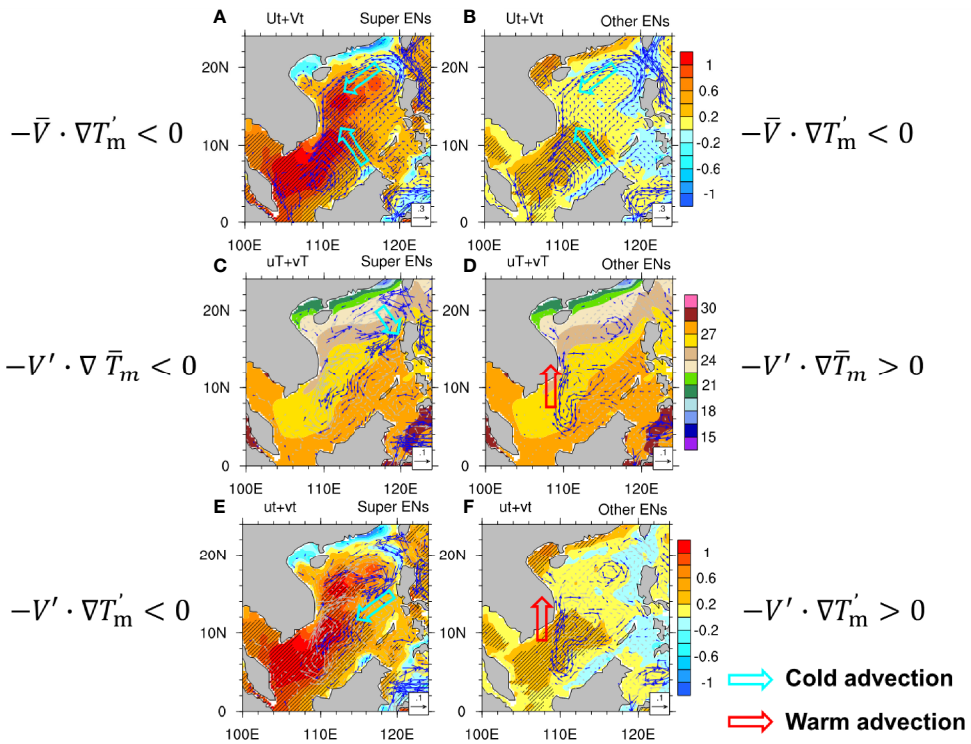

FIGURE 10 | **(A)** The SST anomalies (shading, unit: °C) and mean mixed layer averaged currents (vectors, unit: m/s) over Jan–Feb–Mar [JFM(+1)] for super El Niño composite. **(B)** Same as in **(A)** but for other El Niño composite. **(C)** Mean SST (shading) and mixed layer averaged current anomalies (vectors) over JFM(+1) for super El Niño composite. **(D)** Same as in **(C)** but for other El Niño composite. **(E)** The SST anomalies (shading) and mixed layer averaged current anomalies (vectors) over JFM(+1) for super El Niño composite. **(F)** Same as in **(E)** but for other El Niño composite. The composite SST and current results exceeding the 90% confidence level are hatched and shown in blue vectors based on Student's *t*-test.

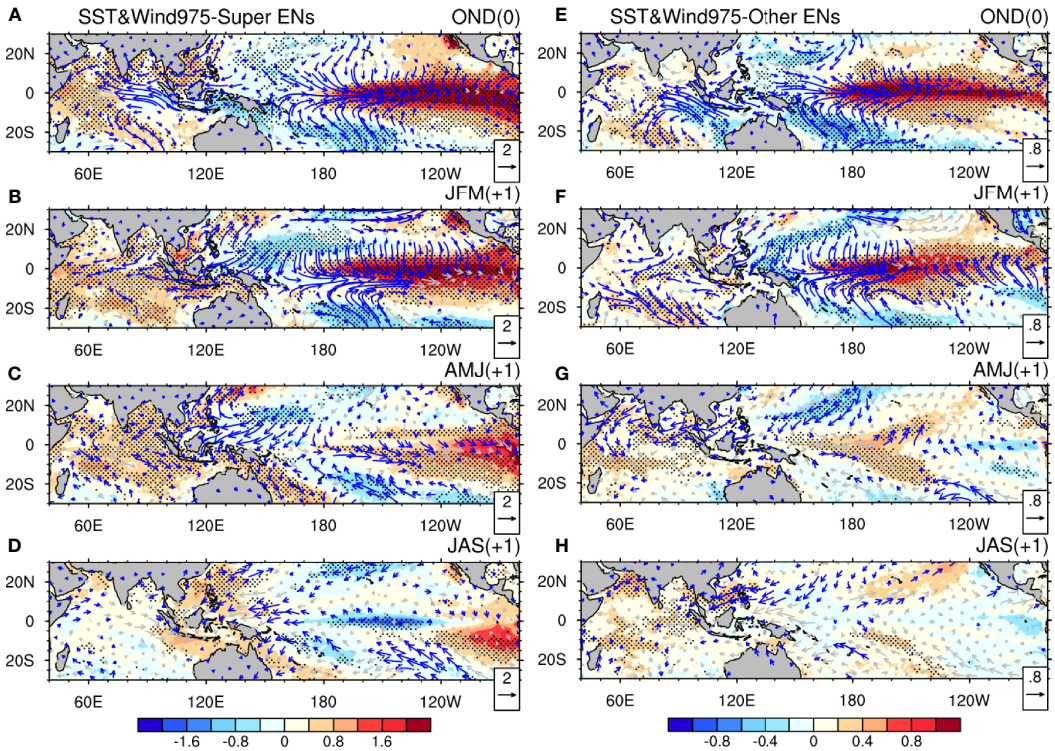

FIGURE 11 | Composited SST anomalies (shading; unit: °C) and 975-hPa wind anomalies (vector; m/s) during **(A)** OND(0), **(B)** JFM(+1), **(C)** AMJ(+1), and **(D)** JAS (+1) for super El Niño events. **(E–H)** Same as in **(A–D)** but for other El Niño events composite. The black dots and blue vectors indicate the composite exceeding the 90% significance level based on Student's *t*-test.

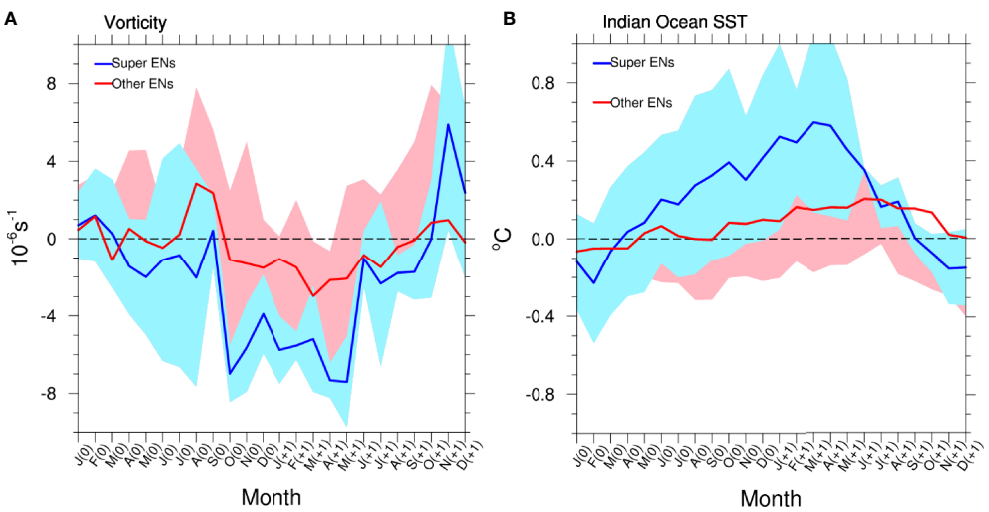

FIGURE 12 | **(A)** The blue and red lines indicate the vorticity anomalies averaged over the SCS for super and other El Niño composite, respectively. **(B)** Same as in **(A)** but for the SST anomalies over the Indian Ocean (20°S–20°N, 40–100°E). Shading indicates ±1 standard deviations of every month.

During the second warming period, the mechanisms for SST warming for super and other El Niños are very similar. The *Qnet* term acts as a damping term, while the warming process could be attributed to the vertical warm advection. Specially, the SCSAC weakened but the anomalous easterly winds strengthened to reduce the upwelling over the SCS, especially off the coast of southeast Vietnam for other El Niño composite. The second warming rate for super El Niño composite is smaller than that of other El Niños,

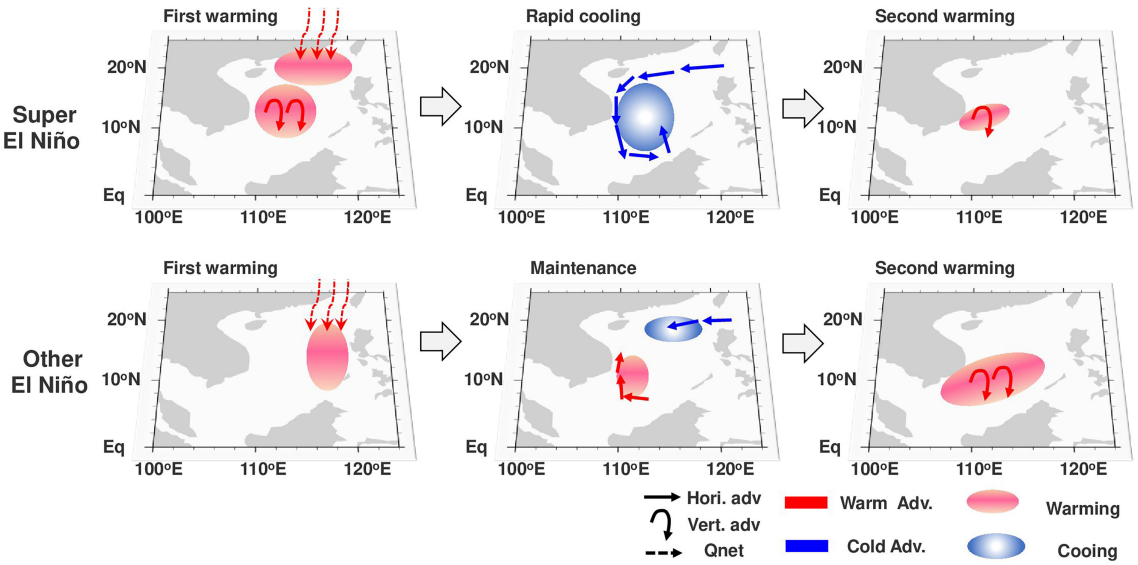

FIGURE 13 | Schematic illustrating the discrepant effects of oceanic advection in the evolution of SCS SST anomalies during El Niño of different intensities.

because the horizontal advection of ATMC offsets the warming partially. The schematic map is shown in **Figure 13**.

From the above results, it is well understood the different influences of El Niño with different intensities on SCS SST were mainly exerted *via* oceanic advection. The different ocean circulations and associated advections are related to the development of SCSAC. Based on the previous studies, the atmospheric response associated with the Indian Ocean warming is a very important factor for SCSAC, especially for super El Niños and the correlation coefficient between the SCSAC and Indian Ocean SST reaches −0.84. It is noteworthy that weaker relationship between the Indian Ocean and SCSAC (r = −0.61) indicates that some other factor could impact the SCSAC for other El Niños, such as the Madden–Julian Oscillation (Xiao et al., 2020c). The evolutions of SCS SST anomalies differ in each El Niño, the monthly-scale characteristics of ENSO's impact on SCS SST will be investigated in future work.

DATA AVAILABILITY STATEMENT

The original contributions presented in the study are included in the article/supplementary material. Further inquiries can be directed to the corresponding author.

AUTHOR CONTRIBUTIONS

FX conducted the analyses and wrote the manuscript. DW read through the manuscript and provided revisions. All authors listed have made a substantial, direct, and intellectual contribution to the work and approved it for publication.

FUNDING

This work was supported by the National Natural Science Foundation of China (Grant Nos. 92158204, 41806027, 42006035), the open fund of State Key Laboratory of Satellite Ocean Environment Dynamics, Second Institute of Oceanography, MNR (Grant No. QNHX2108), the Innovation Group Project of Southern Marine Science and Engineering Guangdong Laboratory (Zhuhai) (Grant No. 311020004), and the GuangzhouU-HKUST Joint Research Fund (Grant Nos. YH202101 and GZU21SC03).

ACKNOWLEDGMENTS

The authors would like to thank two reviewers for their valued criticism and suggestions.

REFERENCES

Alexander M. A., Bladé I., Newman M., Lanzante J. R., Lau N. C., Scott J. D. (2002). The Atmospheric Bridge: The Influence of ENSO Teleconnections on Air–Sea Interaction Over the Global Oceans. *J. Climate* 15 (16), 2205–2231. doi: 10.1175/1520-0442(2002)015<2205:TABTIO>2.0.CO;2

Carton J. A., Chepurin G. A., Chen L. (2018). SODA3: A New Ocean Climate Reanalysis. *J. Climate* 31 (17), 6967–6983. doi: 10.1175/JCLI-D-18-0149.1

Chen J. M., Chang C. P., Li T. (2003). Annual Cycle of the South China Sea Surface Temperature Using the NCEP/NCAR Reanalysis. *J. Meteorol. Soc Jpn. Ser. II* 81 (4), 879–884. doi: 10.2151/jmsj.81.879

Cheng L., Abraham J., Hausfather Z., Trenberth K. E. (2019). How Fast are the Oceans Warming? *Science* 363 (6423), 128–129. doi: 10.1126/science.aav7619

Cheng L., Trenberth K. E., Fasullo J., Boyer T., Abraham J., Zhu J. (2017). Improved Estimates of Ocean Heat Content From 1960 to 2015. *Sci. Adv.* 3 (3), e1601545. doi: 10.1126/sciadv.1601545

Cheng X., Xie S. P., Du Y., Wang J., Chen X., Wang J. (2016). Interannual-To-Decadal Variability and Trends of Sea Level in the South China Sea. *Clim. Dynam.* 46 (9), 3113–3126. doi: 10.1007/s00382-015-2756-1

Chen J. M., Li T., Shih C. F. (2007). Fall Persistence Barrier of Sea Surface Temperature in the South China Sea Associated With ENSO. *J. Climate* 20 (2), 158–172. doi: 10.1175/JCLI4000.1

Chiang T. L., Hsin Y. C., Wu C. R. (2018). Multidecadal Changes of Upper-Ocean Thermal Conditions in the Tropical Northwest Pacific Ocean Versus South China Sea During 1960–2015. *J. Climate* 31 (10), 3999–4016. doi: 10.1175/JCLI-D-17-0394.1

Chu P. C., Edmons N. L., Fan C. (1999). Dynamical Mechanisms for the South China Sea Seasonal Circulation and Thermohaline Variabilities. *J. Phys. Oceanogr.* 29 (11), 2971–2989. doi: 10.1175/1520-0485(1999)029<2971:DMFTSC>2.0.CO;2

Dee D. P., Uppala S. M., Simmons A. J., Berrisford P., Poli P., Kobayashi S., et al. (2011). The ERA-Interim Reanalysis: Configuration and Performance of the Data Assimilation System. *Q. J. R. Meteor. Soc.* 137 (656), 553–597. doi: 10.1002/qj.828

Gill A. (1980). Some Simple Solutions for Heat-Induced Tropical Circulation. *Q. J. R. Meteor. Soc.* 106 (449), 447–462. doi: 10.1002/qj.49710644905

Halliwell G. R. (2004). Evaluation of Vertical Coordinate and Vertical Mixing Algorithms in the HYbrid-Coordinate Ocean Model (HYCOM). *Ocean. Model* 7 (3), 285–322. doi: 10.1016/j.ocemod.2003.10.002

Kim J. W., An S. I. (2019). Western North Pacific Anticyclone Change Associated With the El Niño–Indian Ocean Dipole Coupling. *Int. J. Climatol.* 39 (5), 2505–2521. doi: 10.1002/joc.5967

Klein S. A., Soden B. J., Lau N. C. (1999). Remote Sea Surface Temperature Variations During ENSO: Evidence for a Tropical Atmospheric Bridge. *J. Climate* 12 (4), 917–932. doi: 10.1175/1520-0442(1999)012<0917:RSSTVD>2.0.CO;2

Liang Z., Zeng L., Wang Q., Peng Q., Wang D. (2021). Interpretation of Interannual Variability of the Zonal Contrasting Thermal Conditions in the Winter South China Sea. *Clim. Dynam.* 1-19. doi: 10.1007/s00382-021-05968-6

Liu Q., Jiang X., Xie S.-P., Liu W.-T. L. (2004). A Gap in the Indo-Pacific Warm Pool Over the South China Sea in Boreal Winter: Seasonal Development and Interannual Variability. *J. Geophys. Res.-Oceans* 109 (C7). doi: 10.1029/2003JC002179

Liu Q.-Y., Wang D., Wang X., Shu Y., Xie Q., Chen J. (2014). Thermal Variations in the South China Sea Associated With Eastern and Central Pacific El Niño and Their Mechanisms. *J. Geophys. Res.-Oceans* 119, 8955–8972. doi: 10.1002/2014JC010429

Liu Z., Yang H., Liu Q. (2001). Regional Dynamics of Seasonal Variability in the South China Sea. *J. Phys. Oceanogr.* 31 (1), 272–284. doi: 10.1175/1520-0485(2001)031<0272:RDOSVI>2.0.CO;2

Li T., Zhang Y., Lu E., Wang D. (2002). Relative Role of Dynamic and Thermodynamic Processes in the Development of the Indian Ocean Dipole: An OGCM Diagnosis. *Geophys. Res. Lett.* 29 (23), 25–21. doi: 10.1029/2002GL015789

Matsuno T. (1966). Quasi-Geostrophic Motions in the Equatorial Area. *J. Meteorol. Soc Jpn. Ser. II* 44 (1), 25–43. doi: 10.2151/jmsj1965.44.1_25

Monterey G., Levitus S. (1997). Seasonal Variability of Mixed Layer Depth for the World Ocean. *NOAA Atlas NESDIS* 14. 100 pp. atl. Oceanicand Atmos. Admin., Silver Spring, Md.

Ose T., Song Y., Kitoh A. (1997). Sea Surface Temperature in the South China Sea. *J. Meteorol. Soc Jpn. Ser. II* 75 (6), 1091–1107. doi: 10.2151/jmsj1965.75.6_1091

Qu T. (2001). Role of Ocean Dynamics in Determining the Mean Seasonal Cycle of the South China Sea Surface Temperature. *J. Geophys. Res.-Oceans* 106 (C4), 6943–6955. doi: 10.1029/2000JC000479

Qu T., Kim Y. Y., Yaremchuk M., Tozuka T., Ishida A., Yamagata T. (2004). Can Luzon Strait Transport Play a Role in Conveying the Impact of ENSO to the South China Sea? *J. Climate* 17 (18), 3644–3657. doi: 10.1175/1520-0442(2004)017<3644:CLSTPA>2.0.CO;2

Reynolds R. W., Smith T. M., Liu C., Chelton D. B., Casey K. S., Schlax M. G. (2007). Daily High-Resolution-Blended Analyses for Sea Surface Temperature. *J. Climate* 20 (22), 5473–5496. doi: 10.1175/2007JCLI1824.1

Seow M. X. C., Tozuka T. (2019). Ocean Thermodynamics Behind the Asymmetry of Interannual Variation of South China Sea Winter Cold Tongue Strength. *Clim. Dynam.* 52, 3241–3253. doi: 10.1007/s00382-018-4320-2

Shen S., Lau K. M. (1995). Biennial Oscillation Associated With the East Asian Summer Monsoon and Tropical Sea Surface Temperatures. *J. Meteorol. Soc Jpn. Ser. II* 73 (1), 105–124. doi: 10.2151/jmsj1965.73.1_105

Sverdrup H. U. (1947). Wind-Driven Currents in a Baroclinic Ocean: With Application to the Equatorial Currents of the Eastern Pacific. *P. Natl. Acad. Sci. U.S.A.* 33, 318–326. doi: 10.1073/pnas.33.11.318

Tan W., Wang X., Wang W., Wang C., Zuo J. (2016). Different Responses of Sea Surface Temperature in the South China Sea to Various El Niño Events During Boreal Autumn. *J. Climate* 29 (3), 1127–1142. doi: 10.1175/JCLI-D-15-0338.1

Tian J., Yang Q., Liang X., Xie L., Hu D., Wang F., et al. (2006). Observation of Luzon Strait Transport. *Geophys. Res. Lett.* 33 (19). doi: 10.1029/2006GL026272

Tomita T., Yasunari T. (1996). Role of the Northeast Winter Monsoon on the Biennial Oscillation of the ENSO/monsoon System. *J. Meteorol. Soc Jpn. Ser. II* 74 (4), 399–413. doi: 10.2151/jmsj1965.74.4_399

Trenberth K. E., Branstator G. W., Karoly D., Kumar A., Lau N. C., Ropelewski C. (1998). Progress During TOGA in Understanding and Modeling Global Teleconnections Associated With Tropical Sea Surface Temperatures. *J. Geophys. Res.-Oceans* 103 (C7), 14291–14324. doi: 10.1029/97JC01444

Wang D., Liu Q., Huang R. X., Du Y., Qu T. (2006b). Interannual Variability of the South China Sea Throughflow Inferred From Wind Data and an Ocean Data Assimilation Product. *Geophys. Res. Lett.* 33 (14). doi: 10.1029/2006GL026316

Wang C., Wang W., Wang D., Wang Q. (2006a). Interannual Variability of the South China Sea Associated With El Niño. *J. Geophys. Res.-Oceans* 111, C03023. doi: 10.1029/2005JC003333

Wang B., Wu R., Fu X. (2000). Pacific–East Asian Teleconnection: How Does ENSO Affect East Asian Climate? *J. Climate* 13 (9), 1517–1536. doi: 10.1175/1520-0442(2000)013<1517:PEATHD>2.0.CO;2

Wang B., Wu R., Li T. I. M. (2003). Atmosphere–warm Ocean Interaction and its Impacts on Asian–Australian Monsoon Variation. *J. Climate* 16 (8), 1195–1211. doi: 10.1175/1520-0442(2003)16<1195:AOIAII>2.0.CO;2

Wang D., Xie Q., Du Y., Wang W., Chen J. (2002). The 1997–1998 Warm Event in the South China Sea. *Chin. Sci. Bul.* 47 (14), 1221–1227. doi: 10.1007/BF02907614

Wang B., Zhang Q. (2002). Pacific–East Asian Teleconnection. Part II: How the Philippine Sea Anomalous Anticyclone is Established During El Niño Development. *J. Climate* 15, 3252–3265. doi: 10.1175/1520-0442(2002)015,3252:PEATPI.2.0.CO;2

Watanabe M., Jin F. F. (2002). Role of Indian Ocean Warming in the Development of Philippine Sea Anticyclone During ENSO. *Geophys. Res. Lett.* 29 (10), 116–111. doi: 10.1029/2001GL014318

Wu R., Chen W., Wang G., Hu K. (2014). Relative Contribution of ENSO and East Asian Winter Monsoon to the South China Sea SST Anomalies During ENSO Decaying Years. *J. Geophys. Res.-Atmoss* 119 (9), 5046–5064. doi: 10.1002/2013JD021095

Xiao F., Wang D., Leung M. Y. (2020b). Early and Extreme Warming in the South China Sea During 2015/2016: Role of an Unusual Indian Ocean Dipole Event. *Geophys. Res. Lett.* 47 (17), e2020GL089936. doi: 10.1029/2020GL089936

Xiao F., Wang D., Yang L. (2020a). Can Tropical Pacific Winds Enhance the Footprint of the Interdecadal Pacific Oscillation on the Upper-Ocean Heat Content in the South China Sea? *J. Climate* 33 (10), 4419–4437. doi: 10.1175/JCLI-D-19-0679.1

Xiao F., Wang D., Zeng L., Liu Q.-Y., Zhou W. (2019). Contrasting Changes in the Sea Surface Temperature and Upper Ocean Heat Content in the South China Sea During Recent Decades. *Clim. Dynam.* 53 (3–4), 1597–1612. doi: 10.1007/s00382-019-04697-1

Xiao F., Wu Z., Lyu Y., Zhang Y. (2020c). Abnormal Strong Upwelling Off the Coast of Southeast Vietnam in the Late Summer of 2016: A Comparison With the Case in 1998. *Atmosphere* 11 (9), 940. doi: 10.3390/atmos11090940

Xiao F., Zeng L., Liu Q.-Y., Zhou W., Wang D. (2018). Extreme Subsurface Warm Events in the South China Sea During 1998/99 and 2006/07: Observations and Mechanisms. *Clim. Dynam.* 50 (1–2), 115–128. doi: 10.1007/s00382-017-3588-y

Xie S. P., Hu K., Hafner J., Tokinaga H., Du Y., Huang G., et al. (2009). Indian Ocean Capacitor Effect on Indo–western Pacific Climate During the Summer Following El Niño. *J. Climate* 22 (3), 730–747. doi: 10.1175/2008JCLI2544.1

Xie S. P., Xie Q., Wang D., Liu W. T. (2003). Summer Upwelling in the South China Sea and its Role in Regional Climate Variations. *J. Geophys. Res.-Oceans* 108 (C8). doi: 10.1029/2003JC001867

Yu K., Qu T. (2013). Imprint of the Pacific Decadal Oscillation on the South China Sea Throughflow Variability. *J. Climate* 26 (24), 9797–9805. doi: 10.1175/JCLI-D-12-00785.1

Zhang R., Sumi A., Kimoto M. (1996). Impact of El Niño on the East Asian Monsoon. *J. Meteorol. Soc Jpn. Ser. II* 74 (1), 49–62. doi: 10.2151/jmsj1965.74.1_49

Conflict of Interest: The authors declare that the research was conducted in the absence of any commercial or financial relationships that could be construed as a potential conflict of interest.

Publisher's Note: All claims expressed in this article are solely those of the authors and do not necessarily represent those of their affiliated organizations, or those of the publisher, the editors and the reviewers. Any product that may be evaluated in this article, or claim that may be made by its manufacturer, is not guaranteed or endorsed by the publisher.

Copyright © 2022 Xiao, Wang, Wu, Song, Zeng, Xie and Wang. This is an open-access article distributed under the terms of the Creative Commons Attribution License (CC BY). The use, distribution or reproduction in other forums is permitted, provided the original author(s) and the copyright owner(s) are credited and that the original publication in this journal is cited, in accordance with accepted academic practice. No use, distribution or reproduction is permitted which does not comply with these terms.

frontiers | Frontiers in Marine Science

ORIGINAL RESEARCH
published: 12 April 2022
doi: 10.3389/fmars.2022.882196

Differences of Macroalgal Consumption by Eight Herbivorous Coral Reef Fishes From the Xisha Islands, China

Peng Wu[1,2,3,4], *Teng Wang*[1,2,3,4], *Yong Liu*[1,2,3,4*], *Chunhou Li*[1,2,3,4], *Yayuan Xiao*[1,2,3], *Shannan Xu*[1,2,3], *Tingting Han*[3], *Lin Lin*[1,2,3] *and Qiumei Quan*[1]

[1] *Key Laboratory of South China Sea Fishery Resources Exploitation & Utilization, Ministry of Agriculture and Rural Affairs, South China Sea Fisheries Research Institute, Chinese Academy of Fishery Sciences, Guangzhou, China,* [2] *Southern Marine Science and Engineering Guangdong Laboratory (Guangzhou), Guangzhou, China,* [3] *Scientific Observation and Research Field Station of Pearl River Estuary Ecosystem, Guangdong Province, South China Sea Fisheries Research Institute, Guangzhou, China,* [4] *Guangdong Provincial Key Laboratory of Fishery Ecology and Environment, South China Sea Fisheries Research Institute, Guangzhou, China*

OPEN ACCESS

Edited by:
Meilin WU,
South China Sea Institute of Onceanology (CAS), China

Reviewed by:
Ximei Liang,
Jiangxi Agricultural University, China
Yanjun Shen,
Chongqing Normal University, China
Xuefeng Wang,
Guangdong Ocean University, China

***Correspondence:**
Yong Liu
liuyong@scsfri.ac.cn

Specialty section:
This article was submitted to Marine Pollution, a section of the journal Frontiers in Marine Science

Received: *23 February 2022*
Accepted: *17 March 2022*
Published: *12 April 2022*

Citation:
Wu P, Wang T, Liu Y, Li C, Xiao Y, Xu S, Han T, Lin L and Quan Q (2022) Differences of Macroalgal Consumption by Eight Herbivorous Coral Reef Fishes From the Xisha Islands, China. Front. Mar. Sci. 9:882196. doi: 10.3389/fmars.2022.882196

Herbivorous fishes play an important role in preventing the overabundance of macroalgae on coral reefs. Understanding the feeding selectivity and consumption of macroalgae by herbivorous fishes can be challenging in studies of their ecological role in the preservation and recovery of coral reefs. Coral reef decline, macroalgal overgrowth and overfishing are clearly visible in the Xisha Islands, China. However, there are seldom studies on the feeding behaviors of herbivorous fishes in this area. We used microscopy, 18S rRNA high-throughput sequencing, and stable isotope analyses to comprehensively examine the diet of eight herbivorous reef fish species common in the Xisha Islands, including one parrotfish, two chub, two unicorn fish, and three rabbitfish. Based on microscopic examination, *Siganus argenteus* fed on the highest number of macroalgae species (five species), followed by *Naso unicornis* (four species). *Kyphosus cinerascens*, *K. vaigiensis*, *N. unicornis* and *S. punctatissimus* fed on the entire macroalgal thallus, indicating their greater ecological importance compared with species that only consume algal fronds. According to the 18S rRNA high-throughput sequencing of fish intestinal contents, cluster analysis revealed that consumed macroalgae composition from the eight fishes always grouped together based on the fish species, but with low similarity. *K. vaigiensis* removed the highest diversity of macroalgae species as well as the greatest quantity of macroalgae. *Calotomus carolinus* can consume the red alga *Pneophyllum conicum*, which is widely distributed on Indo-Pacific coral reefs and can overgrow and kill live corals. *N. unicornis* was found to occupy the lowest trophic position based on stable isotope analysis. Multi-technique analyses revealed that *K. vaigiensis*, *N. unicornis* and *S. argenteus* showed a high consumption potential of macroalgae, suggesting that they are the key browsers that should receive priority protection in the Xisha Islands. A diverse herbivorous fish fauna is also very important in the Xisha coral reefs. These results not only demonstrated the

various functions of different herbivorous fish species in macroalgal removal, but also provided insights into the management of herbivorous fishes on the coral reefs of the South China Sea.

Keywords: coral reefs, herbivorous fishes, macroalgal species composition, diet, intestinal contents

INTRODUCTION

Coral reefs are often called the tropical rainforests of the ocean and are the most productive and biologically diverse ecosystem, supporting more than 25% of all known marine species (Moberg and Folke, 1999; Walker and Wood, 2005). However, the world's coral reefs are declining due to numerous anthropogenic activities and global climate disturbances, such as coastal development, land-based and marine pollution, overfishing, tropical storms and thermal stress (Burke et al., 2011; Liu et al., 2021; Souter et al., 2021). There was a massive loss of almost 14% of the coral from the world's coral reefs between 2009 and 2018 (Souter et al., 2021). The decline of coral reefs can involve a shift from coral towards macroalgae as the dominant feature (Cheal et al., 2010; Kopp et al., 2010; Bruno et al., 2019). Macroalgae growth can hinder the settlement, survival, and growth of corals, so that a healthy coral reef ecosystem is difficult to reestablish (Puk et al., 2016; Dell et al., 2020). Phase shifts in the balance of coral/macroalgal species have been attributed to insufficient herbivore activity, eutrophication, environmental disturbances (e.g. typhoons, ocean warming and coral bleaching, etc.), or a combination of these factors (Cheal et al., 2010; Russ et al., 2015; Neilson et al., 2018; Bruno et al., 2019; Adam et al., 2021).

Herbivorous reef fishes are the major consumers of macroalgae on coral reefs (Cheal et al., 2010). Chub (*Kyphosus* spp.) (Dell et al., 2020), unicorn fish (*Naso* spp.) (Lefevre and Bellwood, 2011; Streit et al., 2015) and rabbitfish (*Siganus* spp.) (Bennett and Bellwood, 2011; Streit et al., 2015) are recognized as the important macroalgal grazers on coral reefs. Parrotfish are usually as microphages that target microscopic photoautotrophs, and macroalgae is a low component of diet of Parrotfish (Clements et al., 2017; Nicholson and Clements, 2020). The feeding preferences of herbivorous reef fishes differ at the species level (Hoey and Bellwood, 2009; Duran et al., 2019; Dell et al., 2020). *Naso* spp. and *Kyphosus* spp. generally target brown macroalgae (Puk et al., 2016). Of the over 50 herbivorous fish species identified off Lizard Island, northern Great Barrier Reef (GBR), only one, *Naso unicornis*, fed on the erect brown macroalga *Sargassum* across all habitats (Hoey and Bellwood, 2009). A study of the feeding behaviors of four rabbitfish species in the Seychelles of the Indian Ocean, indicated that *Siganus argenteus* and *S. sutor* were generalist herbivores, foraging on turf algae, macroalgae, seagrass and epiphytic algae, while *S. corallinus* and *S. stellatus* were specialist herbivores foraging primarily on turf algae growing on the reef substrate (Ebrahim et al., 2020). Herbivore species richness appears to be critical in generally lowering macroalgal abundance because of the complementary feeding habits of a diverse assemblage of herbivores (Burkepile and Hay, 2008). Therefore, it is essential to understand the dietary spectra of the various herbivorous reef fishes to understand their cumulative effect on coral reef health. However, very little is currently known about the macroalgal feeding preferences of the herbivorous reef fishes on the coral reefs off the Xisha Islands, and this limits our understanding of their different functional roles in controlling the spread of macroalgae.

The feeding ecology of herbivorous fishes on coral reefs is usually determined by behavioral observations, counting the number of bites taken by fish feeding in the field (Mantyka and Bellwood, 2007; Dell et al., 2020; Ebrahim et al., 2020), or by microscopic examination of intestinal contents (Choat et al., 2002; Dromard et al., 2015). These methods are convenient and provide detailed information on the dietary spectrum of different species (de Carvalho et al., 2019). However, there are some practical problems; small, fragile, or morphologically indistinct organisms are difficult to identify in intestinal samples, especially after digestion (Dromard et al., 2015; Kume et al., 2021). Stable isotope analysis is a powerful tool which can reveal feeding behavior over an extended period, although with some taxonomic limitations (Rodriguez-Barreras et al., 2020; Kume et al., 2021). High-throughput sequencing is emerging as a molecular method to estimate fish dietary composition by identifying the taxa eaten from genomic DNA recovered from fish intestines (Corse et al., 2010; Leray et al., 2015; Lin et al., 2021; Nalley et al., 2022). This molecular method is more efficient for diet evaluation with enrichment of the reference sequence databases such as GenBank (Devloo-Delva et al., 2019). Nalley et al. (2021) also demonstrated that reference sequences were important for metabarcoding sequencing. However, DNA metabarcoding lacks the biomass information of the diet (Lamb et al., 2019). Different approaches on examining the diets of herbivorous fishes may influence the interpretation of diet and function (Nalley et al., 2022). Therefore, using a combination of these three methods allows comprehensive descriptions of the dietary composition of various fish species.

Coral cover off the Xisha Islands has declined dramatically over the past 15 years (Li et al., 2018) and macroalgae have become dominant in many of their coral reef areas (Chen et al., 2019). Macroalgae cover was higher than coral cover in about 30% of the sites (70 sites) in Xisha coral reef island, and macroalgae cover in Qilianyu Islets and Cays can reach to 20% (Chen et al., 2019). Over 100 fish species have been recorded off the Qilianyu Islets and Cays, with the dominant species belonging to the families Pomacentridae and Labridae (Li et al., 2017). Overfishing has become a serious threat for these reefs (Zhao et al., 2016). However, the diet composition of fishes in this area was seldom investigated. Here, we explored the

dietary differences of eight different herbivorous reef fishes common around the Xisha Islands, based on microscopic examination, 18S rRNA high-throughput sequencing and stable isotope analyses. We focused on comparisons of the macroalgal feeding selectivity of herbivores, including one parrotfish (*Calotomus carolinus*), two chub (*Kyphosus cinerascens*, and *K. vaigiensis*), two unicorn fish (*Naso brevirostris*, and *N. unicornis*) and three rabbitfish (*S. argenteus*, *S. puellus*, and *S. punctatissimus*). These fishes cover the herbivorous fishes belonging to different Family in Xisha Islands. Our previous study showed that *K. vaigiensis*, *N. brevirostris* and *N. unicornis* were the abundant herbivorous species in this region, while the others were common species (Wang et al., 2022). In addition, chubs, unicorn fish and rabbitfish were always considered as important herbivores in the Indo-Pacific (Dell et al., 2020). The results provided key information on the ecological function of these herbivorous fishes in removing macroalgae from coral reefs, and gave insights into the most effective overfishing prevention measures to keep the coral reef ecosystem at its most healthy.

MATERIALS AND METHODS

Study Site and Fish Sample Collection

The Xisha Islands, in the central South China Sea, are derived from coral reefs and comprise over 40 islands, reefs and cays, including the Dongdao Atolls, the Huaguang Atolls, the Xuande Atolls, the Yongle Atolls, and some smaller islands (Zhao et al., 2017; Ding et al., 2019; Zhao et al., 2019). The Qilianyu Islets and Cays (16°59′ N, 112°18′ E) of the Xisha Islands comprise an arced reef flat, which extends in a NW-SE direction and curves to the NNE (Shen et al., 2017). Eight herbivorous reef fish species common in the Qilianyu Islets and Cays were collected by SCUBA in June 2020 (**Figure S1**). Fishes were captured by driver with spear guns between the hours of 18:00 and 20:00. All fishes were collected along the shallow waters around the coral reef regions (water depth below 15 m). The details of the fishes sampled in this study, along with their phylogenetic classification and feeding strategies, are shown in **Table 1**. The feeding strategy of each species was determined based on the previous published studies. All fishes collected were kept at -4°C and transported to the laboratory, where they were dissected using sterile scissors. In the dissecting process, all fishes were made sure to have food item in the intestines. The anterior intestinal contents were separated and divided into two subsamples. One subsample was used for microscopic examination, and the another was used for 18S rRNA high-throughput sequencing analysis. A small piece of white muscle tissue near the dorsal fin was sampled from each fish and used for stable isotope analysis.

Intestinal Contents for Microscopical Analysis Examination

Intestinal contents of each fish species were collected for dietary assessment. Intestinal contents of individual fish were spread on glass culture dish and put under a microscope (Zeiss SteREO Discovery.V20, Germany). Photographs of the food items were taken using the microscope. Macrophytes species (Macroalgae and seagrasses) were only observed here, however, quantity analysis of the macrophytes composition wasn't concerned. Macrophytes species were identified according to their morphological traits (Titlyanov et al., 2017; Huang, 2018).

Composition of Intestinal Contents Measured by 18S rRNA High-Throughput Sequencing Analysis

The total DNA of intestinal contents (0.2 g sample) of individual fish was extracted using a QIAamp® Fast DNA Stool Mini Kit (Qiagen, Germantown, MD, USA) according to the manufacturer's protocols. The total DNA recovered from the same fish species was pooled together for PCR amplification which targeted the V4 region of the eukaryotic 18S rRNA gene using primers 528F (5'-GCGGTAATTCCAGCTCCAA-3') and 706R (5'-AATCCRAGAATTTCACCTCT-3'), where the barcodes were an eight-base sequence unique to each sample (Cheung et al., 2010). Amplicons were extracted from 2% agarose gels and purified using the AMPure XP Beads (Beckman, Agencourt, USA). These purified amplicons were pooled in equimolar paired-end sequences (2 × 250) on an Illumina platform (Gene Denovo Co., Guangzhou, China). Raw reads for each fish species were deposited into the NCBI Sequence Read Archive (SRA) database with the accession number PRJNA742779. The representative sequences affiliated to the phyla Chlorophyta, Ochrophyta and Rhodophyta obtained in this study were deposited in the GenBank database under accession numbers MZ481947-MZ481964, MZ481932-MZ481946 and MZ481965-MZ482014, respectively.

TABLE 1 | Basic information on the coral reef fish species sampled in this study.

Fish species	Sampling sites	Sampled number	Total length(mm)	Genus	Family	Source of herbivorous feeding strategy
C. carolinus	Xisha Islands	3	227 ± 8	*Calotomus*	Labridae	Chong-Seng et al., 2014; Sura et al., 2021
K. cinerascens	Xisha Islands	4	291 ± 71	*Kyphosus*	Kyphosidae	Choat et al., 2004
K. vaigiensis	Xisha Islands	3	224 ± 9	*Kyphosus*	Kyphosidae	Choat et al., 2004; Streit et al., 2015
N. brevirostris	Xisha Islands	3	202 ± 15	*Naso*	Acanthuridae	Choat et al., 2004
N. unicornis	Xisha Islands	3	236 ± 20	*Naso*	Acanthuridae	Choat et al., 2004; Streit et al., 2015; Sura et al., 2021
S. argenteus	Xisha Islands	5	248 ± 20	*Siganus*	Siganidae	Hoey et al., 2013
S. puellus	Xisha Islands	3	221 ± 43	*Siganus*	Siganidae	Bennett and Bellwood, 2011; Hoey et al., 2013
S. punctatissimus	Xisha Islands	3	298 ± 18	*Siganus*	Siganidae	Cvitanovic and Bellwood, 2009

Raw reads were filtered using FASTP (V0.18.0) to obtain high quality clean reads according to the following rules: (1) remove reads containing more than 10% of unknown nucleotides and (2) remove reads containing less than 50% of bases with a quality (Q-value)>20 (Chen et al., 2018). Paired-end clean reads were merged as raw tags using FLSAH (V1.2.11) with a minimum overlap of 10 bp and mismatch error rates of 2% or less (Magoc and Salzberg, 2011). Noisy sequences of raw tags were then filtered using QIIME (V1.9.1) (Caporaso et al., 2010) under specific filtering conditions (Bokulich et al., 2013) to obtain high quality clean tags. Clean tags were searched against the reference database (http://drive5.com/uchime/uchime_download.html) to perform reference-based chimera checks, using the UCHIME algorithm (Edgar et al., 2011). All chimeric tags were removed to finally obtain effective tags for further analysis.

The effective tags were clustered into operational taxonomic units (OTUs) of ≥ 97% similarity using UPARSE (V9.2.64) (Edgar, 2013). A dominant sequence was selected within each cluster as a representative sequence. The representative sequences were then picked-out to annotate taxonomic assignments using the RDP classifier (V2.2) (Wang et al., 2007) based on the SILVA database (V132) (Pruesse et al., 2007). The OTU sequences belonging to class Actinopterygii were discarded in further analysis. Moreover, if an OTU sequence could not be assigned to any phylum in the SILVA database, it was subjected to a further BLAST search (http://blast.ncbi.nlm.nih.gov/Blast.cgi). The taxonomic classification was then finally confirmed by its similarity to a BLAST result.

Stable Isotope Analysis

Fish muscle tissue were dried at 60°C to a constant weight. Samples were then ground to a fine, homogeneous powder using an automatic sample grinder (Jxfstprp-24, Jingxin Co., Shanghai, China). Samples were taken for carbon and nitrogen stable isotope analysis using a continuous-flow isotope ratio mass spectrometer (Finnigan MAT 253, Thermo Scientific, USA) coupled to an elemental analyzer (Flash EA 1112, Thermo Scientific, USA). The C and N isotope ratios were determined as $\delta^{13}C$ and $\delta^{15}N$, respectively, according to the following formula:

$$\delta^{13}C \quad \text{or } \delta^{15}N\ (\text{‰}) = \left(\frac{R_{sample}}{R_{standard}} - 1\right) \times 1000,$$

where R is the corresponding ratio $^{13}C/^{12}C$ or $^{15}N/^{14}N$, R_{sample} is measured for fish, and $R_{standard}$ is an international standard (Pee Dee Belemnite for C isotopes and atmospheric N_2 for N isotopes).

Data Analysis

Bar charts of relative abundances of eukaryote sequences found in eight fish intestines and a biplot of stable isotope signatures ($\delta^{13}C$ and $\delta^{15}N$) of fish muscles were constructed using Origin 2018 software (OriginLab Co., Northampton, MA, USA). A phylogenetic tree of 18S rRNA sequences related to the phyla Chlorophyta, Ochrophyta and Rhodophyta was constructed using MEGA X and the neighbor-joining algorithm, and the maximum composite likelihood method with bootstrap analyses for 1,000 replicates (Kumar et al., 2018). A heat map of the relative abundance of the 18S rRNA sequences belonging to the phyla Chlorophyta, Ochrophyta and Rhodophyta was individually generated using the OmicShare tools (http://www.omicshare.com/tools). Dominant OTUs from the heat maps were selected to analyze taxonomic assignments using BLAST research. Based on the relative abundance of macroalgae sequences in eight fish intestines, data were transformed as square root with Bray-Curtis similarity resemblance. Then cluster analysis of the Bray-Curtis similarity was done with the Primer 5 software. Statistical differences about the stable isotope values of $\delta^{13}C$ and $\delta^{15}N$ among the different eight fishes were analyzed, with $p<0.05$ considered significant.

RESULTS

Microscopic Observations of Fish Intestinal Contents

Intestinal contents of the eight fish species collected were analyzed by microscopy. After thorough washing, anterior intestinal contents of fishes were examined and a high proportion of flocculent detritus was found. Coral sand was only detected in the intestinal contents of *C. carolinus* and *S. argenteus*. Importantly, macrophytes (macroalgae or seagrasses) were easily observed in fish intestines (**Table 2**). The number of macrophyte species consumed by the eight herbivorous reef fishes varied. *S. argenteus* consumed the highest number of macrophyte species (six species), followed by *N. unicornis* (four species). However, only a few macrophyte species could be identified morphologically, while other fragments belonging to Chlorophyta, Ochrophyta or Rhodophyta were too small and were difficult to identify. The green algae *Valonia ventricosa* and *Halimeda* sp. were detected in the fish intestines of *N. unicornis* and *S. argenteus*, respectively. The brown alga *Turbinaria ornata* and the red alga *Acanthophora* spp. were observed in the intestinal contents of *N. unicornis* and *S. punctatissimus*, respectively. In addition, the seagrass *Halophila ovalis* was identified as a food source of *S. argenteus*.

Molecular Detection of Macrophyte Species Composition in Fish Intestines

The dietary spectra of the eight fishes were analyzed with 18S rRNA gene high-throughput sequencing at the phylum and class levels (**Figure 1**). The 15 most abundant phyla accounted for 88.2%–99.3% of the total sequences found in the eight fish species' intestines (**Figure 1A**). There were marked differences in the relative abundance of the dominant phyla in each species sample. Porifera was the most abundant taxon in *C. carolinus*, which was further identified as Demospongiae (sponges) (**Figure 1**). The dominant phyla in *K. cinerascens* were Bacillariophyta and Porifera. Ochrophyta, Streptophyta and Bigyra were significantly more abundant in *K. vaigiensis*, *S. argenteus* and *S. punctatissimus*, respectively. However,

TABLE 2 | Macrophyte fragments observed by microscopic examination in the intestinal contents of fishes from the Xisha coral reefs.

Fish species	Number of observed macrophytes species	Photographs of macrophytes fragments in fish intestine
C. carolinus	1	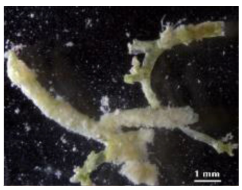
K. cinerascens	2	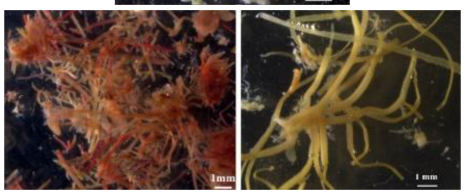
K. vaigiensis	2	
N. brevirostris	2	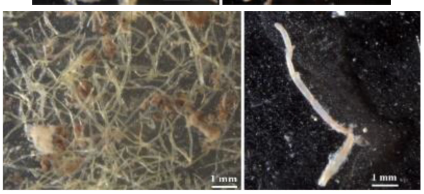
N. unicornis	4	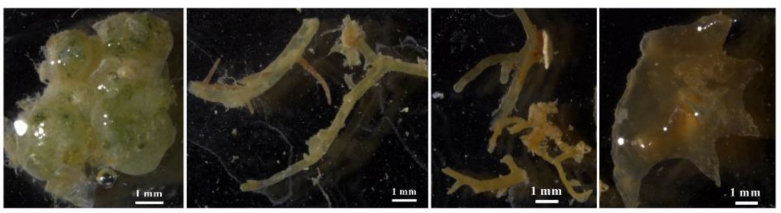 *Valonia ventricosa* *Turbinaria ornata*
S. puellus	2	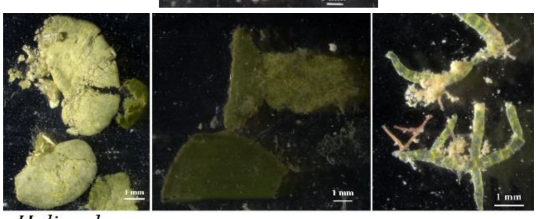 *Halimeda* sp.

(Continued)

TABLE 2 | Continued

Fish species	Number of observed macrophytes species	Photographs of macrophytes fragments in fish intestine
S. argenteus	6	*Halophila ovalis*
S. punctatissimus	1	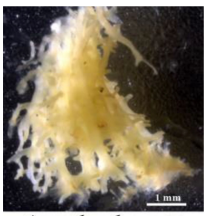 *Acanthophora* sp.

Cnidaria, mainly Anthozoa (corals), were much higher in *S. puellus*, *N. brevirostris*, *N. unicornis* and *C. carolinus* (**Figure 1**). Sequences belonging to Streptophyta were identified as *H. ovalis*, a seagrass species which occurred in the intestines of *C. carolinus*, *N. brevirostris*, *S. argenteus* and *S. punctatissimus*.

Sequences referring to the phyla Chlorophyta, Ochrophyta and Rhodophyta found in the eight fishes were further analyzed (**Figure 2**). A total of 18, 15 and 47 OTUs were observed belonging to Chlorophyta, Ochrophyta and Rhodophyta, respectively (**Figure 2A**). A phylogenetic tree of the observed OTUs was constructed and is shown in **Figure 3**. Chlorophyta OTUs were most diverse in *K. vaigiensis* and *S. argenteus* (≥10 OTUs). The highest numbers of Rhodophyta OTUs (23 OTUs) were observed in *K. cinerascens* and *K. vaigiensis*. Ochrophyta OTUs were most abundant in *K. vaigiensis* (11 OTUs). The relative abundance of macroalgae found in fish intestines are shown in **Figure 2B**. *K. vaigiensis* consumed the greatest abundance of macroalgae (76.9%), followed by *K. cinerascens* (14.5%). *N. unicornis* preferred brown algae, while *S. punctatissimus* consumed more green algae. The diet of *S. argenteus* contained 2.9% green algae, 0.8% brown algae and 1.9% red algae.

The differences in macroalgal composition between the intestinal contents of the eight fish species were analyzed (**Figure 4** and **Table 3**). The species composition of green algae or red algae in the eight herbivorous fishes diets was different (**Figures 4A, C**). Regarding the green algae, Otu000030, identified as *Dictyosphaeria cavernosa*, was abundant in *K. vaigiensis*. Otu000055, which was very similar to *Ulvella leptochaete*, was a dominant component in *S. argenteus* and *K. cinerascens*. Both Otu000067 and Otu000102 were affiliated to the genus *Cladophora*. The occurrence of Otu000067 was higher in *K. cinerascens*, while Otu000102 dominated in *N. brevirostris* and *S. argenteus*. Regarding the red algae (**Figure 4C**), Otu000056 dominated in *S. argenteus* and showed a high similarity to *Spyridia filamentosa*. Otu000077 was related to *Centroceras hyalacanthum*, and was a major component in *S. argenteus* and *S. punctatissimus*. Otu000094 matched with *Ceramium sinicola* and was relatively abundant in *K. cinerascens*. Otu000200 and Otu000260 were relatively abundant in *K. vaigiensis* and were similar to *Peyssonnelia rumoiana* and *P. armorica*, respectively. Otu000535 was identified as the red alga *P. rosenvingei* and was very abundant in *C. carolinus*. The intestinal contents of *C. carolinus* also contained a dominant OTU (Otu000554), which was matched with *Pneophyllum conicum*. The dominant OTUs in *N. unicornis* included Otu000309 and Otu000874, which were similar to *Chondrophycus* cf. *undulates* and *C. sinicola*, respectively. Regarding the brown algae (**Figure 4B**), Otu000009, related to *Lobophora variegate*, was dominant in the intestinal contents of all the fishes, except *S. argenteus*. Otu000014 was also abundant in most fishes, especially *S. argenteus* in which it was most abundant. Cluster analysis indicated that macroalgae consumption from different fish of the same species always grouped together with each other. However, there was a low similarity among the fishes (<52%), only *N. brevirostris* and *N. unicornis* group at a high similarity (50.8%) (**Figure 5**).

Stable Isotope Analysis

Stable isotope values of $\delta^{13}C$ and $\delta^{15}N$ from the eight herbivorous fish species are shown as a bi-plot (**Figure 6**). The $\delta^{13}C$ values across species ranged from -19.2 to -12.3‰. The $\delta^{13}C$ values were more enriched in *C. carolinus* (-12.3 ± 0.8‰), which was significant different with other five species, except for *N. unicornis* (-13.4 ± 2.6‰) and *K. vaigiensis* (-13.8 ± 1.5‰) (**Figure S2**). However, *S. punctatissimus* and *N. brevirostris* had lower enrichment of $\delta^{13}C$ values, with -19.2 ± 0.9‰ and -18.0 ± .02‰, respectively. The $\delta^{15}N$ values of fishes varied from 5.1 to 8.3‰. *K. vaigiensis* (8.3 ± 0.5‰) had significantly higher $\delta^{15}N$ values than others, except for *K. cinerascens* (p>0.05). *N. unicornis* showed the lowest $\delta^{15}N$ values (5.1 ± 0.6‰) and exhibited significant different from most species, but not for *S. punctatissimus* and *K. cinerascens*. *K. cinerascens*, *S. puellus* and *S. argenteus* had generally similar $\delta^{13}C$ and $\delta^{15}N$ values with no significant difference. The differences in $\delta^{15}N$ observed in

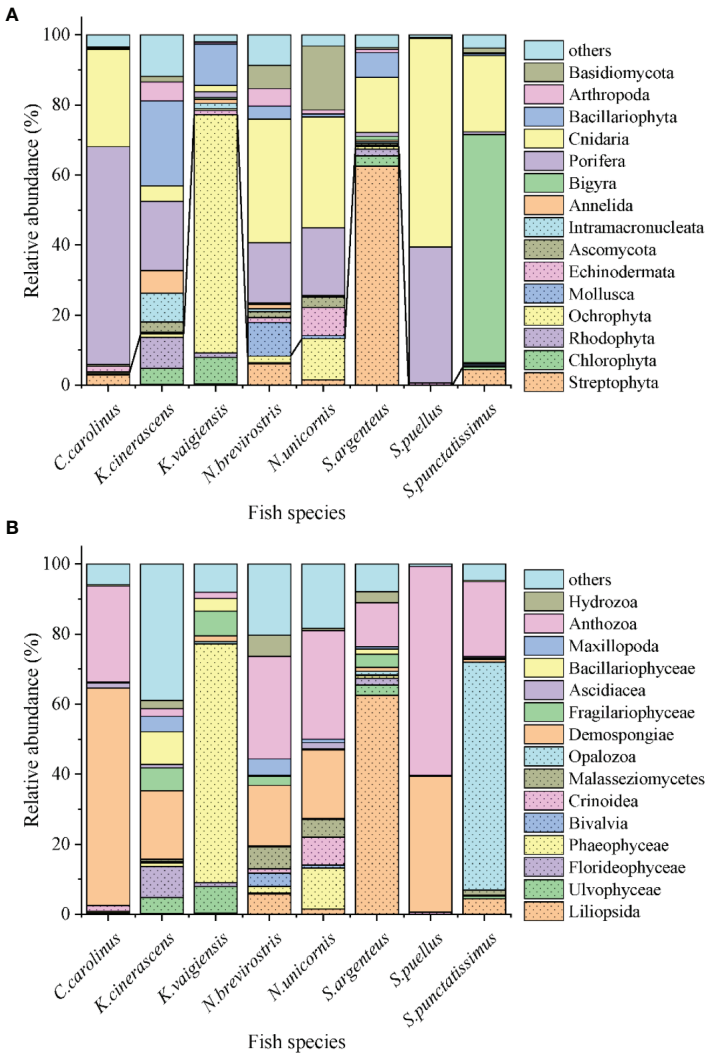

FIGURE 1 | Relative abundances of eukaryote sequences found in fish intestines, determined with 18S rRNA high-throughput sequencing. **(A)** phylum level. Polylines show the sum of the relative abundance of the phyla Streptophyta, Chlorophyta, Ochrophyta and Rhodophyta. **(B)** class level.

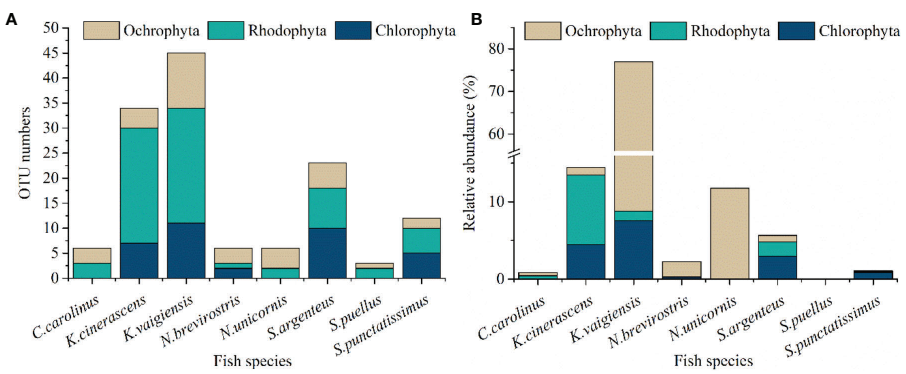

FIGURE 2 | Eukaryote sequences belonging to the phyla Chlorophyta, Ochrophyta and Rhodophyta obtained from intestinal contents of eight coral reef fish species which were collected from the Xisha Islands, China. **(A)** OTU numbers of taxonomic groups. **(B)** Relative abundance of taxonomic groups.

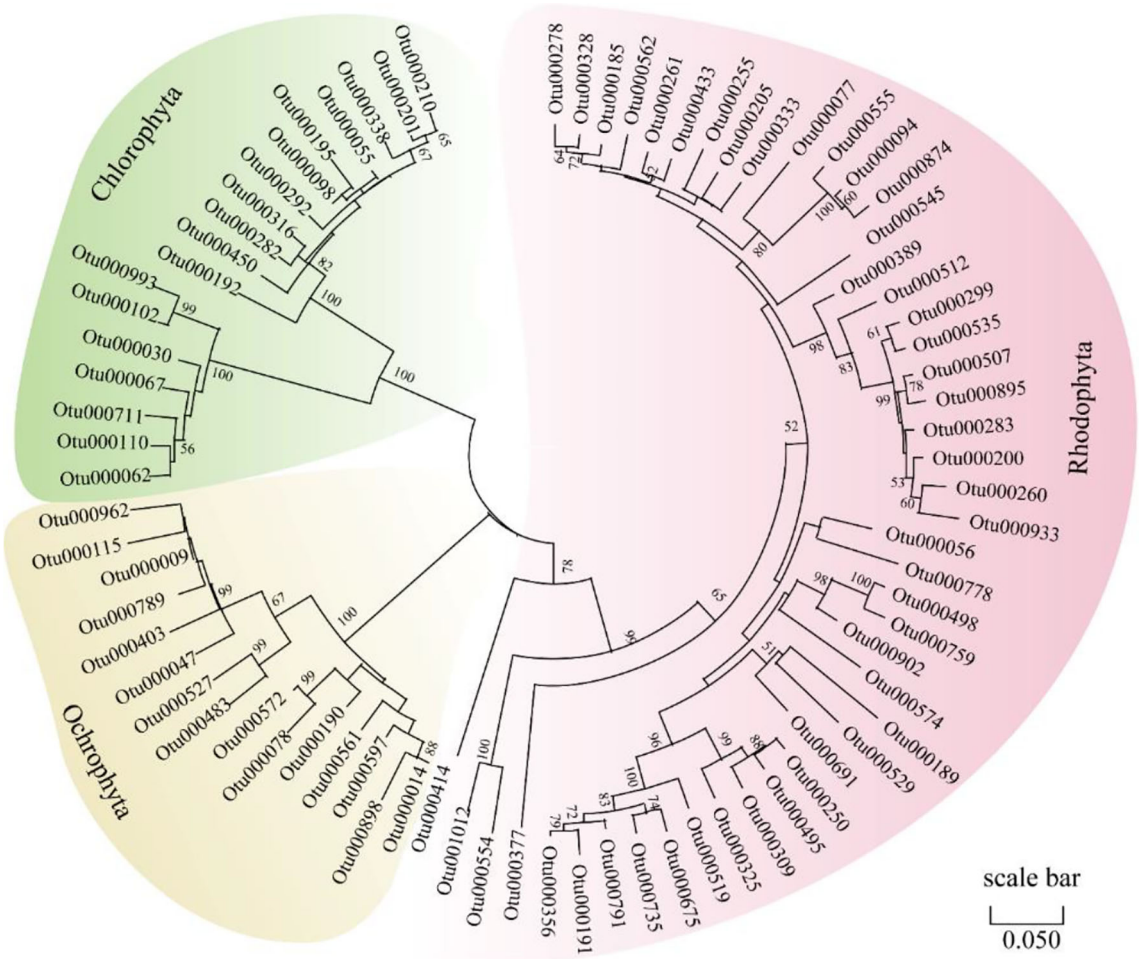

FIGURE 3 | Neighbor-joining tree of 18S rRNA sequences affiliated to the phyla Chlorophyta, Ochrophyta and Rhodophyta obtained from the intestinal contents of eight coral reef fish species which were collected from the Xisha Islands, China. The scale bar represents 5% estimated sequence divergence.

the eight fishes indicated that *N. unicornis* occupied a relatively low trophic position.

DISCUSSION

Microscopic Examination and High-Throughput Sequencing Analyses of Fish Intestinal Contents

Microscopic examination and 18S rRNA high-throughput sequencing analyses were used to investigate the dietary composition of eight herbivorous reef fish species off the Xisha Islands, China. There were some similarities in the results of the two methods. For example, the seagrass *H. ovalis* was observed in the intestinal contents of *S. argenteus* based on microscopic examination, and high-throughput sequencing analysis also found that this seagrass (Liliopsida) dominated the intestinal contents of *S. argenteus*. Microscopic examination revealed coral sand in the intestinal contents of *C. carolinus* and *S. argenteus*. High-throughput sequencing analysis also showed a high abundance of the class Anthozoa (corals) in *C. carolinus* and *S. argenteus*.

However, diet composition and breadth may vary according to the different approach used (Nalley et al., 2021). In this study, 18S rRNA high-throughput sequencing analysis provided higher taxonomic resolution of dietary composition, compared with microscopic examination. For example, some taxa that were found to dominate the intestinal contents using molecular analysis, such as Porifera, Cnidaria, Bacillariophyta were not detected by microscopic examination. The possible reasons were as follows. First, small organisms or digested organisms are too difficult to identify using a microscope (Dromard et al., 2015; Kume et al., 2021). In this study, microscopy detected a large amount of detritus in the fish intestinal contents. Dromard et al. (2015) using microscopy, also observed a high proportion of detritus in the intestines of Scaridae. Second, high-throughput sequencing is highly sensitive and can detect traces of DNA in mixed samples. This molecular technique can discriminate

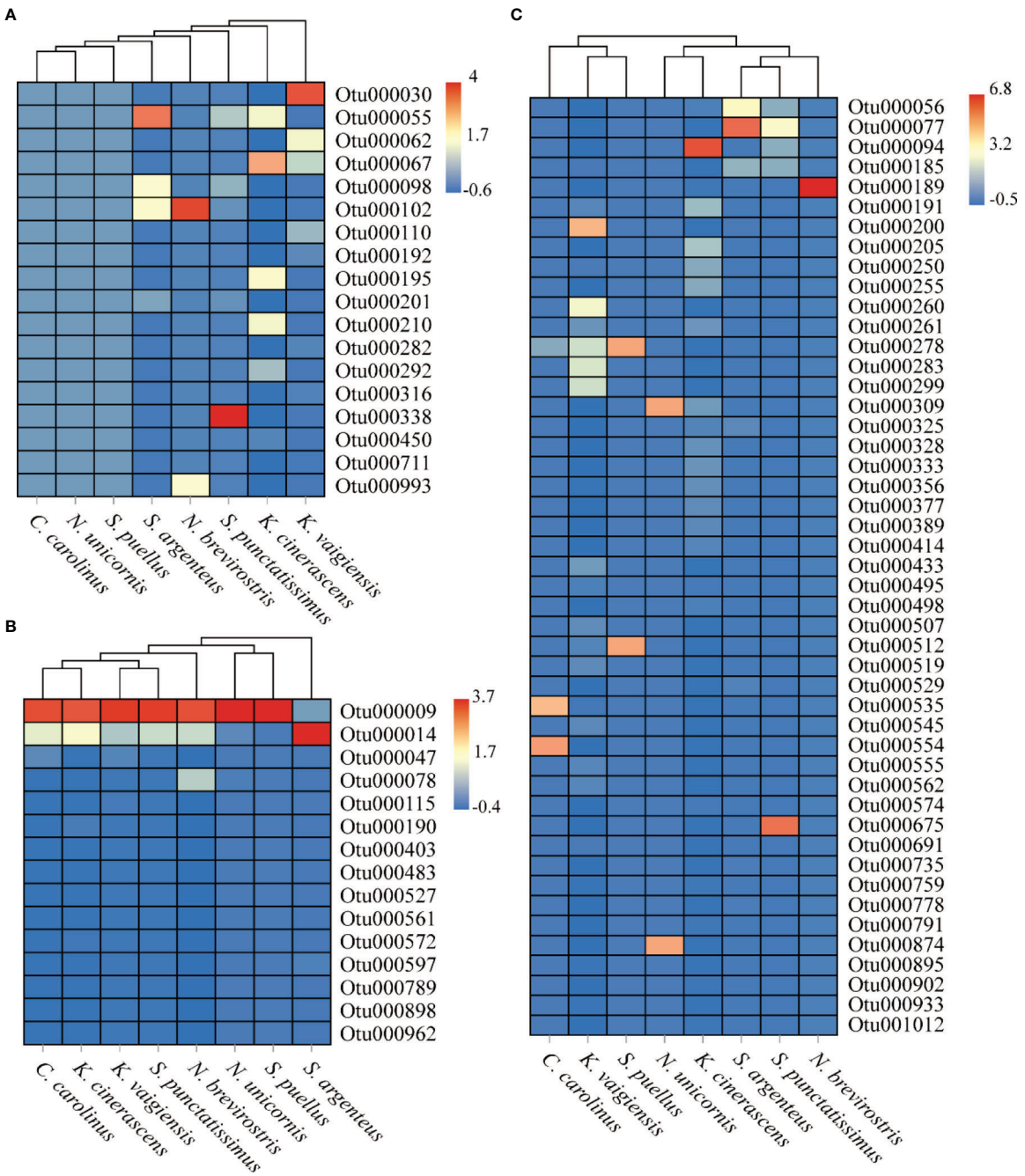

FIGURE 4 | Heat map of the relative abundance of 18S rRNA sequences affiliated with different phyla found in the intestinal contents of eight coral reef fish species which were collected from the Xisha Islands, China. **(A)** Chlorophyta, **(B)** Ochrophyta, **(C)** Rhodophyta.

OTUs with only a single nucleotide variation within the targeted amplified region (Albaina et al., 2016). Third, the number of sampled fishes in this study was small so that some taxa in fish intestine were not observed using the microscope. For example, previous studies have shown that *S. puellus* can consume sponges (Hoey et al., 2013). While microscopic examination did not find any sponge remains in fish intestinal contents, Demospongiae (sponges) were identified as the main food for *S. puellus* using high-throughput sequencing. Leray et al. (2015) also showed that pyrosequencing analysis could broaden the recognition of the food webs of coral-dwelling predatory fish and achieved unprecedented taxonomic resolution of their diets. Nalley et al. (2022) reported that the resolution of metabarcding is greater than visual observation; metabarcding can identify specific taxa

TABLE 3 | Taxonomic assignment of the dominant OTUs affiliated to the phyla Chlorophyta, Ochrophyta and Rhodophyta, found in fish intestines using BLAST methodologies.

Phylum	OTUs	Fish species[a]	Closely related sequence (Accession number)	Similarity
Chlorophyta	Otu000030	KV	*Dictyosphaeria cavernosa* (AM498756)	99.1%
	Otu000055	SA、KC	*Ulvella leptochaete* (LM653280)	97.4%
	Otu000067	KC	*Cladophora socialis* (AM498751)	99.1%
	Otu000102	NB、SA	*Cladophora vagabunda* (LT607383)	100%
Ochrophyta	Otu000009	CC、KV、SPn、NB、NU、Spe、KC	*Lobophora variegate* (AB096086)	99.2%
	Otu000014	SA、CC	*Dictyota linearis* (AB087108)	99.2%
	Otu000078	NB	*Sphacelaria rigidula* (LM653281)	97.5%
Rhodophyta	Otu000056	SA	*Spyridia filamentosa* (EU718707)	99.4%
	Otu000077	SA、SPn	*Centroceras hyalacanthum* (DQ374387)	90.5%
	Otu000094	KC、SPn	*Ceramium sinicola* (AY155519)	88.4%
	Otu000189	NB	*Taenioma perpusillum* (MF093957)	86.7%
	Otu000200	KV	*Peyssonnelia rumoiana* (AB231315)	98.5%
	Otu000260	KV	*Peyssonnelia armorica* (AB231316)	96.8%
	Otu000278	Spe、KV	*Centroceras micracanthum* (DQ374386)	96.8%
	Otu000309	NU	*Chondrophycus* cf. *undulates* (GU223780)	97.1%
	Otu000443	Spe	*Gibsmithia dotyi* (AF317108)	99.1%
	Otu000512	Spe	*Erythrophyllum delesserioides* (AF317105)	97.7%
	Otu000535	CC	*Peyssonnelia rosenvingei* (AB231317)	97.7%
	Otu000554	CC	*Pneophyllum conicum* (MF611677)	100%
	Otu000675	SPn	*Neosiphonia* sp. NDR51A (AB219905)	98.5%
	Otu000874	NU	*Ceramium sinicola* (AY155519)	87.8%

[a]*Symbols of fish species: C. carolinus-CC; K. cinerascens-KC; K. vaigiensis-KV; N. brevirostris-NB; N. unicornis-NU; S. argenteus-SA; S. puellus-Spe; S. punctatissimus-SPn.*

within the categories of turf algae that were targeted by herbivorous coral reef fishes, while visual inspection was limited to the identification of turf algae.

Differences in Macroalgal Consumption Among Herbivorous Coral Reef Fishes

Based on microscopy, 18S rRNA high-throughput sequencing and stable isotope analyses, we suggested that *K. vaigiensis*, *N. unicornis* and *S. argenteus* showed a high consumption potential of macroalgae from the coral reef ecosystem. Similarly, previous studies have also shown that *K. vaigiensis* and *N. unicornis* were highly effective in consuming macroalgae, especially the brown macroalgae (Lefevre and Bellwood, 2011; Streit et al., 2015; Puk et al., 2016). Similarly, we found that *K. vaigiensis* and *N. unicornis* favored brown macroalgae. However, in the northern GBR, Choat et al. (2002) demonstrated the dominant macroalgae genera in the diet of *N. unicornis* and *K. vaigiensis* were *Turbinara* and *Dictyota*, while Cvitanovic and Bellwood (2009) found that *K. vaigiensis* in the central region of the GBR preferred the brown macroalgae *Sargassum*. In this study, *K. vaigiensis* favored *Lobophora* and *Dictyota*, but *N. unicornis* targeted more on *Lobophora* and *Turbinara*. The diet difference of fishes between the GBR and the Xisha Islands may be related with occurrence of the dominant macroalgae in the habitat. Previous study showed that *Sargassum* was one of the abundant species in nearshore reefs of the GBR (McCook, 1997). However, *Sargassum* was seldom founded in the Xisha Islands. As for *S. argenteus*, in the Seychelles of the Indian Ocean, *S. argenteus* removed a range of substrate algae, including turf algae, macroalgae, seagrass and epiphytic algae (Ebrahim et al., 2020). Here, we also showed *S. argenteus* can consume macroalgae and seagrass. Furthermore, *S. argenteus* was supposed to focus more on red and green macroalgae in the northern GBR (Hoey et al., 2013). Here, *S. argenteus* also was found to favor red and green macroalgae. Of course, macroalgal grazing selectivity of herbivorous fishes can vary with location, season, food availability and according to the other fish species present (Puk et al., 2016).

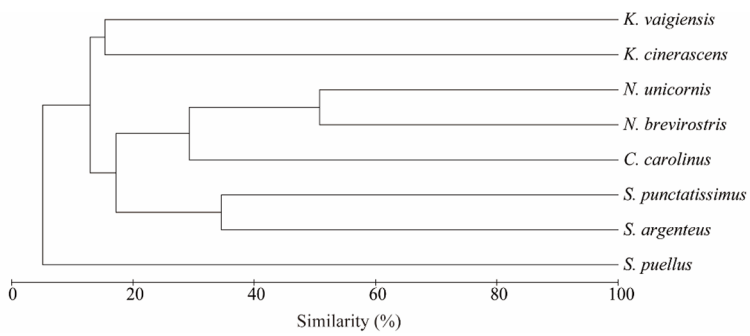

FIGURE 5 | Cluster analysis of macroalgae composition in intestines of eight fish from the Xisha Islands.

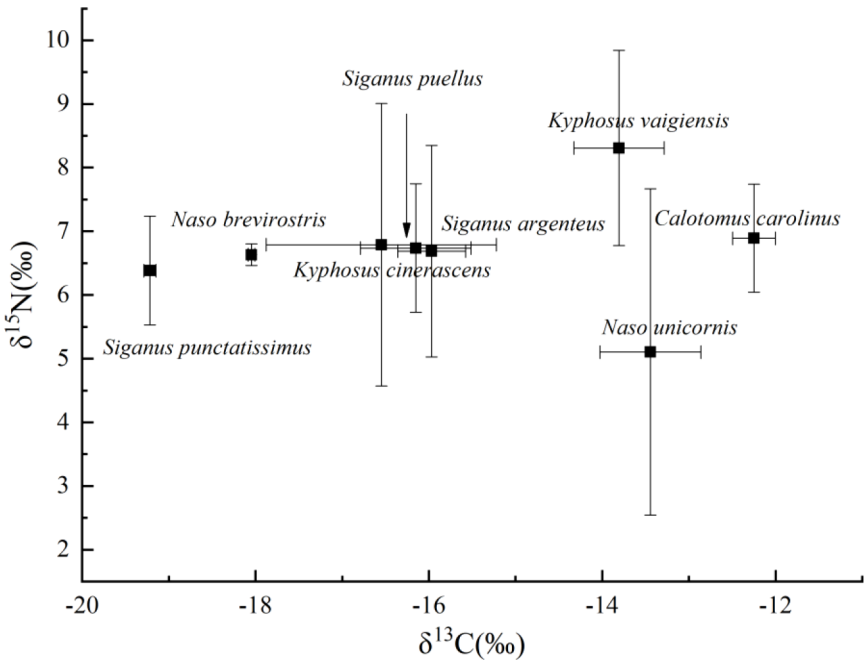

FIGURE 6 | $\delta^{13}C$ and $\delta^{15}N$ isotope values of eight coral reef fish species from the Xisha Islands. Data points are averages with standard error bars.

Ecological Function of Herbivorous Fishes in Removing Macroalgae From Coral Reefs

In addition to identifying the diets of the eight herbivorous reef fishes studied, our results demonstrated the ecological importance of these fishes in removing macroalgae from coral reefs. Herbivorous fishes are broadly classified into four functional groups: excavators, scrapers, grazers, and browsers (Hoey and Bellwood, 2009). Excavators, scrapers and grazers generally consume small macroalgae and algal turfs, while browsers target large, erect macroalgal species and play a critical part in controlling macroalgal spreading (Hoey and Bellwood, 2009; Michael et al., 2013; Ebrahim et al., 2020). Previous studies have shown that *C. carolinus*, *K. cinerascens*, *K. vaigiensis*, *N. brevirostris*, *N. unicornis* and *S. argenteus* in the Moorea, the GBR or other coral reef islands belong to the browser group (Puk et al., 2016; Sura et al., 2021) and this was confirmed in our study. Based on microscopic examination, *N. unicornis* can consume *V. ventricosa* and *T. ornate*, while *S. argenteus* can consume *Halimeda* sp. (**Table 2**). According to the 18S rRNA high-throughput sequencing analysis, we found that *C. carolinus*, *K. cinerascens*, *K. vaigiensis*, *N. brevirostris* and *N. unicornis* consumed the brown alga *L. variegate*, and that *K. vaigiensis* and *N. unicornis* foraged especially heavily on this macroalgae. However, *S. argenteus* fed more on *D. linearis*. *K. vaigiensis* played an important role in removing the green alga *D. cavernosa*, while *S. argenteus* preferred to feed on the red algae *S. filamentosa* and *C. hyalacanthum*. *K. vaigiensis* also preferred to consume *Peyssonnelia* spp. The macroalgae mentioned above all belonged to either the upright calcareous or fleshy macroalgae. These two macroalgae groups are problematic as they probably inhibit coral settlement, while the crustose calcareous algae and algal turfs have only minor negative effects on coral settlement (Diaz-Pulido et al., 2010). Overgrowth of *Lobophora* and *Dictyota* is widely supposed to reduce coral settlement (Foster et al., 2008; Diaz-Pulido et al., 2010; Evensen et al., 2019; Vieira, 2020) and the spread of *Dictyota* can even cause coral disease outbreaks (Brandt et al., 2012). Unfortunately, *Lobophora* and *Dictyota*, are the dominant species on Indo-Pacific coral reefs (Cardoso et al., 2009; Titlyanov et al., 2017). We found that the nitrogen signature ($\delta^{15}N$) of *N. unicornis* was significantly lower than most of the other herbivorous fishes, indicating a high consumption potential of macroalgae. In general, we suggested that *K. vaigiensis*, *N. unicornis* and *S. argenteus* were the key browsers removing macroalgae from reefs off the Xisha Islands. This result is similar to that of a previous view, which recommended that *K. vaigiensis*, *N. unicornis* and *Siganus canaliculatus* were the predominant removers of macroalgae, the "true macroalgae browsers" of coral reefs (Puk et al., 2016). *K. vaigiensis* and *N. unicornis* were commonly considered as important macroalgal consumers in the coral reefs of the GBR (Verges et al., 2012).

Herbivorous fishes that eat the entire macroalgal thallus have a great functional impact on macroalgae removal from coral reefs than species that only consume algal fronds (Streit et al., 2015). In this study, *K. cinerascens*, *K. vaigiensis*, *N. unicornis* and *S. punctatissimus* were found to feed on the entire macroalgal thallus by microscopic examination (**Table 2**). Streit et al. (2015) also showed that *K. vaigiensis* and *N. unicornis* bit on the entire

macroalgal thallus in almost 90% of bites. Body size, tooth shape, and feeding behavior of different herbivores may result in these functional differences (Streit et al., 2015). *S. punctatissimus* can fed on *Acanthophora* sp., while *Acanthophora* can inhibit the successful settlement of coral planulae (Vermeij et al., 2009). The red alga, *P. conicum* is widely distributed on Indo-Pacific coral reefs and can overgrow and kill live corals (Antonius, 2001). Coincidentally, we found that *C. carolinus* consumed *P. conicum*. In addition, herbivorous fishes can selectively remove some macroalgae including *Ulvella*, *Cladophora*, *Sphacelaria*, *Spyridia*, *Centroceras*, *Ceramium* and *Neosiphonia*, which often occur in the Xisha Islands (Titlyanov et al., 2017; Huang, 2018). The spread of macroalgae can negatively affect coral reefs through the inhibition of coral fecundity and growth, the reduction of coral larval settlement and recruitment and the increasing prevalence of coral diseases (Dell et al., 2020). Burkepile and Hay (2008) identified herbivore species richness and feeding complementarity as key factors in the effective suppression of the spread of macroalgae in a coral ecosystem. In summary, we recommend reducing fishing mortality for key browser species, such as *K. vaigiensis*, *N. unicornis* and *S. argenteus*, in order to control the spread of macroalgae on the reefs off the Xisha Islands. Gowri et al. (2016) recommended a ban on fishing herbivorous fishes during the times of spawning aggregations, and a ban on the use of small-mesh gill nets in coral management of India. Dell et al. (2020) also encouraged the government to protect and monitor the key browsers in the coral reefs. Some countries, such as Belize, even have implemented bans on fishing herbivorous fishes (Kramer et al., 2017).

CONCLUSIONS

In this study, for the first time we compared the capability of macroalgal consumption by eight herbivorous coral reef fishes from the Xisha Islands, China, as determined by microscopy, 18S rRNA high-throughput sequencing and stable isotope analyses. The results of the three methods suggested that *K. vaigiensis*, *N. unicornis* and *S. argenteus* potentially consumed macroalgae more effectively. However, high-throughput sequencing showed that macroalgae consumption of the eight fishes in the same species always clustered together. Moreover, *K. vaigiensis* and *N. unicornis* preferred to take brown macroalgae, while *S. argenteus* targeted more on red and green macroalgae. Meanwhile, a high diversity of herbivorous fishes was very important to the health of the Xisha coral reefs. Because we found herbivorous fishes can selectively remove some macroalgae which showed negative influences on the coral growth and coral larval settlement. For example, *C. carolinus* can consume a red alga *P. conicum*, which can directly overgrow and kill live corals. In the future, analysis of feeding behavior of herbivorous fishes should be investigated according to variation of macroalgae composition in Xisha coral reef islands, and macroalgae selectivity for herbivorous fishes should be elaborated in more details.

DATA AVAILABILITY STATEMENT

The datasets presented in this study can be found in online repositories. The names of the repository/repositories and accession number(s) can be found below: NCBI [accession: PRJNA742779, MZ481947-MZ481964, MZ481932-MZ481946 and MZ481965-MZ482014].

ETHICS STATEMENT

All work undertaken in this study complied with the committee on Laboratory Animal Welfare and Ethics of South China Sea Fisheries Research Institute, Chinese Academy of Fishery Sciences (nhdf2022-01).

AUTHOR CONTRIBUTIONS

Conceptualization, PW, YL and CL; investigation, PW, TW, YX, TH and QQ; methodology, PW, TW and TH; formal analysis, PW and QQ; writing original draft, PW and YX; writing-review & editing, PW, LL, YL, CL, SX and TW; data curation, YL and LL; funding acquisition, CL and PW. All authors contributed to the article and approved the submitted version.

FUNDING

This research was supported by the National Key R&D Program of China (2018YFD0900803), Key Special Project for Introduced Talents Team of Southern Marine Science and Engineering Guangdong Laboratory (Guangzhou) (GML2019ZD0605), Central Public-interest Scientific Institution Basal Research Fund, South China Sea Fisheries Research Institute, CAFS (No. 2019TS28, No. 2021SD04), Financial Fund of the Ministry of Agriculture and Rural Affairs, P. R. of China (NFZX2021), Key Laboratory of Tropical Marine Biotechnology of Hainan Province (LTMB202203), Central Public-interest Scientific Institution Basal Research Fund, CAFS (No. 2020TD16), Science and Technology Planning Project of Guangdong Province (2019B121201001) and Fundamental and Applied Fundamental Research Major Program of Guangdong Province (2019B030302004-05).

ACKNOWLEDGMENTS

We thank International Science Editing (http://www.internationalscienceediting.com) for editing this manuscript.

SUPPLEMENTARY MATERIAL

The Supplementary Material for this article can be found online at: https://www.frontiersin.org/articles/10.3389/fmars.2022.882196/full#supplementary-material

REFERENCES

Adam, T. C., Burkepile, D. E., Holbrook, S. J., Carpenter, R. C., Claudet, J., Loiseau, C., et al. (2021). Landscape-Scale Patterns of Nutrient Enrichment in a Coral Reef Ecosystem: Implications for Coral to Algae Phase Shifts. *Ecol. Appl.* 31, 2227. doi: 10.1002/eap.2227

Albaina, A., Aguirre, M., Abad, D., Santos, M., and Estonba, A. (2016). 18s rRNA V9 Metabarcoding for Diet Characterization: A Critical Evaluation With Two Sympatric Zooplanktivorous Fish Species. *Ecol. Evol.* 6, 1809–1824. doi: 10.1002/ece3.1986

Antonius, A. (2001). *Pneophyllum Conicum*, a Coralline Red Alga Causing Coral Reef-Death in Mauritius. *Coral Reefs* 19, 418–418. doi: 10.1007/s003380000126

Bennett, S., and Bellwood, D. R. (2011). Latitudinal Variation in Macroalgal Consumption by Fishes on the Great Barrier Reef. *Mar. Ecol. Prog. Ser.* 426, 241–252. doi: 10.3354/meps09016

Bokulich, N. A., Subramanian, S., Faith, J. J., Gevers, D., Gordon, J. I., Knight, R., et al. (2013). Quality-Filtering Vastly Improves Diversity Estimates From Illumina Amplicon Sequencing. *Nat. Methods* 10, 57–59. doi: 10.1038/nmeth.2276

Brandt, M. E., Ruttenberg, B. I., Waara, R., Miller, J., Witcher, B., Estep, A. J., et al. (2012). Dynamics of an Acute Coral Disease Outbreak Associated With the Macroalgae *Dictyota* Spp. In Dry Tortugas National Park, Florida, USA. *B. Mar. Sci.* 88, 1035–1050. doi: 10.5343/bms.2011.1104

Bruno, J. F., Cote, I. M., and Toth, L. T. (2019). Climate Change, Coral Loss, and the Curious Case of the Parrotfish Paradigm: Why Don't Marine Protected Areas Improve Reef Resilience? *Ann. Rev. Mar. Sci.* 11, 307–334. doi: 10.1146/annurev-marine-010318-095300

Burkepile, D. E., and Hay, M. E. (2008). Herbivore Species Richness and Feeding Complementarity Affect Community Structure and Function on a Coral Reef. *Proc. Natl. Acad. Sci. U.S.A.* 105, 16201–16206. doi: 10.1073/pnas.0801946105

Burke, L., Reytar, K., Spalding, M., and Perry, A. (2011). *Reefs at Risk Revisited* (Washington: World Resources Institute).

Caporaso, J. G., Kuczynski, J., Stombaugh, J., Bittinger, K., Bushman, F. D., Costello, E. K., et al. (2010). QIIME Allows Analysis of High-Throughput Community Sequencing Data. *Nat. Methods* 7, 335–336. doi: 10.1038/nmeth.f.303

Cardoso, S. C., Soares, M. C., Oxenford, H. A., and Côté, I. M. (2009). Interspecific Differences in Foraging Behaviour and Functional Role of Caribbean Parrotfish. *Marine Biodivers. Records* 2, 148. doi: 10.1017/S1755267209990662

Cheal, A. J., MacNeil, M. A., Cripps, E., Emslie, M. J., Jonker, M., Schaffelke, B., et al. (2010). Coral-Macroalgal Phase Shifts or Reef Resilience: Links With Diversity and Functional Roles of Herbivorous Fishes on the Great Barrier Reef. *Coral Reefs* 29, 1005–1015. doi: 10.1007/s00338-010-0661-y

Chen, X. Y., Yu, K. F., Huang, X. Y., Wang, Y. H., Liao, Z. H., Zhang, R. J., et al. (2019). Atmospheric Nitrogen Deposition Increases the Possibility of Macroalgal Dominance on Remote Coral Reefs. *J. Geophys. Res-Biogeo* 124, 1355–1369. doi: 10.1029/2019JG005074

Chen, S., Zhou, Y., Chen, Y., and Gu, J. (2018). Fastp: An Ultra-Fast All-In-One FASTQ Preprocessor. *Bioinformatics* 34, 884–890. doi: 10.1093/bioinformatics/bty560

Cheung, M. K., Au, C. H., Chu, K. H., Kwan, H. S., and Wong, C. K. (2010). Composition and Genetic Diversity of Picoeukaryotes in Subtropical Coastal Waters as Revealed by 454 Pyrosequencing. *ISME. J.* 4, 1053–1059. doi: 10.1038/ismej.2010.26

Choat, J. H., Clements, K. D., and Robbins, W. D. (2002). The Trophic Status of Herbivorous Fishes on Coral Reefs: 1. Dietary Analyses. *Mar. Biol.* 140, 613–623. doi: 10.1007/s00227-001-0715-3

Choat, J. H., Robbins, W. D., and Clements, K. D. (2004). The Trophic Status of Herbivorous Fishes on Coral Reefs: II. Food Processing Modes and Trophodynamics. *Mar. Biol.* 145, 445–454. doi: 10.1007/s00227-004-1341-7

Chong-Seng, K. M., Nash, K. L., Bellwood, D. R., and Graham, N. A. J. (2014). Macroalgal Herbivory on Recovering Versus Degrading Coral Reefs. *Coral Reefs* 33, 409–419. doi: 10.1007/s00338-014-1134-5

Clements, K. D., German, D. P., Piché, J., Tribollet, A., and Choat, J. H. (2017). Integrating Ecological Roles and Trophic Diversification on Coral Reefs: Multiple Lines of Evidence Identify Parrotfishes as Microphages. *Biol. J. Linn. Soc.* 120, 729–751.doi: 10.1111/bij.12914.

Corse, E., Costedoat, C., Chappaz, R., Pech, N., Martin, J. F., and Gilles, A. (2010). A PCR-Based Method for Diet Analysis in Freshwater Organisms Using 18s rDNA Barcoding on Faeces. *Mol. Ecol. Resour.* 10, 96–108. doi: 10.1111/j.1755-0998.2009.02795.x

Cvitanovic, C., and Bellwood, D. R. (2009). Local Variation in Herbivore Feeding Activity on an Inshore Reef of the Great Barrier Reef. *Coral Reefs* 28, 127–133. doi: 10.1007/s00338-008-0433-0

de Carvalho, D. R., de Castro, D. M. P., Callisto, M., Chaves, A. J. D., Moreira, M. Z., and Pompeu, P. S. (2019). Stable Isotopes and Stomach Content Analyses Indicate Omnivorous Habits and Opportunistic Feeding Behavior of an Invasive Fish. *Aquat. Ecol.* 53, 365–381. doi: 10.1007/s10452-019-09695-3

Dell, C. L. A., Longo, G. O., Burkepile, D. E., and Manfrino, C. (2020). Few Herbivore Species Consume Dominant Macroalgae on a Caribbean Coral Reef. *Front. Mar. Sci.* 7, 676. doi: 10.3389/fmars.2020.00676

Devloo-Delva, F., Huerlimann, R., Chua, G., Matley, J. K., Heupel, M. R., Simpfendorfer, C. A., et al. (2019). How Does Marker Choice Affect Your Diet Analysis: Comparing Genetic Markers and Digestion Levels for Diet Metabarcoding of Tropical-Reef Piscivores. *Mar. Freshwater Res.* 70, 8–18. doi: 10.1071/MF17209

Diaz-Pulido, G., Harii, S., McCook, L. J., and Hoegh-Guldberg, O. (2010). The Impact of Benthic Algae on the Settlement of a Reef-Building Coral. *Coral Reefs* 29, 203–208. doi: 10.1007/s00338-009-0573-x

Ding, J. F., Jiang, F. H., Li, J. X., Wang, Z. X., Sun, C. J., Wang, Z. Y., et al. (2019). Microplastics in the Coral Reef Systems From Xisha Islands of South China Sea. *Environ. Sci. Technol.* 53, 8036–8046. doi: 10.1021/acs.est.9b01452

Dromard, C. R., Bouchon-Navaro, Y., Harmelin-Vivien, M., and Bouchon, C. (2015). Diversity of Trophic Niches Among Herbivorous Fishes on a Caribbean Reef (Guadeloupe, Lesser Antilles), Evidenced by Stable Isotope and Gut Content Analyses. *J. Sea Res.* 95, 124–131. doi: 10.1016/j.seares.2014.07.014

Duran, A., Adam, T. C., Palma, L., Moreno, S., Collado-Vides, L., and Burkepile, D. E. (2019). Feeding Behavior in Caribbean Surgeonfishes Varies Across Fish Size, Algal Abundance, and Habitat Characteristics. *Mar. Ecol.* 00, 12561. doi: 10.1111/maec.12561

Ebrahim, A., Martin, T. S. H., Mumby, P. J., Olds, A. D., and Tibbetts, I. R. (2020). Differences in Diet and Foraging Behaviour of Commercially Important Rabbitfish Species on Coral Reefs in the Indian Ocean. *Coral Reefs* 39, 977–988. doi: 10.1007/s00338-020-01918-6

Edgar, R. C. (2013). UPARSE: Highly Accurate OTU Sequences From Microbial Amplicon Reads. *Nat. Methods* 10, 996–998. doi: 10.1038/nmeth.2604

Edgar, R. C., Haas, B. J., Clemente, J. C., Quince, C., and Knight, R. (2011). UCHIME Improves Sensitivity and Speed of Chimera Detection. *Bioinformatics* 27, 2194–2200. doi: 10.1093/bioinformatics/btr381

Evensen, N. R., Doropoulos, C., Wong, K. J., and Mumby, P. J. (2019). Stage-Specific Effects of *Lobophora* on the Recruitment Success of a Reef-Building Coral. *Coral Reefs.* 38, 489–498. doi: 10.1007/s00338-019-01804-w

Foster, N. L., Box, S. J., and Mumby, P. J. (2008). Competitive Effects of Macroalgae on the Fecundity of the Reef-Building Coral *Montastraea Annularis*. *Mar. Ecol. Prog. Ser.* 367, 143–152. doi: 10.3354/meps07594

Gowri, V.S., Pramiladevi, R.R.I., and Nammalwar, P. (2016). Biodiversity of Selected Herbivorous Coral Reef Fishes and Their Role in Coral Management, India. *Int. J. Res. Sci. Innov.* III, 94–100.

Hoey, A. S., and Bellwood, D. R. (2009). Limited Functional Redundancy in a High Diversity System: Single Species Dominates Key Ecological Process on Coral Reefs. *Ecosystems* 12, 1316–1328. doi: 10.1007/s10021-009-9291-z

Hoey, A. S., Brandl, S. J., and Bellwood, D. R. (2013). Diet and Cross-Shelf Distribution of Rabbitfishes (F. Siganidae) on the Northern Great Barrier Reef: Implications for Ecosystem Function. *Coral Reefs.* 32, 973–984. doi: 10.1007/s00338-013-1043-z

Huang, H. (2018). *Coral Reef Atlas of Xisha Islands* (Beijing: Science Press).

Kopp, D., Bouchon-Navaro, Y., Cordonnier, S., Haouisee, A., Louis, M., and Bouchon, C. (2010). Evaluation of Algal Regulation by Herbivorous Fishes on Caribbean Coral Reefs. *Helgoland. Mar. Res.* 64, 181–190. doi: 10.1007/s10152-009-0177-4

Kramer, P., Kramer, P., McField, M., Drysdale, I., Rueda, M., GirÃ, A., et al. (2017). *2015 Report Card for the Mesoamerican Reef* (Washington, DC: The Summit Foundation).

Kumar, S., Stecher, G., Li, M., Knyaz, C., and Tamura, K. (2018). MEGA X: Molecular Evolutionary Genetics Analysis Across Computing Platforms. *Mol. Biol. Evol.* 35, 1547–1549. doi: 10.1093/molbev/msy096

Kume, G., Kobari, T., Hirai, J., Kuroda, H., Takeda, T., Ichinomiya, M., et al. (2021). Diet Niche Segregation of Co-Occurring Larval Stages of Mesopelagic and Commercially Important Fishes in the Osumi Strait Assessed Through Morphological, DNA Metabarcoding, and Stable Isotope Analyses. *Mar. Biol.* 168, 6. doi: 10.1007/s00227-020-03810-x

Lamb, P. D., Hunter, E., Pinnegar, J. K., Creer, S., Davies, R. G., and Taylor, M. I. (2019). How Quantitative Is Metabarcoding: A Meta-Analytical Approach. *Mol. Ecol.* 28, 420–430. doi: 10.1111/mec.14920

Lefevre, C. D., and Bellwood, D. R. (2011). Temporal Variation in Coral Reef Ecosystem Processes: Herbivory of Macroalgae by Fishes. *Mar. Ecol. Prog. Ser.* 422, 239–251. doi: 10.3354/meps08916

Leray, M., Meyer, C. P., and Mills, S. C. (2015). Metabarcoding Dietary Analysis of Coral Dwelling Predatory Fish Demonstrates the Minor Contribution of Coral Mutualists to Their Highly Partitioned, Generalist Diet. *Peer J.* 3, 1047. doi: 10.7717/peerj.1047

Li, Y. C., Chen, S. Q., Zheng, X. Q., Cai, Z. F., Wu, Z. J., Wang, D. R., et al. (2018). Analysis of the Change of Hermatypic Corals in Yongxing Island and Qilianyu Island in Nearly a Decade. *Haiyang Xuebao* 40, 97–109. doi: 10.3969/j.issn.0253-4193.2018.08.010.

Lin, X. Z., Hu, S. M., Liu, Y., Zhang, L., Huang, H., and Liu, S. (2021). Disturbance-Mediated Changes in Coral Reef Habitat Provoke a Positive Feeding Response in a Major Coral Reef Detritivore, *Ctenochaetus Striatus*. *Front. Mar. Sci.* 8, 682697. doi: 10.3389/fmars.2021.682697

Liu, Y., Wu, P., Li, C. H., Xiao, Y. Y., Wang, T., and Lin, L. (2021). The Bacterial Composition Associated With *Atriolum Robustum*, a Common Ascidian From Xisha Coral Reef, China. *Symbiosis* 83, 153–161. doi: 10.1007/s13199-020-00742-4

Li, Y. C., Wu, Z. J., Chen, S. Q., Cai, Z. F., Lan, J. X., Tong, Y. H., et al. (2017). Discussion of the Diversity of the Coral Reef Fish in the Shallow Reefs Along the Yongxing and Qilianyu Island. *Marine Environ. Sci.* 36, 509–516. doi: 10.13634/j.cnki.mes.2017.04.005

Magoc, T., and Salzberg, S. L. (2011). FLASH: Fast Length Adjustment of Short Reads to Improve Genome Assemblies. *Bioinformatics* 27, 2957–2963. doi: 10.1093/bioinformatics/btr507

Mantyka, C. S., and Bellwood, D. R. (2007). Macroalgal Grazing Selectivity Among Herbivorous Coral Reef Fishes. *Mar. Ecol. Prog. Ser.* 352, 177–185. doi: 10.3354/meps07055

McCook, L. J. (1997). Effects of Herbivory on Zonation of *Sargassum* Spp. Within Fringing Reefs of the Central Great Barrier Reef. *Mar. Biol.* 129, 713–722. doi: 10.1007/s002270050214

Michael, P. J., Hyndes, G. A., Vanderklift, M. A., and Verges, A. (2013). Identity and Behaviour of Herbivorous Fish Influence Large-Scale Spatial Patterns of Macroalgal Herbivory in a Coral Reef. *Mar. Ecol. Prog. Ser.* 482, 227–240. doi: 10.3354/meps10262

Moberg, F., and Folke, C. (1999). Ecological Goods and Services of Coral Reef Ecosystems. *Ecol. Econ.* 29, 215–233. doi: 10.1016/S0921-8009(99)00009-9

Nalley,E. M., Donahue, M. J., Heenan, A., and Toonen, R. J. (2022). Quantifying the Diet Diversity of Herbivorous Coral Reef Fishes Using Systematic Review and DNA Metabarcoding. *Environ. DNA* 4, 191–205. doi: 10.1002/edn3.247

Nalley, E. M., Donahue, M. J., and Toonen, R. J. (2021). Metabarcoding as a Tool to Examine Cryptic Algae in the Diets of Two Common Grazing Surgeonfishes, *Acanthurus Triostegus* and *A. Nigrofuscus*. *Environ. DNA* 00, 1–12.doi: 10.1002/edn3.206.

Neilson, B. J., Wall, C. B., Mancini, F. T., and Gewecke, C. A. (2018). Herbivore Biocontrol and Manual Removal Successfully Reduce Invasive Macroalgae on Coral Reefs. *Peer J.* 6, 5332. doi: 10.7717/peerj.5332

Nicholson, G. M., and Clements, K. D. (2020). Resolving Resource Partitioning in Parrotfishes (Scarini) Using Microhistology of Feeding Substrata. *Coral Reefs* 39, 1313–1327. doi: 10.1007/s00338-020-01964-0

Pruesse, E., Quast, C., Knittel, K., Fuchs, B. M., Ludwig, W. G., Peplies, J., et al. (2007). SILVA: A Comprehensive Online Resource for Quality Checked and Aligned Ribosomal RNA Sequence Data Compatible With ARB. *Nucleic. Acids Res.* 35, 7188–7196. doi: 10.1093/nar/gkm864

Puk, L. D., Ferse, S. C. A., and Wild, C. (2016). Patterns and Trends in Coral Reef Macroalgae Browsing: A Review of Browsing Herbivorous Fishes of the Indo-Pacific. *Rev. Fish Biol. Fisher.* 26, 53–70. doi: 10.1007/s11160-015-9412-z

Rodriguez-Barreras, R., Godoy-Vitorino, F., Praebel, K., and Wangensteen, O. S. (2020). DNA Metabarcoding Unveils Niche Overlapping and Competition Among Caribbean Sea Urchins. *Reg. Stud. Mar. Sci.* 40, 101537. doi: 10.1016/j.rsma.2020.101537

Russ, G. R., Questel, S. L., Rizzari, J. R., and Alcala, A. C. (2015). The Parrotfish-Coral Relationship: Refuting the Ubiquity of a Prevailing Paradigm. *Mar. Biol.* 162, 2029–2045. doi: 10.1007/s00227-015-2728-3

Shen, J. W., Wang, Y., Zhao, N., Yang, H. Q., Fu, F. X., and Jin, Y. B. (2017). Carbonate Sedimentary Characteristics of the Beach Rocks Around Qilian Islets and Cays, Xisha Islands: Implication for Coral Reef Development and Decline. *Palaeogeogr. Palaeocl.* 474, 264–278. doi: 10.1016/j.palaeo.2016.05.005

Souter, D., Planes, S., Wicquart, J., Logan, M., Obura, D., and Staub, F. (2021). *Status of Coral Reefs of the World: 2020 Executive Summary* (Townsville: Global Coral Reef Monitoring Network).

Streit, R., Hoey, A., and Bellwood, D. (2015). Feeding Characteristics Reveal Functional Distinctions Among Browsing Herbivorous Fishes on Coral Reefs. *Coral Reefs.* 34, 1037–1047. doi: 10.1007/s00338-015-1322-y

Sura, S. A., Molina, N. E., Blumstein, D. T., and Fong, P. (2021). Selective Consumption of Macroalgal Species by Herbivorous Fishes Suggests Reduced Functional Complementarity on a Fringing Reef in Moorea, French Polynesia. *J. Exp. Mar. Biol. Ecol.* 536, 151508. doi: 10.1016/j.jembe.2020.151508

Titlyanov, A. E., Titlyanova, V. T., Li, X., and Huang, H. (2017). *Coral Reef Marine Plants of Hainan Island* (London: Academic Press).

Verges, A., Bennett, S., and Bellwood, D. R. (2012). Diversity Among Macroalgae-Consuming Fishes on Coral Reefs: A Transcontinental Comparison. *PloS One* 7, 45543. doi: 10.1371/journal.pone.0045543

Vermeij, M. J. A., Smith, J. E., Smith, C. M., Thurber, R. V., and Sandin, S. A. (2009). Survival and Settlement Success of Coral Planulae: Independent and Synergistic Effects of Macroalgae and Microbes. *Oecologia* 159, 325–336. doi: 10.1007/s00442-008-1223-7

Vieira, C. (2020). *Lobophora*-Coral Interactions and Phase Shifts: Summary of Current Knowledge and Future Directions. *Aquat. Ecol.* 54, 1–20. doi: 10.1007/s10452-019-09723-2

Walker, P., and Wood, E. (2005). *The Coral Reef* (New York: Facts on File).

Wang, Q., Garrity, G. M., Tiedje, J. M., and Cole, J. R. (2007). Naive Bayesian Classifier for Rapid Assignment of rRNA Sequences Into the New Bacterial Taxonomy. *Appl. Environ. Microb.* 73, 5261–5267. doi: 10.1128/AEM.00062-07

Wang, T., Liu, Y., Quan, Q. M., Xiao, Y. Y., Wu, P., and Li, C. H. (2022). Species Composition Characteristics Analysis of Qilianyu Reef Fishes of Xisha Islands. *J. Fisher. Sci. China* 29, 102–117. doi: 10.12264/JFSC2021-0122.

Zhao, N., Shen, D. S., and Shen, J. W. (2019). Formation Mechanism of Beach Rocks and Its Controlling Factors in Coral Reef Area, Qilian Islets and Cays, Xisha Islands, China. *J. Earth Sci-China* 30, 728–738. doi: 10.1007/s12583-018-0981-3

Zhao, M. X., Yu, K. F., Shi, Q., Yang, H. Q., Riegl, B., Zhang, Q. M., et al. (2016). The Coral Communities of Yongle Atoll: Status, Threats and Conservation Significance for Coral Reefs in South China Sea. *Mar. Freshwater Res.* 67, 1888–1896. doi: 10.1071/MF15110

Zhao, M. X., Yu, K. F., Shi, Q., Yang, H. Q., Riegl, B., Zhang, Q. M., et al. (2017). Comparison of Coral Diversity Between Big and Small Atolls: A Case Study of Yongle Atoll and Lingyang Reef, Xisha Islands, Central of South China Sea. *Biodivers. Conserv.* 26, 1143–1159. doi: 10.1007/s10531-017-1290-3

Conflict of Interest: The authors declare that the research was conducted in the absence of any commercial or financial relationships that could be construed as a potential conflict of interest.

Publisher's Note: All claims expressed in this article are solely those of the authors and do not necessarily represent those of their affiliated organizations, or those of the publisher, the editors and the reviewers. Any product that may be evaluated in this article, or claim that may be made by its manufacturer, is not guaranteed or endorsed by the publisher.

Copyright © 2022 Wu, Wang, Liu, Li, Xiao, Xu, Han, Lin and Quan. This is an open-access article distributed under the terms of the Creative Commons Attribution License (CC BY). The use, distribution or reproduction in other forums is permitted, provided the original author(s) and the copyright owner(s) are credited and that the original publication in this journal is cited, in accordance with accepted academic practice. No use, distribution or reproduction is permitted which does not comply with these terms.

frontiers | Frontiers in Marine Science

ORIGINAL RESEARCH
published: 10 May 2022
doi: 10.3389/fmars.2022.885037

Comparative Study of Nitrogen Cycling Between a Bay With Riverine Input and a Bay Without Riverine Input, Inferred From Stable Isotopes

Chunqing Chen[1], Qibin Lao[1,2], Youli Shen[2], Guangzhe Jin[1,3,4], Fajin Chen[1,3,4], Qizhong Su[2], Xuetie Lei[2], Xin Zhou[1], Xuan Lu[1], Qingmei Zhu[1,3,4] and Guoqiang Liu[2,5]*

[1] College of Ocean and Meteorology, Guangdong Ocean University, Zhanjiang, China, [2] Marine Environmental Monitoring Centre of Beihai, State Oceanic Administration, Beihai, China, [3] Key Laboratory of Climate, Resources and Environment in Continental Shelf Sea and Deep Sea of Department of Education of Guangdong Province, Guangdong Ocean University, Zhanjiang, China, [4] Laboratory for Coastal Ocean Variation and Disaster Prediction, College of Ocean and Meteorology, Guangdong Ocean University, Zhanjiang, China, [5] Key Laboratory of Marine Environmental Survey Technology and Application, Ministry of Natural Resources, Guangzhou, China

OPEN ACCESS

Edited by:
Meilin Wu,
South China Sea Institute of Oceanology (CAS), China

Reviewed by:
Li-Wei Zheng,
Hainan University, China
Jinlong Wang,
East China Normal University, China

***Correspondence:**
Fajin Chen
fjchen@gdou.edu.cn

Specialty section:
This article was submitted to Marine Pollution, a section of the journal Frontiers in Marine Science

Received: 27 February 2022
Accepted: 31 March 2022
Published: 10 May 2022

Citation:
Chen C, Lao Q, Shen Y, Jin G, Chen F, Su Q, Lei X, Zhou X, Lu X, Zhu Q and Liu G (2022) Comparative Study of Nitrogen Cycling Between a Bay With Riverine Input and a Bay Without Riverine Input, Inferred From Stable Isotopes. Front. Mar. Sci. 9:885037. doi: 10.3389/fmars.2022.885037

The eutrophication degree in the coastal bay has been increasing significantly for the past years, due to the increasing nutrient discharge. However, the factors controlling sources and nitrogen (N) cycling in the different types of bays are still poorly understood. In this comparative study, nitrate dual isotopes ($\delta^{15}N - NO_3^-$ and $\delta^{18}O - NO_3^-$) and ammonium nitrogen isotope ($\delta^{15}N - NH_4^+$), were used to determine the origin of nitrate in Qinzhou Bay (with riverine input) and Tieshangang Bay (without riverine input) in Beibu Gulf and to study biogeochemical processes associated with nitrogen cycling. The nutrient concentrations generally showed a decreased trend from the upper bay to the outer bay. The isotopic values in Tieshangang Bay were generally higher than that in the Qinzhou Bay, suggesting that there are differences in nitrate sources and transformation processes between the two bays. The dominant sources from manure and sewage (41%) and soil N (30%) from runoff input were responsible for the high nitrate observed in the upper Qinzhou Bay. Though manure and sewage (59%) were also dominant nitrate sources in the upper Tieshangang Bay, a decrease in source from soil N (20%) occurred due to less runoff input. Nutrients were retained in the upper Tieshangang Bay due to weak hydrodynamic conditions, which caused higher NH_4^+ concentrations in the upper bay. Significant nitrate loss occurred in the outer Qinzhou Bay, which was related to the intense hydrodynamic condition. Moreover, phytoplankton assimilation mainly utilized NH_4^+ due to sufficient NH_4^+ in the outer Qinzhou Bay. In contrast, nitrate loss was also found in the outer Tieshangang Bay, which is mainly related to the phytoplankton assimilation due to the weak hydrodynamic condition. In addition, the greater enrichment of $\delta^{18}O - NO_3^-$ than $\delta^{15}N - NO_3^-$ during both bays suggests that atmospheric deposition also contributes to the nitrate pool in the water and the impact of atmospheric deposition on the whole Beibu Gulf is relatively consistent. By this comparative study, we found that different nitrate

biogeochemical processes occurred in these two types of bays, which were mainly determined by the difference of human activities and hydrodynamic conditions.

Keywords: nitrogen, stable nitrogen isotopes, biogeochemical processes, nitrogen cycling, Beibu Gulf

INTRODUCTION

As a transition zone between ocean and land, coastal oceans receive anthropogenic nutrient inputs, which have significantly increased over the past decades (Gruber and Galloway, 2008; Sharples et al., 2017; Yan et al., 2017; Lao et al., 2019a; Chen et al., 2020). This has resulted in serious nutrient load in the coastal environment and has caused a host of environmental problems such as eutrophication, harmful algal blooms, and seasonal hypoxia in the coastal areas, which greatly impacts the original functions of coastal ecosystems and biogeochemical cycles (Carstensen and Conley, 2019; Gobler, 2020; Yu et al., 2020; Anderson et al., 2021; Lao et al., 2021a). In addition, nitrogen (N) is also a key element that regulates marine primary productivity and its availability influences the storage of anthropogenic carbon dioxide in coastal areas and climate change (Moore et al., 2013; Tremblay et al., 2015). Thus, tracing nitrogen sources and its cycles are very important to design effective management practices to protect coastal ecosystems.

Among many methods for studying N dynamics, stable nitrogen isotope ($\delta^{15}N$) of various N pools combined with oxygen isotope of nitrate ($\delta^{18}O-NO_3^-$), is considered a powerful tool to trace sources and biogeochemical processes of N. Generally, various sources of N can be distinguished by their different ranges of nitrogen and oxygen isotopic values (Kendall, 1998; Xue et al., 2009). For example, nitrate sources originating from sewage and manure are more enriched in $\delta^{15}N$ (4-25‰) than fertilizer and atmospheric deposition due to the volatilization of ^{15}N-depleted ammonia from human and animal waste (Kendall, 1998; Xue et al., 2009), while $\delta^{18}O-NO_3^-$ values from atmospheric deposition are generally high (>50‰) compared to those from other sources (<25‰) (Ye et al., 2016). In addition, the isotopic ratios can also reflect biological processes. For example, assimilation and denitrification cause a synchronous increase of $\delta^{15}N$ and $\delta^{18}O$ in the residual water NO_3^- as the lighter isotopes (^{14}N and ^{16}O) are preferentially utilized by microorganisms (Granger et al., 2004; Sigman et al., 2005). Therefore, a better understanding of sources and biogeochemical processes of N in the coastal ecosystem could be achieved by the distribution and variation of isotopic signatures of various N pools.

The Beibu Gulf located in the northwestern South China Sea (SCS), is a newly developing port, mariculture, and industrial area in south China. Its rich biology and high productivity make the gulf a key fishing ground and source of fisheries products in China (Liu et al., 2020; Lao et al., 2021b; Xu et al., 2021). However, the increasing population and intensification of industrial and agriculture activities around the coastal gulf for the past years have greatly increased nutrient loading to the gulf (Lao et al., 2020; Lao et al., 2021a; Lao et al., 2021c; Xu et al., 2021). This has resulted in an increase in the degree of eutrophication in the coastal gulf for the past years, particularly in the coastal bay of the Beibu Gulf (Lao et al., 2021a; Lao et al., 2021c). There are several rivers that flow into the Beibu Gulf (**Figure 1**), and the nutrient input into the gulf shows a different seasonal change between the rivers (Lao et al., 2020). However, due to the difference in river distribution (most of which are concentrated in the middle of the Beibu Gulf) and different depths, there are obvious differences in hydrodynamic conditions between the coastal bays of the Beibu Gulf. For example, there are many rivers around the Qinzhou Bay in the gulf (**Figure 1**), which carry a large amount of nutrients such as nitrogen and phosphorus into the bay every year, and thus causing high nutrient load and increasing the eutrophication in the bay (Lao et al., 2020; Lao et al., 2021a; Lao et al., 2021c). Different from Qinzhou Bay, Tieshangang Bay is a natural deep-water port in Guangxi Province and an important port area in the Beibu Gulf. There are no large rivers flowing to the Tieshanggang Bay, thus hydrodynamic conditions are weak and the water exchange is mainly affected by the tide (Jiang et al., 2017). In addition, due to the unique ecological resources and environment of freshwater and saltwater in Qinzhou Bay, the bay is an important aquaculture area in Guangxi Province and the largest natural oyster spawning and breeding area in China (Liu et al., 2020; Xu et al., 2020; Lao et al., 2021c). However, since there is less influence from freshwater input and weak hydrodynamic conditions in the Tieshangang Bay, the aquaculture scale is much smaller than that of Qinzhou Bay. But as an industrial area and port, the ecological environment of the Tieshangang Bay is significantly affected by human activities (Gan et al., 2013; Lao et al., 2019b; Lao et al., 2021d). Thus, with such great differences in hydrological conditions, their nutrient sources are different between the two bays in the Beibu Gulf. However, the factors controlling sources and nitrogen cycling in the different types of bays are still poorly understood.

In this comparative study, nitrate dual isotopes ($\delta^{15}N-NO_3^-$ and $\delta^{18}O-NO_3^-$) and ammonium nitrogen isotope ($\delta^{15}N-NH_4^+$), were used to determine the origin of nitrate in two types of bays in Beibu Gulf (Qinzhou Bay and Tieshanggang Bay) and to study biogeochemical processes associated with nitrogen cycling.

MATERIALS AND METHODS

Study Area and Sampling

The Beibu Gulf is a semi-enclosed gulf located in south China and the northwestern part of the SCS. The climate of Beibu Gulf is affected by the East Asian monsoon, whereas the northeast monsoon prevails in winter and the southwest monsoon prevails

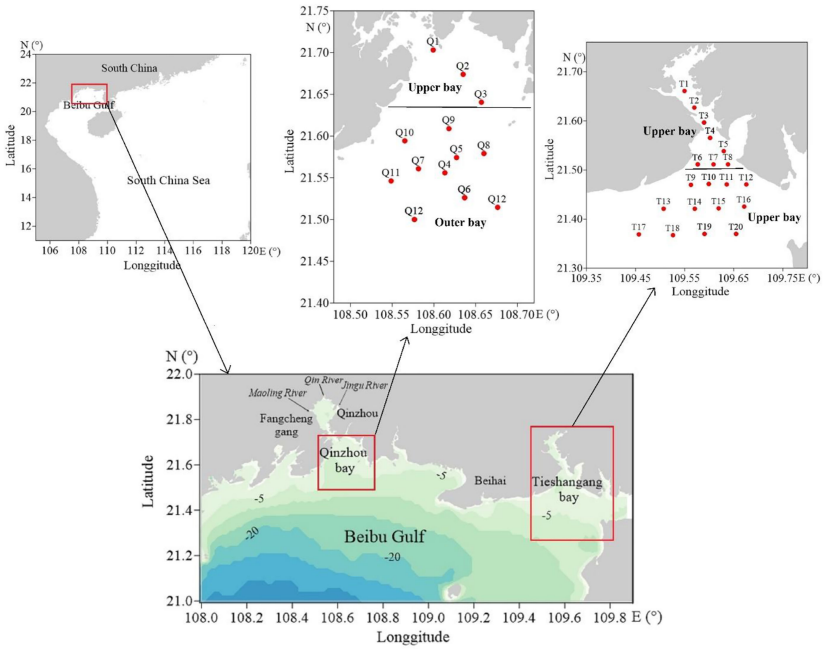

FIGURE 1 | Map of Beibu Gulf and sampling stations. The red boxes are the sampling areas, including Qinzhou Bay and Tieshangang Bay in the Beibu Gulf.

in summer. The annual rainfall in the gulf is 1,775mm and most occurs in the rainy season (April to October, accounting for nearly 90% of the annual total) (http://data.cma.cn). Qinzhou Bay and Tieshangang Bay are two semi-enclosed bays in the center and northeastern coastal Guangxi Province (**Figure 1**). They are all bays that are significantly affected by industrial and aquaculture activities but they are still quite different. Geographically, Qinzhou Bay is a shallow semi-enclosed bay located in the northernmost part of the Beibu Gulf, with a water depth of 2-18 m. In addition, there are many rivers around Qinzhou Bay, including Maoling River, Qin River, Jingu River (**Figure 1**). The annual freshwater discharge from Qin River and Maoling River (the two largest rivers around the bay) is 599.33×10^8 m^3 and 885.98×10^8 m^3, respectively (Lao et al., 2020). By contrast, there are no large river flowing into the Tieshanggang Bay and the hydrodynamic conditions are weak.

In this study, the cruises were carried out in Tieshangang Bay and Qinzhou Bay from March 31 to April 1, 2021 and April 8, 2021, respectively. A total of 13 and 20 stations were conducted in Qinzhou Bay and Tieshangang Bay, respectively (**Figure 1**). A total of 13 and 20 seawater samples were collected from the surface water (0.5 m) in Qinzhou Bay and Tieshangang Bay, respectively, using a rosette sampler fitted with 10 L Niskin bottles. The temperature, salinity, pH, and DO were measured in the field. For nutrients and isotopic samples, seawater was filtered using precombustion (450°C, 4h) glass fiber filters (47 mm diameter, Whatman GF/F). Then, the filtrate was transferred into a precleaned (acid-washed) polyethylene bottle and stored at -20°C until analysis. For Chl *a*, about 1000-2000 mL of seawater samples were filtered using the GF/F and stored at -20°C until further analysis.

Chemical Analysis

The Chl *a* samples of GF/F filter were extracted using 90% acetone and determined by a spectrophotometer (Lorenzen, 1967). DO samples were measured using the Winkler titration method. The nutrient (PO_4^{3-}, NO_2^-, NO_3^- and NH_4^+) samples were measured using a San++ continuous flow analyzer (Skalar, Netherlands), with detection limits for PO_4^{3-}, NO_2^-, NO_3^- and NH_4^+ were 0.02 μmol L^{-1}, 0.1 μmol L^{-1}, 0.1 μmol L^{-1} and 0.1 μmol L^{-1}, respectively. The analysis of $\delta^{15}N-NO_3^-$ and $\delta^{18}O-NO_3^-$ samples were using a cadmium-azide method modified from Mcilvin et al. (2005). The sulfamic acid was added to each sample to remove preexisting NO_2^-, followed the procedure from Granger and Sigman (2009). Spongy cadmium (Cd) was added to reduce NO_3^- to NO_2^-, and further reduce to N_2O, sodium azide buffered with acetic acid to pH 4-5 was added. The $\delta^{15}N-NH_4^+$ samples were first quantitatively oxidized to NO_2^- by adding BrO^- at pH 12, and then excess BrO^- was removed by $NaAsO_2$ and the yield was verified *via* colorimetric nitrite determination. Then, NO_2^- was further reduced to N_2O by adding sodium azide buffered with acetic acid (Zhang et al., 2007). N_2O was separated and analyzed for $\delta^{18}O-NO_3^-$ and $\delta^{15}N-NO_3^-$ by a Precon-GasBench II-253 plus (253 Plus, Thermo Scientific, United States). To ensure the quality of monitoring data, a standard sample (IAEA-N-1) was inserted into each batch of samples (10 samples) to monitor the stability of the instrument. In addition, the $\delta^{15}N-NH_4^+$ values were calibrated by the

international standards of USGS 25, USGS26, and IAEA-N1. The $\delta^{15}N-NO_3^-$ and $\delta^{18}O-NO_3^-$ values were calibrated by the IAEA-N3 international standard. The reproducibility of duplicate analysis of $\delta^{15}N-NH_4^+$, $\delta^{15}N-NO_3^-$, and $\delta^{18}O-NO_3^-$ were <0.3‰ (mean ± 0.1‰), <0.3‰ (mean ± 0.1‰), and <0.6‰ (mean ± 0.3‰), respectively.

Mixing Model

To evaluate the behavior of nitrogen along the salinity gradient, nitrogen concentration and the isotopic values from simple physical mixing between two endmembers (coastal diluted water and outer seawater) can be calculated by a salinity-based conservative mixing model (Fry, 2002), as follows:

$$q_1 + q_2 = 1 \quad (1)$$

$$q_1 S_1 + q_2 S_2 = S_{mix} \quad (2)$$

$$q_1 N_1 + q_2 N_2 = N_{mix} \quad (3)$$

$$q_1 N_1 \delta_1 + q_2 N_2 \delta_2 = N_{mix} \delta_{mix} \quad (4)$$

where q terms denote the fractional contributions of the two endmembers (denoted by the subscripts q_r and q_m). The S, N, δ terms denote the parameters being mixed: salinity, NO_3^- or NH_4^+ concentration and $\delta^{15}N-NO_3^-$ or $\delta^{18}O-NO_3^-$ value. S_{mix}, N_{mix} and δ_{mix} terms denote the theoretical value of a mixture from the two endmembers. Based on equation (1)-(4):

$$q_1 = (S_{mix} - S_2)/(S_1 - S_2) \quad (5)$$

$$N_{mix} = N2 + (N1 - N2)q_1 \quad (6)$$

$$\delta_{mix} = [q_1(\delta_1 N_1 - \delta_2 N_2) + \delta_2 N_2]/N_{mix} \quad (7)$$

According to the above equations, the salinity-based NO_3^- or NH_4^+ mixing shows linear conservative mixing (equation 6), whereas the salinity-based isotopic mixing shows curvilinear, which reflects the $[NO_3^-]$ or $[NH_4^+]$ -based weighting of endmember isotopic contributions. The NO_3^- or NH_4^+ concentration and the isotopic value distributions, are expected to fall on the physical mixing line between the two endmembers. However, deviations from the mixing line indicate the presence of N transformation processes or other sources or both (Wankel et al., 2007). For example, the processes of nitrification and mineralization cause nitrate distribution above the mixing line, whereas $\delta^{15}N-NO_3^-$ and $\delta^{18}O-NO_3^-$ cause distributions below the mixing line (Yang et al., 2018). In contrast, the processes of assimilation and denitrification cause nitrate distribution below the mixing line whereas $\delta^{15}N-NO_3^-$ and $\delta^{18}O-NO_3^-$ distributions above the mixing lines (Yang et al., 2018).

SIAR Mixing Model

The contribution of potential nitrate sources to nitrate in water can be quantified by using a Bayesian mixing model created by and run in the stable isotope analysis in the R (SIAR) package This model has been widely used to estimate the proportional contribution of different nitrate sources (Korth et al., 2014; Davis et al., 2015; Zhang et al., 2018; Lao et al., 2019a; Torres-Martínez et al., 2020; Lao et al., 2021b). The framework is as follows (Moore and Semmens, 2008; Xue et al., 2009):

$$X_{ij} = \sum_{k=1}^{k} P_k(S_{jk} + c_{jk}) + \epsilon_{ij} \quad (8)$$

$$S_{jk} \sim N(\mu_{jk}, \omega_{jk}^2) \quad (9)$$

$$c_{jk} \sim N(\lambda_{jk}, \tau_{jk}^2) \quad (10)$$

$$\epsilon_{jk} \sim N(0, \sigma_j^2) \quad (11)$$

where X_{ij} and S_{jk} represent nitrate dual isotope values in a mixed sample and the values of nitrate dual isotopes from nitrate sources, respectively; μ_{jk} and ω_{jk} represent mean value and standard deviation from the normally distributed of S_{jk}; P_k is the proportional contribution of source k; c_{jk} is the fractionation factor for nitrate dual isotopes on source k; and λ_{jk} and τ_{jk} are the mean value and standard deviation from the normally distributed of c_{jk}; ϵ_{jk} is the residual error of the additional unquantified variation between individual samples, and 0 and σ_j are the normally distributed of ϵ_{jk}. The detail information of the model can be found in Moore and Semmens (2008); Xue et al. (2009) and Zhang et al. (2018).

RESULTS

Distribution Characteristics of Physicochemical Parameters

The distribution characteristics of temperature, salinity, DO, and Chl *a* in Qinzhou Bay and Tieshangang Bay are presented in **Figure 2**. The temperature in Qinzhou Bay and Tieshangang Bay ranged from 24.4°C to 26.0°C and from 24.0°C to 27.3°C, with an average of 24.9°C and 25.3°C, respectively. The salinity in Qinzhou Bay and Tieshangang Bay increases seaward, i.e., from the inner bay to the outer bay, ranging overall from 29.89 to 31.54 and 30.59 to 31.82, with an average of 30.79 and 31.54 during the sampling period, respectively. The lowest salinity was observed in the inner Qinzhou Bay (station Q1), which could be influenced by the freshwater input from the rivers around the bay. The DO levels in Qinzhou Bay (ranging from 6.44 to 7.01 mg L^{-1}, an average of 6.68 mg L^{-1}) were slightly higher than those in Tieshangang Bay (ranging from 5.53 to 7.72 mg L^{-1}, an average of 6.42 mg L^{-1}). A relatively low DO level (< 6.5 mg L^{-1}) was also found in the upper Qinzhou Bay (**Figure 2E**). Similarly, a significantly low DO level (< 6.0 mg L^{-1}) was observed in the upper Tieshanggang Bay, whereas a higher DO level was in the outer bay (**Figure 2F**). The Chl *a* levels in Qinzhou Bay and Tieshangang Bay ranged from 1.70 to 4.50 μg L^{-1} and 0.90 to 2.80 μg L^{-1}, with an average of 2.45 μg L^{-1} and 1.89 μg L^{-1}, respectively. Except for a lower Chl *a* level was found in the station Q12 in the most seaward in Qinzhou Bay, the higher Chl *a* level (>2.0μg L^{-1}) was found in other stations. In contrast, a lower Chl *a* level was

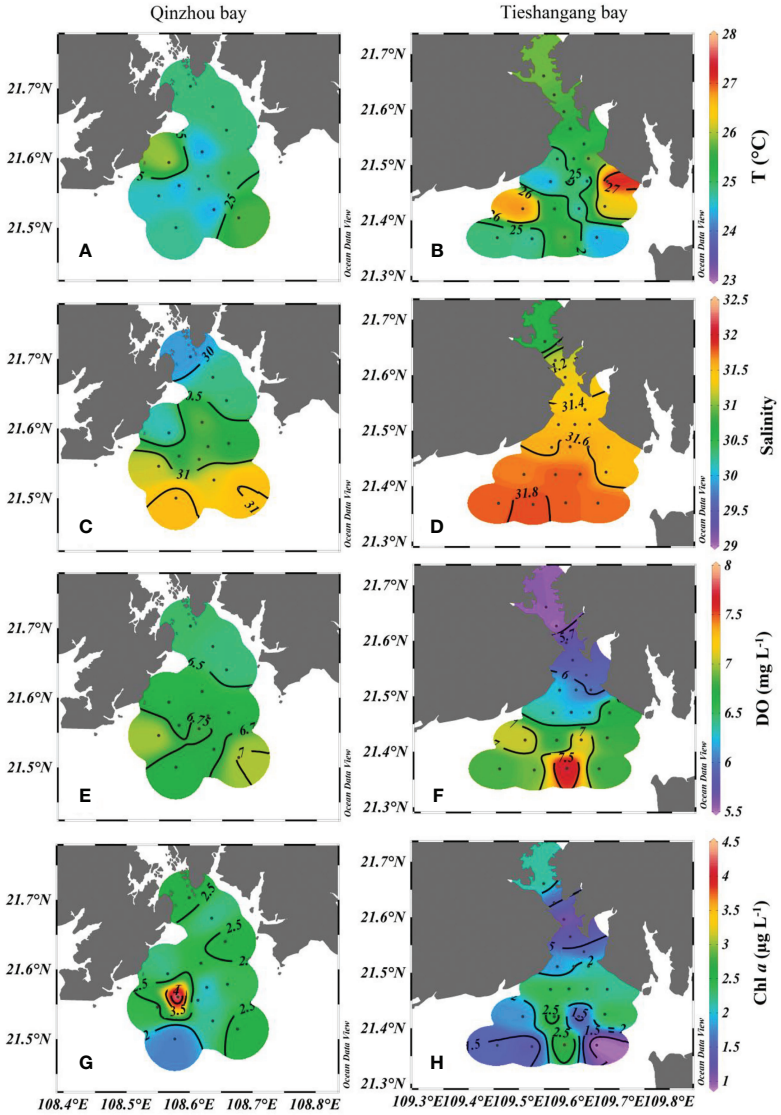

FIGURE 2 | Spatial distributions of temperature **(A, B)**, salinity **(C, D)**, DO **(E, F)** and Chl *a* level **(G, H)** in Qinzhuo Bay and Tieshangang Bay during the sampling period.

found in the inner Tieshangang Bay whereas a higher Chl *a* level in the outer bay (**Figure 2H**). Generally, the Chl *a* level in Qinzhou Bay was higher than that in the Tieshangang Bay. The pH ranged from 7.86 to 8.07 and 7.76 to 8.21 in Qinzhou Bay and Tieshangang Bay, respectively, and generally showed an increasing trend from the upper bay to the outer bay in both bays (**Figures 3A, B**). The total suspended matter (TSM) ranged from 13.7 to 30.8 mg L^{-1} and 16.6 to 37.6 mg L^{-1} in Qinzhou Bay and Tieshangang Bay, respectively. Corresponding to the lower temperature in the outer Qinzhou Bay, a higher TSM level also occurred in the outer bay (**Figure 3C**), suggesting that the vertical mixing of water may be strong in the outer bay. The TSM level in Tieshanggang Bay generally showed a decreasing trend from the upper bay to the outer bay (**Figure 3D**).

Nutrient Concentrations

The distribution characteristics of PO_4^{3-}, NO_2^-, NO_3^- and NH_4^+ concentrations were similar in Qinzhou Bay and Tieshangang Bay, which exhibited the highest concentration in the most upper station (Q1 and T1), and increasing trend from the upper bay to the outer bay (**Figure 4**). The concentrations of PO_4^{3-}, NO_2^-, NO_3^- and NH_4^+ were ranged 0.15 to 1.06 μmol L^{-1}, 0.37 to 0.82 μmol L^{-1}, 1.24 to 19.21 μmol L^{-1} and 0.65 to 1.16 μmol L^{-1}, with an average of 0.48 μmol L^{-1}, 0.53 μmol L^{-1}, 6.23 μmol L^{-1} and 0.93 μmol L^{-1} in Qinzhou bay, respectively; concentrations of PO_4^{3-}, NO_2^-, NO_3^- and NH_4^+ ranged from 0.02 to 0.92 μmol L^{-1}, 0.05 to 1.28 μmol L^{-1}, 0.23 to 10.07 μmol L^{-1} and 0.60 to 2.31 μmol L^{-1}, with an average of 0.25 μmol L^{-1}, 0.46 μmol L^{-1}, 3.17 μmol L^{-1} and 1.21 μmol L^{-1} in Tieshangang Bay, respectively. Generally,

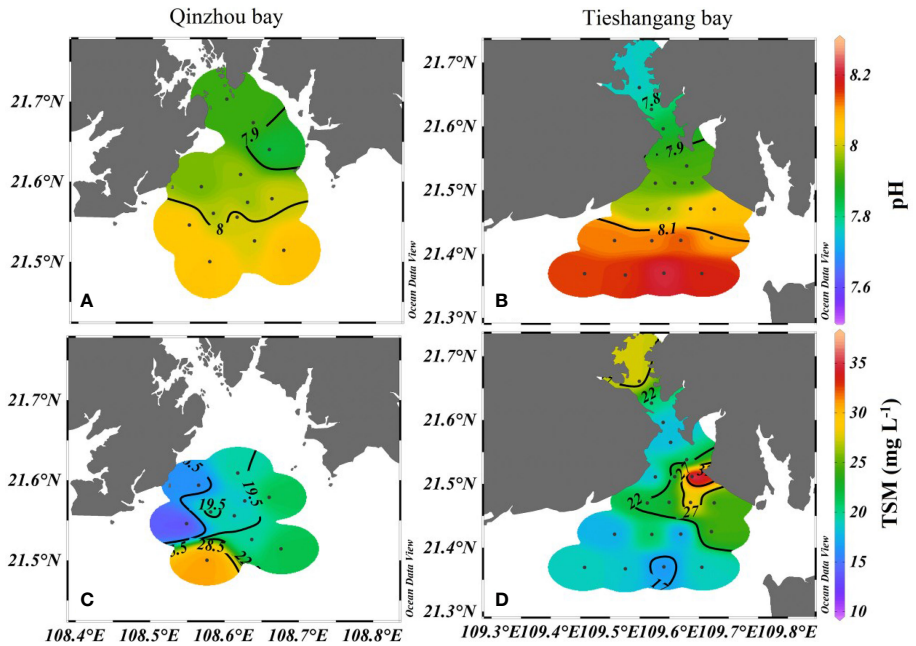

FIGURE 3 | Spatial distributions of pH **(A, B)** and TSM **(C, D)** in Qinzhuo Bay and Tieshangang Bay during the sampling period.

the concentrations of nutrients decreased from the upper bay to outer bay in both Qinzhou Bay and Tieshangang Bay (except for NH_4^+ in Qinzhou Bay) (**Figure 4**). This suggests that it is greatly influenced by terrigenous input in both two bays. However, the hydrodynamic condition may be another important factor affecting the spatial distribution of nutrients. For example, in Qinzhou Bay, with strong hydrodynamic conditions, the difference between nutrient concentration in the upper bay and outer bay is significantly higher than that in Tieshangang Bay. This is mainly due to the strong hydrodynamic conditions, which are conducive to the diffusion of nutrients and easily diluted by the low nutrient concentration in the outer bay seawater. Notably, the NO_3^- concentration in the upper Qinzhou Bay (average of 17.05 μmol L^{-1}) was significantly higher than that in the upper Tieshangang Bay (average of 5.96 μmol L^{-1}). In contrast, the NH_4^+ concentration in the upper Tieshangang Bay (average of 1.74 μmol L^{-1}) was higher than that in the upper Qinzhou Bay (average of 1.05 μmol L^{-1}) (**Figure 4**). Among the components of dissolved inorganic nitrogen (DIN, including NO_2^-, NO_3^- and NH_4^+), the proportion of NO_3^- was the highest in both Qinzhou Bay (80%) and Tieshangang Bay (65%), followed by NH_4^+ (13% in Qinzhou Bay and 25% in Tieshangang Bay), and the lowest by NO_2^- (7% in Qinzhou Bay and 9% in Tieshangang Bay). The ratio of N/P $[(NO_2^-) + (NO_3^-) + (NH_4^+)/(PO_4^{3-})]$ ranged from 6.9 to 36.1 (average of 16.23) in Qinzhou Bay and from 8.4 to 120.4 (average of 29.7) in Tieshangang Bay. The ratios in Qinzhou Bay and Tieshangang Bay were all in the range of previous studies in the Beibu Gulf (Lai et al., 2014; Lao et al., 2021b). Comparing with the rivers around the bay, the N/P ratio in the Qinzhou Bay was higher than that in Maoling River (11) but significantly lower than in the Qin River (145) during a similar period (Lao et al., 2020). This suggested that the river input may change the nutrient structure in the bay. The N/P ratio in Qinzhou Bay was similar to the Redfield ratio (i.e., the ratio of the nutrients utilized by marine phytoplankton) of 16 (Justić et al., 1995). However, the N/P ratio in Tieshangang Bay was higher than the Redfield ratio, suggesting that phosphorus (P) could be limited to producing phytoplankton in the bay; and this is consistent with the results of the previous studies on the coast of Beihai city (Lao et al., 2021b) and the western coastal Beibu Gulf (Lao et al., 2021a).

Isotopic Compositions

The distribution characteristics of $\delta^{15}N - NO_3^-$, $\delta^{18}O - NO_3^-$ and $\delta^{15}N - NH_4^+$ in Qinzhou Bay and Tieshangang Bay during the sampling period were presented in **Figure 5**. The $\delta^{15}N - NO_3^-$, $\delta^{18}O - NO_3^-$ and $\delta^{15}N - NH_4^+$ values in Qinzhou Bay ranged from 11.4 to 14.2‰, 1.3 to 13.5‰ and -35.6 to 16.7‰, with an average of 13.0‰, 8.2‰ and -4.8‰, respectively; the values in Tieshangang Bay ranged from 9.8 to 18.3‰, 2.7 to 18.0‰ ang -18.6 to 18.9‰, with an average of 15.2‰, 11.7‰ and 4.98‰, respectively. The lower $\delta^{15}N - NO_3^-$, and $\delta^{18}O - NO_3^-$ values were found in the upper Qinzhou Bay and Tieshangang Bay and exhibited an increasing trend from the upper bay to the outer bay (**Figures 5A–D**). In contrast, the highest $\delta^{15}N - NH_4^+$ value was found in the upper Tieshangang Bay and the value exhibited a decreasing trend from the upper to the outer bay (**Figure 5F**). While in the Qinzhou Bay, fewer spatial variations of $\delta^{15}N - NH_4^+$ value were found in Qinzhou Bay (**Figure 5E**). Generally, isotopic

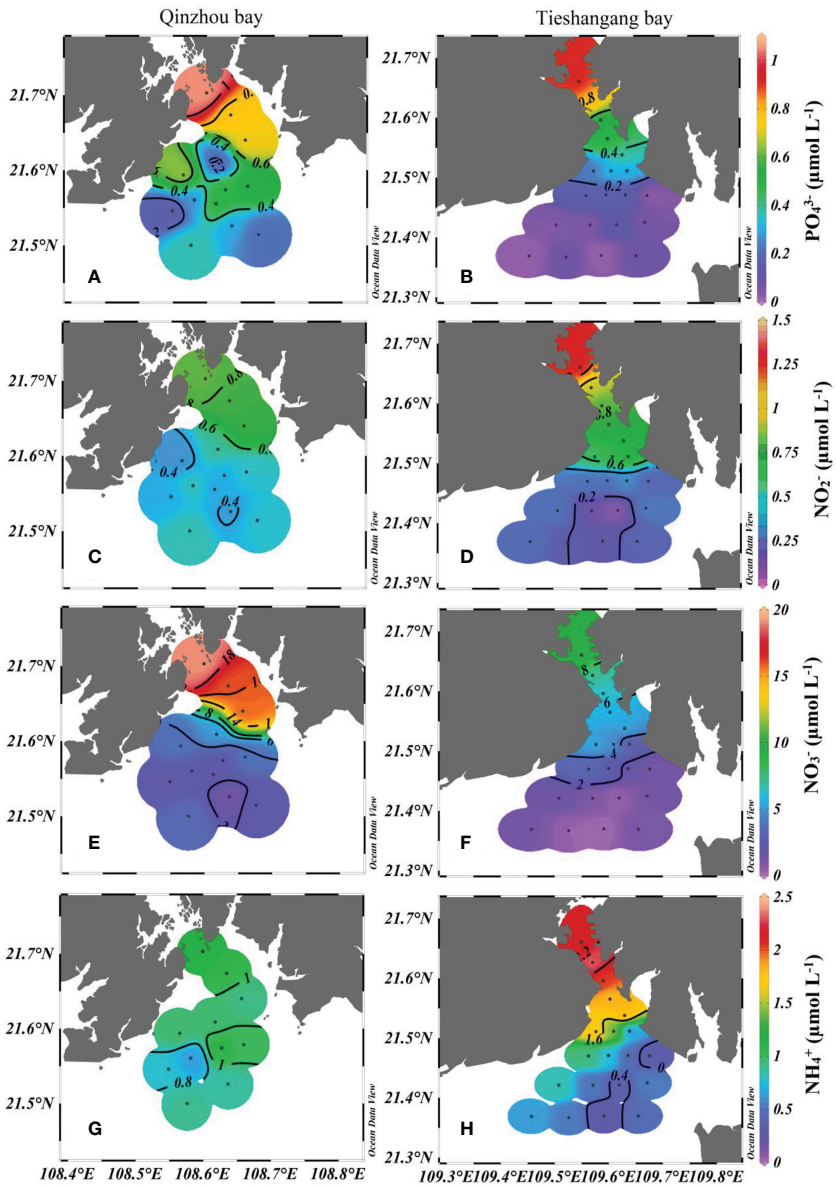

FIGURE 4 | Spatial distributions of nutrients [PO_4^{3-} **(A, B)** NO_2^- **(C, D),** NO_3^- **(E, F)** and NH_4^+ **(G, H)**] in Qinzhuo Bay and Tieshangang Bay during the sampling period.

values in the Tieshangang Bay were higher than those in the Qinzhou Bay, suggesting that there may be differences in nutrient sources and transformation processes between the two bays.

DISCUSSION

To further analyze the nitrogen sources and their biological transformations in the Qinzhou Bay and Tieshangang Bay, we classified the sampling sites into two analysis regions based on the characteristics of physicochemical parameters, nutrients, and isotopic compositions: the upper bay, including stations Q1-Q3 in Qinzhou Bay and stations T1-T8 in Tieshangang Bay, was characterized by the effect of terrestrial freshwater discharge having lower salinity and higher nutrient concentration; and the outer bay, including other stations except for the upper bay in Qinzhou Bay and Tieshangang Bay, was characterized by higher salinity and lower nutrient concentrations (**Figure 1**). The physico-chemical parameters of the two end-members of Tieshangang Bay and Qinzhou Bay are presented in **Table 1**.

Nitrate Sources and Their Biogeochemical Processes in Qinzhou Bay

In the Qinzhou Bay, nutrient concentrations in the upper bay were significantly higher than that in the outer bay (**Figure 4**), which has also been observed previously, particularly in rainy

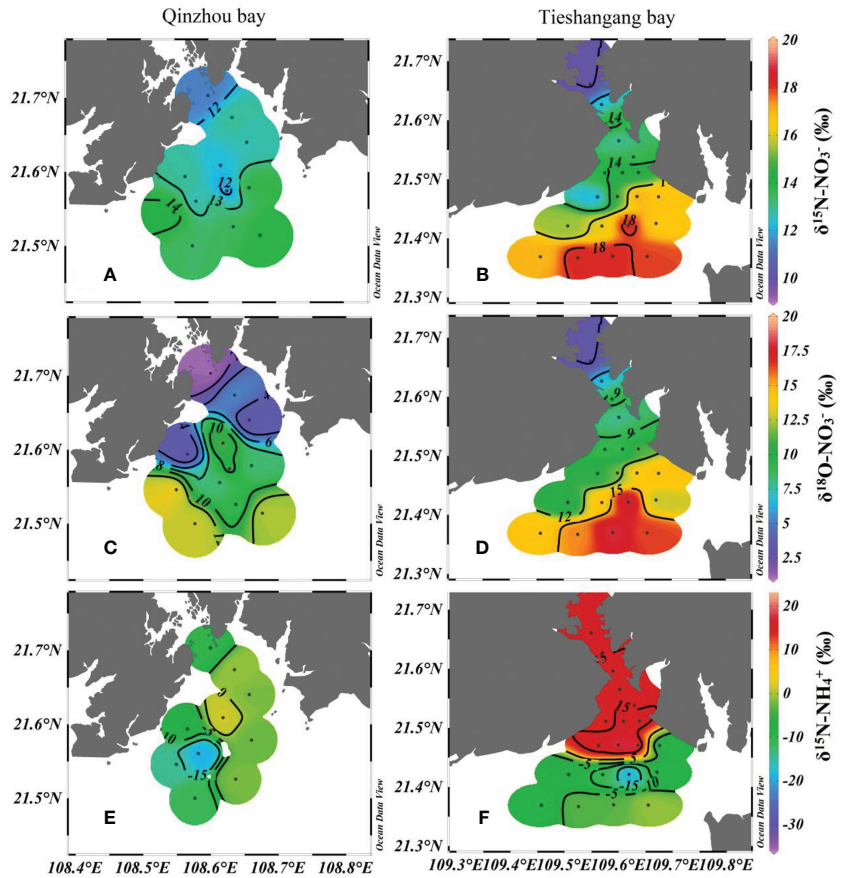

FIGURE 5 | Spatial distributions of $\delta^{15}N - NO_3^-$ **(A, B)**, $\delta^{18}O - NO_3^-$ **(C, D)** and $\delta^{15}N - NH_4^+$ **(E, F)** in Qinzhuo Bay and Tieshangang Bay during the sampling period.

seasons, as reported by Lao et al. (2021a) and Lao et al. (2021c). In addition, the nutrients showed significantly negative correlation with salinity in both Qinzhou Bay and Tieshangang Bay (**Figure 6**), suggesting that the lower salinity water with higher nutrient concentrations in the upper bay is well mixed with the higher salinity water with lower nutrient concentrations in the outer bay. In the Beibu Gulf, the heavy rainfall mainly occurred from April to October, and the runoff in the rivers around the gulf increased significantly from April (Lao et al., 2020). More importantly, although the runoff was higher in the rainy seasons, the nutrient concentrations in some rivers around the Beibu Gulf and the coastal areas during the rainy season were still higher than that in the dry seasons, indicating that the significant influence by the heavy land-sources discharge from anthropogenic activities (Lao et al., 2020; Lao et al., 2021a). Thus, the high nutrient concentration in the upper bay may be largely influenced by the land-source inputs. The increasing land-source input has resulted in the significant increase of eutrophication in Qinzhou Bay over the past 40 years (Lao et al., 2021c). In addition, the submarine groundwater discharge (SGD) was also considered as another nutrient source in the Maowei Sea, which is a semi-enclosed bay located close to the upper Qinzhou Bay, and the SGD-derived nutrients were even more important than the amounts in the local river input (Chen et al., 2018). Thus, the higher nutrient concentration in the upper bay may be also influenced by the SGD. In the upper bay, the N/P (ranged from

TABLE 1 | Endmember parameters of Qinzhou Bay and Tieshangang Bay, including salinity, nutrient concentrations and nitrate dual isotopes, used in the two-endmember mixing model in equation (5–7) .

Areas	Station	Salinity	PO_4^{3-} [μmol L^{-1}]	NH_4^+ [μmol L^{-1}]	NO_2^- [μmol L^{-1}]	NO_3^- [μmol L^{-1}]	$\delta^{15}N - NO_3^-$ [‰]	$\delta^{18}O - NO_3^-$ [‰]	$\delta^{15}N - NH_4^+$ [‰]
Qinzhou bay	Q1	29.89	1.06	1.16	0.82	19.21	11.4	1.3	-10
	Q12	31.54	0.18	0.89	0.45	1.66	13.4	12.8	-11.1
Tieshangang bay	T1	30.59	0.92	2.11	1.28	10.07	9.8	2.7	15.8
	T18	31.82	0.08	0.84	0.20	0.36	18.2	15.6	-3.4

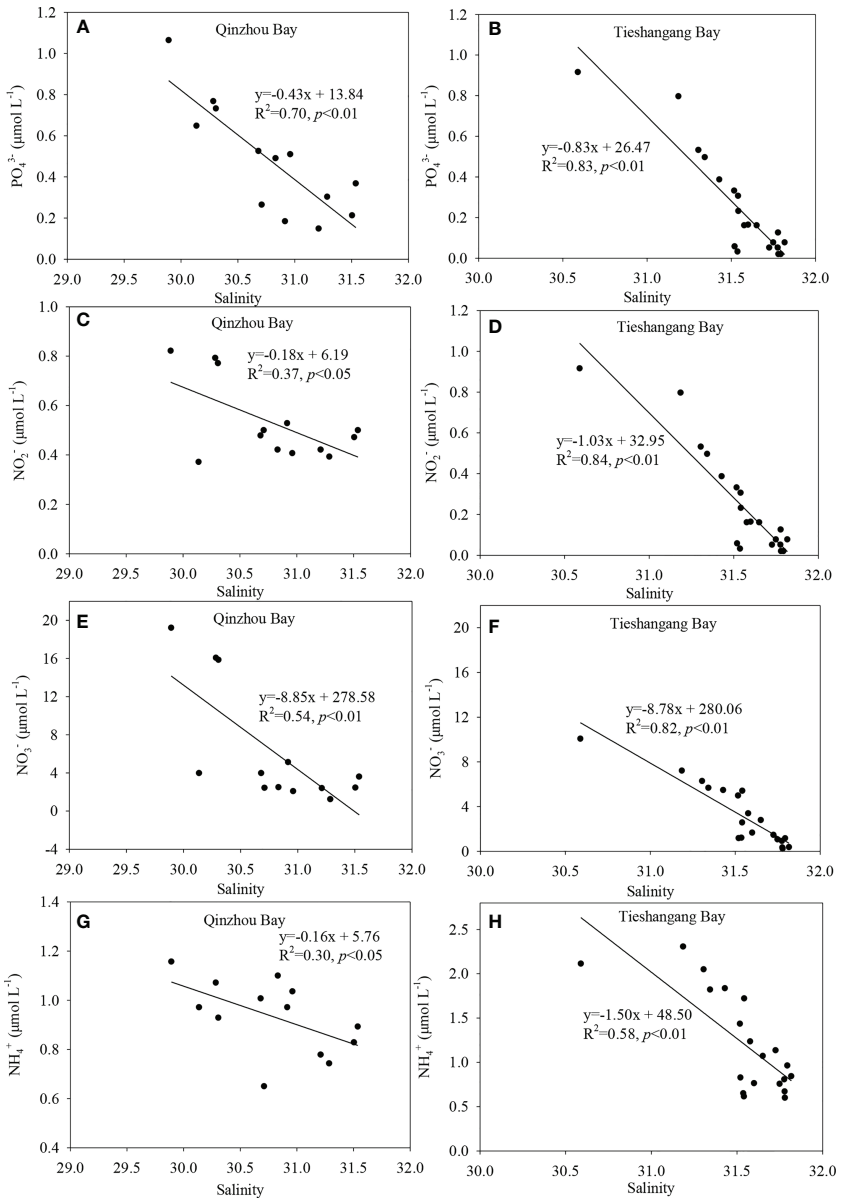

FIGURE 6 | Linear relationship between nutrient [PO_4^{3-} **(A, B),** NO_2^- **(C, D),** NO_3^- **(E, F),** and NH_4^+ **(G, H)**] and salinity in the Qinzhou Bay and Tieshangang Bay.

19.9 to 24.0, an average of 22.4) was higher than the throughout Qinzhou Bay (average of 16.2), as well as the Redfield ratio (16.0), suggesting that higher DIN concentrations input in the upper bay compared to the P. However, the high PO_4^{3-} concentrations [with a minimum (PO_4^{3-}) of >0.70 μmol L^{-1}] suggested that neither N nor P acted as a limiting nutrient in the upper bay, which were suitable for phytoplankton blooms. Notably, the N/P ratio also decreased significantly and closer to the Redfield ratio for the past years, mainly due to the increasing P input (Lao et al., 2021c). This has caused the harmful algal blooms to increase in frequency over the past ten years, particularly in the spring (Xu et al., 2019; Kang et al., 2020; Guan et al., 2022). This may be the reason that the higher Chl *a* level was observed in Qinzhou Bay during the sampling period (**Figure 2G**).

Lower $\delta^{15}N-NO_3^-$ and $\delta^{18}O-NO_3^-$ values but relatively high $\delta^{15}N-NH_4^+$ values were found in the upper bay (**Figures 5A, C, E**), suggesting that nitrification may occur in the area. The light N in the presence of excess NH_4^+ is preferentially used by the microorganisms, which could result in heavier ^{15}N in the residual NH_4^+ pool, whereas adding, depleted ^{14}N to the residual NO_3^- pool (Sigman et al., 2005; Chen et al., 2009; Ye et al., 2016). Isotope fractionation during the biological processes of nitrification can be approximated by

the open-system Rayleigh fractionation (Altabet, 2006; Ye et al., 2016), the equation is as follows:

$$\delta_m = \delta_i + \epsilon \times f_{NH4}$$

where δ_m and δ_i represent the measured and initial values for $\delta^{15}N - NH_4^+$, respectively; ϵ represents the fractionation factor; f_{NH4} represent the fraction of measured $[NH_4^+]$ relative to the initial $[NH_4^+]$ $[(NH_4^+)m/(NH_4^+)i]$. However, there is no relationship between $\delta^{15}N - NH_4^+$ and f_{NH4} ($p>0.05$). Moreover, the overall estimated ϵ (6.7‰) in the upper bay was significantly deviated from the reported values for N fractionation factors in nitrification (-14 to -38‰) (Casciotti et al., 2003; Ye et al., 2016). This suggested that microbial nitrification was not the dominant biological process in the upper bay and the isotopic signal in this area may reflect the mixing of sources. According to a classical nitrate dual isotopic approach (Xue et al., 2009; Zhang et al., 2018), the $\delta^{15}N - NO_3^-$ (from 11.4 to 12.9‰) and $\delta^{18}O - NO_3^-$ (from 1.3 to 5.3‰) values in the upper bay would suggest that sewage and manure might be the dominant nitrate sources to this region (**Figure 7**).

In the outer bay, there was a clear $\delta^{15}N - NO_3^-$ and $\delta^{18}O - NO_3^-$ values increase. In addition, significantly NO_3^- loss and relatively high offset $\delta^{15}N - NO_3^-$ and $\delta^{18}O - NO_3^-$ values were found in the outer Qinzhou Bay (**Figure 8**), suggesting that substantial NO_3^- loss or consumption occurred in the outer bay. There could be several reasons for the increase of isotopic values, including phytoplankton assimilation, denitrification, and intense physical sediment-water interaction. However, denitrification could be firstly ruled out as the cause of the increase of isotopic anomalies due to high DO levels (>6.50 mg L^{-1}) in the outer bay (**Figure 2E**). Hence, phytoplankton assimilation may be responsible for the NO_3^- loss and relatively positive isotope values in the outer bay. Phytoplankton assimilation can cause isotopic enrichment of $\delta^{15}N - NO_3^-$, $\delta^{18}O - NO_3^-$ and $\delta^{15}N - NH_4^+$, during which fractionation factors vary among different species (Granger et al., 2004; Wankel et al., 2009; Yan et al., 2017). Indeed, a spring phytoplankton bloom was indicated by a higher Chl *a* level (average of 2.5 μg L^{-1}) in the outer bay and the highest Chl *a* level (4.5 μg L^{-1}) was observed in station Q7 (**Figure 2G**). However, there is no relationship between $\delta^{15}N - NO_3^-$ and $\delta^{18}O - NO_3^-$ values in the outer bay and the increase of isotopic values were noticeably deviated from the assimilation line (1:1) (**Figure 7**). The uptake of NO_3^- by phytoplankton causes isotope enrichment in the residual NO_3^- pool due to preferential consumption of light nitrate ($^{14}NO_3^-$) by phytoplankton, with coupled $\delta^{15}N - NO_3^-$ and $\delta^{18}O - NO_3^-$ fractionation effects ($^{18}\epsilon$:$^{15}\epsilon$) of ~1 (Sigman et al., 1999; Granger et al., 2004). Moreover, based on the open-system Rayleigh fractionation (equation 10), the fractionation factor

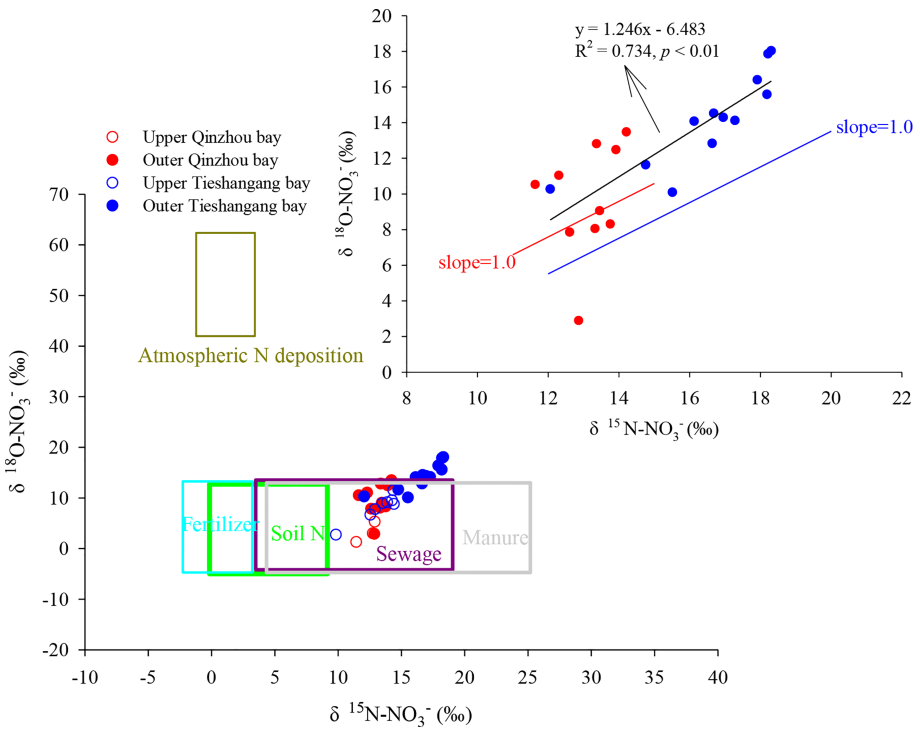

FIGURE 7 | Values of $\delta^{15}N - NO_3^-$ and $\delta^{18}O - NO_3^-$ in Qinzhou Bay (red dots and circles) and Tieshangang Bay (blue dots and circles) and in various source reservoirs (boxes). In the larger graph, the isotopic composition of five potential nitrate sources are adapted from Chen et al. (2019), (Kendall 1998), Xue et al. (2009) and Zhang et al. (2018). The inset in the upper right corner is the plots of $\delta^{15}N - NO_3^-$ and $\delta^{18}O - NO_3^-$ in outer Qinzhou Bay (red dots) and outer Tieshangang Bay (blue dots). Assimilative uptake would cause nitrate dual isotopes to increase along a slope of 1.

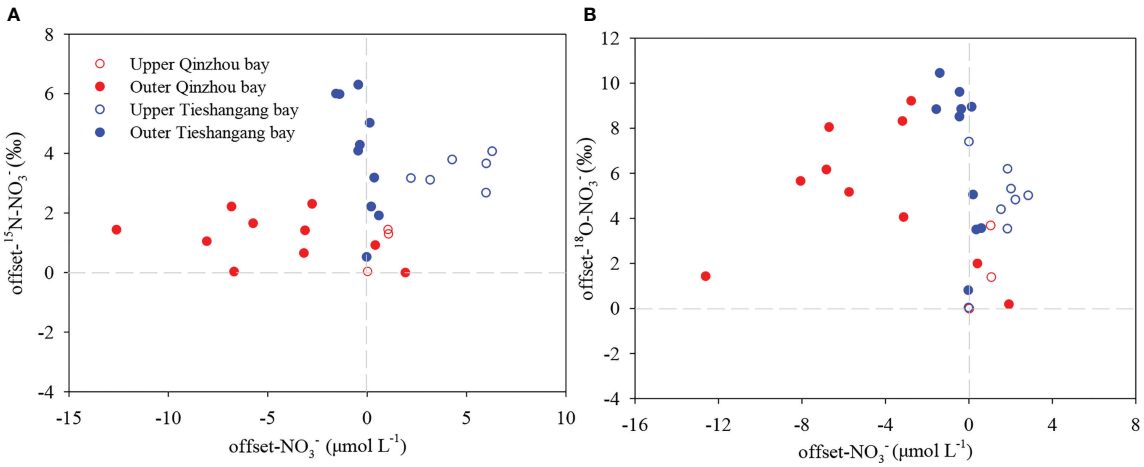

FIGURE 8 | Relationships between offset $\delta^{15}N - NO_3^-$ **(A)** and $\delta^{18}O - NO_3^-$ **(B)** and offset NO_3^- in the Qinzhou Bay and Tieshangang Bay. The offset values are the difference between measured and expected values, which area calculated using the end-member mixing model.

associated with the assimilation process was calculated. No relationship between $\delta^{15}N - NO_3^-$ and f_{NO3} ($p>0.05$) was found in the outer bay and the overall estimated ϵ (-0.7‰) in the outer bay was significantly deviated from the range of reported values (-3 to -9‰) for the process of assimilation (York et al., 2007; Ye et al., 2016). Additionally, the concentration of NH_4^+ does not decrease too much in the outer bay (average of 0.90 μmol L^{-1}, which is close to the upper bay [average of 1.05μmol L^{-1})]. Thus, when NH_4^+ is sufficient, phytoplankton preferentially assimilates NH_4^+ (Glibert et al., 2016). However, the $\delta^{15}N - NH_4^+$ values did not increase significantly in the outer bay (**Figure 5E**), which may be related to the continuous outward transportation of NH_4^+ in the upper bay under the strong hydrodynamic force, resulting in the isotopic signal of NH_4^+ sources covering the signal of isotopic fractionation caused by assimilation. Thus, phytoplankton assimilation is unlikely to be the dominant cause for the increase of nitrate dual isotopes in the outer bay. The intense physical sediment-water interaction may be responsible for the nitrate loss in the outer bay. Previous studies suggest that active consumption of nitrate due to denitrification in the sediments, causing an efflux of nitrate from the water column to the sediments, which resulted in the enrichment of $\delta^{15}N - NO_3^-$ and concurrent nitrate loss in the water (Zhang et al., 2013; Ye et al., 2016). Because advective flux returning nitrate to the upper overlying water environment caused by wind-induced mixing and tidal pumping, $\delta^{15}N - NO_3^-$ and $\delta^{18}O - NO_3^-$ values in the overlying water are substantially high, reflecting more closely nitrate isotopic fractionation by denitrification (Lehmann et al., 2007; Wankel et al., 2009). This suggestion was agreeable with the previous work that suggested the physical perturbation in the surface sediments could be very significant in spring period, when wind-induced mixing and tidal pumping in the northern Beibu Gulf was strong (Lao et al., 2021b). Indeed, the depth of the Qinzhou Bay is shallow (most stations are less than 6m, and the deeper depth in station Q12 is only 10.1m), and wind-induced mixing could aggravate the exchange of bottom and surface water. In addition, the air temperature has increased from the spring (March) in Beibu Gulf, but lower surface temperature (average of 24.7°C) in the Qinzhou Bay was found when compared to that in Tieshangang Bay (average of 25.4°C) during the same sampling period (**Figures 2A, B**), suggesting that the lower surface temperature in Qinzhou Bay originated from the bottom water upwelling. Moreover, an increasing TSP level (average of 20.0 mg L^{-1}) was also found in the outer bay (**Figure 3C**). Such a dynamic environment would result in the bidirectional exchange of substances, including nitrate, between the overlying water and the sediment pore water. This process would finally lead to the increase of nitrate isotopic values but the decrease of nitrate concentration in the bay due to denitrification-induced isotopic enrichment in sediments. However, due to the lack of other water layers in the bay, i.e., the bottom layer, this hypothesis still needs further evaluation in the field investigation.

Nitrate Sources and Its Biogeochemical Processes in Tieshangang Bay

In the Tieshangang Bay, significantly high nutrient concentrations were observed in the upper bay and showed a decrease trend from the upper bay to the outer bay (**Figure 4**). Different from Qinzhou Bay, there is no large rivers around the bay. Thus, the nutrient sources in the bay are mainly influenced by local human activities. In the upper bay, significantly positive offset NO_3^- values were found, with the values ranging from 0.01 to 2.85 μmol L^{-1} (average of 1.77 μmol L^{-1}) (**Figure 8**), which could be new nitrate added into the waters in the upper bay. The new nitrate could be sourced from direct nitrate input, and/or decomposition and/or nitrification of NH_4^+ in the upper bay. Indeed, significantly low DO level (**Figure 2F**) and lower pH (**Figure 3B**) and nitrate dual isotope values (**Figures 4B, D**) were

found in the upper bay. This suggested that oxygen consumption processes could have occurred in the upper bay, which is probably decomposition. Moreover, a lower Chl *a* level was found in the upper bay (**Figure 2H**), indicating that oxygen consumption by decomposition is more important than photosynthesis. A large oxygen consumption and a large amount of CO_2 release caused by the decomposition process could be responsible for the low DO level and pH in the upper bay. Similar results were also reported in the other coastal bays in Beibu Gulf (Lao et al., 2021a; Lao et al., 2021c). Correspondingly, a higher NH_4^+ concentration occurred in the upper bay (**Figure 4H**). The rainy seasons in the coastal Beibu Gulf would carry a relatively huge transport of sewage from the coastal cities and soil organic nitrogen (SON) from the soil to the coastal bay (Lao et al., 2020), where SON could have been easily remineralized due to the priming effect to NH_4^+ (Bianchi et al., 2015), and then nitrified to nitrate in the water (Guo et al., 2015; Ye et al., 2015). However, if the mineralization/nitrification processes are the dominant in the upper bay, the $\delta^{15}N - NO_3^-$ values should be close to 0‰, because the process generally adds isotopically light isotopes to the nitrate pool (Burns and Kendall, 2002; Ye et al., 2015). In contrast, although relatively low $\delta^{15}N - NO_3^-$ values occurred in the upper bay compared to the outer bay, the most values were still higher than 12‰ (average of 13.2‰) (**Figure 5B**), which is much higher than 0‰. This suggests that the mineralization/nitrification processes are unlikely to be the dominant cause for the increase of $\delta^{15}N - NO_3^-$ and $\delta^{18}O - NO_3^-$ in the outer bay. Notably, significantly high $\delta^{15}N - NH_4^+$ values (average of 15.1‰) were also found in the upper bay (**Figure 5F**), which are possibly associated with municipal sewage effluents from the coastal area. Generally, nitrate originated from sewage and manure is usually characterized by high isotopic values of nitrate (4 to 25‰) due to the volatilization of ^{15}N-depleted ammonia formed from human and animal waste, which results in an enrichment of ^{15}N in residual nitrate pool (Xue et al., 2009). Thus, the nitrate sources from sewage and manure may be responsible for the higher isotopic signal in the upper bay (**Figure 7**).

In the outer bay, the nutrient concentrations decrease but nitrate dual isotopic values increase. In addition, a relatively negative offset NO_3^- (average of -0.29 μmol L^{-1}) but positive offset $\delta^{15}N - NO_3^-$ (average of 4.0‰) and $\delta^{18}O - NO_3^-$ value (average of -6.8‰) was found in the outer bay, suggesting that nitrate loss or consumption occurred in the outer bay. However, the denitrification could be ruled out due to the high DO level (>7.0 mg L^{-1}) in the outer bay (**Figure 2F**), which did not favor the occurrence of denitrification. Moreover, the influence of physical sediment-water interaction should be less in the outer bay. Different from the Qinzhou Bay, the depth of outer Tieshangang Bay is deeper (most station >10m, and the deepest station in T19 reach 20m). With the air temperature increasing in spring, the surface water temperature increases in the outer bay (average of 25.4°C), opposite to the outer Qinzhou Bay (**Figures 2A, B**). This suggests that with the increase of surface water temperature, there is no bottom water upwelling in Tieshangang Bay as in Qinzhou Bay. Thus, the phytoplankton assimilation may be related to the nitrate loss but increasing isotopic nitrate values in the outer bay. Indeed, a higher Chl *a* level was found in the outer bay (average 2.41 μg L^{-1}) (**Figure 2H**). In addition, although the slope (1.25) has slightly deviated from the assimilation line (1:1), a significantly positive relationship between $\delta^{15}N - NO_3^-$ and $\delta^{18}O - NO_3^-$ values were found in the outer bay (**Figure 7**). Moreover, the fractionation factor associated with assimilation was calculated and the ^{15}N fractionation with isotope effects of -3.3‰ in the outer bay was also within the range of reported values (-3 to -9‰) for phytoplankton assimilation (York et al., 2007). This suggests that NO_3^- uptake by phytoplankton was the dominant process for NO_3^- decrease and its isotopic increase in the outer bay. However, the $\delta^{15}N - NH_4^+$ value did not increase in the outer bay. This may be because the assimilation by phytoplankton mainly utilizes NO_3^- due to significantly low NH_4^+ concentration in the outer bay (**Figure 4H**). NO_3^- is assimilated by phytoplankton when NH_4^+ is insufficient in the water environment (Glibert et al., 2016). However, extremely higher $\delta^{18}O - NO_3^-$ values were also observed in the outer bay (>10‰, average of 14.1‰) (**Figure 5E**). Neither phytoplankton assimilation nor mixing with other water masses from outer Beibu Gulf or the northern South China Sea is enough to lead to $\delta^{18}O - NO_3^-$ values higher than 10 ‰ (Ye et al., 2015; Ye et al., 2016; Lao et al., 2021b). Synthetic NO_3^- fertilizer and atmospheric N precipitation have much higher $\delta^{18}O - NO_3^-$ values (Chen et al., 2009; Chen et al., 2019), and those sources may be related to the high $\delta^{18}O - NO_3^-$ values in the outer bay. However, the source from synthetic NO_3^- fertilizer can be readily ruled out since it only accounts for <2% of the synthetic N fertilizer applied in China (Chen et al., 2009). Thus, the high $\delta^{18}O - NO_3^-$ values are partly influenced by the atmospheric deposition, which could be responsible for the nitrate dual isotopes slightly deviation of assimilation line (1:1).

To quantify the contribution of atmospheric N deposition to the NO_3^- pool in the outer bay, a simple isotope mass balance model was utilized [equations (11) and (12)]. This model is based on nitrate isotope anomalies, such as the deviation from the conservative mixing, which has also been used to calculate the relative contribution of atmospheric deposition in the coastal area (Ye et al., 2016; Lao et al., 2019a; Lao et al., 2021b). In this model, we assumed that nitrate isotope anomalies are mainly influenced by assimilation and atmospheric deposition in the outer Tieshangang Bay.

$$\Delta\delta^{15}N = \delta^{15}N_{atmosphere} \times N_{atmosphere}/(N_{atmosphere} + N_{mixing}) + 15\epsilon_{assimilation} \times fNO_3, \quad (11)$$

$$\Delta\delta^{18}O = \delta^{18}O_{atmosphere} \times N_{atmosphere}/(N_{atmosphere} + N_{mixing}) + 18\epsilon_{assmilation} \times fNO_3, \quad (12)$$

where $\triangle\delta^{15}N$ and $\triangle\delta^{18}O$ are the measured $\delta^{15}N - NO_3^-$ and $\delta^{18}O - NO_3^-$ anomalies relative to the mixing line. The process of assimilation cause $\delta^{15}N - NO_3^-$ and $\delta^{18}O - NO_3^-$ values increase of 1:1 ($^{15}\epsilon = {}^{18}\epsilon$) (Granger et al., 2004). Thus,

$$\Delta\delta^{15}N - \Delta\delta^{18}O = (\delta^{15}N_{atmosphere} - \delta^{18}O_{atmosphere}) \times N_{atmosphere}/(N_{atmosphere} + N_{mixing})$$

where we define $N_{atmosphere}/(N_{atmosphere} + N_{mixing})$ as $f_{atmosphere}$, and obtained

$$f_{atmosphere} = (\Delta\delta^{15}N - \Delta\delta^{18}O)/(\delta^{15}N_{atmosphere} - \delta^{18}O_{atmosphere}) \quad (13)$$

where $f_{atmosphere}$ is the proportional contribution of atmospheric deposition. The $\delta^{15}N - NO_3^-$ and $\delta^{18}O - NO_3^-$ values of atmospheric deposition (0.8 for $\delta^{15}N - NO_3^-$ and 52.4 for $\delta^{18}O - NO_3^-$ values) were obtained from Zhanjiang, where located at the eastern coast of the Tieshangang Bay (distance less than 60 km). The result shows that the proportional contribution of atmospheric deposition to the NO_3^- pool in the outer bay ranged from 0 to 17%, with an average of 7%. This is similar to the previous study in the northeastern Beibu Gulf (more seaward of Tieshangang Bay), which suggests that the contribution of NO_3^- from atmospheric deposition in the offshore area of Beibu Gulf was 6% (Lao et al., 2021b).

Quantification of Nitrate Sources in Qinzhou Bay and Tieshangang Bay

Since the biological processes were not the dominant factor that affected the nitrate in the upper bay of both Qinzhou Bay and Tieshangang Bay, the isotopic characteristics may provide a signal on the various sources that contributed to the mixture. According to a classical nitrate dual isotopic approach in **Figure 7**, the nitrate dual isotopic values in the two bays were significantly deviated from the potential nitrate source from fertilizer, since the $\delta^{15}N - NO_3^-$ and $\delta^{18}O - NO_3^-$ values were generally higher than that from the fertilizer. Thus, the nitrate source from fertilizer could be less in the Beibu Gulf. Although the manure and sewage might be the dominant nitrate sources in both two upper bays, the isotopic fingerprints in the upper bays were close to the source from soil N, and the extremely high $\delta^{18}O - NO_3^-$ values that were influenced by atmospheric deposition as discussed above, were considered. Thus, four potential nitrate sources, including manure and sewage, soil N, fertilizer, and atmospheric deposition, were applied to quantify the proportional contribution of the nitrate sources by a Bayesian mixing model. The $\delta^{15}N - NO_3^-$ and $\delta^{18}O - NO_3^-$ values of these four potential sources are presented in **Table 2**. The result is presented in **Figure 9**. The manure and sewage are the dominant nitrate sources in the coastal bays and the contribution in Tieshangang Bay (a total of 59%) was higher than that in Qinzhou Bay (41%), while the nitrate source from soil N in Qinzhou Bay (30%) was higher than that in the Tieshangang Bay (20%). Although both bays are affected by industrial and aquaculture activities, Tieshangang Bay does not have the rivers around the bay input as Qinzhou Bay. Thus, less soil N was carried into the Tieshangang Bay, and the dominant sources from sewage and manure could also bring the NH_4^+ into the bay. In addition, the NH_4^+ would retain in the bay due to weak hydrodynamic conditions (Jiang et al., 2017), resulting in a high NH_4^+ concentration in the upper Tieshangang Bay. In contrast, river input could bring more soil nitrogen from the coastal cities into Qinzhou Bay. This may be

TABLE 2 | The values (‰) of dual isotopes for the four potential nitrate sources at the river mouth.

	^{15}N			^{18}O		
Source	**Range**	**Mean ± SD**	**Literature**	**Range**	**Mean ± SD**	**Literature**
AND	-1.8~4.1	0.8 ± 1.5	(Chen et al., 2019)	42.7~61.6	52.4 ± 5.1	(Chen et al., 2019)
Manure and sewage	4~25	10.3 ± 4.0	(Xue et al., 2009)	-5~15	4.08 ± 0.33	(Kendall, 1998; Zhang et al., 2018)
Fertilizer	-1.87~2.96	0.04 ± 1.87	(Kendall, 1998; Zhang et al., 2018)	-5~15	4.08 ± 0.33	(Kendall, 1998; Zhang et al., 2018)
Soil N	-0.05~8.25	4.52 ± 2.67	(Kendall, 1998; Zhang et al., 2018)	-5~15	4.08 ± 0.33	(Kendall, 1998; Zhang et al., 2018)

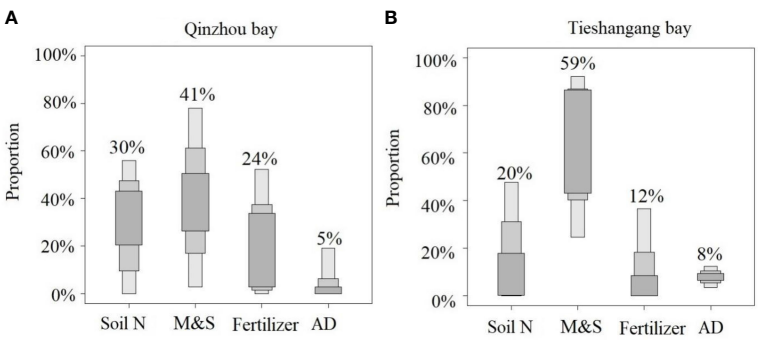

FIGURE 9 | The proportional contribution of potential sources of nitrate in the water of upper bay of Qinzhou Bay **(A)** and Tieshangang Bay **(B)**, including soil N, manure and sewage (M&S), fertilizer, and atmospheric deposition (AD).

responsible for the high NO_3^- concentration observed in the upper Qinzhou Bay. In the river basin, the nitrification coupled denitrification process in the soil can convert ammonium into nitrate and the river can bring it into the coastal environment (Chen et al., 2009). In addition, although the dominant sources from sewage and manure could bring the NH_4^+ into the bay, the strong hydrodynamic conditions accelerate the exchange of seawater between the upper bay and the outer bay, resulting in the dilution of NH_4^+ concentration. Thus, the concentration of NH_4^+ in Qinzhou Bay is not as high as that in Tieshangang Bay due to accumulation. The contribution of atmospheric deposition was similar between the two upper bays (**Figure 9**), and also similar to the outer Tieshanggang Bay (8%) and the offshore area of the northeastern Beibu Gulf (6%) reported by previous studies (Lao et al., 2021b). This suggests that the impact of atmospheric deposition on the Beibu Gulf is relatively consistent.

According to the results of quantitative calculation, the sources of nitrate in the two bays are obviously different. In the Qinzhou Bay with riverine input, the contribution of the soil N and fertilizer is higher than that without riverine input in the Tieshangang Bay, while the source from manure and sewage in the Tieshangang Bay is higher than that in the Qinzhou Bay. This suggests that for the bay with riverine input, rivers can import a large number of land-based pollutants into the coastal waters, while the bay without riverine input reflects the discharge of industrial or urban manure and sewage, which needs the attention of environmental managers.

CONCLUSION

Nitrate dual isotopes ($\delta^{15}N - NO_3^-$ and $\delta^{18}O - NO_3^-$) and ammonium nitrogen isotope ($\delta^{15}N - NH_4^+$), were used to determine the origin of nitrate in the coastal bays of Beibu Gulf (Qinzhou Bay and Tieshanggang Bay) and to study biogeochemical processes associated with nitrogen cycling. The summary of the nitrate sources and its biogeochemical processes is presented in **Figure 10**. The nutrient concentrations generally showed a

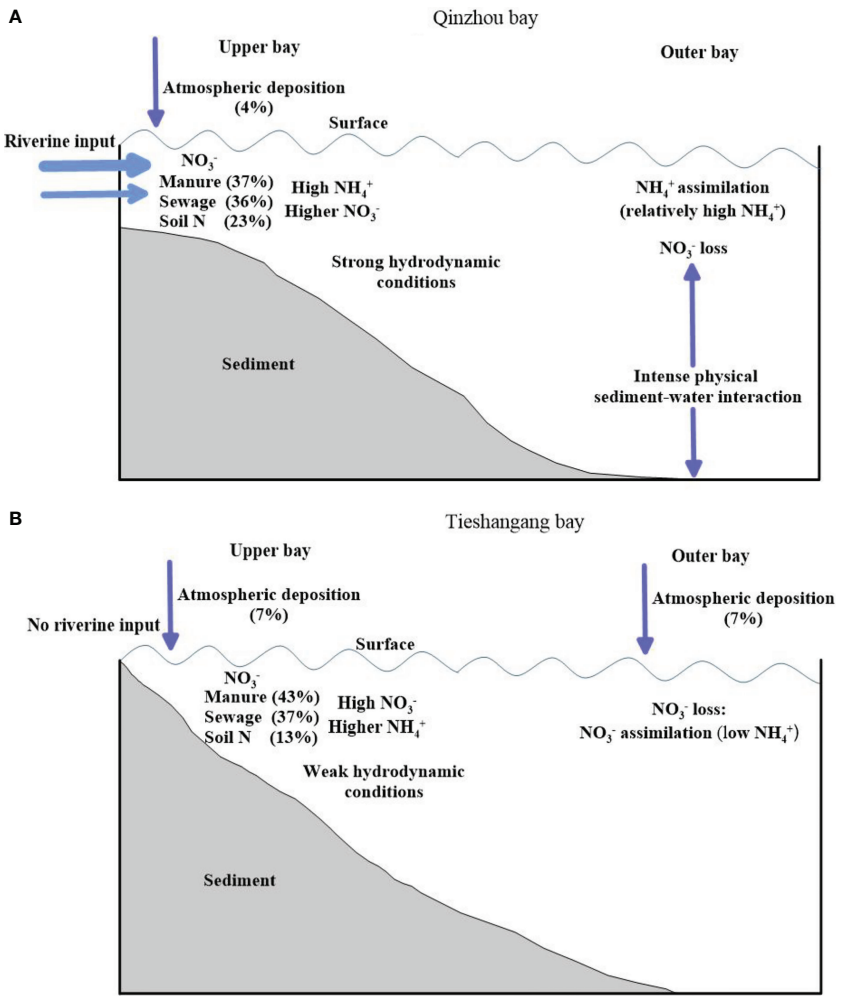

FIGURE 10 | Conceptual diagram of sources and cycling of nitrogen between a bay with riverine input **(A)** and a bay without riverine input **(B)** in the Beibu Gulf.

decreased trend from the upper bay to the outer bay, while the $\delta^{15}N - NO_3^-$ and $\delta^{18}O - NO_3^-$ values increased seaward in both bays. The $\delta^{15}N - NH_4^+$ values decreased from the upper Tieshangang Bay to the outer bay. Although the isotopic distribution trends of the two bays are similar, the isotopic values in Tieshangang Bay were higher than that in the Qinzhou Bay, suggesting that there may be differences in nutrient sources and transformation processes between the two bays. Manure and sewage were the dominant nitrate sources in the both upper bays, but the contribution in Tieshangang Bay (59%) was higher than that in the Qinzhou Bay (41%). While the nitrate source from soil N in upper Qinzhou Bay (30%) was higher than that in the upper Tieshangang Bay (20%), which may relate to the runoff input from the coastal cities around the Qinzhou Bay. Moreover, nutrients were retained in the upper Tieshangang Bay due to weak hydrodynamic conditions, which caused higher NH_4^+ concentrations in the upper bay. Significant nitrate loss occurred in the outer Qinzhou Bay, which is related to the intense physical sediment-water interaction. Moreover, phytoplankton assimilation mainly utilized NH_4^+ due to sufficient NH_4^+ in the outer Qinzhou Bay. Nitrate loss was also found in the outer Tieshangang Bay which mainly related to the phytoplankton assimilation. In addition, the greater enrichment of $\delta^{18}O - NO_3^-$ than $\delta^{15}N - NO_3^-$ in both bays suggests that atmospheric deposition also contributes to the nitrate pool in the water and the impact of atmospheric deposition on the Beibu Gulf is relatively consistent.

DATA AVAILABILITY STATEMENT

The original contributions presented in the study are included in the article/supplementary material. Further inquiries can be directed to the corresponding author.

AUTHOR CONTRIBUTIONS

FC was responsible for the conceptualization. CC and QL prepared and wrote the original draft. QL, FC, and CC wrote, reviewed, and edited the manuscript. YS and GJ were responsible for the data curation. QZ, XLu, and XZ were responsible for the experimental operation. QS, XLe, and GL were responsible for field sampling. FC and QL funded the acquisition. All authors read and approved the final manuscript.

FUNDING

This study was supported by the National Natural Science Foundation of China (U1901213), Guangxi Natural Science Foundation of China (2020GXNSFBA297065), Guangdong Natural Science Foundation of China (2019B1515120066, 2016A030312004), and Scientific Research Start-Up Foundation of Shantou University (NTF20006).

REFERENCES

Altabet, M. A. (2006). "Isotopic Tracers of the Marine Nitrogen Cycle: Present and Past," in *Marine Organic Matter: Biomarkers, Isotopes and DNA* (Berlin, Heidelberg: Springer), 251–293.

Anderson, D. M., Fensin, E., Gobler, C. J., Hoeglund, A. E., Hubbard, K. A., Kulis, D. M., et al. (2021). Marine Harmful Algal Blooms (HABs) in the United States: History, Current Status and Future Trends. *Harmf. Algae.* 102, 101975. doi: 10.1016/j.hal.2021.101975

Bianchi, T. S., Thornton, D. C. O., Yvon-Lewis, S. A., King, G. M., Eglinton, T. I., Shields, M. R., et al. (2015). Positive Priming of Terrestrially Derived Dissolved Organic Matter in a Freshwater Microcosm System. *Geophys. Res. Lett.* 42 (13), 5460–5467. doi: 10.1002/2015GL064765

Burns, D. A., and Kendall, C. (2002). Analysis of δ^{15}n and δ^{18}o to Differentiate NO_3^- Sources in Runoff at Two Watersheds in the Catskill Mountains of New York. *Water Resour. Res.* 38 (5), 9–1. doi: 10.1029/2001WR000292

Carstensen, J., and Conley, D. J. (2019). Baltic Sea Hypoxia Takes Many Shapes and Sizes. *Limnol. Oceanog. Bull.* 28 (4), 125–129. doi: 10.1002/lob.10350

Casciotti, K. L., Sigman, D. M., and Ward, B. B. (2003). Linking Diversity and Stable Isotope Fractionation in Ammonia-Oxidizing Bacteria. *Geomicrobio. J.* 20 (4), 335–353. doi: 10.1080/01490450303895

Chen, F., Jia, G., and Chen, J. (2009). Nitrate Sources and Watershed Denitrification Inferred From Nitrate Dual Isotopes in the Beijiang River, South China. *Biogeochemistry* 94 (2), 163–174. doi: 10.1007/s10533-009-9316-x

Chen, F., Lao, Q., Jia, G., Chen, C., Zhu, Q., and Zhou, X. (2019). Seasonal Variations of Nitrate Dual Isotopes in Wet Deposition in a Tropical City in China. *Atmos. Environ.* 196, 1–9. doi: 10.1016/j.atmosenv.2018.09.061

Chen, X., Lao, Y., Wang, J., Du, J., Liang, M., and Yang, B. (2018). Submarine Groundwater-Borne Nutrients in a Tropical Bay (Maowei Sea, China) and Their Impacts on the Oyster Aquaculture. *Geochem. Geophys. Geosyst.* 19 (3), 932–951. doi: 10.1002/2017GC007330

Chen, F., Lao, Q., Zhang, S., Bian, P., Jin, G., Zhu, Q., et al. (2020). Nitrate Sources and Biogeochemical Processes Identified Using Nitrogen and Oxygen Isotopes on the Eastern Coast of Hainan Island. *Continent. Shelf. Res.* 207, 104209. doi: 10.1016/j.csr.2020.104209

Davis, P., Syme, J., Heikoop, J., Fessenden-Rahn, J., Perkins, G., Newman, B., et al. (2015). Quantifying Uncertainty in Stable Isotope Mixing Models. *J. Geophys. Res.: Biogeosci.* 120 (5), 903–923. doi: 10.1002/2014JG002839

Fry, B. (2002). Conservative Mixing of Stable Isotopes Across Estuarine Salinity Gradients: A Conceptual Framework for Monitoring Watershed Influences on Downstream Fisheries Production. *Estuaries* 25, 264–271. doi: 10.1007/BF02691313

Gan, H., Lin, J., Liang, K., and Xia, Z. (2013). Selected Trace Metals (As, Cd and Hg) Distribution and Contamination in the Coastal Wetland Sediment of the Northern Beibu Gulf, South China Sea. *Mar. Poll. Bull.* 66 (1-2), 252–258. doi: 10.1016/j.marpolbul.2012.09.020

Glibert, P. M., Wilkerson, F. P., Dugdale, R. C., Raven, J. A., Dupont, C. L., Leavitt, P. R., et al. (2016). Pluses and Minuses of Ammonium and Nitrate Uptake and Assimilation by Phytoplankton and Implications for Productivity and Community Composition, With Emphasis on Nitrogen-Enriched Conditions. *Limnol. Oceanog.* 61 (1), 165–197. doi: 10.1002/lno.10203

Gobler, C. J. (2020). Climate Change and Harmful Algal Blooms: Insights and Perspective. *Harmf. Algae.* 91, 101731. doi: 10.1016/j.hal.2019.101731

Granger, J., and Sigman, D. M. (2009). Removal of Nitrite With Sulfamic Acid for Nitrate N and O Isotope Analysis With the Denitrifier Method. *Rapid Commun. Mass. Spectromet.* 23 (23), 3753–3762. doi: 10.1002/rcm.4307

Granger, J., Sigman, D. M., Needoba, J. A., and Harrison, P. J. (2004). Coupled Nitrogen and Oxygen Isotope Fractionation of Nitrate During Assimilation by Cultures of Marine Phytoplankton. *Limnol. Oceanog.* 49 (5), 1763–1773. doi: 10.4319/lo.2004.49.5.1763

Gruber, N., and Galloway, J. N. (2008). An Earth-System Perspective of the Global Nitrogen Cycle. *Nature* 451, 293–296. doi: 10.1038/nature06592

Guan, W., Bao, M., Lou, X., Zhou, Z., and Yin, K. (2022). Monitoring, Modeling and Projection of Harmful Algal Blooms in China. *Harmf. Algae.* 111, 102164. doi: 10.1016/j.hal.2021.102164

Guo, W., Ye, F., Xu, S., and Jia, G. (2015). Seasonal Variation in Sources and Processing of Particulate Organic Carbon in the Pearl River Estuary, South China. *Estua. Coast. Shelf. Sci.* 167, 540–548. doi: 10.1016/j.ecss.2015.11.004

Jiang, C., Liu, Y., Long, Y., and Wu, C. (2017). Estimation of Residence Time and Transport Trajectory in Tieshangang Bay, China. *Water* 9 (5), 321. doi: 10.3390/w9050321

Justić, D., Rabalais, N. N., Turner, R. E., and Dortch, Q. (1995). Changes in Nutrient Structure of River-Dominated Coastal Waters: Stoichiometric Nutrient Balance and its Consequences. *Estua. Coast. Shelf. Sci.* 40 (3), 339–356. doi: 10.1016/S0272-7714(05)80014-9

Kang, Z., Yang, B., Lai, J., Ning, Y., Zhong, Q., Lu, D., et al. (2020). Phaeocystis Globosa Bloom Monitoring: Based on P. Globosa induced seawater viscosity modification adjacent to a nuclear power plant in Qinzhou Bay, China. *J. Ocean. Univ. China* 19 (5), 1207–1220. doi: 10.1007/s11802-020-4481-6

Kendall, C. (1998). "Tracing Nitrogen Sources and Cycling in Catchments," in *Isotope Tracers in Catchment Hydrology*. Eds. C. Kendall and J. J. McDonnel (New York: Elsevier), 519–576.

Korth, F., Deutsch, B., Frey, C., Moros, C., and Voss, M. (2014). Nitrate Source Identification in the Baltic Sea Using its Isotopic Ratios in Combination With a Bayesian Isotope Mixing Model. *Biogeosciences* 11 (17), 4913–4924. doi: 10.5194/bg-11-4913-2014

Lai, J., Jiang, F., Ke, K., Xu, M., Lei, F., and Chen, B. (2014). Nutrients Distribution and Trophic Status Assessment in the Northern Beibu Gulf, China. *Chin. J. Oceanol. Limnol.* 32 (5), 1128–1144. doi: 10.1007/s00343-014-3199-y

Lao, Q., Chen, F., Liu, G., Chen, C., Jin, G., Zhu, Q., et al. (2019a). Isotopic Evidence for the Shift of Nitrate Sources and Active Biological Transformation on the Western Coast of Guangdong Province, South China. *Mar. Poll. Bull.* 142, 603–612. doi: 10.1016/j.marpolbul.2019.04.026

Lao, Q., Liu, G., Gao, J., Shen, Y., Guo, Z., Qing, S., et al. (2021c). Study on the Characteristics and Eutrophication of Nutrients in the Mariculture Farms of Qinzhou Bay, South China. *Mar. Environ. Sci.* 40 (3), 407–416. doi: 10.13634/j.cnki.mes.2021.03.011

Lao, Q., Liu, G., Gao, J., Shen, Y., Su, Q., Chen, C., et al. (2021b). Seasonal Sources and Cycling of Nitrogen Revealed by Stable Isotopes in the Northeastern Beibu Gulf, China. *J. Mar. Sci. Eng.* 9 (10), 1123. doi: 10.3390/jmse9101123

Lao, Q., Liu, G., Shen, Y., Su, Q., Gao, J., and Chen, F. (2020). Distribution Characteristics and Fluxes of Nutrients in the Rivers of the Beibu Gulf. *Haiyang Xuebao* 42 (12), 93–100. doi: 10.3969/j.issn.0253–4193.2020.12.010

Lao, Q., Liu, G., Shen, Y., Su, Q., and Lei, X. (2021a). Biogeochemical Processes and Eutrophication Status of Nutrients in the Northern Beibu Gulf, South China. *J. Earth Syst. Sci.* 130 (4), 1–14. doi: 10.1007/s12040-021-01706-y

Lao, Q., Liu, G., Zhou, X., Chen, F., and Zhang, S. (2021d). Sources of Polychlorinated Biphenyls (PCBs) and Dichlorodiphenyltrichloroethanes (DDTs) Found in Surface Sediment From Coastal Areas of Beibu Gulf: A Reflection on Shipping Activities and Coastal Industries. *Mar. Poll. Bull.* 167, 112318. doi: 10.1016/j.marpolbul.2021.112318

Lao, Q., Su, Q., Liu, G., Shen, Y., Chen, F., Lei, X., et al. (2019b). Spatial Distribution of and Historical Changes in Heavy Metals in the Surface Seawater and Sediments of the Beibu Gulf, China. *Mar. Poll. Bull.* 146, 427–434. doi: 10.1016/j.marpolbul.2019.06.080

Lehmann, M. F., Sigman, D. M., McCorkle, D. C., Granger, J., Hoffmann, S., Cane, G., et al. (2007). The Distribution of Nitrate $^{15}N/^{14}N$ in Marine Sediments and the Impact of Benthic Nitrogen Loss on the Isotopic Composition of Oceanic Nitrate. *Geochim. Cosmochim. Acta* 71 (22), 5384–5404. doi: 10.1016/j.gca.2007.07.025

Liu, G., Lao, Q., Su, Q., Shen, Y., Chen, F., Qing, S., et al. (2020). Spatial and Seasonal Characteristics of Dissolved Heavy Metals in the Aquaculture Areas of Beibu Gulf, South China. *Hum. Ecol. Risk Assess.* 26 (7), 1957–1969. doi: 10.1080/10807039.2019.1629273

Lorenzen, C. J. (1967). Determination of Chlorophyll and Pheopigments: Spectrophotometric Equations. *Limnol. Oceanog.* 12, 343–346. doi: 10.4319/lo.1967.12.2.0343

McIlvin, M. R., and Altabet, M. A. (2005). Chemical Conversion of Nitrate and Nitrite to Nitrous Oxide for Nitrogen and Oxygen Isotopic Analysis in Freshwater and Seawater. *Analytic. Chem.* 77 (17), 5589–5595. doi: 10.1021/ac050528s

Moore, J. M., Mills, M. M., Arrigo, K. R., Berman-Frank, I., Bopp, L., Boyd, P. W., et al. (2013). Processes and Patterns of Oceanic Nutrient Limitation. *Nat. Geosci.* 6 (9), 701–710. doi: 10.1038/ngeo1765

Moore, J. M., and Semmens, B. X. (2008). Incoporating Uncertainty and Prior Information Into Stable Isotope Mixing Models. *Ecol. Lett.* 11, 470–480. doi: 10.1111/j.1461-0248.2008.01163.x

Sharples, J., Middelburg, J. J., Fennel, K., and Jickells, T. D. (2017). What Proportion of Riverine Nutrients Reaches the Open Ocean? *Global Biogeochem. Cycle.* 31, 39–58. doi: 10.1002/2016GB005483

Sigman, D. M., Altabet, M. A., McCorkle, D. C., Francois, R., and Fischer, G. (1999). The $\delta^{15}n$ of Nitrate in the Southern Ocean: Consumption of Nitrate in Surface Waters. *Global Biogeochem. Cycle.* 13 (4), 1149–1166. doi: 10.1029/1999GB900038

Sigman, D. M., Granger, J., DiFiore, P. J., Lehmann, M. M., Ho, R., Cane, G., et al. (2005). Coupled Nitrogen and Oxygen Isotope Measurements of Nitrate Along the Eastern North Pacific Margin. *Global Biogeochem. Cycle.* 19 (4), GB4022. doi: 10.1029/2005GB002458

Torres-Martínez, J. A., Mora, A., Knappett, P. S., Ornelas-Soto, N., and Mahlknecht, J. (2020). Tracking Nitrate and Sulfate Sources in Groundwater of an Urbanized Valley Using a Multi-Tracer Approach Combined With a Bayesian Isotope Mixing Model. *Water Res.* 182, 115962. doi: 10.1016/j.watres.2020.115962

Tremblay, J.É., Anderson, L. G., Matrai, P., Coupel, P., Bélanger, S., Michel, C., et al. (2015). Global and Regional Drivers of Nutrient Supply, Primary Production and CO_2 Drawdown in the Changing Arctic Ocean. *Prog. Oceanog.* 139, 171–196. doi: 10.1016/j.pocean.2015.08.009

Wankel, S. D., Kendall, C., and Paytan, A. (2009). Using Nitrate Dual Isotopic Composition ($\delta^{15}n$ and $\delta^{18}o$) as a Tool for Exploring Sources and Cycling of Nitrate in an Estuarine System: Elkhorn Slough, California. *J. Geophys. Res.* 114, G01011. doi: 10.1029/2008JG000729

Wankel, S. D., Kendall, C., Pennington, J. T., Chavez, F. P., and Paytan, A. (2007). Nitrification in the Euphotic Zone as Evidenced by Nitrate Dual Isotopic Composition: Observations From Monterey Bay, California. *Global Biogeochem. Cycle.* 21, 1–13. doi: 10.1029/2006GB002723

Xu, C., Dan, S. F., Yang, B., Lu, D., Kang, Z., Huang, H., et al. (2021). Biogeochemistry of Dissolved and Particulate Phosphorus Speciation in the Maowei Sea, Northern Beibu Gulf. *J. Hydrolog.* 593, 125822. doi: 10.1016/j.jhydrol.2020.125822

Xue, D., Botte, J., De Baets, B., Accoe, F., Nestler, A., Taylor, P., et al. (2009). Present Limitations and Future Prospects of Stable Isotope Methods for Nitrate Source Identification in Surface-and Groundwater. *Water Res.* 43 (5), 1159–1170. doi: 10.1016/j.watres.2008.12.048

Xu, C., Yang, B., Dan, S. F., Zhang, D., Liao, R., Lu, D., et al. (2020). Spatiotemporal Variations of Biogenic Elements and Sources of Sedimentary Organic Matter in the Largest Oyster Mariculture Bay (Maowei Sea), Southwest China. *Sci. Tot. Environ.* 730, 139056. doi: 10.1016/j.scitotenv.2020.139056

Xu, Y., Zhang, T., and Zhou, J. (2019). Historical Occurrence of Algal Blooms in the Northern Beibu Gulf of China and Implications for Future Trends. *Front. Microbiol.* 10, 451. doi: 10.3389/fmicb.2019.00451

Yan, X., Xu, M. N., Wan, X. S., Yang, J.-Y. T., Trull, T. W., Dai, M., et al. (2017). Dual Isotope Measurements Reveal Zoning of Nitrate Processing in the Summer Changjiang (Yangtze) River Plume. *Geophys. Res. Lett.* 4 (12), 289–12,297. doi: 10.1002/2017GL075951

Yang, Z., Chen, J., Li, H., Jin, H., Gao, S., Ji, Z., et al. (2018). Sources of Nitrate in Xiangshan Bay (China), As Identified Using Nitrogen and Oxygen Isotopes. *Estuar. Coast. Shelf Sci.* 207, 109–118. doi: 10.1016/j.ecss.2018.02.019

Ye, F., Jia, G., Xie, L., Wei, G., and Xu, J. (2016). Isotope Constraints on Seasonal Dynamics of Dissolved and Particulate N in the Pearl River Estuary, South China. *J. Geophys. Res.-Oceans* 121 (12), 8689–8705. doi: 10.1002/2016JC012066

Ye, F., Ni, Z., Xie, L., Wei, G., and Jia, G. (2015). Isotopic Evidence for the Turnover of Biological Reactive Nitrogen in the Pearl River Estuary, South China. *J. Geophys. Res.-Biogeosciences* 120, 661–672. doi: 10.1002/2014JG002842

York, J. K., Tomasky, G., Valiela, I., and Repeta, D. J. (2007). Stable Isotopic Detection of Ammonium and Nitrate Assimilation by Phytoplankton in the Waquoit Bay Estuarine System. *Limnol. Oceanog.* 52, 144–155. doi: 10.4319/lo.2007.52.1.0144

Yu, X., Shen, J., and Du, J. (2020). A Machine-Learning-Based Model for Water Quality in Coastal Waters, Taking Dissolved Oxygen and Hypoxia in Chesapeake Bay as an Example. *Water Resour. Res.* 56 (9), e2020WR027227. doi: 10.1029/2020WR027227

Zhang, L., Altabet, M. A., Wu, T., and Hadas, O. (2007). Sensitive Measurement of NH_4^+ $^{15}n/^{14}n$ ($\delta^{15}nh_4^+$) at Natural Abundance Levels in Fresh and Saltwaters. *Analytic. Chem.* 79 (14), 5297–5303. doi: 10.1021/ac070106d

Zhang, L., Wang, L., Yin, K., Lu, Y., Zhang, D., Yang, Y., et al. (2013). Pore Water Nutrient Characteristics and the Fluxes Across the Sediment in the Pearl River Estuary and Adjacent Waters, China. *Estuar. Coast. Shelf Sci.* 133, 182–192. doi: 10.1016/j.ecss.2013.08.028

Zhang, M., Zhi, Y., Shi, J., and Wu, L. (2018). Apportionment and Uncertainty Analysis of Nitrate Sources Based on the Dual Isotope Approach and a Bayesian Isotope Mixing Model at the Watershed Scale. *Sci. Tot. Environ.* 639, 1175–1187. doi: 10.1016/j.scitotenv.2018.05.239

Conflict of Interest: The authors declare that the research was conducted in the absence of any commercial or financial relationships that could be construed as a potential conflict of interest.

Publisher's Note: All claims expressed in this article are solely those of the authors and do not necessarily represent those of their affiliated organizations, or those of the publisher, the editors and the reviewers. Any product that may be evaluated in this article, or claim that may be made by its manufacturer, is not guaranteed or endorsed by the publisher.

Copyright © 2022 Chen, Lao, Shen, Jin, Chen, Su, Lei, Zhou, Lu, Zhu and Liu. This is an open-access article distributed under the terms of the Creative Commons Attribution License (CC BY). The use, distribution or reproduction in other forums is permitted, provided the original author(s) and the copyright owner(s) are credited and that the original publication in this journal is cited, in accordance with accepted academic practice. No use, distribution or reproduction is permitted which does not comply with these terms.

frontiers | Frontiers in Marine Science

BRIEF RESEARCH REPORT
published: 24 May 2022
doi: 10.3389/fmars.2022.861718

Community Structure of Benthic Macrofauna and the Ecological Quality of Mangrove Wetlands in Hainan, China

Ping Li[1,2,3], Jingli Liu[1,2], Jiankun Bai[3], Yifan Tong[3], Yuchen Meng[3], Xiaoping Diao[4], Ke Pan[1], Xiaoshan Zhu[3,5] and Guanghui Lin[3]*

[1] Shenzhen Key Laboratory of Marine Microbiome Engineering, Institute for Advanced Study, Shenzhen University, Shenzhen, China, [2] Key Laboratory of Optoelectronic Devices and Systems, College of Physics and Optoelectronic Engineering, Shenzhen University, Shenzhen, China, [3] Shenzhen International Graduate School, Tsinghua University, Shenzhen, China, [4] College of Life Science, Hainan Normal University, Haikou, China, [5] South Laboratory of Ocean Science and Engineering (Guangdong, Zhuhai), Zhuhai, China

OPEN ACCESS

Edited by:
Ana Carolina Ruiz-Fernández, National Autonomous University of Mexico, Mexico

Reviewed by:
Michal Kowalewski, University of Florida, United States
Iñigo Muxika, Technological Center Expert in Marine and Food Innovation (AZTI), Spain

***Correspondence:**
Xiaoshan Zhu
zhu.xiaoshan@sz.tsinghua.edu.cn
orcid.org/0000-0003-1223-1415

Specialty section:
This article was submitted to Marine Pollution, a section of the journal Frontiers in Marine Science

Received: 25 January 2022
Accepted: 25 April 2022
Published: 24 May 2022

Citation:
Li P, Liu J, Bai J, Tong Y, Meng Y, Diao X, Pan K, Zhu X and Lin G (2022) Community Structure of Benthic Macrofauna and the Ecological Quality of Mangrove Wetlands in Hainan, China. Front. Mar. Sci. 9:861718. doi: 10.3389/fmars.2022.861718

Few studies have systematically assessed the ecological status of mangrove wetlands following the stress of anthropogenic activities in China. This study investigated the spatial and seasonal distribution of benthic macroinvertebrate communities and assessed the ecological quality of mangrove habitats on an island scale in Hainan, China (containing the third largest mangrove area of China and the highest mangrove species richness). For the benthic macrofauna community structure, a total of 102 macrobenthic taxa belonging to 50 families were identified, with Crustaceans, Molluscs, Polychaetes, and Oligochaeta having relative abundances of 52.3%, 36.1%, 10.8%, and 0.8%, respectively. Decapoda and Gastropoda dominated the benthic community abundance. Non-metric multidimensional scaling and an analysis of similarities revealed significantly different macroinvertebrate assemblages among the regions during the two seasons. The South mangroves had the lowest macrofauna species numbers, biodiversity, richness, and abundance. The macrofaunal species richness, Shannon index, Margalef index, abundance, and biomass markedly affected by region and season. As indicated by the biotic indices AMBI (AZTI's Marine Biotic Index) and M-AMBI, more than half of the mangrove habitats on Hainan Island were slightly to heavily disturbed and had poor to moderate ecological quality. Our results recommend long-term monitoring for evaluating the quality status of mangrove wetlands and avoiding extensive land-use conversion of mangroves. Holistic approaches considering ecological characteristics and combining information on both floral and faunal functionality would contribute to the effective management and conservation of mangroves in disturbed areas.

Keywords: mangrove ecosystems, benthic macrofauna, community structure, ecological status, Hainan Island

INTRODUCTION

Mangrove forests, which are distributed on tropical and subtropical coastlines, provide excellent habitats for marine organisms. Due to the rapid development of coastal regions, mangroves are under increasing threats from human activities (e.g., tourism, industry, agriculture, and aquaculture). To conserve and restore mangrove ecosystems, it is of particular significance to monitor their quality and health under different anthropogenic impacts.

Benthic macrofauna are poorly mobile and sensitive to environmental changes, yet they play an important role in linking the primary producers and higher trophic levels in marine ecosystems (Bouillon et al., 2002; Lee, 2008). Disturbances such as human activities and natural factors can lead to changes in their habitats, which in turn leads to changes in the species composition of macrobenthic communities (Lee et al., 2006). Marine macrobenthos are thus widely used as ecological indicators to assess the health of marine ecosystems (Ni et al., 2019; Dimitriou et al., 2020; Dong et al., 2021).

Hainan Island contains the third largest mangrove area of China and the highest mangrove species richness (Li and Lee, 1997; Chen et al., 2009). In recent decades, due to the rapid development of the economy, mangrove wetlands on Hainan Island have suffered from fragmentation and habitat degradation (Liao et al., 2019; Herbeck et al., 2020). Although previous studies have reported on the diversity of the mangrove benthos (e.g., crabs, mollusks, foraminifera, etc.) in some areas (Gu, 2017; Ma et al., 2018; Li et al., 2021), the benthic macrofauna diversity and ecological status of mangrove wetlands on Hainan Island as a whole are still unclear.

In the present study, we chose Hainan Island as a case study with the aim of (1) investigating the macrofaunal distribution and community composition of the mangrove wetlands on the whole island and (2) evaluating the ecological quality of the mangrove wetlands by examining the changes in species composition of macrobenthic communities over time and space. The biological and nonbiological factors (mangrove vegetation, land usage, and other environmental factors) shaping the composition of the macrofaunal community were also discussed to link mangrove wetland quality with different anthropogenic impact pressures. Given that mangrove system is such an important and distinctive coastal habitat and are currently threatened by natural and anthropogenic pressures, such studies will help to better understand their ecological responses to environmental pressures and guide mangrove wetland management.

MATERIALS AND METHODS

Study Area

Hainan Island (18°10'–20°09' N, 108°37'–111°01' E) is located in the South China Sea, with a coastline of 1944.35 km. In this study, seven mangrove wetlands covering 97.5% of the mangrove areas on Hainan Island were selected (**Figure 1**), and divided into four regions (North, East, West, and South) based on their geographic locations. These were the Dongzhai Harbor Mangrove Reserve with 1508.14 ha of mangroves (North); the Bamen Bay Mangrove Reserve with 1036.03 ha (East); the Danzhou, Lingao, and Chengmai mangroves with 915.35 ha (West); and the Lingshui and Sanya mangroves with 143.5 ha (South) (Wang et al., 2019). The Bamen Bay (35 species), followed by the Dongzhai Harbor mangrove wetlands (23 species) was reported to contain the most number of mangrove species in China (Chen et al., 2009).

Sampling and Analysis

Field campaigns were carried out in these seven mangrove wetlands during December 2018 (dry season) and August 2019 (wet season). As shown in **Figure 1** and **Supplementary Table 1**, a total of 30 sampling sites (transects) were selected as the representative areas

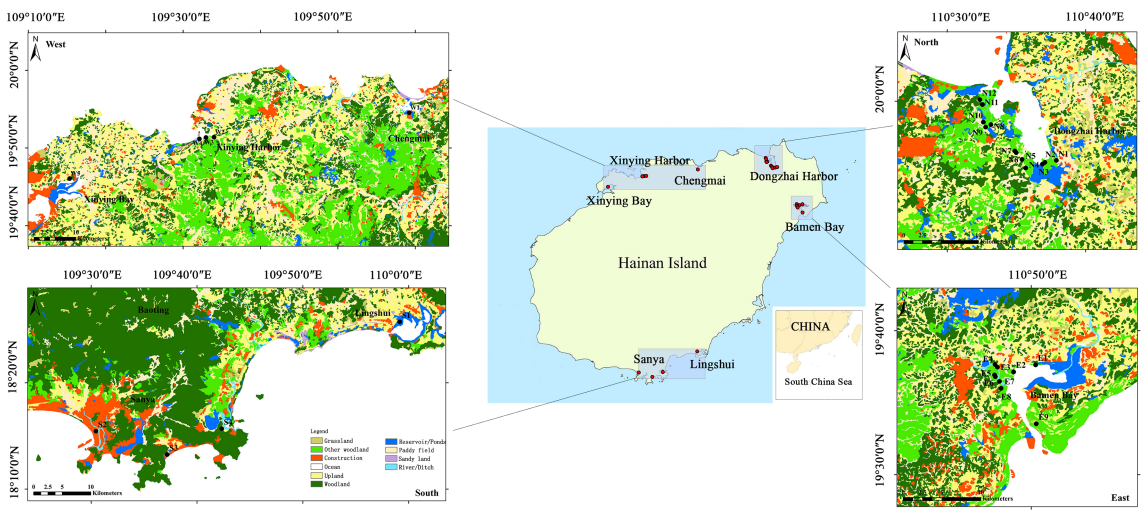

FIGURE 1 | Land use map for mangrove wetlands with the sediment sample locations on Hainan Island in China. Note: mangrove areas are included in the other woodland.

based on "Technical specification for eco-monitoring of mangrove ecosystem" (HY/T 081-2005, China). Surface sediments (0 –5 cm) were collected for determining the heavy metal content (Cr, Zn, Pb, Cu, As, and Cd) and performing other physicochemical analyses such as water content, nitrogen content, carbon content, etc. (Li et al., 2022). Sediment samples were transported in a cooler and stored at -20°C until analysis. The carbon and nitrogen contents of sediment samples were measured based on the combustion method (Schumacher, 2002) by a MARCO Cube Elemental Analyzer (Elementar, Germany). The temperature, pH, and salinity of water and sediments were measured *in situ* using a Thermo Scientific A321 pH Portable Meter (Thermo Fisher, USA), YSI Pro30 Salinity Instrument (YSI Inc, USA), and HM-TY soil salinity instrument (HM Inc, CHN), respectively. Heavy metals in the sediments were extracted according to the US EPA 3052, and determined by ICP-MS (Agilent 7700X, Agilent Technologies, USA). The mangrove species diversity, density, and structural characteristics were also investigated (Bai et al., 2021). The diameters of trees at breast height (DBH) in each plot were measured (Kauffman and Donato, 2012). The species, basal diameter, height and live/dead status of trees were recorded at the same time. More details of methodology were presented in **Supplementary Material**.

Benthic macrofauna samples were collected from the 30 sampling sites mentioned above. Three field plots (10 × 10 m) were designed at each site. Only one field plot could be designed for S2, S4 and W3 sites due to narrow mangrove areas. Three to five sediment samples were collected randomly from each plot using a 25 × 25 cm quadrat at a depth of 25 cm below the sediment surface. All the sediment from a quadrat was passed through a 0.5 mm mesh sieve to retrieve the macrofauna. The macrofauna collected were stored in 70% ethanol and then transported to the laboratory for further analysis. The processing, identification, counting, and weighing of the collected samples were carried out according to the Guidelines for Marine Biological Surveys (GB/T 12763.6-2007). Species richness, abundance, biomass, and diversity were determined to characterize the macrofaunal communities within the different habitats.

Biodiversity Analysis

The dominant macrofaunal species were determined by the Index of Relative Importance (*IRI*) (Pinkas, 1971) as follows: where N and W represents the proportions of abundance and biomass of each species, respectively, and F represents the percentage of each species at all sampling sites.

$$IRI = (N + W) \times F \times 10^4, \quad (1)$$

The diversity of the macrofaunal community was quantified using the Shannon diversity index (H'), Margalef richness index (D), and Pielou evenness index (J). The three indices are most well known and frequently used for biodiversity assessment of benthic macrofauna (Ni et al., 2019; Delfan et al., 2021; Yang et al., 2021).

Shannon index considers the proportional abundances of species and is more sensitive to changes in the rare species (Peet, 1974). It is calculated as follows (Shannon, 1948):Margalef richness index considers both abundances and species numbers, and is calculated as follows (Margalef, 1958):Pielou evenness index considers abundance and species occurrence, displaying the relations between the class frequencies (Palaghianu, 2014). It is calculated as follows (Pielou, 1969):where n_i represents the number of individuals in the ith group, N represents the total number of individuals at each site, and S is the number of species at each site.

$$H' = -\sum_{i=1}^{s} n_i/N \ln \left(\frac{n_i}{N}\right), \quad (2)$$

$$D = (S - 1)/\ln N, \quad (3)$$

$$J = H'/\ln S, \quad (4)$$

Statistical Analysis

Two-way ANOVA was used to assess effects of season and region on macrofaunal species richness, abundance, biomass, and diversity indices. Normality and homogeneity of variances were examined by the Shapiro–Wilk test and Levene's test, respectively. One-way ANOVA with Tukey's HSD test and independent-Samples T Test were applied to evaluate differences in macrofaunal abundance and diversity indices among regions and between seasons. All these analyses were conducted using SPSS 19.0 software. To visualize the spatial differences of the macrofaunal community structures, non-metric multidimensional scaling (NMDS) analyses were performed using Bray-Curtis dissimilarity between samples. For ordination analyses, only sites in which there were more than one species were included. The data was standardized in terms of relative abundance of the identified species in each site prior to analysis. An analysis of similarity (ANOSIM) test on Bray-Curtis distances was conducted to assess significant differences in the community structures between samples. NMDS and ANOSIM analyses were conducted using the vegan package in R 4.1.2 (Oksanen et al., 2019).

To assess the benthic ecological quality of the study area, AZTI's Marine Biotic Index (AMBI) and multivariate AMBI (M-AMBI) were calculated using AMBI version 6.0 (http://ambi.azti.es). Considering that the mangrove areas in Hainan were affected by different levels of human activities, the M-AMBI reference conditions were obtained following the method based on previous studies (Borja and Tunberg, 2011; Cai et al., 2013; Li et al., 2017; Zhou et al., 2018; Yan et al., 2020): the highest values of the Shannon index H' and species richness (S) in the present study were both increased by 15%, and the lowest AMBI value were selected as the M-AMBI reference condition under high quality status, e.g.,AMBI=0, H'=4.42, S = 20; and under bad quality status, AMBI = 6, H'=0, S = 0.

RESULTS

Community Structure and Distribution of Benthic Macrofauna

As shown in **Supplementary Table 2**, a total of 102 species were observed in the four mangrove regions over the two seasons. These consisted of Crustacea (43.1% Decapoda, 9.8% Amphipoda, 3.9%

Isopoda, and 1% each Tanaidacea, Stomatopoda, and Sessilia), Mollusca (20.6% Gastropoda and 10.8% Bivalvia), and Annelida (7.8% Polychaeta and 1.0% Oligochaeta). A total of 67 species were found in the dry season and 59 species in the wet season. Some species were only observed during one season, e.g., *Corophium* sp. and *Audouinia comosa* were only found in the dry season. The number of species found in the Hainan mangrove wetlands followed the order of North (72 species) >East and West (33 species each) > South (25 species). The North mangroves had the highest number of macrofaunal species in both seasons, while the mangroves in the South had the lowest number. Thus, the species richness varied not only by season, but also by region.

In the dry season, Gastropoda (25.7% of total individuals) were the most abundant, followed by Decapoda (23.3%) and Tanaidacea (21.2%) (**Figure 2A**). In the East and North, Tanaidacea predominated, with abundances of 43.2% and 31.9%, respectively. In contrast, Gastropoda (48.1%) dominated in the West and Decapoda (37.7%) in the South. The most abundant species were *Geloina expansa* in the East and South (*IRI* values of 5366.1 and 1543.6, respectively), *Paradoxapseudes mortoni* in the North (*IRI* 3036.8), and *Assiminea* sp. in the West (*IRI* 3256.4; **Supplementary Table 2**).

During the wet season, Decapoda (53.6%) and Gastropoda (25.6%) predominated in the Hainan mangrove wetlands (**Figure 2B**). Decapoda was dominant in all regions, accounting for 77.3%, 49.0%, 52.1%, and 45.8% in the East, North, West, and South, respectively. The most predominant species in the East and North was *Perisesarma bidens*, with *IRI* values of 8327.0 and 4779.9, respectively, while *Geloina expansa* prevailed in the West (*IRI* 4322.3) and South (*IRI* 4202.8).

The NMDS ordinations showed that the four mangrove regions had distinct macrofaunal communities during the two seasons (**Figures 2C, D**). The two-dimensional ordinations had acceptably low stress values: 0.13 for the dry season dataset and 0.15 for the wet season dataset, respectively. The macrofaunal community at Site S3 in the dry season was not subjected to the NMDS analysis, as only one species of macrofauna was found. The statistically significant clustering of the macrofaunal communities was confirmed by an ANOSIM test based on the sample locations in the dry ($R = 0.441$, $p = 0.001$) and wet ($R = 0.385$, $p = 0.001$) seasons.

Abundance, Biomass, and Diversity of Benthic Macrofauna

Macrofaunal species richness, abundance, Shannon index, Margalef index, and Pielou index in the mangrove wetlands on Hainan Island did not differ significantly between seasons (Independent-Samples T Test, $p > 0.05$) (**Figures 3A, B, D–F**). The average biomass of the macrofauna in the Hainan mangroves was 92.3 ± 104.8 $g{\cdot}m^{-2}$ in the dry season, which was significantly lower than that in the wet season (190.0 ± 134.4 $g{\cdot}m^{-2}$) (Independent-Samples T Test, $F = 0.723$, $p = 0.003$) (**Figure 3C**). In the dry season, macrofaunal abundance in the West (One-way ANOVA, $F = 4.022$, $p = 0.018$), species richness ($F = 19.519$, $p < 0.0001$), Shannon index ($F = 3.739$, $p = 0.023$), and Margalef index ($F = 23.099$, $p < 0.0001$) in the North was significantly higher than that in other regions. During the wet season, macrofaunal species richness ($F = 5.310$, $p = 0.005$), Shannon index ($F = 3.464$, $p = 0.031$), and Margalef index ($F = 4.042$, $p = 0.017$) in the West was significantly higher than that in other regions. There was no significant variance observed in the

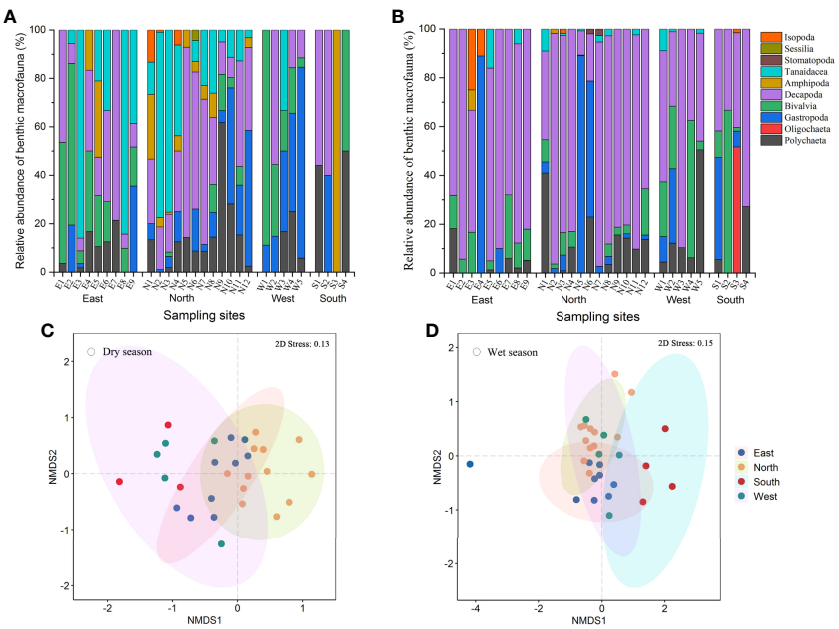

FIGURE 2 | Benthic macrofauna in the mangrove wetlands on Hainan Island in different seasons. Community structure during the **(A)** dry and **(B)** wet seasons and non-metric multidimensional scaling (NMDS) maps during the **(C)** dry and **(D)** wet seasons.

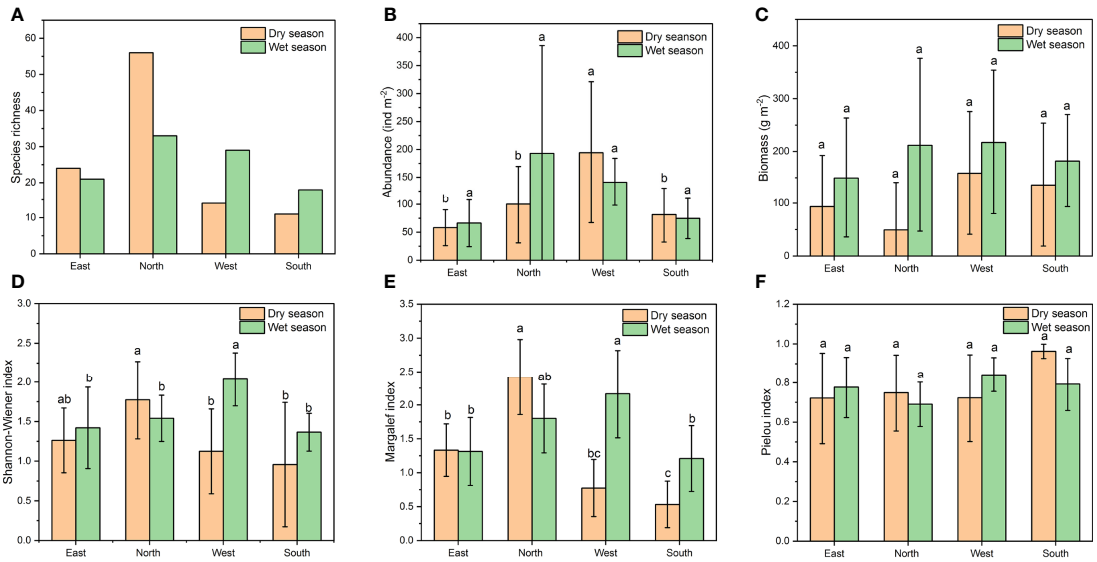

FIGURE 3 | Species richness **(A)**, abundance **(B)**, biomass **(C)**, and diversity indices [**(D)** Shannon-Wiener index; **(E)** Margalef index; **(F)** Pielou index] for the mangrove benthic macrofaunal communities on Hainan Island in different seasons.

macrofaunal biomass and Pielou index among the different regions in either season (One-way ANOVA, $p > 0.05$).

Two-way ANOVA test for effects of region and season revealed that both factors significantly influenced the species richness (region: $F = 14.719$, $p < 0.0001$; season: $F = 9.352$, $p = 0.004$), Shannon index (region: $F = 3.272$, $p = 0.028$; season: $F = 5.852$, $p = 0.019$), and Margalef index (region: $F = 15.460$, $p < 0.0001$; season: $F = 6.126$, $p = 0.017$) for the benthic macrofauna (**Supplementary Table 3**). Moreover, there was significant interaction effect between region and season for the species richness ($F = 5.679$, $p = 0.002$), Shannon index ($F = 4.016$, $p = 0.012$), and Margalef index ($F = 10.253$, $p < 0.0001$). Macrofaunal abundance and biomass was significantly affected by region ($F = 3.450$, $p = 0.023$) and season ($F = 5.485$, $p = 0.023$), respectively. Neither region nor season had a significant effect on the Pielou index (region: $F = 1.641$, $p = 0.191$; season: $F = 0.088$, $p = 0.768$). There was no significant interaction between region and season for the abundance, biomass and Pielou index.

Ecological Quality Status of the Mangrove Habitats

The AMBI and M-AMBI indices were used to evaluate the ecological quality of the mangrove habitats on Hainan Island (**Figure 4**). The AMBI is based on the abundance of ecological macrofaunal groups, from sensitive species to opportunistic species (**Supplementary Figure 1**). Generally, an AMBI <1.2 suggests an undisturbed area, whereas 1.2–3.3, 3.3–4.3, 4.3–5.5, and >5.5 indicate slightly, moderately, heavily, and extremely disturbed areas, respectively (Muxika et al., 2005). The average AMBI value for the mangrove wetlands did not differ significantly between seasons (Independent-Samples T Test, $p = 0.064$), although the average values during the wet season was slightly higher than that in the dry season. In the dry season, 56.7% of the mangrove habitats on Hainan Island were slightly or moderately disturbed ($1.2 < \text{AMBI} < 4.3$). The AMBI values followed the order of South (2.8) > West (1.7) > East (1.5) > North (1.3), indicating the mangrove ecosystem in the South was more strongly disturbed than the other regions. Among the sites, E7, N9, and S1 were moderately disturbed during this season. In the wet season, nearly 86.7% of the mangroves on Hainan Island suffered from slight to heavy disturbances. The East and West had the highest AMBI values (2.5), followed by the North (2.0) and South (1.4), indicating the East and West were more disturbed than other regions. Sites N4 and N9 were moderately disturbed, and W5 was heavily disturbed in this season.

The threshold values for M-AMBI classifications are as follows. An M-AMBI <0.2 refers to bad ecological quality, while 0.20–0.38, 0.38–0.53, 0.53–0.77, and >0.77 indicate poor, moderate, good, and high ecological habitat quality, respectively (Borja et al., 2007; Borja et al., 2009). The average M-AMBI values in the Hainan mangroves were 0.54 ± 0.14 in the dry season and 0.52 ± 0.12 in the wet season, indicating the overall ecological quality was good and moderate, respectively. Over 50.0% of the mangroves on Hainan Island had a poor to moderate ecological quality in both seasons. In the dry season, the M-AMBI values followed the order of North (0.66) > East (0.52) > West (0.43) > South (0.37), which suggests the ecological quality of the mangroves in the North was better than other regions and that the South region was the worst. It should be noted that, the ecological quality of the mangroves at Sites W1 in the West, S3 and S4 in the South was poor (M-AMBI <0.38). In contrast, during the wet season, the M-AMBI values in the West were the highest (0.61), indicating that the West mangrove wetlands had the better ecological quality. The West was

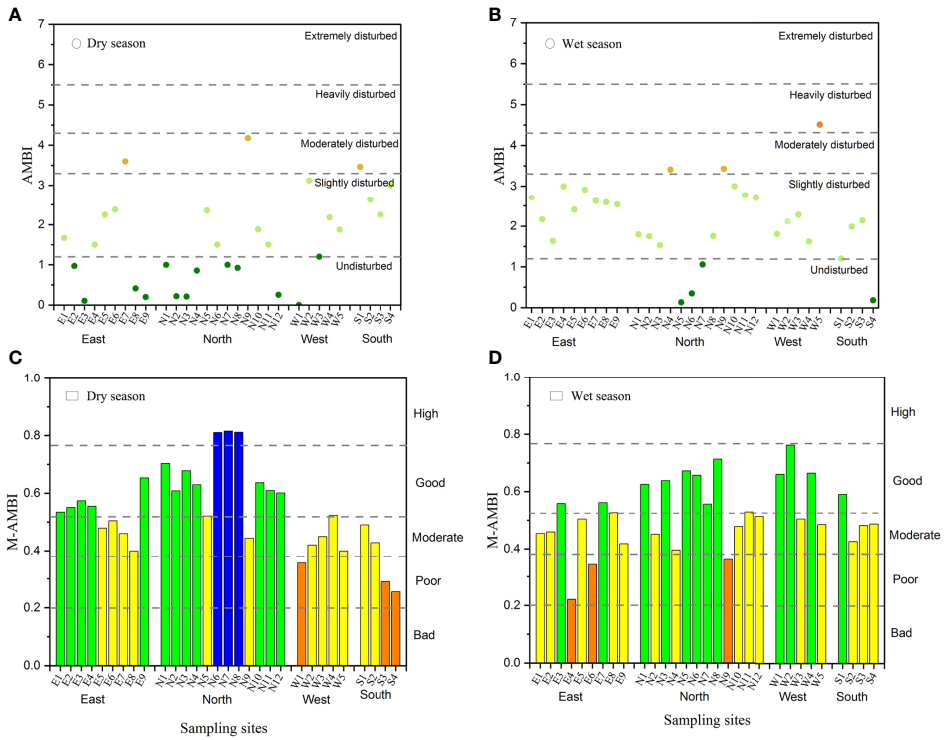

FIGURE 4 | Habitat ecological quality of the mangrove wetlands on Hainan Island based on AZTI's Marine Biotic Index (AMBI) during the **(A)** dry and **(B)** wet seasons and the multivariate AMBI in the **(C)** dry and **(D)** wet seasons.

followed by the North (0.55), South (0.50), and East (0.45), indicating the East had the worst ecological quality, with 77.8% of the mangrove wetlands rated as poor to moderate. In particular, the ecological quality of the mangroves at Sites E4, E6 and N9 was at the poor level (M-AMBI <0.38).

DISCUSSION

The macrofauna communities in the mangrove wetlands of Hainan Island in this study were similar to the one observed in June 2009 (Zhang et al., 2016), which was dominated by polychaetes, crustaceans, and mollusks. Variations in environmental parameters such as rainfall, water temperature, pH, and salinity might contribute to shaping macrofaunal communities in different seasons and regions. Our previous results found that the physicochemical characters of the sediments were significantly distinct between these four regions, e.g., the East sediments were found to contain significantly higher concentrations of total organic nitrogen, total nitrogen, total organic carbon, and total carbon. The mean water salinity and pH in the Hainan mangroves were higher in the dry season than in the wet season, and the water content of the sediments was lower in the dry season (Bai et al., 2021; Wang et al., 2021). Salinity has been reported as the main environmental factor affecting benthic macroinvertebrate community composition and structure in estuarine ecosystems (Conde et al., 2013; Verdelhos et al., 2015; Little et al., 2017). For instance, Mariano and Barros (2014) found that several abundant macrofaunal species showed specific preferences for different salinities along a salinity gradient; among these, the polychaete families Capitellidae, Nereididae, and Spionidae appeared mainly at low salinity.

In addition to variation in environmental parameters, anthropogenic contamination can also affect benthic communities (Johnston and Roberts, 2009). In this study, the sediments in the North contained the highest heavy metal (Cr, Zn, Pb, Cu, As, and Cd) contents (Li et al., 2022), but they also had the higher macrofaunal species richness and diversity. Metal contamination increasing macrofaunal richness may be due to species replacement with those having a higher tolerance to pollutants than others. Infaunal communities in metal-contaminated sediments are generally governed by metal-resistant opportunistic deposit-feeding polychaetes (Belan, 2004; Lancellotti and Stotz, 2004). The high heavy-metal enriched North also showed the clear abundance of *Capitella* sp., which is a typical indicator species for pollution (Grassle and Grassle, 1976; Pearson and Rosenberg, 1977). Metal contamination in the Hainan mangroves is mainly from aquacultural sewage and agricultural runoff (Li et al., 2022), which may lead to the increased availability of nutrients with a concomitant increase in species richness (Grall and Chauvaud, 2002). The presence of these nutrients at low

concentrations does not affect the macrofauna, which may even benefit from the additional supply (Ribeiro et al., 2016); however, an oversupply of nutrients will cause an opposite effect (Giles, 2008), especially in species with low tolerance to stressful conditions (Weisberg et al., 1997; King et al., 2005).

The number of macrofaunal species observed in this study during the wet season was comparable to the same period in 2009 (56 species). The macrofaunal biomass was higher than in 2009, but the average abundance and diversity (Shannon index) were much lower (Zhang et al., 2016). Reduction of macrofaunal diversity might be caused by habitat loss or habitat degradation (Airoldi et al., 2008; Carugati et al., 2018). The mangrove areas in Hainan Island was reported to decrease by 9.3% between 1987 and 2017, which was likely driven by human activities, such as land conversion for aquaculture, tourism development, and wastewater discharge (Liao et al., 2019). Region and season were revealed to significantly influence the species richness, Shannon index, Margalef index, abundance, and biomass for the benthic macrofauna in this study. The macrofaunal biomass during the wet season was higher than those in the dry season, which is consistent with previous findings. Zou et al. (1999) found that macrofaunal biomass in the mud flat of the Dongzhai Harbor mangroves on Hainan Island was higher in summer (June) than in winter (December).

Comparing the benthic macrofauna regionally, the higher species numbers, Shannon index and Margalef index were found in the North, while the lowest were in the South. Such spatial differences may be related to the land-use patterns of the mangrove wetlands in different regions. The North region has a higher proportion of mangrove area (accounting for 30.8% of the total area) than other regions, while the South has the lowest (0.5%) (Li et al., 2022). In general, structurally complex habitats support a higher density of benthic organisms than non-vegetated habitats due to their lower predation pressure, greater number of settlement areas, and enhanced nutrient availability (Alfaro, 2006). The complex structures of mangroves can provide shelter for various benthic fauna from predation, while the mangrove litter provides a direct or indirect food source for some macrobenthos such as gastropods and crabs (Nagelkerken et al., 2008). Thus, the loss of mangroves in the South might have resulted in a reduction in biodiversity and macrofaunal abundance, which is consistent with previous studies' findings (Ribeiro et al., 2016; Carugati et al., 2018).

According to the results of AMBI and M-AMBI analysis, the degree of disturbance to the Hainan mangroves and the ecological quality of the mangrove habitats might be related to the mangrove area and land-use patterns. For instance, Sites S3 and S4, determined as habitats with poor ecological quality, had the smallest mangrove areas (with proportions of the total area of only 0.001% and 2.03%, respectively). Site W5, determined as heavily disturbed area, had a mangrove area ratio of less than 0.001%. Mangrove wetland at W5 was strongly affected by agriculture, aquaculture, and construction activities, which accounted for more than 50% of the total area (Li et al., 2022). It indicates the importance of the mangrove habitat to benthic community structure and that a loss of mangrove habitat can lead to a decline in ecological quality. Importantly, the impact of human activities on the ecological quality of mangroves cannot be ignored.

CONCLUSION

With the current intensive anthropogenic pressures on coastal marine ecosystems, it is crucial to conduct investigations on the quality and health status of these important habitats. Taking Hainan Island as an example, this study provides a comprehensive investigation of the community structure and spatial distribution of benthic macrofauna within different mangrove wetlands and evaluates the ecological status of the mangrove habitats. The results showed that Crustaceans were the most abundant group, followed by Molluscs, Polychaetes, and Oligochaeta. Among them, Decapoda and Gastropoda dominated the benthic community abundance. Except for biomass, macrofaunal species richness, abundance, Shannon index, Margalef index, and Pielou index did not differ significantly between seasons. Macrofaunal species richness, Shannon index, and Margalef index were significantly varied in different regions in both seasons. Seasonal fluctuations of environmental factors and different land usage patterns may explain the macrofaunal community variations by season and region, respectively. Based on the macrofaunal community, the AMBI and M-AMBI indices revealed that more than half of the mangrove habitats on Hainan Island were slightly to heavily disturbed and had poor to moderate ecological quality in both seasons. The study implies that the impact of human activities on the ecological quality of mangroves cannot be ignored. We recommend long-term monitoring of the composition and traits of resident fauna to evaluate the quality status of mangrove ecosystem. Moreover, extensive land-use conversion of mangrove wetlands into aquaculture ponds or construction land etc. should be avoided. Finally, holistic approaches considering ecological characteristics and combining information on both floral and faunal functionality would be benefit for effective management, conservation, and restoration for these threatened mangrove ecosystems.

DATA AVAILABILITY STATEMENT

The original contributions presented in the study are included in the article/**Supplementary Material**. Further inquiries can be directed to the corresponding author.

AUTHOR CONTRIBUTIONS

PL: Conceptualization, Data Curation, Writing-original draft. JL: Visualization, biological data analysis. JB, YT, and YM: Investigation, Formal analysis. XD: Methodology. KP: Validation, Resources. XZ: Project administration, Supervision, Writing- review and editing. GL: Supervision, Resources.

All authors contributed to the article and approved the submitted version.

FUNDING

This study was supported by the Ministry of Science and Technology of China (2017FY100703), Shenzhen Fundamental Research project (WDZC202008191733 45002) and Shenzhen Key Laboratory of Marine IntelliSense and Computation (ZDSYS20200811142605016). It was also supported in part by the fellowship of China Postdoctoral Science Foundation (2020M672780) and Guangdong Basic and Applied Basic Research Foundation (2019A1515110930).

ACKNOWLEDGMENTS

We would like to thank all scientists who participated in sampling throughout the years. We wish to thank the editors and the reviewers for their valuable comments and suggestions on this paper.

SUPPLEMENTARY MATERIAL

The Supplementary Material for this article can be found online at: https://www.frontiersin.org/articles/10.3389/fmars.2022.861718/full#supplementary-material

REFERENCES

Airoldi, L., Balata, D., and Beck, M. W. (2008). The Gray Zone: Relationships Between Habitat Loss and Marine Diversity and Their Applications in Conservation. *J. Exp. Mar. Biol. Ecol.* 366, 8–15. doi: 10.1016/j.jembe.2008.07.034

Alfaro, A. C. (2006). Benthic Macro-Invertebrate Community Composition Within a Mangrove/Seagrass Estuary in Northern New Zealand. *Estuar. Coast. Shelf. Sci.* 66, 97–110. doi: 10.1016/j.ecss.2005.07.024

Bai, J., Meng, Y., Gou, R., Lyu, J., Dai, Z., Diao, X., et al. (2021). Mangrove Diversity Enhances Plant Biomass Production and Carbon Storage in Hainan Island, China. *Funct. Ecol.* 35, 774–786. doi: 10.1111/1365-2435.13753

Belan, T. A. (2004). Marine Environmental Quality Assessment Using Polychaete Taxocene Characteristics in Vancouver Harbour. *Mar. Environ. Res.* 57, 89–101. doi: 10.1016/S0141-1136(03)00062-X

Borja, A., Josefson, A. B., Miles, A., Muxika, I., Olsgard, F., Phillips, G., et al. (2007). An Approach to the Intercalibration of Benthic Ecological Status Assessment in the North Atlantic Ecoregion, According to the European Water Framework Directive. *Mar. Pollut. Bull.* 55, 42–52. doi: 10.1016/j.marpolbul.2006.08.018

Borja, A., Miles, A., Occhipinti-Ambrogi, A., and Berg, T. (2009). Current Status of Macroinvertebrate Methods Used for Assessing the Quality of European Marine Waters: Implementing the Water Framework Directive. *Hydrobiologia* 633, 181–196. doi: 10.1007/s10750-009-9881-y

Borja, A., and Tunberg, B. G. (2011). Assessing Benthic Health in Stressed Subtropical Estuaries, Eastern Florida, USA Using AMBI and M-AMBI. *Ecol. Indic.* 11, 295–303. doi: 10.1016/j.ecolind.2010.05.007

Bouillon, S., Koedam, N., Raman, A., and Dehairs, F. (2002). Primary Producers Sustaining Macro-Invertebrate Communities in Intertidal Mangrove Forests. *Oecologia* 130, 441–448. doi: 10.1007/s004420100814

Cai, W., Meng, W., Zhu, Y., Zhou, J., and Liu, L. (2013). Assessing Benthic Ecological Status in Stressed Liaodong Bay (China) With AMBI and M-AMBI. *Chin. J. Oceanol. Limnol.* 31, 482–492. doi: 10.1007/s00343-013-2177-0

Carugati, L., Gatto, B., Rastelli, E., Lo Martire, M., Coral, C., Greco, S., et al. (2018). Impact of Mangrove Forests Degradation on Biodiversity and Ecosystem Functioning. *Sci. Rep.* 8, 13298. doi: 10.1038/s41598-018-31683-0

Chen, L., Wang, W., Zhang, Y., and Lin, G. (2009). Recent Progresses in Mangrove Conservation, Restoration and Research in China. *J. Plant Ecol.* 2, 45–54. doi: 10.1093/jpe/rtp009

Conde, A., Novais, J. M., and Dominguez, J. (2013). Intertidal Macrofauna and Environmental Stress at a Riverine-Marine Boundary. *Mar. Environ. Res.* 92, 1–9. doi: 10.1016/j.marenvres.2013.07.002

Delfan, N., Shojaei, M. G., and Naderloo, R. (2021). Patterns of Structural and Functional Diversity of Macrofaunal Communities in a Subtropical Mangrove Ecosystem. *Estuar. Coast. Shelf. Sci.* 252, 107288. doi: 10.1016/j.ecss.2021.107288

Dimitriou, P. D., Chatzinikolaou, E., and Arvanitidis, C. (2020). Ecological Status Assessment Based on Benthic Macrofauna of Three Mediterranean Ports: Comparisons Across Seasons, Activities and Regions. *Mar. Pollut. Bull.* 153, 110997. doi: 10.1016/j.marpolbul.2020.110997

Dong, J.-Y., Sun, X., Zhang, Y., Zhan, Q., and Zhang, X. (2021). Assessing Benthic Habitat Ecological Quality Using Four Benthic Indices in the Coastal Waters of Sanshandao, Laizhou Bay, China. *Ecol. Indic.* 129, 107980. doi: 10.1016/j.ecolind.2021.107980

Giles, H. (2008). Using Bayesian Networks to Examine Consistent Trends in Fish Farm Benthic Impact Studies. *Aquaculture* 274, 181–195. doi: 10.1016/j.aquaculture.2007.11.020

Grall, J., and Chauvaud, L. (2002). Marine Eutrophication and Benthos: The Need for New Approaches and Concepts. *Global Change Biol.* 8, 813–830. doi: 10.1046/j.1365-2486.2002.00519.x

Grassle, J. P., and Grassle, J. F. (1976). Sibling Species in the Marine Pollution Indicator Capitella (Polychaeta). *Science* 192, 567–569. doi: 10.1126/science.1257794

Gu, K. (2017). *Distribution Characteristics and Influence Factors of Crabs Among Mangrove Communities* (Dongzhaigang Bay, Hainan: Xiamen University).

Herbeck, L. S., Krumme, U., Andersen, T. J., and Jennerjahn, T. C. (2020). Decadal Trends in Mangrove and Pond Aquaculture Cover on Hainan (China) Since 1966: Mangrove Loss, Fragmentation and Associated Biogeochemical Changes. *Estuar. Coast. Shelf. Sci.* 233, 106531. doi: 10.1016/j.ecss.2019.106531

Johnston, E. L., and Roberts, D. A. (2009). Contaminants Reduce the Richness and Evenness of Marine Communities: A Review and Meta-Analysis. *Environ. Pollut.* 157, 1745–1752. doi: 10.1016/j.envpol.2009.02.017

King, R. S., Hines, A. H., Craige, F. D., and Grap, S. (2005). Regional, Watershed and Local Correlates of Blue Crab and Bivalve Abundances in Subestuaries of Chesapeake Bay, USA. *J. Exp. Mar. Biol. Ecol.* 319, 101–116. doi: 10.1016/j.jembe.2004.05.022

Kauffman, J. B., and Donato, D. C. (2012). Protocols for the Measurement, Monitoring and Reporting of Structure, Biomass and Carbon Stocks in Mangrove Forests. *Working Paper* 86. Bogor, Indonesia: Center for International Forestry Research (CIFOR). Available at: https://www.researchgate.net/publication/264892201_W_o_r_k_i_n_g_P_a_P_e_r_Protocols_for_the_measurement_monitoring_and_reporting_of_structure_biomass_and_carbon_stocks_in_mangrove_forests.

Lancellotti, D., and Stotz, W. (2004). Effects of Shoreline Discharge of Iron Mine Tailings on a Marine Soft-Bottom Community in Northern Chile. *Mar. Pollut. Bull.* 48, 303–312. doi: 10.1016/j.marpolbul.2003.08.005

Lee, S. Y. (2008). Mangrove Macrobenthos: Assemblages, Services, and Linkages. *J. Sea. Res.* 59, 16–29. doi: 10.1016/j.seares.2007.05.002

Lee, S. Y., Dunn, R. J. K., Young, R. A., Connolly, R. M., Dale, P. E. R., Dehayr, R., et al. (2006). Impact of Urbanization on Coastal Wetland Structure and Function. *Austral Ecol.* 31, 149–163. doi: 10.1111/j.1442-9993.2006.01581.x

Liao, J., Zhen, J, Zhang, L., and Metternicht, G. (2019). Understanding Dynamics of Mangrove Forest on Protected Areas of Hainan Island, China: 30 Years of Evidence From Remote Sensing. *Sustainability* 11, 5356. doi: 10.3390/su11195356

Li, T., Cai, G., Zhang, M., Li, S., and Nie, X. (2021). The Response of Benthic Foraminifera to Heavy Metals and Grain Sizes: A Case Study From Hainan Island, China. *Mar. Pollut. Bull.* 167, 112328. doi: 10.1016/j.marpolbul.2021.112328

Li, M. S., and Lee, S. Y. (1997). Mangroves of China: A Brief Review. *For. Ecol. Manage.* 96, 241–259. doi: 10.1016/S0378-1127(97)00054-6

Li, P., Li, X., Bai, J., Meng, Y., Diao, X., Pan, K., et al. (2022). Effects of Land Use on the Heavy Metal Pollution in Mangrove Sediments: Study on a Whole Island Scale in Hainan, China. *Sci. Tot. Environ.* 824, 153856. doi: 10.1016/j.scitotenv.2022.153856

Li, B., Li, X., Bouma, T. J., Soissons, L. M., Cozzoli, F., Wang, Q., et al. (2017). Analysis of Macrobenthic Assemblages and Ecological Health of Yellow River Delta, China, Using AMBI & M-AMBI Assessment Method. *Mar. Pollut. Bull.* 119, 23–32. doi: 10.1016/j.marpolbul.2017.03.044

Little, S., Wood, P. J., and Elliott, M. (2017). Quantifying Salinity-Induced Changes on Estuarine Benthic Fauna: The Potential Implications of Climate Change. *Estuar. Coast. Shelf. Sci.* 198, 610–625. doi: 10.1016/j.ecss.2016.07.020

Margalef, R. (1958). Information Theory in Ecology. *Gen. Syst.* 3, 36–71.

Mariano, D. L. S., and Barros, F. (2014). Intertidal Benthic Macrofaunal Assemblages: Changes in Structure Along Entire Tropical Estuarine Salinity Gradients. *J. Mar. Biol. Assoc. Unit Kingdom.* 95, 5–15. doi: 10.1017/S002531541400126X

Ma, W., Wang, M., Wang, W., Liu, Y., Luo, L., and Tang, C. (2018). Biodiversity of Mangrove Mollusks in the West Coast of Hainan Island, China. *Biodiver. Sci.* 26, 707–716. doi: 10.17520/biods.2018104

Muxika, I., Borja, A., and Bonne, W. (2005). The Suitability of the Marine Biotic Index (AMBI) to New Impact Sources Along European Coasts. *Ecol. Indic.* 5, 19–31. doi: 10.1016/j.ecolind.2004.08.004

Nagelkerken, I., Blaber, S. J. M., Bouillon, S., Green, P., Haywood, M., Kirton, L. G., et al. (2008). The Habitat Function of Mangroves for Terrestrial and Marine Fauna: A Review. *Aquat. Bot.* 89, 155–185. doi: 10.1016/j.aquabot.2007.12.007

Ni, D., Zhang, Z., and Liu, X. (2019). Benthic Ecological Quality Assessment of the Bohai Sea, China Using Marine Biotic Indices. *Mar. Pollut. Bull.* 142, 457–464. doi: 10.1016/j.marpolbul.2019.03.055

Oksanen, J., Blanchet, F., Friendly, M., Kindt, R., Legendre, P., McGlinn, D., et al. (2019). *Vegan: Community Ecology Package. R Package Version 2.5-5.*

Palaghianu, C. (2014). A Tool for Computing Diversity and Consideration on Differences Between Diversity Indices. *J. Landscape Manage.* 5, 78–82. doi: 10.48550/arXiv.1602.04005

Pearson, T. H., and Rosenberg, R. (1977). Macrobenthic Succession in Relation to Organic Enrichment and Pollution of the Marine Environment. *Oceanog. Mar. Biol.: An. Annu. Rev.* 16, 229–311.

Peet, R. K. (1974). The Measurement of Species Diversity. *Annu. Rev. Ecol. Systemat.* 5, 285–307. doi: 10.1146/annurev.es.05.110174.001441

Pielou, E. C. (1969). *An Introduction to Mathematical Ecology*. (New York: Wiley-Interscience), 286.

Pinkas, L. (1971). Food Habits of Albacore, Bluefin Tuna and Bonito in California Waters. *Calif. Dept. Fish. Game. Fish. Bull.* 152, 1–105.

Ribeiro, L. F., Eca, G. F., Barros, F., and Hatje, V. (2016). Impacts of Shrimp Farming Cultivation Cycles on Macrobenthic Assemblages and Chemistry of Sediments. *Environ. Pollut.* 211, 307–315. doi: 10.1016/j.envpol.2015.12.031

Schumacher, B. A. (2002). Methods for the Determination of Total Organic Carbon (TOC) in Soils and Sediments. Ecological Risk Assessment Support Center, Office of Research and Development, US Environmental Protection Agency, NCEA-C-1282, 2002: 1-23. Available at: http://bcodata.whoi.edu/LaurentianGreatLakes_Chemistry/bs116.pdf. (Accessed January 12, 2019).

Shannon, C. E. (1948). A Mathematical Theory of Communication. *Bell. Sys. Tech. J.* 27, 379–423. doi: 10.1002/j.1538-7305.1948.tb01338.x

Verdelhos, T., Marques, J. C., and Anastácio, P. (2015). The Impact of Estuarine Salinity Changes on the Bivalves Scrobicularia Plana and Cerastoderma Edule, Illustrated by Behavioral and Mortality Responses on a Laboratory Assay. *Ecol. Indic.* 52, 96–104. doi: 10.1016/j.ecolind.2014.11.022

Wang, H., Tian, T., Gong, Y., Ma, S., Altaf, M. M., Wu, H., et al. (2021). Both Environmental and Spatial Variables Affect Bacterial Functional Diversity in Mangrove Sediments at an Island Scale. *Sci. Tot. Environ.* 753, 142054. doi: 10.1016/j.scitotenv.2020.142054

Wang, D., Wan, B., Qiu, P., Zuo, Z., Wang, R., and Wu, X. (2019). Mapping Height and Aboveground Biomass of Mangrove Forests on Hainan Island Using UAV-LiDAR Sampling. *Remote Sens.* 11, 2156. doi: 10.3390/rs11182156

Weisberg, S. B., Ranasinghe, J. A., Dauer, D. M., Schaffner, L. C., Diaz, R. J., and Frithsen, J. B. (1997). An Estuarine Benthic Index of Biotic Integrity (B-IBI) for Chesapeake Bay. *Estuaries* 20, 149–158. doi: 10.2307/1352728

Yang, X., Ma, S., Li, T., Gan, M., and Chen, M. (2021). Community Characteristics and Distribution Patterns of Soil Fauna After Vegetation Restoration in the Northern Loess Plateau. *Ecol. Indic.* 122, 107236. doi: 10.1016/j.ecolind.2020.107236

Yan, J., Sui, J., Xu, Y., Li, X., Wang, H., and Zhang, B. (2020). Assessment of the Benthic Ecological Status in Adjacent Areas of the Yangtze River Estuary, China, Using AMBI, M-AMBI and BOPA Biotic Indices. *Mar. Pollut. Bull.* 153, 111020. doi: 10.1016/j.marpolbul.2020.111020

Zhang, G., Lan, J., Wu, R., and Wang, D. (2016). Preliminary Study on Macrozoobenthos Diversity in Mangrove Area of Hainan Province. *Chin. J. Trop. Agric.* 36, 37–42. doi: 10.12008/j.issn.1009-2196.2016.11.008

Zhou, Z., Li, X., Chen, L., Li, B., Liu, T., Ai, B., et al. (2018). Macrobenthic Assemblage Characteristics Under Stressed Waters and Ecological Health Assessment Using AMBI and M-AMBI: A Case Study at the Xin'an River Estuary, Yantai, China. *Acta Oceanol. Sin.* 37, 77–86. doi: 10.1007/s13131-018-1180-x

Zou, F., Song, X., CHen, W., Zheng, X., and Chen, J. (1999). The Diversity of Benthic Macrofauna on Mud Flat in Dongzhaigang Mangrove Reserve, Hainan. *Biodiv. Sci.* 7, 175–180. doi: 10.17520/biods.1999027

Conflict of Interest: The authors declare that the research was conducted in the absence of any commercial or financial relationships that could be construed as a potential conflict of interest.

Publisher's Note: All claims expressed in this article are solely those of the authors and do not necessarily represent those of their affiliated organizations, or those of the publisher, the editors and the reviewers. Any product that may be evaluated in this article, or claim that may be made by its manufacturer, is not guaranteed or endorsed by the publisher.

Copyright © 2022 Li, Liu, Bai, Tong, Meng, Diao, Pan, Zhu and Lin. This is an open-access article distributed under the terms of the Creative Commons Attribution License (CC BY). The use, distribution or reproduction in other forums is permitted, provided the original author(s) and the copyright owner(s) are credited and that the original publication in this journal is cited, in accordance with accepted academic practice. No use, distribution or reproduction is permitted which does not comply with these terms.

frontiers | Frontiers in Marine Science

ORIGINAL RESEARCH
published: 26 May 2022
doi: 10.3389/fmars.2022.891663

Variations and Environmental Controls of Primary Productivity in the Amundsen Sea

Jianlong Feng[1,2], *Delei Li*[3,4], *Jing Zhang*[1] *and Liang Zhao*[1,5]*

[1] Key Laboratory of Marine Resource Chemistry and Food Technology (TUST), Ministry of Education, Tianjin University of Science and Technology, Tianjin, China, [2] Laborator for Marine Fisheries Science and Food Production Process, Pilot National Laboratory for Marine Science and Technology (Qingdao), Qingdao, China, [3] Chinese Academy of Science (CAS) Key Laboratory of Ocean Circulation and Waves, Institute of Oceanology, Chinese Academy of Sciences, Qingdao, China, [4] Center for Ocean Mega-Science, Chinese Academy of Sciences, Qingdao, China, [5] School of Marine Science and Technology, Tianjin University, Tianjin, China

OPEN ACCESS

Edited by:
Biraja Kumar Sahu,
Council of Scientific and Industrial Research (CSIR), India

Reviewed by:
Sanjiba Kumar Baliarsingh,
Indian National Centre for Ocean Information Services, India
Fajin Chen,
Guangdong Ocean University, China

***Correspondence:**
Liang Zhao
zhaoliang@tust.edu.cn

Specialty section:
This article was submitted to Marine Pollution, a section of the journal Frontiers in Marine Science

Received: 08 March 2022
Accepted: 29 April 2022
Published: 26 May 2022

Citation:
Feng J, Li D, Zhang J and Zhao L (2022) Variations and Environmental Controls of Primary Productivity in the Amundsen Sea. Front. Mar. Sci. 9:891663. doi: 10.3389/fmars.2022.891663

The Amundsen Sea is one of the regions with the highest primary productivity in the Antarctic. To better understand the role of the Southern Ocean in the global carbon cycle and in climate regulation, a better understanding of the variations and environmental controls of primary productivity is needed. Using cluster analysis, the Amundsen Sea was divided into nine bioregions. The biophysical differences among bioregions enhanced confidence to identify priorities and regions to study the temporal and spatial variations in primary production. Four nearshore bioregions with high net primary productivity or rapidly increasing rates were selected to analyze temporal and spatial variations in primary productivity in the Amundsen Sea. Due to changes in net solar radiation and sea ice, primary production had significant seasonal variation in these four bioregions. The phenology had changed at two bioregions (6 and 7), which has the third and fourth highest primary production, due to changes in the dissolved iron. Annual primary production showed increasing trends in these four bioregions, and it was significant at three bioregions. The variation in primary production in the bioregion (9), which has the highest primary production, was mainly affected by variations in sea surface temperatures. In the bioregion (8), which has the second-highest primary production, the primary production was significantly positively correlated with sea surface temperature and significantly negatively correlated with sea ice thickness. The long-term changes of primary productivity in bioregions 6 and 7 were thought to be related to changes in the dissolved iron, and dissolved iron was the limiting factor in these two bioregions. Bioregionalization not only disentangles multiple factors that control the spatial differences, but also disentangles limiting factors that affect the phenology, decadal and long-term changes in primary productivity.

Keywords: Amundsen Sea, primary productivity, bioregions, dissolved iron, climate change

INTRODUCTION

The Southern Ocean, also known as the Antarctic Ocean, encompasses 10% of the global ocean and contains parts of the South Pacific Ocean, the South Atlantic Ocean, the South Indian Ocean, and the marginal seas around Antarctica, such as the Ross Sea, Weddell Sea, and the Amundsen Sea. The Southern Ocean contains 40% of the total oceanic inventory of anthropogenic carbon dioxide (Khatiwala et al., 2009), and plays an important role in Earth's climate regulation, especially by neutralizing the effects of rising carbon dioxide concentrations and rising global temperatures (Reid et al., 2009; Ma et al., 2012; Bijma et al., 2013; Petrou et al., 2016). The Amundsen Sea (**Figure 1**) lies between the Cape Flying Fish and Cape Dart on Slip Island, and is one of the most rapidly warming regions on Earth (Bromwich et al., 2013), and it is one of the least studied Antarctic continental shelf regions (Griffiths, 2010; Pabis et al., 2014).

Primary productivity plays an important role in the transformation of dissolved elements in the ocean and in ocean-atmosphere carbon exchange (Amthor and Baldocchi, 2001). Previous studies have indicated that the phenology, decadal and long-term changes in primary productivity in the Southern Ocean have been and will continue to be affected by the current and predicted changes in ocean circulation and hydrology associated with climate variability (Lannuzel et al., 2007; Herraiz-Borreguero et al., 2016; Kim and Kim, 2021). Significant spatial differences exist in the changes in primary productivity in the Southern Ocean, both over large latitudinal scales and at regional scales (Arrigo et al., 2008; Ardyna et al., 2017). These spatial differences are related to nutrient availability (mainly iron and possibly nitrate and silicic acid), temperature, light availability, sea-ice coverage, and mortality factors (Boyd, 2002; Smith Jr. and Comiso, 2008; Behrenfeld and Boss, 2014; Arrigo et al., 2015). These factors are controlled by vertical mixing, advection, sea ice cover, and seasonal variations in solar irradiance (Ardyna et al., 2017). However, studies of the primary productivity of the Southern Ocean have been limited in their ability to assess spatial variabilities over both short and long timescales for a variety of different reasons, such as lack of observation and uneven distribution of surveys (Arrigo et al., 2008). Primary productivity also shows significant spatial differences in the Amundsen Sea. The Amundsen Sea Polynya is the region of particularly high productivity in the Southern Ocean (Arrigo and van Dijken, 2003; Lee et al., 2012). Although some studies have been conducted on primary productivity in the Amundsen Sea (Arrigo and van Dijken, 2003; Arrigo et al., 2012; Lee et al., 2012; Park et al., 2017; Lim et al., 2019; Kwon et al., 2021), the spatial differences and mechanisms that drive differences in phenology, decadal and long-term changes in primary productivity are still not clear.

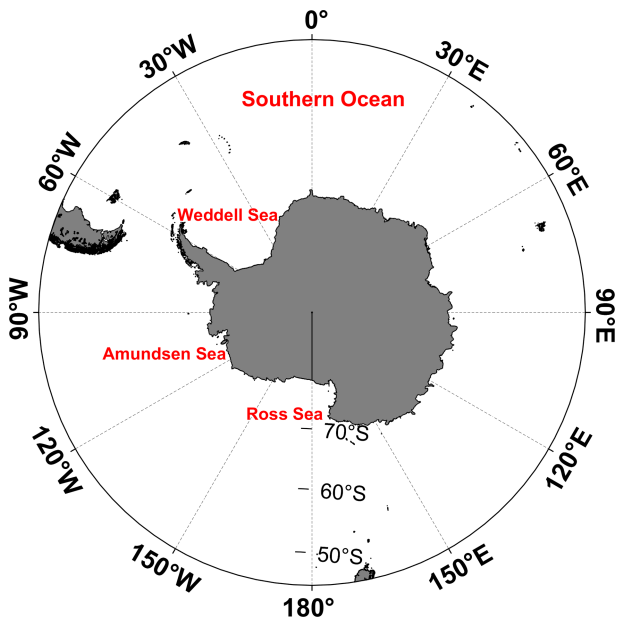

FIGURE 1 | Locations of the Southern Ocean, Weddell Sea, Rose Sea, and Amundsen Sea.

Bioregionalization is one method used to define ecosystems. Under this approach, regions are defined based on physical and biological properties, the method can be defined as the process of delineating the continuous spatial coverage of contiguous spatial units that support distinct biological assemblages (Costello, 2009; Koubbi et al., 2011; Roberson et al., 2017). Usually, the spatial units are delineated using geophysical and biological observation data, modeled data, or a combination of both (Grantham et al., 2010). The obtained bioregions can be used for monitoring and reporting the state of the environment, modeling and predicting the effects of climate changes, and identifying priority areas for protection (Greger and Bodtker, 2007; Spalding et al., 2007; Rice et al., 2011). In recent years, the delimitation of marine bioregions has also been used to disentangle multiple limiting factors that affect the efficiency of biological pumps mediated by phytoplankton (Longhurst, 2007; Ardyna et al., 2017), the spatial and temporal changes of key ecological parameters (Bowman et al., 2018). In the Southern Ocean, bioregionalization has been widely used to identify representative areas for protection at broad and regional scales, such as in the Southern Ocean (Grant et al., 2006), Ross Sea region (Sharp et al., 2010), and Weddell Sea (Teschke et al., 2016). Delineating the effects of environmental forcing on temporal and spatial variations in primary productivity remains challenging and requires novel approaches. We used bioregionalization to provide a basis for understanding variations in primary productivity in the Amundsen Sea.

In this paper, we conducted a cluster analysis using variables from the Global Ocean Reanalysis and Simulations (GLORYS) dataset to obtain a bioregional map of the Amundsen Sea. Using the bioregionalization outputs, we analyzed the limiting factors that affect spatial differences, the phenology, decadal and long-term changes in primary productivity in the Amundsen Sea.

DATA AND METHODOLOGY

Data

The physical and ecological variables used in the bioregionalization were derived from the Global Ocean Reanalysis and Simulation Version 4 (GLORYS2v4) dataset (https://resources.marine.copernicus.eu/?option=com_csw&task=results&pk_vid=f205f72451b76b161622075614d28a7a). GLORYS2v4 is an ocean reanalysis, which is a scientific method that produces a comprehensive record of how ocean properties are changing over time. This reanalysis is performed with the NEMOv3.1 ocean model in configuration ORCA025_LIM. The vertical grid has 75 levels in depth with partial steps at the bottom. GLORYS2v4 has assimilated observations, containing delayed time along-track satellite Sea Level Anomaly, Sea Ice Concentration, Sea Surface Temperature, and *in situ* profiles of temperature and salinity from the Coriolis Ocean dataset for Reanalysis (CORA) 4 database. The monthly mean values from 1993 to 2015 with a resolution of 1/4°×1/4° were used in this work.

In situ observed temperature and salinity data were acquired during the *ANTXXVI/3* from the research ice breaker Polarstern (Gohl, 2010). The Climate Data Record (CDR) of sea ice concentration from obtained from NSIDC (Meier et al., 2017). Chlorophyll-a data were obtained from the Ocean Colour Climate Change Initiative (OC-CCI, http://www.esa-oceancolour-cci.org) project.

Previous studies have shown that variables obtained from GLORY2v4 perform well against observations in the Amundsen Sea (Uotila et al., 2019; Huang et al., 2020). In this work, we also compare the temperature, salinity, sea ice concentration, and chlorophyll against observations in the Amundsen Sea (shown in **Supplementary Figures S1–S3**). Results showed that comparisons between the GLORYS2v4 and *in situ*/satellite measurements of the temperature, salinity, sea ice concentration, and chlorophyll show a good agreement. The temperature of GLORYS2v4 had a good fit to the observed water temperature structure at section S01. The mean temperature obtained from the observation at section S01 was 34.70 ± 0.03°C, and it was 34.70 ± 0.04°C from GLORYS2v4. The sea ice concentration of GLORYS2v4 was significant correlated with sea ice concentration from CDR, the correlation coefficient were larger than 0.9 both in winter and summer. The monthly/annual surface chlorophyll concentrations of GLORYS2v4 had a good fit to the observed monthly/annual surface chlorophyll concentrations distributions. Also, the mixed layer depths were calculated according to Brainerd and Gregg (1995) at the S01 section (**Figure S1**). The mixed layer depths obtained from the observations ranged from 4 to 24 m with a mean of 15 m. At the same time, the mixed layer depths obtained from GLORYS2v4 ranged from 5 to 27 m with a mean of 17m. The above results enhanced the confidence in the quality of the GLORYS2v4 to get the bioregions in the Amundsen Sea.

As variables measured at the ocean surface are strongly correlated with processes at depth, the surface variables can reflect the properties of the water column (Longhurst, 2007; Oliver and Irwin, 2008). Therefore, the variables of the first layer were used in this work. The extents of all variables were clipped to match the study area, ranging from 80°to 150°W and 55°to 80°S. In addition to net primary productivity (nppv in **Table 1**), other physical and biological variables were also selected. These variables were selected according to two principles: first, variables selected by other studies conducted in the Southern Ocean were also selected in this work, including the sea surface temperature (SST), sea surface height (SSH), salinity, water depth, sea ice persistence index, sea bottom temperature, and chlorophyll (**Table 1**); second, variables that could affect primary productivity were also selected, including the mixed layer depth, and dissolved iron (**Table 1**). The parameters used in the clustering analysis contained the average states of the variables (mean value across the time series), their variability (annual maximum mean, annual minimum mean, long-term change rate), and topographic gradient. The sea ice persistence index (ICE) was calculated as the proportion of the overall time during which the grid was covered by sea ice (the sea ice concentration larger than 50%). The index was calculated as ICE=M1/M, where M1 is the number of months which monthly sea ice concentration is less than 50%, M stands for the number of months used in a year. All variables were standardized to zero means and unit standard deviations to eliminate issues associated with units of measurement.

Methodology

Bioregions were obtained in this work using cluster methods. Cluster analysis is a class of techniques in which a set of objects or cases classified in the same group (called a cluster) are more similar to each other than to those in other groups. One advantage of cluster techniques is that they allow for areas with similar characteristics to be defined regardless of their location, thereby producing results representative of intrinsic spatial patterns and environmental variables (Leathwick et al., 2003; Snelder et al., 2007). Cluster analysis has been commonly used to identify bioregions and is still widely used today (Milligan and Cooper, 1987; Ebach et al., 2015; Roberson et al., 2017; Bloomfield and Knerr, 2018). For the Southern Ocean, physical and biological variables, including the water temperature, salinity, depth, chlorophyll, and sea-ice information, were used to obtain the bioregions to facilitate systematic planning for the protection of marine habitat diversity (Grant et al., 2006; Sharp et al., 2010; Teschke et al., 2016; Godet et al., 2020). In this work, hierarchical clustering and the *K*-means clustering method were selected to obtain bioregions in the Amundsen Sea. *K*-means clustering is a data-mining method that classifies objects (variables) into *K* clusters, objects within a given cluster are more similar to each other (in the multivariate

TABLE 1 | Variables from GLORYS2V4 used in pelagic bioregionalization.

Physical	Biological
Temperature (*tem*)	Total Chlorophyll (*chl*)
Salinity (*sal*)	net primary productivity (*nppv*)
Sea surface height (*ssh*)	Dissolved Iron (*fe*)
Density ocean mixed layer thickness (*mlp*)	
Sea floor potential temperature (*bot*)	
Ice concentration (*fice*)	

space) than to those in other clusters. The key advantage of K-mean clustering over other unsupervised approaches are its low complexity, quick computation, capacity to deal with large data sets, and adjustable cluster membership (Govender and Sivakumar, 2020). This approach has been successfully applied in the North Atlantic (Lacour et al., 2015), the Southern Ocean (Ardyna et al., 2017), and the Mediterranean Sea (Mayot et al., 2016) as well as at the global scale (D'Ortenzio and d'Alcalà, 2012). The number of *K* categories used for the *K*-means clustering was determined using the hierarchical clustering method, which depends on the pairwise distances between data points to merge or divide data into a series of clusters (Fraley and Raftery, 1998). The K-mean clustering was carried out using the open source Geoda software (Anselin et al., 2006). In this study, the physical and biological variables listed in **Table 1** were used in the clustering analysis. The long-term change rate was calculated using linear regression. The significance of the correlations and trends identified in this study was checked using t-tests and Mann–Kendall tests (von Storch and Zwiers, 1999; Feng et al., 2015), respectively. The pre-whitening method was used to avoid autocorrelations in the work (Kulkarni and von Storch, 1995). The software of computing hierarchical clustering, linear regression, and significance of correlations was R (https://www.r-project.org/).

The Mann-Kendall test, first introduced by Mann (1945), is a non-parametric statistical method to test the significant of change trend of time series. It is widely utilized to examine climatic factors's long-term trends and abrupt change point of climate factors. The statistic *UFk* is an order normalization parameter of time series *X* calculated in order. If *UFk* is more (or less) than 0, it indicates that the sequence is increasing (decreasing). For a given significant level α, if the absolute

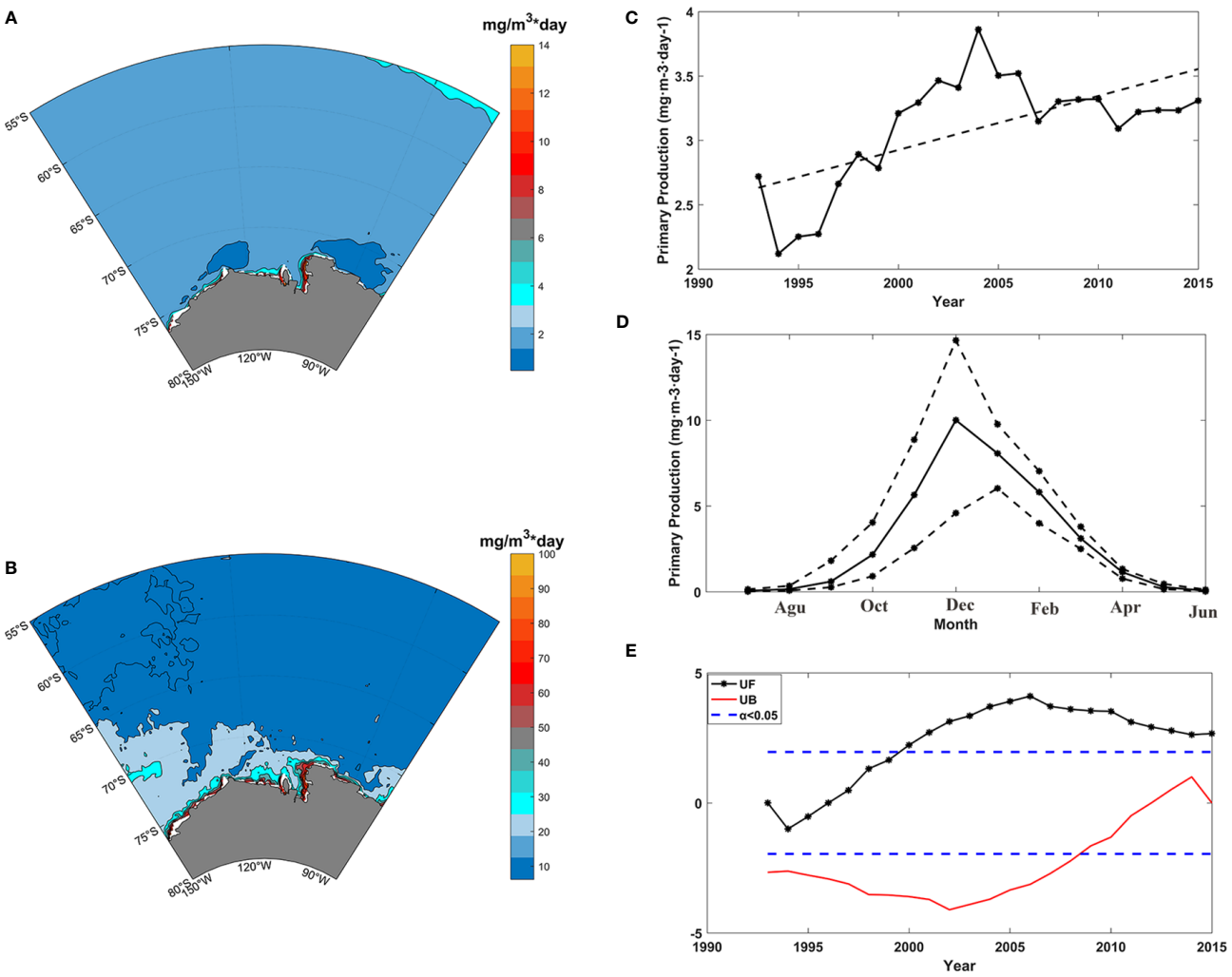

FIGURE 2 | Primary production in the Amundsen Sea, **(A)** mean value of primary production from 1993 to 2015; **(B)** seasonality amplitude of primary production; **(C)** annual values of (black line) and long-term changes in (black dashed line) primary production; **(D)** MK-values (y-axes) obtained from the sequential Mann-Kendall test against time for annual primary production, the black line represents the progressive *UF(t)* and the red line represents the retrograde *UB(t)*; **(E)** monthly primary production values (black line) and amplitudes of the monthly values (black broken line).

value of *UFk* is greater than *U_α* (for α=0.05,U_α= ± 1.96), the sequence has a significant trend. *UBk* is an order normalized parameter calculated in reverse order of time series *X*. If there is an intersection point between the two curves of *UFk* and *UBk*, and the point is between the *U_α*, the point corresponding to the abrupt change point.

RESULTS AND DISCUSSION

Primary Productivity in the Amundsen Sea

The mean value (**Figure 2A**) and seasonality amplitude (the difference between maximum value of monthly mean and minimum value of monthly mean) (**Figure 2B**) of primary production in the Amundsen Sea were calculated using the data obtained from GLORYS2v4. The spatial differences existed in the Amundsen Sea, and the mean primary production values of the Amundsen Sea ranged from 1.5 to 14 mgC m^{-3} day^{-1}. In most areas, the mean value was less than 3 mgC m^{-3} day^{-1}. The primary production was largest in Pine Island Bay, and minimum values occurred on the two areas adjacent to of Pine Island Bay, with a mean value of less than 2 mgC m^{-3} day^{-1}. This distribution was consistent with other studies about primary production in the Amundsen Sea (Park et al., 2019). The seasonality amplitude of primary production (**Figure 2B**) ranged from 10 to 100 mgC m^{-3} day^{-1} and showed some similar spatial characteristics with the mean values, the amplitude was also largest in Pine Island Bay. However, the spatial variations in the seasonality amplitude were more complicated than those of the mean value. The seasonality amplitude was not the smallest in the two areas adjacent to Pine Island Bay, featuring a mean value less than 2 mgC m^{-3} day^{-1}.

The annual primary production showed an increasing trend from 1993 to 2015 (**Figure 2C**). The primary production was relatively high from 2000 to 2006; reached a maximum in 2004, and displayed low values from 1993 to 1996; a minimum occurred in 1994. Furthermore, the progressive *UF(t)* and the retrograde *UB(t)* series of the sequential Mann-Kendall test (Mann, 1945) were calculated against time for the annual mean primary production (**Figure 2E**). The results showed that primary production featured an increasing trend in general. The positive trend was significant after 1999, and no abrupt change existed in the annual primary production. Primary production exhibited clear seasonal variability (**Figure 2D**), it began to increase in August, reached a maximum in December, and began to decrease after December. From April to September, the primary production was less than 2 mgC m^{-3} day^{-1}. The monthly primary production varied greatly in the summer months, and the amplitude was largest in December (ranging from 4.5 to 14.5 mgC m^{-3} day^{-1}). Above results were consistent with previous studies using observations (Arrigo and van Dijken, 2003; Park et al., 2017; Lim et al., 2019; Kwon et al., 2021), and enhanced the confidence in the data quality and in the analysis.

Bioregion Classification and Characterization

To obtain the number of clusters (*K*), hierarchical clustering was carried out in the Amundsen Sea by computing the similarity of all the pixel at the mean values. The dendrogram obtained from the hierarchical clustering algorithm was used to guide the clustering process (**Figure 3**). Norse (2010) indicated that if *K* is too large, important details are overlooked; if K is too small, the result is an unmanageable number of decision-making groups.

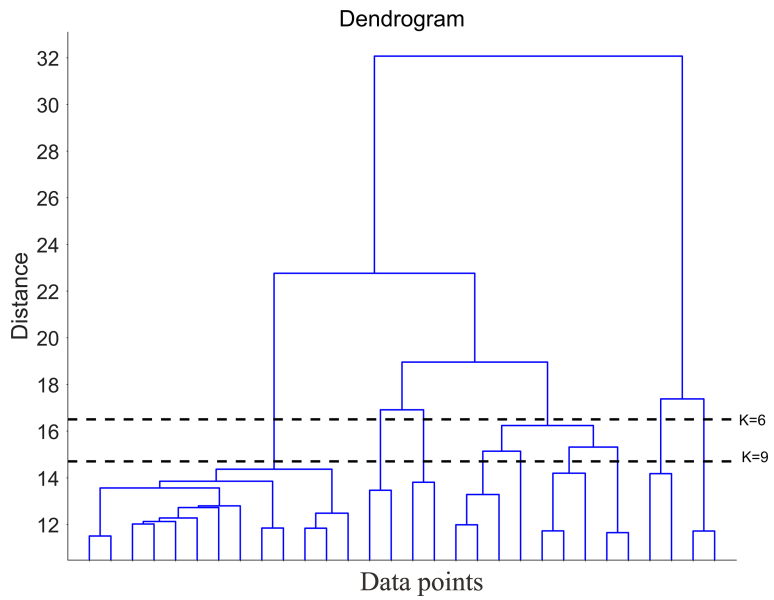

FIGURE 3 | Dendrogram obtained from hierarchical clustering. The dotted lines (*K*=6 and *K*=9) show the levels at which the dendrogram was cut to produce the groups.

To obtain a more reasonable result, *K*-means cluster analyses were carried out twice (*K*=6 and *K*=9) (**Figure 4**). The results show that spatial distribution had similar characteristics between the *K*=6 and *K*=9 results. But differences also existed, when *K*=9 was selected, the coastal area was divided into 2 bioregions (9-8 and 9-9). When *K*=6 was selected, the coastal area was divided into 1 bioregion (6-6). The northern boundary area was divided into two bioregions (6-1and 6-2) when *K*=6, while it was divided into three bioregions (9-1, 9-2, and 9-3) when *K*=9. When *K*=6, the central region was divided into two bioregions (6-3 and 6-4), and when *K*=9, the central region was divided into three bioregions (9-4, 9-5, and 9-6). For comparison, the mean values of the variables in different bioregions were calculated (6-6, 9-8 and 9-9; 6-2, 9-2, and 9-3) (**Table 2**). The results showed that the differences in the physical variables were small among bioregions 6-6, 9-8, and 9-9, while the differences in the biological variables were quite pronounced. The mean values of *chl* and *nppv* were significantly smaller in the 9-8 bioregion than those in the 6-6 and 9-9 bioregions. The differences in biological variables among bioregions 6-2, 9-2, and 9-3 were small, while the differences in physical variables were quite clear, especially the *mlp*, *ssh*, and *fice* variables. The above results indicated that the bioregions obtained from *K*=9 can describe the detailed differences in *fice, mlp, chl* and *nppv* more clearly than the bioregions obtained from *K*=6. All these variables are important in a spatial analysis of primary production in the Amundsen Sea; therefore, we ultimately selected the resulting bioregions when *K*=9.

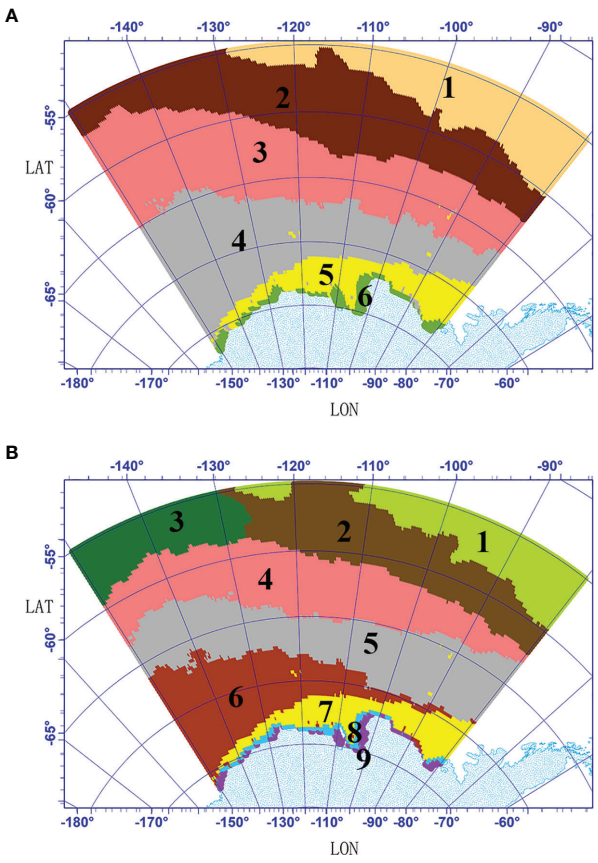

FIGURE 4 | Six bioregions **(A)** and nine subregions **(B)** identified in the *K*-means cluster analysis.

The parameters that characterize the key properties of each bioregion differed among the bioregions (**Supplementary Table S1** and **Figure 5**). Here, we listed four levels of each parameter to help characterize each bioregion relative to the study area: the maximum value, the second-highest value, the minimum value, and the second-lowest value. Bioregions 8 and 9 are associated with the continental shelf and slope edge down to approximately 300 m. The Amundsen Sea Polynya is located in this region (Swalethorp et al., 2019), and these two bioregions are the areas through which the coastal current flows in the Amundsen Sea (Kim et al., 2016). Bioregions 8 and 9 showed some similar features; they were both distinguished by low *tem*, low *mlp*, low *sal*, high *chl*, high *nppv*, high *fe*, and low *dep* values. There were also some differences between bioregions 8 and 9; bioregion 9 had the lowest *bot* value, while bioregion 8 had the second-highest *bot* value. The *fice* values of bioregion 8 were higher than those of bioregion 9, the *tem* values of bioregion 8 were lower than those of bioregion 9, bioregion 9 had the second-highest longitudinal gradient, and bioregion 8 had the second-lowest latitudinal gradient. Although bioregion 8 had the second-highest *nppv* value, the *nppv* value of bioregion 9 (8.51 mgC m^{-3} day^{-1}) was much higher than that of bioregion 8 (5.86 mgC m^{-3} day^{-1}).

Bioregion 7 was located within the continental slope, and its boundary was mostly consistent with the Antarctic Slope Front (Martinson, 2012). Bioregion 7 was distinguished by the lowest *tem*, lowest *mlp*, second-lowest *ssh*, highest *bot*, highest *fice*, lowest *chl*, and lowest *nppv*, the lowest latitudinal gradient and highest longitudinal gradient. In this bioregion, Circumpolar Deep Water (CDW) intrudes onto the shelf, after which it mixes with surrounding water and masses to become Modified Circumpolar Deep Water (MCDW) (Arneborg et al., 2012). MCDW is a potential source of dissolved iron fueling primary productivity in bioregions 8 and 9 (St-Laurent et al., 2017; Dinniman et al., 2020).

Bioregions 1, 2, 3, 4, 5, and 6 were located in the abyssal plain. Bioregion 6 was distinguished by the second-lowest *mlp*, the lowest *ssh*. Bioregion 6 was therefore assumed to be closely associated with the Ross Gyre (Dotto et al., 2018). The Ross Gyre is formed by the interaction between the Antarctic Circumpolar Current and the Antarctic Continental Shelf and rotates clockwise. The northern boundary of bioregion 5 mostly consisted of winter sea ice (Comiso et al., 2003). Bioregion 4 was distinguished by the second-lowest *bot*, the second-lowest *fe*, and the second-lowest annual maximum *chl* values. The sea ice of bioregion 4 decreased from 1993 to 2015 (**Table S1**), and the rate of sea ice decrease was the largest in bioregion 4 among all bioregions. Bioregions 1, 2, and 3 were located at the northern boundary of the study region, and these bioregions are the areas through which Antarctic Circumpolar Current flows. Bioregion 1 was distinguished by the highest *tem*, the highest *mlp*, the highest *ssh*, the lowest *fice*, the highest *sal* and the lowest *dep* values. Bioregion 2 was distinguished by the second-highest *tem*,

TABLE 2 | Mean values of variables at different bioregions.

	ALL	6-6	9-8	9-9	6-2	9-2	9-3
tem (K)	273.86	271.56	271.53	271.57	276.42	277.07	276.03
mlp (m)	66.66	42.71	43.51	43.14	94.69	112.43	67.24
ssh (m)	-1.25	-1.59	-1.59	-1.60	-0.43	-0.77	-1.08
bot (K)	273.46	273.34	274.06	272.97	273.33	273.32	273.63
ice	0.59	0.96	0.97	0.95	0.12	0.05	0.20
sal	33.65	33.22	33.31	33.19	33.92	33.99	33.86
chl (mg m^{-3})	0.38	0.72	0.57	0.76	0.33	0.32	0.36
nppv (mgC m^{-3} day^{-1})	3.64	8.01	5.86	8.51	2.99	3.12	3.19
fe (mmol m-3)	<0.001	0.002	0.001	0.003	<0.001	<0.001	<0.001
depth (m)	-3000	-144	-295	-86	-4448	-3276	-4613

the second-highest *mlp*, the second-highest *ssh*, the second-lowest *fice*, the second-highest *sal*, and the second-lowest *dep* values. Bioregion 3 was distinguished by the lowest *fe* value the lowest longitudinal gradient, and the lowest long-term change rate of *tem*.

The above results indicated that the bioregions differed in their physical and biological characteristics (including primary productivity). These bioregions can be used to study the temporal and spatial variations in primary productivity in the Amundsen Sea. Furthermore, the 9 bioregions had biophysical significance; therefore, they are also useful for systematic conservation planning of marine protected areas (MPAs) in the Amundsen Sea (Fraschetti et al., 2008; Treml and Halpin, 2012).

Variations in Primary Productivity

In the Amundsen Sea, intense phytoplankton blooms occasionally develop, making primary productivity highly variable both temporally and spatially (Moore and Abbott, 2000; Arrigo et al., 2008) (**Figure 2B**). Our results outlined in section 3.2 indicated that the 9 obtained bioregions can be used to reflect the temporal differences in primary productivity in the

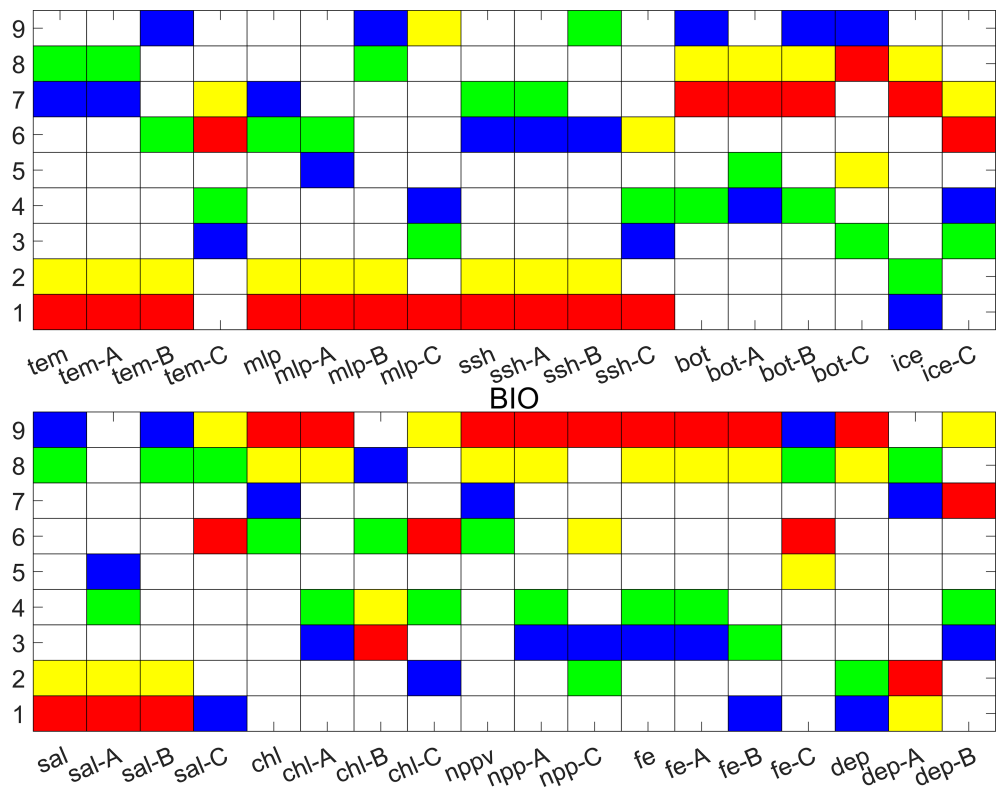

FIGURE 5 | Parameters that characterize the key properties of bioregions, showing the maximum value (red), the second-highest value (yellow), the minimum value (blue) and the second-lowest value (green) of each parameter, including the annual maximum mean **(A)**, annual minimum mean **(B)**, and long-term change rate **(C)** (dep-A: latitudinal gradient, dep-B: longitudinal gradient).

Amundsen Sea. The mean value, annual maximum mean, and long-term change rate of primary production were calculated in the 9 bioregions and are shown in **Figure 6**. The results showed that the mean and annual maximum mean values of primary production in bioregions 8 and 9 were obviously larger than those in other bioregions. This is because the polynyas in the Amundsen Sea are located in bioregion 8 and 9. And the annual maximum mean values of primary production of bioregions 6 and 7 were the third and fourth largest. The long-term change rate of bioregion 9 was the largest, followed by those of bioregions 6 and 7. Therefore, bioregions 6, 7, 8, and 9 were selected as typical bioregions with which to analyze variations in primary productivity in the Amundsen Sea.

Primary productivity exhibited clear seasonal variability in these four bioregions (**Figure 7A**). The primary production was large from November to March, and the monthly variations were more obviously in bioregions 8 and 9 than in the other bioregions. From April to October, the differences among these 4 bioregions became small, and primary production in these 4 bioregions was less than 1 mgC m^{-3} day^{-1}. Seasonal variations in primary productivity in the Amundsen Sea were mainly caused by changes in net solar radiation, sea ice, and iron (Moore and Abbott, 2000; Stammerjohn et al., 2015; Wu and Hou, 2017; St-Laurent et al., 2019). In the Amundsen Sea, the sea ice coverage increased after March and reached a maximum value in austral winter (**Figure 7B**). After September, the sea ice coverage decreased and reached a minimum value in austral summer. The production of meltwater, the generation of a stratified surface layer, and the release of biogenic elements (such as iron) increased phytoplankton growth and accumulation within the marginal ice zone (Ritterhoff and Zauke, 1997; Smith Jr. and Comiso, 2008; St-Laurent et al., 2019). The net solar radiation of the Southern Ocean has significant seasonal variations and is higher in spring (September to November) and summer (December to February) and lower in autumn (March to May) and winter (June to August). At the same time, sea ice coverage can regulate the availability of irradiance to phytoplankton in the Amundsen Sea. Under the effects of polar night and large sea ice coverage, the primary production was close to 0 from May to September in these four bioregions. Results also showed that the dissolved iron also exhibited clear seasonal variability. The iron reached a maximum in November, and then decreased, it reached its minimum in February (**Figure 7C**). The seasonal cycles of Fe

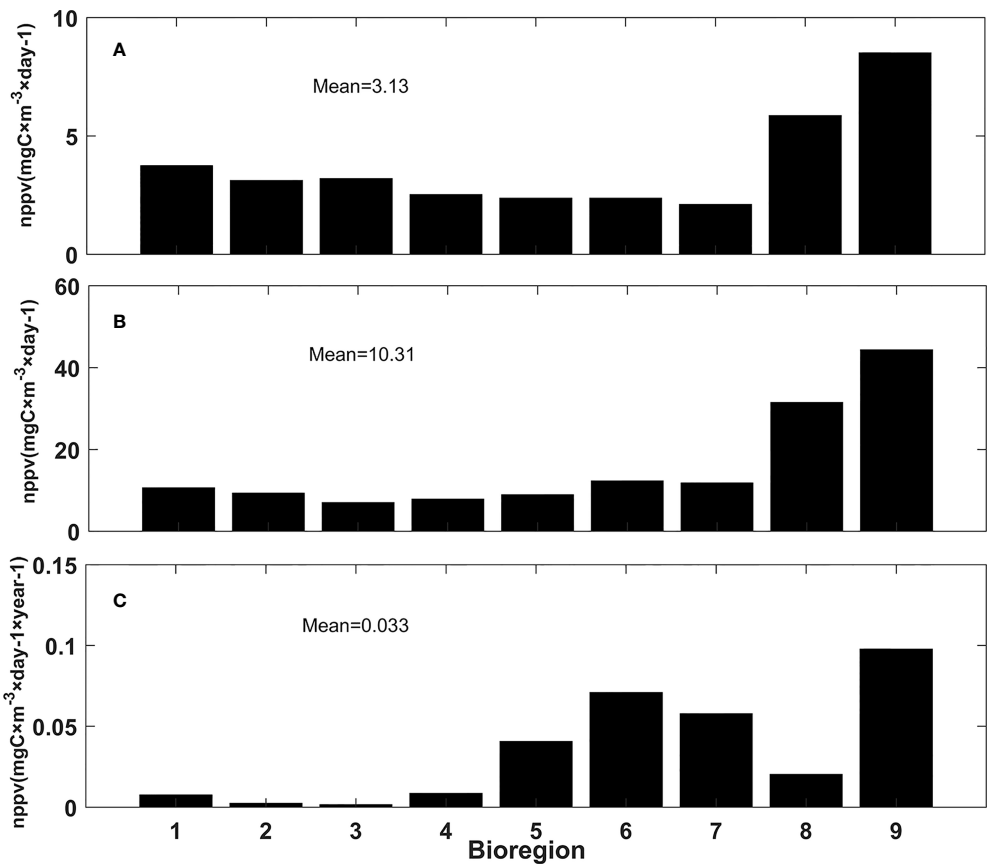

FIGURE 6 | Mean values **(A)**, annual maximum mean values **(B)**, and long-term change rates **(C)** of primary production in 9 bioregions, the mean value of the whole bioregions was also listed in the figure.

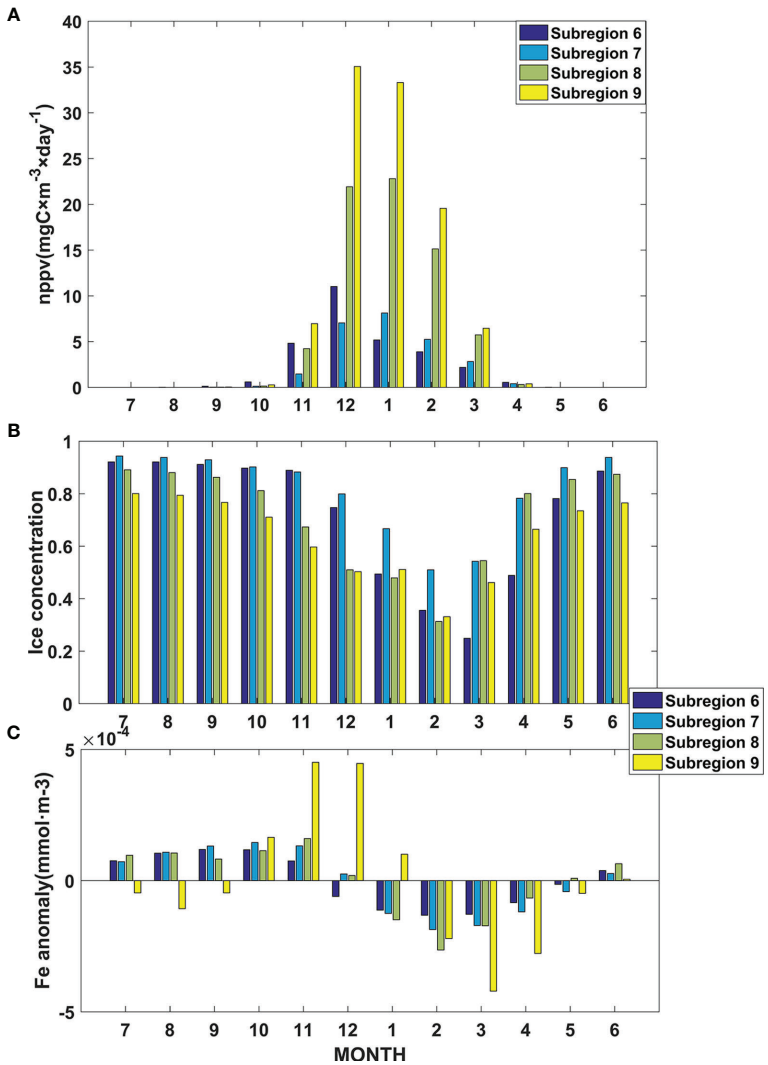

FIGURE 7 | **(A)** Monthly mean net primary productivity values in bioregions 6, 7, 8, and 9 from 1993 to 2015; **(B)** Monthly mean ice concentration in bioregions 6, 7, 8, and 9 from 1993 to 2015; **(C)** Monthly mean dissolved iron anomaly in bioregions 6, 7, 8, and 9 from 1993 to 2015.

are dominated by iron scavenging and by remineralization (St-Laurent et al., 2019). In December and January, the primary production increase rapidly and provided a large inventory of sinking biogenic particles, the scavenging increases rapidly during this period. Over the rest of the year, scavenging decreases gradually. From January to June the Fe gradual recovery through remineralization of organic particles or the dissolution/solubilization of surface bound labile particulate iron. Previous studies of the coastal polynya also found that the phytoplankton bloom is primarily light-limited in its early stages, but as the pool of dissolved iron is depleted by phytoplankton uptake, there is a transition towards iron limitation (St-Laurent et al., 2019).

The results also showed that the phenology changed over the study period in bioregions 6 and 7 (**Figure 8**). In bioregion 3, primary production reached a maximum in January before 1998, while after 1998, maximum primary production occurred in December. In bioregion 6, the primary production rates in November and December increased significantly after 1998. In bioregion 7, primary production reached its maximum in January before 2001; after 2001, the maximum primary production occurred in December. In bioregion 7, primary production increased significantly in November and December after 2001. These variations in primary production in bioregions 6 and 7 were thought to be related to the changes in nutrients (**Figure 9**). In bioregion 6, the dissolved iron concentrations increased significantly in November and December after 1998; these increased values were more than 2 times higher than those recorded before 1998. Increased dissolved iron concentrations resulted in increased primary production in November and December after 1998. In bioregion 7, the dissolved iron concentrations also increased in August, September, November

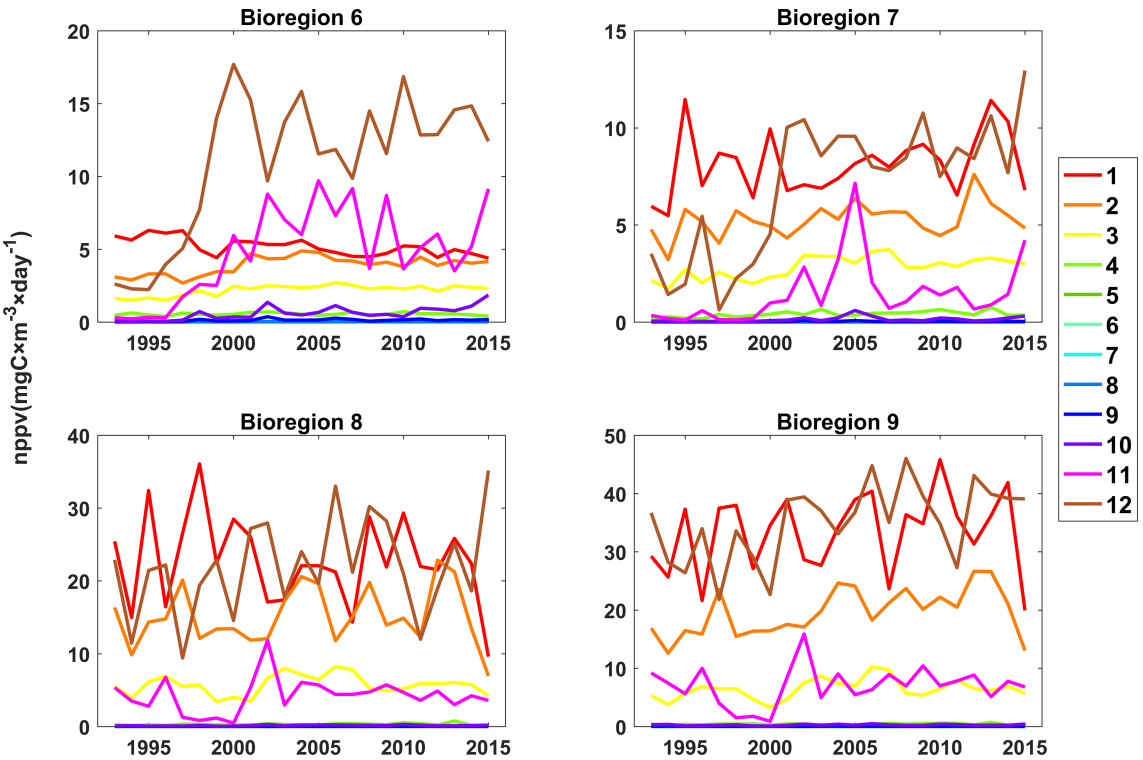

FIGURE 8 | Changes in monthly net primary productivity values in bioregions 6, 7, 8, and 9 from 1993 to 2015 (the colors represent different months).

and December after 1998, and the nitrate, phosphate, and silicate concentrations increased significantly in August, September, November and December after 2000.

The variation of these nutrients was caused by changes of the seasonal cycle of the sea ice in the offshore area in the Amundsen Sea. Stammerjohn et al. (2015) found that the winter ice season duration showed a rapid decrease since 2000 and the summer open duration showed a rapid increase since 2000 in the offshore area in the Amundsen Sea. Previous studies have shown that sea ice coverage in west Antarctica water and in the Amundsen Sea has decreased drastically over the last few decades (Randall-Goodwin et al., 2015; Stammerjohn et al., 2015). On the one hand, the melting sea ice is a potentially important source of dissolved iron, nitrate, phosphate, and silicate (Lannuzel et al., 2010). On the other hand, the melting sea ice can lead to salinity-driven vertical stratification (the "meltwater pump"), it can transport sediment-derived nutrients to the upper water column (St-Laurent et al., 2017; Twelves et al., 2021). Throughout much of the Southern Ocean, macronutrients are abundant and low Fe concentrations limit productivity (Tagliabue et al., 2014). Also, Alderkamp et al. (2015) showed that the primary production is stressed by limited iron availability while macronutrients are generally abundant in the Amundsen Sea. Alderkamp et al. (2015) indicated that primary productivity would be stressed by low iron concentrations during December and January in the Amundsen Sea. So the changes in dissolved iron resulted in increased primary production in November and December after 2000. Kwon et al. (2021) also found that the increase in iron can lead to a shift in the bloom peak timing to earlier than January in the Amundsen Sea continental shelf water (mostly in bioregion 5) using a 1-D pelagic ecosystem model.

The changes in primary production from 1993 to 2015 in bioregions 6, 7, 8, and 9 were also analyzed (**Figure 10**). The results showed that primary production showed positive linear trends in these four bioregions, and these trends were significant at the 95% confidence level in bioregions 6, 7, and 9. Bioregion 9 had the fastest growth rate, and the decadal variations in bioregion 9 were also larger than those in the other 3 bioregions. Primary production reached highest in 2006 and was relatively low in 1994, 1999, 2000, and 2015. The increasing trend observed in bioregion 8 was not significant, but the interannual variations were more significant in bioregion 8 than those in bioregions 6 or 7. The interannual and decadal variations between bioregion 8 and bioregion 9 were quite similar, with a correlation coefficient of approximately 0.75 (calculated using the time series after long-term trend removal). In bioregion 9, a significant positive correlation existed between primary production and sea surface temperatures in summer (from November to March), and the correlation coefficient was 0.46 (**Table 3**). In bioregion 8, the interannual and decadal variations in primary production were positively correlated with the sea surface temperature in summer, and the correlation coefficient was 0.45. These variations in primary

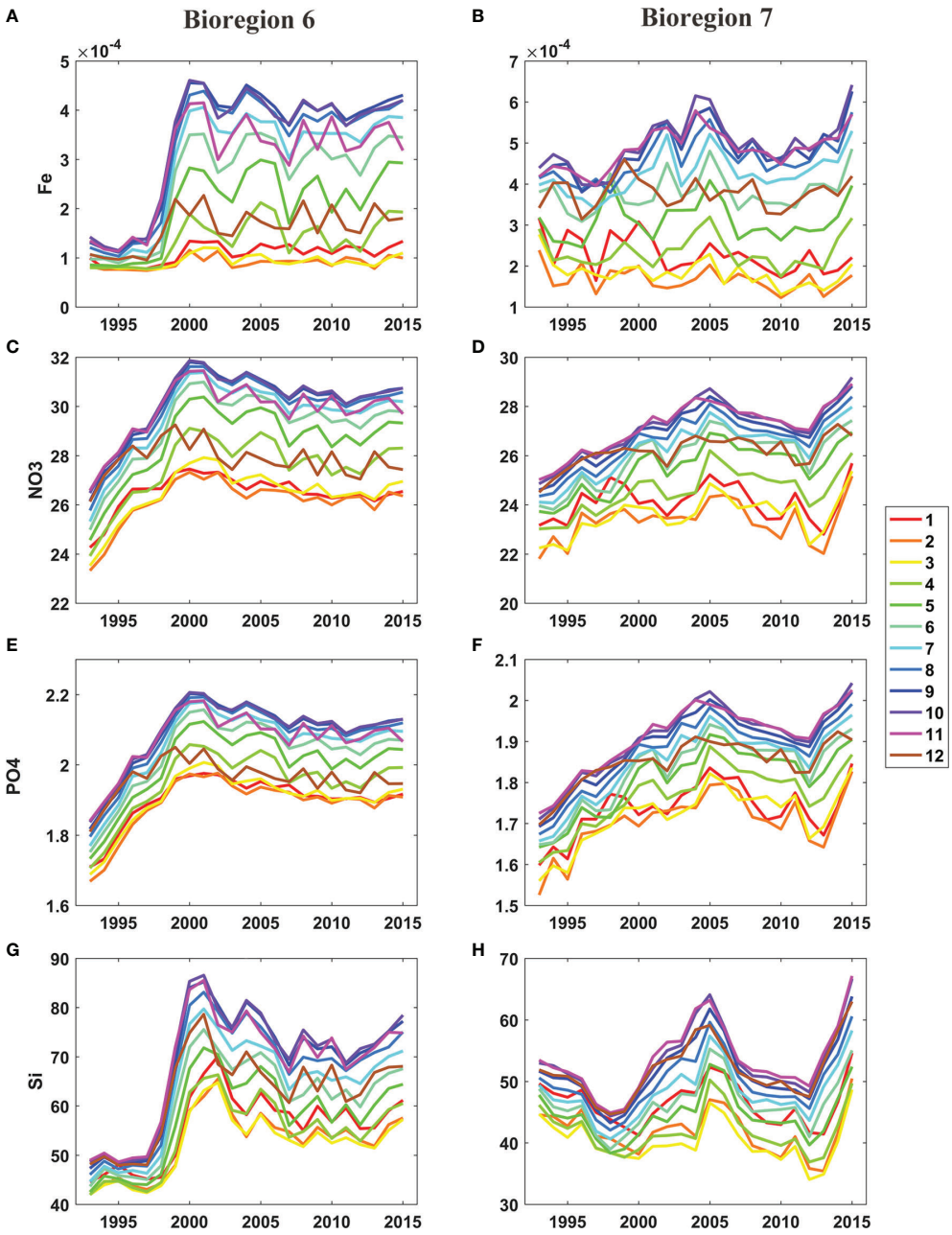

FIGURE 9 | Changes in monthly Fe **(A, B)** (mmol m^{-3}), monthly nitrate **(C, D)** (mmol m^{-3}), month phosphate **(E, F)** (mmol m^{-3}) and monthly silicate **(G, H)** (mmol m^{-3}) in bioregion 6 (left panels) and 7 (right panels).

production were also significantly negatively correlated with sea ice thickness, and the correlation coefficient was -0.54 of bioregion 8 and -0.24 of bioregion 9. Therefore, the changes in primary production recorded in bioregions 8 and 9 may have been caused by changes in the sea surface temperatures in summer and changes of sea ice thickness in these areas. Previous studies have shown that SSTs can impact rates of products directly through the relationship between temperature and phytoplankton metabolic rate; SSTs can also affect surface ocean stratification and sea ice distributions (Arrigo et al., 2008). The decline in sea ice thickness can increase the light availability, which has significant effects on the blooms in the nearshore and coastal polynyas in the Amundsen Sea (Venables et al., 2013; Schofield et al., 2015; Oliver et al., 2019). The growth rate of primary production was calculated using linear regression (**Figure 10**). The growth rate of primary production in bioregion 6 was larger than that in bioregions 7 and 8. This primary production rise accelerated before 2000, while after 2000,

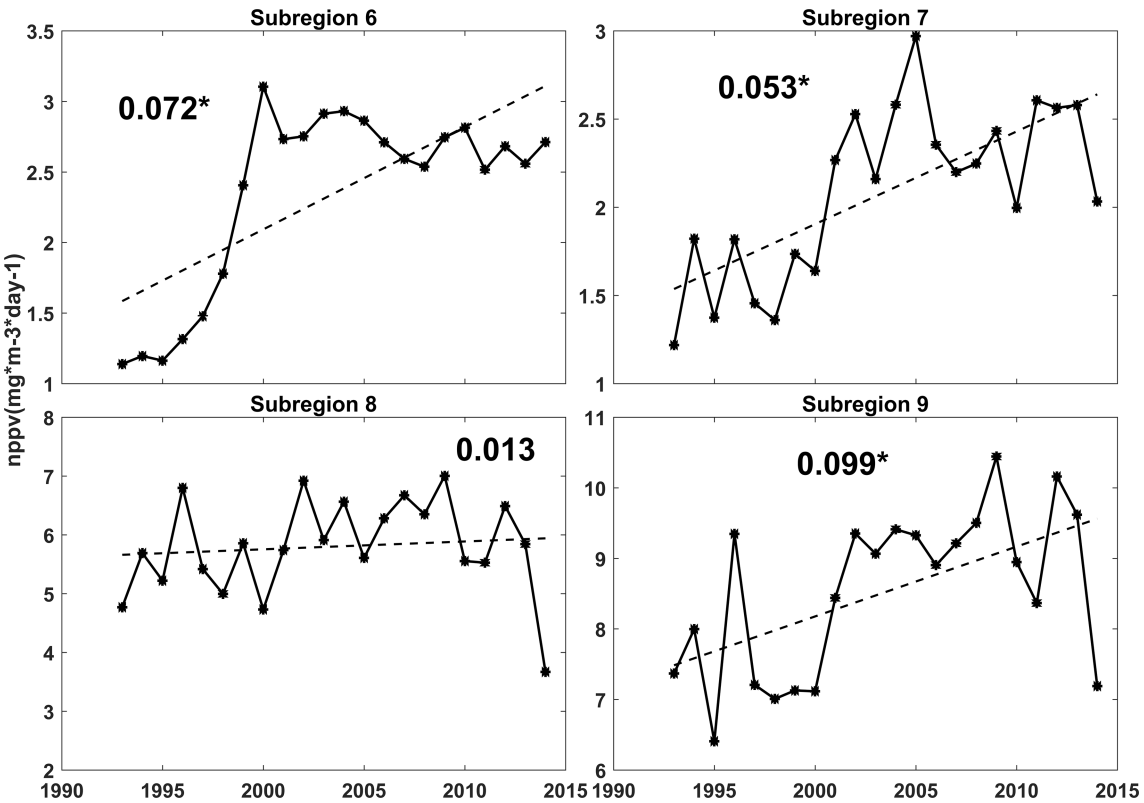

FIGURE 10 | Annual net primary productivity rates (full line) in bioregions 6, 7, 8 and 9 from 1993 to 2015, the dotted lines indicate the linear trends (numbers are the slope of long-term change). The * means that the trend is significant.

TABLE 3 | Correlation between primary production and environmental factors of bioregion 6, 7, 8 and 9.

	SST (Nov-Mar)	Hice	Fe	nitrate	phosphate	silicate	mlp
Bioregion 6	0.12	-0.10	0.96	0.86	0.87	0.94	-0.18
Bioregion 7	0.07	-0.18	0.59	0.78	0.81	0.61	0.11
Bioregion 8	0.45	-0.54	0.11	0.08	0.13	0.07	-0.02
Bioregion 9	0.46	-0.24	-0.25	-0.15	0.20	-0.05	-0.15

A Trends with significance at the 95% level are underlined.

no significant long-term change was observed in bioregion 6. Primary production rose with fluctuations in bioregion 7 and reached a maximum in 2005. The decadal and long-term changes in primary production recorded in bioregions 6 and 7 were thought to be related to changes in dissolved iron. The correlation coefficients between primary production and dissolved iron were 0.96 in bioregion 6 and 0.59 in bioregion 7, indicating that dissolved iron was an important factor limiting primary productivity. We also found that the primary production was significantly positively correlated with nitrate, phosphate, and silicate in bioregions 6 and 7. The correlation coefficients were all larger than 0.6 in bioregions 6 and 7. However, the Southern Ocean is the largest high-nutrient region (Lee et al., 2012). And the differences in nitrate, phosphate, and silicate were quite small among these four bioregions. These positive correlations may be caused by the significant correlation between the dissolved iron and nitrate, phosphate, and silicate in bioregions 6 and 7 (all larger than 0.8). The nitrogen: phosphorus ratios were in the range of 13.5 to 14.5, which was quite near to the Redfield ratio. Justić et al. (1995) indicated that the nutrients will inhibit the growth of phytoplankton when nitrate<1mmol m-3, phosphate<0.1 mmol m-3, silicate<2mmol m-3, respectively. In the Amundsen Sea, the concentrations of nitrate, phosphate and silicate were substantially higher than the limitations (**Figure 9**). As a result, the nitrate, phosphate, and silicate were not thought to be limiting factors of primary productivity in the Amundsen Sea.

The environmental controls of primary productivity of 6 and 7 showed some differences with that of bioregions 8 and 9. These differences may be caused by the differences of the dissolved iron concentrations. The dissolved iron concentrations in bioregions 8 (with mean value of 9.85×10^{-4} mmol m^{-3}) and 9 (with mean

value of 2.5×10^{-3} mmol m^{-3}) were the highest in the Amundsen Sea area (**Figure 5**) and much larger than that of bioregion 6 and 7 (**Figure 9**). So dissolved iron was not the limiting factor for primary productivity in these two bioregions. In bioregion 8 and 9 the decadal and long-term changes of primary productivity were more correlated with the SST and sea ice. In bioregion 6 and 7, the dissolved iron concentrations were much smaller than that of bioregion 8 and 9. The primary productions were also positive correlated with SSTs and negative correlated with sea ice thickness, but the correlation were not significant at 95% confidence levels. So the primary production was mainly controlled by dissolved iron concentrations in bioregions 6 and 7. The spatial differences in the limitation of dissolved iron on the primary productivity of the Amundsen Sea were consistent with previous results (Yager et al., 2012).

CONCLUSION

The Amundsen Sea is one of the least-studied regions in the Southern Ocean and has significant spatial differences in primary productivity. In this work, we used bioregionalization to provide a basis for understanding the temporal and spatial variations in primary productivity in the Amundsen Sea.

The spatial differences were quite significant in the Amundsen Sea; in most areas, the mean primary production was less than 3 mgC m^{-3} day^{-1}. However, near the coast of Pine Island Bay, mean primary production reached 14 mgC m^{-3} day^{-1}. Primary production exhibited clear seasonal variabilities and was largest in December at approximately 10 mgC m^{-3} day^{-1}.

The Amundsen Sea was divided into 9 bioregions using hierarchical clustering and the *K*-means clustering method. Four nearshore bioregions (6, 7, 8, and 9) were selected to analyze variations in primary productivity in the Amundsen Sea. Due to changes in the dissolved iron, the phenology of primary production changed in bioregions 6 and 7. Primary production showed positive linear trends in these four bioregions due to changes in SST, sea ice and dissolved iron. The long-term primary changes of bioregions 6 and 7 were thought to be limited by changes in the dissolved iron concentrations. Our results indicated that although there were some same similar characteristics existed in the changes of primary productions, the spatial differences were quite large in the Amundsen. We thought that our findings, including the spatial differences and mechanisms that drive differences in phenology, decadal and long-term changes in primary productivity, can be helpful for predicting how the primary production will respond to future change, and also for analysis and protection of the ecosystem in the Amundsen Sea.

The above results indicated that in addition to being used in the systematic conservation planning of marine protected areas, bioregionalization is also an effective method to disentangle multiple limiting factors that affect spatial differences, the phenology, decadal and long-term changes in the physical and ecological variables, such as the primary productivity.

DATA AVAILABILITY STATEMENT

The original contributions presented in the study are included in the article/**Supplementary Material**. Further inquiries can be directed to the corresponding author.

AUTHOR CONTRIBUTIONS

JF wrote the first version of the manuscript, DL performed addition analyses, JZ made figures, and LZ revised the text. All authors contributed to the article and approved the submitted version.

FUNDING

This study was supported by impact and response of Antarctic seas to climate change under contract RFSOCC2020-2022-No.18, Project of Scientific Research Program of Tianjin Municipal Education Commission (2017KJ181) and National Science Foundation of Tianjin (19JCZDJC40600).

SUPPLEMENTARY MATERIAL

The Supplementary Material for this article can be found online at: https://www.frontiersin.org/articles/10.3389/fmars.2022.891663/full#supplementary-material

REFERENCES

Alderkamp, A. C., van Dijken, G. L., Lowry, K. E., Connelly, T. L., Lagerström, M., Sherrell, R. M., et al. (2015). *Fe Availability Drives Phytoplankton Photosynthesis Rates During Spring Bloom in the Amundsen Sea Polynya, Antarctica* Vol. 3 (Elementa: Science of the Anthropocene), 000043.

Amthor, J. S., and Baldocchi, D. D. (2001). "Terrestrial Higher Plant Respiration and Net Primary Production," in *Terrestrial Global Productivity* (San Diego: Academic Press), 33–59.

Anselin, L., Syabri, I., and Kho, Y. (2006). Geoda: An Introduction to Spatial Data Analysis. *Geograohic. Anal.* 38 (1), 5–22. doi: 10.1111/j.0016-7363.2005.00671.x

Ardyna, M., Claustre, H., Sallée, J. B., D'Ovidio, F., Gentili, B., van Dijken, G., et al. (2017). Delineating Environmental Control of Phytoplankton Biomass and Phenology in the Southern Ocean. *Geophys. Res. Lett.* 44, 5016–5024. doi: 10.1002/2016GL072428

Arneborg, L., Wåhlin, A. K., Björk, G., Lijebladh, B., and Orsi, A. H. (2012). Persistent Inflow of Warm Water Onto the Central Amundsen Shelf. *Nat. Geosci.* 5 (12), 876–880. doi: 10.1038/ngeo1644

Arrigo, K. R., Lowry, K. E., and van Dijken, G. L. (2012). Annual Changes in Sea Ice and Phytoplankton in Polynyas of the Amundsen Sea, Antarctica. *Deep Sea Res. Part II: Topical Stud. Oceanogr.* 71-76, 5–15. doi: 10.1016/j.dsr2.2012.03.006

Arrigo, K. R., and van Dijken, G. L. (2003). Phytoplankton Dynamics Within 37 Antarctic Coastal Polynya Systems. *J. Geophy. Res.* 108, C83271. doi: 10.1029/2002JC001739

Arrigo, K. R., van Dijken, G. L., and Bushinsky, S. (2008). Primary Production in the Southern Ocean 1997-2006. *J. Geophys. Res.* 113, C08004. doi: 10.1029/2007JC004551

Arrigo, K. R., van Dijken, G. L., and Strong, A. L. (2015). Environmental Controls of Marine Productivity Hot Spots Around Antarctica. *J. Geophys. Res.: Oceans* 120 (8), 5545–5565. doi: 10.1002/2015JC010888

Behrenfeld, M., and Boss, E. (2014). Resurrecting the Ecological Underpinnings of Ocean Plankton Blooms, Annu. *Rev. Mar. Sci.* 6, 167–194. doi: 10.1146/annurev-marine-052913-021325

Bijma, J., Pörtner, H. O., Yesson, C., and Rogers, A. D. (2013). Climate Change and the Oceans – What Does the Future Hold? *Mar. Pollut. Bull.* 74 (2), 495–505. doi: 10.1016/j.marpolbul.2013.07.022

Bloomfield, N. J., and Knerr, N. (2018). And Encinas-Viso, F.: A Comparison of Network and Clustering Methods to Detect Biogeographical Regions. *Ecography* 41, 1–10. doi: 10.1111/ecog.02596

Bowman, J. S., Kavanaugh, M. T., Donsy, S. C., and Ducklow, H. W. (2018). Recurrent Seascape Units Identify Key Ecological Processes Along the Western Antarctic Peninsula. *Global Change Biol.* 24 (7), 3065–3078. doi: 10.1111/gcb.14161

Boyd, P. W. (2002). Environmental Factors Controlling Phytoplankton Processes in the Southern Ocean. *J. Phycol.* 38 (5), 844–861. doi: 10.1046/j.1529-8817.2002.t01-1-01203.x

Brainerd, K. E., and Gregg, M. C. (1995). Surface Mixed and Mixing Layer Depths. *Deep Sea Res. Part I* 42 (9), 1521–1543.

Bromwich, D. H., Nicolas, J. P., Monaghan, A. J., Lazzara, M., Keller, L. M., Weidner, G. A., et al. (2013). Central West Antarctica Among the Most Rapidly Warming Regions on Earth. *Nat. Geosci.* 6, 139–145. doi: 10.1038/ngeo1671

Comiso, J. C., Cavalieri, D. J., and Markus, T. (2003). Sea Ice Concentration, Ice Temperature, and Snow Depth Using AMSR-E Data. *IEEE Trans. Geosci. Remote Sens.* 41 (2), 243–252. doi: 10.1109/TGRS.2002.808317

Costello, M. J. (2009). Distinguishing Marine Habitat Classification Concepts for Ecological Data Management. *Mar. Ecol. Prog. Ser.* 397, 253e268. doi: 10.3354/meps08317

Dinniman, M. S., St-Lauernt, P., Arrigo, K. R., Hofmann, E. E., and van Dijken, G. L. (2020). Analysis of Iron Source in Antarctic Continental Shelf Water. *J. Geophys. Res.: Oceans* e2019JC015736.

D'Ortenzio, F., and d'Alcalà, M. R. (2009). On the Trophic Regimes of the Mediterranean Sea: A Satellite Analysis. *Biogeosciences* 6 (2), 139–148. doi: 10.5194/bg-6-139-2009

Dotto, T. S., Garabato, A. N., Bacon, S., Tsamados, M., Holland, P. R., Hooley, J., et al. (2018). Variability of the Ross Gyre, Southern Ocean: Drivers and Responses Revealed by Satellite Altimetry. *Geophys. Res. Lett.* 45 (12), 6195–6201. doi: 10.1029/2018GL078607

Ebach, M. C., Murphy, D. J., Gonzalez-Orozco, C., and Miller, J. (2015). A Revised Area Taxonomy of Phytogeographical Regions Within the Australian Bioregionalisation Atlas. *Phytotaxa* 208 (4), 261–277. doi: 10.11646/phytotaxa.208.4.2

Feng, J., von Storch, H., Jiang, W., and Weisse, R. (2015). Assessing Changes in Extreme Sea Level Along the Coast of China. *J. Geophys. Res.: Oceans* 120 (12), 8039–8051. doi: 10.1002/2015JC011336

Fraley, C., and Raftery, A. (1998). How Many Clusters? Which Clustering Method? Answers *via* Model-Based Cluster Analysis. *Comput. J.* 41, 578–588. doi: 10.1093/comjnl/41.8.578

Fraschetti, S., Terlizzi, A., and Boero, F. (2008). How Many Habitats are There in the Sea (and Where)? *J. Exp. Mar. Bio. Ecol.* 366, 109.e115. doi: 10.1016/j.jembe.2008.07.015

Godet, C., Robuchon, M., Leroy, B., Cotté, C., Baudena, A., Silva, O. D., et al. (2020). Matching Zooplankton Abundance and Environment in the South Indian Ocean and Southern Ocean. *Deep Sea Res. Part I: Oceanogr. Res. Papers* 163, 103347. doi: 10.1016/j.dsr.2020.103347

Gohl, K. (2010). The Expedition of the Research Vessel Polarstern to the Amundsen Sea, Antatctica, in 2010 (ANT-XXIV/3). *Rep. Polar Mar. Res.* 617, 173.

Govender, P., and Sivakumar, V. (2020). Application of K-Means and Hierarchical Clustering Techniques for Analysis of Air Pollution: A Review, (1980-2019). *Atmos. Pollut. Res.* 11 (1), 40e56. doi: 10.1016/j.apr.2019.09.009

Grant, S., Constable, A., Raymond, B., and Doust, S. (2006). "Bioregionalisation of the Southern Ocean. Report of an Expert Workshop, Hobart, Australia, September 2006," WWF-Australia and ACE CRC.

Grantham, H. S., Pressey, R. L., Wells, J. A., and Beattie, A. J. (2010). Effectiveness of Biodiversity Surrogates for Conservation Planning: Different Measures of Effectiveness Generate a Kaleidoscope of Variation. *PloS One* 5. doi: 10.1371/journal.pone.0011430

Greger, E. J., and Bodtker, K. M. (2007). Adaptive Classification of Marine Ecosystems: Identifying Biological Meaningful Regions in the Marine Environment. *Deep Sea Res. I* 54, 385–402. doi: 10.1016/j.dsr.2006.11.004

Griffiths, H. J. (2010). Antarctic Marine Biodiversity—What do We Know About the Distribution of Life in the Southern Ocean? *PloS One* 5 (7), e1130. doi: 10.1371/journal.pone.0011683

Herraiz-Borreguero, L., Lannuzel, D., van der Merwe, P., Treverrow, A., and Pedro, J. B. (2016). Large flux of Iron From the Amery Ice Shelf Marine Ice to Prydz Bay, East Antarctica. *J. Geophys. Res. Oceans* 121, 6009–6020. doi: 10.1002/2016JC011687

Huang, J., Zhang, Z., and Wang, X. (2020). Evaluation of Four High-Resolution Sea Ice Reanalysis Products in the Ross Sea and Amundsen Sea. *Chin. J. Polar Res.* 32 (4), 452–468. doi: 10.13679/j.jdyj.20200007

Justić, D., Rabalais, N. N., Turner, R. E., and Dortch, Q. (1995). Changes in Nutrient Structure of River-Dominated Coastal Waters: Stoichiometric Nutrient Balance and its Consequences. *Estuarine Coastal Shelf Sci.* 40 (3), 339–356. doi: 10.1016/S0272-7714(05)80014-9

Khatiwala, S., Primeau, F., and Hall, T. (2009). Reconstruction of the History of Anthropogenic CO_2 Concentrations in the Ocean. *Nature* 462 (7271), 346–349. doi: 10.1038/nature08526

Kim, S. U., and Kim, K. Y. (2021). Impact of Climate Change on the Primary Production and Related Biogeochemical Cycles in the Coastal and Sea Ice Zone of the Southern Ocean. *Sci. Total Environ.* 751, 141678. doi: 10.1016/j.scitotenv.2020.141678

Kim, C. S., Kim, T. W., Cho, K. H., Ha, H. K., Lee, S. H., Kim, H. C., et al. (2016). Variability of the Antarctic Coastal Current in the Amundsen Sea. *Estuarine Coastal Shelf Sci.* 181 (5), 123–133. doi: 10.1016/j.ecss.2016.08.004

Koubbi, P., Moteki, M., Duhamel, G., Goarant, A., Hulley, P. A., O'Driscoll, R., et al. (2011). Ecoregionalization of Myctophid Fish in the Indian Sector of the Southern Ocean: Results From Generalized Dissimilarity Models. *Deep. Res. Part II Top. Stud. Oceanogr.* 58, 170e180. doi: 10.1016/j.dsr2.2010.09.007

Kulkarni, A., and von Storch, H. (1995). Monte Carlo Experiments on the Effect of Serial Correlation on the Mann-Kendall-Test of Trends. *Meteor Z.* 4, 82–85. doi: 10.1127/metz/4/1992/82

Kwon, Y. S., La, H. S., Jung, J., Lee, S. H., Kim, T. W., Kang, H. W., et al. (2021). Exploring the Roles of Iron and Irradiance in Dynamics of Diatoms and Phaeocystis in the Amundsen Sea Continental Shelf Water. *J. Geophys. Res.: Oceans* 126 (3), 1–23. doi: 10.1029/2020JC016673

Lacour, L., Claustre, H., Prieur, L., and D'Ortenzio, F. (2015). Phytoplankton Biomass Cycles in the North Atlantic Subpolar Gyre: A Similar Mechanism for Two Different Blooms in the Labrador Sea. *Geophys. Res. Lett.* 42, 5403–5410. doi: 10.1002/2015GL064540

Lannuzel, D., Schoemann, V., de Jong, J., Pasquer, B., van der Merwe, P., Masson, F., et al. (2010). Distribution of Dissolved Iron in Antarctic Sea Ice: Spatial, Seasonal, and Inter-Annual Variability. *J. Geophys Res. Biogeosci.* 115, G03022. doi: 10.1029/2009JG001031

Lannuzel, D., Schoemann, V., De Jong, J., Tison, J. L., and Chou, L. (2007). Distribution and Biogeochemical Behaviour of Iron in the East Ant-Arctic Sea Ice. *Mar. Chem.* 106 (1), 18–32. doi: 10.1016/j.marchem.2006.06.010

Leathwick, J. R., Overton, J., and McLeod, M. (2003). An Environmental Domain Classification of New Zealand and its Use as a Tool for Biodiversity Management. *Conserv. Biol.* 17, 1612–1623. doi: 10.1111/j.1523-1739.2003.00469.x

Lee, S. H., Kim, B. K., Yun, M. S., Joo, H., Yang, E. J., Kim, Y. N., et al. (2012). Spatial Distribution of Phytoplankton Productivity in the Amundsen Sea, Antarctica. *Polar Biol.* 35, 1721–1733. doi: 10.1007/s00300-012-1220-5

Lim, Y. J., Kim, T. W., Lee, S., Lee, D., Park, J., Kim, B., et al. (2019). Seasonal Variations in the Small Phytoplankton Contribution to the Total Primary Production in the Amundsen Sea, Antarctica. *J. Geophys. Res. Oceans* 124 (11), 8324–8341. doi: 10.1029/2019JC015305

Longhurst, A. (2007). *Ecological Geography of the Sea. 2nd ed* (Burlington, Mass: Academic Press), 542.

Mann, H. B. (1945). Nonparametric Tests Against Trend. *Econometrica* 13, 245–259. doi: 10.2307/1907187

Martinson, D. G. (2012). Antarctic Circumpolar Current's Role in the Antarctic Ice System: An Overview. *Palaeogeogr. Palaeoclimatol. Palaeoecol.* 335–336, 71–74. doi: 10.1016/j.palaeo.2011.04.007

Ma, H., Wang, Z., and Shi, J. (2012). The Role of the Southern Ocean Physical Processes in Global Climate System. *Adv. Earth Sci.* 27 (4), 398–412. doi: 10.11867/j.issn.1001-8166.2012.04.0398

Mayot, N., D'Ortenzio, F., d'Alcalà, M. R., Lavigne, H., and Claustre, H. (2016). Interannual Variability of the Mediterranean Trophic Regimes From Ocean Color Satellites. *Biogeosciences* 13 (6), 1901–1917. doi: 10.5194/bg-13-1901-2016

Meier, W. N., Fetterer, F., Savoie, M., Mallory, S., Duerr, R., and Stroeve, J. (2017). *NOAA/NSIDC Climate Data Record of Passive Microwave Sea Ice Concentration, Version 3* (Boulder, Colorado USA: NSIDC: National Snow and Ice Data Center). doi: 10.7265/N59P2ZTG

Milligan, G. W., and Cooper, M. C. (1987). Methodology Review: Clustering Methods. *Appl. Psychol. Meas.* 11, 329–354. doi: 10.1177/014662168701100401

Moore, J. K., and Abbott, M. R. (2000). Phytoplankton Chlorophyll Distributions and Primary Production in the Southern Ocean. *J. Geophys. Res.* 105 (C12), 28709–28722. doi: 10.1029/1999JC000043

Norse, E. A. (2010). Ecosystem-Based Spatial Planning and Management of Marine Fisheries: Why and How. *Mar. Pollut. Bull.* 86 (2), 179–195.

Oliver, M. J., and Irwin, A. J. (2008). Objective Global Ocean Biogeographic Provinces. *Geophys. Res. Lett.* 35, L15601. doi: 10.1029/2008GL034238

Oliver, H., St-Laurent, P., Sherrell, R. M., and Yager, P. L. (2019). Modeling Iron and Light Controls on the Summer Phaeocystis Antarctica Bloom in the Amundsen Sea Polynya. *Global Biogeochem. Cycles* 33 (5), 570–596. doi: 10.1029/2018GB006168

Pabis, K., Hara, U., Presler, P., and Sicinski, J. (2014). Structure of Bryozoan Communities in an Antarctic Glacial Fjord (Admiralty Bay, South Shelands). *Polor Biol.* 37, 737–751.

Park, K., Hahm, D., Choi, J. O., Xu, S., Kim, H. C., and Lee, S. H. (2019). Spatiotemporal Variation in Summer Net Community Production in the Amundsen Sea Polynya: A Self-Organizing Map Analysis Approach. *Continent. Shelf Res.* 184, 21–29. doi: 10.1016/j.csr.2019.07.001

Park, J., Kuzminovm, F. I., Bailleul, B., Yang, E. J., Lee, S., Falkowski, P. G., et al. (2017). Light Availability Rather Than Fe Controls the Magnitude of Massive Phytoplankton Bloom in the Amundsen Sea Polynyas, Antarctica. *Limnol. Oceanogr.* 62 (5), 2260–2276. doi: 10.1002/lno.10565

Petrou, K., Kranz, S. A., Trimborn, S., Hassler, C. S., Ameijeiras, S. B., Sackett, O., et al. (2016). Southern Ocean Phytoplankton Physiology in a Changing Climate. *J. Plant Physiol.* 203, 135–150. doi: 10.1016/j.jplph.2016.05.004

Randall-Goodwin, E., Meredith, M. P., Jenkins, A., Yager, P. L., Sherrell, R. M., Abrahamsen, E. P., et al. (2015). Freshwater Distributions and Water Mass Structure in the Amundsen Sea Polynya Region, Antarctica. *Elem. Sci. Anth.* 3, 000065. doi: 10.12952/journal.elementa.000065

Reid, P. C., Fischer, A. C., Lewis-Brown, E., Meredith, M. P., Sparrow, M., Andersson, A. J., et al. (2009). Impacts of the Oceans on Climate Change. *Adv. Mar. Biol.* 56, 1–150. doi: 10.1016/S0065-2881(09)56001-4

Rice, J., Gjerde, K. M., Ardron, J., Arico, S., Cresswell, I., Escobar, E., et al. (2011). Policy Relevance of Biogeographic Classification for Conservation and Management of Marine Biodiversity Beyond National Jurisdiction, and the GOODS Biogeographic Classification. *Ocean. Coast. Manag.* 54, 110e122. doi: 10.1016/j.ocecoaman.2010.10.010

Ritterhoff, J., and Zauke, G. P. (1997). Trace Metals in Field Samples of Zooplankton From the Fram Strait and the Greenland Sea. *Sci. Total Environ.* 199, 255–270. doi: 10.1016/S0048-9697(97)05457-0

Roberson, L. A., Lagabrielle, E., Lombard, A. T., Sink, K., Livingstone, T., Grantham, H., et al. (2017). Pelagic Bioregionalisation Using Open-Access Data for Better Planning of Marine Protected Area Networks. *Ocean Coastal Manage.* 148, 214–230. doi: 10.1016/j.ocecoaman.2017.08.017

Schofield, O. M., Miles, T., Alderkamp, A.-C., Lee, S., Haskins, C., Rogalsky, E., et al. (2015). *In Situ* Phytoplankton Distributions in the Amundsen Sea Polynya Measured by Autonomous Gliders. *Elementa: Sci. Anthropocene* 3, 000073. doi: 10.12952/journal.elementa.000073

Sharp, B. R., Parker, S. J., Pinkerton, M., Breen, B. A., Cummings, V. J., Dunn, A., et al. (2010). "Bioregionalisation and Spatial Ecosystem Processes in the Ross Sea Region," in *Document WG-EMM-10/30* (Hobart, TAS: CCAMLR).

Smith, W. O. Jr., and Comiso, J. C. (2008). Influence of Sea Ice on Primary Production in the Southern Ocean, A Satellite Perspective. *J. Geophys. Res. Oceans* 113, C05S93. doi: 10.1029/2007JC004251

Snelder, T. H., Leathwick, J., Dey, K., Rowden, A. A., Weatherhead, M. A., Fenwick, G. D., et al. (2007). Development of an Ecological Marine Classification in the New Zealand Region. *Environ. Manage.* 39, 12–29. doi: 10.1007/s00267-005-0206-2

Spalding, M. D., Fox, H. E., Allen, G. R., Davidson, N., FerdaNa, Z., Finlayson, M., et al. (2007). Marine Ecoregions of the World: A Bioregionalization of Coastal and Shelf Areas. *Bioscience* 57, 573–583. doi: 10.1641/B570707

Stammerjohn, S. E., Maksym, T., Lowry, K. E., Arrigo, K. R., Yuan, X., Raphael, M., et al. (2015). Seasonal Sea Ice Changes in the Amundsen Sea, Antarctica, Over the Period of 1979-2014. *Elementa: Sci. Anthropocene* 3, 000055. doi: 10.12952/journal.elementa.000055

St-Laurent, P., Yager, P. L., Sherrell, R. M., Oliver, H., Dinniman, M. S., and Stammerjohn, S. E. (2019). Modeling the Seasonal Cycle of Iron and Carbon Fluxes in the Amundsen Sea Polynya, Antarctica. *J. Geophys. Res.: Oceans* 124 (3), 1544–1565. doi: 10.1029/2018JC014773

St-Laurent, P., Yager, P. L., Sherrell, R. M., Stammerjohn, S. E., and Dinniman, M. S. (2017). Pathways and Supply of Dissolved Iron in the Amundsen Sea (Antarctica). *J. Geophys. Res.: Oceans* 122 (9), 7135–7162. doi: 10.1002/2017JC013162

Swalethorp, R., Dinasquet, J., Logares, R., Bertilsson, S., Kjellerup, S., Krabberød, A. K., et al. (2019). Microzooplankton Distribution in the Amundsen Sea Polynya (Antarctica) During an Extensive Phaeocystis Antarctica Bloom. *Prog. Oceanogr.* 170, 1–10. doi: 10.1016/j.pocean.2018.10.008

Tagliabue, A., Sallée, J. B., Bowie, A., Lévy, M., Swart, S., and Boyd, P. W. (2014). Surface-Water Iron Supplies in the Southern Ocean Sustained By Deep Winter Mixing. *Nat. Geosci.* 7, 314–320.

Teschke, K., Beaver, D., Bester, M. N., Bombosch, A., Boremann, H., Brandt, A., et al. (2016). Scientific Background Document in Support of the Development of a CCAMLR MPA in the Weddell Sea (Antarctica)—version 2016—Part A: General Context of the Establishment of MPAs and Background Information on the Weddell Sea MPA Planning Area. *CCAMLR* SC-CAMLR-XXXV/BG/11, 1–112.

Treml, E. A., and Halpin, P. N. (2012). Marine Population Connectivity Identifies Ecological Neighbors for Conservation Planning in the Coral Triangle. *Conserv. Lett.* 5, 441–449. doi: 10.1111/j.1755-263X.2012.00260.x

Twelves, A. G., Goldberg, D. N., Henley, S. F., Mazloff, M. R., and Jones, D. C. (2021). Self-Shading and Meltwater Spreading Control the Transition From Light to Iron Limitation in an Antarctic Coastal Polynya. *J. Geophys. Res.: Oceans* 126 (2), 1–28. doi: 10.1029/2020JC016636

Uotila, P., Goosse, H., Haines, K., Chevallier, M., Barthélemy, A., Bricaud, C., et al. (2019). An Assessment of Ten Ocean Reanalyses in the Polar Regions. *Clim. Dynam.* 52, 1613–1650. doi: 10.1007/s00382-018-4242-z

Venables, H. J., Clarke, A., and Mereddith, M. P. (2013). Wintertime Controls on Summer Stratification and Productivity at the Western Antarctic Peninsula. *Limnol. Oceanogr.* 58, 1035–1047. doi: 10.4319/lo.2013.58.3.1035

von Storch, H., and Zwiers, F. W. (1999). *Statistical Analysis in Climate Research* (Cambridge: United Kingdom at the University Press).

Wu, S. Y., and Hou, S. (2017). Impact of Icebergs on Net Primary Productivity in the Southern Ocean. *Cryosphere* 11, 707–722. doi: 10.5194/tc-11-707-2017

Yager, P., Sherrell, R. M., Stammerjohn, S. E., Alderkamp, A. C., Schofield, O., Abrahamsen, E. P., et al. (2012). ASPIRE: The Amundsen Sea Polynya International Research Expedition. *Oceanography* 25, 40–53. doi: 10.5670/oceanog.2012.73

Conflict of Interest: The authors declare that the research was conducted in the absence of any commercial or financial relationships that could be construed as a potential conflict of interest.

Publisher's Note: All claims expressed in this article are solely those of the authors and do not necessarily represent those of their affiliated organizations, or those of the publisher, the editors and the reviewers. Any product that may be evaluated in this article, or claim that may be made by its manufacturer, is not guaranteed or endorsed by the publisher.

Copyright © 2022 Feng, Li, Zhang and Zhao. This is an open-access article distributed under the terms of the Creative Commons Attribution License (CC BY). The use, distribution or reproduction in other forums is permitted, provided the original author(s) and the copyright owner(s) are credited and that the original publication in this journal is cited, in accordance with accepted academic practice. No use, distribution or reproduction is permitted which does not comply with these terms.

frontiers | Frontiers in Marine Science

ORIGINAL RESEARCH
published: 27 May 2022
doi: 10.3389/fmars.2022.844970

Plankton Metabolism in Coastal Waters of the Guangdong-Hong Kong-Macao Greater Bay: Regional Variance and Driving Factors

Liangkui Zhang[1,2,3], *Gang Li*[1,2], *Chenhui Xiang*[1,2,4], *Yadong Huang*[1,5], *Xiaoming Fu*[1,5], *Chuanyang Zheng*[1,5], *Zheng Wang*[1,5], *Zhiyuan Ouyang*[1,5] *and Xingyu Song*[1,2,5*]

[1] *Key Laboratory of Tropical Marine Bio-resources and Ecology, South China Sea Institute of Oceanology, Chinese Academy of Sciences, Guangzhou, China,* [2] *Southern Marine Science and Engineering Guangdong Laboratory (Guangzhou), Guangzhou, China,* [3] *University of Chinese Academy of Sciences, Beijing, China,* [4] *Innovation Academy of South China Sea Ecology and Environmental Engineering, Chinese Academy of Sciences, Guangzhou, China,* [5] *Nansha Marne Ecological and Environmental Research Station, South China Sea Institute of Oceanology, Chinese Academy of Sciences, Guangzhou, China*

OPEN ACCESS

Edited by:
Yu-Pin Lin,
National Taiwan University, Taiwan

Reviewed by:
Yuyuan Xie,
University of South Florida, United States
Peng Jin,
University of Guangzhou, China

***Correspondence:**
Xingyu Song
songxy@scsio.ac.cn

Specialty section:
This article was submitted to Marine Pollution, a section of the journal Frontiers in Marine Science

Received: *29 December 2021*
Accepted: *19 April 2022*
Published: *27 May 2022*

Citation:
Zhang L, Li G, Xiang C, Huang Y, Fu X, Zheng C, Wang Z, Ouyang Z and Song X (2022) Plankton Metabolism in Coastal Waters of the Guangdong-Hong Kong-Macao Greater Bay: Regional Variance and Driving Factors. Front. Mar. Sci. 9:844970. doi: 10.3389/fmars.2022.844970

Metabolisms of field plankton community, including gross primary production (GPP), community respiration (CR), and net community production (NCP), usually indicate the status of the health, resource production, and carbon budget of marine ecosystems. In this study, we explored the regional variance and driving forces of plankton metabolism in coastal waters of the Guangdong-Hong Kong-Macao Greater Bay Area (GGBA), a fast-developed area with complex hydrological and environmental states. The results showed that the maximum GPP and CR occurred in the estuarine plume of the GGBA in summer, while in winter the more active metabolisms of plankton community occurred in the Daya Bay, with the GPP and CR being respectively mediated by the nutrient level and temperature. Moreover, four regional zones were divided on the base of the environments and biological factors in surface water of the GGBA i.e., the river-runoff zone, river-plume zone, nearshore and far-offshore zones. The metabolic states in these zones varied significantly due to the regional and seasonal variations of, for example, the nutrient level, temperature, and turbidity driven by multiple factors including land-derived runoffs, anthropogenic activities, the Yuedong Coastal Current, and offshore seawater-intrusions. On the whole, the GGBA areas exhibited the weak heterotrophic processes in both summer (NCP = -24.9 ± 26.7 mg C m^{-3} d^{-1}) and winter (NCP = -51.2 ± 8.51 mg C m^{-3} d^{-1}). In addition, we found that the higher CR occurred to the bottom layers of the river plume and nearshore zones wherein hypoxia happened, indicating a possible attribution of plankton community respiration to the hypoxia in the GGBA.

Keywords: primary production, community respiration, hypoxia, algal bloom, Pearl River Estuary

INTRODUCTION

Rising atmospheric CO_2 causes global climate change, which brings unprecedented challenges to human's sustainable development. As an important carbon reservoir on Earth, the ocean has been estimated to absorb 31 ± 4% of anthropogenic CO_2 from 1994 to 2007 (Gruber et al., 2019), wherein the plankton metabolisms mediate the exchange of CO_2 between air and sea (Odum, 1956; Falkowski, 1998; Duarte et al., 2013). The dynamics of gross primary production (GPP) and community respiration (CR) can directly reflect the carbon metabolism balance in marine ecosystems, as indicated by the net community production (NCP) (Duarte and Regaudie-de-Gioux, 2009; Cai, 2011). When the GPP is over the CR (i.e., NCP>0), marine ecosystem has a potential to absorb CO_2 and export organic matters and is thus autotrophic. When NCP <0, the marine ecosystem emits CO_2 and becomes a carbon source and is thus heterotrophic, and when NCP ≈ 0, the CO_2 absorption and emission tends to be in equilibrium (Duarte and Regaudie-de-Gioux, 2009; Caffrey et al., 2014). The carbon metabolism of the plankton community that often regulates the distribution and variation of carbon flux in marine ecosystem usually influences the evaluations of the carbon cycle and nutrient dynamics in the oceans.

The metabolism status of the marine plankton community is susceptible to multiple factors and shows greatly spatial and temporal changes (Karl et al., 2003). Therefore, it is not surprising that the controversial results often occur among different regions and seasons depended on whether the marine ecosystem is autotrophic or heterotrophic (Ducklow and Doney, 2013; Serret et al., 2015). A famous controversy is about the judgment of autotrophy or heterotrophy in oligotrophic oceans (Duarte et al., 2013; Williams et al., 2013). Such a debate of metabolic status also occurs in estuaries or bays. Many studies suggested that the estuarine and nearshore areas are heterotrophic and are the sources of CO_2 due to the land-derived inputs of excess organic carbon, while the continental shelves are autotrophic and the sinks of CO_2 (Heip et al., 1995; Caffrey, 2004; Borges et al., 2005; Duarte and Prairie, 2005; Chen et al., 2013; Cloern et al., 2014). However, some recent studies showed that some estuaries, coastal and coral reef areas are autotrophic (Bauer et al., 2013; McKinnon et al., 2017; Agusti et al., 2018; Garcia Corral et al., 2020). Such a controversy demonstrates that the metabolic-balanced characteristics, and potential driving mechanisms need to be studied further in combination with specific biological and environmental factors because the regional estuarine and coastal ecosystems are usually affected by various human activities and environmental forces with a spatial variance.

As one of major urban agglomerations in the world, the Guangdong-Hong Kong-Macao Greater Bay Area (GGBA or Greater Bay Area) is one of the regions with the strongest economic vitality and fastest development in China. The coastal area of the GGBA covers the Pearl River Estuary (PRE) and its adjacent waters (**Figure 1**) and forms a coastal ecosystem with diverse habitats (estuary, bay, and offshore waters) and high biodiversity (Yang et al., 2019; Yu, 2019; Wang et al., 2021). Due to the inputs of nutrients and organic matters, the estuarine and nearshore waters are important junction of connecting land to open sea with active biochemical geochemical cycles (Gattuso et al., 1998). Previous studies showed that the greatly regional variances often occurred in physical and chemical environments of the PRE and its

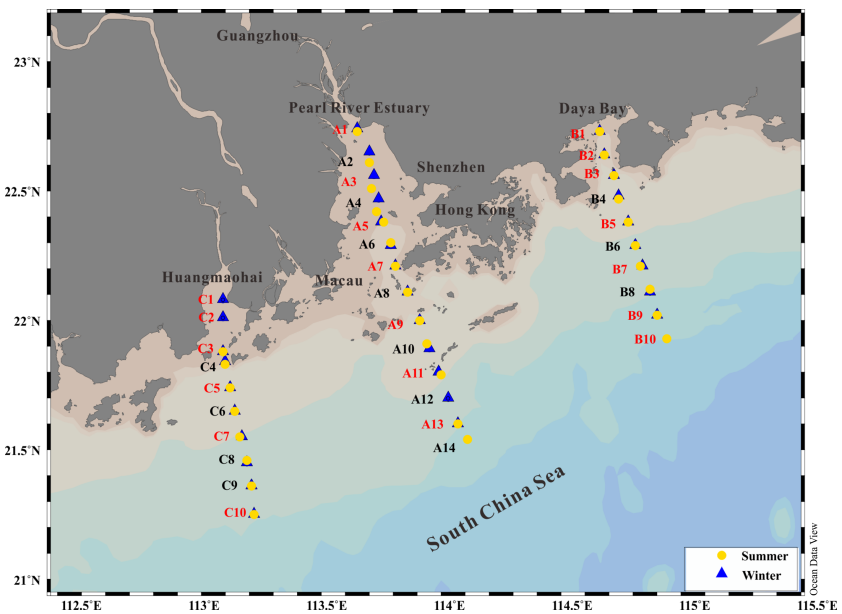

FIGURE 1 | Map indicating the sampling stations during the summer (yellow dots; July 14–24, 2019) and winter periods (blue triangles; December 8–18, 2020). Stations marked in red show where the cell size-fractionated Chl *a* measurements and metabolic experiments (GPP, CR, and NCP) were carried out.

adjacent waters due to the Pearl River runoffs, human activities, and other physical processes (such as coastal current and coastal upwelling), which further affected the carbon fixation process of plankton assemblages (Cai et al., 2002; Song et al., 2004; Song et al., 2011). Many studies also showed that phytoplankton primary production and microbial metabolism mainly mediated the air–sea carbon flux in the PRE (Cai et al., 2004; Guo et al., 2009; Dai et al., 2014; Li et al., 2019), suggesting the importance of plankton metabolisms in this ecosystem. However, there are few studies on the couplings of the respiration and primary production of the plankton community in coastal waters of the GGBA, therefore, the balance of autotrophic and heterotrophic processes and their variations and regulation mechanisms are still unclear as the environments therein are very complicated.

With rapid urbanization and economic growth, eutrophication, algal bloom, and hypoxia have become serious ecological and environmental problems in coastal waters of the GGBA (Yin et al., 2004a; Harrison et al., 2008; Song et al., 2009; Qian et al., 2018). As both algal bloom and hypoxia are closely related to the processes of plankton production and metabolism, studies on the balance between them and the influencing factors will help us to deeply understand the potential formation mechanism of these environmental and ecological events. Therefore, the GPP, CR, and NCP of the plankton community, as well as their associated environmental and biological factors were characterized in coastal waters of the GGBA during both wet (summer) and dry (winter) seasons, to clarify 1) the metabolic balance and carbon budget of plankton community in the GGBA and how the physical-environmental–biological factors shape their spatial and temporal variations; and 2) the relationship of plankton metabolic processes to the ecological risks of e.g., algal blooms and hypoxia events, as well as its potential indicative functions.

MATERIAL AND METHODS

Study Area and Sample Collection

In this study, we carried out the experiments in 3 transactions located in the PRE (A1-A14), Daya Bay (B1–B10), and Huangmaohai Bay (C1–C10) during wet (summer; July 14–24, 2019); and dry seasons (winter; December 8–18, 2020) (**Figure 1**). During the two investigations, the profiles of temperature, salinity, dissolved oxygen (DO), pH, turbidity, nutrients, and chlorophyll *a* (Chl *a*) concentration were obtained at all the 34 stations; and the cell size-fractionated Chl *a*, GPP, CR, and NCP in surface and bottom layers were measured at 20 of the 34 stations (labeled in red color). The seawater in the surface (~0.5 m depth), 5, 10, 15, 20, 30, 50 m, and bottom layers were collected with an acid-cleaned (1N HCl) 5-L polycarbonate bucket for Chl *a* and nutrient analysis as described below.

Environments and Chlorophyll *a* Measurements

At each station, the temperature, salinity, and DO profiles were measured with a multi-parameter water quality monitor Sonde (YSI 6600; Yellow Springs Instruments, Yellow Springs, OH, USA).

For nutrient analysis, the collected seawater from each depth was filtrated through 0.7 μm pore-sized glass fiber filters (25 mm, Whatman GF/F). The filtrate was then dispensed into an 80 ml polycarbonate bottle, frozen immediately, and stored at -20°C for subsequent analysis. Concentrations of NH_4^+, NO_2^-, NO_3^-, PO_4^{3-} (DIP), and SiO_3^{2-} were measured with an automatic nutrient analyzer (AA3; Seal Instruments, Hamburg, Germany) using the traditional colorimetry methods (Hansen and Koroleff, 1999). In this study, the DIN concentration was calculated as the sum of NH_4^+, NO_2^-, and NO_3^- concentrations.

For the Chl *a* measurement, 250 ml of collected seawater was prefiltered through a 200 μm mesh and then sequentially filtrated through a 20 μm pore-sized nylon-net filter (25 mm, Millipore), 3 μm pore-sized polycarbonate filter (25 mm, Millipore), and 0.7 μm pore-sized glass fiber filter (25 mm, Whatman GF/F) to collect micro- (>20 μm), nano- (3–20 μm), and pico cell-sized phytoplankton cells (<3 μm), respectively. The total Chl *a* was obtained by directly filtrating the 200 μm pore-sized mesh-prefiltered seawater onto a 0.7 μm pore-sized GF/F filter. All the filters with phytoplankton cells were stored at -20°C for later analysis. The Chl *a* concentration was measured fluorometrically using a Turner Designs 10 fluorometer (Parsons et al., 1984) after extracting in the dark for 24 h at 4°C in 10 ml acetone (90% v/v).

NCP, CR, and GPP

To measure NCP and CR, the collected seawater was gently siphoned into 6 narrow-mouth 250 ml borosilicate glass Winkler bottles. Approximately 3 of the 6 bottles were wrapped in aluminum foil for dark incubation, and the remaining 3 replicates were incubated with the neutral cloth covered to achieve an *in situ* light level. The *in situ* light conditions were measured with the Secci disk method (Song et al., 2012). After recording the initial DO level with a high-precision fluorescent oxygen probe (Microx 4; PreSens, Regensburg, Germany), all the Winkler bottles were incubated for 24 h in a water tanker with running surface seawater to control temperature. After the incubations, the final DO concentration in each bottle was measured again, and the NCP and CR were calculated as

$$\mathrm{NCP}\ (\mathrm{mg\ O_2\ m^{-3}\ d^{-1}}) = [\mathrm{O_2}]_{t24(\mathrm{Light})} - [\mathrm{O_2}]_{t0(\mathrm{Light})};$$

$$\mathrm{CR}\ (\mathrm{mg\ O_2\ m^{-3}\ d^{-1}}) = [\mathrm{O_2}]_{t0(\mathrm{Dark})} - [\mathrm{O_2}]_{t24(\mathrm{Dark})}$$

where $[O_2]_{t24}$ and $[O_2]_{t0}$ indicate the DO concentration at time 24 h and 0 in the dark or light bottles. The GPP was calculated as

$$\mathrm{GPP} = \mathrm{NCP} + \mathrm{CR}$$

GPP, CR, and NCP were converted to carbon units, assuming a photosynthetic quotient (PQ) of 1.3 and a respiratory quotient (RQ) of 1 (Gazeau et al., 2005; Hopkinson & Smith, 2005).

Statistical Analysis

Before doing analysis, the data were tested for normality (Shapiro–Wilk test) and the homogeneity of variance (Levene's test). Then, the independent *t* test or Mann–Whitney test was

used to identify the seasonal differences of environmental and metabolic factors. Principal component analysis (PCA) for environmental and biological factors was performed with CANOCO 5.0 software (Lepš and Šmilauer, 2003). Data were standardized to minimize the influence of the variances of variables, and the individual transformed observations were named scores (Wu et al., 2016). The GGBA was divided into several zones according to the scores of the first two principal components of each station as well as their actual geographical locations (Song et al., 2011); then, the regional differences of environments and metabolisms were identified between different zones. Tukey's honestly significant difference (HSD) test was used to verify the significance of regional differences of environmental and biological factors, and the results were visualized using "ggplot2" package in R v4.0.5 (Ginestet, 2011; Zhao et al., 2021). Spearman correlation was used to determine the correlation of environment factors to plankton community metabolisms, and the results were visualized using the "ggcor" package in R v4.0.5 (Huang et al., 2020). An optimal multiple regression model was used to evaluate the contribution of environmental factors to the variation of plankton community metabolisms in R v4.0.5 (Grömping, 2006; Field et al., 2012). To estimate the importance of the variables, percentage increases in the mean squared error (MSE) were used: higher MSE% values indicate more important variables, according to the result of Spearman correlation analysis and the optimal multiple regression model with variance decomposition analysis in R v4.0.5 (Jiao et al., 2020). The map of sampling stations, spatial distribution, and transection plots was drawn using Ocean Data View (Schlitzer, 2020).

RESULTS

Environmental Characteristics

In summer, the seawater stratification generally existed in the GGBA according to vertical distributions of salinity and temperature, and all the investigated areas in the PRE, Daya Bay, and Huangmaohai Bay showed clear stratification, especially in nearshore waters (**Figures 2A, B**). The isohaline of 20 psu extended to the distances of over 100 and 40 km in transections A and C, respectively (**Figure 2B**-1, -5), and the salinity was higher than 29 psu in transection B (**Figure 2B**-3). High DO and Chl *a* concentration generally appeared in the surface water , as well as in the offshore areas of transections A and B. Hypoxia events occurred in bottom of all three transections, with the lowest DO level of less than 2.2 mg L^{-1} in transection A (**Figure 2C**-1), less than 3.3 mg L^{-1} in transection B (**Figure 2C**-3), and less than 1.7 mg L^{-1} in transection C, respectively (**Figure 2C**-5). Moreover, the surface water with DIN levels of over 25 μmol L^{-1} extended to the distances of over 100 and 50 km far from the land in transections A and C, respectively (**Figure 2E**-1, -5). In winter, the water column was well mixed than that in summer. The isohaline of 20 psu shrank to the distances of less than 20 and 10 km far from the land in transections A and C, respectively (**Figure 2B**-2, -6).

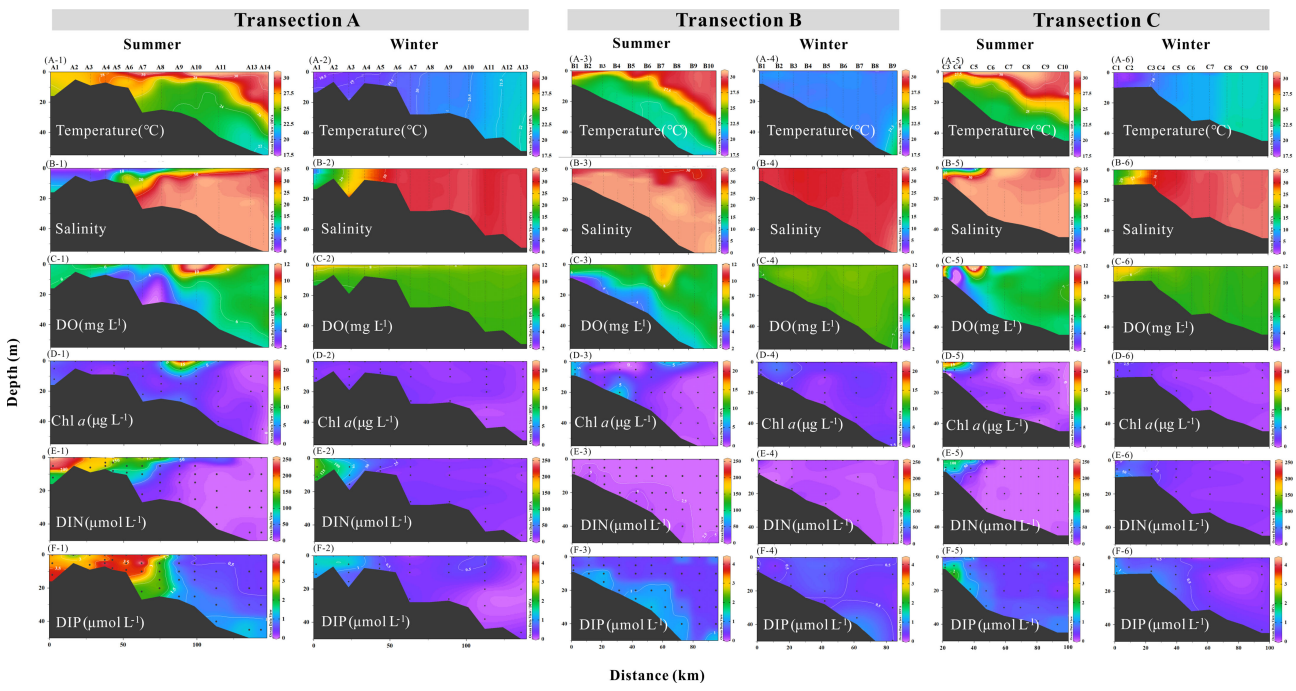

FIGURE 2 | Vertical distributions of temperature (**A**, °C), salinity **(B)**, DO (**C**, mg L^{-1}), Chl *a* concentration (**D**, μg L^{-1}), DIN (**E**, μmol L^{-1}), and DIP (**F**, μmol L^{-1}) along the transections **A**, **B**, and **C** in summer and winter periods.

Consistently, the DO concentration distributed evenly in vertical scale and no hypoxia happened in the bottom layer, and Chl *a* concentration was lower than summer (Mann–Whitney test, $p < 0.05$) especially in nearshore areas (**Figure 2D**). In addition, the surface water with higher DIN level (>25 μmol L^{-1}) in winter just extended to ~50 and ~30 km far from the land in transections A and C, respectively (**Figure 2E**-2, -6).

In general, nano-phytoplankton (3–20 μm) dominated (~60%) both the surface and bottom layers of nearshore waters of all three transections during summer and winter periods, while the pico-phytoplankton (<3 μm) dominated (~50%) both layers of the offshore waters. Moreover, contribution of nano-Chl *a* to total Chl *a* decreased offshore-ward, while that of pico-Chl *a* increased. The contribution of micro-Chl *a* (>20 μm) to total Chl *a* (i.e., varying from 3.17% to 38%) showed no clear spatial change from nearshore to offshore waters (**Figure 3**).

Plankton Community Metabolisms

Coinciding with Chl *a* biomass, the GPP varied from 52.3 to 661 mg C m^{-3} d^{-1} in surface water during the summer period and decreased from nearshore to offshore waters (**Figure 4A**-1). The GPP reached as high as 661 mg C m^{-3} d^{-1} in estuarine–offshore waters, and such high GPP waters extended from southeast to northwest of the investigated area. In winter, however, the GPP ranged from 19.2 to 303 mg C m^{-3} d^{-1} and was significantly lower than that in summer (Mann–Whitney test, $p < 0.05$). The highest GPP (i.e., 303 mg C m^{-3} d^{-1}) was observed in nearshore waters of the Daya Bay (**Figure 4A**-2). Moreover, the GPP in the bottom layer was very low in both summer and winter periods (i.e., summer, 19.5 ± 4.5 mg C m^{-3} d^{-1}; winter, 8.9 ± 1.5 mg C m^{-3} d^{-1}), and displayed less spatial variation than that in surface water (**Figure 4A**-3, -4).

Similarly, surface CR varied from 65.0 to 1,213 mg C m^{-3} d^{-1} in summer, and the active CR co-occurred with high GPP and Chl *a*, e.g., the CR reached up to 1,213 mg C m^{-3} d^{-1} in the

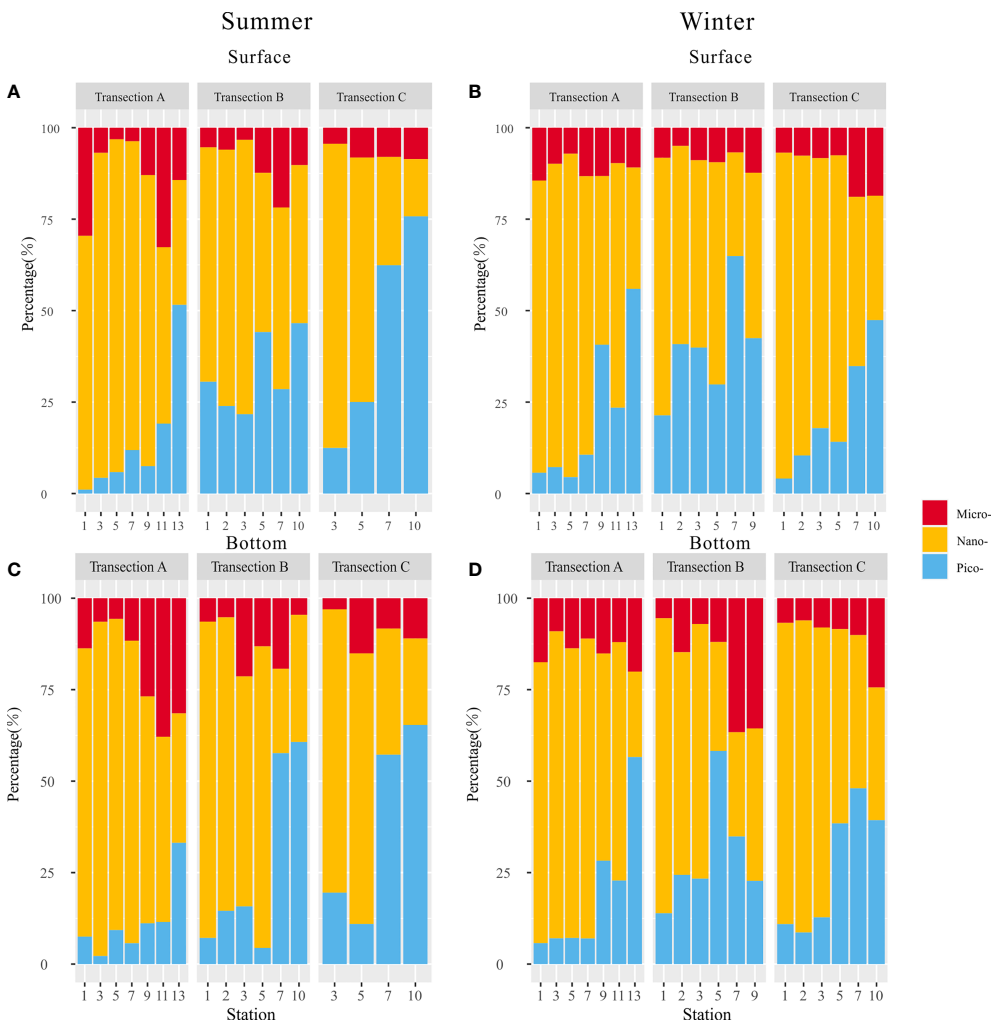

FIGURE 3 | Contribution (%) of three cell size-fractioned Chl *a* in surface and bottom seawater along transections **(A–C)** of the GGBA in summer **(A–C)** and winter **(B, D)** periods.

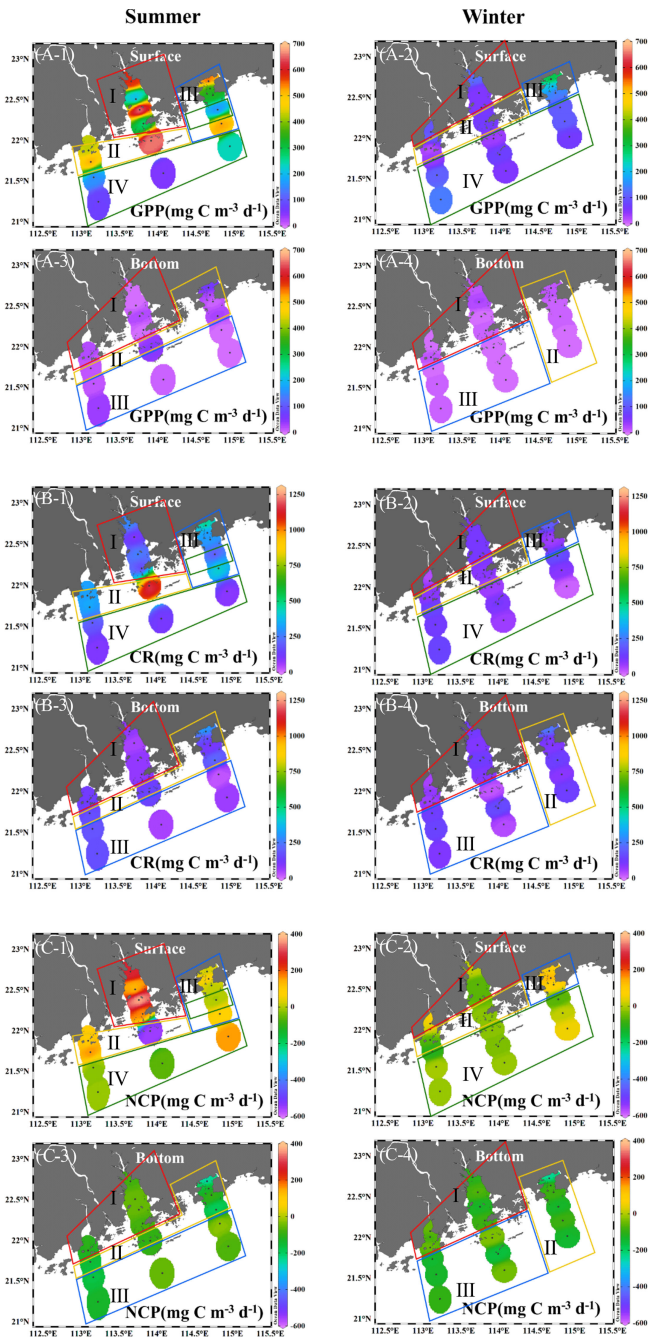

FIGURE 4 | Distribution characteristics of GPP (**A**, mg C m^{-3} d^{-1}), CR (**B**, mg C m^{-3} d^{-1}), and NCP (**C**, mg C m^{-3} d^{-1}) in surface and bottom seawater along transections **(A-C)** of the GGBA in summer and winter periods. The clusters divided here are consistent with the clusters shown in **Figure 5**.

interface of plume- and saline-waters, where the GPP and Chl *a* reached as high as 659 mg C m^{-3} d^{-1} and 21.7 μg L^{-1}, respectively (**Figure 4B**-1). In winter, the surface CR varied from 20.0 to 210 mg C m^{-3} d^{-1} (**Figure 4B**-2). As compared to surface water, the CR in the bottom layer was markedly lower in summer (Mann–Whitney test, $p < 0.05$); however, such a difference did not occur in winter (**Figure 4B**-3, -4) and no significant difference occurred between summer and winter periods either (i.e., 131 ± 79.9 vs. 110 ± 51.4 mg C m^{-3} d^{-1}).

The NCP in surface water ranged from -554 to 377 mg C m^{-3} d^{-1} in summer and showed a similar spatial change as the GPP and CR (**Figure 4C**-1). The highest NCP presented in inner PRE, while the lowest appeared in the interface of plume- and saline- water. In winter, surface NCP varied from -113 to 141 mg C m^{-3} d^{-1} and was

lower than that in summer (Mann–Whitney test, $p < 0.05$) (**Figure 4C**-2). The NCP in the bottom layer appeared to be negative in both summer and winter periods (**Figure 4C**-3, -4), with the lowest values of -245 mg C m^{-3} d^{-1} in summer and of -241 mg C m^{-3} d^{-1} in winter presented in the Daya Bay. Moreover, the surface water of the GGBA was generally autotrophic in summer , and was close to the metabolic balance in winter; while the bottom water was heterotrophic in both investigated periods (**Figure 4C**).

Principal Component Analysis Results on Regional Variances

Based on the PCA results in surface water as well as the geographical locations, the investigated area of the GGBA was divided into four regional zones (**Figures 5A, B**). In summer, Zone I that is located in the PRE had lower salinity and higher DIP, DIN, and SiO_3^{2-} concentrations (**Figures 6B, D, E**; **Table S1**). Zone II had intermediate salinity between Zone I and Zone III or IV, as well as nutrient content. Moreover, Zone II had the highest DO and Chl *a* concentration among all four zones, wherein the GPP was higher as well (**Figures 6C, F, J**). Zones III and IV located in the coastal area of the Daya Bay and the far-offshore area of the GGBA respectively, and had higher salinity and lower nutrient loadings than Zones I and II (**Figures 6B, D, E**; **Table S1**). Zone III had lower temperature but higher DIN, DIP, and SiO_3^{2-}, as compared to Zone IV (**Figures 6A, D, E**; **Table S1**). Moreover, pico-Chl *a* allocation in Zone III was higher than Zones I and II but lower than Zone IV (**Figure 6I**-1). The proportion of nano-phytoplankton in Zone IV was significantly lower, as compared to other zones (**Figure 6H**-1). In addition, Chl *a*, GPP, and CR in Zone IV were lowest among all zones of the GGBA (**Figures 6F, J, K**; **Table S1**).

In winter, the surface water of Zone I is located near the PRE and Huangmaohai Bay and covered a narrower area than summer, and was closer to the upper reaches of the PRE. The salinity in Zone I was significantly lower than that in other zones (**Figure 6B**-2), while the DIP, DIN, and SiO_3^{2-} concentrations were significantly higher (**Figures 6D, E**; **Table S1**) but with moderate Chl *a* and lower GPP and NCP (**Figures 6F, J, L**). Zone II covered the interface area of fresh- and saline-water and was closer to the coast, as compared to summer. The salinity in Zone II was lower than that of Zone III or IV, and the DIN was higher than that of Zone III and IV; however, the DIP was lower, leading to the higher N:P ratio (~82) than that in Zone III (~13) or IV (~31) (**Figures 6B, D, E**; **Table S1**). Surface Chl *a* in Zone II appeared to be moderate, just higher than Zone IV but lower than Zone III (**Figure 6F**-2). The GPP and NCP in Zone II were lower either, while the CR was similar to the other zones (**Figures 6J, K, L**). As compared to summer, Zone III in winter just covered the

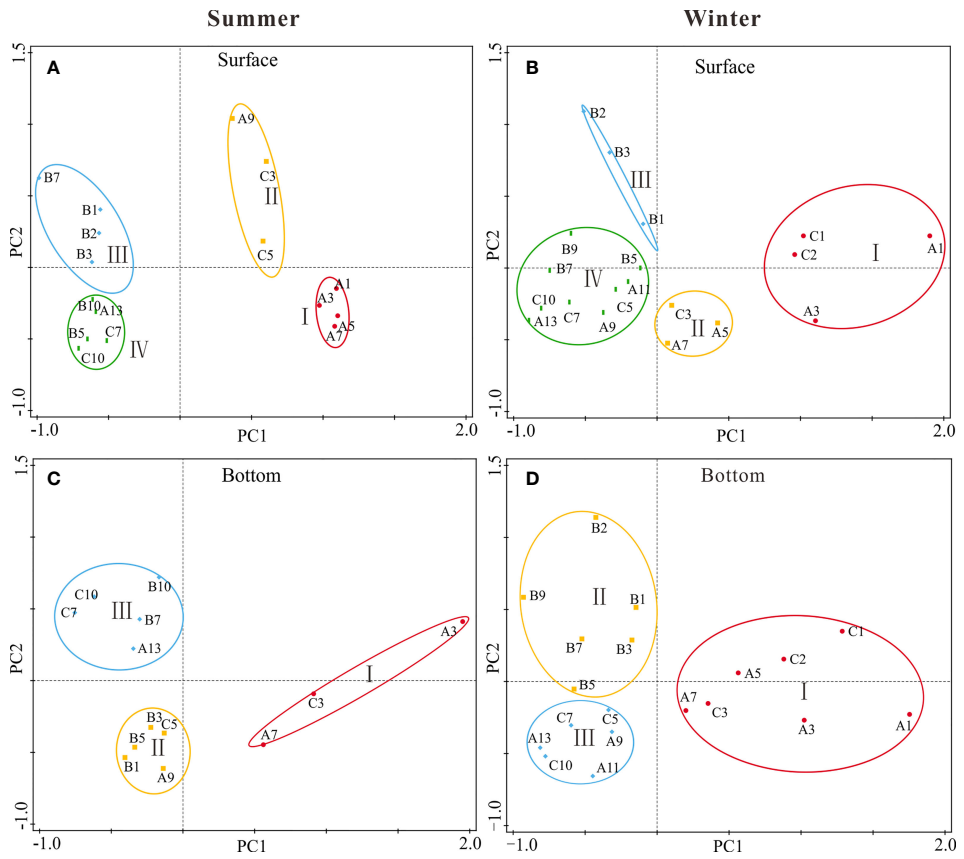

FIGURE 5 | PCA results of environmental and biological characteristics in surface **(A, B)** and bottom **(C, D)** seawater along transections **(A–C)** of the GGBA in summer **(A, C)** and winter **(B, D)** periods.

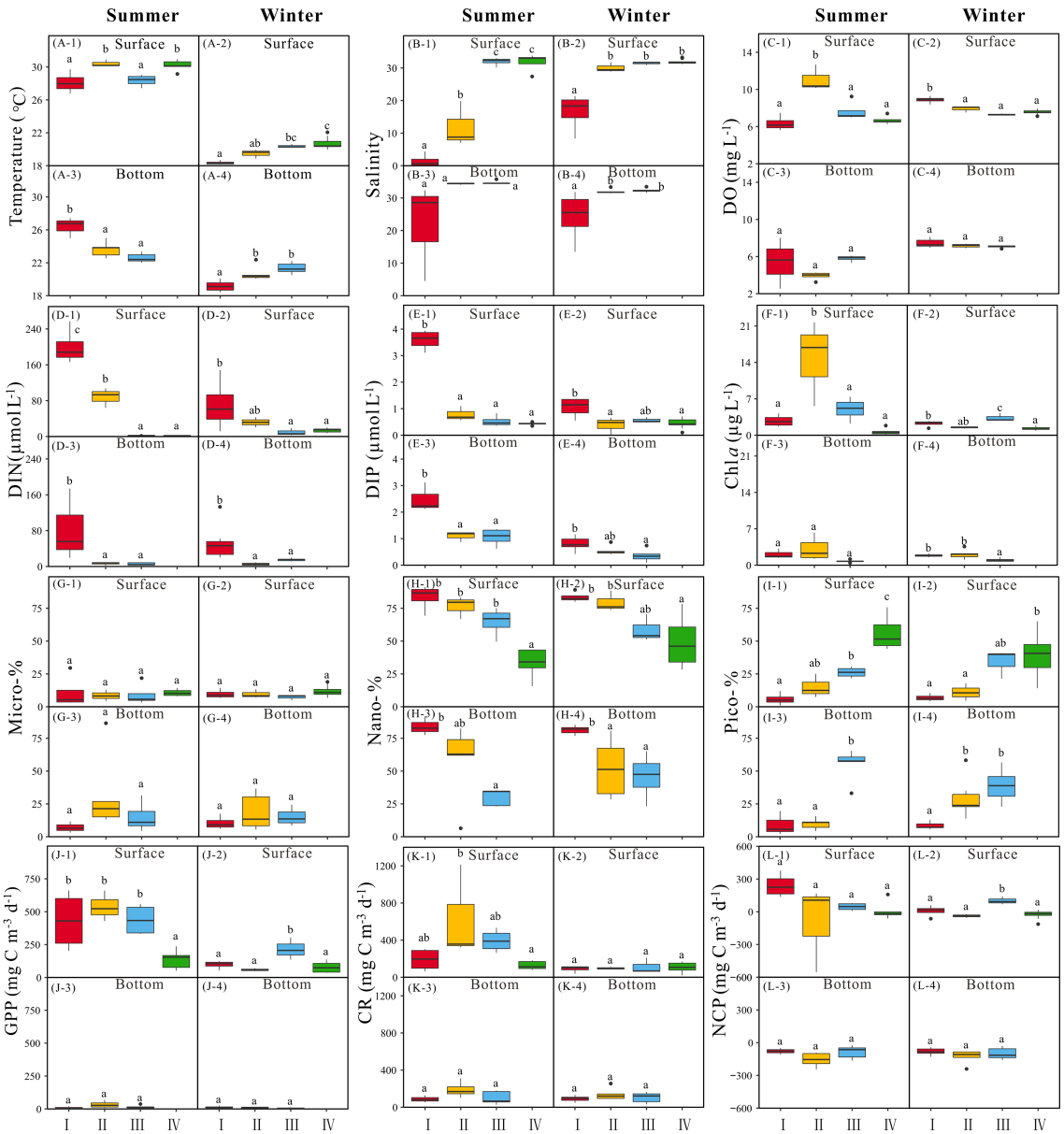

FIGURE 6 | Regional variance of temperature (**A**, °C), salinity **(B)**, DO (**C**, mg L^{-1}), DIN (**D**, μmol L^{-1}), DIP (**E**, μmol L^{-1}), Chl a concentration (**F**, μg L^{-1}), Micro-% **(G)**, Nano-% **(H)**, Pico-% **(I)**, GPP (**J**, mg C m^{-3} d^{-1}), CR (**K**, mg C m^{-3} d^{-1}) and NCP (**L**, mg C m^{-3} d^{-1}) in surface (-1, -2) and bottom (-3, -4) layer along transections of the GGBA in summer (-1, -3) and winter (-2, -4) periods. Different letters in each box plot indicate the significant differences among different groups (Turkey' HSD test, $p < 0.05$)

nearshore area of the Daya Bay, wherein the salinity, temperature, and DIP were higher than Zone II or IV (**Figures 6A, B, E**). The Chl *a*, GPP, and NCP in Zone III were significantly higher than other zones (**Figures 6F, J, L**). Zone IV that covered a wider range of the offshore area in winter than summer had higher temperature and salinity than other zones but lower DIP, DIN and SiO_3^{2-} concentrations. Moreover, Zone IV had the lowest Chl *a*, GPP, and NCP among all zones in winter (**Figure 6**; **Table S1**).

In contrast to surface water, the bottom water that generally had higher salinity and lower temperature (**Figures 6A, B**), as well as lower Chl *a*, GPP, CR, and NCP (**Figures 6F, J, K, L**), was divided into three zones in both summer and winter periods (**Figures 5C, D**). In summer, Zone I that is located in the inner parts of the PRE and Huangmaohai Bay had higher temperature and nutrients, as well as lower salinity (**Figures 6A, B, D, E**; **Table S1**). Zone II covered the inner part of the Daya Bay and the interface area of fresh- and saline-water, wherein it had the lowest DO among all three zones (**Figure 6C**-3). Nano-phytoplankton dominated Zone II, wherein GPP and CR were highest and NCP was most negative (**Figures 6H, J, K, L**). Zone III covered the offshore waters off Zone II and was dominated by pico-phytoplankton and characterized with lower nutrients and Chl *a* (**Figures 6I, D, E, F**). Moreover, the

GPP and CR in Zone III were low too, and the NCP was even closer to zero (**Figures 6J, K, L**).

In winter, the bottom water of Zone I covered similar area as in summer, and had the highest nutrients concentration and lowest temperature and salinity among all three zones (**Figures 6A, B, D, E**). Moreover, the Chl *a* and NCP in Zone I were higher than Zone II or III, and nano-phytoplankton dominated therein (**Figures 6F, H, L**). Zone II is located in the Daya Bay and covered its offshore area, but did not cover the coastal waters of the PRE and Huangmaohai Bay. Zone III covered the offshore waters of the investigated area except that off the Daya Bay. Both the Zones II and III were characterized with the higher temperature and salinity than Zone I, as well as lower nutrients (**Figures 6A, B, D, E**). The pico-Chl *a* allocation was higher in these two zones (**Figure 6I**-4). Finally, the Chl *a* biomass in Zone II was higher than that in Zone III, while the proportion of pico-Chl *a* was lower (**Figure 6**; **Table S1**).

DISCUSSION

Regulation of Plankton Community Metabolisms

The environmental factors that influence the production and consumption of plankton community include temperature, light, nutrients, and turbidity (Rochelle-Newall et al., 2007; Kemp and Testa, 2011). Previous studies showed that temperature and nutrients are key factors to regulate the primary production and community respiration of the estuaries and their adjacent coastal areas (Caffrey, 2004; Caffrey et al., 2014; Hung et al., 2014). Consistently, in this study temperature and nutrients were identified as the key environmental factors for regulating the metabolisms of the plankton community of the GGBA, although the extent of these regulations on the GPP and CR differed greatly. According to the optimal regression model, field temperature explained more variance of the surface CR as compared to other variables, while the nutrients explained more of the GPP (**Figure 7**). Furthermore, the surface NCP was positively correlated to GPP ($p < 0.01$), but not to CR ($p > 0.05$) (**Table S2**), again indicating that the nutrients regulate the GPP and thus vary the NCP of the surface waters of GGBA. However, such differences in regulatory factors between primary production and respiratory metabolism were not obvious in the bottom waters, since the multiple regression analysis result suggests the similar key environmental factors explaining the variation of GPP and CR, both of which are significantly correlated with NCP ($p < 0.01$) (**Figure 7**; **Table S2**).

Coastal ecosystems of the GGBA are usually influenced by the Pearl River runoffs, Yuedong Coastal Current, and intruded oligotrophic oceanic water from the South China Sea (Yin

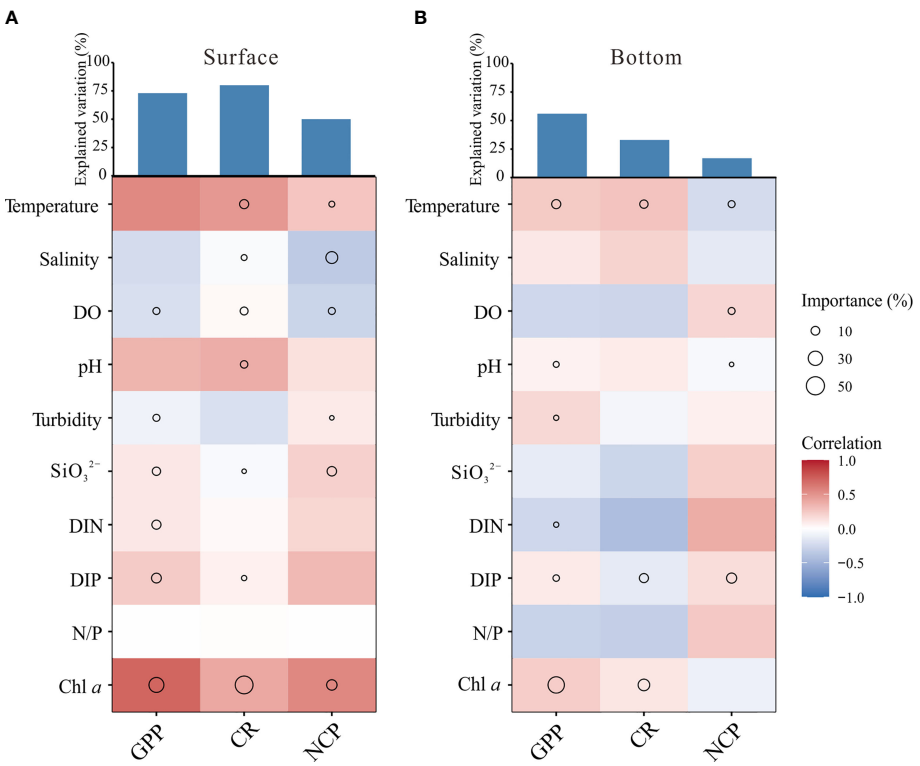

FIGURE 7 | Contribution of environmental factors to variation of GPP, CR, and NCP based on optimal multiple regression model in **(A)** surface and **(B)** bottom layers. The above bar graph indicates the total contribution, and the heat plot indicates the Spearman correlation coefficients. The size of circles indicates the importance of environmental variables.

et al., 2004a; Harrison et al., 2008; Song et al., 2011; Zu et al., 2014; Zu and Gan, 2015). Together with the influences of monsoon, tide, topography, and anthropogenic inputs, the metabolic processes of plankton community in this area varied greatly in spatial and seasonal scales (**Figure 4**). In this case, the regional analysis would be helpful to get a clear understanding about the complex relationship between community metabolism and driving forces in each regions. According to the PCA results, the GGBA was divided into different zones (**Figure 5**), corresponding to the different extent of the comprehensive effects of driving factors like the Pearl River runoffs, anthropogenic activities, and offshore water currents. These regional differences are more obvious in the upper water layer due to the generally higher and more various impacts of the driving factors therein (**Figure 6**; **Table S1**; Song et al., 2011; Dai et al., 2014; Zu et al., 2014).

The upper reach of the PRE (Zone I) was mainly influenced by the runoffs of Pearl River, with the influence range extending more seaward in summer. This region had the highest nutrient level but not highest Chl *a* and GPP (**Figure 6**; **Table S1**), probably due to the restriction of solar irradiation caused by the high turbidity and low transparency and disturbance therein (Lu and Gan, 2015). However, the metabolic state of this region was generally autotrophic in summer, inconsistent to other eutrophic estuaries where they were usually reported to be heterotrophic (Ducklow and McCallister, 2004; Caffrey et al., 2014), which may be explained by the greater negative effect of high disturbance upon the CR than the GPP (Alizadeh et al., 2018).

The river plume-dominated area (Zone II) often expands wider in summer due to the increased land-derived runoffs (**Figure 2**; Zu and Gan, 2015; Zhao et al., 2020) and was characterized with high Chl *a* and primary production (**Figure 6**; **Table S1**), consistent with previous studies (Yin et al., 2000; Yin et al., 2004b; Harrison et al., 2008; Song et al., 2011; Lu and Gan, 2015). Nutrients in this area are plentiful, and the restrictions of temperature, turbidity, and so on are less, probably leading to the higher primary production and plankton respiration (**Figure 4A, B**). In particular, the surface CR in this region is close to or even higher than the GPP, which may be attributed to the active metabolic decomposition during the post-algal bloom period (**Figures 2**, **4**; **Table S1**; Buchan et al., 2014; Wemheuer et al., 2014), thus resulting in the low NCP and even a partially heterotrophic state.

The eastern nearshore area of the GGBA (Zone III) was less affected by the runoffs of Pearl River. So, the nutrient sources of this region are mainly taken from anthropogenic activities and terrigenous inputs, as well as the vertical upwelling in a certain period of rainy season (Song et al., 2015; Wu et al., 2017; Zhang et al., 2019), which may increase the GPP and CR to some extent. Moreover, the metabolic process in this zone was more active than the upper reaches of the PRE as well, possibly due to low turbidity. This coastal water showed an obvious autotrophic state in its surface layer in both summer and winter, being consistent with other coastal waters of e.g., the coastal waters of the Red Sea and the northern Australia (McKinnon et al., 2017; López-Sandoval et al., 2019). The far-offshore region (Zone IV), where had low GPP and CR, is understandable due to the offshore oligotrophic water with low nutrients and organic matters. In addition, a weak heterotrophy occurred in this region, indicating the primary production could not satisfy the requirements of community metabolism. It is consistent with the results from the similar oligotrophic oceanic waters (Duarte et al., 2013; Regaudie-de-gioux and Duarte, 2013).

The bottom water in the GGBA was less influenced by the Pearl River runoffs, and thus more stable than surface water, with the environmental factors varying less in both temporal and spatial scales (**Figures 2**, **6**; Zu et al., 2014). Due to lacking solar light, the GPP therein was low; so, the regional variation of NCP could mainly be dependent on the CR (**Table S2**). Moreover, efficient transport of organic and inorganic nutrients *via* terrestrial inputs or downward depositions from the high-GPP upper water may make the community metabolism more active in nearshore areas (Ke et al., 2019; Dan et al., 2021), while in bottom of the offshore waters, the community metabolism was less active (**Figure 6**; **Table S1**), probably resulting from the lacking nutrient inputs.

The Greater Bay Area covers the coastal areas with spatially environmental diversity. The corresponding spatial variations of key environmental factors, such as nutrient supply, turbidity and temperature lead to the regional complexity of plankton metabolic processes. According to the water-column integrated data, the plankton community metabolisms in winter shifted from heterotrophy in upper reaches of the estuary to autotrophy in nearshore waters and back to heterotrophy again in offshore waters, consistent with other coasts (Gattuso et al., 1998; Ducklow and McCallister, 2004). In summer however, the expansion of river plume led to a large-scale heterotrophy in coastal waters off the PRE accompanying with an algal bloom, which has seldom been reported before. This is possibly because that the heterotrophic processes during the algal bloom are more active than primary production, thus leading to the negative state of metabolic balance (Song et al., 2021).

Plankton Metabolisms as Indicators of Ecosystem Health and Carbon Budget

The metabolic status of the plankton community is an important indicator for the health and carbon budget of an ecosystem. Liu et al. (2012) reported the close relationship between high primary production and algal blooms in nearshore waters of the Daya Bay and suggested the primary production as an index of coastal eutrophication. Similarly, here, an obviously high GPP was associated with an algal bloom [featured as maximum Chl *a* >20 μg L^{-1}, more than twice of the criterion value described by He et al. (2013)] in the Pearl River plume during summer period (**Figures 2**, **4**). Previous studies showed that this area is conducive to the primary production process and biomass accumulation due to the large amount of nutrient inputs from river runoffs, as well as the more stable water column in summer, resulting in the frequent records of algal blooms (Yin et al., 2000; Yin et al., 2004b; Harrison et al., 2008; Song et al., 2011; Lu and Gan, 2015; Alizadeh et al., 2018). In contrast, the upper reaches of the estuary are less likely to form algal blooms, since

phytoplankton production therein are usually limited by turbidity and river-flow disturbance.

Hypoxia often occurs in the bottom water of the GGBA in summer, such as in the PRE and Daya Bay (Yin et al., 2004a; Song et al., 2015; Li et al., 2018; Lu et al., 2018; Qian et al., 2018). In summer, obvious stratification often forms in estuarine and coastal waters, which may block the transportation of oxygen from upper to bottom layers and thus hydrologically increase the probability of hypoxia (**Figure 2**; Lu and Gan, 2015; Zhao et al., 2020). On the other hand, high production in the upper layer usually enhances the downward transportation of organic carbon, which may have favored the community respiration in the bottom layer, and thus led to the negative NCP value and heterotrophy therein (Li et al., 2019). Consistently, the higher bottom CR, as compared to its adjacent waters, occurred around the high surface GPP area within the river plume (**Figure 4**). In addition, the benthic respiration (mainly microbial metabolism) may also benefit from the downward transportation of excess organic matters that are associated with high primary production in surface water (Aller et al., 2008; Zhu et al., 2011). Therefore, the high oxygen consumption in summer due to the active community metabolism and long-term stratification may result in the low DO in bottom water (**Figure 2**). It is also suggested that the formation of hypoxic zone is closely related to the massive growth and reproduction of surface phytoplankton cells (Qian et al., 2018). More interestingly, the bottom hypoxia zone in the estuary was not rightly located under the areas with high surface Chl *a* and primary production but under its adjacent area (**Figure 2**). This can be explained by the saltwater wedge effect that has transported the sinking organic matters to the nearby area through the current intrusion in lower or bottom layer (Hu and Li, 2009). However, this is not the case in the Daya Bay because there is no such wedge effect (**Figure 2**). The hypoxia seldom happened in winter either (**Figure 2**), possibly due to the strong vertical mixing caused by northeastern monsoon that has transported the high DO surface water to the bottom layer and thus enhanced the DO level therein. The lower temperature in winter may be another cause through enhancing oxygen solubility and lowering respiration metabolic rate.

A previous study suggested that annual sea–air CO_2 exchange near the PRE was close to equilibrium, and the CO_2-absorbing capacity was enhanced in summer (Zhai et al., 2013). In this study, the primary production and community respiration in the GGBA is close to be balanced in both winter and summer, and NCP is also higher in summer (Mann-Whitney test, $p < 0.05$), indicating the high similarity and potential correlation between the community metabolic carbon flux and carbon budgets. Moreover, the specific distribution of plankton community carbon budget varied greatly in spatial and temporal scales, making it difficult to exactly evaluate the detailed carbon flux. It is generally believed that the upstream of estuaries is the source of CO_2, while the waters controlled by a river plume is the sink due to the high primary production (Guo et al., 2009; Dai et al., 2014). In this study however, the metabolic respiration appeared to be more active than primary production in river plume in summer, probably contributing to the carbon export of this area. In the eastern coastal part of the GGBA, the plankton community metabolisms were much less affected by the Pearl River runoffs, making this area appear to be a carbon source in both winter and summer (**Figure 4**). This heterotrophy also existed in the nearshore waters of the Daya Bay during a certain summer period (Li et al., 2021), suggesting the complication of ecosystem carbon flux even in a small-scaled area like the GGBA due to its temporal and spatial variations of the impacts of anthropogenic activities and other environmental factors.

In conclusion, we found that the field plankton community metabolisms in the GGBA showed a great regional difference in both summer and winter periods, interactively influenced by the physical–environmental–biological factors. The surface water of the GGBA exhibited autotrophic in summer, while such an autotrophic in summer status was weaker in winter; however, the bottom water exhibited heterotrophic in both summer and winter periods. Our results also showed that the high surface GPP and bottom CR can be considered as the important indicators for the algal blooms and hypoxia events that happened during that time in the GGBA. Further studies on the dynamic variations of plankton metabolism and its driving mechanisms are necessary for an in-depth understanding of the function of coastal ecosystem and better assessment and management of potential ecological risks.

DATA AVAILABILITY STATEMENT

The original contributions presented in the study are included in the article/**Supplementary Material**. Further inquiries can be directed to the corresponding author.

AUTHOR CONTRIBUTIONS

LZ, XS, and GL designed the experiments and analyzed the data. CX, YH, XF, and CZ conducted the shipboard sampling and environmental measurements. LZ and YH performed the *in situ* plankton metabolism measurements. ZW and ZO conducted nutrient measurements. LZ, XS, GL, and CX wrote, discussed, and edited the paper. All authors contributed to the article and approved the submitted version.

FUNDING

This study was supported by National Natural Science Foundation under contract No. 41890853; Southern Marine Science and Engineering Guangdong Laboratory (Guangzhou) under contract No. GML2019ZD0404; Science & Technology Basic Resources Investigation Program of China under contract No. 2018FY100105; Innovation Academy of South China Sea Ecology and Environmental Engineering, Chinese Academy of Sciences (NO. ISEE2018ZD02); the National Key Basic Research Program of China (973 program, No. 2015CB452904), Development Project of China under contract Nos 2017YFC0506302 and 2016YFC0502805.

SUPPLEMENTARY MATERIAL

The Supplementary Material for this article can be found online at: https://www.frontiersin.org/articles/10.3389/fmars.2022.844970/full#supplementary-material

Supplementary Table 1 | Characteristics of environment and plankton community metabolism in different zones of the GGBA.

Supplementary Table 2 | Spearman correlation index of plankton community metabolic parameters and ecological environmental factors in the GGBA * indicates $p < 0.05$; ** indicates $p < 0.01$.

REFERENCES

Agusti, S., Vigoya, L., and Duarte, C. M. (2018). Annual Plankton Community Metabolism in Estuarine and Coastal Waters in Perth (Western Australia). *PeerJ* 6, e5081. doi: 10.7717/peerj.5081

Alizadeh, M. J., Kavianpour, M. R., Danesh, M., Adolf, J., Shamshirband, S., Chau, K. W., et al. (2018). Effect of River Flow on the Quality of Estuarine and Coastal Waters Using Machine Learning Models. *Eng. Appl. Comput. Fluid. Mech.* 12, 810–823. doi: 10.1080/19942060.2018.1528480

Aller, R. C., Blair, N. E., and Brunskill, G. J. (2008). Early Diagenetic Cycling, Incineration, and Burial of Sedimentary Organic Carbon in the Central Gulf of Papua (Papua New Guinea). *J. Geophys. Res.* 113, F01S09. doi: 10.1029/2006jf000689

Bauer, J. E., Cai, W. J., Raymond, P. A., Bianchi, T. S., Hopkinson, C. S., and Regnier, P. A. (2013). The Changing Carbon Cycle of the Coastal Ocean. *Nature* 504, 61–70. doi: 10.1038/nature12857

Borges, A. V., Delille, B., and Frankignoulle, M. (2005). Budgeting Sinks and Sources of CO_2 in the Coastal Ocean: Diversity of Ecosystems Counts. *Geophys. Res. Lett.* 322019, 1–4. doi: 10.1029/2005gl023053

Buchan, A., Lecleir, G. R., Gulvik, C. A., and González, J. M. (2014). Master Recyclers: Features and Functions of Bacteria Associated With Phytoplankton Blooms. *Nat. Rev. Microbiol.* 12, 686–698. doi: 10.1038/nrmicro3326

Caffrey, J. M. (2004). Factors Controlling Net Ecosystem Metabolism in U.S. Estuaries. *Estuaries* 27, 90–101. doi: 10.1007/bf02803563

Caffrey, J. M., Murrell, M. C., Amacker, K. S., Harper, J. W., Phipps, S., and Woodrey, M. S. (2014). Seasonal and Inter-Annual Patterns in Primary Production, Respiration, and Net Ecosystem Metabolism in Three Estuaries in the Northeast Gulf of Mexico. *Estuar. Coast.* 37, 222–241. doi: 10.1007/s12237-013-9701-5

Cai, W.-J. (2011). Estuarine and Coastal Ocean Carbon Paradox: CO_2 Sinks or Sites of Terrestrial Carbon Incineration? *Ann. Rev. Mar. Sci.* 3, 123–145. doi: 10.1146/annurev-marine-120709-142723

Cai, W.-J., Dai, M., Wang, Y., Zhai, W., Huang, T., Chen, S., et al. (2004). The Biogeochemistry of Inorganic Carbon and Nutrients in the Pearl River Estuary and the Adjacent Northern South China Sea. *Cont. Shelf. Res.* 24, 1301–1319. doi: 10.1016/j.csr.2004.04.005

Cai, Y., Ning, X., and Liu, Z. (2002). Studies on Primary Production and New Production of the Zhujiang Estuary, China. *Acta Oceanol. Sin.* 24, 101–111.

Chen, C.-T., Huang, T.-H., Chen, Y.-C., Bai, Y., He, X., and Kang, Y. (2013). Air–sea Exchanges of CO_2 in the World's Coastal Seas. *Biogeosciences* 10, 6509–6544. doi: 10.5194/bg-10-6509-2013

Cloern, J. E., Foster, S. Q., and Kleckner, A. E. (2014). Phytoplankton Primary Production in the World's Estuarine-Coastal Ecosystems. *Biogeosciences* 11, 2477–2501. doi: 10.5194/bg-11-2477-2014

Dai, M., Gan, J., Han, A., Kung, H., and Yin, Z. (2014). "Physical Dynamics and Biogeochemistry of the Pearl River Plume," in *Biogeochemical Dynamics at Large River–Coastal Interfaces*. Eds. T. Bianchi, M. Allison and W. J. Cai (Cambridge University Press, Cambridge), 321–352. doi: 10.1017/CBO9781139136853

Dan, S. F., Li, S., Yang, B., Cui, D., Ning, Z., Huang, H., et al. (2021). Influence of Sedimentary Organic Matter Sources on the Distribution Characteristics and Preservation Status of Organic Carbon, Nitrogen, Phosphorus, and Biogenic Silica in the Daya Bay, Northern South China Sea. *Sci. Tot. Environ.* 783, 146899. doi: 10.1016/j.scitotenv.2021.146899

Duarte, C. M., and Prairie, Y. T. (2005). Prevalence of Heterotrophy and Atmospheric CO_2 Emissions From Aquatic Ecosystems. *Ecosystems* 8, 862–870. doi: 10.1007/s10021-005-0177-4

Duarte, C. M., and Regaudie-De-Gioux, A. (2009). Thresholds of Gross Primary Production for the Metabolic Balance of Marine Planktonic Communities. *Limnol. Oceanogr.* 54, 1015–1022. doi: 10.4319/lo.2009.54.3.1015

Duarte, C. M., Regaudie-De-Gioux, A., Arrieta, J. M., Delgado-Huertas, A., and Agustí, S. (2013). The Oligotrophic Ocean Is Heterotrophic. *Ann. Rev. Mar. Sci.* 5, 551–569. doi: 10.1146/annurev-marine-121211-172337

Ducklow, H. W., and Doney, S. C. (2013). What Is the Metabolic State of the Oligotrophic Ocean? A Debate. *Ann. Rev. Mar. Sci.* 5, 525–533. doi: 10.1146/annurev-marine-121211-172331

Ducklow, H. W., and McCallister, S. L. (2004). "The Biogeochemistry of Carbon Dioxide in the Coastal Oceans," in *The Sea, Volume 13, The Global Coastal Ocean-Multiscale Interdisciplinary Processes*. Eds. A. R. Robinson, K. Brink, J. Wiley and Sons, (New York: Harvard University Press).

Falkowski, P. G. (1998). Biogeochemical Controls and Feedbacks on Ocean Primary Production. *Science* 281, 200–206. doi: 10.1126/science.281.5374.200

Field, A., Miles, J., and Field, Z. (2012). *Discovering Statistics Using R.* (London: Sage Publications).

García Corral, L. S., Agusti, S., and Duarte, C. M. (20201142). Plankton Community Metabolism in Western Australia: Estuarine, Coastal and Oceanic Surface Waters. *Front. Mar. Sci.* 7. doi: 10.3389/fmars.2020.582136

Gattuso, J. P., Frankignoulle, M., and Wollast, R. (1998). Carbon and Carbonate Metabolism in Coastal Aquatic Ecosystems. *Ann. Rev. Ecol. Syst.* 29, 405–434. doi: 10.1146/annurev.ecolsys.29.1.405

Gazeau, F., Borges, A. V., Barrón, C., Duarte, C. M., Iversen, N., Middelburg, J. J., et al. (2005). Net Ecosystem Metabolism in a Micro-Tidal Estuary (Randers Fjord, Denmark): Evaluation of Methods. *Mar. Ecol. Prog. Ser.* 301, 23–41. doi: 10.3354/meps301023

Ginestet, C. (2011). Ggplot2: Elegant Graphics for Data Analysis. *J. R. Stat. Soc Ser.* A174, 245–246. doi: 10.1111/j.1467-985x.2010.00676_9.x

Grömping, U. (2006). Relative Importance for Linear Regression in R: The Package Relaimpo. *J. Stat. Softw.* 17, 1–27. doi: 10.18637/jss.v017.i01

Gruber, N., Clement, D., Carter, B. R., Feely, R. A., Van Heuven, S., Hoppema, M., et al. (2019). The Oceanic Sink for Anthropogenic CO_2 From 1994 to 2007. *Science* 363, 1193–1199. doi: 10.1126/science.aau5153

Guo, X., Dai, M., Zhai, W., Cai, W.-J., and Chen, B. (2009). CO_2 Flux and Seasonal Variability in a Large Subtropical Estuarine System, the Pearl River Estuary, China. *J. Geophys. Res.* 114, G03013. doi: 10.1029/2008jg000905

Hansen, H. P., and Koroleff, F. (1999). "Determination of Nutrients," in *Methods of Seawater Analysis*. Eds. K. Grasshoff, K. Kremling and M. Ehrhard (Wiley-VCH, Weinheim), 159–228.

Harrison, P. J., Yin, K., Lee, J. H. W., Gan, J., and Liu, H. (2008). Physical–biological Coupling in the Pearl River Estuary. *Cont. Shelf. Res.* 28, 1405–1415. doi: 10.1016/j.csr.2007.02.011

He, X., Bai, Y., Pan, D., Chen, C.-T. A., Cheng, Q., Wang, D., et al. (2013). Satellite Views of the Seasonal and Interannual Variability of Phytoplankton Blooms in the Eastern China Seas Over the Past 14 yr 1998–2011). *Biogeosciences* 10, 4721–4739. doi: 10.5194/bg-10-4721-2013

Heip, C., Goosen, N., Herman, P., Kromkamp, J., Middelburg, J., and Soetaert, K. (1995). Production and Consumptionof Biological Particles in Temperate Tidal Estuaries, London. *Oceanogr. Mar. Biol.* 33, 1–150.

Hopkinson, C., and Smith, E. M. (2005). Estuarine Respiration: An Overview of Benthic, Pelagic, and Whole System Respiration. *Respirat. Aquat. Ecosyst.* 8, 122–146.

Huang, H., Zhou, L., Chen, J., and Wei, T. (2020) *Ggcor: Extended Tools for Correlation Analysis and Visualization. R Package Version 0.9.8.1.* Available at: https://cran.r-project.org/web/packages/ggcor/index.html (Accessed July 20, 2021).

Hu, J., and Li, S. (2009). Modeling the Mass Fluxes and Transformations of Nutrients in the Pearl River Delta, China. *J. Mar. Syst.* 78, 146–167. doi: 10.1016/j.jmarsys.2009.05.001

Hung, J.-J., Ho, C.-M., and Shiah, F.-K. (2014). Effects of River Inputs on Nutrient and Organic-Carbon Conditions and Net Ecosystem Metabolism in the Kaoping (Taiwan) Coastal Sea. *Mar. Freshw. Res.* 65, 697–709. doi: 10.1071/MF13183

Jiao, S., Yang, Y., Xu, Y., Zhang, J., and Lu, Y. (2020). Balance Between Community Assembly Processes Mediates Species Coexistence in Agricultural Soil Microbiomes Across Eastern China. *ISME. J.* 14, 202–216. doi: 10.1038/s41396-019-0522-9

Karl, D. M., Laws, E. A., Morris, P., Williams, P. J. L., and Emerson, S. (2003). Metabolic Balance of the Open Sea. *Nature* 426, 32–32. doi: 10.1038/426032a

Kemp, W., and Testa, J. (2011). Metabolic Balance Between Ecosystem Production and Consumption. *Treat. Estuar. Coast. Sci.* 7, 83–118. doi: 10.1016/B978-0-12-374711-2.00706-3

Ke, Z., Tan, Y., Huang, L., Liu, J., Xiang, C., Zhao, C., et al. (2019). Significantly Depleted 15N in Suspended Particulate Organic Matter Indicating a Strong Influence of Sewage Loading in Daya Bay, China. *Sci. Tot. Environ.* 650, 759–768. doi: 10.1016/j.scitotenv.2018.09.076

Lepš, J., and Šmilauer, P. (2003). *Multivariate Analysis of Ecological Data Using CANOCO* (Cambridge: Cambridge University Press). doi: 10.1017/CBO9780511615146

Li, G., Liu, J., Diao, Z., Jiang, X., Li, J., Ke, Z., et al. (2018). Subsurface Low Dissolved Oxygen Occurred at Fresh- and Saline-Water Intersection of the Pearl River Estuary During the Summer Period. *Mar. Pollut. Bull.* 126, 585–591. doi: 10.1016/j.marpolbul.2017.09.061

Liu, H., Song, X., Huang, L., and Zhong, Y. (2012). Using Primary Productivity as an Index of Coastal Eutrophication: A Case Study in Daya Bay. *Water Environ. J.* 26, 235–240. doi: 10.1111/j.1747-6593.2011.00281.x

Li, Y., Xiang, C., Jiang, Z., and Song, X. (2021). Production and Metabolism Characteristics of Planktonic Community and Their Influencing Factors in Daya Bay During Summer. *J. Trop. Oceanogr.* 40, 83–92.

Li, X., Xu, J., Shi, Z., and Li, R. (20191026). Response of Bacterial Metabolic Activity to the River Discharge in the Pearl River Estuary: Implication for CO_2 Degassing Fluxes. *Front. Microbiol.* 10. doi: 10.3389/fmicb.2019.01026

López-Sandoval, D. C., Rowe, K., Carillo-de-Albonoz, P., Duarte, C. M., and Agustí, S. (2019). Rates and Drivers of Red Sea Plankton Community Metabolism. *Biogeosciences* 16 (15), 2983–2995. doi: 10.5194/bg-16-2983-2019

Lu, Z., and Gan, J. (2015). Controls of Seasonal Variability of Phytoplankton Blooms in the Pearl River Estuary. *Deep. Sea. Res. Part II Top. Stud. Oceanogr.* 117, 86–96. doi: 10.1016/j.dsr2.2013.12.011

Lu, Z., Gan, J., Dai, M., Liu, H., and Zhao, X. (2018). Joint Effects of Extrinsic Biophysical Fluxes and Intrinsic Hydrodynamics on the Formation of Hypoxia West Off the Pearl River Estuary. *J. Geophys. Res.: Ocean.* 123, 6241–6259. doi: 10.1029/2018jc014199

McKinnon, A. D., Duggan, S., Logan, M., and Lønborg, C. (2017). Plankton Respiration, Production, and Trophic State in Tropical Coastal and Shelf Waters Adjacent to Northern Australia. *Front. Mar. Sci.* 4. doi: 10.3389/fmars.2017.00346

Odum, H. T. (1956). Primary Production in Flowing Waters1. *Limnol. Oceanogr.* 1, 102–117. doi: 10.4319/lo.1956.1.2.0102

Parsons, T. R., Maita, Y., and Lalli, C. M. (1984). *A Manual of Chemical and Biological Methods for Seawater Analysis* (Oxford: Pergamon Press).

Qian, W., Gan, J., Liu, J., He, B., Lu, Z., Guo, X., et al. (2018). Current Status of Emerging Hypoxia in a Eutrophic Estuary: The Lower Reach of the Pearl River Estuary, China. *Estuar. Coast. Shelf. Sci.* 205, 58–67. doi: 10.1016/j.ecss.2018.03.004

Regaudie-de-Gioux, A., and Duarte, C. M. (2013). Global Patterns in Oceanic Planktonic Metabolism. *Limnol. Oceanogr.* 58, 977–986. doi: 10.4319/lo.2013.58.3.0977

Rochelle-Newall, E. J., Winter, C., Barrón, C., Borges, A. V., Duarte, C. M., Elliott, M., et al. (2007). Artificial Neural Network Analysis of Factors Controlling Ecosystem Metabolism in Coastal Systems. *Ecol. Appl.* 17, S185–S196. doi: 10.1890/05-1769.1

Schlitzer, R. (2020) *Ocean Data View*. Available at: http://odv.awi.de (Accessed October 20, 2021).

Serret, P., Robinson, C., Aranguren-Gassis, M., Garcia-Martin, E. E., Gist, N., Kitidis, V., et al. (2015). Both Respiration and Photosynthesis Determine the Scaling of Plankton Metabolism in the Oligotrophic Ocean. *Nat. Commun.* 6, 1–10. doi: 10.1038/ncomms7961

Song, X., Huang, L., Zhang, J., Huang, H., Li, T., and Su, Q. (2009). Harmful Algal Blooms (HABs) in Daya Bay, China: An *in Situ* Study of Primary Production and Environmental Impacts. *Mar. Pollut. Bull.* 58, 1310–1318. doi: 10.1016/j.marpolbul.2009.04.030

Song, X., Huang, L., Zhang, J., Huang, X., Zhang, J., Yin, J., et al. (2004). Variation of Phytoplankton Biomass and Primary Production in Daya Bay During Spring and Summer. *Mar. Pollut. Bull.* 49, 1036–1044. doi: 10.1016/j.marpolbul.2004.07.008

Song, X., Huang, L., Zhang, J., Yin, K., Liu, S., Tan, Y., et al. (2011). Chemometric Study of Spatial Variations of Environmental and Ecological Characteristics in the Zhujiang River (Pearl River) Estuary and Adjacent Waters. *Acta Oceanol. Sin.* 30, 60–74. doi: 10.1007/s13131-011-0137-0

Song, X., Lai, Z., Ji, R., Chen, C., Zhang, J., Huang, L., et al. (2012). Summertime Primary Production in Northwest South China Sea: Interaction of Coastal Eddy, Upwelling and Biological Processes. *Cont Shelf. Res.* 48, 110–121. doi: 10.1016/j.csr.2012.07.016

Song, X., Liu, H., Zhong, Y., Tan, Y., Qin, G., Li, K., et al. (2015). Bacterial Growth Efficiency in a Partly Eutrophicated Bay of South China Sea: Implication for Anthropogenic Impacts and Potential Hypoxia Events. *Ecotoxicology* 24, 1529–1539. doi: 10.1007/s10646-015-1497-6

Song, X., Li, Y., Xiang, C., Su, X., Xu, G., Tan, M., et al. (2021). Nitrogen and Phosphorus Enrichments Alter the Dynamics of the Plankton Community in Daya Bay, Northern South China Sea: Results of Mesocosm Studies. *Mar. Freshw. Res.* 72, 1632–1642. doi: 10.1071/mf21097

Wang, Q., Wang, X., Xiao, K., Zhang, Y., Luo, M., Zheng, C., et al. (2021). Submarine Groundwater Discharge and Associated Nutrient Fluxes in the Greater Bay Area, China Revealed by Radium and Stable Isotopes. *Geosci. Front.* 12, 101223. doi: 10.1016/j.gsf.2021.101223

Wemheuer, B., Güllert, S., Billerbeck, S., Giebel, H.-A., Voget, S., Simon, M., et al. (2014). Impact of a Phytoplankton Bloom on the Diversity of the Active Bacterial Community in the Southern North Sea as Revealed by Metatranscriptomic Approaches. *FEMS Microbiol. Ecol.* 87, 378–389. doi: 10.1111/1574-6941.12230

Williams, P. J. L. B., Quay, P. D., Westberry, T. K., and Behrenfeld, M. J. (2013). The Oligotrophic Ocean Is Autotrophic. *Ann. Rev. Mar. Sci.* 5, 535–549. doi: 10.1146/annurev-marine-121211-172335

Wu, M. L., Wang, Y. S., Wang, Y. T., Sun, F. L., and Dong, J. D. (2016). Seasonal and Spatial Variations of Water Quality and Trophic Status in Daya Bay, South China Sea. *Mar. Pollut. Bull.* 112 (1), 341–348. doi: 10.1016/j.marpolbul.2016.07.042

Wu, M. L., Wang, Y. S., Wang, Y. T., Yin, J. P., Dong, J. D., Jiang, Z.-Y., et al. (2017). Scenarios of Nutrient Alterations and Responses of Phytoplankton in a Changing Daya Bay, South China Sea. *J. Mar. Syst.* 165, 1–12. doi: 10.1016/j.jmarsys.2016.09.004

Yang, C., Li, Q., Hu, Z., Chen, J., Shi, T., Ding, K., et al. (2019). Spatiotemporal Evolution of Urban Agglomerations in Four Major Bay Areas of US, China and Japan From 1987 to 2017: Evidence From Remote Sensing Images. *Sci. Tot. Environ.* 671, 232–247. doi: 10.1016/j.scitotenv.2019.03.154

Yin, K., Lin, Z., and Ke, Z. (2004a). Temporal and Spatial Distribution of Dissolved Oxygen in the Pearl River Estuary and Adjacent Coastal Waters. *Cont. Shelf. Res.* 24, 1935–1948. doi: 10.1016/j.csr.2004.06.017

Yin, K., Qian, P., Chen, J., Hsieh, D., and Harrison, P. (2000). Dynamics of Nutrients and Phytoplankton Biomass in the Pearl River Estuary and Adjacent Waters of Hong Kong During Summer: Preliminary Evidence for Phosphorus and Silicon Limitation. *Mar. Ecol. Prog. Ser.* 194, 295–305. doi: 10.3354/meps194295

Yin, K., Zhang, J., Qian, P.-Y., Jian, W., Huang, L., Chen, J., et al. (2004b). Effect of Wind Events on Phytoplankton Blooms in the Pearl River Estuary During Summer. *Cont. Shelf. Res.* 24, 1909–1923. doi: 10.1016/j.csr.2004.06.015

Yu, H. (2019). The Guangdong-Hong Kong-Macau Greater Bay Area in the Making: Development Plan and Challenges. *Camb. Rev. Int. Aff.* 34, 1–29. doi: 10.1080/09557571.2019.1679719

Zhai, W. D., Dai, M. H., Chen, B. S., Guo, X. H., Li, Q., Shang, S. L., et al. (2013). Seasonal Variations of Sea–Air CO_2 Fluxes in the Largest Tropical Marginal Sea (South China Sea) Based on Multiple-Year Underway Measurements. *Biogeosciences* 10, 7775–7791. doi: 10.5194/bg-10-7775-2013

Zhang, L., Xiong, L., Zhang, J., Jiang, Z., Zhao, C., Wu, Y., et al. (2019). The Benthic Fluxes of Nutrients and the Potential Influences of Sediment on the Eutrophication in Daya Bay, South China. *Mar. Pollut. Bull.* 149, 110540. doi: 10.1016/j.marpolbul.2019.110540

Zhao, Z., Li, H., Sun, Y., Yang, Q., and Fan, J. (2021). Contrasting the Assembly of Phytoplankton and Zooplankton Communities in a Polluted Semi-Closed Sea: Effects of Marine Compartments and Environmental Selection. *Environ. Pollut.* 285, 117256. doi: 10.1016/j.envpol.2021.117256

Zhao, Y., Liu, J., Uthaipan, K., Song, X., Xu, Y., He, B., et al. (2020). Dynamics of Inorganic Carbon and pH in a Large Subtropical Continental Shelf System: Interaction Between Eutrophication, Hypoxia, and Ocean Acidification. *Limnol. Oceanogr.* 65, 1359–1379. doi: 10.1002/lno.11393

Zhu, Z., Zhang, J., Wu, Y., Zhang, Y., Lin, J., and Liu, S. (2011). Hypoxia Off the Changjiang (Yangtze River) Estuary: Oxygen Depletion and Organic Matter Decomposition. *Mar. Chem.* 125, 108–116. doi: 10.1016/j.marchem.2011.03.005

Zu, T., and Gan, J. (2015). A Numerical Study of Coupled Estuary–Shelf Circulation Around the Pearl River Estuary During Summer: Responses to Variable Winds, Tides and River Discharge. *Deep. Sea. Res. Part II Top. Stud. Oceanogr.* 117, 53–64. doi: 10.1016/j.dsr2.2013.12.010

Zu, T., Wang, D., Gan, J., and Guan, W. (2014). On the Role of Wind and Tide in Generating Variability of Pearl River Plume During Summer in a Coupled Wide Estuary and Shelf System. *J. Mar. Syst.* 136, 65–79. doi: 10.1016/j.jmarsys.2014.03.005

Conflict of Interest: The authors declare that the research was conducted in the absence of any commercial or financial relationships that could be construed as a potential conflict of interest.

Publisher's Note: All claims expressed in this article are solely those of the authors and do not necessarily represent those of their affiliated organizations, or those of the publisher, the editors and the reviewers. Any product that may be evaluated in this article, or claim that may be made by its manufacturer, is not guaranteed or endorsed by the publisher.

Copyright © 2022 Zhang, Li, Xiang, Huang, Fu, Zheng, Wang, Ouyang and Song. This is an open-access article distributed under the terms of the Creative Commons Attribution License (CC BY). The use, distribution or reproduction in other forums is permitted, provided the original author(s) and the copyright owner(s) are credited and that the original publication in this journal is cited, in accordance with accepted academic practice. No use, distribution or reproduction is permitted which does not comply with these terms.

frontiers | Frontiers in Marine Science

ORIGINAL RESEARCH
published: 09 June 2022
doi: 10.3389/fmars.2022.882010

Impact of Environmental Regulation on Coastal Marine Pollution—A Case of Coastal Prefecture-Level Cities in China

Jintao Ma[1], *Qiuguang Hu*[1,2*] *and Xinyi Wei*[1]

[1] School of Business, Ningbo University, Ningbo, China, [2] Marine Economic Research Center, Dong Hai Strategic Research Institute, Ningbo University, Ningbo, China

Based on the data on the level of environmental regulation and the degree of coastal marine pollution in 46 coastal prefecture-level cities in China from 2004 to 2016, this study uses the mediation effect model and the spatial Durbin model to analyze the impact and role of environmental regulation on offshore pollution from multiple dimensions and mechanisms. The findings are as follows: (1) Environmental regulation has an inverted "U"-shaped nonlinear effect on coastal marine pollution, which first intensifies and then inhibits. (2) Promoting green technology innovation is an important mechanism for environmental regulation to improve the quality of the marine environment, and the impact of environmental regulation on green technology innovation is characterized by a "U" shape. (3) Environmental regulation of coastal cities can affect coastal marine pollution in adjacent areas through spatial spillover effects, and the impact trajectory also shows an inverted "U"-shaped curve. This study proposes that in the process of marine environ-mental governance, first, a scientific and strict environmental regulation system should be constructed, and differentiated environmental regulation policies should be implemented. Second, giving full play to the conduction effect of green technology innovation and promoting the research and development, diffusion, and application of green technology are necessary. Third, we must attach importance to the cross-regional transfer and control of offshore pollution and promote regional joint prevention and control work.

Keywords: environmental regulation, coastal marine pollution, green technology innovation, spatial measurement, marine environmental protection

OPEN ACCESS

Edited by:
Tieyu Wang,
Shantou University, China

Reviewed by:
Nitin Agarwala,
National Maritime Foundation, India
Yen-Chiang Chang,
Dalian Maritime University, China

****Correspondence:***
Qiuguang Hu
huqiuguang@nbu.edu.cn

Specialty section:
This article was submitted to Marine Pollution, a section of the journal Frontiers in Marine Science

Received: *23 February 2022*
Accepted: *05 May 2022*
Published: *09 June 2022*

Citation:
Ma J, Hu Q and Wei X (2022) Impact of Environmental Regulation on Coastal Marine Pollution—A Case of Coastal Prefecture-Level Cities in China. Front. Mar. Sci. 9:882010. doi: 10.3389/fmars.2022.882010

1 INTRODUCTION

In order to achieve sustainable marine ecological environment and promote the stable development of China's marine economy, China's coastal cities bear the heavy burden of marine pollution prevention and control. Since the reform and opening up, China's eastern coastal cities, such as Shanghai and Shenzhen, have developed rapidly. However, the long-term use of extensive economic model has exacerbated the generation and discharge of pollutants. Although the level of pollution

treatment technology has gradually improved, due to insufficient technology accumulation and excessive reliance on the self-purification ability of the ocean, land-based pollution with long duration, complexity, and concealment has caused great damage to the marine environment. To curb the deterioration of the ecological environment, the coastal city governments has implemented a series of positive measures. For example, Shanghai has established a marine ecological red line management system, and Shenzhen has improved the marine environmental management mechanism of land-sea coordination. After their long-term efforts, marine environmental protection has achieved phased results. The sea area with water quality worse than Grade IV has dropped significantly. Nevertheless, according to the Bulletin on the State of China's Marine Ecological Environment, the pollution of some sea areas such as the East China Sea is still serious; the direct discharge of pollutants, such as chemical oxygen demand, petroleum, and heavy metals is still high; and the prevention and control of marine pollution undertaken by coastal cities remain arduous. Moreover, due to the strong cross-border flow characteristics of coastal marine pollution and the existence of "Pollution Haven" effect, isolated environmental regulation hardly plays its expected role, and the implementation effect of relevant policies will be influenced by adjacent coastal cities. The " race to the bottom" and "incomplete implementation" of environmental regulation not only aggravate local marine pollution but also restrict the overall governance of marine environment (Zhang et al., 2021; Hu and Ma, 2022). Therefore, analyzing the impact of environmental regulation on coastal marine pollution at the urban level, exploring its action mechanism, emphasizing the direction for follow-up marine environmental protection work, promoting the improvement of marine ecological environment quality, and accelerating the construction of marine ecological civilization are necessary.

Owing to the great differences in research samples, index data, and research perspectives, three main views on the relationship between environmental regulation and environmental pollution exist. (1) Environmental regulation helps reduce environmental pollution. Most relevant literature starts from the "Porter hypothesis," indicating that the strong level of environmental regulation will force enterprises to conduct scientific research innovation and industrial upgrading to realize decoupling between economic development and environmental pollution (Xia and Zhong, 2016; Hui and Zhao, 2017; Sun and Zaenhaer, 2021). On the basis of the perspective of the implementation of industrial policies for environmental protection, Jiang (Jiang and Cui, 2019) found that environmental regulation will guide enterprises to increase environmental protection investment and jointly promote environmental protection and economic development. Wu (Wu and Han, 2020) stated that improving the level of environmental regulation will promote green technology innovation and help improve the ecological environment. Some studies were extended on this basis. Zhang (2017) focused on the externality of policies and emphasized that cooperative governance between cities is the key to giving play to the effectiveness of environmental regulation and improving environmental quality. (2) Environmental regulation is inconducive to reducing environmental pollution. Some scholars have recommended the "green paradox" (Sinn, 2008) and believed that strict environmental regulation fails to effectively promote the improvement of ecological environment quality. That is, with the enhancement of environmental regulation, the production and operation cost of enterprises will increase significantly. When the expected cost increases, enterprises may speed up the exploitation and consumption of resources and increase the emission of pollutants in the short term (Zhang, 2014; Li et al., 2018). In addition, "follow-the-cost effect" may occur. Enterprises will accelerate the release of production capacity to compensate for the increase in cost and follow the development model of "pollution first, treatment later" (Qi and Wang, 2015; Fünfgelt and Schulze, 2016; Xu, 2016), which will aggravate the problem of environmental pollution. Some studies have also performed analyses on the basis of the "Pollution Haven effect," indicating that the improvement of environmental regulation will cause nearby transfer of pollution, resulting in the transfer of polluting industries from areas with high level of environmental regulation to areas with low level (Wu et al., 2017; Shen et al., 2017; Qin and Ge, 2018). In the absence of overall coordination, the environmental regulation policies formulated by cities to achieve local environmental improvement will not be conducive to the overall governance of the ecological environment. (3) The impact of environmental regulation on environmental pollution is uncertain. Many studies have emphasized that a nonlinear relationship exists between the two. For example, Zhang (Zhang and Wei, 2014) believed that the effect of environmental regulation will change from a "green paradox" effect to a "forced emission reduction" effect with the increase in its intensity. Zhou (Zhou et al., 2015) found that low-level environmental regulation will accelerate the consumption of fossil energy. Only after crossing the "threshold" can the energy-saving effect of environmental regulation be brought into play. Moreover, great differences in the impact of different types of environmental regulation tools on the ecological environment exist (Ban and Liu, 2021), and no unified conclusion on which is stronger or weaker between market- and command-based tools has been drawn (Li and Zhang, 2020; Wang and Lu, 2021). Existing research on the spatial effect of environmental regulation also has some differences. Ji (Ji and Song, 2021) regarded the cities in the Yangtze River Delta as a sample and found that the environmental regulation of adjacent cities will aggravate the pollution agglomeration of local cities. Sun (Sun and Zaenhaer, 2021) used the data of national prefecture-level cities to conduct an empirical study and believed that the implementation of environmental regulation will help reduce the level of environmental pollution in adjacent cities.

To sum up, studies have conducted extensive and in-depth discussions on the impact mechanism and transmission path between environmental regulation and environmental pollution. Based on the perspectives of different industries and regions, the theories such as "Porter Hypothesis" and "Following Cost

Theory" are demonstrated in detail. But studies focused on terrestrial pollution, research in the marine field remains lacking. China's academic research in the field of marine ecological environment started in the 1960s, but the progress was slow. After entering the 21st century, with the country's increasing emphasis on marine ecology, related research has ushered in vigorous development (Li et al., 2011; Gao and Gao, 2012; Peng et al., 2018). However, because the statistical standards have not been perfected, marine-related data are still lacking. Existing literature often makes empirical analysis by using coastal provincial data; discusses the impact of environmental regulation on marine economic development, industrial structure, and scientific and technological innovation (Zhao, 2019; Ge et al., 2020; Xu and Lin, 2020; Chen, 2021); or focuses on the influencing factors of coastal marine environment to test the relationship among marine economic growth (Wang et al., 2019), urbanization promotion (Yu et al., 2020), economic growth goal (Shen et al., 2021), and coastal marine pollution. Few studies have analyzed the impact mechanism of environmental regulation on coastal marine pollution on the basis of the data of coastal prefecture-level cities, and research results on the spillover effect of environmental regulation on coastal marine pollution in adjacent areas from a spatial perspective are lacking. Thus, the innovation of this study lies in the following: (1) sink the research object to coastal prefecture-level cities, avoid the deviation of results due to insufficient samples and wide content, fully consider the objective differences within a province, accurately evaluate the impact of environmental regulation on coastal marine pollution, and analyze the action mechanism of environmental regulation on coastal marine environmental pollution from the perspective of green technology innovation; (2) integrate the spatial spillover effect into the research scope, analyze the impact of local environmental regulation on coastal marine pollution in adjacent areas, and comprehensively evaluate the effectiveness of environmental regulation in controlling coastal marine environmental pollution to provide a reference basis for marine ecological environment governance.

2 RESEARCH HYPOTHESES

This study focuses on the coastal marine ecological environment, and discusses the impact of environmental regulation on coastal marine pollution and its mechanism. Based on the environmental Kuznets curve theory (Gene and Alan, 1995), Porter hypothesis (Porter and van der Linde, 1995), and environmental regulation competition theory (Arik, 2003), the corresponding research hypotheses are put forward on the basis of analyzing its influence mechanism, which lays a solid foundation for empirical analysis.

2.1 Nonlinear Characteristics of the Impact of Environmental Regulation

Environmental regulation is an important measure to deal with the negative externality of environmental pollution. The government restricts the production and operation activities of enterprises through administrative punishment, pollutant discharge permit, and pollutant discharge tax, which aims to internalize the environmental cost, guide enterprises to adjust the development mode, and reduce the discharge of wastewater and waste gas and the demand for fossil energy to realize ecological protection and sustainable development. However, in accordance with the environmental Kuznets curve (Gene and Alan, 1995), a nonlinear relationship may exist between environmental regulation and coastal marine pollution. When the level of environmental regulation is low, facing the constraints of environmental regulation, enterprises may choose to reduce scientific research investment, accelerate the release of production capacity, increase pollutant emissions, and compensate for the increased production costs to maximize their own interests, resulting in the intensification of land-based pollution and further deterioration of the marine ecological environment. Nonetheless, with the strengthening of environmental regulation, on the one hand, small enterprises with backward production capacity and serious pollution will hardly bear the rising pollution cost and be gradually eliminated in the market competition. On the other hand, to increase market share and realize long-term benefits, some large-scale enterprises will promote the innovation of production and pollution control technology by optimizing resource allocation and increasing scientific research investment, which will improve urban production efficiency and reduce pollution emissions. From the above discussion, Hypothesis 1 is proposed as follows.Hypothesis 1 (H1). *The impact trajectory of environmental regulation on coastal marine pollution shows an inverted "U" curve.*

2.2 Mechanism of Environmental Regulation

The impact of environmental regulation on green technology innovation is the result of the game between "innovation compensation effect" and "follow-the-cost effect." Improving the level of environmental regulation, on the one hand, will increase the cost of pollution control and emission reduction of enterprises, cause an overall decline in enterprise business performance in the short term, squeeze its investment in scientific and technological research and development (R&D). In particular, small- and medium-sized enterprises with low awareness of environmental protection and shortage of funds and talents often avoid the R&D of green technologies with large investment and high risk. On the other hand, according to Porter hypothesis, the benefits of technological innovation will be significantly higher than the increased environmental costs in the long run. To achieve long-term and stable development, enterprises with a certain foundation in terms of talents, funds, and equipment have the ability and power to carry out green technology innovation and offset the rising cost caused by environmental regulation through improving economic efficiency, promoting pollution reduction, and optimizing resource allocation. Therefore, this study infers that the impact of environmental regulation on green technology innovation has nonlinear characteristics. The improvement of green technology

innovation level is conducive to the improvement of marine ecological environment governance. Studies have shown that 80% of the total amount of marine pollutants comes from land-based pollution, which shows that curbing the discharge of land-based pollution into the sea is an important task to protect the coastal marine environment. Green technology innovation with green development as the core will promote the energy saving and cleaning of enterprise production equipment, technology, and products; accelerate the optimization and upgrading of industrial structure in coastal cities; and reduce land-based pollution from the source, including reducing the direct discharge of sewage into the sea, lowering excessive factors, such as ammonia nitrogen. From the above discussion, Hypothesis 2 is proposed as follows.Hypothesis 2 (H2). *Environmental regulation has an impact on coastal marine pollution through green technology innovation.*

2.3 Spatial Spillover Effect of Environmental Regulation

Coastal marine pollution has strong cross-border flow characteristics, which can break through the spatial constraints and spread to adjacent areas with the help of natural factors, such as ocean current and wind direction. At the same time, enterprises, as the main body of pollutant emission, will also carry out cross land transfer. Therefore, the marine environmental quality of coastal cities is closely related to the spatial adjacent areas. The environmental regulation in these areas will have an impact on the coastal marine pollution in the adjacent areas. The governments of coastal cities restrict the production and operation of enterprises by controlling the total amount of emissions, raising emission standards, and strengthening rewards and punishments to strengthen the remediation of land-based pollution. On the one hand, due to the "bottom-by-bottom competition" and "incomplete implementation" of environmental regulation, to reduce the cost of environmental treatment, some polluting enterprises may relocate and move to adjacent areas with relatively loose environmental regulation to transfer the pollution nearby and form the "Pollution Haven" effect (Shen et al., 2017; Wu and He, 2017), resulting in the deterioration of the ecological environment in adjacent areas. On the other hand, in the long run, environmental regulation will stimulate the enthusiasm of enterprises for green innovation. To improve market competitiveness, enterprises will actively innovate production and environmental protection technologies, which will effectively curb the transfer and diffusion of pollution and strengthen the benign interaction between regions. From the above discussion, Hypothesis 3 is proposed as follows. Hypothesis 3 (H3). *The environmental regulation of coastal cities can affect the coastal marine pollution in adjacent areas through the spatial spillover effect.*

3 METHODOLOGY AND DATA

3.1 Dependent Variable

Existing studies generally use indicators, such as industrial wastewater discharge (He and Chen, 2018) and nonclass water quality and sea area (Zhang et al., 2020), to measure the degree of coastal marine pollution. Although they reflect the coastal marine pollution to a certain extent, the relevant data are relatively general and one-sided and do not sink to the level of coastal cities to reflect the specific changes in coastal marine pollution. In this study, the average concentration data of inorganic nitrogen, active phosphate, petroleum, and chemical oxygen demand were obtained by identifying the histogram of the main exceeding standard factors in the coastal waters of coastal cities in the Bulletin on Environmental Quality of China's Coastal Seas (Yu et al., 2020; Shen et al., 2021). After dimensionless processing of the data, the coastal marine pollution index was constructed by the entropy method, as shown in Equation (1):

$$MP_i = a_1 DIN_i + a_2 PO_i + a_3 OIL_i + a_4 COD_i \quad (1)$$

where *MP* is the coastal marine pollution index, *DIN* is inorganic nitrogen, *PO* is active phosphate, *OIL* is petroleum, and *COD* is the chemical oxygen demand. a_1, a_2, a_3, and a_4 are the weights of each index. According to the Bulletin of Marine Ecology and Environment Status of China, we evaluated the degree of impact on the marine ecological environment by measuring the average point exceeding rate of each factor during the sample period, and set the corresponding weights based on the exceeding conditions, $a_1 = 0.6$, $a_2 = 0.3$, $a_3 = 0.07$, and $a_4 = 0.03$.

3.2 Explanatory Variable

Due to the multi-dimensional nature of environmental regulation and the low availability of relevant data, there is a certain controversy about the measurement of environmental regulation level. Four main methods can be used to measure the level of regional environmental regulation. First, on the basis of the micro level, the intensity of environmental regulation is reflected by the pollution costs of enterprises, such as sewage charges and governance investment (Xie et al., 2014; Chen et al., 2021; Liu and Wan, 2021). Second, the regulation level is evaluated through government pollution control investment (Song and Wang, 2013; Yang and Wen, 2021). Third, a comprehensive index of environmental regulation is established on the basis of the discharge of various pollutants (Ye et al., 2018; Wu et al., 2021). Fourth, the number of environmental protection regulations and the frequency of environmental words in a government work report are used (Chen et al., 2018; Wang, 2018 Zhang and Chen, 2021). Considering the objectivity of indicators and the availability, based on the above analysis, we referred to the research of Shen (Shen et al., 2017), Li (Li and Du, 2014), and selected four single indicators: removal rate of industrial sulfur dioxide, removal rate of industrial smoke, comprehensive utilization rate of industrial solid waste, and sewage treatment rate. We determined the weight of each index by using the improved entropy method and calculated the comprehensive index of environmental regulation to reflect the intensity of environmental regulation level. The specific steps are as follows.

(1)We performed dimensionless processing on the indicator, and shifted the indicator data so that it is concentrated between

30-100. i represents the year, j represents the indicator type, x_{ij}^{*} is the standardized index, x_{ij} is the initial indicator, $x_{max(j)}$ and $x_{min(j)}$ represent the maximum and minimum values of the j index in all cities in the current year, respectively

$$x_{ij}^{*} = \frac{x_{ij} - x_{min(j)}}{x_{max(j)} - x_{min(j)}} * 70 + 30 \quad (2)$$

(2) We calculated the proportion (D_{ij}) of x_{ij}^{*}, the entropy value (k_j) of the j and the difference coefficient (f_j). The larger the difference coefficient (f_j), the more important x_{ij} is in the comprehensive evaluation, and then the weight N_j is determined

$$D_{ij} = \frac{x_{ij}^{*}}{\sum_{i=1}^{n} x_{ij}^{*}},$$
$$k_j = -\left(\frac{1}{lnn}\right)\sum_{i=1}^{n} D_{ij} \ln D_{ij},$$
$$f_j = 1 - k_j \quad (3)$$

$$N_j = \frac{f_j}{\sum_{m=1}^{m} f_j} = \frac{1 - k_j}{\sum_{j=1}^{m}(1 - k_j)} (0 \le N_j \le 1) \quad (4)$$

(3) We calculated comprehensive indicators of environmental regulation. The larger the comprehensive index of environmental regulation (ers_i), the higher the level of environmental regulation.

$$ers_i = \sum_{j=1}^{m} (N_j * 100) * (D_{ij} * 100) \quad (5)$$

3.3. Control Variable

With reference to existing research, the control variables included the following: (1) Economic development (lnpergdp). The development of regional economy has promoted the improvement of living standards and raised the public's requirements for the quality of ecological environment. The government and enterprises have implemented positive measures to respond to social needs. We chose the logarithm of per capita GDP to measure the economic development level of a city. (2) Industrial structure (ind). The industrial structure of a city has a profound impact on the decision-making behavior of the local government. We used the proportion of secondary industry to evaluate the level of urban industrial structure. (3) Foreign capital utilization (fdigdp). The effective utilization of foreign capital has played an important role in enterprise transformation and upgrading, scientific research, development, and utilization. We reflected the utilization of foreign capital by the proportion of actually used foreign capital in GDP. (4) Urbanization level (urban). Urbanization is a complex process that promotes the evolution of social and economic structure. In this process, the various changes in the economy, population, and society of coastal cities will exert an impact on the marine ecological environment. We characterized this index by urbanization rate. (5) Population density (rapopul). A high population density promotes economies of scale and industrial division of labor, as well as intensifies the generation and emission of pollutants. We measured it by the population per square kilometer of a city. (6) Level of marine economic development (reocean). The level of marine economic development can reflect the local attention to marine resources and environment. Considering that coastal cities do not publish the total marine production value, we replaced it with the total marine production value of coastal provinces and reflected this index by the proportion of total marine production value in regional production value. Summary statistics for the data are shown in **Table 1**.

3.4. Data Sources and Model Settings

3.4.1. Data Sources

We regarded the panel data of 46 coastal prefecture-level cities in China from 2004 to 2016 as a sample to evaluate the impact of environmental regulation on coastal marine pollution. The time span has been selected for the following reasons. Firstly, the Bulletin on Environmental Quality of China's Coastal Seas and the Bulletin on the State of China's Marine Environment were merged into the Bulletin on the State of China's Marine Ecological Environment after 2017, and the pollutant concentration is no longer reported in the combined bulletin. Secondly, the serious lack of data before 2004 has forced us to consider this time span. The study includes all coastal cities in China, but the data of some coastal cities are seriously missing (such as Danzhou City) which had to be overlooked. Finally, 46 coastal prefecture-level cities are selected out of the 57 coastal prefecture-level cities in China as the research samples. The data related to the construction of a coastal marine pollution index came from the Bulletin on Environmental Quality of China's Coastal Seas[1]. The index data for evaluating the level of environmental regulation and control variable data came from the statistical yearbooks of China's cities, China's environment, China's oceans, and coastal cities and provinces[2].

3.4.2. Model Settings

To test the above hypotheses, we referred to the research of Li (Li and Zhang, 2020), Yu (Yu et al., 2020) and Wu (Wu et al., 2021), built a model on the basis of the nonlinear impact of environmental regulation on coastal marine environmental pollution. The model was constructed as

$$lnmp_{it} = \alpha_0 + \alpha_1 lners_{it} + \alpha_2 (lners)_{it}^2 + \alpha_3 \sum control_{it} + \gamma_t + \lambda_i + \xi_{it} \quad (6)$$

where *lnmp* is the logarithm of the coastal marine pollution index; *lners* and $(lners)^2$ are the logarithm of the environmental regulation level and its square term, respectively; *control* is the control variable; γ_t and λ_i control the fixed effects of time and city, respectively; ξ_{it} is a random interference item; *i* represents the city; and t represents the year.

[1] Relevant information is obtained by querying the official website of the Ministry of Ecology and Environment of the People's Republic of China.
[2] The statistical yearbook data is obtained by querying EPS database.

TABLE 1 | Summary statistics.

Variables	Variable Definition	Mean	SD	Min	Max
mp	Coastal marine pollution index	0.1555	0.1175	0.0204	0.9242
ers	Environmental regulation level	16.7224	1.9766	8.5160	19.9844
lnpergdp	Logarithm of GDP per capita	10.5449	0.6876	8.5431	13.0557
ind	Proportion of secondary industry to GDP	0.4969	0.0880	0.1857	0.8228
fdigdp	Proportion of foreign capital to GDP	0.0343	0.0452	0.0003	0.5755
urban	Urbanization rate	0.5533	0.1672	0.1123	1.0000
rapopul	Population per square kilometer	6.4158	4.7057	0.4435	34.5354
reocean	Proportion of marine production output to GDP	0.1610	0.0634	0.0524	0.3763

4 EMPIRICAL RESULTS

4.1 Benchmark Estimation Results

In accordance with the benchmark model, this study quantitatively evaluated the relationship between environmental regulation and coastal marine pollution. In order to test whether the influence of the core explanatory variables is robust and improve the stability of the test results, we conducted regression analysis by sequentially increasing the control variables. The empirical results are shown in **Table 2**, where column (1) refers to the regression results without control variables, and columns (2–7) are the regression results with sequentially increasing control variables. In column (1), the primary term coefficient of the core explanatory variable environmental regulation level (lners) is positive, and the square term coefficient is negative. After the control variables are added in turn, the results have not changed significantly. This finding shows that the impact of environmental regulation on coastal marine pollution has the characteristic of inverted "U." The low level of environmental regulation in coastal cities intensifies the problem of coastal marine pollution. With the improvement of the level of environmental regulation, its containment effect on pollution becomes gradually prominent, and Hypothesis 1 is verified. We explain the above results as follows: when the level of environmental regulation is low, although the emission and technical standards formulated by the government increase the environmental cost of enterprises, due to the insufficient punishment of pollution behavior and the limited policy coverage, enterprises are more inclined to increasing product output and pollution emission, especially when environmental regulation is expected to become gradually stricter. In addition, to avoid environmental governance responsibilities, polluting enterprises in areas with strong environmental regulation may choose to migrate across land, making areas with weak environmental regulation "Pollution Haven" However, with the improvement of the level of environmental regulation, some enterprises with high energy consumption, excessive pollution, and low production capacity will hardly bear the rising environmental costs and be gradually eliminated in the market competition. At the same time, enterprises with certain advantages

TABLE 2 | Benchmark estimation results.

Variables	Dependent Variable: Coastal Marine Pollution Index						
	(1)	(2)	(3)	(4)	(5)	(6)	(7)
lners	1.986**	2.130**	2.359***	3.360***	3.793***	3.783***	4.012***
	(0.831)	(0.792)	(0.704)	(0.734)	(0.668)	(0.664)	(0.691)
$(lners)^2$	-0.354**	-0.367**	-0.407**	-0.597***	-0.675***	-0.673***	-0.718***
	(0.158)	(0.150)	(0.134)	(0.137)	(0.124)	(0.122)	(0.128)
lnpergdp		-0.229***	-0.199***	-0.196***	-0.174***	-0.176***	-0.179***
		(0.050)	(0.059)	(0.061)	(0.050)	(0.049)	(0.050)
ind			-0.227	-0.235	-0.281*	-0.280*	-0.326**
			(0.139)	(0.135)	(0.136)	(0.136)	(0.129)
fdigdp				-0.610***	-0.619***	-0.618***	-0.594***
				(0.099)	(0.103)	(0.103)	(0.093)
urban					-0.434***	-0.438***	-0.327***
					(0.085)	(0.080)	(0.066)
rapopul						-0.001	-0.002
						(0.003)	(0.002)
reocean							1.615
							(1.146)
_cons	-5.229***	-3.251***	-3.765***	-5.080***	-5.654***	-5.616***	-6.127***
	(1.097)	(0.970)	(0.900)	(0.790)	(0.700)	(0.684)	(0.762)
Time fixed effect	YES	YES	YES	YES	YES	YES	YES
Urban fixed effect	YES	YES	YES	YES	YES	YES	YES
N	598	598	598	598	598	598	598
Adj R2	0.478	0.483	0.494	0.507	0.527	0.536	0.543

*Figures in () are robust standard error; ***, ** and * indicate significance at the 1%, 5% and 10% levels, respectively.*

in capital, talents, and technology will actively increase R&D investment, promote green technology innovation, and accelerate the application and diffusion of energy-saving and environmental protection technologies to improve market competitiveness and achieve long-term and stable development. In this process, land-based pollution emissions are significantly reduced, marine environmental quality is improved, and the inhibitory effect of environmental regulation on coastal marine pollution is effectively brought into play.

Among the control variables, the coefficient of economic development (lnpergdp) is significantly negative, indicating that the improvement of economic development level will inhibit coastal marine pollution. With the vigorous development of economy, the enthusiasm of the public to participate in environmental governance has gradually increased. The demand for high-quality development will promote the implementation of ecological protection, effectively restrict the production behavior of enterprises, and then reduce the pollution of marine environment. The coefficient of industrial structure (ind) is significantly negative, implying that the increase in the proportion of secondary industry contributes to the reduction in coastal marine pollution. The reason may be that the eastern coastal cities are basically in the late stage of industrialization, that is, the stage of technology intensification. Cities pay attention to the cultivation of high-tech, high-added-value, and low-pollution industries and emphasize innovation and green development. The negative coefficient of foreign capital utilization (fdigdp) is significant, indicating that the effective utilization of foreign capital promotes marine environmental governance, possibly because the inflow of foreign capital helps alleviate the capital constraints of enterprises and increase the investment in environmental protection and green innovation. At the same time, the entry of foreign capital is accompanied by the exchange of knowledge and technology. Through learning advanced environmental protection concepts and management experience, the level of environmental governance will be significantly improved. The coefficient of urbanization level (urban) is significantly negative, demonstrating that the promotion of urbanization has a positive impact on the marine ecological environment, which may be due to the following two aspects. First, the improvement of urbanization level will promote the rational allocation of resources and enhance the efficiency of ecological environment treatment. Second, the promotion of urbanization will contribute to the R&D, application, and diffusion of green technology and encourage cleaner production and end of pipe treatment.

4.2 Robustness Test

To ensure that the regression results accurately reflect the impact of environmental regulation on coastal marine pollution, a robustness test was performed by eliminating sample extreme values and interference samples and replacing core explanatory variables. The specific results are shown in **Table 3**. First, to avoid the impact of sample extreme values on the empirical results, we shrank the tail of the sample by 5%. In column (1), the primary term coefficient of environmental regulation level (lners) is positive, and the secondary term coefficient is negative, which is consistent with the benchmark results. Second, we considered that Shanghai and Tianjin, as municipalities directly under the central government, have higher administrative levels than others and may be subject to greater constraints in terms of economy and environment. Therefore, after excluding Shanghai and Tianjin from the sample, we reassessed the regression results. The regression results in column (2) have not changed significantly. Lastly, referring to the studies of Wu (Wu and Han, 2020), Shen (Shen et al., 2017), and Ye (Ye et al., 2018), we built a comprehensive index of environmental regulation on the basis of the emission and removal rate of various pollutants in cities and tested the robustness by replacing explanatory variables. In accordance with columns (3) and (4), the primary term coefficients of environmental regulation level (er, erh) are significantly positive, and the square term coefficients are significantly negative. The above tests verify the robustness of the benchmark regression results, indicating that the impact trajectory of environmental regulation on coastal marine pollution presents an inverted "U" curve.

4.3 Endogenous Test

A two-way causal relationship may exist between environmental regulation and coastal marine pollution, and endogenous problems will cause errors in the regression results. Therefore, to ensure the reliability of benchmark analysis, we referred to existing studies (Liu and Wan, 2021; Zhang and Chen, 2021) and conducted an endogenous test through lag regression and instrumental variable regression. The specific results are shown in **Table 4**. We regarded the level of environmental regulation lagging behind the first period (l.lners) as the explanatory variable for regression. In accordance with column (1), the primary term coefficient of the index is significantly positive, and the square term coefficient is significantly negative. This result indicates that

TABLE 3 | Robustness test.

Variables	Tail shrinking	Exclude Municipalities	Replace explanatory variables	
	(1)	(2)	(3)	(4)
lners	2.717***	4.174***		
	(0.759)	(0.857)		
$(lners)^2$	-0.502***	-0.751**		
	(0.140)	(0.160)		
er			0.039**	
			(0.017)	
$(er)^2$			-0.001**	
			(0.001)	
erh				0.074**
				(0.041)
$(erh)^2$				-0.015**
				(0.007)
Control	YES	YES	YES	YES
Time fixed effect	YES	YES	YES	YES
Urban fixed effect	YES	YES	YES	YES
N	538	572	598	598
Adj R2	0.467	0.532	0.457	0.439

*Figures in () are robust standard error; ***, ** indicate significance at the 1%, 5% levels, respectively.*

the impact of environmental regulation on coastal marine pollution presents an inverted "U" shape, which proves the robustness of the benchmark results. On this basis, to further eliminate the endogenous impact, we regarded the first and second lag terms of environmental regulation level (lners) as instrumental variables. From column (2), when the instrumental variables meet the statistical requirements, no significant difference exists between the sign and significance of the primary term and square term coefficients of the environmental regulation level (lners) and the benchmark results, which confirms the robustness of the previous conclusions.

4.4 Mechanism Analysis

The internalization of enterprise pollution costs by environmental regulation may lead to capital crowding out effect and inhibit the improvement of green technology innovation level. However, in order to maximize profits, enterprises may increase capital investment in green R&D, so as to improve production efficiency and the innovation effect. Compared with traditional technological innovation, green technological innovation pays more attention to resource protection and pollution control. Its high-efficiency production mode is conducive to energy conservation, emission reduction and cleaner production, curb the damage of land-based pollution to the coastal marine environment. Therefore, it is necessary to further explore the impact mechanism of environmental regulation on coastal marine pollution from the perspective of green innovation. We referred to the "Porter hypothesis" and regarded green technology innovation as an intermediary variable to test whether environmental regulation has an impact on coastal marine pollution through affecting green technology innovation (Wu and Han, 2020; Wu et al., 2021). The mediation effect model was constructed as

$$innov_{it} = \beta_0 + \beta_1 lners_{it} + \beta_2 (lners)^2_{it} + \beta_3 \sum control_{it} + \gamma_t + \lambda_i + \xi_{it} \quad (7)$$

$$lnmp_{it} = v_0 + v_1 innov_{it} + v_2 lners_{it} + v_3 (lners)^2_{it} + v_4 \sum control_{it} + \gamma_t + \lambda_i + \xi_{it} \quad (8)$$

where *innov* is the level of green technology innovation, which is represented by the total number of green patent applications in a city in a year. The relevant data were obtained by querying the State Patent Office. The interpretation of other variables is the same as that in model (6). If the coefficients β_1, β_2, and v_1 are significant, then an intermediary effect exists.

The regression results are shown in **Table 5**. In column (1), the primary term coefficient of environmental regulation level (lners) is negative, and the square term coefficient is positive. This result demonstrates that the impact of environmental regulation on urban green technology innovation is "U" shaped, which first inhibits and then promotes. In column (2), the coefficient of green innovation level (innov) is significantly negative, indicating that improving the green innovation level of coastal cities helps reduce coastal marine pollution. Therefore, Hypothesis 2 is verified. Environmental regulation exerts an impact on coastal marine pollution through affecting green technology innovation. In the absence of external constraints, enterprises often ignore the damage to the ecological environment in the processes of production and operation and lack the enthusiasm to increase investment in green scientific research and promote cleaner production. Hence, the government should urge enterprises to bear environmental social responsibility through environmental regulation. However, when the level of environmental regulation is relatively low, the "innovation compensation effect" hardly covers the "follow-the-cost effect." Enterprises tend to avoid green technology innovation and follow the traditional development model. Nevertheless, with the improvement of environmental regulation intensity, increased pollution emission costs will urge enterprises to adjust their development strategies. To avoid being eliminated from the market or

TABLE 4 | Endogenous test.

Variables	Lag regression	Instrumental variable regression
	(1)	(2)
l.lners	1.722**	
	(0.681)	
l. $(lners)^2$	-0.309**	
	(0.129)	
lners		25.177**
		(12.362)
$(lners)^2$		-4.543**
		(2.235)
Control	43S	YES
Time fixed effect	YES	YES
Urban fixed effect	YES	YES
N	552	495
LM-statistics		36.222
F-statistics		14.211
$\chi 2$ P-value		0.468
Adj R2	0.286	0.029

*Figures in () are robust standard error; ** indicates significance at the, 5% level, respectively.*

TABLE 5 | Mechanism analysis.

Variables	innov	lnmp
	(1)	(2)
lners	-32.952***	3.683***
	(6.443)	(0.613)
$(lners)^2$	5.804***	-0.652***
	(1.194)	(0.114)
innov		-0.006**
		(0.002)
Control	YES	YES
Time fixed effect	YES	YES
Urban fixed effect	YES	YES
N	598	598
Adj R2	0.447	0.547

*Figures in () are robust standard error; ***, ** indicate significance at the 1%, 5% levels, respectively.*

migrating outward, enterprises will pay considerable attention to the R&D and application of green technology; actively develop or introduce green technology by fully considering R&D capacity and economic benefits, promote energy conservation, emission reduction, and cleaner production.

4.5 Spatial Regression Results

4.5.1 Spatial Correlation Test

To analyze whether environmental regulation has a spatial spillover effect on coastal marine pollution, we should test the spatial autocorrelation of the coastal marine pollution index. This study identified the spatial correlation of coastal marine pollution in 46 coastal cities from 2004 to 2016 through Moran's I index. The specific results are shown in **Table 6**. **Table 6** presents that the Moran's I index for coastal marine pollution is significantly positive, except for individual years. This result indicates that a significant spatial positive correlation in the degree of coastal marine pollution exists among China's coastal cities, with evident spatial agglomeration characteristics. This finding lays a theoretical foundation for this study to further explore the impact mechanism of environmental regulation on coastal marine pollution by using a spatial econometric model.

4.5.2 Spatial Model Settings

To accurately evaluate the spatial effect of environmental regulation and avoid influencing the effectiveness of the conclusion due to setting errors, we conducted an identification test on the spatial panel model. The specific test types and results are shown in **Table 7**. First, LM and robust LM were used to test the spatial lag and correlation. The test results show that the model has spatial lag and error terms. On this basis, the appropriate spatial econometric model was selected through LR and Wald tests. Both of them pass the 1% significance test, which implies that choosing the spatial Dobbin model (SDM) for demonstration is more reasonable. Lastly, the Hausman test shows that the result is significant at the level of 1%. Therefore, we chose the fixed effect model of SDM to analyze the spatial effect of environmental regulation on coastal marine pollution. The model was constructed as

$$\begin{aligned} lnmp_{it} = {} & \rho_0 + \rho_1 lners_{it} + \rho_2 (lners)_{it}^2 + \rho_3 \sum controlit \\ & + \delta W lnmp_{it} + \theta_1 W lners_{it} \\ & + \theta_2 W (lners)_{it}^2 + \theta_3 W \sum control_{it} + \gamma t + \lambda_i + \xi_{it} \end{aligned} \quad (9)$$

where δ is the spatial autoregressive coefficient of coastal marine pollution, W is the spatial weight matrix, ρ is the coefficient of the explanatory variable, θ is the coefficient of the spatial interaction term of the explanatory variable, and the interpretation of other variables is the same as that in model (6). The spatial weight matrix selected in this study is the geographical distance weight matrix, which is expressed by the reciprocal of the linear distance between the centers of two regions.

4.5.3 Spatial Correlation Test

We used SDM to test the spatial spillover effect of environmental regulation on coastal marine pollution. The regression results are shown in **Table 8**. From column (1), under the geographical distance matrix, the spatial autoregressive coefficient of coastal marine pollution is significantly positive, the spatial interaction coefficient of the primary term of environmental regulation level (lners) is significantly positive, and the spatial interaction coefficient of the square term is significantly negative. This result shows that the coastal marine pollution of coastal cities not only has an endogenous interaction effect but also has an exogenous interaction effect of environmental regulation. Hypothesis 3 is verified. Environmental regulation can affect coastal marine pollution in adjacent areas through the spatial spillover effect, and the impact trajectory shows an inverted "U" curve. We proposed the following three reasons. First, differences in the implementation of environmental regulations exist among various coastal cities. Under the dual pressure of local finance and promotion championship, " race to the bottom " and "incomplete implementation" of environmental regulation may occur. Polluting enterprises that cannot adapt to the local strict environmental regulation will migrate to the adjacent areas with relatively loose regulation, thus aggravating the marine pollution problem of adjacent coastal cities. Second, because of the spatial spillover of coastal marine pollution itself, with the improvement of environmental regulation level, the quality of marine ecological environment in a region will gradually improve. The emission reduction and pollution control effect brought by environmental regulation will spread to adjacent areas to reduce the coastal marine pollution of adjacent coastal cities. Third, the positive influence of regional interaction effect has been brought into play. Environmental regulation in a region has brought "demonstration effect" and "warning effect" to the governments and enterprises in adjacent regions. At the same time, with the

TABLE 6 | Moran's I index of coastal marine pollution in coastal cities.

Year	Moran's I	p-value	Year	Moran's I	p-value
2004	0.064	0.151	2011	0.236	0.001
2005	0.178	0.009	2012	0.196	0.004
2006	0.171	0.010	2013	0.158	0.015
2007	0.194	0.004	2014	0.173	0.009
2008	0.155	0.016	2015	0.107	0.059
2009	0.240	0.001	2016	0.104	0.062
2010	0.236	0.001			

TABLE 7 | LM, Wald, LR and Hausman Tests.

Type	Z	p-value
Lagrange multiplier (error)	69.629	0.000
Robust Lagrange multiplier (error)	31.981	0.000
Lagrange multiplier (lag)	43.793	0.000
Robust Lagrange multiplier (lag)	6.145	0.013
LR spatial lag	33.04	0.000
LR spatial error	33.06	0.000
Waldspatial lag	21.25	0.003
Waldspatial error	20.88	0.007
Hausman	58.38	0.000

TABLE 8 | Regression results of spatial dobbin model.

Variables	Dependent Variable: Coastal Marine Pollution Index		
	(1)	(2)	(3)
lners	4.793**		
	(2.336)		
$(lners)^2$	-0.863**		
	(0.436)		
W×lners	37.637***		
	(13.477)		
W×$(lners)^2$	-7.037***		
	(2.482)		
erh		0.103**	
		(0.059)	
$(erh)^2$		-0.017**	
		(0.008)	
W×erh		0.563***	
		(0.208)	
W×$(erh)^2$		-0.058**	
		(0.028)	
er			0.084**
			(0.035)
$(er)^2$			-0.003**
			(0.001)
W×er			0.364**
			(0.150)
W×$(er)^2$			-0.014**
			(0.006)
rho	0.229***	0.467***	0.223***
	(0.086)	(0.068)	(0.089)
sigma2_e	0.055***	0.057***	0.055***
	(0.003)	(0.003)	(0.003)
Control	YES	YES	YES
N	598	598	598
Adj R2	0.098	0.109	0.091

*Figures in () are robust standard error; ***, ** indicate significance at the 1%, 5% levels, respectively.*

continuous improvement of the state's attention to ecological and environmental protection, the diffusion and application of green technologies, such as pollution control and cleaner production, will also be accelerated.

To verify the reliability of the results of spatial spillover effect, we tested the robustness by replacing explanatory variables. In columns (2) and (3), the spatial autoregressive coefficients are significantly positive, Hand the spatial interaction term coefficients of the primary term and square term of environmental regulation level (er, erh) are significantly positive and negative, respectively, which is basically consistent with the previous conclusions. Therefore, the test results of environmental regulation on the spatial spillover effect of coastal marine pollution have strong robustness. On this basis, we decomposed the spatial effect to deeply explore the impact of environmental regulation on coastal marine pollution in a region and adjacent areas and explained it through direct and indirect effects. In accordance with **Table 9**, the indirect effect of environmental regulation on coastal marine pollution is significant, which is similar to the impact track of local effect and shows the dynamic characteristic of inverted "U." The indirect effect is significantly greater than the direct effect, which further shows that in geographical space, adjacent coastal cities will jointly bear the pollution of coastal marine environment and enjoy the results of environmental governance.

TABLE 9 | Spatial effect decomposition.

Variables	Direct Effect	Indirect Effect	Total Effect
lners	4.053**	26.750**	30.803***
	(0.061)	(11.125)	(11.168)
$(lners)^2$	-0.726**	-5.021**	-5.748***
	(0.438)	(2.040)	(2.048)
erh	0.130**	1.122***	1.252***
	(0.061)	(0.363)	(0.384)
$(erh)^2$	-0.020**	-0.121**	-0.141**
	(0.008)	(0.048)	(0.050)
er	0.090**	0.473***	0.563***
	(0.035)	(0.180)	(0.186)
$(er)^2$	-0.003**	-0.018***	-0.021***
	(0.001)	(0.007)	(0.007)

*Figures in () are robust standard error; ***, ** indicate significance at the 1%, 5% level, respectively.*

5 DISCUSSION

Improving the governance level and the quality of marine ecological environment is crucial for the development of China's marine cause. After long-term efforts, China's marine environmental protection has achieved phased results (Guan et al., 2019; Li, 2020; Chen and Hu, 2021). However, the pollution of some sea areas is still serious, the marine ecological situation remains severe, and the green paradox and pollution transfer phenomenon exist to a certain extent. The implementation effect and impact mechanism of environmental regulation policies in coastal cities should be analyzed. On the basis of the panel data of 46 coastal prefecture-level cities in China, we explored the impact of environmental regulation on coastal marine pollution from a multidimensional perspective. Definition of symbols in formulas are shown in **Table 10**. Our research contributes to the literature in two important aspects. (1) Existing research on the relationship between environmental regulation and environmental pollution mainly focuses on inland areas, and research focusing on the marine field is lacking. Most of the studies stay at the provincial level, without fully considering the objective differences between coastal cities in economic level, industrial structure, and innovation factors. We sank the analysis object to coastal prefecture-level cities and

TABLE 10 | Nomenclatures.

Symbol used	Definition of the symbol
α	coefficient of variable
β	coefficient of variable
ν	coefficient of variable
ρ	coefficient of variable
γ	fixed effects of time
λ	fixed effects of city
ξ	random interference item
θ	coefficient of the spatial interaction term
δ	spatial autoregressive coefficient
W	spatial weight matrix

quantitatively evaluated the impact of environmental regulation on coastal marine pollution by constructing environmental regulation level indicators and marine pollution indexes. The finding shows that environmental regulation has an inverted "U" effect on coastal marine pollution, which first intensifies and then inhibits. Therefore, coastal cities should improve environmental regulation. While eliminating high-pollution and inefficient industries, the government should force enterprises to independently develop or introduce green technologies to effectively promote cleaner production, energy conservation, and emission reduction. On this basis, we analyzed the mechanism of environmental regulation from the perspective of green technology innovation and found that promoting green technology innovation is an important mechanism for environmental regulation to improve the quality of marine environment. (2) Studies on the effectiveness of environmental regulation in ecological governance are often limited to the direct effect of environmental regulation. Few studies have explored the impact of environmental regulation on the coastal marine environment of surrounding cities from a spatial perspective. In accordance with the geographical distance weight matrix, we used SDM to test the spatial spillover effect of environmental regulation on coastal marine pollution. We found that the coastal marine pollution of coastal cities has not only an endogenous interaction effect but also an exogenous interaction effect of environmental regulation. The indirect effect of environmental regulation on coastal marine pollution is significant and presents the same inverted "U" effect as that of the local one. Thus, the effective implementation of environmental regulation should be based on regional joint prevention and control. Strengthening communication and cooperation and coordinating environmental regulation actions by coastal city governments are important contents to promote the continuous improvement of marine ecological environment quality.

6 CONCLUSIONS

This study used the panel data of 46 coastal prefecture-level cities in China from 2004 to 2016 as samples to quantitatively evaluate the relationship between environmental regulation and coastal marine pollution and explored its role from the perspective of green technology innovation. On this basis, the spatial spillover effect was included in the research scope, and the impact mechanism of environmental regulation on coastal marine pollution was deeply analyzed. We reached the following conclusions: (1) The impact of environmental regulation on coastal marine pollution shows an inverted "U" shape. The low level of environmental regulation in coastal cities intensifies the problem of coastal marine pollution. With the improvement of the level of environmental regulation, its containment effect on coastal marine pollution becomes gradually prominent. (2) Environmental regulation exerts an impact on coastal marine pollution through affecting green technology innovation. When the level of environmental regulation is relatively low, the "innovation compensation effect" hardly covers the "follow-the-cost effect." However, with the improvement of the intensity of environmental regulation, the enthusiasm of enterprises for green technology innovation will gradually increase to promote marine ecological environment protection. (3) The environmental regulation of coastal cities can affect the coastal marine pollution in adjacent areas through the spatial spillover effect. The impact trajectory also shows an inverted "U" curve, and the indirect effect is significantly greater than the direct effect. The adjacent coastal cities share the responsibility of marine pollution and the results of marine governance.

The above conclusions have important implications for controlling land-based pollution emissions and improving marine ecological environment governance:

1. Build a scientific and strict environmental regulation system. Coastal city governments should accurately understand the role of environmental regulation in marine ecological environment protection and implement differentiated environmental regulation policies with comprehensive consideration of regional development level, geographical location, and pollution status. The central government should strengthen environmental protection supervision, enhance the performance evaluation system guided by green transformation, and improve the innovation of local governments in formulating environmental policies and the enthusiasm of implementing environmental policies.
2. Give full play to the conduction effect of green technology innovation in environmental regulation and coastal marine ecological environment. On the one hand, the government should actively promote the establishment of a green technology innovation system with enterprises as the main body. While the government puts forward clear requirements on emission standards and production technology, it should effectively utilize market means, such as environmental protection tax, environmental subsidies, and emission trading, to stimulate the enthusiasm of enterprises to carry out green technology innovation. On the other hand, the government should gradually improve the transformation mechanism of scientific and technological achievements, accelerate the ownership reform of scientific and technological achievements, promote the market-oriented application of green innovation achievements, build a green technology cooperation and exchange platform, and consolidate the foundation for the diffusion and application of green technology.
3. Pay attention to the trans regional transfer and treatment of coastal marine pollution and promote regional joint prevention and control. Coastal city governments should break through the shackles of "mutual prevarication and respective formation," pay attention to the coordination and cooperation with adjacent regions in marine environmental governance, and strengthen joint environmental law enforcement and supervision. Under the overall coordination of the central government, building a platform for environmental protection information exchange and sharing, establishing a coordination mechanism for marine pollution prevention and control, and preparing a

unified plan for regional ecological environment governance are vital.

DATA AVAILABILITY STATEMENT

The original contributions presented in the study are included in the article/supplementary material. Further inquiries can be directed to the corresponding author.

AUTHOR CONTRIBUTIONS

QH put forward the idea and revised the paper; JM analyzed the data and wrote the paper; XW contributed to the conceptual framework of the methodology. All authors have read and approved the final manuscript.

FUNDING

National Natural Science Foundation of China (No. 71874092).

REFERENCES

Arik, L. (2003). Environmental Regulatory Competition: A Status Report and Some New Evidence. *Natl. Tax. J.* 56, 91–106. doi: 10.17310/ntj.2003.1.06

Ban, L., and Liu, X. (2021). The Study of Emission Reduction Effects of Different Environmental Regulations on the Different Environmental Pollution Types. *Ningxia Soc Sci.* 40, 140–151. doi: 10.3969/j.issn.1002-0292.2021.05.016

Chen, J. (2021). The Impact of Environmental Regulation on Green Development Marine Economy. *J. Tech. Econ. Manage.* 42, 103–107. doi: 10.3969/j.issn.1004-292X.2021.12.020

Chen, Q., and Hu, Q. (2021). Evolution Logic, Complementary Needs and Reform Path of China's Marine Ecological Protection System. *Chn. Popu. Res. Envi.* 31, 174–182.

Chen, Z., Kahn, M., Liu, Y., and Wang, Z. (2018). The Consequences of Spatially Differentiated Water Pollution Regulation in China. *J. Envi. Manag.* 88, 468–485. doi: 10.1016/j.jeem.2018.01.010

Chen, S., Zhang, J., and Liu, C. (2021). Environmental Regulation,Financing Constraints,and Enterprise Emission Reduction: Evidence From Pollution Levy Standards Adjustment. *J. Financ. Res.* 64, 51–71.

Fünfgelt, J., and Schulze, G. (2016). Endogenous Environmental Policy for Small Open Economies With Transboundary Pollution. *Econ. Model.* 57, 294–310. doi: 10.1016/j.econmod.2016.03.021

Gao, L., and Gao, Q. (2012). Validation and Calculation of the Coordination Degree of Interactive Relationships in the Marine Eco-Economic System. *Res. Sci.* 34, 173–184.

Gene, M., and Alan, B. (1995). Economic Growth and the Environment. *Q. J. Econ* 110, 353–377. doi: 10.2307/2118443

Ge, H., Zhu, Z., Zhong, C., and Zhu, G. (2020). Study on the Impact of Environmental Regulation on the Transformation of Regional Marine Economy. *Stats. Deci* 36, 111–114. doi: 10.13546/j.cnki.tjyjc.2020.24.024

Guan, D., Liang, B., and Zhang, Z. (2019). Marine Eco-Environmental Protection in China: History, Current Situation and Future. *Environ. Prot.* 47, 27–31. doi: 10.14026/j.cnki.0253-9705.2019.17.006

He, L., and Chen, X. (2018). Empirical Research on the Effect of Marine Environmental Pollution to Marine Economic Development Based on the Panel Data. *Ocean Dev. Manage.* 35, 17–21. doi: 10.3969/j.issn.1005-9857.2018.02.004

Hui, W., and Zhao, G. (2017). Environmental Regulation and Pollution Haven —— An Empirical Analysis Based on Panel Threshold Regression of Chinese Provincial Data. *Econ. Theory Bus. Manage.* 37, 23–33.

Hu, Q., and Ma, J. (2022). Impact of Low-Carbon City Pilot Policies on Green Technology Innovation Efficiency——An Empirical Test Based on the Perspective of Innovation Value Chain. *J. Soc Sci.* 44, 62–72. doi: 10.13644/j.cnki.cn31-1112.2022.01.006

Jiang, Y., and Cui, G. (2019). The Impact of Environmental Industrial Policies on Corporate Environmental Investment: Based on the Empirical Study of Heavily Polluted Companies. *Reform.* 32, 87–101.

Ji, Z., and Song, Y. (2021). Spatial Effect of Pollution Agglomeration of Environmental Regulation in the Yangtze River Delta. *J. Tech. Econ. Manage.* 42, 124–128. doi: 10.3969/j.issn.1004-292X.2021.08.024

Li, Z. (2020). Transition Path of Green Development of Marine Economy in the Perspective of "Ecological+". *Econ. Manag.* 34, 35–41.

Li, M., and Du, W. (2014). Is the Double Dividend of Environmental Regulation and Employment Applicable to China? Empirical Analysis Based on Inter Provincial Panel Data. *Econ. Sci.* 36, 14–26. doi: 10.3969/j.issn.1007-5097.2011.06.003

Li, H., Hu, Q., and Hu, B. (2011). Research of Coordinated Development Between Marine Economy and Ecological Environment in Zhejiang Province——Based on the Perspective of a Low-Carbon Economy. *East Chin. Econ. Manage.* 25, 11–14. doi: doi:10.19523/j.jjkx.2014.04.003

Liu, J., and Wan, G. (2021). Does Environmental Regulation Restrain FDI Inflow? *Res. Econ. Manage.* 42, 20–34. doi: 10.13502/j.cnki.issn1000-7636.2021.11.002

Li, R., and Zhang, J. (2020). The Heterogeneous Impact of Different Types of Environmental Regulations on Local Environmental Governance. *Commer. Res.* 63, 36–45. doi: 10.13902/j.cnki.syyj.2020.07.005

Li, H., Zhang, J., Wang, C., Wang, Y., and Coffey, V. (2018). An Evaluation of the Impact of Environmental Regulation on the Efficiency of Technology Innovation Using the Combined DEA Model: A Case Study of Xi'an, China. *Sustain. Cities Soc* 42, 355–369. doi: 10.1016/j.scs.2018.07.001

Peng, F., Sun, C., Liu, T., Li, Y., and Hu, W. (2018). Temporal and Spatial Evolution of Vulnerability and Coordination of Marine Eco-Economic System in Coastal Area of China. *Econ. Geogr.* 38, 165–174. doi: 10.15957/j.cnki.jjdl.2018.03.021

Porter, M., and van der Linde, C. (1995). Toward a New Conception of the Environment-Competitiveness Relationship. *J. Econ. Perspect.* 9, 97–118. doi: 10.1257/jep.9.4.97

Qin, B., and Ge, L. (2018). Relative Environmental Regulations,Pollution-Intensive Industry Transfer and Pollution Agglomeration in China. *Chn. Popu. Res. Envi.* 28, 52–62.

Qi, H., and Wang, Z. (2015). Research on the Change of Emission Differences and Its Income Partition Countermeasures in China. *J. Quant. Tech. Econ.* 32, 57–72+141. doi: 10.13653/j.cnki.jqte.2015.12.004

Shen, W., Hu, Q., and Yu, X. (2021). Impact of Coastal City Economic Growth Target on Offshore Pollution. *Res. Sci.* 43, 898–908. doi: 10.18402/resci.2021.05.04

Shen, K., Jin, G., and Fang, X. (2017). Does Environmental Regulation Cause Pollution to Transfer Nearby? *Econ. Res. J.* 52, 44–59.

Sinn, H. (2008). Public Policies Against Global Warming:A Supply Side Approach. *Cesifo Work. Paper.* 15, 360–394. doi: 10.1007/s10797-008-9082-z

Song, M., and Wang, S. (2013). Analysis of Environmental Regulation, Technological Progression and Economic Growth From the Perspective of Statistical Tests. *Econ. Res. J.* 48, 122–134.

Sun, H., and Zaenhaer, D. (2021). The Impact of Heterogeneous Environmental Regulation on Urban Environmental Pollution:Research Based on Static and Dynamic Spatial Durbin Model. *East Chin. Econ. Manage.* 35, 75–82. doi: 10.19629/j.cnki.34-1014/f.201120017

Wang, S. (2018). Local Environmental Laws and Regulations,Marketization Process and Pollution Emissions. *East Chin. Econ. Manage.* 32, 70–78. doi: 10.19629/j.cnki.34-1014/f.170910004

Wang, Z., Bu, C., Li, H., and Wei, W. (2019). Seawater Environmental Kuznets Curve: Evidence From Seawater Quality in China's Coastal Waters. *J. Clean. Prod.* 219, 925–935. doi: 10.1016/j.jclepro.2019.02.012

Wang, Y., and Lu, Y. (2021). Fiscal Decentralization,Environmental Regulation and Regional Environmental Quality——Empirical Analysis Based on Mediation Effect and Threshold Effect. *Inq. Econ. Issues*. 42, 120–137.

Wu, H., Guo, H., Zhang, B., and Bu, M. (2017). Westward Movement of New Polluting Firms in China: Pollution Reduction Mandates and Location Choice. *J. Comp. Econ.* 45, 119–138. doi: 10.1016/j.jce.2016.01.001

Wu, L., and Han, H. (2020). Environmental Regulation,Green Technology Innovation and Regional Environmental Quality. *Urban Environ. Stud.* 7, 38–65.

Wu, W., and He, Q. (2017). "Forced Pollution Reduction" or "Regressive" ? Threshold Characteristic and Spatial Spillover of Pollution Reduction Effect From Environmental Regulation. *Econ. Manage.* 39, 20–34. doi: 10.19616/j.cnki.bmj.2017.02.002

Wu, Y., Qian, J., and Zhang, T. (2021). Environmental Regulation,Green Technology Innovation, and High-Quality Economic Development in the Yangtze River Delta. *East Chin. Econ. Manage.* 35, 30–42. doi: 10.19629/j.cnki.34-1014/f.210615027

Xia, Y., and Zhong, M. (2016). The Influence of Environmental Regulation on the Decoupling Between Economic Growth and Environmental Pollution: Analysis Based on Industrial SO2 Emission Data of China's 271 Cities. *J. Bus. Econ.* 36, 69–78. doi: 10.14134/j.cnki.cn33-1336/f.2016.11.007

Xie, M., Wang, J., and Liu, D. (2014). Environment Regulation, Technological Innovation and Corporate Performance. *Nankai Bus. Rev.* 17, 106–113. doi: 10.3969/j.issn.1008-3448.2014.06.012

Xu, Z. (2016). Industrial Economic Development, Environmental Regulation Intensity and Pollution Reduction Effect: Theoretical Analysis and Empirical Test Based on Development Pattern of Treatment After Pollution. *J. Financ. Econ.* 42, 134–144. doi: 10.16538/j.cnki.jfe.2016.03.011

Xu, R., and Lin, X. (2020). Multiple Subjects of Ecological Compensation, Environmental Regulation and Sustainable Development of Marine Economy. *Econ. Prob.* 42, 58–67. doi: 10.16011/j.cnki.jjwt.2020.11.008

Yang, L., and Wen, X. (2021). Does Environmental Regulation Improve Transformation and Upgrading of Marine Industrial Structure ——Based on Selection of Marin Environmental Regulation Tools. *Rev. Econ. Manage.* 37, 38–49. doi: 10.13962/j.cnki.37-1486/f.2021.01.004

Ye, Q., Zeng, G., Dai, S., and Wang, D. (2018). Research on the Effects of Different Policy Tools on China's Emissions Reduction Innovation. *Chn. Popu. Res. Envi.* 28, 115–122.

Yu, X., Shen, M., Xie, H., and Wang, D. (2020). The Impact of China's Coastal Urbanization on Marine Pollution: Based on Panel Spatial Measurement Method. *Chn. J. Environ. Manage.* 12, 95–102. doi: 10.16868/j.cnki.1674-6252.2020.06.095

Zhang, H. (2014). The Green Paradox Puzzle: Interpretation From the Perspective of Local Government Competition. *J. Financ. Econ.* 40, 114–127. doi: 10.16538/j.cnki.jfe.2014.12.001

Zhang, Z. (2017). Does Environmental Regulation Improve the Urban Environmental Quality in China? Evidence Based on a "Quasi-Natural Experiment". *Ind. Econ. Res.* 16, 69–80. doi: 10.13269/j.cnki.ier.2017.03.006

Zhang, J., and Chen, S. (2021). Financial Development, Environmental Regulations and Green Economic Transition. *J. Financ. Econ.* 47, 78–93. doi: 10.16538/j.cnki.jfe.20210918.301

Zhang, H., Liu, M., Zhang, C., and Wang, K. (2020). Study on the Dynamic Impact of Land Industrial Structure Evolution on Marine Environment: A Case Study of the Yangtze Basin and the East China Sea Coast. *Res. Environ. Yangtze Basin.* 29, 1586–1596.

Zhang, H., and Wei, X. (2014). Green Paradox or Forced Emission-Reduction: Dual Effect of Environmental Regulation on Carbon Emissions. *Chn. Popu. Res. Envi.* 24, 21–29. doi: 10.3969/j.issn.1002-2104.2014.09.004

Zhang, M., Zhang, L., and Song, Y. (2021). Heterogeneous Environmental Regulations, Spatial Spillover and Haze Pollution. *Chn. Popu. Res. Envi.* 31, 53–61.

Zhao, Y. (2019). Study on the Induced Marine Technological Innovation and Environmental Regulation. *Ecol. Econ.* 35, 143–153.

Zhou, X., Feng, C., Hu, Y., and Wei, X. (2015). Environmental Regulation and Fossil Energy Consumption: Based on the Perspective of Technological Progress and Economic Structure Transformation. *Chn. Popu. Res. Envi.* 25, 35–44. doi: 10.3969/j.issn.1002-2104.2015.12.005

Conflict of Interest: The authors declare that the research was conducted in the absence of any commercial or financial relationships that could be construed as a potential conflict of interest.

Publisher's Note: All claims expressed in this article are solely those of the authors and do not necessarily represent those of their affiliated organizations, or those of the publisher, the editors and the reviewers. Any product that may be evaluated in this article, or claim that may be made by its manufacturer, is not guaranteed or endorsed by the publisher.

Copyright © 2022 Ma, Hu and Wei. This is an open-access article distributed under the terms of the Creative Commons Attribution License (CC BY). The use, distribution or reproduction in other forums is permitted, provided the original author(s) and the copyright owner(s) are credited and that the original publication in this journal is cited, in accordance with accepted academic practice. No use, distribution or reproduction is permitted which does not comply with these terms.

frontiers | Frontiers in Marine Science

ORIGINAL RESEARCH
published: 13 June 2022
doi: 10.3389/fmars.2022.920069

Conditions of Mainland China's Island Ecosystems and Associated Influencing Factors: Integrated Assessment of 42 Typical Island Ecosystems

Zhiyuan Ma[1,2], Weiwei Yu[1,2], Wanting Zhang[1,2], Feiyang Ge[1], Bin Chen[1,2]*, Wenjia Hu[1,2], Dian Zhang[1], Jianji Liao[1,2], Hao Huang[1,2], Yuanmin Sun[1,2] and Haiping Huang[1]*

[1] Third Institute of Oceanography, Ministry of Natural Resources, Xiamen, China, [2] Key Laboratory of Marine Ecological Conservation and Restoration, Ministry of Natural Resources, Xiamen, China

OPEN ACCESS

Edited by:
Meilin Wu,
Chinese Academy of Sciences, China

Reviewed by:
Chao Chen,
Zhejiang Ocean University, China
Zhaohui Zhang,
First Institute of Oceanography, China
Zeng Jiangning,
Ministry of Natural Resources, China

***Correspondence:**
Weiwei Yu
yuweiwei@tio.org.cn
Bin Chen
chenbin@tio.org.cn

Specialty section:
This article was submitted to Marine Pollution, a section of the journal Frontiers in Marine Science

Received: 14 April 2022
Accepted: 13 May 2022
Published: 13 June 2022

Citation:
Ma Z, Yu W, Zhang W, Ge F, Chen B, Hu W, Zhang D, Liao J, Huang H, Sun Y and Huang H (2022) Conditions of Mainland China's Island Ecosystems and Associated Influencing Factors: Integrated Assessment of 42 Typical Island Ecosystems. Front. Mar. Sci. 9:920069. doi: 10.3389/fmars.2022.920069

Although China possesses a large number of islands, knowledge of their overall ecological condition is limited on a national scale. Accordingly, this study developed a comprehensive and quantitative island ecosystem assessment framework that incorporates environmental quality, biological structure, and landscape patterns. The framework was applied to 42 typical, representative islands within China's coastal regions, including different climatic zones, area sizes, populations, and substratum lithologies. Results showed that the value range of the comprehensive index of island ecosystem condition (CI_{island}) was significant (from 52.33 to 89.53, 71.72 average), and 85.4% of islands scored either "high" or "good," indicative of their exceptional condition. However, conditions varied among different island components, indicating different challenges. Environmental quality index (I_{env}) values ranged from 60.70 to 94.80 (79.72 average), where primary threats were seawater nutrient pollution, petroleum, and marine organism metal contamination. Biological structure index (I_{bio}) values ranged from 43.50 to 89.40 (66.10 average), where primary threats were vegetation destruction and a reduction in marine biodiversity within intertidal and subtidal zones. Landscape pattern index (I_{land}) values varied significantly (from 6 to 100, 72.36 average), where a key characteristic of highly developed islands was low natural landscape (vegetation) coverage. Conditions also varied among island climate zones, lithologies, area sizes, and levels of human habitation. Additionally, island ecosystem conditions were influenced by both natural and anthropogenic factors as well as area size, population, and GDP. Although distance to the mainland significantly correlated to (I_{bio}), and (CI_{island}), these parameters did not significantly correlate to (I_{env}), which might be explained by that environmental quality

was generally conditional on large-scale environments. This assessment is intended to provide a holistic perspective on island conditions in China while identifying key challenges and associated driving factors, which will greatly aid in establishing island-specific sustainable management practices.

Keywords: integrated assessment, ecosystem indicators, island ecosystem, island sustainable management, ecosystem condition

INTRODUCTION

An island is a land body completely surrounded by sea water, which is a complicated ecological-social-economical systems having important ecological and socioeconomic roles. Due to geographic isolation and unique environments, many endemic and specialized species inhabit islands (Weigelt et al., 2013), playing a critical role in global biodiversity maintenance (Veettil et al., 2020). At the same time, island ecosystems also provide valuable goods and services, such as food and water provisioning, erosion and pollination regulation, and recreation and ecotourism (Su et al., 2016; Balzan et al., 2018). However, owing to their isolation and small size, most island ecosystems are ecologically fragile (Brodie et al., 2013), being particularly susceptible to global climate change (Leclerc et al., 2020), land-use intensification (Xie et al., 2021), exotic species invasion (Reaser et al., 2007), etc. Under increasing threat from natural and anthropogenic impacts, there is growing concern regarding island conservation and sustainable development around the world.

Comparatively, China holds many islands. For example, more than 11,000 islands are dispersed around its surrounding seas, among which 7372 have a land area greater than 500 m^2. This equates to an approximate land area of 72,800 km^2 and a coastline of 14217.8 km (Ministry of Natural Resources of the People's Republic of China, 2018). Many of these islands have undergone considerable changes and degradation, mainly due to intensive anthropogenic activities (Zhao et al., 2004; Cao et al., 2017), such as vegetation destruction, endemic species loss, and seawater deterioration. Over time, island management has moved from being hands-off to active management, such as island restoration, island tourism management, and carefully planned and comprehensive management will become more necessary with increasing climate change and anthropogenic pressures (Xie et al., 2021), particularly in a large spatial scale. For better decision making for island management, it is important to determine their ecosystem condition status and baseline.

Since China's First National Island Resources Comprehensive Survey (1988–1996), various aspects of island data have been reported on, including island soil, bird, vegetation, marine organisms, environmental quality, etc. (Yang, 2000; Xu et al., 2017; Tan et al., 2020). In recent years, an increasing number of studies have tended to assess or evaluate island ecosystems quantitatively. For example, Zhan et al. (2019) used emergy analysis modeling to evaluate ecosystem services in Chongming Island. Sun et al. (2020) established an Eco-environmental Quality Index (EQI) model to evaluate the ecological status of Hainan Island. Zhang et al. (2021) applied principal component analysis (PCA) to conduct an island sustainability evaluation in the Zhoushan Archipelago, using 15 island ecosystem indices covering climatic, geographical, landscape, social, and biological dimensions. Chi et al. (2021) applied 12 factors that included vegetation, soil, and landscape factors to evaluate island ecosystems in the Miaodao Archipelago. However, challenges remain: i) most current studies were conducted at a relatively small scale (i.e., island or archipelago scale), and knowledge related to Chinese island ecosystems and associated methodologies are limited on a national scale; ii) only limited knowledge is available on comprehensive island conditions that cover terrestrial, intertidal, and subtidal sub-ecosystems. Accordingly, this study aims to quantitatively explore the condition of Chinese island ecosystems, providing an important baseline to predict prospective effects of anthropogenic disturbances and climate change, which will be of great significance in informing the direction of effective management and sustainable development.

MATERIALS AND METHODS

Selected Islands

A total of 42 islands were selected for this study, exemplifying China's main island characteristics. These are representative island systems from different climatic zones and with varying area sizes, populations, and substratum lithologies (**Table 1** and **Figure 1**). Because China's subtropical zone consists of the largest number of islands overall (i.e., approximately 73% of all of China's islands are distributed off the coast of Zhejiang, Fujian, and Guangdong provinces) (Ministry of Natural Resources of the People's Republic of China, 2018), most islands selected for this study are from the subtropical zone (28 in total). Considering the relative equilibrium of the islands selected among China's different climate zones, subtropical islands were further grouped into three subsets by their location and climate condition, namely, northern subtropical, central subtropical, and southern subtropical subsets. Finally, nine temperate, nine northern subtropical, eight central subtropical, 11 southern subtropical, and five tropical island ecosystems were selected for this investigation. Island area ranged from 0.1 km^2 to 1225 km^2 (63.31 km^2 average), of which 86.36% were less than 100 km^2. Regarding population, most islands were inhabited (i.e., 35 inhabited and seven uninhabited). Based on island substratum lithologies, which express specific island-forming processes, 34

TABLE 1 | Characteristics of the selected islands in this study.

NO.	Island name	Area (km^2)	Climatic zone	Population	Island lithology
1	Dalu Island	3.7	Temperate	Inhabited	Continental
2	Dachangshan Island	25.7	Temperate	Inhabited	Continental
3	Snake Island	0.7	Temperate	Uninhabited	Continental
4	Juhua Island	11.7	Temperate	Inhabited	Continental
5	Shijiutuo Island	3.4	Temperate	Inhabited	Alluvial
6	Sanhe Island	0.1	Temperate	Uninhabited	Alluvial
7	Nanchangshan Island	10.4	Temperate	Inhabited	Continental
8	Liugong Island	1.8	Temperate	Inhabited	Continental
9	Dongxilian Island	5.4	Temperate	Inhabited	Continental
10	Xinglongsha Island	36.6	Northern Subtropical	Inhabited	Alluvial
11	Chongming Island	1225	Northern Subtropical	Inhabited	Alluvial
12	Dajinshan Island	0.2	Northern Subtropical	Uninhabited	Continental
13	Dayangshan Island	6.6	Northern Subtropical	Inhabited	Continental
14	Shengshan Island	4.5	Northern Subtropical	Inhabited	Continental
15	Daxie Island	28.4	Northern Subtropical	Inhabited	Continental
16	Zhoushan Island	502.6	Northern Subtropical	Inhabited	Continental
17	Mount Putuo Island	16	Northern Subtropical	Inhabited	Continental
18	Zhujiajian Island	75.8	Northern Subtropical	Inhabited	Continental
19	Baishishan Island	1.1	Central Subtropical	Inhabited	Continental
20	Wuzhishan Island	4.8	Central Subtropical	Uninhabited	Continental
21	Yuhuan Island	174.3	Central Subtropical	Inhabited	Continental
22	Dachen Islands	17.5	Central Subtropical	Inhabited	Continental
23	Yushan Islands	12	Central Subtropical	Inhabited	Continental
24	Nanji Archipelago	12	Central Subtropical	Inhabited	Continental
25	Xiaoyushan Island	3.3	Central Subtropical	Inhabited	Continental
26	Sandu Island	24.7	Central Subtropical	Inhabited	Continental
27	Langqi Island	72	Southern Subtropical	Inhabited	Continental
28	Meizhou Island	14.2	Southern Subtropical	Inhabited	Continental
29	Xiamen Island	129.5	Southern Subtropical	Inhabited	Continental
30	Zini Island	47	Southern Subtropical	Inhabited	Alluvial
31	Nan'ao Island	105.2	Southern Subtropical	Inhabited	Continental
32	Neilingding Island	5.5	Southern Subtropical	Uninhabited	Continental
33	Guishan Island	3.6	Southern Subtropical	Inhabited	Continental
34	Shangchuan Island	137.2	Southern Subtropical	Inhabited	Continental
35	Techeng Island	3.2	Southern Subtropical	Inhabited	Continental
36	Weizhou Island	25	Southern Subtropical	Inhabited	Continental
37	Jiangpingsan Islands	20.8	Southern Subtropical	Inhabited	Alluvial
38	Guoheyuan Island	1.1	Tropic	Uninhabited	Alluvial
39	Dongyu Island	1.7	Tropic	Inhabited	Alluvial
40	Dazhou Island	4.4	Tropic	Inhabited	Continental
41	Niuqizhou Island	1.1	Tropic	Uninhabited	Continental
42	Ximaozhou Island	2.1	Tropic	Inhabited	Continental

islands were designated continental and seven alluvial. In general, the distribution of all 42 islands selected for this study reflect the uneven distribution of the islands that surround China. In other words, most islands are distributed throughout the southern region of the country while, at the same time, most islands are situated nearshore (compared to offshore).

Data Sources

Data on marine environmental and biological parameters in this study were based on a comprehensive and nationwide marine project (i.e., China's offshore marine investigation and assessment), covering seawater, phytoplankton, and macrobenthos, which were compiled from a series of published provincial and national investigations reports (Offshore Marine Investigation and Assessment Project Office of Jiangsu, 2012; Hebei Oceanic Administration, 2013; Xu et al., 2013; Hou and Ma, 2014; Chen, 2016; Huang et al., 2017; Ma et al., 2017). Marine environmental and biological parameters were obtained during four campaigns conducted in July (summer) 2006, October (autumn) 2006, January (winter) 2007, and April (spring) 2007. Investigation methods used were consistent across all selected islands, following the technical regulations for island investigations (Offshore Marine Investigation and Assessment Project Office of SOA, 2005a), the technical regulations for marine biological and ecological investigations (Offshore Marine Investigation and Assessment Project Office of SOA, 2006a), the technical regulations for marine chemical investigations (Offshore Marine Investigation and Assessment Project Office of SOA, 2006b). Some of the data used in our study are presented in the **Supplementary Tables 1**, **2**.

For island vegetation and landscape parameters, data were interpreted from remote sensing images fused with multi-spectral and panchromatic bands with a resolution of 2.5m using data from 2005, following the technical regulations for aerial remote sensing investigation of islands and coastal zones (Offshore Marine Investigation and Assessment Project Office of SOA, 2005b).

FIGURE 1 | Distribution of the selected islands in this study.

TABLE 2 | Criteria for selecting indicators of island ecosystem condition.

Criteria	Description
Representative	Indicator should be typical for describing a certain aspect of ecosystem condition, and representative for some other related and repeated indicators with the same or similar meaning.
Sensitive	Indicator should be able to provide early warnings and accurately reflects a certain aspect of ecosystem condition.
Measurable	Indicator should be measured by scientific tools or methods and transparent for an easy communication, in order to be applied at different islands.
Data available	The data required for indicators should be easy to attain and interpret by current monitoring efforts.
Comprehensive	Indicator system should be comprehensive to cover the main characteristics of ecosystem, and also reflect the spatial integrity of island ecosystem covering insular land, intertidal and subtidal sub-ecosystems.

In this way, all data described were obtained during the same period with uniform investigation technical regulations, enhancing the data's comparability and reliability.

Integrated Assessment Method

Indicators

An island is a unique ecosystem comprised of complex components in multiple dimensions, which spatially covers various sub-ecosystems, including terrestrial, intertidal, and subtidal sub-ecosystems, biotic and abiotic factors, and the hierarchical ecological organization of individuals, populations, communities, and landscapes. For this study, to simplify complexity, island ecosystem condition was defined and characterized under three specific factors: environmental, biological, and landscape. A set of criteria was then proposed to screen for appropriate indicators that could be used to determine island ecosystem conditions, including representativeness, sensitivity, measurability, data availability, and comprehensiveness (**Table 2**). Based on these criteria, proposed indicators were selected by a panel of experts using

the Delphi method, and a three-hierarchal indicator system was established, covering indicators related to environmental quality, biological structure, and landscape pattern (**Table 3**).

For environmental quality, three subgoals were considered in view of data availability, including the quality of seawater, intertidal sediment, and intertidal organisms, which were measured using typically used chemical parameters. For biological structure, in light of the spatial integrity of biological structure, terrestrial, intertidal, and subtidal biological structures were included. Moreover, two specific species level indicators were also considered, including invasive species and indicator species of important or endangered species. Biological structures were primarily measured respective to the composition, abundance, and diversity of taxonomic entities, where the Shannon index (*H'*) was adopted to calculate diversity (Shen et al., 2010). For landscape pattern, naturalness of landscape was selected, which was measured using natural landscape coverage.

Given the considerable characteristic differences across all selected islands (along with the limited available data of some of them), indicators were defined as either "required" or "optional," where the former was used for all islands while the latter could be applied to a limited number of islands conditional on data availability. This was done to enhance the operability of the indicator system (**Table 3**). For this study, "required" indicators must reflect typical characteristics among all selected islands, have easily obtainable and available raw data, and are strongly representative. Conversely, "optional" indicators are those that represent unique characteristics of certain island ecosystems or where the raw data were difficult to attain.

Reference Values

Ecosystem condition was generally defined as being an observed state to a referenced condition or ecological target (Smit et al., 2021); thus, setting the reference value for all indicators was an essential part of the ecosystem condition assessment. Owing to the natural and anthropogenic heterogeneity across the selected islands, ensuring comparability was the key challenge of this study.

To resolve this challenge, we used consistent standards across the selected islands by adopting current and related standards. Specifically, reference values of island seawater quality, intertidal sediment quality, and intertidal organism quality derived from the national sea water quality standard of China (GB3097-1997), the marine sediment quality standard of China (GB18668-2002), and the marine biological quality standard of China (GB18421-2001), respectively. For biological structure indicators, reference values referred to the guidance for the assessment of coastal marine ecosystem health (HY/T 087-2005). For certain indicators that lacked a current standard, we used data that derived from the First National Island Resources Comprehensive Survey (1988–1996), which provided historical conditions devoid of or with only limited anthropogenic disturbances. For landscape patterns, an absolute boundary was set at 0–100% natural landscape coverage, and therefore, the highest theoretical value (100%) was defined as the reference condition, indicating the best condition without anthropogenic disturbances.

To highlight differences among indicator value intervals, indicator reference values were hierarchized into four categories: class I, class II, class III, and class IV. The final reference values were determined as described in **Supplementary Table 3**.

Indicator Normalization

Indicator normalization was used to reduce measurements to dimensionless data under a standard scale, where, specifically, raw indicator data were rescaled into an identical score scale of 0–100 based on the aforementioned reference values. Being consistent with the four reference value categories, the normalization score range was set correspondingly in **Supplementary Table 3**.

The min-max normalization technique with linear interpolation was used for indicator normalization. Two different formulas were employed for positive (a) and negative (b) indicators, respectively. A positive indicator indicated a positive relationship between raw indicator data and normalization score, a lower indicator data value, and a lower normalization score, reducing the ecological condition. Conversely, a negative indicator yielded a lower raw indicator data value and a higher normalization score, increasing the ecological condition.

TABLE 3 | Island ecosystem assessment indicators.

Goal	Sub-goal	Indicators	Unit	Required (●)/ optional (○)
Environmental quality (A)	Seawater quality (A1)	DO, COD, DIN, PO4-P, Petroleum	mg/L	●
	Intertidal sediment quality (A2)	Organic carbon, Sulfide, Petroleum, Cu, Zn, Pb, Cr, Hg, As, Cd	10^{-6}	●
	Intertidal organism quality (shellfish) (A3)	666, DDT, Cu, Zn, Pb, Cr, Hg, As, Cd, Petroleum	mg/kg	○
Biological structure (B)	Island terrestrial biological structure (B1)	Vegetation coverage	%	●
		Abundance variation of key terrestrial animals	%	○
	Intertidal biological structure (B2)	Intertidal macrobenthos diversity	–	●
	Subtidal biological structure (B3)	Chlorophyll-*a*	mg/m3	●
		Phytoplankton diversity	–	●
		Zooplankton diversity	–	●
		Subtidal diversity	–	●
		Nekton diversity	–	○
	Indicator species (B4)	Abundance variation of important or endangered species	%	●
	Invasive species (B5)	Area coverage invaded by alien species	–	○
Landscape pattern (C)	Naturalness of landscape (C1)	Coverage of natural landscapes	%	●

$$Y_i = \frac{F_{\max} - F_{\min}}{B_{\max} - B_{\min}}(X_i - B_{\min}) + F_{\min} \quad \text{(a)}$$

$$Y_i = F_{\max} - \frac{F_{\max} - F_{\min}}{B_{\max} - B_{\min}}(X_i - B_{\min}) \quad \text{(b)}$$

where Y_i is the normalization score of indicator I; X_i is the observed value of raw data for indicator i; B_{max} and B_{min} are the upper and lower limits of reference values of the condition level interval for indicator i determined by its measurement; F_{max} and F_{min} are the upper and lower limits of normalization score values of the condition level interval for indicator i.

Weight Assignment

Weights reflect the importance of each indicator relative to the upper level composite indicator. The weights on goal and sub-goal levels were determined using the Delphi method through an investigation of greater than 100 questionnaires, covering scientific researchers, students, governmental administrators, protected area managers, etc. An equal weighting scheme was used for indicator levels. In the case of missing data for certain sub-goals or indicators, the weights of other sub-goals or indicators at the same level were adjusted proportionally based on the original weights. The total sum of weights at the same indicator level was 1. The final weights were calculated as shown in **Figure 2**.

Integrated Assessment Model

The aim of this integrated assessment was to aggregate several indicators into a single composite index. The weighted sum model was used to calculate the comprehensive index of island ecosystems, covering the environmental quality index, the biological structure index, and the landscape pattern index. The formulas used are as follows:

FIGURE 2 | Indicator weights of integrated assessment of island ecosystems.

$$CI_{island} = I_{env}W_{env} + I_{bio}W_{bio} + I_{land}W_{land} \quad \text{(c)}$$

$$I_{env} = \sum_{i=1}^{5} I_{env_i} W_{env_i} \quad \text{(d)}$$

$$I_{bio} = \sum_{i=1}^{5} I_{bio} i W_{bio_i} \quad \text{(e)}$$

where (CI_{island}) is the comprehensive index of island ecosystem condition; I_{env} is the environmental quality index; I_{bio} is the biological structure index; I_{land} is the landscape pattern index, W_{env}, $W_{bio,}$ and W_{land} are the weights for environmental quality, biological structure, and landscape patterns. I_{env_i} is the score of sub-goal i for environmental quality; W_{env_i} is the weight of sub-goal i for environmental quality. I_{bio_i} is the score of sub-goal i for biological structure; W_{bio_i} is the weight of sub-goal i for biological structure. Analogously, sub-goal scores were obtained by weighted summation as formal (d) and (e) from corresponding next level indicators.

The value for the composite index, including, (CI_{island}) I_{env}, I_{bio} and I_{land}ranged from 0 to 100. The higher the value, the better the condition, where 0 represents the fully degraded condition and 100 represents the best condition without disturbance and degradation. To further define the condition, the equidistant method was applied to section the value of the composite index into five levels that represent different conditions: very poor (0~20), poor (20~40), moderate (40~60), good (60~80), and high (80~100).

RESULTS

Environmental Quality Index

The value of environmental quality index (I_{env}) ranged from 60.70 to 94.80, with an average of 79.72, indicating good environmental quality, where the condition of 19 islands scored "high" and 23 islands scored "good". Pertaining to the different factors, the value to intertidal sediment quality was highest (87.95 average) under the "high" condition, followed by seawater quality (78.73 average) under the "good" condition, while organism quality was the lowest (66.25 average) under the "good" condition.

For seawater quality, the overall condition of the selected islands was good, where most environmental parameters met the class II national sea water quality standard of China (GB3097-1997), except for DIN and PO_4-P, which were also the primary pollution parameters within China's nearshore waterbodies. In approximately 47.6% of the selected islands, DIN exceeded the class II national sea water quality standard of China (0.3mg/L), where Zini Island, Chongming Island, and Dajinshan Island had particularly high DIN content (>1.0mg/L). In approximately 38.1% of the selected islands, PO_4-P exceeded the class II national sea water quality standard of China (0.03mg/L), where Baishishan Island and Dachangshan Island had particularly high PO_4-P content (>0.05mg/L).

For intertidal sediment quality, sulfide, organic carbon, and heavy metal content was low in most of the selected islands,

where approximately 82% of the selected islands met the class I marine sediment quality standard of China (GB18668-2002). The quality of intertidal shellfish was comparatively lower, where all parameters in greater than 50% of islands exceeded the class I organism marine biological quality standard threshold of China (GB18421-2001).

Furthermore, certain parameters [i.e., petroleum, lead (Pb), zinc (Zn)] had high pollution content, whether for seawater, intertidal sediment, or organisms. Spatially, the environmental quality value was highest in tropical islands, followed by temperate and subtropical islands (**Table 4**). However, significant variation was observed among the different sub-regions in the subtropical zone, where the value of the central subtropical zone was highest overall, particularly regarding its high intertidal sediment quality score. The northern subtropical zone had the lowest overall score, which was mainly due to its comparatively lower intertidal organism quality value.

Biological Structure Index

The biological structure index I_{bio} values varied significantly from 43.50 to 89.40, with an average of 66.10 under the "good" condition, where the condition of 4, 28, and 10 islands scored "high," "good," and "moderate," respectively. Values also varied significantly among the different factors, where values of invasive species were highest overall, with an average value of 96.76 under the "high" condition, followed by indicator species with an average value of 74.88 and island terrestrial biological structure with an average value of 64.32 under the "good" condition. Lower values were observed in subtidal biological structure values (58.08 average) and intertidal biological structure (53.83 average) under the "moderate" condition.

Results showed that the biological condition of marine aquatic island sub-ecosystems (i.e., intertidal and subtidal) was lower than that of island terrestrial sub-ecosystems. Island vegetation coverage varied significantly (from 0 to 100%, 62.64% average), where Snake Island, Dajinshan Island, and Neilingding Island had a vegetation coverage of 100%, all being protected areas, while Wuzhishan Island and Zini Island had a vegetation coverage of 0%. Biological invasion was uncommon across all selected islands. *Mikania micrantha* was the most prominent invasive species found on a limited number of islands, particularly Neilingding Island. For subtidal biological structure, biological conditions differed among biological communities, where higher values were observed in zooplankton diversity (69.20 average) and nekton diversity (62.73 average) under the "good" condition, followed by phytoplankton diversity (58.64 average), chlorophyll-*a* (55.75 average), and macrobenthos diversity (50.21 average) under the "moderate" condition.

Spatially, the biological condition of temperate islands was the highest overall, followed by subtropical and tropical islands (**Table 5**). The low value of tropical islands was the result of a significant reduction in the abundance of important and/or endangered species, particularly in Dong Island and Ximaozhou Island.

Landscape Pattern Index

The value of landscape pattern index I_{land} varied significantly from 6 to 100 (72.36 average) where the value of approximately 47.62% of the selected islands were under the "good" condition, indicating that most islands retained relatively high natural landscape coverage. The condition of two islands scored "very poor" while three islands scored "poor," which were mostly in inhabited islands that surrounded megacities, such as Xinglongsha Island and Chongming Island in Shanghai, indicating that the advantageous geographic location of islands near to large cities often resulted in a reduction in their natural landscapes.

The landscape pattern condition varied spatially, where tropical islands had the highest I_{land} values (91.36 average), followed by subtropical islands (69.69 average) and temperate islands (66.75 average) (**Table 6**). Significant variation was observed among the different subtropical sub-regions, where the highest values were in the central subtropical region (86.02 average), followed by the southern subtropical region (64.65 average) and the northern subtropical region (58.40 average).

Composite Index of Island Ecosystem Conditions

The value of the comprehensive index of the island ecosystem condition (CI_{island}) for all selected islands varied significantly from 52.33 to 89.53 (71.72 average) under the "good" condition (**Table 7**). Specifically, 12 islands were under the "high" condition, 23 islands were under the "good" condition, and seven islands were under the "moderate" condition.

For both indicators and climatic zones, conditions varied slightly (**Table 8** and **Figures 3**, **4**). Environmental quality index

TABLE 4 | Environmental quality assessment scores.

Indicators		Temperate	Subtropical				Tropical
			All	Northern Subtropical	Central Subtropical	Southern Subtropical	
Seawater quality (A1)	range	73.04-88.67	66.27-92.71	68.52-76.19	66.27-82.13	73.13-92.71	53.00-92.23
	average	82.40	76.60	70.65	76.91	82.24	80.39
Intertidal sediment quality (A2)	range	87.73-98.28	65.96-97.68	65.96-95.47	78.14-93.99	67.08-97.68	77.78-99.1
	average	92.17	86.34	84.92	93.99	88.47	85.48
Intertidal organism quality (A3)	range	43.93-66.71	37.17-85.78	37.17-82.34	59.66-85.78	37.06-84.06	69.24-69.24
	average	55.30	66.06	58.00	75.91	64.28	69.24
environmental quality index I_{env}	range	67.95-91.68	60.70-91.78	60.70-80.57	72.57-84.75	66.91-91.78	62.42-92.08
	average	83.80	76.88	72.18	84.75	79.45	81.93

TABLE 5 | Biological structure assessment scores.

Indicators		Temperate	Subtropical				Tropical
			All	Northern Subtropical	Central Subtropical	Southern Subtropical	
Island terrestrial biological structure	range	46.40-100	0-100	0-100	62.68-99.34	0-100	44.70-93.9
	average	73.16	61.04	50.80	81.58	50.75	77.66
Intertidal biological structure	range	28.20-100	23.54-91.39	25.00-66.00	26.16-91.39	23.54-79.15	/
	average	65.87	50.23	45.00	58.20	47.48	/
Subtidal biological structure	range	42.90-69.10	34.00-79.00	34.00-66.00	48.26-72.41	41.85-79.00	57.94-76.00
	average	52.70	58.68	53.50	61.85	60.69	64.13
Indicator species	range	75.00-100	25.00-100	100	30.00-90.00	25.00-90.00	7.92-100
	average	85.63	77.08	100	63.75	67.50	31.32
Invasive species	range	100	20.00-100	100	100	20.00-100	/
	average	100	96.00	100	100	88.00	/
Biological structure index I_{bio}	range	43.50-89.40	46.00-85.22	46.00-74.00	53.99-85.22	49.51-76.25	46.64-85.84
	average	71.50	64.85	60.70	72.64	61.20	64.49

TABLE 6 | Landscape pattern assessment scores.

Indicators		Temperate	Subtropical				Tropic
			All	Northern Subtropical	Central Subtropical	Southern Subtropical	
Naturalness of landscape (C1)	range	19.70-100	6.00-100	6.00-100	57.70-100	27.72-100	82.40-100
	average	66.75	69.69	58.40	86.02	64.65	91.36

TABLE 7 | Integrated assessment scores of island conditions.

Indicators		Temperate	Subtropical				Tropical
			All	Northern Subtropical	Central Subtropical	Southern Subtropical	
Environmental quality index I_{env}	range	67.95-91.68	60.70-91.78	60.70-80.57	72.57-84.75	66.91-91.78	62.42-92.08
	average	83.80	76.88	72.18	84.75	79.45	81.93
Biological structure index I_{bio}	range	43.50-89.40	46.00-85.22	46.00-74.00	53.99-85.22	49.51-76.25	46.64-85.84
	average	71.50	64.85	60.70	72.64	61.20	64.49
Landscape pattern index I_{land}	range	19.70-100	6.00-100	6.00-100	57.70-100	27.72-100	82.40-100
	average	66.75	69.69	58.40	86.02	64.65	91.36
Composite index of island ecosystem condition $CIis_{land}$	range	54.29-88.97	52.33-87.52	52.33-82.29	69.11-87.52	52.51-80.85	64.38-89.53
	average	74.17	70.14	64.29	77.98	68.16	77.14

(I_{env}) values were highest (79.72 average), where all selected islands were under the "good" or "high" condition. Moreover, a comparatively large number of islands were under the "high" condition in the temperate and tropical zones. Although the landscape pattern index I_{land} ranked second (72.36 average), its range was significant. Even though all tropical and central subtropical islands were under the "high" condition, a certain proportion of islands in other climatic zones were degraded with respect to landscape pattern. Biological structure index (I_{bio}) values were lowest (66.10 average), where a high proportion of islands were under the "high" or "good" condition. Tropical island conditions were best overall, followed by temperate and the subtropical islands. Additionally, this also showed that except for "poor" or "very poor" conditions observed in the landscape pattern index (I_{land}) for a limited number of islands, the other sub-goals were comparatively better.

TABLE 8 | Pearson correlation coefficients between island condition indices and geographical-social-economic parameters.

	Area Size	Island Population	Population Density of Island	Island GDP	GDP Density of Island	Distance to Mainland
I_{env}	-0.16	-0.26	-0.29	-0.39	-0.39	-0.29
I_{bio}	-0.03	-0.11	**-0.31***	**-0.54***	**-0.54***	**-0.35***
I_{land}	**-0.47****	**-0.50****	**-0.47****	-0.28	-0.28	**-0.41****
CI_{Island}	**-0.31***	**-0.40****	**-0.48****	**-0.52***	**-0.52***	**-0.47****

**denotes a correlation significance of P<0.05; **denotes a correlation significance of P<0.01.*

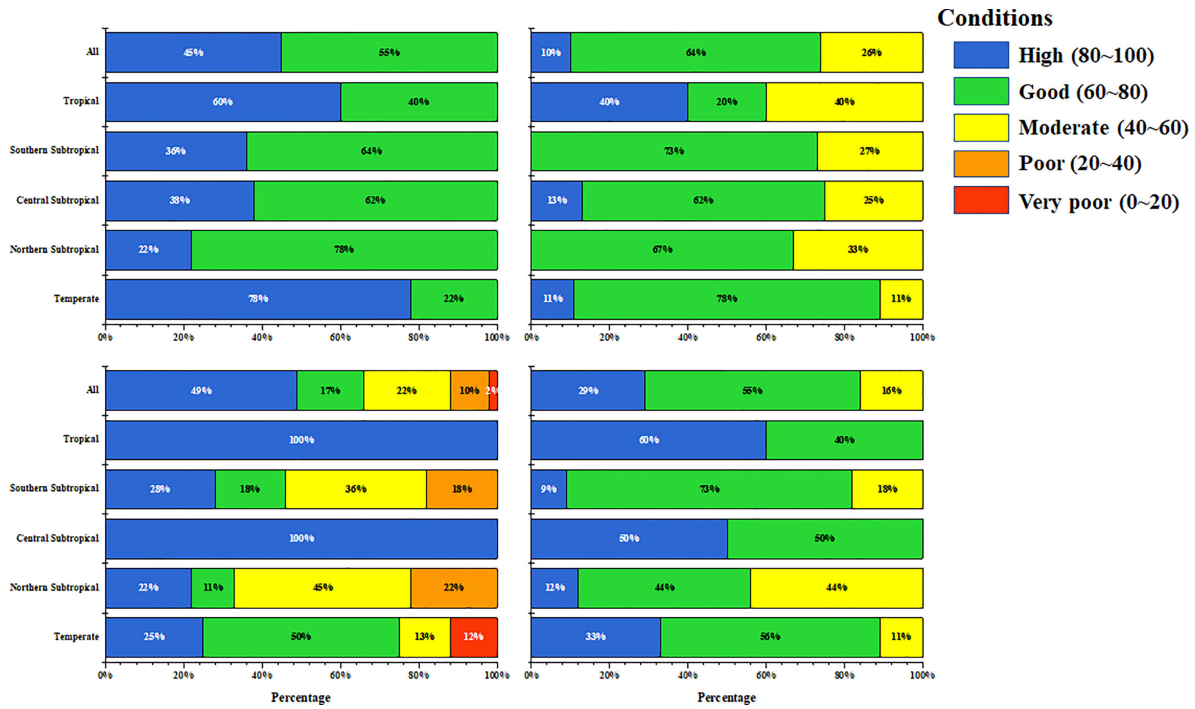

FIGURE 3 | Integrated assessment results of island ecosystem (a:I_{env}, b:I_{bio}, c:I_{land}, d:CI_{land}).

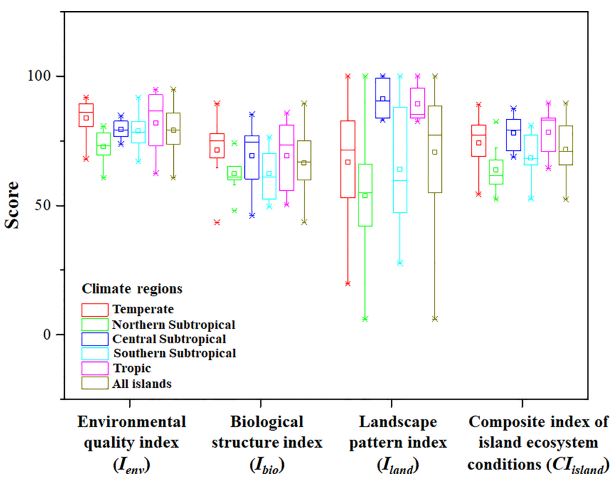

FIGURE 4 | Integrated assessment results of island ecosystem.

DISCUSSION

Overall Condition and Primary Challenges of Chinese Island Ecosystems

Our results showed that approximately 85.4% of the islands investigated were under the "high" and/or "good" condition, indicating that the overall condition of all selected islands was good. Spatially, the condition of subtropical islands was the lowest overall (**Figure 5**). Therefore, some challenges remain with respect to certain island ecosystem components for some islands.

For environmental quality, the main threats were nutrient pollution in seawater and petroleum and marine organism (shellfish) metal contamination. Regarding the different climate regions, the seawater quality condition of subtropical islands was the lowest overall, particularly those in the northern region, being one of China's most densely developed areas (i.e., Yangtze River Delta economic region). Moreover, the seawater quality of coastal island systems was generally lower than that of offshore island systems. Marine organism contamination was severe, particularly regarding petroleum-based and Zn and Pb pollution. This indicates that more effort should be paid to reducing and controlling nutrient, petroleum, and heavy metal pollution to improve conditions of island environmental quality.

For biological structure, the degradation range of most islands varied in biological community structure, covering terrestrial, intertidal, and subtidal sub-ecosystems. It is important to note that biological structure conditions were largely dependent on both natural baselines and levels of anthropogenic disturbance. Under a natural context, biological community baselines differed significantly with respect to island climate conditions, area, substratum lithology, etc. For example, a general trend was observed in subtidal macrobenthos species richness in a northward to southward direction (**Supplementary Table 2**), and similar trends were observed for intertidal macrobenthos as well as subtidal phytoplankton, zooplankton, and nekton species richness. However, no spatial trend was observed in the

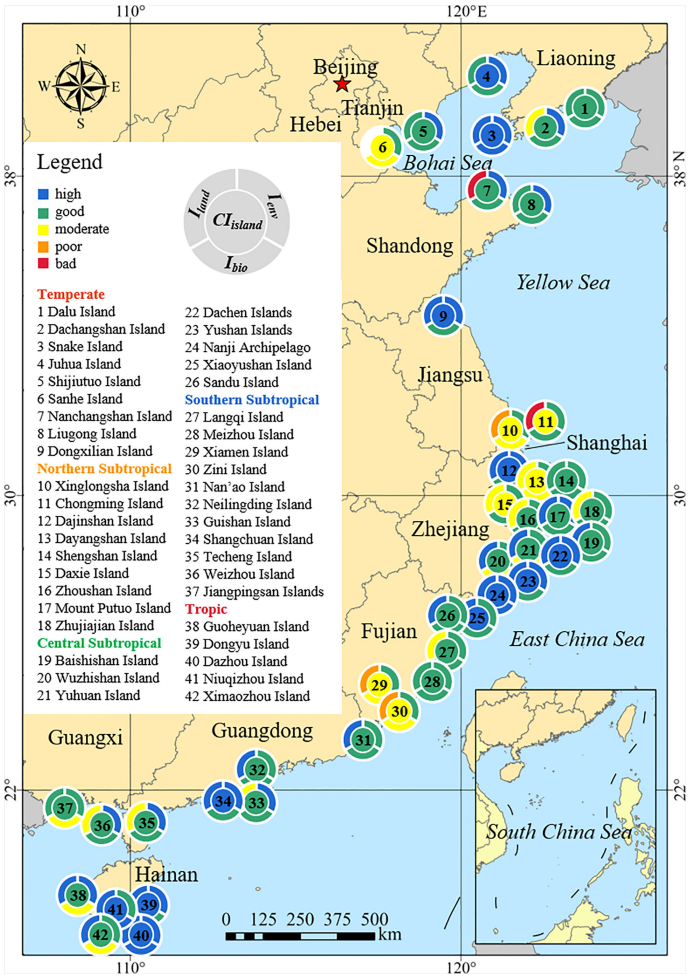

FIGURE 5 | The overall condition of island ecosystem in China mainland.

abundance and density of these communities. Analogously, island vegetation coverage was selected as the single indicator of terrestrial biological structure respective to data availability. This study found that: i) island vegetation coverage was higher in tropical and temperate islands and comparatively higher in subtropical islands; ii) higher vegetation coverage was observed in islands covered in bedrock, while comparatively lower in islands comprised of sediment and corals; iii) uninhabited islands had higher overall vegetation coverage than inhabited islands, which was particularly the case for islands with lower vegetation cover which were developed for agriculture and industry usage. The primary threat to island vegetation coverage was from intensive urban and industrial development, which was common in most inhabited islands, resulting in island vegetation destruction. It is therefore recommended that *in situ* conservation efforts should be strengthened to protect endemic and endangered island species from eradication resulting from invasive species and anthropogenic development.

Landscape patterns were directly indicative of the degree of destruction of natural landscapes, and low vegetation coverage of natural landscapes was typically observed in highly developed islands, such as Nanchangshan Island, Chongming Island, Xiamen Island, and Zini Island. Thus, more effort should be prioritized to ecological restoration to restore the natural habitats and landscapes of these island ecosystems.

Differences Among Different Island Types

Conditions varied across different island ecosystems. Regarding climate, the overall condition of subtropical islands was lower than temperate and tropical islands, indicating that rapid and intensive coastal economic development in subtropical zones affected island ecosystem conditions. Regarding island substratum lithologies, continental island conditions were significantly better than alluvial islands, whether being environmental quality, biological structure, or landscape patterns. Conditions of small-sized islands (with an island area <5 km^2) were better than larger islands (with an island area >5 km^2), which was particularly the case regarding environmental quality and landscape pattern. Conditions of uninhabited islands were better than inhabited islands, being

associated with island area, given that large islands are typically inhabited.

Key Factors Contributing to Ecosystem Conditions

Islands are often geographically remote, connected directly and/or indirectly to the mainland, relatively small, and vary in geological, ecological, economic, human, cultural, and topographical settings. It needs emphasized that islands are complicated ecological-social-economical systems, and island condition is influenced by both natural and anthropogenic factors. Our study indicated that area, population, GDP, and distance to the mainland were significantly correlated to I_{bio}, I_{land}, and CI_{island} (**Table 8**). Results also indicated that anthropogenic development impacts were manifest. I_{bio} was negatively correlated to population density, GDP, and GDP density. This indicated that along with anthropogenic impacts, the impact of natural factors was associated with distance to the mainland, reflective of a negative correlation. This is because certain offshore islands are covered by rocks instead of vegetation, such as Wuzhishan Island. I_{land} negatively correlated to area size, population, population density, and distance to the mainland, indicating that larger island areas, populations, and closer proximity to the mainland are associated with intensive development, resulting in the destruction of natural landscapes. However, results also showed that parameters were not significantly related to; I_{env} thus, it was assumed that large-scale islands were mostly influenced by environmental quality. For example, the "very poor" environment quality of both Chongming Island and Dajinshan Island was largely dependent on the Yangtze Estuary, the region in which China's most severe water-based nutrient pollution occurs.

Limitations and Challenges

This study aimed to develop an applicable framework to comprehensively assess island ecosystems at a national scale, which was largely dependent on data availability. Since the 908 Project has mostly focused on marine aquatic ecosystems, only limited data are available on terrestrial island area. On this account, due to the limited number of terrestrial indicators used in this study, results can be considered slightly biased, particularly concerning environmental quality. This study also highlighted the importance of island soil and freshwater quality. Accordingly, results from this study showed that terrestrial island monitoring should be strengthened respective to national scale monitoring and investigations, particularly regarding island soil and freshwater environments as well as island-specific animal and endemic species. With the rapid development of remote sensing and big data processing technology, there is great potential for the large-scale assessment of island ecosystems in a comprehensive way, particularly along with the impact of climate change and land-use modification, the status of land-sea ecological connectivity and integrity.

CONCLUSIONS

Although China has many island systems, knowledge related to their overall ecological condition is limited on a national scale. Accordingly, this study developed a national scale quantitative assessment framework for island ecosystem conditions, including environmental quality, biological structure, and landscape patterns. Results from the 42 typical, representative island ecosystems indicated that the overall condition of Chinese islands was good, where the condition of approximately 85.4% of all selected islands scored either "high" or "good". The primary challenges mainly included nutrient pollution in seawater environments, petroleum and metal contamination in marine organisms, and vegetation destruction and a reduction in marine biodiversity in intertidal and subtidal zones. Island ecosystem conditions are influenced by both natural and anthropogenic factors, while area size, population, GDP, and distance to the mainland significantly correlated to I_{bio}, I_{land}, and CI_{island}. This proposed framework provides a practical tool to use for island ecosystem condition assessments, which can be widely applied at different scales. However, certain factors require further investigation, such as island soil and freshwater environments as well as animal and endemic species. Additionally, the monitoring of these parameters should be strengthened in future investigations at a national scale. Our study can enrich and extend the methodologies used in island assessments, while offering an effective and versatile tool for which to better instruct island sustainable management practices.

DATA AVAILABILITY STATEMENT

The original contributions presented in the study are included in the article/**Supplementary Material**. Further inquiries can be directed to the corresponding authors.

AUTHOR CONTRIBUTIONS

BC contributed to the study's conception. ZM and WY contributed to the article writing. WZ, FG, and DZ performed the data analyze and figures drawing. WH, JL, and HH (9th Author) performed the indicator selection. YS and HH (11th Author) performed the data collection. All authors contributed to the article and approved the submitted version.

FUNDING

This research was supported by the National Natural Science Foundation of China (42076163); Offshore Marine Investigation and Assessment Project; Asian Cooperation Fund Project-Marine Protected Areas Network in China-ASEAN Countries.

ACKNOWLEDGMENTS

Authors acknowledge all those who contributed to the article. Special thanks to Xinmei Yang, Pifu Cong, and Bin Liang from National Marine Environmental Monitoring Center; Jianqiang Yang, Wei Tang, and Bei Zhao from North China Sea Bureau, Ministry of Natural Resources; Xiaodong Zhu, Yangfan Li, Xiang Sun, and Xiao Yang from Nanjing University; Shengyun Yang, Xiaoming Zhu, Mingru Chen, Jiamei Xiao, and Lu Yang from Xiamen University; Xiaoping Huang, Zhijian Jiang, and Liangmin Huang from Institute of South China Sea, Chinese Academy of Sciences.

SUPPLEMENTARY MATERIAL

The Supplementary Material for this article can be found online at: https://www.frontiersin.org/articles/10.3389/fmars.2022.920069/full#supplementary-material

REFERENCES

Balzan, M. V., Potschin-Young, M., and Haines-Young, R. (2018). Island Ecosystem Services: Insights From a Literature Review on Case-Study Island Ecosystem Services and Future Prospects. *Int. J. Biodivers. Sci. Ecosyst. Serv. Manage.* 14, 71–90. doi: 10.1080/21513732.2018.1439103

Brodie, G., Pikacha, P., and Tuiwawa, M. (2013). Biodiversity and Conservation in the Pacific Islands: Why Are We Not Succeeding? *Conserv. Biol.: Voice. Trop.* Chapter 21, 181–187. doi: 10.1002/9781118679838.ch21

Cao, W., Li, R., Chi, X., Chen, N., Chen, J., Zhang, H., et al. (2017). Island Urbanization and its Ecological Consequences: A Case Study in the Zhoushan Island, East China. *Ecol. Indic.* 76, 1–14. doi: 10.1016/j.ecolind.2017.01.001

Chen, J. (2016). *Fujian Nearshore Comprehensive Investigation and Assessment Report* (Beijing: Ocean Press).

Chi, Y., Liu, D., Xing, W., and Wang, J. (2021). Island Ecosystem Health in the Context of Human Activities With Different Types and Intensities. *J. Clean. Prod.* 281, 125334. doi: 10.1016/j.jclepro.2020.125334

Hebei Oceanic Administration (2013). *Hebei Offshore Marine Investigation and Assessment Report* (Beijing: Ocean Press).

Hou, Y., and Ma, D. (2014). *Shandong Offshore Marine Investigation and Assessment Report* (Beijing: Ocean Press).

Huang, L., Sheng, P., Liu, C., and Tan, Y. (2017). *Guangdong Offshore Marine Investigation and Assessment Report* (Beijing: Ocean Press).

Leclerc, C., Courchamp, F., and Bellard, C. (2020). Future Climate Change Vulnerability of Endemic Island Mammals. *Nat. Commun.* 11, 1–9. doi: 10.1038/s41467-020-18740-x

Ma, Z., Chen, B., and Yu, W. (2017). *Assessment of Island Ecosystem in China* (Beijing: China Ocean Press).

Ministry of Natural Resources, PRC (2018) *Island Survey Statistical Bulletin of 2017*. Available at: http://www.mnr.gov.cn/gk/tzgg/201807/P020180907587895302182.pdf.

Offshore Marine Investigation and Assessment Project Office of Jiangsu (2012). *Jiangsu Offshore Marine Investigation and Assessment Report* (Beijing: Science Press).

Offshore Marine Investigation and Assessment Project Office of SOA (2005a). *Technical Regulations for Aerial Remote Sensing Investigation of Islands and Coastal Zones* (Beijing: Ocean Press).

Offshore Marine Investigation and Assessment Project Office of SOA (2005b). *Technical Regulations for Island Investigation* (Beijing: Ocean Press).

Offshore Marine Investigation and Assessment Project Office of SOA (2006a). *Technical Regulations for Marine Biological and Ecological Investigation* (Beijing: Ocean Press).

Offshore Marine Investigation and Assessment Project Office of SOA (2006b). *Technical Regulations for Marine Chemical Investigation* (Beijing: Ocean Press).

Reaser, J. K., Meyerson, L. A., Cronk, Q., De Poorter, M. A. J., Eldrege, L. G., Green, E., et al. (2007). Ecological and Socioeconomic Impacts of Invasive Alien Species in Island Ecosystems. *Environ. Conserv.* 34, 98–111. doi: 10.1017/S0376892907003815

Shen, G., Huang, L., Guo, F., and Shi, B. (2010). *Marine Ecology* (Beijing: Science Press).

Smit, K. P., Bernard, A. T. F., Lombard, A. T., and Sink, K. J. (2021). Assessing Marine Ecosystem Condition: A Review to Support Indicator Choice and Framework Development. *Ecol. Indic.* 2021, 121. doi: 10.1016/j.ecolind.2020.107148

Sun, R., Wu, Z., Chen, B., Yang, C., Qi, D., Lan, G., et al. (2020). Effects of Land-Use Change on Eco-Environmental Quality in Hainan Island, China. *Ecol. Indic.* 109, 105777. doi: 10.1016/j.ecolind.2019.105777

Su, M., Wall, G., and Jin, M. (2016). Island Livelihoods: Tourism and Fishing at Long Islands, Shandong Province, China. *Ocean. Coast. Manage.* 122, 20–29. doi: 10.1016/j.ocecoaman.2015.11.014

Tan, F., Yang, H., Xu, X., Fang, Z., Xu, H., Shi, Q., et al. (2020). Microplastic Pollution Around Remote Uninhabited Coral Reefs of Nansha Islands, South China Sea. *Sci. Tot. Environ.* 725, 138383. doi: 10.1016/j.scitotenv.2020.138383

Veettil, B. K., Van, D. D., and Quang, N. X. (2020). Biodiversity and Nature Conservation in Island Ecosystems: Spatiotemporal Changes in Socotra Archipelago (Yemen). *J. Coast. Conserv.* 24 (5), 54. doi: 10.1007/s11852-020-00774-4

Weigelt, P., Jetz, W., and Kreft, H. (2013). Bioclimatic and Physical Characterization of the World's Islands. *PNAS.* 110 (38), 15307–15312. doi: 10.1073/pnas.1306309110

Xie, Z., Li, X., Chi, Y., Jiang, D., Zhang, Y., Ma, Y., et al. (2021). Ecosystem Service Value Decreases More Rapidly Under the Dual Pressures of Land Use Change and Ecological Vulnerability: A Case Study in Zhujiajian Island. *Ocean. Coast Manage.* 201, 105493. doi: 10.1016/j.ocecoaman.2020.105493

Xu, Y., Lin, S., He, J., Xin, Y., Zhang, L., Jiang, H., et al. (2017). Tropical Birds are Declining in the Hainan Island of China. *Biol. Conserv.* 210, 9–18. doi: 10.1016/j.biocon.2016.05.029

Xu, R., Ye, S., Jiang, X., Wang, J., Cheng, X., and Liu, Z. (2013). *Shanghai Nearshore Comprehensive Investigation and Assessment Report* (Beijing: Science Press).

Yang, W. (2000). *Chinese Islands* (Beijing: Ocean Press).

Zhang, H., Xiao, Y., and Deng, Y. (2021). Island Ecosystem Evaluation and Sustainable Development Strategies: A Case Study of the Zhoushan Archipelago. *Glob. Ecol. Conserv.* 28, e01603. doi: 10.1016/j.gecco.2021.e01603

Zhan, J., Zhang, F., Chu, X., Liu, W., and Zhang, Y. (2019). Ecosystem Services Assessment Based on Emergy Accounting in Chongming Island, Eastern China. *Ecol. Indic.* 105, 464–473. doi: 10.1016/j.ecolind.2018.04.015

Zhao, B., Kreutur, U., Li, B., Ma, Z., Chen, J., and Nakagoshi, N. (2004). An Ecosystem Service Value Assessment of Land-Use Change on Chongming Island, China. *Land. Use. Policy.* 21, 139–248. doi: 10.1016/j.landusepol.2003.10.003

Conflict of Interest: The authors declare that the research was conducted in the absence of any commercial or financial relationships that could be construed as a potential conflict of interest.

Publisher's Note: All claims expressed in this article are solely those of the authors and do not necessarily represent those of their affiliated organizations, or those of the publisher, the editors and the reviewers. Any product that may be evaluated in this article, or claim that may be made by its manufacturer, is not guaranteed or endorsed by the publisher.

Copyright © 2022 Ma, Yu, Zhang, Ge, Chen, Hu, Zhang, Liao, Huang, Sun and Huang. This is an open-access article distributed under the terms of the Creative Commons Attribution License (CC BY). The use, distribution or reproduction in other forums is permitted, provided the original author(s) and the copyright owner(s) are credited and that the original publication in this journal is cited, in accordance with accepted academic practice. No use, distribution or reproduction is permitted which does not comply with these terms.

frontiers | Frontiers in Marine Science

ORIGINAL RESEARCH
published: 13 June 2022
doi: 10.3389/fmars.2022.912402

Ecological Distribution and Diversity of Key Functional Genes for Denitrification in Surface Sediments of the Northern South China Sea: Implications for Potential N_2O Emissions

Hua Xiang[1,2,3], *Yiguo Hong*[1]*, *Jiapeng Wu*[1] and *Aimin Long*[2,3]*

[1] Key Laboratory for Water Quality and Conservation of the Pearl River Delta, Institute of Environmental Research at Greater Bay Area, Ministry of Education, Guangzhou University, Guangzhou, China, [2] State Key Laboratory of Tropical Oceanography (LTO), South China Sea Institute of Oceanology, Chinese Academy of Sciences, Guangzhou, China, [3] University of Chinese Academy of Sciences, Beijing, China

Denitrification is an important pathway for nitrogen sink and N_2O emissions, but little is known about the ecological distribution of key functional genes of denitrification and their potential N_2O emissions in marine sediments. In this study, we analyzed the abundance, ecological distribution, and diversity of key functional genes (*nir* and *nos*Z) for denitrification in the northern South China Sea (SCS) surface sediments. Our results showed that the gene abundances varied from 10^5 to 10^8 and from 10^6 to 10^7 copies·g^{-1} for the *nir*S and *nir*K, respectively. The *nos*Z II/*nos*Z I gene abundance ratios were 1.28–9.88 in shallow-sea and deep-sea sediments, suggesting that the *nos*Z II gene should play a dominant role in N_2O reduction in the northern SCS sediments. Moreover, the significantly higher abundance ratios of *nir*/*nos*Z in deep-sea surface sediments implied that there might be stronger N_2O emissions potential in deep-sea sediments than in shallow-sea sediments. The ecological distribution profiles of the *nir*S, *nos*Z I, and *nos*Z II gene communities varied with water depth, and denitrification genes in shallow-sea and deep-sea sediments differed in their sensitivity to environmental factors. Water temperature was the major factor affecting both the abundance and the community distribution of the *nir*S gene in deep-sea sediments. Nitrate was the major factor shaping the community of *nos*Z I and *nos*Z II genes in shallow-sea sediments. Our study provides a pattern of ecological distribution and diversity for the *nir* and *nos*Z genes and emphasizes the role of these key functional genes in potential N_2O emissions of the northern SCS surface sediments.

Keywords: denitrification, functional genes, ecological distribution, potential N_2O emissions, South China Sea

OPEN ACCESS

Edited by:
Meilin Wu,
South China Sea Institute of Oceanology (CAS), China

Reviewed by:
Hui Wang,
Shantou University, China
Yanpei Zhuang,
Jimei University, China
Hongpo Dong,
East China Normal University, China

***Correspondence:**
Yiguo Hong
yghong@gzhu.edu.cn
Aimin Long
longam@scsio.ac.cn

Specialty section:
This article was submitted to Marine Pollution, a section of the journal Frontiers in Marine Science

Received: *04 April 2022*
Accepted: *09 May 2022*
Published: *13 June 2022*

Citation:
Xiang H, Hong Y, Wu J and Long A (2022) Ecological Distribution and Diversity of Key Functional Genes for Denitrification in Surface Sediments of the Northern South China Sea: Implications for Potential N_2O Emissions. Front. Mar. Sci. 9:912402. doi: 10.3389/fmars.2022.912402

INTRODUCTION

Nitrogen is essential for all creatures and is a major nutrient supporting marine primary production (Wang et al., 2019a). With the rapid development of industry, increased amounts of reactive nitrogen generated by anthropic activities have flooded into estuaries, coastal bays, and oceans (Seitzinger et al., 2010). Fortunately, 40–50% of the external sources of dissolved inorganic nitrogen (DIN) input can be removed by denitrification and released into the ambient environment as N_2 to maintain the nitrogen cycle balance in marine sediments (Ward, 2013). Meanwhile, N_2O, a powerful and long-lived greenhouse gas with 300 times higher global warming potential than CO_2, may also form during denitrification (Makowski, 2019).

The denitrification process includes four stepwise reduction steps: NO_3^- reduction, NO_2^- reduction, NO reduction, and N_2O reduction (Knowles, 1982). Among them, NO_2^- reduction and N_2O reduction are two key steps. Two enzymes with different structures but similar functions catalyze NO_2^- reduction; the *nir*S gene encodes the copper-containing NO_2^- reductases and the *nir*K gene encodes the cytochrome cd1-containing NO_2^- reductases (Zumft, 1997). In most cases, the *nir*S gene or *nir*K gene occurs in bacteria as a single copy (Jones et al., 2008; Graf et al., 2014); the two genes cannot co-exist in microorganisms (Coyne et al., 1989). However, many research on NO_2^- reductase has only focused on the *nir*S gene (Smith et al., 2007; Christopher et al., 2013). The *nir*K gene was detected in only 30% of denitrifying microorganisms but with a broader range of taxa (Coyne et al., 1989). The *nor*B gene encodes the NO reductase (responsible for the reduction of NO to N_2O), but as compared with the *nir*S or *nir*K genes, research on the potential of the *nor*B gene as a molecular marker started relatively late (Guo et al., 2011). N_2O reductase (Nos), which catalyzes N_2O reduction, is encoded by the *nos*Z gene. The *nos*Z gene generally occurs as a single copy, except in *Pseudomonas raps* and *Thiomonas denitrificans* with the form of a double copy (Sanford et al., 2012). A significant deviation between the predicted N_2O emissions based on the gene abundance and expression of the *nos*Z and the actual N_2O emissions detected (Henderson et al., 2010; Morales et al., 2010), indicating that a class of previously undiscovered functional N_2O reductase genes might exist. Sanford et al. (2012) compared the amino acid sequences of *nos*Z genes in public databases and found that, in addition to the known typical *nos*Z I gene, there was also an emerging atypical *nos*Z II gene. Emerging studies about *nos*Z II have focused on the soil as a significant source of N_2O, such as arable soil (Graf et al., 2016), grassland soil (Di et al., 2014), and salt marsh ecosystems (Dini-Andreote et al., 2016). The *nos*Z II gene has been found to have a particularly significant effect on N_2O reduction in soils (Hallin et al., 2018). However, there is little research on the *nos*Z II gene in oceans whose surfaces cover over 70% of the Earth. The abundance and community diversity of the *nos*Z II gene and its relative importance on N_2O reduction in oceans are poorly understood, as well as how these four genes (*nir*S, *nir*K, *nos*Z I, and *nos*Z II) collectively affect N_2O emissions by denitrification in oceans.

The SCS is a largest marginal sea in China and an ideal region for research on the nitrogen cycle (Su, 2004; Yang et al., 2021). The SCS was reported to be a contributor of atmospheric N_2O, with about 132% N_2O saturation in its waters (Tseng et al., 2016; Ren et al., 2017). The atmospheric contribution of N_2O from the SCS has been estimated to be 0.15-0.24 $Tg{\cdot}a^{-1}$, which was much larger than that of the open ocean (Zheng et al., 2009; Ren et al., 2017). Moreover, the N_2O concentration in coastal waters of northern SCS increased gradually from the surface to the bottom (Xu et al., 2006; Han et al., 2013), suggesting that a source of N_2O might exist in deep waters or sediments. The present research on N_2O in the SCS mainly focuses on the distribution of N_2O in waters and its correlation with apparent oxygen utilization (AOU) (Xu et al., 2006; Zheng et al., 2009; Han et al., 2013; Tseng et al., 2016; Ren et al., 2017). As a hot spot for denitrification, sediment is generally overlooked for N_2O emissions in the SCS. The balance between *nir* (*nir*S and *nir*K) and *nos*Z (*nos*Z I and *nos*Z II) genes should determine N_2O emissions to some extent (Domeignoz-Horta et al., 2015). Combining the abundances and communities of denitrification-related functional genes will provide valuable information to explain potential N_2O emissions driven by the denitrification process.

In this study, we analyzed the distribution and relative importance of key functional genes (*nir* and *nos*Z) in N_2O emissions during denitrification by using qPCR and high-throughput sequencing analysis. We aimed to provide valuable insight into the implications of key functional genes on N_2O emissions by denitrification in marine sediments.

MATERIALS AND METHODS

Sample Collection and Environmental Parameters Measurement

The South China Sea (SCS) lies in the Northwest Pacific Ocean, expanding from the equator to latitude 23°N and from 99°E to 121°E (Su, 2005). It covers an area of about 3.50×10^6 km^2, combined with an average water depth of 1000 m (Chen et al., 2001). A total of 17 surface sediments (0–5 cm) were obtained during 3 cruises of R/V Shiyan 3 (in May 2014, October 2015, and October 2016). The sampling map is shown in **Figure 1**. Site description, sampling details, and methods of analysis are provided by Wu et al. (2019). Water depth and water temperature was continuously recorded, and the salinity and DIN (including NO_3^-, NO_2^-, and NH_4^+) of porewater was examined as described by Wu et al. (2016) and Guan et al. (2017).

DNA Extraction and PCR Amplification

Details of DNA extraction and quality determination processes were described by Wu et al. (2019). The primer pairs cd3aF/R3cd (Throback et al., 2004; Yergeau et al., 2007), *nos*Z 2F/*nos*Z 2R (Henry et al., 2006), *nos*Z IIF/*nos*Z IIR (Jones et al., 2013) were used to amplify the genes of the *nir*S, *nos*Z I, and *nos*Z II, and the products' lengths were 426, 267, 749 bp, respectively. Detailed protocols about PCR amplification are listed in **Supplementary Table 1**. PCR products recovered from gel electrophoresis were

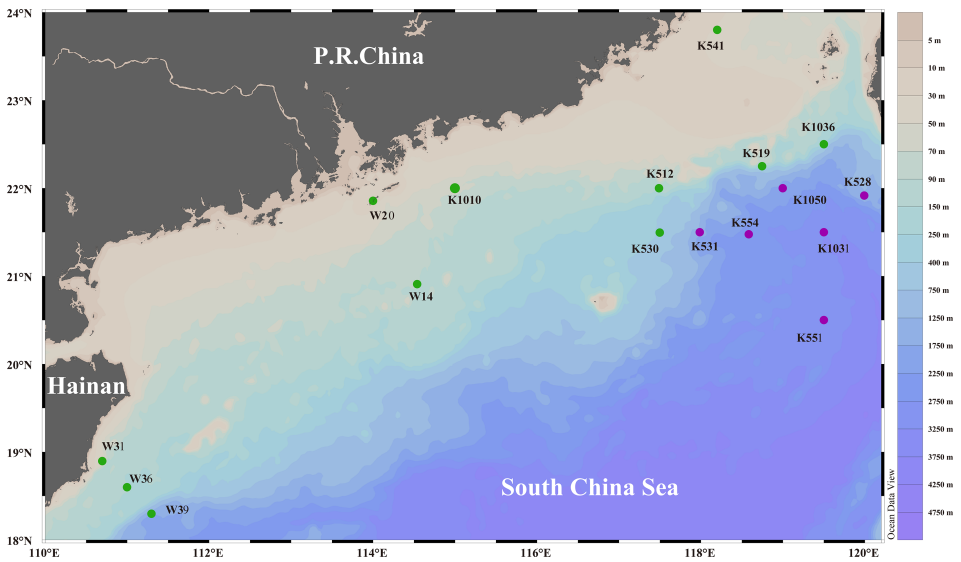

FIGURE 1 | The map of sampling sites. The dots denoted sampling stations (green dots represent shallow-sea stations and purple dots represent deep-sea stations), and the scale bar denoted water depth.

purified with an agarose gel DNA extraction kit (TaKaRa Bio, Japan).

High-Throughput Sequencing Analysis

The purified products were sequenced on an Illumina HiSeq platform (Genewiz Corporation, Suzhou, China) and then analyzed using Mothur (version 1.39.5), according to high-throughput sequencing standard procedures reported by Schloss et al. (2009). The *nos*Z I and *nos*Z II gene sequences were downloaded in Fungene (http://fungene.cme.msu.edu/) as reference sequences, and the reference sequences of *nir*S gene were derived from Fungene and NCBI (https://www.ncbi.nlm.nih.gov/) as described by Liu et al. (2020).

Briefly, valid raw data were derived after the removal of corresponding primers. The trimmed sequences were generated after the processes of binning, denoising, and trimming, and then they were aligned with prepared reference databases. To ensure the quality of the sequences, screen.seqs and chimera.uchime commands were employed to filter out poor-quality reads and to remove chimeric sequences. Finally, the classifying.seqs command was employed and the level of confidence was set at 85% for the *nir*S and *nos*Z genes (Wu et al., 2021a). A 97% sequence identity was used to define the representative sequence of each operational taxon unit (OTU) for these genes for further analysis (Wu et al., 2021a; Wu et al., 2021b). Rarefaction curves, Shannon curves, ranking abundance, and the alpha-diversity index were analyzed by Mothur based on observed OTUs (Schloss et al., 2009) and visualized by Origin 2019b. Origin 2019b was employed to describe the composition of microbial community. The neighbor-joining phylogenetic tree was constructed and visualized using MEGA7.0 (https://www.megasoftware.net/) and EvolView (He et al., 2016). A heat map was plotted by Microsoft Excel (Microsoft Excel 2016).

qPCR Analysis of Key Functional Genes for Denitrification

The abundances of *nir* and *nos*Z genes were detected using a LightCycler ® R480 II Real-Time PCR (Roche, Switzerland), and the primers and detailed protocols are listed in **Supplementary Table 1**. In addition to the primer pairs mentioned above, the *nir*K gene was amplified and quantified by primer sets F1aCu/R3Cu (Hallin and Lindgern, 1999). Each sample was quantified in triplicate, and negative controls were performed simultaneously. A standard curve was constructed with a plasmid DNA of the target gene with known concentration and copy number. The specificity of PCR products was examined by both the melting curve and gel electrophoresis. High amplification efficiencies (90–110%) and correlation coefficients ($R^2 > 0.97$) were shown for the qPCR results.

Statistical Analysis

The map of the sampling area was drawn using Ocean Data View (http://odv.awi.de). Both the bacterial communities and their correlations with environmental variables were explored by canonical correspondence analysis (CCA), redundancy analysis (RDA) and principal coordinates analysis (PCoA) with Canoco 5 (ter Braak and Šmilauer, 2012). The Pearson correlation analysis of abundance and diversity with environmental variables was constructed and visualized using IBM SPSS statistics 19 and Microsoft Excel (Microsoft Excel 2016). Non-parametric test statistics (Mann-Whitney test) was used to examine the differences of gene abundance ratios in shallow-sea and deep-sea sediments as the data did not conform to a normal distribution.

Nucleotide Sequence Accession Numbers

Raw gene sequences of *nir*S, *nos*Z I, and *nos*Z II were deposited in NCBI under the submission numbers PRJNA792035, PRJNA792063, and PRJNA792068, respectively.

RESULTS

Environmental Characteristics of Surface Sediments

The environmental characteristics of surface sediments were described in (Wu et al., 2019). The water depth at the sediments can reach 2,980 m, with water temperatures varying from 1.58 to 25.36°C (**Supplementary Figure 1**). Moreover, the water temperature showed a general drop with water depth (**Supplementary Table 2**), and the average water temperature at depths over 2000 m water was as low as 1.72 ± 0.12°C. Little change was observed in the salinity and pH of porewater, with an average of 35.55 ± 1.65 and 8.31 ± 0.23, respectively. DIN concentrations varied at sampling sites, and mainly existed in the form of NO_3^-, with NO_3^- concentration ranging from 1.8 to 46.43 μM. The concentration of NO_2^- remained at a low level (<1.11 μM) in most samples. The NH_4^+ concentration of the W31 sample was as high as 10.61 μM but consistently low (<1.11 μM) in other samples. In addition, DIN concentrations were positively correlated with the NO_3^- concentrations (r = 0.983 and $p < 0.01$) (**Supplementary Table 2**).

Abundance and Ratios of Key Functional Genes and Their Relationships With Environmental Factors

The *nir* and *nos*Z genes were all detected in sediments (**Figure 2** and **Supplementary Table 3**). An obvious variation was observed in the gene abundance of the *nir*S, ranging from $(6.04 \pm 2.78) \times 10^5$ to $(1.52 \pm 0.05) \times 10^8$ copies·g^{-1}; maximum and minimum values of *nirS* gene abundance were reached in the W20 and K554 samples, respectively. The *nir*S gene abundance inversely correlated with water depth (r = -0.486 and $p < 0.05$) and correlated favorably with water temperature (r = 0.488 and $p < 0.05$) (**Supplementary Table 2**). Moreover, the *nir*S gene abundance showed a favorable correlation with the *nos*Z I gene (r = 0.768 and $p < 0.01$) and the *nos*Z II gene (r = 0.933 and $p < 0.01$) (**Supplementary Table 2**). The *nir*K gene abundance fluctuated between $(1.23 \pm 0.22) \times 10^6$ and $(6.25 \pm 1.60) \times 10^7$ copies·g^{-1}, and it was strongly correlated with the concentration of NH_4^+ (r = 0.752 and $p < 0.01$) (**Supplementary Table 2**). The *nir*K/*nir*S ratios were <1 in shallow-sea surface sediments (except for the W31 and W14 samples) and >1 in deep-sea surface sediments (**Figure 2B** and **Supplementary Table 3**).

The gene abundances of the *nos*Z I and *nos*Z II varied from $(5.51 \pm 0.39) \times 10^5$ to $(7.18 \pm 0.09) \times 10^7$ copies·g^{-1} and from $(3.60 \pm 0.17) \times 10^6$ to $(2.92 \pm 0.41) \times 10^8$ copies·g^{-1}, respectively (**Figure 2A** and **Supplementary Table 2**). The *nos*Z I gene abundance positively correlated with water temperature (r = 0.520 and $p < 0.05$) (**Supplementary Table 2**). Furthermore, the gene abundance of the *nos*Z II was found to be higher than the *nos*Z I, with the *nos*Z II/*nos*Z I ratio >1 in each sample (**Figure 2C**). Gene abundances of the *nir* was calculated as the total gene abundances of the *nir*S and *nir*K, and gene abundances of the *nos*Z as the total gene abundances of the *nos*Z I and *nos*Z II. The gene abundances of the *nir* and *nos*Z varied from 10^6 to 10^8 copies·g^{-1}. The *nir*/*nos*Z gene abundance ratios were >1 in deep-sea surface sediments (except for the K528 sample) and <1 in most shallow-sea surface sediments (**Figure 2D**). Besides, there were significant differences in *nir*K/*nir*S ratios ($p < 0.01$) and *nir*/*nos*Z ratios ($p < 0.05$) between shallow-sea and deep-sea sediments (**Figures 2B, D**).

Community Composition and Diversity of the *nir*S Gene

After executing a series of quality control procedures, an average of 8400 ± 380 high-quality reads of *nir*S gene sequences per sample were screened (**Supplementary Table 4**). Rarefaction curves (**Supplementary Figure 2A**), Shannon index (**Supplementary Figure 2B**), rank abundance (**Supplementary Figure 2C**) and high coverage (**Supplementary Table 4**) all suggested that the sequencing results provided adequate bioinformation to study the *nir*S gene community composition and diversity. Moreover, the community diversity of the *nir*S gene declined with increasing water depth (OTUs, r = -0.722 and $p < 0.01$; Ace, r = -0.753 and $p < 0.01$; Chao1, r = -0.760 and $p < 0.01$; Shannon, r = -0.535 and $p < 0.05$), decreasing water temperature (OTUs, r = 0.55 and $p < 0.05$; Ace r = 0.617 and $p < 0.01$; Chao1, r = 0.608 and $p < 0.05$), and decreasing salinity (Shannon, r = 0.496 and $p < 0.05$; Simpson, r = -0.505 and $p < 0.05$; Evenness, r = -0.250 and $p < 0.05$) (**Supplementary Table 5**).

The dominant OTUs (top 50 OTUs, covering 49.24% of the sequences after removing rare OTUs) of the *nir*S gene were phylogenetically associated with 10 different clusters (**Figures 3A, B** and **Supplementary Figures 3 and 4**). Moreover, only C6 belonged to Alpha-proteobacteria, whereas the other 9 clusters were affiliated to Gamma-proteobacteria (**Figure 3B** and **Supplementary Figure 4**). C6 contained only OTU45 and existed exclusively in the K530 sample, closely affiliated to *Azospirillum* (**Figure 3B** and **Supplementary Figure 4**). C1 (29.59% of the total sequences) and C5 (17.15% of the total sequences) showed some similarity with the uncultured bacteria in Changjiang Estuary and the East China Sea (Dang et al., 2008), San Francisco Bay (Lee and Francis, 2017), respectively. Moreover, C1 and C5 were more abundant in deep-sea surface sediments than those sampled in shallow-sea surface sediments (**Figure 3A** and **Supplementary Figure 3**). C2 (belonging to *Chromohalobacter*), C8 (belonging to *Pseudomonas*), and C9 (belonging to *Thermomonas*) were found almost exclusively in deep-sea surface sediments (**Figures 3A, B**). PCA revealed the *nir*S gene community in deep-sea surface sediments was separated from the shallow-sea surface sediments (accounted for 82.58% of the variance, **Supplementary Figure 5**). For shallow-sea surface sediments, the environmental variables detected in this study explained 47.49% of the total variance, and nitrate was the major factor shaping the spatial distribution of the *nir*S gene community (pseudo-F = 1.5 and $p > 0.05$) (**Figure 3C**). But for deep-sea surface sediments, the environmental variables detected in this study explained 65.66% of the total variance, and water temperature turned to be the major factor affecting the spatial distribution of the *nir*S gene community (pseudo-F = 2.1 and $p < 0.01$) (**Figure 3D**).

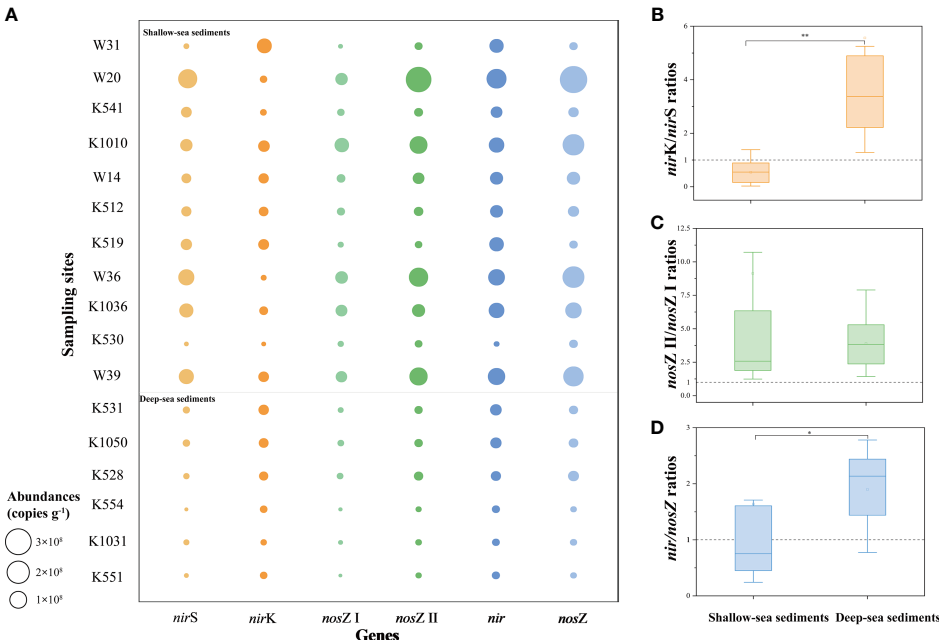

FIGURE 2 | Abundances and ratios of key functional genes for denitrification in surface sediments of SCS. The gene abundances include the *nir* (*nir*S and *nir*K) and *nosZ* (*nosZ* I and *nosZ* II) genes **(A)**, gene ratios include the *nirK*/*nirS* gene abundance ratios **(B)**, the *nosZ* II/*nosZ* I gene abundance ratios **(C)** and the *nir*/*nosZ* gene abundance ratios **(D)**. The asterisks denoted statistically differences by Mann-Whitney test, two asterisks (**) denotes $p < 0.01$ and one asterisk (*) denotes $p < 0.05$.

Community Composition and Diversity of the *nosZ* Gene

A sum of 0.17 million *nosZ* I raw sequences for 17 samples and 0.10 million *nosZ* II raw sequences for 10 samples were detected. Rarefaction curves (**Supplementary Figures 6A, 7A**), Shannon index (**Supplementary Figures 6B, 7B**), and rank abundance (**Supplementary Figures 6C, 7C**) suggested that the sequencing results were sufficient enough to reveal the diversities and community compositions of the *nosZ* gene. The basic alpha diversities of the *nosZ* gene are presented in **Supplementary Tables 6, 7**. Moreover, the coverage of the *nosZ* gene was above 0.99, indicating that the library OTUs of the *nosZ* gene had been adequately captured (**Supplementary Tables 6, 7**). The community diversity of the *nosZ* I gene was impacted by water depth (OUT, r = -0.605 and $p < 0.05$), followed by pH (Shannon, r = 0.499 and $p < 0.05$) (**Supplementary Table 8**). However, for the *nosZ* II gene, its diversity was only affected by water depth (Shannon, r = -0.755 and $p < 0.05$; Simpson, r = 0.694 and $p < 0.05$) (**Supplementary Table 9**).

The dominant OTUs of the *nosZ* I gene were divided into 12 clusters, all of which belonged to *Proteobacteria* (**Figure 4B** and **Supplementary Figure 8**). Extensive sequences of the 50 OTUs, including C1, C4, C6, and C8, matched with soil or sediment samples. Many cultured pure bacteria have also been detected, such as *Aestuarium* (C3), *Azospirillum* (C7), *Ruegeria* (C9), *Polymorphum* (C10), *Rhodobaca* (C11), and *Pseudomonas* (C12). Among the 12 clusters, only *Pseudomonas* (C12) belonged to the Gamma-proteobacteria, whereas the other 11 clusters belonged to Alpha-proteobacteria (**Figure 4B** and **Supplementary Figure 8**). Moreover, *Pseudomonas* (C12) was only observed in deep-sea surface sediments. *Aestuarium* (C3), uncultured pure bacteria (C6), and *Ruegeria* (C9) were detected to be more abundant in surface sediments of deep sea as compared with those in shallow sea. However, the *nosZ* I gene in shallow-sea surface sediments was richer in uncultured *Proteobacteria* (C5) and *Azospirillum* (C7) than those in deep-sea surface sediments (**Figures 4A, B**; **Supplementary Figure 9**).

Dominant OTUs (top 50 OTUs) of *nosZ* II gene sequences were divided into 10 clusters, including *Proteobacteria*, *Chloroflexi*, and *Bacteroidetes* (**Figures 5 A, B** and **Supplementary Figure 10**). C1–C5, containing 69.50% of the total *nosZ* II gene sequences, belonged to *Caldilinea aerophila*. C6 (4.37% of the total sequence) was closely related to *Magnetospirillum gryphiswaldense*. C1, C2, C4, and C6 were richer in shallow-sea surface sediments than deep-sea surface sediments. On the contrary, C3 was only found in deep-sea surface sediments. C7 (9.75% of the total sequence), belonging to *Lutibacter profundi*, was more abundant in deep-sea surface sediments than shallow-sea surface sediments. C8 (*Rhodothermaceae bacterium*), C9 (*Myxococcales* bacterium), and C10 (uncultured bacterium in petrochemical soil and Fyrisan Fen) were just observed in some samples.

PCoA discovered that the gene communities of the *nosZ* I and *nosZ* II in the deep-sea group were separated from the shallow-sea group (explained by 74.22% and 76.49% of the variance for *nosZ* I and *nosZ* II gene, respectively) (**Supplementary Figures 12, 13**). For shallow-sea surface sediments, nitrate was the major factor shaping the community of *nosZ* I gene (pseudo-

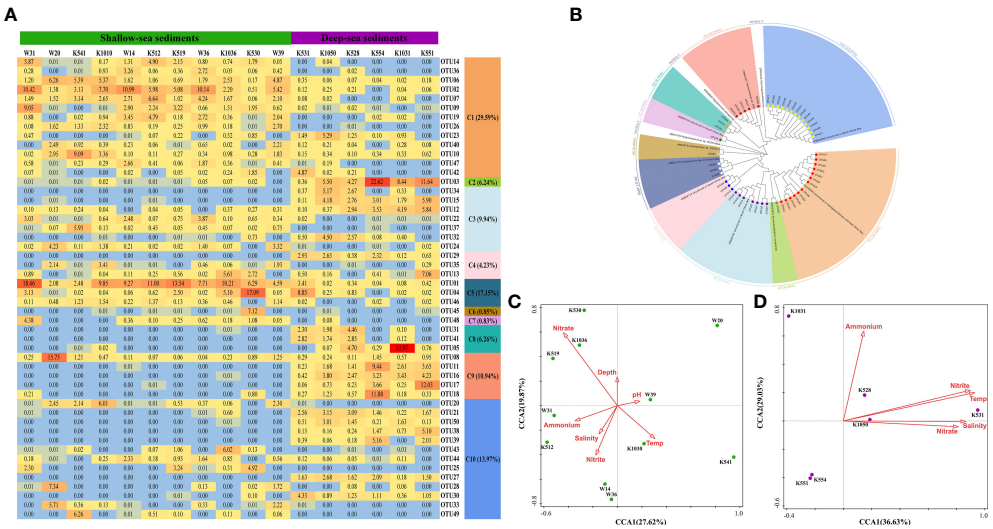

FIGURE 3 | Microbial characteristics of the *nir*S gene in surface sediments of the northern SCS. **(A)** The heat map of dominant OTUs for the *nir*S gene (Top 50 OTUs). **(B)** Neighbor-joining phylogenetic tree of dominant OTUs for the *nir*S gene (Top 50 OTUs) and the reference sequences from Genbank (bootstrap 1000). **(C)** The canonical correspondence analysis (CCA) for the *nir*S gene derived from shallow-sea surface sediments. **(D)** The canonical correspondence analysis (CCA) for the *nir*S gene derived from deep-sea surface sediments.

F = 1.9 and $p < 0.05$) (**Figure 4C**) and *nos*Z II gene (pseudo-F = 1.5 and $p < 0.05$) (**Figure 5C**). And for deep-sea surface sediments, ammonium and water temperature became the most important factor affecting the community of *nos*Z I (pseudo-F = 2.6 and $p > 0.05$) (**Figure 4D**) and *nos*Z II gene (pseudo-F = 5.3 and $p > 0.05$), respectively (**Figure 5D**).

DISCUSSION

Ecological Distribution and Diversity of the *nir* Gene

In this study, the gene abundances of the *nir*S and the *nir*K was focused on in the northern SCS surface sediments, with *nir*S gene abundance ranging from 10^5 to 10^8 copies·g^{-1} and *nir*K gene abundance ranging from 10^6 to 10^7 copies·g^{-1} (**Figure 2** and **Supplementary Table 3**). The gene abundances of the *nir*S and *nir*K were similar to the values shown in Fitzroy Estuary (Abell et al., 2009) and Elkhorn Slough (Smith et al., 2014). The abundances of the *nir*K or *nir*S genes might have been higher than examined, owning to the primer coverage limitations, since the abundances of the *nir*K or *nir*S genes could not be detected with any single universal detection method (Helen et al., 2016). The abundances of *nir* gene indicate the potential of N_2O production in surface sediments of the SCS, as it catalyzes NO_2^- reduction to NO (an essential precursor of N_2O). The *nos*Z gene co-occurred with the *nir*S gene (*nos*Z I, r = 0.768 and $p < 0.01$; *nos*Z II, r = 0.933 and $p < 0.01$) at a relatively higher rate than with the *nir*K gene (*nos*Z I, r = -0.007 and $p > 0.05$; *nos*Z II, r = -0.127 and > 0.05), indicating that the *nir*S gene might share a common regulatory mechanism that inhibits the loss of the *nos*Z gene (**Supplementary Table 2**). However, this mode of genomic linkage was not observed in the *nir*K gene (**Supplementary Table 2**). This result was in accordance with a finding that only 10-30% of *nir*K-harboring bacteria contained the *nos*Z gene (Clark et al., 2012). Meanwhile, there was also a positive correlation between the gene abundance of the *nir*K and N_2O emissions (Clark et al., 2012). Additionally, Cuhel et al. (2010) observed a significant negative correlation between *nir*S gene abundance and the N_2O/N_2 ratio. These results suggested that the *nir*K gene was more prone to be incomplete denitrifiers, therefore, contributed more to N_2O emissions. To some extent, the ratio of *nir*K/*nir*S can be seen as an indicator of the percentage of incomplete denitrification, i.e., potential N_2O emissions. In this study, we found *nir*K/*nir*S >1 in deep-sea surface sediments and *nir*K/*nir*S <1 in shallow-sea surface sediments (except for the W31 and W14 samples) (**Figure 2B**; **Supplementary Table 3**). Moreover, the ratio of *nir*K/*nir*S was around 5.28 in most deep-sea surface sediments (**Figure 2B** and **Supplementary Table 3**). These results suggest that the *nir*K gene cannot be ignored during denitrification, especially in the northern SCS deep-sea surface sediments. More importantly, our study indicated that the northern SCS deep-sea surface sediments had a relatively higher but not strong potential N_2O emissions as compared with the northern SCS shallow-water surface sediments (**Figure 2** and **Supplementary Table 3**).

In addition, the abundance of the *nir*S gene decreased with increasing depth (r = -0.486 and $p < 0.05$) and decreasing water temperature (r = 0.488 and $p < 0.05$) (**Supplementary Table 2**). CCA also showed that water temperature was the major factor affecting the community of *nir*S gene in deep-sea sediments (**Figure 3D**). The results might indicate warm environment is

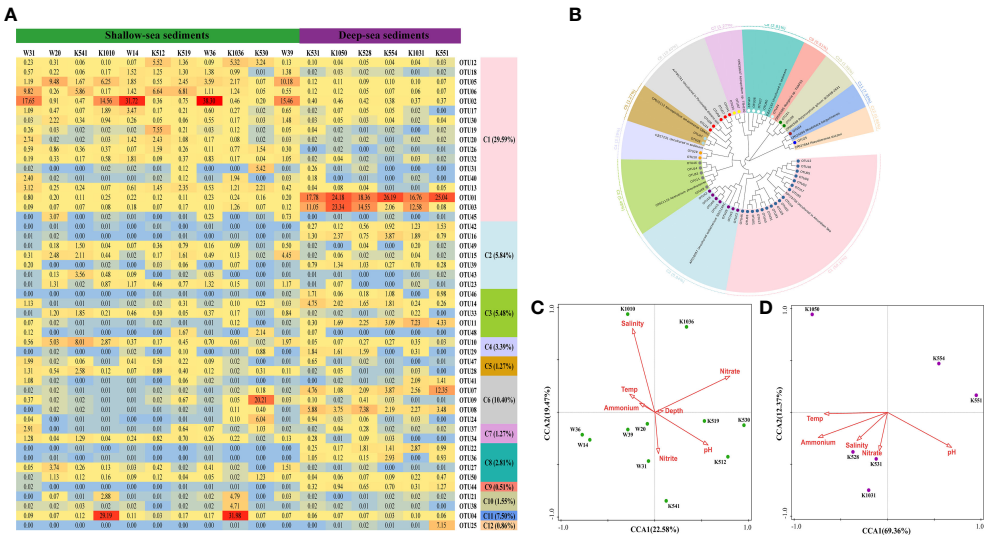

FIGURE 4 | Microbial characteristics of the *nosZ* I gene in surface sediments of the northern SCS. **(A)** The heat map of dominant OTUs for the *nosZ* I gene (Top 50 OTUs). **(B)** Neighbor-joining phylogenetic tree of dominant OTUs (Top 50 OTUs) and the reference sequences from Genbank (bootstrap 1000). **(C)** The canonical correspondence analysis (CCA) for the *nosZ* I gene from shallow-sea surface sediments. **(D)** The canonical correspondence analysis (CCA) for the *nosZ* I gene from deep-sea surface sediments.

more suitable for *nir*S gene to survive, which was consistent with a previous finding that warm incubation enhanced the growth of *nir*S-harboring bacteria (Warneke et al., 2011). The lower abundance of the *nir*S gene in deep-sea sediments also resulted in the significantly higher *nir*K/*nir*S ratios (**Figure 2B**). Some exclusive *nir*S genes were observed in deep-sea surface sediments, such as those in *Chromohalobacter* (C2) and *Pseudomonas aeruginosa* (C8), on average occupying 14.00 ± 9.86% and 17.06 ± 20.30% in the northern SCS deep-sea surface sediments, respectively (**Figures 3A, B** and **Supplementary Figure 3**). Similar to the anammox detected in the SCS, the community shift between shallow-sea and deep-sea sediments of the *nir*S gene might be an adaptation to the low-temperature environment in the deep sea (Oshiki et al., 2016; Wu et al., 2019). Research on surface sediments of San Francisco Bay showed that the environment with higher nitrate and lower water temperature might be more preferred for *nir*S and *nir*K genes, respectively (Lee and Francis, 2017). Our study observed that the *nir*S gene community diversity decreased with increasing salinity (**Supplementary Table 5**, Shannon, r = 0.496 and $p < 0.05$; Simpson, r = -0.505 and $p < 0.05$; Evenness, r = -0.250 and $p < 0.05$). In addition, NH_4^+ concentration was associated with the community composition of the *nir*K gene (Lee and Francis, 2017). In this study, a positive and stronger correlation between *nir*K gene abundance and NH_4^+ concentration was found (r = 0.752 and $p < 0.01$) (**Supplementary Table S2**). Further investigation is needed for a comprehensive understanding between complex environmental characteristics and bacterial community.

Ecological Distribution and Diversity of the *nosZ* Gene

There are biotic processes (denitrification, nitrification, and the reduction of dissimilatory nitrate to ammonium, i.e., DNRA) and an abiotic process (chemodenitrification) that can be the sources of N_2O (Stremińska et al., 2012). However, the only known N_2O sink is the N_2O reduction to N_2 by the N_2O reductase encoded by the genes of *nosZ* I or *nosZ* II (Sanford et al., 2012; Jones et al., 2013). Although the *nosZ* II gene has been found to be a different type of N_2O reductase gene (Sanford et al., 2012; Yoon et al., 2016), many research on the *nosZ* gene still ignored the differences between the two distinctive clades, especially in estuaries and oceans (Wang et al., 2019b; Aamer et al., 2020). In this study, the *nosZ* I and *nosZ* II genes were both widely distributed in the northern SCS surface sediments, with gene abundances ranging from 10^5 to 10^7 copies·g^{-1} and from 10^6 to 10^8 copies·g^{-1}, respectively (**Figure 2** and **Supplementary Table 3**). The gene abundances of the *nosZ* I were higher than the level reported at Gloucester Point (Wu et al., 2021a) but lower than that measured in the rhizosphere (Zhao et al., 2019). The gene abundances of the *nosZ* II were similar to the values detected at Gloucester Point (Wu et al., 2021b) and in the riparian zone (Zhao et al., 2018). The gene abundances of the *nosZ* I were correlated to the *nir*S gene (r = 0.768 and $p < 0.01$) rather than the *nir*K gene (r = -0.007 and $p > 0.05$), and the gene abundances of the *nosZ* II were closely associated with the *nir*S gene (r = 0.933 and $p < 0.01$) rather than the *nir*K gene (r = -0.127 and $p > 0.05$), indicating that the *nosZ* gene might be closely coupled to the *nir*S gene rather than the *nir*K gene during

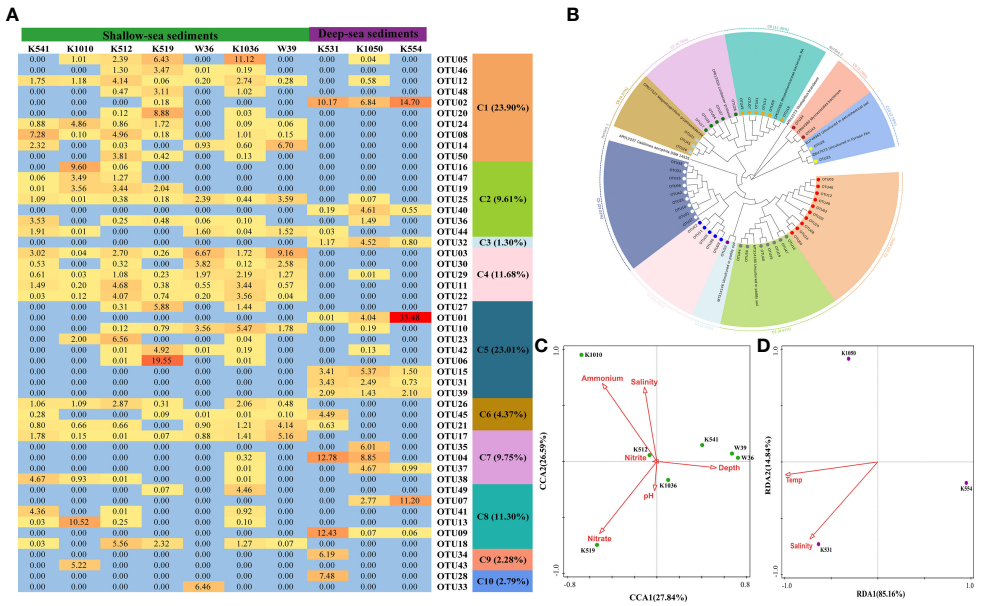

FIGURE 5 | Microbial characteristics of the *nosZ* II gene in surface sediments of the northern SCS. **(A)** The heat map of dominant OTUs (Top 50 OTUs). **(B)** Neighbor-joining phylogenetic tree of dominant OTUs (Top 50 OTUs) and the reference sequences from Genbank (bootstrap 1000). **(C)** The canonical correspondence analysis (CCA) for the *nosZ* II gene from shallow-sea surface sediments. **(D)** The redundancy analysis (RDA) for the *nosZ* II gene from deep-sea surface sediments.

evolution. These results were also observed in Tibetan alpine meadows (Malviya et al., 2016; Samad et al., 2016) and were consistent with a former understanding that *nir*S-carrying bacteria were more potentially complete denitrifiers (Graf et al., 2014).

Although the higher gene abundances of the *nosZ* II over the *nosZ* I at 1.5–10 has been commonly reported in a variety of environments such as soil, sewage treatment plants, wetlands, and rice fields (Tsiknia et al., 2015; Graf et al., 2016), little research has been conducted on the *nosZ* II gene in marine ecosystems. At Gloucester Point, the gene abundance of the *nosZ* II was two orders of magnitude larger than the *nosZ* I based on PCR quantification (Wu et al., 2021a). Another two studies based on metagenomic analysis also supported the dominance of the *nosZ* II gene in the marine oxygen minimum zone (Bertagnolli et al., 2020) and in salt marshes (Graves et al., 2016). In this study, the *nosZ* II/*nosZ* I ratios in the SCS surface sediments were 1.28–9.88, showing that the *nosZ* II gene was dominant in both shallow- and deep-sea surface sediments (**Figure 2C** and **Supplementary Table 3**). The genome of microorganisms can contain different combinations of denitrification genes, and organisms solely equipped with the *nosZ* gene coding Nos are non-denitrifying N_2O microorganisms (Roco et al., 2016; Lycus et al., 2017). Non-denitrifying N_2O microorganisms are more likely to be true N_2O sinks than denitrifying N_2O microorganisms, as they only complete N_2O reduction without contributing to N_2O production (Hallin et al., 2018). Intergenomic comparisons have shown that 51% of microorganisms with the *nosZ* II gene, which lacked the *nir* gene, were non-denitrifying N_2O reducers (Graf et al., 2014); only 17% of microorganisms with the *nosZ* I gene which lacked the *nir* gene were non-denitrifying N_2O reducers (Graf et al., 2014). Pioneering research has also highlighted the role of the *nosZ* II gene instead of the *nosZ* I gene acting as an N_2O sink in soil (Jones et al., 2014).

Coherent with past research (Jones et al., 2014; Wittorf et al., 2016), the community diversity of the *nosZ* II gene was higher than the *nosZ* I gene in the northern SCS surface sediments. At the phylum level, the *nosZ* II gene was detected in *Proteobacteria*, *Chloroflexi*, and *Bacteroidetes* (**Figure 5B** and **Supplementary Figure 10**), and the *nosZ* I gene was only found in *Proteobacteria* (**Figure 4B** and **Supplementary Figure 8**). A competitive advantage might be provided by higher community diversity of the *nosZ* II gene in adjusting to different ecology environments. This hypothesis was supported by the Pearson analysis, i.e., no environmental factors except depth were found to be correlated with the community diversity of the *nosZ* II gene (Shannon, r = -0.755 and $p < 0.05$; Simpson, r = 0.694 and $p < 0.05$; Evenness, r = -0.742 and $p < 0.05$) (**Supplementary Table 9**). For the *nosZ* II gene community, Alphaproteobacteria were more abundant in shallow-sea surface sediments than deep-sea sediments, but the opposite was true for *Bacteroides* (**Figure 5B** and **Supplementary Figure 11**). The high abundance and community diversity of the *nosZ* II gene indicated that strong N_2O reduction potential might exist in the northern SCS surface sediments. For shallow-sea sediments, nitrate was the major factor affecting the community of both *nosZ* I and *nosZ* II gene (**Figures 4C** and **5C**), suggesting nitrate may be in short supply in shallow-sea sediments relative to the demand for denitrifying bacteria.

Implications of Key Functional Genes for Potential N_2O Emissions by Denitrification

N_2O can be produced through nitrification, denitrification, and DNRA; however, N_2O exists as an intermediate product in denitrification and as an end product in nitrification and DNRA processes (Zumft, 1997; Sanford et al., 2012; Harris et al., 2021). These microbial processes involving N_2O can happen simultaneously in the marine ecosystems, an N_2O pool might be formed before it is reduced to N_2 through denitrification. Under such a circumstance, denitrification plays an important role in the conversion of N_2O (Wang et al., 2014; Zhao et al., 2021). Different abundances of denitrifying genes were associated with varying denitrification enzyme activities (Holtan-Hartwig et al., 2000; Rich et al., 2003) and indicated potential N_2O production or consumption (Bergaust et al., 2010; Morales et al., 2010). The abundance analysis of denitrifying genes might offer a closer connection for potential N_2O emissions (Cuhel et al., 2010). The *nir* and *nos*Z genes are vital denitrification genes and closely related to N_2O emissions. The enzyme encoded by *nir* gene produce a precursor for N_2O synthesis; the enzymes encoded by *nos*Z gene reduces N_2O to N_2 (Butterbach-Bahl et al., 2014). The gene abundance ratio of *nir*/*nos*Z can be regarded as an indicator of potential N_2O emissions. Previous research has shown the balance between *nir* and *nos*Z genes can partially determine the level of N_2O emissions in soils and lakes (Domeignoz-Horta et al., 2015; Saarenheimo et al., 2015). In this study, the *nir*/*nos*Z ratios were calculated in the northern SCS sediments. In the shallow-sea surface sediments, the *nir*/*nos*Z ratios ranged from 0.27 ± 0.03 to 5.72 ± 0.51, which was in accordance with the results found in rhizosphere soils (Zhao et al., 2019). Most of the *nir*/*nos*Z ratios in the shallow-sea surface sediments were < 1, implying that the N_2O produced might be reduced in shallow-sea surface sediments. This implication was supported by the relatively low value of N_2O concentration (around 12.5 $nmol{\cdot}L^{-1}$) in shallow-sea water (Tseng et al., 2016). However, in deep-sea surface sediments, the *nir*/*nos*Z ratios were > 1, with the highest value of 2.55 ± 0.33 (except for the K528 sample). These results suggested that potential N_2O production was slightly higher than that of reduction during denitrification, thus, resulting in a small amount of N_2O emissions. This implication was supported by a relatively higher value of N_2O concentration (around 25 $nmol{\cdot}L^{-1}$) in deep-sea waters (Tseng et al., 2016). In this study, the *nir*/*nos*Z ratios suggested that deep-sea surface sediments might have stronger potential N_2O emissions than shallow-sea sediments as the significantly higher *nir*/*nos*Z ratios in deep-sea sediments (**Figure 2D**). Another study also showed N_2O concentrations in bottom waters were about 2.5 times than that of surface water in the northern SCS, indicating that N_2O was abundantly accumulated in deep sea (Zheng et al., 2009; Ren et al., 2017). Although most research based on significant correlations among N_2O, AOU, and NO_3^- has provided circumstantial evidence that N_2O was mainly derived from nitrification (Xu et al., 2006; Tseng et al., 2016; Ren et al., 2017). Marchant et al. (2016) reported N_2O was mainly produced by denitrification in sediments of the Wadden Sea. Denitrification process cannot be excluded in an oxygen-depleted deep sea of the SCS (Xu et al., 2006; Zheng et al., 2009; Tseng et al., 2016; Ren et al., 2017). Denitrification is more likely to occur under low oxygen conditions, and N_2O emissions can be accelerated due to the inhibitory effect of oxygen on the activity of Nos (Körner and Zumft, 1989; Codispoti, 2010). Tseng et al. (2016) reported N_2O maxima peaked at depths where dissolve oxygen was minimal at SCS and the West Philippines Sea. Besides, mineralization of organic matter and the product of nitrate from nitrification in the upper water column may provide substrate for denitrification in deep-sea sediments (Gao et al., 2018), and sediments generally contain minerals which can preserve organic substrates (Kleber et al., 2021). Therefore, the substrate can support the abundance of *nir*K and *nos*Z genes in the deep-sea sediments. Additional direct evidence based on SP values measured for N_2O has verified that both nitrification process and denitrification process can produce N_2O in the SCS waters (Zhang et al., 2019). These results all confirmed our speculation based on *nir*/*nos*Z ratios. The gene analysis may provide new insight and act as an indicator of N_2O emissions, especially when there are difficulties obtaining *in situ* N_2O measurement.

CONCLUSION

In this study, we investigated the ecological distribution and diversity of key functional genes (*nir* and *nos*Z) for denitrification in the northern SCS shallow-sea and deep-sea surface sediments. The results showed that both *nir* (*nir*S and *nir*K) and *nos*Z (*nos*Z I and *nos*Z II) genes were widely distributed in the northern SCS surface sediments. Denitrification genes in shallow-sea and deep-sea sediments differed in their sensitivity to environmental factors. The community distribution and diversity of these genes were affected by water depth, nitrate and water temperature. Furthermore, the significantly higher abundance ratios of *nir*/*nos*Z in deep-sea as compared with shallow-sea sediments suggested that deep-sea sediments might have strong potential N_2O emissions as compared with shallow-sea sediments. In summary, this study provides an ecological distribution pattern of functional genes of denitrification and the implication on N_2O emissions by denitrification in marine sediments.

DATA AVAILABILITY STATEMENT

Raw gene sequences of *nir*S, *nos*Z I, and *nos*Z II were deposited in NCBI under the submission numbers PRJNA792035, PRJNA792063, and PRJNA792068, respectively.

AUTHOR CONTRIBUTIONS

HX conducted the experimental operation and wrote the original draft. YH was responsible for the conceptualization. HX, YH, and AL reviewed and edited the manuscript. JW was responsible

for field sampling. All authors read and approved the final manuscript.

FUNDING

The work was funded by the National Natural Science Foundation of China (No. 31870100, No. 91851111 and No. 42006122), Basic and Applied Basic Research Foundation of Guangdong Province (No. 2019B1515120066 and No. 2020A1515110597), Young Talent Research Project of Guangzhou Education Bureau (No. 202032795), Innovation Team Project of Guangdong Provincial Department of Education (2021KCXTD016).

ACKNOWLEDGMENTS

We would like to thank Yaohao Hu for his kind help in high-throughput sequencing analysis.

SUPPLEMENTARY MATERIAL

The Supplementary Material for this article can be found online at: https://www.frontiersin.org/articles/10.3389/fmars.2022.912402/full#supplementary-material

REFERENCES

Aamer, M., Shaaban, M., Hassan, M. U., Huang, G. Q., Liu, Y., Tang, H. Y., et al. (2020). Biochar Mitigates the N_2O Emissions From Acidic Soil by Increasing the *nos*Z and *nir*K Gene Abundance and Soil pH. *J. Environ. Manage.* 255, 7. doi: 10.1016/j.jenvman.2019.109891

Abell, G. C., Revill, A. T., Smith, C., Bissett, A. P., Volkman, J. K., and Robert, S. S. (2009). Archaeal Ammonia Oxidizers and *nirS*-Type Denitrifiers Dominate Sediment Nitrifying and Denitrifying Populations in a Subtropical Macrotidal Estuary. *ISME J.* 4, 286–300. doi: 10.1038/ismej.2009.105

Bergaust, L., Mao, Y., Bakken, L., and Frostegard, A. (2010). Denitrification Response Patterns During the Transition to Anoxic Respiration and Posttranscriptional Effects of Suboptimal pH on Nitrous Oxide Reductase in *Paracoccus Denitrificans*. *Appl. Environ. Microbiol.* 76 (19), 6387–6396. doi: 10.1128/AEM.00608-10

Bertagnolli, A. D., Konstantinidis, K. T., and Stewart, F. J. (2020). Non-Denitrifier Nitrous Oxide Reductases Dominate Marine Biomes. *Environ. Microbiol. Rep.* 12, 681–692. doi: 10.1111/1758-2229.12879

Butterbach-Bahl, K., Baggs, E. M., Dannenmann, M., Kiese, R., and Zechmeister-Boltenstern, S. (2014). Nitrous Oxide Emissions From Soils: How Well Do We Understand the Processes and Their Controls? *Philos. Trans. R. Soc Lond. B.: Biol. Sci.* 368 (1621), 1–15. doi: 10.1098/rstb.2013.0122

Chen, C. T. A., Wang, S. L., Wang, B. J., and Pai, S. C. (2001). Nutrient Budgets for the South China Sea Basin. *Mar. Chem.* 75 (4), 281–300. doi: 10.1016/S0304-4203(01)00041-X

Christopher, F., Gregory, A. C., Jeffrey, C., and Bess, W. (2013). Transitions in *nirS*-Type Denitrifier Diversity, Community Composition, and Biogeochemical Activity Along the Chesapeake Bay Estuary. *Front. Microbiol.* 4. doi: 10.3389/fmicb.2013.00237

Clark, I. M., Buchkina, N., Jhurreea, D., Goulding, K., and Hirsch, P. R. (2012). Impacts of Nitrogen Application Rates on the Activity and Diversity of Denitrifying Bacteria in the Broadbalk Wheat Experiment. *Philos. Trans. R. Soc B-Biol. Sci.* 367 (1593), 1235–1244. doi: 10.1098/rstb.2011.0314

Codispoti, L. A. (2010). Interesting Times for Marine N_2O. *Science* 327 (5971), 1339–1340. doi: 10.1126/science.1184945

Coyne, M. S., Arunakumari, A., Averill, B. A., and Tiedje, J. M. (1989). Immunological Identification and Distribution of Dissimilatory Heme Cd_1 and Nonheme Copper Nitrite Reductases in Denitrifying Bacteria. *Appl. Environ. Microbiol.* 55 (11), 2924–2931. doi: 10.1128/aem.55.11.2924-2931.1989

Cuhel, J., Simek, M., Laughlin, R. J., Bru, D., Cheneby, D., Watson, C. J., et al. (2010). Insights Into the Effect of Soil pH on N_2O and N_2 Emissions and Denitrifier Community Size and Activity. *Appl. Environ. Microbiol.* 76 (6), 1870–1878. doi: 10.1128/AEM.02484-09

Dang, H., Zhang, X., Sun, J., Li, T., Zhang, Z., and Yang, G. (2008). Diversity and Spatial Distribution of Sediment Ammonia-Oxidizing Crenarchaeota in Response to Estuarine and Environmental Gradients in Changjiang Estuary and East China Sea. *Microbiology* 154, 2084–2095. doi: 10.1099/mic.0.2007/013581-0

Di, H., Cameron, K., Podolyan, A., and Dawson, A. (2014). Effect of Soil Moisture Status and a Nitrification Inhibitor, Dicyandiamide, on Ammonia Oxidizer and Denitrifier Growth and Nitrous Oxide Emissions in a Grassland Soil. *Soil Biol. Biochem.* 73, 59–68. doi: 10.1016/j.soilbio.2014.02.011

Dini-Andreote, F., Brossi, M., van Elsas, J., and Salles, J. (2016). Reconstructing the Geneti Potential of the Microbially-Mediated Nitrogen Cycle in a Salt Marsh Ecosystem. *Front. Microbiol.* 1 (7). doi: 10.3389/fmicb.2016.00902

Domeignoz-Horta, L., Spor, A., Bru, D., Breuil, M., Bizouard, F., Leonard, J., et al. (2015). The Diversity of the N_2O Reducers Matters for the N_2O:N_2 Denitrification End-Product Ratio Across an Annual and a Perennial Cropping Stystem. *Front. Microbiol.* 6, 971. doi: 10.3389/fmicb.2015.00971

Gao, D., Xiaolong, W., Liang, H., Wei, Q., Dou, Y., and Li, L. (2018). Anaerobic Ammonia Oxidizing Bacteria: Ecological Distribution, Metabolism, and Microbial Interactions. *Front. Environ. Sci. Eng.* 12 (3), 10. doi: 10.1007/s11783-018-1035-x

Graf, D., Jones, C., and Hallin, S. (2014). Intergenomic Comparisons Highlight Modularity of the Denitrification Pathway and Underpin the Importance of Community Structure for N_2O Emissions. *PLos One* 9 (12), e114118. doi: 10.1371/journal.pone.0114118

Graf, D. R. H., Zhao, M., Jones, C. M., and Hallin, S. (2016). Soil Type Overrides Plant Effect on Genetic and Enzymatic N_2O Production Potential in Arable Soils. *Soil Biol. Biochem.* 100, 125–128. doi: 10.1016/j.soilbio.2016.06.006

Graves, C. J., Makrides, E. J., Schmidt, V. T., Giblin, A. E., Cardon, Z. G., and Rand, D. M. (2016). Functional Responses of Salt Marsh Microbial Communities to Long-Term Nnutrient Enrichment. *J. Appl. Environ. Microbiol.* 82 (9), 2862–2871. doi: 10.1128/AEM.03990-15

Guan, F. J., Hong, Y. G., Wu, J. P., Wang, Y., Bing, L. Y., Tang, B., et al. (2017). A Fast Sodium Hypobromite Oxidation Method for the Sequential Determination of Ammonia Nitrogen in Small Volume. *Ecol. Sci.* 36 (2), 42–48. doi: 10.14108/j.cnki.1008-8873.2017.02.006

Guo, L. Y., Shi, F., and Yang, L. Y. (2011). Advances in Functional Genes and Molecular Ecology in Denitrifiers. *Microbiol. China* 38 (4), 583–590. doi: 10.3724/SP.J.1011.2011.00462

Hallin, S., and Lindgern, P.-E. (1999). PCR Detection of Genes Encoding Nitrite Reductase in Denitrifying Bacteria. *Appl. Environ. Microbiol.* 65 (4), 1652–1657. doi: 10.1128/AEM.65.4.1652-1657.1999

Hallin, S., Philippot, L., Loffler, F. E., Sanford, R. A., and Jones, C. M. (2018). Genomics and Ecology of Novel N_2O-Reducing Microorganisms. *Trends Microbiol.* 26 (1), 43–55. doi: 10.1016/j.tim.2017.07.003

Han, Y., Zhang, G., Zhao, Y., and Liu, S. (2013). Distributions and Sea-to-Air Fluxes of Nitrous Oxide in the Coastal and Shelf Waters of the Northwestern South China Sea. *Estuar. Coast. Shelf. Sci.* 133, 32–44. doi: 10.1016/j.ecss.2013.08.001

Harris, E., Diaz-Pines, E., Stoll, E., Schloter, M., Schulz, S., Duffner, C., et al. (2021). Denitrifying Pathways Dominate Nitrous Oxide Emissions From Managed Grassland During Drought and Rewetting. *Sci. Adv.* 7 (6), eabb7118. doi: 10.1126/sciadv.abb7118

Helen, D., Heylen, K., Tytgat, B., and Willems, A. (2016). Highly Diverse *nir*K Genes Comprise Two Major Clades That Harbour Ammonium-Producing Denitrifiers. *BMC Genomics* 17, 155. doi: 10.1186/s12864-016-2465-0

Henderson, S. L., Dandie, C. E., Patten, C. L., Zebarth, B. J., Burton, D. L., Trevors, J. T., et al. (2010). Changes in Denitrifier Abundance, Denitrification Gene mRNA Levels, Nitrous Oxide Emissions, and Denitrification in Anoxic Soil

Microcosms Amended With Glucose and Plant Residues. *Appl. Environ. Microbiol.* 76 (7), 2155–2164. doi: 10.1128/AEM.02993-09

Henry, S., Bru, D., Stres, B., Hallet, S., and Philippot, L. (2006). Quantitative Detection of the *nos*Z Gene, Encoding Nitrous Oxide Reductase, and Comparison of the Abundances of 16S rRNA, *Nar*g, *Nir*k, and *nos*Z Genes in Soils. *Appl. Environ. Microbiol.* 72 (8), 5181–5189. doi: 10.1128/AEM.00231-06

He, Z., Zhang, H., Gao, S., Lercher, M. J., Chen, W. H., and Hu, S. (2016). Evolview V2: An Online Visualization and Management Tool for Customized and Annotated Phylogenetic Trees. *Nucleic Acids Res.* 44 (W1), W236–W241. doi: 10.1093/nar/gkw370

Holtan-Hartwig, L., Dörsch, P., and Bakken, L. (2000). Comparison of Denitrifying Communities in Organic Soils: Kinetics of NO_3- and N_2O Reduction. *Soil Biol. Biochem.* 32, 833–843. doi: 10.1016/S0038-0717(99)00213-8

Jones, C. M., Graf, D. R., Bru, D., Philippot, L., and Hallin, S. (2013). The Unaccounted Yet Abundant Nitrous Oxide-Reducing Microbial Community: A Potential Nitrous Oxide Sink. *ISME J.* 7 (2), 417–426. doi: 10.1038/ismej.2012.125

Jones, C. M., Spor, A., Brennan, F. P., Breuil, M.-C., Bru, D., Lemanceau, P., et al. (2014). Recently Identified Microbial Guild Mediates Soil N_2O Sink Capacity. *Nat. Clim. Change* 4 (9), 801–805. doi: 10.1038/nclimate2301

Jones, C., Stres, B., Rosenquist, M., and Hallin, S. (2008). Phylogenetic Analysis of Nitrite, Nitric Oxide, and Nitrous Oxide Respiratory Enzymes Reveal a Complex Evolutionary History for Denitrification. *Mol. Biol. Evol.* 25, 1955–1966. doi: 10.1093/molbev/msn146

Kleber, M., Bourg, I., Coward, E., Hansel, C., Myneni, S., and Nunan, N. (2021). Dynamic Interactions at the Mineral–Organic Matter Interface. *Nat. Rev. Earth Environ.* 2 (6), 402–421. doi: 10.1038/s43017-021-00162-y

Knowles, R. (1982). Denitrification. *Microbiol. Rev.* 46 (1), 43–70. doi: 10.1007/BF02010678

Körner, H., and Zumft, W. (1989). Expression of Denitrification Enzymes in Response to the Dissolved Oxygen Level and Respiratory Substrate in Continuous Culture of *Pseudomonas Stutzeri*. *Appl. Environ. Microbiol.* 55 (7), 1670–1676. doi: 10.1128/AEM.55.7.1670-1676.1989

Lee, J. A., and Francis, C. A. (2017). Spatiotemporal Characterization of San Francisco Bay Denitrifying Communities: A Comparison of *nir*K and *nir*S Diversity and Abundance. *Microb. Ecol.* 73 (2), 271–284. doi: 10.1007/s00248-016-0865-y

Liu, X. H., Wu, J. P., Hong, Y. G., Jiao, L. J., Li, Y. B., Wang, L. M., et al. (2020). Nitrogen Loss by *nir*S-Type Denitrifying Bacterial Communities in Eutrophic Coastal Sediments. *Int. Biodeterior. Biodegrad.* 150, 104955. doi: 10.1016/j.ibiod.2020.104955

Lycus, P., Bøthun, K. L., Bergaust, L., Shapleigh, J. P., Bakken, L. R., and Frostegard, A. (2017). Phenotypic and Genotypic Richness of Denitrifiers Revealed by a Novel Isolation Strategy. *ISME J.* 11 (10), 2219–2232. doi: 10.1038/ismej.2017.82

Makowski, D. (2019). N_2O Increasing Faster Than Expected. *Nat. Clim. Change* 9 (12), 909–910. doi: 10.1038/s41558-019-0642-2

Malviya, S., Scalco, E., Audic, S., Vincent, F., Veluchamy, A., Poulain, J., et al. (2016). Insights Into Global Diatom Distribution and Diversity in the World's Ocean. *Proc. Natl. Acad. Sci. U. S. A.* 113 (11), E1516–E1525. doi: 10.1073/pnas.1509523113

Marchant, H., Holtappels, M., Lavik, G., Ahmerkamp, S., Winter, C., and Kuypers, M. (2016). Coupled Nitrification-Denitrification Leads to Extensive N Loss in Subtidal Permeable Sediments. *Limnol. Oceanogr.* 61(3), 1033–1048. doi: 10.1002/lno.10271

Morales, S. E., Cosart, T., and Holben, W. E. (2010). Bacterial Gene Abundances as Indicators of Greenhouse Gas Emission in Soils. *ISME J.* 4 (6), 799–808. doi: 10.1038/ismej.2010.8

Oshiki, M., Satoh, H., and Okabe, S. J. E. M. (2016). Ecology and Physiology of Anaerobic Ammonium Oxidizing Bacteria. *J. Environ. Microbiol.* 18 (9), 2784–2796. doi: 10.1111/1462-2920.13134

Ren, Y. Y., Zheng, W. J., Ye, W.-W., Zhang, Y. Y., and Zhang, G. (2017). Distribution, Formation and Air-Sea Flux of Dissolved Nitrous Oxide in Northern Continental Slope of South China Sea in Summer and Autumn. *Oceanol. Limnol. Sin.* 48, 29–39. doi: 10.11693/hyhz20160600137

Rich, J., Heichen, R. S., Bottomley, P. J., Cromack, K., and Myrold, D. D. (2003). Community Composition and Functioning of Denitrifying Bacteria From Adjacent Meadow and Forest Soils. *Appl. Environ. Microbiol.* 69, 5974–5982. doi: 10.1128/AEM.69.10.5974-5982.2003

Roco, C. A., Bergaust, L. L., Bakken, L. R., Yavitt, J. B., and Shapleigh, J. P. (2016). Modularity of Nitrogen-Oxide Reducing Soil Bacteria: Linking Phenotype to Genotype. *Environ. Microbiol.* 19 (6), 2507–2519. doi: 10.1111/1462-2920.13250

Saarenheimo, J., Rissanen, A., Arvola, L., Nykänen, H., Lehmann, M., and Tiirola, M. (2015). Genetic and Environmental Controls on Nitrous Oxide Accumulation in Lakes. *PLos One* 10, e0121201. doi: 10.1371/journal.pone.0121201

Samad, M. S., Biswas, A., Bakken, L. R., Clough, T. J., de Klein, C. A., Richards, K. G., et al. (2016). Phylogenetic and Functional Potential Links pH and N_2O Emissions in Pasture Soils. *Sci. Rep.* 6, 35990. doi: 10.1038/srep35990

Sanford, R. A., Wagner, D. D., Wu, Q., Chee-Sanford, J. C., Thomas, S. H., Cruz-Garcia, C., et al. (2012). Unexpected Nondenitrifier Nitrous Oxide Reductase Gene Diversity and Abundance in Soils. *Proc. Natl. Acad. Sci. U. S. A.* 109 (48), 19709–19714. doi: 10.1073/pnas.1211238109

Schloss, P. D., Westcott, S. L., Ryabin, T., Hall, J. R., Hartmann, M., Hollister, E. B., et al. (2009). Introducing Mothur: Open-Source, Platform-Independent, Community-Supported Software for Describing and Comparing Microbial Communities. *Appl. Environ. Microbiol.* 75 (23), 7537–7541. doi: 10.1128/AEM.01541-09

Seitzinger, S. P., Mayorga, E., Bouwman, A. F., Kroeze, C., Beusen, A. H. W., Billen, G., et al. (2010). Global River Nutrient Export: A Scenario Analysis of Past and Future Trends. *Glob. Biogeochem. Cycle* 24 (4), 2621–2628. doi: 10.1029/2009GB003587

Smith, J. M., Mosier, A. C., and Francis, C. A. (2014). Spatiotemporal Relationships Between the Abundance, Distribution, and Potential Activities of Ammonia-Oxidizing and Denitrifying Microorganisms in Intertidal Sediments. *Microb. Ecol.* 69 (1), 13–24. doi: 10.1007/s00248-014-0450-1

Smith, C. J., Nedwell, D. B., Dong, L. F., and Osborn, A. M. (2007). Diversity and Abundance of Nitrate Reductase Genes (*narG* and *Napa*), Nitrite Reductase Genes (*nirS* and *Nrfa*), and Their Transcripts in Estuarine Sediments. *Appl. Environ. Microbiol.* 73 (11), 3612–3622. doi: 10.1128/AEM.02894-06

Stremińska, M. A., Felgate, H., Rowley, G., Richardson, D. J., and Baggs, E. M. (2012). Nitrous Oxide Production in Soil Isolates of Nitrate-Ammonifying Bacteria. *Environ. Microbiol. Rep.* 4 (1), 66–71. doi: 10.1111/j.1758-2229.2011.00302.x

Su, J. L. (2004). Overview of the South China Sea Circulation and Its Influence on the Coastal Physical Oceanography Outside the Pearl River Estuary. *Cont. Shelf. Res.* 24 (16), 1745–1760. doi: 10.1016/j.csr.2004.06.005

Su, J. L. (2005). Overview of the South China Sea Circulation and its Dynamics. *J. Acta Oceanol. Sin.* 27 (6), 1–8. doi: 10.1111/j.1745-7254.2005.00209.x

ter Braak, C., and Šmilauer, P. (2012). *Canoco Reference Manual and User's Guide: Software of Ordination (Version 5.0)* (Ithaca, NY USA: Microcomputer Power).

Throback, I. N., Enwall, K., Jarvis, A., and Hallin, S. (2004). Reassessing PCR Primers Targeting *Nir*s, *nir*K and *nos*Z Genes for Community Surveys of Denitrifying Bacteria With DGGE. *FEMS Microbiol. Ecol.* 49 (3), 401–417. doi: 10.1016/j.femsec.2004.04.011

Tseng, H. C., Chen, C. T. A., Borges, A. V., Delvalls, T. A., Lai, C. M., and Chen, T. Y. (2016). Distributions and Sea-to-Air Fluxes of Nitrous Oxide in the South China Sea and the West Philippines Sea. *Deep-Sea. Res. Part I-Oceanogr. Res. Pap.* 115, 131–144. doi: 10.1016/j.dsr.2016.06.006

Tsiknia, M., Paranychianakis, N., Varouchakis, E. A., and Nikolaidis, N. P. (2015). Environmental Drivers of the Distribution of Nitrogen Functional Genes at a Watershed Scale. *FEMS Microbiol. Ecol.* 91 (6), fiv052. doi: 10.1093/femsec/fiv052

Wang, Q., Jiang, G., Ye, L., Pijuan, M., and Yuan, Z. (2014). Heterotrophic Denitrification Plays an Important Role in N2O Production From Nitritation Reactors Treating Anaerobic Sludge Digestion Liquor. *Water Res.* 62, 202–210. doi: 10.1016/j.watres.2014.06.003

Wang, J., Kan, J. J., Qian, G., Chen, J. F., Xia, Z. Q., Zhang, X. D., et al. (2019b). Denitrification and Anammox: Understanding Nitrogen Loss From Yangtze Estuary to the East China Sea (ECS). *Environ. Pollut.* 252 (Pt B), 1659–1670. doi: 10.1016/j.envpol.2019.06.025

Wang, W. L., Moore, J. K., Martiny, A. C., and Primeau, F. W. (2019a). Convergent Estimates of Marine Nitrogen Fixation. *Nature* 566 (7743), 205–211. doi: 10.1038/s41586-019-0911-2

Ward, B. (2013). How Nitrogen is Lost. *Science* 341, 352–353. doi: 10.2307/23491098

Warneke, S., Schipper, L., Matiasek, M., Scow, K., Cameron, S., Bruesewitz, D., et al. (2011). Nitrate Removal, Communities of Denitrifiers and Adverse Effects in Different Carbon Substrates for Use in Denitrification Beds. *Water Res.* 45 (17), 5463–5475. doi: 10.1016/j.watres.2011.08.007

Wittorf, L., Bonilla-Rosso, G., Jones, C. M., Bäckman, O., Hulth, S., and Hallin, S. (2016). Habitat Partitioning of Marine Benthic Denitrifier Communities in Response to Oxygen Availability. *Environ. Microbiol. Rep.* 8 (5), 486–492. doi: 10.1111/1758-2229.12393

Wu, J. P., Hong, Y. G., Chang, X. Y., Jiao, L. J., Li, Y. B., Liu, X. H., et al. (2019). Unexpectedly High Diversity of Anammox Bacteria Detected in Deep-Sea Surface Sediments of the South China Sea. *FEMS Microbiol. Ecol.* 95 (3), fiz013. doi: 10.1093/femsec/fiz013

Wu, J. P., Hong, Y. G., Guan, F. J., Wang, Y., Tan, Y. H., Yue, W. Z., et al. (2016). A Rapid and High-Throughput Microplate Spectrophotometric Method for Field Measurement of Nitrate in Seawater and Freshwater. *Sci. Rep.* 6 (1), 20165. doi: 10.1038/srep20165

Wu, J. P., Hong, Y. G., Liu, X. H., and Hu, Y. H. (2021b). Variations in Nitrogen Removal Rates and Microbial Communities Over Sediment Depth in Daya Bay, China. *Environ. Pollut.* 286, 117267. doi: 10.1016/j.envpol.2021.117267

Wu, J. P., Hong, Y. G., Wilson, S. J., and Song, B. (2021a). Microbial Nitrogen Loss by Coupled Nitrification to Denitrification and Anammox in a Permeable Subterranean Estuary at Gloucester Point, Virginia. *Mar. Pollut. Bull.* 168, 112440. doi: 10.1016/j.marpolbul.2021.112440

Xu, J. R., Wang, Y. S., Zhang, F. Q., Sun, C. C., Yin, J. P., Wang, Q. J., et al. (2006). Studies on Formation Mechanism and Distribution of Nitrous Oxide in Northeastern South China Sea. *J. Trop. Oceanogr.* 25 (4), 66–74. doi: 10.1111/j.1744-7917.2006.00098.x

Yang, J. Y., Tang, J. M., Guo, X. H., and Kao, S.-J. (2021). Nitrogen Cycling Processes and its Budget in China Marginal Sea: Case Studies in the South China Sea. *Oceanol. Limnol. Sin.* 52 (2), 9. doi: 10.11693/hyhz20200800234

Yergeau, E., Kang, S., He, Z., Zhou, J., and Kowalchuk, G. (2007). Functional Microarray Analysis of Nitrogen and Carbon Cycling Genes Across an Antarctic Latitudinal Transect. *ISME J.* 1 (2), 163–179. doi: 10.1038/ismej.2007.24

Yoon, S., Nissen, S., Park, D., Sanford, R. A., and Löffler, F. E. (2016). Nitrous Oxide Reduction Kinetics Distinguish Bacteria Harboring Clade II NosZ. *Appl. Environ. Microbiol.* 82 (13), 3793–3800. doi: 10.1128/AEM.00409-16

Zhang, G., Liu, S., Casciotti, K. L., Forbes, M. S., Gu, X., Ren, Y., et al. (2019). Distribution of Concentration and Stable Isotopic Composition of N_2O in the Shelf and Slope of the Northern South China Sea: Implications for Production and Emission. *J. Geophys. Res.: Ocean.* 124 (8), 6218–6234. doi: 10.1029/2019jc014947

Zhao, S., Wang, X., Pan, H., Wang, Y., and Zhu, G. (2021). High N_2O Reduction Potential by Denitrification in the Nearshore Site of a Riparian Zone. *Sci. Total. Environ.* 813, 152458. doi: 10.1016/j.scitotenv.2021.152458

Zhao, S., Wang, Q., Zhou, J., Yuan, D., and Zhu, G. (2018). Linking Abundance and Community of Microbial N_2O-Producers and N_2O-Reducers With Enzymatic N_2O Production Potential in a Riparian Zone. *Sci. Total. Environ.* 642, 1090–1099. doi: 10.1016/j.scitotenv.2018.06.110

Zhao, S., Zhou, J., Yuan, D., Wang, W., Zhou, L., Pi, Y., et al. (2019). *NirS*-Type N_2O-Producers and *nosZ* II-Type N_2O-Reducers Determine the N_2O Emission Potential in Farmland Rhizosphere Soils. *J. Soil. Sed.* 20, 461–417. doi: 10.1007/s11368-019-02395-3

Zheng, L., Zhang, G., Xu, J., Zhang, F., and Zhang, J. (2009). Distribution and Air-Sea Fluxes of N_2O in South China Sea in Spring. *Mar. Environ. Sci.* 28 (3), 233–237. doi: 10.3969/j.issn.1007-6336.2009.03.001

Zumft, W. G. (1997). Cell Biology and Molecular Basis of Denitrification. *Microbiol. Mol. Biol. Rev.* 61 (4), 533–536. doi: 10.1128/.61.4.533-616.1997

Conflict of Interest: The authors declare that the research was conducted in the absence of any commercial or financial relationships that could be construed as a potential conflict of interest.

Publisher's Note: All claims expressed in this article are solely those of the authors and do not necessarily represent those of their affiliated organizations, or those of the publisher, the editors and the reviewers. Any product that may be evaluated in this article, or claim that may be made by its manufacturer, is not guaranteed or endorsed by the publisher.

Copyright © 2022 Xiang, Hong, Wu and Long. This is an open-access article distributed under the terms of the Creative Commons Attribution License (CC BY). The use, distribution or reproduction in other forums is permitted, provided the original author(s) and the copyright owner(s) are credited and that the original publication in this journal is cited, in accordance with accepted academic practice. No use, distribution or reproduction is permitted which does not comply with these terms.

frontiers | Frontiers in Marine Science

ORIGINAL RESEARCH
published: 15 June 2022
doi: 10.3389/fmars.2022.923494

Contaminant Characteristics and Influencing Factors of Heavy Metals in Seawater and Sediments in a Typical Mariculture Bay in South China

Qibin Lao[1,2,3], Shangjun Cai[1,2,3], Peng Huang[1,2,3], Fajin Chen[1,2,3], Qizhong Su[4], Xuetie Lei[4], Xin Zhou[1,2,3], Chunqing Chen[1,2,3], Qingmei Zhu[1,2,3], Xuan Lu[1,2,3] and Guoqiang Liu[4,5]*

[1] College of Ocean and Meteorology, Guangdong Ocean University, Zhanjiang, China, [2] Key Laboratory for Coastal Ocean Variation and Disaster Prediction, Guangdong Ocean University, Zhanjiang, China, [3] Key Laboratory of Climate, Resources and Environment in Continental Shelf Sea and Deep Sea of Department of Education of Guangdong Province, Guangdong Ocean University, Zhanjiang, China, [4] Marine Environmental Monitoring Centre of Beihai, State Oceanic Administration, Beihai, China, [5] Key Laboratory of Marine Environmental Survey Technology and Application, Ministry of Natural Resources, Guangzhou, China

OPEN ACCESS

Edited by:
Meilin Wu,
Chinese Academy of Sciences, China

Reviewed by:
Zuhao Zhu,
Ministry of Natural Resources, China
Sucharita Chakraborty,
Indian Institute of Technology Kharagpur, India
Wen Zhuang,
Shandong University, China

***Correspondence:**
Fajin Chen
fjchen@gdou.edu.cn

Specialty section:
This article was submitted to Marine Pollution, a section of the journal Frontiers in Marine Science

Received: 19 April 2022
Accepted: 11 May 2022
Published: 15 June 2022

Citation:
Lao Q, Cai S, Huang P, Chen F, Su Q, Lei X, Zhou X, Chen C, Zhu Q, Lu X and Liu G (2022) Contaminant Characteristics and Influencing Factors of Heavy Metals in Seawater and Sediments in a Typical Mariculture Bay in South China. Front. Mar. Sci. 9:923494. doi: 10.3389/fmars.2022.923494

Heavy metal pollution in the mariculture areas is of considerable attention due to its potential ecological effects and public concern for seafood safety. A better understanding of the current contamination status and historical trend of heavy metals in the ecosystems of mariculture areas has an important implication for the sustainable development of marine ecosystems and for public health concerns. To assess the impact of human activities on heavy metal pollution in the mariculture area, seven metals (Cu, Pb, Zn, Cd, Hg, As, and Cr) and the environmental parameters were seasonally investigated in the surface seawater and sediments in Qinzhou Bay, a typical mariculture bay in South China. Seasonal variations in the concentration of heavy metals were found in both seawater and sediment, which are mainly influenced by seasonal hydrological change, biological activity, and human influence. The concentration of heavy metals in the seawater was at a relatively higher level than that of other mariculture areas in China, while a lower level was found in the sediment. The concentration of Cu increased in both seawater and sediment for the past decades (by nearly 2 times), which is mainly influenced by the mariculture and shipping activities. The concentration of Hg decreased significantly in the seawater for the past 40 years (decreased by 13 times) due to the decrease in production and usage of Hg. However, the concentrations of Pb, Zn, and Cd in seawater showed an increasing trend in the mariculture bay, while the concentrations of Pb, Zn, As, and Cr decreased in the sediment over the past decades. The decrease in pH value (decreasing by 4.7% for the past 20 years) was responsible for the different trend of those metals between seawater and sediment because the decrease in pH could re-release metals from sediments into the water column. Hg and As are the main ecological risk factors in the mariculture bay.

This study suggests that environmental changes, such as ocean acidification, affect the distribution of metals in seawater and sediments, which we should be more vigilant and concerned about under the global climate change.

Keywords: heavy metals, pH, historical trend, mariculture area, ecological risk, Qinzhou Bay

INTRODUCTION

Heavy metal pollution has become a global concern because of their high toxicity, persistence, and bioaccumulation (Duodu et al., 2016; Gong et al., 2018; Alengebawy et al., 2021). The coastal ecological environment is now facing a significant risk due to heavy metal pollution caused by intensive human activities (Wang et al., 2013; Lao et al., 2019; Adyasari et al., 2021; Li et al., 2022). Although many countries have made great efforts to reduce the anthropogenic discharges of heavy metals for the past decades, high levels of heavy metals can still be found in various environmental mediums around the world due to their persistence, particularly in the coastal areas (Chen et al., 2018; Wu et al., 2018; Cai et al., 2019; Kumar et al., 2019; Yan et al., 2022). Excessive amounts of heavy metals in the coastal environment would adversely affect the health of marine organisms and eventually threaten human life (Castro-González and Méndez-Armenta, 2008; Achary et al., 2017; Mishra et al., 2019; Liu et al., 2021).

Seafood from mariculture is an important animal protein source for humans and is a developing industry that greatly contributes to the national economy (Wang et al., 2016). With the global climate change and the continuous expansion of the mariculture scale, various environmental problems have also appeared in the mariculture areas, such as eutrophication (Baquiran and Conaco, 2018; Lao et al., 2021a), hypoxia, ocean acidification (Clements and Chopin, 2017; Ng and Chiu, 2020), and heavy metal pollution (Wang et al., 2016; Liu et al., 2020). Excessive heavy metals are discharged into the mariculture area, which strongly cause accumulation and biomagnification by aquaculture organisms along the water, sediment, and aquatic food (Islam and Tanaka, 2004; Jiang et al., 2018). Moreover, sediments are not only the sink for heavy metals in marine environments but also the source of heavy metals by the disturbance of bottom water and the changes in environmental conditions, such as pH (Ma et al., 2016) because the absorbed heavy metals can be released again with the decrease in pH value in the environment (Kashem and Singh, 2001). Under the stress of anthropogenic input and environmental change, the issue of heavy metal pollution in mariculture areas has become more and more serious. Thus, a better understanding of the current degree of contamination and historical trend of heavy metals in the ecosystems of mariculture areas has an important implication for the seafood industry, the sustainable development of marine ecosystems, and public health concerns.

Qinzhou Bay, located in the northern Beibu Gulf, South China Sea, is one of the most important mariculture grounds in the coast of the South China Sea. The bay is influenced by the discharge of several rivers and tidal influx from outer Beibu Gulf and constitutes a good estuary–bay multi-ecosystem with rich biological diversity (Xu et al., 2020 and Xu et al., 2021). However, with the rapid development of urbanization and industrialization around the coast regions in the Beibu Gulf, a large amount of terrestrial contaminant input resulted in the bay facing many environmental problems now (Gu et al., 2015; Lao et al., 2021a; Lao et al., 2021b and Li et al., 2018; Liu et al., 2020; Lao et al., 2021c). Rivers around the Qinzhou Bay discharged a large amount of terrestrial contaminants into the bay every year, and the contaminant input by the river has shown an increasing trend in the recent two decades (Lao et al., 2020). This resulted in the eutrophication increase over the past 40 years (increased by 18 times) (Lao et al., 2021a), and the pollution of heavy metals in Qinzhou Bay is more serious when compared with that of other bays in Beibu Gulf (Lao et al., 2019; Liu et al., 2020). In addition, a higher level of heavy metal pollution in seawater was found in the Maowei Sea (Upper Qinzhou Bay, **Figure 1**) among the four main mariculture areas in the Guangxi Beibu Gulf, and the level of some metals, such as Cu, was much higher than that found in the past 20 years (Liu et al., 2020). In sediments, high concentrations of Pb, Cr, and Cu were observed in Qinzhou Bay, which is not suitable for mariculture, endangered species reserves, and nature reserves (Gu et al., 2015). However, systematic studies on heavy metal pollution in seawater and sediments, including the estuary and the mariculture areas, have not been reported. The dynamic processes and the internal factors causing the changes of heavy metals between seawater and sediments in the bay are still unclear, which is significantly important for the sustainable development of the mariculture and seafood industry.

In this study, the seasonal concentrations of metals and other physicochemical parameters in seawater and sediments of the Jingu River Estuary and the adjacent mariculture area in Qinzhou Bay were investigated and combined with the historical data to identify the occurrence, potential sources, historical trend and its influencing factors, and ecological risk of heavy metals in the mariculture bay.

MATERIALS AND METHODS

Study Area and Sampling

Qinzhou Bay is s semi-enclosed bay in the northern Beibu Gulf, located at the northwest of South China Sea (**Figure 1**). The area of Qinzhou Bay is 908 km ^{2}, and the water depth is mostly <10 m. The climate in the bay is controlled by the East Asian Monsoon, with the monthly air temperature ranging from 13.9 to 28.6°C (average of 22.5°C) (http://data.cma.cn/site/index.html). The annual rainfall is 2,174 mm, of which over 83% falls during the

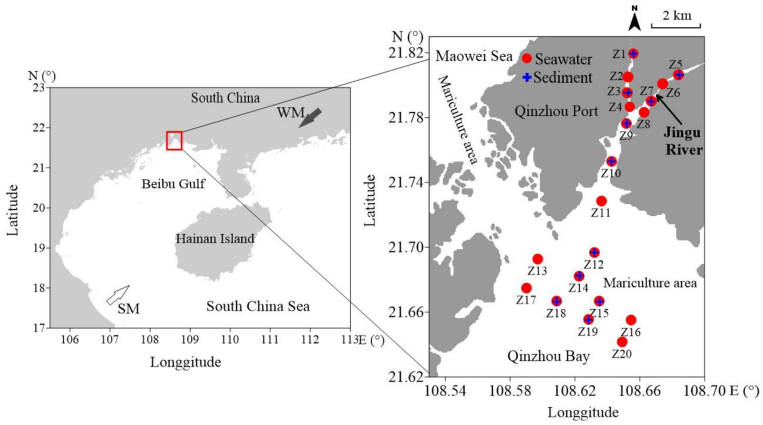

FIGURE 1 | Study area and the sampling stations in the estuarine and the adjacent sea in Qinzhou Bay. The red box in the left is the sampling area, the red dots in the right are the seawater sampling stations, and the blue crosses in the right are the sediment sampling stations. SM, summer monsoon; WM, winter monsoon.

rainy season (from April to September), and the rainfall increased significantly from April [average of 113.8 mm in April, which is significantly higher than that from October to March (average of 54.8 mm)] and decreased significantly after October (http://data.cma.cn/site/index.html). Due to the unique ecological environment and mixture of freshwater and saltwater, Qinzhou Bay and the Maowei Sea in the north of the bay have been used for mariculture over 50 years, and these regions are the largest natural oyster seeding (~2,340 hm^2) and mariculture bay in China (Yang et al., 2019; Xu et al., 2020). The bay represents a significant economic developing area, which has been greatly influenced by anthropogenic activities (Xu et al., 2021).

In this study, two cruises were conducted in the Jingu River Estuary and the adjacent mariculture area in Qinzhou Bay in winter (December 2019, dry season) and spring (the end of April 2020, early rainy season), respectively. A total of 20 seawater stations (20 seawater samples) and 11 sediment stations (11 seawater samples) were investigated during the dry season and early rainy season, respectively (**Figure 1**). In addition, the historical data of the surface water and sediment in 2010 and 2013 were collected in a similar station in Qinzhou Bay (data obtained from the Marine Environmental Monitoring Centre of Beihai, State Oceanic Administration). Surface seawaters (depth of 0.5 m) were collected using a rosette sampler fitted with a 5-L Niskin bottle and then transferred into acid-cleaned polypropylene bottles. The temperature, salinity, dissolved oxygen (DO), and pH were measured on-site. For the chlorophyll *a* (Chl *a*) sample, about 1,000 ml seawater was filtered using glass fiber filters (GF/F, 0.7μm, Whatman) and stored at -20°C until further analysis. The total suspended particulate matter (TSM) samples were filtered through pre-weighed GF/F. For the heavy metal analysis, the seawater samples were filtered through acid-cleaned cellulose acetate filters (0.45-μm pore size and 47-mm diameter, Whatman), and then the filtrate was placed into 250-ml acid-cleaned polyethylene bottles, and HNO_3 was added to the filtrate to achieve a pH of approximately 2. Finally, the filtrate was stored at -20°C until further analysis. Surface sediment (0–5 cm) was collected using a grab sampler. The upper sediment samples (1 to 2 cm) were removed using an acid-washed plastic spoon to avoid any pollution from the metallic sampler, and the sediment sample was placed into a polyethylene bag and stored at -20°C until further analysis. Six metals (Cu, Pb, Zn, Cd, Hg, and As) and seven metals (Cu, Pb, Zn, Cd, Hg, As, and Cr) were measured in the seawater and sediment samples, respectively. The pretreatment and laboratory analyses for the heavy metal samples were conducted according to the method by Lao et al. (2019). The measurement of Cu, Pb, Zn, Cd, As, and Cr in the sediment samples were oven-dried at 105°C for ~72 h, and the sediment samples for Hg were dried naturally at room temperature (24°C). After drying, the sediment samples were ground with a pestle and agate mortar and then sieved through an 80-mesh sieve for Hg and a 160-mesh sieve for Cu, Pb, Zn, Cd, As, and Cr.

Chemical Analysis

Salinity was measured using a salinometer (SYA2-2, Beijing, China), and pH in the field was measured using a pH meter (PHS-3C, Shanghai, China). The DO samples were analyzed by the Winkler titration method with a precision of 0.07 mg L^{-1}. The chemical oxygen demand samples were measured by the potassium permanganate oxidation method with a precision of 0.15 mg L^{-1}. The Chl *a* samples were extracted using 90% acetone solution (*v*/*v*) and measured by a spectrophotometer (Turner Designs Fluorometer, Model 10AU, Shanghai, China). The total organic matter (TOC) in the sediment samples were freeze-dried for the analysis, and the level was determined using the potassium dichromate oxidation–ferrous titration method (GAQS-IQ, 2008). The detection limit of TOC was 0.01%. The sediment samples for the grain size were pretreated according to the Chinese National Standard (GB/T12763.8-2007), and the granulometry was determined by a laser diffractometer (Malvern Mastersizer 3000, UK).

The analysis of heavy metal in the seawater and sediment samples in this study was conducted according to Lao et al. (2019). The measurements of Cu, Pb, Zn, and Cd in seawater were used in anodic stripping voltammetry (797 VA Computrace, Wantong, Switzerland). The measurements of Hg and As were used in atomic fluorescence spectrometry (ASF-9530, Beijing Haiguang Instrument, China). The detection limits of Cu, Pb, Zn, Cd, Hg, and As in the seawater samples were 0.6, 0.1, 1.0, 0.01, 0.007, and 0.5 μg L^{-1}, respectively. During the analysis of heavy metals in the sediment, 0.5 g of processed sediment samples was digested with a mixture containing HCl and HNO_3 at 95°C for 1 h and then diluted to 50 ml with distilled water before the analysis. Cr, Pb, Zn, Cu, and Cd were measured by atomic absorption spectrometry (ZEENH700P, Jena, German). As and Hg were measured by atomic fluorescence spectrometry (ASF-9530, Beijing Haiguang Instrument, China). The detection limits of Cu, Pb, Zn, Cd, Cr, Hg, and As were 2.0, 1.0, 6.0, 0.04, 2.0, 0.002, and 0.06 μg g^{-1}, respectively.

Quality Control and Quality Assurance

All glassware during the experimental procedure were soaked in nitric acid solution (HNO_3, 1:3) for 7 days and then cleaned with ultra-pure water before use. To ensure high accuracy and precision, the number of duplicate samples, blanks, and certified reference material [GBW-07309 from the State Oceanographic Administration of China and GBW(E)-080040 from the Second Institute of Oceanography, Ministry of Natural Resources of China] accounted for 20% of samples in the batch digestion experiments. The results were all blank-corrected in this study. Duplicate samples were analyzed to check the reproducibility, and the relative difference was <5%. Spike recovery test was conducted to test the analytical procedures, and the recoveries in the standard were 99 ± 4% for Cu, 95 ± 5% for Pb, 102 ± 3% for Zn, 98 ± 3% for Cd, 95 ± 6% for Cr, 103 ± 6% for Hg, and 97 ± 3% for As.

Heavy Metal Pollution Assessment

The contaminant degree of heavy metals in seawater was assessed by the ecological risk index (ERI) (Hakanson, 1980). The equation is as follows:

$$\mathrm{ERI} = \sum_{i=1}^{N} E_r^i = \sum_{i=1}^{N} T_f^i \times \frac{C_i}{C_o} \tag{1}$$

where E_r^i, T_f^i, C_i, and C_o represent each heavy metal potential ERI, toxic response factor (TRF), heavy metal value in the seawater, and standard value. The C_o in this study adopted the National Standard of China for Seawater Quality GB 3097-1997, grades I and II (**Table 1**). According to this method, E_r^i <40 and ERI <150 represent a low ecological risk, 40 < E_r^i <80 and 150 < ERI <300 represent a moderate ecological risk, 80 < E_r^i <160 and 300 < ERI <600 represent a high ecological risk, 160 < E_r^i <320 represent a very high ecological risk, and E_r^i ≥320 and ERI ≥600 represent an extremely high ecological risk. The TRF of Cu, Pb, Zn, Cd, Hg, and As are 5, 5, 1, 30, 40, and 10, respectively (Liu et al., 2020).

The contaminant degree of heavy metals in the sediment was assessed by the pollution load index (PLI), geoaccumulation index (I_{geo}), and enrichment factor (EF). The background values of Cu, Pb, Zn, Cd, Cr, Hg, and As in the sediment were from the Beibu Gulf, and the values were 15.8, 28.9, 75.8, 0.09, 35.0, 0.029, and 7.8 μg g^{-1}, respectively (Lao et al., 2019).

The PLI, I_{geo}, and EF values were calculated according to Islam et al. (2015) and Lao et al. (2019). The PLI value was calculated as follows:

$$\mathrm{PLI} = (\mathrm{CF}_1 \times \mathrm{CF}_2 \times \ldots \times \mathrm{CF}_n)^{1/n} \tag{2}$$

where CF denotes the ratio of heavy metal concentration and background value ($\mathrm{CF} = C_{\mathrm{measured}}/C_{\mathrm{background}}$). A PLI value of 0 represents no contamination, a value of 1 represents the presence of only a baseline level of contamination, and >1 represents progressive deterioration. In addition, a CF value <1 represents a low degree, 1 ≤ CF ≤3 represents a moderate degree, 3 ≤ CF ≤6 represents a considerable degree, and CF ≥6 represents a very high degree (Lao et al., 2019).

The I_{geo} value was calculated as follows:

$$I_{\mathrm{geo}} = \log_2\left[\frac{C_n}{1.5B_n}\right] \tag{3}$$

where C_n represents the measured value of each metal in the field, and B_n represents the background value of each metal. I_{geo} ≤0 represents being practically uncontaminated, 0 ≤ I_{geo} ≤1 represents low contamination, 1 ≤ I_{geo} ≤2 represents moderate contamination, 2 ≤ I_{geo} ≤3 represents moderate to heavy contamination, 3 ≤ I_{geo} ≤4 represents heavy contamination, 4 ≤ I_{geo} ≤5 represents heavy to extreme contamination, and I_{geo} ≥5 represents extreme contamination (Islam et al., 2015; Lao et al., 2019).

RESULTS

Environment Background Properties in the Seawater and Sediment

The variations of the physico-chemical parameters in Qinzhou Bay are presented in **Figure 2** and **Table 1**. The temperature in the mariculture area was higher than that in the estuary area during winter, but the opposite feature was found in spring (**Figure 2A**). Salinity exhibited an upward trend from the upper estuary to the mariculture area during both seasons, with higher salinity in the dry season (ranging from 27.59 to 30.75) and lower salinity in the early rainy season (ranging from 23.11 to 27.99) (**Figure 2B**). This suggested that the seawater intruded into the estuary with the decrease in runoff due to the low rainfall in the dry season. The pH and DO values were higher than those in the estuary area during both seasons (**Figures 2C, D**). The TSM concentration in spring was higher than that in winter, while there was a little difference between the values of the estuary and mariculture area during both seasons (**Figure 2E**). The Chl *a* levels were all higher in spring and lower in winter (**Figure 2F**). During spring, phytoplankton blooms occurred in the

TABLE 1 | Summary of the average values of physico-chemical parameters in the seawater of different areas during spring and winter.

		Temperature (°C)	Salinity	pH	Dissolved oxygen (mg L^{-1})	Total suspended particulate matter (mg L^{-1})	Chemical oxygen demand (mg L^{-1})	Chl *a* (μg L^{-1})
Spring	Estuary area	26.45	23.96	7.55	5.93	23.77	1.57	2.13
	Mariculture area	24.42	27.13	8.11	6.99	24.28	1.19	11.18
	Average	25.54	25.38	7.81	6.41	24.00	1.40	6.44
Winter	Estuary area	18.11	28.77	7.83	6.93	20.54	1.09	0.48
	Mariculture area	18.27	30.22	8.08	7.67	20.97	0.84	1.24
	Average	18.18	29.42	7.95	7.27	20.73	0.98	0.83
Annual average		21.86	27.40	7.88	6.84	22.37	1.19	3.63

mariculture area (**Figure 2F**). There was a little difference in the pH values in the sediment between winter (average of 7.67) and spring (average of 7.67), but the value in the mariculture area was higher than that in the estuary area during both seasons. Notably, the pH values in Qinzhou Bay decreased during the rainy seasons for the past 20 years, decreasing by 4.7% (**Figure 3**). The TOC concentrations in the sediment during spring (average of 1.53 μg g^{-1}) were higher than those in winter (average of 1.04 μg g^{-1}). **Figure 4** displays the composition of the grain size of the sediments. The composition of the grain size of the sediments is similar during both seasons, and silt- and sand-sized grains mainly exist in the two regions.

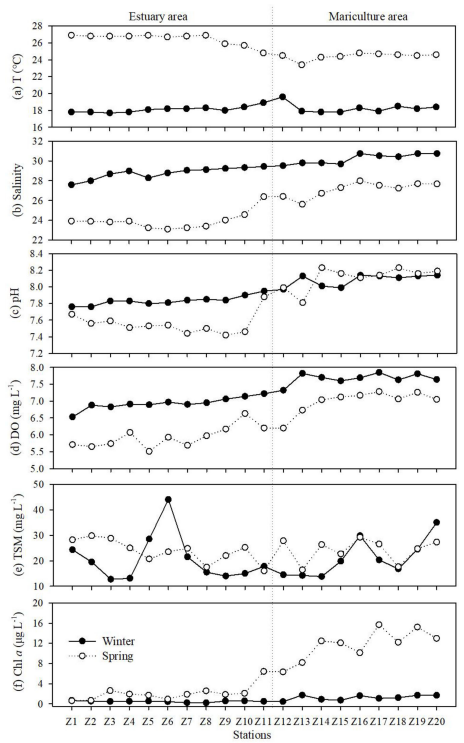

FIGURE 2 | Variations of the physico-chemical parameters in the seawater of the estuary and mariculture area in Qinzhou Bay during winter and spring.

Heavy Metals in the Seawater

The concentrations of six metals in the surface seawater are presented in **Figure 5** and **Table 2**. The average concentration of heavy metals followed a decreasing order of Zn > Cu > Pb > As > Cd > Hg during both seasons. Generally, the concentrations of Cu, Pb, Zn, Cd, and As in winter were higher than those in spring, while the concentration of Hg in spring was higher than that in winter (**Figure 5** and **Table 2**). The concentration of Cu in the mariculture area was higher than that in the estuary, while Zn exhibited an opposite trend during both seasons (**Table 2**). The other metals showed a little difference between mariculture and estuary area. The concentrations of Cu, Zn, Cd, Hg, and As were within the range of grade I in seawater, and the concentration of Pb was within the range of grade II in seawater (**Table 2**). Compared with the other areas, the concentrations of heavy metals were generally lower than those in developed coastal areas, such as the Yellow River Estuary (Wang et al., 2018) and Guangdong coastal area (Zhang et al., 2015), while the level was higher than the other mariculture areas in China (**Table 3**)—for example, all metals except As are higher than those in Laoshan Bay (Wang et al., 2019); the concentrations of Pb, Zn, and Cd are higher than those in Zhanjiang Bay (Zhang et al., 2018) and Lianzhou Bay in northeastern Beibu Gulf (Liu et al., 2020) and Maowei Sea in the upper Qinzhou Bay (Liu et al., 2020); and all metals except Hg are higher than those in Pearl Bay in northwestern Beibu Gulf (Liu et al., 2020). Notably, despite the fluctuation, the concentrations of Cu, Pb, Zn, and Cd showed an increasing trend in the seawater, while the concentration of Hg decreased over the past 40 years (**Table 3**).

Heavy Metals in the Sediments

The concentrations of seven metals in the surface sediments are presented in **Figure 6** and **Table 2**. The average concentrations of the seven metals revealed a decreasing order of Zn > Cr > Cu > Pb > As > Cd > Hg during the spring, while the concentrations showed a decreasing order of Zn > Pb > Cr > As > Cu > Cd > Hg during the winter (**Table 2**). The different orders suggested that different metal sources may occur in different seasons. The concentrations of Cu, Zn, As, and Cr in spring were higher than those in winter, while Pb and Hg exhibited higher concentrations in winter but lower concentrations in spring. The concentration of Cd in winter was similar to that in spring. Differently from those in the seawater, the concentrations of heavy metals in the sediment were more complicated between mariculture and the estuary area. The

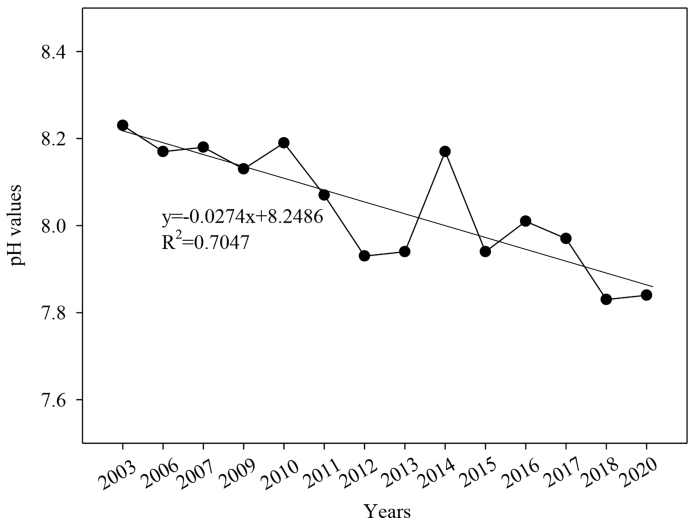

FIGURE 3 | Variations of pH values during the rainy seasons for the past 20 years. Data obtained from the Marine Environmental Monitoring Centre of Beihai, State Oceanic Administration.

concentration of Cu in the estuary area was higher than that in the mariculture area, while the concentration of Zn showed an opposite trend during both seasons (**Table 2**). The concentration of Pb in spring were higher in the estuary area, while higher concentrations in winter were found in the mariculture area. Other metals showed a little difference between mariculture and the estuary areas during both seasons. Differently from those in the seawater, the concentrations of heavy metals in the sediment were generally lower than those in other similar coastal mariculture bays and other coastal regions in China (**Table 4**). The concentrations of all metals in the sediment were within the range of grade I (**Table 4**). In contrast to the tendency of heavy metals in seawater, except for the concentration of Cu which increased, the concentrations of Pb, Zn, As, and Cr generally decreased in the sediment for the past 20 years, and the concentration of Hg in the sediment has a little change for the past years (**Table 4**).

DISCUSSION

The Hydrodynamic and Biological Effects on the Distribution of Heavy Metals in Qinzhou Bay

In the marine environment, the distribution and transportation of heavy metals are greatly influenced by the physicochemical processes (Lao et al., 2019) and the external inputs of heavy metals, including anthropogenic and terrestrial sources, sediment release, biogenic processes, and hydrography (Lao et al., 2019). To better understand the control factors for the distribution of heavy metals in the estuary and adjacent mariculture area in Qinzhou Bay, the relationships between heavy metals and environmental parameters in both seawater and sediment were analyzed, and the results are presented in **Tables 5**, **6**. Zn is not related to the physicochemical factors in

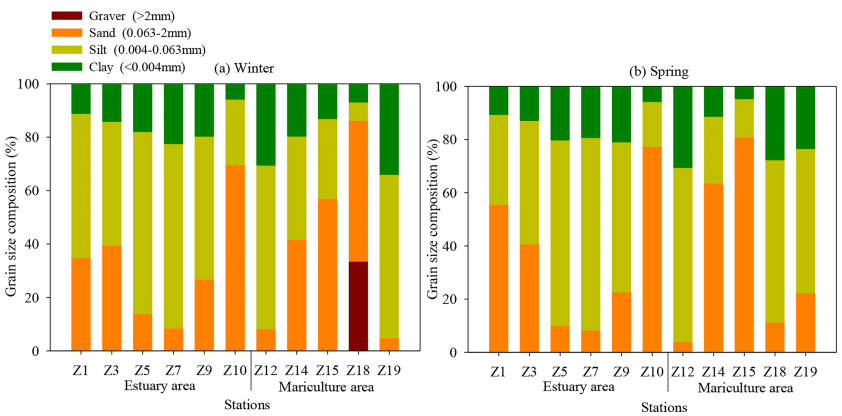

FIGURE 4 | Seasonal and spatial variations of grain size composition in the surface sediment of the estuary and mariculture area in Qinzhou Bay.

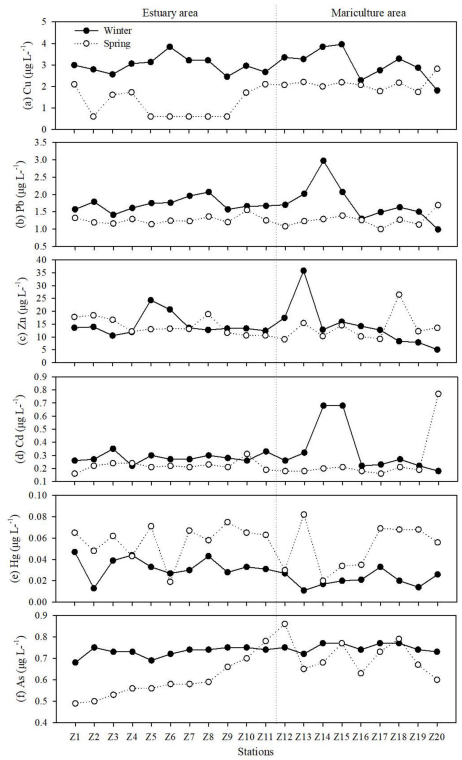

FIGURE 5 | Variations of heavy metals in the seawater of the estuary and mariculture area in Qinzhou Bay during winter and spring.

the seawater. Hg is negatively correlated with salinity, suggesting that the metal is greatly influenced by the terrestrial input. In contrast, there is a significantly positive relationship between Cu, Pb, Cd, and As, and they showed positive correlations with salinity while showing negative correlations with Hg, suggesting that the level of these metals may be influenced by the intrusion of seawater. Previous studies have found that, under the influence of the circulation of Beibu Gulf, a high concentration of heavy metals in the other areas can be introduced into the coastal seawaters of Guangxi Beibu Gulf (Lao et al., 2019; Liu et al., 2020). Correspondingly, Cu, Pb, Cd, and As showed a significantly positive correlation with temperature, indicating that the intrusion of these metals into the coastal mariculture area mainly occurred in winter (dry season). During the dry season, the runoff around the coastal area decreased sharply (Lao et al., 2020; Lao et al., 2021b), and the seawater could intrude into the bay; thus, the salinity increased. In contrast, Hg showed a positive correlation with temperature, indicating that the increase of runoff in the rainy season (higher temperature) could introduce more land-based Hg into the bay. Hg showed a significantly negative correlation with pH. This suggested that, except for the terrestrial input, the Hg level in the estuary and the bay may also be influenced by the water environment. Pb and As showed a significantly negative correlation with TSM level, indicating that Pb and As may be absorbed into the particulate matter under the higher TSM level in the water. According to the partition coefficient (K_d) in the similar semi-enclosed bay in South China, a high ratio of particulate Pb to dissolved Pb was found (higher than other metals), indicating a stronger affinity between Pb and suspended particles (Zhang et al., 2018). A high partition coefficient of Pb was also found in Yangtze Estuary in East China (Feng et al., 2017). In addition, As would be more easily adsorbed onto TSM under the higher TSM level and salinity in the estuary areas (Feng et al., 2017). Although the salinity slightly decreased in spring, the salinity in the study area was still >23 during that season, which was favored by the metal adsorbed onto TSM (Wang and Liu, 2003). Thus, the lower level of Pb and As that was observed in spring

TABLE 2 | Summary of the average value of heavy metals in the seawater (μg L^{-1}) and sediment (μg g^{-1}) of different areas in Qinzhou Bay during spring and winter.

Seawater			Cu	Pb	Zn	Cd	Hg	As	Cr
		Estuary area	1.07	1.27	14.18	0.22	0.058	0.59	
	Spring	Mariculture area	2.11	1.26	13.43	0.25	0.051	0.71	
Seawater		Average	1.60	1.26	13.84	0.24	0.055	0.65	
		Estuary area	2.99	1.71	15.55	0.28	0.033	0.73	
	Winter	Mariculture area	3.05	1.74	14.44	0.34	0.021	0.75	
		Average	3.01	1.72	14.50	0.31	0.028	0.74	
		Annual average	2.31	1.49	14.17	0.27	0.041	0.69	
Seawater		Grade I	5	1	20	1	0.05	20	
		Grade II	10	5	50	5	0.2	30	
		Estuary area	20.33	14.12	56.37	0.10	0.028	12.46	21.55
	Spring	Mariculture area	18.06	13.46	66.60	0.07	0.022	13.58	21.98
Sediment		Average	19.30	13.82	61.02	0.09	0.026	12.97	21.75
		Estuary area	11.93	12.37	37.83	0.09	0.084	12.32	12.62
	Winter	Mariculture area	6.14	16.56	42.86	0.08	0.085	11.39	13.30
		Average	9.30	14.27	40.12	0.09	0.084	11.90	12.93
		Annual average	14.30	14.04	50.57	0.09	0.055	12.43	17.34
Sediment		Grade I[a]	35.0	60.0	150.0	0.50	0.20	20.0	80.0
		Grade II[a]	100.0	130.0	350.0	1.50	0.50	65.0	150.0

[a]*National Standard of China for Seawater Quality (GB 3097-1997).*

TABLE 3 | Comparison of heavy metal levels in seawater with those in other regions (μg L^{-1}).

Area	Period	Cu	Pb	Zn	Cd	Hg	As	Reference
World average		0.25	0.03	0.5-4.9	0.07-0.11	0.00023		(Reimann and De Caritat, 2012)
Zhanjiang Bay, China	2014	4.40	0.23	12.64	0.12			(Zhang et al., 2018)
Xiangshan Bay, China	2011–2016	3.35	1.93	16.75	0.22	0.060	2.58	(Zhao et al., 2018)
Yellow River Estuary, China		11.6	5.61	14.9	0.66	0.24	2.59	(Wang et al., 2018)
East Guangdong coastal area, China	2006–2007	2.24	1.94	14.05	0.11		2.48	(Zhang et al., 2015)
West Guangdong coastal area, China	2006–2007	1.91	1.81	11.86	0.09		1.86	(Zhang et al., 2015)
Laoshan Bay, China	2017–2018	1.50	0.81	1.81	0.12	0.015	1.16	(Wang et al., 2019)
Beibu Gulf, China	2003	1.08	0.74		0.07	0.01	1.24	(Lao et al., 2019)
Beibu Gulf, China	2017	3.03	0.71	10.0	0.17	0.10	0.74	(Lao et al., 2019)
Pearl Bay, China	2018	1.63	0.84	4.77	0.14	0.094	1.56	(Liu et al., 2020)
Lianzhou Bay, China	2018	2.69	0.78	9.62	0.17	0.052	0.89	(Liu et al., 2020)
Maowei Sea, China	2018	3.69	0.85	15.28	0.11	0.099	0.81	(Liu et al., 2020)
Qinzhou Bay, China	1983	1.71	1.00	3.14	0.20	0.48		(Wei and He, 2004)
Qinzhou Bay, China	2003	1.10	0.60		0.01	0.014	1.28	(Lao et al., 2019)
Qinzhou Bay, China	2010	1.12	0.87		0.22	0.017	0.92	This study
Qinzhou Bay, China	2013	2.64	0.68	13.94	0.14	0.044	0.38	This study
Qinzhou Bay, China	2018	1.69	0.79	4.67	0.21	0.033	0.91	(Liu et al., 2020)
Jingu River estuary	2020	2.08	1.49	14.37	0.25	0.046	0.66	This study
Qinzhou Bay	2020	2.58	1.50	13.94	0.30	0.036	0.73	This study

The data in the table are from Beibu Gulf, including the coastal areas of Fangchenggang, Qinzhou, and Beihai in Guangxi province, and the same is true for ***Table 4****.*
ND, not detected.

may be influenced by the higher TSM level due to the increase of runoff in that season. In addition, Cu, Pb, Cd, and As showed positive correlations with DO, while Hg showed a negative correlation with DO. Pb showed a negative correlation with Chl *a*. These results suggest that these metals may present a close relationship with biological activities. The complexation prosperities of heavy metals with organic matter in the marine environment could result in the metal remaining in the water (Baeyens et al., 1998; Lao et al., 2019). In the sediment, Cu, Zn, and Cr showed significantly positive correlations with TOC, indicating that the TOC level greatly influenced their distribution and enrichment. There are significantly positive correlations between Cu, Pb, Cd, and Cr, indicating that there may be similar sources in the sediment. However, Hg showed a negative correlation with Cu, Cd, and TOC, suggesting that other factors influenced the distribution of Hg in the sediment.

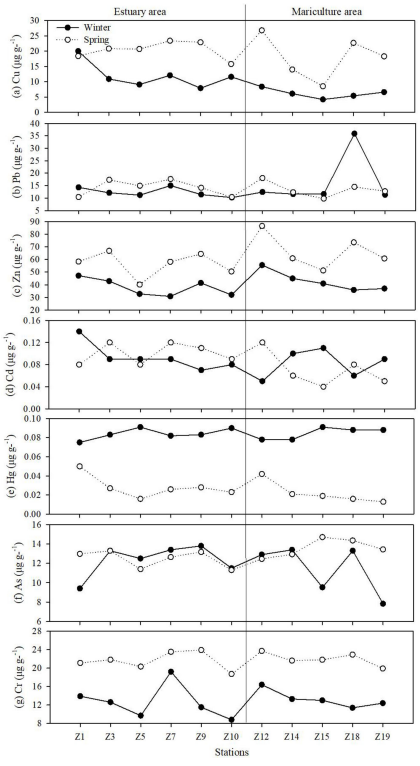

FIGURE 6 | Variations of heavy metals in the sediments of the estuary and mariculture area in Qinzhou Bay during winter and spring.

To further evaluate the correlations and the possible origins of heavy metals in Qinzhou Bay, the principal component analysis (PCA) for heavy metals and the related environmental parameters in the seawater and sediment were analyzed in this study, and the results are presented in **Figure 7**. In the seawater, three principal components that accounted for 73.458% of the total data variance were identified. PC1 accounted for 47.696% of the variance, with high negative loadings for Hg and salinity and high positive loadings for Cu, Pb, and As. This further confirmed that those metals are influenced by their hydrological characteristics. Hg in the seawater may be influenced by the terrestrial inputs, and Cu, Pb, and As may be influenced by the intrusion of water with higher salinity from the outer bay. Pb is widely used as an antiknock agent in diesel fuel and anti-corrosive compound for shipping, Cu and As are constituents of some algaecides and fungicides, and the high concentrations of these two metals are usually found in mariculture areas (Wang et al., 2018). Thus, mariculture and shipping activities mainly contributed to PC1. PC2 accounted for 16.003%, with high negative loadings for Pb, pH, and Chl *a*. PC3 accounted for 9.759%, with high positive

TABLE 4 | Comparison of heavy metal concentrations (μg g^{-1}) in surface sediments with those in other regions.

Area	Period	Cu	Pb	Zn	Cd	Hg	As	Cr	Reference
Zhanjiang Bay, China	2014	18.74	43.89	73.60	0.15			63.83	(Zhang et al., 2018)
Xiangshan Bay, China	2011–2016	36.8	38.5	121	0.15	0.11	12.3	81.7	(Zhao et al., 2018)
Coast of Hainan, China	2012–2014	29.4	19.2	81.4	0.19			57.3	(Xu et al., 2015)
Nan'ao Island, China	2014–2015	15.26	40.81	102.72	0.35				(Luo et al., 2020)
Zhelin Bay, China	2011	32	76	156	0.108	0.08	14.5	31	(Wang et al., 2016)
Zhelin Bay, China	2013	28	56	121	0.082	0.07	11.8	23	(Wang et al., 2016)
Xiamen Bay, China	2004	44.0	54.0	139.0	0.331			74.5	(Zhang et al., 2007)
West Guangdong coastal area, China	2006–2007	43.83	44.29	139.93	0.38	0.13	20.83	86.97	(Zhao et al., 2016)
Pearl River Estuary, China	2007	348.0	102.6	383.4	1.72			93.1	(Niu et al., 2009)
Beibu Gulf	2003	9.57	18.72		0.03	0.03	12.59		(Lao et al., 2019)
Beibu Gulf	2017	15.07	14.64	52.37	0.06	0.06	7.82	44.42	(Lao et al., 2019)
Qinzhou Bay, China	2003	8.6	18.4		0.02	0.027	15.94		(Lao et al., 2019)
Qinzhou Bay, China	2010	15.58	12.42	61.33	0.11	0.050	17.58	61.02	This study
Qinzhou Bay, China	2013	17.7	39.9	61.0	0.10	0.040	13.20	36.50	This study
Qinzhou Bay, China	2017	13.4	14.65	43.20	0.05	0.026	10.79	43.40	(Lao et al., 2019)
Qinzhou Bay, China	2020	12.10	15.01	54.73	0.08	0.050	12.48	17.64	This study
Jingu River Estuary	2020	16.13	13.24	47.10	0.10	0.056	12.39	17.08	This study

TABLE 5 | Correlation analysis between heavy metal concentrations and the physicochemical parameters in surface water.

	T	PH	S	DO	TSM	Chl *a*	Cu	Pb	Zn	Cd	Hg	As
T	1.000	-0.422[a]	-0.889[a]	-0.733[a]	0.261	0.442[a]	-0.819[a]	-0.618[a]	-0.041	-0.293[b]	0.662[a]	-0.653[a]
PH		1.000	0.751[a]	0.813[a]	-0.029	0.507[a]	0.528[a]	0.140	-0.027	0.166	-0.402[a]	0.596[a]
S			1.000	0.920[a]	-0.175	-0.100	0.804[a]	0.486[a]	-0.054	0.279[b]	-0.641[a]	0.740[a]
DO				1.000[a]	-0.162	0.113	0.703[a]	0.445[a]	-0.013	0.307[b]	-0.571[a]	0.693[a]
TSM					1.000	0.153	-0.198	-0.375[a]	-0.075	-0.179	0.026	-0.319[b]
Chl *a*						1.000	-0.193	-0.389[a]	-0.087	-0.082	0.365[a]	0.042
Cu							1.000	0.740[a]	0.161	0.486[a]	-0.556[a]	0.611[a]
Pb								1.000	0.257	0.698[a]	-0.497[a]	0.348[b]
Zn									1.000	0.091	-0.021	-0.122
Cd										1.000	-0.245	0.120
Hg											1.000	-0.451[a]
As												1.000

[a]*Correlation is significant at the 0.01 level.*
[b]*Correlation is significant at the 0.05 level.*

TABLE 6 | Correlation analysis between heavy metal concentrations and the environmental parameters in sediment.

	pH	TOC	Cu	Pb	Zn	Cd	Hg	As	Cr
pH	1.000	-0.079	-0.339	-0.019	0.236	-0.261	-0.032	-0.016	-0.054
TOC		1.000	0.748**	-0.007	0.765**	0.279	-0.453*	0.136	0.482*
Cu			1.000	0.052	0.725**	0.430*	-0.699**	0.133	0.752**
Pb				1.000	0.029	0.036	0.061	0.144	0.007
Zn					1.000	0.164	-0.678**	0.322	0.779**
Cd						1.000	0.106	-0.434*	0.066
Hg							1.000	-0.353	-0.866**
As								1.000	0.371*
Cr									1.000

** Correlation is significant at the 0.05 level; ** correlation is significant at the 0.01 level.*

loadings for Zn, Cd, and Chl *a*. PC2 and PC3 indicated the influence of biological activities. The growth of phytoplankton would not only absorb some metals but also could induce the decomposition of organic matter that releases the metal into the water. The increase of phytoplankton (fresh and labile organic matter) tended to modify and, more generally, increase the decomposition rate of the more recalcitrant organic matter (Fontaine et al., 2003; Guenet et al., 2010). The increase in decomposition rate would result in more specific metals released into the water (Cotrufo et al., 1995; Luo et al., 2022). Thus, except from the influence of hydrological processes, biological activity is another important factor that influences

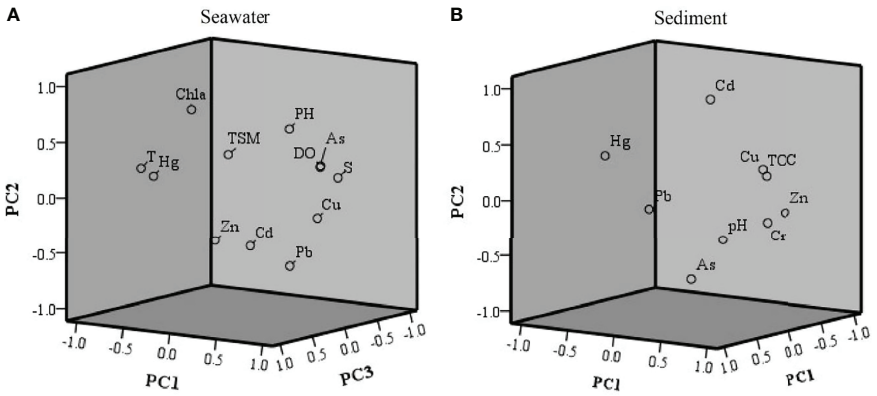

FIGURE 7 | Results of principal component analysis of heavy metal concentrations and environmental parameters in the estuary and the adjacent mariculture in Qinzhou Bay.

the distribution of heavy metals in the seawater. In sediments, three principal components that account for 75.513% of the total variance were identified. PC1 accounted for 43.804% of the variance, with high positive loadings for Cu, Zn, Cr, and TOC and high negative loadings for Hg and TOC, further confirming that TOC was the main controlling factor for the distribution of these metals. PC2 accounted for 19.215% of the total variance, with high negative loadings for Cd and As, suggesting the different fate of these two metals in the sediment. Cd is widely used in chemical plants, and chemical material manufacturing discharges wastewater containing high Cd concentrations (Wang et al., 2018). Thus, Cd reflects the input of terrestrial and industrial sources, while As reflects mariculture activities. Generally, mariculture activity keeps away from urban and industrial wastewater outlets. PC3 accounted for 12.494%, with high negative loadings for Pb and pH, indicating that the sediment environment (acidity and alkalinity) was the main factor influencing the enrichment of Pb in the sediment.

Historical Trend and Its Influencing Factors of Heavy Metals in Qinzhou Bay

The concentration of Cu increased in both seawater and sediment of the mariculture area in Qinzhou Bay over the past years (**Tables 3**, **4**). This is similar to the observation in Beibu Gulf (Lao et al., 2019; Liu et al., 2020). Cu is used as fertilizers and as additive in algaecides and agriculture fungicides (Burgos-Núñez et al., 2017; Wang et al., 2018; Naser, 2013). Previous studies suggested that the concentration of Cu showed a significantly increasing trend in both seawater and sediments of the whole Guangxi Beibu Gulf due to the influence of rapid industrial development and the enhancement and expansion of mariculture activities over the past years (Lao et al., 2019; Liu et al., 2020). In addition, due to the great toxicity and harm of Hg, the production of mercury began to decline as early as 1884, and the usage of Hg has also decreased significantly in the past years (Schuster et al., 2002; Pacyna et al., 2006). Thus, the decrease in production and usage of Hg may be responsible for the decrease in Hg concentration in the seawater over the past 40 years. Notably, the concentration of Hg showed a significantly negative correlation to pH, indicating that pH would directly affect the biosorption of metal ions (Atkinson et al., 2007; Ma et al., 2016; Lao et al., 2019).

However, different variation tendencies of some metals were observed in seawater and sediment according to the historical data. The concentrations of Pb, Zn, and Cd showed an increasing trend in the seawater of Qinzhou Bay for the past 40 years (**Table 3**), while the concentrations of Pb, Zn, As, and Cr in the sediment generally decreased for the past 20 years (**Table 4**). If the increase of terrestrial input and the enhancement of human activity intensity are the dominant factors that result in the increase of those metals in the mariculture area, the level of the metal in both seawater and sediment should be increased. In contrast, the level of some metals decreased in the sediment, indicating that other factors may control such an opposite trend between the seawater and the sediment. The change in the water environment in Qinzhou Bay may be an important factor causing the different change trends of heavy metals in seawater and sediments. For the past 20 years, the pH value of seawater in Qinzhou Bay has decreased significantly (**Figure 3**). In addition, the results of correlation and principal component analyses show that the pH value is the important parameter affecting the distribution of heavy metals in both seawater and sediment (**Tables 5**, **6** and **Figure 7**)—for example, high negative loadings for Pb and pH were found in both sediment and seawater (**Figure 7**), indicating that the increased Pb concentration in seawater and the decrease in the sediment may be greatly influenced by the decrease in pH over the past decades. The pH in the aquatic environment and sediment is very important for the mobility of heavy metals because metal availability is relatively low when the pH value is at a low level (Ma et al., 2016). The absorbed metals can be released into the water again with the change of pH (Kashem and Singh, 2001). The release of heavy metals is associated with a lower pH since the low pH can weaken the strength of heavy metal association and impede the retention of heavy metals by

particulate matter and sediments, while the higher pH value promotes precipitation and adsorption (Ma et al., 2016; Zhang et al., 2014). Thus, the decrease in pH value would lead to the re-release of heavy metals in particles and sediments into the water column, resulting in the decrease of heavy metals in the sediment and an increase in the seawater.

Pollution Status of Heavy Metals and Their Feedback to Environmental Change

In the seawater, the E_r^i in the estuary and the adjacent mariculture area decreased in the order Hg > Cd > Pb > Cu > Zn > As during both seasons. Although the ERI value (60) in spring was higher than that in winter (44), those values were all lower than 150, indicating that the potential risks of the six metals to the aquaculture ecosystem were relatively low. Notably, the E_r^i value for Hg (44) in spring was higher than 40 (at the level of moderate ecological risk), and the contribution for ERI was 73%, showing a potential ecological risk.

In the sediment, the mean values for the seven metals were in the decreasing order of Hg (2.91) > As (1.53) > Cd (0.98) > Cu (0.59) > Zn (0.53) > Pb (0.49) > Cr (0.37) during winter and As (1.66) > Cu (1.22) > Cd (0.96) > Hg (0.88) > Zn (0.80) > Cr (0.62) > Pb (0.48) during spring. Hg and As in winter and As and Cu in spring exhibited a moderate degree of contamination. The PLI values of those seven metals ranged from 0.70 to 0.96 (an average of 0.79) and from 0.64 to 1.14 (an average of 0.86) during winter and spring, respectively. The PLI level is an important reference index to decision-makers about pollution status and can provide inhabitants with an understanding of the environmental quality of the mariculture area (Islam et al., 2015; Lao et al., 2019). The lower PLI values (<1) in both seasons indicated the presence of only the baseline levels of pollutants.

The I_{geo} values for Hg are in the range of 0.79 to 1.06 (an average of 0.95), while the average I_{geo} values for other metals are all lower than 0 in winter. This indicates that Hg is moderately contaminated, while the other metals are uncontaminated in the sediment. In the spring, the I_{geo} values for As are in the range of -0.05 to 0.33 (an average of 0.15), indicating that As is a potential ecological risk factor during that season. However, the average I_{geo} values for other metals are all lower than 0, suggesting that those metals are uncontaminated in the sediment during spring. Overall, Hg and As presented a higher risk in both the seawater and sediment of the mariculture area, and the heavy metal contamination in the mariculture area must not be ignored.

Environmental change, such as the decrease in pH and seasonal hypoxia, likely changes the heavy metal status in aquatic systems (Atkinson et al., 2007; Chakraborty et al., 2016; Ma et al., 2016; Lao et al., 2019). Previous studies have found that the DO level is a key factor controlling the stability and lability of metals in the sediment (Chakraborty et al., 2016)—for example, some metals, such as Pb, associated with Fe/Mn-oxyhydroxide phases in the sediment would reduce with the decreasing DO level of the overlying water because of the dissolution of the Fe/Mn-oxyhydroxide phase (Chakraborty et al., 2016). In Qinzhou Bay, the eutrophication degree has increased in the past few decades due to the rapid development of industrialization and urbanization and the continuous expansion of aquaculture activities (Lao et al., 2021a), which may induce seasonal hypoxia in the bay (Howarth et al., 2011). Moreover, the pH value has decreased significantly over the past 20 years in Qinzhou Bay, which may cause more metals to be released into the water environment. In addition, Qinzhou Bay is a sea area with strong hydrodynamic conditions in Beibu Gulf (Chen et al., 2022). Particularly under the influence of the northeast monsoon in winter, the bottom sediment is resuspended into the water column, which may also lead to the increase of heavy metal release in a more acidic environment. The increase of heavy metal concentrations in seawater would lead to the increase of heavy metal absorption by aquaculture organisms, which poses a great threat to the health of organisms and ultimately endangers human health. Especially under global climate change, the acidification of seawater in most aquaculture areas in the world is aggravated (Clements and Chopin, 2017; Ng and Chiu, 2020; Jin et al., 2020; Swezey et al., 2020), which may also lead to the increase of heavy metal released into the seawater. This problem should be more vigilant and concerned in the future.

CONCLUSION

Seasonal changes in the concentrations of heavy metals were found in Qinzhou Bay. The concentrations of heavy metals in the seawater were higher, while the levels in the sediment were lower than that in other mariculture areas in China. The concentration of Cu in the seawater and sediment increased over the past decades, mainly influenced by the enhancement and expansion of mariculture and shipping activities. The concentration of Hg has decreased significantly in the seawater over the past 40 years due to the decrease in production and usage of Hg. However, the concentrations of Pb, Zn, and Cd in the seawater showed an increasing trend over the past 40 years, while the concentrations of Pb, Zn, As, and Cr in the sediment generally decreased over the past 20 years. The decrease in pH value (by 4.7%) over the past 20 years was responsible for the different trends of those metals between seawater and sediment. Hg and As presented a higher risk in both the seawater and sediment of the mariculture area. Overall, this study suggests that environmental changes, such as decrease in pH, affect the distribution of heavy metals in water and sediments, which we should be more vigilant and concerned about under the global climate change.

DATA AVAILABILITY STATEMENT

The original contributions presented in the study are included in the article/supplementary material. Further inquiries can be directed to the corresponding author.

AUTHOR CONTRIBUTIONS

FC was responsible for the conceptualization. QL prepared and wrote the original draft. QL and FC wrote, reviewed, and edited

the manuscript. SC and PH were responsible for the data curation. QS, XLe, CC, QZ, XLu, and XZ were responsible for the experimental operation. QS, XLe, and GL were responsible for field sampling. FC and QL funded the acquisition. All authors contributed to the article and approved the submitted version.

FUNDING

This study was supported by the National Natural Science Foundation of China (U1901213 and 92158201), Guangdong Natural Science Foundation of China (2019B1515120066), Innovation and Entrepreneurship Project of Shantou (2021112176541391), and Guangxi Natural Science Foundation of China (2020GXNSFBA297065).

ACKNOWLEDGMENTS

We would like to thank the Marine Environmental Monitoring Centre of Beihai, State Oceanic Administration, for their support in collecting seawater and sediment samples and their supply in historical data.

REFERENCES

Achary, M. S., Satpathy, K. K., Panigrahi, S., Mohanty, A. K., Padhi, R. K., Biswas, S., et al. (2017). Concentration of Heavy Metals in the Food Chain Components of the Nearshore Coastal Waters of Kalpakkam, Southeast Coast of India. *Food Contr.* 72, 232–243. doi: 10.1016/j.foodcont.2016.04.028

Adyasari, D., Pratama, M. A., Teguh, N. A., Sabdaningsih, A., Kusumaningtyas, M. A., and Dimova, N. (2021). Anthropogenic Impact on Indonesian Coastal Water and Ecosystems: Current Status and Future Opportunities. *Mar. Poll. Bull.* 171, 112689. doi: 10.1016/j.marpolbul.2021.112689

Alengebawy, A., Abdelkhalek, S. T., Qureshi, S. R., and Wang, M. Q. (2021). Heavy Metals and Pesticides Toxicity in Agricultural Soil and Plants: Ecological Risks and Human Health Implications. *Toxics* 9 (3), 42. doi: 10.3390/toxics9030042

Atkinson, C. A., Jolley, D. F., and Simpson, S. L. (2007). Effect of Overlying Water Ph, Dissolved Oxygen, Salinity and Sediment Disturbances on Metal Release and Sequestration From Metal Contaminated Marine Sediments. *Chemosphere* 69 (9), 1428–1437. doi: 10.1016/j.chemosphere.2007.04.068

Baeyens, W., Elskens, M., Gillain, G., and Goeyens, L. (1998). "Biogeochemical Behaviour of Cd, Cu, Pb and Zn in the Scheldt Estuary During the Period 1981–1983," in *In Trace Metals in the Westerschelde Estuary: A Case-Study of a Polluted, Partially Anoxic Estuary* (Dordrecht: Springer), 15–44.

Baquiran, J. I. P., and Conaco, C. (2018). Sponge-Microbe Partnerships are Stable Under Eutrophication Pressure From Mariculture. *Mar. Poll. Bull.* 136, 125–134. doi: 10.1016/j.marpolbul.2018.09.011

Burgos-Núñez, S., Navarro-Frómeta, A., Marrugo-Negrete, J., Enamorado-Montes, G., and Urango-Cárdenas, I. (2017). Polycyclic Aromatic Hydrocarbons and Heavy Metals in the Cispata Bay, Colombia: A Marine Tropical Ecosystem. *Mar. Poll. Bull.* 120 (1-2), 379–386. doi: 10.1016/j.marpolbul.2017.05.016

Cai, L. M., Wang, Q. S., Luo, J., Chen, L. G., Zhu, R. L., Wang, S., et al. (2019). Heavy Metal Contamination and Health Risk Assessment for Children Near a Large Cu-Smelter in Central China. *Sci. Total. Environ.* 650, 725–733. doi: 10.1016/j.scitotenv.2018.09.081

Castro-González, M. I., and Méndez-Armenta, M. (2008). Heavy Metals: Implications Associated to Fish Consumption. *Environ. Toxicol. Pharmacol.* 26 (3), 263–271. doi: 10.1016/j.etap.2008.06.001

Chakraborty, P., Chakraborty, S., Jayachandran, S., Madan, R., Sarkar, A., Linsy, P., et al. (2016). Effects of Bottom Water Dissolved Oxygen Variability on Copper and Lead Fractionation in the Sediments Across the Oxygen Minimum Zone, Western Continental Margin of India. *Sci. Total. Environ.* 566, 1052–1061. doi: 10.1016/j.scitotenv.2016.05.125

Chen, C., Lao, Q., Shen, Y., Jin, G., Chen, F., Su, Q., et al. (2022). Comparative Study of Nitrogen Cycling Between a Bay With Riverine Input and a Bay Without Riverine Input, Inferred From Stable Isotopes. *Front. Mar. Sci* 9, 885037. doi: 10.3389/fmars.2022.885037

Chen, F., Lin, J., Qian, B., Wu, Z., Huang, P., Chen, K., et al. (2018). Geochemical Assessment and Spatial Analysis of Heavy Metals in the Surface Sediments in the Eastern Beibu Gulf: A Reflection on the Industrial Development of the South China Coast. *Int. J. Environ. Res. Public Health* 15 (3), 496. doi: 10.3390/ijerph15030496

Clements, J. C., and Chopin, T. (2017). Ocean Acidification and Marine Aquaculture in North America: Potential Impacts and Mitigation Strategies. *Rev. Aquacult.* 9 (4), 326–341. doi: 10.1111/raq.12140

Cotrufo, M. F., De Santo, A. V., Alfani, A., Bartoli, G., and De Cristofaro, A. (1995). Effects of Urban Heavy Metal Pollution on Organic Matter Decomposition in Quercus Ilex L. Woods. *Environ. Poll.* 89 (1), 81–87. doi: 10.1016/0269-7491(94)00041-B

Duodu, G. O., Goonetilleke, A., and Ayoko, G. A. (2016). Comparison of Pollution Indices for the Assessment of Heavy Metal in Brisbane River Sediment. *Environ. Poll.* 219, 1077–1091. doi: 10.1016/j.envpol.2016.09.008

Feng, C., Guo, X., Yin, S., Tian, C., Li, Y., and Shen, Z. (2017). Heavy Metal Partitioning of Suspended Particulate Matter–Water and Sediment–Water in the Yangtze Estuary. *Chemosphere* 185, 717–725. doi: 10.1016/j.chemosphere.2017.07.075

Fontaine, S., Mariotti, A., and Abbadie, L. (2003). The Priming Effect of Organic Matter: A Question of Microbial Competition? *Soil Biol. Biochem.* 35 (6), 837–843. doi: 10.1016/S0038-0717(03)00123-8

Gong, Y., Zhao, D., and Wang, Q. (2018). An Overview of Field-Scale Studies on Remediation of Soil Contaminated With Heavy Metals and Metalloids: Technical Progress Over the Last Decade. *Water Res.* 147, 440–460. doi: 10.1016/j.watres.2018.10.024

Guenet, B., Danger, M., Abbadie, L., and Lacroix, G. (2010). Priming Effect: Bridging the Gap Between Terrestrial and Aquatic Ecology. *Ecology* 91 (10), 2850–2861. doi: 10.1890/09-1968.1

Gu, Y. G., Lin, Q., Yu, Z. L., Wang, X. N., Ke, C. L., and Ning, J. J. (2015). Speciation and Risk of Heavy Metals in Sediments and Human Health Implications of Heavy Metals in Edible Nekton in Beibu Gulf, China: A Case Study of Qinzhou Bay. *Mar. Poll. Bull.* 101 (2), 852–859. doi: 10.1016/j.marpolbul.2015.11.019

Hakanson, L. (1980). An Ecological Risk Index for Aquatic Pollution Control. A Sedimentological Approach. *Water Res.* 14 (8), 975–1001.

Howarth, R., Chan, F., Conley, D. J., Garnier, J., Doney, S. C., Marino, R., et al. (2011). Coupled Biogeochemical Cycles: Eutrophication and Hypoxia in Temperate Estuaries and Coastal Marine Ecosystems. *Front. Ecol. Environ.* 9 (1), 18–26. doi: 10.1890/100008

Islam, M. S., Ahmed, M. K., Raknuzzaman, M., Habibullah-Al-Mamun, M., and Islam, M. K. (2015). Heavy Metal Pollution in Surface Water and Sediment: A Preliminary Assessment of an Urban River in a Developing Country. *Ecol. Indic.* 48, 282–291. doi: 10.1016/j.ecolind.2014.08.016

Islam, M. S., and Tanaka, M. (2004). Impacts of Pollution on Coastal and Marine Ecosystems Including Coastal and Marine Fisheries and Approach for Management: A Review and Synthesis. *Mar. Poll. Bull.* 48 (7-8), 624–649. doi: 10.1016/j.marpolbul.2003.12.004

Jiang, Z., Xu, N., Liu, B., Zhou, L., Wang, J., Wang, C., et al. (2018). Metal Concentrations and Risk Assessment in Water, Sediment and Economic Fish Species With Various Habitat Preferences and Trophic Guilds From Lake Caizi, Southeast China. *Ecotoxicol. Environ. Saf.* 157, 1–8. doi: 10.1016/j.ecoenv.2018.03.078

Jin, P., Hutchins, D. A., and Gao, K. (2020). The Impacts of Ocean Acidification on Marine Food Quality and its Potential Food Chain Consequences. *Front. Mar. Sci.* 7, 543979. doi: 10.3389/fmars.2020.543979

Kashem, M. A., and Singh, B. R. (2001). Metal Availability in Contaminated Soils: I. Effects of Floodingand Organic Matter on Changes in Eh, pH and Solubility of Cd, Ni andZn. *Nutri. Cycl. Agroecosyst.* 61 (3), 247–255.

Kumar, V., Parihar, R. D., Sharma, A., Bakshi, P., Sidhu, G. P. S., Bali, A. S., et al. (2019). Global Evaluation of Heavy Metal Content in Surface Water Bodies: A Meta-Analysis Using Heavy Metal Pollution Indices and Multivariate Statistical Analyses. *Chemosphere* 236, 124364. doi: 10.1016/j.chemosphere.2019.124364

Lao, Q., Liu, G., Gao, J., Shen, Y., Guo, Z., Qing, S., et al. (2021a). Study on the Characteristics and Eutrophication of Nutrients in the Mariculture Farms of Qinzhou Bay, South China. *Mar. Environ. Sci.* 40 (3), 407–416. doi: 10.13634/j.cnki.mes.2021.03.011

Lao, Q., Liu, G., Shen, Y., Su, Q., Gao, J., and Chen, F. (2020). Distribution Characteristics and Fluxes of Nutrients in the Rivers of the Beibu Gulf. *Haiyang Xuebao* 42 (12), 93–100. doi: 10.3969/j.issn.0253–4193.2020.12.010

Lao, Q., Liu, G., Shen, Y., Su, Q., and Lei, X. (2021b). Biogeochemical Processes and Eutrophication Status of Nutrients in the Northern Beibu Gulf, South China. *J. Earth Syst. Sci.* 130 (4), 1–14. doi: 10.1007/s12040-021-01706-y

Lao, Q., Liu, G., Zhou, X., Chen, F., and Zhang, S. (2021c). Sources of Polychlorinated Biphenyls (PCBs) and Dichlorodiphenyltrichloroethanes (DDTs) Found in Surface Sediment From Coastal Areas of Beibu Gulf: A Reflection on Shipping Activities and Coastal Industries. *Mar. Poll. Bull.* 167, 112318. doi: 10.1016/j.marpolbul.2021.112318

Lao, Q., Su, Q., Liu, G., Shen, Y., Chen, F., Lei, X., et al. (2019). Spatial Distribution of and Historical Changes in Heavy Metals in the Surface Seawater and Sediments of the Beibu Gulf, China. *Mar. Poll. Bull.* 146, 427–434. doi: 10.1016/j.marpolbul.2019.06.080

Liu, G., Lao, Q., Su, Q., Shen, Y., Chen, F., Qing, S., et al. (2020). Spatial and Seasonal Characteristics of Dissolved Heavy Metals in the Aquaculture Areas of Beibu Gulf, South China. *Hum. Ecol. Risk Assess.: Int. J.* 26 (7), 1957–1969. doi: 10.1080/10807039.2019.1629273

Liu, S., Shi, J., Wang, J., Dai, Y., Li, H., Li, J., et al. (2021). Interactions Between Microplastics and Heavy Metals in Aquatic Environments: A Review. *Front. Microbiol.* 12, 730. doi: 10.3389/fmicb.2021.652520

Li, C., Wang, H., Liao, X., Xiao, R., Liu, K., Bai, J., et al. (2022). Heavy Metal Pollution in Coastal Wetlands: A Systematic Review of Studies Globally Over the Past Three Decades. *J. Hazard. Material.* 424, 127312. doi: 10.1016/j.jhazmat.2021.127312

Li, J., Zhang, H., Zhang, K., Yang, R., Li, R., and Li, Y. (2018). Characterization, Source, and Retention of Microplastic in Sandy Beaches and Mangrove Wetlands of the Qinzhou Bay, China. *Mar. Poll. Bull.* 136, 401–406. doi: 10.1016/j.marpolbul.2018.09.025

Luo, H., Wang, Q., Liu, Z., Wang, S., Long, A., and Yang, Y. (2020). Potential Bioremediation Effects of Seaweed Gracilaria Lemaneiformis on Heavy Metals in Coastal Sediment From a Typical Mariculture Zone. *Chemosphere* 245, 125636. doi: 10.1016/j.chemosphere.2019.125636

Luo, H., Xie, S., Dai, X., Wang, Q., and Yang, Y. (2022). Biomass Decomposition and Heavy Metal Release From Seaweed Litter, Gracilaria Lemaneiformis, and Secondary Pollution Evaluation. *J. Environ. Manage.* 310, 114729. doi: 10.1016/j.jenvman.2022.114729

Ma, X., Zuo, H., Tian, M., Zhang, L., Meng, J., Zhou, X., et al. (2016). Assessment of Heavy Metals Contamination in Sediments From Three Adjacent Regions of the Yellow River Using Metal Chemical Fractions and Multivariate Analysis Techniques. *Chemosphere* 144, 264–272. doi: 10.1016/j.chemosphere.2015.08.026

Mishra, S., Bharagava, R. N., More, N., Yadav, A., Zainith, S., Mani, S., et al. (2019). "). Heavy Metal Contamination: An Alarming Threat to Environment and Human Health," in *In Environmental Biotechnology: For Sustainable Future* (Singapore: Springer), 103–125.

Naser, H. A. (2013). Assessment and Management of Heavy Metal Pollution in the Marine Environment of the Arabian Gulf: A Review. *Mar. Poll. Bull.* 72 (1), 6–13. doi: 10.1016/j.marpolbul.2013.04.030

Ng, J. C., and Chiu, J. M. (2020). Changes in Biofilm Bacterial Communities in Response to Combined Effects of Hypoxia, Ocean Acidification and Nutrients From Aquaculture Activity in Three Fathoms Cove. *Mar. Poll. Bull.* 156, 111256. doi: 10.1016/j.marpolbul.2020.111256

Niu, H., Deng, W., Wu, Q., and Chen, X. (2009). Potential Toxic Risk of Heavy Metals From Sediment of the Pearl River in South China. *J. Environ. Sci.* 21, 1053–1058. doi: 10.1016/S1001-0742(08)62381-5

Pacyna, E. G., Pacyna, J. M., Steenhuisen, F., and Wilson, S. (2006). Global Anthropogenic Mercury Emission Inventory for 2000. *Atmos. Environ.* 40 (22), 4048–4063. doi: 10.1016/j.atmosenv.2006.03.041

Reimann, C., and De Caritat, P. (2012). *Chemical Elements in the Environment: Factsheets for the Geochemist and Environmental Scientist* (Springer, Berlin: Springer Science & Business Media), 398 p

Schuster, P. F., Krabbenhoft, D. P., Naftz, D. L., Cecil, L. D., Olson, M. L., Dewild, J. F., et al. (2002). Atmospheric Mercury Deposition During the Last 270 Years: A Glacial Ice Core Record of Natural and Anthropogenic Sources. *Environ. Sci. Technol.* 36 (11), 2303–2310. doi: 10.1021/es0157503

Swezey, D. S., Boles, S. E., Aquilino, K. M., Stott, H. K., Bush, D., Whitehead, A., et al. (2020). Evolved Differences in Energy Metabolism and Growth Dictate the Impacts of Ocean Acidification on Abalone Aquaculture. *Proc. Natl. Acad. Sci.* 117 (42), 26513–26519. doi: 10.1073/pnas.2006910117

Wang, Z. L., and Liu, C. Q. (2003). Distribution and Partition Behavior of Heavy Metals Between Dissolved and Acid-Soluble Fractions Along a Salinity Gradient in the Changjiang Estuary, Eastern China. *Chem. Geol.* 202 (3-4), 383–396. doi: 10.1016/j.chemgeo.2002.05.001

Wang, X., Liu, L., Zhao, L., Xu, H., and Zhang, X. (2019). Assessment of Dissolved Heavy Metals in the Laoshan Bay, China. *Mar. Poll. Bull.* 149, 110608. doi: 10.1016/j.marpolbul.2019.110608

Wang, Y., Wei, Y., Guo, P., Pan, J., Wu, Q., and Liu, N. (2016). Distribution Variation of Heavy Metals in Maricultural Sediments and Their Enrichment, Ecological Risk and Possible Source—A Case Study From Zhelin Bay in Southern China. *Mar. Poll. Bull.* 113 (1-2), 240–246. doi: 10.1016/j.marpolbul.2016.09.028

Wang, S. L., Xu, X. R., Sun, Y. X., Liu, J. L., and Li, H. B. (2013). Heavy Metal Pollution in Coastal Areas of South China: A Review. *Mar. Poll. Bull.* 76 (1-2), 7–15. doi: 10.1016/j.marpolbul.2013.08.025

Wang, X., Zhao, L., Xu, H., and Zhang, X. (2018). Spatial and Seasonal Characteristics of Dissolved Heavy Metals in the Surface Seawater of the Yellow River Estuary, China. *Mar. Poll. Bull.* 137, 465–473. doi: 10.1016/j.marpolbul.2018.10.052

Wei, M., and He, B. (2004). Change Trend of Water Environment Index in Recent 20a in Qinzhou Bay-III Content Distribution of Trace Metal and its Source Analysis. *Mar. Environ. Sci.* 23 (1), 29–32. doi: 10.3969/j.issn.1007-6336.2004.01.009

Wu, J., Lu, J., Li, L., Min, X., and Luo, Y. (2018). Pollution, Ecological-Health Risks, and Sources of Heavy Metals in Soil of the Northeastern Qinghai-Tibet Plateau. *Chemosphere* 201, 234–242. doi: 10.1016/j.chemosphere.2018.02.122

Xu, C., Dan, S. F., Yang, B., Lu, D., Kang, Z., Huang, H., et al. (2021). Biogeochemistry of Dissolved and Particulate Phosphorus Speciation in the Maowei Sea, Northern Beibu Gulf. *J. Hydrol.* 593, 125822. doi: 10.1016/j.jhydrol.2020.125822

Xu, F., Tian, X., Yin, X., Yan, H., Yin, F., and Liu, Z. (2015). Trace Metals in the Surface Sediments of the Eastern Continental Shelf of Hainan Island: Sources and Contamination. *Mar. Poll. Bull.* 99, 276–283. doi: 10.1016/j.marpolbul.2015.07.055

Xu, C., Yang, B., Dan, S. F., Zhang, D., Liao, R., Lu, D., et al. (2020). Spatiotemporal Variations of Biogenic Elements and Sources of Sedimentary Organic Matter in the Largest Oyster Mariculture Bay (Maowei Sea), Southwest China. *Sci. Total. Environ.* 730, 139056. doi: 10.1016/j.scitotenv.2020.139056

Yan, X., An, J., Yin, Y., Gao, C., Wang, B., and Wei, S. (2022). Heavy Metals Uptake and Translocation of Typical Wetland Plants and Their Ecological Effects on the Coastal Soil of a Contaminated Bay in Northeast China. *Sci. Total. Environ.* 803, 149871. doi: 10.1016/j.scitotenv.2021.149871

Yang, B., Lan, R. Z., Lu, D. L., Dan, S. F., Kang, Z. J., Jiang, Q. C., et al. (2019). Phosphorus Biogeochemical Cycling in Intertidal Surface Sediments From the Maowei Sea in the Northern Beibu Gulf. *Reg. Stud. Mar. Sci.* 28, 100624. doi: 10.1016/j.rsma.2019.100624

Zhang, C., Yu, Z. G., Zeng, G. M., Jiang, M., Yang, Z. Z., Cui, F, et al(2014). Effects of Sediment Geochemical Properties on Heavy Metal Bioavailability. *Environment international.* 73, 270-281. doi: 10.1016/j.envint.2014.08.010.x

Zhang, L., Shi, Z., Zhang, J. P., Jiang, Z., Wang, F., and Huang, X. (2015). Spatial and Seasonal Characteristics of Dissolved Heavy Metals in the East and West

Guangdong Coastal Waters, South China. *Mar. Poll. Bull.* 95, 419–426. doi: 10.1016/j.marpolbul.2015.03.035

Zhang, L., Ye, X., Feng, H., Jing, Y., Ouyang, T., Yu, X., et al. (2007). Heavy Metal Contamination in Western Xiamen Bay Sediments and its Vicinity, China. *Mar. Poll. Bull.* 54, 974–982. doi: 10.1016/j.marpolbul.2007.02.010

Zhang, J., Zhou, F., Chen, C., Sun, X., Shi, Y., Hui, Z., et al. (2018). Spatial Distribution and Correlation Characteristics of Heavy Metals in the Seawater, Suspended Particulate Matter and Sediments in Zhanjiang Bay, China. *PloS One* 13, e0201414. doi: 10.1371/journal.pone.0201414

Zhao, G., Lu, Q., Ye, S., Yuan, H., Ding, X., and Wang, J. (2016). Assessment of Heavy Metal Contamination in Surface Sediments of the West Guangdong Coastal Region, China. *Mar. Poll. Bull.* 108, 268–274. doi: 10.1016/j.marpolbul.2016.04.057

Zhao, B., Wang, X., Jin, H., Feng, H., Shen, G., Cao, Y., et al. (2018). Spatiotemporal Variation and Potential Risks of Seven Heavy Metals in Seawater, Sediment, and Seafood in Xiangshan Bay, China, (2011–2016). *Chemosphere* 212, 1163–1171. doi: 10.1016/j.chemosphere.2018.09.020

Conflict of Interest: The authors declare that the research was conducted in the absence of any commercial or financial relationships that could be construed as a potential conflict of interest.

Publisher's Note: All claims expressed in this article are solely those of the authors and do not necessarily represent those of their affiliated organizations, or those of the publisher, the editors and the reviewers. Any product that may be evaluated in this article, or claim that may be made by its manufacturer, is not guaranteed or endorsed by the publisher.

Copyright © 2022 Lao, Cai, Huang, Chen, Su, Lei, Zhou, Chen, Zhu, Lu and Liu. This is an open-access article distributed under the terms of the Creative Commons Attribution License (CC BY). The use, distribution or reproduction in other forums is permitted, provided the original author(s) and the copyright owner(s) are credited and that the original publication in this journal is cited, in accordance with accepted academic practice. No use, distribution or reproduction is permitted which does not comply with these terms.

frontiers | Frontiers in Marine Science

BRIEF RESEARCH REPORT
published: 16 June 2022
doi: 10.3389/fmars.2022.937477

Organic Enrichment Induces Shifts in the Trophic Position of Infauna in a Subtropical Benthic Food Web, Hong Kong

Wenzhe Xu[1,2]*, *Paul K. S. Shin*[3] and *Jun Sun*[1,2]

[1] College of Marine and Environmental Sciences, Tianjin University of Science and Technology, Tianjin, China, [2] Tianjin Key Laboratory of Marine Resources and Chemistry, Tianjin University of Science and Technology, Tianjin, China, [3] Department of Biology and Chemistry, City University of Hong Kong, Kowloon, Hong Kong SAR, China

Anthropogenic nutrient input to coastal waters is one of the most common disturbances within inshore marine benthic communities. Organic enrichment in sediments leads to the reduction or disappearance of sensitive organisms, and influences the quality and quantity of primary producers which serve as food sources for the benthic fauna. Such changes, in turn, affect the energy flow and food-web interactions in benthic communities. To examine how organic enrichment may alter marine benthic trophic relationship, a stable isotope ($\delta^{13}C$ and $\delta^{15}N$) analysis of the potential food sources and a range of meiofauna and polychaetes from an organically polluted and a relatively unpolluted site was compared in subtropical waters of Hong Kong. Results indicated that some omnivorous infauna shifted from a mainly carnivorous diet at the unpolluted site to a largely herbivorous diet at the organically polluted site. This dietary shift is likely to be related to the oxygen stress, prey limitation and increased abundance and nutritional quality of primary producers in the eutrophic area, resulting in an increase in utilization of plant materials as the major food source. The present findings suggest that such changes in trophic position induced by organic enrichment can provide further insights into the structure and function of coastal benthic communities under pollution stress.

Keywords: organic enrichment, benthic community, nematodes, polychaetes, food web, trophic structure

OPEN ACCESS

Edited by:
Meilin Wu,
South China Sea Institute of Oceanology (CAS), China

Reviewed by:
Yongfen Du,
Nanjing University, China
Haichao Zhou,
Shenzhen University, China
Er Hua,
Ocean University of China, China

***Correspondence:**
Wenzhe Xu
xuwenzhe@tust.edu.cn

Specialty section:
This article was submitted to Marine Pollution, a section of the journal Frontiers in Marine Science

Received: *06 May 2022*
Accepted: *23 May 2022*
Published: *16 June 2022*

Citation:
Xu W, Shin PKS and Sun J (2022) Organic Enrichment Induces Shifts in the Trophic Position of Infauna in a Subtropical Benthic Food Web, Hong Kong. Front. Mar. Sci. 9:937477. doi: 10.3389/fmars.2022.937477

INTRODUCTION

Anthropogenic nutrient inputs to the coastal ecosystems particularly from discharges of untreated domestic sewage have led to widespread organic enrichment in inshore marine environments (Souza et al., 2013; Altieri and Diaz, 2019; Brauko et al., 2020). Such nutrient enrichment has impacted many biological communities, ranging from depletion of native populations, extinction of sensitive species to disappearance of diverse community structure (Nordström and Bonsdorff, 2017; Caswell et al., 2018; Culhane et al., 2019; Drylie et al., 2020). This becomes increasing important to understand how the species, community and ecosystem levels respond to such human-induced changes and whether ecosystem functions and services can be maintained (Riedel et al., 2014; Johansen et al., 2018; Guan et al., 2020).

The increase in nutrients can have both positive and negative effects on marine pelagic and benthic communities. Higher nutrient input can stimulate primary production in the water column, resulting in further deposition of organic matter onto the sediment that benefits both benthic grazers and detritus feeders (Aberson et al., 2016). However, increased sedimentation of organic matter can also lead to reduction or disappearance of some sensitive organisms through siltation, habitat modification and depletion of oxygen due to enhanced metabolic activities of microorganisms (Grall and Chauvaud, 2002; Dorgham, 2014; Hale et al., 2016). Changes in species composition and abundance associated with hypoxia caused by organic enrichment may in turn result in limitation of prey availability and alter consumers' feeding habits (Fox et al., 2009; Zheng et al., 2020). Under low oxygen supply, there is also a change in predator-prey dynamics, in which the foraging ability of predators is reduced due to slower mobility (Riedel et al., 2014; Briggs et al., 2017). These changes in composition and feeding behaviour of consumers may alter trophic relationships in coastal areas subject to eutrophication.

Stable isotope analyses of carbon and nitrogen are commonly used to reveal trophic interactions of natural populations of consumers in the field (Lepoint et al., 2004; Braeckman et al., 2015; Du et al., 2020). $\delta^{13}C$ is absorbed in the animal tissues with little or no change as compared to their food sources, so it can be used to determine the food sources; whereas $\delta^{15}N$ is absorbed in the animals with constant trophic shift, so it can be used to determine the trophic level (Fry, 2006). Using stable isotope analysis, the diets of benthic consumers have been shown to follow the changes in primary producers under nutrient enrichment, resulting in different benthic pathways that may explain modifications in community diversity and food web structure (Armitage and Fourqurean, 2009; Mitwally and Fleeger, 2015).

Victoria Harbour in subtropical Hong Kong (**Figure 1**) is one of the busiest and heavily populated ports in the world. Historically, the harbour has received substantial loadings of pollutants from sewage discharge, leading to severe pollution especially within the harbour centre where water movement is restricted by embayments and vessel anchorage shelters (Nicholson et al., 2011). At present most sewage is treated and discharged *via* a submarine outfall west of the harbour and the general water quality in the harbour has been improved (Xu et al., 2011). However, the sediments there still contain high levels of organic matter in the central harbour area resulting in lower diversity and different benthic community structure compared with that outside the harbour (Liu et al., 2011; Xu et al., 2014).

In the present study, we took advantages of coastal areas with different levels of pollution to examine whether increased organic enrichment can alter the benthic trophic relationship. To determine food web linkages, we measured stable isotopes ($\delta^{13}C$ and $\delta^{15}N$) of the particulate organic matter (POM), sediment organic matter (SOM) and primary and secondary consumers at an organically enriched site within the harbour area and a relative unpolluted site outside the harbour. Identifying and understanding the shifts in food source availability and the feeding modes of the animals in inshore areas can help to assess how coastal ecosystems respond under a long history of organic enrichment, sedimentation and other anthropogenic disturbances.

MATERIALS AND METHODS

Study Sites

The investigation and collection of samples for benthic infaunal community and stable isotope analysis were conducted in August 2010 at two sites around Victoria Harbour at a depth of 15-20 m (**Figure 1**). Tung Lung Chau (TLC) is located on the east outside the harbour, where anthropogenic activities are minimal and can be regarded as a relatively unpolluted site with low sediment nutrient levels. Sai Wan Ho (SWH) is located inside the harbour, where the sediment is organically enriched. A preliminary study on the taxonomic composition of macrofauna and nematode communities in relation to a number of sediment parameters were conducted at the same locations as in the present study (Xu et al., 2014). Data from the preliminary study showed that the sediment at TLC contained relative low nutrient levels (total organic carbon content: 0.37%, total

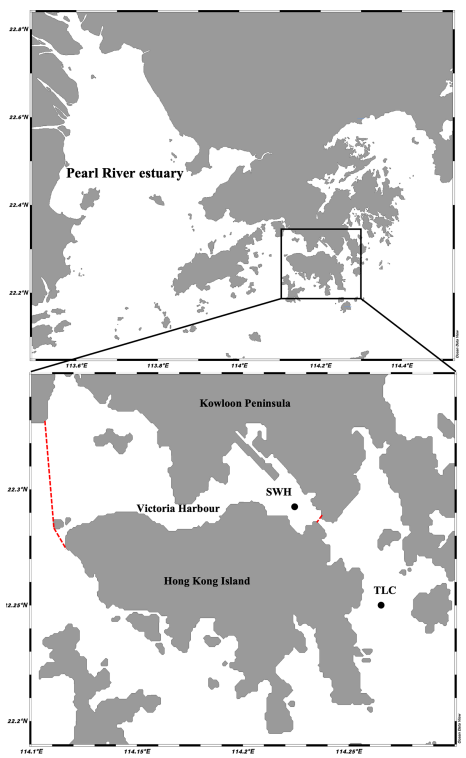

FIGURE 1 | Map showing the relatively unpolluted site TLC and organically enriched site SWH in subtropical Hong Kong, the red dotted lines indicate the boundary of Victoria Harbour.

phosphorus: 374.68 mg/kg, total Kjeldahl nitrogen: 632.97 mg/kg) and higher benthic faunal diversity (Shannon index $H' = 2.74$ for polychaetes and 3.61 for nematodes) as compared to that at SWH, with higher nutrient levels (total organic carbon content: 1.71%, total phosphorus: 807.07 mg/kg, total Kjeldahl nitrogen: 1926.72 mg/kg) and lower benthic faunal diversity (Shannon index $H' = 2.35$ for polychaetes and 2.59 for nematodes). The results also showed that the low diversity and different benthic community structure in the inner-harbour area were highly correlated with increased sediment nutrient levels.

Sampling

Triplicate water samples (~10 L per replicate) for particulate organic matter (POM) were collected at about 1 m above the sea bottom at each site using a water sampler. Sediment samples were collected with a 0.1 m^2 van Veen grab. A total of twelve grab sediment samples were retrieved at each site. For the first three grab samples, the upper 8 cm of sediment was scraped and stored in plastic bags for subsequent collection of copepod and free-living nematode specimens. For the next three grab samples, sediment was sieved through a 0.5 mm screen and the residues retained were transferred into plastic bags for collection of polychaete specimens. For the following three grab samples, about 400 g surface sediment was scooped by a spatula for later sediment organic matter (SOM) analysis. Benthic microalgae (BMA) were sampled from the sediment in the last three grab samples using the method modified from Wainright et al. (2000) and Doi et al. (2005). In brief, surface sediment was scraped to a depth of 1 cm, and spread into a 1 cm thin layer on a 0.1 m^2 plastic flat plate on board. For each plate sample, sediment was covered with a thin layer of silica sand (pre-combusted at 500°C for 2 h), a piece of 63 μm nylon screen, and another thin layer of silica sand. The plates were placed under sunlight for 2 h with continuous moisture from filtered seawater to allow vertical phototactic migration of microalgae onto the nylon screen. Then the screen was peeled off and stored in an ice box.

In the laboratory, meiofaunal nematodes and harpacticoid copepods were extracted from the sediment samples using the centrifugation technique with colloidal Ludox solution (Heip et al., 1985). Moens et al. (2002) showed that the isotopic values of meiofauna obtained under such handling procedures were not affected as compared with similar analysis of live specimens. Sorting of nematodes was restricted to species which were easily recognizable under a stereomicroscope and available in sufficient biomass. In order to obtain enough biomass, for the large nematodes *Halichoanolaimus* and *Sphaerolaimus* spp., at least 50 individuals were pooled. For the average-sized nematode *Daptonema*, *Dorylaimopsis*, *Paradontophora* and *Terschellingia* spp., at least 500 individuals were pooled. Harpacticoid copepods were pooled with at least 500 individuals, without identification to genus or species level. For macrofauna, only polychaetes were sorted and identified to species as far as practicable. The whole body of polychaetes was used for subsequent stable isotope analysis. At least five individuals per species were pooled to obtain enough biomass. All sorted faunal samples were then oven dried at 60°C and 1 mg of the homogenized samples was placed in pre-combusted aluminium cups and stored in screw-cap glass tubes for subsequent stable isotope analysis. Gut contents of all collected meio- and macrofaunal specimens were not separated from the tissue. Hence, the reported stable isotope ratios of these animals referred to the signatures of both assimilated and ingested matter.

In order to obtain enough BMA, the benthic microalgae and silica sand from the three screen replicates were rinsed by distilled water into one beaker, then swirled, and the suspended (non-sand) materials were filtered onto a pre-combusted Whatman GF/F glass fiber filter paper (0.7 μm porosity). For collection of POM, water samples obtained from each site were rinsed through a 63 μm screen to remove larger zooplankton before filtration on pre-combusted Whatman GF/F glass fiber filters (0.7 μm porosity). Sediment samples for SOM analysis were processed following the method of Riera et al. (1996). Each sediment sample was homogenized, freeze-dried and ground using a mortar and pestle. BMA, POM and SOM samples were acidified with 1.2 N HCl to remove inorganic carbon. To prevent any loss of dissolved organics, samples were not rinsed, but were dried overnight at 60°C under a fume extractor to evaporate the acid.

Stable Isotope Analysis

^{13}C and ^{15}N isotopic ratios of food source and consumer samples were determined using a PDZ Europa ANCA-GSL elemental analyzer interfaced to a PDZ Europa 20-20 isotope ratio mass spectrometer (Sercon Ltd., Cheshire, UK) in the Stable Isotope Facility, University of California, Davies, USA. Results of isotopic ratios were expressed in standard δ-unit notation, which is defined as follows:

$$\delta X = \left[\left(R_{sample}/R_{reference}\right) - 1\right] \times 1000‰$$

where X is ^{13}C or ^{15}N, and R is either the ^{13}C:^{12}C ratio for carbon or the ^{15}N:^{14}N ratio for nitrogen. These values were reported relative to the Vienna-PeeDee Belemnite (V-PDB) standard for C and to air N_2 for N.

Data Analysis

The use of different food sources by the meio- and macrofauna at each of the two sites was investigated by measurements of the isotopic niche widths. A small sample-size corrected standard ellipse area (SEAc) was calculated by the values of $\delta^{13}C$ versus $\delta^{15}N$ of all taxa at the two sites (Jackson et al., 2011; Jackson et al., 2012). This metric represents a measure of the total amount of niche occupied in the isotopic space and can be used to investigate the distinct food sources and their utilization (Layman et al., 2007; Layman et al., 2012). It also allows calculating the overlapping area of the standard ellipses between the two study sites, which can be used as a measure of diet similarity between the consumers. In addition, the Laymen's metrics (Layman et al., 2007) can be estimated to describe these ellipses, as follows: (1) mean distance to centroid (CD), giving additional information about the isotopic niche amplitude and

spacing between taxa; and (2) standard deviation of nearest neighbour distance (SDNND), a measure of the evenness of taxa displaying in a bi-plot space. All the metrics proposed by Layman et al. (2007), SEAc and overlapping of standard ellipses were calculated using the SIAR package (Jackson et al., 2011; Jackson et al., 2012) in R 3.10 software (R Development Core Team, 2014).

RESULTS

Stable Isotope of Food Sources and Benthic Fauna

From the stable isotope food web bi-plot (**Figure 2A**), the $\delta^{13}C$ and $\delta^{15}N$ values of primary producers at the two sites were close to each other. At the relatively unpolluted TLC, the stable isotope

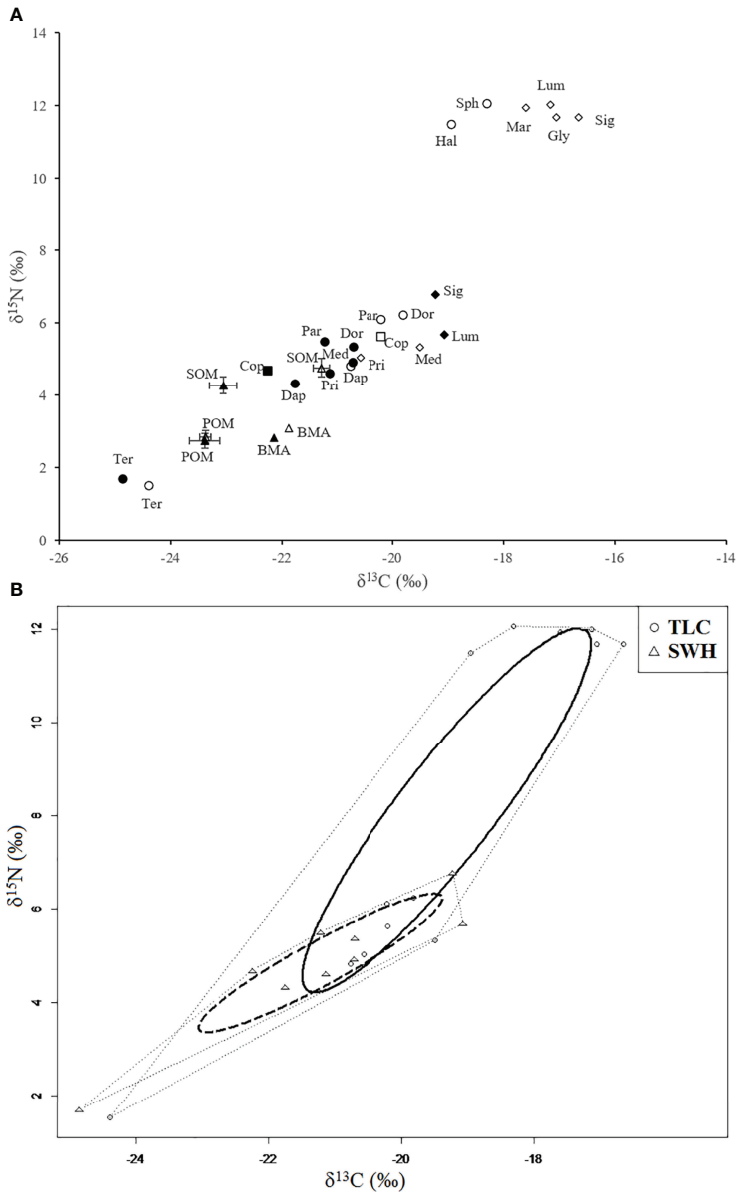

FIGURE 2 | Stable isotope food web bi-plot for **(A)** all consumers and potential food sources at TLC (open symbols) and SWH (solid symbols). Each symbol represents the $\delta^{13}C$ and $\delta^{15}N$ values for nematodes (circles), copepods (squares), polychaetes (diamonds) and primary producers (triangles). Cop, Copepods; Dap, *Daptonema* sp.; Dor, *Dorylaimopsis* sp.; Gly, *Glycera* sp.; Hal, *Halichoanolaimus* sp.; Lum, *Lumbrineris* sp.; Mar, *Marphysa stragulum*; Med, *Mediomastus* sp.; Par, *Paradontophora* sp.; Pri, *Prionospio* sp.; Sig, *Sigambra hanaokai*; Sph, *Sphaerolaimus* sp.; Ter, *Terschellingia* sp.; **(B)** convex hull areas (thin dotted lines) and corrected standard ellipses areas (SEAc: bold lines) in the isotopic space for benthic communities sampled at the relatively unpolluted site TLC (circle) and organically enriched site SWH (triangle).

ratios of the food sources ranged from -23.4‰ (POM) to -21.3‰ (SOM) and from 2.9‰ (POM) to 4.8‰ (SOM) for $\delta^{13}C$ and $\delta^{15}N$, respectively. At the organically enriched SWH, the stable isotope ratios of the food sources ranged from -23.4‰ (POM) to -22.1‰ (BMA) and from 2.7‰ (POM) to 4.3‰ (SOM) for $\delta^{13}C$ and $\delta^{15}N$, respectively. The stable isotope values of SOM at SWH were lighter than that at TLC (**Table 1**).

Table 1 also shows the $\delta^{13}C$ and $\delta^{15}N$ values of the consumers inhabiting in the sediments at TLC and SWH, together with their feeding types according to literature information. The number of species found at TLC was higher than that of species occurring at SWH. For nematodes, there were 6 abundant species (2 carnivores and 4 herbivores) included in the present analysis, with all the 6 species found at TLC and 4 at SWH (4 herbivores). For polychaetes, there were also 6 abundant species (1 carnivore, 3 omnivores and 2 herbivores) at the study sites, with all the 6 species found at TLC and 4 at SWH (2 omnivores and 2 herbivores). At TLC, $\delta^{13}C$ ranged from -24.4‰ (nematode *Terschellingia* sp.) to -16.6‰ (polychaete *Sigambra hanaokai*) and $\delta^{15}N$ ranged from 1.5‰ (nematode *Terschellingia* sp.) to 12.1‰ (nematode *Sphaerolaimus* sp.). At SWH, $\delta^{13}C$ ranged from -24.9‰ (nematode *Terschellingia* sp.) to -19.1‰ (polychaete *Lumbrineris* sp.) and $\delta^{15}N$ ranged from 1.7‰ (nematode *Terschellingia* sp.) to 6.8‰ (polychaete *Sigambra hanaokai*). The $\delta^{15}N$ values of the consumers spanned 10.6‰ at TLC, while 5.1‰ at SWH. Most consumers in a given trophic level at the two sites had similar $\delta^{15}N$ values. However, the $\delta^{15}N$ values of omnivorous polychaetes *Lumbrineris* sp. and *Sigambra hanaokai* were about 5-7‰ lower at SWH compared to that at TLC. These two omnivorous polychaete species tended to become solely herbivorous at the organically enriched SWH, while they remained omnivorous with more prey in their diet and less primary producers at the relatively unpolluted TLC.

Community-Wide Dynamics of Benthic Communities

Layman's metrics for benthic fauna sampled at TLC showed larger values than that at SWH (**Table 2**). The CD value at TLC (3.8‰) was more than two times larger than that at SWH (1.5‰). In contrast, SEAc measure was more than three times larger at TLC than that at SWH (SEAc = 11.0‰ and 3.1‰, respectively; **Table 2**). However, the ellipses overlapping area was lower (15.0%) for benthic fauna present at TLC as compared to that at SWH (53.2%) (**Table 2**). Comparing the relatively unpolluted TLC to the organically enriched SWH sites, there was a shift of the ellipse towards food sources with lower $\delta^{13}C$ values and a shift towards low trophic levels at SWH (**Figure 2B**).

DISCUSSION

Food Sources for Benthic Consumers

Previous studies of benthic communities in subtidal sediment have emphasized the importance of the phytoplankton pathway as an energy source for the benthic food web (Thimdee et al., 2004; Jeffreys et al., 2013; Careddu et al., 2015). In the present study, POM was collected as an indication of phytoplankton content and detritus material. The composition of SOM is usually highly heterogeneous, which includes both *in situ* primary producers, i.e., microphytobenthos, microorganisms, sedimentation of phytoplankton, nutrients from human

TABLE 1 | Stable isotope composition of food sources and consumers in subtidal sediments at the relatively unpolluted site TLC and organically enriched site SWH in subtropical Hong Kong.

	TLC		SWH		Feeding type
	$\delta^{13}C$ (‰)	$\delta^{15}N$ (‰)	$\delta^{13}C$ (‰)	$\delta^{15}N$ (‰)	
Food Sources					
BMA	-21.9	3.1	-22.1	2.8	NA
POM	-23.4 ± 0.1(3)	2.9 ± 0.2(3)	-23.4 ± 0.3(3)	2.7 ± 0.2(3)	NA
SOM	-21.3 ± 0.1(3)	4.8 ± 0.3(3)	-23.1 ± 0.2(3)	4.3 ± 0.2(3)	NA
Consumers					
(1) Nematodes					
Paradontophora sp.	-20.2	6.1	-21.2	5.5	Herbivore/Epigrowth feeder (grazer)[1]
Halichoanolaimus sp.	-18.9	11.5	–	–	Carnivore[1]
Dorylaimopsis sp.	-19.8	6.2	-20.7	5.4	Herbivore/Epigrowth feeder (grazer)[1]
Daptonema sp.	-20.8	4.8	-21.8	4.3	Herbivore/Non-selective deposit feeder[1]
Terschellingia sp.	-24.4	1.5	-24.9	1.7	Herbivore/Non-selective deposit feeder[1]
Sphaerolaimus sp.	-18.3	12.1	–	–	Carnivore[1]
(2) Copepods	-20.2	5.6	-22.3	4.7	Herbivore/omnivore[2]
(3) Polychaetes					
Lumbrineris sp.	-17.1	12.0	-19.1	5.7	Omnivore[3]
Marphysa stragulum	-17.6	11.9	–	–	Omnivore[3]
Glycera sp.	-17.1	11.7	–	–	Carnivore[3]
Sigambra hanaokai	-16.6	11.7	-19.2	6.8	Omnivore[3]
Mediomastus sp.	-19.5	5.3	-20.7	4.9	Subsurface deposit feeder[3]
Prionospio sp.	-20.6	5.0	-21.1	4.6	Surface deposit feeder[3]

[1]*Wieser (1953);* [2]*De Troch (2006b);* [3]*Fauchald and Jumars (1979), Jumars et al. (2015).*

The number of replicates is shown in brackets only for samples contained more than 1 replicate (NA = not applicable; - = not collected).

TABLE 2 | Summary of niche community metrics of benthic communities sampled at the relatively unpolluted site TLC and organically enriched site SWH in subtidal sediments of subtropical Hong Kong.

Metrics	TLC	SWH
CD (‰)	3.8	1.5
SDNND (‰)	1.2	1.1
SEAc (‰)	11.0	3.1
Overlapping SEAc (‰)	1.7	
Total overlapping[a] (%)	15.0	53.2

[a]*Total overlapping (%) = [overlapping SEAc (‰)/SEAc (‰)] ×100%.*

CD, mean distance to centroid; SDNND, standard deviation of nearest neighbour distance; SEAc, standard ellipse area corrected.

activities, and detritus from other origins. Increases in nutrient loading in coastal waters from anthropogenic activities can influence the quality and quantity of the primary producers (e.g. phytoplankton), and together with less prey availability due to hypoxic condition resulting from organic enrichment can further affect consumer population structure and diets (Tewfik et al., 2005; Fox et al., 2009; van der Lee et al., 2021).

Taking an average trophic level increase in $\delta^{15}N$ of about 3‰ (Post, 2002), the within-site range of $\delta^{15}N$ of consumers (7.3‰ at TLC and 2.5‰ at SWH, excluding the nematode *Terschellingia* sp.) spanned two trophic steps at the relatively unpolluted site TLC and one step at the organically enriched site SWH. Although feeding behaviour of species from the same trophic level may be different, most consumers in a given trophic level at these two sites had similar $\delta^{15}N$ values.

In the present study, organisms that are regarded as herbivores from literature had relatively lower $\delta^{15}N$ values than that of omnivores and carnivores. The nematode *Daptonema* sp. is a non-selective deposit feeder (Wieser, 1953), ingesting suitably-sized food particulates like microalgae (Moens et al., 2014; Xu et al., 2018). The stable isotope values of *Daptonema* sp. obtained from the present study also reflected BMA as its main diet. The nematode *Dorylaimopsis* and *Paradontophora* spp. are considered as epigrowth feeders or grazers based on their buccal morphology (Wieser, 1953). This was also confirmed from the isotopic values of these nematodes in this study, with BMA and other detritus in sediment as their major diet. In a microcosm experiment, Moens et al. (2014) found that epigrowth feeders can either ingest whole diatoms or use their teeth to puncture and suck out the cell contents. With similar isotope values, the harpacticoid copepods collected in the present study also mainly feed on BMA. Our results thus coincided with data from other studies that BMA was an important food source to many harpacticoid copepods (De Troch et al., 2006a; Cnudde et al., 2015) and epigrowth feeding nematodes (Moens and Vincx, 1997). The polychaete *Prionospio* sp. is considered a typical surface deposit feeder based on the study of its biology (Jumars et al., 2015), and its feeding mode was confirmed from the stable isotope values in the present study. The polychaete *Mediomastus* sp. is a small to medium-sized worm living in permanent sandy tubes in fine sand and mud, where it exploits subsurface diatoms and detritus as food sources (Hansen, 1993). Its stable isotope values obtained in the present study also revealed that BMA and other detritus in sediments are the major food sources.

The strongly depleted $\delta^{13}C$ value of the nematode *Terschellingia* sp. suggested a different trophic pathway involving utilization of a carbon source that might not be included in the present study. Several chemoautotrophic processes could yield depleted $\delta^{13}C$ values, such as sulphide-oxidizing bacteria, with $\delta^{13}C$ values below -30‰ (Robinson and Cavanaugh, 1995). Therefore, our data could imply that *Terschellingia* sp. relies on such bacteria as a food source for its diets, as reported from a mangrove ecosystem in India (Bouillon et al., 2002), an estuarine intertidal flat in the Netherlands (Moens et al., 2011), and an estuarine *Zostera noltii* seagrass bed in Portugal (Vafeiadou et al., 2014).

Predators are usually more sensitive to stress due to increased metabolic demand, longer lifespan and late maturity (Mor et al., 2022). All the six carnivorous/omnivorous species (2 carnivorous nematodes, 1 carnivorous polychaete and 3 omnivorous polychaetes) involved in the present study were found at the relatively unpolluted site TLC, while only two omnivorous polychaetes were present at the organically enriched site SWH. At TLC, the $\delta^{15}N$ values of omnivores overlapped with that of carnivores, whereas at SWH, the $\delta^{15}N$ values of omnivores were considerably similar to that of herbivores. The nematodes *Sphaerolaimus* and *Halichoanolaimus* spp. were only found at TLC. Their higher $\delta^{15}N$ values indicated a carnivorous role, which is in agreement with the trophic guild classification based on buccal morphology (Wieser, 1953; Moens and Vincx, 1997) and field observations (Chitwood and Timm, 1954). The nematode *Sphaerolaimus* sp. has also been reported having a predacious feeding mode from a stable isotope study from the Scheldt estuary, the Netherlands (Moens et al., 2005), a mudflat in Marennes-Oléron Bay, French Atlantic coast (Rzeznik-Orignac et al., 2008), and *Zostera noltii* seagrass beds and adjacent bare sediments in Mira estuary, Portugal (Vafeiadou et al., 2014). The polychaetes *Marphysa stragulum*, *Sigambra hanaokai* and *Lumbrineris* sp. are considered to be omnivores, whereas *Glycera* sp. is a carnivore (Fauchald and Jumars, 1979; Jumars et al., 2015). At TLC, the $\delta^{15}N$ values of these omnivorous polychaetes were similar to those of carnivorous polychaete and nematodes, suggesting that they tend to rely on other animals as their main food source. In contrast, the polychaetes *Sigambra hanaokai* and *Lumbrineris* sp. at SWH had depleted $\delta^{15}N$ values as compared to that collected at TLC, implying that they may assume mainly a herbivore role. Fox et al. (2009) observed organisms that have been reported to feed omnivorously shifted their diets from mainly a carnivorous diet in an oligotrophic estuary to mainly a herbivorous diet in an eutrophic estuary, where prey were limited and macroalgae were abundant. It thus suggested that under organically enriched condition in which the availability of prey is limited, some omnivores can alter their feeding mode to become herbivores by taking advantage of the increase in primary production so as to survive in such stressed environment (Zheng et al., 2020). A similar case was also noted from the present study.

Community-Wide Dynamics of Benthic Food Web

Larger CD and SDNND values were found in the benthic community sampled at the relatively unpolluted site TLC than those at the organically enriched site SWH, indicating a more complex functional community at TLC than that at SWH. This could be directly related to the presence of more trophic levels from herbivores to carnivores at TLC, as reflected in their wider isotopic niche. The largely narrower isotopic niche as revealed in the benthic community at SWH could be related to the high organic enrichment in the sediment, which is characterized by the presence of smaller organisms, usually deposit feeders (Mucha and Costa, 1999; Aberson et al., 2016). Larger SEAc measure was also found in the benthic community at TLC, further suggesting a more complex functional community there. Furthermore, the overlapping area of the ellipses of niche areas at TLC and SWH indicated the niches of benthic communities at the two sites can be different, owing to the different functional structures in their benthic community.

Apart from causing hypoxia with subsequent decrease in prey availability (Riedel et al., 2014) and predator foraging activity (Sagasti et al., 2001; Stover et al., 2013), nutrient enrichment can also lead to changes in the abundance and nutritional quality of primary producers, providing another explanation for the shifts in trophic position of some benthic omnivores (van der Lee et al., 2021). The evidence of a higher reliance on POM as the major food source at SWH can be indicated from difference in the position of the ellipse areas depicted from TLC and SWH (**Figure 2B**). Such change in food source reliance may also be reflected from the different $\delta^{13}C$ values of SOM from the two sites, probably due to a higher contribution of phytoplankton-derived detritus to the overall resource pool at the organically enriched SWH. These dietary differences may be linked to the increase in phytoplankton production which is frequently occurred in eutrophic coastal waters, especially in harbour centre where water movement is restricted by embayments and breakwaters (Nixon and Buckley, 2002). It is noted that there has been an increase in algal biomass within Victoria Harbour in recent years, likely owing to the nutrients brought by the nearby Pearl River estuary from west of the harbour (**Figure 1**) and increased water transparency as a result of improvement in water quality (Xu et al., 2010). In contrast, chlorophyll *a* biomass is low in relatively open eastern waters at TLC which are dominated by nutrient-poor oceanic seawater off the coast (Ho et al., 2008). The bulk of the increased primary production may not be directly utilized as living phytoplankton, but may enter the benthic food web as an allochthonous subsidy of POM falling from the water column, and finally settle on the sediment and support the benthic community there (Bouillon et al., 2002; Tewfik et al., 2005). Moreover, the tidal-induced vertical mixing can breakdown the stratification in the water column and transport phytoplankton below the photic zone, as indicated by the fairly high chlorophyll *a* concentration at the bottom water of Victoria Harbour in summer (Yin and Harrison, 2007; Xu et al., 2010). Such process could increase the sinking rate of microalgae from the water column to the sediment. In addition, the dietary shift of benthic omnivores is likely to be related to the increased nutritional quality of primary producers in more eutrophic waters caused by urban expansion, which allows for an enhanced consumption of plant material (van der Lee et al., 2021). With the shift of the feeding preference of omnivores in organically enriched sediment, the energy flow through the trophic web thus changed by transferring energy from primary production directly to omnivores instead of the functional and trophic roles of herbivores under unpolluted conditions (Fox et al., 2009). Our present findings revealed that the ability of some benthic invertebrate omnivores to change their trophic position in response to organic enrichment, which results in the limited availability of prey and variation in the abundance and nutritional quality of primary producers, may have important implications for our understanding of changes to the structure and function of benthic communities under such pollution stress. Additionally, the traditional feeding type classification based on buccal morphology should be combined with empirical information such as stable isotope signatures in order to decipher the food web structure in areas suffering from prolonged organic enrichment.

DATA AVAILABILITY STATEMENT

The original contributions presented in the study are included in the article/supplementary material. Further inquiries can be directed to the corresponding author.

AUTHOR CONTRIBUTIONS

PS designed the experiment and revised the manuscript. WX conducted the experiment and wrote the manuscript. JS gave constructive comments and revised the manuscript. All the authors approved the final manuscript.

FUNDING

This work was supported by the Natural Science Foundation of China (No. 41706184), the Natural Science Foundation of Tianjin (18JCQNJC79000), and the General Research Fund (No. CityU 161009) from the Research Grants Council of the HKSAR Government.

ACKNOWLEDGMENTS

Thanks for Ankang Teng for his technical assistance in the field and laboratory.

REFERENCES

Aberson, M. J. R., Bolam, S. G., and Hughes, R. G. (2016). The Effect of Sewage Pollution on the Feeding Behaviour and Diet of *Hediste* (*Nereis Diversicolor* (O.F. Müller 1776)) in Three Estuaries in South-East England, With Implications for Saltmarsh Erosion. *Mar. Pollut. Bull.* 105 (1), 150–160. doi: 10.1016/j.marpolbul.2016.02.033

Altieri, A. H., and Diaz, R. J. (2019). "Chapter 24 Dead Zones: Oxygen Depletion in Coastal Ecosystems," in *World Seas: An Environmental Evaluation*, *2nd ed*. Ed. C. Sheppard (Massachusetts, MA: Academic Press), 453–473. doi: 10.1016/B978-0-12-805052-1.00021-8

Armitage, A. R., and Fourqurean, J. W. (2009). Stable Isotopes Reveal Complex Changes in Trophic Relationships Following Nutrient Addition in a Coastal Marine Ecosystem. *Estuar. Coast.* 32 (6), 1152–1164. doi: 10.1007/s12237-009-9219-z

Bouillon, S., Koedam, N., Raman, A., and Dehairs, F. (2002). Primary Producers Sustaining Macro-Invertebrate Communities in Intertidal Mangrove Forests. *Oecologia* 130 (3), 441–448. doi: 10.1007/s004420100814

Braeckman, U., Provoost, P., Sabbe, K., Soetaert, K., Middelburg, J. J., Vincx, M., et al. (2015). Temporal Dynamics in a Shallow Coastal Benthic Food Web: Insights From Fatty Acid Biomarkers and Their Stable Isotopes. *Mar. Environ. Res.* 108, 55–68. doi: 10.1016/j.marenvres.2015.04.010

Brauko, K. M., Cerveira, A. F., Freitas, R. F., Hadlich, H. L., Beras, T., Fonseca, A. L., et al. (2020). Comparing Structural and Functional Approaches to Distinguish Benthic Communities From Nutrient and non-Eutrophic Estuaries. *Mar. Pollut. Bull.* 157, 111290. doi: 10.1016/j.marpolbul.2020.111290

Briggs, K. B., Craig, J. K., Shivarudrappa, S., and Richards, T. M. (2017). Macrobenthos and Megabenthos Responses to Long-Term, Large-Scale Hypoxia on the Louisiana Continental Shelf. *Mar. Environ. Res.* 123, 38–52. doi: 10.1016/j.marenvres.2016.11.008

Careddu, G., Costantini, M. L., Calizza, E., Carlino, P., Bentivoglio, F., Orlandi, L., et al. (2015). Effects of Terrestrial Input on Macrobenthic Food Webs of Coastal Sea are Detected by Stable Isotope Analysis in Gaeta Gulf. *Estuar. Coast. Shelf. Sci.* 154, 158–168. doi: 10.1016/j.ecss.2015.01.013

Caswell, B. A., Paine, M., and Frid, C. L. J. (2018). Seafloor Ecological Functioning Over Two Decades of Organic Enrichment. *Mar. Pollut. Bull.* 136, 212–229. doi: 10.1016/j.marpolbul.2018.08.041

Chitwood, B., and Timm, R. (1954). "Free-Living Nematodes of the Gulf of Mexico," in *Gulf of Mexico Its Origins, Waters and Marine Life. Fishery Bulletin of the Fish and Wildlife Service*, vol. 55 . Ed. P. S. Galtsoff (USA: United States Government Printing Office), 313–323.

Cnudde, C., Moens, T., Werbrouck, E., Lepoint, G., Van Gansbeke, D., and De Troch, M. (2015). Trophodynamics of Estuarine Intertidal Harpacticoid Copepods Based on Stable Isotope Composition and Fatty Acid Profiles. *Mar. Ecol. Prog. Ser.* 524, 225–239. doi: 10.3354/meps11161

Culhane, F. E., Briers, R. A., Tett, P., and Fernandes, T. F. (2019). Response of a Marine Benthic Invertebrate Community and Biotic Indices to Organic Enrichment From Sewage Disposal. *J. Mar. Biol. Assoc. U. K.* 99, 1721–1734. doi: 10.1017/S0025315419000857

De Troch, M., Chepurnov, V., Gheerardyn, H., Vanreusel, A., and Ólafsson, E. (2006a). Is Diatom Size Selection by Harpacticoid Copepods Related to Grazer Body Size? *J. Exp. Mar. Biol. Ecol.* 332 (1), 1–11. doi: 10.1016/j.jembe.2005.10.017

De Troch, M., Houthoofd, L., Chepurnov, V., and Vanreusel, A. (2006b). Does Sediment Grain Size Affect Diatom Grazing by Harpacticoid Copepods? *Mar. Environ. Res.* 61, 265–277. doi: 10.1016/j.marenvres.2005.10.004

Doi, H., Matsumasa, M., Toya, T., Satoh, N., Mizota, C., Maki, Y., et al. (2005). Spatial Shifts in Food Sources for Macrozoobenthos in an Estuarine Ecosystem: Carbon and Nitrogen Stable Isotope Analyses. *Estuar. Coast. Shelf. Sci.* 64 (2), 316–322. doi: 10.1016/j.ecss.2005.02.028

Dorgham, M. M. (2014). "Effects of Eutrophication," in *Eutrophication: Causes, Consequences and Control*, vol. Vol. 2 . Eds. A. A. Ansari and S. S. Gill (Dordrecht: Springer), 29–44. doi: 10.1007/978-94-007-7814-6_3

Drylie, T. P., Lohrer, A. M., Needham, H. R., and Pilditch, C. A. (2020). Taxonomic and Functional Response of Estuarine Benthic Communities to Experimental Organic Enrichment: Consequences for Ecosystem Function. *J. Exp. Mar. Biol. Ecol.* 532, 151455. doi: 10.1016/jembe.2020.151455

Du, J. G., Makatipu, P. C., Tao, L. S. R., Pauly, D., Cheung, W. W. L., Peristiwady, T., et al. (2020). Comparing Trophic Levels Estimated From a Tropical Marine Food Web Using an Ecosystem Model and Stable Isotopes. *Estuar. Coast. Shelf. Sci.* 233, 106518. doi: 10.1016/j.ecss.2019.106518

Fauchald, K., and Jumars, P. A. (1979). The Diet of Worms: A Study of Polychaete Feeding Guilds. *Oceanogr. Mar. Biol. Annu. Rev.* 17, 193–284.

Fox, S. E., Teichberg, M., Olsen, Y. S., Heffner, L., and Valiela, I. (2009). Restructuring of Benthic Communities in Eutrophic Estuaries: Lower Abundance of Prey Leads to Trophic Shifts From Omnivory to Grazing. *Mar. Ecol. Prog. Ser.* 380, 43–57. doi: 10.3354/meps07917

Fry, B. (2006). *Stable Isotope Ecology* (New York, NY: Springer).

Grall, J., and Chauvaud, L. (2002). Marine Eutrophication and Benthos: The Need for New Approaches and Concepts. *Glob. Change Biol.* 8 (9), 813–830. doi: 10.1046/j.1365-2486.2002.00519.x

Guan, Y., Hohn, S., Wild, C., and Merico, A. (2020). Vulnerability of Global Coral Reef Habitat Suitability to Ocean Warming, Acidification and Eutrophication. *Glob. Change Biol.* 26 (10), 5646–5660. doi: 10.1111/gcb.15293

Hale, S. S., Cicchetti, G., and Deacutis, C. F. (2016). Eutrophication and Hypoxia Diminish Ecosystem Functions of Benthic Communities in a New England Estuary. *Front. Mar. Sci.* 3. doi: 10.3389/fmars.2016.00249

Hansen, B. (1993). Aspects of Feeding, Growth and Stage Development by Trochophora Larvae of the Boreal Polychaete *Mediomastus Fragile* (Rasmussen) (Capitellidae). *J. Exp. Mar. Biol. Ecol.* 166 (2), 273–288. doi: 10.1016/0022-0981(93)90224-C

Heip, C., Vincx, M., and Vranken, G. (1985). The Ecology of Marine Nematodes. *Oceanogr. Mar. Biol. Annu. Rev.* 23, 313–328.

Ho, A. Y. T., Xu, J., Yin, K., Yuan, X. C., He, L., Jiang, Y. L., et al. (2008). Seasonal and Spatial Dynamics of Nutrients and Phytoplankton Biomass in Victoria Harbour and its Vicinity Before and After Sewage Abatement. *Mar. Pollut. Bull.* 57 (6), 313–324. doi: 10.1016/j.marpolbul.2008.04.035

Jackson, M. C., Donohue, I., Jackson, A. L., Britton, J. R., Harper, D. M., and Grey, J. (2012). Population-Level Metrics of Trophic Structure Based on Stable Isotopes and Their Application to Invasion Ecology. *PLoS One* 7 (2), e31757. doi: 10.1371/journal.pone.0031757

Jackson, A. L., Inger, R., Parnell, A. C., and Bearhop, S. (2011). Comparing Isotopic Niche Widths Among and Within Communities: SIBER – Stable Isotope Bayesian Ellipses in R. *J. Anim. Ecol.* 80 (3), 595–602. doi: 10.1111/j.1365-2656.2011.01806.x

Jeffreys, R. M., Burke, C., Jamieson, A. J., Narayanaswamy, B. E., Ruhl, H. A., Smith, K. L.Jr., et al. (2013). Feeding Preferences of Abyssal Macrofauna Inferred From *in Situ* Pulse Chase Experiments. *PLoS One* 8 (11), e80510. doi: 10.1371/journal.pone.0080510

Johansen, P.-O., Isaksen, T. E., Bye-Ingebrigtsen, E., Haave, M., Dahlgren, T. G., Kvalø, S. E., et al. (2018). Temporal Changes in Benthic Macrofauna on the West Coast of Norway Resulting From Human Activities. *Mar. Pollut. Bull.* 128, 483–495. doi: 10.1016/j.marpolbul.2018.01.063

Jumars, P. A., Dorgan, K. M., and Lindsay, S. M. (2015). Diet of Worms Emended: An Update of Polychaete Feeding Guilds. *Annu. Rev. Mar. Sci.* 7 (1), 497–520. doi: 10.1146/annurev-marine-010814-020007

Layman, C. A., Araujo, M. S., Boucek, R., Hammerschlag-Peyer, C. M., Harrison, E., Jud, Z. R., et al. (2012). Applying Stable Isotopes to Examine Food-Web Structure: An Overview of Analytical Tools. *Biol. Rev.* 87, 545–562. doi: 10.1111/j.1469-185X.2011.00208.x

Layman, C. A., Arrington, D. A., Montaña, C. G., and Post, D. M. (2007). Can Stable Isotope Ratios Provide for Community-Wide Measures of Trophic Structure? *Ecology* 88 (1), 42–48. doi: 10.1890/0012-9658(2007)88[42:csirpf]2.0.co;2

Lepoint, G., Dauby, P., and Gobert, S. (2004). Applications of C and N Stable Isotopes to Ecological and Environmental Studies in Seagrass Ecosystems. *Mar. Pollut. Bull.* 49 (11), 887–891. doi: 10.1016/j.marpolbul.2004.07.005

Liu, X. S., Xu, W. Z., Cheung, S. G., and Shin, P. K. (2011). Marine Meiobenthic and Nematode Community Structure in Victoria Harbour, Hong Kong Upon Recovery From Sewage Pollution. *Mar. Pollut. Bull.* 63 (5-12), 318–325. doi: 10.1016/j.marpolbul.2011.03.027

Mitwally, H. M., and Fleeger, J. W. (2015). Long-Term Nutrient Enrichment Alters Nematode Trophic Structure and Body Size in a *Spartina Alterniflora* Salt Marsh. *Mar. Ecol.* 36 (4), 910–925. doi: 10.1111/maec.12181

Moens, T., Bouillon, S., and Gallucci, F. (2005). Dual Stable Isotope Abundances Unravel Trophic Position of Estuarine Nematodes. *J. Mar. Biol. Assoc. U. K.* 85 (6), 1401–1407. doi: 10.1017/S0025315405012580

Moens, T., Luyten, C., Middelburg, J. J., Herman, P. M. J., and Vincx, M. (2002). Tracing Organic Matter Sources of Estuarine Tidal Flat Nematodes With Stable Carbon Isotopes. *Mar. Ecol. Prog. Ser.* 234, 127–137. doi: 10.3354/meps234127

Moens, T., Moodley, L., Steyaert, M., Van Colen, C., Van Oevelen, D., Boschker, H. T., et al. (2011). "The Structure and Functional Roles of Tidal Flat Meiobenthos," in *Aspects of Coastal Research in Contribution to LOICZ in the Netherlands and Flanders, (2002–2010). LOICZ Reports and Studies*, vol. 38 . Eds. C. Heip and R. Laane (Helmholtz-Zentrum Geesthacht, Germany: LOICZ International Project Office), 171–184.

Moens, T., Vafeiadou, A.-M., De Geyter, E., Vanormelingen, P., Sabbe, K., and De Troch, M. (2014). Diatom Feeding Across Trophic Guilds in Tidal Flat Nematodes, and the Importance of Diatom Cell Size. *J. Sea. Res.* 92, 125–133. doi: 10.1016/j.seares.2013.08.007

Moens, T., and Vincx, M. (1997). Observations on the Feeding Ecology of Estuarine Nematodes. *J. Mar. Biol. Assoc. U. K.* 77 (1), 211–227. doi: 10.1017/S0025315400033889

Mor, J. R., Muñoz, I., Sabater, S., Zamora, L., and Ruhi, A. (2022). Energy Limitation or Sensitive Predators? Trophic and non-Trophic Impacts of Wastewater Pollution on Stream Food Webs. *Ecology* 103 (2), e03587. doi: 10.1002/ecy.3587

Mucha, A. P., and Costa, M. H. (1999). Macrobenthic Community Structure in Two Portuguese Estuaries: Relationship With Organic Enrichment and Nutrient Gradients. *Acta Oecol.* 20 (4), 363–376. doi: 10.1016/S1146-609X(99)00130-7

Nicholson, S., Hui, Y. H., and Lam, P. K. S. (2011). Pollution in the Coastal Waters of Hong Kong: Case Studies of the Urban Victoria and Tolo Harbours. *Water Environ. J.* 25 (3), 387–399. doi: 10.1111/j.1747-6593.2010.00234.x

Nixon, S. W., and Buckley, B. A. (2002). "A Strikingly Rich Zone" - Nutrient Enrichment and Secondary Production in Coastal Marine Ecosystems. *Estuaries* 25 (4), 782–796. doi: 10.1007/BF02804905

Nordström, M. C., and Bonsdorff, E. (2017). Organic Enrichment Simplies Marine Benthic Food Web. *Limnol. Oceanogr.* 62 (5), 2179–2188. doi: 10.1002/lno.10558

Post, D. M. (2002). Using Stable Isotopes to Estimate Trophic Position: Models, Methods, and Assumptions. *Ecology* 83, 703–718. doi: 10.1890/0012-9658(2002)083[0703:usitet]2.0.co;2

R Development Core Team (2014). *R: A Language and Environment for Statistical Computing* (Vienna, Austria: R Foundation for Statistical Computing). Available at: http://www.R-project.org/.

Riedel, B., Pados, T., Pretterebner, K., Schiemer, L., Steckbauer, A., Haselmair, A., et al. (2014). Effect of Hypoxia and Anoxia on Invertebrate Behaviour: Ecological Perspectives From Species to Community Level. *Biogeosciences* 11 (6), 1491–1518. doi: 10.5194/bg-11-1491-2014

Riera, P., Richard, P., Grémare, A., and Blanchard, G. (1996). Food Source of Intertidal Nematodes in the Bay of Marennes-Oleron (France), as Determined by Dual Stable Isotope Analysis. *Mar. Ecol. Prog. Ser.* 142, 303–309. doi: 10.3354/meps142303

Robinson, J. J., and Cavanaugh, C. M. (1995). Expression of Form I and Form II Rubisco in Chemoautotrophic Symbioses: Implications for the Interpretation of Stable Carbon Isotope Values. *Limnol. Oceanogr.* 40 (8), 1496–1502. doi: 10.4319/lo.1995.40.8.1496

Rzeznik Orignac, J., Boucher, G., Fichet, D., and Richard, P. (2008). Stable Isotope Analysis Position of Intertidal of Food Source and Trophic Nematodes and Copepods. *Mar. Ecol. Prog. Ser.* 359, 145–150. doi: 10.3354/meps07328

Sagasti, A., Schaffner, L. C., and Duffy, J. E. (2001). Effects of Periodic Hypoxia on Mortality, Feeding and Predation in an Estuarine Epifaunal Community. *J. Exp. Mar. Biol. Ecol.* 258 (2), 257–283. doi: 10.1016/S0022-0981(01)00220-9

Souza, F. M., Brauko, K. M., Lana, P. C., Muniz, P., and Camargo, M. G. (2013). The Effect of Urban Sewage on Benthic Macrofauna: A Multiple Spatial Scale Approach. *Mar. Pollut. Bull.* 67 (1-2), 234–240. doi: 10.1016/j.marpolbul.2012.10.021

Stover, K. K., Burnett, K. G., McElroy, E. J., and Burnett, L. E. (2013). Locomotory Fatigue During Moderate and Severe Hypoxia and Hypercapnia in the Atlantic Blue Crab, *Callinectes Sapidus*. *Biol. Bull.* 224 (2), 68–78. doi: 10.1086/BBLv224n2p68

Tewfik, A., Rasmussen, J., and McCann, K. S. (2005). Anthropogenic Enrichment Alters a Marine Benthic Food Web. *Ecology* 86 (10), 2726–2736. doi: 10.1890/04-1537

Thimdee, W., Deein, G., Sangrungruang, C., and Matsunaga, K. (2004). Analysis of Primary Food Sources and Trophic Relationships of Aquatic Animals in a Mangrove-Fringed Estuary, Khung Krabaen Bay (Thailand) Using Dual Stable Isotope Techniques. *Wetl. Ecol. Manage.* 12 (2), 135–144. doi: 10.1023/b:wetl.0000021674.76171.69

Vafeiadou, A. M., Materatski, P., Adão, H., De Troch, M., and Moens, T. (2014). Resource Utilization and Trophic Position of Nematodes and Harpacticoid Copepods in and Adjacent to *Zostera Noltii* Beds. *Biogeosciences* 11 (14), 4001–4014. doi: 10.5194/bg-11-4001-2014

van der Lee, G. H., Vonk, J. A., Verdonschot, R. C., Kraak, M. H., Verdonschot, P. F., and Huisman, J. (2021). Eutrophication Induces Shifts in the Trophic Position of Invertebrates in Aquatic Food Webs. *Ecology* 102 (3), e03275. doi: 10.1002/ecy.3275

Wainright, S. C., Weinstein, M. P., Able, K. W., and Currin, C. A. (2000). Relative Importance of Benthic Microalgae, Phytoplankton and the Detritus of Smooth Cordgrass *Spartina Alterniflora* and the Common Reed *Phragmites Australis* to Brackish-Marsh Food Webs. *Mar. Ecol. Prog. Ser.* 200, 77–91. doi: 10.3354/meps200077

Wieser, W. (1953). Die Beziehungen Zwischen Mundhohlengestalt, Ernahrungsweise Und Vorkommen Beifreilebenden Marinen Nematoden. *Ark. Zool.* 4, 439–484.

Xu, W. Z., Cheung, S. G., and Shin, P. K. S. (2014). Structure and Taxonomic Composition of Free-Living Nematode and Macrofaunal Assemblages in a Eutrophic Subtropical Harbour, Hong Kong. *Mar. pollut. Bull.* 85 (2), 764–773. doi: 10.1016/j.marpolbul.2014.01.023

Xu, W. Z., Cheung, S. G., Zhang, Z. N., and Shin, P. K. (2018). Dual Isotope Assessment of Trophic Dynamics of an Intertidal Infaunal Community With Seasonal Shifts in Food Sources. *Mar. Biol.* 165 (1), 1–13. doi: 10.1007/s00227-017-3278-7

Xu, J., Lee, J. H., Yin, K., Liu, H., and Harrison, P. J. (2011). Environmental Response to Sewage Treatment Strategies: Hong Kong's Experience in Long Term Water Quality Monitoring. *Mar. Pollut. Bull.* 62 (11), 2275–2287. doi: 10.1016/j.marpolbul.2011.07.020

Xu, J., Yin, K., Liu, H., Lee, J. H. W., Anderson, D. M., Ho, A. Y. T., et al. (2010). A Comparison of Eutrophication Impacts in Two Harbours in Hong Kong With Different Hydrodynamics. *J. Mar. Syst.* 83 (3), 276–286. doi: 10.1016/j.jmarsys.2010.04.002

Yin, K., and Harrison, P. J. (2007). Influence of the Pearl River Estuary and Vertical Mixing in Victoria Harbor on Water Quality in Relation to Eutrophication Impacts in Hong Kong Waters. *Mar. Pollut. Bull.* 54 (6), 646–656. doi: 10.1016/j.marpolbul.2007.03.001

Zheng, X., Como, S., Huang, L., and Magni, P. (2020). Temporal Changes of a Food Web Structure Driven by Different Primary Producers in a Subtropical Eutrophic Lagoon. *Mar. Environ. Res.* 161, 105128. doi: 10.1016/j.marenvres.2020.105128

Conflict of Interest: The authors declare that the research was conducted in the absence of any commercial or financial relationships that could be construed as a potential conflict of interest.

Publisher's Note: All claims expressed in this article are solely those of the authors and do not necessarily represent those of their affiliated organizations, or those of the publisher, the editors and the reviewers. Any product that may be evaluated in this article, or claim that may be made by its manufacturer, is not guaranteed or endorsed by the publisher.

Copyright © 2022 Xu, Shin and Sun. This is an open-access article distributed under the terms of the Creative Commons Attribution License (CC BY). The use, distribution or reproduction in other forums is permitted, provided the original author(s) and the copyright owner(s) are credited and that the original publication in this journal is cited, in accordance with accepted academic practice. No use, distribution or reproduction is permitted which does not comply with these terms.

frontiers | Frontiers in Marine Science

ORIGINAL RESEARCH
published: 27 June 2022
doi: 10.3389/fmars.2022.925567

Impacts of Human Activities and Environmental Changes on Spatial-Seasonal Variations of Metals in Surface Sediments of Zhanjiang Bay, China

Fengxia Zhou[1,2,3], *Mengqi Xiong*[1,2,3], *Shuangling Wang*[1,2,3], *Sheng Tian*[1,2,3], *Guangzhe Jin*[1,2,3]*, *Fajin Chen*[1,2,3], *Chunqing Chen*[1,2,3], *Xuan Lu*[1,2,3], *Qingmei Zhu*[1,2,3] *and Yafei Meng*[1,2,3]

[1] College of Ocean and Meteorology, Guangdong Ocean University, Zhanjiang, China, [2] Key Laboratory for Coastal Ocean Variation and Disaster Prediction, Guangdong Ocean University, Zhanjiang, China, [3] Key Laboratory of Climate, Resources and Environment in Continental Shelf Sea and Deep Sea of Department of Education of Guangdong Province, Guangdong Ocean University, Zhanjiang, China

OPEN ACCESS

Edited by:
Meilin Wu,
South China Sea Institute of Oceanology (CAS), China

Reviewed by:
Arindam Sarkar,
Bidhan Chandra Krishi Viswavidyalaya, India
Antonio Cobelo-Garcia,
Spanish National Research Council (CSIC), Spain
Md. Solaiman Hossain,
Shahjalal University of Science and Technology, Bangladesh
Anandkumar Arumugam,
Bar-Ilan University, Israel

***Correspondence:**
Guangzhe Jin
jinguangzhe@live.cn

Specialty section:
This article was submitted to Marine Pollution, a section of the journal Frontiers in Marine Science

Received: 21 April 2022
Accepted: 26 May 2022
Published: 27 June 2022

Citation:
Zhou F, Xiong M, Wang S, Tian S, Jin G, Chen F, Chen C, Lu X, Zhu Q and Meng Y (2022) Impacts of Human Activities and Environmental Changes on Spatial-Seasonal Variations of Metals in Surface Sediments of Zhanjiang Bay, China. Front. Mar. Sci. 9:925567. doi: 10.3389/fmars.2022.925567

This study investigated the total concentrations and geochemical compositions of metals (Cd, Cr, Cu, Ni, Pb, Zn, Fe and Mn) in surface sediments of Zhanjiang Bay (ZJB) in spring and summer, to assess the contamination status, mobility and influencing factors of spatial-seasonal changes of these metals. The average total concentration for each studied metal in the surface sediments of ZJB was 0.173 μg/g for Cd, 58.25 μg/g for Cr, 17.11 μg/g for Cu, 16.89 μg/g for Ni, 28.70 μg/g for Pb, 67.91 μg/g for Zn, 30.18 mg/g for Fe, and 275.5 μg/g for Mn during the investigation period. Generally higher total concentrations of metals were found in the channel and coastal sediments of ZJB compared with those in the central ZJB, which may be probably resulted by the input of Suixi river, domestic sewage and industrial wastewater. The grain size compositions and TOC contents also had influences on the distributions of metals in ZJB. In the channel, total metals and reducible and bioavailable fractions of metals generally showed decreased concentrations in summer compared with those in spring, suggesting the release of metals from sediments. Organic matter degradation and Fe and Mn (hydr) oxides reduction processes may contribute much to this phenomenon. Relatively high proportions of Cd and Zn (average of 21.7% and 14.6%, respectively) were associated with the acid soluble fraction, indicating their high risk to the environment. The combined assessment results of enrichment factor, contaminated factor and the percentages of acid soluble fraction indicated that Cd and Zn in the surface sediments of ZJB were generally contaminated and they had medium to high risk to the environment. The average values of pollution load index in the channel, coastal and central ZJB were 1.28, 0.93 and 0.81, respectively, indicating the deterioration of surface sediments in the channel of ZJB. More attention should be paid on the metals in surface sediments of the channel of ZJB.

Keywords: metals, distribution, geochemical forms, environmental assessment, seasonal variations, influencing factors

1. INTRODUCTION

Metals are one of the major anthropogenic contaminants in coastal environments (Yu et al., 2008; Hossain et al., 2020). Some metals (e.g. Fe, Mn, Zn etc.) are essential for living organisms when they are in very low concentrations (Hossain et al., 2020). While some metals (e.g. Cd, Cu, Zn etc.) are very toxic when they are supplied above a certain concentration (Pais and Jones, 1997; USEPA, 2000). For example, Cu is an essential element which serves as a cofactor in a number of enzyme systems. However, high intake of Cu can cause adverse health effect problems for most living organisms (Mohanraj et al., 2021). Therefore, assessment of metals in marine environments is useful to determine contamination levels and provide information for determining health risks.

Metals in the coastal environment have natural and anthropogenic sources. With the rapid industrialization and economic development in coastal regions, metals are continuing to be introduced to coastal environment through river runoff and land-based point source discharge (Yu et al., 2008; Anandkumar et al., 2018; Hossain et al., 2020). Anthropogenic sources such as industrial sewage and domestic sewage have led to an increase of metal concentrations in the coastal environments (Gao et al., 2014; Freitas et al., 2019). A major fraction of metals entering into the aquatic systems are rapidly transported into sediments (Wang and Chen, 2000; Gu et al., 2016). Sediments are recognized as an important sink of heavy metals in coastal ecosystems (Pekey, 2006; Hossain et al., 2020).

In sediments, metals can exist in many chemical species and exhibit different behaviors (Akcay et al., 2003; Gao et al., 2010). Investigations on the geochemical forms of metals by sequential extraction give further information about the fundamental reactions that govern the behavior of metals in sediments (Tessier et al., 1979; Gao and Chen, 2012; Prabakaran et al., 2020; Shibini Mol and Sujatha, 2020; Chakraborty et al., 2021; Zhao et al., 2021). The study of metal speciation in sediments is essential for estimating the mobility and bioavailability of metals (Chakraborty et al., 2015; Chakraborty et al., 2017). The chemical forms that are weakly bounded to the sediment (such as acid soluble, reducible and oxidizable forms) are considered as the bioavailable forms (Peña-lcart et al., 2014; Freitas et al., 2019). Under certain conditions, the bioavailable forms of metals in sediments can be released from sediment. For, example, changes in the redox conditions of sediment can lead to the reductive dissolution of Fe and Mn (hydr)oxides in sediments and result in the release of associated metals from sediment to water (Charriau et al., 2011; Dang et al., 2015). The study of Duan et al. (2019) found that obvious seasonal variations of metals occurred at the surface sediments of Changjiang Estuary, which was related to the seasonal variation of temperature, dissolved oxygen (DO) and organic matter in the overlying waters. Many previous studies also indicated that, benthic diffusive fluxes of metals from sediments to water column are equivalent to or even exceed riverine influxes in many coastal areas (Rivera-Duarte and Flegal, 1997; Santos-Echeandia et al., 2009; Duan et al., 2019). Therefore, the release of metals from sediment can cause water quality and ecosystem degradation (Lee et al., 2017; Nagarajan et al., 2019; Li et al., 2020).

Coastal areas, especially the semi-enclosed bays, are particularly at risk from metal contamination since the strong influence of anthropogenic activities in these areas (Gao et al., 2014; Hossain et al., 2020). The Zhanjiang bay (ZJB), located at the northwestern South China Sea, is a typical semi-enclosed bay with a very narrow entrance (< 2 km). It is also an important aquaculture area in China. However, it has been increasingly contaminated by the industrial, agricultural and domestic wastes. Industries discharges hazardous contaminants like metals into ZJB, which may be consumed by planktons, shellfishes or fishes, and finally magnified and transferred to humans. Metal contamination is one of the key environmental problems for ZJB. Zhang et al. (2018) reported the total metal concentrations in the surface sediments of ZJB. A combined study that addresses the seasonal variations and mobility of metals in the sediments of ZJB is limited. In addition, the influences of anthropogenic activities and environmental changes on the spatial-seasonal variations of metals in sediments of ZJB are not completely understood.

The main objectives of this study were to assess the spatial and seasonal variations of metals (Cd, Cr, Cu, Ni, Pb, Zn, Fe and Mn) in surface sediments of ZJB, to assess the potential mobility/bioavailability of metals in different subregions of ZJB, to identify possible sources of metals in ZJB, and to evaluate the contamination status of metals in sediments of ZJB based on different evaluation methods. The results of this study will provide scientific basis for improving the environment of ZJB and protection of aquatic flora and fauna.

2. MATERIALS AND METHODS

2.1. Study Area

Zhanjiang Bay is influenced by seasonally reversing monsoon winds and has a dynamic environment. It has higher precipitation in summer than other seasons. The water temperature, DO concentration and chlorophyll a (Chl *a*) concentration of water in ZJB also vary seasonally (Zhou et al., 2020). The water of ZJB is mainly influenced by the freshwater from Suixi river and seawater from South China Sea (**Figure 1**). These environmental characteristics of ZJB may probably have significant influences on the spatial-seasonal variations of metals in the surface sediments of ZJB.

According to the environmental characteristics of ZJB, the study area can be divided into three subregions: channel, coastal bay and central bay (**Figure 1**). Suixi river has a strong influence on the channel. Besides, large amounts of domestic sewage from Zhanjiang city have been discharged to this area. There are many factories along the coast of ZJB, especially the south coast of ZJB (**Figure 1**). Baosteel Zhanjiang Iron Steel Co., Ltd. (Baosteel, an iron and steel company) and Zhongke (Guangdong) Refining and Chemical Co., Ltd (Zhongke, a refining and chemical company) are two of the large enterprises locating at the south coast of ZJB (**Figure 1**). Large amounts of industrial sewage have been

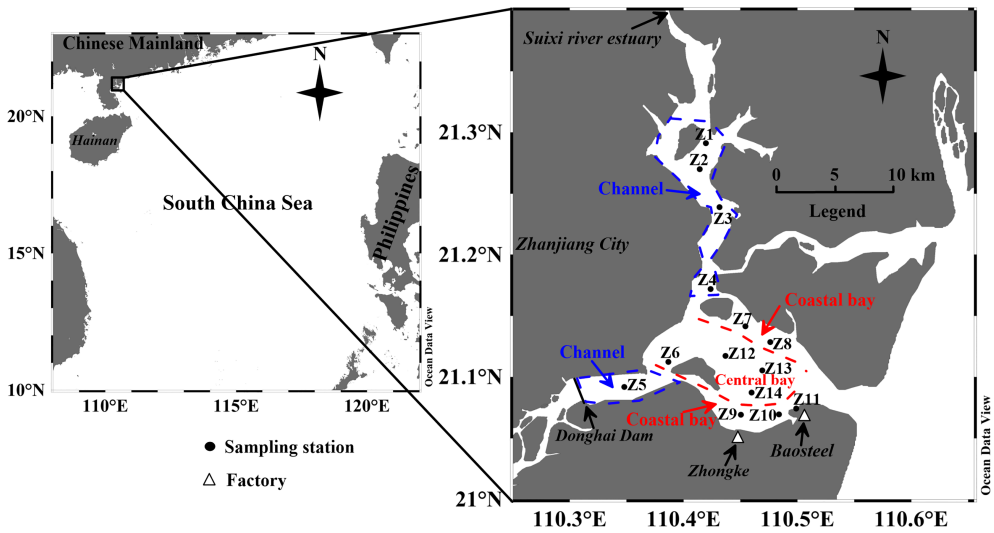

FIGURE 1 | Sampling stations in the Zhanjiang Bay. The Zhanjiang bay is divided into three subregions: channel, coastal bay and central bay. Zhongke: Zhongke (Guangdong) Refining and Chemical Co., Ltd. Baosteel: Baosteel Zhanjiang Iron Steel Co., Ltd.

discharged into the coastal area of ZJB. The central bay is relatively less influenced by river runoff and sewage input.

2.2. Sampling and Analysis

Bottom water and surface sediment samples were collected from ZJB during two cruises in April (spring) and August (summer) 2017. A total of fourteen stations were selected for investigation according to the environment of ZJB. The sampling stations Z1, Z2, Z3, Z4 and Z5 were located in the channel, stations Z7, Z8, Z9, Z10 and Z11 in the coastal bay, and stations Z6, Z12, Z13 and Z14 in the central bay. The temperature of bottom water was measured by a conductivity-temperature-depth meter *in situ*. Bottom water was collected by a plexiglass water sampler for the measurements of DO and Chl *a*. The depths of the collected bottom water samples ranged from 3 to 18 m. The bottom water samples for DO analysis were collected first. DO was determined by the Winkler method. Water samples for Chl *a* analysis were filtered by glass-fiber filters immediately after collection. The filter was extracted with 90% acetone in laboratory. The extract solution was measured for Chl *a* concentration using a Turner fluorometer. A stainless steel grab sampler was used to collect sediment. The surface sediment (0-2 cm) was collected using a plastic spatula at each station, and packed in polyethylene bags. Then the samples were kept on ice in a cooler and immediately transported to the laboratory. In laboratory, the samples were kept frozen at -20°C until further analysis.

A portion of each sediment sample was first pretreated with 30% H_2O_2 to remove organic matter and then with 1 M HCl to remove carbonates. The pretreated samples were washed to neutral with deionized water. Then, the solids were dispersed with 0.05 M $(NaPO_3)_6$ and analyzed for grain size using a Malvern Masterizer 2000 laser diffractometer (Malvern Instruments, UK). The percentages of the clay (< 4 μm), silt (4 – 63 μm) and sand (> 63 μm) fractions were determined. For the analysis of TOC and metal concentrations, sediment samples were freeze-dried and grounded, then passed through a mesh sieve (150 μm in pore size). They were stored in cleaned polyethylene bags until further analysis. For the analysis of TOC, the freeze-dried and grounded sediment samples were treated with 1M HCl to remove carbonates. Then they were washed to neutral with deionized water and dried at 60°C. Concentrations of TOC were determined using an elemental analyzer (Flash EA 1112 HT, Thermo Fisher Scientific, USA). Replicate analysis of one sample (n = 5) gave a relative standard deviation less than 0.8% for TOC.

For the analysis of total metal concentrations, the sediment samples were freeze-dried and grounded. Then, they were digested with HNO_3-HCl-HF (3:1:2) using microwave high-pressure digestion (Multiwave PRO 41HVT56, Austria). The digestion was diluted and determined by inductively coupled plasma mass spectrometry (ICP-MS, Agilent 7500cx, USA) for metals (Cd, Cr, Cu, Ni, Pb, Zn, Fe and Mn). The fractionation of metals in the sediment was determined according to the method reported by Rauret et al. (1999), which has been successfully applied in many studies (Zhuang and Gao, 2014; Akhbarizadeh et al., 2017; Anandkumar et al., 2022). Cd, Cr, Cu, Ni, Pb and Zn associated with four operationally defined geochemical fractions (acid soluble, reducible, oxidizable and residual) were identified by this method. For the acid soluble fraction, 0.5 g sediment was extracted with 0.11 M acetic acid (Step 1). The residual of Step 1 was shaken with 0.5 M hydroxylamine hydrochloride for 16 h to extract the reducible fraction (Step 2). The residual of Step 2 was digested with 8.8 M hydrogen peroxide and then shaken with 1 M ammonium acetate for 16 h to extract the oxidizable fraction. The detailed sequential extraction protocol has been described by Gao et al. (2010). The metal concentration of the extraction solution for each step was determined by ICP-MS (Agilent 7500cx, USA). The residual fraction was calculated by the

difference between the total concentrations of metals and the sums of the acid soluble, reducible and oxidizable fractions.

For the measurement of metals, each sample was analyzed at least in duplicate. The precision of the analysis was <10%. Procedural blanks were analyzed with each batch of samples. Certified reference material for coastal sediment (GBW07314, the Chinese national reference material) was analyzed to control metal analytical quality. The determined values for all metals were consistent with the reference values (**Table S1**). All plastic and glassware were soaked for at least 2 days in 10% HNO_3, followed by soaking and rinsing with de-ionized water.

2.3. Assessment Methods of Metal Contamination

Several methods have been used to evaluate the contamination status, potential risk, enrichment and sources of metals in surface sediments of ZJB, including comparison with related sediment quality guidelines, enrichment factor analysis, contamination factor analysis, pollution load index, and potential risk assessment based on geochemical compositions of metals.

The National Standard of China for Marine Sediment Quality (MSQ) (SEPA, 2002) can be used to assess the potential risk of metals in sediments (Gao et al., 2014). This standard classifies marine sediments into three classes based on the function and protection targets of the area (SEPA, 2002). Enrichment factor (EF) is an important tool to assess metal enrichment. It can be used to determine the anthropogenic influence and the contamination status of sediments. The following equation was used to estimate the EF of metals in sediments using Fe as a normalizer (Ergin et al., 1991; Mucha et al., 2003; Keskin, 2012; Shibini Mol and Sujatha, 2020).

$$EF = (M_s/N_s)/(M_b/N_b)$$

where M_s and M_s represent metal concentration of sample and background concentration respectively, and N_s and N_b are the metal concentration used for normalization in the sample and the background respectively. The metal concentration of China Shelf Sea sediment (Zhao et al., 1995) was used as the background concentration in this study. The EF is classified into many groups to denote the degree of enrichment factor (Chen et al., 2007). EF ≤ 1 denotes no enrichment; 1< EF ≤ 3 denotes minor enrichment; 3< EF ≤ 5 denotes moderate enrichment; 5< EF ≤ 10 denotes moderately severe enrichment; 10 < EF ≤ 25 denotes severe enrichment; 25 < EF ≤ 50 denotes very severe enrichment; and EF > 50 denotes extremely severe enrichment.

Contamination factor (CF) can be used to assess contamination level (Pekey et al., 2004). The following equation was used to estimate the CF of metals (Shibini Mol and Sujatha, 2020).

$$CF = M_s/M_b$$

where M_s and M_b represent metal concentration of sample and background concentration. The metal concentration of Chin Shelf Sea sediment (Zhao et al., 1995) was used as the background concentration in this study. CF ≤ 1 denotes low contamination; 1< CF ≤3 denotes moderate contamination; 3 < CF ≤ 6 denotes considerable contamination; and CF > 6 denotes high contamination. Pollution load index (PLI) can be used to assess the contamination extent of metals in surface sediments of ZJB. It can provide an overall indication of metal pollution contamination (Tomlinson et al., 1980). The following equation was used to calculate PLI.

$$PLI = \sqrt[n]{CF_1 CF_2 CF_3 \cdots \cdots CF_n}$$

where n is the number of studied metals and the *CF* is the contamination factor of the metal calculated as above. PLI provides a comparative mean for assessing a site quality. PLI < 1 denotes uncontaminated area; PLI = 1 denotes baseline level of pollutants; and PLI > 1 denotes deterioration of site quality (Tomlinson et al., 1980).

The former assessment methods of sediment metal contamination are based on the total concentrations of metals. In addition to the total concentrations, the geochemical composition of metals is equally important to determine their potential toxicity and threat to ecosystems (Sahuquillo et al., 2003; Gao et al., 2016). According to the study of Perin et al. (1985), the acid soluble fraction (F1) of metal with no more than 1% of its total concentration is considered to have no risk to the environment; the percentage of metal in this fraction falling in the range of 1-10% indicates a low risk to the environment; its falling in the range of 10-30% indicates a medium risk to the environment; its falling in the range of 30-50% indicates a high risk to the environment; and the percentage higher than 50% indicates a very high risk to the environment.

3. RESULTS AND DISCUSSION

3.1. General Characteristics of the Surface Sediment and Bottom Water in Zhanjiang Bay

The surface sediments of ZJB were mainly composed of silt fraction (average of 60.0% and 63.3% in spring and summer, respectively); the clay and sand fractions were generally lesser than 40% (**Table 1**). Based on the environmental characteristics, the ZJB was divided into three subregions – channel, coastal bay and central bay (Section 2.1; **Figure 1**). In spring, the channel had relatively fine sediments (average of fine (clay + silt) fraction: 46.1%) compared with the coastal bay (33.8%) and central bay (38.3%). Similar distribution pattern was also found in summer. The reason is that the flow of Suixi river is small. The fine particles from Suixi river are mainly settled at the channel of ZJB (Lu et al., 2020). Besides, the channel has large-scale, cage-based mariculture, which can weaken the hydrodynamic conditions and contribute to the settlement of fine particles (Cai et al., 2006; Ke et al., 2014; Pondell and Canuel, 2017; Pan et al., 2019). EBCBS (1999) also indicated that the channel of ZJB had finer sediments compared with the other regions of ZJB. The TOC content in surface sediments of ZJB ranged from 0.10% to 1.46% (average: 0.74%) in spring and from 0.15% to 1.04% (average: 0.60%) in summer (**Table 1**). The decreased average TOC content in summer indicates organic matter degradation in

TABLE 1 | Average (minimum-maximum) of surface sediment and bottom water parameters in Zhanjiang bay in spring and summer.

	Zhanjiang bay	Channel	Coastal bay	Central bay
Sediment in spring				
Clay (%)	18.9 (6.7-35.5)	22.4 (14.4-32.7)	18.5 (6.7-35.5)	15.1 (13.4-16.7)
Silt (%)	60.0 (24.6-76.5)	69.7 (55.2-76.5)	49.0 (24.6-70.2)	61.6 (49.5-67.5)
Sand (%)	21.1 (0.0-68.8)	7.81 (0-30.4)	32.4 (0.00-68.8)	23.4 (19.1-35.2)
TOC (%)	0.74 (0.10-1.46)	1.05 (0.64-1.46)	0.60 (0.10-1.07)	0.52 (0.36-0.86)
Water in spring				
Temperature (°C)	24.23 (24.01-24.51)	24.20 (24.04-24.51)	24.26 (24.20-24.34)	24.25 (24.01-24.42)
Chl a (μg/L)	1.39 (0.47-3.50)	0.79 (0.47-1.50)	1.34 (0.85-1.69)	2.21 (1.21-3.50)
DO (mg/L)	7.15 (6.32-10.48)	7.59 (6.32-10.48)	6.88 (6.65-6.98)	6.88 (6.57-7.29)
Sediment in summer				
Clay (%)	21.2 (0.0-32.2)	29.8 (26.3-32.2)	16.7 (5.4-25.0)	17.2 (11.5-21.0)
Silt (%)	63.4 (21.9-79.6)	68.0 (66.0-70.5)	54.7 (21.9-72.1)	71.6 (65.7-79.6)
Sand (%)	15.4 (1.4-72.8)	2.1 (1.5-3.2)	28.6 (4.8-72.8)	11.2 (1.4-18.9)
TOC (%)	0.60 (0.15-1.04)	0.77 (0.35-1.04)	0.50 (0.15-0.91)	0.50 (0.40-0.61)
Water in summer				
Temperature (°C)	30.20 (29.31-31.01)	30.42 (29.68-31.01)	29.83 (29.31-30.04)	30.39 (29.87-30.69)
Chl a (μg/L)	11.54 (4.34-37.17)	6.33 (4.34-11.32)	9.29 (7.78-12.39)	20.31 (12.71-37.17)
DO (mg/L)	5.99 (4.07-7.57)	5.14 (4.07-6.10)	6.51 (5.94-7.57)	6.41 (5.57-7.20)

this season. Higher TOC content was observed at the channel compared with those of the other two subregions, indicating the strong influences of river input and/or anthropogenic activities (Lu et al., 2020).

The temperature of bottom water in ZJB ranged from 24.01 to 24.51°C (average: 24.23 °C) in spring and from 29.31 to 31.01 °C (average: 30.20 °C) in summer (**Table 1**). Significant increase of temperature was found in summer compared with that in spring. The Chl *a* concentration of bottom water in ZJB ranged from 0.47 to 3.50 μg/L (average: 1.39 μg/L) in spring and from 4.34 to 37.17 μg/L (average: 11.54 μg/L) in summer (**Table 1**). Significant increase of Chl *a* was found in summer compared with that in spring. This indicates that the supply of organic matter in summer increased compared with that in spring. The DO of bottom water in ZJB ranged from 6.32 to 10.48 mg/L (average: 7.15 mg/L) in spring and from 4.07 to 7.57 mg/L (average: 5.99 mg/L) in summer (**Table 1**). This indicates an aerobic environment of the bottom water in ZJB in both spring and summer. In channel, the average DO of bottom water decreased obviously in summer compared with that in spring (**Table 1**). Increased water temperature and organic matter decomposition may contribute to the decrease of DO in bottom water of this area. The seasonal variations of bottom water environment may have significant influences on the concentrations of metals in surface sediments of ZJB.

3.2. Spatial and Seasonal Variations of Total Metal Concentrations in Surface Sediments of Zhanjiang Bay

Total metal concentrations in sediments collected from ZJB in spring and summer are summarized in **Table 2** and **Figures 2**, **S1**. The concentration range for each studied metal in the surface sediments of ZJB was 0.023 to 0.464 μg/g for Cd, 1.67 to 100.71 μg/g for Cr, 1.86 to 37.36 μg/g for Cu, 3.88 to 30.49 μg/g for Ni, 4.72 to 70.10 μg/g for Pb, 8.38 to 161.18 μg/g for Zn, 7.99 to 45.73 mg/g for Fe, and 125.1 to 584.5 μg/g for Mn during the investigation period. In comparison with the previous work of ZJB, the concentrations of the studied metals in this study were generally comparable with those reported by Zhang et al. (2018) (**Table 2**). **Table 2** also shows the metal values of other coastal areas in China. The average concentrations of the studied metals in this study were comparable to the values reported for the surface sediments of the Taiwan Strait (Gao et al., 2016), Xiamen bay (Lin et al., 2014), and Laizhou Bay (Zhuang and Gao, 2014) (**Table 2**). The metal concentrations in this study were apparently lower than the values reported for the Jinzhou Bay (Li et al., 2012), which is one of the most heavily polluted coastal region in China (Gao et al., 2014; Gao et al., 2016).

The distribution patterns of studied metals were generally similar with relatively high concentrations at the channel and coastal bay, and relatively low concentrations in the central bay (**Figures 2**, **S1**). Spatial distribution is a useful tool for determining hotspot area with high metal concentrations (Hossain et al., 2020). The high concentrations of metals at the north channel may probably be resulted by the input of Suixi river and/or the discharge of domestic sewage from coastal area. The high concentrations of metals at the south channel (station Z5) may probably be related to the construction of the Donghai Dam. Previous studies indicated that the construction of the Donghai Dam could lead to long residence time of water near the Donghai Dam (Li, 2008; Zhou et al., 2020), which is conducive to the settlement of fine particles (Lu et al., 2020; Anandkumar et al., 2022). Fine grained sediments are conducive to adsorb more metals (Salomons and Förstner, 1984). Therefore, high metal concentrations can be found in the south channel of ZJB (**Figures 2**, **3**; Lu et al., 2020). Besides, point sources of metals may also contribute to the high concentrations of metals in this area. More research should be carried out to find the possible sources of metals in the south channel of ZJB. Chemical manufacturing units can act as point sources of metal contamination. Many factories are located on the south coast of ZJB (**Figure 1**). The high concentrations of almost all studied metals at the south coast of ZJB (station Z9) may probably

TABLE 2 | Metal concentrations in the surface sediments of ZJB and other coastal areas of China. Related sediment quality guidelines are also shown for comparison purpose.

Location	Sampling date		Cd μg/g	Cr μg/g	Cu μg/g	Ni μg/g	Pb μg/g	Zn μg/g	Fe mg/g	Mn μg/g	References
Zhanjiang bay	Apr. 2017	Range	0.023-0.339	1.67-100.71	1.86-37.36	3.88-30.49	8.50-62.09	8.38-161.18	7.99-45.73	125.1-584.5	This study
		Mean	0.175	59.56	19.03	17.67	31.55	70.18	31.23	304.5	
	Aug. 2017	Range	0.039-0.464	12.67-98.88	2.19-34.20	4.14-28.25	4.72-70.10	17.04-139.60	11.61-44.36	135.5-438.3	
		Mean	0.171	56.94	15.18	16.12	25.85	65.64	29.12	246.6	
	Apr. and Aug. 2017	Range	0.023-0.464	1.67-100.71	1.86-37.36	3.88-30.49	4.72-70.10	8.38-161.18	7.99-45.73	125.1-584.5	
		Mean	0.173	58.25	17.11	16.89	28.70	67.91	30.18	275.5	
Zhanjiang bay	Jan. 2014	Mean	0.15	63.83	18.74	22.43	43.89	73.6	38.28	420	Zhang et al. (2018)
Taiwan Strait, China	May, 2007	Range	0.067-0.27	9.9-80.6	1.3-33.8	4.8-44.7	9.8-39.6	6.9-108	na[a]	na	Gao et al. (2016)
		Mean	0.16	50.9	17.5	26.4	24.0	68.1	na	na	
Xiamen Bay, China	Oct.-Nov. 2011	Range	0.022-1.30	17.5-93.9	5.25-69.2	na	20.1-67.5	17.7-196	na	na	Lin et al. (2014)
		Mean	0.18	53.5	23.4	na	40.2	107	na	na	
Laizhou Bay, China	Oct. 2011	Range	0.09-0.38	32.4-90.0	2.9-28.7	14.1-47.1	11.4-34.0	12.8-88.6	na	na	Zhuang and Gao (2014)
		Mean	0.22	56.7	12.0	25.9	19.4	41.5	na	na	
Jinzhou Bay, China	Oct. 2009	Range	7.9-105	na	24.5-327	26.3-86	29.2-523	168-2506	na	na	Li et al. (2012)
		Mean	26.8	na	74.1	43.5	124.0	689.4	na	na	
China Shelf Sea			0.065	60	15	24	20	65	31.0	530	Zhao et al. (1995)
MSQ Grade I [b]			≤0.5	≤80	≤35	na[a]	≤60	≤150	na	na	SEPA (2002)
MSQ Grade II [b]			≤1.5	≤150	≤100	na	≤130	≤350	na	na	
MSQ Grade III [b]			≤5	≤270	≤200	na	≤250	≤600	na	na	

[a]*na, not available.*
[b]*MSQ Grade I-III, National Standard of China for Marine Sediment Quality GB 18668-2002 Grade I-III.*

indicate the influence of industrial wastewater from coastal factories.

Table 3 showed the average total concentrations of metals in different subregions. In spring, the average total concentrations of Cd, Cr, Cu, Ni, Pb, Zn and Fe in different subregions followed the order of channel > coastal bay > central bay, while for Mn, the order is coastal bay > channel > central bay. This indicates that in spring the main source of Cd, Cr, Cu, Ni, Pb, Zn and Fe in surface sediments of ZJB was probably the input of Suixi river, while for Mn the main source was probably the industrial wastewater from south coast. In summer, the average total concentrations of Cd, Cr, and Cu in different subregions followed the order of channel > coastal bay > central bay; for Ni, Pb and Fe, the order is channel > central bay > coastal bay; for Zn, the order is coastal bay > channel > central bay; and for Mn, the order is coastal bay > central bay > channel (**Table 3**). The distribution pattern of Cd, Cr and Cu in summer was similar with that in spring, while the distribution pattern of Ni, Pb, Fe, Zn and Mn showed some differences compared with that in spring. For Ni, Pb and Fe, the average total concentrations in central bay were higher than those in coastal bay and lower than those in channel. This distribution pattern suggests that the central bay may probably be influenced by river runoff in summer. High rainfall in summer could cause high river runoff, resulting in terrestrial materials transporting to a far distance from Suixi river estuary. This phenomenon has also been found in the study of Zhou et al. (2020). For Zn, the average total concentration in coastal area was higher than that in channel and central bay. This indicates that the main source of Zn in summer was industrial waste from coastal factories, which was different from that in spring. For Mn, the average total concentration in central area was higher than that in channel and lower than that in coastal bay. This indicates that industrial waste water can also be transported to the central bay from the coastal bay in summer. The dynamic environment of ZJB between spring and summer (e.g. increased river runoff in summer) contributed to the spatial variations of Ni, Pb, Zn, Fe and Mn in these two seasons. In spring, due to the low rainfall in this season, the Suixi river had a small runoff and the surface runoff was also weak. The influence from the Suixi river was mainly trapped in the channel, resulting in relatively high metal concentrations in this area, and the pollutants from coastal area cannot be transported far away from coast. While in summer, increased rainfall resulted in increased terrestrial input (Zhou et al., 2020), which may bring pollutants to the central ZJB through river input and/or coastal transportation.

In addition to the variations of spatial distribution pattern of some metals, the average total concentrations of the studied metals in different subregions also showed variations (**Table 3**). For the channel, all the studied metals showed decreasement in summer compared with those in spring, with the maximum decrease of 32.4% for Zn. Similar seasonal variations of metals were also found in the surface sediment of Changjiang Estuary (Duan et al., 2019). Though increased rainfall in summer

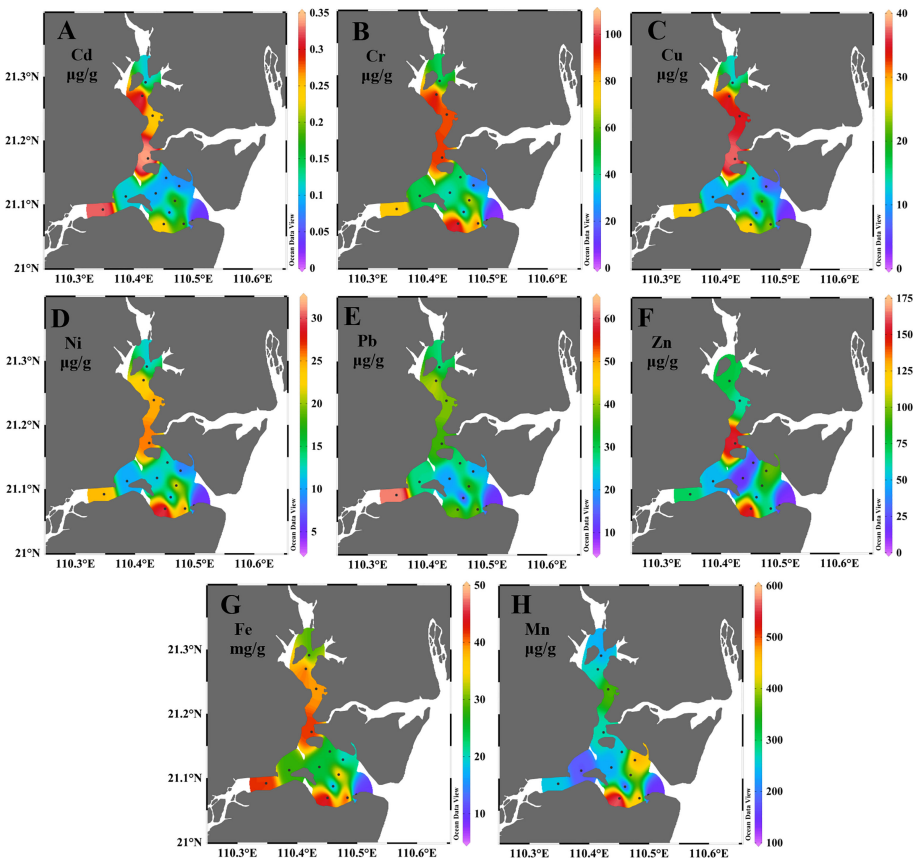

FIGURE 2 | The distribution of total metal concentrations for Cd **(A)**, Cr **(B)**, Cu **(C)**, Ni **(D)**, Pb **(E)**, Zn **(F)**, Fe **(G)** and Mn **(H)** in surface sediments of Zhanjiang bay in spring.

brought terrigenous pollutants to the surface sediment of channel bay, seasonal variations of environmental characteristics promoted metal release from sediment (**Table 1**, Section 3.1; Duan et al., 2019). The reduced Fe, Mn and TOC concentration in surface sediment, increased Chl *a* concentration in bottom water and the aerobic environment of bottom water in summer in the channel may probably indicate that the increase in organic matter degradation resulted in some Fe and Mn (hydr) oxides being reduced and released into the water (**Table 1**, Section 3.1; Duan et al., 2019). The decrease of other studied metals in channel may probably be related to organic matter degradation and Fe and Mn (hydr)oxides reduction processes. High temperature in summer enhanced bacterial activities, which may also contribute to the release of metals in summer (**Table 1**; Duan et al., 2019).

However, in the central bay, Cr, Ni and Zn showed some increases in summer compared with those in spring. These increases of metals in the central bay may be mainly due to the increased discharge of river input (Zhou et al., 2020) and/or industrial sewage from coastal areas in summer. In the coastal bay, the total concentrations of Cu, Ni, Pb, Fe and Mn decreased and Cd, Cr and Zn increased in summer compared with those corresponding concentrations in spring. These metals' seasonal variations in the coastal area may be the comprehensive impact of environmental changes (the change of temperature, DO and/or organic matter degradation) and increased terrigenous input, with the former five metals mainly influenced by environmental changes and the latter three metals mainly influenced by increased terrigenous input.

Correlation analysis was made based on the spring and summer data. Most of the studied metals showed significant positive correlations with each other (**Table 4**), indicating their similar sources and/or behaviors. Besides, almost all the studied metals showed significant positive correlations with TOC content, clay fraction and silt fraction, and showed significant negative correlations with sand fraction. This indicates that sediment grain size and TOC content both had significant influences on the distribution of metals in the surface sediments of ZJB, which has also been found in other areas such as the coastal Bohai Bay (Gao and Chen, 2012) and the mouth of São Francisco Channel (Freitas et al., 2019). Fine-grained sediments (clay + silt) have a larger specific surface area than coarser fraction of sediments (sand), providing them with more binding sites for the adsorption of organic matter and

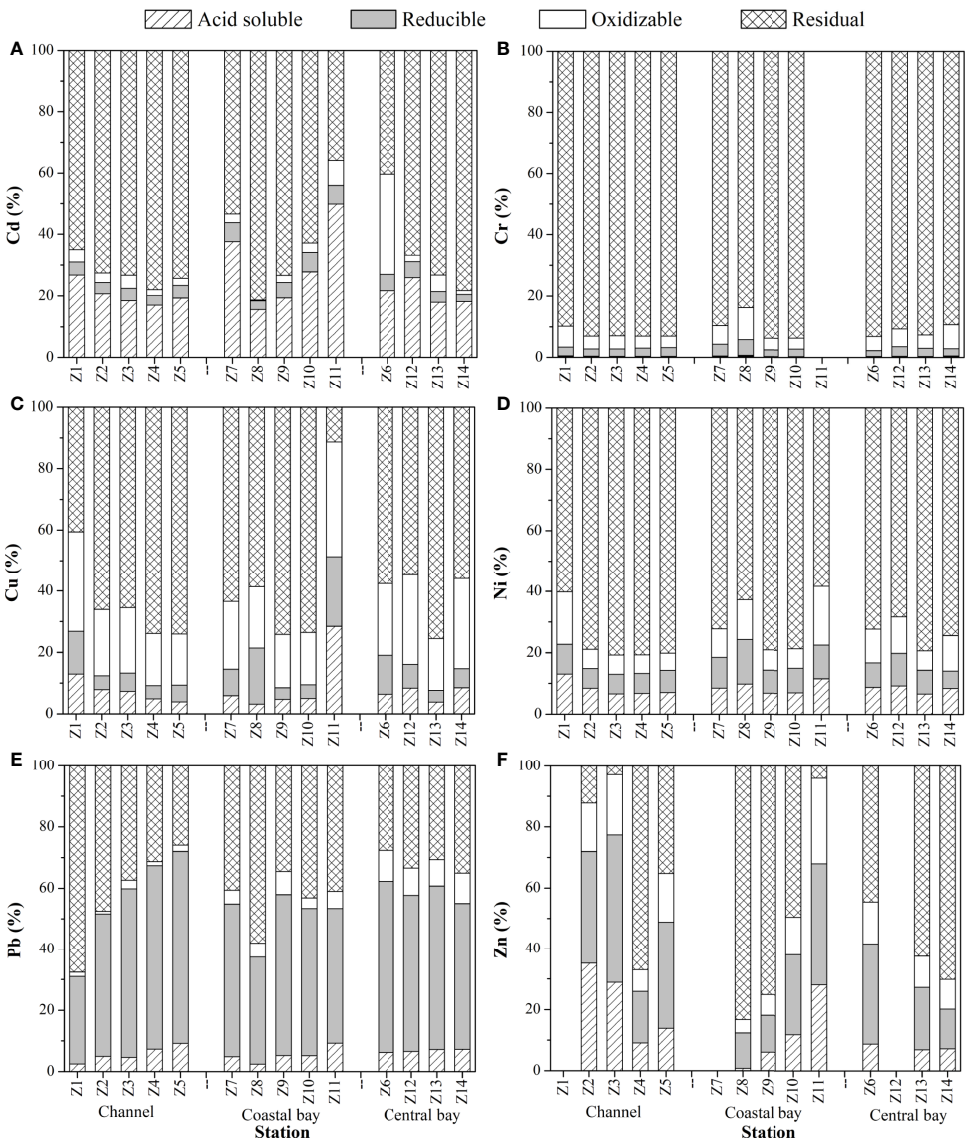

FIGURE 3 | Distributions of Cd **(A)**, Cr **(B)**, Cu **(C)**, Ni **(D)**, Pb **(E)** and Zn **(F)** in different geochemical fractions in the surface sediments of Zhanjiang bay in spring.

TABLE 3 | The average concentrations of total metals in different subregions of Zhanjiang bay.

		Cd μg/g	Cr μg/g	Cu μg/g	Ni μg/g	Pb μg/g	Zn μg/g	Fe mg/g	Mn μg/g
Apr. 2017	Channel	0.267	78.74	29.31	22.17	41.39	90.74	38.36	279.1
	Coastal bay	0.127	51.49	14.74	16.41	27.66	71.71	28.21	382.5
	Central bay	0.120	45.67	11.54	13.64	24.11	47.72	26.11	238.6
Aug. 2017	Channel	0.245	67.59	22.68	18.98	32.23	61.32	35.27	232.4
	Coastal bay	0.144	53.44	11.45	14.44	21.63	82.28	25.40	269.5
	Central bay	0.112	47.98	10.47	14.63	23.15	54.42	26.07	235.6

metals (Salomons and Förstner, 1984; Keil et al., 1994; Mayer, 1994). Organic matter is also an important mechanism of metals complexation in sediment (Freitas et al., 2019). The high concentrations of studied metals in the channel and coastal sediments of Zhanjiang bay were also related to the grain size compositions and TOC contents of sediments in these areas. Under oxidizing conditions, Fe and Mn tend to precipitate in the forms of oxides/hydroxides (Salomons and Förstner, 1984;

TABLE 4 | Pearson correlation analysis for total concentrations of metals and related parameters (n = 28).

	Cr	Cu	Ni	Pb	Zn	Fe	Mn	Clay	Silt	Sand	TOC
Cd	0.844[a]	0.888[a]	0.829[a]	0.862[a]	0.600[b]	0.785[a]	0.394[c]	0.720[a]	0.526[b]	-0.662[a]	0.759[a]
Cr		0.907[a]	0.964[a]	0.783[a]	0.721[a]	0.950[a]	0.571[b]	0.684[a]	0.638[a]	-0.743[a]	0.867[a]
Cu			0.906[a]	0.777[a]	0.636[a]	0.857[a]	0.453[c]	0.710[a]	0.608[b]	-0.716[a]	0.924[a]
Ni				0.809[a]	0.754[a]	0.903[a]	0.652[a]	0.711[a]	0.628[b]	-0.743[a]	0.885[a]
Pb					0.505[b]	0.788[a]	0.557[b]	0.664[a]	0.460[c]	-0.595[b]	0.733[a]
Zn						0.657[a]	0.695[a]	0.458[c]	0.180	-0.331	0.520[b]
Fe							0.563[b]	0.691[a]	0.612[b]	-0.725[a]	0.821[a]
Mn								0.292	0.039	-0.151	0.495[b]

[a] $P < 0.001$; [b] $0.001 < P < 0.01$; [c] $0.01 < P < 0.05$.

Freitas et al., 2019). In this study, significant positive correlations between Fe, Mn and other studied trace metals were found (**Table 4**). This suggests that metals in surface sediment of ZJB were related to Fe and Mn oxides and hydroxides (Freitas et al., 2019).

Principal component analysis (PCA) was used to identify principal components from the studied metals and related environmental parameters in surface sediments of ZJB (**Table 5**). Based on the results of PCA, two principal components (PC1 and PC2) were identified which accounted for 84.6% of the total data variance. PC1, accounting for 71.6% of the total data variance, had high positive loadings for TOC, Clay, silt and all studied metals. Considering the spatial distributions of these parameters (**Table 1** and **Figures 2**, **S1**) and the aforementioned discussion, we think that PC1 mainly represented the sources of river input and/or domestic sewage from Zhanjiang city. PC2, accounting for 12.9% of the total data variance, had high positive loadings for Mn, Zn and sand. Considering their high concentrations in the coastal bay (**Tables 1**, **3**), we think that PC1 represented the sources from coastal region.

3.3. Geochemical Compositions of Metals in Surface Sediments of Zhanjiang Bay

The geochemical compositions of Fe and Mn were not determined in sediments of ZJB. The average values of metal fractions in surface sediments of ZJB are summarized in **Table S2**. Among the studied metals, Pb and Zn were mainly associated with non-residual fractions (acid soluble fraction, reducible fraction and oxidizable fraction), and Cd, Cr, Cu and Ni were mainly associated with the residual fraction (**Table S2**).

TABLE 5 | Loadings of experimental variables on significant principal components for the data from Zhanjiang bay.

Parameter	PC1	PC2
Cd	**0.882**	0.001
Cr	**0.972**	0.081
Cu	**0.936**	-0.013
Ni	**0.975**	0.120
Pb	**0.850**	0.101
Zn	**0.703**	**0.488**
Fe	**0.972**	0.132
Mn	**0.607**	**0.648**
TOC	**0.896**	-0.059
Clay	**0.821**	-0.238
Silt	**0.644**	**-0.677**
Sand	**-0.789**	**0.572**
Percentage of variances	71.6%	12.9%
Cumulative variances	71.6%	84.6%

Bold values indicate strong loadings.

The acid soluble fraction (F1) of metals in sediments (exchangeable and bound to carbonates components) is in equilibrium with metals dissolved in water. It is labile, highly toxic and is the most bioavailable fraction. In the surface sediments of ZJB, the mean proportion of metals in F1 was Cd 24.0%, Cr 0.4%, Cu 7.9%, Ni 8.5%, Pb 5.9%, Zn 14.3% in spring, and Cd 19.4%, Cr 0.6%, Cu 5.8%, Ni 6.8%, Pb 6.5%, Zn 14.8% in summer. Relatively high proportions of Cd and Zn were associated with F1, indicating their high risk to the environment of ZJB. Low proportions of Cr, Cu, Ni and Pb were associated with F1. This indicates that these metals had low risk to the environment of ZJB.

The distribution of metal fractions is presented in **Figures 3**, **S2**. In spring, the average percentage of Zn in F1 was 21.8% at the channel, which was higher than that in the coastal bay (average: 11.7%) and the central bay (average: 7.6%). The acid soluble fraction has the greatest tendency to move from sediment to overlying water (Wang et al., 2011). This indicates that the channel was subject to more anthropogenic inputs of Zn compared with the coastal and central bay. Similar phenomenon was found in summer. In spring, a considerable fraction of Cd in F1 was observed at the coast of ZJB (average: 30.0%), which was higher than that in the channel (average: 20.4%) and the central bay (average: 20.9%). This suggests that the coastal bay was subject to more anthropogenic inputs of Cd compared with the channel and central bay. While in summer, relatively high percentage of Cd in F1 was observed at the channel. This indicates the main sources of acid soluble fraction of Cd varied with seasons.

Reducible fraction (F2) of metal is bound to amorphous Fe and Mn oxides and hydroxides (Rauret et al., 1999; Nemati et al., 2011). This fraction can become dissolved under reducing environment (Morillo et al., 2004). Among the studied metals, Pb had the highest percentage in this fraction (average of 47.4% in spring and summer) in the surface sediments of ZJB, indicating its potential risk to the environment under reducing conditions. Other studied metals had low proportions in F2. The average proportion in this fraction for both seasons can be summarized as: Pb (49.4%) > Zn (26.6%) > Cu (8.7%) > Ni (8.5%) > Cd (4.4%) > Cr (2.8%) in spring and Pb (45.2%) > Zn

(16.4%) > Ni (3.9%) > Cd (3.8%) > Cu (3.4%) > Cr (2.5%) in summer.

The oxidizable fraction (F3) of metal is bound to organic matter and sulfides components (Rauret et al., 1999; Nemati et al., 2011). Cu in this fraction was generally higher in surface sediments of ZJB, with an average proportion of 23.0% in spring and 32.8% in summer. The presence of other metals in this fraction was generally low in both seasons. The average proportion of metals in this fraction can be summarized as follows: Cu (23.0%) > Zn (13.1%) > Ni (9.8%) > Cr (5.4%) > Cd (5.3%) > Pb (5.1%) (spring) and Cu (32.8%) > Zn (15.2%) > Pb (9.9%) > Ni (8.4%) > Cr (4.5%) (summer). Due to contamination in the operation process, Cd in oxidizable fraction in summer was not available. Related parameters (Cd in residual and bioavailable fraction in summer) were also not available.

Metals in the residual fraction (F4) are associated with silicate mineral lattices (Rauret et al., 1999; Nemati et al., 2011). A major proportion of Cr (average of 91.4% and 92.4% in spring and summer, respectively) and Ni (average of 73.2% and 81.0% in spring and summer, respectively) were associated with this fraction, indicating their less mobility and bioavailability in the surface sediments of ZJB. The average proportion of studied metals in residual fraction was summarized as follows: Cr (91.4%) > Ni (73.2%) > Cd (66.3%) > Cu (60.4%) > Zn (46.0%) > Pb (39.6%) (spring) and Cr (92.4%) > Ni (81.0%) > Cu (58.0%) > Zn (53.5%) > Pb (38.4%) (summer).

The bioavailable fraction (BF) of metals is the summing results of the acid soluble, reducible and oxidizable fraction. The residual fraction is the non-bioavailable fraction. Metals associated with BF are bounded through weak bonds on sediments and are readily available to aquatic biota (Forstner, 1989; Pempkowiase et al., 1999). The concentration of metals in the BF is a serious environmental concern (Sundaray et al., 2011).

The average concentrations of bioavailable metals in different subregions are shown in **Figures 4A, B**. All the studied metals in BF had the highest concentrations in the channel sediments, suggesting that terrestrial input and/or domestic sewage may be their main sources. The percentage of the metals in BF decreased in the order of Pb (60.4%) > Zn (54.0%) > Cu (39.6%) > Cd (33.7%) > Ni (26.8%) > Cr (8.6%) in spring and Pb (61.6%) > Zn (46.5%) > Cu (42.0%) > Ni (19.0%) > Cr (7.6%) in summer (**Table S2**). This indicates that Cr and Ni were the least bioavailable studied metals in the sediments of ZJB. High percentages of Pb and Zn recorded in the BF indicate their greater mobility in the sediments of ZJB, which may be mainly from shipping activities (ship repair or painting), industrial effluent or domestic sewage.

Seasonal changes on bioavailability of metals were observed in the surface sediments of ZJB. The average concentrations of bioavailable fractions for all studied metals (except for Cd) decreased in summer compared with those in spring, with the maximum decrease of 52% for bioavailable Zn (**Figures 4A, B**).

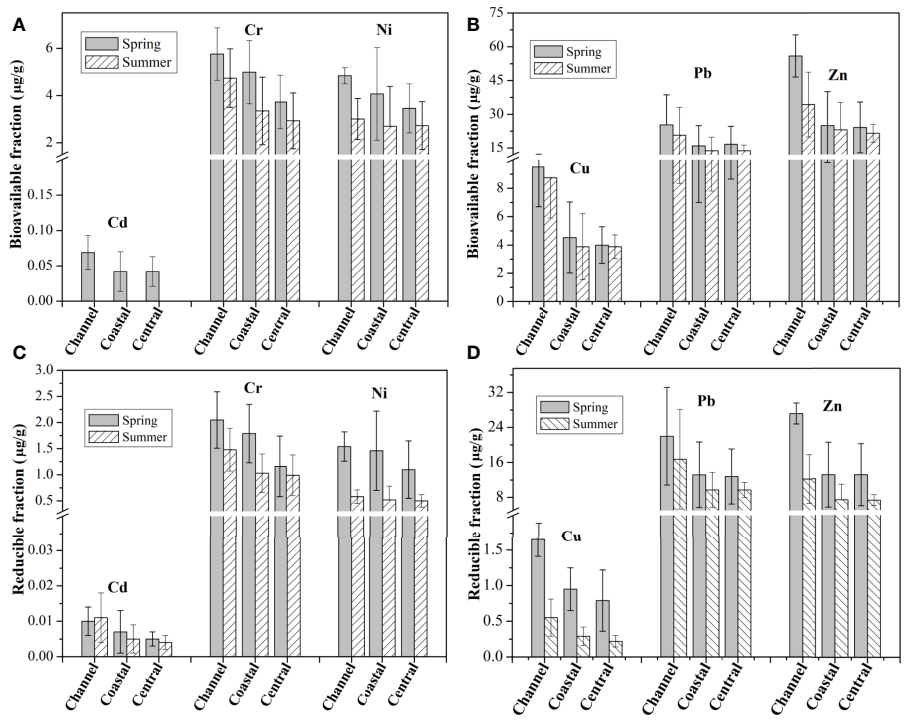

FIGURE 4 | Average concentrations of bioavailable **(A, B)** and reducible **(C, D)** fraction of metals in different subregions of Zhanjiang bay.

These changes indicate the release of bioavailable metals in summer, which were able to increase ecological risks. The concentrations of reducible fraction (bound to Fe/Mn oxyhydroxides components) for all studied metals (except for Cd) decreased in summer compared with those in spring (**Figures 4C, D**). For example, the average concentration of reducible Zn in channel was 27.19 μg/g in spring and 12.21 μg/g in summer. The seasonal variations of metals in this fraction may indicate the influence of relatively low DO in summer (**Table 1**). Decreased DO concentration in summer can promote the reduction of Fe and Mn oxides and hydroxides and the release of related metals (Morillo et al., 2004; Duan et al., 2019).

3.4. Assessment of Contamination Status of Metals in Surface Sediments of Zhanjiang Bay

The average total concentrations of Cd, Cr, Cu, Pb and Zn in the surface sediments of ZJB in both seasons were all within the range of MSQ Grade I (**Table 2**), suggesting that the surface

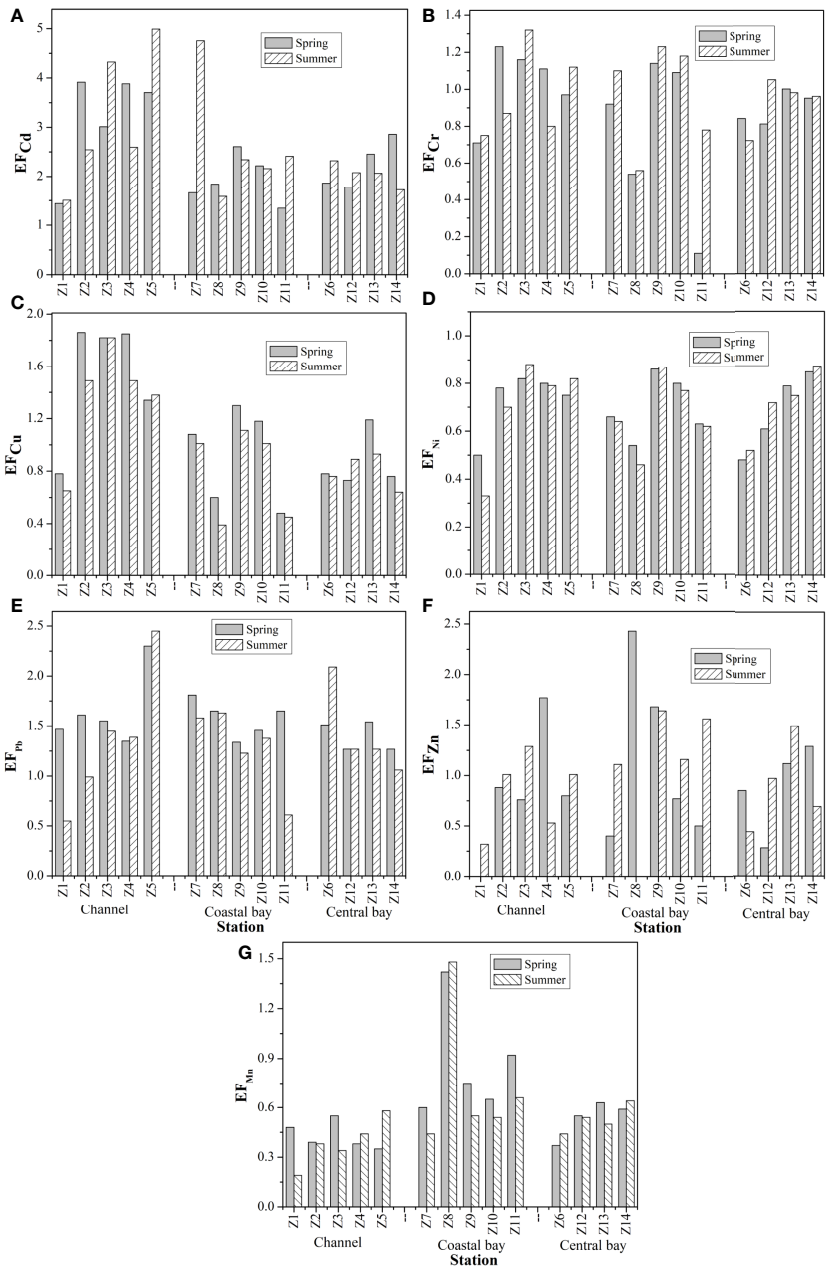

FIGURE 5 | Distributions of enrichment factor (EF) for Cd **(A)**, Cr **(B)**, Cu **(C)**, Ni **(D)**, Pb **(E)**, Zn **(F)** and Mn **(G)** in surface sediments of Zhanjiang bay.

sediments of ZJB were generally not contaminated by these metals.

According to the calculated EF values (**Figure 5**), Cr, Ni and Mn in the sediment of ZJB (average of 0.93, 0.70 and 0.58, respectively) generally showed no enrichment in both spring and summer; Cu showed minor enrichment in spring (average: 1.12); and Cd, Pb and Zn showed minor enrichment in both spring and summer. Overall, the calculated average EF values were in the descending order of Cd (2.47) > Pb (1.56) > Cu (1.12) > Zn (1.04) > Cr (0.90) > Ni (0.71) > Mn (0.62) in spring and Cd (2.61) > Pb (1.33) > Zn (1.05) > Cu (0.97) > Cr (0.96) > Ni (0.70) > Mn (0.54) in summer. Cr, Ni and Mn in the sediment of ZJB originated mainly from the natural input. Cd, Cu, Pb and Zn were influenced by anthropogenic activities to some extent.

The average CF values of the studied metals decreased in the order of Cd (2.69) > Pb (1.58) > Cu (1.27) > Zn (1.08) > Fe (1.01) > Cr (0.99) > Ni (0.74) > Mn (0.57) in spring and Cd (2.63) > Pb (1.29) > Zn (1.01) = Cu (1.01) > Cr (0.95) > Fe (0.94) > Ni (0.67) > Mn (0.47) in summer (**Figure 6**). The channel sediments of ZJB were considerably contaminated by Cd during both seasons (average CF of 4.10 in spring and 3.76 in summer) (**Figure 6**). The coastal and central bay sediments are moderately contaminated

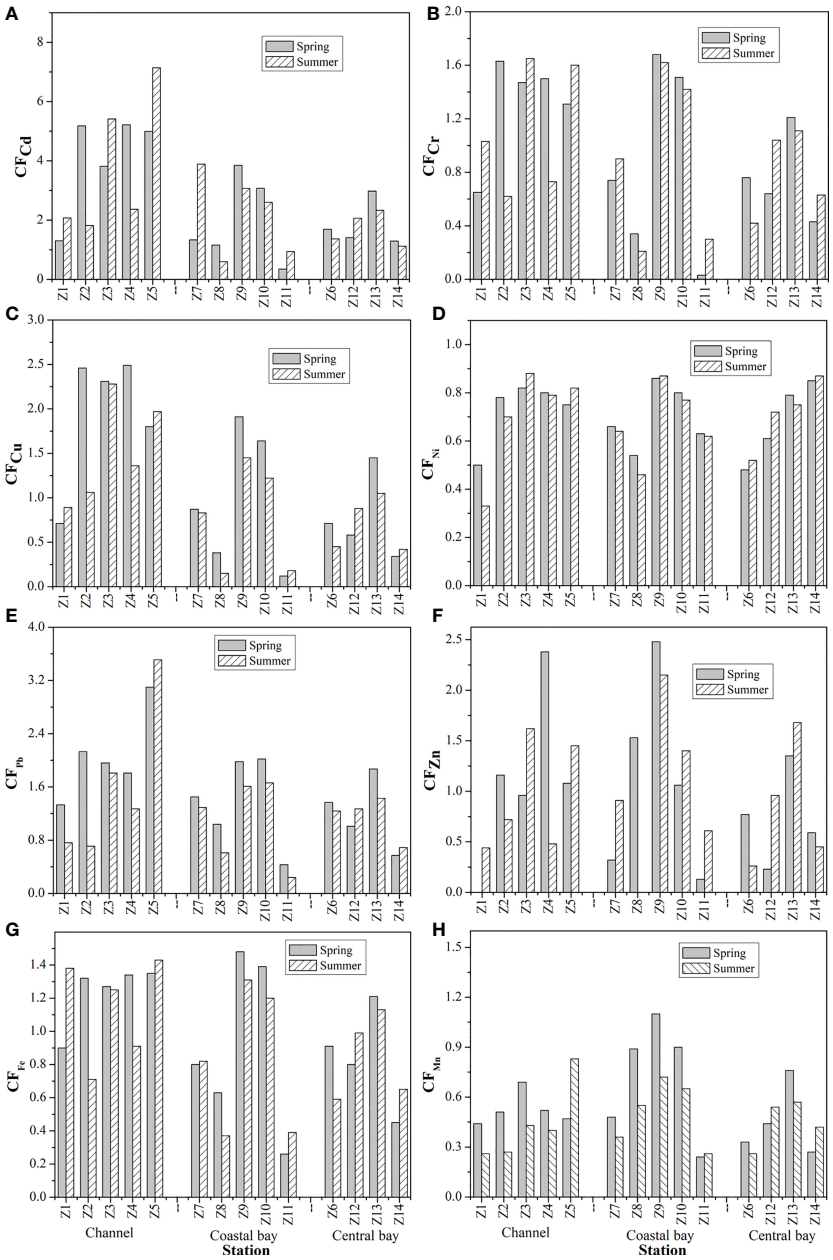

FIGURE 6 | Distributions of contamination factor (CF) for Cd **(A)**, Cr **(B)**, Cu **(C)**, Ni **(D)**, Pb **(E)**, Zn **(F)**, Fe **(G)** and Mn **(H)** in surface sediments of Zhanjiang bay.

by Cd. The three subregions of ZJB were moderately contaminated by Pb. For Cu, only the channel sediments showed moderately contaminated by this metal. For Zn, the station (Z9) near the Zhongke (Guangdong) Refining and Chemical Co., Ltd recorded the highest CF values in both spring and summer (2.48 in spring and 2.15 in summer) (**Figures 1**, **6**). This indicates that station Z9 was moderately contaminated by Zn, which may be probably sourced from the sewage of Zhongke (Guangdong) Refining and Chemical Co., Ltd. Other studied metals generally had low contamination to the surface sediments of ZJB (**Figure 6**).

The result of the hierarchical cluster analysis of the sampling stations based on the calculated CF in the surface sediment of ZJB in spring and summer is shown in **Figure 7**. Three main different clusters could be observed. Cluster 1 involved several stations (Z1, Z6, Z7, Z8, Z11, Z12, Z14) which were less contaminated. Cluster 2 involved several stations (Z2, Z3, Z4, Z9, Z10, Z13) which were generally contaminated. Cluster 3 involved one station (Z5) near the Donghai Dam which was moderately contaminated according to the calculated CF.

The calculated PLI values for metals in the surface sediment of ZJB are summarized in **Figure 8**. PLI ranged from 0.17 to 1.83 in spring and from 0.33 to 1.88 in summer. The average PLI values in the channel, coastal and central ZJB were 1.28, 0.93 and 0.81, respectively (spring and summer). This indicates that the channel of ZJB was contaminated by the studied metals. Besides, the two stations locating at the south coast of ZJB also had PLI values larger than 1, indicating the deterioration of sediment quality in this area.

The risk of metals in surface sediments of ZJB was evaluated based on the percentage of acid soluble fraction (F1) of metals (Section 2.3). The percentages of Cd in F1 in the channel and coastal bay and the percentages of Zn in F1 in the channel were generally in the range of 30-50% (**Figures 3**, **S2**), indicating the high risk of Cd and Zn to the environment in these subregions of ZJB. The percentages of Cd in F1 in the central bay and the percentages of Zn in F1 in the coastal and central bay were generally in the range of 10-30% (**Figures 3**, **S2**), indicating their medium risk to the environment in these subregions. Cu, Ni, Pb and Cr in the surface sediments of Zhanjiang bay generally had low risk or no risk to the environment based on their percentages in F1 (**Figures 3**, **S2**).

The results of EF and CF, which were calculated based on total metal concentrations, also indicated the contamination of Cd and Zn in surface sediments of ZJB (Section 3.5.1 and 3.5.2). Combined the assessment results of EF, CF and the percentages of acid soluble fraction, we concluded that Cd and Zn in the surface sediments of Zhanjiang bay were generally contaminated and they had medium to high risk to the environment.

4. CONCLUSIONS

Total concentrations and geochemical compositions of metals in surface sediments of Zhanjiang bay were studied. The total concentrations of metals were generally higher in the channel and coastal sediments of Zhanjiang bay. River discharge, domestic sewage, industrial wastewater, grain size compositions and TOC contents of sediments contributed much to the high concentrations of metals in these subregions of Zhanjiang bay. The spatial distribution pattern of some studied metals (Ni, Pb, Fe, Zn and Mn) showed seasonal variations. The dynamic environment of Zhanjiang bay

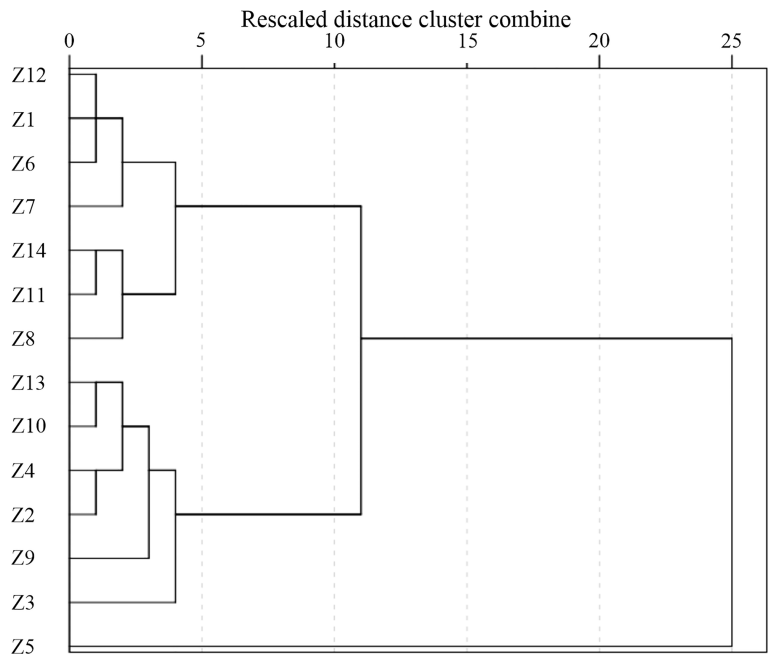

FIGURE 7 | Hierarchical dendrogram in terms of the sampling stations based on the data of contaminant factor in spring and summer.

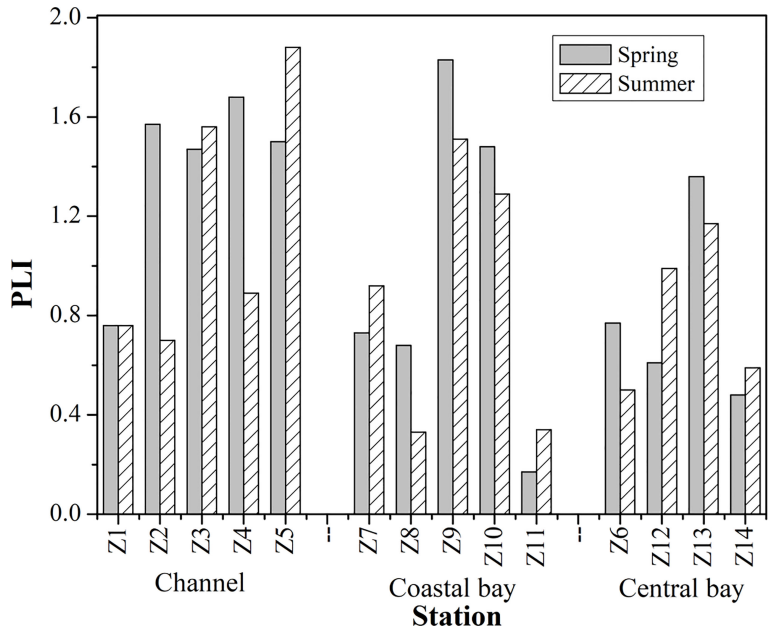

FIGURE 8 | Distributions of pollution load index (PLI) for metals in surface sediments of Zhanjiang bay.

between spring and summer contributed to the spatial variations of these metals. In the channel, all the studied metals showed decreased concentrations in summer compared with those in spring, indicating the release of metals from sediments. Organic matter degradation and Fe and Mn (hydr)oxides reduction processes contributed to that phenomenon.

Relatively high proportions of Cd and Zn were associated with the acid soluble fraction (average of 21.7% and 14.6%, respectively), indicating their high risk to the environment of Zhanjiang bay. The concentrations of reducible and bioavailable fractions of metals generally decreased in summer compared with those in spring. These changes may probably suggest the release of bioavailable metals in summer, which could be able to increase ecological risks. More research should be conducted to confirm this conclusion. Based on the assessment results of enrichment factor, contamination factor and the percentages of acid soluble fraction, Cd and Zn in the surface sediments of Zhanjiang bay were generally contaminated and they had medium to high risk to the environment. The pollution load index indicated the deterioration of sediment quality in the channel and the south coast of Zhanjiang bay. More attention should be paid on these contaminated areas in Zhanjiang bay. Some bioremediation techniques like using aquatic plants to remove the contaminated metals can be used to reduce the contamination of Zhanjiang bay.

DATA AVAILABILITY STATEMENT

The raw data supporting the conclusions of this article will be made available by the authors, without undue reservation.

AUTHOR CONTRIBUTIONS

Conceptualization: FZ. Data curation: FZ, MX, SW, and ST. Funding acquisition: FZ, SW, and FC. Investigation: FZ, GJ, FC, XL, QZ, and YM. Methodology: FZ, MX, ST, and CC. Writing – original draft: FZ. Writing – review and editing: FZ, GJ, and FC. All authors contributed to the article and approved the submitted version.

FUNDING

This work was supported by the Foundation for Young Talents in General Colleges and Universities of Guangdong Province (2019KQNCX044), the Guangdong Povincial College Innovation Team Project (2019KCXTF021), the Guangdong Basic and Applied Basic Research Foundation (2021A1515110172), the National Natural Science Foundation of China (U1901213), the Guangdong Natural Science Foundation of China (2019B1515120066, 2016A030312004), and the First-class Discipline Plan of Guangdong Province (080503032101, 231420003).

SUPPLEMENTARY MATERIAL

The Supplementary Material for this article can be found online at: https://www.frontiersin.org/articles/10.3389/fmars.2022.925567/full#supplementary-material

REFERENCES

Akcay, H., Oguz, A., and Karapire, C. (2003). Study of Heavy Metal Pollution and Speciation in Buyak Menderes and Gediz River Sediments. *Water Res.* 37, 813–822. doi: 10.1016/S0043-1354(02)00392-5

Akhbarizadeh, R., Moore, F., Keshavarzi, B., and Moeinpour, A. (2017). Microplastics and Potentially Toxic Elements in Coastal Sediments of Iran's Main Oil Terminal (Khark Island). *Environ. pollut.* 220, 720–731. doi: 10.1016/j

Anandkumar, A., Nagarajan, R., Gounder, E. S., and Prabakaran, K. (2022). Seasonal Variation and Mobility of Trace Metals in the Beach Sediments of NW Borneo. *Chemosphere* 287, 132069. doi: 10.1016/j.chemosphere.2021.132069

Anandkumar, A., Nagarajan, R., Prabakaran, K., Bing, C. H., and Rajaram, R. (2018). Human Health Risk Assessment and Bioaccumulation of Trace Metals in Fish Species Collected From the Miri Coast, Sarawak, Borneo. *Mar. pollut. Bull.* 133, 655–663. doi: 10.1016/j.marpolbul.2018.06.033

Cai, J. G., Xu, J. L., Yang, S. Y., Bao, Y. J., and Lu, L. F. (2006). The Fractionation of an Argillaceous Sediment and Difference in Organic Matter Enrichment in Different Fractions. *Geological. J. China Universities.* 12, 234–241. doi: 10.1111/j.1745-4557.2006.00081.x

Chakraborty, S., Chakraborty, P., Hathorne, E., Sarkar, A., Linsy, P., Frank, M., et al. (2021). Evidence for Increasing Anthropogenic Pb Concentrations in Indian Shelf Sediments During the Last Century. *Sci. Total. Environ.* 760, 143833. doi: 10.1016/j.scitotenv.2020.143833

Chakraborty, S., Chakraborty, P., Sarkar, A., and Nagender Nath, B. (2017). Kinetic and Equilibrium Based Fractionation Study of Pb in Continental Shelf Sediment of India. *Mar. pollut. Bull.* 123 (1-2), 188–196. doi: 10.1016/j.marpolbul.2017.08.063

Chakraborty, P., Sarkar, A., Vudamala, K., Naik, R., and Nagender Nath, B. (2015). Organic Matter — A Key Factor in Controlling Mercury Distribution in Estuarine Sediment. *Mar. Chem.* 173 (20), 302–309. doi: 10.1016/j.marchem.2014.10.005

Charriau, A., Lesven, L., Gao, Y., Leermakers, M., Baeyens, W., Ouddane, B., et al. (2011). Trace Metal Behavior in Riverine Sediments: Role of Organic Matter and Sulfides. *Appl. Geochem.* 26, 80–90. doi: 10.1016/j.apgeochem.2010.11.005

Chen, C. W., Kao, C. M., Chen, C. F., and Dong, C. D. (2007). Distribution and Accumulation of Heavy Metals in the Sediments of Kaohsiung Harbor, Taiwan. *Chemosphere* 66, 1431–1440. doi: 10.1016/j.chemosphere.2006.09.030

Dang, D. H., Lenoble, V., Durrieu, G., Omanović, D., Mullot, J. U., Mounier, S., et al. (2015). Seasonal Variations of Coastal Sedimentary Trace Metals Cycling: Insight on the Effect of Manganese and Iron (Oxy) Hydroxides, Sulphide and Organic Matter. *Mar. pollut. Bull.* 92, 113–124. doi: 10.1016/j.marpolbul.2014.12.048

Duan, L. Q., Song, J. M., Liang, X. M., Yin, M. L., Yuan, H. M., Li, X. G., et al. (2019). Dynamics and Diagenesis of Trace Metals in Sediments of the Changjiang Estuary. *Sci. Total. Environ.* 675, 247–259. doi: 10.1016/j.scitotenv.2019.04.190

EBCBS (Editorial Board of China Bay Survey) (1999). *Survey of China Bays* Vol. Vol. 10: Western Gulf of Guangdong Province) (Beijing: China Ocean Press).

Ergin, M., Saydam, C., Ba¸stürk, O., Erdem, E., and Yörük, R. (1991). Heavy Metal Concentrations in Surface Sediments From the Two Coastal Inlets (Golden Horn Estuary and Izmit Bay) of the Northeastern Sea of Marmara. *Chem. Geology.* 91 (3), 269–285. doi: 10.1016/0009-2541(91)90004-B

Forstner, U. (1989). *Contaminated Sediments* (Berlin: Springer-verlag), p157.

Freitas, A. R. D., Rodrigues, A. P. D. C., Monte, C. D. N., Freire, A. S., Santelli, R. E., Machado, W., et al. (2019). Increase in the Bioavailability of Trace Metals After Sediment Resuspension. *SN. Appl. Sci.* 1, 1288. doi: 10.1007/s42452-019-1276-8

Gao, X. L., and Chen, C. T. A. (2012). Heavy Metal Pollution Status in Surface Sediments of the Coastal Bohai Bay. *Water Res.* 46, 1901–1911. doi: 10.1016/j.watres.2012.01.007

Gao, X. L., Chen, C. T. A., Wang, G., Xue, Q. Z., Tang, C., and Chen, S. Y. (2010). Environmental Status of Daya Bay Surface Sediment Inferred From a Sequential Extraction Technique. *Estuarine. Coast. Shelf. Sci.* 86 (3), 369–378. doi: 10.1016/j.ecss.2009.10.012

Gao, X. L., Zhou, F. X., and Chen, C. T. A. (2014). Pollution Status of the Bohai Sea: An Overview of the Environmental Quality Assessment Related Trace Metals. *Environ. Int.* 62, 12–30. doi: 10.1016/j.envint.2013.09.019

Gao, X. L., Zhou, F. X., Lui, H. K., Lou, J. Y., Chen, C. T. A., and Zhuang, W. (2016). Trace Metals in Surface Sediments of the Taiwan Strait: Geochemical Characteristics and Environmental Indication. *Environ. Sci. Pollut. Res.* 23, 10494–10503. doi: 10.1007/s11356-015-5669-y

Gu, Y. G., Wang, X. N., Lin, Q., Du, F. Y., Ning, J. J., and Li, Y. F. (2016). Fuzzy Comprehensive Assessment of Heavy Metals and Pb Isotopic Signature in Surface Sediments From a Bay Under Serious Anthropogenic Influences: Daya Bay, China. *Ecotoxicol. Environ. Saf.* 126, 38–44. doi: 10.1016/j.ecoenv.2015.12.011

Hossain, M. S., Ahmed, M. K., Sarker, S., and Rahman, M. S. (2020). Seasonal Variations of Trace Metals From Water and Sediment Samples in the Northern Bay of Bengal. *Ecotoxicol. Environ. Saf.* 193, 110347. doi: 10.1016/j.ecoenv.2020.110347

Ke, S., Zhao, L. R., and Sun, S. L. (2014). Distribution characteristics and sources of PAHs in sea water of the land-based outlet of Zhanjiang Bay. *Marine Environ. Sci.* 33, 71–77. doi: CNKI:SUN:HYHJ.0.2014-01-013

Keil, R. G., Montluçon, D. B., Prahl, F. G., and Hedges, J. I. (1994). Sorptive Preservation of Labile Organic Matter in Marine Sediments. *Nature* 370, 549–552. doi: 10.1038/370549a0

Keskin, S. (2012). Distribution and Accumulation of Heavy Metals in the Sediments of Akkaya Dam, Nigde, Turkey. *Environ. Monit. Assess.* 184, 449–460. doi: 10.1007/s10661-011-1979-9

Lee, P. K., Kang, M. J., Yu, S., Ko, K. S., Ha, K., Shin, S. C., et al. (2017). Enrichment and Geochemical Mobility of Heavy Metals in Bottom Sediment of the Hoedong Reservoir, Korea and Their Source Apportionment. *Chemosphere* 184, 74–85. doi: 10.1016/j.chemosphere.2017.05.124

Li, X. B. (2008). *Research on the Effects of Donghai Dam on the Hydrodynamic Environment of Zhanjiang Bay. Master's Thesis* (China: Ocean University of China, Qingdao).

Li, Y. Y., Gao, B., Xu, D. Y., Peng, W. Q., Liu, X. B., Qu, X. D., et al. (2020). Hydrodynamic Impact on Trace Metals in Sediments in the Cascade Reservoirs, North China. *Sci. total. Environ.* 716, 136914. doi: 10.1016/j.scitotenv.2020.136914

Li, X. Y., Liu, L. J., Wang, Y. G., Luo, G. P., Chen, X., Yang, X. L., et al. (2012). Integrated Assessment of Heavy Metal Contamination in Sediments From a Coastal Industrial Basin, NE China. *PloS One* 7, e39690. doi: 10.1371/journal.pone.0039690

Lin, C., Liu, Y., Li, W. Q., Sun, X. W., and Ji, W. D. (2014). Speciation, Distribution, and Potential Ecological Risk Assessment of Heavy Metals in Xiamen Bay Surface Sediment. *Acta Oceanol. Sin.* 33 (4), 13–21. doi: 10.1007/s13131-014-0453-2

Lu, X., Zhou, F. X., Chen, F. J., Lao, Q. B., Zhu, Q. M., Meng, Y. F., et al. (2020). Spatial and Seasonal Variations of Sedimentary Organic Matter in a Subtropical Bay: Implication for Human Interventions. *Int. J. Environ. Res. Public Health* 17, 1362. doi: 10.3390/ijerph17041362

Mayer, L. M. (1994). Surface Area Control of Organic Carbon Accumulation in Continental Shelf Sediments. *Geochimica. Cosmochimica. Acta* 58, 1271–1284. doi: 10.1016/0016-7037(94)90381-6

Mohanraj, T., Sheeba, M., Cross, S. R. T. S., and Rajathy, T. J. (2021). Seasonal Variation of Heavy Metals in the Intertidal Gastropod Trochus Radiatus of Gulf of Mannar. *Open Jornal. Mar. Sci.* 11, 92–102. doi: 10.4236/ojms.2021.112007

Morillo, J., Usero, J., and Gracia, I. (2004). Heavy Metal Distribution in Marine Sediments From the Southwest Coast of Spain. *Chemosphere* 55 (3), 431–442. doi: 10.1016/j.chemosphere.2003.10.047

Mucha, A. P., Vasconcelos, M. T. S. D., and Bordalo, A. A. (2003). Macrobenthic Community in the Douro Estuary: Relations With Trace Metals and Natural Sediment Characteristics. *Environ. pollut.* 121 (2), 169–180. doi: 10.1016/S0269-7491(02)00229-4

Nagarajan, R., Kumar, A., Hussain, S. M., Jonathan, M. P., Ramkumar, M., Gounder, E. S., et al. (2019). "Geochemical Characterization of Beach Sediments of Miri, NW Borneo, SE Asia: Implications on Provenance, Weathering Intensity, and Assessment of Coastal Environmental Status," in *Coastal Zone Management* (Amsterdam, The Netherlands: Elsevier), 279–330.

Nemati, K., Bakar, N. K. A., Abas, M. R., and Sobhanzadeh, E. (2011). Speciation of Heavy Metals by Modified BCR Sequential Extraction Procedure in Different

Depths of Sediments From Sungai Buloh, Selangor, Malaysia. *J. Hazardous. Materials.* 192 (1), 402–410. doi: 10.1016/j.jhazmat.2011.05.039

Pais, I., and Jones, J. R. (1997). *The Handbook of Trace Elements* (Boca Raton: St. Lucie Press).

Pan, Z., Gao, Q. F., Dong, S. L., Wang, F., Li, D. H., Zhao, K., et al. (2019). Effects of Abalone (Haliotis Discus Hannai Ino) and Kelp (Saccharina Japonica) Mariculture on Sources, Distribution, and Preservation of Sedimentary Organic Carbon in Ailian Bay, China: Identified by Coupling Stable Isotopes (δ^{13}c and δ^{15}n) With C/N Ratio Analyses. *Mar. pollut. Bull.* 141, 387–397. doi: 10.1016/j.marpolbul.2019.02.053

Pekey, H. (2006). The Distribution and Sources of Heavy Metals in Izmit Bay Surface Sediments Affected by a Polluted Stream. *Mar. pollut. Bull.* 52 (10), 1197–1208. doi: 10.1016/j.marpolbul.2006.02.012

Pekey, H., Karakaş, D., Ayberk, S., Tolun, L., and Bakoğlu, M. (2004). Ecological risk assessment using trace elements from surface sediments of Izmit Bay (Northeastern Marmara Sea) Turkey. *Mar. Pollut. Bull.* 48 (9–10), 946–953. doi: 10.1016/j.marpolbul.2003.11.023

Pempkowiase, J., Sikora, A., and Biernacka, E. (1999). Speciation of Heavy Metals in Marine Sediments vs Their Bioaccumulation by Mussels. *Chemosphere* 39 (2), 313–321. doi: 10.1016/S0045-6535(99)00112-5

Peña-lcart, M., Mendiguchía, C., Villanueva-tagle, M. E., Pomares-Alfonso, M. S., and Moreno, C. (2014). Revisiting Methods for the Determination of Bioavailable Metals in Coastal Sediments. *Mar. Pollut. Bull.* 89 (1-2), 67–74. doi: 10.1016/j.marpolbul.2014.10.034

Perin, G., Craboledda, L., Lucchese, L., Cirillo, R., Dotta, L., Zanette, M. L., et al. (1985). "Heavy metal speciation in the sediments of Northern Adriatic Sea: a new approach for environmental toxicity determination," in *Heavy metal in the environment*, vol. vol 2 . Ed. T. D. Lekkas (Edinburgh: CEP Consultant), pp 454–pp 456.

Pondell, C. R., and Canuel, E. A. (2017). The Role of Hydrodynamic Sorting on the Accumulation and Distribution of Organic Carbon in an Impoundment: Englebright Lake, California, USA. *Biogeochemistry* 133, 129–145. doi: 10.1007/s10533-017-0319-8

Prabakaran, K., Eswaramoorthi, S., Nagarajan, R., Anandkumar, A., and Franco, F. M. (2020). Geochemical Behaviour and Risk Assessment of Trace Elements in a Tropical River, Northwest Borneo. *Chemosphere* 252, 126430. doi: 10.1016/j.chemosphere.2020.126430

Rauret, G., Lopez-Sanchez, J. F., Sahuquillo, A., Rubio, R., Davidson, C., Ure, A., et al. (1999). Improvement of the BCR Three Step Sequential Extraction Procedure Prior to the Certification of New Sediment and Soil Reference Materials. *J. Environ. Monit.* 1 (1), 57–61. doi: 10.1039/a807854h

Rivera-Duarte, I., and Flegal, A. R. (1997). Porewater Gradients and Diffusive Benthic Fluxes of Co, Ni, Cu, Zn, and Cd in San Francisco Bay. *Croatica. Chemica. Acta* 70, 389–417.

Sahuquillo, A., Rigol, A., and Rauret, G. (2003). Overview of the Use of Leaching/Extraction Tests for Risk Assessment of Trace Metals in Contaminated Soils and Sediments. *TrAC. Trends Analytical. Chem.* 22 (3), 152–159. doi: 10.1016/S0165-9936(03)00303-0

Salomons, W., and Förstner, U. (1984). *Metals in the Hydrocycle* (Berlin: Springer).

Santos-Echeandia, J., Prego, R., Cobelo-García, A., and Millward, G. E. (2009). Porewater Geochemistry in a Galician Ria (NW Iberian Peninsula): Implications for Benthic Fluxes of Dissolved Trace Elements (Co, Cu, Ni, Pb, V, Zn). *Mar. Chem.* 117, 77–87. doi: 10.1016/j.marchem.2009.05.001

SEPA (State Environmental Protection Administration of China) (2002). *Marine Sediment Quality (GB 18668-2002)* (Beijing: Standards Press of China).

Shibini Mol, P. A., and Sujatha, C. H. (2020). Distribution and Geochemical Speciation of Sediment Bound Heavy Metals in the Specific Zones of Central Kerala, India. *Environ. Nanotechn. Monit. Manage.* 14, 100358. doi: 10.1016/j.enmm.2020.100358

Sundaray, S. K., Nayak, B. B., Lin, S., and Bhatta, D. (2011). Geochemical Speciation and Risk Assessment of Heavy Metals in the River Estuarine Sediments-a Case Study: Mahanadi Basin. India. *J. Hazardous. Materials.* 186, 1837–1846. doi: 10.1016/j.jhazmat.2010.12.081

Tessier, A., Campbell, P. G. C., and Blsson, M. (1979). Sequential Extraction Procedure for the Speciation of Particulate Trace Metals. *Analytical. Chem.* 51 (7), 844–851. doi: 10.1021/ac50043a017

Tomlinson, D. L., Wilson, J. G., Harris, C. R., and Jeffrey, D. W. (1980). Problems in the Assessment of Heavy Metal Levels in Estuaries and the Formation of a Pollution Index. *Helgoland. Mar. Res.* 33, 566–575. doi: 10.1007/BF02414780

USEPA, United States Environmental Protection Agency (2000). "Guidance for Assessing Chemical Contaminant Data for Use in Fish Advisories," in *Fish Sampling and Analysis, 3rd edition*, vol. Volume I. (Washington, D.C: Office of Science and Technology).

Wang, F., and Chen, J. (2000). Relation of Sediment Characteristics to Trace Metal Concentrations: A Statistical Study. *Water Res.* 34 (2), 694–698. doi: 10.1016/S0043-1354(99)00184-0

Wang, Y., Yang, Z., Shen, Z., Tang, Z., Niu, J., and Gao, F. (2011). Assessment of Heavy Metals in Sediments From a Typical Catchment of the Yangtze River, China. *Environ. Monit. Assess.* 172, 407–417. doi: 10.1007/s10661-010-1343-5

Yu, R., Yuan, X., Zhao, Y., Hu, G., and Tu, X. (2008). Heavy Metal Pollution in Intertidal Sediments From Quanzhou Bay, China. *J. Environ. Sci.* 20 (6), 664–669. doi: 10.1016/S1001-0742(08)62110-5

Zhang, J. B., Zhou, F. X., Chen, C. L., Sun, X. L., Shi, Y. Z., Zhao, H., et al. (2018). Spatial Distribution and Correlation Characteristics of Heavy Metals in the Seawater, Suspended Particulate Matter and Sediments in Zhanjiang Bay, China. *PloS One* 13 (8), e0201414. doi: 10.1371/journal.pone.0201414

Zhao, M., Shenghui, Z., Haitao, H., and Pan, D. (2021). Heavy Metals in Sediments of Yellow Sea and East China Sea: Chemical Speciation, Distribution, Influence Factor, and Contamination. *J. Oceanol. Limnol.* 39, 1277–1292. doi: 10.1007/s00343-020-0237-9

Zhao, Y. Y., Yan, M. C., and Jiang, R. H. (1995). Abundance of Chemical Elements in Continental Shelf Sediment of China. *Geo-Marine. Lett.* 15, 71–76. doi: 10.1007/BF01275409

Zhou, F. X., Lu, X., Chen, F. J., Zhu, Q. M., Meng, Y. F., Chen, C. Q., et al. (2020). Spatial-Monthly Variations and Influencing Factors of Dissolved Oxygen in Surface Water of Zhanjiang Bay, China. *J. Mar. Sci. Eng.* 8, 403. doi: 10.3390/jmse8060403

Zhuang, W., and Gao, X. L. (2014). Integrated Assessment of Heavy Metal Pollution in the Surface Sediments of the Laizhou Bay and the Coastal Waters of the Zhangzi Island, China: Comparison Among Typical Marine Sediment Quality Indices. *PloS One* 9 (4), e94145. doi: 10.1371/journal.pone.0094145

Conflict of Interest: The authors declare that the research was conducted in the absence of any commercial or financial relationships that could be construed as a potential conflict of interest.

Publisher's Note: All claims expressed in this article are solely those of the authors and do not necessarily represent those of their affiliated organizations, or those of the publisher, the editors and the reviewers. Any product that may be evaluated in this article, or claim that may be made by its manufacturer, is not guaranteed or endorsed by the publisher.

Copyright © 2022 Zhou, Xiong, Wang, Tian, Jin, Chen, Chen, Lu, Zhu and Meng. This is an open-access article distributed under the terms of the Creative Commons Attribution License (CC BY). The use, distribution or reproduction in other forums is permitted, provided the original author(s) and the copyright owner(s) are credited and that the original publication in this journal is cited, in accordance with accepted academic practice. No use, distribution or reproduction is permitted which does not comply with these terms.

frontiers | Frontiers in Marine Science

ORIGINAL RESEARCH
published: 28 June 2022
doi: 10.3389/fmars.2022.872077

Application of Microalgae Assemblages' Parameters for Ecological Monitoring in Mangrove Forest

Aniefiok Ini Inyang[1,2,3,4,5], *You-Shao Wang*[1,2,3,4*] *and Hao Cheng*[1,2,3,4]

[1] State Key Laboratory of Tropical Oceanography, South China Sea Institute of Oceanology, Chinese Academy of Sciences, Guangzhou, China, [2] Daya Bay Marine Biology Research Station, Chinese Academy of Sciences, Shenzhen, China, [3] Southern Marine Science and Engineering Guangdong Laboratory (Guangzhou), Guangzhou, China, [4] Innovation Academy of South China Sea Ecology and Environmental Engineering, Chinese Academy of Sciences, Guangzhou, China, [5] University of Chinese Academy of Sciences, Beijing, China

OPEN ACCESS

Edited by:
Ana Carolina Ruiz-Fernández, National Autonomous University of Mexico, Mexico

Reviewed by:
Chao Wang, Chinese Academy of Fishery Sciences, China
Biraja Kumar Sahu, Council of Scientific and Industrial Research (CSIR), India
Rosalba Alonso-Rodríguez, National Autonomous University of Mexico, Mexico

***Correspondence:**
You-Shao Wang
yswang@scsio.ac.cn

Specialty section:
This article was submitted to Marine Pollution, a section of the journal Frontiers in Marine Science

Received: *09 February 2022*
Accepted: *23 May 2022*
Published: *28 June 2022*

Citation:
Inyang AI, Wang Y-S and Cheng H (2022) Application of Microalgae Assemblages' Parameters for Ecological Monitoring in Mangrove Forest. Front. Mar. Sci. 9:872077. doi: 10.3389/fmars.2022.872077

Although the relationship between biodiversity and ecological functioning is a vital issue in coastal water ecology, how this relationship is influenced by environmental conditions is still unknown. It was investigated for the dynamics of algal diversity and algal pollution indices, as well as their relationships with trophic state, in a mangrove forest along the Guangdong coast, South China. It is hypothesized that the phytoplankton alpha-diversity indices and algal pollution indices have the potential to provide a signal linking trophic state and water quality variation in the mangrove forest. The *t*-test showed that phytoplankton alpha-diversity indices and algal pollution indices varied significantly between the dry and wet seasons ($p < 0.01$ or $p < 0.05$). The trophic state index record confirmed that the mangrove forest was mesotrophic to eutrophic during study periods while the CCME: WQI revealed that the water quality in the forest was under *poor* and *marginal* conditions in both seasons. Multivariate analysis revealed that the dynamics of phytoplankton alpha-diversity and algal pollution indices was closely related to trophic states change and influenced by environmental conditions. The results indicated that pH, total dissolved solids, salinity, electrical conductivity, turbidity, nitrate, and phosphate were the main factors affecting algal assemblages in the mangrove forest. The indices were confirmed as a quicker, faster, and reliable approach to appropriately describe and measure the trophic state variations in the mangrove ecosystem, though an integrated approach may be required in the future.

Keywords: alpha-diversity indices, algal pollution indices, mangrove forest, trophic state index, coastal water

1 INTRODUCTION

Mangroves, which can be found in tropical and subtropical regions, serve as buffer zones between freshwater and marine biomes, providing habitat for a variety of life (Wang, 2019), and providing natural sewage treatment systems that have been utilized over decades (Wong et al., 1997; Carlos et al., 2007; Wu et al., 2008; Wang and Gu, 2021). Due to the mixing of these distinct water bodies, they are

characterized by pronounced gradients of physical, chemical (McLusky, 1993), and biological components (Inyang and Wang, 2020). Ecosystem assessment is typically conducted using ecological indicators (Rapport and Hildén, 2013), which provide tools for managerial decisions by providing information about a specific area of interest (Jørgensen et al., 2013). Hence, ecological indicators are often based on the biological community at a site, and variation in community characteristics is used to compare the ecological state of that site to those of other sites. Over time, it has been reasoned that environmental parameters and changes therein determine the characteristics of biological communities (Friberg, 2014). Microalgae communities are known to respond rapidly to environmental variation, their short life cycle being sensitive to ecosystem changes (Marchetto et al., 2009; Taipale et al., 2019; Bergstrom et al., 2020; Inyang and Wang, 2020).

Globally, different mangrove forests have been stressed with a significant impact of algal bloom in the forest (Adhavan et al., 2015; Kamalifar et al., 2016; Temino-Boes et al., 2019). The anthropogenic eutrophication impact on coastal waters has always been a global issue before the 2000s, due to wastewater discharge from urban cities, agricultural activities (Meng et al., 2020), and aquaculture facilities into rivers, lakes, and wetlands directly; these also result in algal blooms, mainly of cyanobacteria and diatoms. Meanwhile, this phenomenon has been reported across numerous coastal waters in China (Yang et al., 2004; Xiao et al., 2007; Meng et al., 2020). The anthropogenic nutrient enrichment in coastal waters may cause an extensive impact on the nitrogen cycle (Reis et al., 2017), which could lead to accelerated changes (Geedicke et al., 2018) in the mangrove forest.

Generally, the eutrophication phenomenon has led to ecosystem imbalance, establishment of tolerance species, and disappearance of sensitive taxa (Gu and Wang, 2015). Meanwhile, the application of microalgae for ecosystem monitoring has a long history (Lepisto, 1999) where numerous indices have been developed but none have become widely accepted. Nevertheless, the application of alpha biodiversity indices (i.e., Magarlef index, Shannon index, Pielou's index, and Simpson diversity) to study the characteristics of the microalgae community structure in different water bodies has just been established (Mulder et al., 2001; Weis et al., 2007; Meng et al., 2020), but the application of these indices in ecological study of the mangrove forest is lacking. This study is the first to establish the response mechanism of alpha-diversity indices to changes in water quality parameters in the mangrove forest. Though the diversity based on species richness (number of taxa) and evenness (taxa distribution) can reflect microalgae community composition and could also describe the impacts of water pollution on biotic communities (Hooper et al., 2005), these indices require a high level of taxonomic classification. The degree to which physical and chemical variables affect microalgae alpha-diversity indices is different across different aquatic habitats (Meng et al., 2020). The knowledge of the biotic indicators to explore microalgae assemblage response to environmental change in the mangrove forest is a fundamental research objective in the ecology of the ecosystem.

Therefore, microalgae alpha-diversity indices, algal biomass, algal pollution indices, single-factor trophic state index (TSI Chl *a*), and Canadian Council of Ministers of the Environment Water Quality Index (WQI: CCME) were evaluated in the mangrove forest along the Guangdong coast, South China. Correlation analysis (Pearson correlation) and multivariate analysis were applied to understand the response of microalgae alpha-diversity indices and algal pollution indices to nutrients and other environmental parameters. Microalgae alpha-diversity indices and WQI: CCME were compared during the wet and dry seasons across the mangrove forest. The purposes of the study are as follows: (i) to explore the impact of hydrological parameters on microalgae indicator species; (ii) to understand alpha-diversity indices and algal pollution indices in relation to nutrient distribution; (iii) to establish trophic conditions of the mangrove forest through evaluation of algal pollution indices, algal diversity indices, and TSI (Chl *a*); and (iv) to evaluate the WQI: CCME across the mangrove forest.

2 MATERIALS AND METHODS

The samplings were collected for 34 different locations throughout the Guangdong mangrove forest, at latitude 20°12'–25°31' N and longitude 109°45'–117°20' E (**Figure 1**). The sampling sites are characterized by different species of true mangroves, such as *Acrostichum aureum*, *Excoecaria agallocha*, *Bruguiera gymnorrhiza*, *Kandelia obovata*, *Rizhophora stylosa*, *Lumnizera racemosa*, *Aegicera corniculatum*, *Avicennia marina*, and *Acanthus ilicifolius*, and non-true mangrove species, e.g., *Pongamia pinnata*, *Hibiscus tiliaceus*, *Thespesia populnes*, *Herltiera littoralis*, *Cerbera manghas*, *Clerodendrum inerme*, and *Pluchea indica* (Inyang and Wang, 2020). Guangdong's mangrove forest is influenced by semidiurnal to mixed tides all year, with a tidal range of 0.8 m during neap tides and 4.0 m during spring tides. The average annual precipitation in the study region is ~2,000 mm (Liu, 2013), and approximately 85% of the total rainfall is concentrated in the rainy season from April to September.

The study locations were selected across the mangroves from the Leizhou Peninsula in the west to the east. A total of 34 locations were selected spatially across the mangroves to evaluate the spatial and temporal change in phytoplankton community and variation in trophic state (**Figure 1**). **Figures 2A–D** show algal bloom formation in some parts of the mangrove forest along the Leizhou Peninsula and across the eastern part of the Guangdong coast.

2.1 Sampling Procedure

The sampling and monitoring studies were carried out across 34 stations (30 stations selected during the dry season and 23 stations selected during the wet season) within the mid-section of the mangrove forest from October 2017 to January 2018 (for the dry season) and July to August 2018 (for the wet season). At each station, measurement of environmental parameters and collection of phytoplankton samples were obtained during flood tide.

2.2.1 Measurement of Water Quality Parameters

At each site, *in situ* measurement of water quality parameters such as water temperature, pH, salinity, electrical conductivity (EC), turbidity, and total dissolved solids (TDS) were measured by using a Quanta® Water Quality Monitoring System

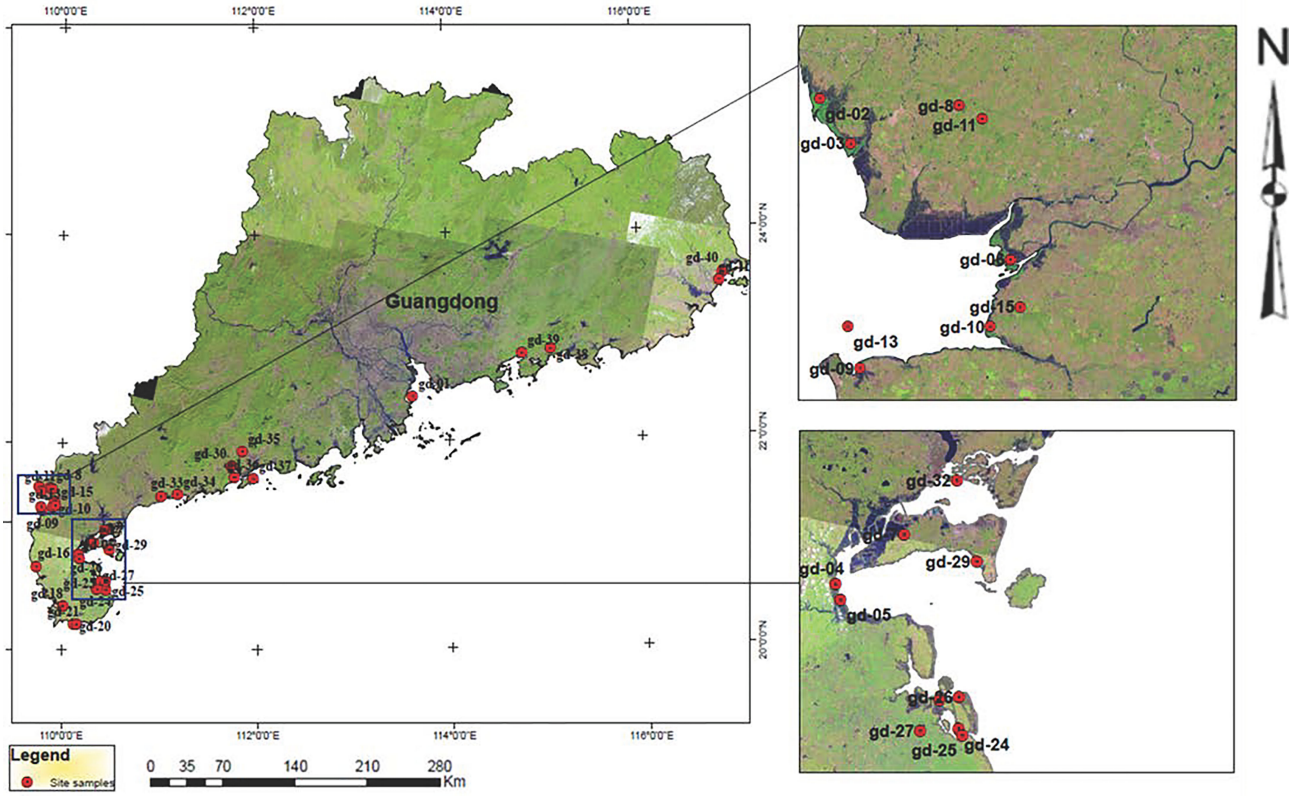

FIGURE 1 | Study area and sampling stations identified by the red dots on the map.

(Hydrolab Corporation, USA) during flood water level within the depth of 1 m. Three hundred milliliters of surface water was collected by using sampling plastic bottles for analysis of nutrients (phosphate, nitrate, nitrite, and silicate). The water samples were filtered using 0.22-µm Whatman® GF/F filters before analysis. Within 2–3 h after sampling, nitrate (NO_3-N), nitrite (NO_2-N), phosphate (PO_4-P), and silicate (SiO_3-Si) were analyzed with a SKALAR auto-analyzer (Skalar Analytical B.V. SanPlus, Holland). Chlorophyll *a* (Chl *a*) analysis was carried out according to HELCOM (2015) using a SHIMADZU Spectrophotometer (UV-1700-Japan) and calculated as follows:

$$Cv = \frac{10^3 \,.\, e \,.\, a(665K)}{83.V \,.\, L} \quad (1)$$

where:

Cv = Chl *a* concentration, mg/m^3; e = volume of ethanol, cm^3; a (665K) = absorbance at 665 nm (the peak) minus the absorbance at 750 nm after correction by the cell-to-cell blank; L = length of the curette, cm; V = water volume filtered, dm^3; 83 = absorption coefficient in 96% ethanol.

2.2.2 Microalgae Analysis

The microalgae samples were collected during flooding tide by vertically hauling within the depth of 1 m, using a plankton net of 0.045 mm size. Approximately 90 L of water was filtered at each station, and the net was rinsed before new sampling to avoid contamination of the new sample by the previous one. The collected phytoplankton samples in 300-ml plastic bottles were preserved with neutral Lugol's solution of 10% concentration for further analysis. Further analysis and identification were conducted as described by Inyang and Wang (2020).

2.3 Evaluation of Algal Pollution Indices

The algal genera and species mentioned by Palmer (1969) as pollution indicators were investigated in the study areas. This technique is considered to be a rapid, reliable, and relatively inexpensive way to record water pollution probability across a number of sites (Noel and Rajan, 2015). It can be applied with other indices of inorganic pollution and eutrophication level (Bellinger and Sigee, 2010). Palmer (1969) compiled a list of 60 genera and 80 species as pollution-tolerant individuals, of which he used 20 genera and 20 species to compute the pollution index score. However, only 17 genera and 16 species (**Table 1**) appeared in the study areas out of the 20 genera and 20 species mentioned in the Palmer pollution index (Palmer, 1969). The taxon was considered significant if its concentration was at least (>10) cells per ml. The final Palmer pollution index value is the summation of the scores of all the present taxa in a given station. Palmer index numerical values were calculated for both species and genera and compared to Palmer's proposed reference values

FIGURE 2 | Different sections of the mangrove forest. **(A)** Mangrove pneumatophores covered with algal bloom. **(B)** *Avecinnia marina* bed covered with algal bloom and the plant burdened with high density of barnacles species. **(C)** *Rhizophora* forest during low water level with a eutrophic pool of water at high tide. **(D)** *Sonneratia* and *Avecinnia* forest during high water level.

TABLE 1 | Water quality objective used in this assessment according to Chinese Environmental Protection Agency, 2002 (GB3838-2002).

Water quality parameters	WQOs
pH	6 – 9
EC (μs/cm)	1000
TDS (mg/L)	1000
Turbidity (NTU)	25
Nitrate (mg/L)	0.5 - 1
Phosphate (mg/L)	0.05

(0–10 indicated no evidence of organic pollution, 10–5 indicated moderate pollution, 15–20 indicated likely high organic pollution, and 20 or more indicated high organic pollution).

2.4 Trophic State Index

Trophic state index (TSI) using single factor (Chl *a*) was used to describe the trophic status (Wang, 2002) in the mangrove forest according to the equation:

$$\mathrm{TSI}(\mathrm{Chl}\,a) = 10(2.5 + 1.086 \ln \mathrm{Chl}\,a) \quad (2)$$

Evaluation standard: $0 < \mathrm{TSI} \leq 30$ oligotrophic, $30 < \mathrm{TSI} \leq 50$ mesotrophic, $\mathrm{TSI} > 50$ eutrophic, > 70 high eutrophic.

2.5 Canadian Council of Ministers of the Environment Water Quality Index

The evaluation of index scores in CCME WQI is obtained as stated in the literature (CCME, Canadian Council of Ministers of the Environment, 2001; Feng et al., 2018; Zhu et al., 2019):

$$\mathrm{WQI} = 100 - \frac{\sqrt{\left(F_1^2 + F_2^2 + F_3^2\right)}}{1.732} \quad (3)$$

where F_1^2, F_2^2 , and F_3^2 represent scope (number of variables, whose objectives are not met), frequency (number of times by which the objectives are not met), and amplitude (the amount by which the objectives are not met), respectively, and are calculated as follows:

$$F_1 = \frac{no.\ of\ failed\ variables}{total\ no.\ of\ variables} \times 100 \quad (4)$$

$$F_2 = \frac{no.\ of\ failed\ tests}{total\ no.\ of\ tests} \times 100 \quad (5)$$

$$F_3 = \frac{nse}{0.01nse + 0.01} \quad (6)$$

$$nse = \frac{\sum excursion}{total\ no.\ of\ tests} \quad (7)$$

$$excursion = \frac{failed\ tests\ test}{standard\ value} - 1 \quad (8)$$

Water quality is categorized into five different categories based on the WQI scores: *Poor* (0–44), *Marginal* (45–64), *Fair* (65–79), *Good* (80–94), and *Excellent* (95–100). According to the environmental quality standards for surface waters (GB3838–2002) (**Table 1**) in China, the water quality in the mangrove forest during both seasons were classified as grade III with a nitrogen concentration limit of 1 mg/L and a phosphorus concentration limit of 0.05 mg/L (Ministry of Environment Protection of the People's Republic, 2010; Ministry of Environment Protection of the People's Republic, 2011).

2.6 Phytoplankton Alpha-Diversity Indices

The phytoplankton assemblage diversity was measured using univariate statistics, such as alpha-diversity indices. This was made possible using the software package PRIMER© version 7 (Plymouth Marine Laboratory, U.K.), and following the methods described in Clarke and Warwick (2001) and Clarke and Gorley (2006). Besides the Species richness (*S*), expressed as the number of species per sample, the alpha-diversity indices were also evaluated. These included the Shannon index (H'), the Margalef index (d), Pielou's (J') diversity, Simpson's (λ) dominance, and inverted Simpson's ($1 - \lambda$) index.

2.7 Statistical Analysis

Statistical analysis was carried out with the aid of XLSTAT (2016 version), SPSS (version 22.0), PAST 3, and PRIMER 7. Student's *t*-test analysis was carried out with the aid of XLSTAT (2016 version), while Pearson's correlation was performed *via* SPSS (version 22.0) at a significant level ($p < 0.01$) and ($p < 0.05$). CCA ordination plot was carried through PAST 3.

3. RESULTS

3.1 Environmental Characteristics and Pollution Indices Fluctuation

The univariate statistics of the environmental characteristics of the 11 water quality parameters including pollution indices across the mangrove forest in two different seasons (dry and wet) are given in **Table 2**. The pH was within the range for surface water standard limit and showed no significant difference between the two seasons ($p < 0.05$) while turbidity fluctuated above the limit across most of the sampling sites during both seasons and showed no significant difference between the two seasons. Electrical conductivity, total dissolved solids, nitrate, and phosphate were significantly different between the two seasons ($p < 0.05$ or $p < 0.01$). However, EC, TDS, and phosphate values in most of the sampling sites were above the standard limit, whereas nitrate was below the limit value in most of the sites during the wet season but above its limit value in the Pearl River axis of the Guangdong coast during the dry season.

The calculated surface water quality index according to the CCME method (**Figure 3**) showed no significant difference between the two seasons ($p < 0.05$) (**Tables 3**, **4**). These values were basically within the range of *poor* and *marginal* category. Meanwhile, only at sites gd-21 in the wet season and gd-27 in the dry season was the water quality index recorded > 70 (*fair*). The sampling sites gd-33 to gd-38 were under *poor* water quality category during both seasons. The single-factor trophic state index analysis (TSI Chl *a*) showed a significant difference between the two seasons ($p < 0.01$). Its index value in the dry season was under mesotrophic to eutrophic state, while in the wet season, it was basically mesotrophic to oligotrophic (**Figure 4**). Based on environmental variable pattern and TSI, we found that pH, TDS/salinity, nitrate, and phosphate were positively correlated with TSI, and were vital components of an ecological process that influenced the trophic state in the mangrove forest.

According to Palmer (1969), a total of 18 species and 18 genera were identified as pollution-tolerant indicators during the wet season, whereas in the dry season, a total of 14 species and 16 genera were identified (**Table 5**). These indicator species consist of diatoms, cyanobacteria, green algae, and euglena (e.g., *Cyclotella*, *Navicula*, *Nitzschia* and *Synedra*, *Gomphonema*,

TABLE 2 | The temporal and spatial variation of environmental parameters and pollution indices during study period.

	pH	Temp (°C)	EC (µs/cm)	TDS (ppt)	Salinity	Turbidity (NTU)	Nitrate (mg/L)	Nitrite (mg/L)	Phosphate (mg/L)	Silicate (mg/L)	Chl. *A* (mg/m³)	CCME: WQI	TSI (Chl.*A*)	AGPI	ASPI
Dry season	8.04 ±0.39	20.38 ±3.88	33.11 ±14.52	10.44 ±5.89	18.96 ±6.97	80.48 ±94.05	2.31 ±3.18	0.04 ±0.03	0.65±0.72	1.79 ±0.54	8.38 ±8.78	47.84 ±10.86	43.31 ±10.76	19.10 ±5.06	13.03 ±6.75
Wet season	7.96 ±0.33	30.09 ±2.45	3745 ±1966.2	14.67 ±5.96	12.67 ±7.54	59.26 ±41.23	0.13 ±0.46	0.11 ±0.37	0.46±0.69	2.25 ±0.37	1.8±2.79	47.96 ±12.99	25.11 ±11.17	23.82 ±6.54	16.57 ±6.36
T-test	Not Sign.	Sign	Sign.	Not Sign.	Sign.	Sign.	Sign.	Sign.	Sign.	Sign.	Sign.	Not Sign.	Sign.	Sign.	Sign.
Dry x Wet	p < 0.05	p < 0.01	p < 0.01	p < 0.05	p < 0.01	p < 0.05	p < 0.01	p < 0.01	p < 0.01	p < 0.01	p < 0.01	p < 0.05	p < 0.01	p < 0.01	p < 0.05

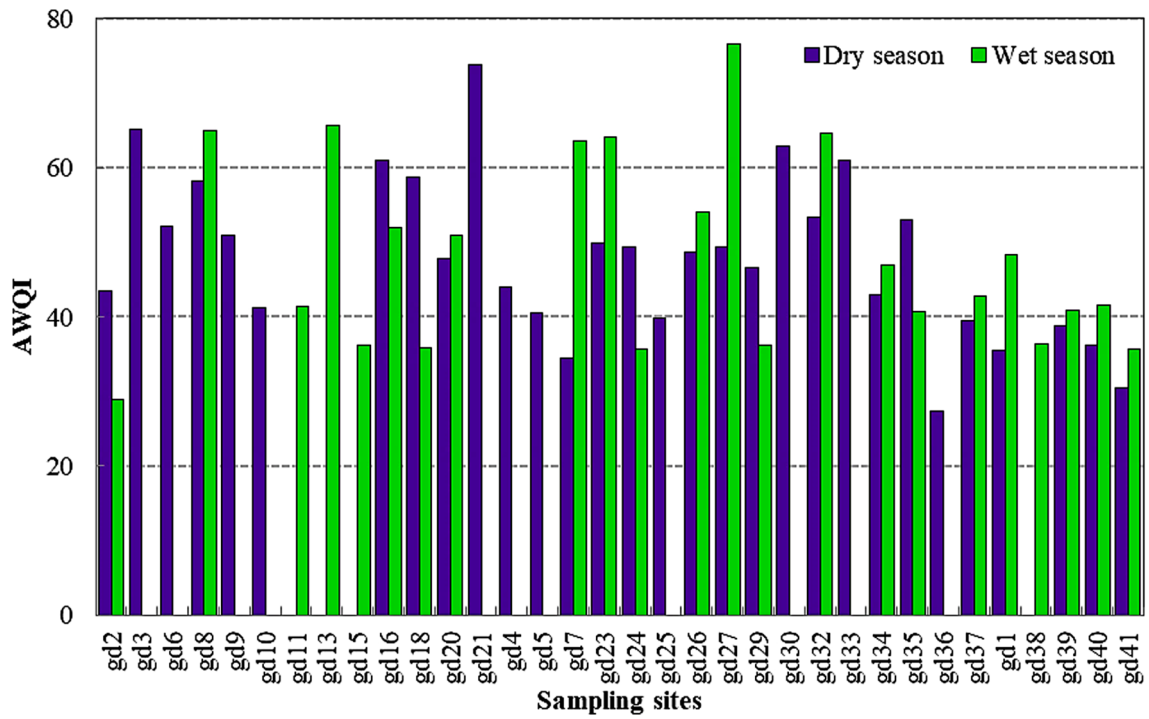

FIGURE 3 | Aquatic water quality index of the mangrove forest at different locations using the CCME method.

TABLE 3 | Algal Genera and species of pollution interest that are included in the Palmer, 1969 and were detected in the mangroves.

Taxa number	Genera index	Pollution index value	Species index	Pollution index value
1	*Microcystis*	1	*Ankistrodesmus falcatus*	3
2	*Ankistrodesmus*	2	*Cyclotella meneghiniana*	2
3	*Closterium*	1	*Euglena gracilis*	1
4	*Cyclotella*	1	*Euglena viridis*	6
5	*Euglena*	5	*Gomphonema parvulum*	1
6	*Gomphonema*	1	*Melosira varians*	2
7	*Lepocinclis*	1	*Navicula crptocaphala*	1
8	*Melosira*	1	*Nitzschia acicularis*	1
9	*Navicula*	3	*Nitzschia palea*	5
10	*Nitzschia*	3	*Oscillatoria limosa*	4
11	*Oscillatoria*	5	*Oscillatoria princeps*	1
12	*Pandorina*	1	*Oscillatoria tenuis*	4
13	*Phacus*	2	*Pandorina morum*	3
14	*Phormidium*	1	*Scenedesmus quadricauda*	4
15	*Scenedesmus*	4	*Stigeoclonium tenue*	3
16	*Stigeoclonium*	2	*Synedra ulna*	3
17	*Synedra*	2	*Arthrospira jenneri*	2
18	*Micractinium*	1	*Chlorella vulgaris*	2
19	*Chlorella*	2	**Total**	**48**
	Total	**39**		

The bold values are the summation value of all the species index values at Genera index and Species index respectively.

Melosira, *Microcystis*, *Oscillatoria*, *Phormidium*, *Scenedesmus Closterium*, *Pandorina*, *Stigeoclonium*, *Lepocinclis*, and *Phacus*). The micro plates of these species are given in **Plate 1**.

Moreover, the spatial and temporal variation of the algal genus pollution index (AGPI) in the mangrove forest was significantly different between the two seasons ($p < 0.01$) (**Table 2**). The mean AGPI in the dry season was 19.10 ± 5.06, significantly lower than that in the wet season (mean = 23.82 ± 6.54) ($p < 0.01$). The AGPI confirmed that all sampling sites in the dry season experienced moderate to very high organic

TABLE 4 | The correlation coefficients found by Pearson's correlation analysis of alpha diversity indices, CCME-WQI, AGPI, ASPI, and TSI (Chl*A*) in the mangrove forest.

Dry season																		
	pH	**TDS**	**Salinity**	**Turbidity**	**Tem**	**EC**	**Phosphate**	**Nitrate**	**Nitrite**	**Silicate**	**Chl*A***	**d**	**J'**	**H'**	**1-λ**	**CCME**	**TSI**	**AGPI**
d	-0.109	0.057	-0.051	-0.078	-0.037	-0.054	-0.426*	-0.105	-0.286	0.118	-0.476**	1						
J'	-0.239	-0.084	-0.125	0.322	-0.380*	0.338	-0.685**	-0.275	-0.239	0.203	-0.474**	0.573**	1					
H'	-0.225	-0.045	-0.122	0.262	-0.329	0.284	-0.680**	-0.248	-0.301	0.201	-0.506**	0.741**	0.973**	1				
1-λ	-0.227	-0.076	-0.175	0.134	-0.316	0.129	-0.628**	-0.185	-0.185	0.225	-0.471**	0.625**	0.918**	0.920**	1			
CCME	-0.045	0.020	0.109	0.325	-0.515**	0.432*	-0.570**	-0.340	-0.507**	0.150	-0.308	0.230	0.538**	0.515**	0.429*	1		
TSI	0.509**	-0.319	0.235	0.259	-0.110	0.266	0.472**	0.406*	0.070	-0.089	0.841**	-0.339	-0.232	-0.261	-0.194	-0.085	1	
AGPI	-0.118	0.102	-0.137	-0.459*	0.020	-0.570**	-0.037	-0.071	0.363*	-0.324	-0.307	0.148	-0.132	-0.089	0.053	-0.273	-0.330	1
ASPI	-0.222	0.229	-0.091	-0.333	-0.001	-0.378*	-0.065	-0.059	-0.073	-0.096	-0.280	0.331	-0.136	-0.007	0.095	-0.062	-0.189	0.572**
Wet season																		
	pH	TDS	Salinity	Turbidity	Tem	EC	Phosphate	Nitrate	Nitrite	Silicate	Chl*A*	d	J'	H'	1-λ	CCME	TSI	AGPI
d	-0.471*	-0.322	-0.347	-0.055	-0.194	0.211	0.080	-0.013	0.053	0.377	-0.425*	1						
J'	-0.486*	-0.257	-0.303	-0.058	-0.172	0.094	-0.040	0.044	0.166	0.105	-0.073	0.518*	1					
H'	-0.538**	-0.296	-0.343	-0.069	-0.203	0.142	0.013	0.044	0.171	0.167	-0.200	.695**	.972**	1				
1-λ	-0.471*	-0.329	-0.374	-0.079	-0.181	0.177	0.026	0.105	0.191	0.190	-0.068	.592**	.891**	.903**	1			
CCME	0.284	0.134	0.172	-0.111	0.210	-0.254	-0.831**	-0.322	-0.374	-0.204	-0.015	-0.172	0.001	-0.061	-0.06	1		
TSI	0.064	0.174	0.185	0.178	0.107	-0.007	-0.080	0.063	0.028	-0.069	0.794**	-0.320	-0.121	-0.202	-0.110	0.087	1	
AGPI	-0.654**	-0.582**	-0.654**	-0.011	-0.183	0.215	-0.009	0.142	0.278	-0.089	-0.264	0.630**	0.602**	0.674**	0.553**	-0.079	-0.193	1
ASPI	-0.433*	-0.468*	-0.525*	-0.153	-0.293	0.419*	0.068	0.429*	0.455*	0.177	-0.286	0.662**	0.327	0.454*	0.434*	-0.264	-0.12	0.694**

*Correlation is significant at the 0.05 level (2-tailed). **Correlation is significant at the 0.01 level (2-tailed).

pollution (**Figure 5**). More so, all the sampling sites in the wet season experienced moderate to very high organic pollution except gd-23, where no evidence of organic pollution was detected (**Figure 5**). Furthermore, the evaluation of organic pollution status at the algal species level in the mangrove forest revealed that numerous sampling sites were organically threatened during the dry and wet season (**Figure 6**). The spatiotemporal distribution of the organic pollution indicator genera and species (**Table 5**) was significantly affected by water quality parameters ($p < 0.05$ or $p < 0.01$) (**Table 6**).

3.2 Alpha-Diversity Index and Its Relationship With Water Quality Parameters

The *t*-test results showed no significant difference in the spatiotemporal variation of alpha-diversity indices across the mangrove forest ($p < 0.05$) (**Table 2**). The mean value of the Margalef index was 16.71 ± 4.78 in the dry season and 14.82 ± 3.38 in the wet season. The peak value of the Margalef index was reported at the Leizhou Peninsula (gd-9: 26.91) during the dry season and at the midsection of the Guangdong coast (gd-34: 21.05) during the wet season (**Figure 7**). We noted that different environmental variables affected the species richness during the dry and wet season. TDS/salinity, nitrate, phosphate, and silicate affected the Margalef index during the dry season while pH, EC, TDS/salinity, and silicate significantly affected it during the wet season (**Table 6**). These results revealed that increased EC and nutrient concentrations promote the phytoplankton species richness in the mangrove forest. The Pielou index was 0.68 ± 0.17 in the dry season and 0.62 ± 0.12 in the wet season. Like the Margalef index, the maximum value of the Pielou index was recorded at the midsection of the Guangdong coast (gd-34: 0.85) during the wet season and at the Leizhou Peninsula (gd-21: 0.91) during the dry season (**Figure 7**). The Pielou index is a signal to indicate community species evenness. Our results confirmed that increased salinity in the dry season and EC in the wet season are beneficial factors for species evenness across the mangrove forest (**Table 6**). Variation on the Shannon–Weaver index (species diversity) across the mangrove forest was influenced by different environmental variables, which included the Margalef and Pielou indices. However, the *t*-test showed that seasonal change had a slight influence on the Shannon–Weaver index ($p > 0.05$). The mean value of the Shannon–Weaver index during the dry season and wet season was 3.29 ± 0.86 and 3.02 ± 0.63, respectively (**Figure 7**). Our results confirmed that the Shannon–Weaver index was controlled by increased TDS/salinity and nutrient salts during the dry season, and by increased EC level and nutrient salts concentration in the wet season ($p < 0.05$) (**Table 6**). pH and salinity played a negative significant influence on the Shannon–Weaver index during the wet season ($p < 0.01$) (**Table 6**). The spatial distribution of the Simpson index in both dry and wet periods in the mangrove forest was very similar to that of the Shannon–Weaver index (**Figure 7**). Like the Shannon–Weaver index, the variation of the Simpson index was influenced by the same environmental variables during the dry and wet seasons, respectively (**Table 6**) ($p < 0.05$). The Simpson index mean value

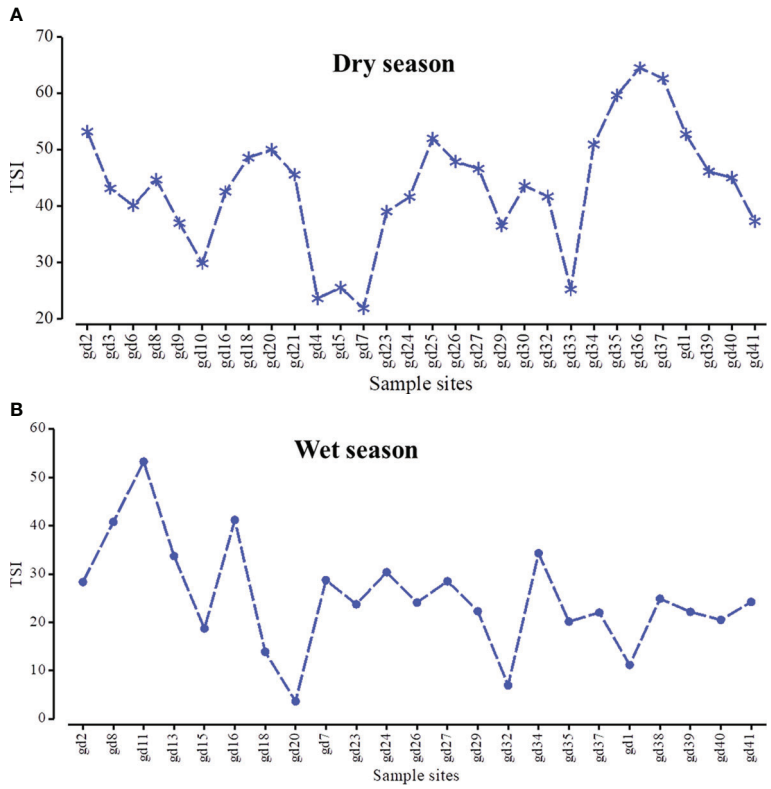

FIGURE 4 | The spatial distribution of trophic state index in dry **(A)** and wet **(B)** seasons across the mangrove forest.

TABLE 5 | The calculated indices values during the dry season across the mangroves.

Sites	CCEM	TSI (Chl.*A*)	AGPI	ASPI	d	J'	H'	1-λ
gd2	43.48	53.21	16	18	12.99	0.65	3.05	0.93
gd3	65.07	43.17	19	8	13.63	0.69	3.2	0.88
gd6	52.08	40.12	20	11	19.31	0.77	3.83	0.95
gd8	58.25	44.68	19	14	11.37	0.67	3.03	0.92
dgd9	50.99	37.02	15	16	26.91	0.82	4.41	0.98
gd10	41.12	29.85	26	2	10.44	0.81	3.42	0.95
gd16	60.9	42.57	25	24	12.5	0.69	3.17	0.93
gd18	58.72	48.62	17	11	19.05	0.8	3.98	0.96
gd20	47.83	50.03	14	8	15.42	0.79	3.72	0.95
gd21	73.73	45.57	17	13	21.33	0.91	4.52	0.98
gd4	44.02	23.65	27	24	21.85	0.58	3.08	0.89
gd5	40.46	25.56	27	14	23.56	0.75	3.93	0.95
gd7	34.48	21.9	16	9	8.743	0.31	1.3	0.52
gd23	49.82	39.04	15	16	20.11	0.74	3.78	0.95
gd24	49.29	41.63	15	16	17.49	0.74	3.64	0.94
gd25	39.77	52.03	15	2	20.58	0.81	4.03	0.95
gd26	48.6	47.88	13	6	14.87	0.83	3.84	0.97
gd27	49.43	46.66	17	21	17.36	0.65	3.32	0.91
gd29	46.52	36.51	20	13	22.15	0.84	4.28	0.97
gd30	62.82	43.61	15	13	21.31	0.73	3.73	0.95
gd32	53.32	41.72	16	7	17.9	0.75	3.67	0.94
gd33	60.89	25.26	15	8	17.11	0.84	3.98	0.97
gd34	42.89	50.93	27	19	19.09	0.58	3.01	0.89
gd35	52.95	59.68	20	10	14.37	0.57	2.73	0.84
gd36	27.4	64.53	14	7	11.72	0.48	2.18	0.79

(Continued)

TABLE 5 | Continued

Sites	CCEM	TSI (Chl.A)	AGPI	ASPI	d	J'	H'	1-λ
gd37	39.38	62.65	14	7	5.44	0.21	0.8	0.36
gd1	35.43	52.76	22	12	12.87	0.69	3.14	0.91
gd39	38.85	46.14	19	10	14.98	0.59	2.87	0.89
gd40	36.18	45.05	27	20	16.58	0.35	1.77	0.68
gd41	30.44	37.32	31	32	20.25	0.63	3.29	0.9

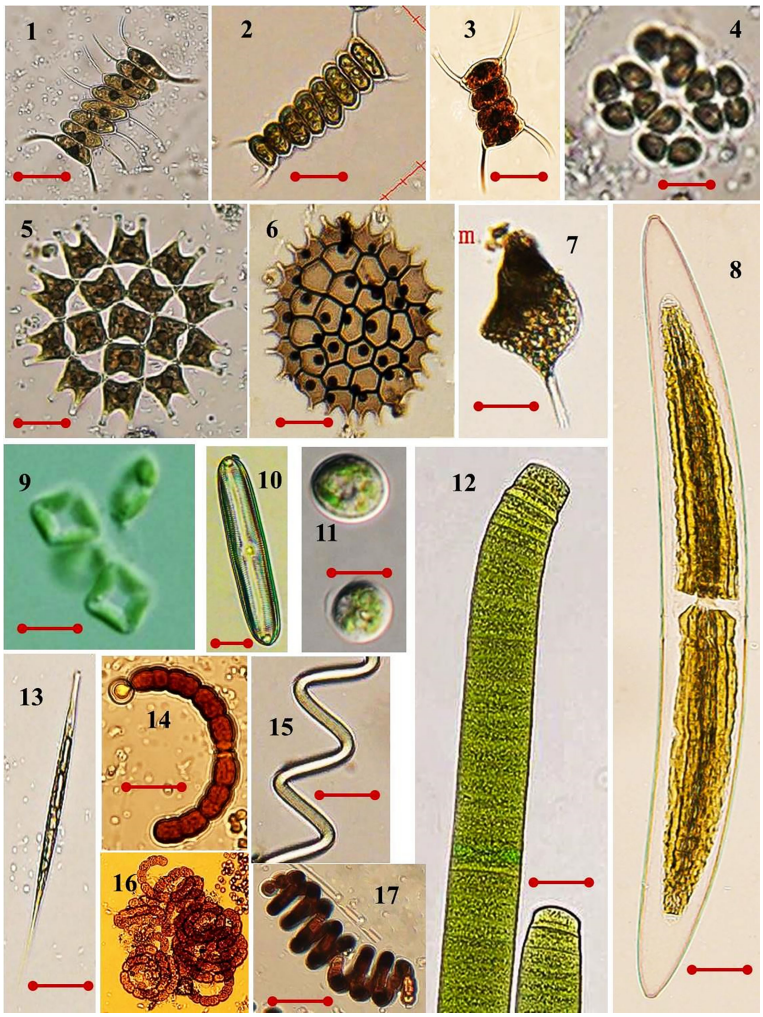

PLATE 1 | Some optical images of high organic tolerant microalgae that was present in the studied area. (1) *Scenedesmus quadricauda* var. *biornatus* f. *giganticus* (av. diam. 10 μm); (2) *S. armatus* (av. diam. 6.5 μm); (3) *S. quadricauda* (av. diam. 6 μm); (4) *Crucigenia quadrata* (av. diam. 5.5 μm); (5) *Pediastrum duplex* (av. diam. 13.5 μm); (6) *Pediastrum boryanum* (av. diam. 16 μm); (7) *Phacus longicauda* (av. diam. 31 μm); (8) *Closterium acerosum* (av. diam. 53 μm); (9) *Crucigenia fenestrate* (av. diam. 3.5 μm); (10) *Pinnularia viridis* (av. diam. 20.7 μm); (11) *Scenedesmus obliquus* (av. diam. 16 μm); (12) *Oscillatoria princeps* (av. diam. 25 μm); (13) *Lepocinclis acus* (av. diam. 15 μm); (14) *Anabaena circinalis* (av. diam. 10 μm); (15) *Arthrospira jenneri* (av. diam. 4 μm); (16) *A. spiraoides* (av. diam. 8 μm); (17) *S. subsalsa* (av. diam. 4 μm). Scale bar = 10 μm. LM magnification ×200.

was 0.89 ± 0.14 in the dry season and 0.87 ± 0.09 in the wet season. The correlation analysis showed that the alpha-diversity indices across the mangrove forest were significantly positively correlated with each other in both seasons ($p < 0.01$) (**Table 6**).

3.3 Relationship Between Alpha-Diversity Indices and Water Quality Indices

Correlation analysis showed that the CCME: WQI in the dry season was significantly positively correlated with the Pielou

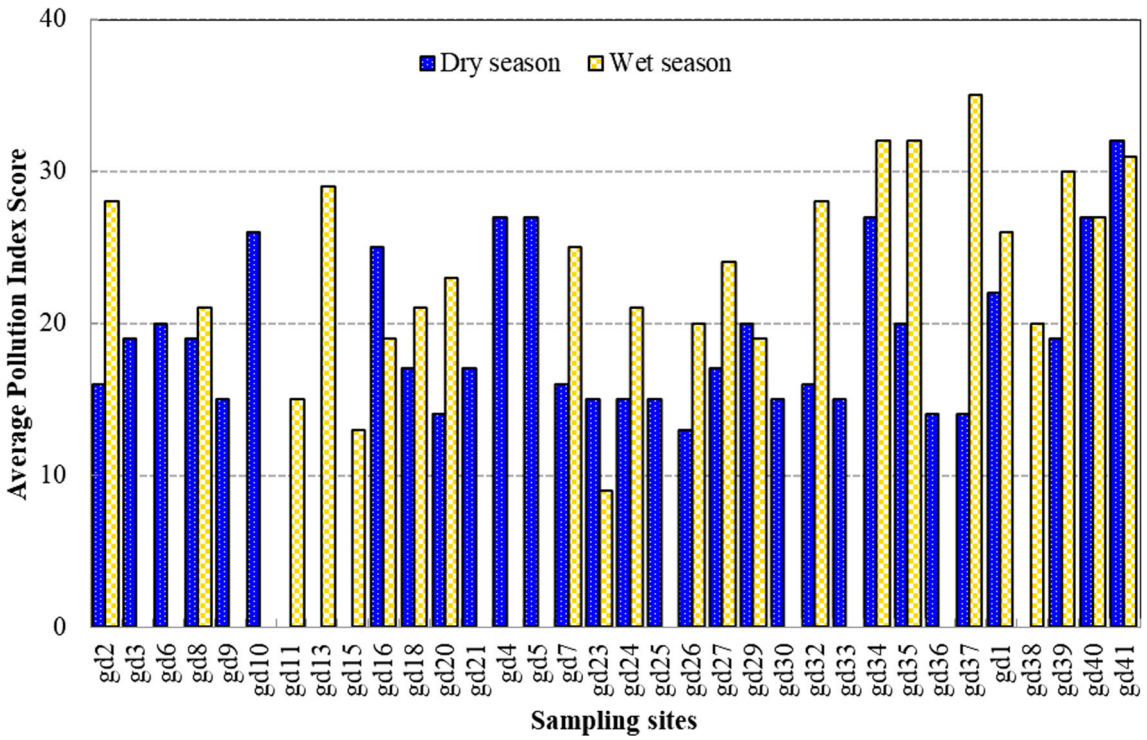

FIGURE 5 | The temporal and spatial variation of the algal genera pollution index score during the study period.

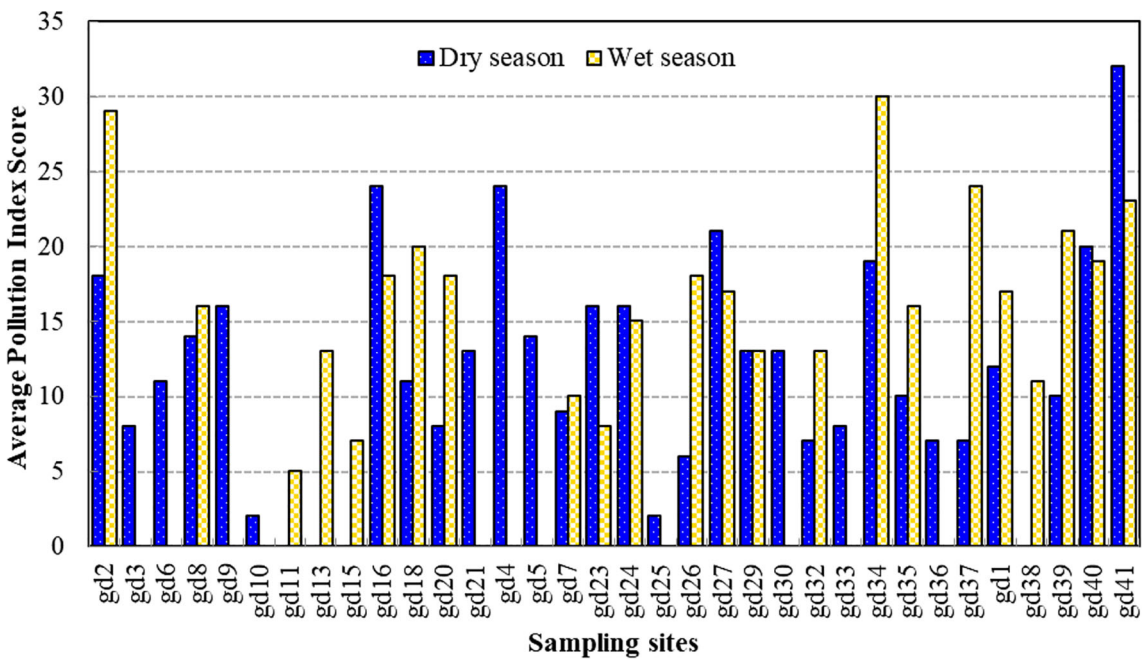

FIGURE 6 | The temporal and spatial variation of the algal species pollution index score during the study period.

TABLE 6 | The calculated indices values during the wet season across the mangroves.

Sites	CCEM	TSI (Chl.*A*)	AGPI	ASPI	d	J'	H'	1-λ
gd2	28.91	28.34	28	29	14.6	0.65	3.14	0.91
gd8	65.04	40.76	21	16	11.41	0.69	3.12	0.91
gd11	41.33	53.27	15	5	7.425	0.56	2.33	0.83
gd13	65.63	33.71	29	13	14.35	0.62	2.96	0.84
gd15	36.2	18.7	13	7	8.693	0.36	1.65	0.66
gd16	51.92	41.19	19	18	17.49	0.61	3.08	0.87
gd18	35.82	13.9	21	20	14.87	0.61	2.94	0.85
gd20	50.83	3.65	23	18	17.44	0.51	2.62	0.86
gd7	63.54	28.73	25	10	11.15	0.49	2.26	0.73
gd23	64.04	23.73	9	8	9.669	0.51	2.29	0.83
gd24	35.57	30.37	21	15	15.8	0.54	2.74	0.87
gd26	53.96	24.09	20	18	13.66	0.46	2.22	0.68
gd27	76.62	28.5	24	17	14.69	0.64	3.12	0.93
gd29	36.2	22.3	19	13	14.37	0.49	2.39	0.84
gd32	64.63	6.96	28	13	16.3	0.85	4.05	0.97
gd34	46.92	34.28	32	30	21.05	0.62	3.28	0.91
gd35	40.64	20.15	32	16	15.44	0.76	3.63	0.93
gd37	42.77	22.02	35	24	19.06	0.68	3.52	0.94
gd1	48.23	11.18	26	17	17.21	0.69	3.45	0.93
gd38	36.28	24.89	20	11	19.65	0.78	3.98	0.96
gd39	40.92	22.16	30	21	14.81	0.7	3.42	0.95
gd40	41.53	20.49	27	19	15.7	0.77	3.75	0.95
gd41	35.63	24.21	31	23	16.06	0.72	3.55	0.94

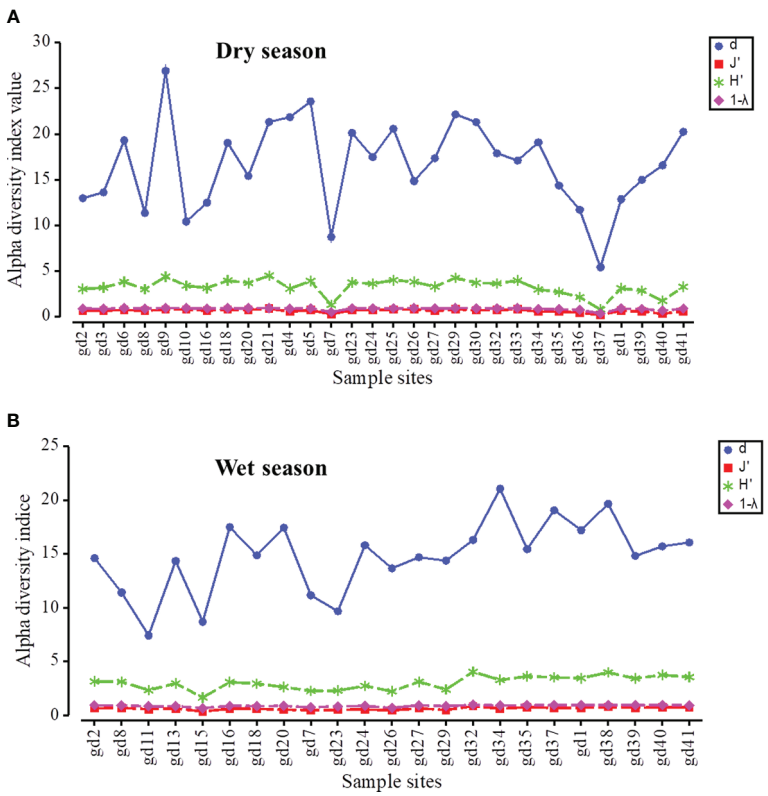

FIGURE 7 | The spatial distribution of phytoplankton alpha-diversity indices during dry **(A)** and wet **(B)** seasons. (*d* = Margalef index; *J′* = Pielou index; *H′* = Shannon–Weaver index; 1 − *λ* = Simpson index).

index, Shannon index, and Simpson index ($p < 0.05$ or $p < 0.01$) (**Table 6**). This implies that the water quality (*poor* to *marginal* category) factors during the dry season influenced the species evenness, diversity, and dominance. The TSI was negatively correlated with the alpha-diversity indices in both seasons ($p < 0.05$) (**Table 6**). The correlation analysis of AGPI and ASPI during the dry season showed no significant relationship with all the diversity indices; instead, a significant positive correlation was recorded in the wet season ($p < 0.01$). This implies that a greater proportion of the phytoplankton species in the mangrove forest were made up of organic pollution indicators.

The multivariate statistical relationships of the algal indices, algal pollution indices, trophic state index, and environmental parameters revealed that the canonical axes of algal indices/environmental parameters during the dry and wet season significantly accounted for 97.56% (*pseudo-F* = 0.27, $p < 0.001$), whose axes 1 and 2 explained 95.22% (Eigenval = 0.26, $p = 0.001$) and 2.34% (Eigenval = 0.006, $p = 0.033$) variation, respectively (**Figure 8**). This explains the fact that the applied indices and TSI during both seasons related positively to the environmental parameters on each axis.

4 DISCUSSION

Phytoplankton diversity indices have been shown to be a useful approach in the evaluation of community structure (e.g., evenness, richness, function, and stability) (Mousing et al., 2016); specifically, phytoplankton alpha-diversity indices have been applied as a tool for trophic state assessment and monitoring of the potential harmful algae blooms (Yang et al., 2016; Katsiapi et al., 2020; Meng et al., 2020). Deduction of ecological traits, which include ecological information of richness, abundance, and evenness, is the main advantage of phytoplankton alpha-diversity index evaluation (Mousing et al., 2016; Tian et al., 2017). Also, the evaluation of algal pollution indices that make use of pollution-tolerant taxa as developed by Palmer (1969) has the potential of detecting early signs of organic pollution in coastal ecosystems before reaching eutrophication state without chemical analysis of the water body. Organic pollution has become a major concern in the mangrove forest due to increased urbanization, aquaculture, agricultural activities, and tourism (Adam et al., 2018; Temino-Boes et al., 2019; Inyang and Wang, 2020). In this study, it is hypothesized that the phytoplankton alpha-diversity indices and algal pollution indices have the potential to provide a signal linking trophic state and water quality index variation in the mangrove forest. Moreover, our results showed that the phytoplankton alpha-diversity indices and algal pollution indices relate to the water quality parameters, presenting an obvious variation in seasonal scale. In addition, the phytoplankton alpha-diversity indices and algal pollution indices had a close relation with the trophic states index and CCME: WQI as revealed by the multivariate analysis. All of these findings verified our hypothesis that the phytoplankton alpha-diversity indices and algal pollution indices were a potential signal for indicating environmental variations in the mangrove forest.

4.1 Impact of Water Quality Fluctuation on Algal Indicator Species

The mangrove forest in China had been burdened by sewage (Wong et al., 1997; Wu et al., 2008) from households and

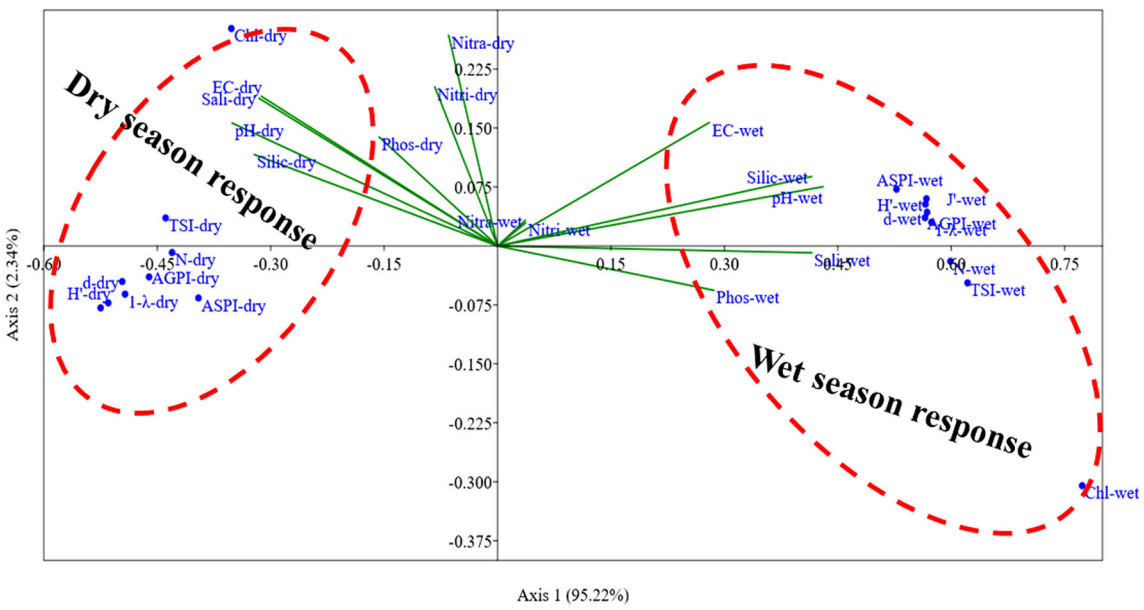

FIGURE 8 | CCA ordination showing the response relationship of the biodiversity indices, trophic state indices, and environmental variables in the mangrove ecosystem during dry and wet seasons. (N, algal abundance; *d*, Margalef index; *J'*, Pielou index; *H'*, Shannon–Weaver index; 1 – λ, Simpson index; AGPI, Algal genus pollution index; ASPI, Algal species pollution index; EC, Electrical conductivity; Sali, salinity; Chl, Chlorophyll-*a*; Nitra, Nitrate; Nitri, Nitrite; Phos, phosphate; Silic, Silicate).

industries, and by aquaculture wastewater, which has resulted in the deterioration of the forest in some places (**Figure 2**). Regina et al. (2019) pointed out that the development of tourism, agricultural facilities, and urban cities along the coast causes serious mangrove degradation in Mexico. The CCME: WQI had revealed that the water quality in the mangrove forest remained under *poor* and *marginal* conditions in both seasons, indicating the impact of the discharged effluent from the river, aquaculture facilities, farmland, and coastal industries (Inyang and Wang, 2020). In the present study, the nutrient parameters, EC, TDS, and turbidity showed a significant spatiotemporal difference ($p < 0.05$), which directly affects the diversity and dispersal of phytoplankton in the forest (Saifullah et al., 2014). Thus, the dynamics of algal assemblage can be an excellent bio-indicator in spatial and temporal monitoring of the forest.

The changes in hydrodynamics and the seasonal environmental change act as driving factors for phytoplankton abundance (Mohammad-Noor et al., 2013) and productivity (Pradhan and Shaikh, 2011). This indicates that the dynamic characteristics of the phytoplankton community in the mangrove forest are closely linked to the water quality parameter fluctuation. It was found that diatom indicator species dominate the plankton community and are more abundant in the wet season than in the dry season ($p < 0.05$). In contrast, indicator species of cyanobacteria and euglena showed no significant variation in abundance during wet and dry periods. It was noted that the motile species of cyanobacteria and euglena were predominant in the forest. During the wet season, it was discovered for low concentrations of nitrate and nitrite, which corresponded with a high abundance of *Pseudanabaena* sp. The EC and nutrients strongly influenced indicator species of cyanobacteria, green algae, and euglena (Yuan et al., 2018; Meng et al., 2020).

4.2 Alpha-Diversity Indices and Algal Pollution Indices' Response to Water Quality Indices

Recent studies suggest that environmental variables may be vital for influencing phytoplankton alpha-diversity patterns (Yang et al., 2016; Tian et al., 2017). In this study, which is based on spatial correlation analysis, it was found that EC, turbidity, and temperature were considerable factors in the fluctuation range of the phytoplankton alpha-diversity pattern other than nutrient salts in the dry season. pH, TDS, and salinity affect the phytoplankton alpha-diversity pattern in the wet season. These results showed that alpha-diversity was not significantly different between the two seasons, suggesting that the seasonal changes in hydrological characteristics did not necessarily promote the richness and evenness in the phytoplankton community temporally. Meanwhile, alpha-diversity is considered positively dependent on catchment characteristics (Stefanidou et al., 2020). Increases in the Shannon–Weaver, Simpson, and Pielou indices were primarily interpreted as indicators of community stability and improved trophic status (Yang et al., 2020).

The Simpson, Margalef, and Pielou indices were negatively correlated with TSI during both seasons, and positively significantly correlated with CCME: WQI in the dry season ($p < 0.01$). Meanwhile, the Margalef index is recorded as a signal for indicating the richness of the community in aquatic and terrestrial ecosystems (Yang et al., 2016). It also was found that pH, TDS, and salinity relatively influenced the phytoplankton richness through the exchange of water and nutrients in the wet season. High EC and trophic state with low salinity and pH provide an appropriate condition for colonization of cyanobacteria and green algae indicator species. The mangrove forest's environmental conditions, such as shallow and calm water and a high trophic state, create a unique habitat and provide ambient conditions for phytoplankton proliferation. This study revealed that the Margalef and Pielou indices presented a significant correlation with pollution indices (AGPI and ASPI). This implied that the main Palmer pollution indices depend on the species richness and the presence of individual indicator taxa. This correlation is governed by water quality variation. In addition, we inferred that the relevant phytoplankton index assessment could be made by a corresponding ordination analysis for visualizing the interaction of phytoplankton diversity, trophic indices, and nutrient concentrations through multivariate statistical methods. However, our ordination evaluation revealed that the trophic state indices relate significantly with the alpha indices and with the nutrient variation during both seasons (**Figure 8**) ($p < 0.001$). Understanding the relationships between diversity indices and trophic state aspects remains a challenge in coastal water research, and at the same time, it is essential for establishing water management databases on a larger spatial and temporal scale.

5 CONCLUSIONS

The possibility of algal indices (alpha-diversity and algal pollution indices) to serve as a biological indicator to assess water quality variation in the mangrove forest was investigated in the present study. The multivariate statistical analysis revealed that environmental variables (like pH, TDS, salinity, EC, and nutrients) strongly influenced the alpha-diversity indices and trophic states during different sampling seasons. Spatially, the water quality variables relatively impacted the algal indices during the dry and wet season due to the differences in catchment characteristics. Based on the CCME: WQI evaluation, the surface water of the Guangdong mangrove forest experiences various levels of enrichment across the sampling sites. TDS, EC, turbidity, nitrate, and phosphate were above the surface water standard limit in most of the studied sites during both seasons. Because of the pressure from fish farming facilities, tourist activities, agricultural activities, and urban cities, the Leizhou Peninsula and other parts of the Guangdong coast experienced mesotrophic to eutrophic state pollution during both seasons. The pollution indicator species showed a seasonal variation in its distribution pattern, probably due to the temporary changes in water quality variables. The development of integrated algal indices is beneficial for environmental regulation since the mangrove forest is very important for the production, diversity, relative abundance, and fecundity of phytoplankton.

DATA AVAILABILITY STATEMENT

The raw data supporting the conclusions of this article will be made available by the authors, without undue reservation.

AUTHOR CONTRIBUTIONS

AI: methodology, software, data curation, and writing—original draft preparation. Y-SW: conceptualization, supervision, and writing—reviewing and editing. HC: investigation and writing—reviewing. All authors contributed to the article and approved the submitted version.

FUNDING

This research was supported by the National Key Research and Development Program of China (No. 2017FY100700), the National Natural Science Foundation of China (No. U1901211 and No. 41876126), the International Partnership Program of Chinese Academy of Sciences (No. 133244KYSB20180012), the Key Special Project for Introduced Talents Team of Southern Marine Science and Engineering Guangdong Laboratory (Guangzhou) (No. GML2019ZD0305), and the Strategic Priority Research Program of the Chinese Academy of Sciences (No. XDA23050200 and No. XDA19060201).

REFERENCES

Adam, M. F., Najera, E., Lovelock, C. E., and Brown, C. J. (2018). Avoided Emissions and Conservation of Scrub Mangroves: Potential for a Blue Carbon Project in the Gulf of California, Mexico. *Biol. Lett.* 14, 20180400. doi: 10.1098/rsbl.2018.0400

Adhavan, D., Marimuthu, N., Tikadar, S., and Sivakumar, K. (2015). Impact of Algal Bloom on Mangrove and Coral Reef Ecosystem in the Marine National Park, Gulf of Kachchh, Gujarat, India. *J. Mar. Biol. Aquacult.* 1, 1–2. doi: 10.15436/2381-0750.15.006

Bellinger, E., and Sigee, D. (2010). "Algae as Bioindicators," in *Freshwater Algae: Identification and Use as Bioindicators*. Eds. E. Bellinger and D. Sigee (Chichester: John Wiley & Sons, Ltd Inc), 99–136.

Bergstrom, A. K., Jonsson, A., Isles, P. D. F., Creed, I. F., and Lau, D. C. P. (2020). Changes in Nutritional Quality and Nutrient Limitation Regimes of Phytoplankton in Response to Declining N Deposition in Mountain Lakes. *Aquat. Sci.* 82, 31–47. doi: 10.1007/s00027-020-0697-1

Carlos, A. R. S., Sérgio, R. O., Ronaldo, D. P. R., and Antonio, A. M. (2007). Dynamics of Phosphorus and Nitrogen Through Litter Fall and Decomposition in a Tropical Mangrove Forest. *Mar. Environ. Res.* 64, 4524–4534. doi: 10.1016/j.marenvres.2007.04.007

CCME (Canadian Council of Ministers of the Environment) (2001). "Canadian Water Quality Guidelines for the Protection of Aquatic Life: CCME Water Quality Index 1.0, User's Manual," in *Canadian Environmental Quality Guidelines* (Winnipeg: Canadian Council of Ministers of the Environment) 1999.

Clarke, K. R., and Gorley, R. N. (2006). *PRIMER V6: User Manual/Tutorial* (Plymouth, UK: PRIMER-E).

Clarke, K. R., and Warwick, R. M. (2001). *Change in Marine Communities: An Approach to Statistical Analysis and Interpretation* (Plymouth, UK: PRIMER-E).

Feng, Y., Bao, Q., Chenglin, L., Bowen, W., and Zhang, Y. (2018). Introducing Biological Indicators Into CCME WQI Using Variable Fuzzy Set Method. *Water Resour. Manag.* 32, 2901– 2915. doi: 10.1007/s11269-018-1965-x

Friberg, N. (2014). Impacts and Indicators of Change in Lotic Ecosystems. *Wire. Water*. 1, 513–531. doi: 10.1002/wat2.1040

Geedicke, I., Oldeland, J., and Leishman, M. R. (2018). Urban Stormwater Run-Off Promotes Compression of Saltmarshes by Freshwater Plants and Mangrove Forests. *Sci. Total. Environ.* 637, 137–144. doi: 10.1016/j.scitotenv.2018.04.357

Gu, J. D., and Wang, Y. S. (2015). Coastal and Marine Pollution and Ecotoxicology. *Ecotoxicology* 24, 1407–1410. doi: 10.1007/s10646-015-1528-3

HELCOM (2015). "Guidelines Concerning Phytoplankton Species Composition, Abundance and Biomass," in *Manual for Marine Monitoring in the COMBINE Programme of HELCOM*. Available at: http://www.helcom.fi/action-areas/monitoring-andassessment/manuals-and-guidelines/combine-manual. Annex C-6.

Hooper, D. U., Chapin, F. S.III, Ewel, J. J., Hector, A., Inchausti, P., Lavorel, S., et al. (2005). Effects of Biodiversity on Ecosystem Functioning: A Consensus of Current Knowledge. *Ecol. Monogr.* 75, 3–35. doi: 10.1890/04-0922

Inyang, A. I., and Wang, Y. S. (2020). Phytoplankton Diversity and Community Responses to Physicochemical Variables in Mangrove Zones of Guangzhou Province, China. *Ecotoxicology* 29, 650–668. doi: 10.1007/s10646-020-02209-0

Jørgensen, S. E., Burkhard, B., and Müller, F. (2013). Twenty Volumes of Ecological Indicators – An Accounting Short Review. *Ecol. Indic.* 28, 4–9. doi: 10.1016/j.ecolind.2012.12.018

Kamalifar, R., Aeinjamshid, K., Nurinejad, M., Dehghan-Mediseh, S., and Vazirizadeh, A. (2016). Ecological Status Assessment of Bidkhun Mangrove Swamp From Bushehr Province, Persian Gulf, Using Macrofauna Community Structure. *AAC Bioflux.* 9, 8– 18.

Katsiapi, M., Genitsaris, S., Stefanidou, N., Tsavdaridou, A., Giannopoulou, I., Stamou, G., et al. (2020). Ecological Connectivity in Two Ancient Lakes: Impact Upon Planktonic Cyanobacteria and Water Quality. *Water* 12, 18–30. doi: 10.3390/w12010018

Lepisto, L. (1999). "Phytoplankton Assemblages Reflecting the Ecological Status of Lakes in Finland," in *Monographs of the Boreal Environment Research 16* (Tampere). Finland: Finnish Environment Institute

Liu, J. Y. (2013). Status of Marine Biodiversity of the China Seas. *PloS One* 8, 50719 – 50743. doi: 10.1371/journal.pone.0050719

Marchetto, A., Padedda, B. M., Mariani, M. A., Luglie, A., and Sechi, N. (2009). A Numerical Index for Evaluating Phytoplankton Response to Changes in Nutrient Levels in Deep Mediterranean Reservoirs. *J. Limnol.* 68, 106–121. doi: 10.4081/jlimnol.2009.106

McLusky, D. S. (1993). Marine and Estuarine Gradients-an Overview. *Netherlands J. Aquat. Ecol.* 27, 489–493. doi: 10.1007/BF02334809

Meng, F., Li, Z., Li, L., Lu, F., Liu, Y., Lu, X., et al. (2020). Phytoplankton Alpha Diversity Indices Response the Trophic State Variation in Hydrologically Connected Aquatic Habitats in the Harbin Section of the Songhua River. *Scien. Rep.* 10, 21337–21350. doi: 10.1038/s41598-020-78300-7

Ministry of Environmental Protection of the People's Republic of China (MEPPRC) (2010). *Gazette of Ecoenvironmental Monitoring of Three Gorges Project, Yangzi River, China 2009*. Beijing, China

Ministry of Environmental Protection of the People's Republic of China (MEPPRC) (2011). *Gazette of Ecoenvironmental Monitoring of Three Gorges Project, Yangzi River, China 2010*. Beijing, China.

Mohammad-Noor, N., Harun, S. N. R., Lazim, Z. M., Mukai, Y., Mohamad, N. T., and Saad, S. (2013). Diversity of Phytoplankton in Coastal Water of Kuantan, Pahang, Malaysia. *Malay. J. Sci.* 32, 29–37. doi: 10.22452/mjs.vol32no1.6

Mousing, E. A., Richardson, K., Bendtsen, J., Cetinic, I., and Perry, M. J. (2016). Evidence of Small-Scale Spatial Structuring of Phytoplankton Alpha- and Beta-Diversity in the Open Ocean. *J. Ecol.* 104, 1682–1695. doi: 10.1111/1365-2745.12634

Mulder, T., Migeon, S., Savoye, B., and Faugeres, C. (2001). Inversely Graded Turbidite Sequences in the Deep Mediterranean. A Record of Deposits From Flood Generated Turbidity Currents? *Geo-Maine. Lett.* 21, 86–93. doi: 10.1007/s003670100071

Noel, S. D., and Rajan, M. R. (2015). Evaluation of Organic Pollution by Palmer's Algal Genus Index and Physico-Chemical Analysis of Vaigai River at Madurai, India. *Natural Resour. Conserv.* 3, 7–10. doi: 10.13189/nrc.2015.030102

Palmer, C. M. (1969). A Composite Rating of Algae Tolerating Organic Pollution. *J. Phycol.* 5, 78–82. doi: 10.1111/j.1529-8817.1969.tb02581.x

Pradhan, V., and Shaikh, J. D. (2011). Seasonal Fluctuation of Plankton Population Correlated With Physico-Chemical Factors in Backwards of Jaikwadi Dam (Kaigaon). *J. Chem. Biol. Phys. Sci.* 1, 270–274.

Rapport, D. J., and Hildén, M. (2013). An Evolving Role for Ecological Indicators: From Documenting Ecological Conditions to Monitoring Drivers and Policy Responses. *Ecol. Indic.* 28, 10–15. doi: 10.1016/j.ecolind.2012.05.015

Reis, C. R. G., Nardoto, G. B., and Oliveira, R. S. (2017). Global Overview on Nitrogen Dynamics in Mangroves and Consequences of Increasing Nitrogen Availability for These Systems. *Plant Soil* 410, 1–19. doi: 10.1007/s11104-016-3123-7

Stefanidou, N., Katsiapi, M., Tsianis, D., Demertzioglou, M., Michaloudi, E., and Moustaka-Gouni, M. (2020). Patterns in Alpha and Beta Phytoplankton Diversity Along a Conductivity Gradient in Coastal Mediterranean Lagoons. *Diversity* 12, 38–54. doi: 10.3390/d12010038

Taipale, S. J., Vuorio, K., Aalto, S. L., Peltomaa, E., and Tiirola, M. (2019). Eutrophication Reduces the Nutritional Value of Phytoplankton in Boreal Lakes. *Environ. Res.* 179, 108836–108849. doi: 10.1016/j.envres.2019.108836

Temino-Boes, R., Romero-López, R., and Romero, I. (2019). A Spatiotemporal Analysis of Nitrogen Pollution in a Coastal Region With Mangroves of the Southern Gulf of Mexico. *Water* 11, 2143–2159. doi: 10.3390/w1110214

Tian, W., Zhang, H. Y., Zhao, L., Zhang, F. F., and Huang, H. (2017). Phytoplankton Diversity Effects on Community Biomass and Stability Along Nutrient Gradients in a Eutrophic Lake. *Int. J. Environ. Res. Public Health* 14, 15–30. doi: 10.3390/ijerph14010095

Wang, M. (2002). Evaluate Method and Classification Standard on Lake Eutrophication. *Environ. Monit, China* 18, 47–49. doi: 10.3969/j.issn.1002-6002.2002.05.018

Wang, Y. S. (2019). *Molecular Ecology of Mangroves* (Beijing, China: The Science Publishing Company).

Wang, Y. S., and Gu, J. D. (2021). Ecological Responses, Adaptation and Mechanisms of Mangrove Wetland Ecosystem to the Global Climate Change and Anthropogenic Activities. *Int. Biodeterior. Biodegrad.* 162, 105248. doi: 10.1016/j.ibiod.2021.105248

Weis, J. J., Cardinale, B. J., Forshay, K. J., and Ives, A. R. (2007). Effects of Species Diversity on Community Biomass Production Change Over the Course of Succession. *Ecology* 88, 929–939. doi: 10.1890/06-0943

Wong, Y. S., Tam, N. F. Y., and Lan, C. Y. (1997). Mangrove Wetlands as Wastewater Treatment Facility: A Field Trial. *Hydrobiologia* 352, 49–59. doi: 10.1023/A:1003040920173

Wu, Y., Chung, A., Tam, N. F. Y., Pi, N., and Wong, M. H. (2008). Constructed Mangrove Wetland as Secondary Treatment System for Municipal Wastewater. *Ecol. Eng.* 38, 137–146. doi: 10.1016/j.ecoleng.2008.07.010

Xiao, Y. J., Ferreira, J. G., Bricker, S. B., Nunes, J. P., Zhu, M. Y., and Zhang, X. L. (2007). Trophic Assessment in Chinese Coastal Systems-Review of Methods and Application to the Changjiang (Yangtze) Estuary and Jiaozhou Bay. *Estuar. Coast.* 60, 901–908. doi: 10.1007/BF02841384

Yang, B., Jiang, Y. J., He, W., Liu, W. X., Kong, X. Z., Jørgensen, E. J., et al. (2016). The Tempo-Spatial Variations of Phytoplankton Diversities and Their Correlation With Trophic State Levels in a Large Eutrophic Chinese Lake. *Ecol. Indic.* 66, 153–162. doi: 10.1016/j.ecolind.2016.01.013

Yang, Y. F., Li, C. H., Nie, X. P., Tang, D. L., and Chung, I. K. (2004). Development of Mariculture and its Impacts in Chinese Coastal Waters. *Rev. Fish. Biol. Fish.* 14, 1–10. doi: 10.1007/s11160-004-3539-7

Yuan, Y. X., et al. (2018). Environmental Variables Influencing Phytoplankton Communities in Hydrologically Connected Aquatic Habitats in the Lake Xingkai Basin. *Ecol. Indic.* 91, 1–12. doi: 10.1016/j.ecolind.2018.03.085

Zhu, S., Mostafaei, A., Luo, W., Jia, B., and Dai, J. (2019). Assessing Water Quality for Urban Tributaries of the Three Gorges Reservoir, China. *J. Water Reuse. Desalinat.* 1, 105– 114. doi: 10.1007/s11269-013-0425-x

Conflict of Interest: The authors declare that the research was conducted in the absence of any commercial or financial relationships that could be construed as a potential conflict of interest.

Publisher's Note: All claims expressed in this article are solely those of the authors and do not necessarily represent those of their affiliated organizations, or those of the publisher, the editors and the reviewers. Any product that may be evaluated in this article, or claim that may be made by its manufacturer, is not guaranteed or endorsed by the publisher.

Copyright © 2022 Inyang, Wang and Cheng. This is an open-access article distributed under the terms of the Creative Commons Attribution License (CC BY). The use, distribution or reproduction in other forums is permitted, provided the original author(s) and the copyright owner(s) are credited and that the original publication in this journal is cited, in accordance with accepted academic practice. No use, distribution or reproduction is permitted which does not comply with these terms.

frontiers | Frontiers in Marine Science

ORIGINAL RESEARCH
published: 15 July 2022
doi: 10.3389/fmars.2022.933561

Linkages Between Optical and Molecular Signatures of Dissolved Organic Matter Along the Yangtze River Estuary-to-East China Sea Continuum

Xingnian Sun[1], Penghui Li[2,3], Yuping Zhou[4,5], Chen He[6], Fang Cao[7], Yuntao Wang[8], Quan Shi[6] and Ding He[4,8,9*]*

[1] Shenzhen Marine Environment Monitoring Center, State Oceanic Administration of China, Shenzhen, China, [2] School of Marine Sciences, Sun Yat-Sen University, Zhuhai, China, [3] Southern Marine Science and Engineering Guangdong Laboratory (Zhuhai), Zhuhai, China, [4] School of Earth Science, Zhejiang University, Hangzhou, China, [5] School of Environmental and Municipal Engineering, Qingdao University of Technology, Qingdao, China, [6] State Key Laboratory of Heavy Oil Processing, China University of Petroleum, Beijing, China, [7] State Key Laboratory of Estuarine and Coastal Research, East China Normal University, Shanghai, China, [8] State Key Laboratory of Satellite Ocean Environment Dynamics, Second Institute of Oceanography, Ministry of Natural Resources, Hangzhou, China, [9] Department of Ocean Science and Hong Kong Branch of the Southern Marine Science and Engineering Guangdong Laboratory (Guangzhou), The Hong Kong University of Science and Technology, Hong Kong, Hong Kong SAR, China

OPEN ACCESS

Edited by:
Meilin Wu,
South China Sea Institute of Oceanology (CAS), China

Reviewed by:
Wei He,
China University of Geosciences, China,
Ruanhong Cai,
Xiamen University, China

***Correspondence:**
Ding He
dinghe@ust.hk
Penghui Li
liph8@mail.sysu.edu.cn

Specialty section:
This article was submitted to Marine Pollution, a section of the journal Frontiers in Marine Science

Received: *01 May 2022*
Accepted: *15 June 2022*
Published: *15 July 2022*

Citation:
Sun X, Li P, Zhou Y, He C, Cao F, Wang Y, Shi Q and He D (2022) Linkages Between Optical and Molecular Signatures of Dissolved Organic Matter Along the Yangtze River Estuary-to-East China Sea Continuum. Front. Mar. Sci. 9:933561. doi: 10.3389/fmars.2022.933561

Changes in the molecular composition of dissolved organic matter (DOM) and its light-absorbing component (CDOM) along the river–coastal ocean continuum are crucial for better understanding the source and fate of DOM in coastal oceans. Both optical (absorbance and fluorescence) techniques and ultrahigh-resolution mass spectrometry have been widely used to trace DOM cycling. However, to the best of our knowledge, the linkage between these two techniques is rarely investigated along the river–coastal ocean continuum. In this regard, bulk characterization, optical techniques, and ultrahigh-resolution mass spectrometry [Fourier transform ion cyclotron resonance mass spectrometer (FT-ICR MS)] were applied to determine the DOM chemistry along a spatial transect from the Yangtze River Estuary (YRE) to the East China Sea. The results showed that DOM in the YRE was mainly controlled by the mixing of freshwater and seawater. Besides terrestrial input, multiple sources (tributary input from the Huangpu River, wastewater input, and sediment resuspension and subsequent release at the turbidity maximum zone) have been identified. In addition, the linkages between CDOM and thousands of formulas were developed based on Spearman's rank correlations between optical parameters and FT-ICR MS peaks. The linkages showed that the molecular groups associated with the optical parameters generally agreed with conventional biogeochemical interpretations. Nevertheless, each technique has its unique advantage and weakness in interpreting DOM composition. Therefore, the combination of the untargeted FT-ICR MS approach and optical techniques could be valuable for studying the DOM sources and transformation in large river estuarine systems.

Keywords: Yangtze River Estuary, East China Sea, dissolved organic matter (DOM), optical properties, molecular composition

INTRODUCTION

Estuaries are the major channels transferring dissolved organic matter (DOM) from land to the coastal ocean, playing a crucial role in biogeochemical element cycling (Li et al., 2015). The transport of DOM from estuaries to coastal oceans represents a fundamental component of the global biogeochemical cycle (Bianchi, 2011; Cao et al., 2018), which has gained increasing attention (Hedges et al., 1997; Benner, 2004). DOM provides an essential source of energy and nutrients, and affects nutrient cycles, oxygen levels, and microbial communities in aquatic environments (Findlay and Sinsabaugh, 2003). The extent of these influences relies not only on the abundance but also on the sources and chemical composition of DOM (Hansell and Carlson, 2015). Primary sources of DOM in estuaries and coastal oceans include terrestrial plants, soils, sediment resuspension, microbes, and marine phytoplankton (Li et al., 2015; Canuel and Hardison, 2016). Moreover, anthropogenic activities such as urban and industrial runoff (wastewater discharges) can further complexify the DOM abundance, chemical composition, and bioavailability, especially in densely populated estuaries (Spencer et al., 2007; He et al., 2020).

In the estuarine zone, the salinity, ion strength, and oxidation–reduction potential changed sharply, which affected the transformation, adsorption, desorption, and sedimentation of organic matter (OM) (Canuel et al., 2012). Although the physical mixing of freshwater and marine water is usually one of the dominant processes affecting the DOM distribution and transformations, other processes have been noted to play important roles, including removal processes such as photochemical and biological degradation, and adsorption to particles, and addition processes such as *in situ* production and sediment resuspension (Li et al., 2015). All these removal and addition processes highly affect DOM composition and sources. In this context, assessing the DOM composition and source would be the first step to understand its transformation in estuaries. The carbon isotopic composition is a well-established tool for differentiating DOM sources, with marine DOM having higher $\delta^{13}C$ values than terrestrial DOM (Hedges et al., 1997; Lalonde et al., 2014). The UV–Vis absorbance and fluorescence spectroscopy were widely used in characterizing the chromophoric DOM (CDOM), an optically active fraction of DOM, and thus infer the overall DOM source and its biogeochemical cycling (Coble, 2007; Li and Hur, 2017). Moreover, excitation–emission matrix coupled with parallel factor analysis (EEM-PARAFAC) was applied in combination with $\delta^{13}C$ to further constrain the DOM sources (Osburn and Stedmon, 2011; Cawley et al., 2012; Ya et al., 2015). Both conservative and non-conservative mixing behaviors of various fluorescent components have been observed spatially from the freshwater to seawater regions (Stedmon and Markager, 2005; Yang et al., 2013; Li et al., 2015), suggesting complex factors controlling the DOM dynamics in estuaries.

Although stable carbon isotopes and optical techniques are helpful in elucidating spatial and temporal variations in DOM sources, they cannot provide the molecular composition of DOM, which is an important determinant of DOM lability and fate (Hansell and Carlson, 2015; Mostovaya et al., 2017). Ultrahigh-resolution mass spectrometry [e.g., Fourier transform ion cyclotron resonance mass spectrometer (FT-ICR MS)] is introduced to investigate the molecular composition of DOM (Kujawinski et al., 2004; Koch and Dittmar, 2006), and has shown promising applications in various aquatic environments (Nebbioso and Piccolo, 2013; Minor et al., 2014). FT-ICR MS has aided in identifying DOM transformation processes from terrestrial to marine biomes (Sleighter and Hatcher, 2008; Medeiros et al., 2015; Seidel et al., 2015). In addition, the linkage between optical and molecular properties of DOM in natural aquatic systems is a subject with rising interest in the aquatic biogeochemistry field (Osburn and Bianchi, 2016). For instance, the combination of optical properties and FT-ICR MS has been applied recently to a few natural systems, such as a boreal river, a subtropical wetland, and the Mediterranean Sea, in order to further understand the chemical composition and transformation of DOM (Stubbins et al., 2014; Wagner et al., 2015; Martínez-Pérez et al., 2017). These studies have recognized that chemical composition at the molecular level is closely associated with many optical indices (e.g., absorbance, relative abundance of fluorescent components) (Stubbins et al., 2014; Kellerman et al., 2015). However, previous studies usually focused on freshwater or marine water systems (Stubbins et al., 2014; Martínez-Pérez et al., 2017). It remains unclear whether many previously reported relationships are still applicable to a typical large estuary–coastal ocean transect (Martínez-Pérez et al., 2017).

The Yangtze (Changjiang) River is the longest river in China and the third-largest river in the world. The average discharge is about 9.03×10^{11} m^3 per year, consisting of more than 80% of the total freshwater discharged into the East China Sea (Yu et al., 2011). The Yangtze River estuary (YRE) is located at the subtropical zone. The east part of YRE is affected by Kuroshio water and upwelling. The western side is affected by Qiantang River, while Taiwan Warm Current also affects this area, making YRE one of the most complex continental shelf coastal areas (Zhang et al., 2007). Previous studies primarily focused on the spatiotemporal variations of DOM in the YRE using optical techniques and high-resolution mass spectrometry and identified both conservative and non-conservative behaviors (Sun et al., 2014; Li et al., 2015; Chen et al., 2016; Zhu et al., 2018; Zhou et al., 2021). Li et al. (2015) suggested that the turbidity maximum zone (TMZ) played a key role in affecting the optical properties of surface water DOM. However, there exist multiple DOM sources, such as tributary input, wastewater discharge, and nearby salt marsh in the YRE, which could result in the complex dynamics of DOM (Li et al., 2015; Chen et al., 2016). Previous studies mostly focused on the bulk [e.g., dissolved organic carbon (DOC)] and optical properties of DOM (Gan et al., 2016; Song et al., 2017), presenting limited information on DOM molecular composition. Although an increasing number of studies have explored the molecular composition of DOM in estuarine environments such as a river to ocean transect at the lower Chesapeake Bay (Sleighter and Hatcher, 2008), the Amazon River to the West Atlantic Ocean (Seidel et al., 2015), and the Delaware Estuary (Osterholz et al., 2016), only two

molecular-level studies have been performed in the YRE (Zhou et al., 2021; Zhou et al., 2022). However, the linkages between optical and molecular composition of DOM are still not explored, limiting our understanding of the organic matter sources and transformation across this typical large estuary and oceanic continuum. Therefore, combining bulk, optical, and molecular approaches, this study aims to (i) determine the molecular diversity of DOM in the YRE and East China Sea and its major controlling factors, and (ii) identify the linkages of the isotopic and optical properties with the molecular composition along this typical large river to coastal ocean continuum system.

MATERIALS AND METHODS

Study Area and Sampling Strategy

The study area included the entire YRE and part of the East China Sea (**Figure 1**). During the 2017 summer cruise, water samples were collected from YE1 to YE18 Surface water (1.5 m below surface) samples were collected at all stations, while samples at middle and bottom depths were collected at some stations. This collecting strategy allowed us to obtain 38 samples in total (Zhou et al., 2021). All water samples were collected by Nalgene bottles [cleaned with acidified ultrapure water (pH = 2) and ultrapure water]. Bottles were rinsed with sample water before sampling. *In situ* water temperature, salinity, turbidity, and dissolved oxygen concentration were obtained from conductivity–temperature–depth (CTD) equipment (SBE-25 plus, Sea-Bird, USA) on board. Water samples were immediately filtered with precombusted 0.7-μm glass fiber filters (Whatman GF/F) and 0.22-μm membrane filters (Millipore) subsequently to remove particles, algal aggregates, and most bacteria. The filtrates were then stored at −20°C in the dark before further analysis.

Nutrients and DOC Measurements

Concentrations of nutrients (NO_3^-, NO_2^-, NH_4^+, PO_4^{3-}, and SiO_3^{2-}) were measured by UV–Vis microplate spectroscopy (Multiscan Spectrum, Thermo Scientific) following a modified method by Grasshoff et al. (2009). The dissolved inorganic nitrogen (DIN) concentration is the total of NH_4^+, NO_2^-, and NO_3^-, and is reported as μM. DOC concentrations were measured as non-purgeable organic carbon (NPOC) on a Shimadzu TOC-L instrument by high-temperature catalytic oxidation (Huguet et al., 2009). Standard solutions of DOC were prepared by dissolving potassium hydrogen phthalate into ultrapure water and used as DOC references. In addition, international reference low-carbon water and deep seawater (provided by Prof. D. Hansell at the University of Miami, USA) are measured as additional control to calibrate the instrument, with variation coefficient less than 5%.

Absorbance and Fluorescence Measurements

The UV–Vis absorbance and fluorescence spectral measurements were performed on an Aqualog (Horiba, Japan) absorbance–fluorescence spectrometer with 1-cm path length quartz cuvettes. Milli-Q water was used as a reference. The absorption coefficient was converted from absorbance, by multiplying the conversion factor 2.303 and dividing by the path length. In this study, the absorption coefficient at 254 nm (a_{254}) was taken as a quantitative measure of CDOM (Li and Hur, 2017). Excitation emission–matrices (EEMs) of fluorescence spectra were generated following the settings described by Wang et al. (2019). The fluorescence intensity was divided by the area of the Raman peak and thus reported in Raman units (RU). Various commonly used compositionally based absorbance and fluorescence optical indices were calculated following the equations as previously

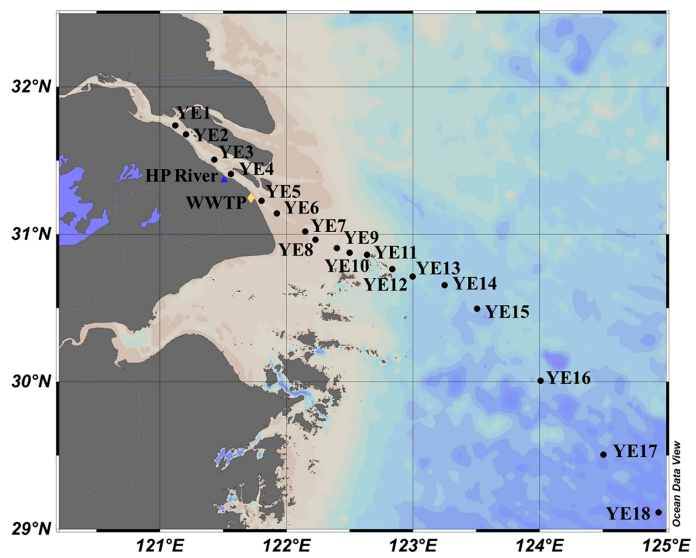

FIGURE 1 | Sampling stations in the Yangtze Estuary and East China Sea. The confluence of the Huangpu River (HP) and the Yangtze River is marked with a blue triangle, and the location of Bailonggang wastewater treatment plant (WWTP) is marked with a yellow diamond.

described (**Table S1**). Specifically, the specific ultraviolet absorbance at 254 nm [$SUVA_{254}$ (L mg C^{-1} m^{-1})] was positively associated with aromatic content, with a higher number indicating greater aromatic content (Weishaar et al., 2003). The slope ratio (S_R) was calculated based on Helms et al. (2008) to assess the average molecular weight of DOM. Fluorescence index (FI) indicates the relative contribution of terrestrial and microbial sources (Mcknight et al., 2001; Cory et al., 2010); humification index (HIX) indicates the humic substance content or the extent of humification (Ohno, 2002), which has been shown to increase with the increasing degree of DOM aromaticity. Both the biological index (BIX) and freshness index (FrI) are calculated to indicate autotrophic productivity and the proportion of recently produced DOM (Parlanti et al., 2000; Huguet et al., 2009; Wilson and Xenopoulos, 2009). In addition, all EEMs were subjected to parallel factor analysis (PARAFAC) using the DOMFluor toolbox (Stedmon and Bro, 2008), following the procedures described in previous studies in the YRE (Li et al., 2015).

Stable Carbon Isotope Measurements of SPE-DOM

DOM was extracted from 1 L of water using solid-phase extraction (SPE) with cartridges filled with a styrene divinyl benzene polymer (Agilent Bond Elut PPL, 500 mg, 6 ml), as described by Dittmar et al. (2008). The stable carbon isotope ratios ($\delta^{13}C$) of SPE-DOM were measured in duplicates on an isotope ratio-monitoring mass spectrometer (Finnigan MAT 253, Thermal Scientific, USA) and were reported in δ notation relative to the Vienna Pee Dee Belemnite. Precision and accuracy were within 0.2‰, and procedural blanks did not yield detectable amounts of contamination (Zhou et al., 2021).

Molecular Composition of SPE-DOM Revealed by FT-ICR MS

A 9.4-T electrospray ionization Bruker Apex FT-ICR MS at the State Key Laboratory of Heavy Oil Processing, China University of Petroleum-Beijing, was used to precisely characterize the molecular composition of SPE-DOM using negative electrospray ionization mode. The procedure followed a previous study by He et al. (2020). Relative peak intensities were calculated based on the summed intensities of all assigned peaks in each sample to assess DOM composition semi-quantitatively. The elements (C, H, O, N, and S), formulas (CHO, CHON, CHOS, and CHONS), and others [the ratio of hydrogen to carbon (H/C), the ratio of oxygen to carbon (O/C), double bond equivalent (DBE), and aromaticity index (AI_{mod})] were obtained based on the magnitude-weighted calculation to the analysis of DOM composition (Koch and Dittmar, 2006; Koch and Dittmar, 2016). Assigned molecular formulas were categorized into different compound groups (Martínez-Pérez et al., 2017; Li et al., 2019): sugars ($1.6 < H/C < 2.0$, $0.7 < O/C < 1.0$, and $N = 0$), peptides ($1.5 < H/C < 2.0$, $O/C < 0.9$, and $N > 0$), highly aromatic compounds with aliphatic side chains such as polyphenols ($0.50 < AI_{mod} < 0.66$), condensed combustion-derived dissolved black carbon (BC, $AI_{mod} \geq 0.66$), highly unsaturated compounds (HU, $AI_{mod} < 0.50$, $H/C < 1.5$, and $O/C < 0.9$), unsaturated aliphatic compounds (UA, $1.5 < H/C \leq 2$, $O/C < 0.9$, and $N = 0$), and carboxyl-rich alicyclic molecules (CRAM, $0.3 < DBE/C < 0.68$, $0.2 < DBE/H < 0.95$, and $0.77 < DBE/O < 1.75$). The molecular lability index (MLB_L, the relative abundance of molecular formulas with $H/C \geq 1.5$) was calculated to evaluate the overall lability of DOM (D'andrilli et al., 2015). The degradation index (I_{DEG}) was calculated to indicate the degradation state of the DOM (Flerus et al., 2012). The relative intensity of t-peaks (RA_{terr}) and the ratio of terrestrial peaks to marine peaks (I_{terr}) were calculated to trace the terrestrial DOM along the transect (Medeiros et al., 2016).

Statistical Analyses

The relative abundance (%) of each PARAFAC component was calculated by dividing the PARAFAC component intensity by the sum of all components' fluorescence intensities within a sample. Pearson correlations were conducted among isotopic, optic, and molecular parameters using MATLAB. Pairwise Spearman's rank correlations were obtained between optical indices and normalized mass peak intensities (Wagner et al., 2015). In this study, correlations were considered significant at the 99% confidence level ($p < 0.01$).

RESULTS

Hydrography Background

The surface water salinity ranged from 0.2 to 35.5 and showed an increasing trend seaward (**Figure S1**). Based on previous studies (Li et al., 2015; Zhou et al., 2021) and the turbidity measured in this study, the turbidity maximum zone is mainly confirmed to be located at YE5 to YE11 during this sampling event (**Figure S1**), although this zone is also dynamically fluctuated depending on the river discharge and tidal effects (Li et al., 2015).

DOC and Bulk Physicochemical Background

The DIN (the sum of NO_3^-, NO_2^-, and NH_4^+), PO_4^{3-}, and SiO_3^{2-} concentrations all showed decreasing trends with increasing salinity, suggesting the dilution of freshwater from the Yangtze River with high nutrient concentrations by seawater with low nutrient concentrations (**Figure S1**). The NO_3^- is the dominant DIN form, and it also showed the highest concentration at the TMZ (YE6). Similarly, both NH_4^+ and NO_2^- showed the highest concentrations at YE7, located at the TMZ. The concentrations of SiO_3^{2-} ranged from 0.5 to 129.6 μM, and they negatively correlated with salinity. The highest concentrations of SiO_3^{2-} were also observed at YE5 and YE6. The primary source of SiO_3^{2-} was from the weathering of rocks, suggesting the dilution of SiO_3^{2-} with marine water.

The DOC concentrations were from 62.9 to 123.3 μM, 68.0 to 93.4 μM, and 60.0 to 114.7 μM in the surface, middle, and bottom water layers, respectively (**Figure S1**). In general, a negative correlation ($p < 0.01$) between concentrations of DOC and salinity was observed.

Spatial Variations of Stable Carbon Isotopic Composition of SPE-DOM

The $\delta^{13}C$ values ranged from −28.0‰ to −23.4‰, −26.3‰ to −23.5‰, and −28.2‰ to −23.2‰ for the surface, middle, and bottom samples, respectively (**Figure S2**). The $\delta^{13}C$ values of terrestrial and marine DOM usually ranged from −28‰ to −25‰, and from −22‰ to −19‰, respectively (Raymond and Bauer, 2001; Osburn and Stedmon, 2011). Therefore, the $\delta^{13}C$ values obtained in this study indicated the mixing of OM from both terrestrial and marine inputs. There is a positive correlation ($p < 0.01$) between $\delta^{13}C$ and salinity.

Optical Properties: UV–Vis Absorbance and Fluorescence

The CDOM absorption coefficient a_{254} was from 1.15 to 8.98 m^{-1}; the $SUVA_{254}$ ranged from 0.59 to 3.32 L mg^{-1} m^{-1}. Both a_{254} and $SUVA_{254}$ decreased with increasing salinity (**Figure S2**) and showed negative correlations with salinity ($R^2 = 0.94$ for a_{254} and $R^2 = 0.80$ for $SUVA_{254}$, both $p < 0.01$). The slope ratios (S_R) were from 0.95 to 5.37, 1.09 to 5.53, and 0.83 to 5.30, in surface, middle, and bottom layer samples, respectively. S_R showed a sharp increase in high-salinity area, suggesting decreasing averaged molecular weight of CDOM with increasing salinity (Helms et al., 2008).

HIX ranged from 0.24 to 0.74, 0.24 to 0.65, and 0.30 to 0.72 from the surface, middle, and bottom layers, respectively. BIX ranged from 0.89 to 1.40, 0.99 to 1.28, and 0.89 to 1.36 for the surface, middle, and bottom layers, respectively (**Figure S2**).

Four fluorescent components were identified by PARAFAC, including two humic-like components (C2 and C3), one tyrosine-like component (C1), and one tryptophan-like component (C4) (**Figure 2**). Further comparisons with previous studies using the OpenFluor database (**Table S2**) revealed that C1 is associated with free and protein-bound amino acids, which are usually ascribed to autochthonous DOM (Coble, 1996; Cory and Mcknight, 2005). C4 had a fluorescence signal similar to the tyrosine-like signal (Stedmon et al., 2011). C2 represents terrestrial humic-like fluorescence in high nutrient and wastewater impacted environments, while C3 represents microbial humic-like fluorescence (Murphy et al., 2011).

The fluorescence intensities of C2 and C3 were closely correlated ($R^2 = 0.99$, $p < 0.001$), suggesting that they could be derived from a similar source and controlled by similar factors (Stedmon and Markager, 2005). They both negatively correlated with salinity ($p < 0.001$). In contrast, although both C1 and C4 belong to protein-like components, they showed distinct behaviors (**Figure 2**). The absolute intensity of C1 showed a weak negative correlation with salinity ($R^2 = 0.52$, $p < 0.01$), whereas no correlation was observed between the salinity and fluorescence intensity of C4. The relative percentages of C2 and C3 both showed negative correlations with salinity. There was no significant correlation between the salinity and relative percentage of C1, whereas a significant positive correlation was observed between the salinity and relative percentage of C4.

Molecular Compositions

The FT-ICR MS technique applied here allowed for the assignment of 7,398 unique molecular formulas in the mass range of 210–730 Da in the 38 DOM samples of the Yangtze River to East China Sea continuum (**Table 1**), providing a fingerprint to assess its sources and alterations (Stubbins et al., 2010). Although only 1,117 common molecular formulas were present in all samples, they account for >50% of the intensity in each sample.

Most molecular parameters such as AI_{mod}, DBE, black carbon, and polyphenols showed negative correlations with salinity ($p < 0.01$). In contrast, H atom number, H/C, and HU showed positive correlations with salinity ($p < 0.01$). The lowest AI_{mod} values and highest H/C were observed at the surface layer of YE16-YE18.

TABLE 1 | Number, average molecular mass, molecular properties, heteroatom, and formula grouping of molecular formulas that correlated positively ($r > 0$, $p < 0.01$) with optical indices (absorption coefficient, relative abundance of PARAFAC components, $SUVA_{254}$, FI, BIX, HIX, and FrI).

	All	Common	%C1	%C2	%C3	%C4	FI	BIX	HIX	FrI	a_{254}	$SUVA_{254}$
Total no. of formulas	7,398 (100)	1,117 (76)	50 (1)	2,356 (27)	2,322 (26)	991 (55)	31 (2)	1,064 (55)	2,318 (26)	1,085 (55)	2,348 (26)	2,224 (26)
MW (Da)	440.2	421.2	460.2	406.9	407.3	479.9	437.7	482.3	406.8	481.1	409.5	408.1
H/C	1.17	1.28	1.52	0.98	0.98	1.36	1.36	1.37	0.98	1.37	0.99	0.99
O/C	0.5	0.49	0.55	0.51	0.51	0.51	0.48	0.5	0.51	0.51	0.51	0.51
DBE	9.7	8.3	6.6	10.8	10.9	8.3	7.9	8.3	10.9	8.2	10.8	10.8
Almod	0.283	0.209	0.169	0.416	0.419	0.16	0.215	0.159	0.419	0.159	0.417	0.415
CHO	2,586 (100)	651 (64)	18 (0)	1,059 (26)	1,039 (25)	446 (61)	12 (3)	486 (60)	1,027 (25)	483 (60)	1,087 (25)	1,052 (25)
CHON	3,085 (100)	366 (10)	17 (1)	767 (25)	758 (24)	410 (46)	17 (1)	441 (47)	766 (24)	451 (47)	747 (23)	711 (24)
CHOS	1,315 (100)	100 (3)	15 (2)	437 (41)	429 (40)	135 (25)	2 (0)	137 (23)	426 (40)	151 (24)	432 (40)	388 (37)
CHONS	412 (100)	0 (0)	0	93	96	0	0	0	99	0	82	73
Black carbon (BC)	435 (100)	0 (0)	0	153	156	0	0	0	164	0	153	138
Polyphenols	849 (100)	0 (0)	0 (0)	493 (94)	492 (94)	0 (0)	0 (0)	0 (0)	490 (94)	0 (0)	495 (95)	471 (94)
Highly unsaturated (HU)	4,654 (100)	969 (71)	25 (0)	1,503 (26)	1,480 (25)	824 (58)	25 (3)	857 (57)	1,471 (25)	859 (57)	1,479 (25)	1,418 (24)
Unsaturated aliphatic (UA)	777 (100)	125 (5)	16 (3)	110 (17)	97 (15)	113 (48)	0 (0)	138 (54)	98 (15)	149 (55)	124 (18)	102 (16)
Saturated fatty acids (SatFA)	64 (100)	0 (0)	5	2	2	0	0	3	2	4	1	2
Sugars	58 (100)	0 (0)	0	0	0	0	0	0	0	0	0	0
Peptides	353 (100)	13 (0)	3 (1)	0 (0)	0 (0)	39 (49)	5 (6)	48 (56)	0 (0)	54 (59)	0 (0)	1 (15)
CRAM	3,711 (100)	715 (52)	18 (0)	1,389 (29)	1,362 (28)	457 (52)	19 (3)	488 (52)	1,358 (29)	488 (52)	1,386 (28)	1,322 (28)

The value within parentheses indicates the contribution of the correlated formulas to their corresponding group (herein the row names of the corresponding rows).

DISCUSSION

Evaluations of DOM Sources Combining Isotopic, Optical, and Molecular Signatures

The YRE has multiple DOM sources, including allochthonous (terrestrial) DOM from riverine discharge and autochthonous DOM from local primary production. The DOC concentration and CDOM abundance (a_{254} and four PARAFAC components) all showed negative correlations with salinity, indicating that DOM in the estuary is mainly controlled by terrestrial input and the physical dilution of freshwater DOM by seawater (Yang et al., 2013; Li et al., 2015; Medeiros et al., 2015), which has been described and discussed in a previous study (Zhou et al., 2021). The increasing $\delta^{13}C$ indicated the decreasing contribution of terrestrial DOM with increasing salinity in the YRE (Fichot and Benner, 2012; Li et al., 2021). Humic-like C2 and C3 have also been reported as terrestrial-derived organic matter (Li et al., 2015). In this study, the significant negative Pearson correlations between $\delta^{13}C$ and C2% ($R^2 = 0.86$, $p < 0.01$) and C3% ($R^2 = 0.84$, $p < 0.01$) further confirm the terrestrial signature of C2 and C3 components. Although naturally terrestrial input has been suggested as the primary source of DOM at the YRE, the sharp increase of protein-like C1 from YE3 to YE6 (**Figure 2**) indicated that the anthropogenic DOM could also introduce a significant portion of DOM. A previous study showed that there is high abundance of protein-like components in the Huangpu River, which flows into the Yangtze River between YE3 and YE4 (Dong et al., 2014). In addition, protein-like fluorescence components were found to be enriched in domestic wastewater (Yin et al., 2020), and one large wastewater treatment plant with a wastewater loading of 2.8 million m^3/d is located nearby YE6. Therefore, the increase of C1 could be possibly attributed to the inputs of the Huangpu River (YE3 station) and the domestic wastewater treatment plant (YE6 station). Moreover, the relative abundance of surfactant-like O_3S and O_5S formulas and the ratios of their abundance to the relative abundance of other organic sulfur (Other OS: CHOS + CHONS, except O_3S and O_5S) increased sharply from YE4 to YE6. The O_3S formulas are likely associated with linear alkylbenzene sulfonates (LAS), which is widely used in detergents and existed commonly in domestic sewage (Gong et al., 2022). The O_5S formulas could be possible degradation products of LAS, and both O_3S and O_5S formulas have been found to be enriched in domestic sewage (Gonsior et al., 2011; Melendez-Perez et al., 2016). Therefore, the wastewater inputs could be supported by the sharp increase in the relative abundance of surfactant-like O_3S and O_5S formulas from YE4 to YE6 (Ye et al., 2019) (**Figure 2**).

Besides tributary and wastewater input, sediment resuspension and subsequent release located at the TMZ could be another source of DOM in the YRE (Yang et al., 2013; Li et al., 2015). In this study, the highest PARAFAC components were found at the TMZ, which could be easily attributed to the sediment resuspension (Li et al., 2015). However, the wastewater input is also located nearby the TMZ, resulting in the complexity of DOM sources in this region. To elucidate the DOM source in this region, further detailed analysis was conducted (**Figure 2**). Protein-like components (C1 and C4) increased sharply at YE4, while C1 and humic-like C2 showed large increase (~10%) at YE6, suggesting that there must be other DOM sources at YE6 besides anthropogenic inputs. Compared to C2, C3 remained relatively stable from YE5 to YE6 with the decrease of average C3:C2 from 0.81 at YE1–YE5 to 0.75 at YE6–YE8. One previous study showed that sediment-extracted organic matter is rich in humic-like components (similar to C2 in this study) at the TMZ of YRE (Han et al., 2021). Therefore, this increase of C2 at YE6 could be partly attributed to the sediment resuspension and subsequent dissolution or desorption.

Linkages Between Optical and Molecular Signatures of DOM

Both optical methods and FT-ICR MS were widely used to characterize DOM in natural ecosystems, demonstrating their potential in studying the source, bioavailability, and terrestrial signature of DOM (Fellman et al., 2008; D'andrilli et al., 2015; Medeiros et al., 2016; Zhang et al., 2018). In our study, various significant correlations were observed between optical and molecular parameters (**Figure 3**). For example, humic-like components (C2 and C3) and their relative abundance (%C2 and %C3) were positively correlated with DBE, AI_{mod}, RA_{terr}, and I_{terr}. Accordingly, a_{254}, $SUVA_{254}$, and HIX behaved similarly to humic-like components, thus correlating similarly with molecular parameters. Contrastingly, protein-like components C1 and C4 showed distinctive correlations with molecular parameters. For arbitrary abundance, C1 exhibited similar correlations with molecular parameters as humic-like C2 and C3 due to their significant positive correlations (C1 vs C2: $R^2 = 0.64$, $p < 0.01$; C1 vs C3: $R^2 = 0.62$, $p < 0.01$), while there was none for C4. However, when shifted to relative abundance, %C4 correlated with various molecular parameters, while none was for %C1. Therefore, the calculation (arbitrary or relative) of PARAFAC components should be carefully checked when discussing the correlations between PARAFAC components and molecular parameters.

The associations between optical and molecular parameters would facilitate the understanding of DOM composition. For example, the significant positive correlations between AI_{mod} and humic-like components (either arbitrary C2 and C3, or relative C2% and C3%) (**Figure 3**) suggested that humic-like components were associated with aromatic compounds, in agreement with previous studies observed in boreal waters and subtropical coastal wetlands (Stubbins et al., 2014; Wagner et al., 2015). Meanwhile, both HIX and $SUVA_{254}$ correlated positively with AI_{mod} and DBE, indicating that aromaticity derived from both optical methods and high-resolution mass spectrometry were consistent with each other, which has been widely reported in previous studies (Maizel and Remucal, 2017; Kellerman et al., 2018).

A significant positive correlation was identified between S_R from UV–Vis absorbance and averaged MW of molecular formulas detected by FT-ICR MS (**Figure 3**), in contrast with the inverse relationship between DOM weight-average MW and S_R for size-fractionated Suwannee River natural OM (Helms et al., 2008). This inconsistency could be partly attributed to the

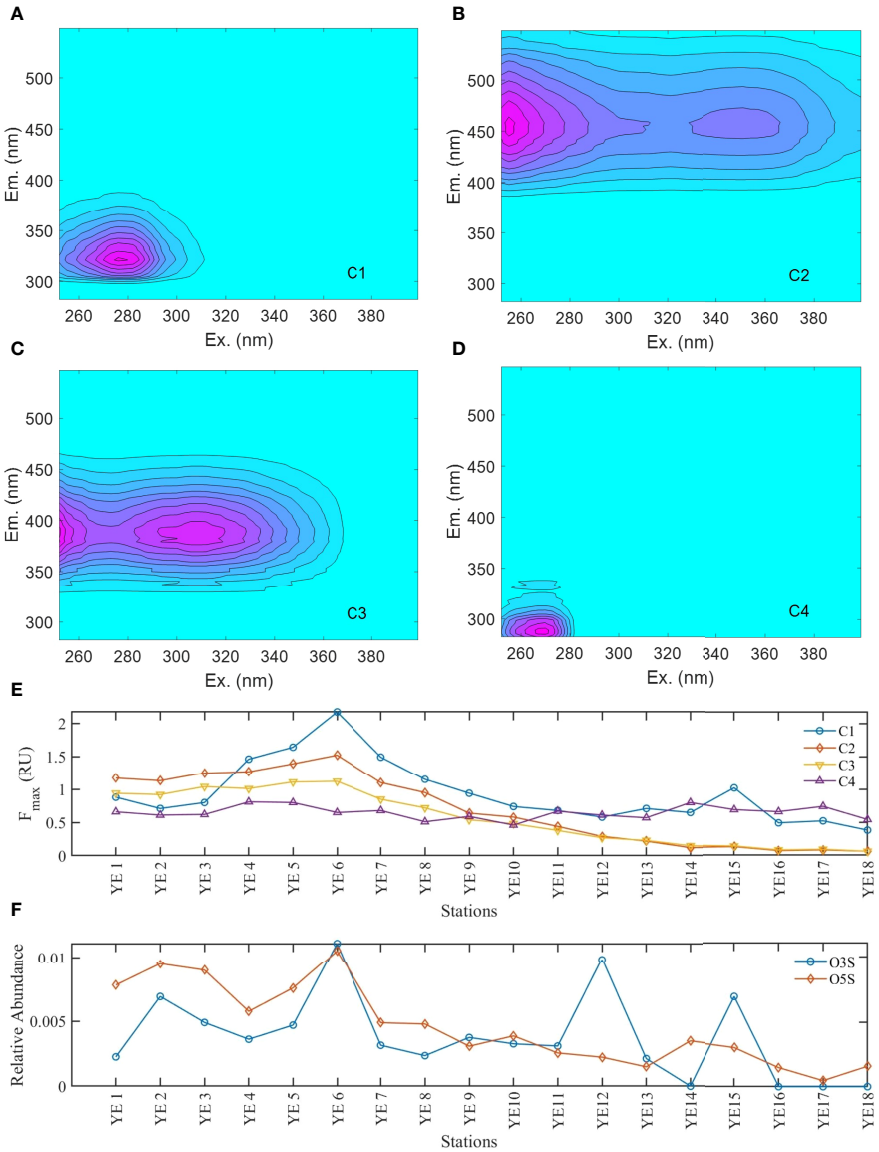

FIGURE 2 | Fluorescence spectra of four PARAFAC components **(A–D)**, F_{max} of four PARAFAC components **(E)**, relative abundance of O_3S and O_5S formulas **(F)**, and the ratios of relative abundance of O_3S and O_5S formulas to other organic sulfurs **(G)** along the Yangtze Estuary transect.

different methods utilized (Wünsch et al., 2018; Li et al., 2019). The MW utilized for the development of S_R has been characterized based on gel permeation chromatography (GPC), ranging from 1,000 to 4,000 Da (Helms et al., 2008). However, in this study, the MW was obtained from FT-ICR MS with a range of 200 to ~800 Da. Moreover, both UV–Vis absorbance spectroscopy and FT-ICR MS only characterize the specific fraction of DOM. The absorbance spectroscopy focuses on the light-absorbing fraction of DOM, while FT-ICR MS mainly characterizes the PPL-adsorbed and negatively ionized fraction. Therefore, the methods should be clearly stated, and the bias should be acknowledged when discussing the MW of DOM in aquatic ecosystems. In addition, one previous study demonstrated that the molecular formulas positively correlated with S_R had lower MW compared to their negatively correlated counterparts in coastal wetlands (Wagner et al., 2015), which is contradictory to our results in YRE, suggesting that the relationship between molecular formulas and S_R could vary with different ecosystems.

To further elucidate the linkages between optical indices and molecular composition of DOM, Spearman correlations have been conducted between optical indices and the relative abundance of all assigned formulas (**Table 1** and **Figure 4**). The results showed that most optical indices (except %C1 and FI) correlated well with the relative abundance of assigned formulas. On the other hand, molecular formulas associated with humic-like (%C2 and %C3) and protein-like (%C4) components showed significant differences in their composition. However, molecular formulas associated with %C2 and %C3 exhibited low MW, low

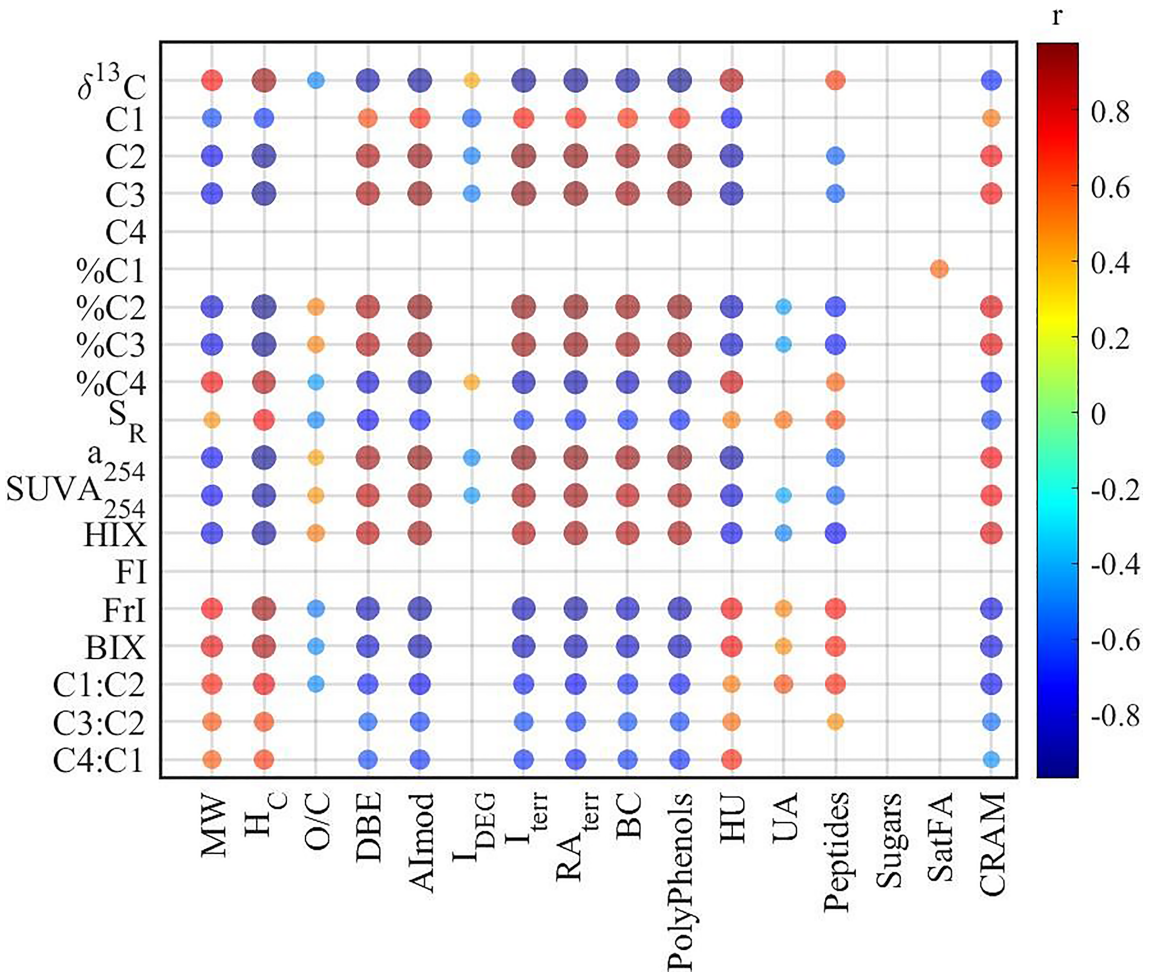

FIGURE 3 | Correlations (Pearson) among different isotopic and optical parameters.

bio-lability (low H/C), and high aromaticity (high DBE and AI_{mod}), while %C4 exhibited high MW, high bio-lability, and low aromaticity. This contrasts with previous studies in which the humic-like fluorescent components are usually associated with high-MW compounds, and protein-like components are commonly related to low-MW compounds (Stubbins et al., 2014; Wagner et al., 2015; Martínez-Pérez et al., 2017). In addition, this is contradictory to the results that recalcitrant deep-ocean enriched formulas exhibited higher MW than surface-enriched formulas (Li et al., 2019). However, the humic-like components have been regarded as biologically recalcitrant (Zhang et al., 2018), and thus should be of low MW according to the size reactivity continuum (SRC) model (Benner and Amon, 2015). Based on the SRC model, the MW of the labile fraction (C4) of DOM should be higher than their corresponding recalcitrant fraction (C2 and C3) (Benner and Amon, 2015), consistent with our results. Moreover, relatively lower MW was identified for molecular formulas positively correlated with humic-like components (C_{420}, C_{460}, and C_{510}) than protein-like components (C_{310}) (Wünsch et al., 2018). These inconsistencies suggest the importance of local calibration of correlations between optical and molecular parameters to further understand DOM cycling in a specific ecosystem.

Furthermore, the contribution of associated formulas to their class has been calculated (**Table 1**). There were 127 black carbon-like formulas and 553 polyphenol formulas associated with %C2, contributing 66% and 94% of black carbon and polyphenol peak intensities. This indicated that humic-like components could be an effective proxy for black carbon and polyphenol in aquatic ecosystems (Stubbins et al., 2014). There were also 1,459 HU and 1,374 CRAM formulas associated with %C2, representing 23% and 25% of the relative abundance of each group of formulas. With a significant correlation with %C2, %C3 formulas shared a large fraction with %C2 (**Figure 5**). Contrastingly, %C4 formulas showed good representativeness of HU (58% of relative abundance), CRAM (52%), peptides (49%), and UA (48%) though %C4 correlated with less HU and CRAM formulas than %C2 and %C3. This suggests that we must check both the number and the relative abundance of the associated formulas when optical indices and molecular formulas are

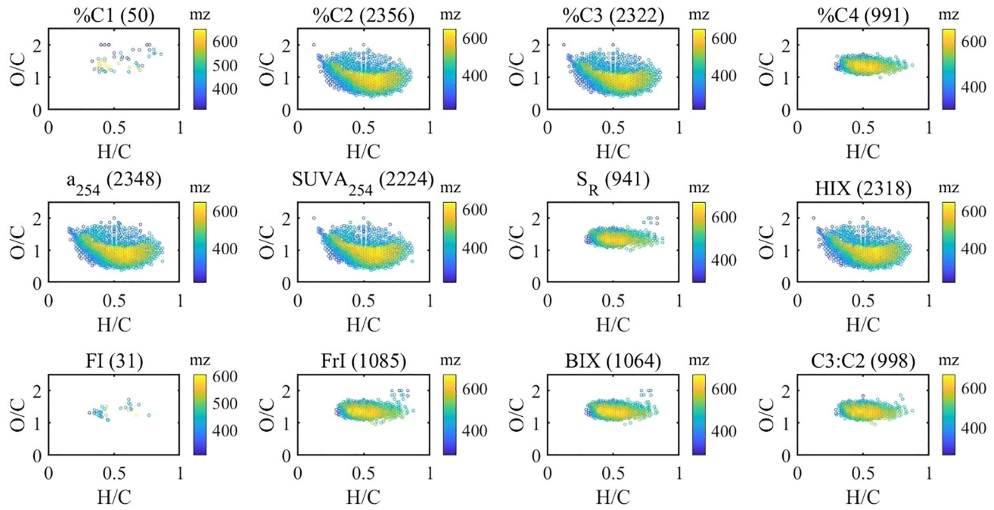

FIGURE 4 | Van Krevelen distributions of molecular formulas positively correlated (Spearman) with optical indices (the numbers in brackets indicate the number of correlated molecular formulas).

correlated, which is not emphasized in previous studies (Wagner et al., 2015). Interestingly, the formulas positively correlated with C3:C2 showed remarkable similarity with %C4 formulas. This indicated that the ratio of different humic-like components could be a valuable indicator of DOM molecular composition. Similarly, a_{254}, $SUVA_{254}$, and HIX shared a large fraction (>90%) of formulas with %C2 and %C3 formulas. BIX and freshness index shared a large fraction of formulas with %C4. However, FI, used to assess relative inputs from microbial vs. terrestrial precursor OM (Mcknight et al., 2001), only correlates with 31 formulas of 2.4% by intensity.

All these correlations indicate the strong linkages between optical indices and molecular parameters. Furthermore, these inconsistencies stated above further suggest the complementary characteristics of optical and molecular techniques in large estuaries with complex DOM sources, or the limitation of Spearman's rank correlation to elucidate the associations between optical and molecular techniques in this study (Wünsch et al., 2018).

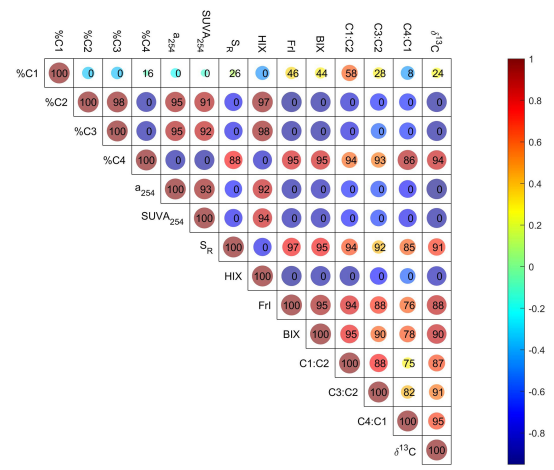

FIGURE 5 | Correlations (Pearson) among isotopic parameters and optical indices, and the similarities of their positively correlated (Spearman) formulas. The size and color of the circle are related to the correlation coefficient. The number in the circle indicates the similarity of correlated molecular formulas associated with the corresponding two parameters; 100 means the formulas associated with these two parameters are the same, and 0 means there is no common formula.

CONCLUSIONS

In this study, the composition of DOM along the Yangtze River to East China Sea continuum was analyzed by a suite of complementary techniques, including the bulk, optical techniques, and FT-ICR MS to further understand DOM cycling. The DOM abundance (DOC, a_{254}, and four PARAFAC components) decreased with increasing salinity, suggesting that DOM in the YRE is mainly controlled by mixing between freshwater and seawater. Moreover, multiple DOM sources (tributary input from the Huangpu River, wastewater input and sediment resuspension, and subsequent release at the TMZ) have been identified in the YRE.

In addition, various correlations have been found between optical indices and molecular parameters derived from FT-ICR MS. Humic-like components (C2 and C3), HIX, and $SUVA_{254}$ all showed significant positive correlations with AI_{mod} and DBE, indicating consistency between optical and molecular methods. Contrastingly, the molecular weight derived from absorbance spectroscopy and FT-ICR MS showed inconsistency, which could be attributed to the specific selectivity of both methods. Finally, Spearman correlations between optical indices and the relative abundance of identified molecular formulas have been

conducted. The results demonstrate that optical indices could be an effective tool to elucidate the molecular composition of DOM. For example, formulas associated with humic-like components could contribute more than 90% to polyphenols derived from FT-ICR MS. However, FI, an index to differentiate terrestrial and microbial sources of DOM, correlated with only a few formulas and contributed a little by peak intensity. Taken together, the association between optical indices and molecular composition further suggests the complementary characteristics for both techniques and the necessity of using multiple approaches in this complex estuarine system, providing the foundation for further understanding the carbon cycling in the large river estuaries and coastal oceans.

DATA AVAILABILITY STATEMENT

The original contributions presented in the study are included in the article/**Supplementary Material**. Further inquiries can be directed to the corresponding authors.

AUTHOR CONTRIBUTIONS

DH contributed to the design of the study. All authors performed the experiment. PL, XS, and DH analyzed the data. PL, XS, and DH prepared the manuscript. All authors contributed to the revision.

FUNDING

This work was supported by the National Science Foundation of China (41973070 and 41906031), Guangdong Basic and Applied Basic Research Foundation (2020A1515110194), Science and Technology Program of Guangzhou (202102021142), the open fund of State Key Laboratory of Satellite Ocean Environment Dynamics, Second Institute of Oceanography, MNR (No. QNHX1912), the Hong Kong Branch of Southern Marine Science and Engineering Guangdong Laboratory (Guangzhou) (SMSEGL20SC01), and funding support from the Center for Ocean Research in Hong Kong and Macau (CORE).

ACKNOWLEDGMENTS

We acknowledge the "YES" cruise for the sampling.

SUPPLEMENTARY MATERIAL

The Supplementary Material for this article can be found online at: https://www.frontiersin.org/articles/10.3389/fmars.2022.933561/full#supplementary-material

REFERENCES

Benner, R. (2004). What Happens to Terrestrial Organic Matter in the Ocean? *Mar. Chem.* 92, 307–310. doi: 10.1016/S0146-6380(97)00066-1

Benner, R. and Amon, R. M. W. (2015). The Size-Reactivity Continuum of Major Bioelements in the Ocean. *Annu. Rev. Mar. Sci.* 7, 185–205. doi: 10.1146/annurev-marine-010213-135126

Bianchi, T. S. (2011). The Role of Terrestrially Derived Organic Carbon in the Coastal Ocean: A Changing Paradigm and the Priming Effect. *Proc. Natl. Acad. Sci. United States America* 108, 19473–19481. doi: 10.1073/pnas.1017982108

Canuel, E. A., Cammer, S. S., Mcintosh, H. A. and Pondell, C. R. (2012). Climate Change Impacts on the Organic Carbon Cycle at the Land-Ocean Interface. *Annu. Rev. Earth Planetary Sci.* 40, 685–711. doi: 10.1146/annurev-earth-042711-105511

Canuel, E. A. and Hardison, A. K. (2016). Sources, Ages, and Alteration of Organic Matter in Estuaries. *Annu. Rev. Mar. Sci.* 8, 409–434. doi: 10.1146/annurev-marine-122414-034058

Cao, X., Aiken, G. R., Butler, K. D., Huntington, T. G., Balch, W. M., Mao, J., et al. (2018). Evidence for Major Input of Riverine Organic Matter Into the Ocean. *Organic Geochem.* 116, 62–76. doi: 10.1016/j.orggeochem.2017.11.001

Cawley, K. M., Ding, Y., Fourqurean, J. and Jaffé, R. (2012). Characterising the Sources and Fate of Dissolved Organic Matter in Shark Bay, Australia: A Preliminary Study Using Optical Properties and Stable Carbon Isotopes. *Mar. Freshw. Res.* 63, 1098–1107. doi: 10.1071/MF12028

Chen, Y., Yang, G.-P., Liu, L., Zhang, P.-Y. and Leng, W.-S. (2016). Sources, Behaviors and Degradation of Dissolved Organic Matter in the East China Sea. *J. Mar. Syst.* 155, 84–97. doi: 10.1016/j.jmarsys.2015.11.005

Coble, P. G. (1996). Characterization of Marine and Terrestrial DOM in Seawater Using Excitation Emission Matrix Spectroscopy. *Mar. Chem.* 51, 325–346. doi: 10.1016/0304-4203(95)00062-3

Coble, P. G. (2007). Marine Optical Biogeochemistry: The Chemistry of Ocean Color. *Chem. Rev.* 107, 402–418. doi: 10.1021/cr050350+

Cory, R. M. and Mcknight, D. M. (2005). Fluorescence Spectroscopy Reveals Ubiquitous Presence of Oxidized and Reduced Quinones in Dissolved Organic Matter. *Environ. Sci. Technol.* 39, 8142–8149. doi: 10.1021/es0506962

Cory, R. M., Miller, M. P., Mcknight, D. M., Guerard, J. J. and Miller, P. L. (2010). Effect of Instrument-Specific Response on the Analysis of Fulvic Acid Fluorescence Spectra. *Limnol. Oceanogr.: Methods.* 8, 67–78. doi: 10.4319/lom.2010.8.67

D'andrilli, J., Cooper, W. T., Foreman, C. M. and Marshall, A. G. (2015). An Ultrahigh-Resolution Mass Spectrometry Index to Estimate Natural Organic Matter Lability. *Rapid Commun. Mass Spectrom.* 29, 2385–2401. doi: 10.1002/rcm.7400

Dittmar, T., Koch, B., Hertkorn, N. and Kattner, G. (2008). A Simple and Efficient Method for the Solid-Phase Extraction of Dissolved Organic Matter (SPE-DOM) From Seawater. *Limnol. Oceanogr.: Methods* 6, 230–235. doi: 10.4319/lom.2008.6.230

Dong, Q., Li, P., Huang, Q., Abdelhafez, A. A. and Chen, L. (2014). Occurrence, Polarity and Bioavailability of Dissolved Organic Matter in the Huangpu River, China. *J. Environ. Sci.* 26, 1843–1850. doi: 10.1016/j.jes.2014.06.020

Fellman, J.B., D'amore, D.V., Hood, E., and Boone, R.D. (2008). Fluorescence characteristics and biodegradability of dissolved organic matter in forest and wetland soils from coastal temperate watersheds in southeast Alaska. *Biogeochemistry* 88, 169-184.

Fichot, C. G. and Benner, R. (2012). The Spectral Slope Coefficient of Chromophoric Dissolved Organic Matter (S275-295) as a Tracer of Terrigenous Dissolved Organic Carbon in River-Influenced Ocean Margins. *Limnol. Oceanogr.* 57, 1453–1466. doi: 10.4319/lo.2012.57.5.1453

Findlay, S. E. and Sinsabaugh, R. L. (2003). *Aquatic Ecosystems: Interactivity of Dissolved Organic Matter* (Burlington: Academic Press).

Flerus, R., Lechtenfeld, O. J., Koch, B. P., Mccallister, S. L., Schmitt-Kopplin, P., Benner, R., et al. (2012). A Molecular Perspective on the Ageing of Marine Dissolved Organic Matter. *Biogeosciences* 9, 1935–1955. doi: 10.5194/bg-9-1935-2012

Gan, S., Wu, Y. and Zhang, J. (2016). Bioavailability of Dissolved Organic Carbon Linked With the Regional Carbon Cycle in the East China Sea. *Deep Sea Res. Part II: Topical Stud. Oceanogr.* 124, 19–28. doi: 10.1016/j.dsr2.2015.06.024

Grasshoff, K., Kremling, K. and Ehrhardt, M. (2009). *Methods of Seawater Analysis* Weinheim; New York; Chichester; Brisbane; Singapore; Toronto: (John Wiley & Sons).

Gonsior, M., Zwartjes, M., Cooper, W.J., Song, W., Ishida, K.P., Tseng, L.Y., et al. (2011). Molecular characterization of effluent organic matter identified by ultrahigh resolution mass spectrometry. *Water Research* 45, 2943-2953.

Gong, C., Jiao, R., Yan, W., Yu, Q., Li, Q., Zhang, P., et al. (2022). Enhanced chemodiversity, distinctive molecular signature and diurnal dynamics of dissolved organic matter in streams of two headwater catchments, Southeastern China. *Water Research*, 118052.

Hansell, D. A. and Carlson, C. A. (2015). *Biogeochemistry of Marine Dissolved Organic Matter* (Amsterdam Boston: Academic Press).

Han, L., Wang, Y., Xu, Y., Wang, Y., Zheng, Y. and Wu, J. (2021). Water- and Base-Extractable Organic Matter in Sediments From Lower Yangtze River–Estuary–East China Sea Continuum: Insight Into Accumulation of Organic Carbon in the River-Dominated Margin. *Front. Mar. Sci.* 8. doi: 10.3389/fmars.2021.617241

Hedges, J. I., Keil, R. G. and Benner, R. (1997). What Happens to Terrestrial Organic Matter in the Ocean? *Organic Geochem.* 27, 195–212. doi: 10.1016/S0146-6380(97)00066-1

Helms, J. R., Stubbins, A., Ritchie, J. D., Minor, E. C., Kieber, D. J. and Mopper, K. (2008). Absorption Spectral Slopes and Slope Ratios as Indicators of Molecular Weight, Source, and Photobleaching of Chromophoric Dissolved Organic Matter. *Limnol. Oceanogr.* 53, 955–969. doi: 10.4319/lo.2008.53.3.0955

He, C., Pan, Q., Li, P., Xie, W., He, D., Zhang, C., et al. (2020). Molecular Composition and Spatial Distribution of Dissolved Organic Matter (DOM) in the Pearl River Estuary, China. *Environ. Chem.* 17, 240–251. doi: 10.1071/EN19051

Huguet, A., Vacher, L., Relexans, S., Saubusse, S., Froidefond, J. M. and Parlanti, E. (2009). Properties of Fluorescent Dissolved Organic Matter in the Gironde Estuary. *Organic Geochem.* 40, 706–719. doi: 10.1016/j.orggeochem.2009.03.002

Kellerman, A. M., Guillemette, F., Podgorski, D. C., Aiken, G. R., Butler, K. D. and Spencer, R. G. M. (2018). Unifying Concepts Linking Dissolved Organic Matter Composition to Persistence in Aquatic Ecosystems. *Environ. Sci. Technol.* 52, 2538–2548. doi: 10.1021/acs.est.7b05513

Kellerman, A. M., Kothawala, D. N., Dittmar, T. and Tranvik, L. J. (2015). Persistence of Dissolved Organic Matter in Lakes Related to its Molecular Characteristics. *Nat. Geosci.* 8, 454–457. doi: 10.1038/ngeo2440

Koch, B. P. and Dittmar, T. (2006). From Mass to Structure: An Aromaticity Index for High-Resolution Mass Data of Natural Organic Matter. *Rapid Commun. Mass Spectrom.* 20, 926–932. doi: 10.1002/rcm.2386

Koch, B. P. and Dittmar, T. (2016). From Mass to Structure: An Aromaticity Index for High-Resolution Mass Data of Natural Organic Matter. *Rapid Commun. Mass Spectrom.* 30, 250–250. doi: 10.1002/rcm.7433

Kujawinski, E. B., Del Vecchio, R., Blough, N. V., Klein, G. C. and Marshall, A. G. (2004). Probing Molecular-Level Transformations of Dissolved Organic Matter: Insights on Photochemical Degradation and Protozoan Modification of DOM From Electrospray Ionization Fourier Transform Ion Cyclotron Resonance Mass Spectrometry. *Mar. Chem.* 92, 23–37. doi: 10.1016/j.marchem.2004.06.038

Lalonde, K., Vähätalo, A. V. and Gélinas, Y. (2014). Revisiting the Disappearance of Terrestrial Dissolved Organic Matter in the Ocean: A δ13c Study. *Biogeosciences* 10, 17117–17144. doi: 10.5194/bg-11-3707-2014

Li, P., Chen, L., Zhang, W. and Huang, Q. (2015). Spatiotemporal Distribution, Sources, and Photobleaching Imprint of Dissolved Organic Matter in the Yangtze Estuary and Its Adjacent Sea Using Fluorescence and Parallel Factor Analysis. *PLos One* 10. doi: 10.1371/journal.pone.0130852

Li, P. and Hur, J. (2017). Utilization of UV-Vis Spectroscopy and Related Data Analyses for Dissolved Organic Matter (DOM) Studies: A Review. *Crit. Rev. Environ. Sci. Technol.* 47, 131–154. doi: 10.1080/10643389.2017.1309186

Li, P., Tao, J., Lin, J., He, C., Shi, Q., Li, X., et al. (2019). Stratification of Dissolved Organic Matter in the Upper 2000 M Water Column at the Mariana Trench. *Sci. Total Environ.* 668, 1222–1231. doi: 10.1016/j.scitotenv.2019.03.094

Li, P., Zhao, C., Liu, K., Xiao, X., Wang, Y., Wang, Y., et al. (2021). Anthropogenic Influences on Dissolved Organic Matter in Three Coastal Bays, North China. *Front. Earth Sci.* 9. doi: 10.3389/feart.2021.697758

Maizel, A. C. and Remucal, C. K. (2017). Molecular Composition and Photochemical Reactivity of Size-Fractionated Dissolved Organic Matter. *Environ. Sci. Technol.* 51, 2113–2123. doi: 10.1021/acs.est.6b05140

Martínez-Pérez, A. M., Nieto-Cid, M., Osterholz, H., Catalá, T. S., Reche, I., Dittmar, T., et al. (2017). Linking Optical and Molecular Signatures of Dissolved Organic Matter in the Mediterranean Sea. *Sci. Rep.* 73436. doi: 10.1038/s41598-017-03735-4

Mcknight, D. M., Boyer, E. W., Westerhoff, P. K., Doran, P. T., Kulbe, T. and Andersen, D. T. (2001). Spectrofluorometric Characterization of Dissolved Organic Matter for Indication of Precursor Organic Material and Aromaticity. *Limnol. Oceanogr.* 46, 38–48. doi: 10.4319/lo.2001.46.1.0038

Medeiros, P. M., Seidel, M., Niggemann, J., Spencer, R. G. M., Hernes, P. J., Yager, P. L., et al. (2016). A Novel Molecular Approach for Tracing Terrigenous Dissolved Organic Matter Into the Deep Ocean. *Global Biogeochemical Cycles* 30, 689–699. doi: 10.1002/2015GB005320

Medeiros, P. M., Seidel, M., Ward, N. D., Carpenter, E. J., Gomes, H. R., Niggemann, J., et al. (2015). Fate of the Amazon River Dissolved Organic Matter in the Tropical Atlantic Ocean. *Global Biogeochemical Cycles* 29, 677–690. doi: 10.1002/2015GB005115

Melendez-Perez, J.J., Martínez-Mejía, M.J., Awan, A.T., Fadini, P.S., Mozeto, A.A., and Eberlin, M.N. (2016). Characterization and comparison of riverine, lacustrine, marine and estuarine dissolved organic matter by ultra-high resolution and accuracy Fourier transform mass spectrometry. *Organic Geochemistry* 101, 99-107.

Minor, E. C., Swenson, M. M., Mattson, B. M. and Oyler, A. R. (2014). Structural Characterization of Dissolved Organic Matter: A Review of Current Techniques for Isolation and Analysis. *Environ. Science-Processes Impacts* 16, 2064–2079. doi: 10.1039/C4EM00062E

Mostovaya, A., Hawkes, J. A., Dittmar, T. and Tranvik, L. J. (2017). Molecular Determinants of Dissolved Organic Matter Reactivity in Lake Water. *Front. Earth Sci.* 5. doi: 10.3389/feart.2017.00106

Murphy, K. R., Hambly, A., Singh, S., Henderson, R. K., Baker, A., Stuetz, R., et al. (2011). Organic Matter Fluorescence in Municipal Water Recycling Schemes: Toward a Unified PARAFAC Model. *Environ. Sci. Technol.* 45, 2909–2916. doi: 10.1021/es103015e

Nebbioso, A. and Piccolo, A. (2013). Molecular Characterization of Dissolved Organic Matter (DOM): A Critical Review. *Analytical Bioanal Chem.* 405, 109–124. doi: 10.1007/s00216-012-6363-2

Ohno, T. (2002). Fluorescence Inner-Filtering Correction for Determining the Humification Index of Dissolved Organic Matter. *Environ. Sci. Technol.* 36, 742–746. doi: 10.1021/es0155276

Osburn, C. and Bianchi, T. (2016). Linking Optical and Chemical Properties of Dissolved Organic Matter in Natural Waters. *Front. Mar. Sci.* 3. doi: 10.3389/fmars.2016.00223

Osburn, C. L. and Stedmon, C. A. (2011). Linking the Chemical and Optical Properties of Dissolved Organic Matter in the Baltic–North Sea Transition Zone to Differentiate Three Allochthonous Inputs. *Mar. Chem.* 126, 281–294. doi: 10.1016/j.marchem.2011.06.007

Osterholz, H., Kirchman, D. L., Niggemann, J. and Dittmar, T. (2016). Environmental Drivers of Dissolved Organic Matter Molecular Composition in the Delaware Estuary. *Front. Earth Sci.* 4. doi: 10.3389/feart.2016.00095

Parlanti, E., Worz, K., Geoffroy, L. and Lamotte, M. (2000). Dissolved Organic Matter Fluorescence Spectroscopy as a Tool to Estimate Biological Activity in a Coastal Zone Submitted to Anthropogenic Inputs. *Organic Geochem.* 31, 1765–1781. doi: 10.1016/S0146-6380(00)00124-8

Raymond, P. A. and Bauer, J. E. (2001). Use of 14C and 13C Natural Abundances for Evaluating Riverine, Estuarine, and Coastal DOC and POC Sources and Cycling: A Review and Synthesis. *Organic Geochem.* 32, 469–485. doi: 10.1016/S0146-6380(00)00190-X

Seidel, M., Yager, P. L., Ward, N. D., Carpenter, E. J., Gomes, H. R., Krusche, A. V., et al. (2015). Molecular-Level Changes of Dissolved Organic Matter Along the Amazon River-To-Ocean Continuum. *Mar. Chem.* 177, Part 2, 218–231. doi: 10.1016/j.marchem.2015.06.019

Sleighter, R. L. and Hatcher, P. G. (2008). Molecular Characterization of Dissolved Organic Matter (DOM) Along a River to Ocean Transect of the Lower Chesapeake Bay by Ultrahigh Resolution Electrospray Ionization Fourier Transform Ion Cyclotron Resonance Mass Spectrometry. *Mar. Chem.* 110, 140–152. doi: 10.1016/j.marchem.2008.04.008

Song, G., Li, Y., Hu, S., Li, G., Zhao, R., Sun, X., et al. (2017). Photobleaching of Chromophoric Dissolved Organic Matter (CDOM) in the Yangtze River Estuary: Kinetics and Effects of Temperature, Ph, and Salinity. *Environ. Science: Processes Impacts* 19, 861–873. doi: 10.1039/C6EM00682E

Spencer, R. G. M., Baker, A., Ahad, J. M. E., Cowie, G. L., Ganeshram, R., Upstill-Goddard, R. C., et al. (2007). Discriminatory Classification of Natural and

Anthropogenic Waters in Two U.K. Estuaries. *Sci. Total Environ.* 373, 305–323. doi: 10.1016/j.scitotenv.2006.10.052

Stedmon, C. A. and Bro, R. (2008). Characterizing Dissolved Organic Matter Fluorescence With Parallel Factor Analysis: A Tutorial. *Limnol. Oceanography-Methods* 6, 572–579. doi: 10.4319/lom.2008.6.572

Stedmon, C. A. and Markager, S. (2005). Resolving the Variability in Dissolved Organic Matter Fluorescence in a Temperate Estuary and its Catchment Using PARAFAC Analysis. *Limnol. Oceanogr.* 50, 686–697. doi: 10.4319/lo.2005.50.2.0686

Stedmon, C. A., Seredyńska-Sobecka, B., Boe-Hansen, R., Le Tallec, N., Waul, C. K. and Arvin, E. (2011). A Potential Approach for Monitoring Drinking Water Quality From Groundwater Systems Using Organic Matter Fluorescence as an Early Warning for Contamination Events. *Water Res.* 45, 6030–6038. doi: 10.1016/j.watres.2011.08.066

Stubbins, A., Lapierre, J. F., Berggren, M., Prairie, Y. T., Dittmar, T. and Del Giorgio, P. A. (2014). What's in an EEM? Molecular Signatures Associated With Dissolved Organic Fluorescence in Boreal Canada. *Environ. Sci. Technol.* 48, 10598–10606. doi: 10.1021/es502086e

Stubbins, A., Spencer, R. G. M., Chen, H., Hatcher, P. G., Mopper, K., Hernes, P. J., et al. (2010). Illuminated Darkness: Molecular Signatures of Congo River Dissolved Organic Matter and its Photochemical Alteration as Revealed by Ultrahigh Precision Mass Spectrometry. *Limnol. Oceanogr.* 55, 1467–1477. doi: 10.4319/lo.2010.55.4.1467

Sun, Q. Y., Wang, C., Wang, P. F., Hou, J. and Ao, Y. H. (2014). Absorption and Fluorescence Characteristics of Chromophoric Dissolved Organic Matter in the Yangtze Estuary. *Environ. Sci. pollut. Res.* 21, 3460–3473. doi: 10.1007/s11356-013-2287-4

Wagner, S., Jaffe, R., Cawley, K., Dittmar, T. and Stubbins, A. (2015). Associations Between the Molecular and Optical Properties of Dissolved Organic Matter in the Florida Everglades, a Model Coastal Wetland System. *Front. Chem.* 3, 66. doi: 10.3389/fchem.2015.00066

Wang, K., Pang, Y., He, C., Li, P., Xiao, S., Sun, Y., et al. (2019). Optical and Molecular Signatures of Dissolved Organic Matter in Xiangxi Bay and Mainstream of Three Gorges Reservoir, China: Spatial Variations and Environmental Implications. *Sci. Total Environ.* 657, 1274–1284. doi: 10.1016/j.scitotenv.2018.12.117

Weishaar, J. L., Aiken, G. R., Bergamaschi, B. A., Fram, M. S., Fujii, R. and Mopper, K. (2003). Evaluation of Specific Ultraviolet Absorbance as an Indicator of the Chemical Composition and Reactivity of Dissolved Organic Carbon. *Environ. Sci. Technol.* 37, 4702–4708. doi: 10.1021/es030360x

Wilson, H. F. and Xenopoulos, M. A. (2009). Effects of Agricultural Land Use on the Composition of Fluvial Dissolved Organic Matter. *Nat. Geosci.* 2, 37–41. doi: 10.1038/ngeo391

Wünsch, U. J., Acar, E., Koch, B. P., Murphy, K. R., Schmitt-Kopplin, P. and Stedmon, C. A. (2018). The Molecular Fingerprint of Fluorescent Natural Organic Matter Offers Insight Into Biogeochemical Sources and Diagenetic State. *Analytical Chem.* 90, 14188–14197. doi: 10.1021/acs.analchem.8b02863

Ya, C., Anderson, W. and Jaffé, R. (2015). Assessing Dissolved Organic Matter Dynamics and Source Strengths in a Subtropical Estuary: Application of Stable Carbon Isotopes and Optical Properties. *Continental Shelf Res.* 92, 98–107. doi: 10.1016/j.csr.2014.10.005

Yang, L. Y., Guo, W. D., Hong, H. S. and Wang, G. Z. (2013). Non-Conservative Behaviors of Chromophoric Dissolved Organic Matter in a Turbid Estuary: Roles of Multiple Biogeochemical Processes. *Estuar. Coast. Shelf Sci.* 133, 285–292. doi: 10.1016/j.ecss.2013.09.007

Ye, Q., Zhang, Z.-T., Liu, Y.-C., Wang, Y.-H., Zhang, S., He, C., et al. (2019). Spectroscopic and Molecular-Level Characteristics of Dissolved Organic Matter in a Highly Polluted Urban River in South China. *ACS Earth Space Chem.* 3, 2033–2044. doi: 10.1021/acsearthspacechem.9b00151

Yin, H., Wang, Y., Yang, Y., Huang, J., and Xu, Z. (2020). Tryptophan-like fluorescence as a fingerprint of dry-weather misconnections into storm drainage system. *ENVIRONMENTAL SCIENCES EUROPE* 32.

Yu, H., Wu, Y., Zhang, J., Deng, B. and Zhu, Z. (2011). Impact of Extreme Drought and the Three Gorges Dam on Transport of Particulate Terrestrial Organic Carbon in the Changjiang (Yangtze) River. *J. Geophys. Research: Earth Surface* 116. doi: 10.1029/2011JF002012

Zhang, C., Dang, H., Azam, F., Benner, R., Legendre, L., Passow, U., et al. (2018). Evolving Paradigms in Biological Carbon Cycling in the Ocean. *Natl. Sci. Rev.* 5, 481–499. doi: 10.1093/nsr/nwy074

Zhang, J., Liu, S. M., Ren, J. L., Wu, Y. and Zhang, G. L. (2007). Nutrient Gradients From the Eutrophic Changjiang (Yangtze River) Estuary to the Oligotrophic Kuroshio Waters and Re-Evaluation of Budgets for the East China Sea Shelf. *Prog. Oceanogr.* 74, 449–478. doi: 10.1016/j.pocean.2007.04.019

Zhou, Y., He, D., He, C., Li, P., Fan, D., Wang, A., et al. (2021). Spatial Changes in Molecular Composition of Dissolved Organic Matter in the Yangtze River Estuary: Implications for the Seaward Transport of Estuarine DOM. *Sci. Total Environ.* 143531. doi: 10.1016/j.scitotenv.2020.143531

Zhou, Y., Zhao, C., He, C., Li, P., Wang, Y., Pang, Y., et al. (2022). Characterization of Dissolved Organic Matter Processing Between Surface Sediment Porewater and Overlying Bottom Water in the Yangtze River Estuary. *Water Res.* 118260. doi: 10.1016/j.watres.2022.118260

Zhu, W.-Z., Zhang, J. and Yang, G.-P. (2018). Mixing Behavior and Photobleaching of Chromophoric Dissolved Organic Matter in the Changjiang River Estuary and the Adjacent East China Sea. *Estuarine Coast. Shelf Sci.* 207, 422–434. doi: 10.1016/j.ecss.2017.07.019

Conflict of Interest: The authors declare that the research was conducted in the absence of any commercial or financial relationships that could be construed as a potential conflict of interest.

Publisher's Note: All claims expressed in this article are solely those of the authors and do not necessarily represent those of their affiliated organizations, or those of the publisher, the editors and the reviewers. Any product that may be evaluated in this article, or claim that may be made by its manufacturer, is not guaranteed or endorsed by the publisher.

Copyright © 2022 Sun, Li, Zhou, He, Cao, Wang, Shi and He. This is an open-access article distributed under the terms of the Creative Commons Attribution License (CC BY). The use, distribution or reproduction in other forums is permitted, provided the original author(s) and the copyright owner(s) are credited and that the original publication in this journal is cited, in accordance with accepted academic practice. No use, distribution or reproduction is permitted which does not comply with these terms.

frontiers | Frontiers in Marine Science

ORIGINAL RESEARCH
published: 15 July 2022
doi: 10.3389/fmars.2022.909839

Distribution, Sources, and Biogeochemistry of Carbon Pools (DIC, DOC, and POC) in the Mangrove-Fringed Zhangjiang Estuary, China

Ran Yan[1], *Jianxiang Feng*[2,3,4*], *Yuming Wang*[2], *Linxi Fu*[1,3], *Xiangxin Luo*[1,3], *Lixia Niu*[1,3] *and Qingshu Yang*[1,3*]

[1] Institute of Estuarine and Coastal Research, School of Marine Engineering and Technology, Sun Yat-sen University, Guangzhou, China, [2] School of Marine Sciences, Sun Yat-Sen University, Zhuhai, China, [3] Southern Marine Science and Engineering Guangdong Laboratory (Zhuhai), Zhuhai, China, [4] Guangdong Provincial Key Laboratory of Marine Resources and Coastal Engineering, Sun Yat-sen University, Zhuhai, China

The lateral carbon export related to mangroves is of great scientific significance and ecological value in the global carbon cycle. The dissolved inorganic carbon (DIC), dissolved organic carbon (DOC), particulate organic carbon (POC), and stable isotopes ($\delta^{13}C_{POC}$) of water samples were quantified in the flood (September 2020) and dry (January 2021) seasons in Zhangjiang Estuary. The results revealed that the carbon compositions in the tidal channel of the Zhangjiang Estuary are as follows: DIC > DOC > POC in both seasons. Except for the POC in the site near the sluice, the contents of all carbon compositions were significantly larger in the flood season than those in the dry season ($p < 0.05$). In the flood season, the POC and DOC exhibited similar spatial characteristics that all sites from the lower sites to the mouth were significantly larger than the site near the sluice. The DIC had an increasing trend from the upper site to the mouth. In the dry season, DIC and DOC displayed patchy distribution under the influence of mariculture and the sluice, while the POC had a decreasing trend from the upper site to the mouth. The MixSIAR model indicates that the source of the POC is overwhelmingly the mariculture, averagely accounting for 42.7% in the flood season and 52.6% in the dry season, mainly in the form of microalgae. The average contribution of mangrove to POC was 33.1% in the flood season and 39.3% in the dry season. The DIC-$\delta^{13}C_{POC}$ and DOC-POC relationships represent the biogeochemical process of microbial photosynthesis and the physical process of adsorption-desorption of organic carbon by redundancy analysis, respectively. This initial dataset for this region should be included in other studies to improve the mangrove outwelling estimate.

Keywords: carbon pools, mangroves, spatiotemporal distribution, sources, anthropogenic activities

OPEN ACCESS

Edited by:
Meilin Wu,
Chinese Academy of Sciences, China

Reviewed by:
Jiafang Huang,
Fujian Normal University, China
Qian Huang,
Johannes Gutenberg University Mainz, Germany

***Correspondence:**
Jianxiang Feng
fengjx23@mail.sysu.edu.cn
Qingshu Yang
yangqsh@mail.sysu.edu.cn

Specialty section:
This article was submitted to Marine Pollution, a section of the journal Frontiers in Marine Science

Received: *31 March 2022*
Accepted: *06 June 2022*
Published: *15 July 2022*

Citation:
Yan R, Feng J, Wang Y, Fu L, Luo X, Niu L and Yang Q (2022) Distribution, Sources, and Biogeochemistry of Carbon Pools (DIC, DOC, and POC) in the Mangrove-Fringed Zhangjiang Estuary, China. Front. Mar. Sci. 9:909839. doi: 10.3389/fmars.2022.909839

INTRODUCTION

Increasing carbon emissions from human activities and the resulting global climate change are of concern in both political and scientific communities (Rani et al., 2021). Thus, it is of great significance to explore the potentials of different types of ecosystems for mitigating global warming. As the largest carbon sink in the world, the ocean can absorb one-third of the global CO_2 emissions per year, and it is defined as blue carbon (McLeod et al., 2011). Estuaries are transitional regions linking the terrestrial environment and continental shelf, and they play a vital role in the global carbon cycle, with an annual net carbon flux of 0.85 Pg C (Bauer et al., 2013) into the ocean. However, the carbon cycle and flux in estuaries are regulated by many factors owing to their complex hydrodynamic conditions. This also leads to the biogeochemical parameters, including carbon, nitrogen, phosphorus, salinity, temperature, and chlorophyll, having different spatial and temporal gradients in different regions. For example, with the largest runoff of 80,000–250,000 m^3/s in the world, the Amazon Estuary mouth and the offshore displayed a CO_2 sink by the dilution of seawater and high chlorophyll contents (Lefèvre et al., 2017). However, in the Altamaha Estuary, the amount of dissolved organic matter (DOM) decreases from the upstream area to the estuary, which is mainly driven by seasonal variations in the river runoff (Letourneau et al., 2021). In addition, anthropogenic activities have a strong influence on the spatiotemporal distribution of estuarine biogenic matter. Owing to anthropogenic perturbation, the carbon pool has decreased by 25%–50% in the past 100 years, and an extra 0.2 Pg C $year^{-1}$ has been exported into the ocean (Regnier et al., 2013). However, the types and intensity of human activities vary in different regions, so it is necessary to focus on the spatiotemporal characteristics, sources, and biogeochemistry of the carbon pool based on the specific characteristics of each estuary to reveal the migration and transformation mechanisms.

Mangroves, a typical blue carbon ecosystem located in estuaries and coastal areas, occupy only 0.5% of the world's coastal area, but they contribute 10%–15% to their total carbon sequestration (Alongi, 2014). Compared with salt marshes (593 Mg C ha^{-1}), seagrass beds (142 Mg C ha^{-1}), and other types of forest systems (200–400 Mg C ha^{-1}), mangrove carbon stocks are remarkably high (956 Mg C ha^{-1}) owing to the burying of organic carbon in anoxic sediment, and thus, mangroves play an irreplaceable role in mitigating climate change. Studies had quantified the carbon stock of mangroves and the carbon exchange (Bouillon et al., 2007a; Bauer et al., 2013; Feng et al., 2017; Jeffrey et al., 2018). The lateral exchange in mangroves is also particularly important to scientific issues related to the global carbon cycling (Donato et al., 2011; Alongi, 2014). However, the hydrodynamic and sedimentary processes change significantly. In particular, the mangrove ecosystem in small estuaries is very sensitive to anthropogenic perturbations. Owing to the complex conditions of the mangrove carbon exchange, the carbon source, carbon export, and controlling mechanisms require further investigation.

The vertical carbon accumulation in mangroves, such as the net primary productivity and biomass, carbon stocks, and storage rates between species or communities, has been frequently reported in previous studies (Donato et al., 2011; Alongi, 2014; Feng et al., 2017; Kamruzzaman et al., 2017; Zhang et al., 2021). It has been found that the vertical carbon sink formed by a mangrove forest can export half of its detritus to the adjacent water environment, accounting for 10%–11% of the total carbon (Odum and Heald, 1975; Alongi, 2014), and thus, it appears to be a lateral carbon source. The mangrove outwelling hypothesis proposes that most of the mangrove detritus is transported to the coastal area in the form of dissolved inorganic carbon (DIC), dissolved organic carbon (DOC), and particulate organic carbon (POC) and maintains the function and stability of the estuary ecosystem through a series of physical and biogeochemical processes. Bouillon et al. (2007b) found that organic carbon can be mineralized and converted into DIC in estuaries. As they reported, DIC is considered to be the main form of estuary carbon export, accounting for more than 50% (Cai et al., 2008) of the total carbon exported from mangrove ecosystems globally, which may contribute to the missing carbon part of the budget. Additionally, the export of mangrove detritus is an important part of the carbon cycle. The contribution of mangrove to POC has been challenged based on stable isotope analysis and has been reported to be very limited (Lee, 1995). Most estuaries have tremendous internal spatial and temporal heterogeneity in terms of carbon processing and fluxes, making it difficult to quantify the net carbon balance of even an individual estuary. Therefore, the contribution of and lateral export from mangrove in estuaries need to be determined to enable further regional and global extrapolation (Bauer et al., 2013).

Stable isotope analysis is an effective tracing method for inferring the relative contributions of different carbon sources to particulate organic matter in aquatic ecosystems, especially complex estuaries. Schulte et al. (2011) found that the $\delta^{13}C_{POC}$ ($^{13}C/^{12}C$) value gradually increased from land to sea, indicating the transport distance of the terrestrial organic matter. On the Atlantic coast of the United States, the $\delta^{13}C_{POC}$ values of the sediment suggest that terrestrial organic matter cannot be transported to the estuaries (Hunt, 1970). Stable isotopes are effective only when the isotopic values of each source are significantly different, and the utilization of multiple isotopic indices can produce more accurate results. For example, multiple isotopes ($^{\delta 13}C_{POC}$, $\delta^{15}N$, and $\delta^{18}O$) have been combined to identify the sources of sewage (Cabral et al., 2019), organic matter in sediments, and consumers (Zhou et al., 2006). The C_4 *Spartina alterniflora* and phytoplankton have been found to be the main sources for filter-feeding mollusks based on $\delta^{13}C_{POC}$, $\delta^{15}N$, and $\delta^{34}S$ data for mangrove ecosystems (Peterson et al., 1985).

Anthropogenic perturbations have increased the flux of carbon to water bodies by as much as 1.0 Pg C $year^{-1}$ since pre-industrial times (Regnier et al., 2013), which has altered the flux from land to sea and the global carbon budget. There

is a large area of mangroves in the Zhangjiang Estuary (ZJE), which is also under the influence of strong human activities, including sluice construction, aquaculture, and invasion of *S. alterniflora*, making it even more complicated to determine the sources and contributors of the organic matter. The sluice built in 1966 prevents the saline sea water from retreating (Zhang and Deng, 2019) and decreases the discharge, transforming the ZJE into a typical tidally controlled area. In the past two decades, a large area of bare tidal flats has been invaded by *S. alterniflora*, as well as mangrove (Bouillon et al., 2008b; Alongi, 2014). The changes in the estuary's hydrodynamics and vegetation definitely altered the biochemical processes and the lateral carbon flux and sources. Furthermore, the coastal mariculture ponds occupied 981 ha, accounting for 41% of the entire ZJE. Therefore, the increased organic matter input from the mariculture may greatly affect the estuarine carbon cycle.

The objectives of this study were as follows: 1) to investigate the spatiotemporal features and sources of the DIC, DOC, and POC and the related estuarine processes under the effects of the sluice and mariculture; and 2) to determine the mangrove outwelling in the ZJE. Therefore, we attempted to reveal the fate of the laterally transported carbon in the ZJE and its critical mechanisms and to further understand the carbon cycle in small estuaries worldwide.

MATERIALS AND METHODS

Study Area

The ZJE (23°54'00"–23°58'00"N, 117°22'00"–117°30'00"E) is located in Yunxiao, Fujian Province, on the southeastern coast of China (**Figure 1**). It has a subtropical monsoon climate with an annual average temperature of 21.2°C (27.1°C in summer and 18.6°C in winter), an average annual precipitation of 1,714.5 mm, which is concentrated from April to September, a relative humidity of 79%, and an annual discharge of 1.0×10^9 m^3 in the estuary. The ZJE is a semi-enclosed, semi-diurnal tidal estuary, with a tidal range of 0.43–4.67 m (average of 2.32 m) and a salinity of 0‰–30‰. It occupies ~2,360 ha and is bordered by 117.9 ha of mangrove. The dominant species are *Avicennia marina*, *Kandelia obovata*, and *Aegiceras corniculatum*. *S. alterniflora* has been introduced into the region since the 1990s, has expanded at a rate of 4.28 m/year (Zhu et al., 2019), occupies 49.7 ha, and even has the potential to replace entire mangrove forests under the influence of strong human activities (Feng et al., 2017). In addition, the mariculture ponds distributed along the two sides of the ZJE and Dongshan Bay outside the estuary cover areas of 980 and 7,380 ha, respectively (Gao et al., 2021).

Sample Collection and Pretreatment

From the upper boundary to the mouth of the ZJE, eight sampling sites were chosen in two creeks. Sites N1, N2, N3, N4, and #5 were located in north Creek 1 from upstream to the estuarine mouth; and sites S1, S2, and S3 were located in south Creek 2 from the mangrove area to the bare flat (**Figure 1**).

Water samples and filter film samples were collected using Niskin bottles (1 L) from 10 to 20 cm below the surface during both ebb and flood in June 2020 (the flood season) and January 2021 (the dry season). The physicochemical parameters (temperature, salinity, and pH) of the water samples from each site were measured using a WTW Multi 3630 instrument (Weilheim, Germany). Total phosphorus (TP) was analyzed using the ammonium molybdate spectrophotometric method. The concentrations of nitrate–nitrogen (NO_3^--N) and ammonia–nitrogen (NH_4^+-N) in the water were determined using the ultraviolet spectrophotometric method and the sodium salicylate-sodium hypochlorite spectrophotometric method, respectively. Before further treatment, referring to Call et al. (2019), the water samples were collected using a polypropylene syringe (previously rinsed with sample), filtered through 0.7-μm Whatman GF/F filters, and stored in a 4°C incubator. The suspended particulate matter (SPM) was weighed after drying at 60°C.

The samples used to determine the POC content and for the stable carbon isotope analysis were then treated with 1 M HCl solution for 24 h to remove inorganic carbon. The organic carbon and total nitrogen contents were determined using an elemental analyzer (Elementar Macrocube, Germany). The stable carbon isotopes were measured using an elemental analyzer coupled with an isotope ratio mass spectrometer (Finnigan Delta V Advantage, Thermo Fisher Scientific, Inc.) in the stable isotope laboratory jointly operated by Shenzhen City Huake Precision Testing, Inc., and the Graduate School in Shenzhen, Tsinghua University. The stable isotope ratios are reported in delta notation as follows:

$$\boldsymbol{\delta}^{13} = \left[\left(\delta^{13}C_{sample} / \delta^{13}C_{standard}\right) - 1\right] \times 1000‰.$$

The DIC and DOC were collected in precombusted 50-ml borosilicate vials containing 100 μl of saturated $HgCl_2$ solution, with no headspace or bubbles. These samples were stored at 4°C in a refrigerator (Call et al., 2019). The DIC and DOC were both analyzed using an organic carbon analyzer (TOCL CSH CSN; Shimadzu Corp., Japan) with precisions of 0.01 and 0.02 mM, respectively.

Statistical Analysis

For POC source analysis, firstly, one-way analysis of variance (ANOVA) revealed that the $\delta^{13}C_{POC}$ and $\delta^{15}N$ values of the mariculture organic matter, marine phytoplankton, mangrove plants, and *S. alterniflora* in the ZJE were all significantly different from each other ($p < 0.05$). A Bayesian-mixing isotope model, MixSIAR, was used to estimate the probability distributions of the contributions of the sources to the mixtures (Moore and Semmens, 2008). We set the isotope fractionation as 0‰. The $\delta^{13}C_{POC}$ and $\delta^{15}N$ of the sources are presented in **Table 1**. The spatiotemporal features of the carbon components were analyzed using kriging interpolation (Arcgis10.2, Esri USA). Two-way ANOVA was conducted to determine the

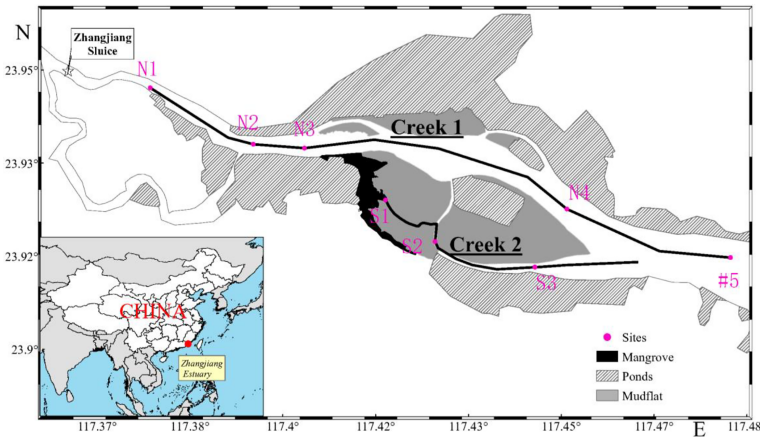

FIGURE 1 | Map of sampling sites in ZJE, Fujian, China.

seasonal and spatial effects on the physicochemical parameters, carbon contents, and stable isotope signatures using the SPSS 22 software (SPSS for Windows, SPSS, Inc.). Redundancy analysis (RDA) was also conducted to explore the relationships between the carbon content and environmental parameters using Canoco 4.5.

RESULTS

Physicochemical Properties of the Water Samples

The salinity (8.3‰–26.7‰), SPM (17.3–36.9 mg/L), temperature (16.2°C–22.9°C), pH (7.8–8.7), dissolved oxygen (DO; 5.6–13.4 mg/L), particulate nitrogen (PN; 0.08–0.6 mg/L), dissolved inorganic nitrogen (DIN; 0.6–4.3 mg/L), and dissolved inorganic phosphorus (DIP; 0.5–10.9 μmol/L) all exhibited significant seasonal differences ($p< 0.01$, **Table 2**). Except for PN and DIP, all of the components exhibited spatial differences, which may be the result of the mariculture drainage and its low DIP content.

Spatial and Seasonal Variability of Carbon Composition

In this study, the proportions of the carbon components were found to be as follows: DIC (70%) > DOC (21%) > POC (9%) (**Figure 2B**). In terms of seasonal variations, except for POC in N1, the POC, DOC, and DIC contents of were significantly higher in the flood season than those in the dry season ($p< 0.05$, **Table 3**; **Figure 2A**).

The average DIC was 11.8 mg/L, accounting for 44%–82% of the total carbon. The DOC was significantly (about 2.8-fold) higher in the flood season than that in the dry season (**Table 3**). The DIC showed an increasing trend in both north Creek 1 (12.8–29.1 mg/L) and south Creek 2 (20.4–24.8 mg/L) in the flood season (**Figure 3C**; **Table 3**). In the dry season, the DIC contents ranged from 2.7 to 3.9 mg/L. The sites near the fringed mangrove (N3 and S1–S3) and the sluice (N1) showed significantly higher DOC contents than the other sites (**Table 3**; **Figure 3F**), indicating that the DIC may have been correlated with the mangrove in the dry season.

The average DOC content was 3.5 mg/L, accounting for 13%–44% of the total carbon. The DOC was significantly (about 2.8-fold) higher in the flood season than that in the dry season (**Table 3**). In the flood season, the DOC contents in all sites were significantly larger than that in N1 ($p< 0.05$), but no significant difference was found among them. The DOC exhibited a patchy distribution owing to the drainage from the mariculture ponds in the dry season.

The average POC content was 1.57 mg/L, accounting for 3%–22% of the total carbon. The POC was significantly higher in the flood season than that in the dry season (about 5.1-fold that in the dry season; **Table 3**). The POC contents from N3 to the mouth #5 were significantly higher than that from N1 in the flood season ($p< 0.05$), while POC contents in the sites of N1–N3 were significantly higher than those in the other sites in the dry season ($p< 0.05$).

TABLE 1 | Signatures of $\delta^{13}C_{POC}$ and $\delta^{15}N$ of organic detritus.

Detritus	Values	Sample size	Reference
Ponds	$\delta^{13}C_{POC}$ = -23.0 ± 0.5 $\delta^{15}N$ = 7.0 ± 3.0	5	(Huang, 2013)
Marine phytoplankton	$\delta^{13}C_{POC}$ = -21.2 ± 0.2 $\delta^{15}N$ = 10.0 ± 0.2	3	
Mangrove	$\delta^{13}C_{POC}$ = -28.6 ± 2.1 $\delta^{15}N$ = 7.1 ± 1.0	5	
Spartina alterniflora	$\delta^{13}C_{POC}$ = -14.5 ± 0.2 $\delta^{15}N$ = 6.7 ± 1.0	5	

TABLE 2 | Two-way ANOVA results of site and season on carbon and physicochemical properties.

Factor	Season			Sites			Season * Sites		
	F	p	df	F	p	df	F	p	df
S	1,657	<0.001	1	3,603.5	<0.001	7	493.8	<0.001	7
SPM	73,225.3	<0.001	1	27,891	<0.001	7	16,510.3	<0.001	7
T	2,673.8	<0.001	1	19.8	<0.001	7	12	<0.001	7
pH	12.3	<0.001	1	3.1	<0.001	7	1.8	<0.001	7
DO	53.9	<0.001	1	69.5	<0.001	7	69.7	<0.001	7
PN	54.5	<0.001	1	0.9	>0.05	7	1.9	<0.001	7
DIN	316.3	<0.001	1	76.2	<0.001	7	103.8	<0.001	7
DIP	0.1	<0.001	1	0.1	>0.05	7	0.1	>0.05	7
POC	107.6	<0.001	1	6	>0.05	7	4	<0.001	7
DOC	247.4	<0.001	1	30.3	<0.001	7	5.8	<0.001	7
DIC	6,921.2	<0.001	1	781	<0.001	7	123.8	<0.001	7
$\delta^{13}C_{POC}$	21.3	<0.001	1	23.9	<0.001	7	9	<0.001	7

S, Salinity; SPM, Suspended particulate matter; T, Temperature; pH; DO, Dossilved oxygen; PN, Particulate nitrogen; DIN, Dissolved inorganic nitrogen; DIP, Dissolved Inorganic Phosphorus; POC, Particulate organic carbon; DOC, Dissolved organic carbon; DIC, Dissolved inorganic carbon; δ13CPOC.

Stable Isotope Values and Sources of Particulate Organic Carbon

With average values of −25.4‰ to −22.5‰, the $\delta^{13}C_{POC}$ values decreased successively from the upper reaches to the mouth. We divided the values into three groups according to the characteristics of the spatial differences, and the decreasing trend was as follows: Group 1 (S3, N4, #5) > Group 2 (N3, S1, S2) > Group 3 (N1, N2).

The contributions of the different sources to the POC in the ZJE in the flood season decreased in the following order: mariculture > mangrove > *S. alterniflora* > marine phytoplankton, with average values of 42.7%, 39.4%, 13.7%, and 4.1%, respectively. The contributions in the dry season changed to mariculture > mangrove > marine phytoplankton > *S. alterniflora*, with average values of 52.6%, 39.2%, 5.5%, and 2.5%, respectively. These results show that the POC mainly came from the mariculture ponds in the ZJE, mainly in the form of microalgae. As for the *S. alterniflora* and marine phytoplankton, both contributions exhibited seasonal variations. The decrease in the contribution from the mariculture and the increase in the contribution of the vegetation (mangrove, *S. alterniflora*) reflect the transition in the POC sources from the upper reaches to the mouth.

Relationship Between Carbon and Environmental Factors

The first two RDA dimensions were greater than 60% (**Figure 4**), so they can explain the carbon estuarine processes in the ZJE well. Negative relationships were observed between $\delta^{13}C_{POC}$ and DIC and between POC and DOC ($p < 0.05$), reflecting the biochemical (such as microbial photosynthesis) and physical processes related to organic carbon.

The temperature, salinity, DO, and DIN controlled the carbon composition. The highly negative correlation between the DIC and pH ($p < 0.05$), especially in the dry season, indicates that the pH directly affected the DIC in the water. The DOC was positively correlated with the DO, T, and C:N ratio in both the flood and dry seasons ($p < 0.05$). Moreover, the POC was positively correlated with the SPM and salinity ($p < 0.05$).

DISCUSSION

Comparison With Carbon Compositions of Other Estuaries

The composition, spatial distribution, and transformation of carbon in the water in estuaries are closely related to the weathering degree of the basin, the dynamics, and the biochemical conditions (Adame and Lovelock, 2011; Bianchi and Bauer, 2011; Bauer et al., 2013; Borges et al., 2018; Pierre et al., 2018; Ray et al., 2018; Spivak et al., 2018). Globally, estuarine water is usually enriched in DIC (2.4–72 mg/L) (Lefèvre et al., 2017; Borges et al., 2018; Liu et al., 2018) owing to the net heterotrophic (Bauer et al., 2013) conditions, high pCO_2, and correspondingly high rates of CO_2 degassing in estuaries. Large estuaries, such as the Yangtze River Estuary and the Pearl River Estuary, have greater buffering capacities and retain CO_2 in the water longer, leading to higher DIC contents (Cai, 2003). In this study, the water in the ZJE was found to have a relatively low DIC content (11.7 mg/L), which is similar to those of the Jiulong Estuary (13.85 mg/L), Sinnamary Estuary (13.38 mg/L), and Mekong Estuary (12.31 mg/L), but it is higher than that of the Hanjiang Estuary (7.96 mg/L), which does not contain mangrove (**Figure 5**). This indicates that the mangrove wetlands may act as an important net source of DIC. As the main form of carbon exported, DIC is mostly derived from mangrove mineralization and groundwater export (Bauer et al., 2013) in estuaries with mangrove ecosystems, contributing nearly 50% in the tidal channel (Bouillon et al., 2007a; Maher et al., 2013; Jeffrey et al., 2018).

In terms of DOC, the DOC contents of tropical mangrove estuaries [such as the Sinnamary Estuary (5.52 mg/L) and Mekong Estuary (4.43 mg/L)] are much higher than those of other estuaries, regardless of the size of the estuary (**Figure 5**), indicating that the DOC content is sensitive to the climate zone of the estuaries. The Sinnamary Estuary is one of the

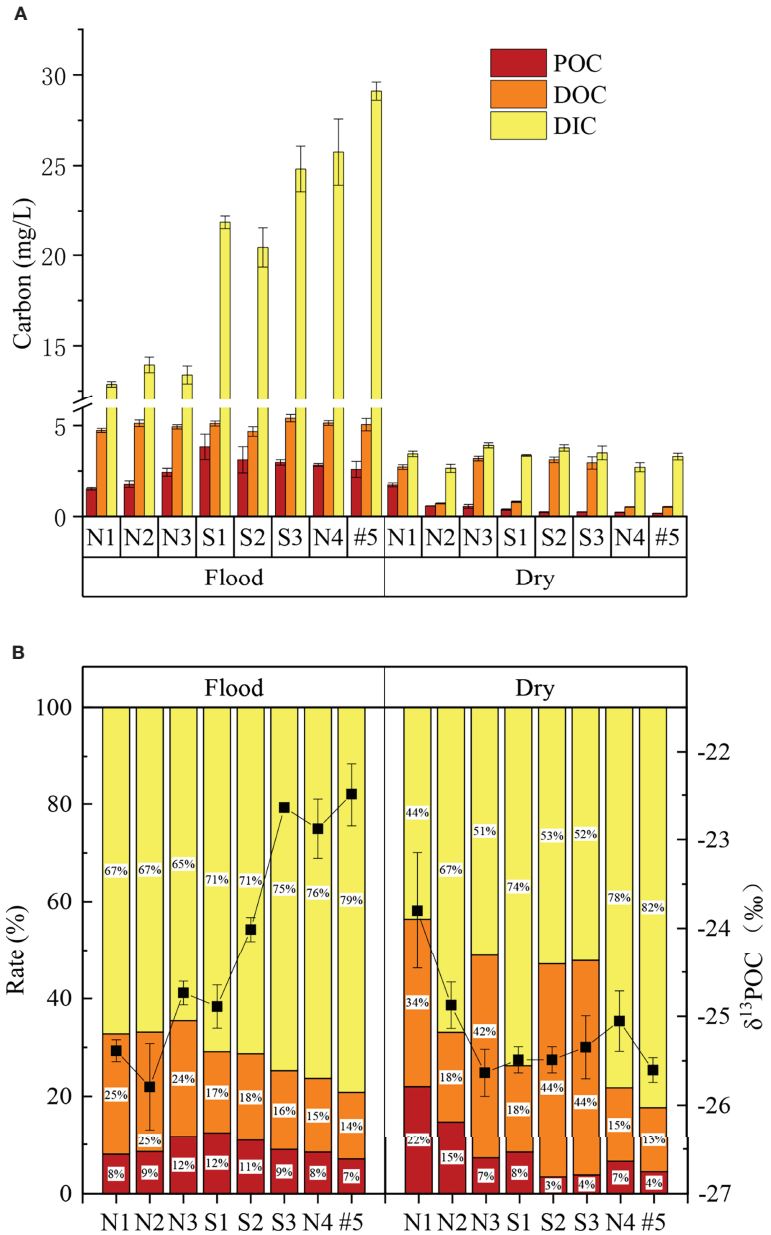

FIGURE 2 | Carbon statistics (**A**, mean and standard error are shown), stacking plot of carbon rate and δ^{13}POC (**B**, mean and standard error are shown) in the flood and dry seasons.

mangrove areas with the highest growth rate (150 cm year^{-1}) in the tropical regions (Ray et al., 2020). The hot and rainy climate accelerates leaching of the humus and organic detritus, and this included a series of processes (e.g., autotrophic activities, seawater mixing and dilution), resulting in the export of more DOC. The tidal dynamics and the mangrove area are secondary factors. The tidal range was found to influence the intensity of the pore water output because it controls the following: 1) the volume and surface area of the water in contact with the mangrove sediments at high tide and 2) the period and vertical extent of the pore water discharge based on the hydraulic advection phenomenon at low tide (Pierre et al., 2018). Thus, the larger the mangrove area is, the larger the contribution of the mangrove is. Under the same tidal amplitude, the water in the ZJE had a higher DOC content (3.42 mg/L) than that in the Jiulong Estuary (Liu et al., 2018) (1.69 mg/L) and the Hanjiang Estuary (Liu et al., 2018) (1.26 mg/L). This may be because the mangrove area is larger in the ZJE (660 ha) than those in the Jiulongjiang Estuary (360 ha) and the Hanjiang Estuary (0 ha).

The POC supports microbial degradation and high trophic biological feeding. Earlier outwelling investigations have focused on detritus or POC and their uptake by consumers (Gattuso et al., 1998), and less attention has been paid to POC sources. Generally, primary producers (e.g., microalgae) wetland plants,

TABLE 3 | Statistics of significant difference in the flood and dry seasons (mean ± SE, the uppercase and lowercase letters indicate the spatial difference in the flood season and dry season, respectively, and * indicates the seasonal difference at the same station, the differences are significant at $p < 0.05$).

		N1	N2	N3	S1	S2	S3	N4	#5
Flood	DIC (mg/L)	12.9 ± 0.2 d*	14.0 ± 0.4 d*	13.4 ± 0.5 d*	21.8 ± 0.3 c*	20.4 ± 1.1 c*	24.8 ± 1.3 b*	25.7 ± 1.8 b*	29.1 ± 0.5 a*
	DOC (mg/L)	4.7 ± 0.1 c*	5.1 ± 0.2 ab*	4.9 ± 0.1 ab*	5.1 ± 0.1 ab*	5.1 ± 0.3 ab*	5.4 ± 0.2 a*	5.2 ± 0.1 ab*	5.1 ± 0.3 ab*
	POC (mg/L)	1.5 ± 0.1 d	1.8 ± 0.2 cd*	2.4 ± 0.2 bc*	3.8 ± 0.7 a*	3.1 ± 0.7 ab*	3.0 ± 0.2 abc*	2.8 ± 0.1 abc*	2.6 ± 0.4 abc*
	δ^{13}POC (‰)	-25.4 ± 0.1 d*	-25.8 ± 0.5 d*	-24.7 ± 0.1 bc*	-24.9 ± 0.2 bc	-24.0 ± 0.1 b*	-22.6 ± 0.1 a*	-22.9 ± 0.3 a*	-22.5 ± 0.4 a*
Dry	DIC (mg/L)	3.4 ± 0.2 ABC	2.7 ± 0.2 C	3.9 ± 0.1 A	3.4 ± 0.1 ABC	3.8 ± 0.2 A	3.5 ± 0.4 AB	2.7 ± 0.3 C	3.3 ± 0.2 BC
	DOC (mg/L)	2.7 ± 0.1 B	0.7 ± 0.0 C	3.2 ± 0.1 A	0.8 ± 0.0 C	3.1 ± 0.2 A	3.0 ± 0.3 AB	0.5 ± 0.0 C	0.5 ± 0.0 C
	POC (mg/L)	1.7 ± 0.1 A	0.6 ± 0.0 B	0.6 ± 0.1 B	0.4 ± 0.0 C	0.2 ± 0.0 CD	0.3 ± 0.0 CD	0.2 ± 0.1 CD	0.2 ± 0.0 D
	δ^{13}POC (‰)	-23.8 ± 0.7 A	-24.9 ± 0.3 C	-25.6 ± 0.3 B	-25.5 ± 0.2 A	-25.5 ± 0.2 CD	-25.3 ± 0.4 D	-25.1 ± 0.3 BC	-25.6 ± 0.1 A

and woody plants are the primary POC sources, so their relative abundances and compositions determine the amounts and forms of organic materials that persist and comprise the standing POC pool (Bianchi and Bauer, 2011). For estuaries with high runoffs (>270 km^3 year^{-1}), such as the Yangtze Estuary, the dominant input of terrestrial POC occurs during the high discharge period, and they account for 72%–86% total organic carbon (Bianchi and Bauer, 2011; Wang et al., 2012). This demonstrates the importance of allochthonous POC sources. However, the POC in the ZJE (1.58 mg/L) and the terrestrial-dominated POC in the Yangtze Estuary (1.67 mg/L) are approximately the same, indicating that POC derived from the coastal wetlands can be equal to that supplied by the river. For small estuaries with limited inflow of sediment, the coastal wetlands provide 90% of the organic carbon for the heterotrophic activities in these estuaries (Regnier et al., 2013), and thus, the larger the mangrove area is, the higher the organic detritus is, and the larger the POC content is. Additionally, the Jiulong Estuary is a small macro-tidal estuary (Wang et al., 2017), belonging to the same dynamic type with the ZJE that both estuaries have no riverine POC. Since 1995, the POC average content in Jiulong Estuary has little changed under normal conditions, and the in-suit POC production from phytoplankton can contribute 44% (Cai et al., 1998). While up to 86% POC was derived from mariculture activities in the ZJE, which may result in 2-fold higher POC content in ZJE water than that in Jiulong Estuary. However, the Sinnamary Estuary has one of the largest mangrove areas (1,134 ha), and the resulting high mineralization and respiration rate consume large amounts of POC (Bouillon et al., 2007a; Bouillon et al., 2007b; Liu et al., 2018), so the content is not as expected.

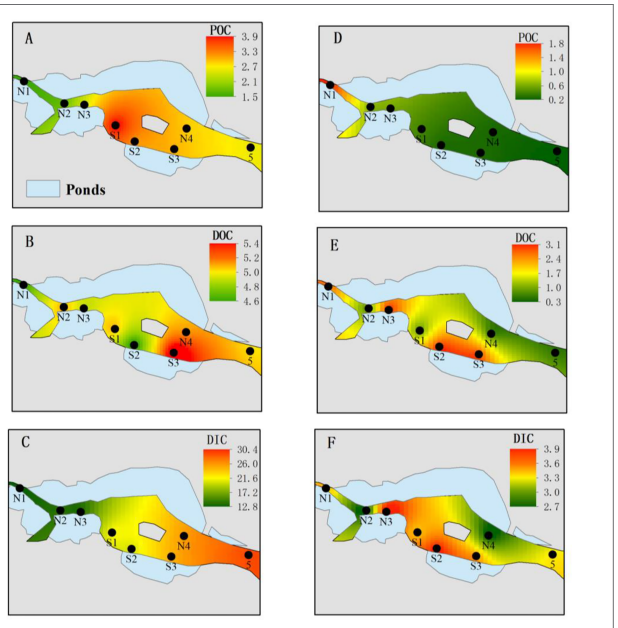

FIGURE 3 | Spatial distribution of various carbons in ZJE during the flood **(A–C)** and dry **(D–F)** seasons. **(A, D)** Particulate organic carbon (POC; mg/L); **(B, E)** dissolved organic carbon (DOC; mg/L); **(C, F)** dissolved inorganic carbon (DIC; mg/L).

Carbon Dynamics in the Two Creeks in Zhangjiang Estuary

The two creeks in the ZJE have different hydrodynamics, which are reflected by their salinity (Pierre et al., 2018). North Creek 1, the main channel connecting the upper reaches to the downstream Dongshan Bay (a semi-enclosed bay), is heavily influenced by the input of seawater and mariculture effluents. From sites N1 to #5, the salinity ranges from 3‰ to 30‰, which is slightly below the salinity of marine water (35‰). This is likely because Dongshan Bay acts as a buffer, and it has been reported to have a water residence time, suggesting incomplete tidal flushing within this small bay (Call et al., 2019), and thus, the seawater salinity at site #5 is relatively low. The upper reaches, sites N1–N3, are distinctly influenced by the surrounding ponds. In addition, the adjacent steep topography may enhance the surface water runoff from the adjacent terrestrial environment into north Creek 1 (no rivers discharge into the upstream area). In contrast, the salinity of south creek 2 (S1–S3), representing the dynamic evolution of the tidal system, ranges from 6‰ to 22‰. Abundant evidence suggests that the composition of carbon in the creek water is controlled by the pore water input (Bouillon et al., 2007b; Sippo et al., 2017; Pierre et al., 2018; Call et al., 2019), despite the freshwater input during the flood season and the *in situ* biogeochemical processes.

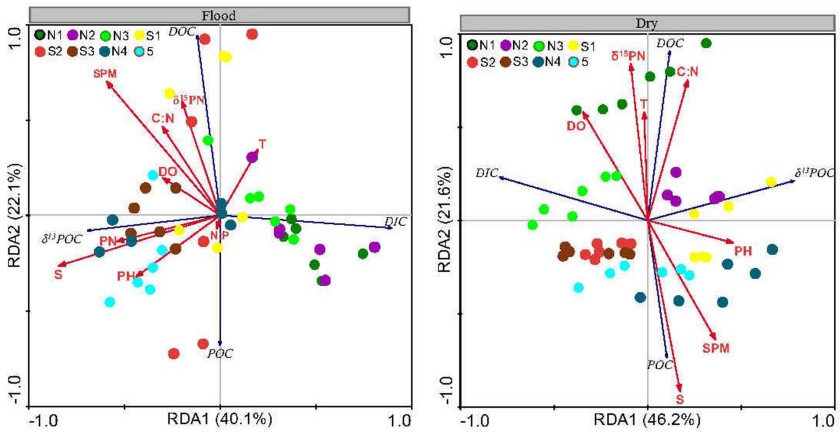

FIGURE 4 | Redundancy analysis ordination showing the relationship between carbon elements and the environmental parameters in the flood and dry seasons (The colors mean different sites).

The observations were conducted in both the flood and dry seasons. The POC distribution was found to be completely complementary despite the existing seasonal variations. In the flood season, the POC content was higher from the intertidal zone to both creeks (Creek 1: N4–#5, Creek 2: S1–S3). While in the dry season, the POC content had an decreasing trend from N1 to #5, and the POC content was significantly higher ($p < 0.05$) in the estuarine upper reaches (N1–N2). This indicates a high sediment load (associated with POC) from the mouth outside and that deposition-resuspension is also a very common phenomenon (María et al., 2016; Ray et al., 2020; Gao et al., 2021). This potential remobilization of sediments was observed to have a maximum velocity of 1 m/s, which is fast enough to exceed the threshold for the erosion of the sediments, resulting in an increase in the POC content. In addition, the vegetated tidal area (i.e., mangrove, *S. alterniflora*) had the maximum POC contents of 3.8 mg/L, which demonstrates the increase in the carbon storage capacity due to the interception and deposition of exogenous carbon (Li and Gao, 2013; Jiang et al., 2020; Zhang et al., 2021). In the dry season, the maximum POC content occurred in the upper reaches of Creek 1 (N1) (1.74 mg/L), but no seasonal difference was observed ($p < 0.05$). This indicates that the construction of the Beijiang sluice contributed to the change in the dynamic depositional conditions (Maavara et al., 2017; Pan et al., 2020; Gao et al., 2021). Before construction, the ZJE was affected by the fluvial runoff. After construction, the sediment dispersal was cut off, resulting in the accumulation of fine-grained sediments, i.e., a local POC sink.

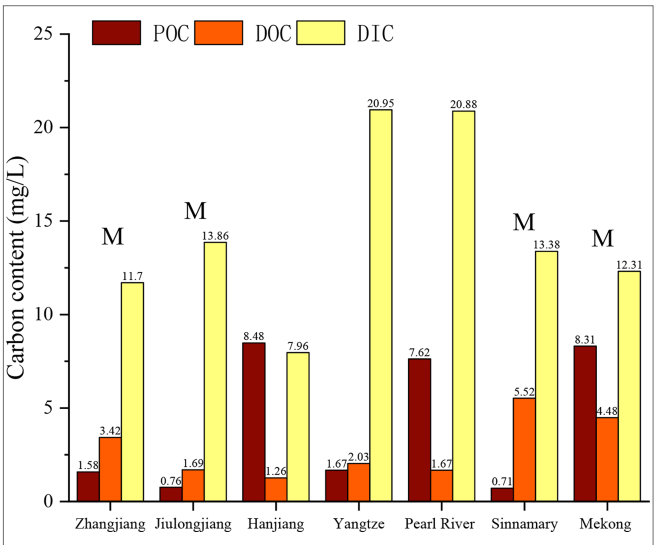

FIGURE 5 | Comparison of carbon compositions in different estuarine regions including ZJE, Jiulong Estuary (Liu et al., 2018), Hanjiang Estuary (Liu et al., 2018), Yangtze, Pearl River Estuary (Liu et al., 2018), Sinnamary Estuary (Ray et al., 2018), and Mekong Estuary (Liu et al., 2018). M indicates that there are mangroves located in the estuary.

In this study, it was found that mariculture contributed a large amount of POC to the water in the coastal wetlands, i.e., 24.6%–86.7% based on the MixSIAR model. The POM in the ponds included microalga, fish bait residue, animal manure, and other substances from natural sources. The excessive food supply and metabolic by-products resulted in the increase in the POC content of the water (Li et al., 2016). In the Mahakam Delta in Indonesia, the carbon output from aquaculture ponds was found to be 525 Mg C ha^{-1}, which is greater than that from mangrove and is equivalent to 266 years of carbon accumulation from natural mangrove (Arifanti et al., 2019). Feng et al. (2017) used MixSIR to analyze the food sources of the fish in the ZJE and found that the contribution of benthic microalgae was up to 80%. Baiting behavior is generally selective, and the contribution of POC to the food web is controversial. The suspended particles in ponds are similar to those of benthic microalgae in terms of their stable isotope compositions and C/N ratios (Spivak et al., 2018). Therefore, most of the POC in the ZJE may come from ponds, and the outwelling form could be microalgae.

The DOC and DIC exhibited different spatial patterns in both seasons. In the flood season, except for N1, DOC in all sites had no significant differences, and DIC had an upward trend with salinity increasing. However, the DOC contents in both mangrove creeks, N3–#5 in Creek 1 and S1–S3 in Creek

2, had no significant differences (**Table 3**). This may be due to the input of pore water *via* the tidal pump. In mangrove creeks, many studies have shown that the DOC is controlled by the pore water (Bouillon et al., 2007a; Bouillon et al., 2007b; Maher et al., 2013; Pierre et al., 2018; Call et al., 2019; Ohtsuka et al., 2020). During ebb tides, the water that retreats from the tidal creek has a composition similar to that of the pore water, which explains >60% of the DOC and >90% of the DIC (Bouillon et al., 2007a; Maher et al., 2013; Pierre et al., 2018; Call et al., 2019; Ohtsuka et al., 2020).

In the dry season, the effects of sluice construction and mariculture should be taken into account. The high DOC and DIC contents occurred near the Beijiang sluice (i.e., site N1) and the area with intensive mariculture (i.e., sites N3, S2, and S3). Under the closure effect of the Bejiang sluice, compared with the POC, the water exchange was limited and the residence time was longer, resulting in enrichment of terrestrial DOC and DIC near the sluice (i.e., 2.7 and 3.4 mg/L, respectively). The mariculture drainage resulted in the patchy distribution of the DOC. In southern China, aquaculture ponds are usually located adjacent to mangroves, and they are constructed by simply excavating mangrove forests. Sites N3, S2, and S3 were located close to aquaculture pond drainage outlets, resulting in DOC contents of 3.2, 3.1, and 2.9 mg/L, respectively, that is, 3.6–6.4-fold increases compared to the other sites. Following the decreasing trend of the nutrient concentration (Wu et al., 2014), the propagation distance of the DOC from the ponds was found to be about 3 km in the direction toward the sea. Although this is less than the distance to the coast, under certain conditions (such as typhoons, astronomical tides, and human activities), this carbon may be transported to the open sea. The short transport distance may be continuous and could lead to secondary pollution of the organic matter in the estuary.

Effects of Mangrove on Carbon Outwelling

Undoubtedly, mangrove forests have large organic carbon reserves, with a global mean total forest carbon reserve of 692. 8 ± 23.1 Mg C ha^{-1}. However, sequestered carbon, especially at depths of 0–1 m, is susceptible to remineralization and tidal export of DOC and DIC, since nearly all of this carbon respired within the entire soil horizon is released in a dissolved form (Bouillon et al., 2007b; Borges et al., 2018; Pierre et al., 2018; Alongi, 2022). The export of leaves, bark, branches, twigs, and other plant litter represents the most obvious loss of POC from mangrove, accounting for roughly 50% of the mangrove litterfall (Alongi, 2014). This indicates that mangrove can act as an important POC source.

In this study, site S1, which was located near the mangrove outwelling outlet during the flood season, had DOC, DIC, and POC contents that were on average 6.3-, 6.6-, and 10-fold higher, respectively, than those of the other sites. Two different processes may explain the similar ranges of the seasonal concentrations. First, litterfall is expected to be higher during the flood season as a result of the higher mangrove-derived organic matter driven by rainfall and temperature (Alongi, 2014). This litter is rapidly decomposed and leached, resulting in the greater contribution of the mangrove during the flood season (52.2% in the flood season, >27.5% in the dry season; **Table 4**). Second, the significantly negative relationship between the $\delta^{13}C_{POC}$ and DIC ($r^2 = 0.85$; **Figure 4**) explains the $\delta^{13}C$ of the microbial autotrophic activity under sufficient DIC. Identically, the highest $\delta^{13}C_{POC}$ values and lowest DIC occurred during the cyanobacteria bloom (Chomicki, 2010). Even in arid mangrove, planktonic particles contributed mostly to the POC pool (10%–65%) (Ray and Weigt, 2018). In addition, the relationships between $\delta^{13}C_{POC}$ and the other parameters (i.e., PN, DO, and C/N) illustrate the need for microbial autotrophic processes, implying the existence of this microbial activity.

Mangroves cover only 0.3% of the global ocean coastal areas, but they contribute 41% of the DIC + DOC + POC export to the adjacent coastal areas of ocean globally (Alongi, 2020). The high concentrations of DIC and DOC in the pore water pool and the subsurface transport result in a significant export of DIC and DOC to the adjacent tidal waters of the ocean in many places (Maher

TABLE 4 | Proportional contributions of different sources to POC in the flood and dry seasons (aquaculture, mangroves, *S. alterniflora,* and marine phytoplankton).

		df	Contributions(%, mean and range 5th~95th percentile)			
			Mariculture	**Mangroves plants**	***S. alterniflora***	**Marine phytoplankton**
N1	Flood	6	53.7 (37.8~68.3)	40.9 (28.3~53.1)	4.2 (0.9~9.9)	1.2 (0.0~4.8)
	Dry	6	86.7 (71.7~96.7)	10.2 (1.9~22.3)	1.2 (0.0~4.4)	1.9 (0.1~6.5)
N2	Flood	6	48.8 (33.6~63.1)	46.1 (33.4~57.9)	3.8 (0.8~8.9)	1.3 (0.0~4.5)
	Dry	6	53.1 (27.6~73.3)	38.1 (23.6~53.7)	3.1 (0.1~11.3)	5.7 (0.3~18.8)
N3	Flood	6	42.2 (34.0~69.0)	48.7 (25.7~53.9)	7.1 (1.7~14.6)	2.0 (0.0~8.4)
	Dry	6	48.8 (31.3~64.1)	46.0 (33.3~59.5)	1.8 (0.1~6.6)	3.4 (0.1~11.4)
S1	Flood	6	32.3 (12.4~53.2)	52.2 (37.5~65.4)	11.9 (2.7~22.0)	3.6 (0.1~16.0)
	Dry	6	66.8 (47.6~84.4)	27.5 (12.7~41.9)	2.0 (0.1~7.4)	3.7 (0.3~12.0)
S2	Flood	6	24.6 (4.1~40.5)	44.7 (34.4~56.7)	21.6 (5.3~30.9)	9.1 (0.1~37.1)
	Dry	6	46.5 (26.9~63.6)	46.6 (33.6~59.6)	2.1 (0.1~8.1)	4.7 (0.1~16.1)
S3	Flood	6	36.8 (12.7~66.7)	31.8 (7.8~49.8)	23.6 (3.7~37.9)	7.8 (0.1~30.6)
	Dry	6	40.0 (15.4~61.2)	48.9 (34.4~63.9)	3.2 (0.1~12.3)	7.8 (0.3~25.0)
N4	Flood	6	54.2 (27.0~84.6)	24.4 (5.7~42.2)	16.8 (3.6~30.3)	4.6 (0.1~19.2)
	Dry	6	36.0 (9.9~62.5)	48.2 (33.0~66.5)	4.7 (0.1~17.1)	11.1 (0.2~32.0)
#5	Flood	6	49.1 (33.0~67.8)	26.8 (15.2~37.1)	21.0 (11.1~30.5)	3.1 (0.1~12.6)
	Dry	6	43.4 (28.0~60.6)	48.5 (35.8~60.8)	2.5 (0.3~7.3)	5.7 (0.5~14.0)

et al., 2013; Ray et al., 2015; Liu et al., 2018; Pierre et al., 2018; Ray et al., 2018; Call et al., 2019; Santos et al., 2019). These results are consistent in revealing the high rates of export, and the mean DIC and DOC contents were found to be 339.6 and 229.1 mg/L, respectively. Large amounts of dissolved carbon may be exported from mangroves, possibly accounting for as much as 112–160 Tg a^{-1} of mangrove carbon, which could help to balance the budgets constructed by Bouillon et al. (2008a). As was reported, 41% of the litter produced is exported to the adjacent tidal waters, with 25.1 mmol m^{-2} d^{-1}. In this study, the mangrove-derived POC was determined to be 10.2%–52.2%. Even in the world's largest mangrove region (e.g., Sundarbans), the mangroves contribute ~60% (Ray et al., 2015), while in the Sinnamary Estuary, South America, the contribution is 70%, including terrestrial and benthic microalgae (Ray et al., 2018). Therefore, we confirm the viewpoint that mangrove contributions are conservative.

In this study, we investigated the three types of carbon involved in estuary processes, the source contributions, and the contents of the carbon components in different regions. However, we prefer to obtain the net flux, that is, the total carbon outwelling to the ocean every year. We suggest that the tidal flux at the mouth of the cross section be estimated to measure the carbon flux in the tidal cycle, which may provide a scientific basis for understanding the carbon budget and outwelling estimates from the mangroves in the ZJE.

CONCLUSIONS

In this paper, the spatiotemporal variability and mangrove outwelling of DOC, DIC, and POC in a mangrove-fringed estuary in Zhangjiang, China, were examined. DIC was the dominant form in the water. The content of all of the types of carbon was significantly higher in the flood season than in the dry season. The POC exhibited seasonally complementary features, that is, the contents were high in the middle reaches and mouth in the flood season and in the upper reaches in the dry season. The DOC and DIC both increased with increasing salinity during the flood season, but they exhibited patchy and fringed-patchy distributions, respectively. The spatial characteristics of the DIC, DOC, and POC reveal the profound effects of the Beijiang sluice and mariculture. Specifically, an average of 47.7% of the POC was from the mariculture effluent based on the stable isotope compositions, mainly in the form of microalgae. Additionally, the contribution of the mangrove was relatively limited, with 36.2% on average. Thus, global carbon outwelling estimates from mangroves differ owing to differences in the methodologies and hydroclimatic settings. An overall understanding of mangrove outwelling on the semi-diurnal and spring-neap-spring timescales in the ZJE will be obtained in future studies.

DATA AVAILABILITY STATEMENT

The original contributions presented in the study are included in the article/supplementary material. Further inquiries can be directed to the corresponding authors.

AUTHOR CONTRIBUTIONS

RY: study conception, investigation, data analysis and manuscript draft preparation. JF, QY and LN: project administration, funding support, conceptualization, supervision, and writing—review and editing. RY, JF, YW, LF, XL: sampling support and methodology. All authors contributed to the article and approved the submitted version of the manuscript.

FUNDING

This study was financially supported by grants by the National Natural Science Foundation of China (Grant No. 41976160, 41706090, 51709289) and the Fundamental Research Funds for the Central Universities, Sun Yat-sen University (Grant No. 22qntd2202).

ACKNOWLEDGMENTS

We were sincerely grateful for the support provided by Shuai Hu, Hao Yang, Ping Zhang, Haiwei Li, Tao Zhang, Ou Chen, Jie Huang, Fangting He, Enmao Huang, Tao Fu, Da Wan, Jiamin Yuan etc. for the field work and data acquisition. We also appreciate the anonymous reviewers for their constructive suggestions.

REFERENCES

Adame, M. F. and Lovelock, C. E. (2011). Carbon and Nutrient Exchange of Mangrove Forests With the Coastal Ocean. *Hydrobiologia* 663, 23–50. doi: 10.1007/s10750-010-0554-7

Alongi, D. M. (2014). Carbon Cycling and Storage in Mangrove Forests. *Annu. Rev. Mar. Sci.* 6, 195–219. doi: 10.1146/annurev-marine-010213-135020

Alongi, D. M. (2020). Carbon Cycling in the World's Mangrove Ecosystems Revisited: Significance of Non-Steady State Diagenesis and Subsurface Linkages Between the Forest Floor and the Coastal Ocean. *Forests* 11 (9), 977. doi: 10.3390/f11090977

Alongi, D. M. (2022). Impacts of Climate Change on Blue Carbon Stocks and Fluxes in Mangrove Forests. *Forests* 13(2), 149. doi: 10.3390/f13020149

Arifanti, V. B., Kauffman, J. B., Hadriyanto, D., Murdiyarso, D. and Diana, R. (2019). Carbon Dynamics and Land Use Carbon Footprints in Mangrove-Converted Aquaculture: The Case of the Mahakam Delta, Indonesia. *For. Ecol. Manage.* 432, 17–29. doi: 10.1016/j.foreco.2018.08.047

Bauer, J. E., Cai, W.-J., Raymond, P. A., Bianchi, T. S., Hopkinson, C. S. and Regnier, P. (2013). The Changing Carbon Cycle of the Coastal Ocean. *Nature* 504, 61–70. doi: 10.1038/nature12857

Bianchi, T. S. and Bauer, J. E. (2011). "Particulate Organic Carbon Cycling and Transformation," in *Treatise on Estuarine and Coastal Science*, vol. Vol 5. (Waltham: Academic Press), 69–117.

Borges, A., Abril, G. and Bouillon, S. (2018). Carbon Dynamics and CO2 and CH4 Outgassing in the Mekong Delta. *Biogeosciences* 15, 1093–1114. doi: 10.5194/bg-15-1093-2018

Bouillon, S., Borges, A. V., Castañeda-Moya, E., Diele, K., Dittmar, T., Duke, N. C., et al. (2008a). Mangrove Production and Carbon Sinks: A Revision of Global Budget Estimates. *Global Biogeochem. Cycles.* 22, GB2013. doi: 10.1029/2007GB003052

Bouillon, S., Connolly, R. M. and Lee, S. Y. (2008b). Organic Matter Exchange and Cycling in Mangrove Ecosystems: Recent Insights From Stable Isotope Studies. *J. Sea. Res.* 59, 44–58. doi: 10.1016/J.SEARES.2007.05.001

Bouillon, S., Dehairs, F., Velimirov, B., Abril, G. and Borges, A. V. (2007a). Dynamics of Organic and Inorganic Carbon Across Contiguous Mangrove and Seagrass Systems (Gazi Bay, Kenya). *J. Geophys. Res.: Biogeosci.* 112, GO2018. doi: 10.1029/2006JG000325

Bouillon, S., Middelburg, J. J., Dehairs, F., Borges, A. V., Abril, G., Flindt, M. R., et al. (2007b). Importance of Intertidal Sediment Processes and Porewater Exchange on the Water Column Biogeochemistry in a Pristine Mangrove Creek (Ras Dege, Tanzania). *Biogeosciences* 4, 311–322. doi: 10.5194/bg-4-311-2007

Cabral, A. C., Wilhelm, M. M., Figueira, R. C. L. and Martins, C. C. (2019). Tracking the Historical Sewage Input in South American Subtropical Estuarine Systems Based on Faecal Sterols and Bulk Organic Matter Stable Isotopes (δ^{13}c and δ^{15}n). *Sci. Total. Environ.* 655, 855–864. doi: 10.1016/j.scitotenv.2018.11.150

Cai, W.-J. (2003). Riverine Inorganic Carbon Flux and Rate of Biological Uptake in the Mississippi River Plume. *Geophys. Res. Lett.* 30 (2), 1032. doi: 10.1029/2002GL016312

Cai, Y., Guo, L. and Douglas, T. A. (2008). Temporal Variations in Organic Carbon Species and Fluxes From the Chena River, Alaska. *Limnol. Oceanogr.* 53, 1408–1419. doi: 10.4319/lo.2008.53.4.1408

Cai, A., Li, W., Chen, Q. and Wang, X. (1998). Studies of Particulate Organic Carbon in the Xiamen Western Harbour and the Jiulong River Estuary. *Mar. Sci.* 2, 37-41.

Call, M., Sanders, C. J., Macklin, P. A., Santos, I. R. and Maher, D. T. (2019). Carbon Outwelling and Emissions From Two Contrasting Mangrove Creeks During the Monsoon Storm Season in Palau, Micronesia. *Estuarine. Coast. Shelf. Sci.* 218, 340–348. doi: 10.1016/j.ecss.2019.01.002

Chomicki, K. (2010). The Use of Stable Carbon and Oxygen Isotopes to Examine the Fate of Dissolved Organic Matter in Two Small, Oligotrophic Canadian Shield Lakes. [dissertation/doctor's thesis]. [Ontario (IL)]: University of Waterloo.

Donato, D. C., Kauffman, J. B., Murdiyarso, D., Kurnianto, S., Stidham, M. and Kanninen, M. (2011). Mangroves Among the Most Carbon-Rich Forests in the Tropics. *Nat. Geosci.* 4, 293–297. doi: 10.1038/ngeo1123

Feng, J., Zhou, J., Wang, L., Cui, X., Ning, C., Wu, H., et al. (2017). Effects of Short-Term Invasion of Spartina Alterniflora and the Subsequent Restoration of Native Mangroves on the Soil Organic Carbon, Nitrogen and Phosphorus Stock. *Chemosphere* 184, 774–783. doi: 10.1016/j.chemosphere.2017.06.060

Gao, C., Yu, F., Chen, J., Huang, Z., Jiang, Y., Zhuang, Z., et al. (2021). Anthropogenic Impact on the Organic Carbon Sources, Transport and Distribution in a Subtropical Semi-Enclosed Bay. *Sci. Total. Environ.* 767, 145047. doi: 10.1016/j.scitotenv.2021.145047

Gattuso, J. P., Frankignoulle, M. and Wollast, R. (1998). Carbon and Carbonate Metabolism in Coastal Aquatic Ecosystems. *Annu. Rev. Ecol. Systematics.* 29, 405–434. doi: 10.1146/annurev.ecolsys.29.1.405

Huang, Q. (2013). Stable Isotope Studies on Food Sources of the Razor Clams (Sinonovacula constricta) in Two Cultivation Modes in Zhangjiangkou Estuary, Fujian. [dissertation/master's thesis]. [Xiamen (IL)]: Xiamen University

Hunt, J. (1970). The Significance of Carbon Isotope Variations in Marine Sediments. *Adv. Organic. Geochem.*, 27–35.

Hunt, J. (1970). *Advances in Organic Geochemistry. London: Pergamon Press* (1966). 27 p.

Jeffrey, L. C., Maher, D. T., Santos, I. R., Call, M., Reading, M. J., Holloway, C., et al. (2018). The Spatial and Temporal Drivers of Pco_2, Pch_4 and Gas Transfer Velocity Within a Subtropical Estuary. *Estuarine. Coast. Shelf. Sci.* 208, 83–95. doi: 10.1016/j.ecss.2018.04.022

Jiang, R., Cheng, P., Gao, J. and Wang, A. (2020). Impacts of Mangrove on the Dynamic Process of Bottom Boundary Layer. *Mar. Geo. Front.* 36, 37–44. doi: 10.16028/j.1009-2722.2019.108

Kamruzzaman, M., Ahmed, S. and Osawa, A. (2017). Biomass and Net Primary Productivity of Mangrove Communities Along the Oligohaline Zone of Sundarbans, Bangladesh. *For. Ecosyst.* 4, 16. doi: 10.1186/s40663-017-0104-0

Lee, S. Y. (1995). Mangrove Outwelling: A Review. *Hydrobiologia* 295, 203–212. doi: 10.1007/BF00029127

Lefèvre, N., Flores, M., Gaspar, F., Rocha, C., Jiang, S., Araujo, M., et al. (2017). Net Heterotrophy in the Amazon Continental Shelf Changes Rapidly to a Sink of CO2 in the Outer Amazon Plume. *Front. Mar. Sci.* 4. doi: 10.3389/fmars.2017.00278

Letourneau, M. L., Schaefer, S. C., Chen, H., Mckenna, A. M., Alber, M. and Medeiros, P. M. (2021). Spatio-Temporal Changes in Dissolved Organic Matter Composition Along the Salinity Gradient of a Marsh-Influenced Estuarine Complex. *Limnol. Oceanogr.* 66, 3040–3054. doi: 10.1002/lno.11857

Li, J. and Gao, S. (2013). Estimating Deposition Rates Using a Morphological Proxy of Spartina Alterniflora Plants. *J. Coast. Res.* 29, 1452–1463. doi: 10.2112/JCOASTRES-D-12-00186.1

Li, R., Liu, S., Zhang, J., Jiang, Z. and Fang, J. (2016). Sources and Export of Nutrients Associated With Integrated Multi-Trophic Aquaculture in Sanggou Bay, China. *Aquacult. Environ. Interact.* 8, 285–309. doi: 10.3354/aei00177

Liu, Q., Guo, X., Yin, Z., Zhou, K., Roberts, E. and Dai, M. (2018). Carbon Fluxes in the China Seas: An Overview and Perspective. *Sci. China Earth Sci.* 61, 1564−1582. doi: 10.1007/s11430-017-9267-4

Maavara, T., Lauerwald, R., Regnier, P. and Van Cappellen, P. (2017). Global Perturbation of Organic Carbon Cycling by River Damming. *Nat. Commun.* 8, 15347. doi: 10.1038/ncomms15347

Maher, D. T., Santos, I. R., Golsby-Smith, L., Gleeson, J. and Eyre, B. D. (2013). Groundwater-Derived Dissolved Inorganic and Organic Carbon Exports From a Mangrove Tidal Creek: The Missing Mangrove Carbon Sink? *Limnol. Oceanogr.* 58, 457–488. doi: 10.4319/lo.2013.58.2.0475

María, C. M., Ana, L. D., Anabela, A. B., María, C. P. and Mónica, S. H. (2016). Seasonal and Tidal Dynamics of Water Temperature, Salinity, Chlorophyll-A, Suspended Particulate Matter, Particulate Organic Matter, and Zooplankton Abundance in a Shallow, Mixed Estuary (Bahía Blanca, Argentina). *J. Coast. Res.* 32, 1051–1061. doi: 10.2112/JCOASTRES-D-14-00236.1

Mcleod, E., Chmura, G. L., Bouillon, S., Salm, R., Björk, M., Duarte, C. M., et al. (2011). A Blueprint for Blue Carbon: Toward an Improved Understanding of the Role of Vegetated Coastal Habitats in Sequestering CO2. *Front. Ecol. Environ.* 9, 552–560. doi: 10.1890/110004

Moore, J. W. and Semmens, B. X. (2008). Incorporating Uncertainty and Prior Information Into Stable Isotope Mixing Models. *Ecol. Lett.* 11, 470–480. doi: 10.1111/j.1461-0248.2008.01163.x

Odum, W. and Heald, E. Estuarine Research. London: Academic Press (1975). 265 p.

Ohtsuka, T., Onishi, T., Yoshitake, S., Tomotsune, M., Kida, M. , Iimura, Y., et al. (2020). Lateral Export of Dissolved Inorganic and Organic Carbon From a Small Mangrove Estuary With Tidal Fluctuation. *Forests* 11(10) 1041. doi: 10.3390/f11101041

Pan, D., Wang, Z., Zhan, Q., Saito, Y., Wu, H., Yang, S., et al. (2020). Organic Geochemical Evidence of Past Changes in Hydro- and Sediment-Dynamic Processes at River Mouths: A Case Study of Holocene Sedimentary Records in the Changjiang River Delta, China. *Continent. Shelf. Res.* 204, 104189. doi: 10.1016/j.csr.2020.104189

Peterson, B., Howarth, R. and Garritt, H. (1985). Multiple Stable Isotopes Used to Trace the Flow of Organic Matter in Estuarine Food Webs. *Sci. (New. York. N.Y.)* 227, 1361–1363. doi: 10.1126/science.227.4692.1361

Pierre, T., Ziegler, A. D., Friess, D. A., David, W., Vinh, T. V., Frank, D., et al. (2018). Carbon Dynamics and Inconstant Porewater Input in a Mangrove Tidal Creek Over Contrasting Seasons and Tidal Amplitudes. *Geochimica. Cosmochimica. Acta* 237, 32–48. doi: 10.1016/j.gca.2018.06.012

Rani, V., Bijoy Nandan, S. and Schwing, P. T. (2021). Carbon Source Characterisation and Historical Carbon Burial in Three Mangrove Ecosystems on the South West Coast of India. *CATENA* 197, 104980. doi: 10.1016/j.catena.2020.104980

Ray, R., Michaud, E., Aller, R. C., Vantrepotte, V., Gleixner, G., Walcker, R., et al. (2018). The Sources and Distribution of Carbon (DOC, POC, DIC) in a Mangrove Dominated Estuary (French Guiana, South America). *Biogeochemistry* 138, 297–321. doi: 10.1007/s10533-018-0447-9

Ray, R., Rixen, T., Baum, A., Gleixner, and Jana, T. K. (2015). Distribution, Sources and Biogeochemistry of Organic Matter in a Mangrove Dominated Estuarine System (Indian Sundarbans) During the Pre-Monsoon. *Estuar. Coast. Shelf. Sci.* 167, 404–413. doi: 10.1016/j.ecss.2015.10.017

Ray, R., Thouzeau, G., Walcker, R., Vantrepotte, V., Gleixner, G., Morvan, S., et al. (2020). Mangrove-Derived Organic and Inorganic Carbon Exchanges Between the Sinnamary Estuarine System (French Guiana, South America) and the Atlantic Ocean. *J. Geophys. Res.: Biogeosci.* 125, e2020JG005739. doi: 10.1029/2020JG005739

Ray, R. and Weigt, M. (2018). Seasonal and Habitat-Wise Variations of Creek Water Particulate and Dissolved Organic Carbon in Arid Mangrove (the Persian Gulf). *Continent. Shelf. Res.* 165, 60–70. doi: 10.1016/j.csr.2018.06.009

Regnier, P., Friedlingstein, P., Ciais, P., Mackenzie, F. T., Gruber, N., Janssens, I. A., et al. (2013). Anthropogenic Perturbation of the Carbon Fluxes From Land to Ocean. *Nat. Geosci.* 6, 597–607. doi: 10.1038/ngeo1830

Santos, I. R., Maher, D. T., Larkin, R., Webb, J. R. and Sanders, C. J. (2019). Carbon Outwelling and Outgassing vs. Burial in an Estuarine Tidal Creek Surrounded by Mangrove and Saltmarsh Wetlands. *Limnol. Oceanogr.* 64, 996–1013. doi: 10.1002/lno.11090

Schulte, P., Van Geldern, R., Freitag, H., Karim, A., Négrel, P., Petelet-Giraud, E., et al. (2011). Applications of Stable Water and Carbon Isotopes in Watershed Research: Weathering, Carbon Cycling, and Water Balances. *Earth-Science. Rev.* 109, 20–31. doi: 10.1016/j.earscirev.2011.07.003

Sippo, J. Z., Maher, D. T., Tait, D. R., Ruiz-Halpern, S., Sanders, C. J. and Santos, I. R. (2017). Mangrove Outwelling is a Significant Source of Oceanic Exchangeable Organic Carbon. *Limnol. Oceanogr. Lett.* 2, 1–8. doi: 10.1002/lol2.10031

Spivak, A. C., Gosselin, K. M. and Sylva, S. P. (2018). Shallow Ponds are Biogeochemically Distinct Habitats in Salt Marsh Ecosystems. *Limnol. Oceanogr.* 63, 1622–1642. doi: 10.1002/lno.10797

Wang, X., Ma, H., Li, R., Song, Z. and Wu, J. (2012). Seasonal Fluxes and Source Variation of Organic Carbon Transported by Two Major Chinese Rivers: The Yellow River and Changjiang (Yangtze) River. *Global Biogeochem. Cycles.* 26, 1−10 GB2025. doi: 10.1029/2011GB004130

Wang, A., Ye, X., Cheng, P. and Wang, L. (2017). Trapping Effect of Estuarine Turbidity Maximum on Particulate Organic Carbon and its Response to a Typhoon Event in a Macro-Tidal Estuary. in 19th EGU General Assembly, EGU2017: Proceedings from the Conference, 2017 April 23-28; Vienna, Austria: 2017. p. 115. URL: https://ui.adsabs.harvard.edu/abs/2017EGUGA..19..115W

Wu, H., Peng, R., Yang, Y., He, L., Wang, W., Zheng, T., et al. (2014). Mariculture Pond Influence on Mangrove Areas in South China: Significantly Larger Nitrogen and Phosphorus Loadings From Sediment Wash-Out Than From Tidal Water Exchange. *Aquaculture* 426-427, 204–212. doi: 10.1016/j.aquaculture.2014.02.009

Zhang, Y. M. and Deng, H. H. (2019). Preliminary Analysis and Calculation of Runoff About Yunxiao Pumped Storage Hydropower Station in Fujian Province. *Guangdong. Water Resour. Hydropowe.* 04, 44–48. doi: 10.11905/j.issn.1008-0112.2019.04.011

Zhang, Y., Yu, C., Xie, J., Du, S., Feng, J. and Guan, D. (2021). Comparison of Fine Root Biomass and Soil Organic Carbon Stock Between Exotic and Native Mangrove. *CATENA* 204, 105423. doi: 10.1016/j.catena.2021.105423

Zhou, J., Wu, Y., Zhang, J., Kang, Q. and Liu, Z. (2006). Carbon and Nitrogen Composition and Stable Isotope as Potential Indicators of Source and Fate of Organic Matter in the Salt Marsh of the Changjiang Estuary, China. *Chemosphere* 65, 310–317. doi: 10.1016/j.chemosphere.2006.02.026

Zhu, X., Hou, Y., Weng, Q. and Chen, L. (2019). Integrating UAV Optical Imagery and LiDAR Data for Assessing the Spatial Relationship Between Mangrove and Inundation Across a Subtropical Estuarine Wetland. *ISPRS. J. Photogrammetry. Remote Sens.* 149, 146–156. doi: 10.1016/j.jmarsys.2017.12.003

Conflict of Interest: The authors declare that the research was conducted in the absence of any commercial or financial relationships that could be construed as a potential conflict of interest.

Publisher's Note: All claims expressed in this article are solely those of the authors and do not necessarily represent those of their affiliated organizations, or those of the publisher, the editors and the reviewers. Any product that may be evaluated in this article, or claim that may be made by its manufacturer, is not guaranteed or endorsed by the publisher.

Copyright © 2022 Yan, Feng, Wang, Fu, Luo, Niu and Yang. This is an open-access article distributed under the terms of the Creative Commons Attribution License (CC BY). The use, distribution or reproduction in other forums is permitted, provided the original author(s) and the copyright owner(s) are credited and that the original publication in this journal is cited, in accordance with accepted academic practice. No use, distribution or reproduction is permitted which does not comply with these terms.

frontiers | Frontiers in Marine Science

DATA REPORT
published: 18 July 2022
doi: 10.3389/fmars.2022.945495

Investigation of Coastal Water Characteristics Along the Southeast Coast of India: A Multivariate Approach

Dilip Kumar Jha[1], Vikas Pandey[1], Chandrasekaran Muthukumar[2], Ponnusamy Sathish Kumar[1], Srinivas Venkatnarayanan[1], Jebarathnam Prince Prakash Jebakumar[3] and Gopal Dharani[1]*

[1] Ocean Science and Technology for Islands, National Institute of Ocean Technology, Ministry of Earth Sciences, Government of India, Chennai, India, [2] National Centre for Coastal Research, Ministry of Earth Sciences, Government of India, Chennai, India, [3] Coastal and Environmental Engineering, National Institute of Ocean Technology, Ministry of Earth Sciences, Government of India, Chennai, India

OPEN ACCESS

Edited by:
Meilin Wu, South China Sea Institute of Oceanology (CAS), China

Reviewed by:
Gopalakrishnan Thilagam, Pachaiyappa's College for Men, India
Prashanthi Devi Marimuthu, Bharathidasan University, India;
Ganesh Thiruchitrambalam, Pondicherry University, Port Blair Campus, India

***Correspondence:**
Dilip Kumar Jha
dilipjhaniot@gmail.com

Specialty section:
This article was submitted to Marine Pollution, a section of the journal Frontiers in Marine Science

Received: *16 May 2022*
Accepted: *08 June 2022*
Published: *18 July 2022*

Citation:
Jha DK, Pandey V, Muthukumar C, Sathish Kumar P, Venkatnarayanan S, Jebakumar JPP and Dharani G (2022) Investigation of Coastal Water Characteristics Along the Southeast Coast of India: A Multivariate Approach. Front. Mar. Sci. 9:945495. doi: 10.3389/fmars.2022.945495

Keywords: environmental quality, coastal, multivariate, Principal Component Analysis, Tamil Nadu coast

INTRODUCTION

Coastal waters support a diverse range of marine life and contribute to the country's economy. Seawater quality has a significant impact on the ecological sustainability and biological productivity of coastal and marine ecosystems (Dheenan et al., 2014; Dheenan et al., 2016). However, population growth and industrialization in the coastal regions have steadily increased the anthropogenic pressure, resulting in seawater quality degradation along the coast. Anthropogenic activities such as land-based runoff, sewage discharge, industrial & aquaculture effluent and eutrophication in the coastal environment could impact the aquatic biota of the region. Consequently, coastal pollution has become a global issue that requires intervention through the application of monitoring programs and improvement of the seawater quality through a mitigation management system.

The combined effects of salinity and temperature influence the coastal water, and nutrient content is responsible for productivity, therefore information on these parameter's distribution in different coastal ecosystems is important (Satpathy et al., 1986). Among the numerous inorganic elements required for life support in marine coastal ecosystems, nitrogen, phosphorous, and silicates are believed to be more significant than the others because they play a vital role in phytoplankton abundance, growth, and metabolism (Barath Kumar et al., 2018). The distribution and behavior of nutrients in the coastal environment, particularly in the nearshore environment, varies greatly depending on local variables such as anthropogenic activities, fresh water influx, tidal variation, and biological activity such as phytoplankton intake and regeneration.

Although several studies on water quality have been conducted in other Indian coastal regions (Renjith et al., 2015; Jha et al., 2015; Yuvaraj et al., 2018; Satheeswaran et al., 2019; Ratnam et al., 2022), there is relatively less work carried out on the seawater quality characteristics for such a long coastal stretch in this region. Recently, Barath Kumar et al. (2018) have studied seawater characteristics at 8 locations over a 300 km coastal stretch along the Tamil Nadu coast. In the present study, we have monitored over 537 km of stretch spreading in five coastal districts. The objective of this study is to understand the spatial variation of physicochemical and biological characteristics in the seawater of five coastal districts in southeast coast India. The data gathered might be useful for comparative research aimed at evaluating the environmental conditions of other tropical coastal locations. The pattern of physicochemical characteristics of coastal waters along the southeast coast

of India was evaluated using analysis of variance (ANOVA-one way), box-whisker plots, principal component analysis (PCA), and N/P ratio.

METHODS

Tamil Nadu has a coastal length of 1076 Km and stretches along the Bay of Bengal, Arabian Sea and the India Ocean. Palk Bay (PB) and the Gulf of Mannar (GoM), which are located along India's southeast coast, form a significant part of of the country's entire coastline length (Barath Kumar et al., 2018; Pandey et al., 2022; Jha et al., 2022). Thanjavur (THA), Pudukottai (PUD), Ramanathapuram (RAM), Thoothukudi (THO), and Tirunelveli (TIR) were five coastal districts (hereafter 'locations') surveyed during the pre monsoon period (January to March) of 2020 to evaluate the seawater quality (**Figure 1A**). Surface and bottom seawater samples were collected from near shore and offshore sites (n= 168 samples). A hand-held GPS (Garmin eTrex Vista; ± 5 m) was used to record the sampling position in the present study.

Sample Collection and Analysis

A Niskin's water sampler was used from a boat to collect seawater samples in polypropylene bottles for nutrient analysis. The titration method of Winkler (Winkler, 1888) was used to assess samples for dissolved oxygen (DO) and biochemical oxygen demand (BOD). The argentometric titration technique was used to determine salinity. Onboard, a calibrated thermometer and a pH meter were used to measure temperature and pH, respectively. To estimate total suspended solids (TSS), 1 L of seawater was filtered using 0.45 µm Millipore GF/C filter paper and rinsed with Milli-Q water to eliminate salt content (APHA, 2005). The nutrients namely nitrite, nitrate, inorganic phosphate (IP), silicate, total nitrogen (TN), ammonia, and total phosphorus (TP) were measured in seawater samples using procedures of Grasshoff et al. (1999). The Redfield ratio (N:P = 16:1) was used to compare nutrient ratio of dissolved inorganic nitrogen (nitrate + nitrite + ammonium = N) and phosphate to assess possible nutritional control on biological production (Van Nieuwerburgh et al., 2004). The spectrophotometric approach was used to examine chlorophyll-a (chl-a) and phaeophytin content (Parsons et al., 1992). Triplicate samples were analyzed, with quality control techniques including thorough standardization and blank measurements. To test spatial variations of physicochemical parameters, one-way ANOVA was employed. The Euclidean distance (ED) based hierarchical agglomerative cluster analysis (CA) (Ward, 1963) from normalized dataset was used to generated dendrogram. The dendrogram is a useful graphical tool for determining the number of clusters that explain the underlying mechanism that causes spatial patterns (Shrestha and Kazama, 2007; Yang et al., 2010). The same ED matrix was used for the non-metric multidimensional scaling (NMDS) ordination plot to corroborate the results of CA. Factor analysis (FA) is one of the most effective approach for decreasing the dimensionality of enormous datasets while preserving their content (Wunderlin et al., 2001). Strong (> 0.75), moderate (0.75–0.50), and weak (0.50–0.30) factor loadings were classified according to Liu et al. (2003) criteria. To establish sample adequacy, the Kaiser–Meyer–Olkin (KMO) criterion was used. To reduce the impact of discrepancies in measurement units and variance, all parameters were normalized using a Z-scale transformation (mean = 0; variance = 1), which rendered the data dimensionless for factor analysis. The analyses were conducted using SPSS software (version 18.0).

RESULTS AND DISCUSSION

The physicochemical parameters of five coastal locations are summarized in **Table S1** (**Supplemental Material**); the concentrations are shown as range and mean (± standard deviation [SD]). The presence of spatial variability induced by polluting sources and/or climatic conditions is indicated by environmental metrics with a high SD (Vega et al., 1998). At Ramanathapuram, the mean TSS (40.49 ± 10.09 mg/L), salinity (31.73 ± 1.52 PSU), and DO (5.93 ± 0.65 mg/L) were high compared to the other locations. The elevated TSS might be attributable to the persistent operation of fishing trawlers and tourist activities, which disturbed the water column in the study region. It was observed that mean AT (30.04 ± 0.73°C) and WT (28.47 ± 0.82°C) were comparatively higher at Tirunelveli and Ramanathapuram, respectively. The mean pH value (8.33 ± 0.10) was comparatively high at Pudukottai. The BOD varied significantly (F=7.011, $p < 0.05$) and was comparatively high (1.80 ± 0.73 mg/L) at Thanjavur, however, it was well within the prescribed limits of the Central Pollution Control Board (CPCB). The nutrients such as nitrite (0.27 ± 0.07 µM), nitrate (3.32 ± 0.27 µM), phosphate (1.75 ± 0.57 µM), total nitrogen (10.70 ± 4.43 µM), and total phosphate (2.28 ± 0.63 µM) concentrations were found higher in Thanjavur while silicate (18.34 ± 5.60 µM) was higher in Pudukottai. This might be due to more anthropogenic activity such as agriculture based land discharge and sewage mixing in the coastal water bodies. Chlorophyll-a, and phaeophytin content were comparatively high in Tirunelveli. In the present study, the spatial variation of all the physicochemical and biological parameters was significant ($p < 0.05$) among different locations except WT, DO, and ammonia ($p > 0.05$).

The **Figures 1B–I** shows box-whisker plots for selected seawater quality parameters. A box plot with no upper whisker indicates that the upper quartile is equal to the maximum [such as that of WT (**Figure 1B**). Long whiskers at the top of the box plot [such as that for TSS (**Figure 1I**) & phosphate (**Figure 1G**) and the bottom [such as salinity (**Figure 1C**) and chl-a (**Figure 1D**), indicate the underlying distribution is skewed toward the high and low range, respectively. Comparatively higher values of BOD (**Figure 1E**) were observed in near-shore samples. The box plots with wide spread revealed spatial deviation in sample distribution which was evident in the nitrate (**Figure 1F**) at Thanjavur.

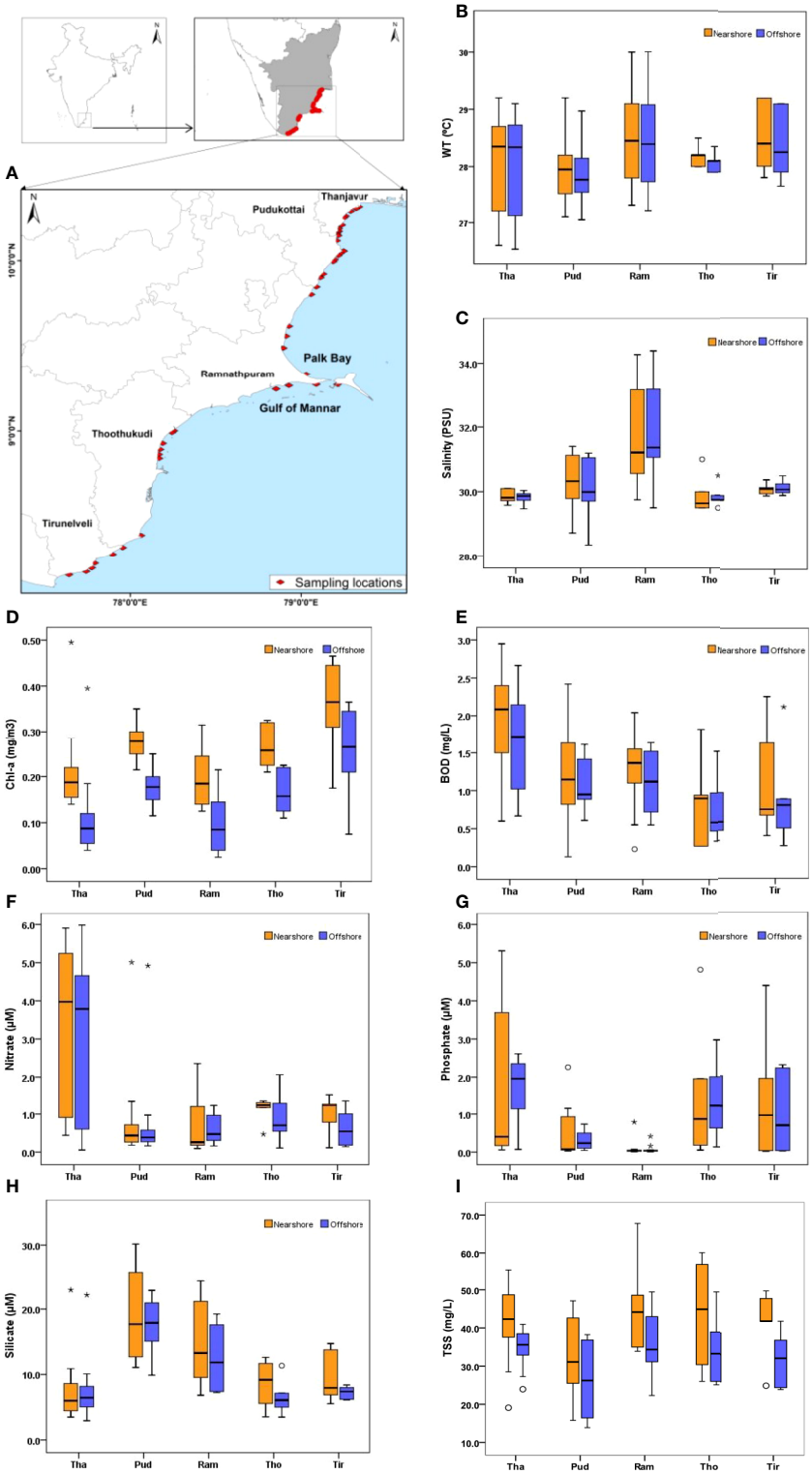

FIGURE 1 | Study area map and box-whisker plots display variations for selected physiochemical variables. **(A)** sampling locations, **(B)** WT, **(C)** salinity, **(D)** chl-a, **(E)** BOD, **(F)** nitrate, **(G)** phosphate, **(H)** silicate and **(I)** TSS. In each plot, the median is represented by the central point, the interval is represented by the rectangle (i.e. 25% and 75% percentiles), and range indicated by the whisker [(*: extreme outlier; ◦: mild outlier); Sampling locations: THA, Thanjavur; PUD, Pudukottai; RAM, Ramanathapuram; THO, Thoothukudi; and TIR, Tirunelveli.

Box plots showed higher silicate in Pudukottai (**Figure 1H**). Further, the selected environmental parameters showed higher concentration towards the nearshore compared to the offshore. The mild (circles) and extreme outliers (asterisks) are indicating a difference in the observed factors at a few sampling stations that might be influenced by some human activities (Jha et al., 2014).

The cluster analysis generated a dendrogram with only one cluster containing THO & TIR which might be explained by the similarity in average values of physicochemical characteristics and dissimilarity from the other locations. The other locations i.e. THA, PUD and RAM were outliers **Figure 2A**. The PUD and RAM, however, showed closed distance on the dendrogram with the cluster formed between THO & TIR. On the other hand, THA showed maximum distance from the cluster resulting from the significant differences in physicochemical values at this location when compared to the other locations. The distance between PUD and RAM was very less which could be attributed to the similar values of silicate compared to other locations. The physiochemical variables depicted a comparable pattern to that of cluster analysis while exposed to 2D nMDS analysis (**Figure 2B**).

The KMO criterion values of 0.550 revealed that by factor analysis, a considerable diminution in the dimensionality of the data set has been obtained (Wu et al., 2010) for the Tamil Nadu coast. Through FA seven significant factors (Eigenvalue >1) were obtained which elucidating 79.83% of the total variation among the dataset along the southeast coast of India. The factor loadings and communality of environmental variables are given in **Table S2** (**Supplemental Material**). Factor 1 elucidates 22.34% of the total variance and reveals moderate positive loading of nitrate (0.693), phosphate (0.700), total phosphorus (0.694), and moderate negative loadings of silicate (-0.556) whereas strong positive loadings of sewage discharge (0.836) and industrial units (0.825) (**Figure 2C**). Factor 2 elucidates 14.46% of the total variance and revealed a moderate positive loading of AT (0.625) and ammonia (0.688) whereas moderate negative loading of pH (-0.619). It might be explained by the natural co-existence of increased ammonia levels in seawater and a high pH value, owing to heavy anthropogenic input in the coastal environment.

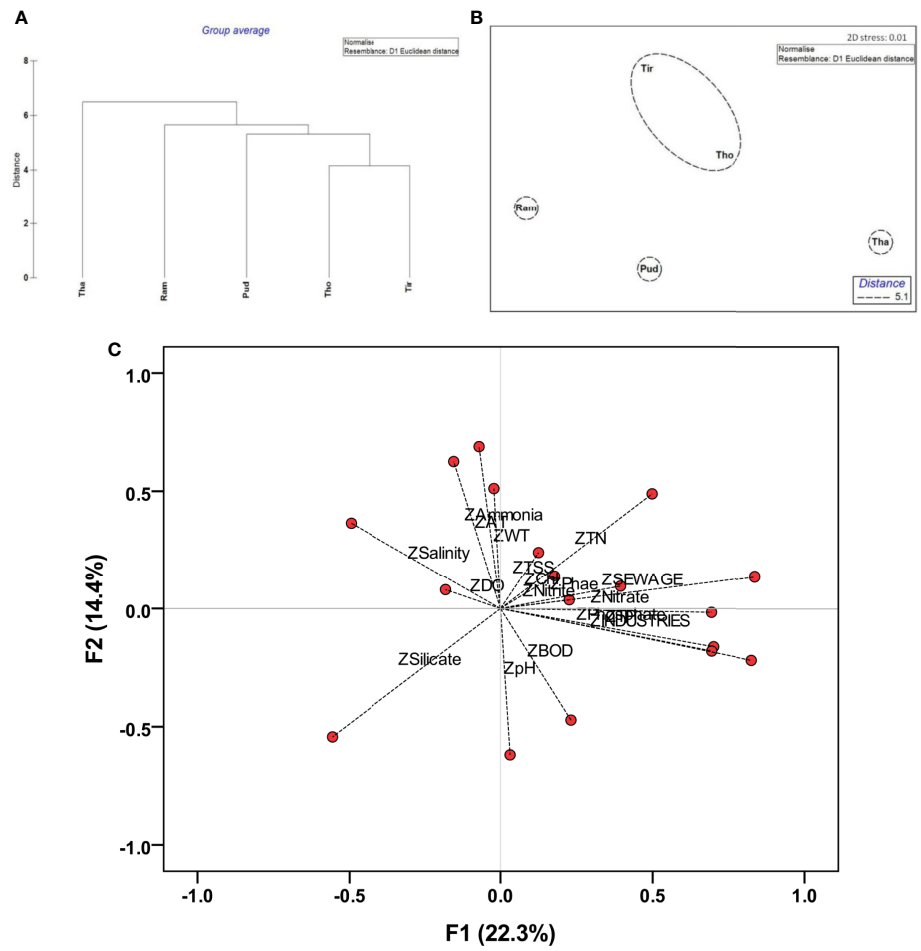

FIGURE 2 | Cluster analysis, 2D NMDS and factor analysis; **(A)** dendrogram of the physiochemical variables in seawater, **(B)** non-metric multidimensional scaling resemblance of physiochemical variables in seawater, and **(C)** factor loading F1 and F2 for environmental parameters.

The Redfield ratio (1934; 1958) in the present study for N/P was 3.68, 9.44, 56.29, 3.55, and 4.54 at Thanjavur, Pudukottai, Ramanathapuram, Toothukodi, and Tirunelveli, respectively. It is stated that the N/P ratio lesser than 16 specify nitrate could be a limiting factor. However, except at Ramanathapuram, the N/P ratio was lesser than 16 which revealed that nitrate was the limiting factor at all the stations except Ramanathapuram where phosphate was the limiting factor. It is reported that an undisturbed location will have phosphate limitation whereas at disturbed location nitrate will be the limiting factor (Gupta et al., 1981). Rivers and sewage channels deliver nutrients to coastal bays under certain environmental circumstances (Xu, 1989). Our observation depicted that anthropogenic impact plays a vital role in regulating the physicochemical parameters, barring the environmental parameters such as temperature and salinity, which were demonstrated through the multivariate approach in a more significant way and is comparable with the earlier scientific studies conducted in other coastal locations (Barath Kumar et al., 2018; Pandey et al., 2022). Regular monitoring will help to maintain the seawater quality, promote healthy habitats for flora and fauna, and contribute to coastal conservation and fisheries management (Vijayakumaran et al., 2005; Murugan et al., 2005; Kumar et al., 2009).

CONCLUSION

To evaluate, coastal water characteristics, sampling was conducted along the five coastal districts in the southeast coast of India. The results obtained through the multivariate tool indicated a good seawater quality at all the sites except near-shore sites of the Thanjavur. In Thanjavur, noticeable variations in the physicochemical parameters were observed in CA and therefore it resulted in an outlier. When the data was subjected to 2D nMDS ordinations, it showed a similar pattern to the CA. Strong factor loadings of sewage discharge (0.836) and industrial units (0.825) illustrated that the variability is due to the influence of physicochemical concentration in the coastal environment. The results revealed higher values near the coast whereas it was oligotrophic towards the offshore waters. The findings will be significant for comparing to other tropical coastal environments.

DATA AVAILABILITY STATEMENT

The original contributions presented in the study are included in the article/**Supplementary Material**. Further inquiries can be directed to the corresponding author.

AUTHOR CONTRIBUTIONS

DJ: Conceptualization, sampling design, data validation, multivariate analysis, and writing-original draft. VP: Collection of samples, analysis of samples, and processing of data. CM: Analysis of sample and data processing. PS: Field investigation and analysis. SV: Field survey and analysis. PJ: Coordination of field survey and reviewing the data. GD: Suggestion to review the manuscript, technical input, and project management. All authors contributed to the article and approved the submitted version.

ACKNOWLEDGMENTS

The authors are thankful to the Ministry of Earth Sciences, Govt. of India, for extending their support for the present study. Dr. G. A. Ramadass, Director, NIOT, Chennai, is to be thanked for his continual encouragement, support, and guidance. We are grateful to Dr. Vijaya Ravichandran, Scientist-G, NIOT, for her guidance and support for this research. We thank Dr. Pravakar Mishra, Scientist-F, NCCR for his critical review on the manuscript. We thank our colleagues Mr. S. Ragumaran, Mr. G. Nanadhagopal, and Mr. B. Ranjan Babu for their support during the survey. We also like to thank the scientific and supporting staff of NIOT's MBT and CEE Groups in Chennai, India, for their timely help.

SUPPLEMENTARY MATERIAL

The Supplementary Material for this article can be found online at: https://www.frontiersin.org/articles/10.3389/fmars.2022.945495/full#supplementary-material

REFERENCES

APHA (American Public Health Association) (2005). "Standard Methods for the Examination of Water and Wastewater," in *American Works Association and Water Environmental Federation*, (APHA-AWWA-WEF) 21th Edition(Washington, D.C).

Barath Kumar, S., Mohanty, A. K., Padhi, R. K., Selvanayagam, M. and Satpathy, K. K. (2018). Coastal Water Characteristics Along Tamil Nadu, East Coast of India During Pre-Northeast Monsoon Period. *Indian Jour. Geo Mar. Sci.* 47 (2), 308–318.

Dheenan, P. S., Jha, D. K., Das, A. K., Vinithkumar, N. V., Prashanthi Devi, M. and Kirubagaran, R. (2016). Geographic Information Systems and Multivariate Analysis to Evaluate Fecal Bacterial Pollution in Coastal Waters of Andaman, India, *Environmental Pollution* 214, 45–53. doi: 10.1016/j.envpol.2016.03.065

Dheenan, P. S., Jha, D. K., Vinithkumar, N. V., Ponmalar, A. A., Venkateshwaran, P. and Kirubagaran, R. (2014). Spatial Variation of Physicochemical and Bacteriological Parameters Elucidation With GIS in Rangat Bay, Middle Andaman. *India J. Sea Res.* 85, 534–541. doi: 10.1016/j.seares.2013.09.001

Grasshoff, K., Kremling, K. and Ehrhardt, M. (1999). *Methods of Seawater Analysis, Third Ed* (Weinheim, Germany: Verlag Chemie).

Gupta, R. S., Moraes, C., George, M. D., Kureishy, T. W., Noronha, R. J. and Fondekar, S. P. (1981). Chemistry & Hydrography of the Andaman Sea. *Indian J. Mar. Sci.* 10, 228–233.

Jha, D. K., Pandey, V., Santhanakumar, J., Sathish Kumar, P., Venkatnarayanan, S., Jebakumar, J. P. P., et al. (2022). Evaluation of Site Suitability for Artificial Reefs Deployment in Southeast Coast of India Using Geographical Information System as a Management Tool. *Front. Mar. Sci.* 8. doi: 10.3389/fmars.2021.817975

Jha, D. K., Vinithkumar, N. V., Sahu, B. K., Das, A. K., Dheenan, P. S., Venkateshwaran, P., et al. (2014). Multivariate Statistical Approach to Identify Significant Sources Influencing the Physic-Chemical Variables in Aerial Bay, North Andaman, India. *Mar. pollut. Bull.* 85, 261–267. doi: 10.1016/j.marpolbul.2014.06.007

Jha, D. K., Vinithkumar, N. V., Sahu, B. K., Dheenan, P. S., Das, A. K., Mehmuna Begum, , et al. (2015). Multivariate and Geo-Spatial Approach for Seawater Quality of Chidiyatappu Bay, South Andaman Islands, India. *Mar. pollut. Bull.* 96(1–2), 463–470. doi: 10.1016/j.marpolbul.2015.05.004

Kumar, T. S., Vijayakumaran, M., Murugan, T. S., Jha, D. K., Sreeraj, G. and Muthukumar, S. (2009). Captive Breeding and Larval Development of the Scyllarine Lobster Petrarctusrugosus , New Zealand. *J. Mar. Freshw. Res.* 43:1, 101–112. doi: 10.1080/00288330909509985

Liu, C. W., Lin, K. H. and Kuo, Y. M. (2003). Application of Factor Analysis in the Assessment of Groundwater Quality in a Blackfoot Disease Area in Taiwan. *Sci. Total Environ.* 313, 77–89. doi: 10.1016/S0048-9697(02)00683-6

Murugan, T. S., Remany, M. C., Mary Leema, T., Jha, D. K., Santhanakumar, J., Vijayakumaran, M., et al. (2005). Growth, Repetitive Breeding, and Aquaculture Potential of the Spiny Lobster, Panulirus Ornatus, New Zealand. *J. Mar. Freshw.* 39:2, 311–315. doi: 10.1080/00288330.2005.9517311

Pandey, V., Jha, D. K., Sathish Kumar, P., Santhanakumar, J., Venkatnarayanan, S.J, et al. (2022). Effect of Multiple Stressors on the Functional Traits of Sub-Tidal Macrobenthic Fauna: A Case Study of the Southeast Coast of India. *Mar. pollut. Bull.* 175, 113355. doi: 10.1016/j.marpolbul.2022.113355

Parsons, T. R., Maita, Y. and Lalli, C. M. (1992). *A Manual of Chemical and Biological Methods for Sea Water Analysis* (Oxford, New York: Pergamon Press).

Ratnam, K., Jha, D. K., Prashanthi Devi, M. and Dharani, G. (2022). Evaluation of Physicochemical Characteristics of Coastal Waters of Nellore, Southeast Coast of India, by a Multivariate Statistical Approach. *Front. Mar. Sci.* 9. doi: 10.3389/fmars.2022.857957

Redfield, A. C. (1934). "On the Proportions of Organic Derivatives in the Sea Water and Their Relation to the Composition of Plankton," in *James Johnstone Memorial Volume*, vol. 176–192 . Ed. Daniel, R. J. (Liverpool: University Press of Liverpool).

Redfield, A. C. (1958). The Biological Control of Chemical Factors in the Environment. *Am. Sci.* 46, 205–221. http://www.jstor.org/stable/27827150

Renjith, V., Sarma, K., Thresyamma, D. D., Geroge, G. and Vethamony, P. (2015). Natural Hazards. *Influence of Natural and Anthropogenic Factors on the Water Quality of the Coastal Waters Around the South Andaman in the Bay of Bengal.* doi: 10.1007/s11069-015-1715-9

Satheeswaran, T., Yuvaraj, P., Damotharan, P., Karthikeyan, V., Jha, D. K., Dharani, G., et al. (2019). Assessment of Trace Metal Contamination in the Marine Sediment, Seawater, and Bivalves of Parangipettai, Southeast Coast of India. *Mar. pollut. Bull.* 149, 110499.doi: 10.1016/j.marpolbul.2019.110499

Satpathy, K. K., Eswaran, M. S. and Nair, K. V. K. (1986). Distribution of Temperature in the Vicinity of Condenser Outfall in Kalpakkam Coastal Waters. *J.Mar. Biol. Ass. India* 28, 151–158. http://mbai.org.in/php/journaldload.php?id=1249&bkid=67

Shrestha, S. and Kazama, F. (2007). Assessment of Surface Water Quality Using Multivariate Statistical Techniques: A Case Study of the Fuji River Basin. *Jpn. Environ. Model. Software* 22, 464–475. doi: 10.1016/j.envsoft.2006.02.001

Van Nieuwerburgh, L., Wanstrand, I. and Snoeijs, P. (2004). Growth and C:N:P Ratios in Copepods Grazing on N- or Si-Limited Phytoplankton Blooms. *Hydrobiologia* 514, 57–/72. doi:10.1007/978-94-017-0920-0_5

Vega, M., Pardo, R., Barrado, E. and Deban, L. (1998). Assessment of Seasonal and Polluting Effects on the Quality of River Water by Exploratory Data Analysis. *Water Res.* 32, 3581–3592. doi: 10.1016/S0043-1354(98)00138-9

Vijayakumaran, M., Murugan, T. S., Remany, M. C., Mary Leema, T., Jha, D. K., Santhanakumar, J., et al. (2005). Captive Breeding of the Spiny Lobster, Panulirus Homarus, New Zealand. *J. Mar. Freshw. Res.* 39:2, 325–334.

Ward Jr., J.H. (1963) Hierarchical Grouping to Optimize an Objective Function. *Journal of the American Statistical Association*, 58, 236-244. doi: 10.1080/01621459.1963.10500845

Winkler, L. W. (1888). Die Bestimmung Des Im Wassergelösten Sauerstoffen. *Ber. Dtsche. Chem. Ges.* 21, 2843–2855. doi:10.1002/cber.188802102122

Wunderlin, D. A., Diaz, M. P., Ame, M. V., Pesce, S. F., Hued, A. C. and Bistoni, M. (2001). Pattern Recognition Techniques for the Evaluation of Spatial and Temporal Variation in Water Quality. *A Case study: Suquia river basin (Cordoba Argentina). Water Res.* 35, 2881–2894. doi: 10.1016/s0043-1354(00)00592-3

Wu, M. L., Wang, Y. S., Sun, C. C., Wang, H., Dong, J. D., Yin, J. P., et al. (2010). Identification of Coastal Water Quality by Statistical Analysis Methods in Daya Bay, South China Sea. *Mar. pollut. Bull.* 60, 852–860. doi: 10.1016/j.marpolbul.2010.01.007

Xu, G. Z. (1989). *Environments and Resources of Daya Bay* (HeFei, China: Anhui Science Publishing House).

Yang, Y., Zhou, F., Guo, H. C., Sheng, H., Liu, H., Dao, X., et al. (2010). Analysis of Spatial and Temporal Water Pollution Patterns in Lake Dianchi Using Multivariate Statistical Methods. *Environ. Monit. Assess.* 170, 407–416. doi: 10.1007/s10661-009-1242-9

Yuvaraj, P., Satheeswaran, T., Damotharan, P., Karthikeyan, V., Jha, D. K., Dharani, G., et al. (2018). Evaluation of the Environmental Quality of Parangipettai, Southeast Coast of India, by Using Multivariate and Geospatial Tool. *Mar. Pollut. Bull.* 131, 239–247. doi: 10.1016/j.marpolbul.2018.04.022

Conflict of Interest: The authors declare that the research was conducted in the absence of any commercial or financial relationships that could be construed as a potential conflict of interest.

Publisher's Note: All claims expressed in this article are solely those of the authors and do not necessarily represent those of their affiliated organizations, or those of the publisher, the editors and the reviewers. Any product that may be evaluated in this article, or claim that may be made by its manufacturer, is not guaranteed or endorsed by the publisher.

Copyright © 2022 Jha, Pandey, Muthukumar, Sathish Kumar, Venkatnarayanan, Jebakumar and Dharani. This is an open-access article distributed under the terms of the Creative Commons Attribution License (CC BY). The use, distribution or reproduction in other forums is permitted, provided the original author(s) and the copyright owner(s) are credited and that the original publication in this journal is cited, in accordance with accepted academic practice. No use, distribution or reproduction is permitted which does not comply with these terms.

frontiers | Frontiers in Marine Science

TYPE Brief Research Report
PUBLISHED 22 July 2022
DOI 10.3389/fmars.2022.955770

Check for updates

OPEN ACCESS

EDITED BY
Meilin Wu,
South China Sea Institute of Oceanology (CAS), China

REVIEWED BY
Kit Yue Kwan,
Beibu Gulf University, China
Youji Wang,
Shanghai Ocean University, China
Xiaoshou Liu,
Ocean University of China, China

*CORRESPONDENCE
Ying Wang
yingwang@tjcu.edu.cn
Nora Fung-Yee Tam
fytam@hkmu.edu.hk

SPECIALTY SECTION
This article was submitted to Marine Pollution, a section of the journal Frontiers in Marine Science

RECEIVED 29 May 2022
ACCEPTED 01 July 2022
PUBLISHED 22 July 2022

CITATION
Wang Y, Du Y-T and Tam NFY (2022) Effects of decabromodiphenyl ether (BDE-209) on a mangrove plant, *Kandelia obovata* and the uptake, translocation and accumulation of BDE-209.
Front. Mar. Sci. 9:955770.
doi: 10.3389/fmars.2022.955770

COPYRIGHT
© 2022 Wang, Du and Tam. This is an open-access article distributed under the terms of the Creative Commons Attribution License (CC BY). The use, distribution or reproduction in other forums is permitted, provided the original author(s) and the copyright owner(s) are credited and that the original publication in this journal is cited, in accordance with accepted academic practice. No use, distribution or reproduction is permitted which does not comply with these terms.

Effects of decabromodiphenyl ether (BDE-209) on a mangrove plant, *Kandelia obovata* and the uptake, translocation and accumulation of BDE-209

Ying Wang[1]*, Yi-Tong Du[1] and Nora Fung-Yee Tam[2,3]*

[1]Tianjin International Joint Research & Development Center of Food Science and Engineering, Tianjin Key Laboratory of Food Biotechnology, College of Biotechnology and Food Science, Tianjin University of Commerce, Tianjin, China, [2]Department of Science, School of Science and Technology, Hong Kong Metropolitan University, Kowloon, Hong Kong SAR, China, [3]State Key Laboratory of Marine Pollution and Department of Chemistry, City University of Hong Kong, Kowloon, Hong Kong SAR, China

Due to close proximity to urban development, mangroves exposed to the contamination of polybrominated diphenyl ethers (PBDEs). Decabromodiphenyl ether (BDE-209) is one of the most predominant PBDE congener. The present study aimed to investigate the toxic effects of BDE-209 on the antioxidative and non-antioxidative responses of *Kandelia obovata*, a very common mangrove species, under different concentrations of BDE-209, 0.1, 1, 5 and 10 mg l^{-1}. BDE-209 did not exhibit any negative effects on the growth of *K. obovata* seedlings. The stimulatory effects of BDE-209 on the enzymes including superoxide dismutase, peroxidase and catalase only occurred in weeks 1 and 4 and diminished in week 8. The concentrations of total polyphenols (TP) and extractable condensed tannins (ECT) were not affected by BDE-209. The production of $O_2^{\cdot -}$ was induced only at the very high level of BDE-209 (10 mg l^{-1}). H_2O_2 was induced only in weeks 1 and 4 under BDE-209 treatment. BDE-209 was taken up by the roots of *K. obovata*, translocated to above-ground tissues, and accumulated in plant tissues with the concentrations declined in the order of root > propagule > stem > leaf. Although BDE-209 has higher molecular weight and higher log Kow than other PBDE congeners, the *K. obovata* seedlings could absorb, translocate and accumulate BDE-209. These findings suggested that mangrove plants could take up, accumulate PBDEs, and BDE-209 are less toxic than other congeners but more difficult to be removed by mangrove systems.

KEYWORDS

Mangroves, *Kandelia obovata*, BDE-209, ecotoxicology, uptake, accumulate

Introduction

Polybrominated diphenyl ethers (PBDEs) are manufactured as additive brominated flame retardants and widely distributed in the environment (Alaee et al., 2003; Portet-Koltalo et al., 2021). Mangroves often receive anthropogenic contamination as they are usually convenient discharge sites for waste and wastewater (Qiu et al., 2010; Ouyang and Guo, 2016), and PBDEs have been recorded in mangrove sediments (Binelli et al., 2007; Qiu et al., 2010). The problems of PBDE contamination in mangroves and their harmful effects on our environment cannot be ignored.

PBDEs pose oxidative stresses to organisms by over-production of reactive oxygen species (ROS), which might lead to poor growth or even death (Zezza et al., 2019). However, few studies reported the effects of PBDEs on plants and their antioxidative responses. Huang et al. (2013) found that PBDEs could increase the activities of nitro-reductase and glutathione-transferase in roots of ryegrass, pumpkin and maize. Our previous study (Wang et al., 2014a) showed BDE-47 posed significantly effects of the activities of three antioxidative enzymes, superoxide dismutase (SOD), peroxidase (POD) and catalase (CAT) of two mangrove plant species, *Kandelia obovata* (*K. obovata*) and *Avicennia marina* (*A. marina*). Knowledge on the role of antioxidative enzymes in mangrove plants to remove excess ROS produced by PBDE contamination is limited. Not only enzymatic antioxidants, non-enzymatic antioxidants in mangrove plants, such as tannins were commonly found and related to their tolerance (Huang et al., 2010a). Whether the non-enzymatic antioxidative defense system of mangrove plants could be induced to combat the oxidative stress posed by PBDE contamination has rarely been reported. Only Zhou et al. (2019) in our group reported the implication of tannin changes in two mangrove plants, *K. obovata* and *Bruguiera gymnorhiza* under PBDE contamination.

It is also important to understand the fate of PBDEs in the environment, particularly, bioaccumulation, transformation and elimination, as these are useful information in determining how the burdens and associated health risks of PBDEs change over time (Mueller et al., 2006). The predominant congeners of PBDEs in environmental samples, such as air, sewage sludge, soil and sediment, were BDE-209 and BDE-47 (Ramu et al., 2005; Li et al., 2009; Jin et al., 2010). The most dominant congener in many sediment samples was BDE-209, followed by BDE-47, BDE-99 and BDE-100 (Mai et al., 2005; Luo et al., 2007; Wang et al., 2007; Chen et al., 2009; Sun et al., 2013a). The accumulation of BDE-209 and BDE-47 in sediment could be due to the more extensive uses and the global BFRs consumption pattern of these commercial PBDE products (Wang et al., 2007). The former is the main component of a commercial product deca-BDEs, while the latter is the main component of another commercial product penta-BDEs, according to the file of US Environmental Protection Agency (EPA).

Therefore, attention should be paid to the toxic effects of BDE-209 and -47, and we reported the effects of BDE-47 on two mangrove plant species, *K. obovata* and *A. marina* (Wang and Tam, 2013; Wang et al., 2014a). Here we aimed to study the effects of BDE-209 on the growth of the seedlings of *K. obovata* during an eight-week hydroponic culture, and compare with BDE-47 (Wang et al., 2014a). In the present study, the hydroponic was used instead of soil culture, since the latter might reduce the toxicity and bioavailability of PBDEs (Mueller et al., 2006). It is also common to use a hydroponic culture to examine the direct toxicity of persistent organic pollutants (Liu and Schnoor, 2008; Wang et al., 2012). *K. obovata*, belonging to *Rhizophoraceae* family, is a very common mangrove species distributed along the coastlines of East-Pacific Archipelagos and Asia. It also can be found in all mangrove associations in south China. Therefore, *K. obovata* is chosen as a model mangrove plant in the present study.

Materials and methods

Chemicals

Spiked BDE-209 was purchased from Dr. Ehrenstorfer (Germany) (purity > 99%). The analytical reagent (AR) grade Tween 20 and butanol were obtained from Sigma. Enzyme kits for SOD, POD and CAT measurements were purchased from Nanjing Jiancheng Bioengineering Institute, China. All chemicals and reagents were of analytical reagent grades. Deionized water was used throughout the experiment.

Experiment setup and sampling

One year old *K. obovata* seedlings were collected (the details have been listed in SI 2.1) and treated with four contamination levels of BDE-209 were 0.1 (low, L), 1 (medium, M), 5 (high, H) and 10 (very high, VH) mg l^{-1}. Preliminary experiments showed that 0.5% of Tween 20 were sufficient to dissolve the highest contamination level used in this experiment for BDE-209, and the recovery percentages of 10 mg l^{-1} BDE-209 was 78.1%. Positive control with nutrient solution and solvent control with nutrient solution plus 0.5% Tween 20 for BDE-209 were prepared in the same way as the treatments but without BDE-209. The sampling days were at the end of weeks 1, 4 and 8.

Plant growth

The dry weight and Chlorophyll a (Chl a) and chlorophyll b (Chl b) were measured, and the details have been listed in SI 2.2.

Determination of antioxidative enzymes

The fresh samples of roots and leaves were used to assay the activities of different antioxidative enzymes (SOD, POD and CAT), and the details have been listed in SI 2.3.

Determination of malondialdehyde (MDA)

Malondialdehyde (MDA) is a final decomposition product of lipid peroxidation and has been used as an index for the status of lipid peroxidation. The details of MDA measurement have been listed in SI 2.4.

Determination of ROS production ($O_2 \cdot^-$ and H_2O_2)

The fresh samples of roots and leaves were used to determine ROS production, that is, superoxide radical ($O_2 \cdot^-$) and hydrogen peroxide (H_2O_2). They were measured, and the details have been listed in SI 2.5.

Determination of tannins and related polyphenols

Total polyphenols (TP) and extractable condensed tannins (ECT) were measured, and the details have been listed in SI 2.6.

Determination of uptake, translocation and debromination of BDE-209

Extraction of BDE-209 in plant samples was performed by accelerated solvent extraction (ASE) purchased from Dionex (USA) according to the method described by our previous work Zhu et al. (2014a); Zhu et al. (2014b) with some modifications. In brief, 0.1 g freeze-dried plant sample was spiked with 10 μl PCB-209 in acetone (10 μg ml^{-1}) as a surrogate standard. The sample mixture was then loaded into the ASE cell fitted with an ASE filter. Two cycles of plant sample extraction were performed using n-hexane as the solvent at a pressure of 1500 psi and temperature of 100 °C, each with a static time of five minutes. The extract was reduced to 1 ml by slow rotary evaporation. All the concentrated extracts were cleaned on a 10 mm i.d. florisil column (5 g, pre-washed by actone), eluted with 20 ml of n-hexane and concentrated to 1 ml prior to gas chromatography-mass spectrometry (GC-MS) analysis. The BDE-209 remained in the hydroponic culture solution was extracted three times by liquid-liquid extraction, using 10 ml of hexane as the solvent and 10 μl of PCB-209 (10 μg ml^{-1}) as the surrogate standard, each at 15 minutes. The extract was concentrated by rotary evaporation to an accurate 1 ml for GC-MS analysis.

GC-MS 6890N/5975 of Agilent Technologies (Palo Alto, CA, USA) equipped with an Agilent 7638B series auto-injector Agilent Technologies and a capillary column (DB-5HT, crosslined 5% phenyl methyl siloxane, 15 m × 0.25 mm, 0.1 μm film thickness) was used to determine the concentration of BDE-209 in the extract. Helium and methane (Hong Kong Oxygen & Acetylene Co., Ltd) with a purity of 99.999% were used as carrier gases with a flow rate of 1.5 ml min^{-1}. GC conditions were as follows: The column was coupled directly to the mass, and the flow rate for the helium carrier gas was 1.5 ml min^{-1}. The injector temperature was 240°C. 2 μl of sample was injected in the splitless mode. The purge flow rate was 50 ml min^{-1}. The temperature was programmed from 150°C (held isothermal for two minutes) to 300°C at a rate of 6°C/min, held isothermal for three minutes. MS condition: The Negative Chemical Ionization (NCI) source was used, and the temperature of both ion source and interface was 250°C. The mass selective detector (MSD) was operated in a selected ion monitoring (SIM) mode. The quantitative ions m/z 79, 81, 487 and 489 were selected for the detection of BDE-209, while ions m/z 464, 498 and 500 were used to monitor PCB-209. Solvent delay time was three minutes. The standard curves were made every time before and after the samples were run.

The limits of detection (LOD) of BDE-209, defined as a signal of three times the noise level, in roots, propagules, stems and leaves of *K. obovata*, were 0.680, 0.701, 0.683 and 0.695 ng g^{-1}. In hydroponic culture solution, the LOD values of BDE-209 were 0.820 μg l^{-1}. For the quality control, a matrix-spike recovery test was used to determine the recovery of the method. In brief, 0.1 grams of the freeze-dried mangrove plant sample cultured in the green house without PBDE spike was spiked with the mixed standard of 1 μg ml^{-1} BDE-209 and 0.1 μg ml^{-1} PCB-209. The same plant sample, but without PBDE spike, was used as the blank. The hydroponic culture solution was also spiked with the same concentration of BDE-209 and PCB-209 as mentioned above, while the solution without PBDE spike was used as the blank. The recoveries (n = 6) of BDE-209 and PCB-209 in plant tissues and hydroponic culture solution were in the range of 70.1 to 89.3 and 94.3 to 102.0%, respectively. Most of the recovery percentages were close to 90%, so the reported concentrations were not corrected by the surrogate recovery rate obtained from the matrix spiked test.

Statistical analyses

Mean and standard deviation of the three replicates for each treatment or control at each sampling time were calculated. A parametric two-way analysis of variance (ANOVA) followed by a Tukey's multiple comparison test were performed to test any

significant differences in the dependent variables (i.e., biomass, Chl a, Chl b, SOD, POD, CAT, MDA, $O_2^{\cdot-}$, H_2O_2, TP and ECT) with BDE-209 treatments and sampling times as the two fixed factors. If interactions between these two factors were significant at $p \leq 0.05$, the differences among BDE-209 treatments at the same sampling time were compared by a parametric one-way ANOVA. Data were tested for the normality and homogeneity of variance assumption of the parametric ANOVA test, and no transformation was needed. All statistical analyses were done by a Statistical Package for Social Science (SPSS Version 16.0), USA.

Results

Effects of BDE-209 on *K. obovata*

Growth

All treatment groups with different concentrations of BDE-209 in this experiment had no significant differences were observed for all growth parameters of *K. obovata* during the 8-week experiment, indicating that the growth of *K. obovata* seedlings may not be affected by BDE-209 contamination. The dry weight of root, propagule, stem and leaf of all treatments and the controls were comparable, ranging from 0.92-1.03, 6.41-6.99, 0.67-0.85 and 0.89-1.13 g, respectively. Similarly, the leaf number, ranging from 4-6, Chl a, b, a+b and a/b of the leaves in the ranges of 0.85-1.23, 0.30-0.52, 1.22-1.80 mg g^{-1} and 2.41-3.29, respectively, were not significantly different among all samples (Table 1).

Antioxidative enzymes

The effects of BDE-209 on SOD were only observed under 10 mg l^{-1} BDE-209 in the root and leaf samples at weeks 1 and 4 (Figure S1). POD activities in both root and leaf samples at weeks 1 and 4 were significantly enhanced by BDE-209 contamination, even at 0.1 mg l^{-1} BDE-209 (Figure S1), but no effects were found on POD in week 8 (Figure S1). Similarly, CAT activity increased according to the levels of BDE-209 in weeks 1 and 4 but BDE-209 had no effects on CAT in week 8 (Figure S1). The two-way ANOVA statistical analyses showed that the effects of BDE-209 treatments, sampling times and interaction on SOD, POD and CAT activities were all significant at $p \leq 0.001$, suggesting that the enzymatic responses were both time- and BDE-209 level-specific (Table 1). The enzymatic responses of roots to BDE-209 were comparable to that of leaves.

MDA

MDA contents in roots and leaves showed little changes during the experiment and were not affected by the contamination levels of BDE-209. The MDA content in roots and leaves in all samples ranged from 10.7-11.8 and 5.2-5.5 nmol g^{-1} FW, respectively.

TABLE 1 F-values of two-way ANOVA tests showing the effects of sampling times and BDE-209 treatments on different parameters in roots and leaves of *K. obovata* (*: $p \leq 0.05$; **: $p \leq 0.01$; ***: $p \leq 0.001$; NS: Not significant; df: Degree of freedom).

Parameters \ Sources of variations	Sampling times (df = 2)	BDE-209 treatments (df = 5)	Sampling times × BDE-209 treatments (df = 10)
Dry weight of root	2.60*	1.80^{NS}	0.30^{NS}
Dry weight of propagule	28.9***	0.70^{NS}	0.40^{NS}
Dry weight of stem	4.10*	1.60^{NS}	1.50^{NS}
Dry weight of leaf	39.1***	0.80^{NS}	0.80^{NS}
Dry weight of total biomass	54.3***	0.70^{NS}	0.40^{NS}
Leaf number	32.8***	0.80^{NS}	0.50^{NS}
Chl a	0.60^{NS}	2.00^{NS}	0.50^{NS}
Chl b	0.30^{NS}	1.50^{NS}	0.30^{NS}
Chl a+ Chl b	0.60^{NS}	2.00^{NS}	0.40^{NS}
Chl a/Chl b	0.30^{NS}	1.30^{NS}	0.60^{NS}
SOD in root	146***	208**	121***
SOD in leaf	52.3***	129***	44.6**
POD in root	99.6***	68.6***	19.1***
POD in leaf	182***	88.1**	22.6***
CAT in root	29.0***	62.1**	12.7***
CAT in leaf	109.0***	110**	16.6***
MDA in root	0.80^{NS}	0.90^{NS}	0.50^{NS}
MDA in leaf	0.30^{NS}	0.20^{NS}	0.50^{NS}
$O_2^{\cdot-}$ release in root	1.20^{NS}	15.4**	2.90**
$O_2^{\cdot-}$ release in leaf	1.30^{NS}	15.4**	1.80^{NS}
H_2O_2 in root	5.40**	10.4***	1.50^{NS}
H_2O_2 in leaf	29.3***	13.9**	3.50***

ROS production

The responses of the $O_2^{\cdot-}$ release and H_2O_2 content of roots to BDE-209 treatments were comparable to those of leaves (Figure S2). Only the very high level of BDE-209 (10 mg l^{-1}) caused significant increases in $O_2^{\cdot-}$ release in roots and leaves in weeks 1 and 4, but dropped to the same level as the control in week 8 (Figure S2). This pattern was similar to that of SOD activity (Figure S1). The content of H_2O_2 in both roots and leaves of *K. obovata* seedlings increased with the contamination levels of BDE-209 during the first four weeks, but BDE-209 did not have any significant effects in week 8 (Figure S2). Such trend was more or less the same as that of POD and CAT activities (Figure S1). BDE-209 treatments could stimulate the production of ROS in both leaves and roots of *K. obovata* seedlings, but the seedlings could recover from the oxidative stress of BDE-209 with the ROS levels returned to the control level in week 8. This implied that the excess ROS induced by BDE-209 might have been scavenged by the antioxidative defense system of *K. obovata* or the seedlings might have adapted to BDE-209 as the experiment progressed. Such short-term effect of BDE-209

on the production of ROS in *K. obovata* seedlings was different from that of BDE-47 (Wang et al., 2014a), which enhanced the production of ROS throughout the entire study period.

The correlation coefficients among antioxidative enzymes (SOD, POD and CAT), MDA and ROS production ($O_2^{\cdot-}$ release and H_2O_2) in the roots and leaves of *K. obovata* under BDE-209 exposure are summarized in **Table S1**. All three antioxidative enzymes were significantly correlated with each other, suggesting that they functioned together to counter-balance the harmful effects caused by ROS under BDE-209 treatments. The correlation coefficient values were comparable between the roots and leaves in *K. obovata* under BDE-209 exposure, implying that the two tissues had similar antioxidative enzyme responses to BDE-209.

Tannins and related polyphenols

Figure S3 showed that BDE-209 at 10 mg l^{-1} did not have any significant effects on TP and ECT contents during the 8-week experiment.

BDE-209 remained in hydroponic culture solution and accumulated in tissues of *K. obovata*

The residual concentrations of BDE-209 in the hydroponic culture solution did not have any significant changes with sampling time (**Figure 1** and **Table S2**). This trend was different from that of BDE-47, which decreased significantly with sampling time under the two highest contamination levels, 5 and 10 mg l^{-1} BDE-47 (Wang et al., 2014b). The concentrations of BDE-209 remained in the hydroponic culture solution at the end of the experiment were significantly higher than that of BDE-47. Compared with the tissue concentrations of BDE-47, the concentrations of BDE-209 accumulated in the plant tissues of *K. obovata* were significantly lower (Wang et al., 2014b), even though the plant concentrations of BDE-209 increased significantly with time and contamination levels according to one-way ANOVA at $p \leq 0.05$ (**Table S2**). Among plant tissues, the concentration of BDE-209 in root was much higher than that in propagule, followed by stem, and leaf had the least uptake (**Figure 2**).

The mass balance calculation of BDE-209 during the 8-week experiment showed that the residual BDE-209 remained in the hydroponic culture solution varied from 81.1 to 91.3% of the total inputs (**Table 2**), which were significantly higher than those of BDE-47 (11.5 to 27.7%) (Wang et al., 2014b). The amounts of BDE-209 remained in the hydroponic culture solution continuously increased from weeks 1 to 8 according to one-way ANOVA at $p \leq 0.05$. The amounts of BDE-209 accumulated in plants increased significantly with contamination levels, and also from weeks 1 to 4, but no further increase thereafter according to one-way ANOVA at $p \leq 0.05$ (**Table 2**). These results suggested that the plant uptake of BDE-209 might become slower as the experiment progressed. The total uptake of BDE-209 in plant tissues of *K. obovata* ranging from 2.70 to 14.9% (**Table 2**), as well as the net losses of BDE-209 (0.40 - 11.3%) were significantly lower than those of BDE-47 (Wang et al., 2014b) according to Student t-test at $p \leq 0.05$ level. These findings indicated that the uptake and transformation of BDE-209 by *K. obovata* seedlings were less than that of BDE-47 under hydroponic culture. The losses of BDE-209 increased with time like those of BDE-47 but became relatively stable from week 4 onwards. Same as BDE-47, no new peaks with less bromine atoms were found in different tissues of *K. obovata* and in the hydroponic culture solution according to the GC-MS total ion

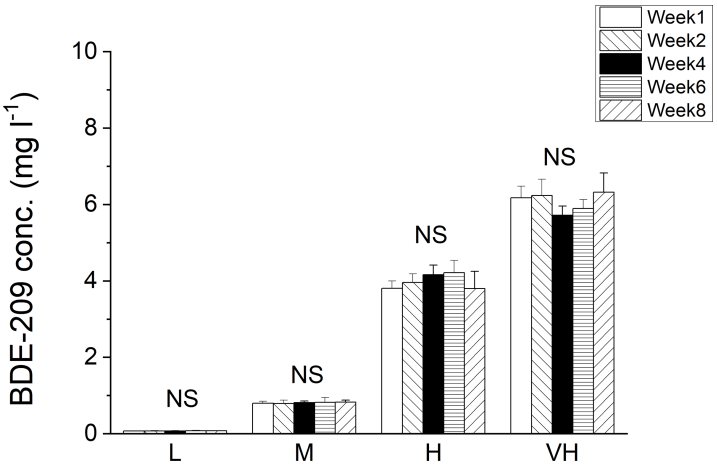

FIGURE 1
Concentrations of BDE-209 (mg l^{-1}) remained in hydroponic culture solution under different contamination levels of BDE-209 (L: 0.1 mg l^{-1} BDE-209, M: 1 mg l^{-1} BDE-209, H: 5 mg l^{-1} BDE-209, VH: 10 mg l^{-1} BDE-209; NS: No significant difference among sampling times under the same treatment at $p > 0.05$ according to one-way ANOVA; Mean and standard deviation of three replicates are shown).

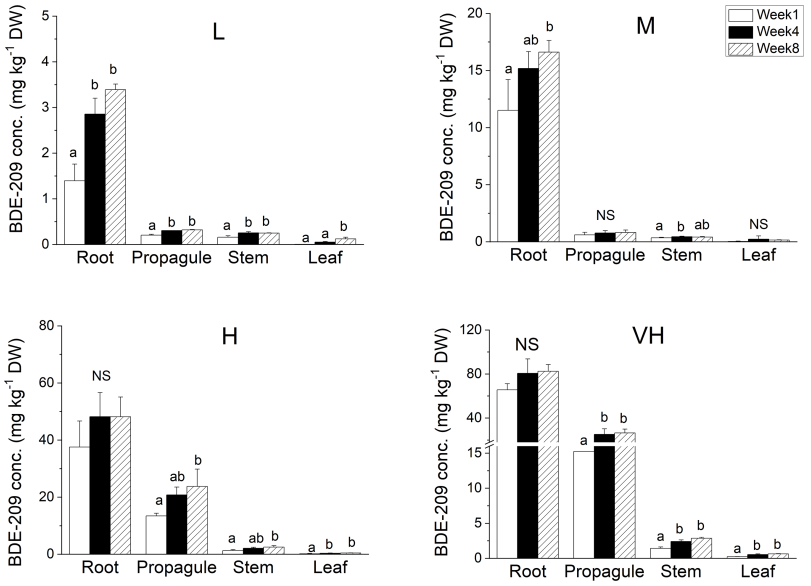

FIGURE 2
Concentrations of BDE-209 (mg kg^{-1} DW) in different tissues of *K. obovata* seedlings under different contamination levels of BDE-209 (L: 0.1 mg l^{-1} BDE-209, M: 1 mg l^{-1} BDE-209, H: 5 mg l^{-1} BDE-209, VH: 10 mg l^{-1} BDE-209; In the same tissue under the same treatment, bars with different letters show significant differences among sampling times at $p \leq 0.05$ according to one-way ANOVA followed by Tukey's tests; NS: Not significant; Mean and standard deviation of three replicates are shown).

chromatograms of BDE-209, suggesting that debromination did not occur in the present study lasted only eight weeks.

Discussion

Toxic effects of BDE-209

BDE-209 did not observe significant differences in growth and non-enzymatic antioxidants and may not have any effect on it, while the effects of BDE-47 on the growth, enzymatic and non-enzymatic antioxidants of *K. obovata* were concentration-dependent and lasted throughout the 8-week experiment (Wang et al., 2014a). The stimulatory effects of BDE-209 on SOD, POD and CAT in both leaves and roots of *K. obovata* were only significant in weeks 1 and 4. After 8-week experiment, the antioxidative enzymes of *K. obovata* exposed to BDE-209, even at the very high level (10 mg l^{-1}) returned to the same values as the control. The more toxic and longer-lasting effects of BDE-47 than BDE-209 might be explained by two reasons: First, the uptake of BDE-47 by *K. obovata* would be higher than BDE-209, due to its lower log Kow value and higher solubility as reported by previous studies (Rahman et al., 2001; Teclechiel et al., 2009). Zhang et al. (2013) also suggested that the lower toxicity of BDE-209 was likely due to its high molecular weight or size, resulting small uptake by organisms. Second, BDE-47 and BDE-209 had different chemical structures leading to different stabilities between BDE-209 and BDE-47. Br and O are atoms with high electronegativity, while H has low electronegativity. As all the carbons on BDE-209 are connected with Br or O, the electrons are well spreaded, thus lowering the electrostatic potential and the reactivity, BDE-209 is thus the most stable PBDE congener (Huang et al., 2011). Higher stability of BDE-209 might also lead to lower bioavailability to the living organisms than BDE-47. Previous studies reported that BDE-47 was more toxic and bioaccumulative than BDE-209 (Gandhi et al., 2011).

Uptake of toxic pollutants by plants

Toxic contaminants such as persistent organic pollutants (POPs) and heavy metals in soil could be taken up by plants (Prasad, 2004; Yan and Tam, 2011). A wide range of terrestrial plant species, such as radish, zucchini, tobacco, nightshade, ryegrass, alfalfa, pumpkin, summer squash, maize, etc., could take up diverse groups of toxic pollutants, including PBDEs but with different abilities (Mueller et al., 2006; Huang et al., 2010b; Sun et al., 2013b). Especially, as wetland plants, many mangrove plant species were reported to uptake and bioaccumulate POPs. The root of *B. gymnorrhiza* accumulated more pyrene than that of *K. candel* grown in pyrene bottom-contaminated sediments (Ke et al., 2003). Pi et al. (2017) reported that two mangrove species, *Excoecaria agallocha* L. and *K. obovata* could uptake of mixed polycyclic aromatic hydrocarbons (PAHs) and PBDEs in wastewater. Chen et al. (2015) reported that nitrogen addition

TABLE 2 Amounts of BDE-209 (μg) and percentages to total inputs (in brackets) remained in hydroponic culture solution, uptake in *K. obovata* seedlings and loss during an 8-week hydroponic experiment.

Treatment	Input	Cumulative outputs		Cumulative loss= Input-Output
	Hydroponic culture	Remained in culture	Plant uptake	
		At the end of week 1 (week 1)		
L	22.0 ± 1.20	18.5 ± 1.10^{a} (84.4%)	2.8 ± 0.4^{a} (14.9%)	0.70 ± 1.90^{a} (3.10%)
M	223 ± 11.4	199 ± 14.3^{b} (89.3%)	15.2 ± 3.3^{b} (7.70%)	8.70 ± 9.20^{a} (3.90%)
H	1094 ± 38.7	951 ± 48.6^{c} (87.0%)	124 ± 6.5^{c} (13.1%)	18.6 ± 52.0^{a} (1.60%)
VH	1848 ± 117	1544 ± 75.9^{d} (83.9%)	162 ± 13.6^{d} (10.5%)	143 ± 165^{a} (7.40%)
		At the end of week 4 (weeks 2 and 4)		
L	44.8 ± 1.90	37.2 ± 1.90^{a} (83.1%)	5.0 ± 0.4^{a} (13.4%)	2.60 ± 2.70^{a} (5.70%)
M	459 ± 18.6	407 ± 20.7^{b} (88.5%)	20.6 ± 0.6^{b} (5.10%)	32.2 ± 14.9^{a} (7.00%)
H	2298 ± 213	2081 ± 125^{c} (91.3%)	187 ± 18.1^{c} (9.00%)	29.9 ± 32.4^{a} (0.40%)
VH	3537 ± 321	2861 ± 119^{d} (81.1%)	243 ± 42.9^{d} (8.50%)	433 ± 164^{b} (12.0%)
		At the end of week 8 (weeks 2, 4, 6 and 8)		
L	90.7 ± 7.40	74.8 ± 1.70^{a} (82.7%)	5.80 ± 0.20^{a} (7.80%)	10.1 ± 6.60^{a} (10.8%)
M	958 ± 23.1	827 ± 51.5^{b} (86.4%)	22.6 ± 0.60^{b} (2.70%)	109 ± 74.9^{a} (11.3%)
H	4389± 429	3801 ± 447.3^{c} (86.7%)	214 ± 31.5^{c} (5.70%)	374 ± 307^{ab} (8.40%)
VH	7275 ± 666	6321 ± 502^{d} (87.0%)	262 ± 23.5^{c} (4.10%)	692 ± 347^{b} (9.40%)

L: 0.1 mg l^{-1} BDE-209, M: 1 mg l^{-1} BDE-209, H: 5 mg l^{-1} BDE-209, VH: 10 mg l^{-1} BDE-209; Mean and standard deviation of three replicates are shown; Values at the same sampling time with lower case letters at superscript position shows significant differences among contamination levels according to one-way ANOVA test.

affected the uptake of PBDEs by a mangrove plant, *Aegiceras corniculatum*. All these indicated that plant uptake of POPs was species-specific. In the present study, *K. obovata*, the two commonest mangrove species in Hong Kong SAR, also took up BDE-209 from hydroponic culture. The mechanisms controlling the uptake of PBDEs in plant species are still unresolved, and one possible mechanism is that Fe plaque formed on root surfaces of mangroves could effectively immobilize organic pollutants (Pi et al., 2017). More research is needed to understand what causes the species-specificity of plant uptake.

Following uptake, toxic chemicals are translocated and accumulated in plants but at different amounts among tissues. The accumulation of PBDEs in stems and leaves may result from a combination of uptake through the root uptake from the soil pathway and foliar uptake from the air (Huang et al., 2011). In the control (without any spiking of PBDEs), no BDE-209 were detected in any plant tissue, indicating that the route of foliar uptake from the air to the aboveground accumulation could be neglected. The highest BDE-209 concentrations were in root, followed by propagule, stem, and the lowest in leaf. Similar declining trends of accumulation from root to leaf were recorded in the uptake of PCBs, DDTs and PBDEs in plants grown directly in contaminated soils (Lunney et al., 2004; Huang et al., 2011; Zhao et al., 2012). These declining trends further supported that the accumulation of PBDEs in plants was mainly due to the root uptake, followed by gradual transfer, to propagules, stems, and then to the leaves.

The total uptake and accumulation of BDE-209 in plant tissues of *K. obovata* increased with the initial contamination levels in the hydroponic culture solution. Similarly, Prasad (2004) also reported that the metal uptake increased with increasing metal concentrations in external medium. The uptake of PCB in the genus of *Luzula* exhibited a great increase relative to increasing soil PCB concentrations (Dawn Pier et al., 2002). The availability of the chemical and the factors restricted its bioavailability such as the lipid content and morphology of roots, the acquisition and/or translocation mechanisms of the plants, etc., may also affect the plant uptake.

Biotransformation of toxic pollutants in plants

Volatilization, degradation and metabolism are important processes determining the fate of pollutants following the uptake, translocation and accumulation of toxic pollutants in plants. It has been demonstrated that PBDEs could be degraded/debrominated into more toxic lower brominated congeners (de-PBDE products) in plants (Wang et al., 2011). The debrominated products of BDE-28, -47 and -99 were recorded in maize (Zhao et al., 2012), and a debromination product (BDE-28) was also identified in the young whole pumpkin plant after exposure to BDE-47 (Sun et al., 2013b). These studies showed that the debromination of PBDEs occurred but its rates and pathways varied from plant species to species.

In the present study, BDE-209 was not debrominated and no newly-borne lower brominated congeners were found in plant tissues and in the hydroponic culture. Previous research showed that the debromination of PBDEs took long time and was more preferably under anaerobic condition (Robrock et al., 2008; Zhu et al., 2014b). As the studies on the degradation, metabolism and fate of PBDEs are still limited to terrestrial plants with very few studies in aquatic ecosystems (Huang et al., 2010b; Wang et al., 2011; Wang et al., 2012; Sun et al., 2013b), the debromination of PBDEs in mangrove plants which are saline, aquatic and ligneous deserves more attention and future study.

The toxic effects of only one PBDE congener were examined in the present study. However, natural environments are often contaminated by a mixture of PBDE congeners. The behavior of PBDE mixture in mangrove soil and the interactions between different PBDE congeners should be further studied. Additionally, the present mangrove microcosm work only investigated the responses of mangrove seedlings to a single addition of BDE-209 to the hydroponic culture at the beginning of the study. However, in natural environments, PBDE contamination from waste dumping or wastewater discharge may occur from time to time. The effects of intermittent and/or continuous discharges of PBDEs on mangrove plants merit further research.

Conclusions

When compared with BDE-47, BDE-209 did not observe any significant negative effects on the growth of *K. obovata* seedlings. Our results suggested that BDE-209 was less toxic to *K. obovata* than BDE-47.

The *K. obovata* seedlings could also absorb, translocate and accumulate BDE-209 from the culture solution. However, most of the spiked BDE-209 was still remained in the hydroponic culture solution. These results suggested that BDE-209, due to its higher molecular weight and higher log Kow, was more difficult to be removed by mangrove system than BDE-47.

This was the first comprehensive study revealing the effects of PBDEs on the growth, enzymatic and non-enzymatic antioxidative responses of mangrove seedlings, as well as their tolerance to PBDE stresses. The abilities of mangrove species to remove, uptake and accumulate PBDEs were reported. The work provided important information on the fate of PBDEs, which could be used for selecting the appropriate species for phytoremediation.

Data availability statement

The original contributions presented in the study are included in the article/**Supplementary Material**. Further inquiries can be directed to the corresponding authors.

Author contributions

YW, conceptualization, methodology, software, writing - original draft, and visualization. Y-TD, software, validation, and investigation. NT, writing - review and editing. All authors contributed to the article and approved the submitted version.

Funding

This work was supported by the Natural Science Foundation of Tianjin (grant numbers 17JCQNJC02400 and 18JCYBJC96000), the National Training Programs for Innovation and Entrepreneurship of Undergraduates (grant number 202110069002 and 202210069014).

Conflict of interest

The authors declare that the research was conducted in the absence of any commercial or financial relationships that could be construed as a potential conflict of interest.

Publisher's note

All claims expressed in this article are solely those of the authors and do not necessarily represent those of their affiliated organizations, or those of the publisher, the editors and the reviewers. Any product that may be evaluated in this article, or claim that may be made by its manufacturer, is not guaranteed or endorsed by the publisher.

Supplementary material

The Supplementary Material for this article can be found online at: https://www.frontiersin.org/articles/10.3389/fmars.2022.955770/full#supplementary-material

References

Alaee, M., Arias, P., Sjodin, A., and Bergman, A. (2003). An overview of commercially used brominated flame retardants, their applications, their use patterns in different countries/regions and possible modes of release. *Environ. Int.* 29, 683–689. doi: 10.1016/S0160-4120(03)00121-1

Binelli, A., Sarkar, S. K., Chatterjee, M., Riva, C., Parolini, M., and Bhattacharya, B. D. (2007). Concentration of polybrominated diphenyl ethers (PBDEs) in sediment cores of sundarban mangrove wetland, northeastern part of bay of

Bengal (India). *Mar. Pollut. Bull.* 54, 1220–1229. doi: 10.1016/j.marpolbul.2007.03.021

Chen, J., Zhou, H. C., Wang, C., Zhu, C. Q., and Tam, N. F.Y. (2015). Short-term enhancement effect of nitrogen addition on microbial degradation and plant uptake of polybrominated diphenyl ethers (PBDEs) in contaminated mangrove soil. *J. Hazardous Materials* 300, 84–92. doi: 10.1016/j.jhazmat.2015.06.053

Chen, L. G., Huang, Y. M., Peng, X. C., Xu, Z. C., Zhang, S. K., and Ren, M. Z. (2009). PBDEs in sediments of the beijiang river, China: Levels, distribution, and influence of total organic carbon. *Chemosphere* 76, 226–231. doi: 10.1016/j.chemosphere.2009.03.033

Dawn Pier, M., Zeeb, B. A., and Reimer, K. J. (2002). Patterns of contamination among vascular plants exposed to local sources of polychlorinated biphenyls in the Canadian Arctic and subarctic. *Sci. Total Environ.* 297, 215–227. doi: 10.1016/S0048-9697(02)00134-1

Gandhi, N., Bhavsar, S. P., Gewurtz, S. B., and Tomy, G. T. (2011). Can biotransformation of BDE-209 in lake trout cause bioaccumulation of more toxic, lower-brominated PBDEs (BDE-47, -99) over the long term? *Environ. Int.* 37, 170–177. doi: 10.1016/j.envint.2010.08.013

Huang, G. Y., Wang, Y. S., Sun, C. C., Dong, J. D., and Sun, Z. X. (2010a). The effect of multiple heavy metals on ascorbate, glutathione and related enzymes in two mangrove plant seedlings (*Kandelia candel* and *Bruguiera gymnorrhiza*). *Oceanol Hydrobiol Stud.* 39, 11–25. doi: 10.2478/v10009-010-0010-z

Huang, H. L., Zhang, S. Z., and Christie, P. (2011). Plant uptake and dissipation of PBDEs in the soils of electronic waste recycling sites. *Environ. pollut.* 159, 238–243. doi: 10.1016/j.envpol.2010.08.034

Huang, H. L., Zhang, S. Z., Christie, P., Wang, S., and Xie, M. (2010b). Behavior of decabromodiphenyl ether (BDE-209) in the soil-plant system: Uptake, translocation, and metabolism in plants and dissipation in soil. *Environ. Sci. Technol.* 44, 663–667. doi: 10.1021/es901860r

Huang, H. L., Zhang, S. Z., Wang, S., and Lv, J. T. (2013). *In vitro* biotransformation of PBDEs by root crude enzyme extracts: Potential role of nitrate reductase (NaR) and glutathione *S*-transferase (GST) in their debromination. *Chemosphere* 90, 1885–18922. doi: 10.1016/j.chemosphere.2012.10.013

Jin, S. W., Yang, F. X., Hui, Y., Xu, Y., Lu, Y. A., and Liu, J. K. (2010). Cytotoxicity and apoptosis induction on RTG-2 cells of 2,2',4,4'-tetrabromodiphenyl ether (BDE-47) and decabromated diphenyl ether (BDE-209). *Toxicol. Vitro* 24, 1190–1196. doi: 10.1016/j.tiv.2010.02.012

Ke, L., Wang, W. Q., Wong, T. W. Y., Wong, Y. S., and Tam, N. F. Y. (2003). Removal of pyrene from contaminated sediments by mangrove microcosms. *Chemosphere* 51, 25–34. doi: 10.1016/S0045-6535(02)00811-1

Li, J., Liu, X., Yu, L. L., Zhang, G., Li, X. D., Lee, C. S. L., et al. (2009). Comparing polybrominated diphenyl ethers (PBDEs) in airborne particles in guangzhou and Hong Kong: Sources, seasonal variations and inland outflow. *J. Environ. Monit.* 11, 1185–1191. doi: 10.1039/B900525K

Liu, J., and Schnoor, J. L. (2008). Uptake and translocation of lesser-chlorinated polychlorinated biphenyls (PCBs) in whole hybrid poplar plants after hydroponic exposure. *Chemosphere* 73, 1608–1616. doi: 10.1016/j.chemosphere.2008.08.009

Lunney, A. I., Zeeb, B. A., and Reimer, K. J. (2004). Uptake of weathered DDT in vascular plants: Potential for phytoremediation. *Environ. Sci. Technol.* 38, 6147–6154. doi: 10.1021/es030705b

Luo, Q., Cai, Z. W., and Wong, M. H. (2007). Polybrominated diphenyl ethers in fish and sediment from river polluted by electronic waste. *Sci. Total Environ.* 383, 115–127. doi: 10.1016/j.scitotenv.2007.05.009

Mai, B. X., Chen, S. J., Luo, X. J., Chen, L. G., Yang, Q. S., and Sheng, G. Y. (2005). Distribution of polybrominated diphenyl ethers in sediments of the pearl river delta and adjacent south China Sea. *Environ. Sci. Technol.* 39, 3521–3527. doi: 10.1021/es048083x

Mueller, K. E., Mueller-Spitz, S. R., Henry, H. F., Vonderheide, A. P., Soman, R. S., Kinkle, B. K., et al. (2006). Fate of pentabrominated diphenyl ethers in soil: Abiotic sorption, plant uptake, and the impact of interspecific plant interactions. *Environ. Sci. Technol.* 40, 6662–6667. doi: 10.1021/es060776l

Ouyang, X., and Guo, F. (2016). Paradigms of mangroves in treatment of anthropogenic wastewater pollution. *Sci. Total Environ.* 544, 971–979. doi: 10.1016/j.scitotenv.2015.12.013

Pi, N., Wu, Y., Zhu, H. W., Wong, Y. S., and Tam, N. F.Y. (2017). The uptake of mixed PAHs and PBDEs in wastewater by mangrove plants under different tidal flushing regimes. *Environment. Pollut.* 231, 104–114. doi: 10.1016/j.envpol.2017.07.085

Portet-Koltalo, F., Guibert, N., Morin, C., de Mengin-Fondragon, F., and Frouard, A. (2021). Evaluation of polybrominated diphenyl ether (PBDE) flame retardants from various materials in professional seating furnishing wastes from French flows. *Waste Manage.* 131, 108–116. doi: 10.1016/j.wasman.2021.05.038

Prasad, M. N. V. (2004). *Heavy metal stress in plants: From biomolecules to ecosystems. 2nd Ed* (Heidelberg: Springer-verlag), 462–465.

Qiu, Y. W., Zhang, G., Guo, L. L., Zheng, G. J., and Cai, S. Q. (2010). Bioaccumulation and historical deposition of polybrominated diphenyl ethers (PBDEs) in deep bay, south China. *Mar. Environ. Res.* 70, 219–226. doi: 10.1016/j.marenvres.2010.05.004

Rahman, F., Langford, K. H., Scrimshaw, M. D., and Lester, J. N. (2001). Polybrominated diphenyl ether (PBDE) flame retardants. *Sci. Total Environ.* 275, 1–17. doi: 10.1016/S0048-9697(01)00852-X

Ramu, K., Kajiwara, N., Tanabe, S., Lam, P. K. S., and Jefferson, T. A. (2005). Polybrominated diphenyl ethers (PBDEs) and organochlorines in small cetaceans from Hong Kong waters: Levels, profiles and distribution. *Mar. Pollut. Bull.* 51, 669–676. doi: 10.1016/j.marpolbul.2005.02.041

Robrock, K. R., Korytar, P., and Alvarez-Cohen, L. (2008). Pathways for the anaerobic microbial debromination of polybrominated diphenyl ethers. *Environ. Sci. Technol.* 42, 2845–2852. doi: 10.1021/es0720917

Sun, J. L., Chen, Z. X., Ni, H. G., and Zeng, H. (2013a). PBDEs as indicator chemicals of urbanization along an urban/rural gradient in south China. *Chemosphere* 92, 471–476. doi: 10.1016/j.chemosphere.2013.01.036

Sun, J. T., Liu, J. Y., Yu, M., Wang, C., Sun, Y. Z., Zhang, A. Q., et al. (2013b). *In vivo* metabolism of 2,2',4,4'-tetrabromodiphenyl ether (BDE-47) in young whole pumpkin plant. *Environ. Sci. Technol.* 47, 3701–3707. doi: 10.1021/es4003263

Teclechiel, D., Sundstrom, M., and Marsh, G. (2009). Synthesis of polybrominated diphenyl ethers *via* symmetrical tetra- and hexabrominated diphenyliodonium salts. *Chemosphere* 74, 421–427. doi: 10.1016/j.chemosphere.2008.09.046

Wang, Y. W., Jiang, G. B., Lam, P. K. S., and Li, A. (2007). Polybrominated diphenyl ether in the East Asian environment: A critical review. *Environ. Int.* 33, 963–973. doi: 10.1016/j.envint.2007.03.016

Wang, Y., and Tam, N. F. Y. (2013). "Effects of a congener of polybrominated diphenyl ethers (BDE-47) on the growth of two mangrove plant species, their uptake, translocation and biotransformation," in *In 13th International Conference on Environmental Science and Technology (CEST 2013)*. Athens, Greece.

Wang, S., Zhang, S. Z., Huang, H. L., Lu, A. X., and Ping, H. (2012). Debrominated, hydroxylated and methoxylated metabolism in maize (*Zea mays* l.) exposed to lesser polybrominated diphenyl ethers (PBDEs). *Chemosphere* 89, 1295–1301. doi: 10.1016/j.chemosphere.2012.05.026

Wang, S., Zhang, S. Z., Huang, H. L., Zhao, M. M., and Lv, J. T. (2011). Uptake, translocation and metabolism of polybrominated diphenyl ethers (PBDEs) and polychlorinated biphenyls (PCBs) in maize (*Zea mays* l.). *Chemosphere* 85, 379–385. doi: 10.1016/j.chemosphere.2011.07.002

Wang, Y., Zhu, H., and Tam, N. F. Y. (2014a). Effect of a polybrominated diphenyl ether congener (BDE-47) on growth and antioxidative enzymes of two mangrove plant species, *Kandelia obovata* and *Avicennia marina*, in south China. *Mar. pollut. Bull.* 85 (2), 376–384. doi: 10.1016/j.marpolbul.2014.02.012

Wang, Y., Zhu, H., and Tam, N. F. Y. (2014b). Polyphenols, tannins and antioxidant activities of eight true mangrove plant species in south China. *Plant Soil* 374 (1), 549–563. doi: 10.1007/s11104-013-1912-9

Yan, Z. Z., and Tam, N. F. Y. (2011). Temporal changes of polyphenols and enzyme activities in seedlings of *Kandelia obovata* under lead and manganese stresses. *Mar. pollut. Bull.* 63, 438–444. doi: 10.1016/j.marpolbul.2011.04.027

Zezza, D., Tait, S., Della Salda, L., Amorena, M., Merola, C., and Perugini, M. (2019). Toxicological, gene expression and histopathological evaluations of environmentally realistic concentrations of polybrominated diphenyl ethers PBDE-47, PBDE-99 and PBDE-209 on zebrafish embryos. *Ecotoxicol Environ. Saf.* 183, 109566. doi: 10.1016/j.ecoenv.2019.109566

Zhang, X. X., Tang, X. X., Zhou, B., and Wang, Y. (2013). Effects of decabromodiphenyl ether (BDE-209) on inter-specific competition between two species of marine bloom-forming microalgae. *PloS One* 8, e56084. doi: 10.1371/journal.pone.0056084

Zhao, M. M., Zhang, S. Z., Wang, S., and Huang, H. L. (2012). Uptake, translocation, and debromination of polybrominated diphenyl ethers in maize. *J. Environ. Sci.* 24, 402–409. doi: 10.1016/S1001-0742(11)60748-1

Zhou, H. C., Tam, F. Y. N., and Cheung, S. G. (2019). "Implication of tannin changes in two mangrove plants, *Kandelia obovata* and *Bruguiera gymnorhiza* under PBDE contamination," in *In 9th International Conference on Marine Pollution and Ecotoxicology (ICMPE-9)*. O–37. University of Hong Kong, Hong Kong

Zhu, H. W., Wang, Y., and Tam, N. F. Y. (2014a). Microcosm study on fate of polybrominated diphenyl ethers (PBDEs) in contaminated mangrove sediment. *J. Hazardous Mater* 265, 61–68. doi: 10.1016/j.jhazmat.2013.11.046

Zhu, H. W., Wang, Y., Wang, X. W., Luan, T. G., and Tam, N. F. Y. (2014b). Distribution and accumulation of polybrominated diphenyl ethers (PBDEs) in Hong Kong mangrove sediments. *Sci. Total Environ.* 468, 130–139. doi: 10.1016/j.scitotenv.2013.08.021

frontiers | Frontiers in Marine Science

TYPE Original Research
PUBLISHED 26 July 2022
DOI 10.3389/fmars.2022.956474

Check for updates

OPEN ACCESS

EDITED BY
Meilin Wu,
South China Sea Institute of Oceanology, Chinese Academy of Sciences, China

REVIEWED BY
Jia Renming,
Ministry of Natural Resources, China
Rong Yi,
Gannan Medical University, China
Xin Liu,
University of Shiga Prefecture, Japan
Jiaxi Tang,
Liaoning Technical University, China

*CORRESPONDENCE
Guangzhe Jin
jinguangzhe@live.cn
jingz@gdou.edu.cn

SPECIALTY SECTION
This article was submitted to Marine Pollution, a section of the journal Frontiers in Marine Science

RECEIVED 30 May 2022
ACCEPTED 28 June 2022
PUBLISHED 26 July 2022

CITATION
Cai S, Lao Q, Jin G, Chen C, Zhou X, Zhu Q and Lu X (2022) Sources of nitrate in a heavily nitrogen pollution bay in Beibu Gulf, as identified using stable isotopes.
Front. Mar. Sci. 9:956474.
doi: 10.3389/fmars.2022.956474

COPYRIGHT
© 2022 Cai, Lao, Jin, Chen, Zhou, Zhu and Lu. This is an open-access article distributed under the terms of the Creative Commons Attribution License (CC BY). The use, distribution or reproduction in other forums is permitted, provided the original author (s) and the copyright owner(s) are credited and that the original publication in this journal is cited, in accordance with accepted academic practice. No use, distribution or reproduction is permitted which does not comply with these terms.

Sources of nitrate in a heavily nitrogen pollution bay in Beibu Gulf, as identified using stable isotopes

Shangjun Cai[1,2], Qibin Lao[1,2], Guangzhe Jin[1,2]*, Chunqing Chen[1,2], Xin Zhou[1,2], Qingmei Zhu[1,2] and Xuan Lu[1,2]

[1]Key Laboratory for Coastal Ocean Variation and Disaster Prediction, College of Ocean and meteorology, Guangdong Ocean University, Zhanjiang, China, [2]Key Laboratory of Climate, Resources and Environment in Continental Shelf Sea and Deep Sea of Department of Education of Guangdong Province, Guangdong Ocean University, Zhanjiang, China

Eutrophication, mainly caused by the oversupply of inorganic nitrogen and phosphate, has increased and become a serious environmental problem in the coastal bays of Beibu Gulf, a newly developing industry and port in South China. However, the sources of nitrate are poorly understood in the gulf. In this study, nitrate dual isotopes (δ^{15}N-NO_3^- and δ^{18}O-NO_3^-) and ammonium isotopes (δ^{15}N-NH_4^+) were measured during the rainy season to identify the nitrate sources and elucidate their biogeochemical processes in Xi Bay, a semi-enclosed bay that is strongly affected by human activities in the Beibu Gulf. The results showed that a high dissolved inorganic nitrogen (DIN, 10.24-99.09 μmol L^{-1}) was observed in Xi Bay, particularly in the bay mouth. The concentrations of DIN in the bay were 1.5 times higher than that in Qinzhou Bay and 1.7 times than that in Tieshangang Bay, which mainly influenced by the intensive human activities (i.e., industrial and port activities). In addition, lower values of δ^{15}N-NO_3^- and δ^{18}O-NO_3^- and higher values of δ^{15}N-NH_4^+ were observed in the upper bay, suggesting that microbial nitrification occurs in the upper bay, which was the dominant nitrate source in the upper bay (39%). In addition to nitrification, external sources, including sewage and manure (33%), soil N (15%) and fertilizer (11%), contributed to the higher nutrients in the upper bay. In the lower bay, severe nitrogen pollution led to a weaker impact of biological processes on isotopic fractionation, although a high Chl *a* level (average of 7.47 μg L^{-1}) was found in this region. The heavy nitrate pollution in the lower bay mainly originated from sewage and manure (54%), followed by soil N (26%) and fertilizer (17%). The contribution of the nitrate source from atmospheric deposition was relatively low in the bay (<3%). This study suggests that biogeochemical processes have little impact on nitrate dual isotopes under heavy nitrogen pollution, and isotopes are an ideal proxy for tracing nitrogen sources.

KEYWORDS

nitrate dual isotopes, ammonium isotope, nitrogen pollution, source, Beibu Gulf

Introduction

Coastal bays receive terrestrial and riverine nutrient inputs, which have increased considerably in recent decades (Jickells, 1998; Gruber and Galloway, 2008; Savage et al., 2010; Yan et al., 2017). The increase in anthropogenic inputs has resulted in a host of environmental problems, such as eutrophication (Malone and Newton, 2020; Zhou et al., 2020), seasonal hypoxia (Rabalais et al., 2002; Howarth et al., 2011; Yu et al., 2021) and harmful algal blooms (Li et al., 2014; Glibert et al., 2014), in coastal bays, which greatly affect biogeochemical cycles and coastal ecosystems. Nitrogen (N) plays a key role in regulating marine primary productivity (Falkowski et al., 1998; Moore et al., 2013), and thus, its availability influences the sequestration of anthropogenic CO_2 in coastal seas and climate changes. However, increasing N loads to coastal bays, associated with industrial, agricultural, urban and domestic waste, have aroused widespread public concern (Yang et al., 2018). Therefore, a better understanding of N sources and their recycling processes is beneficial for designing effective management practices to protect and improve aquatic ecosystems.

The stable N isotopes ($\delta^{15}N$) of various pools of N, combined with the oxygen isotope of nitrate ($\delta^{18}O\text{-}NO_3^-$), have been proven to be useful in identifying nitrogen sources and their biogeochemical processes (Kendall, 1998; Ye et al., 2016; Yan et al., 2017; Yang et al., 2018; Lao et al., 2019a; Chen et al., 2020). For example, sewage and manure have higher $\delta^{15}N$ values (4-25‰) than soil N (-0.1-8.3‰), fertilizer (-1.9-3.0‰) and atmospheric deposition (-1.8-4.1‰) (Chen et al., 2019a; Kendall, 1998; Xue et al., 2009; Zhang et al., 2018) because the volatilization of $\delta^{15}N$-depleted ammonia is produced from human and animal waste and thus results in the enrichment of $\delta^{15}N$ in the residual N pools (Xue et al., 2009; Yang et al., 2018). In addition, the applicability of this technique can also reflect biogeochemical transformations associated with N cycles. Nitrification first oxidizes ammonia to nitrite and then further oxidizes it to nitrate (Casciotti et al., 2011). A nitrogen isotope effect of 14-42‰ has been found for the former step (Casciotti et al., 2003 and Casciotti et al., 2010), whereas an inverse kinetic isotope effect occurs for the latter step (Casciotti, 2009); thus, $\delta^{15}N\text{-}NO_3^-$ values are close to 0‰ during nitrification (Sigman et al., 2005 and Sigman et al., 2009; Smart et al., 2015). In addition, oxygen (O) is sourced from water (H_2O) and dioxygen (O_2) during nitrification. Typically, one-third of O in the newly formed nitrate is considered to originate from O_2, with two-thirds originating from H_2O, and $\delta^{18}O\text{-}NO_3^-$ values are 7.8‰ during nitrification (Kendall, 1998; Wankel et al., 2006; Chen et al., 2009). Moreover, assimilation and denitrification cause an increase in $\delta^{15}N\text{-}NO_3^-$ and $\delta^{18}O\text{-}NO_3^-$ values in the residual nitrate pool, as lighter isotopes (^{14}N and ^{16}O) are preferentially utilized by phytoplankton and microorganisms, with an increase in the $\delta^{15}N\text{-}NO_3^-$:$\delta^{18}O\text{-}NO_3^-$ ratio of 1 (Granger et al., 2004; Sigman et al., 2005; Granger et al., 2008). Thus, stable isotopes can serve as a useful tool in advancing our understanding of nitrogen dynamics in coastal bays.

Beibu Gulf is a semi-enclosed gulf and a newly developing industry and port area in the northwestern South China Sea (SCS). There are several rivers around the northern Beibu Gulf, and the influence of runoff input by the rivers and tidal influx from the outer gulf constitutes a well estuary-bay multi-ecosystem and has become an important mariculture area in China (Lao et al., 2020 and Liu et al., 2020; Xu et al., 2020: Xu et al., 2021; Lao et al., 2021a; Lao et al., 2022a and 2022b). However, with the rapid development of local urbanization and industrialization, the coastal bays in Beibu Gulf have been subjected to a high loading of contaminants from anthropogenic inputs, such as domestic, industrial, port and agricultural waste (Lao et al., 2019b; Xu et al., 2020: Lao et al., 2021a; Lao et al., 2021b; Lao et al., 2021c; Lao et al., 2021d: Xu et al., 2021 and Lao et al., 2022a). The nutrients discharged into coastal bays from runoff input have increased over the past 20 years, and the increase in phosphorus input has decreased the N/P ratios in several coastal bays in the Beibu Gulf (Lao et al., 2020 and Lao et al., 2021c). Moreover, the eutrophication of some coastal bays in the Beibu Gulf has increased in recent decades due to the increase in terrestrial nutrient input, particularly the nitrogen input (Lai et al., 2014; Guo et al., 2020; Lao et al., 2021a and Lao et al., 2021c; Pan et al., 2021). In addition, sewage is the dominant nitrate source in most bays/areas in the Beibu Gulf, which is identified by the dual nitrate isotopes (Pan et al., 2021; Lao et al., 2021b; Chen et al., 2022). This has resulted in an increase in the frequency of harmful algal blooms in the Beibu Gulf over the past decades, particularly in the past ten years (Xu et al., 2019).

Xi Bay is a semi-enclosed bay located on the coast of Fangchenggang city, which is an important industrial and port area in the northwestern Beibu Gulf. In addition to being affected by industrial activities, Xi Bay is also affected by a large amount of terrestrial contaminant input from the Fangcheng River in the upper bay (Lao et al., 2020). It is reported that a higher contaminant level was found in the coastal bay, including high nutrient loads, particularly in the rainy seasons (Lao et al., 2019b; Lao et al., 2021a). This is mainly affected by the heavy land-source discharge during the rainy seasons (Lao et al., 2021a). However, in such bays that are seriously affected by intensive human activities (i.e., industrial and port activities), the sources of nitrate are poorly understood. In this study, nitrate dual isotopes ($\delta^{15}N\text{-}NO_3^-$ and $\delta^{18}O\text{-}NO_3^-$) and ammonium isotopes ($\delta^{15}N\text{-}NH_4^+$) were measured during the rainy season (July 2021) to determine the nitrate sources and their biogeochemical processes in Xi Bay.

Materials and methods

Study area and sampling

Xi Bay is a semi-enclosed bay in the northern Beibu Gulf, located on the coast of Fangchenggang city, South China. The

climate of the bay is influenced by the East Asian monsoon, and the southwest monsoon prevails during summer and the northeast monsoon prevails during winter. The annual rainfall in the bay is 2441 mm; most rainfall occurs in the rainy season (April to October, accounting for 91% of the annual rainfall), and the highest rainfall occurs in July (accounting for 23% of the annual rainfall) (China Meteorological Data Sharing Service System, http://data.cma.cn/site/index.html). The monthly mean air temperature ranges from 14.3 to 28.6 °C, with an annual average of 22.7 °C. There is the Fangcheng River in the upper bay (**Figure 1**). The Fangcheng River is approximately 98 km long with a drainage area of 843 km^2. The annual runoff of the Fangcheng River is 542.25 × 10^8 m^3, with the highest runoff in July (127.41 × 10^8 m^3), and flows into the northern end of Xi Bay (Lao et al., 2020; Lao et al., 2022b). The eastern part of Xi Bay is the urban center of Fangchenggang city. The eastern bay mouth of Xi Bay is the industrial and port area. Thus, Xi Bay is a coastal bay greatly affected by human activities in the Beibu Gulf.

In this study, a cruise was conducted in Xi Bay in July (rainy season) 2021. A total of 16 seawater stations were collected in the bay, including a station (X1) in the Fangcheng River estuary and a station (X16) in the outer bay, using a rosette sampler fitted with 5-L Niskin bottles. The pH was measured in-suit with a pH meter (PHS-3C, Shanghai, China), and salinity was measured with a salinometer (SYA2-2). Dissolved oxygen (DO) was immediately determined using the Winkler titration method, with a precision of 0.07mg L^{-1}. COD samples were determined by the potassium permanganate oxidation method with a precision of 0.15 mg L^{-1}. The seawater samples for the dual nitrate isotopes ($\delta^{15}N\text{-}NO_3^-$ and $\delta^{18}O\text{-}NO_3^-$) and ammonium isotope ($\delta^{15}N\text{-}NH_4^+$) were filtered by precombustion (450°C, 4 h) GF/F (glass fiber filters, 47-mm diameter, Whatman). The filtrate was transferred into a 250-ml precleaned (acid clean) polyethylene bottle and stored at -20°C until further analysis. Seawater was filtered by GF/F for the chlorophyll *a* (Chl *a*) sample, and the filtered GF/F was stored at -20°C until further analysis.

Chemical analysis

DO samples were measured on site by using the Winkler titration method. The Chl *a* samples were extracted by acetone (9:1) and measured by a spectrophotometer (Lorenzen, 1967). Nutrients, including PO_4^{3-}, NO_2^-, NO_3^- and NH_4^+, were determined using a San++ continuous flow analyzer (Skalar, Netherlands). The detection limit of PO_4^{3-} was 0.02 μg L^{-1}, and the detection limits of NO_2^-, NO_3^- and NH_4^+ were 0.1 μg L^{-1}. The $\delta^{15}N\text{-}NO_3^-$ and $\delta^{18}O\text{-}NO_3^-$values were measured by the cadmium-azide method (McIlvin and Altabet, 2005) using a GasBench II-MAT 253 (253 Plus, Thermo Scientific, United States). Briefly, the NO_2^- in the seawater was removed by sulfamic acid (Granger et al., 2008). NO_3^- was reduced to NO_2^-

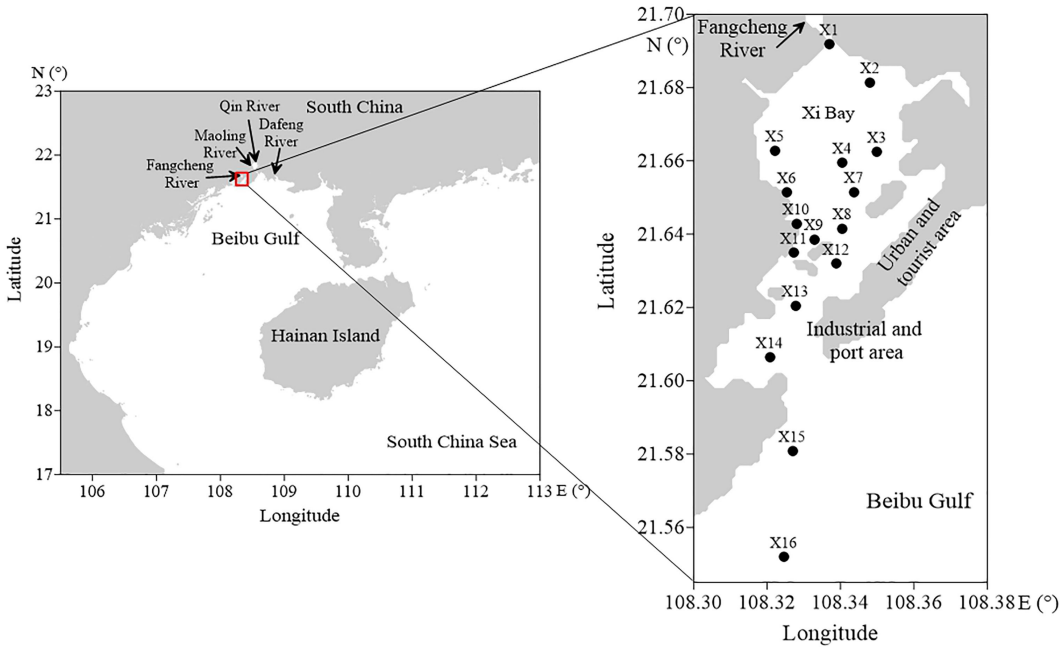

FIGURE 1
Study area and the sampling stations in Xi Bay, Beibu Gulf.

by adding Cd and then further reduced to N_2O by adding sodium azide buffer. For the analysis of $\delta^{15}N\text{-}NH_4^+$, BrO^- (pH 12) was added to the seawater to oxidize NH_4^+ to NO_2^-, and then NaAsO2 was added to remove excess $NaAsO_2$. The yield was verified *via* colorimetric nitrite determination. Then, sodium azide buffered with acetic acid was added to reduce NO_2^- to N_2O (Zhang et al., 2007). The N_2O was purified and separated by TraceGas (Isoprime), and the compositions of $\delta^{15}N\text{-}NO_3^-$, $\delta^{18}O\text{-}NO_3^-$ and $\delta^{15}N\text{-}NH_4^+$ were determined by GasBench II-MAT 253. The IAEA-N3 international standard was used to calibrate the values of $\delta^{15}N\text{-}NO_3^-$ and $\delta^{18}O\text{-}NO_3^-$, and the international standards of USGS 25, USGS26 and IAEA-N1 were used to calibrate the values of $\delta^{15}N\text{-}NH_4^+$. The reproducibility of duplicate analysis of $\delta^{15}N\text{-}NO_3^-$, $\delta^{18}O\text{-}NO_3^-$ and $\delta^{15}N\text{-}NH_4^+$ was<0.3‰ (mean ± 0.1‰),<0.6‰ (mean ± 0.3‰) and<0.3‰ (mean ± 0.1‰), respectively.

Salinity-based conservative mixing model

Isotopic values and nutrient concentrations from simple physical mixing can be calculated by the salinity-based conservative mixing model (Fry, 2002; Ye et al., 2016; Lao et al., 2019a). The equation is as follows:

$$q_1 + q_2 = 1 \tag{1}$$

$$q_1 S_1 + q_2 S_2 = S_{mix} \tag{2}$$

$$q_1 N_1 + q_2 N_2 = N_{mix} \tag{3}$$

$$q_1 N_1 \delta_1 + q_2 N_2 \delta_2 = N_{mix} \delta_{mix} \tag{4}$$

where q is the proportional contributions of the two endmembers. The terms S, N and δ are the salinity, nutrient and isotopic values of the two endmembers, and S_{mix}, N_{mix} and δ_{mix} are the theoretical values of mixing of the two endmembers. According to equations (1) to (4):

$$q_1 = (S_{mix} - S_2)/(S_1 - S_2) \tag{5}$$

$$N_{mix} = N2 + (N1 - N2)q_1 \tag{6}$$

$$\delta_{mix} = [q_1(\delta_1 N_1 - \delta_2 N_2) + \delta_2 N_2]/N_{mix} \tag{7}$$

Thus, salinity-based nutrient mixing exhibits linear conservative mixing (6), whereas isotopic mixing exhibits curvilinear mixing. The distributions of isotopic values and nutrient levels are expected to fall on the mixing line between two endmembers. The deviation from the mixing line suggests external sources or the presence of transformation processes (Wankel et al., 2006; Yang et al., 2018; Lao et al., 2019a; Lao et al., 2021b; Chen et al., 2022).

The Bayesian mixing model

The proportional contributions of potential nitrate sources can be quantified by a Bayesian mixing model, which was created and run in the SIAR (stable isotope analysis in R 4.1.2) package. This model has been widely used to quantify the potential nitrate sources in marine systems (Xue et al., 2009; Korth et al., 2014; Davis et al., 2015; Zhang et al., 2018: Lao et al., 2019a; Lao et al., 2021b and Chen et al., 2022). The framework can be found in Xue et al. (2009) and Moore and Semmens (2008) as follows:

$$X_{ij} = \sum_{k=1}^{k} P_k(S_{jk} + \quad c_{jk}) + \epsilon_{ij} \tag{8}$$

$$S_{jk} \sim N(\mu_{jk},\ \omega_{jk}^2) \tag{9}$$

$$c_{jk} \sim N(\lambda_{jk},\ \tau_{jk}^2) \tag{10}$$

$$\epsilon_{jk} \sim N(0,\ \sigma_j^2) \tag{11}$$

where X_{ij} represents the isotopic value j of the mixed water i (i =1, 2, 3,…, N and j =1, 2, 3,…, j), S_{jk} represents the source value k (k =1, 2, 3,…, k) on isotope j and represents the normal distribution with an average of μ and a standard deviation of ω, P_k represents the proportional contribution of source k, c_{jk} represents the fractionation factor and represents a normal distribution with an average of λ and a standard deviation of τ, and ϵ_{jk} represents the residual error of the additional unquantified variation between individual mixed samples and represents a normal distribution with an average of 0 and a standard deviation of σ.

Statistical analyses

Statistical analyses were conducted by the software SPSS 19.0 for Windows. The linear regression in this study was conducted by SigmaPlot 11.0.

Results

Physicochemical characteristics

The distributions of physicochemical parameters are presented in **Figure 2**. The surface seawater temperature ranged from 31.90 to 32.40 °C (an average of 32.13 °C). The salinity ranged from 8.97 to 24.22 (an average of 18.60), with a decreasing trend from the upper bay to the outer bay and the lowest salinity in the Fangcheng River estuary and the highest salinity in the outer bay. This suggests that the seawater in Xi Bay

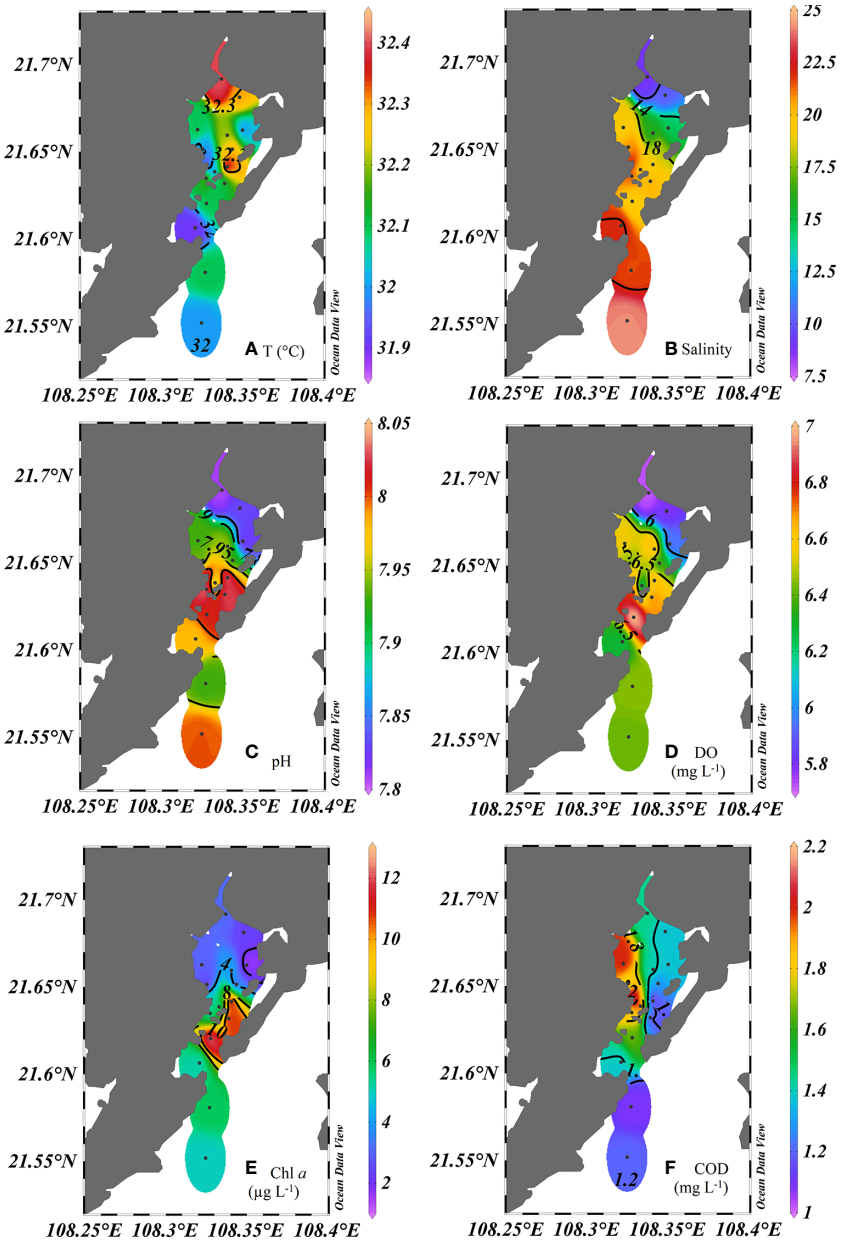

FIGURE 2
Spatial distributions of physicochemical parameters, including temperature **(A)**, salinity **(B)**, pH **(C)**, DO **(D)**, Chl *a* **(E)** and COD **(F)**, in Xi Bay during the rainy season.

is greatly affected by freshwater input from the Fangcheng River. The pH values ranged from 7.81 to 8.04, with an average of 7.95. The DO level ranged from 5.73 mg L^{-1} to 7.00 mg L^{-1} (an average of 6.41 mg L^{-1}), with a lower DO level in the upper bay (< 6 mg L^{-1}). The Chl *a* level ranged from 1.60 to 12.30 μg L^{-1} (average of 5.41 μg L^{-1}), and a higher Chl *a* level was found in the bay mouth. The COD concentrations ranged from 1.09 to 2.18 mg L^{-1}, with an average of 1.52 mg L^{-1}.

Characteristics and distributions of nutrients

The distributions of nutrients are presented in **Figure 3**. The concentrations of PO_4^{3-} ranged from 0.36 to 1.17 μmol L^{-1} (an average of 0.67 μmol L^{-1}). A higher PO_4^{3-} concentration was found in the estuary and the upper bay and exhibited a decreasing trend from the upper bay to the outer bay

(Figure 3A). This result suggests that the PO_4^{3-} in Xi Bay is mainly influenced by the runoff input. High DIN (dissolved inorganic nitrogen, the sum of NO_3^-, NO_2^- and NH_4^+) concentrations were found in Xi Bay. The concentration of NO_3^- ranged from 8.21 to 89.93 μmol L^{-1}, with an average of 31.05 μmol L^{-1}. Although the NO_3^- concentration exhibited a decreasing trend from the upper bay to near the bay mouth, a significantly high NO_3^- concentration was found in the bay mouth (stations X13, X14 and X15, over 3 times than that in the Fangcheng River estuary), which is located in the industrial and port areas (Figures 3B, C). Similar distribution patterns were also found in the concentrations of NO_2^- and NH_4^+ (Figure 3). The concentrations of NO_2^- and NH_4^+ ranged from 0.61 to 2.54 μmol L^{-1} (an average of 1.11 μmol L^{-1}) and 1.26 to 7.36 μmol L^{-1} (an average of 3.01 μmol L^{-1}), and high concentrations were all found in the bay mouth. Notably, the concentrations of DIN in the bay mouth (an average of 98.28 μmol L^{-1}) were significantly higher than those in the Fangcheng River (an average of 58.64 μmol L^{-1}) during a similar rainy month (Lao et al., 2020). This result suggests that the discharge of DIN caused by intensive human activities (i.e., industrial and port activities) in the bay mouth is much higher than the runoff input in Xi Bay. In addition, the concentrations of DIN in Xi Bay (an average of 35.17 μmol L^{-1}) during a similar rainy month (August 2018) were 1.5 times those in Qinzhou Bay (22.99 μmol L^{-1}) and 1.7 times those in Tieshangang Bay (20.51 μmol L^{-1}) (Lao et al., 2021a), which are semi-enclosed bays that are greatly affected by intensive human activities in the northern Beibu Gulf (Chen et al., 2022). Thus, it can be concluded that Xi Bay is a bay seriously affected by artificial inorganic nitrogen input in the Beibu Gulf.

Characteristics and distributions of isotopic compositions

The distribution characteristics of $\delta^{15}N\text{-}NO_3^-$, $\delta^{18}O\text{-}NO_3^-$ and $\delta^{15}N\text{-}NH_4^+$ in Xi Bay during the rainy season are presented in Figure 4. The values of $\delta^{15}N\text{-}NO_3^-$, $\delta^{18}O\text{-}NO_3^-$ and $\delta^{15}N\text{-}NH_4^+$ ranged from 4.6 to 13.7‰, 3.1 to 15.3‰ and -3.0 to 26.3‰, with averages of 7.5‰, 7.1‰ and 13.5‰, respectively. Generally, the values of $\delta^{15}N\text{-}NO_3^-$ and $\delta^{18}O\text{-}NO_3^-$ were lower in the upper bay and exhibited an increasing trend to the bay mouth (Figure 4). Corresponding to the DIN, the highest values

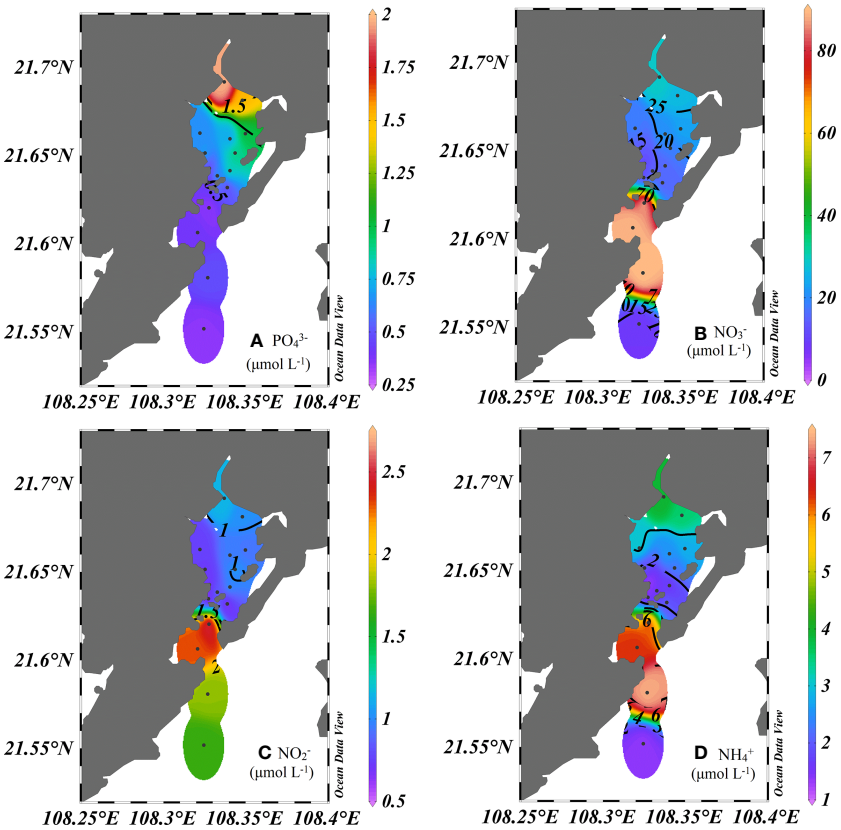

FIGURE 3
Spatial distributions of nutrients in Xi Bay during the rainy season. **(A)**,PO_4^{3-} **(B)**, NO_3^-**(C)**, NO_2^- **(D)**, NH_4^+.

of $\delta^{15}N\text{-}NO_3^-$ and $\delta^{18}O\text{-}NO_3^-$ were all observed in the bay mouth. In contrast, higher values of $\delta^{15}N\text{-}NH_4^+$ were observed in the upper bay (Figure 4A). The difference in isotopic values in the upper bay and bay mouth suggests that different biogeochemical processes or sources of nitrogen could have occurred in the two regions.

Riverine and marine endmember mixing in the bay

In this study, the lowest salinity at station X1 was selected as the freshwater endmember, and the highest salinity at the outer bay (station X16) was selected as the marine endmember. The hydrological characteristics, nutrient concentrations and isotopic values of freshwater and marine endmembers are presented in Table 1.

Discussion

Characteristics of nutrients in Xi Bay

Higher nutrient concentrations were also observed in the other coastal bays of Beibu Gulf during the rainy seasons (Lai et al., 2014; Lao et al., 2021a and Lao et al., 2021c), which were

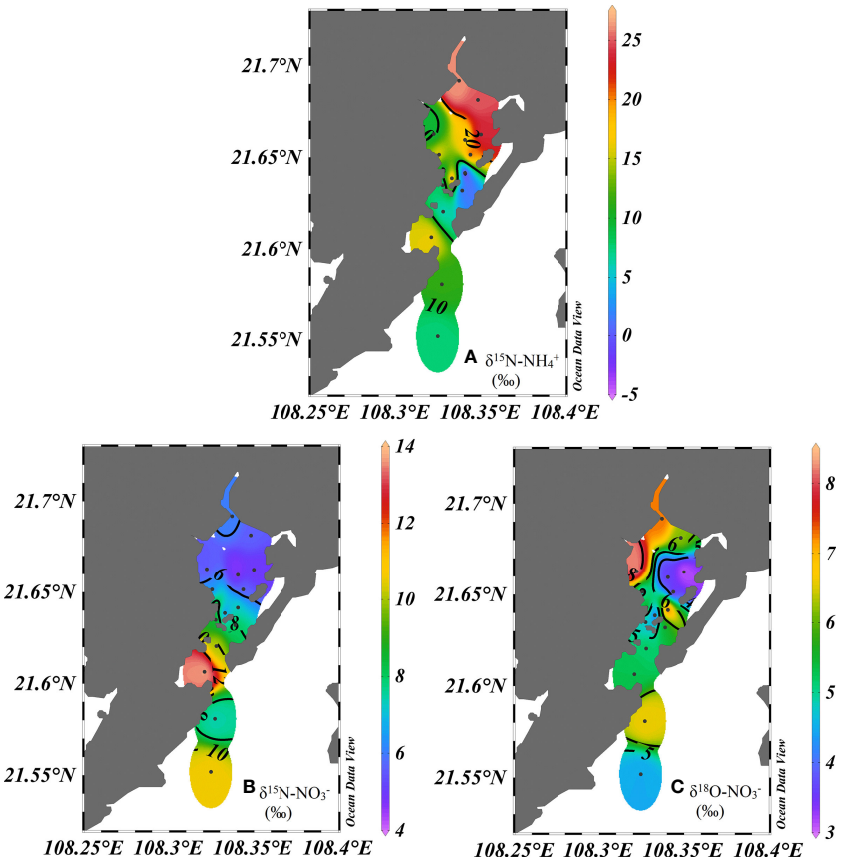

FIGURE 4
Spatial distributions of nutrients in Xi Bay during the rainy season. **(A)**, δ15N-NO_3^- **(B)**, δ18O-NO_3-**(C)**, δ15N-NH4$^+$

TABLE 1 The hydrological characteristics, nutrient concentrations and isotopic values of freshwater and marine endmembers of Xi Bay.

Station	Salinity	PO_4^{3-}	NH_4^+[μmol L^{-1}]	NO_2^-	NO_3^-	$\delta^{15}N\text{-}NO_3^-$ [‰]	$\delta^{18}O\text{-}NO_3^-$ [‰]	$\delta^{15}N\text{-}NH_4^+$ [‰]
X1	8.97	1.17	3.15	1.15	29.22	6.1	7.3	26.3
X16	24.22	0.36	1.38	0.65	8.21	10.6	4.5	7.6

mainly related to the heavy land-source discharge induced by the increasing runoff around the coastal Beibu Gulf (Lao et al., 2020; Lao et al., 2021a). Particularly in Qinzhou Bay, because there are several rivers, such as the Qin River, Maoling River and Dafeng River, that directly input a large amount of terrestrial contaminants into the bay (Chen et al., 2019a; Zhang et al., 2019; Lao et al., 2020; Lao et al., 2021c; Lao et al., 2022b; Lyu et al., 2022). However, heavier DIN pollution was found in Xi Bay. Similarly, there is a Fangcheng River that directly inputs into Xi Bay, and 626,669 t of nitrogen and 4,987 t of phosphorus are discharged directly into the bay every year, including 69% of nitrogen and 60% of phosphorus in the rainy season (Lao et al., 2020). In addition, a significant correlation between PO_4^{3-} concentrations and salinity was found in Xi Bay (**Figure 5A**), suggesting that the PO_4^{3-} in the bay was mainly affected by terrestrial input. There was no relationship between DIN concentration and salinity (**Figure 5B**). This was mainly because the high DIN concentration occurred in the bay mouth. However, if the stations in the bay mouth (X13, X14 and X15) were excluded, a significant correlation between DIN concentration and salinity was found in Xi Bay (**Figure 5C**). This result suggests that the DIN in the bay is also affected by terrestrial input. An extremely high DIN level was observed in the bay mouth, suggesting that the DIN in Xi Bay was also greatly influenced by anthropogenic discharge. Fangchenggang is a major industrial and port city in the Beibu Gulf, and industrial and port transportation activities may cause a great load of environmental pollution in the coastal area (Lai et al., 2014; Chen et al., 2019a; Lao et al., 2021a and Xu et al., 2019; Lao et al., 2021d). Thus, except for the runoff input, industrial and port transportation also contributed greatly to the DIN load in Xi Bay, which could be responsible for the high DIN pollution compared to the other coastal bays in the Beibu Gulf. In addition, the N/P ratios were high in Xi Bay (ranging from 21 to 272, with an average of 69), particularly in the bay mouth (an average of 241), which was significantly higher than the Redfield ratio of 16 (the ratio at which nutrients are utilized by phytoplankton). This result is similar to previous studies in coastal Fangchenggang city (Lai et al., 2014; Lao et al., 2021a). The high DIN discharge could be responsible for the high N/P ratios in the coastal bay. Moreover, Fangchenggang city is an important production area of phosphate fertilizer around the Beibu Gulf urban agglomeration, and the PO_4^{3-} concentration in the coastal area is relatively higher than that in other coastal bays in the Beibu Gulf, which is mainly influenced by the waste produced from the phosphate fertilizer plant in the city (Lai

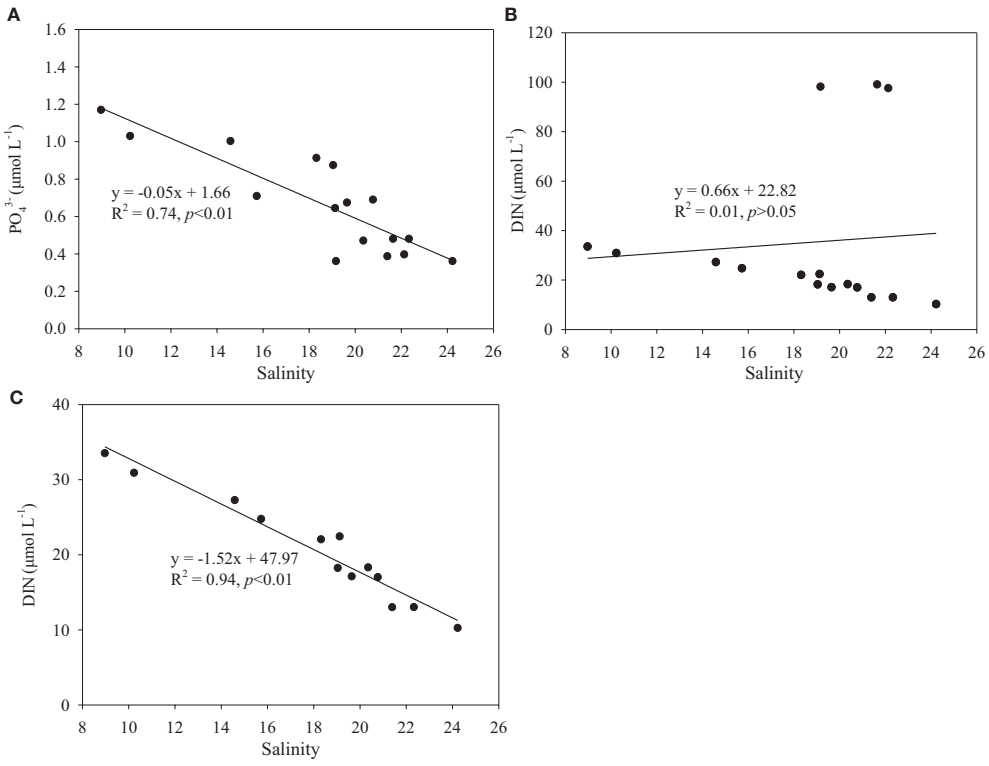

FIGURE 5
The linear relationship between PO_4^{3-} and salinity all stations of Xi Bay **(A)**; the linear relationship between DIN and salinity all stations of Xi Bay **(B)**; the linear relationship between DIN and salinity in Xi bay that exclude the stations in the bay mouth **(C)**.

et al., 2014; Lao et al., 2021a). In this study, higher PO_4^{3-} concentrations (with a minimum [PO_4^{3-}] of >0.4 μmol L^{-1}) suggest that neither P nor N acted as a limiting nutrient in this ecosystem despite higher N/P ratios found in the bay and that environmental conditions were favorable for phytoplankton blooms. In addition, a decreasing N/P ratio was found in the coastal bays of Beibu Gulf due to increasing P input (Lao et al., 2021a and Lao et al., 2021c; Chen et al., 2022), which has resulted in harmful algal blooms increasing in frequency in recent years, especially in the past ten years (Xu et al., 2019; Kang et al., 2020; Guan et al., 2022). This could be responsible for the high Chl *a* level in the bay, particularly in the bay mouth (**Figure 2**). A similar situation has been documented in Xiangshan Bay of the East China Sea (Yang et al., 2018).

Sources and biogeochemical processes of nitrate in Xi Bay

Lower values of dual nitrate isotopes ($\delta^{15}N\text{-}NO_3^-$ and $\delta^{18}O\text{-}NO_3^-$) were observed, whereas higher $\delta^{15}N\text{-}NH_4^+$ values were observed in the upper bay (stations X1 to X7). In addition, the nutrients in the bay are slightly above the mixing lines, particularly in the bay mouth (except for PO_4^{3-}) (**Figure 6**). These results suggest that decomposition/nitrification and/or external sources may occur in the bay. During the nitrification process, light N ($\delta^{14}N$) in the NH_4^+ pool is preferentially utilized by microorganisms, resulting in the enrichment of $\delta^{15}N\text{-}NH_4^+$ while adding depleted $\delta^{14}N$ to the residual nitrate pool (Sigman et al., 2005; Chen et al., 2009; Ye et al., 2016; Lao et al., 2021b). If nitrification is the dominant process in the bay, isotopic fractionation during the process can be estimated by open-system Rayleigh fractionation (Altabet, 2006; Ye et al., 2016; Chen et al., 2022) as follows:

$$\delta_m = \delta_i + \epsilon \times f_{NH4} \quad (12)$$

where δ_m is the measured $\delta^{15}N\text{-}NH_4^+$ value; δ_i is the initial $\delta^{15}N\text{-}NH_4^+$ value; ϵ is the fractionation factor; and f_{NH4} is the fraction of measured NH_4^+ concentration relative to the initial NH_4^+ concentration ($[NH_4^+]_m/[NH_4^+]_i$). The slope of the $\delta^{15}N\text{-}NH_4^+$-$f_{NH4}$ linear regression line corresponds to the isotopic effects of NH_4^+ oxidation in seawater (Ye et al., 2016). In our results, a weak but still significant correlation was found between $\delta^{15}N\text{-}NH_4^+$ values and f_{NH4} in the upper bay (**Figure 7**). In addition, the overall estimated ϵ (-25.21‰) falls well within the reported values for N fractionation factors during nitrification in field studies (-14 to -38‰) (Casciotti et al., 2003; Ye et al., 2016). This further suggests that microbial nitrification occurs in the upper bay. Microbial decomposition/nitrification could consume oxygen and release carbon dioxide in the water column, which may be responsible for the lower DO level (an average of 6.20) and pH value (an average of 7.88) in the upper bay (**Figure 2**).

However, if nitrification was the dominant process in the upper bay, the $\delta^{15}N\text{-}NO_3^-$ values should be close to 0‰ (Sigman et al., 2005 and Sigman et al., 2009; Smart et al., 2015). Higher $\delta^{15}N\text{-}NO_3^-$ (ranging from 4.9 to 6.1‰) and $\delta^{18}O\text{-}NO_3^-$ (ranging from 3.1 to 8.4‰) values were found in the upper bay. This indicates that other processes or external sources may also occur in the bay. Both the processes of assimilation and denitrification can enrich the dual nitrate isotopes in the residual water column, with coupled $\delta^{15}N\text{-}NO_3^-$ and $\delta^{18}O\text{-}NO_3^-$ fractionation effects of ~1 (Granger et al., 2004; Sigman et al., 2005; Granger et al., 2011). However, both assimilation and denitrification consume nutrients, which is consistent with the distribution of nutrients above the mixing lines (**Figure 6**). In addition, there is no relationship between $\delta^{15}N\text{-}NO_3^-$ and $\delta^{18}O\text{-}NO_3^-$ values (R^2 = 0.13, p>0.05). This further confirms that the processes of assimilation and denitrification are not responsible for the slight enrichment of dual nitrate isotopes in the upper bay, which can be related to external sources. Sewage and manure are usually characterized by relatively high $\delta^{15}N\text{-}NO_3^-$ values (4‰ to 25‰) because of the volatilization of $\delta^{15}N$-depleted ammonia produced from human and animal waste (Xue et al., 2009). Soil N is another source that is characterized by relatively higher $\delta^{15}N\text{-}NO_3^-$ values (0‰ to 8‰) (Xue et al., 2009). Previous studies suggested that a higher proportional contribution of soil N (30%) was found in strong hydrodynamic conditions with several river inputs in Qinzhou Bay, whereas a lower contribution of soil N (20%) was found in weak hydrodynamic conditions with river inputs in Tieshanggang Bay (Chen et al., 2022). Particularly in the rainy seasons, heavy rainfall could carry more land-source nutrients into the coastal Beibu Gulf (Lao et al., 2021a). In addition, manure and sewage were the dominant nitrate sources in the coastal bays of Beibu Gulf, which were mainly influenced by intensive human activities, such as mariculture, industrial and shipping activities (Lao et al., 2021b; Chen et al., 2022).

In the lower bay (stations X8 to X12) and the bay mouth (stations X13 to X15), the increased $\delta^{15}N\text{-}NO_3^-$ and $\delta^{18}O\text{-}NO_3^-$ values may be influenced by the characteristics of high isotopic nitrate sources (i.e., sewage and manure) and/or the processes of denitrification and assimilation. However, denitrification in water column can be first ruled out due to the high DO levels (> 6 mg L^{-1}) in the lower bay and the bay mouth. The high Chl *a* level indicates that assimilation may occur in the lower bay and the bay mouth. In addition, the PO_4^{3-} concentrations were below the mixing line (**Figure 6**), which may be related to consumption by phytoplankton. However, there is no correlation between $\delta^{15}N\text{-}NO_3^-$ and $\delta^{18}O\text{-}NO_3^-$ values (R^2 = 0.07, p>0.05). In addition, according to the open-system Rayleigh fractionation (equation 12), the fractionation during the process of assimilation can be calculated. There is no relationship between $\delta^{15}N\text{-}NO_3^-$ and f_{NO3} (R^2 = 0.25, p>0.05) in the lower bay and the bay mouth, and the overall estimated ϵ (0.7‰) significantly deviates from the range of reported values (-3 to

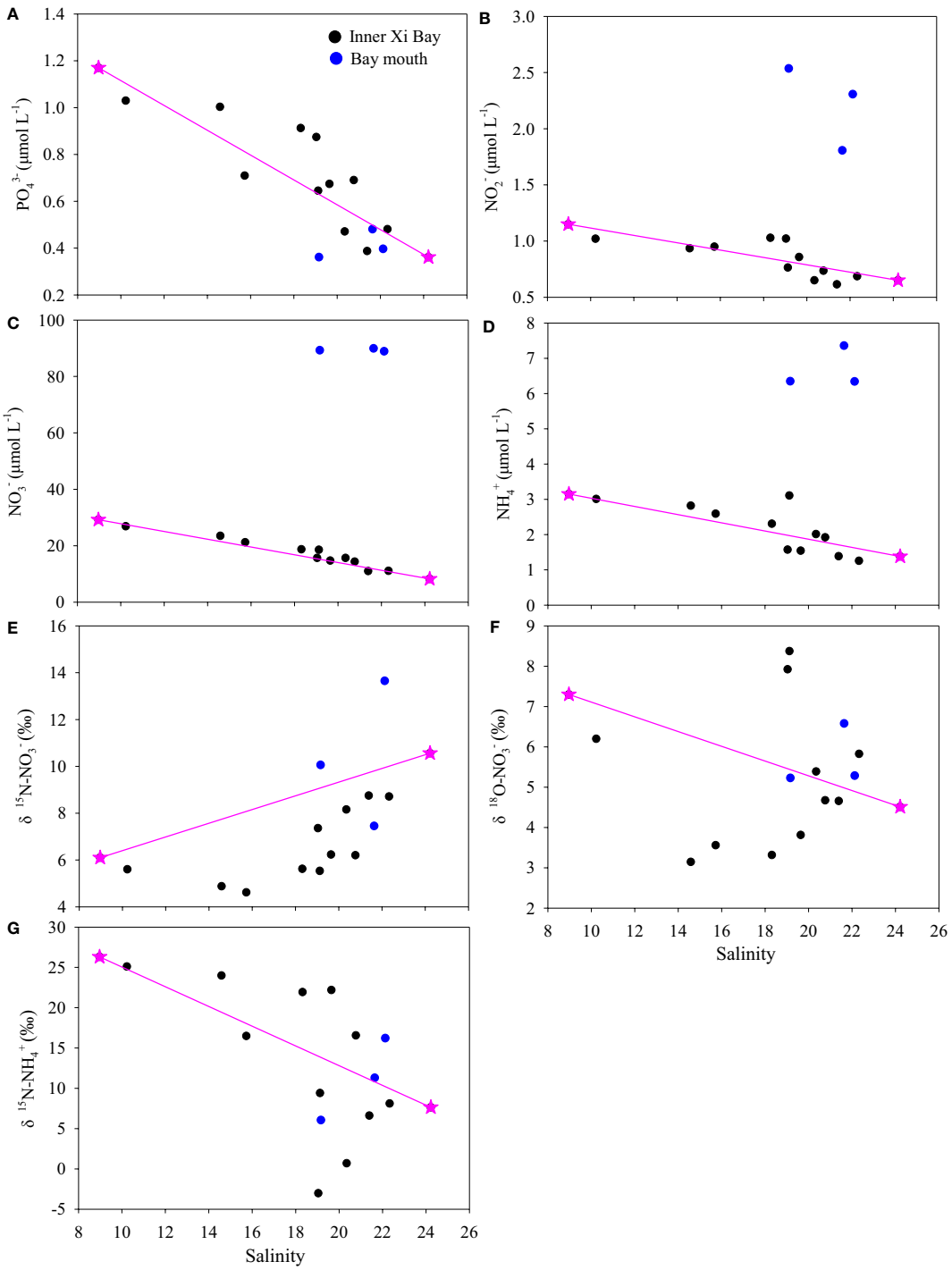

FIGURE 6
Distribution of nutrients and isotopic values against salinity in Xi Bay. The black dots are the samples excluding the stations in the bay mouth of Xi Bay; the blue dots are the samples in the bay mouth. The pink lines indicate the mixing line. The inner bay includes the upper bay and lower bay (stations X1 to X12); the bay mouth includes stations X13 to X15. **(A)**, PO_{43}^- **(B)**, NO_2^- **(C)** NO_3^- **(D)** NH_4^+ **(E)**, δ15N-NO_3^- **(F)**, δ18O-NO_3^- **(G)**, δ15N-NH_4^+

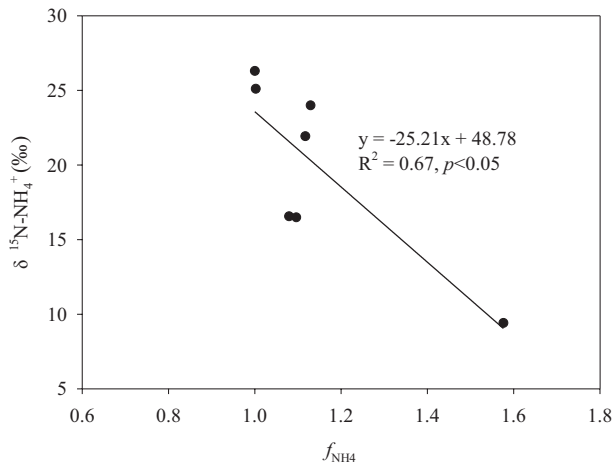

FIGURE 7
Linear relationship between $\delta^{15}N\text{-}NH_4^+$ and f_{NH4} in the upper bay.

-9‰) during assimilation (York et al., 2007; Ye et al., 2016; Chen et al., 2022). This suggests that assimilation is unlikely to be the dominant process causing the increase in $\delta^{15}N\text{-}NO_3^-$ and $\delta^{18}O\text{-}NO_3^-$ values in the lower bay and the bay mouth. Moreover, a high NH_4^+ concentration (>6.30 μmol L^{-1}) was found in the bay mouth, indicating that NH_4^+ is sufficient, and phytoplankton preferentially assimilate NH_4^+ (Glibert et al., 2016). However, if the assimilated NH_4^+ by phytoplankton was the dominant process in the lower bay and the bay mouth, increasing $\delta^{15}N\text{-}NH_4^+$ values can be expected. In contrast, lower $\delta^{15}N\text{-}NH_4^+$ values were found in the lower bay and the bay mouth (**Figure 4**). Thus, the external DIN sources could be responsible for the high DIN level in the bay mouth. The coast of the bay mouth is an important port and industrial area in Fangchenggang city. Intensive human activities and industrial emissions may be responsible for the high DIN concentration in the bay mouth (Lao et al., 2021a). In addition, heavy rainfall during the rainy seasons could also scour masses of pollutants into the bay, particularly in heavily polluted wharves and industrial areas (Lao et al., 2021a).

Quantification of nitrate sources in Xi Bay

Because of the lower influence of isotopic fractionation caused by biological processes, such as denitrification and assimilation, isotopic characteristics may provide a signal on the various nitrate sources in Xi Bay, and the Bayesian mixing model can be used to quantify the potential nitrate sources (Lao et al., 2019a). In previous studies, potential nitrate sources, including sewage and manure, soil N, fertilizer and atmospheric deposition, have been reported in the coastal Beibu Gulf (Lao et al., 2021b; Chen et al., 2022). In Beibu Gulf, sewage and manure are considered as the most important nitrate sources in the coastal areas (Pan et al., 2021; Lao et al., 2021b; Chen et al., 2022). In addition, due to the input of many rivers into the Beibu Gulf, the rivers can input a large amount of agricultural nitrogen fertilizer and soil N into the coastal waters (Pan et al., 2021; Chen et al., 2022). Therefore, based on previous literature, we carried out a Bayesian mixed model calculation for four potential sources that may affect nitrate content in Xi Bay. In this study, the potential nitrate source from sewage and manure was selected from the measured values in the Beibu Gulf (Pan et al., 2021), and nitrate sources from soil N and fertilizer were selected from the coastal areas in the gulf (Jin et al., 2020), and the source from precipitation was selected near the Beibu Gulf in Zhanjiang city (Chen et al., 2019c). The $\delta^{15}N\text{-}NO_3^-$ and $\delta^{18}O\text{-}NO_3^-$ values of these four potential sources are presented in **Table 2**. As discussed above, nitrification is another important nitrate source in the upper bay, and thus, the isotopic values of $\delta^{15}N\text{-}NO_3^-$ (0‰) and $\delta^{18}O\text{-}NO_3^-$ (7.8‰) (Chen et al., 2009 and Chen et al., 2019b) are considered a nitrate source endmember in the upper bay. The results of the quantification of potential nitrate sources in Xi Bay are presented in **Figure 8**. In the upper bay, the nitrate is mainly formed by nitrification (accounted for 39%). Except for the nitrate formed by nitrification, the nitrate from sewage and manure was another dominant external source in the upper bay (ranging from 28% to 38%, average of 33%), followed by soil N (ranging from 0% to 31%, average of 15%) and fertilizer (ranging from 0% to 29%, average of 11%), while the source from atmospheric deposition was the lowest (2%). In the lower bay and the bay mouth, due to the influence of intensive human activities, heavy nitrate pollution mainly originated from sewage and manure (ranging from 44% to 64%, average of 54%),

TABLE 2 The values (‰) of dual isotopes for the four potential nitrate sources at the river mouth.

Source	$\delta^{15}N\text{-}NO_3^-$			$\delta^{18}O\text{-}NO_3^-$		
	Range	Mean ± SD	Reference	Range	Mean ± SD	Reference
Manure and sewage	–	15.5 ± 0.5	(Pan et al., 2021)	–	-1.2 ± 0.2	(Pan et al., 2021)
Soil N	-6.2~9.0	2.9 ± 4.0	(Jin et al., 2020)	1.0~16.4	8.2 ± 4.4	(Jin et al., 2020)
Fertilizer	-0.2~0.9	0.4 ± 0.5	(Jin et al., 2020)	14.2~15.1	14.7 ± 0.4	(Jin et al., 2020)
Atmospheric deposition	-1.8~4.1	0.8 ± 1.5	(Chen et al., 2019c)	42.7~61.6	52.4 ± 5.1	(Chen et al., 2019c)

followed by soil N (ranging from 4% to 45%, average of 26%) and fertilizer (ranging from 1% to 33%, average of 17%), and atmospheric deposition accounted for only 3%. According to the calculated results, the high proportion of sewage and manure was responsible for the high DIN pollution in Xi Bay, particularly in the bay moth. Similar results were also reported in the other coastal bays in the Beibu Gulf, which suggests that sewage and manure were the dominant nitrate sources (Lao et al., 2021b; Pan et al., 2021; Chen et al., 2022). With the rapid development of urbanization and industrialization in the Beibu Gulf, the population density of coastal cities has gradually increased, and land-based wastewater discharge has increased (Lao et al., 2019a; Lao et al., 2020; Liu et al., 2020; Lao et al., 2021d), resulting in an increase in eutrophication in the coastal seawater of Beibu Gulf in recent decades (Lao et al., 2021a and Lao et al., 2021c). In addition, soil N was another important source that contributed to the heavy nitrogen pollution in the bay. With the increase in rainfall in the rainy season, a large amount of soil N on the land can be washed away and enter the coastal bay with the river (Lao et al., 2022b). Previous studies suggested that the nitrate source from the soil N in a coastal bay with riverine input was significantly higher than that in a bay without riverine input during the same period (Chen et al., 2022; Lao et al., 2022b). Moreover, nitrogen fertilizer (almost in the reduced form) is heavily applied in catchment agriculture in the Beibu Gulf during the rainy seasons (Xia et al., 2011; Kaiser et al., 2014; Lao et al., 2021a: Lao et al., 2021b), which could leak and contribute to the bay in this rainy season.

Conclusion

Nitrate and aammonium isotopes ($\delta^{15}N\text{-}NO_3^-$, $\delta^{18}O\text{-}NO_3^-$ and $\delta^{15}N\text{-}NH_4^+$) were measured to determine the nitrate sources and the biogeochemical processes associated with nitrogen cycling in Xi Bay in Beibu Gulf, a semi-enclosed bay strongly affected by human activities. A high DIN concentration was observed in Xi Bay, particularly in the bay mouth. In addition, the DIN concentration was significantly higher than that in the other coastal bays in Beibu Gulf (the concentration in Xi Bay is 1.5 times that in Qinzhou Bay and 1.7 times that in Tieshangang Bay), suggesting high nitrogen pollution in the bay due to intensive human activities (i.e., industrial and port activities). Lower values of $\delta^{15}N\text{-}NO_3^-$ and $\delta^{18}O\text{-}NO_3^-$ and higher $\delta^{15}N\text{-}NH_4^+$ values were observed in the upper bay, suggesting that microbial nitrification occurs in the upper bay, and the nitrate

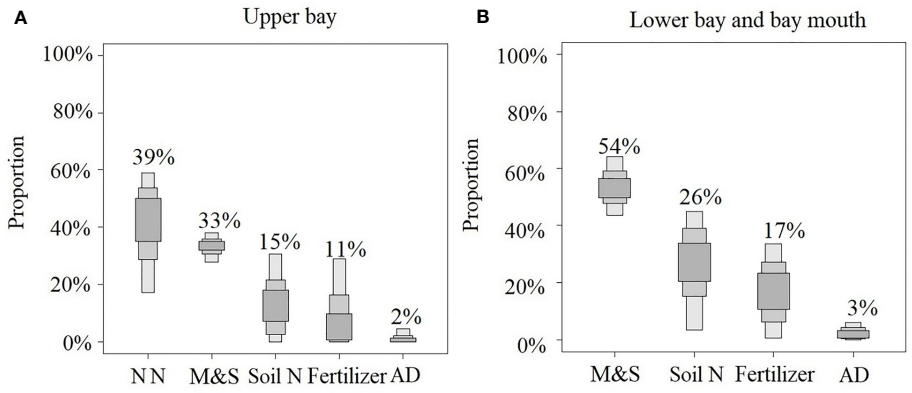

FIGURE 8
Proportion of potential nitrate sources in bay A during rainy season. **(A)** Proportion of potential nitrate sources in Upper bay, **(B)** Proportion of potential nitrate sources in Low bay and bay mouth. NN: nitrate from nitrification.

formed by nitrification accounted for 39%, which is the dominant nitrate source in the upper bay. Except for nitrification, external sources, including sewage and manure (accounting for 33%), soil N (accounting for 15%) and fertilizer (accounting for 11%), contributed to the higher nutrients in the upper bay. In the lower bay and the bay mouth, severe nitrogen pollution resulted in less impact of biological processes on isotopic fractionation. The heavy nitrate pollution in the lower bay and the bay mouth mainly originated from sewage and manure (accounting for 54%), followed by soil N (accounting for 26%) and fertilizer (accounting for 17%), and atmospheric deposition accounted for only 3%. Overall, biogeochemical processes have little impact on nitrate dual isotopes under heavy nitrogen pollution, and isotopes are an ideal proxy for tracing nitrogen sources.

Data availability statement

The original contributions presented in the study are included in the article/supplementary material. Further inquiries can be directed to the corresponding author.

Author contributions

GJ was responsible for the conceptualization. SC and QL prepared and wrote the original draft. SC, QL and GJ wrote, reviewed, and edited the manuscript. QL were responsible for the data curation. CC, QZ and XL were responsible for the experimental operation. SC, QL and XL were responsible for field sampling. QL and GJ funded the acquisition. All authors contributed to the article and approved the submitted version.

Acknowledgments

We would like to thank Marine Environmental Monitoring Centre of Beihai, State Oceanic Administration, for their support in collecting water samples. This study was supported by the Guangdong Provincial College Innovation Team Project (2019KCXTF021), the Guangxi Natural Science Foundation of China (2020GXNSFBA297065) and First-class Discipline Plan of Guangdong Province (080503032101, 231420003).

Conflict of interest

The authors declare that the research was conducted in the absence of any commercial or financial relationships that could be construed as a potential conflict of interest.

Publisher's note

All claims expressed in this article are solely those of the authors and do not necessarily represent those of their affiliated organizations, or those of the publisher, the editors and the reviewers. Any product that may be evaluated in this article, or claim that may be made by its manufacturer, is not guaranteed or endorsed by the publisher.

References

Casciotti, K. L. (2009). Inverse kinetic isotope fractionation during bacterial nitrite oxidation. *Geochimica Cosmochimica Acta* 73 (7), 2061–2076. doi: 10.1016/j.gca.2008.12.022

Casciotti, K. L., Buchwald, C., Santoro, A. E., and Frame, C. (2011). Assessment of nitrogen and oxygen isotopic fractionation during nitrification and its expression in the marine environment. *Methods enzygogy* 486, 253–280. doi: 10.1016/B978-0-12-381294-0.00011-0

Casciotti, K. L., McIlvin, M., and Buchwald, C. (2010). Oxygen isotopic exchange and fractionation during bacterial ammonia oxidation. *Limnology Oceanography* 55 (2), 753–762. doi: 10.4319/lo.2010.55.2.0753

Casciotti, K. L., Sigman, D. M., and Ward, B. B. (2003). Linking diversity and stable isotope fractionation in ammonia-oxidizing bacteria. *Geomicrobiology J.* 20 (4), 335–353. doi: 10.1080/01490450303895

Chen, B., Dong, D., Qin, X., Xu, M., Chen, X., and Shi, M. (2019a). Relationship between the occurrence of red tides and the dynamic response mechanisms in the northern beibu gulf. *J. Coast. Res.* 93 (SI), 185–193. doi: 10.2112/SI93-026.1

Chen, F., Jia, G., and Chen, J. (2009). Nitrate sources and watershed denitrification inferred from nitrate dual isotopes in the beijiang river, south China. *Biogeochemistry* 94 (2), 163–174. doi: 10.1007/s10533-009-9316-x

Chen, F., Lao, Q., Jia, G., Chen, C., Zhu, Q., and Zhou, X. (2019c). Seasonal variations of nitrate dual isotopes in wet deposition in a tropical city in China. *Atmospheric Environ.* 196, 1–9. doi: 10.1016/j.atmosenv.2018.09.061

Chen, C., Lao, Q., Shen, Y., Jin, G., Chen, F., Su, Q., et al. (2022). Comparative study of nitrogen cycling between a bay with riverine input and a bay without riverine input, inferred from stable isotopes. *Front. Mar. Sci.* 9, 885037. doi: 10.3389/fmars.2022.885037

Chen, F., Lao, Q., Zhang, S., Bian, P., Jin, G., Zhu, Q., et al. (2020). Nitrate sources and biogeochemical processes identified using nitrogen and oxygen isotopes on the eastern coast of hainan island. *Continental Shelf Res.* 207, 104209. doi: 10.1016/j.csr.2020.104209

Chen, F., Zhou, X., Lao, Q., Wang, S., Jin, G., Chen, C., et al. (2019b). Dual isotopic evidence for nitrate sources and active biological transformation in the northern south China Sea in summer. *PloS One* 14 (1), e0209287. doi: 10.1371/journal.pone.0209287

Davis, P., Syme, J., Heikoop, J., Fessenden-Rahn, J., Perkins, G., Newman, B., et al. (2015). Quantifying uncertainty in stable isotope mixing models. *J. Geophysical Research: Biogeosciences* 120 (5), 903–923. doi: 10.1002/2014JG002839

Falkowski, P. G., Barber, R. T., and Smetacek, V. (1998). Biogeochemical controls and feedbacks on ocean primary production. *science* 281 (5374), 200–206. doi: 10.1126/science.281.5374.200

Fry, B. (2002). Conservative mixing of stable isotopes across estuarine salinity gradients: A conceptual framework for monitoring watershed influences on downstream fisheries production. *Estuaries* 25, 264–271. doi: 10.1007/BF02691313

Glibert, P. M., Icarus Allen, J., Artioli, Y., Beusen, A., Bouwman, L., Harle, J., et al. (2014). Vulnerability of coastal ecosystems to changes in harmful algal bloom distribution in response to climate change: projections based on model analysis. *Global Change Biol.* 20 (12), 3845–3858. doi: 10.1111/gcb.12662

Glibert, P. M., Wilkerson, F. P., Dugdale, R. C., Raven, J. A., Dupont, C. L., Leavitt, P. R., et al. (2016). Pluses and minuses of ammonium and nitrate uptake and assimilation by phytoplankton and implications for productivity and community composition, with emphasis on nitrogen-enriched conditions. *Limnology Oceanography* 61 (1), 165–197. doi: 10.1002/lno.10203

Granger, J., Prokopenko, M. G., Sigman, D. M., Mordy, C. W., Morse, Z. M., Morales, L. V., et al. (2011). Coupled nitrification-denitrification in sediment of the eastern Bering Sea shelf leads to 15N enrichment of fixed n in shelf waters. *J. Geophysical Research: Oceans* 116 (C11). doi: 10.1029/2010jc006751

Granger, J., Sigman, D. M., Lehmann, M. F., and Tortell, P. D. (2008). Nitrogen and oxygen isotope fractionation during dissimilatory nitrate reduction by denitrifying bacteria. *Limnology Oceanography* 53 (6), 2533–2545. doi: 10.4319/lo.2008.53.6.2533

Granger, J., Sigman, D. M., Needoba, J. A., and Harrison, P. J. (2004). Coupled nitrogen and oxygen isotope fractionation of nitrate during assimilation by cultures of marine phytoplankton. *Limnology Oceanography* 49 (5), 1763–1773. doi: 10.4319/lo.2004.49.5.1763

Gruber, N., and Galloway, J. N. (2008). An earth-system perspective of the global nitrogen cycle. *Nature* 451, 293–296. doi: 10.1038/nature06592

Guan, W., Bao, M., Lou, X., Zhou, Z., and Yin, K. (2022). Monitoring, modeling and projection of harmful algal blooms in China. *Harmful Algae* 111, 102164. doi: 10.1016/j.hal.2021.102164

Guo, J., Wang, Y., Lai, J., Pan, C., Wang, S., Fu, H., et al. (2020). Spatiotemporal distribution of nitrogen biogeochemical processes in the coastal regions of northern beibu gulf, south China sea. *Chemosphere* 239, 124803. doi: 10.1016/j.chemosphere.2019.124803

Howarth, R., Chan, F., Conley, D. J., Garnier, J., Doney, S. C., Marino, R., et al. (2011). Coupled biogeochemical cycles: eutrophication and hypoxia in temperate estuaries and coastal marine ecosystems. *Front. Ecol. Environ.* 9 (1), 18–26. doi: 10.1890/100008

Jickells, T. D. (1998). Nutrient biogeochemistry of the coastal zone. *Science* 281 (5374), 217–222. doi: 10.1126/science.281.5374.217

Jin, Z., Wang, J., Chen, J., Zhang, R., Li, Y., Yaoting, L., et al. (2020). Identifying the sources of nitrate in a small watershed using δ15N-δ18O isotopes of nitrate in the kelan reservoir, guangxi, China. *Agric. Ecosyst. Environ.* 297, 106936. doi: 10.1016/j.agee.2020.106936

Kaiser, D., Unger, D., and Qiu, G. (2014). Particulate organic matter dynamics in coastal systems of the northern beibu gulf. *Continental Shelf Res.* 82, 99–118. doi: 10.1016/j.csr.2014.04.006

Kendall, C. (1998). "Tracing nitrogen sources and cycling in catchments," in *Isotope tracers in catchment hydrology*. Eds. C. Kendall and J. J. McDonnel (New York: Elsevier), 519–576.

Korth, F., Deutsch, B., Frey, C., Moros, C., and Voss, M. (2014). Nitrate source identification in the Baltic Sea using its isotopic ratios in combination with a Bayesian isotope mixing model. *Biogeosciences* 11 (17), 4913–4924. doi: 10.5194/bg-11-4913-2014

Lai, J., Jiang, F., Ke, K., Xu, M., Lei, F., and Chen, B. (2014). Nutrients distribution and trophic status assessment in the northern beibu gulf, China. *Chin. J. oceanology limnology* 32 (5), 1128–1144. doi: 10.1007/s00343-014-3199-y

Lao, Q., Cai, S., Huang, P., Chen, F., Su, Q., Lei, X., et al. (2022a). Contaminant characteristics and influencing factors of heavy metals in seawater and sediments in a typical mariculture bay in south China. *Front. Mar. Sci.* 9. doi: 10.3389/fmars.2022.923494

Lao, Q., Zhang, S., Li, Z., Chen, F., Zhou, X., Jin, G., et al. (2022b). Quantification of the seasonal intrusion of water masses and their impact on nutrients in the Beibu Gulf using dual water isotopes. *J. Geophys. Res. Oceans* 127, e2021JC018065. doi: 10.1029/2021JC018065

Lao, Q., Chen, F., Liu, G., Chen, C., Jin, G., Zhu, Q., et al. (2019a). Isotopic evidence for the shift of nitrate sources and active biological transformation on the western coast of guangdong province, south China. *Mar. pollut. Bull.* 142, 603–612. doi: 10.1016/j.marpolbul.2019.04.026

Lao, Q., Liu, G., Gao, J., Shen, Y., Guo, Z., Qing, S., et al. (2021c). Study on the characteristics and eutrophication of nutrients in the mariculture farms of qinzhou bay, south China. *Mar. Environ. Sci.* 40 (3), 407–416. doi: 10.13634/j.cnki.mes.2021.03.011

Lao, Q., Liu, G., Gao, J., Shen, Y., Su, Q., Chen, C., et al. (2021b). Seasonal sources and cycling of nitrogen revealed by stable isotopes in the northeastern beibu gulf, China. *J. Mar. Sci. Eng.* 9 (10), 1123. doi: 10.3390/jmse9101123

Lao, Q., Liu, G., Shen, Y., Su, Q., Gao, J., and Chen, F. (2020). Distribution characteristics and fluxes of nutrients in the rivers of the beibu gulf. *Haiyang Xuebao* 42 (12), 93–100. doi: 10.3969/j.issn.0253–4193.2020.12.010

Lao, Q., Liu, G., Shen, Y., Su, Q., and Lei, X. (2021a). Biogeochemical processes and eutrophication status of nutrients in the northern beibu gulf, south China. *J. Earth System Sci.* 130 (4), 1–14. doi: 10.1007/s12040-021-01706-y

Lao, Q., Liu, G., Zhou, X., Chen, F., and Zhang, S. (2021d). Sources of polychlorinated biphenyls (PCBs) and dichlorodiphenyltrichloroethanes (DDTs) found in surface sediment from coastal areas of beibu gulf: A reflection on shipping activities and coastal industries. *Mar. pollut. Bull.* 167, 112318. doi: 10.1016/j.marpolbul.2021.112318

Lao, Q., Su, Q., Liu, G., Shen, Y., Chen, F., Lei, X., et al. (2019b). Spatial distribution of and historical changes in heavy metals in the surface seawater and sediments of the beibu gulf, China. *Mar. pollut. Bull.* 146, 427–434. doi: 10.1016/j.marpolbul.2019.06.080

Li, H. M., Tang, H. J., Shi, X. Y., Zhang, C. S., and Wang, X. L. (2014). Increased nutrient loads from the changjiang (Yangtze) river have led to increased harmful algal blooms. *Harmful Algae* 39, 92–101. doi: 10.1016/j.hal.2014.07.002

Liu, G., Lao, Q., Su, Q., Shen, Y., Chen, F., Qing, S., et al. (2020). Spatial and seasonal characteristics of dissolved heavy metals in the aquaculture areas of beibu gulf, south China. *Hum. Ecol. Risk Assessment: Int. J.* 26 (7), 1957–1969. doi: 10.1080/10807039.2019.1629273

Lorenzen, C. J. (1967). Determination of chlorophyll and pheopigments: spectrophotometric equations. *Limnol Oceanogr* 12, 343–346. doi: 10.4319/lo.1967.12.2.0343

Lyu, H., Song, D., Zhang, S., Wu, W., and Bao, X. (2022). Compound effect of land reclamation and land-based pollutant input on water quality in qinzhou bay, China. *Sci. Total Environ.* 826, 154183. doi: 10.1016/j.scitotenv.2022.154183

Malone, T. C., and Newton, A. (2020). The globalization of cultural eutrophication in the coastal ocean: causes and consequences. *Front. Mar. Sci.* 7, 670. doi: 10.3389/fmars.2020.00670

McIlvin, M. R., and Altabet, M. A. (2005). Chemical conversion of nitrate and nitrite to nitrous oxide for nitrogen and oxygen isotopic analysis in freshwater and seawater. *Analytical Chem.* 77 (17), 5589–5595. doi: 10.1021/ac050528s

Moore, C. M., Mills, M. M., Arrigo, K. R., Berman-Frank, I., Bopp, L., Boyd, P. W., et al. (2013). Processes and patterns of oceanic nutrient limitation. *Nat. Geosci.* 6 (9), 701–710. doi: 10.1038/ngeo1765

Moore, J. W., and Semmens, B. X. (2008). Incoporating uncertainty and prior information into stable isotope mixing models. *Ecol. Lett.* 11, 470–480. doi: 10.1111/j.1461-0248.2008.01163.x

Pan, K., Zheng, X., Liu, X., and Jiang, H. (2021). Nitrogen cycling in a tropical coral reef ecosystem under severe anthropogenic disturbance in summer: Insights from isotopic compositions. *Water Res.* 207, 117824. doi: 10.1016/j.watres.2021.117824

Rabalais, N. N., Turner, R. E., and Wiseman, W. J.Jr. (2002). Gulf of Mexico hypoxia, aka "The dead zone". *Annu. Rev. Ecol. Systematics* 33 (1), 235–263. doi: 10.1146/annurev.ecolsys.33.010802.150513

Savage, C., Leavitt, P. R., and Elmgren, R. (2010). Effects of land use, urbanization, and climate variability on coastal eutrophication in the Baltic Sea. *Limnology Oceanography* 55 (3), 1033–1046. doi: 10.4319/lo.2010.55.3.1033

Sigman, D. M., DiFiore, P. J., Hain, M. P., Deutsch, C., Wang, Y., Karl, D. M., et al. (2009). The dual isotopes of deep nitrate as a constraint on the cycle and budget of oceanic fixed nitrogen. *Deep Sea Res. Part I: Oceanographic Res. Papers* 56 (9), 1419–1439. doi: 10.1016/j.dsr.2009.04.007

Sigman, D. M., Granger, J., DiFiore, P. J., Lehmann, M. M., Ho, R., Cane, G., et al. (2005). Coupled nitrogen and oxygen isotope measurements of nitrate along the eastern north pacific margin. *Global Biogeochemical Cycles* 19 (4), GB4022. doi: 10.1029/2005GB002458

Smart, S. M., Fawcett, S. E., Thomalla, S. J., Weigand, M. A., Reason, C. J., and Sigman, D. M. (2015). Isotopic evidence for nitrification in the Antarctic winter mixed layer. *Global Biogeochemical Cycles* 29 (4), 427–445. doi: 10.1002/2014GB005013

Wankel, S. D., Kendall, C., Francis, C. A., and Paytan, A. (2006). Nitrogen sources and cycling in the San Francisco bay estuary: A nitrate dual isotopic composition approach. *Limnology Oceanography* 51 (4), 1654–1664. doi: 10.4319/lo.2006.51.4.1654

Xia, P., Meng, X., Yin, P., Cao, Z., and Wang, X. (2011). Eighty-year sedimentary record of heavy metal inputs in the intertidal sediments from the nanliu river estuary, beibu gulf of south China Sea. *Environ. pollut.* 159 (1), 92–99. doi: 10.1016/j.envpol.2010.09.014

Xu, C., Dan, S. F., Yang, B., Lu, D., Kang, Z., Huang, H., et al. (2021). Biogeochemistry of dissolved and particulate phosphorus speciation in the maowei Sea, northern beibu gulf. *J. Hydrology* 593, 125822. doi: 10.1016/j.jhydrol.2020.125822

Xue, D., Botte, J., De Baets, B., Accoe, F., Nestler, A., Taylor, P., et al. (2009). Present limitations and future prospects of stable isotope methods for nitrate

source identification in surface-and groundwater. *Water Res.* 43 (5), 1159–1170. doi: 10.1016/j.watres.2008.12.048

Xu, C., Yang, B., Dan, S. F., Zhang, D., Liao, R., Lu, D., et al. (2020). Spatiotemporal variations of biogenic elements and sources of sedimentary organic matter in the largest oyster mariculture bay (Maowei Sea), southwest China. *Sci. Total Environ.* 730, 139056. doi: 10.1016/j.scitotenv.2020.139056

Xu, Y., Zhang, T., and Zhou, J. (2019). Historical occurrence of algal blooms in the northern beibu gulf of China and implications for future trends. *Front. Microbiol.* 10, 451. doi: 10.3389/fmicb.2019.00451

Yang, Z., Chen, J., Li, H., Jin, H., Gao, S., Ji, Z., et al. (2018). Sources of nitrate in xiangshan bay (China), as identified using nitrogen and oxygen isotopes. *Estuarine Coast. Shelf Sci.* 207, 109–118. doi: 10.1016/j.ecss.2018.02.019

Yan, X., Xu, M. N., Wan, X. S., Yang, J. Y. T., Trull, T. W., Dai, M., et al. (2017). Dual isotope measurements reveal zoning of nitrate processing in the summer changjiang (Yangtze) river plume. *Geophysical Res. Lett.* 44 (24), 12–289. doi: 10.1002/2017GL075951

Ye, F., Jia, G., Xie, L., Wei, G., and Xu, J. (2016). Isotope constraints on seasonal dynamics of dissolved and particulate n in the pearl river estuary, south China. *J. Geophysical Research: Oceans* 121 (12), 8689–8705. doi: 10.1002/2016JC012066

York, J. K., Tomasky, G., Valiela, I., and Repeta, D. J. (2007). Stable isotopic detection of ammonium and nitrate assimilation by phytoplankton in the waquoit bay estuarine system. *Limnology Oceanography* 52, 144–155. doi: 10.4319/lo.2007.52.1.0144

Yu, L., Gan, J., Dai, M., Hui, C. R., Lu, Z., and Li, D. (2021). Modeling the role of riverine organic matter in hypoxia formation within the coastal transition zone off the pearl river estuary. *Limnology Oceanography* 66 (2), 452–468. doi: 10.1002/lno.11616

Zhang, L., Altabet, M. A., Wu, T., and Hadas, O. (2007). Sensitive measurement of NH4+ 15N/14N (δ15NH4+) at natural abundance levels in fresh and saltwaters. *Analytical Chem.* 79 (14), 5297–5303. doi: 10.1021/ac070106d

Zhang, D., Lu, D., Yang, B., Zhang, J., Ning, Z., and Yu, K. (2019). Influence of natural and anthropogenic factors on spatial-temporal hydrochemistry and the susceptibility to nutrient enrichment in a subtropical estuary. *Mar. pollut. Bull.* 146, 945–954. doi: 10.1016/j.marpolbul.2019.07.056

Zhang, M., Zhi, Y., Shi, J., and Wu, L. (2018). Apportionment and uncertainty analysis of nitrate sources based on the dual isotope approach and a Bayesian isotope mixing model at the watershed scale. *Sci. Total Environ.* 639, 1175–1187. doi: 10.1016/j.scitotenv.2018.05.239

Zhou, Y., Wang, L., Zhou, Y., and Mao, X. Z. (2020). Eutrophication control strategies for highly anthropogenic influenced coastal waters. *Sci. Total Environ.* 705, 135760. doi: 10.1016/j.scitotenv.2019.135760

frontiers | Frontiers in Marine Science

ORIGINAL RESEARCH
published: 26 July 2022
doi: 10.3389/fmars.2022.956930

Characteristics of Dissolved Organic Matter in a Semi-closed Bay in Summer: Insights from Stable Isotope and Optical Analyses

Yafeng Zhong[1], *Gang Pan*[2,3], *Hui Zhao*[1,2*] *and Chao Wang*[4,5,6*]

[1]College of Chemistry and Environmental Science, Guangdong Ocean University, Zhanjiang, China, [2]Research Center for Coastal Environmental Protection and Ecological Resilience, Guangdong Ocean University, Zhanjiang, China, [3]School of Humanities, York St. John University, York, United Kingdom, [4]Laboratory for Coastal Ocean Variation and Disaster Prediction, College of Ocean and Meteorology, Guangdong Ocean University, Zhanjiang, China, [5]Key Laboratory of Climate, Resources and Environment in Continental Shelf Sea and Deep Sea of Department of Education of Guangdong Province, Guangdong Ocean University, Zhanjiang, China, [6]Key Laboratory of Space Ocean Remote Sensing and Application, Ministry of Natural Resources, Beijing, China

Dissolved organic matter (DOM) serves as the most active and sensitive organic component in the bay, and its biogeochemical characteristics and reactivity are affected by the properties of terrestrial and marine substances significantly. In this study, in order to study the distribution and characteristics of DOM in a semi-closed bay, 34 water samples from 19 stations were collected from Zhanjiang Bay and analyzed for $\delta^{13}C$ of dissolved inorganic carbon (DIC) and fluorescent components of DOM. The results showed that there were many sources of organic matter in the bay, including soil input, algae input, and sewage input. Influenced by freshwater input, DOM in the bay decreased from the upper bay to the outer bay. The organic matter in the bay displayed two characteristics, where the northern bay is composed of terrigenous organic matter mainly with high humus, while the southern bay is more inclined to marine sources with a high biological index (BIX) and low humification index (HIX). The correlation between organic matter with different characteristics and environmental parameters such as salinity, pH, and chlorophyll *a* was analyzed. The discrepancy may be caused by the weak turbulent mixing in the semi-closed bay.

Keywords: dissolved organic matter, characteristic, stable isotope, Zhanjiang Bay, semi-closed bay

OPEN ACCESS

Edited by:
Meilin Wu,
South China Sea Institute of Oceanology (CAS), China

Reviewed by:
Yong Zhang,
Shandong University, China
Dongliang Lu,
Beibu Gulf University, China
Wen-zhuo Zhu,
Zhejiang Ocean University, China

***Correspondence:**
Hui Zhao
huizhao1978@163.com
Chao Wang
chaowang@gdou.edu.cn

Specialty section:
This article was submitted to Marine Pollution, a section of the journal Frontiers in Marine Science

Received: *30 May 2022*
Accepted: *20 June 2022*
Published: *26 July 2022*

Citation:
Zhong Y, Pan G, Zhao H and Wang C (2022) Characteristics of Dissolved Organic Matter in a Semi-closed Bay in Summer: Insights from Stable Isotope and Optical Analyses. Front. Mar. Sci. 9:956930. doi: 10.3389/fmars.2022.956930

1 INTRODUCTION

Estuaries serve as the important hubs of the global carbon cycle, linking multiple ecosystems such as land, atmosphere, and ocean (Bianchi, 2007). As an ecosystem affected by terrestrial runoff and ocean tides, estuaries have sensitive characteristics of distinct physical–chemical and biological conditions (He et al., 2016; Chen et al., 2018). Estuaries also have frequent biological activities and possess high primary productivity and redox capacity as reaction pools of terrestrial and marine materials (Bianchi, 2011; Gireeshkumar et al., 2013). Driven by climate changes and anthropogenic activities, tremendous alterations in physical–chemical and biological conditions occur in estuaries (Najjar et al., 2010; Kerr, 2011; Canuel et al., 2012; Cabral et al., 2019).

Dissolved organic matter (DOM) serves as the most active and sensitive organic component; its biogeochemical characteristics and reactivity can be affected by the properties of allochthonous and

local substances significantly (Murphy et al., 2008; Ya et al., 2015; Lloret et al., 2016; Lee et al., 2020). Being surrounded by frequent human activity and diverse environments, estuarine DOM is provided with complex sources including primary productivity, river input, and sewage input (Hudson et al., 2007; Guo et al., 2014; Kinsey et al., 2018). As a matter of fact, more and more allochthonous DOM is imported into estuarine systems with the increase of anthropogenic activities like industrialization, urbanization, and agricultural practices (Boesch, 2002; Felgate et al., 2021). They will change the quality and quantity of DOM, which in turn impact the biogeochemical cycle, decomposition of organic matter, and recycling of chemical elements in sediments (Spilling et al., 2018; Felgate et al., 2021; García-Martín et al., 2021). Due to the different sources of DOM, their conversion, retention, and output fluxes in biogeochemical processes including flocculation, photochemistry, and biodegradation in estuaries also differ (Carlson and Hansell, 2015; García-Martín et al., 2021). Therefore, discriminating main sources of DOM and their contributions will be an important basis for evaluating the fate of estuarine DOM, which also is of great significance to evaluate the effects of terrestrial runoff and ocean tides on estuarine organic matter (Zhou, 2021).

Stable carbon isotope analysis is widely used to identify the origin of DOM because of the selective utilization of HCO_3^- by algae (Andrews et al., 1998; Beer et al., 2014; Lee et al., 2020). In terms of spectrophotometry, the composition of DOM is evaluated by detecting fluorescent DOM (FDOM) and various established optical indexes, such as fluorescence index (FI), humification index (HIX), and biological index (BIX) (Coble, 1996; Stedmon et al., 2003; Coble et al., 2014; Amaral et al., 2020). Those methods have been widely used to elucidate the contribution of DOM from different sources in estuaries, helping to track the transition and transportation of DOM from a river to an ocean (Coble, 1996; Jørgensen et al., 2011; Coble et al., 2014). A semi-closed bay is usually accompanied by closed topography and weak hydrodynamic conditions (Xue et al., 2021). In this case, Zhanjiang Bay was studied as a semi-closed bay, and the total amount of DOM and its main sources through spatial were investigated, paying attention to the transition and characteristics of DOM from a river to an ocean. The combination of stable carbon isotope and spectrophotometry was used to evaluate the distribution and source of DOM and clarify the characteristics and relationship with environmental factors of DOM in Zhanjiang Bay.

2 MATERIALS AND METHODS

2.1 Study Area and Sampling Collection

Zhanjiang Bay, located in the east of Leizhou Peninsula in China, is a typical semi-closed bay surrounded by islands and a peninsula. In this study, Zhanjiang Bay is divided into two parts according to the terrain: the northern bay and the southern bay (**Figure 1**). The northern bay is mainly composed of the estuary of the Suixi River, with shallow water depth. Among them, the Suixi River, the main river of Zhanjiang Bay, is about 80 km long with an annual average flow of 10.4×10^8 m^3. The southern bay is the major broad water in the bay, which is connected with the South China Sea through the southeastern bay mouth. Affected by narrow terrain, poor hydrodynamic conditions, and the influence of steady wind–east wind, the half exchange time of water in the northern bay was more than 100 days, and that in the southern bay was 30 days (Li, 2012). Zhanjiang Bay is also a bay deeply affected by human activities, where the degree of eutrophication of the bay is high, and many sewage outlets in the northern bay exist (Yu et al., 2017; Yu et al., 2021; Zhang et al., 2021).

A cruise was carried out during the summer (June 2021), mainly sampling from the estuary of the Suixi River to the southeastern bay mouth, and 34 water samples from 19 stations were collected from Zhanjiang Bay. The surface water and bottom water were collected with a 10-L Plexiglass water sampler during the cruise. The full-depth profiles of temperature, salinity, and water depth were determined using an SBE37 conductivity–temperature–depth (CTD) meter (Sea-Bird Scientific, Bellevue, WA, USA). The pH was measured on site with a pre-calibrated pH measuring instrument (Thermo Fisher Scientific, Waltham, MA, USA) and then corrected on site with temperature data. The water samples for dissolved oxygen (DO) analysis were collected first. Water from the Plexiglass water sampler was slowly drained into brown glass bottles and allowed to overflow for several minutes. Manganous sulfate and alkaline iodide solutions were then added. Titration was conducted in the laboratory within 24 h after taking the sample. The seawater samples for DOM were filtered using filters (Millipore, Billerica, MA, USA; 0.22 μm, PC Membrane) and stored at −20°C for analysis. For chlorophyll *a* (Chl-*a*), water samples (approximately 1,000 ml) were filtered

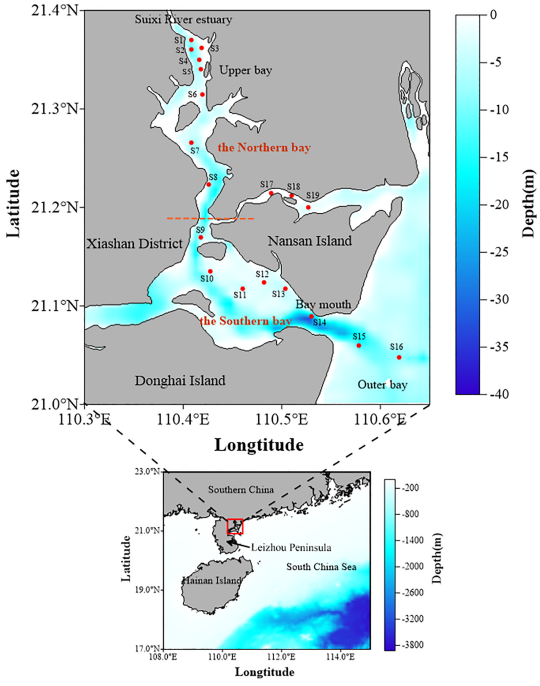

FIGURE 1 | Map of Zhanjiang Bay and sampling sites.

using pre-combusted (450°C, 4 h) glass-fiber filters (Whatman, 0.7 μm, GF/F) and stored at −20°C before further processing and analysis. Water samples for $\delta^{13}C_{DIC}$ measurements were collected in 60-ml glass bottles. Soon after collection, the samples were poisoned with $HgCl_2$, sealed with a rubber septum-aluminum cap, and wrapped with thick black paper. In the laboratory, the samples were kept refrigerated until analysis.

2.2 Chemical analysis

In the laboratory, after the sample was extracted in 90% acetone, the concentration of Chl-*a* was determined using a Turner fluorometer (Lorenzen and Jeffrey, 1980). The concentration of DO was determined using the Winkler method (Montgomery et al., 1964). The stable carbon isotope values of inorganic–organic carbon ($\delta^{13}C_{DIC}$) were determined using an elemental analysis isotope ratio mass spectrometer (GasBench II-IRMS). The precision based on replicate analysis was ±0.1‰ for $\delta^{13}C_{DIC}$ measurements.

2.3 Fluorescence Measurements and Excitation–Emission Matrix–PARAFAC Modeling

The FDOM excitation–emission matrices (EEMs) of 34 water samples were determined by an F-7100 fluorescence spectrofluorometer (Hitachi, Tokyo, Japan). The blank sample was prepared using Milli-Q water (Millipore, 18.2 MΩ/cm), and samples were placed into fused silica cells with a 1-cm path length. The EEM fluorescence was obtained by scanning excitation spectra (Ex) at 5-nm intervals of 240–450 nm and the emission wavelength (Em) at 2-nm intervals of 280–600 nm. The blank subtracted, normalized, and PARAFAC models of 34 EEMs were analyzed by the water Raman signals using MATLAB software (R2014b, MathWorks, Natick, MA, USA) (Stedmon and Bro, 2008). The reliability of the PARAFAC model was verified by residual and split-half analyses.

2.4 Optical Index Analysis

The optical indexes could provide effective information for the study of the composition and properties of DOM. FI was the ratio of emission intensity at 450 and 500 nm when the excitation wavelength was 370 nm, which could effectively indicate the source and degradation degree of DOM [Eq. (1)] (McKnight et al., 2001). The BIX implied the relative contributions of fresh DOM by the ratio of the emission at 380 nm to that at 430 nm for an excitation wavelength of 310 nm [Eq. (2)] (Huguet et al., 2009). The HIX could judge the degree of humification of DOM by calculating the ratios of two integrated sections of emission wavelengths (the summed emissions from 435 to 480 nm divided by the summed emissions from 300 to 345 nm) for an excitation wavelength at 254 nm (Zsolnay et al., 1999). Since FDOM was measured every 5 nm for excitation, leading to the excitation wavelength at 254 nm, which was not measured in the study, the adjacent excitation wavelength at 255 nm was used to replace the 254-nm wavelength here Eq. (3).

$$FI = \left[F_{\lambda em} = 450nm\right] / \left[F_{\lambda em} = 500nm\right], \lambda_{ex} = 370nm \quad (1)$$

$$BIX = \left[F_{\lambda em} = 380nm\right] / \left[F_{\lambda em} = 430nm\right], \lambda_{ex} = 310nm \quad (2)$$

$$HIX = \left[F_{\lambda em} = 435 \sim 480nm\right] / \left[F_{\lambda em} = 300 \sim 345nm\right], \lambda_{ex} = 255nm \quad (3)$$

2.5 Statistical analysis

Hierarchical cluster analysis (HCA) was performed to reveal the intrinsic correlation or similarity between sampling sites of different regions by Origin 2021b. Redundancy analysis (RDA) was applied to investigate the effects of environmental variables on fluorescence components by CANOCO 5.

3 RESULTS

3.1 Distributions of Salinity, Temperature, and pH

As shown in **Figure 2**, the salinity of Zhanjiang Bay ranged from 19.89 to 31.82 (with an average of 26.71 ± 3.50). A lower salinity was found from the northern bay, particularly in the

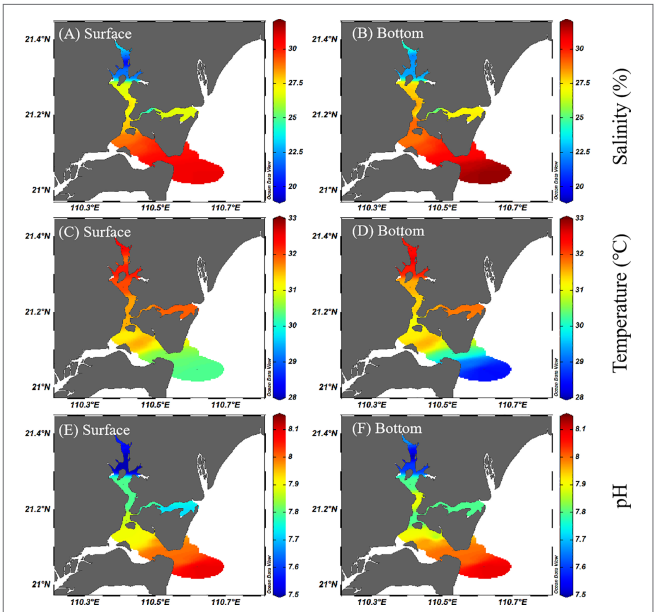

FIGURE 2 | Spatial distributions of salinity **(A, B)**, temperature **(C, D)** and pH **(E, F)** in the surface and bottom water of Zhanjiang Bay during the sampling period.

estuary of the Suixi River, suggesting that it was affected by the coastal freshwater discharge. On the whole, the salinity difference between the surface water and the bottom water was very small, indicating that the water in the bay may be mixed evenly. The water temperature of Zhanjiang Bay ranged from 28.41°C to 32.64°C (with an average of 31.52°C ± 0.93°C), and the temperature in the southern bay was lower than that in the northern bay. The pH ranged from 7.46 to 8.09 (with an average of 7.78 ± 0.18) in Zhanjiang Bay. Similar to salinity, the spatial distribution of pH also showed an obvious increasing trend and the lowest pH value corresponding to the lowest salinity, which indicated that the Suixi River is the region with the lowest pH value in Zhanjiang Bay.

3.2 Distributions of Chlorophyll-*A*, Dissolved Oxygen, and Stable Isotope

The Chl-*a* ranged from 0.6 to 10.06 μg L^{-1} (with an average of 2.00 ± 2.13 μg L^{-1}), and the high-value area was located in the Nansan islands (**Figure 3**). Compared with salinity and temperature, the spatial distribution of Chl-*a* did not show an obvious increasing or decreasing trend, and the overall distribution was relatively even.Lower DO values were observed from the estuary of the Suixi River and displayed a seaward increasing trend from the upper bay to the outer bay (3.67–5.79 mg L–1, with an average of 4.79 ± 0.59 mg L–1) (**Figure 3**). Although the salinity difference between the surface water and the bottom water was very small, the difference between DO was obvious. The correlation between DO and salinity was relatively weak (r^2 = 0.56, p< 0.01, n = 34), and that between DO and Chl-*a* was small (r^2 = 0.05, p< 0.01, n = 34), indicating that freshwater input and algae growth did not have a decisive influence on the distribution of DO. Combined with the fact that the DO of Zhanjiang Bay was all in unsaturated states (DO saturation: 57.84%–94.82%) (**Figure S1**), the DO may be affected by the consumption of organic matter in the degradation process. The concentration of DO near the estuary of the Suixi River was low, and the saturation of DO was also the lowest (**Figure S1**), which may be due to the fact that it had the highest concentration of DOM and was most severely affected by the degradation of organic matter. The $\delta^{13}C$ of dissolved inorganic carbon (DIC) values varied from −4.9‰ to 0.3‰ (with an average of −2.1‰ ± 1.57‰) and showed an increasing trend from the upper bay to the outer bay (**Figure 3**).

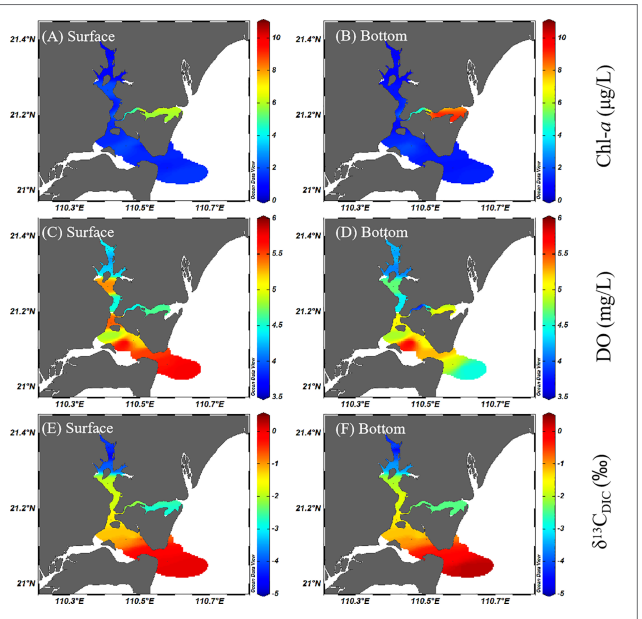

FIGURE 3 | Spatial distributions of Chl-a **(A, B)**, DO **(C, D)**, and stable isotope of DIC **(E, F)** in surface and bottom water of Zhanjiang Bay during the sampling period. Chl-a, chlorophyll a; DO, dissolved oxygen; DIC, dissolved inorganic carbon.

3.3 Distributions of Fluorescent Dissolved Organic Matter

Two humic-like components (C1–C2) and two protein-like components (C3–C4) were identified using the PARAFAC model in this study (**Figure 4**). C1 showed an excitation maximum at ≤240 nm and an emission maximum at 400 nm, which had been considered a marine humic-like fluorescence peak M previously (Coble, 1996). C2 displayed an excitation maximum at 250 nm and an emission maximum at 456 nm, which used to be classified into a mixture of terrestrial humic-like fluorescence peak C and peak A (Coble, 1996). C3 has two excitation maxima at ≤240 and 280 nm and an emission maximum at 356 nm, which have previously been reported as tryptophan-like fluorescence peak T (Coble, 1996). C4 had an excitation/emission maximum at 270/324 nm, which was attributed to protein-like fluorescence peak B and peak T (Coble, 1996).

The fluorescence intensity of humic-like C1 and C2 ranged from 5.90 to 50.99 (10^{-2} RU) and 3.90 to 32.95 (10^{-2} RU) (**Figure 5**), which had strong correlation between each other (r^2 = 0.99, p< 0.01, n = 34). Combined with their similar distribution, C1 and C2 should have the same source. The intensity of tryptophan-like C3 ranged from 4.84 to 28.48 (10^{-2} RU) (with an average of 13.90 ± 0.07 (10^{-2} RU)), and the intensity of protein-like C4 ranged from 5.23 to 13.67 (10^{-2} RU) (with an average of 8.92 ± 0.02 (10^{-2} RU)). The salinity showed a great negative correlation with the four fluorescent components (C1, r = −0.91, p< 0.01; C2, r = −0.91, p< 0.01; C3, r = −0.92, p< 0.01; C4, r = −0.87, p< 0.01). There were strong negative correlations between salinity and C1–C3 components, indicating that these three components may mainly come from the river, while the correlation between C4 and salinity decreased, indicating that freshwater had weakened the effect for C4 components. The four fluorescent components all showed a decreasing trend from the upper bay to the outer bay, and the decreasing amount was relatively large. In general, the fluorescence intensity of surface water was slightly lower than that of bottom water.

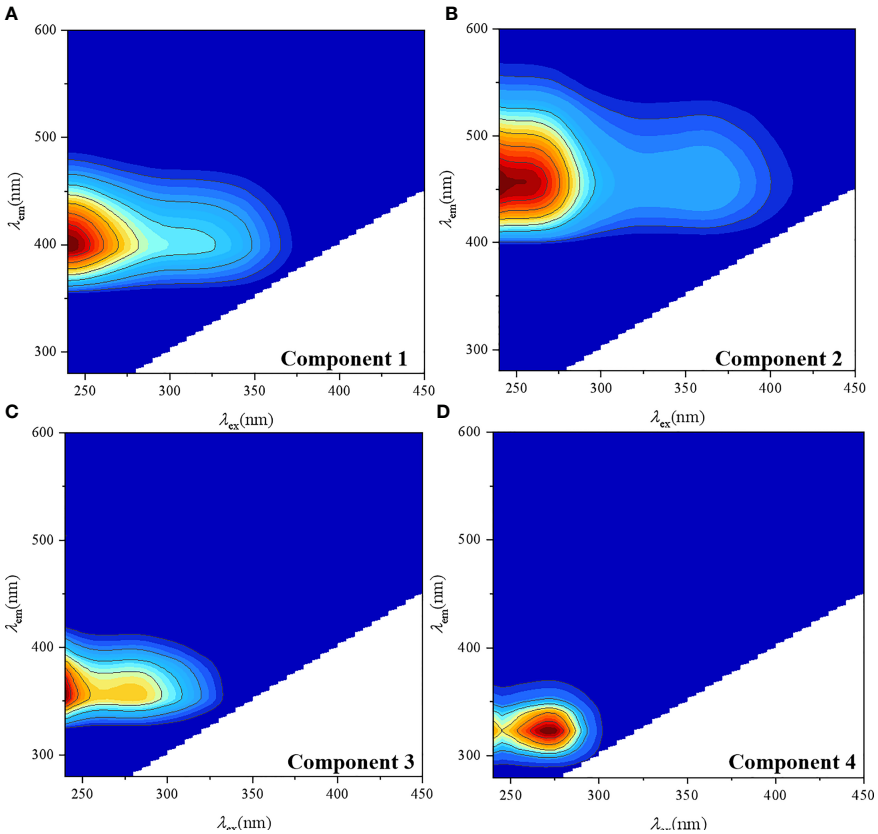

FIGURE 4 | Fluorescence components identified of C1 **(A)**, C2 **(B)**, C3 **(C)** and C4 **(D)** by the PARAFAC modeling in Zhanjiang Bay.

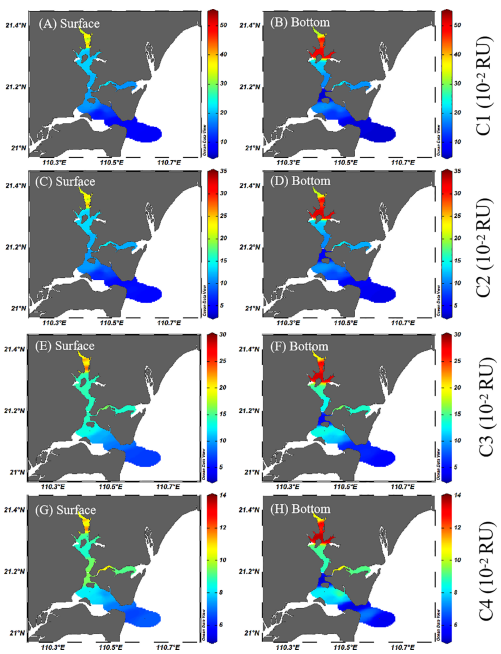

FIGURE 5 | Spatial distributions of fluorescence components C1 **(A, B)**, C2 **(C, D)**, C3 **(E, F)** and C4 **(G, H)** in the surface and bottom water of Zhanjiang Bay during the sampling period.

4 DISCUSSION

4.1 Sources and Characteristics of Dissolved Organic Matter in Zhanjiang Bay

Stable carbon isotope ($\delta^{13}C$) was an indicator of the source of organic matter. Algae utilized DIC as a substrate during photosynthesis and distinguished ^{12}C and ^{13}C with a kinetic classification of 20‰–21‰ (Chanton and Lewis, 1999; Hoffman and Bronk, 2006). In general, marine phytoplankton utilized HCO_3^- ($\delta^{13}C = 0‰$) in water for photosynthesis, while terrestrial plants used atmospheric CO_2 ($\delta^{13}C = -8‰$); thus, aquatic microorganisms tended to have heavier $\delta^{13}C$ values (Bouillon et al., 2011; Remeikaitė-Nikienė;, 2017). The $\delta^{13}C$ values of marine phytoplankton were relatively high, ranging from −23‰ to −16‰, while those of freshwater phytoplankton were low, ranging from −33‰ to −25‰ (Wang et al., 2004; Hoffman and Bronk, 2006; Bianchi, 2011; Yang et al., 2014). The variation of DIC stable carbon isotope ($\delta^{13}C_{DIC}$) in summer ranged from −4.9‰ to 0.32‰, displaying an increasing tendency from the upper bay to the outer bay (**Figure 3**). Assuming the fractionation of algae production was −21‰, the $\delta^{13}C$ of organic matter from Zhanjiang Bay in this study ranged from −25.9‰ to −20.68‰, with the mixture of terrigenous (higher plant debris, soil input) and authigenic (phytoplankton input, microbial input) characteristics. There were significant differences in $\delta^{13}C_{DIC}$

among the stations, meaning that the source of organic matter may be obviously different. The $\delta^{13}C_{DIC}$ increased from the upper bay to the outer bay as a whole; the contribution of terrigenous input gradually decreased from the estuary of the Suixi River to the bay mouth. Among them, the Suixi River, as the largest source of freshwater input to Zhanjiang Bay, inputted a large amount of land-based materials such as higher plant debris and soil humus into Zhanjiang Bay. In the location of stations S1 and S2 closest to the estuary of the Suixi River, the $\delta^{13}C_{DIC}$ was relatively low (−4.9‰ to −3.8‰), and the kinetic fractionation of $\delta^{13}C$ was −25.9‰ to −24.8‰, which was closer to freshwater phytoplankton ($\delta^{13}C$ = −33‰ to −25‰) and soil humus ($\delta^{13}C$ = −25‰ to −22‰) (Kendall, 1998; Chanton and Lewis, 1999; Zhang et al., 2018). The $\delta^{13}C_{DIC}$ in bay mouth ranged from 0‰ to 0.5‰, which belonged to the range of marine algae, indicating that phytoplankton contributed to the organic matter (Bouillon et al., 2011; Remeikaitė-Nikienė, 2017).

Generally speaking, phytoplankton absorbed ^{12}C preferentially during photosynthesis, resulting in relatively enriched ^{13}C in water (Bouillon et al., 2011). Therefore, phytoplankton photosynthesis in surface water was more intense than in bottom water, and $\delta^{13}C$ was relatively positive (Hoffman and Bronk, 2006). However, for some stations (S3–S6) in Zhanjiang Bay, the $\delta^{13}C_{DIC}$ of surface water was significantly lower than that of bottom water, which indicated that abiotic processes were more strongly affecting these regions. As this region was near the sewage outlet of Zhanjiang Bay (Zhang et al., 2021), the difference between surface and bottom water may be affected by sewage discharge, and the kinetic fractionation of $\delta^{13}C$ in surface water was in the range of sewage ($\delta^{13}C$ = −26‰ to −22‰). The C3 component, which was attributed to protein-like fluorescence (Coble, 1996; Ye et al., 2019), also had strong fluorescence intensity in this region at the same time. Furthermore, in abiotic sources of DOM, there was a considerable amount of DOM in surface sediments at times, which may be diffused into the water with the concentration gradient and had a significant impact on the properties of organic matter in the sea (Burdige and Komada, 2015). The $\delta^{13}C_{DIC}$ values in this region ranged from −4.9‰ to −3.6‰, and the values of $\delta^{13}C$ dynamic fractionation ranged from −25.9‰ to −24.6‰, which were consistent with the previously reported $\delta^{13}C$ range of surface sediments in Zhanjiang Bay (Zhou et al., 2021). However, this region had narrow terrain and relatively closed and poor hydrodynamic conditions (Li, 2012; Shi et al., 2015). Moreover, the salinity difference of these stations was relatively small, and the stirring effect of the salt wedge on sediment should be small, so it did not have the dynamic conditions to cause sediment resuspension. In addition, the bay mouth, which was more susceptible to tidal oscillation and had strong hydrodynamic conditions, did not show this characteristic; thus, the possibility of sediment resuspension could be ruled out.

HCA was performed using optical indexes (FI, BIX, and HIX) and fluorescent components (C1 to C4) to explore the source and characteristic similarity or difference of DOM for Zhanjiang Bay (**Figure 6**). The Ward clustering method of Euclidean distance was selected to generate the tree graph of the samples, and the relationship among the 7 indicators was discussed by the Ward clustering method of Pearson's correlation coefficient. The data set was standardized before performing HCA, avoiding errors caused by the range of values and units of the original variables.

The 7 indicators fall into three categories. Cluster I had C1, C2, C3, C4, and HIX, all of which included microbial origin, phytoplanktonic origin, and terrestrial origin, representing the mixed sources of organic matter. Cluster II was the BIX, representing the primary source of DOM, which usually means a large input of fresh antigenic organic matter with a high index (Huguet et al., 2009). Cluster III was composed of the FI, which reflected the relative contribution rate of aromatic amino acids and non-aromatic substances to DOM fluorescence intensity, so it could be used as an indicator of the source of substances and the degradation degree of DOM (Chin et al., 1994; McKnight, et al., 2001; Mladenov et al., 2007). DOM was derived from the biological activity and sediment release when the FI was high, and sewage discharge may also be its source (McKnight, et al., 2001; Dong and Rosario-Ortiz, 2012; Ye et al., 2019).

In HCA results, the 34 water samples were distinctly divided into three clusters according to their variations of optical indexes and fluorescent components (**Figure 6**). Among them, 8 water samples were clustered into the red cluster with a higher value of indicators of cluster I, 19 water samples were clustered into the blue cluster with indicators of cluster II exhibiting a higher value, and 7 water samples were clustered in the green cluster with higher value of indicators of cluster III. The red clustering data, accompanying higher values of indicators for cluster I, were mainly concentrated in the upper bay (S1–S5), where the C1 component representing the microbial source, the C2 component representing the terrestrial source, and the C4 component representing phytoplanktonic source all had high fluorescence intensity (**Figure 6**). Thus, there was a typically mixed source in the red cluster. In addition, the red cluster had the characteristics of high HIX and low BIX, indicating that the region was affected

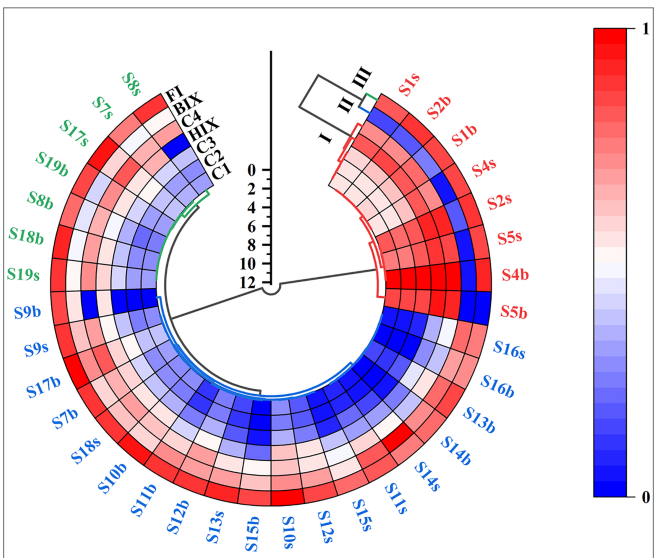

FIGURE 6 | A dendrogram with heatmap of DOM fluorescent components and optical indexes at each sampling site in Zhanjiang Bay. DOM, dissolved organic matter.

by terrestrial freshwater input and had more terrigenous humus. The high $\delta^{13}C_{DIC}$ in the region also supported this view.

BIX of cluster II could be used as an indicator of DOM traceability in water (Chiu et al., 2019), where high values (>0.8) corresponded to DOM of *in situin-situ* origin, while low BIX (<0.8) indicated allochthonous origin (Catalán, 2014). In this study, the blue clustering stations (S9–S16) were mainly concentrated in the southern bay, and the water samples of BIX between 1.1 and 1.19 were mainly distributed here (**Figure S1**), implying the that highest-value area of BIX was concentrated in the southern bay. These indicated that the input of a large amount of fresh autogenous organic matter made the newly generated DOM into the southern bay, especially protein-like DOM, and had a high proportion in the overall DOM (Huguet et al., 2009). Compared with the red cluster, the fluorescence intensity of C1, C2, and C3 components in the blue cluster was lower, and the HIX was lower at the same time, which means that the terrestrial input was weakened in this region. Moreover, the decreasing trend of C1, C2, and C3 components from the upper bay to the outer bay also confirmed that (**Figure 5**). In the meantime, higher C4 component and BIX showed a significant role in algal activity in the southern bay, explaining that phytoplankton growth had an important impact on the southern bay. On the whole, although the southern bay was part of the semi-closed bay, its organic matter sources were more marine than terrestrial and displayed a characteristic of the high BIX and low HIX, which tended to be marine water (Huguet et al., 2009).

FI usually had multiple meanings, including that organic matter may be derived from biological activities, sediment release, or sewage discharge (Chin et al., 1994; McKnigh, et al., 2001; Dong and Rosario-Ortiz, 2012). The green clustering data were mainly concentrated on the Nansan islands, where the area was narrow and the water depth was less than 5 m on the whole (**Figure 1**), which means that the weak turbulence mixing did not have the dynamic conditions to cause sediment resuspension, so the release of sediment may not be the cause of high FI. The FI in the green cluster showed a decreasing trend from west to east (**Figure S1**), indicating that the source of the high FI may be at station S17. The lowest salinity at station S17 indicated that freshwater should be coming into a bay here (**Figure 2**), but there were no rivers in the area; thus, the effects of the river could be excluded. A large number of artificially reclaimed fishponds were distributed on both sides of the green clustering stations, and aquaculture sewage would be discharged from time to time, which seemed to explain the freshwater input. Moreover, the FI in this area ranged from 2.00 to 2.10, with an average of 2.04 ± 0.04, exceeding the range limit of ordinary natural water, which could be from sewage possibly (Dong and Rosario-Ortiz, 2012; Ye et al., 2019). Combined with the high value of Chl-*a* in this area, it was possible that the FI of green clustering was influenced by sewage input and phytoplankton. In addition, although the C4 component representing protein-like organic matter had a high value in the green cluster and was close to the bay mouth, the phytoplankton growth activity here may be promoted by the high concentration of nutrients brought by sewage instead of by the offshore input, so the maximum value of Chl-*a* corresponded to the lowest value of salinity. Thus, the green cluster also embodied the dominance of freshwater.

4.2 Interactions Between Fluorescence Parameters of Dissolved Organic Matter and Environmental Variables

RDA was conducted to explain the combined correlation and impacted between response variables (PARAFAC composition and optical index) and environmental variables (water quality index)(**Figure 7**). In the RDA diagram, the length of the arrow indicated the importance of the factor, and the angle or coordinate axis between the arrow and another arrow indicated the correlation between them (Ouyang et al., 2018). When the angle was smaller, the relationship was stronger. The DOM of the red clustering site and green clustering site may be caused by mixed sources and sewage, respectively; that these areas were affected by human activities was relatively obvious. Therefore, the two clustering data were merged for analysis in RDA, summarized as the northern bay and the blue clustering site for the southern bay, to enhance the credibility of the results. RDA determined the relationship between DOM fluorescence parameters and water quality parameters through Canoco5.0 software. Log(x + 1) conversion was performed on the original optical parameters and water quality parameters before RDA so that these parameters were normally distributed (Ramette, 2007).

In general, freshwater inputs from the land were rich in organic matter and served as important sources of DOM in estuaries. The salinity in the northern and southern bays was

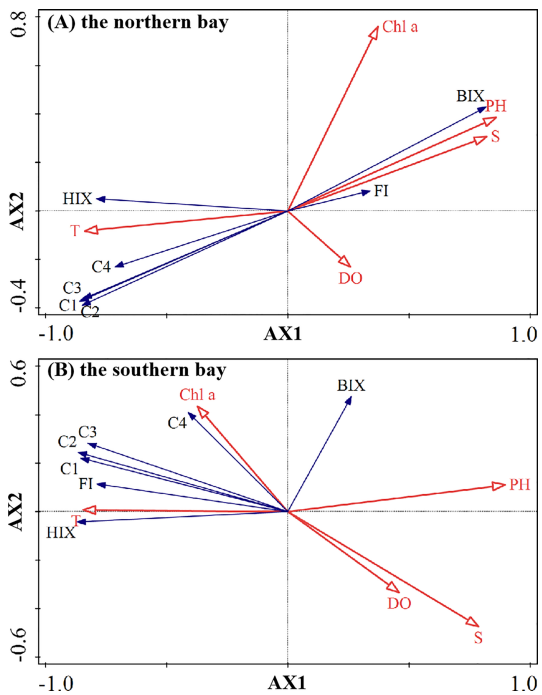

FIGURE 7 | The plots based on redundancy analysis in Zhanjiang Bay (the solid arrows with blue fonts are the response variables, and the hollow arrows with red fonts are the environmental variables).

opposite to the direction of the arrow of the four fluorescent components, and the included angle of the extension line was small, indicating that terrigenous input served as the important source of Zhanjiang Bay. Among them, the angle between C1–C4 fluorescence components and reverse extension line of salinity in the southern bay was slightly larger than that in the northern bay, signifying that the terrigenous input had weakened in the southern bay. Compared with the upper bay, the fluorescence intensity of C1–C4 components in the bay mouth decreased by 80%, 79%, 69%, and 42%, respectively, on average, further indicating that terrigenous organic matter was greatly diluted from the bay mouth and the concentration of organic matter decreased significantly. Terrigenous DOM in Zhanjiang Bay had limited influence on the outside bay, which may be due to the fact that Zhanjiang Bay served as a typical semi-closed bay with a narrow bay mouth of only 2 km, where only a small amount of water could flow out of the bay to participate in water exchange each time (Shi et al., 2015), or it may also be affected by seawater intrusion.

The pH value of seawater was mainly controlled by the dissociation equilibrium of dissolved inorganic carbonate (Zeebe and Wolf-Gladrow, 2001), so any action which could change the dissolution equilibrium of inorganic carbonate also was able to further affectting the pH value of seawater. In theory, many processes were equipped to affect the relative concentration of carbonate in seawater systems, such as temperature, hydrostatic pressure, salinity, and consumption by life activities, as well as to change the pH value of seawater ulteriorly (Zeebe and Wolf-Gladrow, 2001). The pH of the northern bay was in the same direction as the arrow of salinity, and the angle between pH and salinity was less than 20°, existing as a strong positive correlation; that is, the change of pH was affected by salinity. The pH value of the northern bay increased with the increase of the salinity of the mixed water, showing a trend of moving from the upper bay to the outer bay. They were strongly correlated and presented a conservative mixing condition, which means that the mechanical mixing of water played a leading role in the changing trend of pH in the northern bay. In the southern bay, the pH was in the same direction as the arrow of salinity, and the included angle with salinity was greater than 60°, which means that the positive correlation between pH and salinity was not as strong as that in the northern bay, and mechanical mixing of water may not play a leading role in the changing trend of pH in the southern bay. Moreover, the angle between pH, HIX, and reverse extension line of temperature was small, which signified that humus organic matter and temperature may have an important influence on pH change.

The direction of Chl-*a* and BIX in the northern bay was the same as that of the arrow of salinity but opposite to that of the arrow of each fluorescence component. The included angle between BIX and salinity was small, and the occurrence of high Chl-*a* values at sites with high salinity also indicated this, which seemed to signify that seawater had a relatively important influence on the input of fresh antigenic organic matter. In fact, the correlation was more likely due to sewage discharge in the green cluster. The angle between the BIX and salinity arrow was 90° nearly in the southern bay, and the BIX showed the characteristics of neither marine sources nor terrigenous sources, which may be due to two reasons. On the one hand, the contribution of freshwater to nutrients in Zhanjiang Bay (about 54%–90%) was much higher than that in the seawater (about 18%–45%) in summer (unpublished data from our previous survey). However, freshwater from rivers accounts for only a small proportion in summer, about 7% (unpublished data from our previous survey). When the salinity of seawater increased, the terrigenous signal was weakened by the dilution of seawater. As the result, the influence of terrigenous organic matter in the southern bay could not be as strong as that in the northern bay. On the other hand, as the salinity of seawater increased, the autogenous contribution of phytoplankton in the ocean gradually became dominant (Seidel et al., 2014; Medeiros et al., 2015), at which time organic matters may show characteristics of the high BIX and low HIX (Huguet et al., 2009; Milbrandt et al., 2010). Therefore, with the weakening of terrestrial organic matter and the enhancement of marine organic matter, the BIX of the southern bay may be affected by the organic matter at both ends.

4.3 Weak Turbulent Mixing of Dissolved Organic Matter in Semi-Closed Bay

Influenced by freshwater input, the DOM of Zhanjiang Bay displayed a decreasing trend from the upper bay to the outer bay on the whole. However, the organic matter in the bay displayed different characteristics, and the correlation between organic matter with different characteristics and environmental parameters was also different. This phenomenon may be caused by the fact that Zhanjiang Bay was a typical semi-closed bay with weak turbulent mixing.

Meanwhile, with the tidal driving effect, seawater as the medium could effectively transport the terrigenous matter from the estuary to the outer bay at low tide (Lin et al., 2019; Iglesias et al., 2020). The northern part of Zhanjiang Bay had a long and narrow terrain, while the southern part had a small bay mouth and a large stomach. Coupled with the influence of summer monsoon easterly winds, the turbulent mixing was weak, while the semi-exchange time of water in the northern bay was more than 100 days, and that in the southern bay was 30 days (Li, 2012). Thus, the tide may not dilute and replace the water in the northern bay in time. Terrigenous organic matter was mainly trapped in the northern narrow sea area and had limited influence on the southern bay. Most of the marine source features in the southern bay came from algae, which may be produced *in situ* by seawater inside the bay, brought in by seawater outside the bay during high tide, or both.

As a general rule, more and more terrestrial DOM is being imported from the river into the estuary and then into the ocean, with the increase of anthropogenic activities (Hudson et al., 2007; Guo et al., 2014). However, the weak turbulent mixing of semi-closed bay may not be effective in facilitating the dispersal of terrigenous material all the time, even during the summer when river flows were at their greatest. In seasons or years with less rainfall, changes in organic matter characteristics of semi-closed bays and their response to the marine environment are worthy of our continued attention in future research.

5 CONCLUSION

By measuring $\delta^{13}C$ of DIC and fluorescent components of DOM, the distribution and characteristics of DOM in Zhanjiang Bay were discussed. The following conclusions were drawn based on the results presented in this study: 1) there were several organic matter sources in Zhanjiang Bay, including river input, algae input, and sewage input, but freshwater inputs serve as an important source of DOM on the whole. Among them, the DOM in the bay displayed two characteristics in different parts. The DOM in the northern bay was composed of terrigenous organic matter mainly with high humus, while that in the southern bay was more inclined to marine sources with high BIX and low HIX. 2) The correlation between DOM with different characteristics and environmental parameters was also different. On the one hand, the salinity, pH, and Chl-*a* in the northern bay were correlated with DOM strongly, indicating that freshwater input had a profound impact on the relationship between organic matter and the environment. On the other hand, the correlation in the southern bay was weakened or even disappeared, meaning that with decreased freshwater input, DOM had changed from being dominated by freshwater input to being affected by the joint action of terrace and ocean. 3) The discrepancy between bays may be caused by the weak turbulent mixing in the semi-closed bay, where terrigenous organic matter was mostly trapped in the northern bay because of the narrow terrain, causing the southern bay to be affected by terrigenous and marine organic matter.

DATA AVAILABILITY STATEMENT

The raw data supporting the conclusions of this article will be made available by the authors, without undue reservation.

AUTHOR CONTRIBUTIONS

YZ, HZ, and CW conceived of the presented idea. HZ and CW performed the analysis of the manuscript. YZ processed the data, drafted the manuscript, and designed the figures. GP was involved in planning and supervising the funding of this work. All authors listed made a substantial, direct, and intellectual contribution to the work and approved it for publication.

FUNDING

The present research is supported by the National Natural Science Foundation of China (No. 42076162), Natural Science Foundation of Guangdong Province, China (No. 2020A1515010496), Postgraduate Education Innovation Project of Guangdong Ocean University (202145), and a project supported by Innovation Group Project of Southern Marine Science and Engineering Guangdong Laboratory (Zhuhai) (No. 311020004).

SUPPLEMENTARY MATERIAL

The Supplementary Material for this article can be found online at: https://www.frontiersin.org/articles/10.3389/fmars.2022.956930/full#supplementary-material

REFERENCES

Amaral, V., Romera-Castillo, C. and Forja, J. (2020). Dissolved Organic Matter in the Gulf of Cádiz: Distribution and Drivers of Chromophoric and Fluorescent Properties. *Front. Mar. Sci.* 7, 126. doi: 10.3389/fmars.2020.00126

Andrews, J. E., Greenaway, A. M. and Dennis, P. F. (1998). Combined Carbon Isotope and C/N Ratios as Indicators of Source and Fate of Organic Matter in a Poorly Flushed, Tropical Estuary: Hunts Bay, Kingston Harbour, Jamaica. *Estuarine. Coast. Shelf. Sci.* 46 (5), 743–756. doi: 10.1006/ecss.1997.0305

Beer, S., Björk, M. and Beardall, J. (2014). *Photosynthesis in the Marine Environment* New Jersey: Wiley-Blackwell.

Bianchi, T. S. (2007). *Biogeochemistry of Estuaries, Oxford:* Oxford University Press.

Bianchi, T. S. (2011). The Role of Terrestrially Derived Organic Carbon in the Coastal Ocean: A Changing Paradigm and the Priming Effect. *Proc. Natl. Acad. Sci. U.S.A.* 108 (49), 19473–19481. doi: 10.1073/pnas.1017982108

Boesch, D. F. (2002). Challenges and Opportunities for Science in Reducing Nutrient Over-Enrichment of Coastal Ecosystems. *Estuaries* 25 (4), 886–900. doi: 10.1007/BF02804914

Bouillon, S., Connolly, R. M. and Gillikin, D. P. (2011). 7.07 Use of Stable Isotopes to Understand Food Webs and Ecosystem Functioning in Estuaries. *Treatise. Estuar. Coast. Sci.* 7 (13-14):143-173. doi: 10.1016/B978-0-12-374711-2.00711-7

Burdige, D. J. and Komada, T. (2015). "Sediment Pore Waters," in *Biogeochemistry of Marine Dissolved Organic Matter*: Academic Press.

Cabral, H., Fonseca, V., Sousa, T. and Costa Leal, M. (2019). Synergistic Effects of Climate Change and Marine Pollution: An Overlooked Interaction in Coastal and Estuarine Areas. *Int. J. Environ. Res. Public Health* 16 (15), 2737. doi: 10.3390/ijerph16152737

Canuel, E. A., Cammer, S. S., McIntosh, H. A. and Pondell, C. R. (2012). Climate Change Impacts on the Organic Carbon Cycle at the Land-Ocean Interface. *Annu. Rev. Earth Planet. Sci.* 40(685), 2012. doi: 10.1146/annurev-earth-042711-105511

Carlson, C. A. and Hansell, D. A. (2015). DOM Sources, Sinks, Reactivity, and Budgets. *Biogeochem. Mar. Dissolved Org. Matter*, 65-126. doi: 10.1016/B978-0-12-405940-5.00003-0

Catalán, Núria, Biel Obrador, and Joan Ll Pretus, (2014). "Ecosystem processes drive dissolved organic matter quality in a highly dynamic water body." *Hydrobiologia* 728(1) 111-124. doi: 10.1007/S10750-014-1811-Y

Chanton, J. P. and Lewis, F. G. (1999). Plankton and Dissolved Inorganic Carbon Isotopic Composition in a River-Dominated Estuary: Apalachicola Bay, Florida. *Estuaries* 22 (3), 575–583. doi: 10.2307/1353045

Chen, N., Krom, M. D., Wu, Y., Yu, D. and Hong, H. (2018). Storm Induced Estuarine Turbidity Maxima and Controls on Nutrient Fluxes Across River-Estuary-Coast Continuum. *Sci. Total. Environ.* 628, 1108–1120. doi: 10.1016/j.scitotenv.2018.02.060

Chin, Y. P., Aiken, G. and O'Loughlin, E. (1994). Molecular Weight, Polydispersity, and Spectroscopic Properties of Aquatic Humic Substances. *Environ. Sci. Technol.* 28 (11), 1853–1858. doi: 10.1021/es00060a015

Chiu, T. P., Huang, W. S., Chen, T. C., and Yeh, Y. L. (2019). Fluorescence Characteristics of Dissolved Organic Matter (DOM) in Percolation Water and Lateral Seepage Affected by Soil Solution (SS) In A Lysimeter Test. Sensors, 19(18), 4016. doi: 10.3390/s19184016

Coble, P. G. (1996). Characterization of Marine and Terrestrial DOM in Seawater Using Excitation-Emission Matrix Spectroscopy. *Mar. Chem.* 51 (4), 325–346. doi: 10.1016/0304-4203(95)00062-3

Coble, P. G., Lead, J., Baker, A., Reynolds, D. M. and Spencer, R. G. (Eds.)(2014). *Aquatic Organic Matter Fluorescence*. (Cambridge University Press).

Dong, M. M. and Rosario-Ortiz, F. L. (2012). Photochemical Formation of Hydroxyl Radical From Effluent Organic Matter. *Environ. Sci. Technol.* 46 (7), 3788–3794. doi: 10.1021/es2043454

Felgate, S. L., Barry, C. D., Mayor, D. J., Sanders, R., Carrias, A., Young, A., et al. (2021). Conversion of Forest to Agriculture Increases Colored Dissolved Organic Matter in a Subtropical Catchment and Adjacent Coastal Environment. *J. Geophys. Res.: Biogeosci.* 126 (6), e2021JG006295. doi: 10.1029/2021JG006295

García-Martín, E. E., Sanders, R., Evans, C. D., Kitidis, V., Lapworth, D. J., Rees, A. P., et al. (2021). Contrasting Estuarine Processing of Dissolved Organic Matter Derived From Natural and Human-Impacted Landscapes. *Global Biogeochem. Cycles* 35 (10), e2021GB007023. doi: 10.1029/2021GB007023

Gireeshkumar, T. R., Deepulal, P. M. and Chandramohanakumar, N. (2013). Distribution and Sources of Sedimentary Organic Matter in a Tropical Estuary, South West Coast of India (Cochin Estuary): A Baseline Study. *Mar. pollut. Bull.* 66 (1-2), 239–245. doi: 10.1016/j.marpolbul.2012.10.002

Guo, W., Yang, L., Zhai, W., Chen, W., Osburn, C. L., Huang, X., et al. (2014). Runoff-Mediated Seasonal Oscillation in the Dynamics of Dissolved Organic Matter in Different Branches of a Large Bifurcated Estuary—The Changjiang Estuary. *J. Geophys. Res.: Biogeosci.* 119 (5), 776–793. doi: 10.1002/2013JG002540

He, W., Chen, M., Schlautman, M. A. and Hur, J. (2016). Dynamic Exchanges Between DOM and POM Pools in Coastal and Inland Aquatic Ecosystems: A Review. *Sci. Total. Environ.* 551, 415–428. doi: 10.1016/j.scitotenv.2016.02.031

Hoffman, J. C. and Bronk, D. A. (2006). Interannual Variation in Stable Carbon and Nitrogen Isotope Biogeochemistry of the Mattaponi River, Virginia. *Limnol. Oceanogr.* 51 (5), 2319–2332. doi: 10.4319/lo.2006.51.5.2319

Hudson, N., Baker, A. and Reynolds, D. (2007). Fluorescence Analysis of Dissolved Organic Matter in Natural, Waste and Polluted Waters—a Review. *River. Res. Appl.* 23 (6), 631–649. doi: 10.1002/rra.1005

Huguet, A., Vacher, L., Relexans, S., Saubusse, S., Froidefond, J. M. and Parlanti, E. (2009). Properties of Fluorescent Dissolved Organic Matter in the Gironde Estuary. *Org. Geochem.* 40 (6), 706–719. doi: 10.1016/j.orggeochem.2009.03.002

Iglesias, I., Almeida, C. M. R., Teixeira, C., Mucha, A. P., Magalhães, A., Bio, A., et al. (2020). Linking Contaminant Distribution to Hydrodynamic Patterns in an Urban Estuary: The Douro Estuary Test Case. *Sci. Total. Environ.* 707, 135792. doi: 10.1016/j.scitotenv.2019.135792

Jørgensen, L., Stedmon, C. A., Kragh, T., Markager, S., Middelboe, M. and Søndergaard, M. (2011). Global Trends in the Fluorescence Characteristics and Distribution of Marine Dissolved Organic Matter. *Mar. Chem.* 126 (1-4), 139–148. doi: 10.1016/j.marchem.2011.05.002

Kendall, C. (1998). "Tracing Nitrogen Sources and Cycling in Catchments," in *Isotope Tracers in Catchment Hydrology Amsterdam:* Elsevier, 519–576.

Kerr, R. A. (2011). Humans are Driving Extreme Weather; Time to Prepare. *Science* 334 (6059), 1040. doi: 10.1126/science.334.6059.1040

Kinsey, J. D., Corradino, G., Ziervogel, K., Schnetzer, A., Osburn, C. (2018). Formation of Chromophoric Dissolved Organic Matter by Bacterial Degradation of Phytoplankton-Derived Aggregates. *Front. Mar. Sci.* 4, 430. doi: 10.3389/fmars.2017.00430

Lee, S. A., Kim, T. H. and Kim, G. (2020). Tracing Terrestrial Versus Marine Sources of Dissolved Organic Carbon in a Coastal Bay Using Stable Carbon Isotopes. *Biogeosciences* 17 (1), 135–144. doi: 10.5194/bg-17-135-2020

Li, X. ,. (2012). Numerical Study on the Water Exchange of a Semi-Closed Bay. *Mar. Sci. Bull.* 31 (03), 248–254.

Lin, Y., Li, Y., Zheng, B., Yin, X., Wang, L., He, J., et al. (2019). Evolution of Sedimentary Organic Matter in a Small River Estuary After the Typhoon Process: A Case Study of Quanzhou Bay. *Sci. Total. Environ.* 686, 290–300. doi: 10.1016/j.scitotenv.2019.05.452

Lloret, E., Dessert, C., Buss, H. L., Chaduteau, C., Huon, S., Alberic, P., et al. (2016). Sources of Dissolved Organic Carbon in Small Volcanic Mountainous Tropical Rivers, Examples From Guadeloupe (French West Indies). *Geoderma* 282, 129–138. doi: 10.1016/j.geoderma.2016.07.014

Lorenzen, C. J. and Jeffrey, S. W. (1980). Determination of Chlorophyll in Seawater. *Unesco. tech. pap. Mar. Sci.* 35 (1), 1–20. doi: 10.1556/Nano.2008.00001

McKnight, D. M., Boyer, E. W., Westerhoff, P. K., Doran, P. T., Kulbe, T. and Andersen, D. T. (2001). Spectrofluorometric Characterization of Dissolved Organic Matter for Indication of Precursor Organic Material and Aromaticity. *Limnol. Oceanogr.* 46 (1), 38–48. doi: 10.4319/lo.2001.46.1.0038

Medeiros, P. M., Seidel, M., Ward, N. D., Carpenter, E. J., Gomes, H. R., Niggemann, J., et al. (2015). Fate of the Amazon River Dissolved Organic Matter in the Tropical Atlantic Ocean. *Global Biogeochem. Cycles* 29 (5), 677–690. doi: 10.1002/2015GB005115

Milbrandt, E. C., Coble, P. G., Conmy, R. N., Martignette, A. J. and Siwicke, J. J. (2010). Evidence for the Production of Marine Fluorescent Dissolved Organic Matter in Coastal Environments and a Possible Mechanism for Formation and Dispersion. *Limnol. Oceanogr.* 55 (5), 2037–2051. doi: 10.4319/lo.2010.55.5.2037

Mladenov, N., McKnight, D. M., Macko, S. A., Norris, M., Cory, R. M. and Ramberg, L. (2007). Chemical Characterization of DOM in Channels of a Seasonal Wetland. *Aquat. Sci.* 69 (4), 456–471. doi: 10.1007/s00027-007-0905-2

Montgomery, H., Thom, N. S. and Cockburn, A. (1964). Determination of Dissolved Oxygen by the Winkler Method and the Solubility of Oxygen in Pure Water and Sea Water. *J. Appl. Chem.* 14 (7). 280-296 doi: 10.1002/jctb.5010140704

Murphy, K. R., Stedmon, C. A., Waite, T. D. and Ruiz, G. M. (2008). Distinguishing Between Terrestrial and Autochthonous Organic Matter Sources in Marine Environments Using Fluorescence Spectroscopy. *Mar. Chem.* 108 (1-2), 40–58. doi: 10.1016/j.marchem.2007.10.003

Najjar, R. G., Pyke, C. R., Adams, M. B., Breitburg, D., Hershner, C., Kemp, M., et al. (2010). Potential Climate-Change Impacts on the Chesapeake Bay. *Estuarine. Coast. Shelf. Sci.* 86 (1), 1–20. doi: 10.1016/j.ecss.2009.09.026

Ouyang, W., Yang, W., Tysklind, M., Xu, Y., Lin, C., Gao, X., et al. (2018). Using River Sediments to Analyze the Driving Force Difference for non-Point Source Pollution Dynamics Between Two Scales of Watersheds. *Water Res.* 139, 311–320. doi: 10.1016/j.watres.2018.04.020

Ramette, A. (2007). Multivariate Analyses in Microbial Ecology. *FEMS Microbiol. Ecol.* 62 (2), 142–160. doi: 10.1111/j.1574-6941.2007.00375.x

Remeikaitė-Nikienė;, N. (2017). *Distribution of Organic Matter and Metals in the South-Eastern Baltic Sea (Lithuanian Zone) Lithuania:* (Doctoral dissertation, Vilniaus universitetas).

Seidel, M., Beck, M., Riedel, T., Waska, H., Suryaputra, I. G., Schnetger, B., et al. (2014). Biogeochemistry of Dissolved Organic Matter in an Anoxic Intertidal Creek Bank. *Geochim. Cosmochim. Acta* 140, 418–434. doi: 10.1016/j.gca.2014.05.038

Shi, Y., Zhang, Y. and Sun, X. (2015). Spatiotemporal Distribution of Eutrophication and Its Relationship With Environmental Factors in Zhanjiang Sea Bay Area. *Environ. Sci. Technol.* 38 (12), 90–96+122. doi: CNKI:SUN:FJKS.0.2015-12-017

Spilling, K., Olli, K., Lehtoranta, J., Kremp, A., Tedesco, L., Tamelander, T., et al. (2018). Shifting Diatom—Dinoflagellate Dominance During Spring Bloom in the Baltic Sea and its Potential Effects on Biogeochemical Cycling. *Front. Mar. Sci.* 5, 327. doi: 10.3389/fmars.2018.00327

Stedmon, C. A. and Bro, R. (2008). Characterizing Dissolved Organic Matter Fluorescence With Parallel Factor Analysis: A Tutorial. *Limnol. Oceanogr.: Methods* 6 (11), 572–579. doi: 10.4319/lom.2008.6.572

Stedmon, C. A., Markager, S. and Bro, R. (2003). Tracing Dissolved Organic Matter in Aquatic Environments Using a New Approach to Fluorescence Spectroscopy. *Mar. Chem.* 82 (3-4), 239–254. doi: 10.1016/S0304-4203(03)00072-0

Wang, X. C., Chen, R. F., and Gardner, G. B. (2004). Sources and Transport of Dissolved and Particulate Organic Carbon in the Mississippi River Estuary and Adjacent Coastal Waters of the Northern Gulf of Mexico. *Mar. Chem.* 89(1-4), 241-256. doi: 10.1016/j.marchem.2004.02.014

Xue, Y., Zhang, Z. M., Zhang, R. R., Li, Y. Q., Sun, A. L., Shi, X. Z., et al. (2021). Aquaculture-Derived Distribution, Partitioning, Migration, and Transformation of Atrazine and its Metabolites in Seawater, Sediment, and Organisms From a Typical Semi-Closed Mariculture Bay. *Environ. pollut.* 271, 116362. doi: 10.1016/j.envpol.2020.116362

Ya, C., Anderson, W. and Jaffé, R. (2015). Assessing Dissolved Organic Matter Dynamics and Source Strengths in a Subtropical Estuary: Application of Stable Carbon Isotopes and Optical Properties. *Cont. Shelf. Res.* 92, 98–107. doi: 10.1016/j.csr.2014.10.005

Yang, J., Gao, J., Liu, B., and Zhang, W. (2014). Sediment deposits and organic carbon sequestration along mangrove coasts of the Leizhou Peninsula, Southern China. Estuarine, *Coastal Shelf Sci.* 136, 3-10. doi: 10.1016/j.ecss.2013.11.020

Ye, Q., Zhang, Z. T., Liu, Y. C., Wang, Y. H., Zhang, S., He, C., et al. (2019). Spectroscopic and Molecular-Level Characteristics of Dissolved Organic Matter in a Highly Polluted Urban River in South China. *ACS Earth Space. Chem.* 3 (9), 2033–2044. doi: 10.1021/acsearthspacechem.9b00151

Yu, G., Fu, D., Zhong, Y. and Luo, Y. (2021). Optical Characteristics of Colored Dissolved Organic Matter in Zhanjiang Bay and Its Adjacent Sea Areas. *J. Guangdong Ocean. Univ.* 41 (01), 55–62. doi: 10.3969/j.issn.1673-9159.2021.01.008

Yu, G., Liao, S., Fu, D. and Li, X. (2017). Remote Sensing Retrieval of Colored Dissolved Organic Matter in Zhanjiang Coastal Area. *J. Guangdong Ocean. Univ.* 37 (04), 123–127. doi: 10.3969/j.issn.1673-9159.2017.04.019

Zeebe, R. E. and Wolf-Gladrow, D. (2001). *CO_2 in Seawater: Equilibrium, Kinetics, Isotopes, Amsterdam:* Elsevier.

Zhang, J., Wei, L., Lai, Y., Dai, P., Chen, Y. and Zhang, J. (2021). Concentration, Composition and Fluxes of Land-Based Nitrogen and Phosphorus Source Pollutants Input Into Zhanjiang Bay in Summer. *J. Guangdong Ocean. Univ.* 39 (4), 63–72. doi: 10.3969/j.issn.1673-9159.2019.04.010

Zhang, M., Zhi, Y., Shi, J. and Wu, L. (2018). Apportionment and Uncertainty Analysis of Nitrate Sources Based on the Dual Isotope Approach and a Bayesian Isotope Mixing Model at the Watershed Scale. *Sci. Total. Environ.* 639, 1175–1187. doi: 10.1016/j.scitotenv.2018.05.239

Zhou, Y., He, D., He, C., Li, P., Fan, D., Wang, A., et al. (2021). Spatial Changes in Molecular Composition of Dissolved Organic Matter in the Yangtze River Estuary: Implications for the Seaward Transport of Estuarine DOM. *Sci. Total. Environ.* 759, 143531. doi: 10.1016/j.scitotenv.2020.143531

Zhou, X., Jin, G., Li, J., Song, Z., Zhang, S., Chen, C., et al. (2021). Effects of Typhoon Mujigae on the Biogeochemistry and Ecology of a Semi-Enclosed Bay in the Northern South China Sea. *J. Geophys. Res.: Biogeosci.* 126 (7), e2020JG006031. doi: 10.1029/2020JG006031

Zsolnay, A., Baigar, E., Jimenez, M., Steinweg, B. and Saccomandi, F. (1999). Differentiating With Fluorescence Spectroscopy the Sources of Dissolved Organic Matter in Soils Subjected to Drying. *Chemosphere* 38 (1), 45–50. doi: 10.1016/S0045-6535(98)00166-0

Conflict of Interest: The authors declare that the research was conducted in the absence of any commercial or financial relationships that could be construed as a potential conflict of interest.

Publisher's Note: All claims expressed in this article are solely those of the authors and do not necessarily represent those of their affiliated organizations, or those of the publisher, the editors and the reviewers. Any product that may be evaluated in this article, or claim that may be made by its manufacturer, is not guaranteed or endorsed by the publisher.

Copyright © 2022 Zhong, Pan, Zhao and Wang. This is an open-access article distributed under the terms of the Creative Commons Attribution License (CC BY). The use, distribution or reproduction in other forums is permitted, provided the original author(s) and the copyright owner(s) are credited and that the original publication in this journal is cited, in accordance with accepted academic practice. No use, distribution or reproduction is permitted which does not comply with these terms.

frontiers | Frontiers in Marine Science

TYPE Original Research
PUBLISHED 28 July 2022
DOI 10.3389/fmars.2022.932984

Check for updates

OPEN ACCESS

EDITED BY
Meilin WU,
Chinese Academy of Sciences, China

REVIEWED BY
Yunwei Dong,
Ocean University of China, China
Feixue Li,
Nanjing University, China
Hanzhi Lin,
Science Systems and Applications, Inc., United States
Baowen Liao,
Chinese Academy of Forestry, China

*CORRESPONDENCE
Fengxia Wang
summer_wangfx@126.com

†These authors have contributed equally to this work and share first authorship

SPECIALTY SECTION
This article was submitted to Marine Pollution, a section of the journal Frontiers in Marine Science

RECEIVED 30 April 2022
ACCEPTED 05 July 2022
PUBLISHED 28 July 2022

CITATION
Zhao P, Ge S, He D, Zhong C, Wang B, Wang X, Wang F and Kao S (2022) Incorporating coastal blue carbon into subnational greenhouse gas inventories.
Front. Mar. Sci. 9:932984.
doi: 10.3389/fmars.2022.932984

COPYRIGHT
© 2022 Zhao, Ge, He, Zhong, Wang, Wang, Wang and Kao. This is an open-access article distributed under the terms of the Creative Commons Attribution License (CC BY). The use, distribution or reproduction in other forums is permitted, provided the original author(s) and the copyright owner(s) are credited and that the original publication in this journal is cited, in accordance with accepted academic practice. No use, distribution or reproduction is permitted which does not comply with these terms.

Incorporating coastal blue carbon into subnational greenhouse gas inventories

Peng Zhao[1†], Song Ge[2†], Dinghua He[2†], Cairong Zhong[3†], Boyan Wang[4], Xiaokang Wang[1], Fengxia Wang[2*] and Shuhji Kao[1]

[1]State Key Laboratory of Marine Resource Utilization in the South China Sea, Hainan University, Haikou, China, [2]College of Tourism, Hainan University, Haikou, China, [3]Forestry Academy of Hainan, Haikou, China, [4]HNU-ASU Joint International Tourism College, Hainan University, Haikou, China

The climate mitigation potential of coastal blue carbon including mangroves, seagrasses and tidal marshes have been widely recognized, and guidelines for incorporating coastal wetlands into greenhouse gas inventories released by IPCC in 2014 make it possible to bring coastal blue carbon into multilevel climate governance regimes. However, the intricate guidelines and inadequate data block governments from accounting and reporting their coastal blue carbon in inventories. In this research, we integrated and simplified the equations and assumptions of IPCC inventory guidance on coastal wetlands, and took Hainan province of China as a case study by (1) formulating a land use change matrix from high resolution satellite imagery for the years of 2010 to 2020, (2) compiling dataset of emission factors for coastal wetlands of Hainan, and (3) estimating CO_2, CH_4, and N_2O emissions from coastal wetlands in Hainan. We reveal that the mangroves' area increased from 4,190.7 ha in 2010 to 4,644.1 ha in 2020, with a net increase of 483.9 ha from tidal flats and aquaculture ponds. The weighted average EF_{AGB} and EF_{soil} of Hainan is 61.7 MgC ha^{-1} and 227.4 MgC ha^{-1}, respectively,estimated from peer-reviewed literature in both Chinese and English. The annual average net CO_2 emission of mangroves of Hainan is -26974.3 $MgCO_2e$ yr^{-1}. CO_2 emission from mangrove deforestation and N_2O emission from shrimp aquaculture in coastal aeras may offset the efforts of coastal wetlands conservation and restoration. Countries and sub-country regions are encouraged to bring coastal blue carbon into greenhouse gases inventories as soon as possible, and to take a bottom-up strategy to initiate the task at a local level.

KEYWORDS

coastal wetlands, mangrove, Hainan, climate change, land use change (LUC), biomass carbon accumulation, soil carbon sequestration

Introduction

Vegetated coastal wetlands, including mangroves, seagrasses and salt marshes are recognized as coastal blue carbon ecosystems, are one of the most biologically productive ecosystems in the world (Costanza et al., 1997; Howard et al., 2017). Despite occupying just 0.2% of the ocean surface, coastal blue carbon ecosystems contribute about 50% the yearly carbon burial in the ocean, despite occupying just 0.2% of the ocean surface (Duarte et al., 2013). Due to the reason that organic carbon decomposes slowly in coastal wetlands with negligible amounts of CO_2 being released (Chmura et al., 2003). Moreover, these ecosystems function across a long carbon storage timeframe (Feller et al., 2007; Iacono et al., 2008), making a disproportionately significant contribution to global carbon sequestration (Macreadie et al., 2019). Therefore, the restoration of coastal blue carbon ecosystems is recommended as a regretless mitigation option at the national level for coastal countries by IPCC (Bindoff et al., 2019).

United Nations Framework Convention on Climate Change (UNFCCC) sets the regime of international climate change governance, and all parties to the convention are obligated to regularly report their GHGs emissions or removals from six sectors in their national GHGs inventories (Wilson et al., 2015). In order to include significant land-use and already occurring management activities in wetlands into inventories, the Intergovernmental Panel on Climate Change (IPCC) released the *2013 Supplement to the 2006 IPCC Guidelines for National Greenhouse Gas Inventories: Wetlands*, Chapter 4 of which provides guidance on methodologies for estimating the carbon stock changes and CH_4 emissions from mangroves, tidal marshes and seagrasses, and the N_2O emissions from aquaculture in coastal wetlands (IPCC, 2014). Incorporating coastal blue carbon into GHGs Inventories helps explain human-induced emissions and removals of the coastal vegetated wetlands, while also informing society and professionals of climate change mitigation strategies, which are critical to producing an effective nature-based solution under the UNFCCC and its Paris Agreement (Crooks et al., 2018). The United States and Australia have incorporated coastal wetlands into their nventories since 2017 (Crooks et al., 2018). Net emissions from extraction and the regeneration of mangroves, conversion of tidal marshes and aquaculture was initially reported, with continuous improvements including consideration of seagrass drainage as well as methods and data renewal having been added to successive inventories.

The coasts of China span 18,000 km from temperate to tropical zones, and comprise a coastal wetland area of approximately 5.8×10^6 ha which nourish vast, diverse and ecologically important mangroves, seagrasses and tidal marshes (Sun et al., 2015; Meng et al., 2019). There have been four periods of large-scale sea reclamation which, during 1960s to 2000s, reduced coastal ecological systems as well as vegetated coastal wetlands by >60% (Zhao et al., 2016). Such plummeting of natural coastlines has been ceased since 2013 due to the national call upon ecological civilization by China authority (Wang et al., 2021). Successive policies and legislation including the ban of sea reclamation, the nation-wide mangrove restoration plan and the goal of carbon neutrality by 2060, as well as the introduction of the Wetlands Protection Law, further strengthened the conservation, rehabilitation and restoration of vegetated coastal wetlands (Liu et al., 2020; Pan et al., 2022). Although China included blue carbon actions among its Nationally Determined Contributions (Gallo et al., 2017) and encouragement in blue carbon have been written into many national-level and provincial-level policies and plans, blue carbon's absence from China's national GHGs inventory continues to inhibit the development of a clear picture that indicates the shifting emphasis on blue carbon in official documents and research papers to an emphasis on climate actions and practices.

The effort of incorporating blue carbon into China's national GHGs inventory has met with some difficulties. Firstly, data from national surveys and statistics on natural resources, wetlands and forests cannot fully support the needs and requirements of inventory compilation (Wang et al., 2020). For example, there is no information on tidal marshes and seagrasses, and there is no information on land-use change in mangroves in the decennial *National Land Resource Survey*. Second, the national default values of emission factors related to coastal wetlands have not been systematically reported according to the guidance of *IPCC 2013 Supplement*. Additionally, both rapid coastal zone development and its utilization during recent decades have reduced and broken up the vegetated coastal areas, with small areas possibly being left out and not added to national data. Here, we suggest taking a bottom-up strategy by beginning the research and practice with the local incorporation of blue carbon sequestration activities, and expanding the experience and knowledge across the national domain.

In this study, we followed the guidance of the IPCC on coastal wetlands, simplified the equations and assumptions, and took Hainan as an case study in order to estimate the GHG emissions of coastal wetlands by (1) acquiring activity data on the land use change matrix between 2010 and 2020 from high resolution satellite imagery, (2) summarizing emission factors of above-ground biomass storage and soil carbon storage of Hainan and its coastal regions, and (3) estimating CO_2, CH_4 and N_2O emissions of coastal wetlands in Hainan. This study will not only provide methods for reporting on the coastal wetlands section of a provincial inventory and enlightening the national inventory compilation in a much more technician-friendly way, but it will also provide an example of how to assess the coastal wetlands protection and restoration from the perspective of climate change mitigation.

Material and methods

Study area

Hainan, the second largest island of China, is the youngest coastal province with an area of 33,900 km^2 and 1,823 km of coastline. This island has a tropical monsoon climate with an average annual temperature of 25.7°C, and is famous for its rainforests and marine ecosystems such as mangroves, seagrasses and coral reefs (Gao et al., 2018). Mangroves and seagrasses are two of the main kinds of coastal blue carbon ecosystems in Hainan, the biodiversity of which ranks top in China (Chen et al., 2009). These mangroves are mainly distributed in the Dongzhai, Qinglan, Xinying, Huachang, Xinying, Qingmei and Tielu coastal areas (see Figure 1); the total area of which shows a U shape fluctuation since the 1950s due to land reclamation, and aquaculture during the 1960s through to the 2000s and mangrove restoration over the last 20 years (Liao et al., 2019). Seagrasses grow in the shallow water of lagoons, bays and on the fringes of coral reef flats along Hainan Island. Due to imprecise information on their distribution and areas still being insufficient (Hu et al., 2021), seagrasses are not included in this study.

Methodology for GHGs emission estimation

We followed the reporting framework of the *2006 Inventory Guidelines* and the methodology provided in the *2013 Supplement* in this study. A connection between the land-use change categories in *2006 Inventory Guidelines* and the land-use categories in the *2013 Supplement* (Table 1) was built to minimize the gap between the activity data acquisition and inventory reporting. The land use change categories are coastal wetlands that remain coastal wetlands (CC), non-coastal wetlands to coastal wetlands (NC), and coastal wetlands to non-coastal wetlands (CN) which should be reported in other relevant categories according to the Guidelines. We have followed practices of the United States to report the CN category under the coastal wetland category for a comprehensive understanding of change in the Hainan coastal wetlands.

It is thought that the CO_2, CH_4 and N_2O emissions (see Equation 1), induced by human activities in coastal wetlands, should be reported. With respect to CO_2 emissions, there are five carbon pools including above-ground biomass, below-ground biomass, soil, dead wood and litter (see Equation 2). The below-ground biomass is inferred from the above-ground biomass with

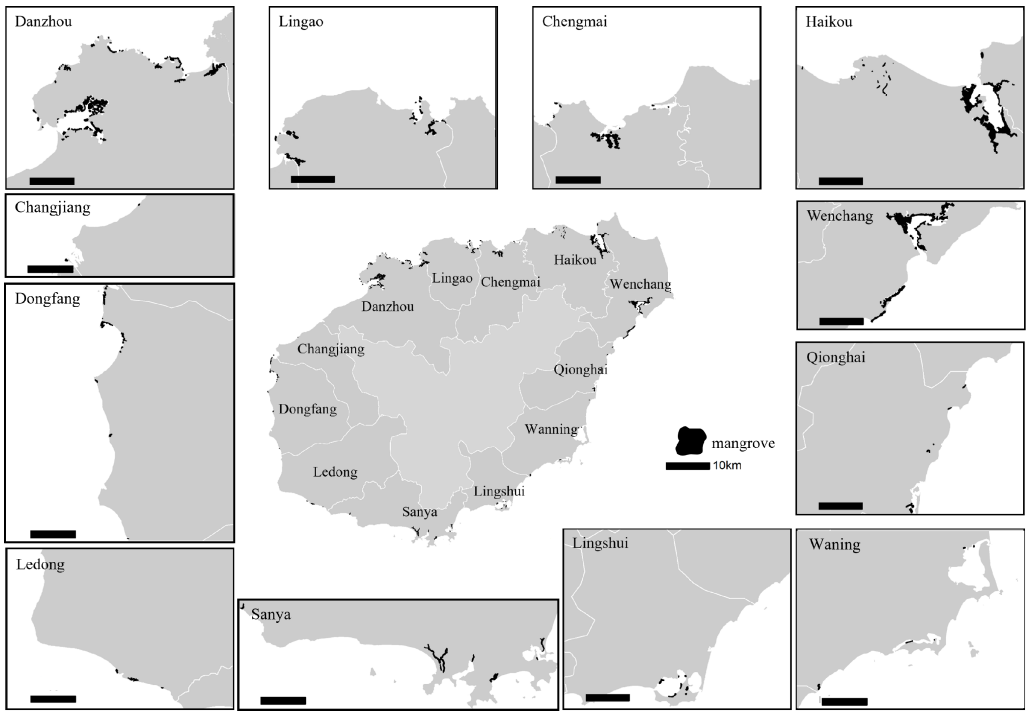

FIGURE 1
Mangrove distribution of Hainan in 2020.

TABLE 1 EM_{CO_2} calculation methods for different land-use change categories.

Land use change (*i*)	Land use	EM_{AGB}	EM_{soil}	$EM_{DW} + EM_{litter}$
CC	Forestry/ecological management	$-EF_{AGB}\times A_{CC}\times \frac{(a_{t_2}-a_{t_1})}{(t_2-t_1)}\times 3.67$	0	0
CN	Drainage (agriculture, forestry, mosquito control) Extraction (port, harbour and marina construction, aquaculture, salt production)	$EF_{AGB}\times(t_2-t_1)\times 3.67$	$EF_{soil}\times A_{CN}/(t_2-t_1)\times 3.67$	$ER_{DW}+EF_{litter}\times A_{CN}/(t_2-t_1)\times 3.67$
NC	Rewetting, revegetation and creation	$-EF_{GR}\times A_{NC}\times 3.67$	$-EF_{rewet}\times A_{NC}\times 3.67$	0

EF_{AGB}: above-ground biomass carbon storage per area, t C ha^{-1} yr^{-1}; a_{t_1} , a_{t_2} : the vegetation coverage at time t_1, t_2; EF_{GR}: carbon stock from annual aboveground biomass growth, a default value of 9.9 MgC ha^{-1} yr^{-1} for mangroves is used here (IPCC, 2014); EF_{rewet}: carbon stock from aggregated soils influenced by rewetting and revegetation activities, a local value of 1.56 MgC ha^{-1} yr^{-1} for mangroves is used here (see Supplementary Information Table S1); to the default values of EM_{DW} and $EM_{Llitter}$ are 10.7 MgC ha^{-1} and 0.7 MgC ha^{-1} for mangroves (IPCC, 2014).

a root-shoot ratio (*R*) of underground biomass to above-ground biomass. Due to the strong inverse relationship between salinity and CH_4 emissions, the rewetting and revegetation activities in freshwater and brackish waters with salinity<18 ppt (Equation 3) should be considered. N_2O is produced by the denitrification process of residual diets and feces from aquaculture animals including those of fish and shrimps, and their emission from aquaculture activities in coastal wetlands should be considered in the inventory (see Equation 4). The emission of GHGs is calculated by multiplying an emission factor (*EF*) with an activity data.

$$EM = EM_{CO_2} + EM_{CH_4} + EM_{N_2O} \quad (1)$$

$$EM_{CO_2} = \sum EM_{AGB_i}(1+R) + EM_{soil_i} + EM_{DW_i} + EM_{litter_i} \quad (2)$$

$$EM_{CH_4} = EF_{CH_4} \times A_{LS} \times 28 \quad (3)$$

$$EM_{N_2O} = EF_{N_2O} \times P_a \times 265 \quad (4)$$

In which,

EM is the total emission of GHGs from coastal wetlands, in which EM_{CO_2} , $EM_{N_2}O$, EM_{CH_4} are the emissions of CO_2, CH_4, N_2O correspondingly, $MgCO_2e{\cdot}yr^{-1}$

EM_{AGB} is CO_2 emission from above-ground biomass pool, $MgCO_2{\cdot}yr^{-1}$;

i is a category of land use change, including CC, CN, and NC.

R is the ratio of below-ground biomass to above-ground biomass, and a default value of 0.49 is used in this study (IPCC, 2014).

EM_{soil} is CO_2 emission from soil pool, $MgCO_2{\cdot}yr^{-1}$;

EM_{DW} is CO_2 emission from the dead wood pool, $MgCO_2{\cdot}yr^{-1}$;

EM_{litter} is CO_2 emission from litter pool, $MgCO_2{\cdot}yr^{-1}$;

EF_{CH4} is the emission factor of CH_4 from rewetted soils in freshwater and brackish water with salinity<18, and a default value of 0.1937 $MgCH_4$ ha^{-1} $yr^{-1}$is used in this study (IPCC, 2014).

A_{LS} is the area of rewetted soils in freshwater and brackish water with salinity<18, which has been interpreted using remote sensing imagery, ha; $EF_{N_2}O$ is the emission factor of N_2O from aquaculture production, with a default value of 0.00169 Mg N_2O-N per t aquaculture product (IPCC, 2014)

P_a is the annual cultured fish and shrimp production, the data of which is available in the Hainan Statistics Yearly Book, t/yr

There are two kinds of emission factors for the CO_2 emission estimation. The factor with the unit MgC ha^{-1} yr^{-1} on annual carbon flux is multiplied by the activity data (see Equation 5). And the factor with the unit MgC ha^{-1} on the carbon storage is used using the Stock-Difference method (IPCC, 2006) (see Equation 6).

For the *EF* representing annual carbon flux per area:

$$EM_{CO_2 i,j} = EF_{i,j} \times A_i \times 3.67 \quad (5)$$

For the *EF* representing carbon storage per area:

$$EM_{CO_2 i,j} = EF_{i,j} \times A_i/(t_2 - t_1) \times 3.67 \quad (6)$$

In which,

$EM_{i,j}$ is the emission of CO_2 of the *j* carbon pool in the *i* category, MgC ha^{-1};

$EF_{i,j}$ is CO_2 emission factors of the *j* carbon pool in the *i* category, MgC ha^{-1} or MgC ha^{-1} yr^{-1};

A_i is the area of the *i* category of land-use change during t_1 and t_2, ha;

j is one category of the 5 carbon pools;

3.67 is the transfer factor for transferring carbon to carbon dioxide.

For simplifying the complicated guidance of the *2013 Supplement*, we use the tier 1 method and relevant assumptions. Biomass is the only carbon pool considered in CC, and coverage change is used for estimating change of carbon storage in this pool; all carbon storage in the 5 carbon pools is assumed to be depleted and emitted as CO_2 during the period of extraction in CN, and the carbon sequestration induced by rewetting and revegetation, and creation is calculated yearly in NC.

Activity data

Activity data is defined as the magnitude of human activity resulting in emissions or removals during a given period. For coastal wetlands, data on land areas, management systems and fertilizer use are activity data. The activity data used in this study includes A_{CC}, A_{NC}, A_{CN}, A_{LS} and P_{α}. Satellite imagery was used to estimate areas of the three land-use change categories and relevant sub-categories. The data for two periods of satellite imagery (2010 and 2020) with a 1.2m resolution covering the whole coastal area of Hainan were downloaded from Google Earth. The cloud coverage of imagery is less than 10%. A vector of mangrove distribution in 2020, from an official survey, was introduced in the study for ensuring data consistency and accuracy. The vector overlapped with the imagery from 2020, and the surface factures within the vectors were classified into mangroves, tidal flats, aquaculture ponds and construction lands. Then, the vector was overlapped with imagery from 2010, and the surface factures were classified as the same to get A_{CC} and A_{NC}, while mangroves outside the vector were added to map the 2010 mangrove distribution. Then the vector of mangrove distribution in 2010 was overlapped with imagery from 2020 to figure out the areas (A_{CN}) of mangroves, measured in 2010, that had changed to other land-use categories. The areas (A_{LS}) of mangroves restored in freshwaters and brackish waters were calculated to estimate the CH_4 emissions. For the CC category, pixel-based classification using the Maximum Likelihood Method was used for calculating the vegetation coverage rate (a_{t_1} , a_{t_2}) of mangroves in the two periods. The classification accuracies were over 85%. Data from the Hainan Statistics Yearbook on the production of shrimp was used as P_{α} because shrimp aquaculture is the main aquaculture activity in the coastal areas of Hainan, with fish aquaculture often being conducted in aquaculture farms on land or in offshore cages at the depth > 6m.

Emissions factors

An emission factor (EF) is a coefficient that relates the activity data to the amount of greenhouse gases or its precursors and is calculated at an average emission rate, which is often based on published measurement data. In this study, EFs, including mangrove above-ground biomass carbon storage (EF_{AGB}), soil carbon storage (EF_{soil}) and the soil carbon sequestration rate (EF_{rewet}) have been assembled through a synthesis of peer-reviewed literatures. Default values from the *2013 Supplement* were applied to other EFs which are not available in the literature, such as to EF_{DW}, EF_{litter}, EF_{GR}, EF_{CH_4} , and EF_{N_2O} . We searched the literature on the Web of Science using the search topic "TS=(carbon OR biomass) AND mangrove* AND (China OR Hainan)", and in the CNKI (www.cnki.net), a Chinese literature database, using the search topic "SU=红树林*海南*(碳+生物量)". Data from 20 informative papers (10 from the Web of Science, and 10 from CNKI) were compiled and assimilated (Supplementary Information Tables S2 and Table S3). We followed the suggestion of the *2013 Supplement* and set the depth of the soil carbon pool at 1 m, and data of soil carbon storage at a depth of more or less than 1 m were transferred to 1 m depth with the assumption that the soil organic carbon content with the depth > 0.5 m is stable. For regions lacking local data on emission factors, the values of adjacent regions were used as a default value. Considering that the mangroves are distributed unevenly in Hainan, we calculated the weighted average EF_{AGB} and EF_{soil} for Hainan Province as below:

$$EF_{AGB,Hainan} = \sum EF_{AGB,k} \times (A_k \; A_{Hainan}) \quad (7)$$

$$EF_{soil,Hainan} = \sum EF_{soil,k} \times (A_k \; A_{Hainan}) \quad (8)$$

In which:

$EF_{AGB,Hainan}$ is the average above-ground biomass carbon storage per area of Hainan, MgC ha^{-1};

$EF_{soil,Hainan}$ is the average soil organic carbon storage per area of Hainan, MgC ha^{-1};

$EF_{AGB,k}$ is the average aboveground biomass carbon storage per area of the *k* region, MgC ha^{-1};

$EF_{soil,k}$ is the average organic soil carbon storage per area of the *k* region, MgC ha^{-1};

A_k is the area of mangroves in the *k* region, ha;

A_{Hainan} is the total area of mangroves in Hainan, ha.

Results

The land-use change of mangroves between 2010 and 2020

Mangroves are distributed in all coastal regions of Hainan province (see Figure 1), 81.7% of which are located in the northern regions of Haikou, Wenchang and Danzhou, while the other areas of mangroves are scattered across 9 other coastal regions (see Table 2). The total area of mangroves in 2010 increased from 4,190.7ha to 4,644.1 ha in 2020, with an average annual growth rate of 1.1%. 4,175.4 ha of mangroves fall into the category of CC. The vegetation coverage rate increased from 91.4% to 91.5% province-wide, but it decreased in Haikou, Wenchang, Chengmai, Lingao and Ledong. A total of 483.9 ha of tidal flats (A_{FC}) and aquaculture ponds (A_{PC}) have been revegetated into mangroves, in which, 70.3 ha we created in freshwater and brackish water. 15.3 ha of mangroves have been transformed into aquaculture ponds and construction lands. The net increased area of mangroves is 453.3 ha, while another 4.1 ha

TABLE 2 Land-use change of coastal wetlands of Hainan between 2010 and 2020. Unit: ha.

Region	A_{CC}	A_{NC}			A_{CN}		A_{2010}	A_{2020}	ΔA	a_{2010}(%)	a_{2020}(%)	ΔA_{CC}	$\Delta A+\Delta A_{CC}$
		A_{FC}	A_{LS}	A_{PC}	A_{CP}	A_{CL}							
Haikou	1676.2	79.7	6.7	35.0	0.8	1.4	1678.4	1788.7	110.3	93.3	92.1	-19.4	90.9
Wenchang	1105.9	59.3	7.8	15.8	9.9	1.0	1116.8	1170.1	53.3	99.9	98.6	-14.8	38.5
Danzhou	779.1	54.8	2.6	0.3	0	0	779.1	834.2	55.1	79.8	86.0	48.8	103.9
Lingao	206.1	43.6	10.8	0	0.2	0	206.3	249.5	43.2	86.8	85.8	-2.1	41.1
Chengmai	194.9	47.7	3.2	1.1	0	0	194.9	243.7	48.8	85.9	76.3	-18.7	30.0
Sanya	79.0	44.1	29.0	0	0	0	79.0	123.1	44.1	80.1	85.9	4.5	48.6
Dongfang	58.5	46.1	0	23.0	0.3	0	58.8	127.3	68.5	96.0	99.0	1.7	70.2
Lingshui	30.4	7.9	1.4	0	0	0	30.4	38.3	7.9	80.8	88.6	2.4	10.3
Wanning	27.7	4.5	4.5	0	0	0	27.7	32.2	4.5	68.4	75.0	1.8	6.3
Qionghai	10.6	9.1	2.2	0	1.7	0	12.3	18.0	5.7	94.3	94.2	0	5.7
Ledong	3.7	4.5	1.8	1.3	0	0	3.7	9.5	5.8	100.0	97.2	-0.1	5.7
Changjiang	3.4	6.1	0.3	0	0	0	3.4	9.5	6.1	100.0	100.0	0	6.1
Hainan	4175.4	407.4	70.3	76.5	12.9	2.4	4190.7	4644.1	453.3	91.4	91.5	4.1	457.4

A_{FC}: the area from tidal flats to coastal wetlands; **A_{PC}:** the area from aquaculture ponds to coastal wetlands; **A_{CP}:** the area from coastal wetlands to aquaculture ponds; **A_{CL}:** the area from coastal wetlands to construction land; **ΔA:** total changed area between 2010 and 2020; **ΔAcc:** changed area due to vegetation coverage change.

will be added in consideration of the change in vegetation coverage between 2010 and 2020.

Emission factors relating to Hainan and its coastal regions

There are 103 AGB data and 159 soil organic carbon storage data in peer-review literatures in English and Chinese. 94% of the AGB data and 96% of the soil carbon storage data relate to mangroves in Haikou, Wenchang, Danzhou and Sanya. The weighted average EF_{AGB} and EF_{soil} of Hainan is 61.7 MgC ha^{-1} and 227.4 MgC ha^{-1}. By using the default value (0.49) of *R*, the sum of the weighted average of biomass and soil carbon storage is 319.3 MgC ha^{-1} (see Figure 2). The highest average EF_{AGB} is EF_{AGB} as recorded in Qionghai, while the average EF_{soil} of Wenchang is also the highest among this category. EF_{AGB} relating to Dongfang is close to that of Qionghai, and the EF_{AGB} in the remaining regions are between 52.6 and 66.2 MgC ha^{-1}. EF_{soil} in Wenchang and Qionghai ranks the second highest in Hainan; while the EF_{soil} in Haikou, Chengmai, Danzhou and Sanya is less than 200 MgC ha^{-1} (see Table 3).

The GHGs inventory for coastal wetlands in Hainan

The annual average net CO_2 emission of mangroves of Hainan is -26974.3 $MgCO_2e\ yr^{-1}$ during 2010 to 2020 (See Table 4). The CO_2 emissions (-27355.6 $MgCO_2e\ yr^{-1}$) from biomass, soil, dead woods and litters in the mangroves is offset by the CH_4 emissions (381.3 $MgCO_2e\ yr^{-1}$) resulting from the rewetting and restoration activities in the areas which registered a salinity of<18 ppt. The soil carbon pool in the mangroves in Wenchang and Qionghai emitted CO_2 due to 9.9 ha and 1.7 ha of mangroves becoming transformed into ponds, which, in turn, also enhanced the emissions of biomass carbon pool. With more unvegetated lands transferring to mangroves, we can see Haikou, Danzhou and Dongfang as the top three regions in their net contribution of CO_2 removals. Because two-thirds of the mangroves restoration in Sanya occurred in freshwaters, the CH_4 emission was the highest for Hainan.

Discussion

The important role of coastal blue carbon in climate mitigation has been widely accepted and passionately discussed domestically in China and worldwide (Wu et al., 2020; Macreadie et al., 2021). More and more countries include the blue carbon into their Nationally Determined Contributions, however most of countries have not reported coastal blue carbon in national inventories as the United States and Australia have done on account of them lacking qualified national activity data and an assembly of local emission factors (Yona et al., 2020). Sub-national policies and actions on blue carbon without waiting for instruction from higher authorities should be the choice for dealing locally with the climate crisis (Wedding et al., 2021), and incorporating coastal blue carbon into inventories is essential for the achievement of this goal. Compared to the national inventory, sub-national inventory reporting requires detailed tier 3 data from remote sensing and on-site studies that is not only informative for climate mitigation but is also informative of land-use changes, biodiversity conservation, industrial development, and so on.

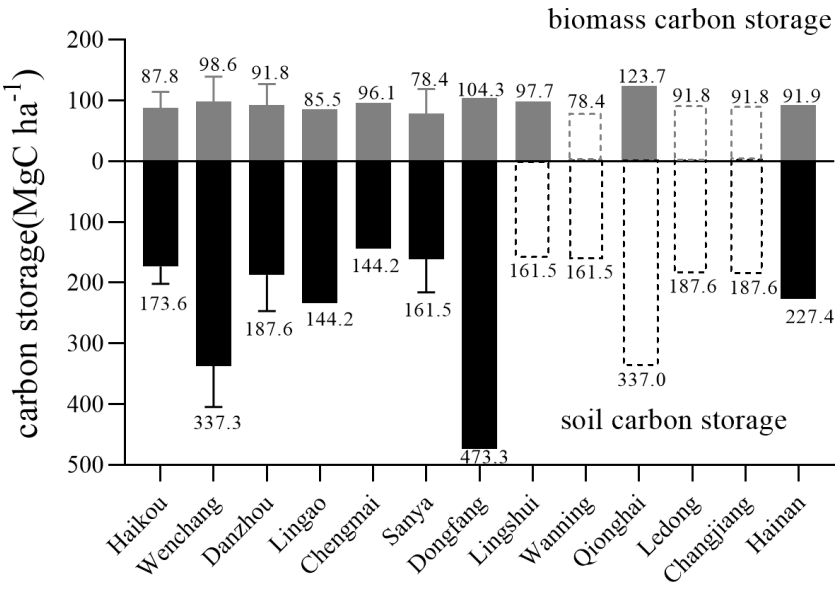

FIGURE 2
The average carbon storage of biomass and soil in the mangroves in Hainan. Dash lines indicate the value of adjacent regions is cited.

This study reports on the GHG emissions or removals from mangroves affected by human activities in Hainan, which demonstrated a net sink capacity of CO_2e during the 2010 to 2020 period, where the total area of mangroves and vegetation coverage has increased, reflecting the efforts of mangroves protection, rehabilitation and restoration in both Hainan and China in general. However, the local figures of land-use change also alert us to the impact of CO_2 emissions. For example, the descending coverage rates in Haikou, Wenchang, Chengmai and Lingao, four regions north of Hainan, may have been caused by a sea-level rise, pests and diseases or liana (*Derris trifoliate*), meaning the necessary adaption measures should be considered and implemented. Although the Hainan Province Mangrove Protection Regulations was adopted in 1998, some mangroves have nevertheless been destroyed in Haikou, Wenchang, Qionghai, Lingao and Dongfang. The 13.9% removal of mangrove reforestation on aquaculture ponds in Wenchang, Dongfang and Haikou is offset by emissions from deforestation for the purpose of establishing aquaculture, even if A_{CN}/A_{NC} is 0.03, we are reminded that we need to strengthen the protection of mangroves and avoid deforestation in these areas.

TABLE 3 The EF_{AGB} and EF_{SOC} of mangroves in Hainan

Regions	EF_{AGB} (MgC ha^{-1})			EF_{soil} (MgC ha^{-1})		
	Mean	95% CI	n	Mean	95% CI	n
Haikou	58.9	[41.2,76.53]	52	173.6	[145.1,202.2]	100
Wenchang	66.2	[39.2,93.2]	34	337.0	[269.1,405.0]	32
Danzhou	61.6	[37.9,85.28]	4	187.6	[128.4,246.8]	10
Lingao	57.4	–	1	233.9	–	1
Chengmai	64.5	–	2	144.2	–	1
Sanya	52.6	[25.4,79.8]	6	161.5	[106.7,216.4]	11
Dongfang	70.0	–	1	473.3	–	4
Lingshui	65.6	–	1	161.5	–	0
Wanning	52.6	–	0	161.5	–	0
Qionghai	83.0	–	1	337.0	–	0
Ledong	61.6	–	0	187.6	–	0
Changjiang	61.6	–	0	187.6	–	0
Hainan	61.7	–	102	227.4	–	159

TABLE 4 The CO_2 and CH_4 inventory for mangroves in Hainan. Unit: MgCO2e yr-1.

regions	CC		CN				NC			In total		
	EM_{AGB}× (1 + R)	EM_{CO_2}	EM_{AGB}× (1 + R) (1)	EM_{soil} (2)	EM_{DW} + EM_{litter}(3)	EM_{CO_2} (1)+(2) +(3)	EM_{AGB}× (1 + R) (4)	EM_{soil} (5)	EM_{CO_2} (4) + (5)	EM_{CH_4}	EM_{CO_2}	EM_{CO_2}+ EM_{CH_4}
Haikou	625.9	625.9	70.9	140.2	9.2	220.3	-6209.4	-656.7	-6866.1	36.3	-6019.9	-5983.6
Wenchang	536.9	536.9	394.6	1348.1	45.6	1788.3	-4065.6	-430.0	-4495.6	42.3	-2170.4	-2128.1
Danzhou	-1642.7	-1642.7	0	0	0	0	-2982.9	-315.5	-3298.4	14.1	-4941.1	-4927.0
Lingao	64.6	64.6	6.3	17.2	0.8	24.3	-2360.3	-249.6	-2609.9	58.6	-2521	-2462.4
Chengmai	661.2	661.2	0	0	0	0	-2641.7	-279.4	-2921.1	17.4	-2259.9	-2242.5
Sanya	-130.8	-130.8	0	0	0	0	-2387.4	-252.5	-2639.9	157.3	-2770.7	-2613.4
Dongfang	-66.5	-66.5	11.5	52.1	1.3	64.9	-3740.8	-395.6	-4136.4	0	-4138.0	-4138.0
Lingshui	-84.7	-84.7	0	0	0	0	-427.7	-45.2	-472.9	7.6	-557.6	-550.0
Wanning	-52.9	-52.9	0	0	0	0	-243.6	-25.8	-269.4	24.4	-322.3	-297.9
Qionghai	0.3	0.3	77.2	210.3	7.1	294.6	-492.6	-52.1	-544.7	11.9	-249.8	-237.9
Ledong	3.5	3.5	0	0	0	0	-314.0	-33.2	-347.2	9.8	-343.7	-333.9
Changjiang	0	0	0	0	0	0	-331.9	-35.1	-367.0	1.6	-367	-365.4
Hainan	-137.5	-137.5	516.1	1276.8	64.0	1856.9	-26197.9	-2770.6	-28968.5	381.3	-27249.1	-26867.8

The N_2O emissions from shrimp aquaculture in Hainan fluctuated, during 2010 to 2020, with an average of 47538 $MgCO_2e\ yr^{-1}$ (See Table 5). The data from Wenchang accounts for one-third of the total emissions in the province, while illustrating a descending trend, which even reaches zero in the tropical tourism cities of Lingshui and Sanya.

N_2O emissions from aquaculture in coastal wetlands is about two times that of the CO_2 removal facilitated by managed mangroves, which, in turn, has a significant impact on the inventory. This problem should be taken into serious consideration by leading countries in aquaculture production. Descending shrimp production in Sanya and Lingshui, since 2019, represents the initial 'transferring ponds to wetlands' across the whole province. Since most of ponds on tidal flats have been dismantled and reforested with mangrove, the N_2O emissions in these regions will plummet in the near future. According to the National Action Plan of Mangroves Protection and Restoration Plan (2020-2025), 5200 ha of mangroves will have been rehabilitated and restored in Hainan, and 18800 ha in China by 2025. This increase of CO_2 removal will be accompanied by a decrease in N_2O emissions.

This study also illustrates that there are data gaps that need to be addressed to reduce uncertainty of local inventory, which would also be informative on the national level. Some default values from *IPCC 2013 Supplement* have to be used as emission factors because there is a lack of national and local data, which may produce uncertainty in the inventory. It is suggested that the default values should be replaced with local data as far as possible. Meanwhile, investigation on the carbon storage of different carbon pools and the sequestration rate of above-ground biomass and soil are necessary to fill data gaps in other regions besides those of Haikou, Wenchang and Sanya, as emission factors for coastal blue carbon is highly impacted by environmental factors and plant species (Wang et al., 2019). For countries and regions that have no land-use change data or the land-use categories that are consistent with the *2006 Guidelines*

TABLE 5 N_2O emissions of shrimp aquaculture in Hainan. Unit: $MgCO_2e\ yr^{-1}$.

Region	2010	2011	2012	2013	2014	2015	2016	2017	2018	2019	2020
Haikou	2664.3	3124.2	4281.9	5545.7	3535.8	4641.1	3694.8	5070.6	4825.6	5160.6	3615.5
Wenchang	7179.5	7827.1	7933.7	8813.7	7250.2	8618.9	9026.9	14998.5	13086.6	16125.7	15454.9
Danzhou	8274.0	12415.7	11114.3	12328.4	10832.6	11046.2	9883.2	10639.6	8318.8	8331.4	8442.9
Lingao	4002.9	3583.2	5486.2	5091.6	3272.4	3294.4	2979.1	3107.2	1996.5	2037.3	1830.4
Chengmai	2843.0	3364.7	2943.3	5374.2	3502.2	3609.2	3868.1	3743.1	3916.4	3529.1	3095.1
Sanya	1086.0	983.9	644.9	1314.9	507.4	628.3	100.8	421.4	107.5	313.5	26.9
Dongfang	1630.6	0	2685.3	2237.5	2222.7	2255.8	2261.6	2751.1	2316.7	1870.7	1232.9
Lingshui	726.0	0	729.5	797.2	365.9	315.7	322.5	67.2	0	0	0
Wanning	7386.4	7072.9	7710.2	8525.7	5050.4	7007.1	6575.3	6623.3	6269.9	6126.1	5792.9
Qionghai	1718.8	1727.4	1948.1	2054.7	1611.4	2004.1	1981.7	1569.7	1496.7	1587.6	1599.7
Ledong	2378.5	1929.3	2101.3	2114.3	2107.6	2198.5	2274.2	2340.9	2304.2	1841.6	1778.0
Changjiang	1428.6	0	1750.2	2535.3	1773.5	1911.4	2109.4	2872.1	3447.5	3829.6	2958.9
Hainan	41318.6	42028.5	49328.9	56733.2	42032.1	47530.8	45077.4	54204.6	48086.6	50753.0	45828.0

and the *2013 Supplement*, it is suggested that a land-use change matrix be built based on official survey vectors. While it is common that countries lack spatially explicit seagrass data because of economic and technical difficulties (Unsworth et al., 2019), the Australia Inventory established a good practice of reporting on the areas of drained seagrasses, an activity which requires collaboration between different government agencies. As a comprehensive solution for Hainan and China, as well as other countries and sub-national regions, it is suggested that there be a compilation of a EFs database that incorporates the main locations, species, salinities and latitudes, which models the prediction of the EFs of certain independent variables. The development of an automatic imagery analysis system supported by machine learning continues to be a necessity for efficiently and promptly monitoring land-use change and the production activity data.

We suggest countries and sub-country regions should begin bringing coastal blue carbon into their GHGs inventories as soon as possible, and that they should take a bottom-up strategy to addressing this task. This will not only be helpful to stakeholders and decision-makers when needing to learn what has happened to coastal wetlands as a result of climate changes, but this initiative will also make nature-based solutions computable and visible, which, in the end, will inform climate change mitigation and adaptation strategies.

Data availability statement

The original contributions presented in the study are included in the article/Supplementary Material. Further inquiries can be directed to the corresponding author.

Author contributions

PZ and FW conceived and designed the study. SG, XW and BW collected and analyzed the data. PZ, SG, and CZ drafted the manuscript. PZ, FW and SK revised the manuscript. All authors contributed to the article and approved the submitted version.

Funding

This study was supported by the Key R & D Plan of Hainan Province (ZDYF2021SHFZ255), the S & T Plan of Beihai City (BKH2020165011), the Open Research of State Key Laboratory of Marine Resource Utilization in the South China Sea (MRUKF2021013), the Blue Planet Project (PORO000642) supported by WWF and OPF and the Research on Coastal Blue Carbon Status and Development Strategy of China supported by Paulson Institute and Heren Charitable Foundation.

Conflict of interest

The authors declare that the research was conducted in the absence of any commercial or financial relationships that could be construed as a potential conflict of interest.

Publisher's note

All claims expressed in this article are solely those of the authors and do not necessarily represent those of their affiliated organizations, or those of the publisher, the editors and the reviewers. Any product that may be evaluated in this article, or claim that may be made by its manufacturer, is not guaranteed or endorsed by the publisher.

Supplementary material

The Supplementary Material for this article can be found online at: https://www.frontiersin.org/articles/10.3389/fmars.2022.932984/full#supplementary-material

References

Bindoff, N., Cheung, W. W. L., Kairo, J. G., Aristegui, J., Guinder, V., Hilmi, N., et al. (2019). *Changing ocean, marine ecosystems, and dependent communities," in The ocean and cryosphere in a changing climate: special report of the intergovernmental panel on climate change.* (Cambridge: Cambridge University Press), 447–588. doi: 10.1017/9781009157964.013

Chen, L., Wang, W., Zhang, Y., and Lin, G. (2009). Recent progresses in mangrove conservation, restoration and research in China. *J. Plant Ecol.* 2, 45–54. doi: 10.1093/jpe/rtp009

Chmura, G. L., Anisfeld, S. C., Cahoon, D. R., and Lynch, J. C. (2003). Global carbon sequestration in tidal, saline wetland soils. *Global Biogeochemical Cycles* 17, 1111. doi: 10.1029/2002GB001917

Costanza, R., Arge„ Groot, R. D., Farberk, S., and Belt, M. (1997). The value of the world's ecosystem services and natural capital. *Nature* 387, 253–260. doi: 10.1038/387253a0

Crooks, S., Sutton-Grier, A. E., Troxler, T. G., Herold, N., and Wirth, T. (2018). Coastal wetland management as a contribution to the US national greenhouse gas inventory. *Nat. Climate Change* 8, 1109–1112. doi: 10.1038/s41558-018-0345-0

Duarte, C. M., Losada, I. J., Hendriks, I. E., Mazarrasa, I., and Marba, N. (2013). The role of coastal plant communities for climate change mitigation and adaptation. *Nat. Climate Change* 3, 961–968. doi: 10.1038/nclimate1970

Feller, I. C., McKee, K. L., and Cahoon, D. (2007). Caribbean Mangroves adjust to rising sea level through biotic controls on change in soil elevation. *Global Ecol. Biogeography* 16, 545–556. doi: 10.1111/j.1466-8238.2007.00317.x

Gallo, N. D., Victor, D. G., and Levin, L. A. (2017). Ocean commitments under the Paris agreement. *Nat. Climate Change* 7, nclimate3422. doi: 10.1038/nclimate3422

Gao, T., Ding, D., Guan, W., and Liao, B. (2018). Carbon stocks of coastal wetland ecosystems on hainan island, China. *Polish J. Environ. Stud.* 27, 1061–1069. doi: 10.15244/pjoes/76501

Howard, J., Sutton-Grier, A., Herr, D., Kleypas, J., Landis, E., Mcleod, E., et al. (2017). Clarifying the role of coastal and marine systems in climate mitigation. *Front. Ecol. Environ.* 15. doi: 10.1002/fee.1451

Hu, W., Zhang, D., Chen, B., Liu, X., Ye, X., Jiang, Q., et al. (2021). Mapping the seagrass conservation and restoration priorities: Coupling habitat suitability and anthropogenic pressures. *Ecol. Indic.* 129, 107960. doi: 10.1016/j.ecolind.2021.107960

Iacono, C. L., Mateo, M. A., Gràcia, E., Guasch, L., Carbonell, R., Serrano, L., et al. (2008). Very high-resolution seismo-acoustic imaging of seagrass meadows (Mediterranean sea): Implications for carbon sink estimates. *Geophysical Res. Lett.* 35, 102–102. doi: 10.1029/2008GL034773

IPCC (2014). *2013 supplement to the 2006 IPCC guidelines for national greenhouse gas inventories* (Switzerland: Wetlands).

Liao, J., Zhen, J., Zhang, L., and Metternicht, G. (2019). Understanding dynamics of mangrove forest on protected areas of hainan island, China: 30 years of evidence from remote sensing. *Sustainability* 11, 5356. doi: 10.3390/su11195356

Liu, L., Wang, H.-J., and Yue, Q. (2020). China's coastal wetlands: Ecological challenges, restoration, and management suggestions. *Regional Stud. Mar. Sci.* 37, 101337. doi: 10.1016/j.rsma.2020.101337

Macreadie, P. I., Anton, A., Raven, J. A., Beaumont, N., Connolly, R. M., Friess, D. A., et al. (2019). The future of blue carbon science. *Nat. Commun.* 10, 3998. doi: 10.1038/s41467-019-11693-w

Macreadie, P. I., Costa, M. D. P., Atwood, T. B., Friess, D. A., Kelleway, J. J., Kennedy, H., et al. (2021). Blue carbon as a natural climate solution. *Nat. Rev. Earth Environ.* 2, 826–839. doi: 10.1038/s43017-021-00224-1

Meng, W., Feagin, R. A., Hu, B., He, M., and Li, H. (2019). The spatial distribution of blue carbon in the coastal wetlands of China. *Estuarine Coast. Shelf Sci.* 222, 13–20. doi: 10.1016/j.ecss.2019.03.010

Pan, W., Gulzar, M. A., Wang, Z., and Guo, C. (2022). Spatial distribution and regional difference of environmental efficiency based on carbon reduction goals: Evidence from China. *Front. Environ. Sci.* 9. doi: 10.3389/fenvs.2021.816071

Sun, Z., Sun, W., Tong, C., Zeng, C., Yu, X., and Mou, X. (2015). China's coastal wetlands: Conservation history, implementation efforts, existing issues and strategies for future improvement. *Environ. Int.* 79, 25–41. doi: 10.1016/j.envint.2015.02.017

Unsworth, R. K. F., Nordlund, L. M., and Cullen-Unsworth, L. C. (2019). Seagrass meadows support global fisheries production. *Conserv. Lett.* e12566. doi: 10.1111/conl.12566

Wang, G., Guan, D., Xiao, L., and Peart, M. R. (2019). Ecosystem carbon storage affected by intertidal locations and climatic factors in three estuarine mangrove forests of south China. *Regional Environ. Change* 19, 1701–1712. doi: 10.1007/s10113-019-01515-6

Wang, X., Xiao, X., Xu, X., Zou, Z., Chen, B., Qin, Y., et al. (2021). Rebound in china's coastal wetlands following conservation and restoration. *Nat. Sustainability* 4, 1076–1083. doi: 10.1038/s41893-021-00793-5

Wang, X., Xiao, X., Zou, Z., Hou, L., and Li, B. (2020). Mapping coastal wetlands of China using time series landsat images in 2018 and Google earth engine. *ISPRS J. Photogrammetry Remote Sens.* 163, 312–26. doi: 10.1016/j.isprsjprs.2020.03.014

Wedding, L. M., Moritsch, M., Verutes, G., Arkema, K., Hartge, E., Reiblich, J., et al. (2021). Incorporating blue carbon sequestration benefits into sub-national climate policies. *Global Environ. Change-Human Policy Dimensions* 69, 102206. doi: 10.1016/j.gloenvcha.2020.102206

Wilson, D., Dixon, S. D., Artz, R. R. E., Smith, T. E. L., Evans, C. D., Owen, H. J. F., et al. (2015). Derivation of greenhouse gas emission factors for peatlands managed for extraction in the republic of Ireland and the united kingdom. *Biogeosciences* 12, 5291–5308. doi: 10.5194/bg-12-5291-2015

Wu, J. P., Zhang, H. B., Pan, Y. W., Krause-Jensen, D., He, Z. G., Fan, W., et al. (2020). Opportunities for blue carbon strategies in China. *Ocean Coast. Manage.* 194, 105241. doi: 10.1016/j.ocecoaman.2020.105241

Yona, L., Cashore, B., Jackson, R. B., Ometto, J., and Bradford, M. A. (2020). Refining national greenhouse gas inventories. *Ambio* 49, 1581–1586. doi: 10.1007/s13280-019-01312-9

Zhao, P., Lu, W., Song, J., Stuart, P., and Yang, H. (2016). Natural coast protection and use in China: Implications of resource protection "Redline" policies. *Coast. Manage.* 44, 21–35. doi: 10.1080/08920753.2016.1116668

frontiers | Frontiers in Marine Science

TYPE Data Report
PUBLISHED 28 July 2022
DOI 10.3389/fmars.2022.953985

Check for updates

OPEN ACCESS

EDITED BY
Biraja Kumar Sahu,
Council of Scientific and Industrial Research (CSIR), India

REVIEWED BY
Sadayan Paramasivam,
Alagappa University, India
Thadickal V. Joydas,
King Fahd University of Petroleum and Minerals, India

*CORRESPONDENCE
Ganesh Thiruchitrambalam
ganesht.omb@pondiuni.edu.in

SPECIALTY SECTION
This article was submitted to Marine Pollution, a section of the journal Frontiers in Marine Science

RECEIVED 26 May 2022
ACCEPTED 27 June 2022
PUBLISHED 28 July 2022

CITATION
Sahu N, Lakra RK and Thiruchitrambalam G (2022) Effect of cyclonic storm *Vardah* on the community structure and ecosystem functioning of macrobenthic fauna in the intertidal region of South Andaman Islands. *Front. Mar. Sci.* 9:953985. doi: 10.3389/fmars.2022.953985

COPYRIGHT
© 2022 Sahu, Lakra and Thiruchitrambalam. This is an open-access article distributed under the terms of the Creative Commons Attribution License (CC BY). The use, distribution or reproduction in other forums is permitted, provided the original author(s) and the copyright owner(s) are credited and that the original publication in this journal is cited, in accordance with accepted academic practice. No use, distribution or reproduction is permitted which does not comply with these terms.

Effect of cyclonic storm *Vardah* on the community structure and ecosystem functioning of macrobenthic fauna in the intertidal region of South Andaman Islands

Nosad Sahu, Raj Kiran Lakra and Ganesh Thiruchitrambalam*

Department of Ocean Studies and Marine Biology, Pondicherry University, Port Blair, India

An investigation was carried out to understand the effect of a cyclone *Vardah* on the functioning of macrobenthos. The assessment was accomplished by comparing before cyclone (BC) and after cyclone (AC) data of macrobenthos. Additionally, temporal changes in the faunal assemblages were evident through multivariate techniques. Five distinguished assemblages could be noticed through the Bray–Curtis similarity representing different phases of the cyclone. The cyclonic effect also resulted in the recruitment of some macrobenthic species and the loss of a few during the study period. Biological trait analysis identified subsurface deposit feeders, upward and downward conveyers, Ecological Group IV, mid-mobile macrobenthos and size class of 2–4 cm as the important groups that dominated the functioning of the macrobenthic community immediately after the cyclone. The resilience and recruitment of macrobenthos were explained using functional redundancy.

KEYWORDS

biological trait analysis, cyclone effects, macrobenthic fauna, ecosystem functioning, functional redundancy

Introduction

A storm or a tropical cyclone is one of the phenomena that frequently occur in the tropical region. The Arabian Sea and the Bay of Bengal of the Indian subcontinent account for about 4.8% of total storms worldwide (Aguttes et al., 2000). For example, between 2011 and 2016, the Arabian Sea and Bay of Bengal encountered 20 mild and

severe tropical cyclones (Vasudha, 2017). Storms have a big impact on the coastal areas, especially the sedimentary shoreline, and can alter coastal community structure temporally (Balica et al., 2012). Storms cause drastic shifting in sediment, salinity changes in tidal flats, and redistribution of the macrobenthic community, resulting in low species diversity and distribution and dominance of opportunistic species (Posey et al., 1996; Sukumaran et al., 2016). The impacts of storm disturbance on the macrobenthic community vary depending on the time of disturbances, including frequency and timing relative to recruitment events and life histories of resident fauna (Levin, 1984). The majority of the studies on the storm impact on coastal community structure are focused on the diversity, distribution, and assemblage patterns of benthic communities (Sukumaran et al., 2016). Although a few studies attempted to define the functional nature of the coastal community in response to storms (Posey et al., 1996; Sukumaran et al., 2016), there was a lack of explanation for the ecosystem functioning and the impact of disruption. Species diversity, composition, and abundance have long been utilized in traditional biodiversity research (Reizopoulou & Nicolaidou, 2007). Its findings were insufficient to describe the functioning of the entire ecosystem. Functional diversity (FD) (Petchey & Gaston, 2002; Villéger et al., 2008; Linden et al., 2012; Delfan et al., 2021) was introduced to describe the diversity of functional traits found among a group of species in a given ecosystem (Petchey & Gaston, 2002; Villéger et al., 2008; Linden et al., 2012; Mouillot et al., 2013; Delfan et al., 2021). Functional redundancy is mainly used to describe the resilience of lost species due to any perturbation.

Biological trait analysis (BTA) (Bremner et al., 2006) was used to characterize how the macrobenthic population responds to the storm. The trait-based approach establishes a more systematic connection between ecosystem services and species traits, as the species trait is the primary characteristic by which the organism influences ecosystem processes (Petchey & Gaston, 2002). Most of the studies were based on the feeding habitat trait approach (Posey et al., 1996; Jumars et al., 2016; Sukumaran et al., 2016). Apart from the trophic structure, the functioning of the benthic community is dependent on bioturbation, habitat, mobility, mortality rate, and body size (Donadi et al., 2015). There have been few studies to validate the ecosystem functioning in India's marine benthic system (Vijapure et al., 2019; Bhowmik & Mandal, 2021; Sivadas et al., 2021). This study is the first attempt to investigate the functioning of the marine benthic community in the Andaman and Nicobar Islands. The objective of the present study is to access the effects of the cyclone *Vardah* on the assemblage pattern and the functioning of intertidal soft-bottom macrofauna. We hypothesized that extreme weather events like cyclones can disrupt the functioning of the macrobenthic community by creating a void in niche space and giving the opportunity to other species to fill the niche space.

Sampling and methodology

Study area

The Andaman and Nicobar group of islands is a union territory of India, and its geographical position borders are the Southeast Asian countries (i.e., Thailand, Indonesia, and Myanmar). The archipelago is oriented north–south, coordinates between 6°N and 14°N, and 92°E and 94°E and also covers an area of 8,249 km2. The archipelago consists of 572 islands and islets, out of which 38 are permanently inhabited islands. The Andaman and Nicobar Islands comprise both critical and pristine intertidal ecosystems. On 4th December 2016, a low-pressure area developed over the south Andaman sea, later it turned into a very severe cyclonic storm *Vardah*. At midnight of 7th December, it became a cyclonic storm *Vardah*. On 8th December, it passed the Port Blair coast with a wind speed of 50–60 kph (IMD, 2017). Sampling was conducted at Chatham (CH), Port Blair coast; it was a part of an ongoing investigation on the efficiency of sampling gear (Nosad et al., 2021) for macrobenthic fauna. Hence, only biological samples were collected for the analysis. CH (N11°41′08″ and E092°43′ 23″) was selected for the collection of macrobenthic faunal samples (**Figure 1**). It is located in the northeast part of the Port Blair coast, characterized by the presence of a vast exposed intertidal area, very fine sand sediment, and dissipative beach (Pandey & Thiruchitrambalam, 2019). The lush vegetation of seagrasses (e.g., *Halodule uninervis* and *Thalassia hemprichii*) covers the mid and low tide zone.

Sampling methods

Initial sampling was conducted monthly for 7 months (September 2016–March 2017). Bimonthly sampling was conducted to assess the recruitment time for the macrobenthos for 2 years (April 2017–March 2019) because the recruitment time for the lost species due to perturbation may take several months to years. A total of 171 samples (1 station × 3 replicates × 3 waterlines × 19 samplings) were collected using a 25 × 25 cm quadrate during the study period. The collected sediment was screened through a test sieve with a mesh size of 0.5 mm, Magnesium chloride solution was added as a relaxant. Fixation was done with 5% buffered formalin mixed with rose bengal stain. Faunal groups were separated from the residue, enumerated, labeled, and stored in 70% ethanol for further examination. All taxa were identified up to a possible lower level of Linnaean classification (genus or species).

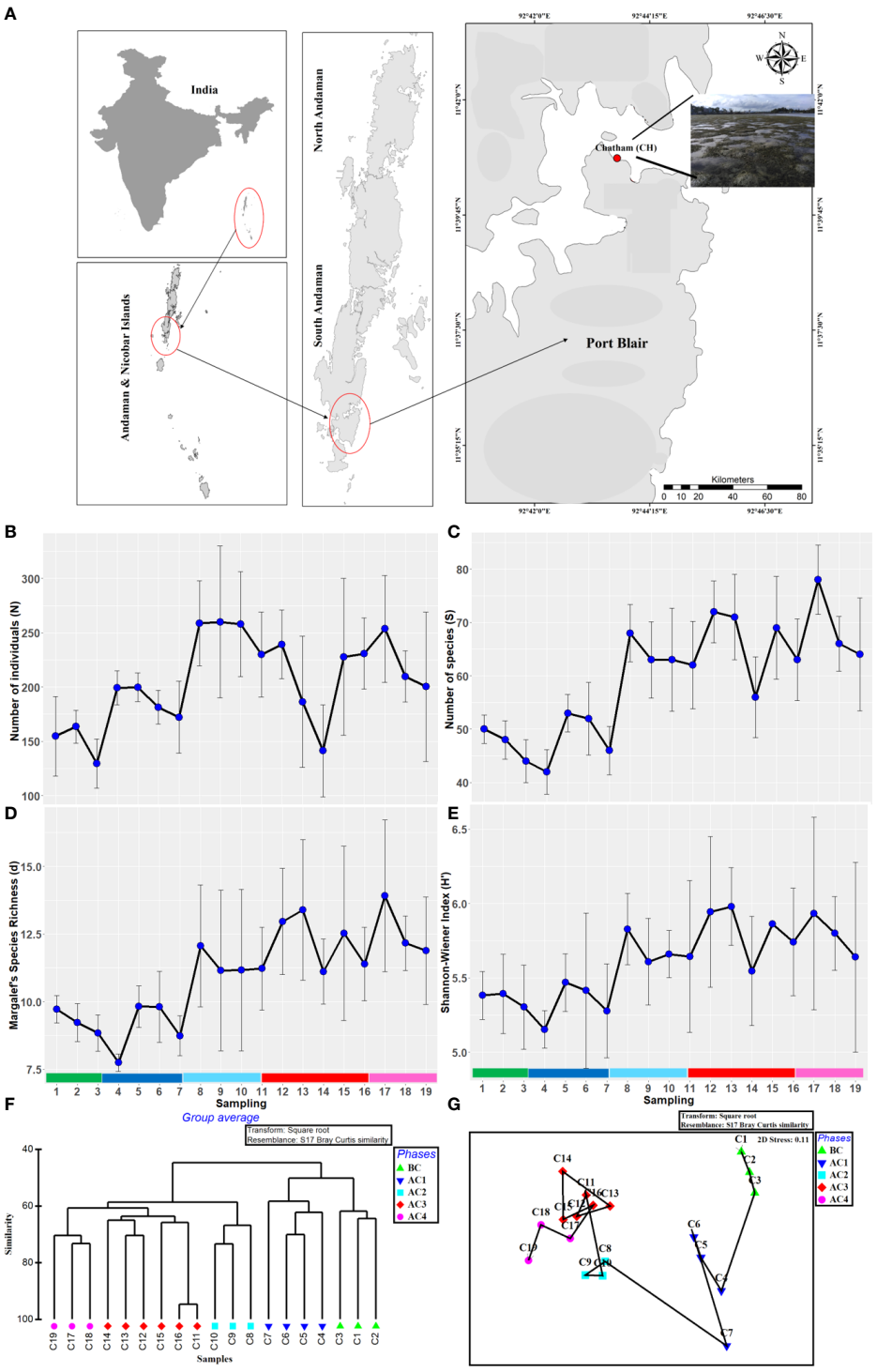

FIGURE 1
(A) Study area map. Macrobenthic community attributes: **(B)** number of individuals, **(C)** number of species, **(D)** Margalef's index, **(E)** Shannon–Wiener index, **(F)** BC similarity dendrogram, and **(G)** nMDS plot. Sample size, n = 9 for panels **(B–E)**. The color shades on the x-axis of line diagram depict cyclonic phases as shown in dendrogram and nMDS plot. BC, before cyclone; AC1, after cyclone phase 1; AC2, after cyclone phase 2; AC3, after cyclone phase 3; AC4, after cyclone phase 4.

Data analysis

Univariate measures include the number of individuals (N ind.m^{-2}), number of species (S), Margalef's species richness (d), Shannon–Wiener diversity (H′ log2), and Evenness (j ′) and Simpson's dominance index (1-Lambda). The collected raw data were pooled into time-series data of 19 samplings (mean of replicates per waterlines). The Bray–Curtis similarity resemblance matrix (after root transformed abundance data) was used to construct a dendrogram and non-metric multidimensional scaling (nMDS) plot. ANOSIM was used to determine the significant difference between the groups. All the analyses were performed using PRIMER v.6 (Clarke and Gorley, 2015). Six biological traits (i.e., bioturbation, ecological group, habitat, mobility, size, and feeding guild) were used for BTA and further subdivided into several modalities according to individual traits (Supplementary Table 1). The Fuzzy coding (Chevene et al., 1994) was implemented to process the abundance data for BTA. Trait data were collected from the online library and online software (e.g., AMBI; MarLIN BIOTIC; http://www.species-identification.org/) and literature (Queirós et al., 2013; Jumars et al., 2016; Ríos-Jara et al., 2009). Principal components analysis (PCA) bi-plot was constructed using CANOCO v4.5. FD was estimated using Rao's quadratic entropy (RaoQ) (Rao, 1982). FD analysis was performed using "FD Package" (Laliberté et al., 2014) in R studio v 4.0.1. Functional redundancy was estimated by taking the ratio between FD and the Shannon–Wiener diversity index (FD/H`) (Linden et al., 2012). Linear regression was applied between FD and H` (Micheli & Halpern, 2005). All the line diagrams and linear regression were done using the "ggplot2" package in R studio v 4.0.1.

Results

Macrobenthic community structure

A total of 96 taxa belonging to 37 families under seven phyla were recorded during the study. Among the groups, *Polychaeta* contributed the highest number of taxa (73 taxa) followed by *Amphipoda* (8 taxa) and *Gastropoda* (6 taxa). A reduction in the species richness of total macrofauna from 45 into 42 taxa and an increase in the number of polychaete taxa from 29 to 35 taxa were noted immediately after the cyclone (AC1). The reduction in the number of taxa was observed immediately after the cyclone in Decapoda and Bivalvia. The number of taxa was increased from the fifth sampling after cyclone (AC) due to the recruitment of additional species in the area (Table 1). A total of 19,949 individuals were recorded during the study. Overall, the number of individuals ranged between 469 and 1,709 ind.m^{-2} (mean: 1050 ± 354 ind.m^{-2}). Polychaetes were numerically important contributing 71% of the total population. The number of individuals increased up to 4% just after the cyclone occurred. Values of diversity indices were decreased after the cyclone; in contrast, the number of individuals increased (5.11%). H` was recorded lowest (5.13 ± 0.12) during the cyclone compared to other sampling periods. Margalef's d values were recorded at all-time low during the cyclone. The number of species, Margalef's d, and Shannon–Wiener diversity showed an increasing trend after AC1 (Figures 1B–D).

At 58% Bray–Curtis similarity, the resulting dendrogram showed five groups representing before the cyclone (BC), after the cyclone phase 1 (AC1), phase 2 (AC2), phase 3 (AC3), and phase 4 (AC4) (Figure 1F). ANOSIM showed a significant difference between these groups (Global R = 0.868, $p < 0.001$), implying distinct assemblages occurred during the timeline of the cyclone. On the nMDS plot, a trajectory was drawn from the first sampling to the last and showed a clear temporal pattern in the macrobenthic faunal assemblages (Figure 1G). The discriminating and characterizing species for each group were listed (Supplementary Table 2).

Biological trait analysis

The results of BTA showed that all traits exhibited more than 80% of the variation in the first two axes of PCA (Supplementary Table 3). Overall crawlers, bio-diffusors, surface deposit feeders, ecological group I, low mobile macrobenthos, and size class of <2cm were characteristics of BC, which were replaced by subsurface deposit feeders, upward and downward conveyers, ecological group IV, mid-mobile macrobenthos, and size class of 2–4 cm immediately after the cyclone (AC1). From the PCA analysis, it was observed that the feeding trait and ecological groups were the important traits for explaining the changes in BC and AC (Figures 2A, B). The most notable observation was that the predominant opportunistic Sub-surface deposit feeders (Ssdf) was represented by *Capitellidae* BC, which was replaced by *Spionidae* immediately AC. Similarly, the predominant bio-diffusors BC was replaced by UC/DC (*Prionospio cirrifera*, *Prionospio pinnata*, etc.) AC. The PCA results for all the traits showed a mixed pattern of trait distribution indicating that the traits in the area are contributing collectively to the functioning of macrobenthos community and are not affected by the temporal variations (Figures 2A–F). Although the trait distribution did not show any changes, variation in faunal assemblages was noticed, implying that the niche spaces of lost species were being filled by new recruits. For example, Sub-surface deposit feeders (Ssdf) was the dominant feeding modality in both the AC3 and AC4 phases where Sub-surface deposit feeders (Ssdf) was represented by *Paradonis armata* and *Orbinia* sp.1 in AC3 and were replaced by *Boccardia* cf. *polybranchia* and *M.indicus* in the AC4 phase. Sometimes, changes in assemblage

TABLE 1 Summary of numerically important species, species that lost due to cyclone and recovered, and new recruit to the station.

	BC	AC1	AC2	AC3	AC4
Phase Duration	Sep. 2016- Nov.2016 (3 months)	Dec.2016-Mar.2017 (4 months)	Apr.2017-Sep.2017 (6 months)	Oct.2017-Sep.2018 (1 year)	Oct.2018-Mar.2019 (6 months)
Numerically Important Species (Means ± SD)	*Notomastus aberrans* (58.66 ± 33.91), *Capitella minima* (43.25 ± 20.6), *Orbinia* sp.1 (31.40 ± 14.63), *Nassarius globusus* (30.22 ± 21.62), *Orbinia* sp.2 (23.11 ± 20.45)	*Malacoceros indicus* (128 ± 58.47), *Orbinia* sp.1 (100.44 ± 78.44), *Prionospio cirrifera* (68 ± 45.56), *P. pinnata* (36.88 ± 29.15), *Syllis* sp. (33.77 ± 15.7)	*Malacoceros indicus* (191.11 ± 27.93), *P. cirrifera* (169.67 ± 77.27), *Orbinia* sp.1 (128.59 ± 14.47), *P. pinnata* (98.07 ± 21), *Capitella singularis* (70.96 ± 39.13)	*Paradonis armata* (693.33 ± 163.36), *Orbinia* sp.1 (563.11 ± 27.25), *Marphysa singuenea* (332.44 ± 24.75), *Armandia intermedia* (310.22 ± 49.45), *Sipuncula nudus* (251.55 ± 16,32)	*Boccardia* cf. *polybranchia* (146.66 ± 52.34), *M. indicus* (105.77 ± 98.66), *C. singularis* (89.33 ± 40.18), *Hyale* sp.1 (61.92 ± 12.74), *Exogone* sp. (57.48 ± 26.9)
New Recruit to the Study Area		*P.*cirrifera[#], *P.*pinnata[#], *Spio* sp.[#], *Pectineria* sp.[#], *Glycera trydactyla*[#], *Urothoe* sp.[#], *Cirriformia filigera*[#], and *Arecidea lopazi*[#]	*Dosnia* sp.[##], *Armandia intermediate*[##], *Odontosyllis* sp.[##], *Chone* sp.[##], *Glycera oxycephala*[##], and 25 other species[##]		
Lost Species		*Nerita* sp*., *Strombus* sp.*, *Dotilla myctiroides**, *Ophiocoma* sp.*, *Microphthalmus convexus**, *Barbita* sp., *Microspio* sp.*, *Paraprionospio* sp.*, and seven other species*	*Ophiocoma* sp.**, *Maldane* sp.**, Spio sp.**, *Pectineria* sp.**, *Phyllodoce* sp.**, and *Prionospio* sp.		
Recovered Species		*Nerita* sp.[$], *Strombus* sp.[$], *Dotilla myctiroides*[$], *Ophiocoma* sp.[$], *Meretrix* sp.[$], *Maldane* sp.[$], *Glycera alba*[$], *Glycera africana*[$], and *Peresiella spatulata*[$]	*Microphthalmus convexus*[$$], *Mututa vector*[$$], *Barbita* sp.[$$], *Trion* sp.[$$], *Microspio* sp.[$$], and *Paraprionospio* sp.[$$]		

[#]New recruited immediately after the cyclone (AC1 phase).
[##]Recruited in phase AC2.
*Lost immediately after the cyclone (AC1 phase).
**Lost during phase 2 (AC2) and never recovered.
[$]Recovered within 1–2 months after cyclone (in AC1).
[$$]Recovered after 4–5 months (in AC2).
Spio sp. and Pectineria sp. were recruited immediately after the cyclone but never recorded after AC1.

patterns are reflected in the modalities for a few traits such as bioturbation. In the PCA, the assemblage of AC2 is dominated by UC/DC but replaced by surface depositors and BD in AC3 (Figure 2E).

Functional diversity, functional redundancy, and recovery

The FD decreased immediately after the cyclone; moreover, the FD was showing a declining trend after the cyclone. However, the FD value was increased after the phase of AC2 (Supplementary Figure 1A). Similarly, the ratio between FD and H` showed a declining pattern immediately after the cyclone until the AC2 phase, it tends to increase afterward, and the highest value was recorded during AC4 (Supplementary Figure 1B). The low FD/H` value indicates high redundancy after the cyclone and the redundancy decreased during the AC4 phase. The linear regression model (Supplementary Figure 1C) showed a positive relationship between H` and FD (R Square: 0.387) with a low slope value of 0.057, indicating the high functional redundancy of macrobenthos during the study period. The high functional redundancy supports the resilience of species in an ecosystem, which was seen during the study. A total of 32 macrobenthos were recruited out of which three opportunistic species were recruited immediately and 29 were recruited in AC2. Seventeen macrobenthos species were lost when the cyclone encountered out of which 10 recovered immediately, whereas 7 species took 4–5 months for recovery. Two species *Spio* sp. and *Prionospio* sp. were encountered for a very short period (only in AC1) and lost throughout the study period (Table 1).

Discussion

An immediate effect of cyclone *Vardah* was observed in both the structure and the function of the macrobenthic community. The resilience of species was observed in the form of shared niches between species. Several studies have concluded that disturbances such as cyclones or tsunamis alter the sediment texture, grain size, and availability of organic matter and other

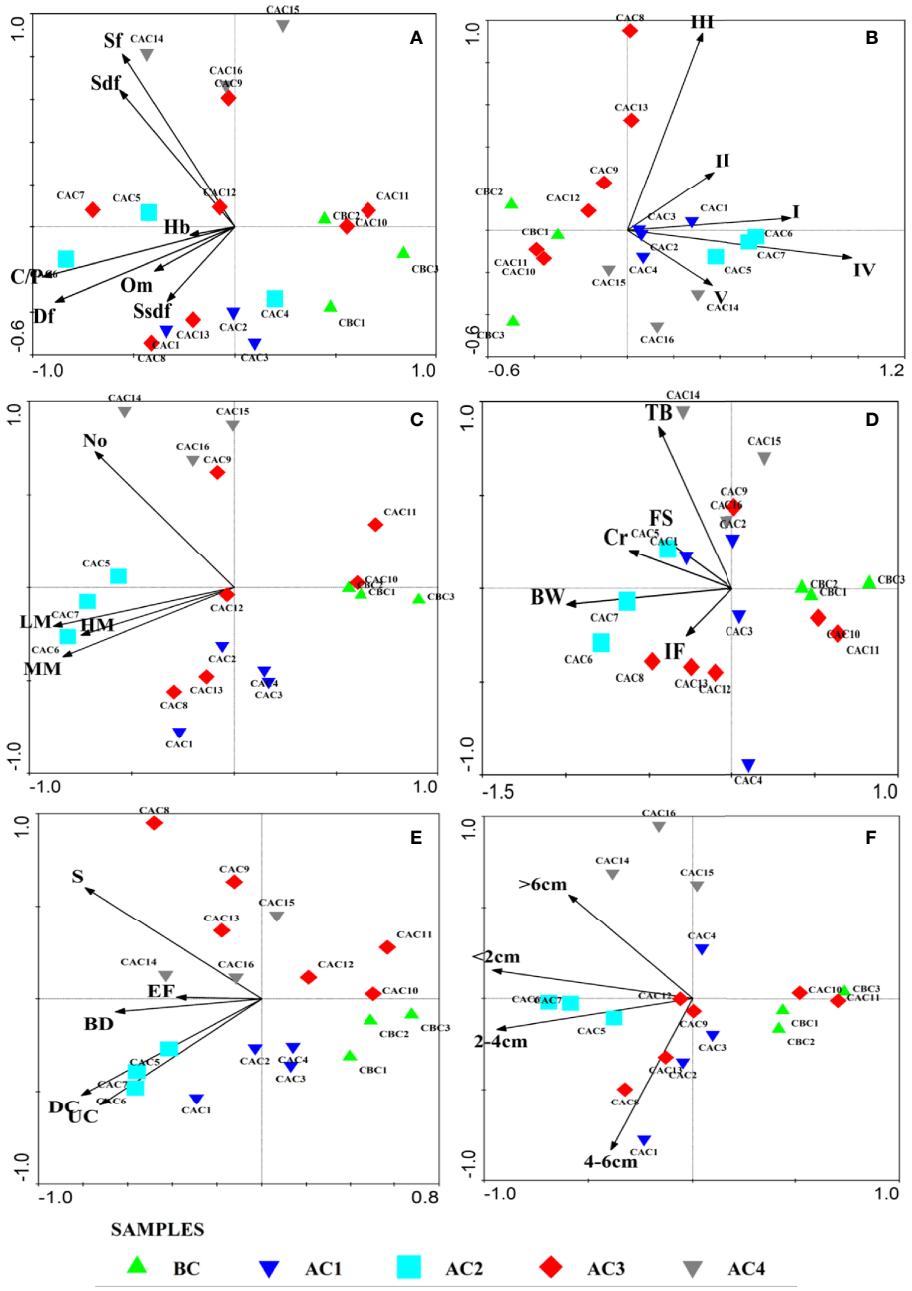

FIGURE 2
PCA bi-plot of different traits. **(A)** Feeding trait, **(B)** ecological groups, **(C)** locomotion, **(D)** habitat, **(E)** bioturbation, and **(F)** size. BC, before cyclone; AC1, after cyclone phase 1; AC2, after cyclone phase 2; AC3, after cyclone phase 3; AC4, after cyclone phase 4.

environmental parameters, which are essential factors for stabilizing the benthic faunal community (Lomovasky et al., 2011; Sukumaran et al., 2016; Sugumaran et al., 2019). The physical disturbance may cause defaunation effects on a large area (Lu & Wu, 2000), which led to the dominance of opportunistic species. The present study found immediate recruitment of opportunistic species such as *P. cirifera*, *P. pinnata*, and *Spio* sp. After the cyclone, which leads to a reduction of species diversity, a similar increase in opportunistic species due to perturbation was recorded elsewhere (Lomovasky et al., 2011; Sukumaran et al., 2016).

Feeding traits and ecological groups were the characterizing functions working immediately AC. It is already established that feeding traits can explain the resource utilization post cyclone

(Sukumaran et al., 2016); however, the use of more traits gives a better picture of ecosystem functioning (Bremner et al., 2006). In most of the studies, it was noticed that the dominance of opportunistic species often leads to a decrease in the number of feeding modalities (Peng et al., 2013). In the current study, feeding modalities were high immediately after the cyclone suggesting opportunistic species performing multiple functions in the ecosystem. Bioturbation is mainly influenced by the size of the organisms, density, and the mode of bioturbation of the residence macrofaunal group (Griffiths et al., 2017). An increase in a large size class, which was mostly predator glycerids, was observed immediately AC, which may be the reason for the increase in the bioturbation trait. All opportunistic species were Ssdf and SDF, and Karlson et al. (2010) have suggested an increase in Ssdf and SDF prevalence in the secondary producers. An increase in secondary producers lures the predators; hence, there was an increase in large size carnivorous group AC. The burrowing activity of organisms can disrupt the sediment and allow the oxygen and detritus penetration to go deep inside the sediment, which further helps in enriching the sediment with organic matter (Aller, 1983). The present study noted an increase in burrowing activities suggesting the reworking of sediment. Moreover, the burrowing activities support other organisms to settle which may be reflected in an increase in diversity in the AC2 phase.

FD is an essential tool to understand the ecosystem functioning (Degen et al., 2018); several studies have been carried out to understand the ecosystem functioning in response to any disturbance or habitat heterogeneity or environmental changes (Micheli & Halpern, 2005; Delfan et al., 2021). The dominance of opportunistic species with the same trait in the community and low species richness can cause a decrease in FD (Leung & Cheung, 2017). A similar reduction in FD was observed immediately AC due to an increase in the number of opportunistic species. Species diversity and FD are linearly correlated (Wong & Dowd, 2015; Leung & Cheung, 2017), so a decrease in species diversity can also cause a decrease in FD. The low FD can also define that the community relies on local retention rather than dispersal species from other areas (Boström et al., 2010). This can lead to the recovery of lost species due to the cyclone. Functional redundancy positively affects species resilience due to any perturbation (Biggs et al., 2020). The present study showed a high FD/H` value during AC4 and a low value up to the AC2 phase which means that the redundancy was highest immediately after the cyclone and gradually reduced in time. The value of slope obtained from the linear regression was close to zero, which denotes a high-redundancy value. High redundancy suggests that the availability of niche space is also high and multiple species have similar functions (Mason et al., 2005; Micheli & Halpern, 2005). The low FD and high redundancy during the cyclone imply an immediate effect of the cyclone on the macrobenthic community. The retention of local species made the platform for the resilience of lost species. Ecological communities with more redundant species are more likely to display resilience or gather stability than the community having low redundant species (Biggs et al., 2020). Although there are limited studies on the impact of the cyclone on the ecosystem functioning of the benthic organisms, we can still relate a part of our results to Sukumaran et al. (2016), where the cyclone *Phyan* affected the feeding trait of the polychaete community. The present study found similar results where feeding traits shifted due to the effect of cyclone *Vardah*. Gamito et al. (2012) suggested that a large-scale meteorological disturbance can cause recolonization by introducing larvae, juveniles, or adults from a faraway area to the location and can alter the species composition of the area. Similar results were observed during the study where six species were recruited newly to the location in the AC1 phase.

Conclusion

An immediate reduction in the diversity indices and shifting assemblage pattern of macrobenthos was observed, suggesting that cyclone has an immediate effect on macrobenthos rather than the long term. The effect resulted in the loss of species and a new recruit of species to the station. The dominant of opportunistic species demonstrated performing multiple functions aiming to occupy the niche space of lost species. Overall, the functional approach was more evident and explanatory in detecting the impact than general community attributes; hence, the use of the functional approach is recommended in similar studies. Finally, the recovery time for the lost species differs for different species as some recovered immediately, some took 4–5 months, and some species never recovered. The lack of environmental variables is a limitation of this study.

Data availability statement

The original contributions presented in the study are included in the article/supplementary material. Further inquiries can be directed to the corresponding author.

Author contributions

NS: Collection and analysis of samples, processing of data, writing-original draft, statistical analysis. RL: Analysis and taxonomic identification of macrobenthos. GT: Conceptualization, sampling design, data validation and reviewing and editing. All authors contributed to the article and approved the submitted version.

Acknowledgments

The authors are thankful to the authorities of Pondicherry University for providing the laboratory facilities and the University fellowship to (SN) for carrying out this research work. We thank the reviewers for their valuable suggestions. This work is dedicated to Late Prof. Akkur V. Raman, Andhra University, Visakhapatnam, an eminent marine biologist and a pioneer in the field of marine benthic ecology and coastal pollution research in India.

Conflict of interest

The authors declare that the research was conducted in the absence of any commercial or financial relationships that could be construed as a potential conflict of interest.

Publisher's note

All claims expressed in this article are solely those of the authors and do not necessarily represent those of their affiliated organizations, or those of the publisher, the editors and the reviewers. Any product that may be evaluated in this article, or claim that may be made by its manufacturer, is not guaranteed or endorsed by the publisher.

Supplementary material

The Supplementary Material for this article can be found online at: https://www.frontiersin.org/articles/10.3389/fmars.2022.953985/full#supplementary-material

References

Aguttes, J. P., Schrive, J., Goldstein, C., Rouze, M., and Raju, G. (2000). MEGHA- TROPIQUES, a satellite for studying the water cycle and energy exchanges in the tropiques. *Int. Geosci. Remote Sens. Symposium (IGARSS)* 7, 3042–3044. doi: 10.1109/igarss.2000.860329

Aller, R. C. (1983). The importance of the diffusive permeability of animal burrow linings in determining marine sediment chemistry. *J. Mar. Res.* 41 (2), 299–322. doi: 10.1357/002224083788520225

Balica, S. F., Wright, N. G., and van der Meulen, F. (2012). A flood vulnerability index for coastal cities and its use in assessing climate change impacts. (*Natural Hazards*), 64(1), 73–105. doi: 10.1007/s11069-012-0234-1

Bhowmik, M., and Mandal, S. (2021). Do seasonal dynamics influence traits and composition of macrobenthic assemblages of sundarbans estuarine system, India? *Oceanologia* 63 (1), 80–98. doi: 10.1016/j.oceano.2020.10.002

Biggs, C. R., Yeager, L. A., Bolser, D. G., Bonsell, C., Dichiera, A. M., Hou, Z., et al. (2020). Does functional redundancy affect ecological stability and resilience? a review and meta-analysis. *Ecosphere* 11 (7), e03184. doi: 10.1002/ecs2.3184

Boström, C., Törnroos, A., and Bonsdorff, E. (2010). Invertebrate dispersal and habitat heterogeneity: expression of biological traits in a seagrass landscape. *J. Exp. Mar. Biol. Ecol.* 390 (2), 106–117. doi: 10.1016/j.jembe.2010.05.008

Bremner, J., Rogers, S. I., and Frid, C. L. J. (2006). Matching biological traits to environmental conditions in marine benthic ecosystems. *J. Mar. Syst.* 60, 302–316. doi: 10.1016/j.jmarsys.2006.02.004

Chevene, F., Doleadec, S., and Chessel, D. (1994). A fuzzy coding approach for the analysis of long-term ecological data. *Freshw. Biol.* 31 (3), 295–309. doi: 10.1111/j.1365-2427.1994.tb01742.x

Clarke, K. R., and Gorley, R. N. (2015). *Primer v.7: User Manual/Tutorial* (Plymouth: PRIMER-e), 296pp.

Degen, R., Aune, M., Bluhm, B. A., Cassidy, C., Kędra, M., Kraan, C., et al. (2018). Trait-based approaches in rapidly changing ecosystems: A roadmap to the future polar oceans. *Ecol. Indic.* 91 (1), 722–736. doi: 10.1016/j.ecolind.2018.04.050

Delfan, N., Ghodrati, M., and Naderloo, R. (2021). Patterns of structural and functional diversity of macrofaunal communities in a subtropical mangrove ecosystem. *Estuarine Coast. Shelf Sci.* 252, 107288. doi: 10.1016/j.ecss.2021.107288

Donadi, S., Klemens, B., Alexander, K., and Dorothee, L. (2015). The body-size structure of macrobenthos changes predictably along gradients of hydrodynamic stress and organic enrichment. *Mar. Biol.* 162, 675–685. doi: 10.1007/s00227-015-2614-z

Gamito, S., Patrício, J., Neto, J. M., Teixeira, H., and Carlos, J. (2012). Feeding diversity index as complementary information in the assessment of ecological quality status. *Ecol. Indic.* 19, 73–78. doi: 10.1016/j.ecolind.2011.08.003

Griffiths, J. R., Kadin, M., Nascimento, F. J. A., Tamelander, T., Törnroos, A., Bonaglia, S., et al. (2017). The importance of benthic–pelagic coupling for marine ecosystem functioning in a changing world. *Global Change Biol.* 23 (6), 2179–2196. doi: 10.1111/gcb.13642

IMD (2017) *India Meteorological department, cyclone warning division, government of India new Delhi*. Available at: https://rsmcnewdelhi.imd.gov.in/uploads/report/26/26_af079d_vardah.pdf.

Jumars, P. A., Dorgan, K. M., and Lindsay, S. M. (2016). Diet of worms emended: An update of polychaete feeding guilds diet of worms emended: An update of polychaete feeding guilds. *Annu. Rev. Mar. Sci.* 7, 497–520. doi: 10.1146/annurev-marine-010814-020007

Karlson, A. M. L., Nascimento, F. J. A., Näslund, J., and Elmgren, R. (2010). Higher diversity of deposit-feeding macrofauna enhances phytodetritus processing. *Ecology* 91 (5), 1414–1423. doi: 10.1890/09-0660.1

Laliberté, E., Legendre, P., and Shipley, B. (2014). FD: measuring functional diversity from multiple traits, and other tools for functional ecology. r package version 1.0-12. *Ecology* 91, 299–305.

Leung, J. Y. S., and Cheung, N. K. M. (2017). Can mangrove plantations enhance the functional diversity of macrobenthic community in polluted mangroves? *Mar. pollut. Bull.*, 116 (1–2), 454–461. doi: 10.1016/j.marpolbul.2017.01.043

Levin, L. A. (1984). Life history and dispersal patterns in a dense infaunal polychaete assemblage: Community structure and response to disturbance ecology, vol. *65 No. 4 (Aug. 1984)* pp, 1185–1200.

Linden, P., Patrício, J., Marchini, A., Cid, N., Magalhães, J., and Carlos, J. (2012). A biological trait approach to assess the functional composition of subtidal benthic communities in an estuarine ecosystem. *Ecol. Indic.* 20, 121–133. doi: 10.1016/j.ecolind.2012.02.004

Lomovasky, B. J., Firstater, F. N., Gamarra, A., Mendo, J., and Iribarne, O. O. (2011). Macro benthic community assemblage before and after the 2007 tsunami and earthquake at paracas bay, Peru. *J. Sea Res.* 65 (2), 205–212. doi: 10.1016/j.seares.2010.10.002

Lu, L., and Wu, R. S. S. (2000). An experimental study on recolonization and succession of marine macrobenthos in defaunated sediment. *Mar. Biol.* 136 (2), 291–302. doi: 10.1007/s002270050687

Mason, N. W. H., Mouillot, D., Lee, W. G., and Wilson, J. B. (2005). Functional richness, functional evenness and functional divergence: The primary components of functional diversity. *Oikos* 111 (1), 112–118. doi: 10.1111/j.0030-1299.2005.13886.x

Micheli, F., and Halpern, B. S. (2005). Low functional redundancy in coastal marine assemblages. *Ecol. Lett.* 8 (4), 391–400. doi: 10.1111/j.1461-0248.2005.00731.x

Mouillot, D., Graham, N. A. J., Villéger, S., Mason, N. W. H., and Bellwood, D. R. (2013). A functional approach reveals community responses to disturbances. *Trends Ecol. Evol.* 28 (3), 167–177. doi: 10.1016/j.tree.2012.10.004

Nosad, S., Ganesh, T., and Kiran, L. R. (2021). Efficiency of sampling gears (Quadrate and core) and taxonomic resolution on the soft bottom intertidal macrobenthic community of port Blair coast. *Res. J. Chem. Environ.* 25 (11), 93–103. doi: 10.25303/2511rjce93103

Pandey, V., and Thiruchitrambalam, G. (2019). Spatial and temporal variability of sandy intertidal macrobenthic communities and their relationship with environmental factors in a tropical island. *Estuarine Coast. Shelf Sci.* 224, 73–83. doi: 10.1016/j.ecss.2019.04.045

Peng, S., Zhou, R., Qin, X., Shi, H., and Ding, D. (2013). Application of macrobenthos functional groups to estimate the ecosystem health in a semi-enclosed bay. *Mar. pollut. Bull.* 74 (1), 302–310. doi: 10.1016/J.MARPOLBUL.2013.06.037

Petchey, O. L., and Gaston, K. J. (2002). Functional diversity (FD), species richness and community composition. *Ecol. Lett.* 5 (3), 402–411. doi: 10.1046/j.1461-0248.2002.00339.x

Posey, M., Lindberg, W., Alphin, T., and Vose, F. (1996). Influence of storm disturbance on an offshore benthic community. *Bull. Mar. Science.* 59 (3), 523–529.

Queirós, A. M., Birchenough, S. N. R., Bremner, J., Godbold, J. A., Parker, R. E., Romero- Ramirez, A., et al. (2013). A bioturbation classification of European marine infaunal invertebrates. *Ecol. Evol.* 3 (11), 3958–3985. doi: 10.1002/ece3.769

Rao, C. R. (1982). Diversity and dissimilarity coefficients: A unified approach. *Theor. Population Biol.* 21 (1), 24–43. doi: 10.1016/0040-5809(82)90004-1

Reizopoulou, S., and Nicolaidou, A. (2007). Index of size distribution (ISD): A method of quality assessment for coastal lagoons. *Hydrobiologia* 577 (1), 141–149. doi: 10.1007/s10750-006-0423-6

Ríos-Jara, E., Ceciel-M. Navarro-Caravantes, Cristian-M. Galván-Villa and Ernesto Lopez-Uriarte, (2009). Bivalves and gastropods of the gulf of tehuantepec, mexico: A checklist of species with notes on their habitat and local distribution. *J. Mar. Sci.* vol. 2009, Article ID 176801, 12. doi: 10.1155/2009/176801

Sivadas, S. K., Gupta, G. V. M., Kumar, S., and Ingole, B. S. (2021). Trait-based and taxonomic macrofauna community patterns in the upwelling ecosystem of the southeastern Arabian sea. *Mar. Environ. Res.* 170, 105431. doi: 10.1016/j.marenvres.2021.105431

Sugumaran, J., Padmasai, R., and Altaff, K. (2019). The effects of tropical cyclone gaja on sandy beach meiofauna of palk. *Region. Stud. Mar. Sci.* 31, 100747. doi: 10.1016/j.rsma.2019.100747

Sukumaran, S., Vijapure, T., Kubal, P., Mulik, J., Rokade, M. A., Salvi, S., et al. (2016). Polychaete community of a marine protected area along the West coast of India-prior and post the tropical cyclone, phyan. *PLoS One* 11 (8), 1–18. doi: 10.1371/journal.pone.0159368

Vasudha, M. (2017). Observation of cyclone occurred in Arabian Sea and bay of Bengal from SAPHIR sensor data. *Int. J. Appl. Eng. Res.* 12 (22), 12821–12832.

Vijapure, T., Sukumaran, S., Neetu, S., and Chandel, K. (2019). Macrobenthos at marine hotspots along the northwest Indian inner shelf: Patterns and drivers. *Mar. Environ. Res. 144(August* 2018), 111–124. doi: 10.1016/j.marenvres.2018.12.007

Villéger, S., Mason, N. W. H., and Mouillot, D. (2008). New multidimensional functional diversity indices for a multifaceted framework in functional ecology. *Ecology* 89 (8), 2290–2301. doi: 10.1890/07-1206.1

Wong, M. C., and Dowd, M. (2015). Patterns in taxonomic and functional diversity of macrobenthic invertebrates across seagrass habitats: A case study in Atlantic Canada. *Estuaries Coasts* 38, 2323–2336. doi: 10.1007/s12237-015-9967-x

frontiers | Frontiers in Marine Science

TYPE Original Research
PUBLISHED 24 August 2022
DOI 10.3389/fmars.2022.919423

Check for updates

OPEN ACCESS

EDITED BY
Meilin Wu,
South China Sea Institute of Oceanology (CAS), China

REVIEWED BY
Guangzhe Jin,
Guangdong Ocean University, China
Rui Bao,
Ocean University of China, China
Yongquan Yuan,
Institute of Oceanology (CAS), China
Chin-Chang Hung,
National Sun Yat-sen University, Taiwan

*CORRESPONDENCE
Weidong Zhai
wdzhai@126.com

SPECIALTY SECTION
This article was submitted to Marine Pollution, a section of the journal Frontiers in Marine Science

RECEIVED 13 April 2022
ACCEPTED 01 August 2022
PUBLISHED 24 August 2022

CITATION
Guo C, Yang S, Zhai W, Niu Y and Liu C (2022) Biological–physical oceanographic coupling influencing particulate organic matter in the South Yellow Sea.
Front. Mar. Sci. 9:919423.
doi: 10.3389/fmars.2022.919423

COPYRIGHT
© 2022 Guo, Yang, Zhai, Niu and Liu. This is an open-access article distributed under the terms of the Creative Commons Attribution License (CC BY). The use, distribution or reproduction in other forums is permitted, provided the original author(s) and the copyright owner(s) are credited and that the original publication in this journal is cited, in accordance with accepted academic practice. No use, distribution or reproduction is permitted which does not comply with these terms.

Biological–physical oceanographic coupling influencing particulate organic matter in the South Yellow Sea

Congcong Guo[1], Shu Yang[1], Weidong Zhai[1,2]*, Yao Niu[3] and Chunli Liu[3]

[1]Institute of Marine Science and Technology, Shandong University, Qingdao, China, [2]Frontier Research Center, Southern Marine Science and Engineering Guangdong Laboratory (Zhuhai), Zhuhai, China, [3]Marine College, Shandong University, Weihai, China

Using total suspended matter (TSM), particulate organic carbon (POC), and particulate nitrogen data, this study investigated the potential vertical POC flux and transport in the South Yellow Sea (SYS). The biogenic production and resuspension fraction (i.e., the proportion of resuspended particles in TSM) were estimated using an ecosystem model and a vertical mixing model. They were verified against reported sediment trap and primary productivity data. The estimates of resuspension fraction showed substantial uncertainty of 50% in summer likely owing to the potential errors of model parameter estimation and the influence of other unexplored biophysical processes such as biological degradation, upwelling, and monsoons; however, the estimates of resuspension fraction showed less uncertainty in other seasons (<20%). Few previous studies have considered the specific influence of resuspension on the dynamics and budget of particulate organic matter (POM) in the SYS. This study proposed a reasonably simple and effective method to address this issue, which was applied to systematic examination of the variation of vertical POM flux with the change of coupled biological–physical oceanographic processes along the Subei coast and in the SYS central basin. The influence of horizontal transport from the Subei coast to the central basin may cause an overestimation of >10% of the resuspension fraction. It will be necessary to acquire additional field data covering a larger spatiotemporal scale to establish an integrated network of the SYS carbon budget.

KEYWORDS

particulate organic matter, biogeochemical modeling, biophysical processes, South Yellow Sea, particle flux, horizontal transport

1 Introduction

The continental shelf and marginal seas receive large amounts of particulate organic matter (POM) and nutrients from terrestrial systems (Walsh, 1991; Brink, 2016), contributing up to 14%–30% of global primary production (Longhurst, 1995; Hedges et al., 1997; Gattuso et al., 1998; Wieder et al., 2015). Terrestrial inputs and primary production provide multiple sources of coastal POM, inducing remarkable spatiotemporal variations (Wassmann, 1990; Trefry et al., 1994; McKee et al., 2004). Such terrestrial and biogenic materials can be transported to the open ocean by alongshore flows and cross-shelf water exchange (Zhou F. et al., 2015; Brink, 2016). The notable biogeochemical dynamics in these shelf regions are important for the production, deposition, degradation, and burial of organic carbon/nitrogen (Ducklow et al., 2001; Volkman and Tanoue, 2002; Oguri et al., 2003; Zhao et al., 2021).

The regional variability in carbon reservoirs from the continental shelf to the open ocean and the preservation/burial of organic carbon are associated with hydrodynamics, sedimentary dynamics, and water column depth (Oguri et al., 2003; Zhou C. et al., 2015; Liénart et al., 2018). For example, large amounts of POM in the water column of shallow shelf systems are derived from tide-induced and/or current-induced sediment resuspension (Bale and Morris, 1998; Hung et al., 2013; Bian et al., 2013a). Therefore, POM dynamics in marginal seas are subject to both vertical (surface–bottom water) and horizontal (inshore–offshore and/or alongshore) transport and exchanges (Schneider et al., 2003; Wang et al., 2008; Ye et al., 2017; Liénart et al., 2018).

The South Yellow Sea (SYS) and the adjacent East China Sea (ECS) are both important marginal seas of the western North Pacific. They receive large amounts of soil-derived and marine-derived particulate matter *via* the discharge of large rivers and local phytoplankton blooms (Beardsley et al., 1985; Zhu et al., 2009; Milliman and Farnsworth, 2011). Sediment traps and ^{234}Th/^{238}U disequilibrium have been adopted to estimate the carbon fluxes in the SYS and ECS (Sheu et al., 1999; Iseki et al., 2003; Oguri et al., 2003; Guo et al., 2010). In the SYS, the downward particulate organic carbon (POC) flux at the bottom of the euphotic zone and/or at the bottom of the thermocline is in the range of 176–342 mg C m^{-2} d^{-1} (Zhang et al., 2004; Guo et al., 2010). In the ECS, the sediment-trap-based POC flux varies from 600 mg C m^{-2} d^{-1} on the inner shelf to 52 mg C m^{-2} d^{-1} at the shelf break (Iseki et al., 2003), with the averaged ^{234}Th-derived POC flux (based on the ^{234}Th deficit relative to ^{238}U and the POC to ^{234}Th ratio) of 99 mg C m^{-2} d^{-1} in the offshore region (Bi et al., 2013). Additionally, the combination of primary production and sediment oxygen consumption and accumulation rates can also provide a perspective of the carbon budget regarding POC production and burial (Song et al., 2016; Qiao et al., 2017). Other than interpretation of direct observations, both hydrodynamic and ecosystem dynamic models have been applied to study POC dynamics in terms of cross-shelf transport, sediment resuspension, and biological production in marginal seas (Schartau et al., 2007; Zhou C. et al., 2015; Zhang and Wu, 2018).

Earlier studies have conducted comprehensive assessment of the carbon fluxes on the continental shelf and at the Okinawa Trough in the ECS, revealing substantial dynamics in cross-shelf transport, deposition, and resuspension under the combined influence of the Changjiang water discharge and the Kuroshio Current (Iseki et al., 2003; Zhu et al., 2006; Li et al., 2016). In the SYS, the fluxes and components of sinking particles have also been studied using sediment trap data (Guo and Zhang, 2005; Guo et al., 2010), but the relationship between the fluxes and biological and physical forcings remains unclear. Wan et al. (2005) used a box model in examining the variability of biomass carbon in the central cold water mass and its correlation with the POC pool, but they overlooked the influence of physical processes. Some other studies have used hydrodynamic models in analyzing the route of suspended sediment transport (Li et al., 2016; Zhong et al., 2020). Unfortunately, such models require complex parameterization, and they aim at understanding physical forcings.

The quantitative estimation of resuspension ratio is challenging, as the resuspension process is highly related to bottom shear stress, sediment grain size, and wind–wave conditions (Bengtsson et al., 1990; Evans, 1994). Previous studies have seldom quantitatively estimated sediment resuspension in the SYS and ECS. Guo and Zhang (2005); Guo et al. (2010); Hung et al. (2013), and Hung et al. (2016) have estimated resuspension ratios and used them in correcting the sediment trap-based sinking flux estimation. However, these resuspension ratios are site-specific and thus highly variable in a given region. An integrated evaluation of the resuspension activity over the SYS/ECS is necessary for better understanding of the framework of sediment resuspension. Additionally, the measurements of radiocarbon (Δ^{14}C) and aluminum contents in sinking particles have suggested that lithogenic particles derived from the adjacent riverine discharges may contribute sinking fluxes over the continental shelves (Hwang et al., 2008; Hwang et al., 2010), indicating that the lateral transport needs to be considered as a potential influencing factor when calculating the resuspension ratio.

The present study addressed this important issue using total suspended matter (TSM), POC, and particulate nitrogen (PN) data and examined the potential vertical POC flux and subsequent transport in the SYS using different models. We combined an ecosystem model and a vertical mixing model to investigate how biogenic processes, resuspension, and potential horizontal cross-shelf transport (i.e., from coastal areas to the

central region) might contribute to the carbon budget between the Subei coast and central SYS basin. The ecosystem model was used to estimate the carbon/nitrogen dynamics of phytoplankton, heterotrophs, and detritus, although we had no means of judging the accuracy of the model results because it is difficult for us to precisely divide TSM into contributions of phytoplankton, heterotrophs, and detritus. However, the findings of this study support a comprehensive understanding of how POM dynamics and stoichiometries reflect a coupled response to biological and physical forcings both seasonally and spatially (from the Subei coast to the central SYS basin) in a marginal sea.

2.Materials and methods

2.1. Study area

This study focused on two subregions of the SYS: the Subei coast region and the central basin (Figure 1). The Subei coast region is near the Subei Shoal with a hydrological regime driven by vertical mixing and coastal currents. Its average depth is <20 m, which means robust resuspension due to strong bottom stress and turbulent kinetic energy (Graber et al., 1989; Bian et al., 2013a). The region has been affected by large-scale green macroalgal blooms (i.e., green tides of *Ulva prolifera*) since 2007 owing to eutrophication (Liu et al., 2009; Liu et al., 2013; Wang et al., 2015). The central basin has an average depth of >70 m. Its variability of biogeochemical dynamics is substantial with moderate mixing in winter, phytoplankton blooms in spring/autumn, and stratification in summer (Lin et al., 2005; Fu et al., 2009).

The study area exhibits distinct hydrodynamic patterns in the spatial framework between western coastal waters and offshore waters (Figure 1A). The coastal currents include principally the Subei Coastal Current (SCC) and Changjiang Diluted Water (CDW), which carry large amounts of nutrients and terrestrial material, thereby notably shaping the biogeochemical characteristics of these biogenic elements and thus the phytoplankton community (Shi et al., 2003; Lin et al., 2005; Zhou et al., 2008; Wang et al., 2013). The Subei Shoal near the Jiangsu coast is characterized by sandy and tidal hydrology with a depth of <10 m, presenting a marked pattern of sediment transport dynamics (Wang et al., 2011; Liu et al., 2013b). The central region of the SYS constitutes a stratified and enclosed regime accompanied by seasonal variation of the Yellow Sea Cold Water Mass (YSCWM). Substantial water exchange occurs with the ambient seas on the southern or southeastern side of the SYS, e.g., intrusion of the Taiwan Warm Current through the SYS–ECS boundary (Chen, 2009) and invasion of the Yellow Sea Warm Current (Figure 1A) that originates from the Tsushima Current.

The environmental conditions have distinct seasonal variation in the central basin and the Subei coast region (Figure 2). Temporal variation of sea surface temperature (SST) shows a seasonal cycle from low values in winter (~7°C) to high values in summer (~27°C) (Figure 2A). The SSTs of the central basin and the Subei coast are similar throughout the year, and the seasonal cycle is notable for photosynthetic active radiation (PAR), with maximum and minimum values occurring in spring/summer (49 mol photons m^{-2} d^{-1}) and winter/autumn (14 mol photons m^{-2} d^{-1}), respectively (Figure 2B). The mixed layer depth (MLD) in the central basin has marked seasonal contrast, deepening in winter (71 m) and shallowing in summer (12 m), whereas the seasonal variation of MLD is small in the Subei coast region throughout the year (Figure 2C). Dissolved inorganic nitrogen (DIN) in the central

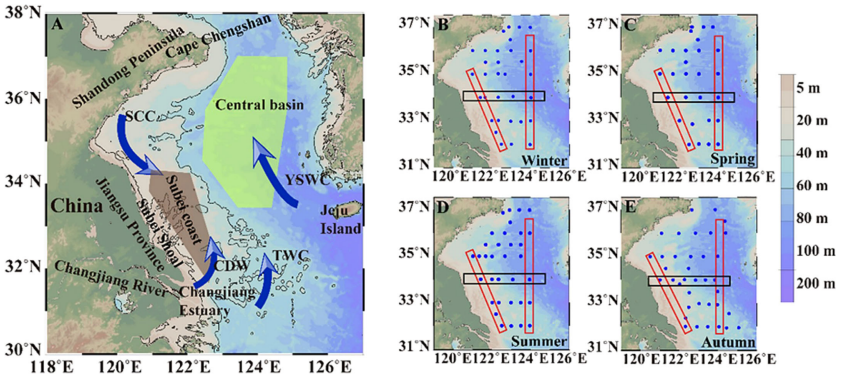

FIGURE 1
Area map and sampling stations. The Subei coast region and central basin are marked by colored polygons. The arrows in panel **(A)** denote the main ocean currents: SCC, Subei Coastal Current; CDW, Changjiang Diluted Water; TWC, Taiwan Warm Current; YSWC, Yellow Sea Warm Current. In panels **(B–E)**, red and black rectangles sketch those featured transects, including coastal and central sections (red rectangles) and the 34°N section (black rectangles).

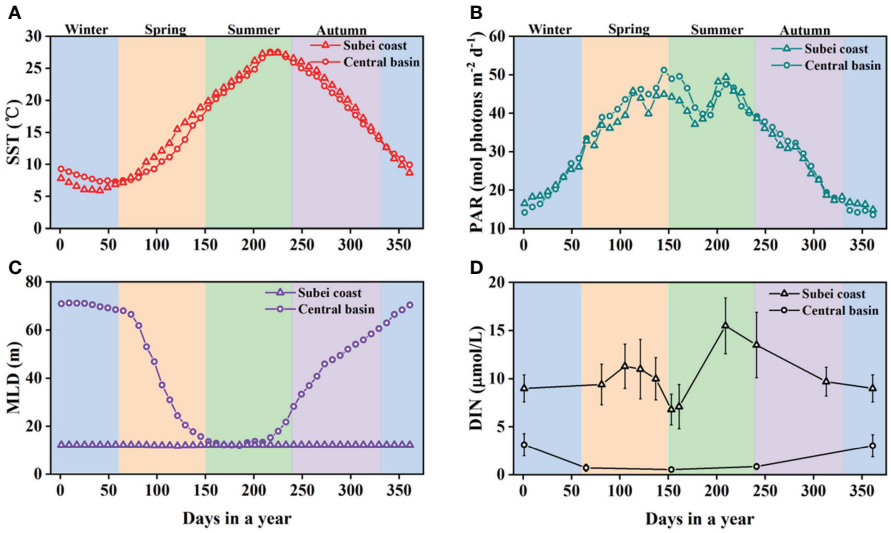

FIGURE 2
Temporal variations of sea surface temperature (SST, **A**), photosynthetic active radiation (PAR, **B**), mixed layer depth (MLD, **C**), and dissolved inorganic nitrogen (DIN, **D**) in the central basin of the South Yellow Sea (SYS) and the Subei coast region. Remote sensing data of 8-day SST, PAR, and MLD with 4-km spatial resolution were used to present their temporal variations throughout the year (https://oceancolor.gsfc.nasa.gov/). The SST, PAR, and MLD data are displayed as mean climatological data from the previous two decades, as reported by Niu et al. (2021). Observational DIN data are obtained from those seasonal sampling surveys at the surface or above the mixed layer (Shi et al., 2015; Guo et al., 2020; Wang et al., 2020). The continuous change of DIN throughout a year was derived by linearly interpolating the seasonal average.

basin decreases with seasonal progression from winter to summer (Figure 2D). However, DIN in the Subei coast region exhibits little seasonal change because of the multiple nutrient sources, e.g., the SCC and vertical mixing during winter and autumn and the CDW during spring and summer. The reported DIN concentration in the Subei coast region has an annual average value of ~10 μmol L^{-1}. During summer, the phenomena of high and low DIN concentrations in the Subei coast region and the central basin are correlated with the robust nutrient input from the CDW in the former and the stratified water column in the latter, respectively.

2.2. Sampling and analyses

Four field surveys were conducted in the SYS between late 2017 and 2019, covering the four seasons (Figures 1B–E). The winter, spring, and summer cruises were conducted by the R/V "*Dongfanghong 2*" during 18 December 2017 to 18 January 2018, 28 March to 16 April 2018, and 24 July to 8 August 2018, respectively. The autumn survey was performed by the R/V "*Lanhai 101*" during 10–19 October 2019. Three water depth samples were collected at each station in the coastal region (surface layer, 2–4 m; middle layer, 7–10 m; bottom layer, 13–25 m), and three or four water depth samples were collected in the central region (surface layer, 2–5 m; subsurface layer, 15–20 m; middle layer, 30–45 m; bottom layer, 55–75 m). Water samples were collected using an onboard Rosette sample system equipped with a conductivity–temperature–depth (CTD) instrument (Seabird 19 Plus). Additional hydrological parameters including temperature, salinity, turbidity, and depth were also measured simultaneously *via* the CTD sensors. High-resolution CTD data were not acquired during autumn. Turbidity data were corrected using the measured TSM (Figure S1) and presented with the unit of milligrams of TSM per liter (mg TSM L^{-1}). Water turbidity values of the middle/bottom layers in the coastal SYS during summer were above the measurement range of the CTD probe when TSM was >10 mg L^{-1} (Figure S1B). Therefore, the CTD turbidity data were available for the central SYS only during summer. The MLD was defined as the depth at which the temperature changed by 0.2°C relative to that at the reference depth of 3 m (Chu et al., 1997). The total number of samples obtained in this study were 108 (9 in the Subei coast region and 47 in the central basin), 84 (9 in the Subei coast region and 33 in the central basin), 116 (8 in the Subei coast region and 41 in the central basin), and 124 (9 in the Subei coast region and 39 in the central basin) in winter, spring, summer, and autumn, respectively.

A certain volume of each sample, extracted for particulate matter analysis (depending on the site: 0.5–2 L in the coastal region; 3–5 L in the central region), was filtered through glass fiber filters (GF/F, 47-mm diameter, Whatman). These filters were preweighed and precombusted in a muffle furnace at 450°C for 5 h. After filtration, these filters were rinsed three

times with ultrapure water. Subsequently, they were folded and wrapped in precombusted aluminum foil and then preserved at −20°C until required for analysis in the laboratory. Prior to analysis, filters were fully dried in a vacuum freeze dryer for at least 24 h. Each dried filter was weighed and then quantitatively divided into two parts. The first part was used to determine particulate carbon and nitrogen; the second part was fumed with 15 ml of 36% HCl for removal of carbonate and then redried for POC measurement. Determination of these elements was performed using a Costech ECS4024 Elemental Analyzer following the standard CHN analysis method by combusting the filters at high temperature (Sharp, 1991). The standard curve was obtained using standard methionine (NC Technologies). The detection limit for carbon was 0.002 mg C ($R^2 > 0.99$) and that for nitrogen was 0.005 mg N ($R^2 > 0.99$). A methodological problem is that the protocol for removing carbonate is inefficient for the removal of inorganic N, which means that the residual N after fuming is actually the total nitrogen consisting of both organic and inorganic parts (Meyers, 2003; Bianchi and Bauer, 2011). Hence, the N composition of the suspended POM is hereafter represented by PN. The mass of TSM was taken as the dry weight difference of the filters before and after filtration.

2.3. Model construction and parameter selection

We combined a simplified ecosystem model and vertical mixing model to estimate how biological processes and resuspension might shape the distributions of POM. We assumed that POC and PN in the water column were dominated by biogenic and resuspension sources. Additionally, the biogenic part of POM was considered principally influenced by biological production, respiration, and aggregation (phytoplankton and heterotrophs), as well as by the formation and decay of detritus; the resuspension part was considered to originate from surface sediments when they were suspended by turbulence and thus reentered the water column.

The ecosystem model includes those state variables, parameters, and kinetics related to important biological production of POC and PN in the water column. The associated pools of POC and PN were modeled in carbon and nitrogen units, respectively. The set of model equations showing the dynamics of the biogenic state variables ($Phy_{C,\ N}$, phytoplankton carbon and nitrogen; $Het_{C,\ N}$, heterotrophs carbon and nitrogen; $Det_{C,\ N}$, detritus carbon and nitrogen) can be expressed as follows:

$$dPhy_C/dt = \left(C_{phot} - R_{phy} - E_C\right) \cdot Phy_C - \left(A_C + G_C\right), \quad (1)$$

$$dHet_C/dt = G_C - \left(R_{het} + E_{het}\right) \cdot Het_C, \quad (2)$$

$$dDet_C/dt = A_C - \omega_C \cdot T_f \cdot Det_C, \quad (3)$$

$$dPhy_N/dt = \left(N_C - E_N\right) \cdot Phy_N - \left(A_N + G_N\right), \quad (4)$$

$$dHet_N/dt = G_N - E_{het} \cdot Het_N, \quad (5)$$

$$dDet_N/dt = A_N - \omega_N \cdot T_f \cdot Det_N, \quad (6)$$

where C_{phot} is the carbon-specific photosynthesis rate (d^{-1}); R_{phy} is the phytoplankton respiration rate (d^{-1}); $E_{C,\ N}$ is the carbon and nitrogen loss rate of phytoplankton due to exudation (d^{-1}); R_{het} is the heterotrophic respiration rate (d^{-1}); E_{het} is the loss rate of heterotrophs (d^{-1}); T_f is the temperature-response function; N_C is the carbon-specific nitrogen assimilation of phytoplankton (d^{-1}); $\omega_{C,\ N}$ is the remineralization of detrital carbon or nitrogen (d^{-1}); $A_{C,\ N}$ is the carbon or nitrogen loss due to aggregation of phytoplankton cells (mmol C m^{-3} d^{-1}/mmol N m^{-3} d^{-1}); and $G_{C,\ N}$ is the carbon or nitrogen loss due to heterotroph grazing (mmol C m^{-3} d^{-1}/mmol N m^{-3} d^{-1}). The detailed parameterizations for biological growth and kinetics are shown in Text S1 in Supplementary Materials. The model was started running in winter with the initial value of the state variables prescribed as follows: 1 mmol Phy_C m^{-3}; 1 mmol Het_C m^{-3}; 2 mmol Det_C m^{-3}; 0.2 mmol Phy_N m^{-3}; 0.1 mmol Het_N m^{-3}; and 0.1 mmol Det_N m^{-3}.

Some model parameters were estimated from earlier studies, e.g., Schartau et al. (2007) and Geider et al. (1998), and fixed values were assigned to these parameters (Table S1). The values of certain parameters that are difficult to measure directly were estimated *via* optimization (Table S1). In the ecosystem model, SST, PAR, and DIN are important factors that affect biological production. The mean climatological data (8-day remote sensing data with 4-km spatial resolution, https://oceancolor.gsfc.nasa.gov/) of SST and PAR over the previous two decades (Figure 2) were reported by Niu et al. (2021). Observational data of DIN (Figure 2D) were taken from those seasonal sampling surveys at sea surface or above the mixed layer (Shi et al., 2015; Guo et al., 2020; Wang et al., 2020). These parameters were input as a forcing function to constrain the model output.

The vertical mixing model, based on a statistical result of observational data, provides a macroscopic perspective from which to estimate the proportion of particles resuspended from the surface sediment and reintroduced into the water column. It is a two end-member mixing model based on an assumption that suspended particles are from a mixture of materials from upper-layer phytoplankton and surface sediment (Bloesch, 1994; Hung et al., 2013). The POC concentration (%, mg mg^{-1}) in the mixture is expressed as follows:

$$POC(\%) = \frac{S_p \times \left(f_p - f_s\right)}{TSM} + f_s, \quad (7)$$

where S_p is the upper-layer phytoplankton concentration (mg L^{-1}), f_p is the POC fraction of phytoplankton (%), and f_s is the POC fraction of surface sediment (%).

By plotting POC (%) against 1/TSM, we can obtain related information of the two endmember values (f_p and f_s). The ratio of resuspended particles to total sinking particles can be determined as follows:

$$f_R = \frac{f_t - f_p}{f_s - f_p} \times 100\,\%, \tag{8}$$

where f_t is the POC fraction of sinking particles (%). Therefore, f_R was used to estimate the POC pools from the benthic system to the water column due to vertical mixing. This model is based on the assumption that particles have unchanged chemical components during/after sinking and resuspension, and it also neglects the potential influence of horizontal transport.

3.Results

3.1. Data overview

Generally, concentrations of TSM, POC, and PN all peaked in the Subei coast region and decreased seaward (Figure 3). The distinct geographical location of the Subei coast makes it the most POM-rich region in the SYS. Apart from the transport of

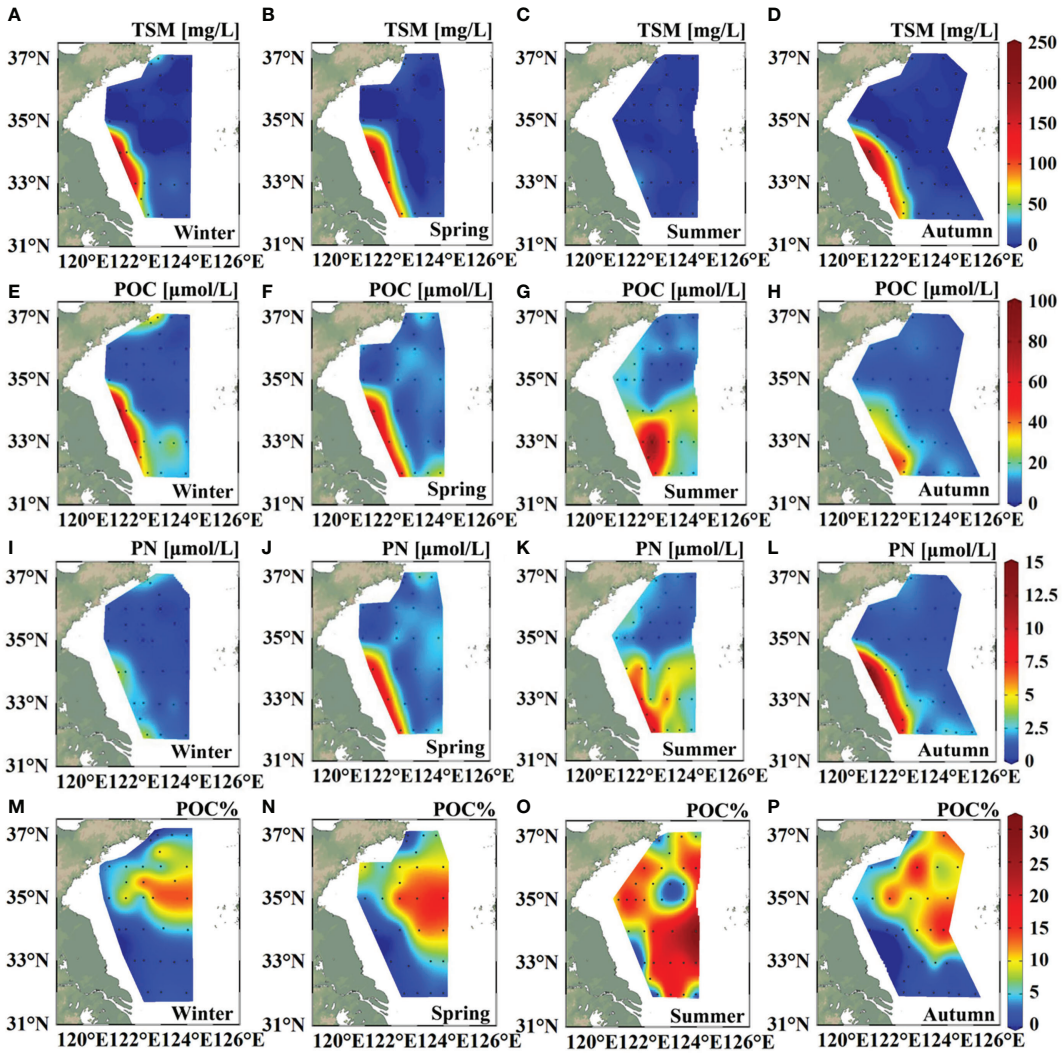

FIGURE 3
Sea surface distributions of total suspended matter (TSM) concentration **(A–D)**, particulate organic carbon (POC) concentration **(E–H)**, particulate nitrogen concentration **(I–L)**, and percentage content of POC in the TSM **(M–P)** in the four seasons.

the sandy sediment, the Subei Shoal is also a region of origin of green tides, and these floating algal mats can drift further offshore into the SYS and the open ocean (Liu et al., 2009; Wang et al., 2015). The propagation of both the muddy and turbid waters and the suspended sediments of this region is robust along the shoreline and toward the offshore sea owing to the wind-driven coastal currents (Wang et al., 2011). We found seaward propagation of high-value patches of POC and PN during summer (Figures 3G, K); however, the lowest concentrations all occurred in the central basin, where weak physical and biological processes make it a POM-poor region.

The lowest upper-layer percentage content of POC in the TSM (POC%) was observed in the Subei coast region (Figures 3M–P). A notable gradient of upper-layer POC% was observed in winter, spring, and autumn from the coastal region to the central SYS. By contrast, low-POC% patches occurred both in the central basin and in the Subei coast region in summer (Figure 3O). The central basin had lower POC% in summer than those in spring and autumn, which could be expected because the upper-layer high-POC% POM provided by biological processes decreased in the nutrient-depleted condition during summer.

For the central section, the signal of warm and saline water was evident in winter to the south of 34°N (Figures 4A, E), indicating invasion of the Taiwan Warm Current from the ECS. The input of saline water south of 34°N remained notable during spring, although the temperature was low (Figures 4B, F). Stratification was robust during summer, with the depth of the thermocline in the range of 30–40 m and the depth of the halocline in the range of 20–30 m (Figures 4C, G). The highest turbidity occurred at the bottom between 32°N and 34°N and decreased from 50–80 mg TSM L^{-1} during spring and winter to <10 mg TSM L^{-1} during summer (Figure S2). The MLD was shallow during spring (11–19 m) and summer (5–16 m) in the central section of 33°N–36°N (Figure S3A). During winter, the MLD deepened to the near-bottom layer (50–60 m) to the north of 34°N, and the water column was uniformly mixed vertically to the south of 34°N (Figure S3B).

For the coastal section, we found no marked vertical variability of temperature and salinity in winter, spring, and autumn (Figure 5). The surface warm and less-saline water was notable at stations between 32°N and 33°N during summer, demonstrating the potential influence of the SCC (Figures 5C, G). The turbidity was considerably high (150–200 mg TSM L^{-1}) throughout the water column between 33°N and 34°N (Figures S2D, S2E). The pattern of uniform mixing was marked for the entire coastal section during winter and spring (Figure S3B). The water column in the area of shallow topography (33°N–34°N) could still be mixed vertically during summer (Figure S3B). The high turbidity and deep mixed layer demonstrated the robust resuspension in the area of shallow topography (<20 m) throughout the year.

Figure 6 shows the vertical distributions of temperature, salinity, and TSM/turbidity along the 34°N to elucidate the potential influence of horizontal cross-shelf transport. In winter, seaward invasion of cold and less-saline coastal waters was notable, with the temperature contour of 10.5°C spreading to the area of 122.3°E (Figures 6A, E). By contrast, seaward invasion of warm and low-salinity coastal waters was observed in summer (Figures 6C, G). Additionally, the low-salinity signal was notable to the east of 123.5°E in summer (Figure 6G).

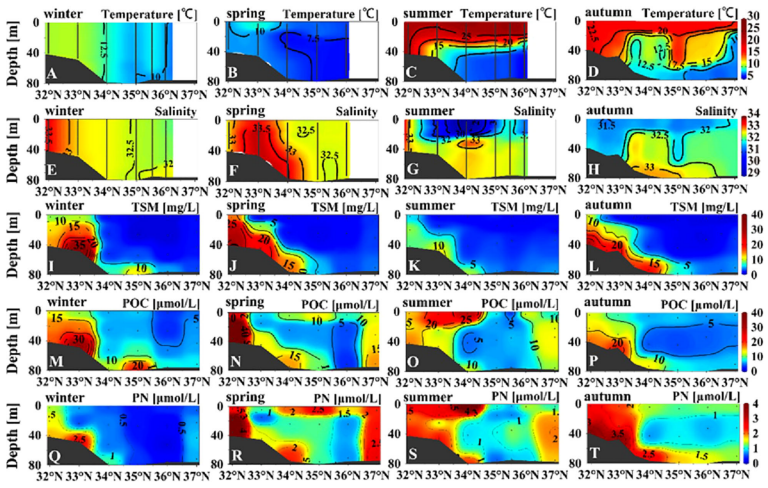

FIGURE 4
Vertical distribution of temperature **(A–D)**, salinity **(E–H)**, total suspended matter **(I–L)**, particulate organic carbon **(M–P)**, and particulate nitrogen **(Q–T)** concentrations in the central section (Figure 1) in the four seasons.

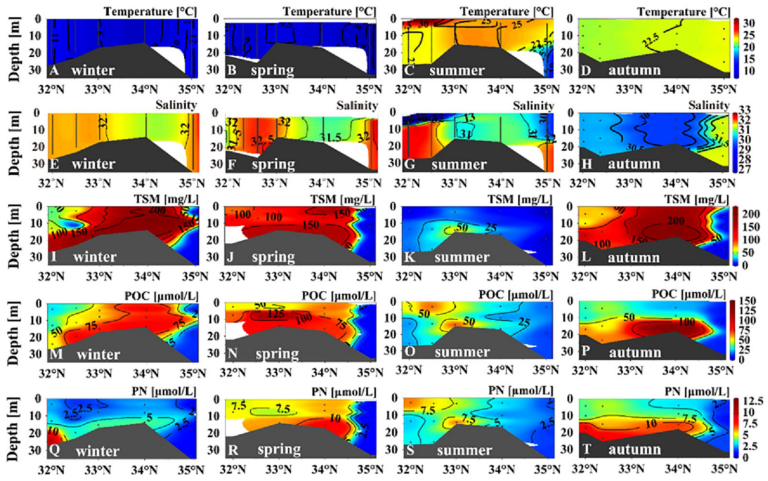

FIGURE 5
Vertical distribution of temperature **(A–D)**, salinity **(E–H)**, total suspended matter **(I–L)**, particulate organic carbon **(M–P)**, and particulate nitrogen **(Q–T)** concentrations in the coastal section (Figure 1) in the four seasons.

3.2. Characteristics of particulate organic matter dynamics

To the south of 34°N along the central section, the concentrations of TSM, POC, and PN all peaked at the bottom during winter, spring, and autumn (Figure 4). The concentrations of POC and PN peaked at the sea surface during summer (Figures 4O, S), demonstrating substantial biological production in summer. By contrast, the concentration differences between the sea surface and the bottom water were small to the north of 34°N along the central section. High values of TSM and POC occurred in the bottom water at 35°N during winter (Figures 4I, M), indicating moderate influence of resuspension. High values of POC and PN occurred at the sea surface in the region 34°N–36°N during spring (Figures 4N, R), indicating increased biological production (Jin et al., 2013).

In comparison with the central section, the coastal section had higher concentrations of TSM, POC, and PN. The vertical distribution of TSM was similar to that of turbidity, showing a relatively high value across the water column between 33°N and 34°N in winter, spring, and autumn (Figures 5I, J, L). High values of TSM occurred only at the bottom in summer

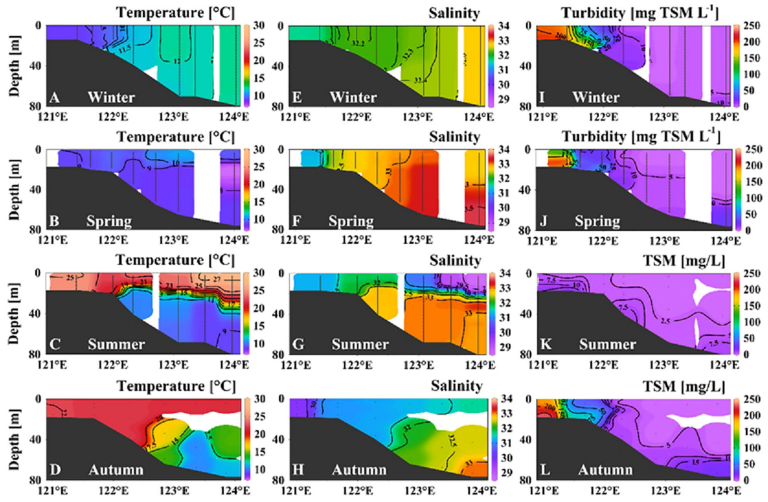

FIGURE 6
Vertical distributions of temperature **(A–D)**, salinity **(E–H)**, and total suspended matter (TSM) concentration **(I–L)** along the 34°N section (Figure 1) in different seasons. In winter and spring, high-resolution turbidity data were used instead of discrete TSM to better show the vertical variations.

(Figure 5K), demonstrating weakened resuspension. Generally, the coastal section showed higher POC and TSM in winter and spring, and the lowest values occurred in summer. The turbulent water column in seasons other than summer contributed to higher supplies of POM from the bottom. In summer, high values of POC and PN were present at both the sea surface and the bottom water (Figures 5O, S), which means joint influence of biological processes and resuspension on POM dynamics. The increase of upper-layer biogenic elements in the Subei coast region and the central basin coincided with the rises in temperature and PAR during spring and summer (Figures 2A, B).

Along the 34°N section, the turbidity contours of 15–50 mg TSM L^{-1} spread out from the high-turbidity region (west of 122° E) at depth of >15 m in winter (Figure 6I). This phenomenon corresponded to seaward invasion of cold coastal waters (Figure 6A). Thus, the horizontal transport of POM was related to freshwater movement driven by hydrodynamic processes. In spring, the seaward-spreading turbidity contours were not notable (Figure 6J). Specifically, the 50 mg TSM L^{-1} contour occurred only at the bottom at 122°E (~20 m) during spring, whereas it spread seaward to the area near 122.2°E at a depth of ~14 m during winter (Figures 6I, J). Thus, horizontal transport in winter was more substantial than that in spring. In summer, the resuspension and seaward spread were not important (Figure 6K). In autumn, seaward-spreading TSM contours (<50 mg/L) were observed at 122°E (Figure 6L), although the spreading range was less than that in winter.

The Subei coast region showed extremely low POC% in winter, spring, and autumn (<1%, Figure 7), indicating robust

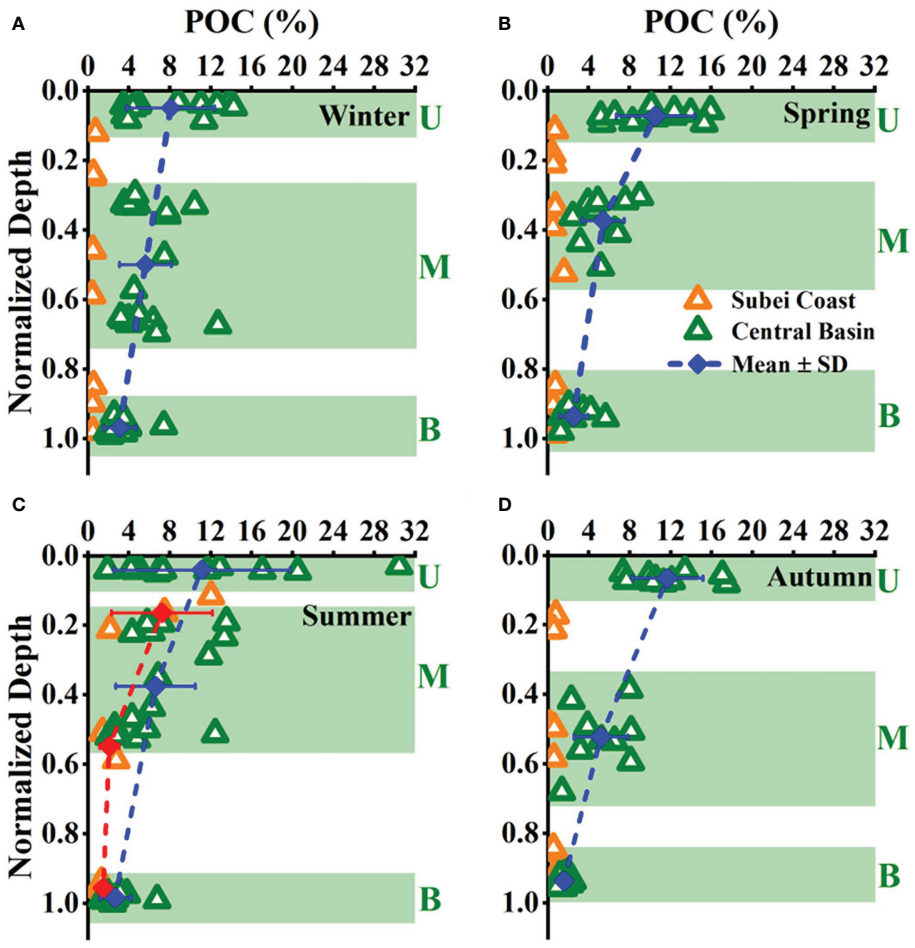

FIGURE 7
Vertical patterns of percentage content of particulate organic carbon (POC%) in the total suspended matters with normalized depth among seasons **(A–D)**. Triangles with different colors represent different areas (orange, Subei coast; olive, central basin). The vertical distribution in the central basin showed a three-layer structure, as marked by the light green frames. U, upper layer; M, middle layer; B, bottom layer. Blue points connected by a dashed line show the change of the mean values in each layer of the central basin. Red points connected by a dashed line in panel **C** show the change of the mean values in each layer of the Subei coast region during summer.

resuspension across the water column. The POC fractions of surface sediments reported in the Yellow Sea (Hu et al., 2013), Changjiang Estuary (Zhang et al., 2007), and ECS (Kao et al., 2003) were usually <1%. This phenomenon corresponded to the high TSM (Figures 5I, J) and deepened MLD (Figure S3B) during winter and spring. Bottom stress and turbulent kinetic energy have been reported to be strong in the continental shelf areas west of 125.5°E, demonstrating robust vertical mixing (Bian et al., 2013a).

Biogenic particles have markedly high POC% (approximately 10%–16%) compared with that of surface sediments (Hung et al., 2013). In summer, upper-layer POC% in the Subei coast region reached up to ~12% (Figure 7C), indicating the increased contribution of upper-layer biogenic POM in the shallow coastal regime. The warm and slightly stratified water column was conducive to the development of phytoplankton blooms when additional nutrients were supplied from CDW in the Subei coast region in summer (Figure 2), demonstrating the increased contribution of biogenic production to the POC pool. However, the robust mixing resulted in a large fraction of resuspended particles in the other seasons, i.e., low POC%, even though the phytoplankton abundance could increase in the Subei coast region. In the central basin, the maximum POC% occurred in the upper layer (average: 10%–12% in spring, summer, and autumn and 8% in winter) and then decreased with depth. Less sediment-dominated POM was mixed in the middle layer during summer because it had higher average POC% (6.6%) than in the other seasons (5.6% in winter, 5.4% in spring, and 5.5% in autumn).

3.3. Variations of particulate organic matter stoichiometries

The C/N ratio based on the data at all sampling depths also showed notable spatial and seasonal variations (Figure 8), indicating that these particles might differ in composition.

The C/N ratio in the Subei coast region displayed the highest value in winter (18.4), which then decreased slightly in spring, deviating by three points from the Redfield ratio (Figures 8A, B). During winter, robust mixing in the Subei coast region could resuspend more sediment carbon into the water column. The three points were in the bottom layers, indicating that bottom resuspension could be notable in spring.

The detritus-rich POM further resulted in a regime with a C/N ratio higher than the Redfield ratio. For example, the extracellular mucilage of these primary producers, known as transparent exopolymer particles, has a high carbon content (on average: C:N >20) and high concentration in productive estuaries and coastal waters (Engel and Passow, 2001;

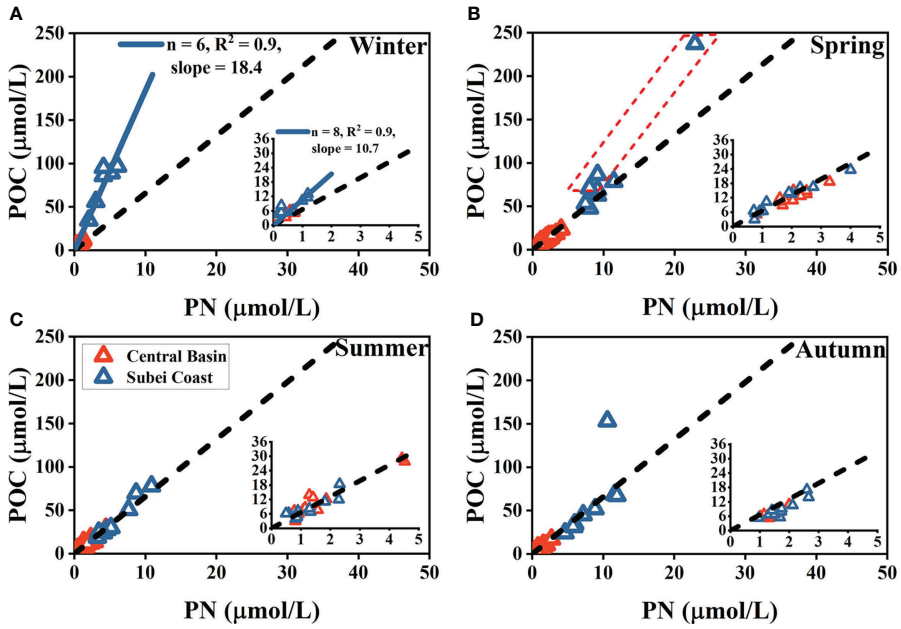

FIGURE 8
Particulate organic carbon (POC) vs. particulate nitrogen (PN) in the Subei coast region and the central basin in the four seasons **(A–D)**. The inset view in each panel shows an enlarged version for POC vs. PN in the central basin between the surface and bottom layers. Orange/blue triangles in the inset views denote surface/bottom data. The slope of the blue fitted line denotes the corresponding mean elemental ratio. The black dashed lines represent the Redfield ratio of POC: PN (6.6). Three outliers marked by a red dashed frame in panel **B** are from the bottom layers in the Subei coast region.

Taylor et al., 2014; Zäncker et al., 2017). Detritus-rich POM was verified by Guo et al. (2010), who identified that settling particles trapped within the SYS and the ECS consisted of substantial particle aggregates (e.g., diatom aggregates, fecal pellets, and tintinnids) that showed a mean C/N ratio of >12. It has been reported that turbulent mixing in coastal systems facilitates the formation of these particle aggregates by increasing the collision and coagulation rates (Kiorboe, 1998).

In summer and autumn, however, the C/N ratio in the Subei coast region did not deviate markedly from the Redfield ratio (Figures 8C, D), demonstrating weakened physical mixing. The increased SST and freshwater inputs by the CDW and Subei local rivers were responsible for the increased stratification in summer and early autumn (Zhu and Wu, 2018). The shallowed MLD in the Subei coast region during summer might indicate the increased stratification (Figure S3A). The occurrence of increased sea surface POC% in the Subei coast region during summer corresponded to the weakened physical mixing (Figure 7C). Similarly, the C/N ratio of the central basin was close to the Redfield ratio in all seasons, demonstrating the notable contribution of biogenic sources to POM pools in the stratified central basin. Furthermore, the C/N ratios in the central basin between the surface and bottom layers are shown in Figure 8 (inset views). Only the bottom C/N ratio showed notable deviation from the Redfield ratio during winter (10.7; Figure 8A), indicating that the influence of resuspended particles (responsible for the increased C/N ratio) might be important in bottom waters in the central basin in winter.

3.4. Modeling results

3.4.1. Results of the ecosystem model

The modeled biogenic POC and PN were contributed by three components: phytoplankton (Phy_C and Phy_N), heterotrophs (Het_C and Het_N), and detritus (Det_C and Det_N). By considering resuspension, we were able to calculate the total POC or PN (biogenic + resuspension, shown as dashed curves in Figure 9) and then perform a comparison with the linear interpolation of the observed values (shown as points in Figure 9) according to Eq. S9 in Supplementary Materials. The calculated C_f is 3.1 ($R^2 = 0.96$) and 0.6 ($R^2 = 0.83$) for POC and PN, respectively, in the Subei coast region and 1.5 ($R^2 = 0.81$) and 0.2 ($R^2 = 0.92$) for POC and PN, respectively, in the central basin. The low C_f and

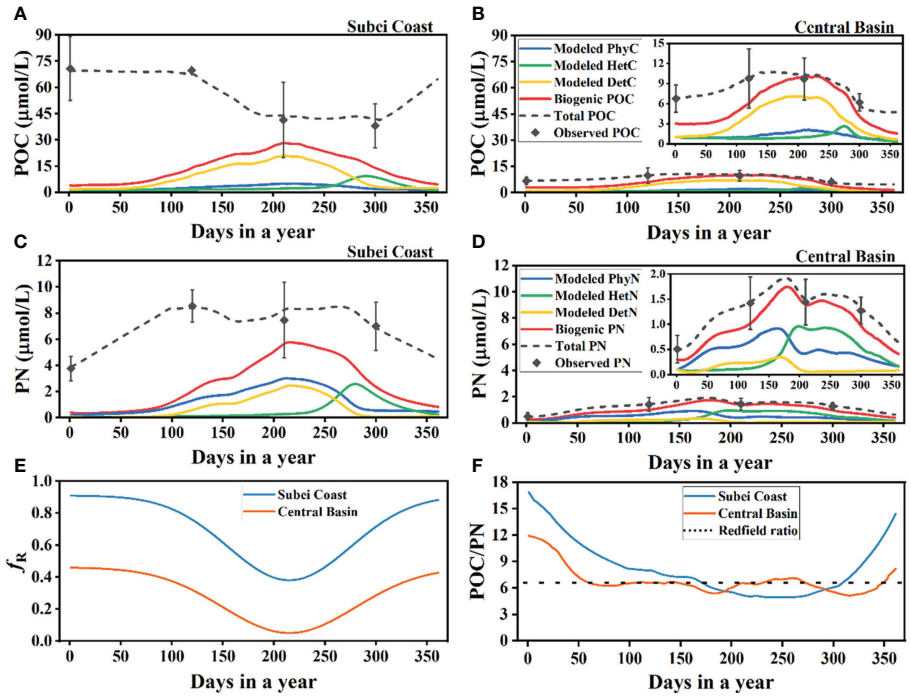

FIGURE 9
Results of the ecosystem model. **(A, B)** Modeling results of particulate organic carbon (POC) in the Subei coast region and central basin. **(C, D)** Modeling results of particulate nitrogen (PN) in the Subei coast region and central basin. The inset view in panels **(B)** or **(D)** shows a related enlarged version. **(E)** Modeling results of f_R after optimization in the Subei coast region and central basin. **(F)** Modeling results of the POC/PN ratio in the Subei coast region and central basin. Phy_C and Phy_N , phytoplankton carbon and nitrogen; Het_C and Het_N , heterotrophs carbon and nitrogen; Det_C and Det_N , detritus carbon and nitrogen; Biogenic POC (PN) = modeled Phy_C + modeled Het_C + modeled Det_C (modeled Phy_N + modeled Het_N + modeled Det_N); Total POC or PN, the sum of biogenic and resuspended POC or PN; Observed POC and PN, observed value of POC and PN *in situ* (means ± SD of all stations in a given region after depth-weighted averaging for each station); f_R , the ratio of resuspended particles to total suspended particles.

high R^2 values indicate that the model results matched the observed values.

The modeling was based on some idealized assumptions such as no horizontal transport. The influence of horizontal transport (mainly from terrestrial input) will be analyzed in *Section 4.3* the biogenic POC of the Subei coast region was approximately 26% higher than that in the central basin. Because resuspended particles contributed more POC than PN (PN is more easily degraded during sedimentation) in the Subei coast region, PN dynamics tended to be determined by biogenic inputs, whereas POC dynamics tended to be determined by resuspended inputs. This resulted in a different trend of the seasonal variation between the total POC and PN (dashed black lines in Figures 9A, C), i.e., the variation of total POC had a reversed trend in comparison with that of biogenic POC, whereas the variation of total PN was in accord with that of biogenic PN. The influence of biogenic input could be more important in the central basin because the variations of the total POC and PN were comparable to those of biogenic POC and PN, respectively (Figures 9B, D). In terms of PN dynamics, biogenic PN contributed more than 56% of the total PN in winter and almost all of the total PN in summer (Figure 9D). The sediments might have less PN content in the central basin because sinking particles have longer residence time in comparison with those in the coastal regions (Guo and Zhang, 2005; Guo et al., 2010), which means that most organic nitrogen will be degraded before particles settle to the seabed.

The model also showed seasonal variation of f_R by optimization (Figure 9E). In the Subei coast region, approximately 90% of the total POM was provided by resuspension during winter, but the resuspension fraction decreased to 38% during late summer. By contrast, resuspension contributed less to the total POM in the central basin, and it decreased from 45% in winter to 5% in late summer. The variation of f_R was largely consistent with the change of MLD in the central basin (Figure S3A). The difference in the resuspension fraction between the Subei coast region (38%) and the central basin (5%) in summer could be the result of different hydrological characteristics. First, stratification in the Subei coast region during summer was not as strong as that in the central basin, which is dominated by the YSCWM. This can be demonstrated by the lower sea surface POC% in the Subei coast region than that in the central basin in summer (Figure 7C). Second, the shallow topography and tidal currents make surface sediment resuspension easier in the Subei coast region than that in the central basin, which has deeper topography (Song et al., 2018; Zhu and Wu, 2018). The modeled POC/PN ratio also showed notable seasonal variation (Figure 9F), which corresponded to the variations of the observed values (Figure 8). The modeled POC/PN ratio in the Subei coast region was markedly higher than the Redfield ratio during winter and spring. The central basin had a lower POC/PN ratio in comparison with that of the Subei coast region, and it presented a ratio close to the Redfield ratio in most seasons.

The influences of environmental factors and model parameters were estimated based on the sensitivity analysis. The detailed information is presented in Text S3 in Supplementary Materials.

3.4.2. Results of the vertical mixing model

According to Eq. 7, the slope of the linear fitting for POC (%) vs. 1/TSM equals to $S_p \times (f_p - f_s)$, and the intercept equals to f_s. The variable slopes of the linear fitting showed regional and seasonal variations (Figure 10). The Subei coast region showed notably larger slopes (19.4–25.1) than those of the central basin (5.1–9.4) principally because the Subei coast region had more upper-layer phytoplankton (S_p) than the central basin. The central basin showed sharp seasonal contrast, whereas the seasonal difference was small in the Subei coast region. The linear fitting also showed a larger intercept in the central basin (0.7–1.1) than that in the Subei coast region (0.3–0.6), indicating that the surface sediments of the central basin had a higher POC content. The mud area in the central SYS largely consists of organic-rich fine-grained sediments originating from the Huanghe River, whereas the Subei coast region is characterized by coarse sediments or transitional sediments (between coarse and fine types) (Lee and Chough, 1989; Yang and Youn, 2007; Qiao et al., 2017).

The parameters used to calculate the resuspension fraction using Eq. 8 are shown in Table 1. It is difficult to measure S_p *in situ* because we have no means to separate phytoplankton from the suspended POM and then to weigh each fraction. For the central basin, we assumed that the upper-layer phytoplankton accounted for a substantial proportion of sea surface TSM, expressed as follows: $S_p = TSM_s \times (1 - f_R)$, where TSM_s is the averaged sea surface TSM in the central basin. The values of TSM_s were taken as 0.96 mg L^{-1} in winter, 1.58 mg L^{-1} in spring and summer, and 0.74 mg L^{-1} in autumn. This assumption is based on recent studies suggesting that living planktonic cells account for most of the POM pools in unproductive regions (Martiny et al., 2013a; Martiny et al., 2013b). For the Subei coast region, we assumed S_p to be directly proportional to the modeled Phy_C. This is based on the fact that the growth of the upper-layer phytoplankton is largely controlled by photosynthesis (i.e., controlled by SST and PAR) in nutrient-rich coastal regions.

The calculated S_p for the central basin (Table 1) was close to the range of 0.25–0.75 mg L^{-1} given by Hung et al. (2013) for the offshore region of the ECS. We have no observed values of the POC% of the total sinking particles (f_t) and no reported data to indicate their seasonal variation in the SYS. We assumed that the sinking particles collected by sediment traps comprised a mixture from three layers (upper, middle, and bottom layers in Figures 7A–D). The depth-weighted average POC% across the

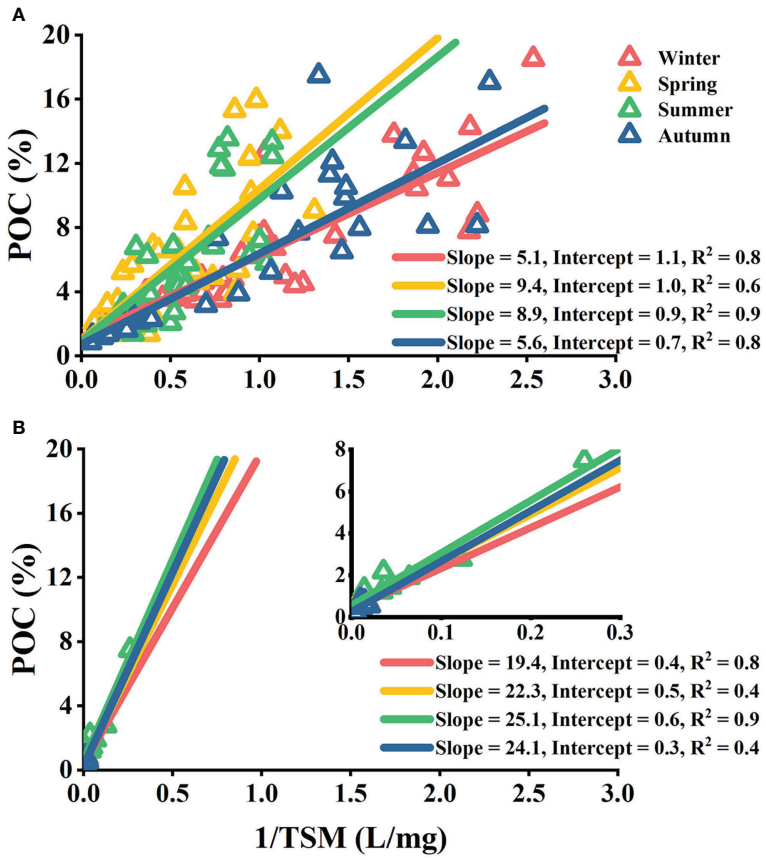

FIGURE 10
Fitting results of POC (%) vs. 1/TSM in the central basin **(A)** and the Subei coast region **(B)**. According to Eq. 7, the slope of the linear fitting for POC (%) vs. 1/TSM is equal to $S_{px}(f_p - f_s)$, and the intercept of that is equal to f_s , where S_p is the upper-layer phytoplankton concentration (mg L^{-1}), f_p is the POC fraction of phytoplankton (%), and f_s is the POC fraction of surface sediment (%). Seasons are distinguished by different colors. The inset view in panel **(B)** shows a related enlarged version.

water column in a given region was calculated to represent f_t (Table 1). Sinking particles in the offshore waters of the ECS showed a POC fraction of 4.2%–7.3% (Hung et al., 2013). Guo et al. (2010) collected sinking particles in a sediment trap in the central SYS during September and showed that sinking particles had POC contents of 7.9% (at 28 m), 4.1% (at 45 m), and 1.3% (at 69 m). These reported data coincided with the presented vertical distribution of POC% (Figure 7) and the calculated f_t (Table 1) in this study. Generally, the resuspension fraction (f_R in Table 1) calculated using the vertical mixing model matched well with the f_R obtained from ecosystem model optimization (Figure 9E).

4. Discussion

4.1. Model validation

The modeled results are based on certain assumptions that might potentially introduce errors and uncertainties. Because no measured vertical flux datasets were available in this study, we compared our modeled results with those of previous studies that used other methods (modeling and observation) to estimate POC fluxes.

It is difficult to demonstrate the accuracy of the result of ecosystem model because we cannot precisely divide TSM into contributions from phytoplankton, heterotrophs, or detritus. Thus, we can only compare the model result with other reported data derived from field observation or modeling. Wan et al. (2005) used a coupled pelagic–benthic ecosystem model to estimate phytoplankton biomass carbon in the central SYS and showed that the modeled biomass was highest in summer and spring (1.1–3.4 mmol C m^{-3}) and lowest in winter (~1.0 mmol C m^{-3}). The results conformed to the variation range of modeled Phy_C in the central basin from winter to late summer (1–3 mmol C m^{-3}). Additionally, the carbon content of phytoplankton can be estimated using a carbon-to-chlorophyll a ratio (C:Chl *a*), which varies from 10 to 100 g g^{-1} in different marine systems (Geider, 1993; Taylor et al., 1997). Chang et al.

TABLE 1 Parameters used in the vertical mixing model.

Region	Seasons	Slope($S_p \times (f_p - f_s)$)	S_p (mg/L)	f_s (%)	f_t (%)	f_R (%)
Central basin	Winter	5.1	0.5	1.1	5.8	53.9
	Spring	9.4	1.1	1.0	6.2	39.1
	Summer	8.9	1.4	0.9	6.8	7.2
	Autumn	5.6	0.6	0.7	6.2	41.1
Subei coast	Winter	19.4	2.4	0.4	0.5	98.8
	Spring	22.3	5.3	0.5	0.8	92.8
	Summer	25.1	5.5	0.6	2.6	56.2
	Autumn	24.1	5.4	0.3	0.6	93.3

Slope is derived from the fitting results in Figures 10A, B. The slope of the linear fitting for POC (%) vs. 1/TSM equals to $S_p \times (f_p - f_s)$ according to Eq. 7. S_p is the upper-layer phytoplankton concentration. f_p is the POC fraction of phytoplankton (%). f_s is the POC% in surface sediments and equals to the intercept of the regression line in Figures 10A and B. f_t is the POC% of the total sinking particles. f_R is the resuspension fraction calculated using Eq. 8.

(2003) estimated that the values of C:Chl *a* were 18.0 and 67.4 g g^{-1} for coastal and offshore waters in the ECS during summer. We assumed that these values were applicable to the SYS. The average Chl *a* concentrations during summer, taken from Fu et al. (2009), were 0.4 mg m^{-3} (in the central SYS) and 2.5 mg m^{-3} (in the coastal SYS), and the calculated biomass carbon values were 2.2 mmol C m^{-3} (in the central SYS) and 3.8 mmol C m^{-3} (in the coastal SYS), which were also comparable with the model results. Using the ratio of POC/Chl *a* in the northern ECS in summer and winter, i.e., ~70 and 16, respectively (Hung et al. (2009), we calculated similar values of phytoplankton biomass carbon, i.e., 2.3 and 3.3 mmol C m^{-3}.

The reported sediment trap data and depth-integrated primary productivity (PP) were used to estimate the potential resuspension fraction and POC export ratio (Table 2). The POC export ratio is equal to the ratio of net POC flux/PP. Guo and Zhang (2005) estimated a net POC flux (NPOC) of 172–342 mg C m^{-2} d^{-1} in a section across the SYS (from the Shandong Peninsula to Jeju Island) by calculating the difference between the total settling flux and the resuspension flux. This range of NPOC corresponded to the POC fluxes estimated by $^{234}Th/^{238}U$ disequilibrium and rare earth elements in the offshore ECS (Bi et al., 2013; Hung et al., 2016). The NPOC can fluctuate in the SYS. As analyzed by Guo and Zhang (2005), the high flux (342 mg C m^{-2} d^{-1}) in the central SYS is associated with the potential influence of YSCWM upwelling. Thus, we used a range (172–342 mg C m^{-2} d^{-1}) instead of a specific value to represent the NPOC in the SYS. Similarly, the NPOC in the coastal ECS was reported as 486–785 mg C m^{-2} d^{-1} by Hung et al. (2013). Actually, the PP (unit: mg C m^{-2} d^{-1}) is a depth-integrated value of the measured PP (unit: mg C m^{-3} d^{-1}) across the water column. Thus, the depth-integrated PP (PP_i) at a certain depth (i) can be calculated as follows:

$$PP_i = PP_b \times \frac{i}{b}, \quad (9)$$

where PP_b is the depth-integrated PP at the bottom (i.e., across the water column), and b is the bottom depth (m). Based on Eq. 9, the PP_i at both the upper layer and the lower layer of the thermocline (ULT and LLT, respectively) was calculated, as shown in Table 2. Similarly, the net POC fluxes estimated by Guo and Zhang (2005) and by Hung et al. (2013) are actually the net fluxes at the bottom (where the influence of resuspension is largest). Thus, we calculated the net fluxes of the ULT or LLT according to Eq. 9 (Table 2).

As shown in Table 2, the estimated f_R varied in the different layers. The lowest f_R occurred in the ULT in the central SYS (12% in summer, 20% in autumn). The f_R increased in the LLT, with a range of 29%–73%. The f_R was high in the ULT in the coastal SYS and the ECS (70%–85% at 20 m, 85%–90% at 10 m) and showed only a slight difference with that at the bottom. Generally, the f_R was considerably high at the bottom in both the coastal and the central regions (82%–96%), even in the central SYS during summer. Similarly, the resuspension flux was estimated to account for more than 90% of the total flux using sediment trap data and $^{234}Th/^{238}U$ disequilibrium in the central SYS during summer (Guo and Zhang, 2005).

Generally, the f_R estimated using the vertical mixing model in this study can better represent the variations of the resuspension fraction in the ULT or the LLT. For example, the estimated f_R was 7.2% in the central basin during summer (Table 1), which was close to the lowest value (12%) shown in Table 2. The f_R in the central SYS during autumn was 20% and 42% at the ULT and LLT, respectively (Table 2), which was comparable to that shown in Table 1 (41.1%). Because reported flux data were unavailable for the Subei coast region, we used data from the coastal ECS as an alternative. The high f_R (92.8%–98.8%) shown in Table 1 demonstrated that the influence of resuspension was important throughout the entire water column, which corresponded to the high f_R and slight difference between the upper layer (10 m) and bottom layer (18 m) in the coastal ECS shown in Table 2. Additionally, the high turbidity and/or TSM and deepened MLD supported this conclusion (Figure 5; Figures S2, S3).

The residence time (τ) of suspended POM can be used to evaluate resuspension. The standing stocks per unit area divided

TABLE 2 Estimated resuspension ratio (f_R) and particulate organic carbon (POC) export ratio based on reported sediment trap data and depth-integrated primary productivity (PP).

Region	Station location	Month	Bottom depth (m)	Trap depth (m)	TPOC (mg m^{-2} d^{-1})	NPOC (mg m^{-2} d^{-1})	PP (mg C m^{-2} d^{-1})	f_R(%)	$f_R^{'}$(%)	POC export ratio	Reference
Coastal SYS	121°E, 35°N	September	38	20	657	98–195	318	70–85	N/A	0.31–0.61	Guo et al. (2010)
				35 (BL)	3,148	172–342	556	89–95	N/A		
Central SYS	124.5°E, 33°N	April	60	60 (BL)	479	172–342	937	29–64	N/A	0.18–0.36	Wang et al. (2002)
Central SYS	123°E, 34.8°N	August	73	21 (ULT)	120	53–106	184	12–56	N/A	0.29–0.58	Guo and Zhang (2005)
				48 (LLT)	340	121–241	421	29–64	N/A		
				68 (BL)	4,081	172–342	596	92–96	93–94		
	124°E, 34.1°N	August	81	15 (ULT)	109	34–68	119	37–68	N/A		
				40 (LLT)	342	92–182	318	47–73	N/A		
				75 (BL)	3,410	172–342	596	90–95	90–94		
Central SYS	123°E, 34.4°N	September	73	28 (ULT)	87	70–139	253	20	N/A	0.28–0.55	Guo et al. (2010)
				45 (LLT)	192	112–223	406	42	N/A		
				69 (BL)	2,218	172–342	623	85–92	94		
Central NYS	123.5°E, 38°N	July	65	50 (BL)	740	172–342	596	54–77	N/A	0.29–0.57	Wang et al. (2002)
		October	65	50 (BL)	2,310	172–342	623	85–93	N/A	0.28–0.55	
Coastal ECS	122.6°E, 31°N	September	23	10	2,918	270–436	889	85–90	N/A	0.30–0.49	Guo et al. (2010)
				18 (BL)	4,401	486–785	1,600	82–90	N/A		

N/A, no data were reported in the corresponding reference.

The PP data refer to the studies of Hama et al. (1997) and Wen et al. (2012). The $f_R^{'}$ is the resuspension ratio of the bottom layer calculated by resuspension models in the corresponding references of Guo and Zhang (2005) and Guo et al. (2010). SYS, South Yellow Sea; ECS, East China Sea; NYS = North Yellow Sea; BL, bottom layer; ULT, upper layer of the thermocline; LLT, lower layer of the thermocline; TPOC, total POC flux based on sediment strap data; NPOC, net POC flux, i.e., the difference between total settling and resuspension fluxes; f_R = (TPOC-NPOC)/TPOC; NPOC/PP, POC export ratio.

10.3389/fmars.2022.919423

by flux can provide the residence time in a given layer. The standing stocks were calculated from the depth-integrated POC concentrations (mg m^{-2}) over a given depth. No significant thermocline occurred in the Subei coast region (Figures 5A–D). Generally, the water column can be divided into two categories: the nepheloid layer and non-nepheloid layer. The nepheloid layer shows a near-bottom maximum of TSM reflecting direct disturbance driven by resuspension. The criterion for partitioning the two layers was based on the study of Guo et al. (2010). The nepheloid depth in the coastal SYS and ECS can account for ~47% and 57% of the total water depth, respectively. The shallowest water depth in the Subei coast region was <20 m. This means that the nepheloid layer in the Subei coast region can account for ~60% of the total water depth, and that this fraction might increase further during winter. Accordingly, we assumed that our sampling depths at the subsurface/middle layer and the bottom layer in the Subei coast region were broadly within the estimated non-nepheloid depth and nepheloid depth, respectively. Considering that the Subei coast region is between the two stations in the coastal SYS and ECS (Table 2), we took the average of the values from the two stations to obtain the TPOC and NPOC in the Subei coast region, i.e., 1,788 (TPOC) and 184–316 (NPOC) mg m^{-2} d^{-1} in the non-nepheloid depth; 3,775 (TPOC) and 329–564 (NPOC) mg m^{-2} d^{-1} in the nepheloid depth. In the central basin, the water column can be divided into the mixing layer (above the MLD) and the bottom layer (below the MLD). Our sampling depths at the subsurface or middle layers in the central basin are broadly within or close to the MLD (Figure S3).

Similarly, we calculated the mixed- and bottom-layer residence times in the central basin (Table S3). Data from the central North Yellow Sea, shown in Table 2, were used for the central SYS because the two regions exhibit similar hydrological characteristics. Because of limited observational data, we estimated the residence time only for summer and autumn. To better constrain the estimation, both the TPOC and NPOC were used to calculate the τ in Table S3 (expressed as τ^a and τ^b, respectively).

TABLE 3 Literature trap fluxes and resuspension ratios estimated by total suspended matter (TSM) or particulate organic carbon (POC) data in different regions.

Region		Bottom depth (m)	Trap depth (m)	Trap flux (g TSM m^{-2} d^{-1})	Trap flux (mg POC m^{-2} d^{-1})	Corrected trap flux (g TSM m^{-2} d^{-1}/mg POC m^{-2} d^{-1})	Resuspension ratio (%) or rates (g m^{-2} d^{-1})	Reference
East China Sea	Coastal region	55	50	79	2,319	696 (POC)	70% (POC)	Guo et al. (2010)
		38–60	20–30	No data	200–7,300	69–785 (POC)	57%–93% (POC)	Hung et al. (2013)
		40	20	No data	4,846	291 (POC)	94% (POC)	Hung et al. (2016)
	Offshore region	88	83	18	280	31 (POC)	89% (POC)	Guo et al. (2010)
		118–154	100–120	No data	80–150	58–63 (POC)	27%–58% (POC)	Hung et al. (2013)
		104/107	50/70	No data	356/262	46/47 (POC)	87%/82% (POC)	Hung et al. (2016)
Faeroe–Shetland Channel		700–800	570–770	~100	300–1,200	~30 (TSM)	70% (TSM)	Bonnin et al. (2002)
Gulf of Lions	Entrance	1,030	500/1,000	0.7/1.0	6.2/4.7	0.4/0.7 (TSM)	32%–41% (TSM)	Heussner et al. (2006)
	Exit	1,030	500/1,000	1.7/3.8	4.8/3.2	0.7/1.2 (TSM)	60%–67% (TSM)	
Lake Arresø		No data	No data	No data	No data	No data	300 g m^{-2} d^{-1} (TSM)*	Kristensen et al. (1992)
Lake Ontario		23	20	17	554	2.6 (TSM), 205 (POC)	85% (TSM), 63% (POC)	Rosa (1985)
		130	125	2.1	193	1.4 (TSM), 176 (POC)	33% (TSM), 9% (POC)	
Lake Eric		9	7–8	6.9	315	0.07 (TSM), 16 (POC)	99% (TSM), 95% (POC)	Bloesch (1982)
		25	22	4.3	232	0.2 (TSM), 51 (POC)	95% (TSM), 78% (POC)	
		40	37	6.1	322	0.7 (TSM), 145 (POC)	88% (TSM), 55% (POC)	

*This value is estimated by an empirical model that describes the relationship between suspended solids and settling velocity and wind velocity. Corrected trap flux = Trap flux × (1 - Resuspension ratio).

The calculated τ showed a larger difference between layers in the central basin in comparison with that of the Subei coast region (Table S3). The τ estimated by the TPOC and NPOC in the mixing layer of the central basin (21.3–27.1 and 12.2–75.3 d, respectively) was markedly higher than that in the non-nepheloid layer of the Subei coast region (1.5 and 8.7–15.1 d, respectively). By contrast, the τ in the bottom layer in the central basin was notably diminished (1.1–1.3 d) and equal to that in the Subei coast region (1.1 d). The τ estimated by the NPOC increased substantially, especially in the bottom layer (an increase of 1–3 times that in the mixing layer and of 6–25 times that in the bottom layer). The large increase of τ in the bottom layer was because the NPOC was potentially unaffected by resuspension. Generally, biogenic particles have fluffy and ductile states and relatively light density and thus show a larger τ than resuspended sediment (Simon et al., 2002; Wurl et al., 2009; Verdugo, 2012). The higher resuspension flux could result in a lower residence time. The estimated average residence time in the mixing layer of the central basin (~1–2 months) matched the reported particle residence time obtained *via* the ^{210}Po/^{210}Pb disequilibria method for the SYS (Zhong et al., 2019) and the offshore ECS (Hung et al., 2000) but was shorter than that reported for the South China Sea (Yang et al., 2006), Southern California Bight (Eppley et al., 1983), and Western North Pacific Ocean (Zhong et al., 2021). Although the potential error could be large (>50%) because the estimated results were based on different datasets, such notable regional variability still indicated the potential influence of resuspension and biological production.

We further compared the estimated results in this study with observed (or measured) datasets in other regions (Table 3). It is noted that these reported resuspension ratios are estimated by sediment trap data in the bottom layer, which can be site-specific and thus variable in a given region (Table 3). For example, the resuspension ratio varies from 27% to 58% as estimated by Hung et al. (2013) to 87%/82% as estimated by Hung et al. (2016) in the offshore ECS (Table 3); however, the corrected POC fluxes reported by Hung et al. (2013) and Hung et al. (2016) are similar (58–63 mg m^{-2} d^{-1} vs. 46/47 mg m^{-2} d^{-1}, Table 3), which indicate that the estimation of resuspension ratio is necessary in correcting trap flux when using sediment trap data. Additionally, the corrected POC fluxes in the offshore ECS are less than the value estimated by Guo and Zhang (2005) in the central SYS (172–342 mg m^{-2} d^{-1}, Table 2). Bengtsson et al. (1990) found that resuspension occurred only a few times in the entire Swedish lake but more frequently in some specific smaller areas. However, we estimated the integrated resuspension activity across the entire subregions (Subei coast region and central basin) in the SYS. The estimated results in this study can only represent the resuspension episode that occurred during the field surveys. It has been suggested that sediment entrainment rates are highly variable on a short timescale (days to weeks) (Chung et al., 2009). Given the highly variable resuspension rate, the estimated f_R in the bottom layer (Table 2) matched the observed datasets (Table 3). The considerably high resuspension rate (300 g m^{-2} d^{-1}) observed in Lake Arresø is because of the shallow water depth (mean depth 3 m) and the influence of storm events (Kristensen et al., 1992). The estimated f_R in the ULT and LLT (Table 2) was lower than those in the bottom layer of coastal ECS, Faeroe–Shetland Channel, and most lakes (Table 3), which was expected because the resuspended material might decrease with the increase of distance above the seafloor, e.g., Kerfoot et al. (2004) found that the log-transformed abundance of *Daphnia* ephippia in resuspension assemblages correlated negatively with the water column depth. It has been suggested that the pulses of resuspension occurring above the thermocline are governed by thermal conditions and wind events (Evans, 1994). The entrance of the Gulf of Lions (1,000-m trap depth) and Lake Ontario (125-m trap depth) also shows relatively low resuspension ratios (Table 3).

4.2. Uncertainty and potential factors influencing the estimated particulate organic matter flux

It is difficult to obtain an accurate value of S_p , and the uncertainty in estimating the value of S_p is approximately 50% according to Hung et al. (2013). Additionally, the uncertainty is derived from the estimation of POC content of phytoplankton. For example, the estimated S_p in the Subei coast region in summer (5.5 mg L^{-1} phytoplankton) might be overestimated. If the POC content of phytoplankton is 10%–17%, then the phytoplankton contribution will be 0.6–0.9 mg L^{-1} POC, whereas the highest POC concentration was ~70 μmol L^{-1} (i.e., 0.84 mg L^{-1}). However, from the perspective of TSM, the S_p accounted for 43% of sea surface TSM (average: 12.9 mg L^{-1} in summer), i.e., with a resuspension fraction of 57%. The results of the two estimation methods showed a deviation of ~50% (all contributed by phytoplankton vs. 43% contributed by phytoplankton), which is close to the 50% uncertainty estimated by Hung et al. (2013). Actually, this mixing model did not consider the influence of degradation of biogenic materials. Biological degradation can be substantial in coastal systems, which means that a certain proportion of phytoplankton-derived POC might be degraded after entering the water column. Hence, the 0.6–0.9 mg L^{-1} POC contributed by phytoplankton was potentially overestimated. Generally, the potential errors in estimating S_p and the POC content of phytoplankton and the influence of biological degradation can result in uncertainty of >50%.

Comparison of the results shown in Tables 1, 2 revealed that the largest difference occurred in summer. For example, the lowest f_R was 12%–37% in the ULT in the central basin (Table 2), which was 67%–414% higher than the value in Table 1 (7.2%). By contrast, the difference in estimated f_R in autumn was lower, i.e., 41.1% (Table 1) vs. 20% and 42% in the ULT and LLT,

respectively (Table 2). The estimated f_R was more sensitive to S_p in summer than in other seasons, which demonstrated that the large uncertainty potentially resulted from the variability of S_p . For example, a 14% decrease of S_p (from 1.4 to 1.2 in Table 1) in the central basin in summer resulted in a 183% increase of f_R (from 7.2% to 20.4%). The value of 20.4% seemed to match better the estimated value in Table 2. However, in the other seasons, a 20% change of S_p resulted in only a <20% change of f_R in the central basin and a <5% change of f_R in the Subei coast region. Thus, we speculated that the uncertainty of the estimated f_R was <20% in the other seasons; however, accurate estimation of S_p in the central basin during summer is necessary.

The important role of S_p in the central basin demonstrated that biogenic inputs have an important influence on POM dynamics. Thus, the community composition of phytoplankton and the category of biogenic materials could be important factors influencing the estimated fluxes. Guo et al. (2010) found that diatom aggregates, fecal pellets, and tintinnids contributed most of the trapped particles in both the ULT and the LLT in the central SYS and that the fraction of mineral particles increased substantially at the bottom layer. Additionally, Hung et al. (2009) found that the concentrations of particulate carbohydrates (PCHOs) and uronic acids (PURAs) in the northern ECS were associated with phytoplankton abundance and bacterial biomass and that they were higher in summer than in winter. We assumed that the same situation might exist in the Yellow Sea. Because PCHO and PURA show roles similar to that of transparent exopolymer particles, the increased PCHO and PURA potentially increased the coagulation kernel (β), as shown in Eq. S7 in Supplementary Materials, which could have further promoted the formation of Det_C according to Eq. 3. Further details can be found in Text S3 in Supplementary Materials. This explains why a large amount of biogenic POC existed in the form of detritus carbon (Figures 9A, C). The diatom- or dinoflagellate-dominated phytoplankton community is a potential factor controlling detritus flux, e.g., diatom aggregates act as an important means of transporting carbon and other nutrients from the euphotic zone to the seabed (Hung et al., 2009; Liu et al., 2015; Turner, 2015). The salinity gradient and turbulence can also influence aggregation dynamics (Beauvais et al., 2006; Mari et al., 2012). Hence, the diatom-dominated phytoplankton community and the turbulent hydrology in the coastal regime meant that more detritus carbon formed and sank in the Subei coast region than in the central basin.

The assumption that resuspension was weakest in summer under robust influence of stratification also resulted in potential errors. Although the model results indicated that strong stratification restricted upward diffusion of sediment (Luo et al., 2017) and that the thermal front around the YSCWM affected sediment resuspension by reducing bottom shear stresses (Zhong et al., 2020), the POC sinking flux and resuspension fraction were still high at the bottom layer in the central SYS during summer (Table 2). This meant that other hydrodynamic processes could result in increased resuspension at the bottom, e.g., the southwestern monsoon in summer and the typhoon season in summer and autumn, which might cause strong vertical mixing in these shallow waters (Lee and Chao, 2003; Hung et al., 2010). Bian et al. (2010) found that typhoon-induced waves deepened the thermocline and caused notable resuspension of sediment. Hoshika et al. (2003) found that the monsoon-derived bottom current was highly correlated with the suspended particle flux in the ECS. The decreased resuspension in the ULT and LLT (Table 2) demonstrated that robust stratification might influence the resuspension flux above the thermocline but not at the bottom. It has been suggested that suspended sediments in the shelf areas of the SYS and the ECS are driven by tidal currents (Yuan et al., 2008; Bian et al., 2013b). Moreover, sedimentary conditions such as bedforms and mixed sediment classes might be important in driving the resuspension of sediment (Graber et al., 1989). To better understand the complex processes of resuspension and transport of sediment in this coastal ocean under investigation, additional detailed observations and enhanced modeling methodology are still needed in future comprehensive studies.

4.3. Potential impact of horizontal transport on particulate organic matter dynamics

In addition to vertical processes, cross-shelf horizontal transport related to suspended POM and sediments in the SYS can be important, e.g., terrigenous materials transported from the Yellow River to Cape Chengshan and the Shandong subaqueous delta (Cai et al., 2003; Xing et al., 2014) and nutrients and POM carried by the northeastward branch of the CDW (Beardsley et al., 1985; Chen et al., 2008; Wei et al., 2017). Sediment transport processes can be influenced by many physical forcings, such as the East Asian Monsoon, tides and river discharges, and there is no consensus regarding their relative importance in the shelf areas of the SYS and the ECS (Bian et al., 2013b). Traditionally, suspended sediment in the Changjiang Estuary is thought to be transported by the wind-induced coastal current of the ECS to the coast of Zhejiang Province and/or to the Okinawa Trough mud area in winter (Milliman et al., 1985; Peng and Hu, 1997). However, studies based on stable organic carbon isotopes and rare earth elements showed that the Changjiang Estuary sediment is transported to the central SYS (Cai et al., 2003; Lan et al., 2009). The model result showed that the tidal residual current can drive the Changjiang River Plume to flow northward and then turn offshore, thus transporting freshwater into the interior SYS during winter (Li et al., 2016; Zhu and Wu, 2018). Additionally, it is suggested that wind-driven downwelling in combination with lateral Ekman transport could probably cause sediment dispersion and transport to the shelf (Liu et al., 2007; Dong

et al., 2011). The notable seaward-spreading turbidity contours and cold/low-salinity water demonstrated the potential horizontal transport driven by physical forcing in winter (Figures 6A, E, I).

Wei et al. (2020) observed a northeast/southeast transport route of suspended particles in the 10-m layer from the Subei coast to the offshore SYS during spring–autumn; however, the range of spread might be limited owing to the evolution of the YSCWM. The YSCWM thermal front, observed from spring–autumn, potentially affects the distribution and transport of suspended sediment (Zhong et al., 2020). The temperature contour of 9°C and the contours of 11°C–21°C spread from the central SYS to the area near 122°E in spring and summer, respectively (Figures 6B, C). The observed turbidity/TSM fronts (50 mg L^{-1}) were also located in the area near 122°E (Figures 6J, L). Therefore, the YSCWM thermal front might prevent seaward extension of suspended particles. Dong et al. (2011) also observed that suspended sediments appeared trapped on the shallow water side of the YSCWM front when transported from the Subei coast to the central SYS.

The resuspension and horizontal transport were reasonably weak in summer (Figure 6K); however, the high-POC/high-PN and high-POC% sea surface patches spreading from the southwest SYS to the central SYS were notable (Figures 3G, K, O). These patches matched the northeastward route of extension of CDW from the Changjiang Estuary to Jeju Island (Beardsley et al., 1985; Lie et al., 2003). The detached CDW can be verified by the low-salinity water to the east of 123.5°E (Figure 6G). Wind, tide-induced mixing, and Changjiang water discharge play important roles in detaching low-salinity water from the CDW plume toward the SYS and Jeju Island (Chen et al., 2008; Moon et al., 2009). The detached CDW creates a condition with moderate nutrients and adequate light, resulting in high primary production and Chl *a* in surrounding offshore regions. Therefore, the observed high-POC% sea surface patches might result from enhanced local biological production that provides large amounts of biogenic materials.

Generally, we considered that cross-shelf horizontal transport (from the Subei coast to the central basin) principally influenced POM dynamics in the area to the west of 122°E (deeper than 20 m) during spring and autumn and that this area extended to 122.5°E during winter. The horizontal transport can result in potential overestimation of the resuspension fraction. For example, if the turbidity contours were vertical lines (i.e., no seaward spread) at the location of 122°E, the TSM would be 50–75 mg L^{-1} and 20–25 mg L^{-1} in the bottom (~20 m) and upper (<14 m) layers, respectively (Figure 6A), similar to the situation in spring (i.e., ~50 mg L^{-1} and 20–25 mg L^{-1} in the bottom and upper layers, respectively). This indicates that the increased TSM flux in the upper layer at the location of 122°E might be contributed by the flux of horizontal transport rather than by resuspension flux. The model results showed that the f_R was 98.8% in winter and 92.8% in spring (Table 1). By assuming that the increased f_R was contributed totally by horizontal transport, the calculated contribution of resuspension might be overestimated by 6%. The particle deposition rate from the water column and the horizontal transportation rate were estimated as 0.33 and 0.02 g cm^{-2} $year^{-1}$ in the shelf edge of the ECS (Iseki et al., 2003), i.e., ~6% of depositing particles were transported to the offshore area, which matched our estimation. Additionally, it is estimated that cross-boundary transport contributes ~5% of the organic carbon transported to the continental slope (Chen, 2010; Song et al., 2016). The location at 122°E was somewhat distant from the shallowest area (~15 m) in the Subei coast region. Therefore, the influence of tidal currents should be considerable, inducing substantial vertical fluxes after the horizontal transport. Ignoring the potential influence of horizontal transport, the resuspension ratio may have been overestimated by >10% in the Subei coast region.

This is a rough estimation because we have no detailed hydrodynamic parameters and methods with which to make a quantitative assessment. Horizontal transport includes sediment transport from land to the ocean and sediment deposition and remobilization in the marine environment (Anderson et al., 2018). The sediment class influences deposition because coarse-grained sediments will deposit quickly, while only fine-grained types will be transported to reach the central SYS (Dong et al., 2011). The composition and age of organic carbon in sediments reflect the potential sediment transport from land to the ocean (Li et al., 2012). The benthic organic carbon mineralization is also an important factor in driving sediment storage/remobilization, and a higher rate of mineralization means that more POM can be decomposed during transportation (Zhao et al., 2018). More comprehensive assessment of these related processes is necessary to constrain the potential influence of horizontal transport.

4.4. Comparison with other marginal seas

The source and fate of POM in the SYS reflect substantial cross-shelf transport and vertical export, which help elucidate the roles of marginal seas as a sink for continental inputs and biological production and a source for offshore open regions (Heussner et al., 2006). The Subei coast, as a shallow coastal area, is an important sink of POM received *via* large depositions of sediment from the Changjiang River and the Old Yellow River (Liu et al., 2013b; Qiao et al., 2017), freshwater inputs from the Subei local rivers (Zhu and Wu, 2018), and biogenic materials from algal blooms (Fan et al., 2015; Wang et al., 2015). The sandy and tidal hydrological characteristics of the region result in intensive vertical and lateral transport of sediments and biogenic elements and make it a substantial source of POM for the central basin (Song et al., 2018; Wei et al., 2020).

The role and function of the Subei coast are similar to those of the typical estuaries and banks in the other marginal seas. The substantial sediment plume formed in the Changjiang Estuary and the adjacent Changjiang bank can extend southeastward to the open sea driven by the cross-shelf circulation (Lie et al., 2003; Luo et al., 2017). The high-nutrient inputs from the CDW are highly correlated with the high primary production, which contributes to the large amounts of biogenic POM in the Changjiang Estuary and adjacent offshore area (Zhou et al., 2008; Zhu et al., 2009). This off-shelf transport and seasonal variability of riverine and marine-derived POM can be considerable in the other river-dominated ocean margins, e.g., the Mississippi River delta and the Gulf of Mexico (Trefry et al., 1994; Wang et al., 2004; Corbett et al., 2006), U.S. West Coast (Hwang et al., 2005; Mollenhauer and Eglinton, 2007), Chesapeake Bay (Fisher et al., 1998; Zhang and Blomquist, 2018), and Baltic Sea (Winogradow et al., 2019; Nilsson et al., 2021).

From a global perspective, the carbon budgets in the SYS and ECS are under the influence of western boundary currents. Another typical marginal sea in a western boundary current system is the South Atlantic Bight. The robust freshwater discharge and tidal dynamics facilitate vertical mixing and resuspension of fine-grained particles in the shelf region of the South Atlantic Bight (Lee et al., 1989). The increased nutrient loads *via* river discharge are reasonable for the high PP in the inner-shelf areas [1,698 mg C m^{-2} d^{-1} (Chen, 2010)], which matches the value in the coastal ECS (Table 2). By contrast, eastern boundary current systems, which are usually zones of upwelling, exhibit very high potential productivity of >3,000 mg C m^{-2} day^{-1} (Carr, 2001), i.e., twice that of the coastal ECS and five times that of the SYS (Table 2).

Most river-dominated ocean margins show seasonal hypoxia/deoxygenation in adjacent offshore stratified zones, which means that large amounts of terrigenous and marine POM can be decomposed to fuel oxygen depletion. However, seasonal hypoxia is not evident in the stratified central SYS. The estimated sediment oxygen consumption in the central SYS was significantly lower than that of typical hypoxia zones (Song et al., 2016), which demonstrates that the remineralization of biogenic POM provided by spring blooms might be limited. Additionally, cross-shelf transport between the Subei coast and the central basin could be restricted by the thermal front around the YSCWM (Wei et al., 2016; Zhong et al., 2020). Therefore, systematic evaluation of the sources and sinks of POM in the SYS could provide a reference for the biogeochemical cycle of organic carbon and oxygen consumption in shelf waters. Further efforts should be dedicated to clarifying the influence of coupled biological–physical oceanographic processes on the POM budgets in these marginal seas.

5. Summary and implications

Based on field observations and modeling, we estimated the influence of coupled biological–physical oceanographic processes on potential POM dynamics, fluxes, and horizontal transport in the SYS. The Subei coast region had considerably higher POM than that found in other subregions of the SYS. The C/N ratio in the Subei coast region deviated more or less from the Redfield ratio during winter and spring, indicating the potential impact of robust physical forcing. The effect of biological processes was notable in the central basin with the C/N ratio broadly matching the Redfield ratio, which can also be proven by the vertical distribution of POC%.

The modeled biogenic POC and PN showed substantial temporal variations, which all peaked in spring and summer. Detritus carbon contributed the most biogenic POC (up to 78%) and phytoplankton nitrogen contributed the most biogenic PN (31%–78%) during spring and summer. The sensitivity analysis results indicated that biological production was affected by environmental factors (temperature, light, and DIN) and key kinetics (nutrient uptake rate, aggregation, and grazing rate). The production of PN was more sensitive to the change of DIN in the nutrient-depleted central basin than in the nutrient-rich Subei coast region. The production of POC was principally controlled by temperature and light. With greater aggregation and a higher grazing rate, the Subei coast region exhibited more detritus and heterotroph carbon than those found in the central basin. The modeled C/N ratio also showed substantial seasonal variability, which deviated from the Redfield ratio in winter and then approached it with the progression of the seasons.

The f_R estimated by ecosystem model optimization matched well with the result calculated by the statistical approach in the vertical mixing model. The resuspension fraction peaked in winter and decreased to a minimum in summer, with the range varying between the seasons from >90% to ~50% in the Subei coast region and from ~50% to <10% in the central basin. Through comparison with reported sediment trap and PP data, we found that the estimated resuspension fraction showed large uncertainty (>50%) in summer because of potential errors in model parameter estimation and the influence of other unexplored biophysical processes (e.g., biological degradation, upwelling, and monsoons); however, the degree of uncertainty was lower in the other seasons (<20%).

Cross-shelf horizontal transport principally influenced POM dynamics in the area to the west of 122°E (deeper than 20 m) during spring and autumn, and this area extended to the west of 122.5°E during winter. We estimated that the contribution of resuspension was potentially overestimated by >10% in the Subei coast region because of the influence of horizontal transport. Given the complex characteristics of resuspension and

horizontal transport, acquisition of additional observational data over a larger spatiotemporal scale will be necessary to establish an integrated network of the carbon budget in the SYS.

Data availability statement

The raw data of particulate parameters reported in this study is available at figshare.com via https://doi.org/10.6084/m9.figshare.20486022.

Author contributions

WZ designed the field surveys and supervised the research. SY maintained the operation of instrument. CG finalized the data set, designed the modeling and drafted an early version of the manuscript. YN contributed to the autumn data collection. YN and CL supported the satellite-derived data. All authors contributed to discussion and revision of the manuscript.

Funding

This research was jointly funded by the National Key Research and Development Program of China (contract no. 2020YFA0608301) and the National Natural Science Foundation of China (grant nos. 42141001 and 91751207).

Acknowledgments

Sampling surveys were supported by the National Natural Science Foundation of China (grant nos. 41649901, 41749901, and 41849901) through ship-time sharing projects *via* Open Research Cruises conducted in the Bohai and Yellow seas onboard R/V *Dongfanghong 2* in 2017–2018 (cruise nos. NORC2017-01 and NORC2018-01) and onboard R/V *Lanhai 101* in October 2019 (cruise no. NORC2019-01). Jing Lang is appreciated for field sampling and most laboratory determination. We thank James Buxton for editing the English text of a draft of this paper and the reviewers for their thoughtful and constructive comments, which improved the quality of this paper.

Conflict of interest

The authors declare that the research was conducted in the absence of any commercial or financial relationships that could be construed as a potential conflict of interest.

Publisher's note

All claims expressed in this article are solely those of the authors and do not necessarily represent those of their affiliated organizations, or those of the publisher, the editors and the reviewers. Any product that may be evaluated in this article, or claim that may be made by its manufacturer, is not guaranteed or endorsed by the publisher.

Supplementary material

The Supplementary Material for this article can be found online at: https://www.frontiersin.org/articles/10.3389/fmars.2022.919423/full#supplementary-material

References

Anderson, C., Murray, R., Dunlea, A., Giosan, L., Kinsley, C., McGee, D., et al. (2018). Climatically driven changes in the supply of terrigenous sediment to the East China Sea. *Geochem. Geophys. Geosyst.* 19, 2463–2477. doi: 10.1029/2017GC007339

Bale, A. J., and Morris, A. W. (1998). Organic carbon in suspended particulate material in the North Sea: Effect of mixing resuspended and background particles. *Continent. Shelf Res.* 18, 1333–1345. doi: 10.1016/S0278-4343(98)00046-6

Beardsley, R., Limeburner, R., Yu, H., and Cannon, G. (1985). Discharge of the Changjiang (Yangtze River) into the East China sea. *Continent. Shelf Res.* 4, 57–76. doi: 10.1016/0278-4343(85)90022-6

Beauvais, S., Pedrotti, M. L., Egge, J., Iversen, K., and Marrasé, C. (2006). Effects of turbulence on TEP dynamics under contrasting nutrient conditions: implications for aggregation and sedimentation processes. *Mar. Ecol. Prog. Ser.* 323, 47–57. doi: 10.3354/meps323047

Bengtsson, L., Hellström, T., and Rakoczi, L. (1990). Redistribution of sediments in three Swedish lakes. *Hydrobiologia* 192, 167–181. doi: 10.1007/BF00006012

Bianchi, T. S., and Bauer, J. E. (2011). "Particulate organic carbon cycling and transformation," in *Treatise on estuarine and coastal science volume 5: Biogeochemistry*. Eds. E. Wolanski and D. McLusky (Waltham:Academic Press), 69–117. doi: 10.1016/B978-0-12-374711-2.00503-9

Bian, C., Jiang, W., Greatbatch, R. J., and Ding, H. (2013a). The suspended sediment concentration distribution in the Bohai Sea, Yellow Sea and East China Sea. *J. Ocean Univ. China* 12, 345–354. doi: 10.1007/s11802-013-1916-3

Bian, C., Jiang, W., Quan, Q., Wang, T., Greatbatch, R. J., and Li, W. (2013b). Distributions of suspended sediment concentration in the Yellow Sea and the East China Sea based on field surveys during the four seasons of 2011. *J. Mar. Syst.* 121, 24–35. doi: 10.1016/j.jmarsys.2013.03.013

Bian, C., Jiang, W., and Song, D. (2010). Terrigenous transportation to the Okinawa Trough and the influence of typhoons on suspended sediment concentration. *Continent. Shelf Res.* 30, 1189–1199. doi: 10.1016/j.csr.2010.03.008

Bi, Q., Du, J., Wu, Y., Zhou, J., and Zhang, J. (2013). Particulate organic carbon export flux by $^{234}Th/^{238}U$ disequilibrium in the continental slope of the East China Sea. *Acta Oceanol. Sin.* 32 (10), 67–73. doi: 10.1007/s13131-013-0303-7

Bloesch, J. (1982). Inshore–offshore sedimentation differences resulting from resuspension in the eastern basin of Lake Erie. *Can. J. Fish. Aquat. Sci.* 39, 748–759. doi: 10.1139/f82-103

Bloesch, J. (1994). A review of methods used to measure sediment resuspension. *Hydrobiologia* 284, 13–18. doi: 10.1007/BF00005728

Bonnin, J., Van Raaphorst, W., Brummer, G.-J., van Haren, H., and Malschaert, H. (2002). Intense mid-slope resuspension of particulate matter in the Faeroe–Shetland channel: short-term deployment of near-bottom sediment traps. *Deep Sea Res. Part I: Oceanogr. Res. Pap.* 49, 1485–1505. doi: 10.1016/S0967-0637(02)00030-4

Brink, K. H. (2016). Cross-shelf exchange. *Annu. Rev. Mar. Sci.* 8, 59–78. doi: 10.1146/annurev-marine-010814-015717

Cai, D., Shi, X., Zhou, W., Liu, W., Zhang, S., Cao, Y., et al. (2003). Sources and transportation of suspended matter and sediment in the southern Yellow Sea: Evidence from stable carbon isotopes. *Chin. Sci. Bull.* 48 (S1), 21–29. doi: 10.1007/BF02900936

Carr, M.-E. (2001). Estimation of potential productivity in Eastern boundary currents using remote sensing. *Deep Sea Res. Part II: Topical Stud. Oceanogr.* 49, 59–80. doi: 10.1016/S0967-0645(01)00094-7

Chang, J., Shiah, F.-K., Gong, G.-C., and Chiang, K. P. (2003). Cross-shelf variation in carbon-to-chlorophyll a ratios in the East China Sea, summer 1998. *Deep Sea Res. Part II: Topical Stud. Oceanogr.* 50, 1237–1247. doi: 10.1016/S0967-0645(03)00020-1

Chen, C. A. (2009). Chemical and physical fronts in the Bohai, Yellow and East China seas. *J. Mar. Syst.* 78, 394–410. doi: 10.1016/j.jmarsys.2008.11.016

Chen, C.-T. A. (2010). "Cross-boundary exchanges of carbon and nitrogen in continental margins," in *Carbon and nutrient fluxes in continental margins: A global synthesis. global change – the IGBP series*. Eds. K.-K. Liu, L. Atkinson, R. Quiñones and L. Talaue-McManus (Berlin, Heidelberg: Springer Berlin Heidelberg), 561–574. doi: 10.1007/978-3-540-92735-8_13

Chen, C., Xue, P., Ding, P., Beardsley, R. C., Xu, Q., Mao, X., et al. (2008). Physical mechanisms for the offshore detachment of the Changjiang diluted water in the East China Sea. *J. Geophys. Res.* 113 (C2), C02002. doi: 10.1029/2006JC003994

Chu, P. C., Fralick, C. R., Haeger, S. D., and Carron, M. J. (1997). A parametric model for the Yellow Sea thermal variability. *J. Geophys. Res.* 102 (C5), 10499–10507. doi: 10.1029/97JC00444

Chung, E. G., Bombardelli, F. A., and Schladow, S. G. (2009). Sediment resuspension in a shallow lake. *Water Resour. Res.* 45, W05422. doi: 10.1029/2007WR006585

Corbett, D. R., McKee, B., and Allison, M. (2006). Nature of decadal-scale sediment accumulation on the western shelf of the Mississippi River delta. *Continent. Shelf Res.* 26, 2125–2140. doi: 10.1016/j.csr.2006.07.012

Dong, L., Guan, W., Chen, Q., Li, X., Liu, X., and Zeng, X. (2011). Sediment transport in the Yellow Sea and East China Sea. *Estuarine Coast. Shelf Sci.* 93, 248–258. doi: 10.1016/j.ecss.2011.04.003

Ducklow, H. W., Steinberg, D. K., and Buesseler, K. O. (2001). Upper ocean carbon export and the biological pump. *Oceanography* 14 (4), 50–58. doi: 10.5670/oceanog.2001.06

Engel, A., and Passow, U. (2001). Carbon and nitrogen content of transparent exopolymer particles (TEP) in relation to their alcian blue adsorption. *Mar. Ecol. Prog. Ser.* 219, 1–10. doi: 10.3354/meps219001

Eppley, R. W., Renger, E. H., and Betzer, P. R. (1983). The residence time of particulate organic carbon in the surface layer of the ocean. Deep Sea Res part A. *Oceanogr. Res. Pap.* 30, 311–323. doi: 10.1016/0198-0149(83)90013-4

Evans, R. D. (1994). Empirical evidence of the importance of sediment resuspension in lakes. *Hydrobiologia* 284, 5–12. doi: 10.1007/BF00005727

Fan, S., Fu, M., Wang, Z., Zhang, X., Song, W., Li, Y., et al. (2015). Temporal variation of green macroalgal assemblage on *Porphyra* aquaculture rafts in the Subei Shoal, China. *Estuarine Coast. Shelf Sci.* 163, 23–28. doi: 10.1016/j.ecss.2015.03.016

Fisher, T. R., Hagy, J. D., and Rochelle-Newall, E. (1998). Dissolved and particulate organic carbon in Chesapeake Bay. *Estuaries* 21, 215–229. doi: 10.2307/1352470

Fu, M., Wang, Z., Li, Y., Li, R., Sun, P., Wei, X., et al. (2009). Phytoplankton biomass size structure and its regulation in the southern Yellow Sea (China): Seasonal variability. *Continent. Shelf Res.* 29, 2178–2194. doi: 10.1016/j.csr.2009.08.010

Gattuso, J.-P., Frankignoulle, M., and Wollast, R. (1998). Carbon and carbonate metabolism in coastal aquatic ecosystems. *Annu. Rev. Ecol. Syst.* 29, 405–434. doi: 10.1146/annurev.ecolsys.29.1.405

Geider, R. J. (1993). Quantitative phytoplankton physiology: implications for primary production and phytoplankton growth. *ICES Mar. Sci. Symp.* 197, 52–62.

Geider, R. J., Maclntyre, H. L., and Kana, T. M. (1998). A dynamic regulatory model of phytoplanktonic acclimation to light, nutrients, and temperature. *Limnol. Oceanogr.* 43, 679–694. doi: 10.4319/lo.1998.43.4.0679

Graber, H. C., Beardsley, R. C., and Grant, W. D. (1989). Storm-generated surface waves and sediment resuspension in the East China and Yellow seas. *J. Phys. Oceanogr.* 19, 1039–1059. doi: 10.1175/1520-0485(1989)0192.0.CO;2

Guo, X., and Zhang, Y. (2005). Particle flux through the Huanghai Sea cold water mass. *Acta Oceanol. Sin.* 24 (5), 78–88.

Guo, C., Zhang, G., Sun, J., Leng, X., Xu, W., Wu, C., et al. (2020). Seasonal responses of nutrient to hydrology and biology in the southern Yellow Sea. *Continent. Shelf Res.* 206, 104207. doi: 10.1016/j.csr.2020.104207

Guo, X., Zhang, Y., Zhang, F., and Cao, Q. (2010). Characteristics and flux of settling particulate matter in neritic waters: The southern Yellow Sea and the East China Sea. *Deep Sea Res. Part II: Topical Stud. Oceanogr.* 57, 1058–1063. doi: 10.1016/j.dsr2.2010.02.007

Hama, T., Shin, K., and Handa, N. (1997). Spatial variability in the primary productivity in the East China Sea and its adjacent waters. *J. Oceanogr.* 53, 41–51. doi: 10.1007/BF02700748

Hedges, J. I., Keil, R. G., and Benner, R. (1997). What happens to terrestrial organic matter in the ocean? *Organic Geochem.* 27, 195–212. doi: 10.1016/S0146-6380(97)00066-1

Heussner, S., de Madron, X. D., Calafat, A., Canals, M., Carbonne, J., Delsaut, N., et al. (2006). Spatial and temporal variability of downward particle fluxes on a continental slope: Lessons from an 8-yr experiment in the Gulf of Lions (NW Mediterranean). *Mar. Geol.* 234, 63–92. doi: 10.1016/j.margeo.2006.09.003

Hoshika, A., Tanimoto, T., Mishima, Y., Iseki, K., and Okamura, K. (2003). Variation of turbidity and particle transport in the bottom layer of the East China Sea. *Deep Sea Res. Part II: Topical Stud. Oceanogr.* 50, 443–455. doi: 10.1016/S0967-0645(02)00462-9

Hung, C.-C., Chen, Y.-F., Hsu, S.-C., Wang, K., Chen, J., and Burdige, D. J. (2016). Using rare earth elements to constrain particulate organic carbon flux in the East China Sea. *Sci. Rep.* 6, 33880. doi: 10.1038/srep33880

Hung, C.-C., Gong, G.-C., Chiang, K.-P., Chen, H.-Y., and Yeager, K. M. (2009). Particulate carbohydrates and uronic acids in the northern East China Sea. *Estuarine Coast. Shelf Sci.* 84, 565–572. doi: 10.1016/j.ecss.2009.07.025

Hung, C.-C., Gong, G.-C., Chou, W.-C., Chung, C.-C., Lee, M.-A., Chang, Y., et al. (2010). The effect of typhoon on particulate organic carbon flux in the southern East China Sea. *Biogeosciences* 7, 3007–3018. doi: 10.5194/bg-7-3007-2010

Hung, J.-J., Lin, P.-L., and Liu, K.-K. (2000). Dissolved and particulate organic carbon in the southern East China Sea. *Continent. Shelf Res.* 20, 545–569. doi: 10.1016/S0278-4343(99)00085-0

Hung, C.-C., Tseng, C.-W., Gong, G.-C., Chen, K.-S., Chen, M.-H., and Hsu, S.-C. (2013). Fluxes of particulate organic carbon in the East China Sea in summer. *Biogeosciences* 10, 6469–6484. doi: 10.5194/bg-10-6469-2013

Hu, L., Shi, X., Guo, Z., Wang, H., and Yang, Z. (2013). Sources, dispersal and preservation of sedimentary organic matter in the Yellow Sea: The importance of depositional hydrodynamic forcing. *Mar. Geol.* 335, 52–63. doi: 10.1016/j.margeo.2012.10.008

Hwang, J., Druffel, E. R., and Eglinton, T. I. (2010). Widespread influence of resuspended sediments on oceanic particulate organic carbon: Insights from radiocarbon and aluminum contents in sinking particles. *Global Biogeochem. Cycles* 24, GB4016. doi: 10.1029/2010GB003802

Hwang, J., Druffel, E. R., and Komada, T. (2005). Transport of organic carbon from the California coast to the slope region: A study of $\Delta^{14}C$ and $\delta^{13}C$ signatures of organic compound classes. *Global Biogeochem. Cycles* 19, GB2018. doi: 10.1029/2004GB002422

Hwang, J., Eglinton, T. I., Krishfield, R. A., Manganini, S. J., and Honjo, S. (2008). Lateral organic carbon supply to the deep Canada basin. *Geophys. Res. Lett.* 35, L11607. doi: 10.1029/2008GL034271

Iseki, K., Okamura, K., and Kiyomoto, Y. (2003). Seasonality and composition of downward particulate fluxes at the continental shelf and Okinawa Trough in the East China Sea. *Deep Sea Res. Part II: Topical Stud. Oceanogr.* 50, 457–473. doi: 10.1016/S0967-0645(02)00468-X

Jin, J., Liu, S. M., Ren, J. L., Liu, C. G., Zhang, J., and Zhang, G. L. (2013). Nutrient dynamics and coupling with phytoplankton species composition during the spring blooms in the Yellow Sea. *Deep Sea Res. Part II: Topical Stud. Oceanogr.* 97, 16–32. doi: 10.1016/j.dsr2.2013.05.002

Kao, S., Lin, F., and Liu, K. (2003). Organic carbon and nitrogen contents and their isotopic compositions in surficial sediments from the East China Sea shelf and the southern Okinawa Trough. *Deep Sea Res. Part II: Topical Stud. Oceanogr.* 50, 1203–1217. doi: 10.1016/S0967-0645(03)00018-3

Kerfoot, W. C., Budd, J. W., Eadie, B. J., Vanderploeg, H. A., and Agy, M. (2004). Winter storms: Sequential sediment traps record *Daphnia* ephippial

production, resuspension, and sediment interactions. *Limnol. Oceanogr.* 49, 1365–1381. doi: 10.4319/lo.2004.49.4_part_2.1365

Kiorboe, T. (1998). Small-scale turbulence, marine snow formation, and planktivorous feeding. *Sci. Marina* 61, 141–158. doi: 10.1023/A:1018427509311

Kristensen, P., Søndergaard, M., and Jeppesen, E. (1992). Resuspension in a shallow eutrophic lake. *Hydrobiologia* 228, 101–109. doi: 10.1007/BF00006481

Lan, X., Zhang, X., Zhao, G., and Zhang, Z. (2009). Distributions of rare earth elements in sediments from core NT1 of the South Yellow Sea and their provenance discrimination. *Geochimica* 38, 123–132. doi: 10.1016/S1874-8651(10)60080-4

Lee, H.-J., and Chao, S.-Y. (2003). A climatological description of circulation in and around the East China Sea. *Deep Sea Res. Part II: Topical Stud. Oceanogr.* 50, 1065–1084. doi: 10.1016/S0967-0645(03)00010-9

Lee, H. J., and Chough, S. K. (1989). Sediment distribution, dispersal and budget in the Yellow Sea. *Mar. Geol.* 87, 195–205. doi: 10.1016/0025-3227(89)90061-3

Lee, T. N., Williams, E., Wang, J., Evans, R., and Atkinson, L. (1989). Response of South Carolina continental shelf waters to wind and Gulf Stream forcing during winter of 1986. *J. Geophys. Res.* 94 (C8), 10715–10754. doi: 10.1029/JC094iC08p10715

Li, X., Bianchi, T. S., Allison, M. A., Chapman, P., Mitra, S., Zhang, Z., et al. (2012). Composition, abundance and age of total organic carbon in surface sediments from the inner shelf of the East China Sea. *Mar. Chem.* 145, 37–52. doi: 10.1016/j.marchem.2012.10.001

Lie, H.-J., Cho, C.-H., Lee, J.-H., and Lee, S. (2003). Structure and eastward extension of the Changjiang River plume in the East China Sea. *J. Geophys. Res.* 108 (C3), 3077. doi: 10.1029/2001JC001194

Liénart, C., Savoye, N., David, V., Ramond, P., Tress, P. R., Hanquiez, V., et al. (2018). Dynamics of particulate organic matter composition in coastal systems: Forcing of spatio-temporal variability at multi-systems scale. *Prog. Oceanogr.* 162, 271–289. doi: 10.1016/j.pocean.2018.02.026

Lin, C., Ning, X., Su, J., Lin, Y., and Xu, B. (2005). Environmental changes and the responses of the ecosystems of the Yellow Sea during 1976–2000. *J. Mar. Syst.* 55, 223–234. doi: 10.1016/j.jmarsys.2004.08.001

Li, G., Qiao, L., Dong, P., Ma, Y., Xu, J., Liu, S., et al. (2016). Hydrodynamic condition and suspended sediment diffusion in the Yellow Sea and East China Sea. *J. Geophys. Res.: Oceans* 121, 6204–6222. doi: 10.1002/2015JC011442

Liu, H., Huang, Y., Zhai, W., Guo, S., Jin, H., and Sun, J. (2015). Phytoplankton communities and its controlling factors in summer and autumn in the southern Yellow Sea, China. *Acta Oceanol. Sin.* 34 (2), 114–123. doi: 10.1007/s13131-015-0620-0

Liu, D., Keesing, J. K., He, P., Wang, Z., Shi, Y., and Wang, Y. (2013). The world's largest macroalgal bloom in the Yellow Sea, China: formation and implications. *Estuarine Coast. Shelf Sci.* 129, 2–10. doi: 10.1016/j.ecss.2013.05.021

Liu, D., Keesing, J. K., Xing, Q., and Shi, P. (2009). World's largest macroalgal bloom caused by expansion of seaweed aquaculture in China. *Mar. Pollut. Bull.* 58, 888–895. doi: 10.1016/j.marpolbul.2009.01.013

Liu, J., Kong, X., Saito, Y., Liu, J. P., Yang, Z., and Wen, C. (2013b). Subaqueous deltaic formation of the Old Yellow River (AD 1128–1855) on the western South Yellow Sea. *Mar. Geol.* 344, 19–33. doi: 10.1016/j.margeo.2013.07.003

Liu, J., Xu, K., Li, A., Milliman, J., Velozzi, D., Xiao, S., et al. (2007). Flux and fate of Yangtze River sediment delivered to the East China Sea. *Geomorphology* 85, 208–224. doi: 10.1016/j.geomorph.2006.03.023

Longhurst, A. (1995). Seasonal cycles of pelagic production and consumption. *Prog. Oceanogr.* 36, 77–167. doi: 10.1016/0079-6611(95)00015-1

Luo, Z., Zhu, J., Wu, H., and Li, X. (2017). Dynamics of the sediment plume over the Yangtze bank in the Yellow and East China seas. *J. Geophys. Res.: Oceans* 122, 10073–10090. doi: 10.1002/2017JC013215

Mari, X., Torreton, J. P., Claire, B. T. T., Bouvier, T., Thuoc, C. V., Lefebvre, J. P., et al. (2012). Aggregation dynamics along a salinity gradient in the Bach Dang Estuary, north Vietnam. *Estuarine Coast. Shelf Sci.* 96, 151–158. doi: 10.1016/j.ecss.2011.10.028

Martiny, A. C., Pham, C. T., Primeau, F. W., Vrugt, J. A., Moore, J. K., Levin, S. A., et al. (2013b). Strong latitudinal patterns in the elemental ratios of marine plankton and organic matter. *Nat. Geosci.* 6, 279–283. doi: 10.1038/NGEO1757

Martiny, A., Vrugt, J. A., Primeau, F. W., and Lomas, M. W. (2013a). Regional variation in the particulate organic carbon to nitrogen ratio in the surface ocean. *Global Biogeochem. Cycles* 27, 723–731. doi: 10.1002/gbc.20061

McKee, B. A., Aller, R., Allison, M., Bianchi, T., and Kineke, G. (2004). Transport and transformation of dissolved and particulate materials on continental margins influenced by major Rivers: benthic boundary layer and seabed processes. *Continent. Shelf Res.* 24, 899–926. doi: 10.1016/j.csr.2004.02.009

Meyers, P. A. (2003). Applications of organic geochemistry to paleolimnological reconstructions: a summary of examples from the Laurentian Great Lakes. *Organic Geochem.* 34, 261–289. doi: 10.1016/S0146-6380(02)00168-7

Milliman, J. D., and Farnsworth, K. L. (2011). *River discharge to the coastal ocean: A global synthesis* (UK: Cambridge University Press), 394pp. doi: 10.1017/CBO9780511781247

Milliman, J. D., Huang-ting, S., Zuo-sheng, Y., and Mead, R. H. (1985). Transport and deposition of river sediment in the Changjiang estuary and adjacent continental shelf. *Continent. Shelf Res.* 4, 37–45. doi: 10.1016/0278-4343(85)90020-2

Mollenhauer, G., and Eglinton, T. I. (2007). Diagenetic and sedimentological controls on the composition of organic matter preserved in California borderland basin sediments. *Limnol. Oceanogr.* 52, 558–576. doi: 10.2307/40006106

Moon, J.-H., Pang, I.-C., and Yoon, J.-H. (2009). Response of the Changjiang diluted water around Jeju Island to external forcings: A modeling study of 2002 and 2006. *Continent. Shelf Res.* 29, 1549–1564. doi: 10.1016/j.csr.2009.04.007

Nilsson, M. M., Hylén, A., Ekeroth, N., Kononets, M. Y., Viktorsson, L., Almroth-Rosell, E., et al. (2021). Particle shuttling and oxidation capacity of sedimentary organic carbon on the Baltic Sea system scale. *Mar. Chem.* 232, 103963. doi: 10.1016/j.marchem.2021.103963

Niu, Y., Liu, C., Lu, X., Zhu, L., Sun, Q., and Wang, S. (2021). Phytoplankton blooms and its influencing environmental factors in the southern Yellow Sea. *Regional Stud. Mar. Sci.* 47, 101916. doi: 10.1016/j.rsma.2021.101916

Oguri, K., Matsumoto, E., Yamada, M., Saito, Y., and Iseki, K. (2003). Sediment accumulation rates and budgets of depositing particles of the East China Sea. *Deep Sea Res. Part II: Topical Stud. Oceanogr.* 50, 513–528. doi: 10.1016/S0967-0645(02)00465-4

Peleg, M., Normand, M. D., and Corradini, M. G. (2012).). The Arrhenius Equation revisited. *Crit. Rev. Food Sci. Nutr.* 52, 830–851. doi: 10.1080/10408398.2012.667460

Peng, M.-C., and Hu, D.-X. (1997). Outflow of suspended materials from the Changjiang River mouth. *Chin. J. Oceanol. Limnol.* 15, 258–263. doi: 10.1007/BF02850882

Qiao, S., Shi, X., Wang, G., Zhou, L., Hu, B., Hu, L., et al. (2017). Sediment accumulation and budget in the Bohai Sea, Yellow Sea and East China Sea. *Mar. Geol.* 390, 270–281. doi: 10.1016/j.margeo.2017.06.004

Rosa, F. (1985). Sedimentation and sediment resuspension in Lake Ontario. *J. Great Lakes Res.* 11, 13–25. doi: 10.1016/S0380-1330(85)71738-8

Schartau, M., Engel, A., Schröter, J., Thoms, S., Völker, C., and Wolf-Gladrow, D. (2007). Modelling carbon overconsumption and the formation of extracellular particulate organic carbon. *Biogeosciences* 4, 433–454. doi: 10.5194/bg-4-433-2007

Schneider, B., Schlitzer, R., Fischer, G., and Nöthig, E. M. (2003). Depth-dependent elemental compositions of particulate organic matter (POM) in the ocean. *Global Biogeochem. Cycles* 17, 1032. doi: 10.1029/2002GB001871

Sharp, J. H. (1991). "Total mass and particulate carbon, nitrogen and phosphorus," in *Marine particles: Analysis and characterization*, vol. 63 . Eds. D. C. Hurd and D. W. Spencer, (Washington, D.C.:American Geophysical Union)87–90. doi: 10.1029/GM063p0087

Sheu, D., Jou, W., Chung, Y., Tang, T., and Hung, J. (1999). Geochemical and carbon isotopic characterization of particles collected in sediment traps from the East China Sea continental slope and the Okinawa Trough northeast of Taiwan. *Continent. Shelf Res.* 19, 183–203. doi: 10.1016/S0278-4343(98)00081-8

Shi, X., Qi, M., Tang, H., and Han, X. (2015). Spatial and temporal nutrient variations in the Yellow Sea and their effects on *Ulva prolifera* blooms. *Estuarine Coast. Shelf Sci.* 163, 36–43. doi: 10.1016/j.ecss.2015.02.007

Shi, X., Wang, X., Han, X., Zhu, C., Sun, X., and Zhang, C. (2003). Nutrient distribution and its controlling mechanism in the adjacent area of Changjiang River Estuary. *J. Appl. Ecol.* 14, 1086–1092. doi: 10.1007/BF02860423

Simon, M., Grossart, H.-P., Schweitzer, B., and Ploug, H. (2002). Microbial ecology of organic aggregates in aquatic ecosystems. *Aquat. Microbial. Ecol.* 28, 175–211. doi: 10.3354/ame028175

Song, Z., Li, J., Meng, F., Tang, W., and Yuan, X. (2018). Seasonal distribution of suspended particulate matter off China's Subei coast. *Polish J. Environ. Stud.* 27, 845–852. doi: 10.15244/pjoes/75826

Song, G., Liu, S., Zhu, Z., Zhai, W., Zhu, C., and Zhang, J. (2016). Sediment oxygen consumption and benthic organic carbon mineralization on the continental shelves of the East China Sea and the Yellow Sea. *Deep Sea Res. Part II: Topical Stud. Oceanogr.* 124, 53–63. doi: 10.1016/j.dsr2.2015.04.012

Taylor, J., Cottingham, S., Billinge, J., and Cunliffe, M. (2014). Seasonal microbial community dynamics correlate with phytoplankton-derived polysaccharides in surface coastal waters. *ISME J.* 8, 245–248. doi: 10.1038/ismej.2013.178

Taylor, A. H., Geider, R. J., and Gilbert, F. J. (1997). Seasonal and latitudinal dependencies of phytoplankton carbon-to-chlorophyll a ratios: results of a modelling study. *Mar. Ecol. Prog. Ser.* 152, 51–66. doi: 10.3354/meps152051

Trefry, J. H., Metz, S., Nelsen, T. A., Trocine, R. P., and Eadie, B. J. (1994). Transport of particulate organic carbon by the Mississippi River and its fate in the Gulf of Mexico. *Estuaries* 17, 839–849. doi: 10.2307/1352752

Turner, J. T. (2015). Zooplankton fecal pellets, marine snow, phytodetritus and the ocean's biological pump. *Prog. Oceanogr.* 130, 205–248. doi: 10.1016/j.pocean.2014.08.005

Verdugo, P. (2012). Marine microgels. *Annu. Rev. Mar. Sci.* 4, 375–400. doi: 10.1146/annurev-marine-120709-142759

Volkman, J. K., and Tanoue, E. (2002). Chemical and biological studies of particulate organic matter in the ocean. *J. Oceanogr.* 58, 265–279. doi: 10.1023/A:1015809708632

Walsh, J. J. (1991). Importance of continental margins in the marine biogeochemical cycling of carbon and nitrogen. *Nature* 350, 53–55. doi: 10.1038/350053a0

Wang, X., Borgne, R. L., Murtugudde, R., Busalacchi, A., and Behrenfeld, M. (2008). Spatial and temporal variations in dissolved and particulate organic nitrogen in the equatorial Pacific: Biological and physical influences. *Biogeosciences* 5, 1705–1721. doi: 10.5194/bg-5-1705-2008

Wang, X.-C., Chen, R. F., and Gardner, G. B. (2004). Sources and transport of dissolved and particulate organic carbon in the Mississippi River estuary and adjacent coastal waters of the northern Gulf of Mexico. *Mar. Chem.* 89, 241–256. doi: 10.1016/j.marchem.2004.02.014

Wang, Y., Liu, D., Richard, P., and Li, X. (2013). A geochemical record of environmental changes in sediments from Sishili Bay, northern Yellow Sea, China: Anthropogenic influence on organic matter sources and composition over the last 100 years. *Mar. Pollut. Bull.* 77, 227–236. doi: 10.1016/j.marpolbul.2013.10.001

Wang, X. H., Qiao, F., Lu, J., and Gong, F. (2011). The turbidity maxima of the northern Jiangsu shoal-water in the Yellow Sea, China. *Estuarine Coast. Shelf Sci.* 93, 202–211. doi: 10.1016/j.ecss.2010.10.020

Wang, Z., Xiao, J., Fan, S., Li, Y., Liu, X., and Liu, D. (2015). Who made the world's largest green tide in China?–an integrated study on the initiation and early development of the green tide in Yellow Sea. *Limnol. Oceanogr.* 60, 1105–1117. doi: 10.1002/lno.10083

Wang, J., Yu, Z., Wei, Q., Yang, F., Dong, M., Li, D., et al. (2020). Intra- and inter-seasonal variations in the hydrological characteristics and nutrient conditions in the southwestern Yellow Sea during spring to summer. *Mar. Pollut. Bull.* 156, 111139. doi: 10.1016/j.marpolbul.2020.111139

Wang, B.-D., Zhan, R., and Xu, M.-D. (2002). Molar ratios of C, N, P of particulate matter and their vertical fluxes in the Yellow Sea. *Chin. J. Oceanol. Limnol.* 20 (1), 91–96. doi: 10.1007/BF02846617

Wan, X., Wu, Z., Zhang, Z., and Li, J. (2005). Simulation of coupled pelagic-benthic ecosystem of the Yellow Sea cold water mass. *Chin. J. Oceanol. Limnol.* 23, 393–399. doi: 10.1007/BF02842682

Wassmann, P. (1990). Calculating the load of organic carbon to the aphotic zone in eutrophicated coastal waters. *Mar. Pollut. Bull.* 21, 183–187. doi: 10.1016/0025-326X(90)90499-X

Wei, Q., Wang, B., Fu, M., Sun, J., Yao, Q., Xin, M., et al. (2020). Spatiotemporal variability of physical-biogeochemical processes and intrinsic correlations in the semi-enclosed South Yellow Sea. *Acta Oceanol. Sin.* 39 (10), 11–26. doi: 10.1007/s13131-020-1656-3

Wei, Q., Yu, Z., Wang, B., Fu, M., Xia, C., Liu, L., et al. (2016). Coupling of the spatial–temporal distributions of nutrients and physical conditions in the southern Yellow Sea. *J. Mar. Syst.* 156, 30–45. doi: 10.1016/j.jmarsys.2015.12.001

Wei, Q., Yu, Z., Wang, B., Wu, H., Sun, J., Zhang, X., et al. (2017). Offshore detachment of the Changjiang River plume and its ecological impacts in summer. *J. Oceanogr.* 73, 277–294. doi: 10.1007/s10872-016-0402-0

Wen, F., Sun, X., Zheng, S., Luo, X., Feng, Q., and Sun, S. (2012). Spatial and seasonal variations of chlorophyll a and primary productivity in spring and summer in the yelow Sea and East China Sea (in Chinese). *Oceanol. Limnol. Sin.* 43 (3), 438–444.

Wieder, W. R., Cleveland, C. C., Smith, W. K., and Todd-Brown, K. (2015). Future productivity and carbon storage limited by terrestrial nutrient availability. *Nat. Geosci.* 8, 441–444. doi: 10.1038/NGEO2413

Winogradow, A., Mackiewicz, A., and Pempkowiak, J. (2019). Seasonal changes in particulate organic matter (POM) concentrations and properties measured from deep areas of the Baltic Sea. *Oceanologia* 61, 505–521. doi: 10.1016/j.oceano.2019.05.004

Wurl, O., Miller, L., Röttgers, R., and Vagle, S. (2009). The distribution and fate of surface-active substances in the sea-surface microlayer and water column. *Mar. Chem.* 115, 1–9. doi: 10.1016/j.marchem.2009.04.007

Xing, L., Zhao, M., Gao, W., Wang, F., Zhang, H., Li, L., et al. (2014). Multiple proxy estimates of source and spatial variation in organic matter in surface sediments from the southern Yellow Sea. *Organic Geochem.* 76, 72–81. doi: 10.1016/j.orggeochem.2014.07.005

Yang, W., Huang, Y., Chen, M., Zhang, L., Li, H., Liu, G., et al. (2006). Disequilibria between ^{210}Po and ^{210}Pb in surface waters of the southern South China Sea and their implications. *Sci. China Ser. D* 49, 103–112. doi: 10.1007/s11430-004-5233-y

Yang, S., and Youn, J.-S. (2007). Geochemical compositions and provenance discrimination of the central South Yellow Sea sediments. *Mar. Geol.* 243, 229–241. doi: 10.1016/j.margeo.2007.05.001

Ye, F., Guo, W., Shi, Z., Jia, G., and Wei, G. (2017). Seasonal dynamics of particulate organic matter and its response to flooding in the Peal River Estuary, China, revealed by stable isotope (δ^{13}c and δ^{15}n) analyses. *J. Geophys. Res.: Oceans* 122, 6835–6856. doi: 10.1002/2017JC012931

Yuan, D., Zhu, J., Li, C., and Hu, D. (2008). Cross-shelf circulation in the Yellow and East China seas indicated by MODIS satellite observations. *J. Mar. Syst.* 70, 134–149. doi: 10.1016/j.jmarsys.2007.04.002

Zäncker, B., Bracher, A., Röttgers, R., and Engel, A. (2017). Variations of the organic matter composition in the sea surface microlayer: A comparison between open ocean, coastal, and upwelling sites off the Peruvian coast. *Front. Microbiol.* 8. doi: 10.3389/fmicb.2017.02369

Zhang, Q., and Blomquist, J. D. (2018). Watershed export of fine sediment, organic carbon, and chlorophyll-a to Chesapeake Bay: Spatial and temporal patterns in 1984–2016. *Sci. Total Environ.* 619-620, 1066–1078. doi: 10.1016/j.scitotenv.2017.10.279

Zhang, Q., and Wu, J. (2018). Sediment suspension by straining-induced convection at the head of salinity intrusion. *J. Geophys. Res.: Oceans* 123, 656–671. doi: 10.1002/2017JC013192

Zhang, J., Wu, Y., Jennerjahn, T. C., Ittekkot, V., and He, Q. (2007). Distribution of organic matter in the Changjiang (Yangtze River) Estuary and their stable carbon and nitrogen isotopic ratios: Implications for source discrimination and sedimentary dynamics. *Mar. Chem.* 106, 111–126. doi: 10.1016/j.marchem.2007.02.003

Zhang, Y.-S., Zhang, F.-J., Guo, X.-W., and Zhang, M.-P. (2004). Vertical flux of the settling particulate matter in the water column of the Yellow Sea in summer. *Oceanol. Limnol. Sin.* 35 (3), 230–38.

Zhao, B., Yao, P., Bianchi, T. S., Arellano, A. R., Wang, X., Yang, J., et al. (2018). The remineralization of sedimentary organic carbon in different sedimentary regimes of the Yellow and East China seas. *Chem. Geol.* 495, 104–117. doi: 10.1016/j.chemgeo.2018.08.012

Zhao, B., Yao, P., Bianchi, T., and Yu, Z. (2021). Controls on organic carbon burial in the Eastern China marginal seas: A regional synthesis. *Global Biogeochem. Cycles* 35, e2020GB006608. doi: 10.1029/2020GB006608

Zhong, Y., Qiao, L., Song, D., Ding, Y., Xu, J., Xue, W., et al. (2020). Impact of cold water mass on suspended sediment transport in the South Yellow Sea. *Mar. Geol.* 428, 106244. doi: 10.1016/j.margeo.2020.106244

Zhong, Q., Wang, J., Du, J., Bi, Q., and Zhao, F. (2019). The ^{210}Po/^{210}Pb disequilibrium in a spring-blooming marginal sea, the southern Yellow Sea. *J. Environ. Radioact.* 207, 15–26. doi: 10.1016/j.jenvrad.2019.05.017

Zhong, Q., Yu, T., Lin, H., Lin, J., Ji, J., Ni, J., et al. (2021). ^{210}Po-^{210}Pb disequilibrium in the western North Pacific Ocean: particle cycling and POC export. *Front. Mar. Sci.* 8. doi: 10.3389/fmars.2021.700524

Zhou, C., Dong, P., and Li, G. (2015). Hydrodynamic processes and their impacts on the mud deposit in the southern Yellow Sea. *Mar. Geol.* 360, 1–16. doi: 10.1016/j.margeo.2014.11.012

Zhou, M., Shen, Z., and Yu, R. (2008). Responses of a coastal phytoplankton community to increased nutrient input from the Changjiang (Yangtze) River. *Continent. Shelf Res.* 28, 1483–1489. doi: 10.1016/j.csr.2007.02.009

Zhou, F., Xue, H., Huang, D., Xuan, J., Ni, X., Xiu, P., et al. (2015). Cross-shelf exchange in the shelf of the East China Sea. *J. Geophys. Res.: Oceans* 120, 1545–1572. doi: 10.1002/2014JC010567

Zhu, Z.-Y., Ng, W.-M., Liu, S.-M., Zhang, J., Chen, J.-C., and Wu, Y. (2009). Estuarine phytoplankton dynamics and shift of limiting factors: A study in the Changjiang (Yangtze River) Estuary and adjacent area. *Estuarine Coast. Shelf Sci.* 84, 393–401. doi: 10.1016/j.ecss.2009.07.005

Zhu, P., and Wu, H. (2018). Origins and transports of the low-salinity coastal water in the southwestern Yellow Sea. *Acta Oceanol. Sin.* 37 (4), 1–11. doi: 10.1007/s13131-018-1200-x

Zhu, Z. Y., Zhang, J., Wu, Y., and Lin, J. (2006). Bulk particulate organic carbon in the East China Sea: tidal influence and bottom transport. *Prog. Oceanogr.* 69, 37–60. doi: 10.1016/j.pocean.2006.02.014

frontiers | Frontiers in Marine Science

TYPE Original Research
PUBLISHED 26 September 2022
DOI 10.3389/fmars.2022.953648

Check for updates

OPEN ACCESS

EDITED BY
Ana Carolina Ruiz-Fernández,
National Autonomous University of Mexico, Mexico

REVIEWED BY
Peng Zhang,
Guangdong Ocean University, China
Pradipta Ranjan Muduli,
Chilika Development Authority, India
Fajin Chen,
Guangdong Ocean University, China

*CORRESPONDENCE
Hyun Je Park
phj13579@gwnu.ac.kr

†These authors have contributed equally to this work

SPECIALTY SECTION
This article was submitted to Marine Pollution, a section of the journal Frontiers in Marine Science

RECEIVED 26 May 2022
ACCEPTED 07 September 2022
PUBLISHED 26 September 2022

CITATION
Lee D-Y, Kwak JH, Park TH, Kang HY, Kim D, Hwang S and Park HJ (2022) Seasonal variations in biochemical and stable isotope compositions of particulate organic matter in two contrasting temperate coastal lagoons of Korea.
Front. Mar. Sci. 9:953648.
doi: 10.3389/fmars.2022.953648

COPYRIGHT
© 2022 Lee, Kwak, Park, Kang, Kim, Hwang and Park. This is an open-access article distributed under the terms of the Creative Commons Attribution License (CC BY). The use, distribution or reproduction in other forums is permitted, provided the original author(s) and the copyright owner(s) are credited and that the original publication in this journal is cited, in accordance with accepted academic practice. No use, distribution or reproduction is permitted which does not comply with these terms.

Seasonal variations in biochemical and stable isotope compositions of particulate organic matter in two contrasting temperate coastal lagoons of Korea

Dong-Young Lee[1†], Jung Hyun Kwak[2†], Tae Hee Park[1], Hee Yoon Kang[3], Dongyoung Kim[4], Sungmin Hwang[5] and Hyun Je Park[1*]

[1]Department of Marine Ecology and Environment, Gangneung-Wonju National University, Gangneung, South Korea, [2]Jeju Fisheries Research Institute, National Institute of Fisheries Science, Jeju, South Korea, [3]Department of Oceanography, Chonnam National University, Gwangju, South Korea, [4]School of Earth Sciences & Environmental Engineering, Gwangju Institute of Science and Technology (GIST), Gwangju, South Korea, [5]Clean Energy Research Center, Korea Institute for Science and Technology (KIST), Seoul, South Korea

The geomorphology of coastal lagoons has an important effect on the hydrological balance between fresh water and seawater, which exhibit a wide range of salinity from nearly fresh water to hypersaline water. The present study aimed to characterize seasonal biogeochemical properties of suspended particulate organic matter (POM) in response to environmental variability driven by hydrological dynamics in contrasting coastal lagoon systems. We selected two lagoons distinguished by their geomorphological features, a permanently open artificial lagoon (Gyeongpoho) and an intermittently open natural lagoon (Hyangho), analyzed environmental characteristics, and compared the seasonal differences in the biochemical compositions of POM. Variations in temperature and precipitation in both lagoons showed the characteristics of a typical monsoon climate but variation in salinity differed 6.5–35.0 in Gyeongpoho and 1.1–10.8 in Hyangho. A self-organizing map analysis using the environmental data revealed that the spatiotemporal variations in salinity and nutrient concentrations differed significantly between the two lagoon systems, indicating a difference in hydrologic connectivity between lagoons and marine systems. Furthermore, a canonical correlation analysis highlighted that the POM properties differed according to physicochemical factors. The differing environmental conditions may affect the spatial and temporal variations in organic matter composition, resulting in significant differences in the biochemical composition of POM

between two lagoon systems. Overall, this information provides insight into the origin and transport process of POM under changing coastal lagoon environments caused by climatic and human activities.

KEYWORDS

Lagoons, suspended particulate organic matter, stable isotopes, biochemical composition, hydrologic connectivity

Introduction

Coastal lagoons are highly heterogeneous aquatic ecosystems formed as a result of the input of variable amounts of freshwater and seawater as transition zones between terrestrial and marine systems (Kjerfve, 1994). These coastal lagoons are among the most productive ecosystems which promote the biological activities of primary producers, owing to a great input of nutrients and organic matter (Pérez-Ruzafa et al., 2019). However, the estimated primary production in such coastal systems generally has highly variable ranges with spatiotemporal variability in biotic and abiotic factors (Carrasco Navas-Parejo et al., 2020). These drivers are significantly influenced by the geomorphological features of lagoons, which can control the hydrological balance between freshwater and seawater (Kjerfve, 1994). Furthermore, the degree of mixing between freshwater and seawater may lead to dynamic ecological processes causing high biodiversity due to environmental heterogeneity and habitat diversity (Pérez-Ruzafa et al., 2011; Lopes and Dias, 2015). As a result, coastal lagoon ecosystems are strongly influenced by hydrogeomorphological dynamics with high intrinsic variability in physicochemical factors at a regional scale, resulting in significant changes in the entire ecosystem.

The particulate organic matter (POM) in coastal waters is affected by a series of physicochemical and biological processes (Chen et al., 2021; Lu et al., 2021). The origins of POM in coastal lagoons are heterogeneous because of the influence of different sources of organic matter on the dynamics of physical, chemical, and biological factors (Rossi et al., 2003; Cresson et al., 2012; Lønborg et al., 2017; Garcia et al., 2018). Primary production by phytoplankton is a major source of POM in coastal lagoons. In addition, local benthic primary producers, such as macroalgae and marsh plants, and input of terrestrial material by freshwater discharge, also considerably contribute to the POM pool in the lagoons. Temporal changes in the diverse sources related to hydrological variations in lagoon systems may lead to a complex mixture of POM (Garcia et al., 2017; Lønborg et al., 2017). The POM in coastal environments exhibits seasonal variability in both quantitative and qualitative characteristics (Grémare et al., 1997; Rossi et al., 2003). Such seasonality in POM can influence the abundance, biomass, and recruitment of pelagic and benthic animal communities, and are major factors controlling food availability for consumer species (Kleppel and Burkart, 1995; Grémare et al., 1997). However, because of the complexity of the POM pool, it is very difficult to assess its quantity, quality, and relative importance for consumers in coastal lagoon systems.

Carbon and nitrogen stable isotope analysis has been successfully used to describe the source of organic matter in coastal environments, which varies with the spatial and temporal heterogeneity of biotic and abiotic factors (Cresson et al., 2012; Briand et al., 2015; Ke et al., 2017). Because marine and terrestrial primary producers have different photosynthetic pathways, they have distinct isotope ratios ($\delta^{13}C$ and $\delta^{15}N$) from each other (Peterson and Fry, 1987). In general, marine-derived organic matter has higher $\delta^{13}C$ and $\delta^{15}N$ values than terrestrial-derived organic matter. Moreover, major primary producers in temperate coastal systems may have highly variable $\delta^{13}C$ values; green macroalgae (−12‰ to −10‰) and microphytobenthos (−20‰ to −10‰) are more ^{13}C-enriched than marine phytoplankton (−24‰ to − 18‰) and marsh plants (−23‰ to − 29‰) (Fry and Sherr, 1984; Kang et al., 2003; Park et al., 2015; Park et al., 2016). The $\delta^{15}N$ values of primary producers may also reflect the source of inorganic nutrients and the magnitude of discrimination based on nutrient concentrations (McClelland and Valiela, 1998). The $\delta^{15}N$ values have been used as indicators of anthropogenic effects on coastal ecosystems because organic matter derived from anthropogenic sources (e.g., artificial fertilizer and sewage) is usually more ^{15}N-enriched than that from natural sources (Cole et al., 2004; Ke et al., 2017). Accordingly, the $\delta^{13}C$ and $\delta^{15}N$ values of POM are representative of the relative contribution of each of the diverse sources in complex coastal lagoon systems.

Analysis of the biochemical compositions of POM pools has been used to assess the origin of organic matter and its nutritional value as a basal food source available to primary consumers (Navarro and Thompson, 1995; Danovaro et al., 2000; Cresson et al., 2012). Labile compounds such as proteins, lipids, and carbohydrates of POM are metabolically utilized by consumers as readily bioavailable fractions (Mazzola

et al., 2001). In general, labile POM, which is a recently synthesized organic matter, is produced by phytoplankton photosynthesis. The biochemical composition of POM may reflect the physiological status and nutritional value of phytoplankton species in response to diverse environmental conditions, such as light, river discharge, and nutrient availability (Danovaro et al., 2000; Lee et al., 2017; Bhavya et al., 2019). Thus, this approach can provide useful information on the ambient environmental conditions and/or changes related to biogeochemical processes in complex coastal ecosystems.

Gyeongpoho and Hyangho, located adjacent to each other, have different ecological environments due to their hydrological characteristics (Park et al., 2020). However, there is no study on spatiotemporal variations in carbon and nitrogen dynamics of POM that could explain the ecosystem structure and function of the lagoons as a transition zone between ocean and land (Chen et al., 2021; Lu et al., 2022). The present study aimed to characterize the seasonal biogeochemical processes of POM in coastal lagoon systems in response to environmental variability using hydrological dynamics. We hypothesized that the biogeochemical characteristics of POM may be seasonally different depending on lagoon-specific processes, reflecting the hydrological conditions. To test this hypothesis, we compared the seasonal differences in isotopic signatures and biochemical compositions of POM with variations in environmental parameters between two permanently and intermittently open lagoons distinguished by the hydrological features. This information provides insight into the origin and transport process of POM under changing coastal lagoon environments caused by climatic and human activities.

Materials and methods

Study area

The sampling sites were located in two coastal lagoons [Gyeongpoho (sites Ga–c) and Hyangho (sites Ha–b)] on the eastern coast of the Korean Peninsula (Figure 1). The two lagoons have different environmental characteristics due to presence or absence of artificial channel that cause differences in salinity gradients, although the depth ranges in both lagoons were generally below 1.0 m. Gyeongpoho has an area of 0.90 km^2, and has several inlets through which freshwater inflows, and is connected to the sea *via* single artificial channel (WREO, 2008; Yoon et al., 2008). The artificial channel allows for continuous exchange of freshwater with seawater, which increases the freshwater's salinity. In contrast, Hyangho has an area of 0.14 km^2, and is usually separated from the sea by sand dunes, but is seasonally connected to the sea by a channel generated by heavy rainfall during summer monsoons (Park et al., 2020).

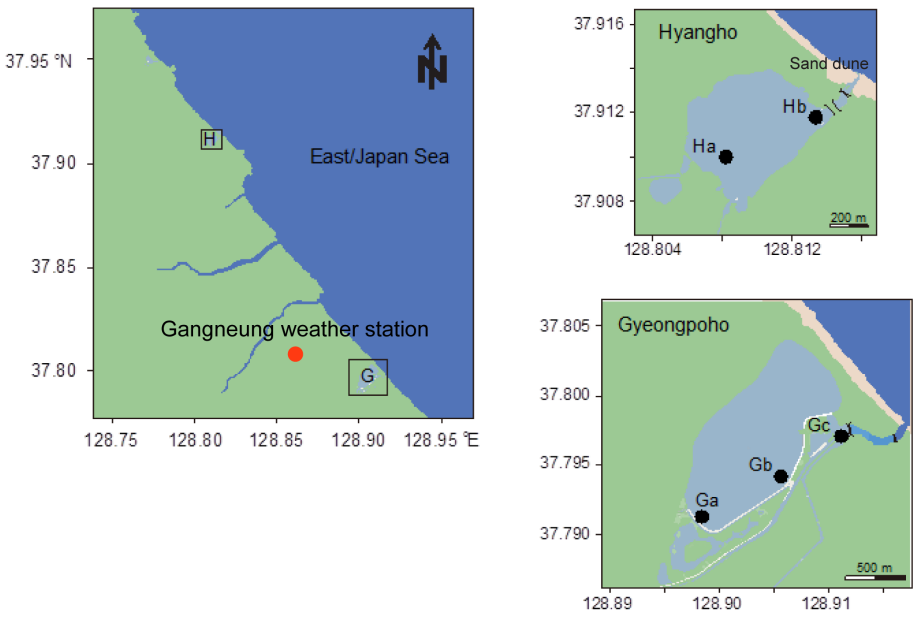

FIGURE 1
Map of the two coastal lagoons located along the eastern coast of the Korean peninsula.

Precipitation, sampling, and laboratory processing

Samplings were conducted monthly from June 2019 to April 2020 at three and two sites in Gyeongpoho and Hyangho, respectively, depending on their distance from the sea. Water samples for nutrient, POC, PON, biochemical composition (PCHO, PPr, and PLip), and Chl-*a* analyses were collected from the surface of each study site. Monthly precipitation and atmospheric temperature data for the study area were obtained from the Korean Meteorological Administration (https://data.kma.go.kr/data/grnd/selectAsosRltmList.do?pgmNo=36).

The water temperature and salinity were measured using a YSI 30 handheld meter (YSI Inc., Yellow Springs, OH, USA). Samples for Chl-*a* and biochemical composition analyses were filtered through 47 mm Whatman GF/F filters. Samples for POC analyses were pre-filtration through a 200 μm net for eliminating large debris and any zooplankton and then gently filtered through 25 mm pre-combusted (450°C, 2 h) Whatman GF/F filters. The filtered water samples for dissolved inorganic nutrient analyses were transferred into acid-washed polyethylene bottles and frozen at −20°C, and the filter samples were wrapped in aluminum foil and then kept in a deep freezer (at −80°C) until the analysis.

POC, PON, and C and N stable isotope analyses of POM

The filtered samples for POC, PON, and ^{13}C and ^{15}N isotope ratio analyses were fumed with HCl for 12 h to remove carbonate and were subsequently freeze-dried. The dried samples were sealed within a tin disk and analyzed using an elemental analyzer (Vario MICRO Cube; Elementar, Hanau, Germany) coupled to a continuous-flow isotope ratio mass spectrometer (CF-IRMS; Isoprime 100; Cheadle Hulme, UK). The samples were oxidized at high temperature (1150°C) using an elemental analyzer. The resultant CO_2 and N_2 gases were separated using an adsorption column and then moved into the CF-IRMS using a He carrier gas. The C and N stable isotope ratios are expressed as δ notation relative to Pee Dee Belemnite for C and atmospheric air for N, using the equation $\delta(‰) = [(R_{sample}/R_{standard})-1] \times 10^3$, where R is the $^{13}C/^{12}C$ or $^{15}N/^{14}N$ ratio. International standards of reference materials sucrose [8542 ANU, $\delta^{13}C = -10.47 \pm 0.13‰$, National Institute of Standards and Technology (NIST), Gaithersburg, MD, USA; RM 8568 UG, $\delta^{15}N = -1.8 \pm 0.1‰$, NIST] were used for calibration after analyzing every 10th unknown sample. The precision based on repeated analyses of acetanilide (Thermo Scientific) as an internal standard was within 0.07‰ for $\delta^{13}C$ and 0.11‰ for $\delta^{15}N$.

Biochemical composition of POM

The filter samples for carbohydrates, proteins, and lipids of POM (PCHO, PPr, and PLip, respectively) were analyzed according to Lowry et al. (1951); Dubois et al. (1956); Bligh and Dyer (1959), and Marsh and Weinstein (1966), respectively.

The samples for PCHO were put into 15 mL PP tubes containing 1 mL of deionized water and triturated using a glass rod. Next, 1 mL of 5% phenol was added for PCHO extraction, and the solutions were stored at room temperature for 40 min. Subsequently, 5 mL sulfuric acid was added to the solution and mixed using a vortex mixer. The mixture was centrifuged at 3500 rpm for 10 min. The PCHO concentration of POM was determined based on the absorbance at 490 nm using a UV spectrophotometer (Labomed Inc., Los Angeles, CA, USA) and quantified as glucose equivalents (Sigma-Aldrich, St. Louis, MO, USA).

The PPr samples were placed in centrifuge tubes containing 1 ml of deionized water. For PPr extraction, the filter was triturated using glass rod and 5 mL of an alkaline copper solution (a mixture of 2% Na_2CO_3 in 0.1 N NaOH with 0.5% $CuSO_4{\cdot}5H_2O$ in 1% sodium tartrate; 50:1, v/v) was added to the tube. The solution was mixed using a vortex mixer and maintained at room temperature for 10 min. Subsequently, 0.5 mL of Folin–Ciocalteu phenol reagent was added to the solution. The solution was then centrifuged at 3000 rpm for 10 min. The PPr concentration of POM was determined based on the absorbance at 750 nm using a UV spectrophotometer and quantified as bovine serum albumin equivalents (Sigma-Aldrich).

For extraction of PLip, the samples were put in 16 mL glass tubes containing 3 mL of chloroform-methan (1:2, v/v), followed by triturating using a glass rod and mixing using a vortex mixer. The solutions were allowed to stand for 1 h in a refrigerator (4°C) to prevent evaporation loss. Subsequently, the solutions were centrifuged at 2000 rpm for 10 min and the supernatants were collected and transferred into new tubes. The extraction procedure was performed immediately and repeated. After completing the extraction, 4 mL of deionized water was added to new tubes containing the extractant. The solution was then homogenized using a vortex mixer and centrifuged at 2000 rpm to separate the solvents into two phases (chloroform for lipids and methanol + water). The methanol/water phase was removed from the solvent using a Pasteur pipette. The tubes containing the chloroform phase were exposed to N_2 gas and were placed in a dry oven at 40°C to remove chloroform. After the chloroform phase was completely dried, 2 mL H_2SO_4 was added to the tubes. The tubes were heated to 200°C for 15 min using a heating block and cooled to room temperature. When the heating procedure was completed, the tubes were placed in a water bath at room temperature, and 3 ml of deionized water was added to the tubes. After all bubbles in the

tubes disappeared, the PLip concentrations of POM were analyzed based on the absorbance at a wavelength of 375 nm and quantified as tripalmitin equivalents.

Dissolved inorganic nutrient and Chl-a

Water samples for dissolved inorganic nutrients were analyzed using a QuAAtro nutrient analyzer (SEAL Analytical GmbH, Norderstedt, Germany) to determine ammonium (NH_4), nitrate (NO_3), nitrate (NO_2), phosphate (PO_4), and silicate (SiO_4) concentrations, according to the procedures developed for automated chemical analysis, with detection limits for 0.01 μM, 0.1 μM, 0.1 μM, 0.02 μM, and 0.1 μM, respectively (Murphy and Riley, 1962; Helder and De Vries, 1979; Hansen and Koroleff, 1999). Filter samples for Chl-*a* were extracted with 90% acetone in the dark at 4°C for 20 h and the concentrations of Chl-*a* were determined fluorometrically using a fluorometer (Turner Designs, Sunnyvale, CA) (Parsons et al., 1984).

Data analysis

Student *t* tests were performed to test variations in salinity data which were normal distribution. For data not normality distributed, Mann–Whitney *U* tests were performed to test the differences in C/N ratios and $\delta^{13}C$ and $\delta^{15}N$ values between the Gyeonghoho and Hyangho samples, and Kruskal–Wallis analysis of variance (ANOVA) was used to compare spatial and temporal variations in nutrients, Chl-*a*, POC, and PON concentrations, C/N ratios, and biochemical compositions among the study sites.

The environmental characteristics of the study sites were classified using a self-organizing map algorithm (SOM), which is a heuristic model used to visualize linear and nonlinear relationships in high-dimensional datasets (Kohonen, 1982). During the training process of the SOM, the data were assigned to neurons (processing units) in the input layer. After coarse training and fine-tuning steps, an output layer composed of output neurons was generated. In the output layer, a real sample was allocated to the most similar neuron, and samples with similar characteristics were arranged in adjacent neurons, which were placed in a two-dimensional grid. The number of output neurons was chosen according to the heuristic rule $5\sqrt{n}$, where n is the number of training samples (Vesanto and Alhoniemi, 2000; Park et al., 2006). Subsequently, the entire procedure was performed several times to determine the final size of the SOM at the minimum levels of the quantization error and topographic error by running the entire procedure several times (Park et al., 2003). Here, 4 5 output neurons were used for clustering of physicochemical data in this study (7 variables, 33 samples from Gyeongpoho and 22 samples from 7 variables in Hyangho). After training the SOM, the cluster boundaries between different SOM units were determined using Ward's linkage method with Euclidean distance measurements. The SOM training and clustering procedures were performed using version 4.0.2 of the R software (Licen et al., 2021).

Canonical correspondence analysis (CCA) using the CANOCO program was applied to outline the relationships between environmental factors (seven variables) and POM properties (six variables) at each study site (Ter Braak, 1986; Sundbäck and Snoeijs, 1991).

Results

Precipitation and physical factors

Variations in precipitation and air temperature in Gangneung City during the study period showed the characteristics of a typical monsoon climate (Figure 2). Precipitation increased rapidly from June 2019 with increasing temperature, peaked at 432 mm in October, and then decreased in winter. In both lagoons, temporal variations in water temperature in the study area represented also typical seasonality ranging from 3.6°C to 30.8°C (Figure 3).

The monthly variations in salinity showed different patterns between the two lagoons. In Gyeongpoho, salinity remained low during the summer monsoon period (from July to October 2019) and increased with decreasing precipitation in the fall and winter. Spatial variation in salinity among sites in Gyeongpoho was different, ranging from 6.5–21.2 at St. Ga, 11.6–26.9 at St. Gb, and 14.8–35 at St. Gc (Figure 3A). On the contrary, spatial differences in salinity between St. Ha (ranging 1.1–8.8) and St. Hb (1.1–10.8) were not significant (Student *t*-test, $p = 0.437$). At the Hyangho sites, salinity increased in September, three months after the increase in precipitation.

Properties of chemical factors

Widespread spatiotemporal variations in nutrient concentrations were observed in the study regions (Figures 4A–E). The maximum concentrations of ammonium (78.1 μM at St. Hb in August), nitrate (39.2 μM at St. Gc in July), nitrate (3.4 μM St. Gc in July), phosphate (4.1 μM at St. Gc in August), and silicate (82.5 μM at St. Ha in October) were recorded during the summer monsoon period. Significant differences in the nutrient concentrations (Kruskal–Wallis test, $p < 0.05$) among the study sites were detected, except for silicate during the non-monsoon period. These differences were attributed to the relatively high nutrient concentrations at St. Gc.

Chl-*a* concentrations peaked in March at St. Ga (15.0 μg L^{-1}), St. Ha (18.5 μg L^{-1}), and St. Hb (17.9 μg L^{-1}), showing no significant spatiotemporal variations (Kruskal–Wallis test, $p >$

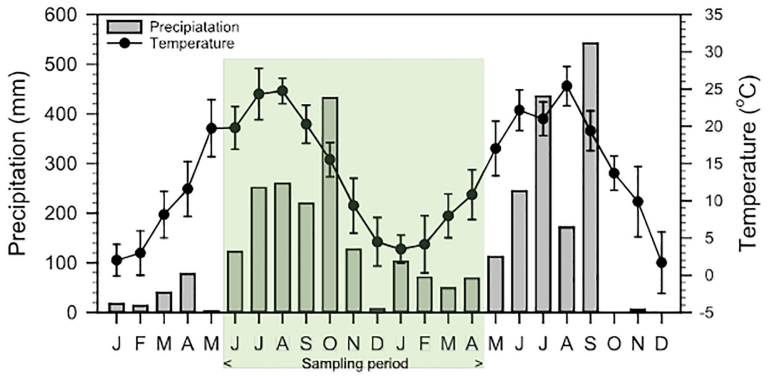

FIGURE 2
Monthly precipitation and average of atmospheric temperature variations from January 2019 to December 2020 in Gangneung city. Green box represents sampling period.

0.05) among the study sites (Figure 4F). Although the temporal variations in Chl-*a* concentrations among the study sites were not consistent, the concentrations tended to increase in July and March, except for St. Gc.

POC and PON concentrations at the study sites peaked in March 2020, except for St. Gc. The highest POC and PON concentrations were observed in March at St. Ga (9.20 mg C L^{-1}) and St. Gb (2.02 mg N L^{-1}), respectively. Interestingly, there were no significant differences (Kruskal-Wallis test, $p > 0.05$) among the study sites in both POC and PON concentrations during the monsoon period, but significant differences (Kruskal-Wallis test, $p < 0.05$) were observed during the non-monsoon period (Figures 4G, H). The C/N ratios in both lagoons tended to be higher (Mann–Whitney *U* test, $p = 0.01$) in the summer monsoon period than in the non-monsoon period (Figure 4I). Spatial variations in the ratios at Gyeongpoho sites (6.7 ± 2.4) were lower (Mann–Whitney *U* test, $p = 0.08$) than those at Hyangho sites (9.7 ± 4.2).

PCHO, PPr, and PLip concentrations varied 6.3–96.9 μg L^{-1}, 1.1–53.1 μg L^{-1}, 2.9–6.2 μg L^{-1}, respectively. Large variations in

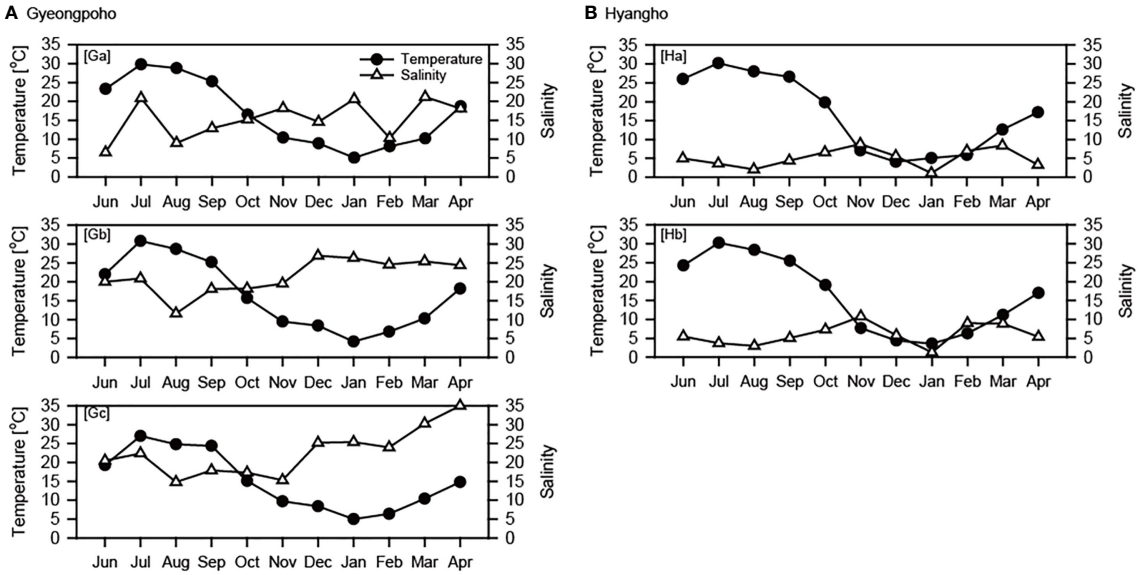

FIGURE 3
Monthly variations in water temperature and salinity at study sites in Gyeongpoho **(A)** and Hyangho **(B)** during sampling period.

10.3389/fmars.2022.953648

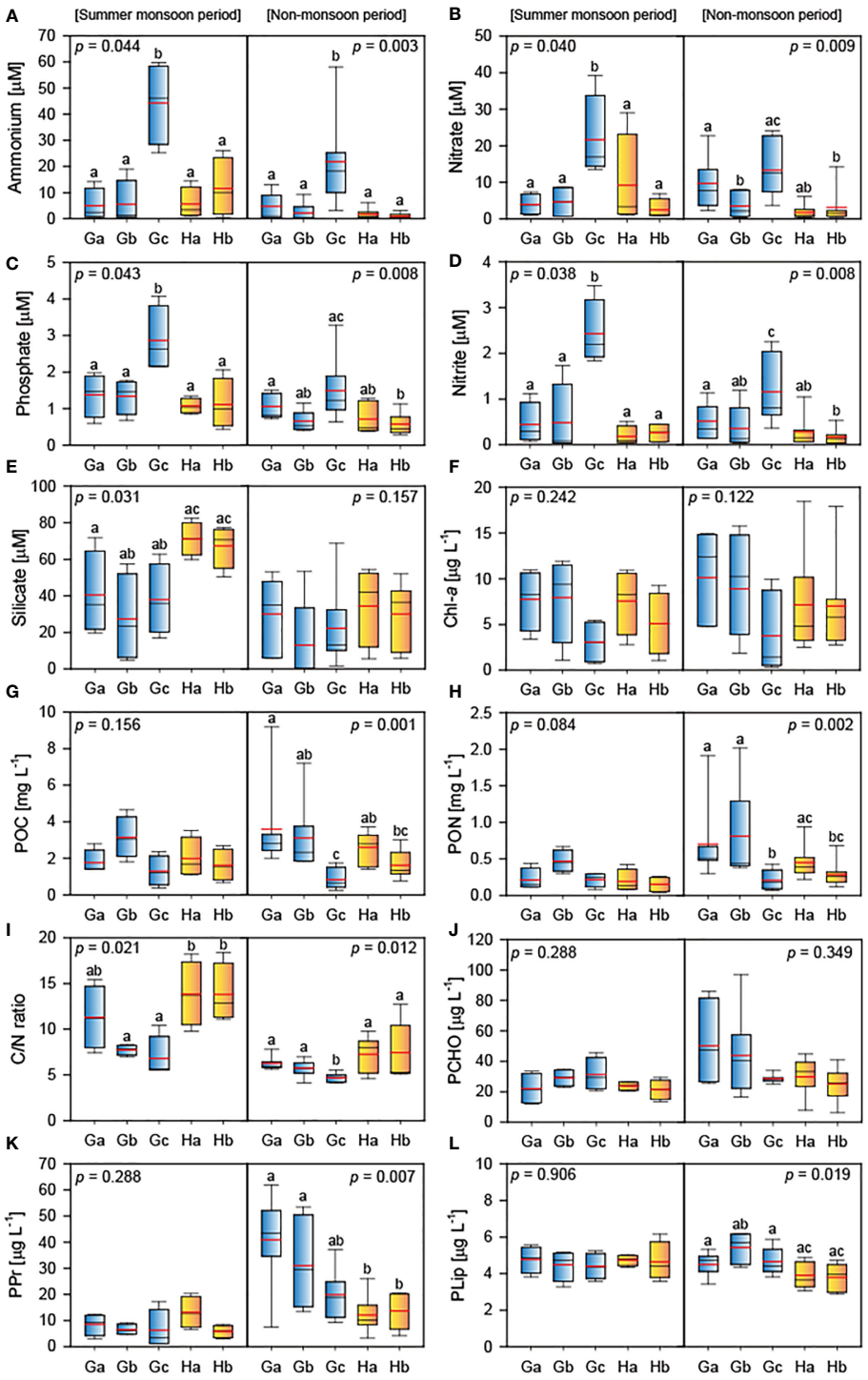

FIGURE 4
Box plots of data for summer monsoon and non-monsoon periods showing **(A)** ammonium, **(B)** nitrate, **(C)** phosphate, **(D)** nitrite, **(E)** silicate, **(F)** Chl-*a*, **(G)** POC, **(H)** PON, **(I)** C/N ratio, **(J)** PCHO, **(K)** PPr, and **(L)** PLip. The blue and yellow boxes represent the sites of Gyeongpoho, and Hyanho, respectively. The median and average values are displayed with the black and red horizontal bar inside the box.

PCHO and PPr concentrations were observed at St. Ga and St. Gb during the non-monsoon period. However, there were no significant differences in these concentrations (Kruskal–Wallis test, $p > 0.05$) between the study sites during the monsoon period (Figures 4J–L).

The $\delta^{13}C$ values for POM tended to decrease gradually during summer and increase in fall and winter in both lagoons (Figure 5). In contrast, $\delta^{15}N$ values for POM showed opposite trends to temporal changes in $\delta^{13}C$ values. The $\delta^{13}C$ and $\delta^{15}N$ values were higher (Mann–Whitney U test, $p < 0.001$) in Gyeongpoho sites (−24.2 ± 2.5‰ and 4.9 ± 1.0‰, respectively) than in Hyanho sites (−26.4 ± 0.6‰ and 3.8± 0.5‰, respectively).

Self-organizing map and canonical correspondence analysis

SOM training results were condensed onto 4×5 rectangular grid maps based on 33 datasets (three stations over 11 months) and 22 datasets (two stations over 11 months) of seven physicochemical variables in Gyeongpoho and Hyangho, respectively (Figure 6). In both lagoons, the dendrograms of SOM results grouped major 2 cluster coinciding with monsoon and non-monsoon periods, reflecting temperature and salinity variations and minor 2 clusters with high nutrient concentrations.

Canonical correspondence analysis (CCA) was applied to investigate the relationships between environmental factors (water temperature, salinity, and nutrients) and biogeochemical properties (POC, PON, Chl-*a*, PCHO, PPr, and PLip) (Figure 7 and Table 1). The first two ordination axes of the CCA explained 96.5%, 87.5%, and 94.3% of the factors in biogeochemical properties at St. Ga and St. Gb, St. Gc, and St. Ha and St. Hb, respectively, with respect to environmental factors. Samples with each dataset, represented by colored circles, were dispersed on CCA diagrams according to the characteristics of environmental and biochemical factors. The samples were closely distributed and coincided with the clusters classified in SOM analysis. In St. Ga and St. Gb, Chl-*a* and PLip are located opposite other biogeochemical properties along axis 1 of the diagram reflecting negative correlation, and PPr is highly related to dissolved inorganic nitrogen. At St. Gc, salinity and PPr were negatively correlated with other environmental factors and biogeochemical properties, respectively. At St. Ha and Hb, PCHO was negatively correlated with other biogeochemical properties.

Discussion

The present study assessed both seasonal and spatial dynamics of the biochemical and isotopic characteristics of suspended POM in the coastal lagoons of Korea by comparing environmental conditions and biological variabilities between permanently and intermittently open lagoons. Our study showed that seasonal and spatial biogeochemical variations in POM are closely associated with changes in freshwater input after the monsoon period and hydrologic connectivity between

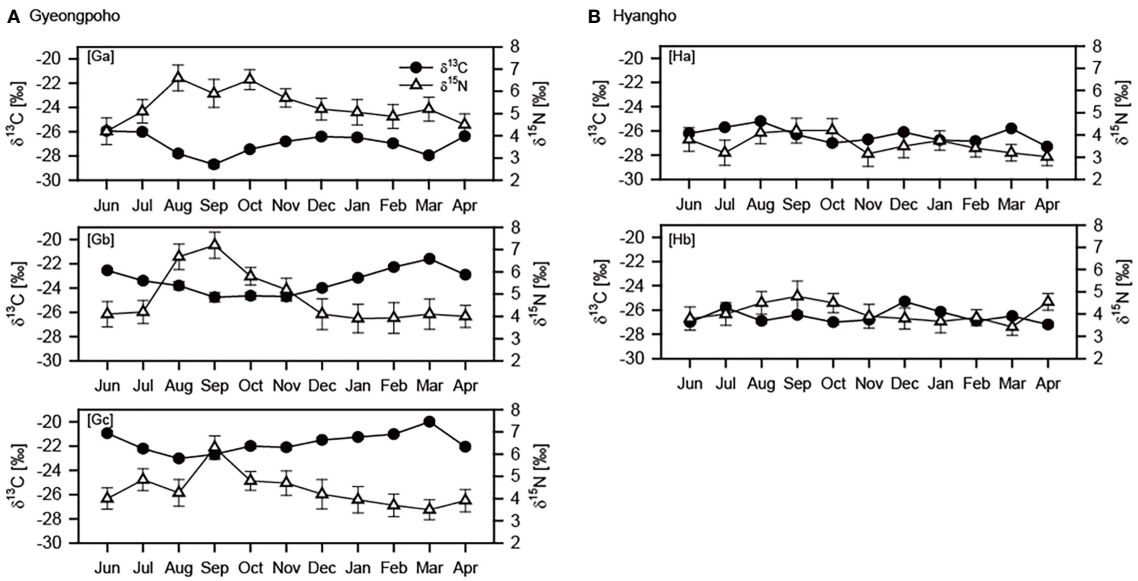

FIGURE 5
Monthly variations in $\delta^{13}C$ and $\delta^{15}N$ variations at study sites in Gyeongpoho **(A)** and Hyangho **(B)** during sampling period.

10.3389/fmars.2022.953648

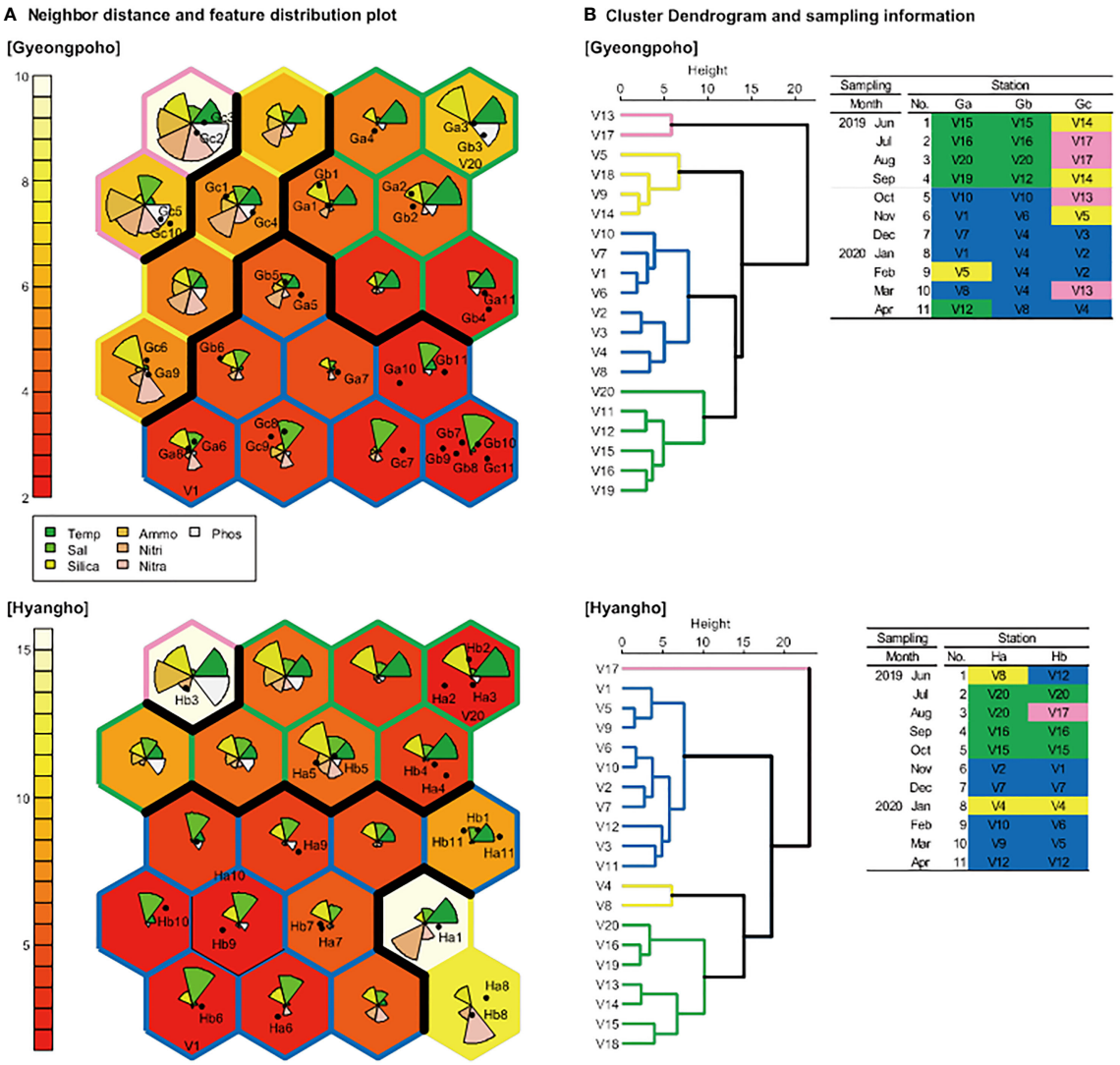

FIGURE 6
(A) Grouping of characteristics in study sites according to time and space on the Kohonen self-organizing map algorithm (SOM) trained with environmental factors. Gradient of unit box color (white-red) represents neighbor distance. Dendrogram of the trained SOM groups based on Ward's linkage method and information table of individual samples **(B)**.

lagoons and marine systems. The seasonal dynamics of environmental conditions resulting from a response to the variation in the hydrological balance between freshwater and seawater might affect the biogeochemical composition of POM, which is comprised of diverse organic matter sources. In addition, multivariate analysis allowed us to better understand the relationships between environmental factors and POM characteristics in the lagoons. The SOM results confirmed that the variations in environmental factors at the study sites were differentiated by the monsoon and non-monsoon periods. As results of CCA, POM characteristics in the lagoons varied according to the changes of environmental factors and there were no significant correlations between Chl-*a* and the other biogeochemical properties, reflecting high contribution of anthropogenic sources for POM (Pérez-Ruzafa et al., 2019). Overall, the seasonal difference in the degree of mixing of freshwater and seawater by geomorphological lagoon features may lead to spatial and temporal heterogeneity in POM composition with environmental conditions.

Spatial and temporal variability in the biogeochemical characteristics of POM

In general, the biogeochemical characteristics of POM in a variety of coastal areas show high spatial and temporal

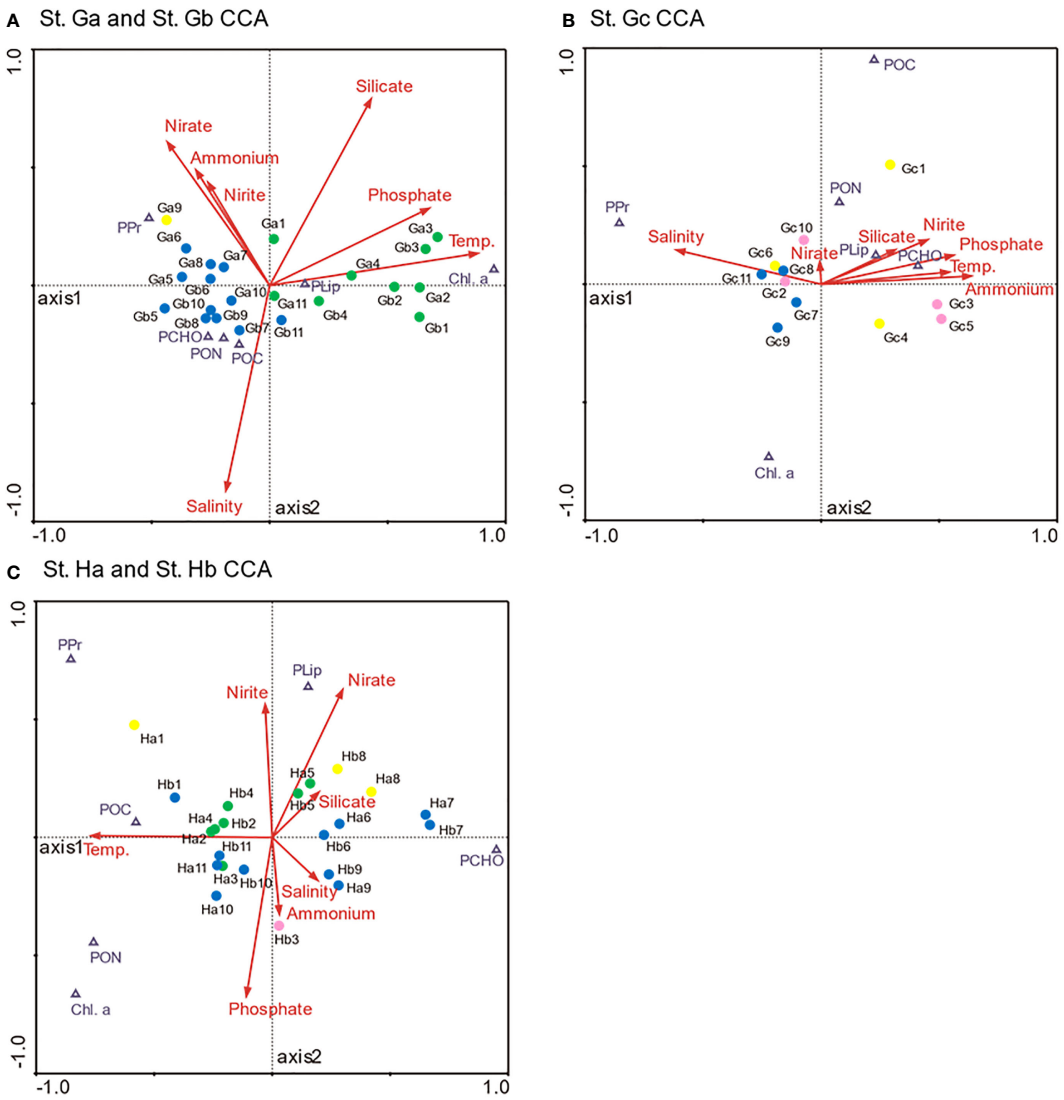

FIGURE 7
Ordination diagram obtained from canonical correspondence analysis based on Chl-*a*, POC, PON, PCHO, PPr, and PLip located in St. Ga and Gb **(A)**, St. Gc **(B)**, and St. Ha and St. Hb **(C)** with respect to environmental factors.

variability (Vizzini and Mazzola, 2003; Bănaru et al., 2007). Environmental factors and hydrodynamic regimes may lead to differences in the origin, distribution, and transfer of POM within coastal areas (Deegan and Garritt, 1997; Vizzini and Mazzola, 2006). POM in coastal lagoons is generally a heterogeneous pool consisting of a mixture of living phytoplankton and detrital material derived from terrestrial and/or marsh organic matter (Berto et al., 2013; Escalas et al., 2015; Garcia et al., 2017). Seasonal and spatial variations in the relative contribution of each organic matter source to POM pools may reflect their isotopic signatures (Fichez et al., 1993; Cresson et al., 2012).

The $\delta^{13}C$ and $\delta^{15}N$ ranges of POM as a tracer for the source identification have been reported for spatio-temporal variations in different lagoons under various environmental conditions (Table 2). In the present study, the $\delta^{13}C$ values for POM during all sampling periods almost showed more positive at the Gyeongpoho sites (−24.2 ± 2.5‰) than at the Hyangho sites (−26.4 ± 0.6‰). These results may be explained by the difference in salinity distribution between the lagoons, showing that Hyangho had a much lower salinity than Gyeongpoho. The Hyangho sites were characterized by oligohaline conditions, whereas the Gyeongpoho sites exhibited a wide range of salinity from nearly freshwater to hypersaline seawater. At the

TABLE 1 Summary of the results from canonical correspondence analysis.

St. Ga and St. Gb	Axes 1	Axes 2	Axes 3	Axes 4	Total inertia
Eigenvalues	0.067	0.028	0.003	0.001	0.171
Species-environment correlations	0.876	0.767	0.346	0.48	
Cumulative percentage variance					
of species data	39.3	56	57.6	57.9	
of species environment relation	67.7	96.5	99.3	99.9	
Sum of all unconstrained eigenvalues					0.171
Sum of all canonical eigenvalues					0.099
St. Gc	**Axes 1**	**Axes 2**	**Axes 3**	**Axes 4**	**Total inertia**
Eigenvalues	0.094	0.02	0.013	0.002	0.225
Species-environment correlations	0.854	0.723	0.589	0.377	
Cumulative percentage variance					
of species data	41.8	50.9	56.9	57.6	
of species environment relation	71.9	87.5	97.8	99.1	
Sum of all unconstrained eigenvalues					0.225
Sum of all canonical eigenvalues					0.131
St. Ha and St. Hb	**Axes 1**	**Axes 2**	**Axes 3**	**Axes 4**	**Total inertia**
Eigenvalues	0.045	0.022	0.002	0.001	0.189
Species-environment correlations	0.803	0.5	0.784	0.277	
Cumulative percentage variance					
of species data	24.1	35.6	36.9	37.5	
of species environment relation	63.8	94.3	97.6	99.2	
Sum of all unconstrained eigenvalues					0.189
Sum of all canonical eigenvalues					0.071

Gyeongpoho sites, the POM composition may reflect the spatial variation in $\delta^{13}C$ values with a diverse mixture of organic matter sources along the salinity gradient (Park et al., 2020). In contrast, the ^{13}C-depletion of POM at the Hyangho sites may be explained by freshwater-dominated conditions resulting from the blocking of seawater intrusion by the presence of sand bars during most of the sampling periods. Such lower $\delta^{13}C$ values suggested the prevalence of organic matter derived from terrestrial and marsh plants within the intermittently open lagoons. Several studies have reported that the connection or separation of the lagoon from the ocean by geomorphological characteristics can result in changes in the POM composition due to seasonal and spatial variations in the distribution and productivity of primary producers (Hoeinghaus et al., 2011; Escalas et al., 2015; Pelage et al., 2021). Thus, the isotopic difference in POM between the two lagoons is likely due to the differences in the mixing degree of seawater and freshwater by the geomorphology for physical connectivity with the adjacent coast.

C/N ratios between 6 and 10 have been usually are characteristic of the predominance of phytoplanktonic cells in POM (Cifuentes et al., 1988; Cresson et al., 2012; Berto et al., 2013; Remeikaitė-Nikienė et al., 2017). Relatively high C/N ratios of more than 30 have been found in marsh vascular plants and terrestrial organic matter (Wainright et al., 2000; Kang et al., 2003). The relatively high C/N values for POM throughout the sampling period at all sites in Hyangho suggested the dominance of non-living detrital materials. In contrast, Gyeongpoho displayed different patterns in C/N values for POM among the within-lagoon sites. Freshwater input with terrestrial organic matter at the upper site of Gyeongpoho (St. Ga) may be responsible for the increase in C/N values for POM, which are similar to those at the Hyangho sites during the monsoon period. The high contribution of phytoplankton to the POM pool at the lower site (St. Gc) suggested that the intrusion of seawater mainly consisted of phytoplanktonic material owing to the permanently open system.

The biochemical composition of POM may be significantly influenced by environmental conditions such as salinity, temperature, light conditions, terrestrial inputs, and species composition of phytoplankton, which can allow us to distinguish phytoplankton production from refractory organic

TABLE 2 Previous results of $\delta^{13}C$ and $\delta^{15}N$ values for particulate organic matter in other lagoon ecosystems.

Study area			Sampling period	Particulate organic matter		References
Region	Lagoon	Location		$\delta^{13}C$ (‰)	$\delta^{15}N$ (‰)	
India (Bay of Bengal)	Chilika lagoon	Whole lagoon	June 2015	−29.17 ~ −20.50	1.34 ~ 8.31	Mukherjee et al. (2019)
		Outer channel		−21.61 ± 0.38	6.91 ± 1.98	
		Southern sector		−23.18 ± 1.79	3.01 ± 1.76	
		Central sector		−23.60 ± 1.20	3.91 ± 1.04	
		Northern sector		−26.14 ± 2.65	3.54 ± 0.74	
France (Mediterranean Sea)	Mauguio lagoon	North-central	February 2002	−26.3 ± 0.9	11.7 ± 0.5	Vizzini et al. (2005)
		South-west		−25.8 ± 0.4	12.3 ± 1.0	
		North-central	July 2002	−25.8 ± 0.4	12.8 ± 0.5	
		South-west		−24.9 ± 0.3	12.0 ± 0.3	
Portugal (Atlantic Ocean)	Ria Formosa	Outlet area	Summer 1995	−20.9	4.6	Machás and Santos (1999)
		Outlet-middle area		−20.9	5.3	
		Middle-inside area		−20.9	4.4	
		Inside channel		−21.1	5.0	
Italy (Adriatic Sea)	Venice lagoon	Whole lagoon	Four seasons (May 2011, August 2011, November 2011, and February 2012)	−25.78 ~ −20.27	−6.60 ~ 18.15	Berto et al. (2013)

matter (Danovaro et al., 2000; Cresson et al., 2012; Lee et al., 2017). In the present study, the POM biochemical compositions in both lagoons displayed relatively high concentrations of PCHO compared with those of PPr and PLip. The dominance of PCHO is likely due to a major contribution of terrestrial matter to the POM pool, as shown by the lower $\delta^{13}C$ values at most sampling sites, which may be linked to freshwater inputs from upstream. As terrestrial and marsh plant-derived organic matter is known to have very low $\delta^{13}C$ values, ranging between −23‰ and −30‰ (Fry and Sherr, 1984; Park et al., 2020), the high concentrations of PCHO support this explanation. In addition, the presence of POM in PPr and PLip has been reported to increase the number of phytoplanktonic cells along with phytoplankton blooms (Pusceddu et al., 1996). Similar to the C/N values for POM, however, there were different patterns in the concentrations of biochemical components between the two lagoons. In Gyeongpoho, under the influence of freshwater and seawater, significant $\delta^{13}C$ differences for POM among sites were observed, and relatively high concentrations of PCHO and PPr at the upper and lower sites appeared to be driven by the proximity of upstream and marine zones out of the lagoon, respectively. A comparable pattern was observed in the two different lagoon systems, where the existence of consistent connectivity between the freshwater wetland and marine systems was demonstrated to be the major contributor to the spatial differences in the isotopic and biochemical characteristics of POM.

Factors controlling the biogeochemical characteristics of POM

In both lagoons, freshwater input following the monsoon period may have resulted in high nutrient concentrations. Despite the apparent evidence of rainfall effects (e.g., low salinity and high inorganic nutrients) on both lagoon systems, isotopic signatures and biochemical concentrations for POM showed seasonally different patterns between them. The enrichment in $\delta^{15}N$ of POM during monsoon period are consistent with the general results for freshwater inputs influenced by anthropogenic nitrogen (McClelland et al., 1997), Seasonal pattern of the $\delta^{15}N$ of POM in both systems may be explained by the differences in complex microbial processes by bacterial community and rapid interactions between nutrients and phytoplankton within each lagoon (Cifuentes et al., 1988). Our results suggested that seasonality in POM characteristics was clearer in Gyeongpoho than in Hyangho. At the Gyeongpoho site, the lowest $\delta^{13}C$ values of POM were recorded immediately after the monsoon period, which may reflect the input of terrestrial organic matter by heavy rainfall (Riera and Richard, 1996; Berto et al., 2013). The input of terrestrial organic matter is known to increase the trophic contribution to consumer production at the upper site of Gyeongpoho, and macroalgal blooms caused by nutrient enrichment can also appear after the monsoon period (Park et al., 2020). For Gyeongpoho, the highly variable salinity was

positively correlated with the $\delta^{13}C$ values of POM. However, the lower site of Gyeongpoho is commonly characterized by organic matter transport from neighboring outer marine systems, as supported by the $\delta^{13}C$ and C/N values of POM being close to those of typical marine phytoplankton, even during the monsoon period. In contrast, the isotopic variations for POM at the Hyangho sites showed little significance monthly, despite the occurrence of the heavy rainfall event. Although the POM composition may be linked with freshwater inputs during the monsoon period, this was mainly influenced by the presence of terrestrial and marsh plant-derived organic matter. In these environments, organic matter derived from primary producers such as seagrasses and terrestrial and marsh plants are generally known to mainly constitute high molecular weights of carbohydrates, which are difficult to use by consumer species, may be sustained throughout the seasons, and may reflect the isotopic and biochemical signatures of POM (Boudouresque et al., 2006; Cresson et al., 2012). These results can also be explained by the different systems open and semi-closed to the sea by distinguishing geomorphological features. Slightly more ^{13}C-enriched POM values at the Hyangho sites following the monsoon period likely reflect the increased marine-derived organic matter transport *via* the intrusion of sea water when the lagoon inlet was opened due to a sustained flood pulse from heavy rainfall (Garcia et al., 2017; Park et al., 2020). Accordingly, the increase in terrestrial organic matter and the timing of inlet opening by heavy rainfall may be the main drivers of seasonal variation in POM characteristics in permanently and intermittently open systems, respectively.

Conclusions

This study provides a biogeochemical characterization of the seasonal and spatial dynamics of POM in permanently and intermittently open coastal lagoons of Korea using isotopic and biochemical tracers for the first time. The environmental conditions and POM compositions showed different seasonal and spatial patterns in the two lagoons during the sampling period. Our results estimated the seasonal and spatial differences in the POM composition influenced by the input of allochthonous materials (terrestrial and marine-derived organic matter) with respect to the geomorphological features of each lagoon. The degree of hydrological connectivity between freshwater and seawater may play an important role in determining the different POM pool compositions between permanently and intermittently open lagoon systems. The isotopic and biochemical signatures in the intermittently open lagoon suggested the prevalence of organic matter derived from terrestrial and marsh plants during most periods, while its temporary opening period (following the post-monsoon period) may provide organic matter transport from the sea. In the permanently open lagoon, these tracers provide evidence of the connectivity between lagoon systems and marine systems by the artificially constructed open inlet during most periods, and thereby, the highly transient pool of POM by the mixing degree of freshwater and seawater along the salinity gradient. Thus, these geomorphological characteristics may contribute to the contrasting biogeochemical responses of POM pools in the two lagoon systems to summer monsoon rainfall. Further studies are needed to assess the global climate effects due to the altered frequency and intensity of heavy rainfall events on the differential integration of POM pools within lagoon trophic networks, which may provide an integrated ecosystem-based management of temperate coastal lagoon systems.

Data availability statement

The original contributions presented in the study are included in the article/Supplementary Material. Further inquiries can be directed to the corresponding author.

Author contributions

D-YL, JHK, and HJP designed the experiments and drafted the manuscript. D-YL and JHK carried out for field observation and sample collection. THP, HYK, and DK analyzed the biochemical and stable isotope compositions of POM samples. JHK and SH performed the statistical analyses. D-YL, JHK, and HJP wrote the main manuscript text. HJP supervised all processes. All authors contributed to the article and approved the submitted version.

Funding

This work was supported by the National Institute of Fisheries Science, Ministry of Oceans and Fisheries, Korea (R2022038) and the National Research Foundation of Korea grant (NRF-2018R1C1B6004501) funded by the Ministry of Science and ICT, Korea.

Conflict of interest

The authors declare that the research was conducted in the absence of any commercial or financial relationships that could be construed as a potential conflict of interest.

Publisher's note

All claims expressed in this article are solely those of the authors and do not necessarily represent those of their affiliated organizations, or those of the publisher, the editors and the reviewers. Any product that may be evaluated in this article, or claim that may be made by its manufacturer, is not guaranteed or endorsed by the publisher.

References

Bănaru, D., Harmelin-Vivien, M., Gomoiu, M. T., and Onciu, T. M. (2007). Influence of the Danube river inputs on c and n stable isotope ratios of the Romanian coastal waters and sediment (Black Sea). *Mar. Pollut. Bull.* 54, 1385–1394. doi: 10.1016/j.marpolbul.2007.05.022

Berto, D., Rampazzo, F., Noventa, S., Cacciatore, F., Gabellini, M., Aubry, F. B., et al. (2013). Stable carbon and nitrogen isotope ratios as tools to evaluate the nature of particulate organic matter in the Venice lagoon. *Estuar. Coast. Shelf Sci.* 135, 66–76. doi: 10.1016/j.ecss.2013.06.021

Bhavya, P. S., Kim, B. K., Jo, N., Kim, K., Kang, J. J., Lee, J. H., et al. (2019). A review on the macromolecular compositions of phytoplankton and the implications for aquatic biogeochemistry. *Ocean Sci. J.* 54, 1–14. doi: 10.1007/s12601-018-0061-8

Bligh, E. G., and Dyer, W. J. (1959). A rapid method of total lipid extraction and purification. *Can. J. Biochem. Physiol.* 37, 911–917. doi: 10.1139/o59-099

Boudouresque, C., Mayot, N., and Pergent, G. (2006). The outstanding traits of the functioning of the posidonia oceanica seagrass ecosystem. *Biol. Mar. Mediterr.* 13, 109–113.

Briand, M. J., Bonnet, X., Goiran, C., Guillou, G., and Letourneur, Y. (2015). Major sources of organic matter in a complex coral reef lagoon: identification from isotopic signatures ($\delta^{13}C$ and $\delta^{15}N$). *PloS One* 10, e0131555. doi: 10.1371/journal.pone.0131555

Carrasco Navas-Parejo, J. C., Corzo, A., and Papaspyrou, S. (2020). Seasonal cycles of phytoplankton biomass and primary production in a tropical temporarily open-closed estuarine lagoon–the effect of an extreme climatic event. *Sci. Total Environ.* 723. doi: 10.1016/j.scitotenv.2020.138014

Chen, F., Lu, X., Song, Z., Huang, C., Jin, G., Chen, C., et al. (2021). Coastal currents regulate the distribution of the particulate organic matter in western guangdong offshore waters as evidenced by carbon and nitrogen isotopes. *Mar. Pollut. Bull.* 172, 112856. doi: 10.1016/j.marpolbul.2021.112856

Cifuentes, L. A., Sharp, J. H., and Fogel, M. L. (1988). Stable carbon and nitrogen isotope biogeochemistry in the Delaware estuary. *Limnol. Oceanogr.* 33, 1102–1115. doi: 10.4319/lo.1988.33.5.1102

Cole, M. L., Valiela, I., Kroeger, K. D., Tomasky, G. L., Cebrian, J., Wigand, C., et al. (2004). Assessment of a $\delta^{15}N$ isotopic method to indicate anthropogenic eutrophication in aquatic ecosystems. *J. Environ. Qual.* 33, 124–132. doi: 10.2134/jeq2004.1240

Cresson, P., Ruitton, S., Fontaine, M. F., and Harmelin-Vivien, M. (2012). Spatio-temporal variation of suspended and sedimentary organic matter quality in the bay of Marseilles (NW Mediterranean) assessed by biochemical and isotopic analyses. *Mar. Pollut. Bull.* 64, 1112–1121. doi: 10.1016/j.marpolbul.2012.04.003

Danovaro, R., Dell'Anno, A., Pusceddu, A., Daniela Marrale, D., Della Croce, N., Fabiano, M., et al. (2000). Biochemical composition of pico-, nano- and micro-particulate organic matter and bacterioplankton biomass in the oligotrophic Cretan Sea (NE Mediterranean). *Prog. Oceanogr.* 46, 279–310. doi: 10.1016/S0079-6611(00)00023-9

Deegan, L. A., and Garritt, R. H. (1997). Evidence for spatial variability in estuarine food webs. *Mar. Ecol. Prog. Ser.* 147, 31–47. doi: 10.3354/meps147031

Dubois, M., Gilles, K. A., Hamilton, J. K., Rebers, P. A., and Smith, F. (1956). Colorimetric method for determination of sugars and related substances. *Anal. Chem.* 28, 350–356. doi: 10.1021/ac60111a017

Escalas, A., Ferraton, F., Paillon, C., Vidy, G., Carcaillet, F., Salen-Picard, C., et al. (2015). Spatial variations in dietary organic matter sources modulate the size and condition of fish juveniles in temperate lagoon nursery sites. *Estuar. Coast. Shelf Sci.* 152, 78–90. doi: 10.1016/j.ecss.2014.11.021

Fichez, R., Dennis, P., Fontaine, M. F., and Jickells, T. D. (1993). Isotopic and biochemical composition of particulate organic matter in a shallow water estuary (Great ouse, north Sea, England). *Mar. Chem.* 43, 263–276. doi: 10.1016/0304-4203(93)90231-C

Fry, B., and Sherr, E. (1984). $\delta^{13}C$ measurements as indicators of carbon flow in marine and freshwater ecosystems. *Contribution Mar. Sci.* 27, 13–47.

Garcia, C. A., Baer, S. E., Garcia, N. S., Rauschenberg, S., Twining, B. S., Lomas, M. W., et al. (2018). Nutrient supply controls particulate elemental concentrations and ratios in the low latitude eastern Indian ocean. *Nat. Commun.* 9, 1–10. doi: 10.1038/s41467-018-06892-w

Garcia, A. M., Winemiller, K., Hoeinghaus, D., Claudino, M., Bastos, R., Correa, F., et al. (2017). Hydrologic pulsing promotes spatial connectivity and food web subsidies in a subtropical coastal ecosystem. *Mar. Ecol. Prog. Ser.* 567, 17–28. doi: 10.3354/meps12060

Grémare, A., Amouroux, J. M., Charles, F., Dinet, A., Riaux-Gobin, C., Baudart, J., et al. (1997). Temporal changes in the biochemical composition and nutritional value of the particulate organic matter available to surface deposit-feeders: a two year study. *Mar. Ecol. Prog. Ser.* 150, 195–206. doi: 10.3354/meps150195

Hansen, H. P., and Koroleff, F. (1999). "Determination of nutrients," in *Methods of seawater analysis*. Eds. K. Grasshoff, K. Kremling and M. Ehrhardt (Weinheim: Wiley-VCH Verlag), 159–228.

Helder, W., and De Vries, R. T. P. (1979). An automatic phenol-hypochlorite method for the determination of ammonia in sea- and brackish waters. *Neth. J. Sea Res.* 13, 154–160. doi: 10.1016/0077-7579(79)90038-3

Hoeinghaus, D. J., Vieira, J. P., Costa, C. S., Bemvenuti, C. E., Winemiller, K. O., and Garcia, A. M. (2011). Estuary hydrogeomorphology affects carbon sources supporting aquatic consumers within and among ecological guilds. *Hydrobiologia.* 673, 79–92. doi: 10.1007/s10750-011-0751-z

Kang, C.-K., Kim, J. B., Lee, K.-S., Kim, J. B., Lee, P.-Y., and Hong, J.-S. (2003). Trophic importance of benthic microalgae to macrozoobenthos in coastal bay systems in Korea: Dual stable c and n isotope analyses. *Mar. Ecol. Prog. Ser.* 259, 79–92. doi: 10.3354/meps259079

Ke, Z., Tan, Y., Huang, L., Zhao, C., and Jiang, X. (2017). Spatial distributions of $\delta^{13}C$, $\delta^{15}N$ and C/N ratios in suspended particulate organic matter of a bay under serious anthropogenic influences: Daya bay, China. *Mar. Pollut. Bull.* 114, 183–191. doi: 10.1016/j.marpolbul.2016.08.078

Kjerfve, B. (1994). "Coastal lagoons," in *Coastal lagoon processes*. Ed. B. Kjerfve (Amsterdam: Elsevier), 1–8. doi: 10.1016/s0422-9894(08)70006-0

Kleppel, G. S., and Burkart, C. A. (1995). Egg production and the nutritional environment of acartia tonsa: The role of food quality in copepod nutrition. *ICES J. Mar. Sci.* 52, 297–304. doi: 10.1016/1054-3139(95)80045-X

Kohonen, T. (1982). Self-organized formation of topologically correct feature maps. *Biol. Cybern.* 43, 59–69. doi: 10.1007/BF00337288

Lønborg, C., Doyle, J., Furnas, M., Menendez, P., Benthuysen, J. A., and Carreira, C. (2017). Seasonal organic matter dynamics in the great barrier reef lagoon: contribution of carbohydrates and proteins. *Contin. Shelf Res.* 138, 95–105. doi: 10.1016/j.csr.2017.01.010

Lee, J. H., Lee, D., Kang, J. J., Joo, H. T., Lee, J. H., Lee, H. W., et al. (2017). The effects of different environmental factors on the biochemical composition of particulate organic matter in gwangyang bay, south Korea. *Biogeosciences*. 14, 1903–1917. doi: 10.5194/bg-14-1903-2017

Licen, S., Franzon, M., Rodani, T., and Barbieri, P. (2021). SOMEnv: an r package for mining environmental monitoring datasets by self-organizing map and k-means algorithms with a graphical user interface. *Microchem. J.* 165, 106181. doi: 10.1016/j.microc.2021.106181

Lopes, C. L., and Dias, J. M. (2015). Assessment of flood hazard during extreme sea levels in a tidally dominated lagoon. *Nat. Hazards* 77, 1345–1364. doi: 10.1007/s11069-015-1659-0

Lowry, O. H., Rosebrough, N. J., Farr, A. L., and Randall, R. J. (1951). Protein measurement with the folin phenol reagent. *J. Biol. Chem.* 193, 265–275. doi: 10.1016/S0021-9258(19)52451-6

Lu, X., Huang, C., Chen, F., Zhang, S., Lao, Q., Chen, C., et al. (2021). Carbon and nitrogen isotopic compositions of particulate organic matter in the upwelling zone off the east coast of hainan island, China. *Mar. Pollut. Bull.* 167, 112349. doi: 10.1016/j.marpolbul.2021.112349

Lu, X., Zhou, X., Jin, G., Chen, F., Zhang, S., Li, Z., et al. (2022). Biological impact of typhoon wipha in the coastal area of western guangdong: A comparative field

observation perspective. *J. Geophys. Res.-Biogeosci* 127 (2), e2021JG006589. doi: 10.1029/2021JG006589

Machás, R., and Santos, R. (1999). Sources of organic matter in ria Formosa revealed by stable isotope analysis. *Acta Oecol.* 20, 463–469. doi: 10.1016/S1146-609X(99)00122-8

Marsh, J. B., and Weinstein, D. B. (1966). Simple charring method for determination of lipids. *J. Lipid Res.* 7, 574–576. doi: 10.1016/S0022-2275(20)39274-9

Mazzola, A., Fabiano, M., Pusceddu, A., and Sarà, G. (2001). Particulate organic matter composition in a semi-enclosed marine system. *Chem. Ecol.* 17, 315–334. doi: 10.1080/02757540108035561

McClelland, J. W., and Valiela, I. (1998). Linking nitrogen in estuarine producers to land-derived sources. *Limnol. Oceanogr.* 43, 577–585. doi: 10.4319/lo.1998.43.4.0577

McClelland, J. W., Valiela, I., and Michener, R. H. (1997). Nitrogen stable isotope signatures in estuarine food webs: A record of increasing urbanization in coastal watersheds. *Limnol. Oceanogr.* 42, 930–937. doi: 10.4319/lo.1997.42.5.0930

Mukherjee, R., Muduli, P. R., Barik, S. K., and Kumar, S. (2019). Sources and transformations of organic matter in sediments of asia's largest brackish water lagoon (Chilika, India) and nearby mangrove ecosystem. *Environ. Earth Sci.* 78, 332. doi: 10.1007/s12665-019-8329-6

Murphy, J., and Riley, J. P. (1962). A modified single solution method for the determination of phosphate in natural waters. *Anal. Chim. Acta.* 27, 31–36. doi: 10.1016/S0003-2670(00)88444-5

Navarro, J., and Thompson, R. (1995). Seasonal fluctuations in the size spectra, biochemical composition and nutritive value of the seston available to a suspension-feeding bivalve in a subarctic environment. *Mar. Ecol. Prog. Ser.* 125, 95–106. doi: 10.3354/meps125095

Park, Y.-S., Céréghino, R., Compin, A., and Lek, S. (2003). Applications of artificial neural networks for patterning and predicting aquatic insect species richness in running waters. *Ecol. Modell.* 160, 265–280. doi: 10.1016/S0304-3800(02)00258-2

Park, H. J., Han, E., Lee, Y. J., and Kang, C. K. (2016). Trophic linkage of a temperate intertidal macrobenthic food web under opportunistic macroalgal blooms: A stable isotope approach. *Mar. Pollut. Bull.* 111, 86–94. doi: 10.1016/j.marpolbul.2016.07.026

Park, H. J., Kwak, J. H., and Kang, C.-K. (2015). Trophic consistency of benthic invertebrates among diversified vegetational habitats in a temperate coastal wetland of Korea as determined by stable isotopes. *Estuaries Coast.* 38, 599–611. doi: 10.1007/s12237-014-9834-1

Park, H. J., Park, T. H., Kang, H. Y., Lee, C. I., and Kang, C. K. (2020). Shifting resource utilization of the lacustrine shrimp palaemon paucidens in temperate coastal lagoons of Korea as revealed by stable isotopes. *Mar. Pollut. Bull.* 160, 111672. doi: 10.1016/j.marpolbul.2020.111672

Park, Y.-S., Tison, J., Lek, S., Giraudel, J.-L., Coste, M., and Delmas, F. (2006). Application of a self-organizing map to select representative species in multivariate analysis: A case study determining diatom distribution patterns across France. *Ecol. Inform.* 1, 247–257. doi: 10.1016/j.ecoinf.2006.03.005

Parsons, T. R., Maita, Y., and Lalli, C. M. (1984). *A manual of chemical & biological methods for seawater analysis.* (Amsterdam: Pergamon Press).

Pelage, L., Gonzalez, J. G., Le Loc'h. F., Ferreira, V., Munaron, J.-M., Lucena-Fredou, F., et al. (2021). Importance of estuary morphology for ecological connectivity with their adjacent coast: A case study in Brazilian tropical estuaries. *Estuar. Coast. Shelf Sci.* 251, 107184. doi: 10.1016/j.ecss.2021.107184

Pérez-Ruzafa, A., Marcos, C., Pérez-Ruzafa, I. M., and Pérez-Marcos, M. (2011). Coastal lagoons: "Transitional ecosystems" between transitional and coastal waters. *J. Coast. Conserv.* 15, 369–392. doi: 10.1007/s11852-010-0095-2

Pérez-Ruzafa, A., Pérez-Ruzafa, I. M., Newton, A., and Marcos, C. (2019). "Coastal lagoons: environmental variability, ecosystem complexity, and goods and services uniformity," in *Coasts and estuaries, the future*. Eds. E. Wolanski, J. W. Day, M. Elliott and R. Ramesh (New York: Elsevier), 253–276. doi: 10.1016/b978-0-12-814003-1.00015-0

Peterson, B. J., and Fry, B. (1987). Stable isotopes in ecosystem studies. *Annu. Rev. Ecol. Syst.* 18, 293–320. doi: 10.1146/annurev.es.18.110187.001453

Pusceddu, A., Serra, E., Sanna, O., and Fabiano, M. (1996). Seasonal fluctuations in the nutritional value of particulate organic matter in a lagoon. *Chem. Ecol.* 13, 21–37. doi: 10.1080/02757549608039099

Remeikaitė-Nikienė, N., Lujanienė, G., Malejevas, V., Barisevičiūtė, R., Zilius, M., Vybernaitė-Lubienė, I., et al. (2017). Assessing nature and dynamics of POM in transitional environment (the curonian lagoon, SE Baltic Sea) using a stable isotope approach. *Ecol. Indic.* 82, 217–226. doi: 10.1016/j.ecolind.2017.06.035

Riera, P., and Richard, P. (1996). Isotopic determination of food sources ofCrassostrea gigasAlong a trophic gradient in the estuarine bay of marennes-ol éron. *Estuar. Coast. Shelf Sci.* 42, 347–360. doi: 10.1006/ecss.1996.0023

Rossi, S., Grémare, A., Gili, J.-M., Amouroux, J.-M., Jordana, E., and Vétion, G. (2003). Biochemical characteristics of settling particulate organic matter at two north-western Mediterranean sites: a seasonal comparison. *Estuar. Coast. Shelf Sci.* 58, 423–434. doi: 10.1016/S0272-7714(03)00108-2

Sundbäck, K., and Snoeijs, P. (1991). Effects of nutrient enrichment on microalgal community composition in a coastal shallow-water sediment system: An experimental study. *Botanica Marina.* 34:341–358. doi: 10.1515/botm.1991.34.4.341

Ter Braak, C. J. F. (1986). Canonical correspondence analysis: a new eigenvector technique for multivariate direct gradient analysis. *Ecology.* 67, 1167–1179. doi: 10.2307/1938672

Vesanto, J., and Alhoniemi, E. (2000). Clustering of the self-organizing map. *IEEE Trans. Neural Netw.* 11, 586–600. doi: 10.1109/72.846731

Vizzini, S., and Mazzola, A. (2003). Seasonal variations in the stable carbon and nitrogen isotope ratios ($^{13}C/^{12}C$ and $^{15}N/^{14}N$) of primary producers and consumers in a western Mediterranean coastal lagoon. *Mar. Biol.* 142, 1009–1018. doi: 10.1007/s00227-003-1027-6

Vizzini, S., and Mazzola, A. (2006). Sources and transfer of organic matter in food webs of a Mediterranean coastal environment: Evidence for spatial variability. *Estuar. Coast. Shelf Sci.* 66, 459–467. doi: 10.1016/j.ecss.2005.10.004

Vizzini, S., Savona, B., Chi, T. D., and Mazzola, A. (2005). Spatial variability of stable carbon and nitrogen isotope ratios in a Mediterranean coastal lagoon. *Hydrobiologia.* 550, 73–82. doi: 10.1007/s10750-005-4364-2

Wainright, S. C., Weinstein, M. P., Able, K. W., and Currin, C. A. (2000). Relative importance of benthic microalgae, phytoplankton and the detritus of smooth cordgrass spartina alterniflora and the common reed phragmites australis to brackish-marsh food webs. *Mar. Ecol. Prog. Ser.* 200, 77–91. doi: 10.3354/meps200077

WREO (2008). The study of ecosystem scrutiny and management for ecosystem conservation and restoration of lagoons on the East coast (I). (Wonju: Wonju Regional Environmental Office).

Yoon, S.-O., Hwang, S.-I., Park, C.-S., Kim, H.-S., and Moon, Y.-R. (2008). Landscape changes of coastal lagoons during the 20th century in the middle east coast, south Korea. *J. Korean Geogr. Soc* 43, 449–465.

frontiers | Frontiers in Marine Science

TYPE Original Research
PUBLISHED 21 December 2022
DOI 10.3389/fmars.2022.920616

Check for updates

OPEN ACCESS

EDITED BY
Biraja Kumar Sahu,
Council of Scientific and Industrial Research (CSIR), India

REVIEWED BY
Marcus PD Dr Schulz,
Osnabrück University, Germany
Liju Tan,
Ocean University of China, China
Vera Fofonova,
Alfred Wegener Institute Helmholtz Centre for Polar and Marine Research (AWI), Germany

*CORRESPONDENCE
Lőrinc Mészáros
Lorinc.Meszaros@deltares.nl

SPECIALTY SECTION
This article was submitted to Marine Pollution, a section of the journal Frontiers in Marine Science

RECEIVED 14 April 2022
ACCEPTED 10 November 2022
PUBLISHED 21 December 2022

CITATION
Mészáros L, van der Meulen F, Jongbloed G and El Serafy G (2022) Coastal environmental and atmospheric data reduction in the Southern North Sea supporting ecological impact studies. *Front. Mar. Sci.* 9:920616. doi: 10.3389/fmars.2022.920616

COPYRIGHT
© 2022 Mészáros, van der Meulen, Jongbloed and El Serafy. This is an open-access article distributed under the terms of the Creative Commons Attribution License (CC BY). The use, distribution or reproduction in other forums is permitted, provided the original author(s) and the copyright owner(s) are credited and that the original publication in this journal is cited, in accordance with accepted academic practice. No use, distribution or reproduction is permitted which does not comply with these terms.

Coastal environmental and atmospheric data reduction in the Southern North Sea supporting ecological impact studies

Lőrinc Mészáros[1,2]*, Frank van der Meulen[2], Geurt Jongbloed[2] and Ghada El Serafy[1,2]

[1]Marine and Coastal Systems, Deltares, Delft, Netherlands, [2]Applied Mathematics, Delft University of Technology, Delft, Netherlands

Coastal climate impact studies make increasing use of multi-source and multi-dimensional atmospheric and environmental datasets to investigate relationships between climate signals and the ecological response. The large quantity of numerically simulated data may, however, include redundancy, multi-colinearity and excess information not relevant to the studied processes. In such cases techniques for feature extraction and identification of latent processes prove useful. Using dimensionality reduction techniques this research provides a statistical underpinning of variable selection to study the impacts of atmospheric processes on coastal chlorophyll-a concentrations, taking the Dutch Wadden Sea as case study. Dimension reduction techniques are applied to environmental data simulated by the Delft3D coastal water quality model, the HIRLAM numerical weather prediction model and the Euro-CORDEX climate modelling experiment. The dimension reduction techniques were selected for their ability to incorporate (1) spatial correlation *via* multi-way methods (2), temporal correlation through Dynamic Factor Analysis, and (3) functional variability using Functional Data Analysis. The data reduction potential and explanatory value of these methods are showcased and important atmospheric variables affecting the chlorophyll-a concentration are identified. Our results indicate room for dimensionality reduction in the atmospheric variables (2 principle components can explain the majority of variance instead of 7 variables), in the chlorophyll-a time series at different locations (two characteristic patterns can describe the 10 locations), and in the climate projection scenarios of solar radiation and air temperature variables (a single principle component function explains 77% of the variation for solar radiation and 57% of the variation for air temperature). It was also found that solar radiation followed by air temperature are the most important atmospheric variables related to coastal chlorophyll-a concentration, noting that regional differences exist, for instance the importance of air temperature is greater in the Eastern Dutch Wadden Sea at Dantziggat than in the Western Dutch Wadden Sea at Marsdiep Noord. Common trends and different regional system characteristics have also been identified through dynamic factor

analysis between the deeper channels and the shallower intertidal zones, where the onset of spring blooms occurs earlier. The functional analysis of climate data showed clusters of atmospheric variables with similar functional features. Moreover, functional components of Euro-CORDEX climate scenarios have been identified for radiation and temperature variables, which provide information on the dominant mode (pattern) of variation and its uncertainties. The findings suggest that radiation and temperature projections of different Euro-CORDEX scenarios share similar characteristics and mainly differ in their amplitudes and seasonal patterns, offering opportunities to construct statistical models that do not assume independence between climate scenarios but instead borrow information ("borrow strength") from the larger pool of climate scenarios. The presented results were used in follow up studies to construct a Bayesian stochastic generator to complement existing Euro-CORDEX climate change scenarios and to quantify climate change induced trends and uncertainties in phytoplankton spring bloom dynamics in the Dutch Wadden Sea.

KEYWORDS

coastal environment, dimensionality reduction, multivariate analysis, climate change, phytoplankton, eutrophication

1 Introduction

Motivation *- The present study is part of an overarching research investigating possibilities for statistical quantification of climate change induced uncertainties in future coastal ecosystem state. The research builds on a multitude of data sources, prominently using numerical models. As the research focuses on statistical methods to quantify and propagate uncertainties, a proper understanding of the multivariate input data, its redundancy, and most importantly the identification of latent variables and extraction of features is a natural first step in the analysis. A host of methods for dealing with these issues is available in the literature but scattered over various disciplines, such as chemometrics, econometrics and mathematics. This paper investigates how these methods can be applied to achieve the higher level objectives: (1) providing statistical underpinning for atmospheric variables selection to study chlorophyll-a response, and* (2) *identifying important features of the climate projections for further statistical models, for instance the Bayesian stochastic generator implemented in* (Mészáros et al., 2021). *More specifically, in this paper a case study (Dutch Wadden Sea) is presented, first introduce the main idea of selected statistical methods, subsequently applying them to a particular dataset (consisting of coastal biogeochemical model, numerical weatherprediction model and climate model outputs) and interpret the results. While the applied statistical methods are separately well documented in the literature (in their own fields), structured and combined use of them for the multivariate analysis of air-sea interactions to informing ecological impact studies is a novelty to the marine scientific community.*

Scientists aiming to study the air-sea interactions either in (operational) short term or (climate) long term scale often make use of numerical models, which produce approximate solutions to the underlying physical phenomena. The role of these physics-based models is even more prominent with the increasing (cloud) computing capabilities (Vance et al., 2019) that facilitate further refined spatial scales and improved process parametrizations. Using these models, gap-free (in space) and high frequency (in time) fields of atmospheric and environmental datasets can be produced. Such multi-dimensional numerical model simulated dataset often includes several variables at many locations (e.g. three dimensional spatial discretization) over long periods of time and covering different model scenarios (e.g. various model boundary conditions and model initializations). While the increasing volume of marine data contains abundant information and insights into the physical processes (also their interconnections and long term evolution), it must be noted that the processes underlying the variations in these simulated data are complex, the data might be noisy, and not all modelled variables are relevant to the studied processes. Consequently, latent variables can be useful for exploring and reducing the data. Traditionally, dimension reduction methods are used for such purposes.

Dimension reduction is an approach often used in multivariate data analysis and it is implemented for several

reasons. Firstly, using dimension reduction techniques high-dimensional data can often be transformed to a lower dimensional space without significant loss of statistical information (preserving accuracy). Secondly, dimension reduction techniques help in the removal of multi-colinearity in the dataset. The multi-colinearity problem is present if two or more variables are highly correlated, and therefore one can be accurately linearly predicted from the others. This is an unwanted property as it increases the variance in estimates of regression parameters (Maitra and Yan, 2008) and makes interpretation difficult. A further advantage of dimension reduction is that it facilitates the interpretation and visualization of high dimensional data as it is reduced to lower dimensions. Additionally, transforming data into lower dimensions decreases the required processing time and storage, and therefore makes analysis algorithms more efficient.

Various dimension reduction methods exist, some use linear combinations of variables to reduce dimensions (linear methods), whereas others use non-linear functions of variables (non-linear methods). A collection of non-linear dimension reduction methods can be found in (Hastie et al., 2009). The most widely used linear dimension reduction techniques are the Principal Component Analysis (PCA), an unsupervised technique, and the Partial Least Squares (PLS) (Maitra and Yan, 2008), a supervised technique. These are useful dimension reduction methods in regression problems due to the following features. Firstly, applying the transformed principal components instead of the original predictive variables tackles the problem of multi-colinearity since the covariance of principal components is zero. Secondly, the principal components successively capture the maximum variance of the predictor matrix, and therefore it is natural to use the first few components as predictive variables for regression. In most cases the majority of the variance is captured by them.

While their concept offers clear advantages, a practical limitation of these standard dimension reduction methods is that they work with "2-way" matrices. The 2-way structure usually contains the observations as rows and the variables as columns. A third way of the matrix, that could be the temporal or spatial dimension for instance, cannot be explicitly included. Multi-way analysis can help to resolve this issue. Multi-way analysis techniques also project variables to low dimensional spaces, therefore they can be called dimension reduction methods, but they are also able to work with multi-way ($N > 2$) data structures. Similarly to the other dimension reduction techniques, multi-way analysis can create latent variables by transforming the original variables, it can reduce noise, and it can explain which original variables are most important to the latent variables (Smilde et al., 2004). Further purpose of applying multi-way methods is data exploration, which includes finding patterns and interrelations (e.g. temporal and spatial behaviour of the different variables), or summarizing the data through decomposition.

Another missing feature in standard dimension reduction techniques that is quite essential in atmospheric and environmental time series is temporal correlation. For this reason, temporal correlation is included in this research through Dynamic Factor Analysis (DFA). Moreover, in this study the discrete-time data are also investigated using Functional Data Analysis (FDA), after transforming them to functional data through a basis function expansion. This is also motivated by the fact that certain variables display 'strong periodic behaviour', such as the sinusoidal shape of air temperature or solar radiation. Similarly to the dimension reduction techniques on discrete-time data, Functional Data Analysis also aims to find common patterns and underlying functions that can describe the general shape of the curves and explain their variability.

In this paper the above described statistical models are applied to atmospheric and environmental datasets in the Dutch Wadden Sea to investigate the relationships between atmospheric signals and the ecological response. Due to the complex interactions of atmospheric forcing with biological processes, the phytoplankton response is not trivial to understand, especially in our case study area. Considering the system dynamics, the southern North Sea is a tidally mixed region (Longhurst, 2007) but in our study area other shallow water, coastal, and estuarine fronts are also prominent. This makes it possible that certain regions are seasonally stratified while others are permanently mixed (van Leeuwen et al., 2015). Consequently, in the offshore areas surface mixing and convective cooling have a greater impact on phytoplankton biomass (Blauw et al., 2018), while in the highly dynamic coastal systems tidal mixing is more dominant.

The relationship between physical factors (atmospheric and oceanic) and the selected ecological response variable (chlorophyll-a) is well documented in the literature, nevertheless, debates still exist between scientists. In general, chlorophyll-a concentration (a proxy for phytoplankton biomass) is coupled to thermal stratification, resource and energy dynamics, as well as predator-prey interactions (Behrenfeld and Boss, 2018). Based on a cross correlation analysis conducted by (Blauw et al., 2018) in the North Sea (at a site with dynamics similar to our study area), the highest correlations were found with solar radiation, air temperature, turbidity, and tidal mixing. This study considered a range of physical factors (tidal mixing, wind mixing, solar radiation, air temperature, SST, salinity, turbidity) and chlorophyll-a (McQuatters-Gollop and Vermaat, 2011). found that inter-annual variability in phytoplankton dynamics in North Atlantic coastal waters were related to solar radiation, sea surface temperature, as well as Si availability. On the other hand, in the offshore regions it was mainly regulated by temperature, Atlantic inflow, wind stress and North Atlantic Oscillation (NAO). Moreover, in his study describing interannual changes in phytoplankton seasonality due to

climate forcing (González Taboada and Anadón, 2014), used the following variables: sea surface temperature that impacts the physiological and ecological processes and is a tracer of vertical mixing; solar radiation that limits phytoplankton growth rates or increases pigment cell levels; wind that is responsible for surface mixing and turbulence; and ocean current variability impacting stratification (Katara et al., 2008). also found that atmospheric variability are associated with chlorophyll-a concentration changes but the study considered large-scale modes of atmospheric variability. A shortcoming of our study is that it focuses on a small-scale coastal area, therefore large scale processes cannot be revealed.

2 Materials and methods

This research aims to support ecological impact studies in coastal ecosystems by providing a statistical framework for investigating latent processes and selecting important atmospheric variables. This statistical framework contains three types of dimension reduction techniques (Figure 1). Firstly, discrete-time data is considered and temporal correlation is neglected. Supervised and unsupervised techniques are compared and spatial correlation is included through multi-way methods. Secondly, temporal correlation is incorporated by applying dynamic factor models. Lastly, the discrete-time climate data is transformed into functional data representation, by smoothing them with basis function expansion (e.g. Fourier basis expansion), and subsequently study the functional variation with Functional PCA. While discrete-time data is a set of discretely measured values $y_{i1},\ldots,y_{in}$ functional data is when these values are converted to a function x_i with values $x_i(t)$ computable for any desired time t (Ramsay and Silverman, 2005).

2.1 Dataset

Our study is based on data from various numerical models (see Figure 2): a coastal water quality model, a numerical weather prediction model, and a climate model. The ecological indicator variable is chlorophyll-a concentration, a proxy for algal biomass, while the atmospheric variables are air temperature, solar radiation, eastern and northern wind components, air pressure, relative humidity, and total cloud cover. These are standard atmospheric variables simulated by most modelling systems for both operational purposes and climate experiments.

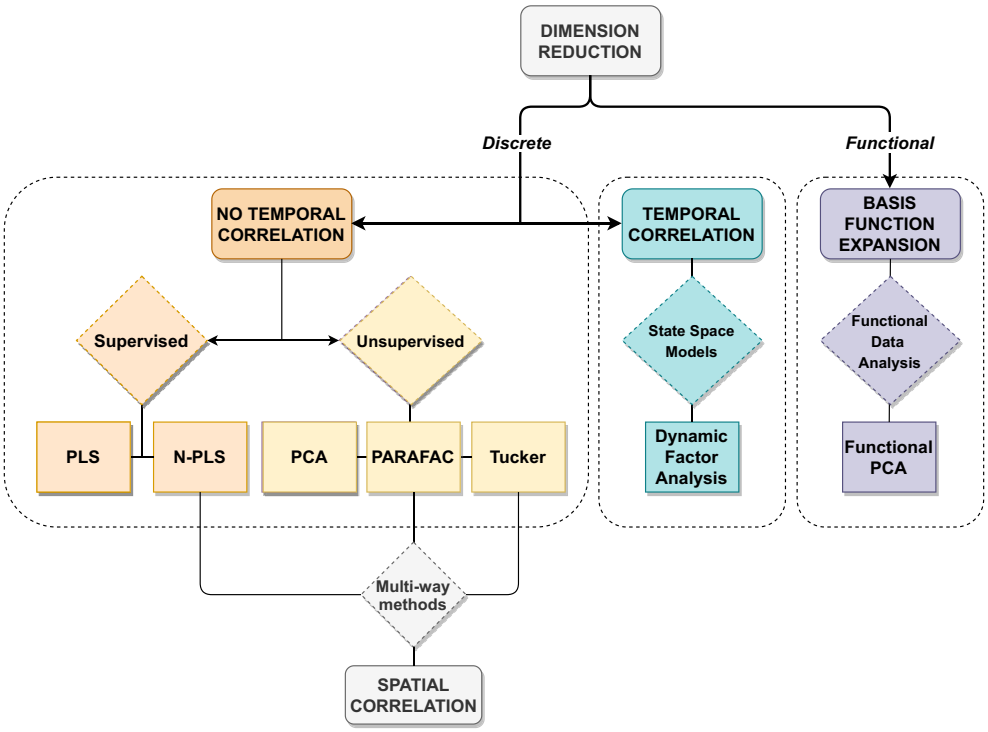

FIGURE 1
Overview of the applied statistical techniques for discrete-time and functional data, including temporal and spatial correlation.

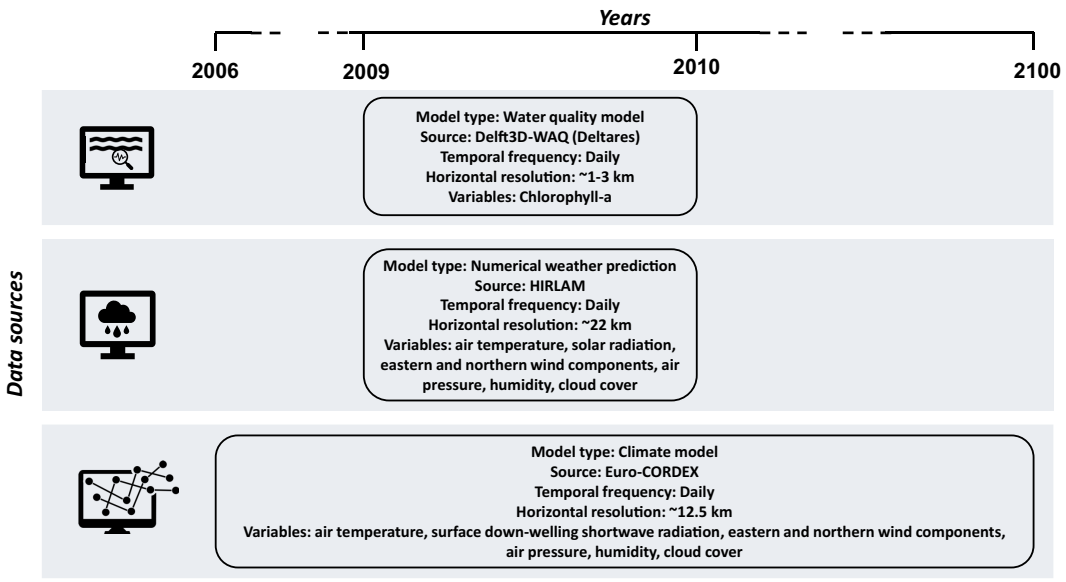

FIGURE 2
Overview of the data used in the study (model type, source, temporal frequency and variables) for the marine water quality model (top), numerical weather prediction model (middle), and climate model (bottom).

2.1.1 Chlorophyll-a concentration data

The chlorophyll-a concentration data is obtained from the water quality sub-module of the Delft3D integrated modelling system, Delft3D-WAQ (https://www.deltares.nl/en/software/158delft3d-4-suite/) (Blauw et al., 2009). In this research an existing model setup is used, which has been previously calibrated and validated for the location of our study area (Los et al., 2008). The spatial domain of the physical model covers the Southern North Sea with coarser horizontal resolution offshore and finer resolution along the Dutch coast, as shown in Figure 3. The model comprises of twelve vertical layers, making it a three dimensional physical model. The horizontal resolution of the water quality model in the Dutch Wadden Sea ranges from 1-by-2 km to 2.5-by-3 km on a curvilinear grid.

Delft3D-WAQ is a comprehensive hybrid ecological model including an array of modules reproducing water quality processes that are then combined with a transport module to calculate advection and dispersion. The model most importantly calculates primary production and chlorophyll-a concentration while integrating dynamic process modules for dissolved oxygen, nutrient availability and phytoplankton species. This Delft3D-WAQ setup includes the phytoplankton module (BLOOM) that simulates the growth, respiration and mortality of phytoplankton. Using this module the species competition and their adaptation to limiting nutrients or light are simulated (Los et al., 2008).

2.1.2 Atmospheric data

Two sources of atmospheric data are used in this study: (1) outputs of an operational numerical weather prediction model, and (2) results of a regional climate modelling experiment. First, the High Resolution Limited Area Model (HIRLAM) model (Meijgaard et al., 2008) output is used, which was applied as atmospheric forcing for the Delft3D-WAQ model setup to compute chlorophyll-a concentration. HIRLAM is a Numerical Weather Prediction (NWP) system developed by the international HIRLAM programme (http://hirlam.org/) (Undén et al., 2002). Since it is the Delft3D-WAQ input data that drives the processes, it allows the exploration of the correlations between atmospheric forcing and numerically computed ecological response. The data for this study are obtained from the 22 km grid resolution HIRLAM model and include near-surface air temperature, solar radiation, eastern and northern near-surface wind components, surface pressure, near-surface relative humidity, and total cloud cover. All HIRLAM model output variables were used in the Delft3D-WAQ model as temporally and spatially variable forcing fields except solar radiation, which is an area average, therefore the same for the entire domain.

Additionally, simulated values of climate variables are acquired from the high resolution 0.11 degree (~12.5 km) EURO-CORDEX Coordinated Regional Downscaling Experiment (https://www.euro-cordex.net/) (Jacob et al., 2014), which uses the Swedish Meteorological and Hydrological Institute Rossby Centre regional atmospheric model (SMHI-

FIGURE 3
Case study area: Dutch Wadden Sea. Delft3D-WAQ model domain in the Southern North Sea and along the Dutch coast (left panel, source: (Mészáros et al., 2021)). Location of the stations where time series data was extracted (right panel).

RCA4) (Samuelsson et al., 2015). In order to produce various regionally downscaled scenarios, EURO-CORDEX applies a range of General Circulation Models (GCMs) to drive the above mentioned Regional Climate Model (RCM). The four driving GCMs in this study are the National Centre for Meteorological Research general circulation model (CNRM-CM5) (Voldoire et al., 2013), the global climate model system from the European EC-Earth consortium (EC-EARTH) (Hazeleger et al., 2012), the Institut Pierre Simon Laplace Climate Model at medium resolution (IPSL-CM5A-MR) (Dufresne et al., 2013), and the Max-Planck-Institute Earth System Model at base resolution (MPI-ESM-LR) (Giorgetta et al., 2013). In addition to the driving models, further scenarios are obtained by considering different socio-economic changes described in the Representative Concentration Pathways (RCPs). RCPs are labeled according to their specific radiative forcing pathway in 2100 relative to pre-industrial values. This study includes RCP8.5 (high), and RCP4.5 (medium-low) (van Vuuren et al., 2011) and four driving GCMs for the projection period between 2006-2100. Together the four different driving GCMs and two RCPs provide us with an ensemble of eight trajectories per climate variable. The climate variables included in the analysis are near-surface air temperature, surface downwelling shortwave radiation, eastern and northern near-surface wind components, surface pressure, near-surface relative humidity, and total cloud cover. For this dataset, near-surface means at a height between 1.5 to 10.0 m.

2.1.3 Data processing

The above introduced datasets are temporally varying multivariate fields covering large domains (see Figure 4). For the purpose of this study, time series data were extracted at ten locations of Rijkswaterstaat monitoring stations in the Dutch Wadden Sea (see Figure 3). Both the atmospheric variables and the chlorophyll-a concentration were provided as 6-hourly datasets. The longer and higher frequency data were sub-sampled to the period between 1st of March and 1st of November, daily at 12:00 (245 time steps). The model simulation year (2009) was chosen based on the fact that a detailed study was conducted (at Deltares) for that year with high resolution information on the suspended matter fields which are crucial for water quality computation in the shallow Wadden Sea. The reason for selecting a reduced time period (9 months) is to concentrate on the season of high phytoplankton productivity and to eliminate near zero chlorophyll-a values during winter. Moreover, the daily time step at 12:00 was selected to eliminate zero radiation values during the night. All variables were then centered to their mean and divided by their standard deviation to eliminate the problem of different measurement units. Finally, the right skewed chlorophyll-a concentration was log transformed to achieve a more symmetrical distribution that may improve the performance of statistical models used in the study. It is a standard practice to log transform chlorophyll-a as it is approximately lognormally distributed in marine waters (Campbell, 1995). The distribution of chlorophyll-a concentration (all locations and all time steps) before and after log transformation are shown in Figure S1 (Supplementary Material). The pair plot of all variables with kernel density estimation is displayed in Figure S2 (Supplementary Material).

Figure 5 shows the Spearman's rank correlation coefficient of all variables after scaling (data taken from all stations). The same plot using Pearson correlation coefficient can be found in Figure S3 (Supplementary Material). It can be observed that solar radiation and air temperature have the highest correlation with chlorophyll-a. Moreover, cross-correlation between the atmospheric data an also be identified, e.g. pressure and northern wind component or humidity and air temperature. It is important to note that while air temperature and solar radiation are positively correlated, they have different impact

10.3389/fmars.2022.920616

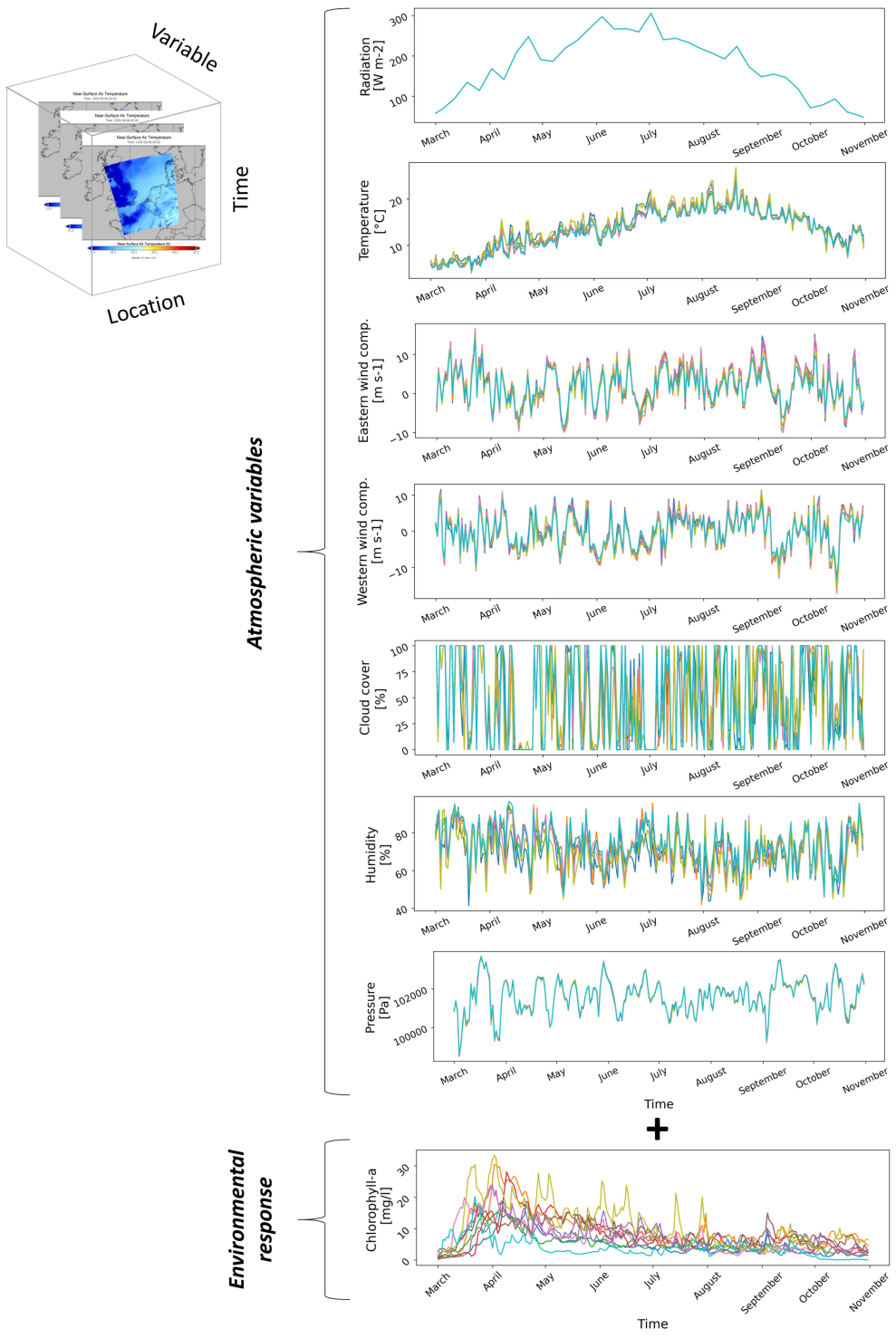

FIGURE 4
Illustration of the atmospheric and environmental variables used in the study.

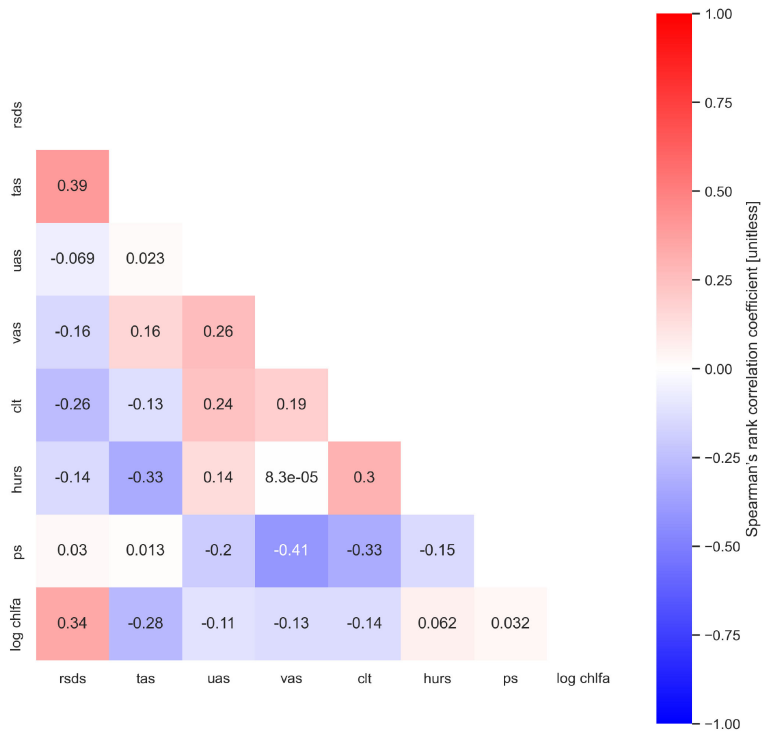

FIGURE 5
Heatmap with Spearman's rank correlation coefficient. Dark red indicates strong positive, while dark blue indicates strong negative correlations. Data from all time series. Abbreviations: solar radiation (rsds), air temperature (tas), eastern (uas) and northern (vas) wind components, cloud cover (clt), humidity (hurs), air pressure (ps), chlorophyll-a (chlfa).

on chlorophyll-a concentration: air temperature has negative correlation, whereas solar radiation has positive correlation with chlorophyll-a. Since in the North Sea the correlation between solar radiation/air temperature and chlorophyll-a concentration highly depends on the region (offshore or coastal) and the temporal scales (short, seasonal, long) there could be various reasons. In our case, it might be attributed to the phenomena reported by Blauw et al. (2018), who found that the thermal mixing of phytoplankton cells (from the deep chlorophyll maximum) into the surface layer is the dominant process explaining the negative correlation between sea surface temperature and the chlorophyll concentration in the daily time series (in the Southern North Sea).

2.2 Two-way and multi-way methods

2.2.1 From PCA to N-PLS

This section briefly introduces the steps to extend the two-way component methods to multi-way regression methods. For convenience, Principal Component Analysis (PCA), Principal Component Regression (PCR) and ordinary PLS regression are introduced briefly, because the N-PLS regression is based on these algorithms. Assuming that $X \in \mathbb{R}^{I \times J}$ and $\underline{y} \in \mathbb{R}^{I}$ are column centred and scaled matrices, the predictor matrix X and response $\underline{y}$ are decomposed as follows:

$$X = TP' + E_X \tag{1}$$

$$\underline{y} = T\underline{q} + e_Y \tag{2}$$

where T is a matrix of scores ($T=XP$); P' is a matrix of X loadings, q is a matrix of $\underline{y}$ loadings, whereas E_X and e_y are the residuals. PCA focuses only on the predictor matrix projecting each data point onto the principal components while preserving as much of the data's variation as possible. PCA finds R components such that they maximize the variance of the projected data in X. The description below is written for R=1. To calculate the 1^{st} PCA component, $\hat{x}_{ij}$ is approximated with t_i core and w_j loading:

$$\hat{x}_{ij} = t_i w_j \tag{3}$$

where $\underline{t} \in \mathbb{R}^I, \underline{w} \in \mathbb{R}^J, i \in \{1,\ldots,I\}, j \in \{1,\ldots,J\}$, and $||w||$=1. Then the score vector and loading vector can be obtained as follows:

$$\underline{t}(w) = \underset{t}{arg\,min} \sum_{i=1}^{I}\sum_{j=1}^{J}\left(x_{ij} - t_i w_j\right)^2 \tag{4}$$

$$\underline{w}^{*} = \underset{\underline{w}:||w||=1}{a\,rgmax}\,\mathrm{var}\;\; \underline{t}(\underline{w}) \tag{5}$$

$$\Rightarrow \underline{t}^{\star} = \underline{t}(w^{\star}) \tag{6}$$

Then the approximation of $\hat{X}$ can be rewritten as:

$$\hat{X} = TP' \tag{7}$$

with $T = \underline{t}$ and $P' = \underline{w}$. Finally, the decomposition of X (for the 1^{st} PC situation) is obtained as:

$$X = \hat{X} + E_X \tag{8}$$

The PCR algorithm is similar to the PCA algorithm except that it is extended with response y using Eq (2). In other words, PCR constructs R components the same way as PCA, but adds a regression step to it. Consequently, the regression coefficient $\underline{q}$ is obtained from regressing $\underline{y}$ on T

$$\underline{q}^{\star} = \underset{q}{a\,rgmin} \parallel \underline{y} - T\underline{q} \parallel^2 = \left(T'T\right)^{-1}T'\underline{y} \tag{9}$$

The PLS regression differs from PCR, due to its supervised nature, as it finds R omponents from both X and $\underline{y}$ such that covariance between the score vector $t(w)$ and $\underline{y}$ is maximized:

$$w^{\star} = \underset{\underline{w}:||w||=1}{a\,rgmax}\mathrm{cov}\left(\underline{t}(\underline{w}), \underline{y}\right) \tag{10}$$

$$\Rightarrow \underline{t}^{\star} = \underline{t}(w^{\star}) \tag{11}$$

Again, rewrite the approximation as Eq (7). with $T = \underline{t}$ and $P = \underline{w}$. Then obtain the decomposition as in Eq (8). Subsequently from Eq (2). the regression coefficient $\underline{q}$ is obtained as in Eq (9). As a consequence, PLS finds loading w that leads to a least squares solution to Eq (3). Moreover, the PLS score vector has maximal covariance with $\underline{y}$. In general, both PCA and PLS achieve dimension reduction by converting highly correlated variables to a set of uncorrelated variables through linear transformation. The difference is that PCA, as an unsupervised technique, captures maximum variance only in the predictor matrix without considering how each predictive variable may be related to the response variable. On the other hand, PLS combines information about the variances of both the predictors and the responses, while also considering the correlations among them (supervised dimension reduction). PLS is considered useful in particular if there are more independent (predictor) variables than dependent (response) variables, and if there is multi-colinearity in the predictors. Since in this study several correlated atmospheric variables are used to estimate one ecological response variable, the use of supervised dimension reduction techniques is preferable.

The N-PLS regression algorithm is an extension of the PLS regression algorithm to multi-way data, where essentially the bilinear model of X is replaced with a multilinear model of X. In case the data is three-way, as in this study, then an appropriate model of X is a trilinear decomposition, as depicted in Eq (16). The model of x_{ij} in ordinary PLS is shown in Eq (3), whereas in three-way PLS the approximation of x_{ijk} is given by the following equation:

$$\hat{x}_{ijk} = t_i w_j^J w_k^K \tag{12}$$

where $\underline{t} \in \mathbb{R}^I, \underline{w}^J \in \mathbb{R}^J, \underline{w}^K \in \mathbb{R}^K$. In this case the three-way decomposition is defined by:

$$\underline{t}\left(w^J, w^K\right) = \underset{t}{a\,rgmin}\sum_{i=1}^{I}\sum_{j=1}^{J}\sum_{k=1}^{K}\left(x_{ijk} - t_i w_j^J w_k^K\right)^2 \tag{13}$$

$$\left(w^{\star J}, w^{\star K}\right) = \underset{||w^J||=1,\,||w^K||=1}{a\,rgmax}\,\mathrm{cov}\left(\underline{t}\left(w^J, w^K\right), \underline{y}\right) \tag{14}$$

$$\Rightarrow \underline{t}^{\star} = \underline{t}(w^{J\star}, w^{K\star}) \tag{15}$$

where $||w^J||=1$ and $||w^K||=1$. The regression coefficient $\underline{q}$ s obtained by regressing $\underline{y}$ on T as in Eq (9), rewriting the approximation as above in Eq (7). with $T=[t]$ and $P=[w]$ subsequently obtaining the decomposition as in Eq (8). Similar to ordinary PLS the resulting score vector has maximal covariance with $\underline{y}$ and the loadings (w_j^J and w_k^K) lead to a least square solution. For $R>1$ further components can be obtained as follows. Rewrite Eq (7) with $T = [\underline{t}_1, \ldots, \underline{t}_R]$, $P = [\underline{w}_1, \ldots, \underline{w}_R]$. Finally, decomposition of X is in Eq (8), and subsequently from Eq (2). the regression coefficient $\underline{q}$ is obtained as in Eq (9).

In summary, the N-PLS model first extracts the important features from the predictor dataset into the loading array P then estimates the regression coefficient vector $\underline{q}$ using least squares. For a more detailed description of the N-PLS algorithm the reader is referred to (de Jong, 1998; Bro, 1996; Smilde, 1997; Bro, 1998; Bro et al., 2001; Smilde et al., 2004).

2.2.2 Comparison of multi-way methods

Atmospheric datasets are often multi-dimensional due to the fact that they contain several variables, which are not only varying over time but also over space. Moreover, often additional dimensions are present such as different climate projection scenarios, or model ensembles, which simulate the same information but use different assumptions or initial conditions. Three-way data that contain information on different variables, over time and space can be organized in a three-way array $\underline{X} = X_{i,j,k}$. In our case the first dimension (mode 1 or index i of the three-way array $\underline{X}$ corresponds to time, the second dimension (mode 2 or index j corresponds to different atmospheric variables, and the third dimension (mode 3 or index k corresponds to location. Consequently, each frontal slice X_k represents a location with variables j sampled over time i.

The distinction between component and regression models should also be noted. The typical purpose of component models

on one block of data is exploring the patterns and interrelations using latent variables (principal components), while regression models are aimed at predicting a block of data (response) using another block of data (predictors) through a prediction model. Consequently, component models require one block data, while regression models need multi block data. The above mentioned dimension reduction methods (PCA and PLS) are two-way component and regression models that cannot be directly applied to multi-way data. The traditional approach to deal with multi-way data is to use unfold methods (sliced analysis) such as the one introduced by Wold et al., (1987). Unfold methods first unfold the multi-way array to a two-way matrix and then perform ordinary PCA and PLS analysis. However, as Bro (1996) has pointed out, the unfolding methods are not favourable since they do not make use of the multi-way structure in the data, they are often complex (using many parameters) and more difficult to interpret compared to the multi-way methods that do not use unfolding.

More appropriate models have been developed for handling multi-way data, which are the so-called multi-way component and regression models, schematized in Figure 6. Multi-way component models are basically generalizations of the two-way solutions to higher order arrays. One generalization of PCA to higher orders is Parallel factor analysis (PARAFAC), also known as trilinear decomposition, with general equation given by:

$$x_{ijk} = \sum_{r=1}^{R} a_{ir} b_{jr} c_{kr} + e_{ijk} \tag{16}$$

where R is the number of components used to fit the model; a_{ir}, b_{jr},c_{kr} are 'triads' (trilinear factors) and e_{ijk} is the residual (see Figure 6). Note that here R>1 s explicitly possible, compare PCA and PLS descriptions above. Another generalization is the Tucker decomposition, also called N-mode Principal Component Analysis (Bro, 1997). For the three-way case, Smilde et al. (2004) describe the Tucker3 model with the following equation:

$$x_{ijk} = \sum_{P=1}^{P}\sum_{q=1}^{Q}\sum_{r=1}^{R} a_{ip} b_{jq} c_{kr} g_{pqr} + e_{ijk} \tag{17}$$

where a_{ip},b_{jq},c_{kr} are elements of the loading matrices A, B, C, g_{pqr} is an element of the core-array G nd e_{ijk} is the residual element in E as depicted in Figure 6.

Similarly, the two-way partial least squares regression was also extended to multi-way data as described in Section 3.2.1. The N-way Partial Least Squares (N-PLS) method was developed by (Bro, 1996) and further elaborated by (de Jong, 1998; Smilde, 1997; Bro, 1998; Bro et al., 2001). A pictorial representation of N-PLS model is shown in Figure 6. Due to its desirable properties, as compared to the unfolding methods, the N-PLS method has been applied in a range of areas such as

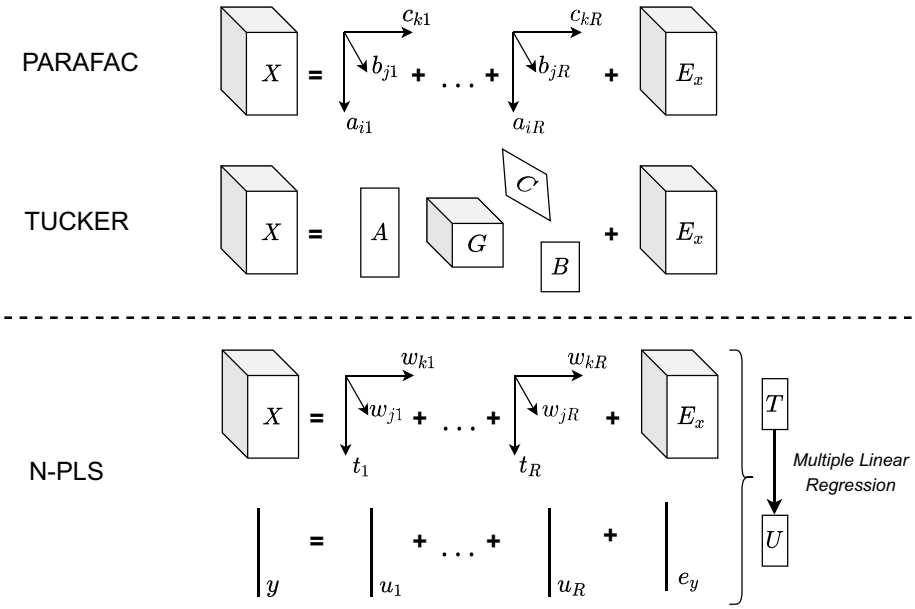

FIGURE 6
Schematization of multi-way models. The cubes (cuboids) represent three dimensional arrays (X denoting the data array, G the core-array for the Tucker model and Ex the residual array for all models), the three arrows represent orthogonal vectors (trilinear factors a1, b1, c1, and loading vectors wk, wj with score vector t), while the lines represent vectors (response vector y, score vector u, and residual vector ey), and the rectangles represent loading matrices for the Tucker model (A, B, C). Adopted from (Fujiwara and Mohr, 2009).

chemometrics, neuroscience and environmental analysis (Bro, 2006), food industry (Favilla et al., 2013), organic pollutants in the environment (Mas et al., 2010) or most recently in agriculture (Lopez-Fornieles et al., 2022).

Moreover, recently another generalized multilinear regression method, the Higher Order Partial Least Squares (HOPLS), was introduced by (Zhao et al., 2013). HOPLS differs substantially from N-PLS in that it uses the Tucker tensor decomposition (see Eq. (17)) instead of the trilinear decomposition (see Eq. (16)), hence, it benefits from the advantages of Tucker over PARAFAC. Zhao et al. (2013) found that HOPLS could outperform N-PLS and PLS in case of small sample sizes and higher order $N>3$ response data $\underline{y}$. While HOPLS appears to be a promising method in those cases, it should be noted that in this study sufficient number of samples is available and the response $\underline{y}$ dataset is not high dimensional $N\leq 3$ The substantial differences between the above mentioned multi-way methods can be seen from their schematic representation (Figure 6). A comprehensive review of other dimension reduction methods for multidimensional data *via* Multilinear Subspace Learning (MSL) can be found in (Lu et al., 2013). In this study the PCA, PLS, PARAFAC and Tucker algorithms were implemented using open source Python packages such as scikit-learn and TensoLy, whereas for the N-PLS algorithm the N-way Toolbox (Andersson et al., 2000) was used in Matlab.

In order to showcase the differences between the various two-way (PCA, PLS) and multi-way (PARAFAC, TUCKER, N-PLS) dimension reduction methods, they were applied on the atmospheric and environmental data (from Section 2.1) for prediction. Their prediction errors were analysed from 10-fold cross-validation. K-fold cross-validation, briefly described in (Hastie et al., 2009), uses a subset of the available data as a training set to fit the model and a different subset as a test set, where the full dataset is split into K qual-sized parts, in this case $K=10$. For the prediction of every $k-th$ subset the model is fitted to the remaining $K-1$ subsets of the data and the prediction error of the fitted model is calculated. This process is repeated for $k=1,2,\ldots,K$ and the K estimates of prediction error are averaged. First the Mean Squared Error (MSE) with only the intercept (no principal components in regression) was calculated, and later on the MSE is computed using 10-fold cross-validation for the principal components, adding one component at the time in increasing order. The error measures of the unsupervised methods were obtained by extracting their computed model factors (with different number of components) which were then used to fit linear regression. The results of estimated mean squared errors of predicting y from 10-fold cross-validation are shown in Figure 7.

Apart from the prediction accuracy, it is also investigated how strongly each component (latent variable) in the two component N-PLS model (the best performing multi-way model) depends on the original variables (see Figure 8).

2.3 Dynamic factor analysis

The previously presented dimension reduction techniques are able to identify unobserved factors that influence a substantial portion of the variation in a larger number of observed variables, and able to summarize the dataset through decomposition. None of these techniques, however, is designed for time series analysis as temporal correlation is neglected. Dynamic Factor Analysis (DFA) is a factor model that explicitly models the transition dynamics of the unobserved factors; hence, it is a dimension reduction technique that is designed for time series data. In fact, DFA is a multivariate time-series analysis technique that estimates underlying common trends in multivariate time series (Harvey, 1990; Mike West, 1997; Lütkepohl, 2005). The time series are modelled using a linear combination of common trends, explanatory variables, and a noise component (Zuur et al., 2003a).

Given N ime series, these could be analysed by univariate models by treating them as N separate univariate time series. However, this would result in N estimated trends without considering the interactions between them. DFA aims to overcome this disadvantage by reducing the N univariate trends to M common trends, where $1\leq M<N$. The main objectives of DFA on environmental time series are therefore identifying underlying common trends (unobserved factors) in the input time series, identifying interactions between the time series, and analysing the effects of explanatory variables.

The basic concept of DFA is to decompose the multivariate data into trends, explanatory variables and noise. Supposing that y_t is a univariate response variable measured in time t where $t=1,\ldots,T$ one of the simplest univariate time series models is given as follows:

$$y_t = \gamma\alpha_t + \in_t \tag{18}$$

$$\alpha_t = \alpha_{t-1} + \eta_t \tag{19}$$

where α_t represents the factor (unknown trend) at time t while $\in_t$ and η_t are error components (noise). This model is called the random walk trend plus noise model. A formulation for the DFA with N time series (N rows) and M common trends (M columns) can be written as:

$$\begin{bmatrix} y_{1t} \\ \vdots \\ y_{Nt} \end{bmatrix} = \begin{bmatrix} \gamma_{11} & \gamma_{1M} \\ \vdots & \vdots \\ \gamma_{N1} & \gamma_{NM} \end{bmatrix} \begin{bmatrix} \alpha_{1t} \\ \vdots \\ \alpha_{Mt} \end{bmatrix} + \in_t \tag{20}$$

$$\begin{bmatrix} \alpha_{1t} \\ \vdots \\ \alpha_{Mt} \end{bmatrix} = \begin{bmatrix} \alpha_{1,t-1} \\ \vdots \\ \alpha_{M,t-1} \end{bmatrix} + \begin{bmatrix} \eta_{1t} \\ \vdots \\ \eta_{Mt} \end{bmatrix} \tag{21}$$

or in generic form:

$$y_t = \Gamma\alpha_t + \in_t \tag{22}$$

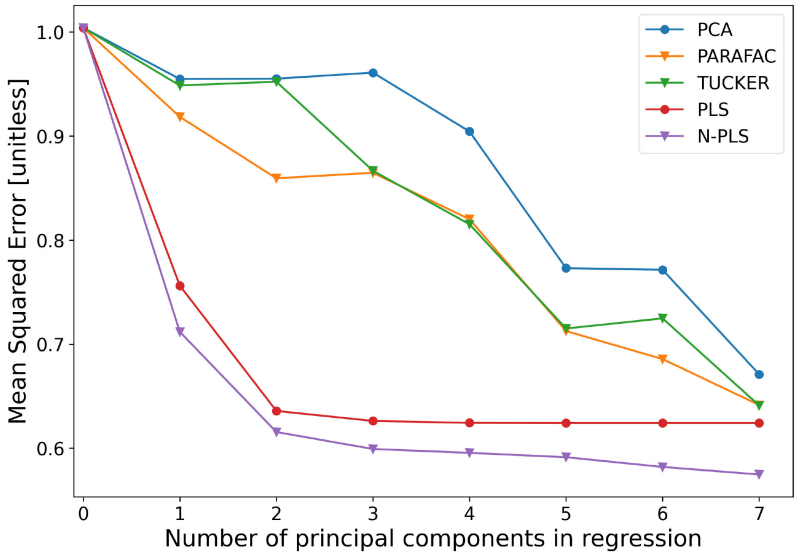

FIGURE 7
Comparison of two-way (point markers) and multi-way (triangle markers), unsupervised (PCA, PARAFAC, TUCKER) and supervised (PLS, N-PLS) dimension reduction models. Prediction errors (MSE) from 10-fold cross-validation with increasing number of components. Prediction is done at Marsdiep Noord station.

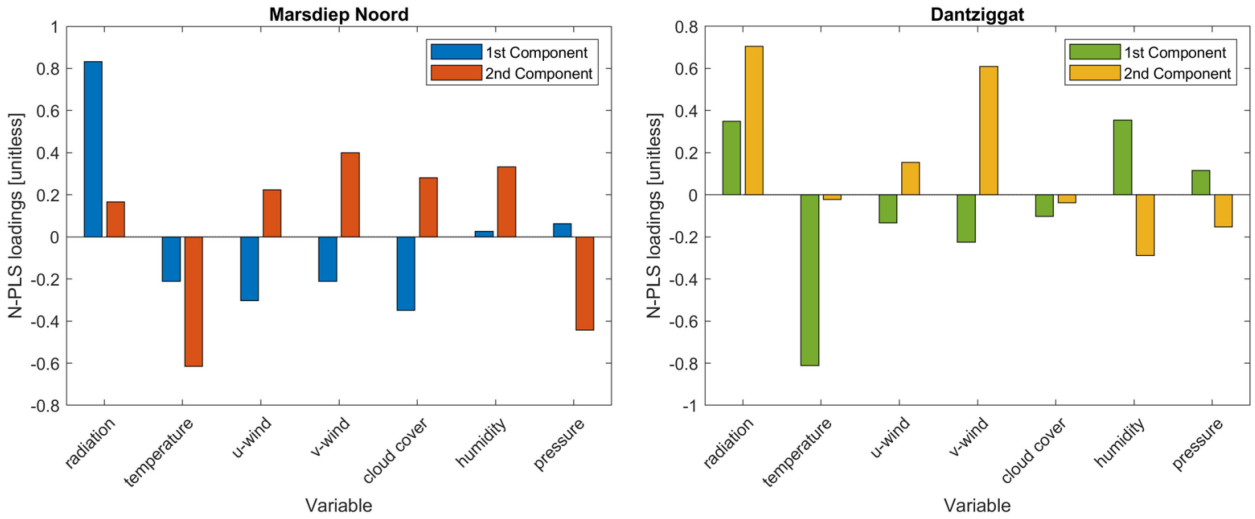

FIGURE 8
Importance of predictor variables in the N-PLS model. Loadings of atmospheric variables in the 1st and 2nd N-PLS components for locations Mardiep Noord (left) and Dantziggat (right). Eastern and northern wind components are denoted by u-wind and v-wind, respectively.

$$\alpha_t = \alpha_{t-1} + \eta_t \tag{23}$$

where Γ is a factor loading matrix with dimension $N \times M$ and contains the unknown factor loadings, which are multiplication factors that determine the linear combination of the original variables; and α_t is a vector of the M common trends at time t with dimension $M \times 1$. It is generally assumed that the error terms are independent, normally distributed with mean 0 and an unknown diagonal or symmetric/non-diagonal covariance matrix: $\in_t \sim N(0,H)$ $\eta \sim N(0,Q)$ and $\alpha_0 \sim N(\alpha_0, V_0)$ where H,Q,V_0 are covariance matrices (Zuur et al., 2003b). Based on these

parameters the covariance matrix of y_t can be written as:

$$cov(yt) = \Gamma\ var(\alpha_t)\Gamma' + H \tag{24}$$

In order to include K explanatory variables in the DFA, equations (22)– (23) can be extended to the following model:

$$y_t = \Gamma\alpha_t + Dx_t + \in_t \tag{25}$$

$$\alpha_t = \alpha_{t-1} + \eta_t \tag{26}$$

where D is an $N\times K$ matrix containing the partial (standardized) regression coefficients, and x_t is a $K\times 1$ vector containing the values of the K explanatory variables at time t. The effects of explanatory variables are modelled as in linear regression, and therefore it depends on the same underlying assumptions, such as normality, independence, and homogeneity of residuals (Zuur et al., 2003a).

Equations (25)- (26) can be cast into state space form, and the unknown trends can be estimated *via* the Kalman filter. The likelihood is then evaluated based on the filtering recursions, and maximum likelihood estimation is used to estimate the parameters. The Kalman Filter and smoother algorithm for the model in equations (25)- (26) can be found in (Zuur et al., 2003b).

The dynamic factor model was applied to the ten chlorophyll-a time series. The main objective was to identify underlying common trends and further analyse the effects of atmospheric variables on chlorophyll-a concentrations, this time considering temporal correlation. Since standard dynamic factor models are not designed for multi-way data, such as N-PLS, the atmospheric data is averaged over the locations. In order to verify that the underlying assumptions of the dynamic factor model are not violated, several tests were conducted. These tests include plotting the standardized residuals over time, checking the normality of the residuals and plotting the correlogram (see Figure S4 in the Supplementary Material). It was verified that residuals are uncorrelated (since the autocorrelations are near zero of all time-lag separations), and normally distributed with mean zero. Thus, underlying assumptions are valid.

2.4 Functional PCA

So far the paper has investigated the features and relationships between short term (1 year long) meteorological data and environmental response. These datasets offered us the opportunity to apply supervised techniques since the environmental response was computed with the meteorological data as input. Moreover, we could consider temporal dependence and compute unobserved factors in the time series due to the reasonable number of time steps that allow us to apply computationally intensive state space models. However, apart from the analysis on short term data, we are also interested in investigating the features of the long term (climate scale) atmospheric projections and potential for data reduction. In order to achieve this, firstly we use Euro-CORDEX climate projections (covering the entire 21st century) instead of numerical weather prediction model outputs. Secondly, we analyse the discretely computed (in time) atmospheric data in the functional data space. This allows us to apply functional data analysis and study functional variation, which is more logical for climate projections that are long time series of modelled variables and are not meant to study short term changes and daily variability. Naturally, an interesting feature of the climate projections is their long term trends. Conclusions on their seasonal variability and the similarities between climate scenarios are less often drawn, however. We aim to reach such conclusions through Functional Data Analysis. By treating these long term climate projections as functional data our objective is to find an underlying function that can characterize the general shape of the time series, explain their variability (functional variation), reduce data complexity, and to aid the interpretation of the underlying variability sources (Ramsay and Silverman, 2005). The findings of the previous analyses and the Functional Data Analysis can be jointly used for climate impact assessment by aiding the atmospheric variables selection for studying chlorophyll-a climate response, as well as the identification of important features of the climate projections for further statistical models.

Functional data representation is commonly done by smoothing the discrete-time data with basis expansion (e.g. constant, polynomial, polygonal, B-splines, power, exponential, Fourier) as a pre-processing step. In our study, a Fourier basis expansion is applied, which has good computational properties especially when the data points are equally spaced. Moreover, Fourier bases are natural for describing periodic data, such as atmospheric variables, and therefore it is commonly used in this domain. The functional basis components can be then estimated through Functional Principal Component Analysis (FPCA).

The underlying idea is that a function $x_i(t)$ can be expressed as a basis expansion:

$$x_i(t) = \bar{x}(t) + \sum_{j=1}^{\infty} f_{ij}\varphi_j(t) \tag{27}$$

And

$$f_{ij} = \int \varphi_j(t)[x_i(t) - \bar{x}(t)]dt \tag{28}$$

where $\bar{x}$(t) is the functional mean (zero if the data is mean centered), $\varphi_j(t)$ are the orthonormal eigenfunctions and f_{ij} are the Functional Principal Component Scores. The first few eigenfunctions and eigenvalues can be used for data reduction and feature extraction, while the Functional Principal Component Scores can be used to describe, cluster and classify the curves (Segovia-Gonzalez et al., 2009). The Functional

Principal component analysis in this research uses an open source Matlab toolbox (Ramsay et al., 2009).

While the other above mentioned methods (multi-way methods and dynamic factor model) are used for identifying the most important atmospheric variables affecting chlorophyll-a concentrations in a shorter time interval, in this research Functional Principal Component Analysis is used to investigate different features of the long term climate projections spanning the 21^{st} entury (from 2006 to 2100). Functional Principal Component Analysis was therefore applied to the Euro-CORDEX climate projections to compare the functional variation of climate variables, and to describe, cluster and classify the climate scenarios for the two most important variables (radiation and temperature).

The discrete-time data points are first transformed to functional data using a Fourier basis expansion. The left panel of Figure 9 shows the atmospheric variables as functional data for an arbitrarily selected year within the 95 year interval. The well distinguishable sinusoidal shapes of solar radiation and temperature can be seen in the figure. Functional Principal Component Analysis with two principal components is then performed on the functional data and the scores of the first two components are plotted to analyse similarities between the variables (right panel of Figure 9). Moreover, as a second experiment, using Functional Principal Component Analysis the aim is to classify and cluster the climate scenarios (Representative Concentration Pathways and driving General Circulation Models) for the two important climate variables (radiation and temperature), see Figures 10, 11.

3 Results

3.1 Comparing two-way and multi-way methods

Another observation is the performance difference between PCA, PARAFAC and Tucker models. Both PARAFAC and TUCKER are generalizations of PCA to a higher order, with the important difference that the PARAFAC model has the attractive feature of providing unique solutions (there is no problem with rotational freedom). If the data are approximately trilinear, the true underlying phenomena can be found if the right number of components is used and the signal-to-noise ratio is appropriate (Bro, 1998). The Tucker model is, however, more flexible and has rotational freedom. It is not structurally unique as PARAFAC. This makes the Tucker model complex and might explain why it has lower performance for this specific example. A restricted Tucker model version exists where domain knowledge is used to restrict the core elements, forcing individual elements to take specific values. This way it is possible to define models that uniquely estimate certain properties. This could be seen as a structural model tailored to a specific problem. In this paper restricted Tucker models were not used.

In Figure 8 the loadings of the first two components of the N-PLS model (the best performing multi-way model) are given for two different locations. By identifying the original predictor variables that weight most heavily one can draw conclusions on the underlying physical processes. Moreover, less important

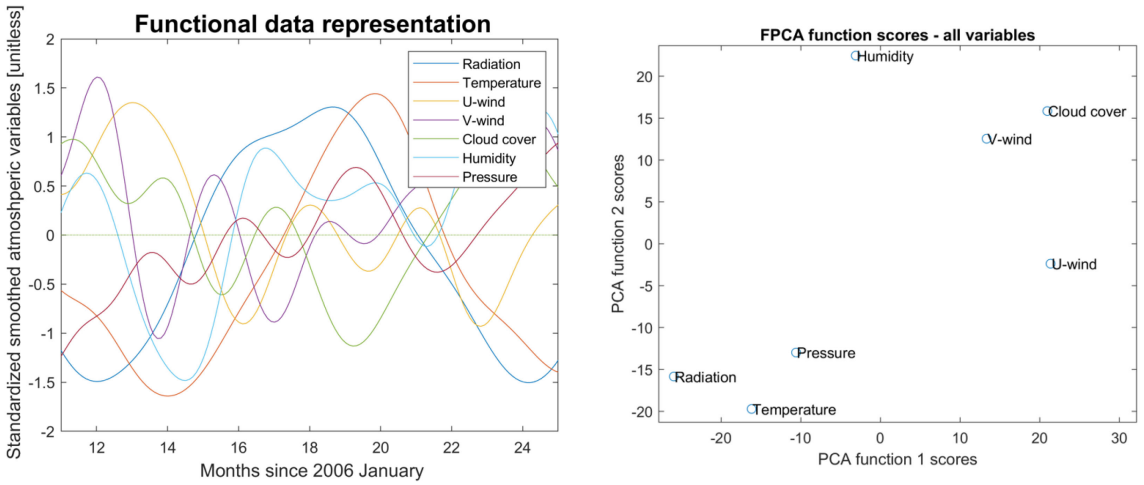

FIGURE 9
Functional Principal Component scores for the Euro-CORDEX climate variables. Atmospheric variables transformed to functional data (for an arbitrarily selected year) on the left panel, and clustering of variables based on the FPCA function scores on the right panel.

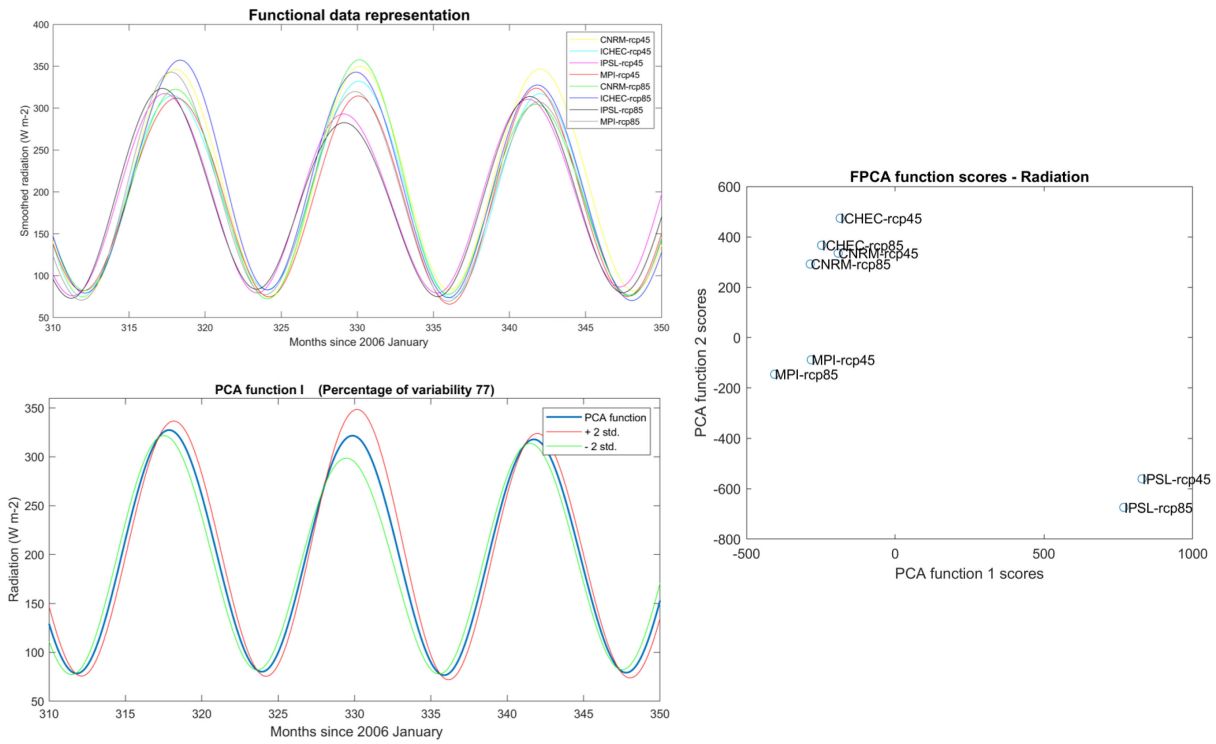

FIGURE 10
Functional Principal Component Analysis for the Euro-CORDEX solar radiation scenarios. Eight solar radiation scenarios transformed to functional data on the upper left panel, the first PCA component with ± two standard deviations on the bottom left panel, and clustering of scenarios based on the PCA function scores on the right panel.

predictors could be excluded from the dataset in order to reduce the number of variables. In Figure 8 it can be observed that at Marsdiep Noord, a location of a deeper tidal inlet, the highest loadings are given to radiation in the first component and to temperature in the second component. On the other hand, at Dantziggat, located in the shallow inter-tidal area, the opposite can be observed: the highest loadings are given to temperature in the first component and to radiation in the second component. Moreover, apart from temperature and radiation which have the highest loadings, northward-wind also has high loading in the second component at Datziggat. The factor loadings indicate the differences in the physical systems between the two locations. In deeper areas (Marsdiep Noord) solar radiation is the primary driver of the onset of phytoplankton blooms, while in shallower areas (Dantzigat) radiation intensity is slightly less limiting and light availability in the water column heavily depend on wind, which influences turbidity due to the mixing of layers and suspension. This could explain the greater importance of wind speed at Dantziggat, especially that northerly winds cause the highest surges of sea water along the Dutch coast (Klein Tank and Lenderink, 2009) that leads to enhanced mixing. In addition, thermal stratification and vertical mixing conditions are different at the two locations, Marsdiep Noord being intermittently stratified and Dantziggat being permanently mixed (van Leeuwen et al., 2015). This influences nutrient availability in the mixed layer depth as well as phytoplankton composition and therefore could be responsible for the greater importance of air temperature at Dantziggat. Moreover, top-down phytoplankton governing factors (e.g. grazing, filter-feeding) are also different at the two locations. For instance the density of filter-feeders is much higher near Dantziggat (Folmer et al., 2014).

3.2 Dynamic factors

Choosing the optimal number of unobserved factors is crucial to find a model that identifies common trends in the dataset without significant loss of statistical information. In order to find the optimal number of factors, the Akaike's Information Criterion (AIC) for each model setup (different number of factors, error covariance matrix diagonal or unstructured) was calculated and the model containing the lowest AIC value was selected as optimal. The selected model contains two factors if the error covariance matrix is set to diagonal. The identified two unobserved factors can be seen in the middle panel of Figure 12. It should be noted that the second

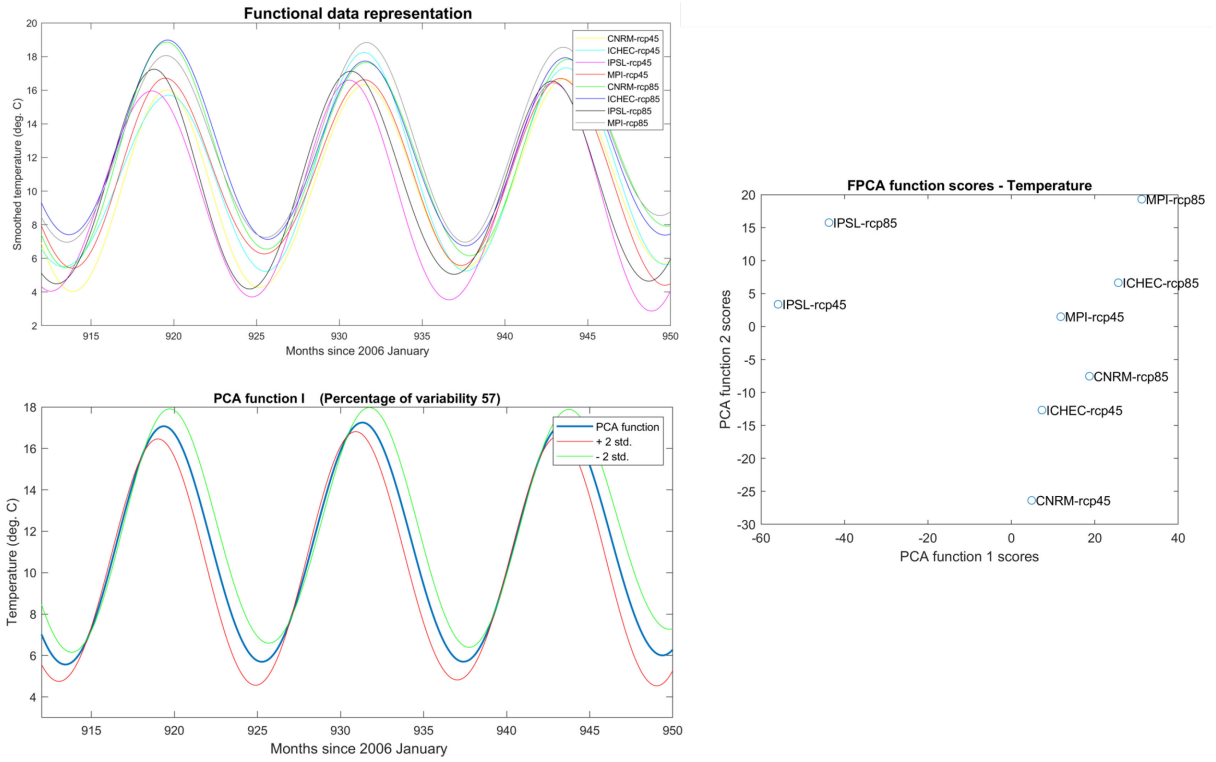

FIGURE 11
Functional Principal Component Analysis for Euro-CORDEX air temperature scenarios. Eight air temperature scenarios transformed to functional data on the upper left panel, the first PCA component with ± two standard deviations on the bottom left panel, and clustering of scenarios based on the PCA function scores on the right panel.

factor has negative factor loadings, and for demonstration purposes, it was plotted with negative sign. The results indicate two well distinguished trends. The first factor represents the trends of those locations where the chlorophyll-a concentration peak (spring bloom) occurs earlier, such as Dantziggat. This is confirmed by the factor loadings Γ. On the other hand, the second factor shows the pattern of the locations where the occurrence of the peak is delayed. The identified temporal shift between locations in the onset of the spring bloom can be explained by the different system dynamics of the areas, for instance shallower intertidal zones and the proximity from river or tidal inlets.

The partial standardized regression coefficients of the dynamic factor model for the two representative stations Marsdiep Noord and Dantziggat (see Figure 13) are in agreement with the findings of N-PLS loadings and confirm that radiation and temperature are the most important atmospheric variables. It is also confirmed that at Dantziggat air temperature has significantly larger impact than at Marsdiep Noord. As mentioned above, this might be related to the differences in thermal stratification, mixing conditions and trophic interactions between the two locations. Nevertheless, considering temporal correlation the relative impact of solar radiation (compared to the other variables) seems to be even more important, especially at station Marsdiep Noord. This finding could be explained by the fact that phytoplankton biomass onset in this coastal ecosystem highly depends on the timing of increased energy from solar radiation during spring (Sommer and Lengfellner, 2008). In fact, it was reported by (Sommer and Lengfellner, 2008) that the (external) light regime appears to play a more important role in the initiation of spring blooms than temperature.

3.3 Functional principal components

An important aspect of FPCA is the examination of the scores of each curve (variable) on each component (here we display the first two). Figure 9 (right panel) shows the scores of the first two components of the Functional Principal Component Analysis applied to Euro-CORDEX climate variables. In order to draw conclusions from this figure, one must take into consideration the inverse correlation between two group of variables: cloud cover and northerly wind on one hand

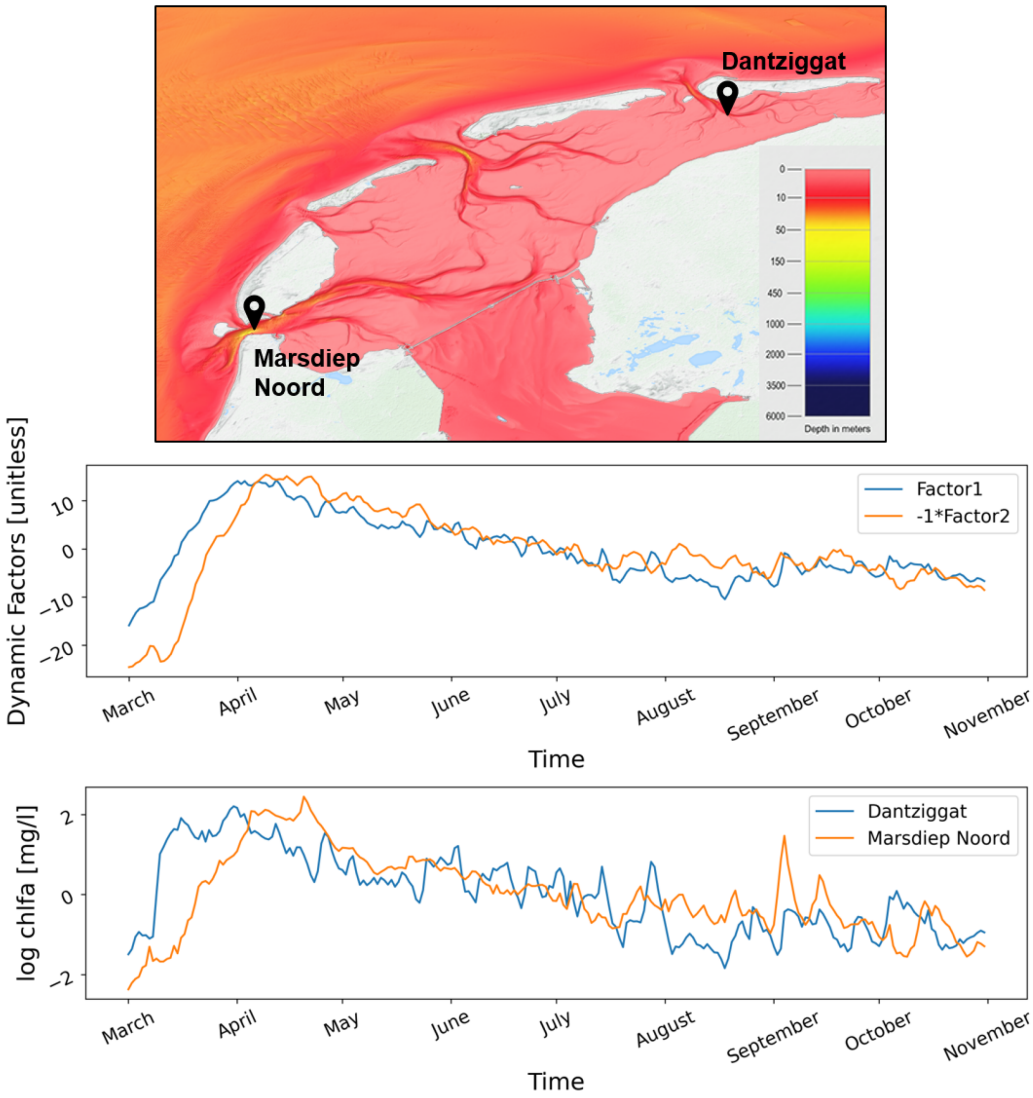

FIGURE 12
Underlying trends in chlorophyll-a time series. First and second factors of the Dynamic Factor model simulating chlorophyll-a trends with atmospheric variables as exogenous variables (middle). Log chlorophyll-a time series at representative stations (bottom). Bathymetry map showing the location of the representative stations (top). Map source is https://portal.emodnet-bathymetry.eu/.

and radiation, temperature, and pressure on the other hand. These variables have relatively similar FPCA function scores but the scores of second group have negative signs (expressing the inverse correlation). Known examples are the anticorrelation of atmospheric pressure and cloud cover (high pressure meaning lower cloudiness), or cloud cover and solar radiation (high cloudiness meaning lower surface downward solar radiation).

After accounting for the sign of the FPCA scores, a single main cluster can be distinguished that group variables (their functional representations) with similar characteristics and two variables, eastern wind and humidity, that are relatively separated. In general the correlation between cloud cover and wind speed is documented (Essenwanger, 1962) but the reason for eastern wind to be separated could be explained by the fact that at this specific location the maritime air mass is mainly brought by the northerly wind from the North Sea to replace the dry continental air mass (Klein Tank and Lenderink, 2009) causing cloud formation. The fact that radiation and temperature are positively correlated and lie near each other is expected, due to their similar sinusoidal functional shapes. The relationship of variations in air temperature to changes in air pressure was also reported in literature (Aguilar and Brunet, 2001) based on the analysis of long historical records. They concluded that changes in atmospheric circulation (influenced

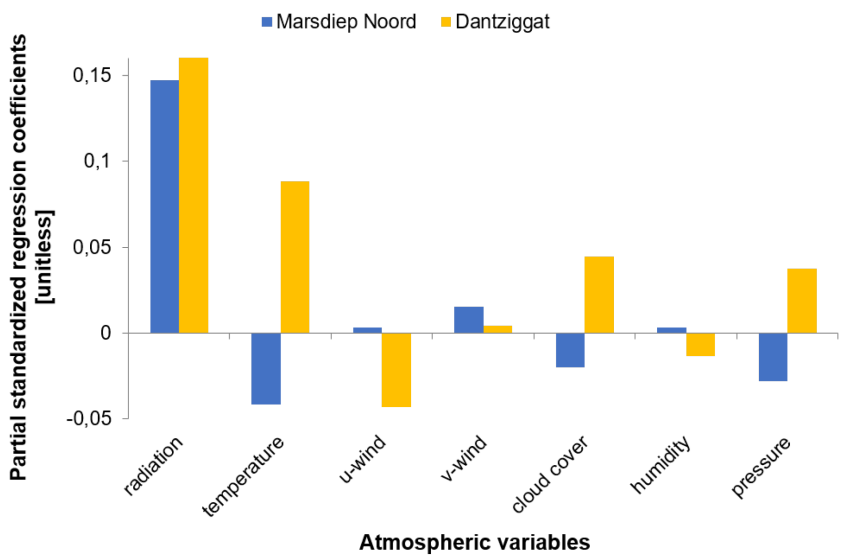

FIGURE 13
Dynamic Factor model partial standardized regression coefficients for Marsdiep Noord and Dantziggat stations demonstrating the effects of atmospheric variables as exogenous variables to model chlorophyll-a trends.

by air pressure) has a key role in air temperature variation, acknowledging that the relationship is seasonally dependent and impacted by the regional topography. Indirect links between air pressure and solar radiation were also discovered by (Klein Tank and Lenderink, 2009). They argue that high pressure systems impact air quality, which in turn affects solar irradiance (Zhang et al., 2022; Yang et al., 2022; Gómez et al., 2023). However, as the considered data are outputs of a climate model, which does not include air quality processes, this could not have been captured in our dataset.

Considering the Functional Principal Component Analysis results for the removal of multi-collinearity, one could expect that using only radiation or temperature might be sufficient without significant loss of statistical information. For climate impact studies at this location it should be considered, however, that solar radiation and temperature display different long term trends in this region and influence the phytoplankton dynamics differently. Based on the Euro-CORDEX projections, long term trends of radiation is constant or slightly decreasing, whereas air temperature trends are increasing.

Figure 10 depicts the functional representation of the eight climate scenarios for solar radiation and the first FPCA function with ± two standard deviations. Most of the variability 77% can be explained by the first FPCA function, which suggest that the scenarios are largely similar. Nevertheless, varying amplitudes and time shifts are observed between scenarios. These deviations from the mean function are depicted in the lower left panel of Figure 10. Furthermore, when comparing the component scores it can be clearly identified that the climate scenarios are clustered based on the driving GCMs, and the two RCP scenarios (RCP4.5 and RCP 8.5) per driving GCM have similar characteristics. This is in line with previous finding that uncertainty in Regional Climate Model projections are primarily influenced by the driving GCMs while the impact of RCPs is less dominant (Morim et al., 2019). The results also suggest that the CNRM and ICHEC driving GCMs are very similar to each other, whereas the IPSL driving GCM is divergent from the other driving GCMs. This was also reported by (Mészáros et al., 2021) based on an in-depth analysis of the characteristics of Euro-CORDEX climate projections.

The same exercise was performed for air temperature and the results are shown in Figure 11. Similarly to the radiation scenarios, the air temperature scenarios also differ in their amplitudes and seasonality (temporal shift). The uncertainty around the mean function (first FPCA component) clearly illustrates this phenomenon. In this case, the variability explained by the first FPCA function is smaller 57% indicating that temperature scenarios are less similar, perhaps due to the long term trends (moderately increasing for RCP4.5 but more sharply increasing for RCP8.5). Surprisingly, the FPCA component scores show a different picture from the results of the radiation variable. While the IPSL driving GCM is still farthest from the others and ICHEC RCP4.5 and CNRM RCP8.5 remain similar, the other scenarios are not clustered by driving GCMs anymore.

These findings indicate that the time series of Euro-CORDEX climate scenarios (for both solar radiation and air temperature) show structural differences across driving GCMs

but full independence between the scenarios cannot be assumed as their functional features are similar. In fact, they can be described with a mean function and varying amplitude plus phase shift. This feature should be incorporated in any statistical model that is aimed at generating new representative climate scenarios similar to the existing Euro-CORDEX projection scenarios. While the results of the Functional Principle Component Analysis do not allow us to draw conclusions about shifting seasonality of radiation scenarios on the long-term, but it does express the strength of the mean signal (77% and 57% variance explained by the first FPCA for radiation and temperature respectively) and highlights the source of the variability around the mean signal.

In a related study (Mészáros et al., 2021) a deeper analysis of the same Euro-CORDEX climate dataset has been performed that reached conclusions on the long term characteristics. In this analysis the radiation projections have been modelled by a structural time series model that has various components accounting for long term trend, seasonal shape with varying amplitude and time shift, and an additive residual term. The parameters of these time series model components have been estimated through Bayesian parameter inference based on the eight Euro-CORDEX climate projection scenarios over the 21st entury. The seasonal shift was represented by the deviations in the (yearly) seasonal cycle lengths. It was observed that the deviations are centered around zero (deviations were maximum around 14 days) and have a negative lag 1 autocorrelation meaning that most positive deviations tend to be followed by negative deviations and vice versa. In this way the yearly cycle lengths remain close to the ideal cycle length (one calendar year) throughout the entire time series. Therefore, no consistent shift in seasonality was identified. Regarding the trend slope, the general expectation that RCP8.5 has steeper slope than RCP4.5 was confirmed for the temperature variable and also for solar radiation but much less pronounced. Finally, regarding the amplitude of the seasonal shape, deviations of up to around 20% were observed but without consistent trend.

4 Discussion

It must be emphasized once again that all statistical techniques applied in this study are well documented in the literature. Consequently, the added value of our research to the marine scientific community is not the development of novel techniques but the application of carefully selected dimension reduction techniques (originating from various domains) to marine and climate big data, in order to provide statistical underpinning for climate variable selection and data reduction to support subsequent ecological impact studies. In addition, our study also offers a framework for the structured application of these dimension reduction techniques to specifically cover three features in marine and climate datasets: (1) spatial correlation, (2) temporal correlation, and (3) functional variability. The paper therefore offers a "dimension reduction tool kit" that goes beyond the standard practice and is suitable to jointly study marine and climate datasets.

For instance, N-PLS was developed in the domain of chemometrics, and while several applications in other domains were reported (Bergant and Kajfež-Bogataj, 2005; Bro, 2006; Mas et al., 2010; Favilla et al., 2013; Lopez-Fornieles et al., 2022), it has not been applied in coastal ecological impact studies, to the best of the author's knowledge. An N-PLS application particularly relevant to our research is the study of Bergant and Kajfež-Bogataj, (2005) in the field of applied climatology that used N-PLS as an empirical downscaling tool for predicting climate variables. That study employed N-PLS regression using average monthly near-ground air temperature, specific humidity and sea-level pressures from Global Climate Models as predictors for downscaled average monthly air temperature, dew temperature, and precipitation. The results of the N-PLS regression were then compared to the ones form Principal Component Regression (PCR). It was concluded that in general N-PLS regression outperforms the commonly used PCR, and therefore presents a promising alternative. While that study presented comparison to PCR, our study extends the comparison of the N-PLS results to a range two-way and multi-way methods. Moreover, the application of N-PLS is also extended by including ecological response apart from the climate data. This provides further evidence on the benefits of N-PLS in the fields of marine and climate sciences.

As opposed to N-PLS, Dynamic Factor Analysis has been more widely used in environmental studies (Fujiwara and Mohr, 2009; Chow et al., 2011; Kuo et al., 2014), including marine ecosystem studies (Zuur et al., 2003b; Zuur et al., 2003a; Ruff et al., 2017), also considering the impact of climate change (Kröncke et al., 2019) to identify general patterns in multivariate time series, interactions between the time series, and the correlation between the time series and explanatory variables. Nevertheless, our application can complement the studies of (Zuur et al., 2003b; Zuur et al., 2003a) that focused on macro zoobenthos and fisheries, as our study describes phytoplankton biomass (via chlorophyll-a as proxy), which has different role in the marine food web.

Our study also advances scientific knowledge related to the analysis (and data reduction) of climate scenarios. In the past, PCA has been applied to various climate multi-model ensembles to reduce the larger ensemble sizes into smaller subsets (Sanderson et al., 2015). applied PCA to define a measure of similarity between models in the Coupled Model Intercomparison Project (CMIP5) (Taylor et al., 2012) (Mendlik and Gobiet, 2016). also used PCA to find common climate change patterns within a multi-model ensemble (ENSEMBLES regional multi-model ensemble), combined with cluster analysis detecting model similarities. Furthermore (Dalelane et al., 2018), presented a methodology using PCA

for reducing the climate projection ensemble size of EURO-CORDEX for subsequent impact studies. There are important differences between our research and these existing studies, however. Firstly, the motivation for those studies to use PCA was to select a subset of scenarios from a larger ensemble while keeping the characteristics representative, whereas our goal is more than just the clustering of climate scenarios. Our study identified features of the radiation and temperature functions such as the sources of variability (e.g. time lag and amplitude shift). These identified properties allow us to construct synthetic realizations of the climate projection scenarios in subsequent studies (using climate generators). Thus, the objectives are in sharp contrast, the former aiming to support scenario studies (based on a reduced number of representative ensemble members) and the latter supporting probabilistic studies (based on numerous synthetic realizations). Secondly, all of these studies used ordinary PCA, not Functional Principal Component analysis. By considering climate data to be functional data, although computed at discrete time intervals, Functional Data Analysis allowed us to represent the entire measured function on a continuum interval. This paradigm shift from discrete-time to functional data presents an alternative approach to the conventional statistical methods, since it provides additional information on the underlying functions. Of course, Functional Data Analysis itself is also not new and has been previously applied in various fields, such as hydrology (Suhaila et al., 2011; Chebana et al., 2012; Suhaila and Yusop, 2017; Alaya et al., 2020; Hael, 2021), climatology (Bonner et al., 2014; Suhaila, 2021), water quality (Henderson, 2006; Gong et al., 2021), and others (Ullah and Finch, 2013) (Suhaila, 2021). already documented the benefits of using Functional Data Analysis to study temporal features of climate data, although in that study Functional PCA was applied to historical data, namely the El Niño Southern Oscillation. In our research Functional PCA is applied to an ensemble of future climate projections.

5 Conclusions

In this paper a variety of statistical methods for the multivariate analysis of air-sea interactions are applied in order to aid the understanding of complex multi-dimensional datasets and to support ecological impact studies. The selected dimension reduction methods were chosen to account for spatial correlation, temporal correlation, and functional variability. The presented methods were found to be useful in exploring the datasets, identifying latent processes, removing multi-collinearity and selecting atmospheric variables that are the most important when predicting chlorophyll-a response. A comparison of standard two-way (PCA, PLS) and less frequently used multi-way methods (PARAFAC, Tucker, N-PLS) showcased the potential of multi-way methods to construct parsimonious data reduction models. The results allow us to conclude that there is room for dimension reduction in the atmospheric dataset since in most cases low prediction errors could be achieved with as few as 2 principal components. Further conclusions could be drawn on the predictors that affect the coastal chlorophyll-a concentration the most. All used methods indicate solar radiation to be the most important influencing factor, followed by air temperature and wind in shallow zones. The dynamic factor model proved to be an appropriate tool to acquire information about underlying common trends in chlorophyll-a time series across stations, and to investigate the effects of atmospheric explanatory variables with the inclusion of temporal structure when constructing unobserved factors. The difference in phytoplankton bloom onset at different parts of the Dutch Wadden Sea was revealed by the dynamic factor model and solar radiation was re-confirmed to be the most dominant atmospheric variable when temporal correlation is considered. Finally, using Functional Principal Component analysis further insights into the Euro-CORDEX regional climate data were gained by identifying features of the climate projection scenarios.

Overall, our findings support the use of solar radiation as the primary driving atmospheric variable to simulate climate impacts on coastal chlorophyll-a concentrations in the Dutch Wadden Sea. Moreover, structural patterns of Euro-CORDEX climate scenarios for solar radiation and air temperature have been determined, which provide information on the mean functions and their uncertainties. In ecological impact studies, uncertainties stemming from the climate scenarios are often only represented by picking few climate ensemble members (some of the driving GCMs and RCPs). Instead of such scenario studies it is advised to use the presented uncertainty intervals in the functional variation of the Euro-CORDEX climate scenarios and perform a fully probabilistic assessment for proper climate uncertainty propagation. In this context, the findings can also inform studies in which climate generators are proposed to produce numerous synthetic realizations of solar radiation and air temperature projections. The underlying structural time series models of such climate generators should incorporate the two identified features: varying amplitudes and time lag (shift) in seasonality. Moreover, due to the identified shared characteristics, climate scenarios seem exchangeable rather than independent, hence, the pooling of scenarios is recommended in hierarchical models to borrow strength and make statistical models more optimal.

Data availability statement

The datasets presented in this study can be found in online repositories. The names of the repository/repositories and accession number(s) can be found below: https://matroos.

deltares.nl/; http://data.dta.cnr.it/ecopotential/wadden_sea/; https://github.com/lorincmeszaros/dimension-reduction. The Matlab and Python scripts used for data processing and analysis can be accessed at: https://github.com/lorincmeszaros/dimension-reduction.

Author contributions

The study was conducted within the PhD research of LM. LM led the data collection, data and results analysis, and manuscript preparation. FM and GJ provided advice on the use of statistical techniques and contributed to their mathematical formulation in Chapter 2. GES advised on the ecological aspects and helped to refine the research objective in order to ensure its applicability to the journal. All authors contributed to the study conception, design and the discussion of results and recommendations. All authors read and approved the final manuscript.

Funding

This research has received funding from the European Union's Horizon 2020 research and innovation programme under grant agreement No 727277. The work was supported by Deltares Theme Enabling Technologies, funded by Deltares - Strategic Research Budget from the Ministry of Economic Affairs and Climate Policy.

Acknowledgments

We are grateful to the reviewers for their comments that helped to improve the quality of the manuscript.

Conflict of interest

The authors declare that the research was conducted in the absence of any commercial or financial relationships that could be construed as a potential conflict of interest.

Junior RE Areti Balconi, Alfred Wegener Institute, Sylt, Germany in collaboration with reviewer VF.

Publisher's note

All claims expressed in this article are solely those of the authors and do not necessarily represent those of their affiliated organizations, or those of the publisher, the editors and the reviewers. Any product that may be evaluated in this article, or claim that may be made by its manufacturer, is not guaranteed or endorsed by the publisher.

Supplementary material

The Supplementary Material for this article can be found online at: https://www.frontiersin.org/articles/10.3389/fmars.2022.920616/full#supplementary-material

References

Aguilar, E., and Brunet, M. (2001). Seasonal patterns of air surface temperature and pressure change in different regions of Antarctica. *Detecting Model. Regional Climate Change* 1, 215–228. doi: 10.1007/978-3-662-04313-419

Alaya, M. A. B., Ternynck, C., Dabo-Niang, S., Chebana, F., and Ouarda, T. B. (2020). Change point detection of flood events using a functional data framework. *Adv. Water Resour.* 103522. doi: 10.1016/J.ADVWATRES.2020.103522

Andersson, C. A., Bro, R.The N-way Toolbox for MATLAB. (2000). *Chemometrics and intelligent laboratory systems* (Amsterdam: Elsevier). 1–4. doi: 10.1016/S0169-7439(00)00071-X

Behrenfeld, M. J., and Boss, E. S. (2018). Student's tutorial on bloom hypotheses in the context of phytoplankton annual cycles. *Global Change Biol.* 24, 55–77. doi: 10.1111/gcb.13858

Bergant, K., and Kajfež-Bogataj, L. (2005). N-PLS regression as empirical downscaling tool in climate change studies. *Theor. Appl. Climatology* 81, 11–23. doi: 10.1007/s00704-004-0083-2

Blauw, A. N., Benincà, E., Laane, R. W., Greenwood, N., and Huisman, J. (2018). Predictability and environmental drivers of chlorophyll fluctuations vary across different time scales and regions of the north Sea. *Prog. Oceanography* 161, 1–18. doi: 10.1016/j.pocean.2018.01.005

Blauw, A. N., Los, H. F. J., Bokhorst, M., and Erftemeijer, P. L. A. (2009). GEM: A generic ecological model for estuaries and coastal waters. *Hydrobiologia* 618, 175–198. doi: 10.1007/s10750-008-9575-x

Bonner, S. J., Newlands, N. K., and Heckman, N. E. (2014). Modeling regional impacts of climate teleconnections using functional data analysis. *Environ. Ecol. Stat.* 21, 1–26. doi: 10.1007/S10651-013-0241-8/FIGURES/6

Bro, R. (1996). Multiway calibration. multilinear PLS. *J. Chemometrics* 10, 47–61. doi: 10.1002/(SICI)1099-128X(199601)10:1<47::AID-CEM400>3.0.CO;2-C

Bro, R. (1997). PARAFAC. tutorial and applications. *Chemometrics Intelligent Lab. Syst.* 38, 149–171. doi: 10.1016/S0169-7439(97)00032-4

Bro, R. (1998). "Multi-way analysis in the food industry," in *Models, algorithms, and applications. Ph.D. thesis* (Amsterdam: Universiteit van Amsterdam).

Bro, R. (2006). Review on multiway analysis in chemistry - 2000-2005. *Crit. Rev. Analytical Chem.* 36, 279–293. doi: 10.1080/10408340600969965

Bro, R., Smilde, A. K., and De Jong, S. (2001). On the difference between low-rank and subspace approximation: Improved model for multi-linear PLS regression. *Chemometrics Intelligent Lab. Syst.* 58, 3–13. doi: 10.1016/S0169-7439(01)00134-4

Campbell, J. W. (1995). The lognormal distribution as a model for bio-optical variability in the sea. *J. Geophysical Research: Oceans* 100, 13237–13254. doi: 10.1029/95JC00458

Chebana, F., Dabo-Niang, S., and Ouarda, T. B. (2012). Exploratory functional flood frequency analysis and outlier detection. *Water Resour. Res.* 4514. doi: 10.1029/2011WR011040

Chow, S. M., Zu, J., Shifren, K., and Zhang, G. (2011). Dynamic factor analysis models with time-varying parameters. *Multivariate Behav. Res.* 46, 303–339. doi: 10.1080/00273171.2011.563697

Dalelane, C., Früh, B., Steger, C., and Walter, A. (2018). A pragmatic approach to build a reduced regional climate projection ensemble for Germany using the EURO-CORDEX 8.5 ensemble. *J. Appl. Meteorology Climatology* 57, 477–491. doi: 10.1175/JAMC-D-17-0141.1

de Jong, S. (1998). Regression coefficients in multilinear PLS. *J. Chemometrics* 12, 77–81. doi: 10.1002/(SICI)1099-128X(199801/02)12:1<77::AID-CEM496>3.0.CO;2-7

Dufresne, J. L., Foujols, M. A., Denvil, S., Caubel, A., Marti, O., Aumont, O., et al. (2013). Climate change projections using the IPSL-CM5 earth system model: From CMIP3 to CMIP5. *Climate Dynamics* 40, 9-10. doi: 10.1007/s00382-012-1636-1

Essenwanger, O. 1962. Correlation of wind direction observations and other surface elements. *Geofisica pura e applicata* 51, 251–290. doi: 10.1007/BF01992668

Favilla, S., Durante, C., Vigni, M. L., and Cocchi, M. (2013). Assessing feature relevance in NPLS models by VIP. *Chemometrics Intelligent Lab. Syst.* 129, 76–86. doi: 10.1016/J.CHEMOLAB.2013.05.013

Folmer, E. O., Drent, J., Troost, K., Büttger, H., Dankers, N., Jansen, J., et al. (2014) Large-Scale spatial dynamics of intertidal mussel (Mytilus edulis l.) bed coverage in the German and Dutch wadden Sea. *Ecosystems* 17, 550–566. doi: 10.1007/s10021-013-9742-4

Fujiwara, M., and Mohr, M. S. (2009). Identifying environmental signals from population abundance data using multivariate time-series analysis. *Oikos* 118, 1712–1720. doi: 10.1111/j.1600-0706.2009.17570.x

Giorgetta, M. A., Jungclaus, J., Reick, C. H., Legutke, S., Bader, J., Böttinger, M., et al. (2013). Climate and carbon cycle changes from 1850 to 2100 in MPI-ESM simulations for the coupled model intercomparison project phase 5. *J. Adv. Modeling Earth Syst* 5, 572–597. doi: 10.1002/jame.20038

Gómez, I., Molina, S., and Galiana-Merino, J. J. (2023). Evaluating the influence of air pollution on solar radiation observations over the coastal region of alicante (Southeastern Spain). *J. Environ. Sci.* 126, 633–643. doi: 10.1016/J.JES.2022.05.004

Gong, M., Miller, C., Scott, M., O'Donnell, R., Simis, S., Groom, S., et al. (2021). State space functional principal component analysis to identify spatiotemporal patterns in remote sensing lake water quality. *Stochastic Environ. Res. Risk Assess.* 35, 2521–2536. doi: 10.1007/S00477-021-02017-W/FIGURES/7

González Taboada, F., and Anadón, R. (2014). Seasonality of north Atlantic phytoplankton from space: impact of environmental forcing on a changing phenology (1998-2012). *Global Change Biol.* 20, 698–712. doi: 10.1111/gcb.12352

Hael, M. A. (2021). Modeling of rainfall variability using functional principal component method: a case study of taiz region, Yemen. *Modeling Earth Syst. Environ.* 7, 17–27. doi: 10.1007/S40808-020-00876-W/FIGURES/6

Harvey, A. C. (1990). *Forecasting, structural time series models and the kalman filter* (Cambridge: Cambridge University Press), 554. doi: 10.1017/CBO9781107049994

Hastie, T., Tibshirani, R., and Friedman, J. (2009). *The elements of statistical learning* Vol. vol. 1 (New York, NY: Springer), 1–694. doi: 10.1007/b94608

Hazeleger, W., Wang, X., Severijns, C., Ştefănescu, S., Bintanja, R., Sterl, A., et al. (2012). EC-Earth V2.2: Description and validation of a new seamless earth system prediction model. *Climate Dynamics* 39, 2611–2629. doi: 10.1007/s00382-011-1228-5

Henderson, B. (2006). Exploring between site differences in water quality trends: a functional data analysis approach. *Environmetrics* 17, 65–80. doi: 10.1002/ENV.750

Jacob, D., Petersen, J., Eggert, B., Alias, A., Christensen, O. B., Bouwer, L. M., et al. (2014). Euro-Cordex: new high-resolution climate change projections for european impact research. *Regional Environ. Change* 14, 563–578. doi: 10.1007/s10113-013-0499-2

Katara, I., Janine, A. E., Ae, I., Pierce, G. J., Beth, A. E., Ae, S., et al. (2008). Atmospheric forcing on chlorophyll concentration in the Mediterranean. *Essential Fish Habitat Mapp. Mediterr.* 203, 33–48. doi: 10.1007/978-1-4020-9141-44

Klein Tank, A. M. G., and Lenderink, G. (2009). Climate change in the netherlands: supplements to the knmi'06 scenarios. *Tech rep KNMI Bilt Netherlands* 1, 1–36.

Kröncke, I., Neumann, H., Dippner, J. W., Holbrook, S., Lamy, T., Miller, R., et al. (2019). Comparison of biological and ecological long-term trends related to northern hemisphere climate in different marine ecosystems. *Nat. Conserv.* 34, 311–341. doi: 10.3897/NATURECONSERVATION.34.30209

Kuo, Y. M., Chu, H. J., and Pan, T. Y. (2014). Temporal precipitation estimation from nearby radar reflectivity using dynamic factor analysis in the mountainous watershed - a case during typhoon morakot. *Hydrological Processes* 28, 999–1008. doi: 10.1002/hyp.9639

Longhurst, A. R. (2007). *Ecological geography of the Sea* (Amsterdam: Elsevier Inc). doi: 10.1016/B978-0-12-455521-1.X5000-1

Lopez-Fornieles, E., Brunel, G., Rancon, F., Gaci, B., Metz, M., Devaux, N., et al. (2022). Potential of multiway PLS (N-PLS) regression method to analyse time-series of multispectral images: A case study in agriculture. *Remote Sens.* 14, 216. doi: 10.3390/RS14010216

Los, F. J., Villars, M. T., and van der Tol, M. W. (2008). A 3-dimensional primary production model (BLOOM/GEM) and its applications to the (southern) north Sea (coupled physical-chemical-ecological model). *J. Mar. Syst.* 74, 259–294. doi: 10.1016/j.jmarsys.2008.01.002

Lu, H., Plataniotis, K. N., and Venetsanopoulos, A. (2013). *Multilinear subspace learning: Dimensionality reduction of multidimensional data* (Boca Raton, Florida, United States: CRC Press), 296.

Lütkepohl, H. (2005). *New introduction to multiple time series analysis* (Berlin, Heidelberg: Springer Berlin Heidelberg), 1–764. doi: 10.1007/978-3-540-27752-1

Maitra, S., and Yan, J. (2008). Principle component analysis and partial least squares: Two dimension reduction techniques for regression. *Casualty Actuarial Society 2008 Discussion Paper Program* 1, 79–90.

Mas, S., de Juan, A., Tauler, R., Olivieri, A. C., and Escandar, G. M. (2010). Application of chemometric methods to environmental analysis of organic pollutants: A review. *Talanta* 80, 1052–1067. doi: 10.1016/J.TALANTA.2009.09.044

McQuatters-Gollop, A., and Vermaat, J. E. (2011). Covariance among north Sea ecosystem state indicators during the past50 years — contrasts between coastal and open waters. *J. Sea Res.* 65, 284–292. doi: 10.1016/J.SEARES.2010.12.004

Meijgaard, E., Ulft, L., Berg, W., Bosvelt, F., Hurk, B., Lenderink, G., et al. (2008). The knmi regional atmospheric model racmo version 2.1. *Tech Rep. 302 KNMI* 1, 1–50.

Mendlik, T., and Gobiet, A. (2016). Selecting climate simulations for impact studies based on multivariate patterns of climate change. *Climatic Change* 135, 381–393. doi: 10.1007/S10584-015-1582-0/FIGURES/5

Mészáros, L., van der Meulen, F., Jongbloed, G., and El Serafy, G. (2021). A Bayesian stochastic generator to complement existing climate change scenarios: supporting uncertainty quantification in marine and coastal ecosystems. *Stochastic Environ. Res. Risk Assess.* 35, 719–736. doi: 10.1007/s00477-020-01935-5

Mike West, J. H. (1997). *Bayesian Forecasting and dynamic models* (New York, NY: Springer), 680. doi: 10.1007/b98971

Morim, J., Hemer, M., Wang, X. L., Cartwright, N., Trenham, C., Semedo, A., et al. (2019). Robustness and uncertainties in global multivariate wind-wave climate projections. *Nat. Climate Change* 9, 711–718. doi: 10.1038/s41558-019-0542-5

Ramsay, J., Hooker, G., and Graves, S. (2009). *Functional data analysis with r and MATLAB* (New York: Springer New York). doi: 10.1007/978-0-387-98185-7

Ramsay, J. O., and Silverman, B. W. (2005). *Functional data analysis* (Springer Series in Statistics (New York, NY: Springer New York). doi: 10.1007/b98888

Ruff, C. P., Anderson, J. H., Kemp, I. M., Kendall, N. W., Mchugh, P. A., Velez-Espino, A., et al. (2017). Salish Sea Chinook salmon exhibit weaker coherence in early marine survival trends than coastal populations. *Fisheries Oceanography* 26, 625–637. doi: 10.1111/FOG.12222

Samuelsson, P., Gollvik, S., Kupiainen, M., Kourzeneva, E., and van de Berg, W. (2015). The surface processes of the rossby centre regional atmospheric climate model (RCA4). *Tech Rep. 1 SMHI* 157, 1–58.

Sanderson, B. M., Knutti, R., and Caldwell, P. (2015). A representative democracy to reduce interdependency in a multimodel ensemble. *J. Climate* 28, 5171–5194. doi: 10.1175/JCLI-D-14-00362.1

Segovia-Gonzalez, M. M., Guerrero, F. M., and Herranz, P. (2009). Explaining functional principal component analysis to actuarial science with an example on vehicle insurance. *Insurance: Mathematics Economics* 45, 278–285. doi: 10.1016/j.insmatheco.2009.07.003

Smilde, A. K. (1997). Comments on multilinear PLS. *J. Chemometrics* 11, 367–377. doi: 10.1002/(SICI)1099-128X(199709/10)11:5<367::AID-CEM481>3.0.CO;2-I

Smilde, A., Bro, R., and Geladi, P. (2004). Multi-way analysis with applications in the chemical sciences. *(J. Wiley)* 381, 1–396. doi: 10.1002/0470012110

Sommer, U., and Lengfellner, K. (2008). Climate change and the timing, magnitude, and composition of the phytoplankton spring bloom. *Global Change Biol.* 14, 1199–1208. doi: 10.1111/J.1365-2486.2008.01571.X

Suhaila, J. (2021). Functional data visualization and outlier detection on the anomaly of El niño southern oscillation. *Climate* 9, 118. doi: 10.3390/CLI9070118

Suhaila, J., Jemain, A. A., Hamdan, M. F., and Wan Zin, W. Z. (2011). Comparing rainfall patterns between regions in peninsular Malaysia via a functional data analysis technique. *J. Hydrology* 411, 197–206. doi: 10.1016/J.JHYDROL.2011.09.043

Suhaila, J., and Yusop, Z. (2017). Spatial and temporal variabilities of rainfall data using functional data analysis. *Theor. Appl. Climatology* 129, 229–242. doi: 10.1007/S00704-016-1778-X/TABLES/4

Taylor, K. E., Stouffer, R. J., and Meehl, G. A. (2012). An overview of CMIP5 and the experiment design. *Bull. Am. Meteorological Soc.* 93, 485–498. doi: 10.1175/BAMS-D-11-00094.1

Ullah, S., and Finch, C. F. (2013). Applications of functional data analysis: A systematic review. *BMC Med. Res. Method.* 13, 1–12. doi: 10.1186/1471-2288-13-43/TABLES/1

Undén, P., Rontu, L., Järvinen, H., Lynch, P., Calvo, J., Cats, G., et al. (2002). *Swedish Meteorological and hydrological institute* (Norrköping, Sweden: Swedish Meteorological and Hydrological Institute), 76. HIRLAM-5 scientific documentation. Tech. repSE-601.

Vance, T. C., Wengren, M., Burger, E. F., Hernandez, D., Kearns, T., Merati, N., et al. (2019). From the oceans to the cloud: Opportunities and challenges for data, models, computation and workflows. *Front. Mar. Sci.* 211. doi: 10.3389/FMARS.2019.00211/BIBTEX

van Leeuwen, S., Tett, P., Mills, D., and van der Molen, J. (2015). Stratified and nonstratified areas in the north Sea: Long-term variability and biological and policy implications. *J. Geophysical Res.: Oceans* 120, 4670–4686. doi: 10.1002/2014JC010485

van Vuuren, D. P., Edmonds, J., Kainuma, M., Riahi, K., Thomson, A., Hibbard, K., et al. (2011). The representative concentration pathways: an overview. *Climatic Change* 5, 5–31. doi: 10.1007/s10584-011-0148-z

Voldoire, A., Sanchez-Gomez, E., Salas y Mélia, D., Decharme, B., Cassou, C., Sénési, S., et al. (2013), The CNRM-CM5.1 global climate model: Description and basic evaluation. *Climate Dynamics* 40, 2091–2121. doi: 10.1007/s00382-011-1259-y

Wold, S., Geladi, P., Esbensen, K., and Öhman, J. (1987). Multi-way principal components-and pls-analysis. *J. Chemometrics* 1, 41–56. doi: 10.1002/cem.1180010107

Yang, L., Gao, X., Li, Z., and Jia, D. (2022). Quantitative effects of air pollution on regional daily global and diffuse solar radiation under clear sky conditions. *Energy Rep.* 8, 1935–1948. doi: 10.1016/J.EGYR.2021.12.081

Zhang, X., Zhang, M., Cui, Y., and He, Y. (2022). Estimation of daily ground-received global solar radiation using air pollutant data. *Front. Public Health* 10, 617. doi: 10.3389/FPUBH.2022.860107/XML/NLM

Zhao, Q., Caiafa, C. F., Mandic, D. P., Chao, Z. C., Nagasaka, Y., Fujii, N., et al. (2013). Higher order partial least squares (HOPLS): A generalized multilinear regression method. *IEEE Trans. Pattern Anal. Mach. Intell.* 35, 1660–1673. doi: 10.1109/TPAMI.2012.254

Zuur, A. F., Fryer, R. J., Jolliffe, I. T., Dekker, R., and Beukema, J. J. (2003b). Estimating common trends in multivariate time series using dynamic factor analysis. *Environmetrics* 14, 665–685. doi: 10.1002/env.611

Zuur, A. F., Tuck, I. D., and Bailey, N. (2003a). Dynamic factor analysis to estimate common trends in fisheries time series. *Can. J. Fisheries Aquat. Sci.* 60, 542–552. doi: 10.1139/f03-030

Frontiers in Marine Science

Explores ocean-based solutions for emerging global challenges

The third most-cited marine and freshwater biology journal, advancing our understanding of marine systems and addressing global challenges including overfishing, pollution, and climate change.

Discover the latest Research Topics

See more →

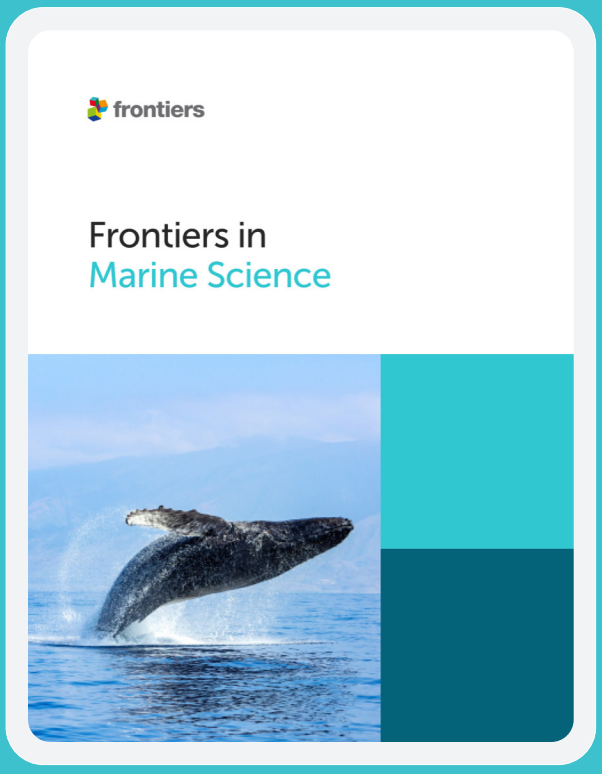

Frontiers

Avenue du Tribunal-Fédéral 34
1005 Lausanne, Switzerland
frontiersin.org

Contact us

+41 (0)21 510 17 00
frontiersin.org/about/contact